RIKEN
Accelerator
Progress Report

2017

vol. 51

理化学研究所　仁科加速器研究センター
RIKEN Nishina Center for Accelerator-Based Science

RIKEN Accelerator Progress Report 2017

vol. **51**

理化学研究所　仁科加速器研究センター
RIKEN Nishina Center for Accelerator-Based Science
Wako, Saitama, 351-0198 JAPAN

RIKEN Accelerator Progress Report 2017 vol.51

This is an unabridged version of the 51st volume of RIKEN Accelerator Progress Report (hereinafter referred to as APR), the official annual report of the Nishina Center for Accelerator-Based Science.

A PDF version of APR can be downloaded from our website.
http://www.nishina.riken.jp/researcher/APR/index_e.html

PREFACE

In 2017, RIKEN celebrated its 100th year. The Nishina Center's history goes back 86 years from the inauguration of Yoshio Nishina's Laboratory in RIKEN.

At the Centennial Exchange Event held on December 21, a rice pounding festival was held in front of the RIBF building. We should be proud of the fact that we have been holding such exchange parties, that is, a barbecue in summer and rice pounding in winter, for a long time. The Nishina Center has borne the history of RIKEN for many years beyond our own research that started with the legacy of Yoshio Nishina. The first cyclotron developed by Nishina and completed in 1937 would now be 80 years old if alive. Its magnet escaped the fate of being thrown into the sea, has been revived as the magnet of the third cyclotron, and is currently being displayed at the site of the Japan Radioisotope Association located in Komagome.

The year 2017 marked the RIKEN Wako campus' 50th anniversary as well. It was Wako where our predecessors completed the 4th cyclotron and to which RIKEN relocated its headquarters. A symbol of RIKEN's relocation to Wako and now a monument in front of the fountain, the 4th cyclotron was the significant backdrop of the tree planting of the "Nishina Tomoka" cherry blossom and the unveiling ceremony of the monument commemorating the discovery of nihonium that took place at the 50th anniversary of the Wako campus held on June 7. Our research, which requires large-scale facilities, cannot be easily conducted in other places and is therefore prone to becoming highly indigenous. For this reason, as in the past, we will continue to lead and represent research history at the Wako campus. As a matter of fact, it has been 30 years since the 5th cyclotron/RIKEN ring cyclotron RRC started its operation.

On December 4 and 5, a symposium commemorating the 10th anniversary of the RIBF was held. It can be said that our RIBF has attained highly remarkable success over the past 10 years since the 9th cyclotron SRC started its operation. All of the experimental facilities have been placed as planned. With the beam intensity increasing every year, the RIBF's performance is unparalleled in the world. International cooperation is further expanding, with experimental equipment brought in from across the globe. The highlighted articles of this volume of the Accelerator Progress Report clearly show the blooming of the RIBF.

So, what will happen in the next ten years? Nuclear research will make a huge leap worldwide. SPIRAL-2 in France, FAIR in Germany, FRIB in the US, and RAON in Korea will begin operations. Such intense competition will surely open a new horizon in the field of nuclear research. With these challenges coming our way, we will need to make new discoveries by taking advantage of our competitive edge and coming up with new research ideas.

On March 14, the "Commemorative Ceremony to Celebrate the Naming of the New Element Nihonium" was held with his Imperial Highness the Crown Prince in attendance. We were honored to have the Crown Prince give a speech about how, as a high school student, he had to draw the periodic table on 30 sheets of paper as homework. From here on, high school students will write "Nh" on the periodic table. With the discovery of nihonium, a supplementary budget of 4 billion yen has been provided. With this budget, a new experimental building has been built GARIS-2 relocated to the E6 Laboratory and has been running smoothly since December, a good start for the experiment to search for element 119.

In fiscal year 2018, RIKEN will enter its 4th midterm, which will last for seven years. It is the aim of the Nishina Center to achieve higher goals, promote the RIBF enhancement plan, and discover elements 119 and 120. Things are looking good for the future of the Nishina Center. Let us all move forward as one.

Hideto En'yo
Director
RIKEN Nishina Center for Accelerator-Based Science

C O N T E N T S

II. RESEARCH ACTIVITIES I (Nuclear, Particle and Astro-Physics)

1. Nuclear Physics

2. Nuclear Physics (Theory)

Ⅲ. RESEARCH ACTIVITIES II (Material Science and Biology)

1. Atomic and Solid State Physics (Ion)

2. Atomic and Solid State Physics (Muon)

3. Radiochemistry and Nuclear Chemistry

4. Radiation Chemistry and Biology

Ⅳ. OPERATION RECORDS

Ⅴ. EVENTS

Ⅵ. ORGANIZATION AND ACTIVITIES OF RIKEN NISHINA CENTER
(Activities, Members, Publications & Presentations)

Ⅶ. LIST OF PREPRINTS

Ⅷ. LIST OF SYMPOSIA, WORKSHOPS & SEMINARS

I. HIGHLIGHTS OF THE YEAR

<< Selection process of highlights >>

Highlights are selected by a two-step process. In the first step, a referee who reviews a manuscript decides whether she/he would recommend it as one of the highlights.
Members of the editorial board then make additional recommendations if they think an important contribution has not been recommended by the referee.

The second step involves the editor-in-chief proposing a list of highlights based on the recommendation given above to the editorial board. After discussing the scientific merits and uniqueness of the manuscripts from viewpoints of experts/non-experts, the editorial board makes the final decision.

Persistence of the $Z = 28$ shell gap around ^{78}Ni: first spectroscopy of ^{79}Cu[†]

L. Olivier,[*1] S. Franchoo,[*1] M. Niikura,[*2] Z. Vajta,[*3] D. Sohler,[*3] P. Doornenbal,[*4] A. Obertelli,[*4,*5]
Y. Tsunoda,[*6] T. Otsuka,[*2,*4,*6] G. Authelet,[*5] H. Baba,[*4] D. Calvet,[*5] F. Château,[*5] A. Corsi,[*5] A. Delbart,[*5]
J.-M. Gheller,[*5] A. Gillibert,[*5] T. Isobe,[*4] V. Lapoux,[*5] M. Matsushita,[*7] S. Momiyama,[*2] T. Motobayashi,[*4]
H. Otsu,[*4] C. Péron,[*5] A. Peyaud,[*5] E. Pollacco,[*5] J.-Y. Roussé,[*5] H. Sakurai,[*2,*4] C. Santamaria,[*4,*5]
M. Sasano,[*4] Y. Shiga,[*4,*8] S. Takeuchi,[*4] R. Taniuchi,[*2,*4] T. Uesaka,[*4] H. Wang,[*4] K. Yoneda,[*4] F. Browne,[*9]
L. Chung,[*10] Z. Dombradi,[*3] F. Flavigny,[*1] F. Giacoppo,[*11] A. Gottardo,[*1] K. Hadyńska-Klęk,[*11] Z. Korkulu,[*3]
S. Koyama,[*2] Y. Kubota,[*4,*7] J. Lee,[*12] M. Lettmann,[*13] C. Louchart,[*13] R. Lozeva,[*14] K. Matsui,[*2,*4]
T. Miyazaki,[*2] S. Nishimura,[*4] K. Ogata,[*15] S. Ota,[*7] Z. Patel,[*16] E. Sahin,[*11] C. Shand,[*16] P.-A. Söderström,[*4]
I. Stefan,[*1] D. Steppenbeck,[*7] T. Sumikama,[*17,*4] D. Suzuki,[*1] V. Werner,[*13] J. Wu,[*4,*18] and Z. Xu[*12]

The shell model constitutes one of the main building blocks of our understanding of nuclear structure. Its robustness is well proven for nuclei close to the valley of stability, where it successfully predicts and explains the occurrence of magic numbers. However, the magic numbers are not universal throughout the nuclear chart and their evolution far from stability, observed experimentally over the last decades, has generated much interest. With 28 protons and 50 neutrons, the ^{78}Ni nucleus is expected to be one of the most neutron-rich doubly magic nuclei. Up to now, no evidence has been found for the disappearance of the shell closures at $Z = 28$ and $N = 50$, even if recent studies hint at a possible weakening of the $N = 50$ magic number below ^{78}Ni. The half-life of ^{78}Ni was determined at 122.2(5.1) ms, rather suggesting a survival of magicity, and calculations predict a first excited state in ^{78}Ni above 2 MeV. But so far no information on the spectroscopy of ^{78}Ni is available and the behavior of the $\pi f_{7/2}$ orbital, of primary importance as one of the orbitals defining the $Z = 28$ gap, is elusive. Access to this hole state is possible through proton transfer or knock-out reactions.

In our experiment performed at the Radioactive Isotope Beam Factory (RIBF), a ^{238}U beam with an energy of 345 MeV per nucleon and an average intensity of 12 pnA was sent on a 3-mm thick ^{9}Be target. The secondary ^{80}Zn beam, with an average intensity of 260 particles per second, was selected in the BigRips separator. The isotopes before and after the secondary target placed at the end of BigRips were identified event-by-event in the BigRips and ZeroDegree spectrometers, respectively, with the tof-$B\rho$-ΔE method. The detector set-up installed between the two spectrometers was composed of the Minos device mounted inside the Dali-2 γ-ray multidetector. Minos consisted of a liquid-hydrogen target of 102 mm long surrounded by a cylindrical time-projection chamber (TPC). The ^{79}Cu nucleus was produced mainly through proton knock-out from the incoming ^{80}Zn isotopes, the (p, 3p) channel contributing with 8%. The emitted protons were tracked in the TPC, while the beam trajectory was given by two parallel-plate avalanche counters before the target. The interaction vertex was reconstructed with 95% efficiency and 5-mm uncertainty FWHM along the beam axis. The Dali-2 array, comprising 186 NaI scintillator crystals, yielded a photopeak efficiency with add-back of 27% and an energy resolution of $\sigma = 45$ keV for a 1 MeV transition emitted at 250 MeV per nucleon.

We carried out the first spectroscopy of ^{79}Cu and compared the results with MCSM calculations. The calculations show the restoration of the single-particle nature of the low-lying states, which is supported by the experiment. There is no significant knock-out feeding to the excited states below 2.2 MeV, indicating that the $Z = 28$ gap remains large. The ability to describe the ^{79}Cu nucleus as a valence proton outside a ^{78}Ni core presents us with indirect evidence of the magic character of the latter.

[*1]   IPN, CNRS and University of Paris-Saclay
[*2]   Department of Physics, University of Tokyo
[*3]   Institute for Nuclear Research, MTA Atomki
[*4]   RIKEN Nishina Center
[*5]   Irfu, CEA and University of Paris-Saclay
[*6]   CNS, University of Tokyo
[*7]   CNS, University of Tokyo
[*8]   Department of Physics, Rikkyo University
[*9]   School of Computing Engineering and Mathematics, University of Brighton
[*10] INST, Vinatom
[*11] Department of Physics, University of Oslo
[*12] Department of Physics, University of Hong Kong
[*13] IKP, Technical University of Darmstadt
[*14] IPHC and University of Strasbourg
[*15] RCNP, Osaka University
[*16] Department of Physics, University of Surrey
[*17] Department of Physics, Tohoku University
[*18] State Key Laboratory of Nuclear Physics and Technology, University of Peking

Decay properties of neutron-rich nuclei around mass $A = 100$

S. Nishimura,[*1] A. Algora,[*2] V. Phong,[*3,*1] S. Go,[*1] J. Liu,[*4,*1] G. Lorusso,[*5,*1] K. P. Rykaczewski,[*6]
J. L. Tain,[*2] R. K. Grzywacz,[*7] J. Agramunt,[*2,*1] N. Brewer,[*6] C. Bruno,[*7] R. Caballero-Folch,[*9]
T. Davinson,[*8] I. Dillmann,[*9] A. Estrade,[*10] N. Fukuda,[*1] G. Kiss,[*11,*1] K. Matsui,[*12,*1] A. I. Morales,[*2]
N. Nepal,[*9] A. Tarifeño-Saldivia,[*13] A. Tolosa-Delgado,[*2] R. Yokoyama,[*7] D. S. Ahn,[*1] H. Baba,[*1]
F. Calvino,[*13] C. Domingo-Pardo,[*2] T. Isobe,[*1] S. Kubono,[*1] H. Sakurai,[*12,*1] P.-A. Söderström,[*14,*1]
T. Sumikama,[*1] H. Suzuki,[*1] H. Takeda,[*1] M. Wolińska-Cichocka,[*15] P. Woods,[*8] J. Wu,[*16,*1]
and the BRIKEN Collaboration

The neutron-rich nuclei around the mass $A \sim 100$ are expected to have rapid changes in nuclear shapes and possible shape coexistence. The decay properties are expected to be sensitive to the structural changes and are desired to be measured experimentally.[1] The β-decay half-lives $T_{1/2}$ and the delayed-neutron emission probabilities P_n in the mass $A = 90-125$ are considered as critical physics inputs in the astrophysical rapid-neutron capture process (r process), where the underestimation of r-process distribution in the mass $A = 110$–125 as well as the origin of elemental deviation of Zr to Cd ($Z = 40$–48) in the extremely metal-poor stars are still open questions.[2]

The BRIKEN project, which aims to survey several hundreds of decay properties toward the neutron drip-line, has been launched at RIBF. The progenitors of the r-process elements in the mass $A = 90$–125 were produced following the projectile fission of a 345 MeV/nucleon ^{238}U beam with primary beam intensity of above 60 pnA. Two data sets centered on ^{100}Br and ^{115}Nb isotopes in the BigRIPS separator were collected with 2- and 2.5-days of measurement times, respectively. The selected and identified isotopes were transported through the ZeroDegree spectrometer and implanted into two types of β-counting systems, namely WAS3ABi Si array[3] and segmented-YSO scintillation detector,[4] which were positioned in the center of the state-of-the-art neutron detector BRIKEN at the F11 focal point. BRIKEN consists of 140 ^{3}He neutron proportional counters arranged in a high-density polyethylene (HDPE: $90\times90\times75$ cm^3) matrix to achieve constant detection efficiency of above 65% up to neutron energies of 1 MeV.[5] In addition,
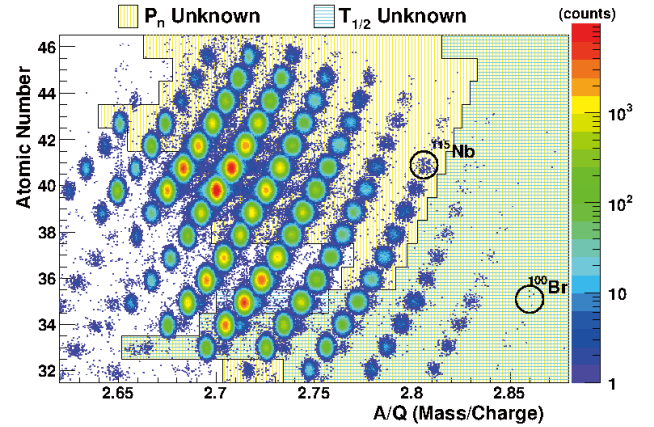
Fig. 1. Particle-identification plot and the areas of isotopes for unknown P_n and unknown $T_{1/2}$, respectively.

two high-purity Ge clover detectors were inserted from side-holes of the HDPE and placed in closed geometry of the β-counters to maximize the γ-ray detection efficiency. The experiment was conducted successfully and the problematic backgrounds of neutrons and light particles were securely reduced by closing the stainless-steel collimators prepared at the F2 focal plane.

The particle identification plot of the accumulated measurement is shown in Fig. 1. A careful analysis of β decay, γ rays, and neutrons in coincident measurement is in progress for one hundred isotopes to deduce $T_{1/2}$, P_n, the multi-neutron emitters (P_{xn}), new isomers, and level schemes of low-lying states. These decay properties are expected to give significant feedback to nuclear theories and improve the reliability of r-process abundance in the network calculations.

*1   RIKEN Nishina Center
*2   Instituto de F
íísica Corpuscular, CSIC-Univ. de Calencia
*3   Dept. of Nuclear Physics, VNU Hanoi Univ. of Science
*4   Dept. Physics, University of Hong Kong
*5   National Physics Laboratory (NPL)
*6   Physics Div., Oak Ridge National Laboratory (ORNL)
*7   Dept. of Physics and Astronomy., Univ. of Tennessee
*8   School of Physics and Astronomy, Univ. of Edinburgh
*9   Dept. of Physical Sciences, TRIUMF
*10 Dept. Physics, Central Michigan Univ.
*11 Institute for Nuclear Research, Atomki
*12 Dept. Physics, Univ. of Tokyo
*13 Univ. Politècnica de Catalunya (UPC)
*14 Technische Univ. Darmstadt
*15 Heavy Ion Lab., Univ. of Warsaw
*16 Physics Div., Argonne National Laboratory (ANL)

References
1) P. Sarriguren, Phys. Rev. C **91**, 044304, 1 (2015).
2) C. Sneden, J. J. Cowan, R. Gallino, Annu. Rev. Astro. Astrophys. **46**, 241 (2008).
3) S. Nishimura *et al.*, RIKEN Accel. Prog. Rep. **46**,182 (2013).
4) R. Grzywacz *et al.*, in this report.
5) A. Tarifeño-Saldivia *et al.*, J. Instrum. **12**, P04006 (2017).

Discovery of new isotopes ^{81,82}Mo and ^{85,86}Ru and a determination of the particle instability of ^{103}Sb†

H. Suzuki,[*1] T. Kubo,[*1] N. Fukuda,[*1] N. Inabe,[*1] D. Kameda,[*1] H. Takeda,[*1] K. Yoshida,[*1] K. Kusaka,[*1] Y. Yanagisawa,[*1] M. Ohtake,[*1] H. Sato,[*1] Y. Shimizu,[*1] H. Baba,[*1] M. Kurokawa,[*1] K. Tanaka,[*1] O. B. Tarasov,[*2] D. P. Bazin,[*2] D. J. Morrissey,[*2] B. M. Sherrill,[*2] K. Ieki,[*3] D. Murai,[*3] N. Iwasa,[*4] A. Chiba,[*4] Y. Ohkoda,[*4] E. Ideguchi,[*5] S. Go,[*5] R. Yokoyama,[*5] T. Fujii,[*5] D. Nishimura,[*6] H. Nishibata,[*7] S. Momota,[*8] M. Lewitowicz,[*9] G. DeFrance,[*9] I. Celikovic,[*9] and K. Steiger[*10]

We discovered four new isotopes, ^{81,82}Mo and ^{85,86}Ru, using the BigRIPS separator[1] at the RIKEN RI Beam Factory. Furthermore, we obtained the first clear evidence for the particle instability of ^{103}Sb. The upper limits of the half-lives of particle-unbound isotopes ^{81}Nb, ^{85}Tc, and ^{103}Sb were deduced.

Proton-rich radioactive isotopes (RI) were produced from a 345-MeV/nucleon 8–9 pnA ^{124}Xe^{52+} beam impinged on a 4-mm-thick Be target by projectile fragmentation. Two BigRIPS settings were conducted; one is ^{85}Ru setting for producing the RIs with atomic numbers $Z = 42$–44, and the other is ^{105}Te setting for $Z = 51$–53. We performed particle identification (PID) by deducing Z and the mass-to-charge ratio, A/Q, of the fragments based on the TOF-$B\rho$-ΔE method in the second stage of the BigRIPS.[2]

In the ^{85}Ru setting, four new isotopes ^{81,82}Mo and ^{85,86}Ru were observed as shown in Fig. 2 of the original article†. The numbers of the observed counts were 1, 6, 1, and 35, respectively. To confirm the existence of the new isotopes, mass number, A, and charge number, Q, were deduced from TOF and TKE measured between the F7 and F12 foci downstream of the BigRIPS. Figure 1 shows the Z vs $A - 2Q$ plot, in which the fully stripped events were selected. The new isotopes were clearly observed again. This re-identification strongly reinforces the discovery of the new isotopes especially for ^{81}Mo and ^{85}Ru, which were observed only 1 count each.

The Z vs A/Q PID plot of ^{105}Te setting is shown in Fig. 2. No new isotopes were observed in this setting. ^{103}Sb was not observed, although the other $N - Z = +1$ isotopes, ^{99}In, ^{101}Sn, and ^{105}Te, were clearly observed, indicating the particle instability of ^{103}Sb. The upper limit of the half life of ^{103}Sb was
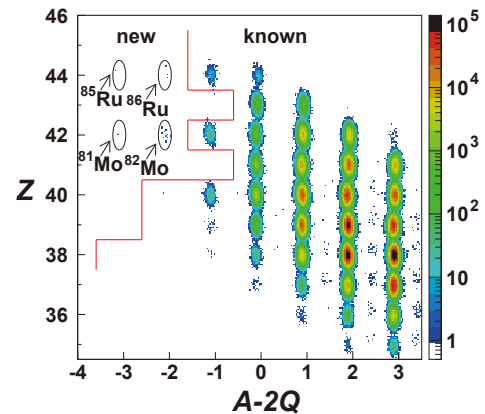
Fig. 1. The Z versus $A - 2Q$ PID plot of the ^{85}Ru setting. The fully stripped events ($Z - Q = 0$) are selected. The solid lines indicate the limits of known isotopes as of June 2017.
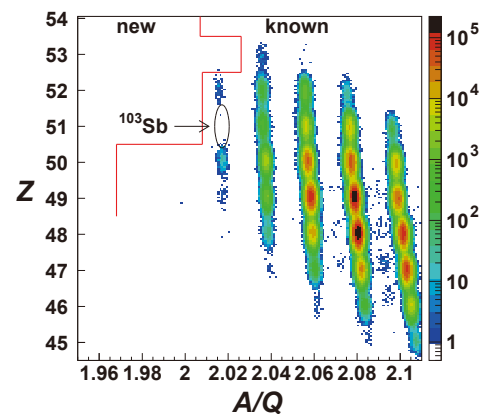
Fig. 2. The Z versus A/Q PID plot of the ^{105}Te setting.

deduced from its expected production-yield based on the yield systematics of neighboring isotopes and the TOF between the target and the F7 focus. Assuming the observation limit of 1 count, the upper limit of its half life was deduced to be 46 ns.

The upper limits of the half-lives of ^{81}Nb and ^{85}Tc were deduced to be 40 and 43 ns, respectively.

References
1) T. Kubo, Nucl. Instrum. Methods Phys. Res. B **204**, 97 (2003).
2) N. Fukuda *et al.*, Nucl. Instrum. Methods Phys. Res. B **317**, 323 (2013).

Discovery of ^{72}Rb: A nuclear sandbank beyond the proton drip line[†]

H. Suzuki,[*1] L. Sinclair,[*1,*2] P.-A. Söderström,[*1,*3,*4] G. Lorusso,[*1,*5,*6] P. Davies,[*2] L. S. Ferreira,[*7]
E. Maglione,[*8] R. Wadsworth,[*2] J. Wu,[*1,*9] Z. Y. Xu,[*10] S. Nishimura,[*1] P. Doornenbal,[*1] D. S. Ahn,[*1]
F. Browne,[*1,*11] N. Fukuda,[*1] N. Inabe,[*1] T. Kubo,[*1] D. Lubos,[*1,*12] Z. Patel,[*1,*6] S. Rice,[*1,*6] Y. Shimizu,[*1]
H. Takeda,[*1] H. Baba,[*1] A. Estrade,[*13] Y. Fang,[*14] J. Henderson,[*2] T. Isobe,[*1] D. Jenkins,[*2] S. Kubono,[*1]
Z. Li,[*9] I. Nishizuka,[*15] H. Sakurai,[*1,*10] P. Schury,[*1,*16] T. Sumikama,[*15,*1] H. Watanabe,[*17,*18] and
V. Werner[*19,*3]

We have discovered two new isotopes, ^{72}Rb and ^{77}Zr, around the proton drip line by using the BigRIPS separator at the RIKEN RI Beam Factory. ^{73}Rb, which is an unbound nuclide, was not observed. The observation of ^{72}Rb, which is an odd-odd nuclide and beyond the unbound nuclide ^{73}Rb, shows the diffuseness of the proton drip line and a possibility of "sandbanks" beyond it.

Proton-rich radioactive isotopes (RI) with atomic numbers $Z = 35$–40 were produced from a 345-MeV/nucleon 30–35 pnA ^{124}Xe^{52+} beam impinging on a 4-mm-thick Be target by projectile fragmentation. We performed the particle identification (PID) by deducing Z and the mass-to-charge ratio, A/Q, of the fragments based on the TOF-$B\rho$-ΔE method[1] using the standard detectors in the second stage of the BigRIPS and F11IC.

The Z vs A/Q PID plot is shown in Fig. 1. One event of ^{77}Zr and 14 events of ^{72}Rb were clearly observed, while ^{73}Rb was not observed. Assuming yield systematics of the neighboring nuclei around ^{73}Rb and its TOF value, the upper limit of the half life was deduced to be 81 ns, which is consistent with the previous result in Ref. 2). The half life of ^{72}Rb was deduced to be 103(22) ns.

The energies of the emitted protons, E_p, were es-
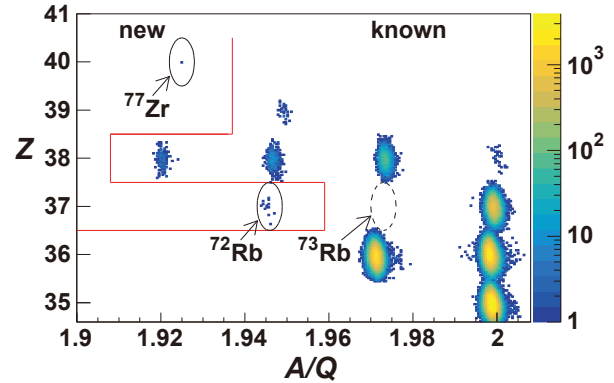
Fig. 1. Z versus A/Q PID plot. The solid lines indicate the limits of known isotopes as of September 2017. ^{73}Rb was evaluated to be a known isotope.[3] A proton-unbound excited state was observed by a beta-delayed proton decay of ^{73}Sr.[4]

timated from the half lives of these proton decays by using the formalism of proton emission from deformed nuclei in Refs. 5, 6). In the ^{72}Rb case, a $5^+ \rightarrow 5/2^-$ proton decay with $E_p = 800$–900 keV was suggested, assuming mirror symmetry in the spin-parity. However, we cannot explicitly exclude the possibility of a transition of the $9^+ \rightarrow 9/2^+$ isomeric state with a broken mirror symmetry. The upper limit of the half life of ^{73}Rb leads to $E_p > 600$ keV, assuming a $3/2^-$ ground state from the mirror nuclide. These E_p values agree well with the values predicted from the atomic mass evaluation.[7,8]

We have estimated the contribution of ^{73}Rb to the two-proton bypass of ^{72}Kr, which is a waiting point in the rapid-proton process in an X-ray burst. From $E_p > 600$ keV in ^{73}Rb, no two-proton capture occurs, implying that ^{72}Kr is a strong waiting point in this nucleosynthetic network.

References
1) N. Fukuda *et al.*, Nucl. Instrum. Methods Phys. Res. B **317**, 323 (2013).
2) R. Pfaff *et al.*, Phys. Rev. C **53**, 1753 (1996).
3) A. M. Parker, M. Thoennessen, At. Data Nucl. Data Tables **98**, 812 (2012).
4) J. C. Batchelder *et al.*, Phys. Rev. C **48**, 2593 (1993).
5) G. Fiorin *et al.*, Phys. Rev. C **67**, 054302 (2003).
6) M. Patial *et al.*, Phys. Rev. C **88**, 054302 (2013).
7) W. J. Huang *et al.*, Chin. Phys. C **41**, 030002 (2017).
8) M. Wang *et al.*, Chin. Phys. C **41**, 030003 (2017).

Determination of fusion barrier distributions from quasielastic scattering cross sections towards superheavy nuclei synthesis[†]

T. Tanaka,[*1,*2] Y. Narikiyo,[*1,*2] K. Morita,[*1,*2] K. Fujita,[*1,*2] D. Kaji,[*1] K. Morimoto,[*1] S. Yamaki,[*1,*3]
Y. Wakabayashi,[*1] K. Tanaka,[*1,*4] M. Takeyama,[*1,*5] A. Yoneda,[*1] H. Haba,[*1] Y. Komori,[*1] S. Yanou,[*1]
B. JP. Gall,[*1,*6] Z. Asfari,[*1,*6] H. Faure,[*1,*6] H. Hasebe,[*1] M. Huang,[*1] J. Kanaya,[*1] M. Murakami,[1]
A. Yoshida,[*1] T. Yamaguchi,[*3] F. Tokanai,[*1,*7] T. Yoshida,[*1,*7] S. Yamamoto,[*1,*2] Y. Yamano,[*1,*2]
K. Watanabe,[*1,*2] S. Ishizawa,[*1,*5] M. Asai,[*8] R. Aono,[*9] S. Goto,[*9] K. Katori,[*1] and K. Hagino[*10,*11]

The excitation functions for quasielastic (QE) cross sections were measured for the reactions relevant to the synthesis of superheavy nuclei, the ^{48}Ca+^{208}Pb, ^{50}Ti+^{208}Pb, and ^{48}Ca+^{248}Cm systems. Owing to the excellent performance of the gas-filled-type recoil ion separator GARIS and the focal plane detector system, the QE scattering events were effectively separated from deep-inelastic (DI) events and precise barrier distributions were deduced for all of these systems.

Coupled-channels calculations[1] were performed by taking into account the couplings to the vibrational and rotational excitations in the colliding nuclei, as well as the neutron transfer processes before contact. The experimental data are well reproduced by the calculations, which demonstrates the importance of including channel couplings in all of the systems. The maxima of the barrier distribution were shown to coincide in energy with the peak of the 2n evaporation residue cross sections[2–5] in the reactions of ^{48}Ca and ^{50}Ti on ^{208}Pb target. For the hot fusion reaction, the evaporation residue cross sections[6,7] peak at an energy well above the barrier region. This clearly suggests that the evaporation residue cross sections are enhanced at energies that correspond to a compact collision geometry with the projectile impacting the side of the deformed target nucleus.

From the results presented in this paper, we conclude that a measurement of the barrier distribution provides a powerful tool for understanding the underlying reaction dynamics for an unknown very heavy nuclei. In particular, it provides an effective way to determine the optimal bombarding energy. Importantly, this determination is independent of theoretical predictions that may include a large model dependence.

Fig. 1. Measured excitation function for the QE scattering cross section relative to the Rutherford cross section $d\sigma_{QE}/d\sigma_R$ (top panels). Left, middle, and right panels are for the ^{48}Ca+^{208}Pb, ^{50}Ti+^{208}Pb, and ^{48}Ca+^{248}Cm systems, respectively. The corresponding QE barrier distribution (middle panels) and the evaporation residue cross sections reported at different center-of-mass energies from the syntheses of No, Rf, and Lv evaporation residues[2–7] (lower panels) are also shown. Red symbols indicate the experimental data from this work, for which the error bars include only the statistical uncertainty. Green symbols indicate the experimental data for mixed QE and DI events. These data points provide an upper limit for $d\sigma_{QE}/d\sigma_R$. Blue solid curves indicate the best fit of the coupled-channels calculation. Blue dashed curves show the results of the single-channel calculations with the same internuclear potential as that used for the blue solid lines.

References
1) K. Hagino *et al.*, Comput. Phys. Commun. **123**, 143 (1999).
2) A. V. Belozerov *et al.*, Eur. Phys. J. A **16**, 447 (2003).
3) H. W. Gaggeler *et al.*, Nucl. Phys. A **502**, 561c (1989).
4) Yu. Ts. Oganessian *et al.*, Phys. Rev. C **64**, 054606 (2001).
5) F. P. Heßberger *et al.*, Eur. Phys. J. A **16**, 57 (2001).
6) Yu. Ts. Oganessian *et al.*, Phys. Rev. C **70**, 064609 (2004).
7) S. Hofmann *et al.*, Eur. Phys. J. A **48**, 62 (2012).

[†] Condensed from the article in J. Phys. Soc. Jpn. **87**, 014201 (2018)
[*1] RIKEN Nishina Center
[*2] Department of Physics, Kyushu University
[*3] Department of Physics, Saitama University
[*4] Faculty of Science and Technology, Tokyo University of Science
[*5] Graduate School of Science and Engineering, Yamagata University
[*6] Université de Strasbourg/IPHC
[*7] Faculty of Science, Yamagata University
[*8] Advanced Science Research Center, JAEA
[*9] Department of Chemistry, Niigata University
[*10] Department of Physics, Tohoku University
[*11] Research Center for Electron Photon Science, Tohoku University

Direct mass measurement of neutron-rich calcium isotopes, $^{55-57}$Ca

S. Michimasa,[*1] M. Kobayashi,[*1] Y. Kiyokawa,[*1] S. Ota,[*1] D. S. Ahn,[*2] H. Baba,[*2] G. P. A. Berg,[*3]
M. Dozono,[*1] N. Fukuda,[*2] T. Furuno,[*4] E. Ideguchi,[*5] N. Inabe,[*2] T. Kawabata,[*4] S. Kawase,[*6] K. Kisamori,[*1]
K. Kobayashi,[*7] T. Kubo,[*8,*9] Y. Kubota,[*2] C. S. Lee,[*1] M. Matsushita,[*1] H. Miya,[*1] A. Mizukami,[*10]
H. Nagakura,[*7] D. Nishimura,[*11] H. Oikawa,[*10] H. Sakai,[*2] Y. Shimizu,[*2] A. Stolz,[*9] H. Suzuki,[*2] M. Takaki,[*1]
H. Takeda,[*2] S. Takeuchi,[*12] H. Tokieda,[*1] T. Uesaka,[*2] K. Yako,[*1] Y. Yamaguchi,[*1] Y. Yanagisawa,[*2]
R. Yokoyama,[*13] K. Yoshida,[*2] and S. Shimoura[*1]

The mass of atomic nuclei is a fundamental quantity as it reflects the sum of all interactions within the nucleus, which is a quantum many-body system comprised of two kinds of fermions, protons and neutrons. Changes in the shell structures in nuclei far from stability can be directly probed by mass measurements.

The shell evolution of the neutron $2p_{1/2}$ and $1f_{5/2}$ orbitals in neutron-rich calcium region has attracted much attention over recent years. The presence of a large sub-shell gap at $N = 34$ between the orbitals in the Ca isotopes was theoretically predicted,[1] and the measurement of $E(2_1^+)$ in ^{54}Ca suggested the possible onset of a sizable subshell closure at $N = 34$.[2] One of the most critical information on existence of the subshell gap at $N = 34$ is the atomic masses of the calcium isotopes beyond $N = 34$. We challenged the first mass measurements of neutron-rich Ca isotopes beyond $N = 34$ to probe shell evolution of the neutron $2p_{1/2}$ and $1f_{5/2}$ orbitals.

The experiment was performed at the Radioactive Isotope Beam Factory (RIBF) at RIKEN, which is operated by RIKEN Nishina Center and Center for Nuclear Study, University of Tokyo. The masses were measured directly by the TOF-$B\rho$ technique. Neutron-rich isotopes were produced by fragmentation of a ^{70}Zn primary beam at 345 MeV/nucleon in a ^{9}Be target. The fragments were separated by the BigRIPS separator,[3] and transported in the High-Resolution Beam Line to the SHARAQ spectrometer.[4] Details on the experimental setup and analysis procedure can be found in the previous report.[5]

We obtained evolution of the two-neutron separation energies (S_{2n}) of neutron-rich Ca isotopes from the atomic masses of $^{55-57}$Ca, as shown in Fig. 1. In the figure, the squares represent the experimental S_{2n} values determined for the first time. The circles are the literature values obtained from AME2016.[6] The solid lines
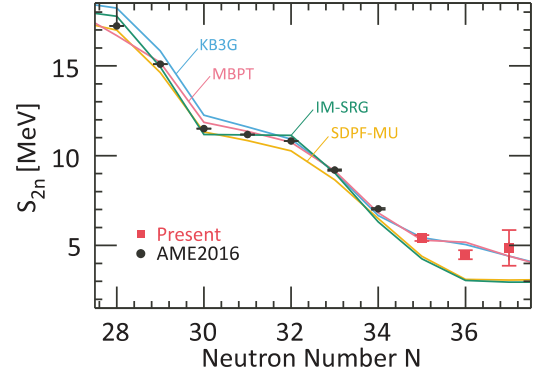
Fig. 1. The two-neutron separation energies in neutron-rich Ca isotopes. Squares indicate values determined for the first time, and circles are literature values from AME2016.[6] The solid lines show theoretical predictions.[7–10]

indicate the theoretical predictions by using KB3G,[7] MBPT,[8] IM-SRG,[9] and modified SDPF-MU[10] interactions. The empirical energy gaps across the Fermi surface in nuclei were evaluated by $S_{2n}(N) - S_{2n}(N+1)$ based on Ref. 11). The empirical energy gap at $N = 34$ is close to that at $N = 32$, and slightly smaller than that at $N = 28$. Therefore, the experimental result indicates a sizable energy gap of subshells in ^{54}Ca, which is comparable to that at ^{52}Ca. However the gap is not as large as recent predictions by SDPF-MU and IM-SRG interactions. We are preparing a physics article to report the shell evolution in neutron-rich Ca isotopes beyond $N = 34$.

References
1) T. Otsuka et al., Phys. Rev. Lett. 87, 082502 (2001).
2) D. Steppenbeck et al., Nature (London) 502, 207 (2013).
3) T. Kubo, Nucl. Instrum. Methods Phys. Res. B 204, 97 (2003).
4) T. Uesaka et al., Prog. Theor. Exp. Phys. 2012, 03C007 (2012).
5) M. Kobayashi et al., RIKEN Accel. Prog. Rep. 50, 59 (2017).
6) M. Wang et al., Chinese Phys. C 41, 030003 (2017).
7) A. Poves et al., Nucl. Phys. 694, 157 (2001).
8) J. D. Holt et al., J. Phys. G: Nucl. Part. Phys. 39, 085111 (2012).
9) S. R. Stroberg et al., Phys. Rev. Lett. 118, 032502 (2017).
10) Y. Utsuno et al., Phys. Rev. C 86, 051301 (2012).
11) W. Satuła et al., Phys. Rev. Lett. 81, 3599 (1998).

*1   Center for Nuclear Study, The University of Tokyo
*2   RIKEN Nishina Center
*3   Dept. of Physics, University of Notre Dame
*4   Dept. of Physics, Kyoto University
*5   RCNP, Osaka University
*6   Dept. of Advanced Energy Engineering Sciences, Kyushu University
*7   Dept. of Physics, Rikkyo University
*8   FRIB, MSU
*9   NSCL, MSU
*10 Dept. of Physics, Tokyo University of Science
*11 Dept. of Physics, Tokyo City University
*12 Dept. of Physics, Tokyo Institute of Technology
*13 Dept. of Physics & Astronomy, University of Tennessee

Observation of new neutron-rich isotopes among fission fragments from in-flight fission of 345 MeV/nucleon ^{238}U: search for new isotopes conducted concurrently with decay measurement campaigns[†]

Y. Shimizu,[*1] T. Kubo,[*1,*18] N. Fukuda,[*1] N. Inabe,[*1] D. Kameda,[*1] H. Sato,[*1] H. Suzuki,[*1] H. Takeda,[*1] K. Yoshida,[*1] G. Lorusso,[*1] H. Watanabe,[*1,*2,*3] G. S. Simpson,[*4] A. Jungclaus,[*5] H. Baba,[*1] F. Browne,[*1,*6] P. Doornenbal,[*1] G. Gey,[*1,*4,*7] T. Isobe,[*1] Z. Li,[*8] S. Nishimura,[*1] P.-A. Söderström,[*1] T. Sumikama,[*1,*9] J. Taprogge,[*1,*5,*10] Zs. Vajta,[*1,*11] J. Wu,[*1,*8] Z. Y. Xu,[*12] A. Odahara,[*13] A. Yagi,[*13] H. Nishibata,[*1] R. Lozeva,[*14,*15] C.-B. Moon,[*16] and H. S. Jung[*17]

The elucidation of the limit of nuclear existence is not only one of the fundamental subjects in nuclear physics but also a method of understanding the nature of nuclei. The search for new isotopes using the in-flight fission of a ^{238}U beam was conducted concurrently with decay measurements, during the so-called EURICA campaigns,[1] at the RIKEN Nishina Center RI Beam Factory. We have identified the following 36 new neutron-rich isotopes: ^{104}Rb, ^{113}Zr, ^{116}Nb, ^{118,119}Mo, ^{121,122}Tc, ^{125}Ru, ^{127,128}Rh, ^{129,130,131}Pd, ^{132}Ag, ^{134}Cd, ^{136,137}In, ^{139,140}Sn, ^{141,142}Sb, ^{144,145}Te, ^{146,147}I, ^{149,150}Xe, ^{149,150,151}Cs, ^{153,154}Ba, and ^{154,155,156,157}La.

The fission fragments produced via in-flight fission of the ^{238}U beam were separated and identified in flight using the BigRIPS separator.[2] We ran five different separator settings, which we refer to as the Sn, Pd, Rh, Nb, and Te settings, respectively, according to the subject of each EURICA experiment. The particle identification (PID) was performed by using the TOF-$B\rho$-ΔE method,[3] in which the mass-to-charge ratio A/Q and the atomic number Z of fragments were derived by measuring the time of flight (TOF), magnetic rigidity ($B\rho$), and energy loss (ΔE).

Figure 1 shows a two-dimensional PID plot of Z versus A/Q for the Sn setting. The red solid lines in the figures indicate the boundary between known isotopes and new isotopes. The relative root-mean-square (rms) Z resolutions and the relative rms A/Q resolutions achieved for fully stripped peaks are typically 0.37 and 0.038%, respectively, for the Sn setting. Owing to the excellent A/Q resolution and background removal that was achieved, we could clearly identify new isotopes.
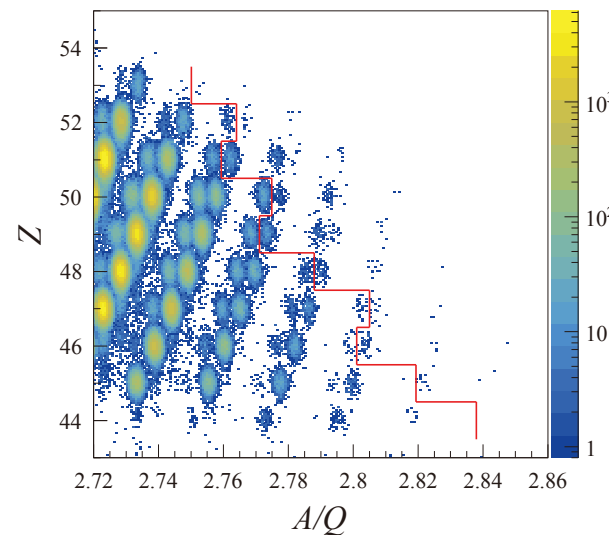
Fig. 1. Z versus A/Q particle identification plots for fission fragments produced in the ^{238}U+Be reaction at 345 MeV/nucleon. The red solid lines indicate the limit of known isotopes. The events whose charge state changed at the F5 focus were excluded.

References
1) S. Nishimura, Prog. Theor. Exp. Phys. **2012**, 03C006 (2012).
2) T. Kubo, Nucl. Instrum. Methods Phys. Res. B **204**, 97 (2003).
3) N. Fukuda *et al.*, Nucl. Instrum. Methods Phys. Res. B **317**, 323 (2013).

† Condensed from the article in J. Phys. Soc. Jpn. **87**, 014203 (2018)
*1 RIKEN Nishina Center
*2 International Research Center for Nuclei and Particles in the Cosmos, Beihang University
*3 School of Physics and Nuclear Energy Engineering, Beihang University
*4 LPSC, Université Joseph Fourier Grenoble
*5 Instituto de Estructura de la Materia, CSIC
*6 School of Computing, Engineering and Mathematics, University of Brighton
*7 Institut Laue-Langevin
*8 Department of Physics, Peking University
*9 Department of Physics, Tohoku University
*10 Departamento de Física Teórica, Universidad Autónoma de Madrid
*11 MTA Atomki
*12 Department of Physics, University of Tokyo
*13 Department of Physics, Osaka University
*14 IPHC, CNRS/IN2PS, Université de Strasbourg
*15 CSNSM, CNRS/IN2PS, Université Paris-sud
*16 Department of Display Engineering, Hoseo University
*17 Department of Physics, Chung-Ang University
*18 Present address: FRIB/NSCL, Michigan State University

Identification of New Neutron-rich Isotopes in the Rare-Earth Region Produced by 345 MeV/nucleon ^{238}U[†]

N. Fukuda,[*1] T. Kubo,[*1,*11] D. Kameda,[*1] N. Inabe,[*1] H. Suzuki,[*1] Y. Shimizu,[*1] H. Takeda,[*1] K. Kusaka,[*1] Y. Yanagisawa,[*1] M. Ohtake,[*1] K. Tanaka,[*1] K. Yoshida,[*1] H. Sato,[*1] H. Baba,[*1] M. Kurokawa,[*1] T. Ohnishi,[*1] N. Iwasa,[*2] A. Chiba,[*2] T. Yamada,[*2] E. Ideguchi,[*3] S. Go,[*3] R. Yokoyama,[*3] T. Fujii,[*3] H. Nishibata,[*4] K. Ieki,[*5] D. Murai,[*5] S. Momota,[*6] D. Nishimura,[*7] Y. Sato,[*8] J. Hwang,[*8] S. Kim,[*8] O. B. Tarasov,[*9] D. J. Morrissey,[*9] and G. Simpson[*10]

Searches for new isotopes at the RIKEN RI Beam Factory[1] have been conducted since its commissioning in 2007, expanding the region of accessible nuclei in the nuclear chart.[2–6] To explore the uncharted region of far-from-stability nuclei, we performed a search for new isotopes in the neutron-rich rare-earth region using a 345 MeV/nucleon ^{238}U beam with the BigRIPS in-flight separator.[7] We observed a total of 29 new neutron-rich isotopes: ^{153}Ba, ^{154,155,156}La, ^{156,157,158}Ce, ^{156,157,158,159,160,161}Pr, ^{162,163}Nd, ^{164,165}Pm, ^{166,167}Sm, ^{169}Eu, ^{171}Gd, ^{173,174}Tb, ^{175,176}Dy, ^{177,178}Ho, and ^{179,180}Er.

Neutron-rich nuclei in the rare-earth region were produced by the in-flight fission of a 345 MeV/nucleon ^{238}U beam with a beryllium target. The intensity of the ^{238}U beam was approximately 0.2–0.3 particle nA. The experiment was carried out with two different settings of the BigRIPS separator, each of which was aimed at the discovery of new neutron-rich isotopes in the region of atomic number Z of around 59 and 64, which are referred to as the Pr and Gd settings, respectively. The target thicknesses were 4.0 mm and 4.9 mm for the Pr and Gd settings, respectively. The particle identification (PID) was performed event-by-event based on the ΔE-TOF-$B\rho$ method, deducing Z and the mass-to-charge ratio A/Q of the fragments.[8]

Figures 1(a) and 1(b) show the Z vs A/Q PID plots obtained with the Pr and Gd settings, respectively. New isotopes are clearly identified in the plots, thanks to the excellent relative A/Q resolutions of 0.034% and 0.036% for the Pr and Gd settings, respectively.
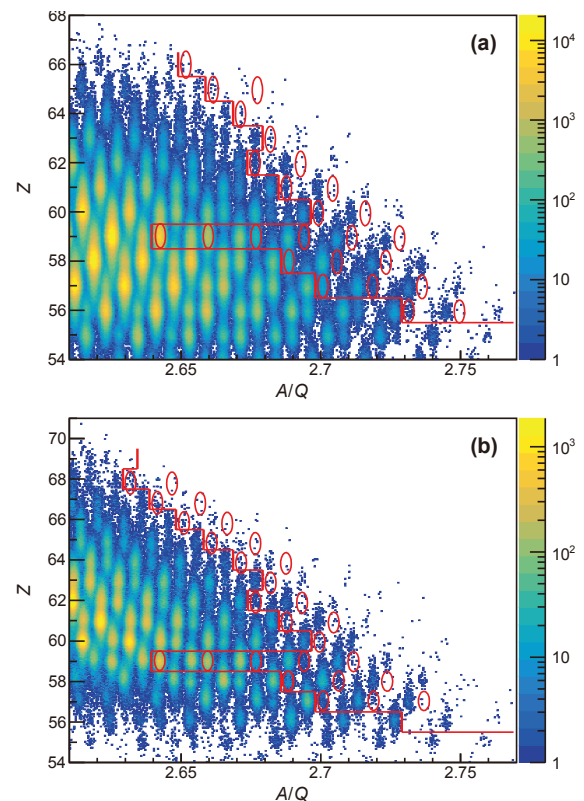
Fig. 1. Particle identification plots of Z vs A/Q for the fragments produced in the ^{238}U + Be reaction at 345 MeV/nucleon: (a) data obtained with the Pr setting during a 54.3-hour measurement period and (b) data obtained with the Er setting during a 45.8-hour measurement period. The red lines indicate the known limit. The new isotopes observed in this work are indicated by the red solid circles.

[*1]   RIKEN Nishina Center
[*2]   Department of Physics, Tohoku University
[*3]   Center for Nuclear Study, University of Tokyo
[*4]   Department of Physics, Osaka University
[*5]   Department of Physics, Rikkyo University
[*6]   School of Environmental Science and Engineering, Kochi University of Technology
[*7]   Department of Physics, Faculty of Liberal Arts and Sciences, Tokyo City University
[*8]   Department of Physics and Astronomy, Seoul National University
[*9]   National Superconducting Cyclotron Laboratory, Michigan State University
[*10] Laboratoire de Physique Subatomique et de Cosmologie de Grenoble
[*11] Present address: FRIB/NSCL, Michigan State University

References
1) Y. Yano, Nucl. Instrum. Methods Phys. Res. B **261**, 1009 (2007).
2) T. Ohnishi et al., J. Phys. Soc. Jpn. **77**, 083201 (2008).
3) T. Ohnishi et al., J. Phys. Soc. Jpn. **79**, 073201 (2010).
4) B. Blank et al., Phys. Rev. C **93**, 061301(R) (2016).
5) H. Suzuki et al., Phys. Rev. C **96**, 034604 (2017).
6) T. Sumikama et al., Phys. Rev. C **95**, 051601(R) (2017).
7) T. Kubo, Nucl. Instrum. Methods Phys. Res. B **204**, 97 (2003).
8) N. Fukuda et al., Nucl. Instrum. Methods Phys. Res. B **317**, 323 (2013).

Direct mass measurement of a $T_{1/2} = 10$ ms nucleus with a relative precision of 10^{-7} level

M. Wada,[*1,*2] Y. Ito,[*2,*8] P. Schury,[*1] S. Kimura,[*2,*6] M. Rosenbusch,[*2] D. Kaji,[*2] K. Morimoto,[*2] H. Haba,[*2] S. Ishizawa,[*2,*4] A. Niwase,[*2,*3] H. Miyatake,[*1] X. Y. Watanabe,[*1] H. Hirayama,[*1] J. Y. Moon,[*7] A. Takamine,[*2] T. Tanaka,[*3,*2] K. Morita,[*3,*2] and H. Wollnik[*5]

Comprehensive mass measurement of all available nuclides is an important mission for nuclear physics, in particular for understanding astronomical nucleosynthesis. So far masses of 2300 nuclei were experimentally determined with relative precisions of better than 1 ppm while other 1000 nuclei were identified; however, the masses are still unknown.[1] The half-lives of those unmeasured nuclei are distributed in a few orders of magnitude, but dominantly in 10–100 ms range (Fig. 1).

In the past, there were no universal mass spectrometers suited for very short-lived nuclei having half-lives of ≈10 ms if a relative precision of 10^{-7} level is required. We developed a multi-reflection time-of-flight (MRTOF) mass spectrograph[2] to cover the *blanc zone* at the GARIS-II facility of RIBF. Fusion-evaporation products were separated from the primary beam by the gas filled recoil ion separator and the energetic RI-beams were then thermalized in a cryogenic gas cell. The thermal ions in the gas cell were extracted by a traveling wave rf carpet and accumulated in the two stages of a triplet rf ion trap system. The bunched ions in the trap were provided to the MRTOF for time of flight measurements. The main purpose of this setup was to measure relatively long-lived trans uranium elements such as Md or Es,[3] so that the setting was not for quick

Fig. 2. ToF spectrum for ^{219}Ra^{2+} ions. A mass precision of 2×10^{-7} was achieved with four sets of spectra.
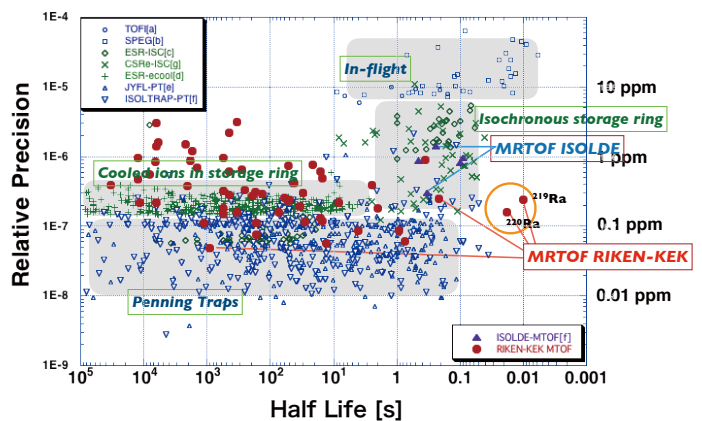
Fig. 3. Plot of mass precision as a function of the half-life with different mass measurement devices. With the MRTOF ≈80 nuclides were measured in FY2016–17.[3–6]

extraction and short trap sequence. The average transport time from GARIS-II to MRTOF was about 30 ms. Even with this condition, we could measure the mass of ^{219}Ra having a half-life of 10 ms with a precision of 2×10^{-7} (Fig. 2).

Figure 3 shows correlations between the mass precisions and half-lives for various mass spectrometers. Present ^{219}Ra measurement placed a milestone at the *blanc zone*.

Fig. 1. Half-lives of mass unknown nuclides (colored ones). Gray boxes indicate masses known with better than 1 ppm precision but the light gray ones are indirectly measured nuclides. Insert shows distribution of half-life for mass unknown nuclides.

*1 KEK, Wako Nuclear Science Center
*2 RIKEN Nishina Center
*3 Department of Physics, Kyushu University
*4 Department of Physics, Yamagata University
*5 Department of Chemistry and Biochemistry, New Mexico State University
*6 Department of Physics, Tsukuba University
*7 Institute for Basic Science
*8 Department of Physics, McGill University

References
1) W. J. Huang *et al.*, Chinese Phys. C **41**, 030002 (2017).
2) P. Schury *et al.*, Nucl. Instrum. Methods B **335**, 39 (2014).
3) Y. Ito *et al.*, Phys. Rev. Lett. **120**, 152501 (2018).
4) P. Schury *et al.*, Phys. Rev. C **95**, 011305(R) (2017).
5) S. Kimura *et al.*, Int. J. Mass Spectrom. **430**, 134 (2018).
6) M. Rosenbusch *et al.*, arXiv: 1801.02823.

Supernova equation of state based on realistic nuclear forces[†]

H. Togashi,[*1,*2] K. Nakazato,[*3] Y. Takehara,[*4] S. Yamamuro,[*4] H. Suzuki,[*4] and M. Takano[*2,*5]

The equation of state (EOS) for hot nuclear matter is one of the main ingredients in astrophysical simulations, such as core-collapse supernovae, cooling of protoneutron stars, black hole formations, and binary neutron star mergers. In order to describe the properties of nuclear matter in these simulations, a nuclear EOS table containing various thermodynamic quantities in wide ranges of the baryon number density n_B, proton fraction Y_p, and temperature T is necessary. Therefore, it is not an easy task to construct a nuclear EOS suitable for the astrophysical simulations. In fact, a limited number of nuclear EOSs are currently available for the core-collapse simulations.[1] Furthermore, high-density uniform matter is treated with the phenomenological models in those EOSs. Under these circumstances, we have recently constructed a new nuclear EOS table based on realistic nuclear forces.[2]

For uniform nuclear matter, the EOS is constructed with the cluster variational method. At zero temperature, we calculate the energy per nucleon as an expectation value of the realistic nuclear Hamiltonian composed of the Argonne v18 two-body and Urbana IX three-body potentials with the Jastrow wave function in the two-body cluster approximation. The obtained energies for pure neutron matter and symmetric nuclear matter are in good agreement with the results of the more sophisticated Fermi hypernetted chain (FHNC) variational calculations by Akmal *et al.*[3] At finite temperature, the free energy per nucleon for uniform nuclear matter was calculated with an extension of the variational method by Schmidt and Pandharipande.[4] The obtained results for pure neutron matter and symmetric nuclear matter are also in good agreement with those obtained using FHNC calculations.[5]

For non-uniform nuclear matter, we adopt the Thomas-Fermi approximation following the method by Shen *et al.*[6] In this method, non-uniform nuclear matter is assumed to be a mixture of free neutrons, free protons, alpha particles, and a single species of heavy nuclei that is located at the center of a Wigner-Seitz cell in a body-centered cubic lattice. We then calculate the free energy per nucleon for non-uniform matter by minimizing the average free energy density of the Wigner-Seitz cell with respect to the parameters specifying the density distributions of particles in the cell.

Table 1. Ranges of temperature T, proton fraction Y_p, and baryon mass density ρ_B in the table of the variational EOS. At the top of the last column, "+1" represents the case at $T = 0$ MeV.

Parameter	Min	Max	Mesh	Number
$\log_{10}(T)$ [MeV]	-1.00	2.60	0.04	$91 + 1$
Y_p	0	0.65	0.01	66
$\log_{10}(\rho_B)$ [g/cm³]	5.1	16.0	0.1	110

Finally, we determine the thermodynamically favorable state for each n_B, Y_p, and T, by comparing the free energy for non-uniform nuclear matter with that for uniform nuclear matter. The obtained free energy and related thermodynamic quantities are tabulated in ranges of n_B, Y_p, and T, as shown in Table 1. Here, the baryon mass density ρ_B is defined as $\rho_B = m_u n_B$ with m_u being the atomic mass unit.

The obtained EOS for various n_B, Y_p, and T is reasonable as compared with the Shen EOS.[6] It is also found that the critical temperature with respect to the liquid–gas phase transition decreases more moderately with Y_p for our EOS. Furthermore, masses of heavy nuclides are slightly larger than those of the Shen EOS in neutron-rich nuclear matter. As reported in Refs. 2, 7), those results are caused by the fact that the density derivative coefficient of the symmetry energy L of our EOS is smaller than that of the Shen EOS.

To the best of our knowledge, this is the first nuclear EOS for astrophysical simulations based on realistic nuclear forces. In the near future, we will extend the present EOS so as to take into account the additional hyperon degrees of freedom at finite temperature, because the hyperon mixing is expected to strongly affect the EOS of dense matter at high densities. In fact, we have already calculated the EOS of hyperonic matter at zero temperature by using the cluster variational method.[8]

The EOS table constructed in this study is open for general use in the studies of nuclear physics and astrophysics. The complete EOS table is available on the Web at `http://www.np.phys.waseda.ac.jp/EOS/`.

References
1) M. Oertel *et al.*, Rev. Mod. Phys. **89**, 015007 (2017).
2) H. Togashi *et al.*, Nucl. Phys. **961**, 78 (2017).
3) A. Akmal *et al.*, Phys. Rev. C **58**, 1804 (1998).
4) K. E. Schmidt, V. R. Pandharipande, Phys. Lett. B **87**, 11 (1979).
5) A. Mukherjee, Phys. Rev. C **79**, 045811 (2009).
6) H. Shen *et al.*, Astrophys. J. Suppl. Ser. **197**, 20 (2011).
7) K. Oyamatsu, K. Iida, Phys. Rev. C **75**, 015801 (2007).
8) H. Togashi *et al.*, Phys. Rev. C **93**, 035808 (2016).

†   Condensed from the article in Nucl. Phys. A **961**, 78 (2017).
*1   RIKEN Nishina Center
*2   Waseda Research Institute for Science and Engineering, Waseda University
*3   Faculty of Arts and Science, Kyushu University
*4   Department of Physics, Tokyo University of Science
*5   Department of Pure and Applied Physics, Waseda University

Single electron yields of charm and bottom hadron decays in central Au+Au collisions at $\sqrt{s_{NN}} = 200$ GeV

K. Nagashima[*1,*2] for the PHENIX collaboration

Heavy quarks (charm and bottom) are sensitive probes of the Quark-Gluon Plasma (QGP) created in high-energy nuclear collisions. The modification of their phase-space distributions in the QGP reflects strongly the dynamics because they are generated in the early stage of collisions, not destroyed by the strong interaction and subsequently propagate through the QGP. Therefore, the transport properties of the QGP, the diffusion coefficient D, can be studied from the measurements of heavy quarks.
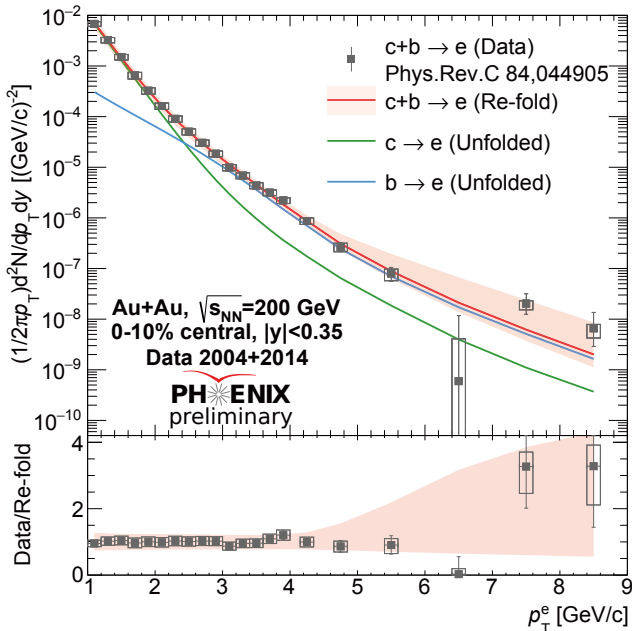
Fig. 1. The invariant yield of charm and bottom hadron decay electrons as a function of p_T.

The PHENIX collaboration at the Relativistic Heavy Ion Collider has measured the large modification of the momentum and angular distributions of inclusive heavy flavor decay electrons in the QGP.[1] Recently the silicon vertex detector was installed in PHENIX to measure precisely the displaced vertices, where the distribution of the distance of closest approach (DCA) of the track to the primary vertex allows the separation of electrons from charm and bottom hadron decays. PHENIX silicon vertex detector has achieved a sufficient DCA resolution, approximately 60 μm at $p_T > 2.5$ GeV/c, for the separation because heavy flavor hadrons have the longer life time, $c\tau(D^0)$ = 123 μm, $c\tau(B^0)$ = 456 μm. PHENIX has estab-

lished the unfolding method to a separation of charm and bottom hadron decay electrons using Bayesian inference techniques applied simultaneously to the yield and DCA distributions.[2]

In 2014–2016, PHENIX collected 20 billion events in Au+Au at $\sqrt{s_{NN}} = 200$ GeV, which is 20 times larger than the 2011 dataset. This dataset allows to measure the charm and bottom yields as a function of a collision centrality and impose a strong constraint on theory. The invariant yield of charm and bottom hadron decay electrons in the most central Au+Au at $\sqrt{s_{NN}} = 200$ GeV is measured in the 2014 data set as shown in Fig. 1.
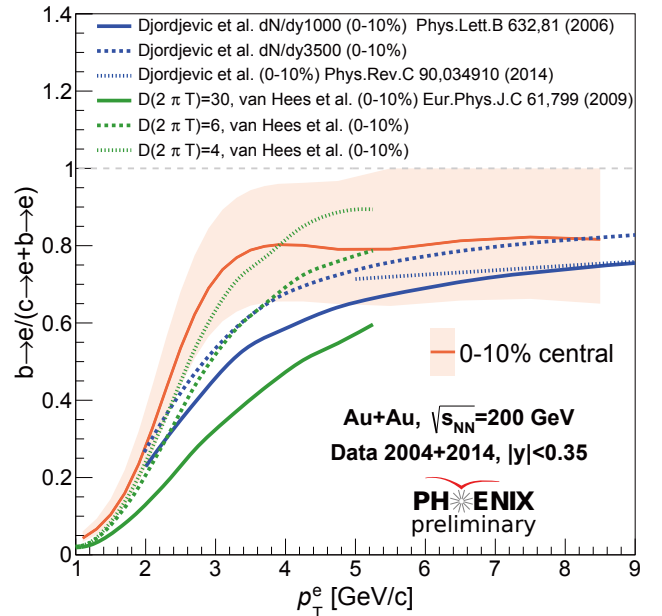
Fig. 2. The bottom electron fraction as a function of p_T compared to model predictions.

The bottom electron fraction (b→e/c + b→e) is compared to model predictions as shown in Fig. 2. Based on model predictions, we find that the diffusion coefficient of QGP is approximately 4 m²/s which indicates the strong coupling of QGP, and the radiative energy loss model can reproduce well at high p_T (> 5 GeV/c).[3]

References
1) A. Adare et al., Phys. Rev. Lett. **98**, 172301 (2006).
2) A. Adare et al., Phys. Rev. C **93**, 034904 (2016).
3) K. Nagashima et al., Nucl. Phys. A **967**, 644 (2017).

*1 Department of Physics, Hiroshima University
*2 RIKEN Nishina Center

Are two nucleons bound in lattice QCD for heavy quark masses?[†]

T. Iritani[*1] for HAL QCD Collaboration

The interactions between hadrons are important for understanding the origin of the matter. These interactions are described by quantum chromodynamics. There are two approaches to study two-hadron systems based on lattice QCD. In the direct method, one extracts the eigenenergy of a two-particle system through temporal correlation. In the HAL QCD method, potential is determined by spatial correlation.

These two methods should be equivalent. However, in the previous studies on heavy quarks masses, deuterons and dineutrons have been found to be bound in the direct method and unbound in the HAL QCD method. In a series of papers,[1,2] we reported that the direct method experiences systematic uncertainties resulting from elastic scattering states.

In the direct method, the energy shift is measured using the temporal correlation where the ground state is dominant. For example, inelastic excitation can be neglected around 1 fm. However, in two-particle systems, there are elastic scattering states, whose gap is considerably smaller than that of inelastic scattering states. Typically, ground state saturation requires $\mathcal{O}(10)$ fm. Owing to its slow convergence, one might misidentify the ground state energy around 1.5 fm.

To resolve such a fake measurement problem, we propose a simple check of the energy shift (ΔE_L) using the scattering phase shift, $\delta_0(k)$, which is given by

$$k \cot \delta_0(k) = \frac{1}{\pi L} \sum_{\vec{n} \in \mathbf{Z}^3} \frac{1}{|\vec{n}|^2 - |kL/(2\pi)|^2} \qquad (1)$$

according to Lüscher's finite volume formula, where k is given by $\Delta E_L = 2\sqrt{m_B^2 + k^2} - 2m_B$ in a finite box of volume L^3. The bound state corresponds to the pole of the S-matrix at $k \cot \delta_0(k)|_{k^2=-\kappa_0^2} = -\sqrt{-k^2}|_{k^2=-\kappa_0^2}$, which is determined by the extrapolation of $k \cot \delta_0(k)$ using effective range expansion (ERE), i.e., $k \cot \delta_0(k) \simeq 1/a_0 + (1/2)r_{\text{eff}}k^2 + \cdots$. In addition, the pole satisfies the physical residue condition by

$$\frac{d}{dk^2}\left[k \cot \delta_0(k)\right]\Big|_{k^2=-\kappa_0^2} < \frac{d}{dk^2}\left[-\sqrt{-k^2}\right]\Big|_{k^2=-\kappa_0^2}. \qquad (2)$$

However, none of the previous works analyze the bound state correctly based on the finite volume method. We re-examine their results carefully. For example, Fig. 1 shows the scattering phase shift obtained by Yamazaki et al.[3] for NN(^{1}S$_0$) and NPLQCD Coll.[4] for NN(^{3}S$_1$). The ERE in the upper panel shows singular behavior, while the EREs in the lower panel are inconsistent with
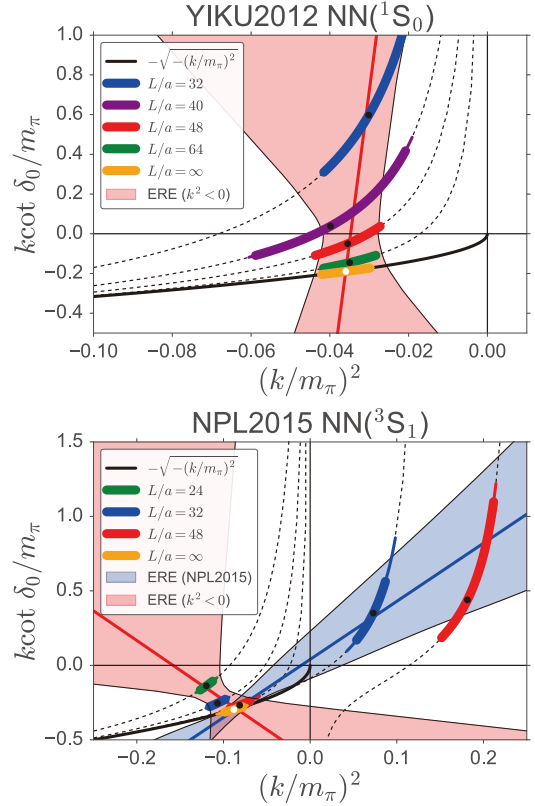
Fig. 1. Scattering phase shift (Upper) NN(^{1}S$_0$) in Yamazaki et al.[3] (Lower) NN(^{3}S$_1$) in NPLQCD Coll.[4] The red (blue) band denotes the fitted ERE for $k^2 < 0$ ($k^2 > 0$).

each other. Moreover, ERE (NPL2015) violates the physical pole condition. These EREs suggest that the ground state is not measured correctly. We have concluded that *there are serious uncertainties about the existence of two-nucleon bound states for heavy quark masses in all previous studies.*[1]

While the temporal correlation in the direct method experiences elastic scattering states, we define potential through spatial correlation in the HAL QCD method, which does not encounter this problem. Furthermore, we show the reliability of the HAL QCD method.[5]

References
1) T. Iritani for HAL QCD Coll., Phys. Rev. D **96**, 034521 (2017).
2) T. Iritani for HAL QCD Coll., J. High Energy Phys. **1610**, 101 (2016).
3) T. Yamazaki et al., Phys. Rev. D **86**, 074514 (2012).
4) S. R. Beane et al. [NPLQCD Coll.], Phys. Rev. D **87**, 034506 (2013).
5) T. Iritani for HAL QCD Coll., arXiv:1710.06147.

---

*1 RIKEN Nishina Center

Origin of the fake eigen energy of the two-baryon system in lattice QCD[†]

T. Iritani[*1] for HAL QCD Collaboration

Both the direct and HAL QCD methods are used to study two-hadron systems in lattice QCD. In previous studies for large pion masses,[2] the direct method showed that both dineutron and deuteron are bound. However, the HAL QCD method suggests that these are unbound. In the series of papers,[3,4] we pointed out that these discrepancies originate from the misidentification of the ground state in the direct method due to the scattering states,[3] which can be revealed by some simple tests using Lüscher's finite volume formula.[4]

In the direct method, one measures the energy eigenvalue. It is estimated by the plateau value of the effective energy shift, which is given by

$$\Delta E_{\mathrm{eff}}(t) \equiv \frac{1}{a} \log \left[\sum_{\vec{r}} R(\vec{r}, t) \right] \Big/ \left[\sum_{\vec{r}} R(\vec{r}, t+a) \right] \quad (1)$$

using the R-correlator

$$R(\vec{r}, t) \equiv \frac{\langle 0 | T\{ B(\vec{x}+\vec{r}, t) B(\vec{x}, t) \} \overline{\mathcal{J}}(0) | 0 \rangle}{\{ C_B(t) \}^2}, \quad (2)$$

where $\mathcal{J}(B)$ is a source(sink) operator and the baryon propagator $C_{\mathrm{B}}(t) \equiv \langle B(t)\bar{B}(0) \rangle$. It converges to the ground state energy at a large time, where the ground state is saturated. For example, the inelastic state becomes negligible around 1 fm, while the elastic excitation in the two-baryon system remains even around $\mathcal{O}(10)$ fm, which causes a fake plateau-like structure around 1.5 fm in the actual calculations.

Such a fake plateau problem can be checked by the source dependence.[3] Figure 1 shows the effective energy shift of $\Xi\Xi(^1S_0)$ at $m_\pi = 0.51$ GeV using the wall and the smeared sources. There is a plateau-like structure around $t \sim 15a \simeq 1.5$ fm, but it depends on the source, which means either (or both) of the results is fake.

Since the time-dependent HAL QCD method uses both the ground and the scattering states simultaneously to extract the interaction, it does not require the ground-state saturation. In this method, the potential is defined from the R-correlator, and some systematic uncertainties are shown to be under control.[1]

Using the correct eigen energies ΔE_n and eigenfunction $\Psi_n(r)$, which are obtained by solving $H \equiv H_0 + V(r)$ with the HAL QCD potential $V(r)$ in the finite box, the R-correlator is expanded by

$$R(\vec{p}=0, t) \simeq \sum_{\vec{r}} \sum_{n} a_n \Psi_n(\vec{r}) e^{-\Delta E_n t} = \sum_n b_n e^{-\Delta E_n t} \quad (3)$$
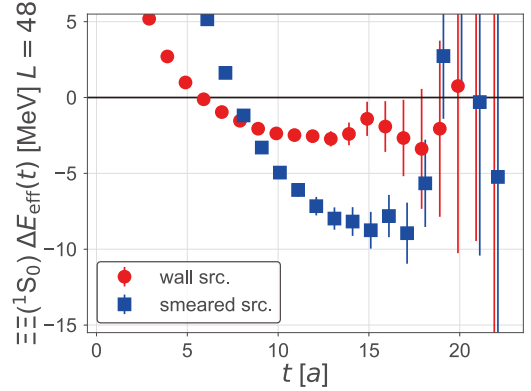
Fig. 1. The effective energy shift using the wall and the smeared source for $\Xi\Xi(^1S_0)$ at $m_\pi = 0.51$ GeV. The lattice size $L = 48$ with the lattice spacing $a \simeq 0.09$ fm.
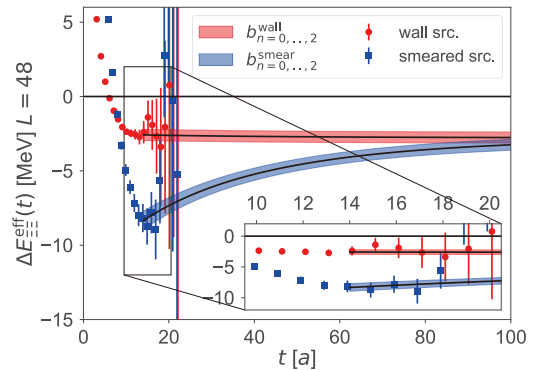
Fig. 2. Reconstructed $\Delta E_{\mathrm{eff}}(t)$ and its convergence.

The contamination coefficients b_n are determined from the orthogonality of $\Psi_n(\vec{r})$.

Figure 2 shows the $\Delta E_{\mathrm{eff}}(t)$ reconstructed using a low-lying b_n and ΔE_n, which well reproduces the fake plateau. The ground-state saturation of the smeared source is estimated to be around $t \sim 100a \sim 10$ fm at $L = 48$. This result proves the advantages of the HAL QCD method, and the direct measurement of the two-baryon system is not practical.

References
1) T. Iritani for HAL QCD Coll., EPS Web Conf. **165**, 05008 (2018).
2) T. Yamazaki, PoS LATTICE **2014**, 009 (2015).
3) T. Iritani for HAL QCD Coll., J. High Energy Phys. **1610**, 101 (2016).
4) T. Iritani for HAL QCD Coll., Phys. Rev. D **96**, 034521 (2017).

$\Lambda_c \to N$ form factors from lattice QCD and phenomenology of $\Lambda_c \to n\,\ell^+\nu_\ell$ and $\Lambda_c \to p\,\mu^+\mu^-$ decays[†]

S. Meinel[*1,*2]

The $\Lambda_c \to N$ transition form factors are relevant both for the charged-current decays $\Lambda_c \to n\,\ell^+\nu_\ell$ and for the GIM-suppressed neutral-current decays $\Lambda_c \to p\,\ell^+\ell^-$. In this work, the first lattice QCD calculation of the $\Lambda_c \to N$ form factors was performed, and predictions were made for the rates and angular distributions of the aforementioned decays. The calculation was based on lattice gauge field ensembles generated by the RBC and UKQCD Collaborations,[1]) with $2+1$ flavors of domain wall fermions. Two lattice spacings, $a \approx 0.11$ fm and $a \approx 0.085$ fm, and pion masses in the range 230 MeV $\lesssim m_\pi \lesssim 350$ MeV were used. The form factors were extrapolated to the continuum limit and the physical pion mass via modified z expansions.

The $\Lambda_c \to n\,e^+\nu_e$ differential decay rate predicted using the form factor results is shown in Fig. 1. This decay not yet been observed in experiments. The integrated decay rate obtained here is higher than most previous theoretical estimates.

In the effective-field-theory analysis, $c \to u\,\ell^+\ell^-$ decays such as $\Lambda_c \to p\,\mu^+\mu^-$ receive contributions both from quark-bilinear operators, whose matrix elements are given by the form factors calculated here, and from four-quark and gluonic operators[2]) that contribute through nonlocal matrix elements containing an additional insertion of the quark electromagnetic current. For the $\Lambda_c \to p\,\mu^+\mu^-$ differential branching fraction, a perturbative treatment of these nonlocal matrix elements[3]) yields the blue dashed curve shown in Fig. 2. It is, however, well known that intermediate light-meson resonances enhance the matrix elements of the four-quark operators by several orders of magnitude. A simple Breit-Wigner model for the contributions from the ρ^0, ω, and ϕ resonances gives the orange curve in Fig. 2.

The LHCb Collaboration recently performed a search for $\Lambda_c \to p\,\mu^+\mu^-$ decays,[4]) and reported an upper limit of $\mathcal{B}(\Lambda_c \to p\,\mu^+\mu^-) < 7.7 \times 10^{-8}$ in the dimuon mass region excluding ± 40 MeV intervals around m_ω and m_ϕ. This measurement constrains new-physics contributions to the Wilson coefficients C_9 and C_{10} to be of order $\mathcal{O}(1)$. While the theoretical predictions for the $\Lambda_c \to p\,\mu^+\mu^-$ decay rate are very unreliable, the forward-backward asymmetry in the angular distribution is nonzero only in the presence of new physics, and a measurement would provide a clean test of the Standard Model.
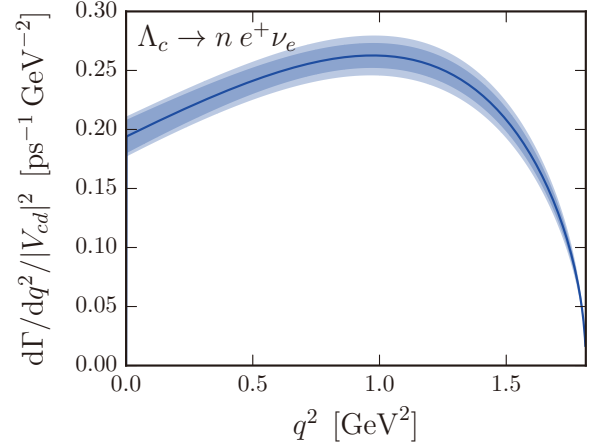
Fig. 1. The $\Lambda_c \to n\,e^+\nu_e$ differential decay rate, without the factor of $|V_{cd}|^2$.
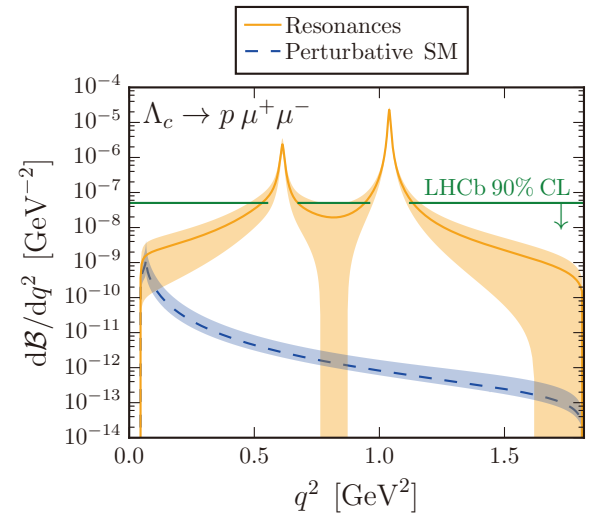
Fig. 2. The $\Lambda_c \to p\,\mu^+\mu^-$ differential branching fraction, calculated using effective Wilson coefficients from perturbation theory (blue dashed curve) or using a Breit-Wigner model for the contributions from the ρ^0, ω, and ϕ resonances. Also indicated is the upper limit obtained by LHCb.[4])

References
1) Y. Aoki *et al.*, (RBC and UKQCD Collaborations), Phys. Rev. D **83**, 074508 (2011).
2) S. de Boer, B. Müller, D. Seidel, J. High Energy Phys. **1608**, 091 (2016).
3) S. de Boer, Eur. Phys. J. C **77**, 11, 801 (2017).
4) R. Aaij *et al.*, (LHCb Collaboration), arXiv:1712.07938.

†   Condensed from the article in arXiv:1712.05783
*1 RIKEN Nishina Center
*2 Department of Physics, University of Arizona

Lattice QCD calculation of neutral D-meson mixing matrix elements[†]

E. T. Neil[*1,*2] for the Fermilab Lattice and MILC Collaborations

The various weak decays of heavy quark flavors provide a stringent test of the electroweak sector of the Standard Model, and can be of great importance in constraining models of new physics beyond the Standard Model (BSM) which have non-trivial flavor structure.[1] In order to interpret experimental results for these decays, it is essential to disentangle the electroweak or BSM effects of interest from the contributions due to the strong force (QCD). Lattice QCD provides a way to numerically calculate the required strong matrix elements at high precision and with full control of systematic effects.

We consider the process of mixing between the neutral D^0 and $\bar{D}^0$ mesons, which is not a decay but does involve flavor-changing weak processes (the charm quantum number changes by $\Delta C = 2$ units.) The presence of down-type quarks in Standard Model contributions to this process through box diagrams allows D mixing to provide unique and complementary information on potential new physics compared to kaon and bottom-quark mixing and decay. Furthermore, the contributions of bottom quarks to D mixing are highly suppressed, which in turn suppresses CP violation from the Standard Model; searches for CP violation in D mixing are therefore very sensitive to new physics.

Our calculation uses lattice gauge theory to compute the set of five QCD matrix elements $\mathcal{O}_1$ through $\mathcal{O}_5$ which contribute to D-mixing. We use a set of gauge ensembles generated by the MILC collaboration with $N_f = 2+1$ dynamical quarks, using the "asqtad" improved staggered fermion formulation and tadpole-improved Luscher-Weisz gauge action. We study 14 ensembles with different values for the lattice spacing a and average pion mass M_π^{RMS}; global fits using staggered chiral perturbation theory then allow us to extrapolate simultaneously to the physical quark mass point and the continuum limit.

Following a careful analysis of sources of systematic error, we obtain for the five matrix elements in the $\overline{\mathrm{MS}}$-NDR scheme at $\mu = 3$ GeV the values $\langle \mathcal{O}_1 \rangle = 0.0805(55)(16)$, $\langle \mathcal{O}_2 \rangle = -0.1561(70)(31)$, $\langle \mathcal{O}_3 \rangle = 0.0464(31)(9)$, $\langle \mathcal{O}_4 \rangle = 0.2747(129)(55)$, $\langle \mathcal{O}_5 \rangle = 0.1035(71)(21)$, where the first error bar shows the combined statistical and systematic error, and the second shows the estimated uncertainty due to quenching of the charm quark in our simulations.

We can apply our matrix element results to place constraints on models of new physics, using the experimental measurements[3] of D-mixing. As an example,
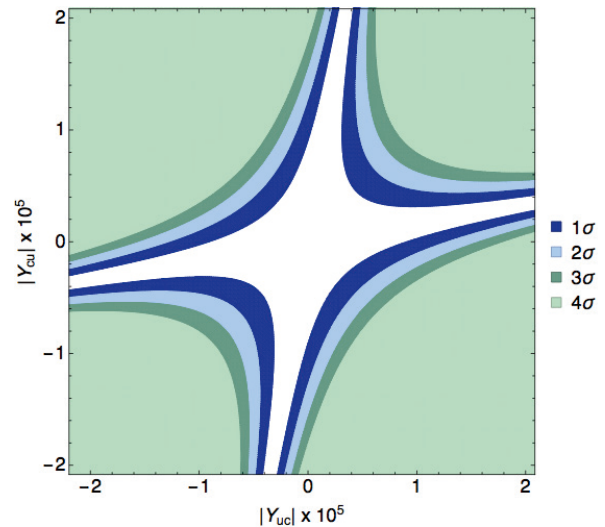
Fig. 1. Bounds on a specific model of new physics in which the Higgs has flavor-violating couplings,[2] using recent experimental results on the complex D-mixing parameter x_{12}[3] and our new lattice QCD results for the D-mixing matrix elements. Colored regions are excluded at the indicated statistical significance. Complex phases of the Yukawa couplings Y_{uc} and Y_{cu} are marginalized over.

we consider a specific model[2] in which the Higgs boson has flavor-violating couplings to quarks and leptons. Integrating out the Higgs field at low energy gives an effective Hamiltonian

$$\mathcal{H}_{\Delta C=2}^{\mathrm{NP}} = -\frac{Y_{uc}^{\star\,2}}{2m_h^2}\mathcal{O}_2 - \frac{Y_{cu}^2}{2m_h^2}\bar{\mathcal{O}}_2 - \frac{Y_{cu}Y_{uc}}{m_h^2}\mathcal{O}_4 \qquad (1)$$

where in front of the operators we show Wilson coefficients at the scale m_h. The Wilson coefficients are run down to a renormalization scale of 3 GeV at which our lattice QCD matrix elements are computed, and then used to convert to an experimental prediction for the D-mixing parameter x_{12} based on the size of the Yukawa couplings Y_{cu} and Y_{uc}. The resulting constraints are shown in Fig. 1.

References
1) M. Antonelli, Phys. Rept. **494**, 197–414 (2010).
2) R. Harnik, J. Kopp, J. Zupan, J. High Energy Phys. **1303**, 026 (2013).
3) Y. Amhis *et al.*, (HFLAV Collaboration), Eur. Phys. J. C **77**, 12, 895 (2017).

---

*1 RIKEN Nishina Center
*2 Department of Physics, University of Colorado, Boulder

A prototype novel laser-melting sampler for analyzing ice cores with high depth resolution and high throughput

M. Maruyama,[*1] M. Yumoto,[*1] K. Kase,[*1] K. Takahashi,[*2] Y. Nakai,[*2] S. Wada,[*1] Y. Yano,[*2] and Y. Motizuki[*2]

A new facility for analyzing ice cores is being prepared jointly by the RIKEN Nishina Center Astro-Glaciology Research Group (AGG) and the RIKEN Center for Advanced Photonics in Room B35 (50 m^2) in the main research building at Wako. The mission of the facility is to analyze ice cores with high depth (temporal) resolution and high throughput to obtain concentration profiles of various isotopes such as ^{18}O/^{16}O and various ions such as SO_4^{2-} and NO_3^-. The ice cores that we study have been drilled by the Japanese Antarctic Research Expedition (JARE) at Dome Fuji station in East Antarctica. From the data obtained, one can elucidate the long-term history of climate changes, and even the history of solar activities and possible supernova explosions in our galaxy. Such astro-related research was initiated by the AGG and their activity so far was summarized in the RIKEN APR special issue.[1]

One of the major components of our facility is a newly installed prefabricated freezer container (3 m wide × 5 m long × 3 m high). The temperature in the container is controlled at −20°C. The inside of this container is partitioned into two areas: a storage area where valuable ice cores are kept clean and frozen, and an ice core sampling area where a new system (under development) for applying the laser-melting technique will be installed. The other components are isotope analyzers and ion chromatography systems for measuring the concentrations of isotopes and ions in the samples collected automatically as described below. They will be placed outside the container at room temperature.

Figure 1 depicts the schematic diagram of a prototype laser-melting sampler. The sampler consists of a continuous wave fiber laser (λ =1.55 μm), optical switching devices, optical fibers (0.25 mm ϕ), needles (0.7 mm ϕ), and a computer that controls the positions of the sampling nozzles and the motorized stage on which an ice core is placed. The laser beam delivered by the optical fiber is radiated on the target ice core surface, and the melted water of 1 mL (enough volume for precision analysis) thereby obtained is sucked up through the needle and transported into a vial bottle by a peristaltic tube pump at a pressure drop of 1 atm. The needle and the tube are kept over 0°C by the heater windings.

We conducted several performance tests for this prototype. Figure 2 shows one of the results: holes as small as 2 mm ϕ were made on ice 5 mm apart by laser-melting. For this performance test, a laser beam with a power of 1 W was irradiated, and the sampling speed was measured to be 26 min/mL. We are optimizing the irradiation conditions via such performance tests. In addition,
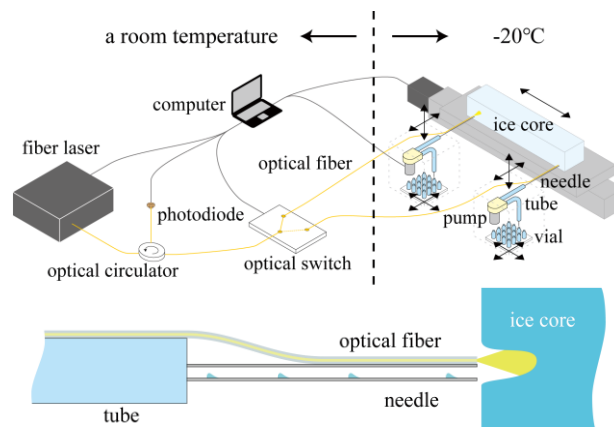
Fig. 1. A schematic view of the ice-core laser-melting sampler. The bottom image shows a sampling nozzle.
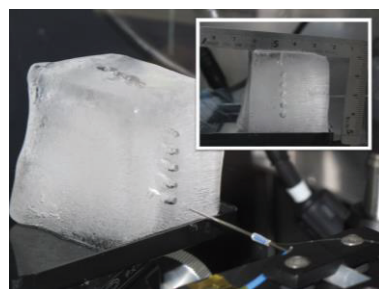
Fig. 2. Photos of a performance test.

we are developing an automated multi-nozzle system to realize high throughput, which is the mission of our facility.

The new system obviously has advantages over our previous work on ice core sampling, which was performed manually using electric band saw machines and ceramic knifes. Our new technique is different from the heater-melting continuous flow analysis method[2] for the following reasons: 1) sampling zones, either holes or horizontal planes, are discrete to avoid mixing with each other, and 2) the amount of sampling ice is adequately minimized for precision analysis.

This system will make it possible to analyze ice cores at a high depth resolution of 1 mm scale, which corresponds to the temporal resolution of ∼1 month in the case of a Dome Fuji ice core. Since the new JARE ice core drilling project has been approved and is in progress, it will become possible to study the correlations between climate and solar activity, and the galactic supernova rate of the past 1,000,000 years. We thank K. Eto and M. Kawada of Tokyo Denki Univ. for helping us with our measurements.

References
1) Y. Motizuki, RIKEN Accel. Prog. Rep. **50**, S-80 (2017).
2) *e.g.*, R. Dallmayr *et al.*, Bulletin of Glac. Res. **34**, 11 (2016).

[*1] RIKEN Center for Advanced Photonics
[*2] RIKEN Nishina Center

Production of vanadium-ion beam from RIKEN 28 GHz SC-ECRIS

Y. Higurashi,*1 J. Ohnishi,*1 and T. Nakagawa*1

Following the last super-heavy element (SHE) ($Z = 113$) search experiment[1] in 2012, an experiment to search for new SHEs ($Z = 119$ and 120) was planned for which intense beams of vanadium (V) and chromium (Cr) ions were strongly required. Therefore, we started test experiments to produce a V-ion beam from RIKEN 28 GHz SC-ECRIS.[2] The main feature of the ion source is that it has six solenoid coils for producing a mirror magnetic field. By using this ion source, we can produce magnetic-field distributions of various shapes from classical $B_{\min}$ to flat $B_{\min}$.[3]

To produce V vapor, we used a high temperature oven[4] of the same type as that used for the production of uranium (U) vapor. The metal V was installed in the crucible of the high-temperature oven and heated by resistance heating up to $\sim 1900°C$. This temperature to obtain sufficient vapor. To avoid the chemical reaction between the metal V and W crucible at the high temperature, we used a ceramic crucible (Y_2O_3) as the W crucible as shown in Fig. 1.

Figure 2 shows the charge state distribution of the highly charged V-ion beam. To produce plasma, we used oxygen gas as an ionized gas. B_{inj}, $B_{\min}$, Br, and B_{ext} were 2.3, 0.5, 1.4, and 1.5 T, respectively. The extraction voltage was 12.6 kV, which is the required extraction voltage to obtain a V-ion beam of 6.0 MeV/nucleon with the RIKEN ring cyclotron for the experiment. The injected microwave power and gas pressure were ~ 1.0 kW and $\sim 7.1 \times 10^{-5}$ Pa, respectively. We used the two-frequency (18 and 28 GHz) plasma heating method[5] to stabilize the beam intensity. The electric power of the high-temperature oven was ~ 720 W. Under this condition, we produced V^{13+} of ~ 100 eμA. In our recent experiment, we observed that the emittance of the ion beam was strongly affected by the aberration of the analyzing magnet. To minimize this effect, we need to provide a focused ion beam. For this reason, to minimize the emittance, we optimized the beam size in the analyzing magnet with a focusing solenoid coil installed after the ion source, and we obtained beam parameter products of 200 mm mrad (four rms x-emittance) and 188 mm mrad (four rms y-emittance) after the analyzing magnet.

In December 2017, a stable V^{13+} beam of ~ 85 eμA was successfully produced for 15 days without break for the experiment. The average consumption rate of the material was ~ 1.9 mg/h. Using the present crucible of the high-temperature oven, metal V of ~ 1.6 gr can be installed. Therefore, it is estimated that one can produce an intense beam (V^{13+} of ~ 85 eμA) for longer than one month without break under the present condition.
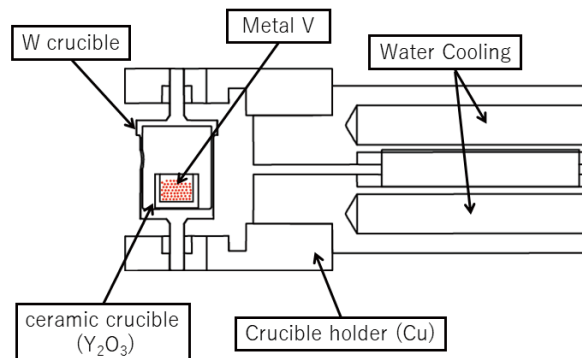
Fig. 1. Schematic of the high-temperature oven.
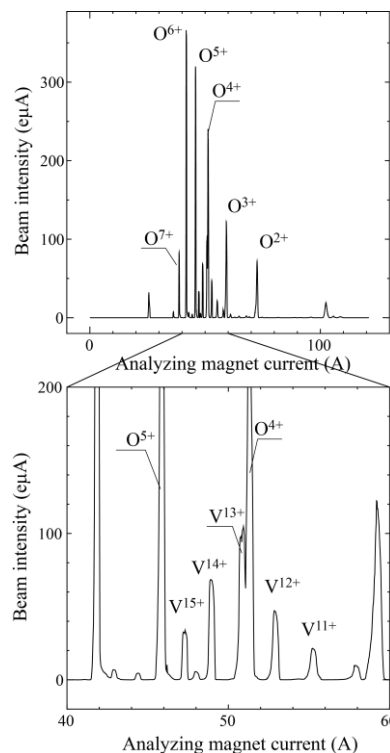
Fig. 2. Charge-state distribution of the highly charged V ion beam.

References
1) Morita *et al.*, J. Phys. Soc. Jpn. **81**, 103201 (2012).
2) Y. Higurashi, J. Ohnishi, K. Ozeki, M. Kidera, T. Nakagawa, Rev. Sci. Instrum. **85**, 02A953 (2014).
3) G. D. Alton, D. N. Smithe, Rev. Sci. Instrum. **65**, 775 (1994).
4) J. Ohnishi *et al.*, Rev. Sci. Instrum. **87**, 02A709 (2016).
5) Z. Q. Xie, C. Lyneis, Rev. Sci. Instrum. **66**, 4218 (1995).

*1 RIKEN Nishina Center

Doughnut-shaped gas cell for KEK Isotope Separation System[†]

Y. Hirayama,[*1] Y.X. Watanabe,[*1] M. Mukai,[*2,*3,*1] M. Oyaizu,[*1] M. Ahmed,[*1,*3] H. Ishiyama,[*4] S.C. Jeong,[*4] Y. Kakiguchi,[*1] S. Kimura,[*2,*3] J.Y. Moon,[*4] J.H. Park,[*4] P. Schury,[*1] M. Wada,[*1,*2] and H. Miyatake[*1]

We have developed the KEK Isotope Separation System (KISS)[1] to study the β-decay properties of neutron-rich isotopes with neutron numbers around $N = 126$ for astrophysics research.[2] KISS uses a laser ion source to produce pure low-energy ion beams of neutron-rich isotopes in the region around $N = 126$, which are produced in multi-nucleon transfer reactions by impinging a stable ^{136}Xe beam with an energy of approximately 10 MeV/nucleon on a ^{198}Pt target.[3] The extraction efficiency from the laser ion source, namely an argon gas cell, was as low as 0.01%. The low extraction efficiency stems from the plasma induced by the primary beam injection into the gas cell, which is believed to reduce the ionization efficiency and selectivity of the laser ionized atoms.

It is straightforward to increase the production yields of unstable nuclei by increasing the primary beam intensity. However, the plasma effect obstructs the increase of beam intensity. To overcome the difficulty, we have developed a doughnut-shaped argon gas cell with a rotating target. Figure 1 shows a schematic 3D view of the doughnut-shaped gas cell. The doughnut-shaped gas cell has an aperture for transporting the primary beam without entering the gas cell and a large window (polyimide foil 5 μm in thickness) for implanting the target-like fragments (TLFs) recoiling out of a rotating ^{198}Pt target. Owing to the characteristic large emission angles of TLFs, the TLFs could be injected into the gas cell with high efficiency.

To study the performance of the doughnut-shaped gas cell with a rotating target, we performed on-line experiments using a ^{136}Xe^{20+} beam with 10.75 MeV/nucleon and a maximum intensity of 60 pnA. Figure 2 shows the measured extraction yield of ^{199}Pt$^+$ as a function of primary beam intensity. The black square and red circles in Fig. 2 indicate the measured extraction yields with the use of the old and new gas cells, respectively. The extraction yields were approximately 20 pps at 20 pnA with the use of the old gas cell and approximately 260 pps at 50 pnA with the use of the new doughnut-shaped gas cell. These results clearly indicate that the doughnut-shaped gas cell increased the extraction efficiency by suppressing
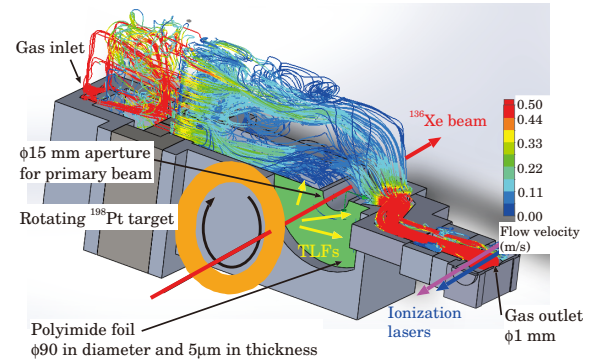
Fig. 1. Schematic view of the doughnut-shaped gas cell. The colored lines indicate the calculated argon gas flow trajectories connected to the gas outlet, based on the exact geometry. The color code indicates the calculated velocity (m/s) of the argon gas flow. Here, the pressure of the argon gas was 88 kPa.

the plasma effect. Moreover, we could increase the extraction yields by increasing the primary beam intensity up to 50 pnA owing to the new gas cell. However, we observed a decrease of the extraction yield as the primary beam intensity was increased beyond 60 pnA. This result indicates that we could not completely suppress the plasma effect, and further improvements are required to the KISS gas cell system. This will be the focus of our future research.
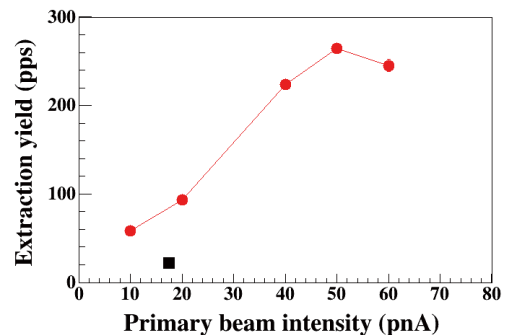
Fig. 2. Measured extraction yields as a function of primary beam intensity with the use of the old and new gas cells. Statistical error bars are smaller than the symbols.

References
1) Y. Hirayama *et al.*, Nucl. Instrum. Methods Phys. Res. B **353**, 4 (2015).
2) S.C. Jeong *et al.*, KEK Report 2010-2, (2010).
3) Y.X. Watanabe *et al.*, Phys. Rev. Lett. **115**, 172503 (2015).

Development of an off-axis electron beam source for cold highly charged ion generation in a linear combined ion trap

N. Kimura,[*1,*2] H. Kato,[*3] K. Okada,[*1] N. Nakamura,[*4] N. Ohmae,[5] H. Katori,[5,*6] and M. Wada[*7,*2]

Some particular transitions in highly charged ions (HCI) are sensitive to possible time variation of the fine structure constant. High-precision spectroscopy of such transitions can be a new probe for the verification of fundamental physics.[1,2] To perform such spectroscopy, ion trapping and cooling of HCI are indispensable. Schmöger et al.[3] observed Coulomb crystallization of highly charged Ar in a linear RF trap; however, no spectroscopy has been performed yet. We designed and constructed a compact cryogenic setup in which a microscopic electron beam ion trap (μ-EBIT) and a linear RF trap are enclosed.[4] In this setup, HCI are generated in the μ-EBIT, while laser-cooled Be$^+$ ions are stored in the linear RF trap. Since the two traps are arranged collinearly, the center axis line must be reserved for the cooling laser path. Additionally, preserving the super-high vacuum necessary for storing HCI precludes the use of any hot electron source. We developed a cold cathode electron beam source with an "off-axis" geometry to fulfill such constraints.

Figure 1 shows the geometry of the electron beam source with electron beam trajectories, which are simulated by SIMION8.0 code. The cold cathode has a through hole for the laser path, and a Coniferous Carbon Nano Structure (CCNS) is generated on the surface in advance.[5] When a high voltage is applied to the anode, field emission electrons are extracted from the cathode surface. The emitted electrons fly according to the electron optics, and some fraction of them will reach the trap region with the energy given by the cathode voltage.

After an aging process was performed by applying high voltages for a long time under ultra-high vacuum condition, we obtained an I-V characteristic plot of the electron beam source, as shown in Fig. 2. The circle plots represent the electron beam intensity reaching the trap region and the square plots represent the total emission from the cold cathode. The electric current (I) and voltage (V) were measured by monitoring the power supply output while changing the anode voltage. The cathode voltage was fixed at 300 V. A typical intensity of >0.1 mA at 300 eV in the trap region with an efficiency of >50% was achieved.

In order to focus the electron beam in the μ-EBIT, a strong magnetic field needs to be applied using hand wound coils of a superconducting wire.[4] As the next step, will generate HCI such as Ho^{14+} in the μ-EBIT, and try to crystallize the HCI in the linear RF trap by sympathetic cooling with laser-cooled Be$^+$.
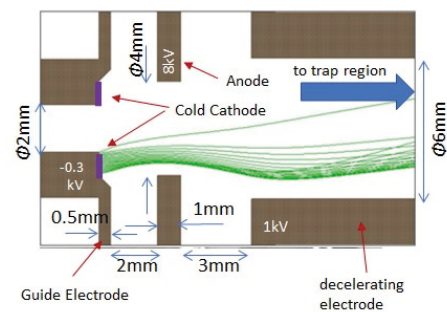
Fig. 1. Sketch of electron beam source with trajectories calculated using SIMION 8.0.
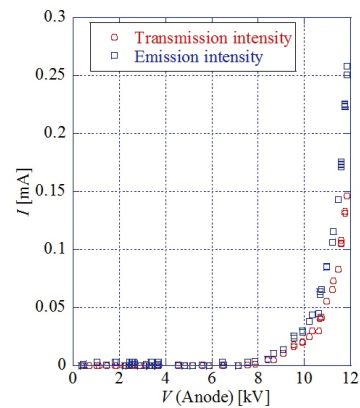
Fig. 2. I-V plot of electron beam of 300 eV.

*1 Department of Physics, Sophia University
*2 RIKEN Nishina Center
*3 Research Institute for Measurement and Analytical Instrumentation (RIMA), National Metrology Institute of Japan (NMIJ), National Institute of Advanced Industrial Science and Technology (AIST)
*4 Institute for Laser Science, The University of Electro-Communications
*5 Quantum Metrology Laboratory, RIKEN
*6 Department of Applied Physics, Graduate School of Engineering, The University of Tokyo
*7 Wako Nuclear Science Center (WNSC), Institute of Particle and Nuclear Studies (IPNS), High Energy Accelerator Research Organization (KEK)

References
1) J. C. Berengut et al., Phys. Rev. Lett. 105, 120801 (2010).
2) V. A. Dzuba et al., Phys. Rev. A 91, 022119 (2015).
3) L. Schmöger, et al., Science 347, 1233–1236 (2015).
4) N. Kimura et al., RIKEN Accel. Prog. Rep. 50, 202 (2016).
5) H. Kato et al., Diamond and Related Materials 55, 41–44 (2015).

TINA - a silicon tracker for transfer reactions

P. Schrock,[*1] Y. Beaujeault-Taudiere,[*2] N. Imai,[*1] K. Iribe,[*3] N. Kitamura,[*1] J. H. Ong,[*4] D. Suzuki,[*5] T. Teranishi,[*3] and K. Wimmer[*6]

Transfer reactions are powerful tools in nuclear physics to study the structure of atomic nuclei. In (d, p) transfer, for instance, one neutron is added to a nucleus populating a single-particle orbital. Respective measurements reveal important information about the shell structure, such as the appearance of closed shells (magic numbers) in exotic nuclear matter.[1]

The recently commissioned OEDO beamline[2] of CNS and RIKEN can provide beams with the necessary intensities at low energies (10–20 MeV/nucleon), offering experimental access to regions of the nuclear chart that were hitherto inaccessible for (d, p) studies.

To utilize OEDO for transfer reactions, the silicon detector setup called TINA has been developed and successfully used in two experiments. TINA is a joint project of CNS, RCNP Osaka, and RIKEN Nishina Center. It is designed for the position and energy measurements of recoiling light particles (protons) from transfer reactions in inverse kinematics.

The first (existing) version of TINA is shown in Fig. 1. It consists of six telescopes, each with a YY1-type silicon strip and CsI detectors. It has been used at Kyushu University Tandem Accelerator and at the OEDO facility. At Kyushu, a ^{12}C beam impinged on a deuterated Ti target.[3] The obtained kinematics curve (energy of YY1 vs. lab angle) of the recoiling light particles is shown in Fig. 2. Deuterons from elastic scattering as well as protons from transfer to the ground state and some excited states were observed.

In the OEDO Day 0 experiment in November 2017, ^{77,79}Se beams were energy-degraded and irradiated onto a CD_2 target. The light recoiling particle identification (PID) plot obtained with TINA is shown in Fig. 3, where the energy loss measured with the silicon detectors are plotted against the remaining energy deposited in the CsI crystals. Protons, deuterons, and tritons can clearly be distiguished.

An upgrade to implement highly granular DSSD detectors with GET readout electronics[4] is ongoing. The upgraded TINA will be well-suited for future transfer studies at OEDO. TINA is also compact enough to be coupled with 4π γ-ray detector arrays.
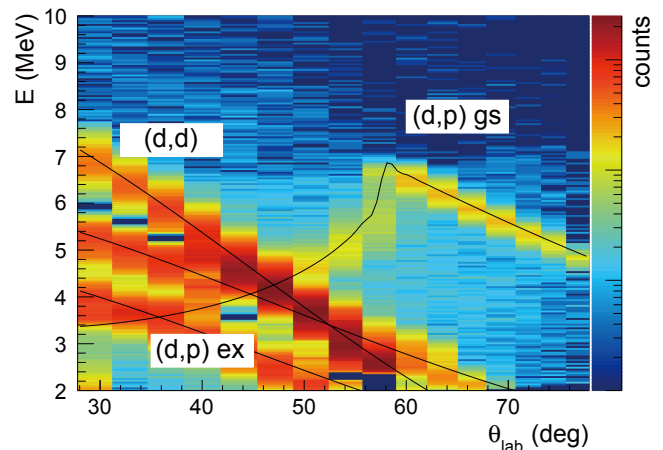
Fig. 2. Kinematics plot of light recoiling particles obtained with a ^{12}C beam on a deuterated target.
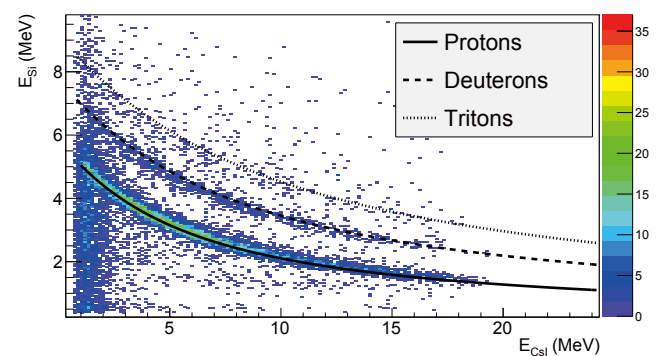
Fig. 3. PID plot for light reaction products obtained in the OEDO Day 0 experiment.

Fig. 1. Photograph of TINA during use in the OEDO Day 0 experiment.

*1　CNS, University of Tokyo
*2　Department of Physics, Universite Paris-Saclay
*3　Department of Physics, Kyushu University
*4　RCNP, Osaka University
*5　RIKEN Nishina Center
*6　Department of Physics, University of Tokyo

References
1) K. L. Jones *et al.*, Nature (London) **465**, 09048 (2010).
2) S. Michimasa (*et al.*), In this report.
3) T. Koiwai *et al.*, RIKEN Accel. Prog. Rep. **50**, 213 (2017).
4) E. C. Pollacco *et al.*, accepted for publication in Nucl. Instrum. Methods A.

Spot size estimation for laser aiming system of ion microbeam irradiation using a tapered glass capillary optics

K. Sato,[*1,*2] T. Ikeda,[*1,*2] K. Hirose,[*1,*2] M. Matsubara,[*2] T. Masuyama,[*2] T. Minowa,[*2] and W.-G. Jin[*2]

In order to investigate the response of living cells to radiation, micrometer-sized beams are used to shoot a small structure inside the cell. A microbeam irradiation system has been developed at RIKEN, employing MeV H/He ions generated by the Pelletron accelerator and tapered glass capillary optics, whose beam inlet and outlet diameters are ∼1 mm and several micrometer, respectively.[1] HeLa cells[2] and *E-coli*. cells[3] were irradiated using this system. Since the high accuracy needed to shoot the targets should be achieved easily, the installation of an aiming system utilizing laser micro spot has been scheduled. The capillary can transmit both ions and laser at the same time. The aiming system provides the laser microbeam needed to spotlight the target prior to ion irradiation. When the excitation light of a specific fluorescent protein or fluorescent dye is selected as the spotlight, only the labeled target in a microscopic view will be irradiated by the ion microbeam.

The laser transmission experiments have been carried out with tapered glass capillary optics in Toho University. The power of the transmitted beam was well-reproduced by a simulation with a precisely measured capillary shape.[4] The beam power was measured by using a power meter based on a photodiode whose sensitive area was 10 mm × 10 mm. In order to determine the laser spot size, a microscopic imaging technique is needed. Figure 1 shows our method, which records the spot shape on a fluorescent-bead screen located L mm-downstream of the capillary outlet; it was set up at the Quantum Electronics Lab. in Toho Univ., using a laser beam from an Ar$^+$ laser source (wavelength $\lambda = 488$ nm, CW power = 15 mW). The screen consists of fluorescent beads, 2 μm in diameter, which can shift the λ from 488 nm (input laser) to around 508 nm (fluorescence). A band pass filter attached at the eye piece suppresses the input laser intensity by 10^{-6}, except for $\lambda = 510$ with a width of 20 nm. The spot images were taken by a digital camera and analyzed for $L > 1$ mm in a previous work.[5]

This year, we introduced another microscope to determine L precisely and succeeded in achieving measurements of L down to 17 μm, which is short enough to spotlight the cell targets in the range of 4 MeV He^{2+} ions in water. The spot shape for $L > 1$ mm was similar to that of a Fraunhofer diffraction pattern, which is known as the ring images for a parallel laser beam entering a small aperture. Although a finite beam divergence during transmission does not follow the Fraunhofer formula, the obtained similarity for $L > 1$ mm inspires Fresnel pattern for $L < 100$ μm, where higher-order outer rings
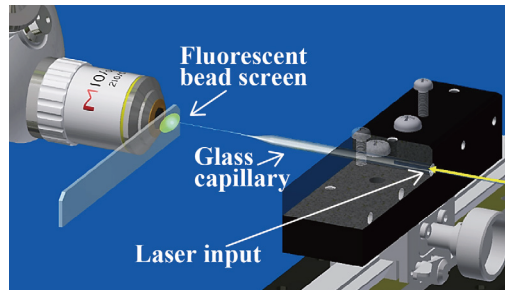
Fig. 1. Fluorescent beads, 2 μm in diameter, shift the wavelength from 488 nm (input laser) to around 508 nm (fluorescence) in order to observe the spot shape at a specific distance.
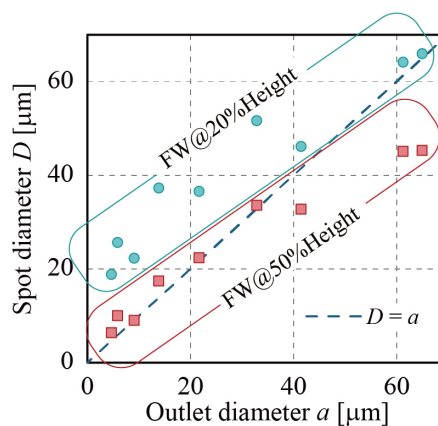
Fig. 2. The spot size as a function of the capillary outlet diameter at $L = 17$ μm and $\lambda = 488$ nm.

are strongly suppressed. This is highly advantageous for spotlighting a small target. We succeeded in performing spot size estimation, for the first time, using the precise L-determination system. Figure 2 shows the results of spot size as a function of outlet diameter at $L = 17$ μm. The full spot width at half (or 20%) maxima for each spot is represented by a square (or circular) symbol. The dashed line is a guide to show the case when the spot size is equal to the outlet size. We confirmed that smaller spots are obtained for smaller outlet capillaries without any higher-order rings. The estimation included the calibration of non-linearity of light intensity at the camera and the suppression of the halation effect due to cross-talk between the fluorescent beads. The installation of the system to a beam line of the Pelletron accelerator is in progress.

References
1) V. Mäckel *et al.*, Rev. Sci. Instrum. **85**, 014302 (2014).
2) Y. Iwai *et al.*, Appl. Phys. Lett. **92**, 023509 (2008).
3) M. Kato *et al.*, Appl. Phys. Lett. **100**, 193702 (2012).
4) W.-G. Jin *et al.*, J. Phys. Soc. Jpn **84**, 114301 (2015).
5) M. Koushima *et al.*, J. Phys. Conf. Ser. **875**, 112004 (2017).

*1 RIKEN Nishina Center
*2 Department of Physics, Toho University

Magnetic moments and ordered states in pyrochlore iridates Nd$_2$Ir$_2$O$_7$ and Sm$_2$Ir$_2$O$_7$ studied by muon-spin relaxation[†]

R. Asih,[*1,*2] N. Adam,[*1,*3] S. S. Mohd-Tajudin,[*1,*3] D. P. Sari,[*1,*2] K. Matsuhira,[*4] H. Guo,[*5]
M. Wakeshima,[*6] Y. Hinatsu,[*6] T. Nakano,[*2] Y. Nozue,[*2] S. Sulaiman,[*3] M. I. Mohammed-Ibrahim,[*3]
P. K. Biswas,[*7] and I. Watanabe[*1,*2,*3,*8]

Pyrochlore iridates, R_2Ir$_2$O$_7$ (R227, R = Nd, Sm, Eu, Gd, Tb, Dy, or Ho), which have the relatively large spin-orbit coupling (SOC) inherent in Ir 5d electrons and a d-f exchange interaction, have been suggested to show peculiar electronic properties.[1] R227 also shows metal-insulator transitions (MITs) at T_{MI}, which seems to be accompanied by magnetic transitions. T_{MI} gradually decreases from 141 K for R = Ho to 117 K for R = Sm with the increasing ionic radius of the trivalent R ion. T_{MI} suddenly drops to 33 K for Nd227, and no MIT is observed in Pr227, which shows metallic behavior.[2] Owing to difficulties in observing Ir magnetic ordering by means of neutron studies in these compounds, muon-spin relaxation (μSR) studies have been proven to directly confirm the appearance of long-range magnetic ordering (LRO) in some of the R227 compounds.[3–5]

In this study, we investigate the magnetic orderings and structures of Nd227 and Sm227, which are particularly important as they lie in the boundary of MIT. In the case of Nd227, we observed the additional LRO of Nd moments below 10 K and found a saturated internal field at the muon site (H_{int}) of approximately 530 G at 1.5 K, which confirmed indications suggested by previous neutron scattering[6] and μSR studies.[5] In the case of Sm227, spontaneous muon-spin precession was observed below T_{MI} = 117 K, which indicated the appearance of LRO of Ir moments below T_{MI}. The parameters obtained from the fitting to the zero-field μSR data on Sm227 are shown in Fig. 1. The solid line in Fig. 1(a) indicates the temperature dependence of the resistivity, showing a clear transition at T_{MI}. The internal field at the muon site, H_{int}, rapidly increases just below T_{MI} and saturates at the temperature region between 60 K and 20 K. With further decrease in temperature, H_{int} decreases below approximately 10 K. As shown in Fig. 1(b), the relaxation rate λ_1 is relatively constant in the paramagnetic region at $T > T_{MI}$ and then increases below T_{MI}, forming a peak at approxi-
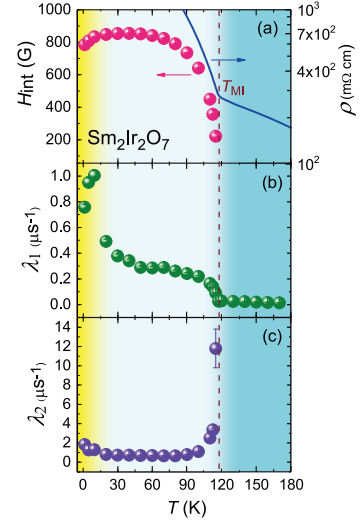
Fig. 1. Temperature dependences of (a) internal field at the muon sites H_{int}, (b) slow relaxation rate λ_1, and (c) damping rate of the muon-spin precession λ_2. The broken line indicates T_{MI} = 117 K. The area $T > T_{MI}$ indicates the paramagnetic region. The temperature dependence of the resistivity of Sm$_2$Ir$_2$O$_7$ is displayed in (a) by the solid line as a reference MIT.

mately 10 K, which indicates a slowing-down behavior toward an LRO below this temperature. This, therefore, suggests the appearance of the additional LRO of Sm moments below 10 K. Increases in the damping rate of the muon-spin precession are also observed below 10 K and near the T_{MI}, as indicated in Fig. 1(c), which further indicates a broadening of the distribution of H_{int}. Dipole-field calculations at the possible muon stopping site show that the all-in all-out spin structure most convincingly explained the present μSR results with the lower limits of the magnetic-ordered moments determined as 0.12 μ_B/Ir^{4+} and 0.2 μ_B/Nd^{3+} in Nd227 and 0.3 μ_B/Ir^{4+} and 0.1 μ_B/Sm^{3+} in Sm227. Further analysis indicated that the spin coupling between Ir and Nd/Sm moments was ferromagnetic for Nd227 and antiferromagnetic for Sm227.

References
1) X. Wan *et al.*, Phys. Rev. B **83**, 205101 (2011).
2) K. Matsuhira *et al.*, J. Phys. Soc. Jpn. **80**, 094701 (2011).
3) S. Zhao *et al.*, Phys. Rev. B **84**, 180402(R) (2011).
4) S. M. Disseler *et al.*, Phys. Rev. B **84** 174441 (2012).
5) H. Guo *et al.*, Phys. Rev. B **88**, 060411(R) (2013).
6) K. Tomiyasu *et al.*, J. Phys. Soc. Jpn. **81**, 034709 (2012).

Effect of Fe substitution on Cu-spin dynamics in the electron-doped cuprates $Eu_{2-x}Ce_xCuO_{4+\alpha-\delta}$

Risdiana,[*1] M. Manawan,[*1] Fitrilawati,[*1] L. Safriani,[*1] T. Saragi,[*1] and I. Watanabe[*2]

The effect of impurities on the Cu-spin dynamics in high-T_c cuprates has attracted great research interest in relation to the mechanism of high-T_c superconductivity. In the hole-doped cuprates of $La_{2-x}Sr_xCu_{1-y}Zn_yO_4$ (LSCZO),[1,2] the non-magnetic imputity Zn tends to slow down the Cu-spin fluctuations in the whole superconducting regime. In the electron-doped cuprates of the $Pr_{1-x}LaCe_xCu_{1-y}Zn_yO_4$,[3] on the other hand, the time spectra are independent of the Zn concentration, which is probably due to the strong effect of the Pr^{3+} moment. For Ni substitution effects, in $La_{2-x}Sr_xCu_{1-y}Ni_yO_4$, a hole-trapping effect together with the stripe-pinning effect of Ni was clearly observed.[4] As an electron doped system, we prepared samples without the Pr^{3+} moment, namely $Eu_{1.85}Ce_{0.15}Cu_{1-y}Ni_yO_{4+\alpha-\delta}$ (ECCNO),[5] in order to clarify the effects of Ni on the Cu-spin dynamics. As shown in Fig. 1, the development of the Cu-spin correlation is induced at low temperatures through Ni substitution. Importantly, in the μSR time spectra of ECCNO, the trace of the development of the Cu-spin correlation was observed at low temperatures for the Ni-substituted samples. However, no clear evidence of the Ni substitution effect on the Cu-spin dynamics has been obtained yet.

The effect of Fe substitution on Cu-spin dynamics has attracted much attention owing to the significant effect of its large magnetic moment on the superconductivity. In hole-doped systems, it has been found that the magnetic transition temperature and magnetic correlation are enhanced through 1% Fe substitution in a wide range of hole concentrations at which superconductivity appears in Fe-free $La_{2-x}Sr_xCuO_4$.[6] On the other hand, the effects of magnetic impurities on the Cu-spin dynamics in electron-doped systems have not yet been reported, which prevents us from drawing a clear conclusion on the relation between the dynamical stripe correlations and superconductivity in electron-doped cuprates. Therefore, partial substitution by Fe in electron-doped cuprates is a potential method of using an impurity to study the Cu-spin dynamics in the electron-doped system.

Figure 2 shows the μSR time spectra of $Eu_{1.85+y}Ce_{0.15-y}Cu_{1-y}Fe_yO_{4+\alpha-\delta}$ (ECCFO) with $y = 0.005, 0.01, 0.02$, and 0.03 at various temperatures. For all samples, the spectra show an exponential-type depolarization behavior at temperatures below $\sim$50 K. Gaussian-type depolarization behavior was only observed at temperatures above $\sim$200 K, which is higher than the corresponding temperature of the ECCNO
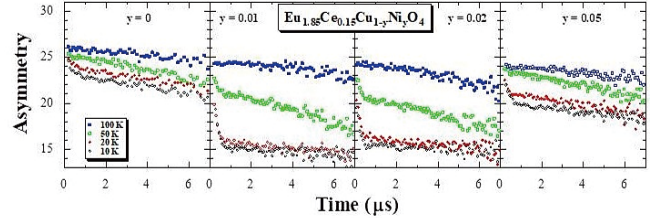
Fig. 1. μSR spectra of $Eu_{1.85}Ce_{0.15}Cu_{1-y}Ni_yO_{4+\alpha-\delta}$ with $y = 0, 0.01, 0.02$, and 0.05 at various temperatures.[5]
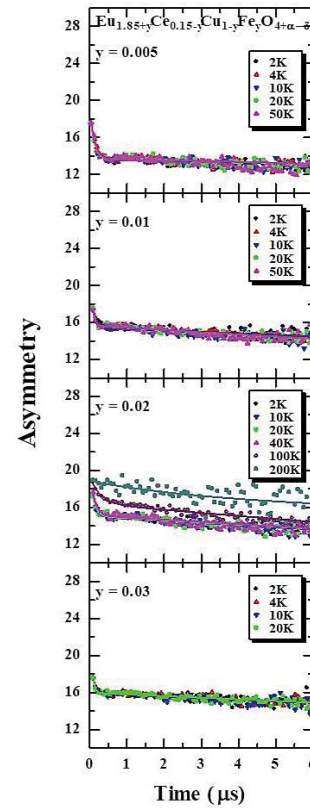
Fig. 2. μSR spectra of $Eu_{1.85+y}Ce_{0.15-y}Cu_{1-y}Fe_yO_{4+\alpha-\delta}$ with $y = 0.005, 0.01, 0.02$, and 0.03 at various temperatures.

sample at $y = 0.02$. These results also indicate the trace of development of the Cu-spin correlation. The coherent precession of muon spins are observed below 50 K, suggesting the existence of a static magnetic ground state.

The trace of stabilization of the Cu-spin fluctuations by Fe substitution indicates a possibility that the stripe model can globally explain high-T_c superconductivity as in the case of hole-doped systems.

References
1) T. Adachi et al., Phys. Rev. B **69**, 184507 (2004).
2) Risdiana et al., Phys. Rev. B **77**, 054516 (2008).
3) Risdiana et al., Phys. Rev. B **82**, 014506 (2010).
4) Y. Tanabe et al., Phys. Rev. B **83**, 144521 (2011).
5) Risdiana et al., Adv. Mat. Res. **896**, 354 (2014).
6) K. M. Suzuki et al., Phys. Rev. B **86**, 014522 (2012).

*1 Department of Physics, Padjadjdaran University, Indonesia
*2 RIKEN Nishina Center

One-pot three-component double-click method for synthesis of [^{67}Cu]-labeled biomolecular radiotherapeutics[†]

K. Fujiki,[*1] S. Yano,[*2] T. Ito,[*3] Y. Kumagai,[*3] Y. Murakami,[*3] O. Kamigaito,[*2] H. Haba,[*2] and K. Tanaka[*1,*4,*5]

A one-pot three-component double-click process to prepare tumor-targeting agents for cancer radiotherapy is described here. By utilizing DOTA (or NOTA) containing tetrazines (DOTA: 1, 4, 7, 10-tetraazadodecane-1, 4, 7, 10-tetraacetic acid, NOTA: 1, 4, 7-triazacyclononane-1, 4, 7-triacetic acid) and the TCO-substituted aldehyde (TCO: trans-cyclooctene), the two click reactions, the tetrazine ligation (an inverse electron-demand Diels-Alder cycloaddition)[1] and the RIKEN click (a rapid 6π-azaelectrocyclization),[2–8] could simultaneously proceed under mild conditions to afford the covalent attachment of the DOTA or NOTA, which forms a bioavailable stable complex with copper (II), to biomolecules such as albumin and anti-IGSF4 antibody without altering their activities (Fig. 1).

Subsequently, the radiolabeling of DOTA- or NOTA-attached albumin and anti-IGSF4 antibody (a tumor-targeting antibody) with ^{67}Cu as a promising β^-/γ-e-mitting theranostic radionuclide having a half-life of 62 h, which is compatible with radioimmunotherapy, could be achieved by mixing DOTA- or NOTA-attached albumin and anti-IGSF4 antibody with RIs and subsequent purification by Amicon filtration; a separate experiment with ^{65}Zn was conducted for comparison (Fig. 2 and Table 1). ^{67}Cu and ^{65}Zn could be produced in the ^{70}Zn$(d, \alpha n)^{67}$Cu and ^{nat}Cu$(d, x)^{65}$Zn reactions at the AVF cyclotron. Our work provides a new and operationally simple method for introducing ^{67}Cu to biomolecules, which is an important process for preparing clinically relevant tumor-targeting agents.
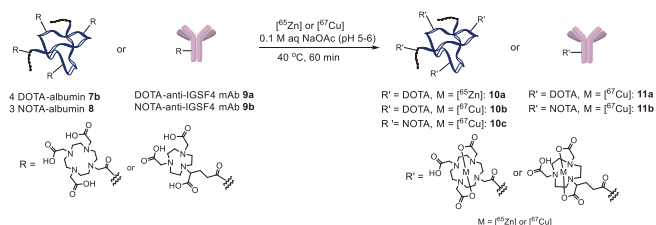
Fig. 2. Radiolabelings of DOTA or NOTA-attached albumins and anti-IGSF4 antibody.
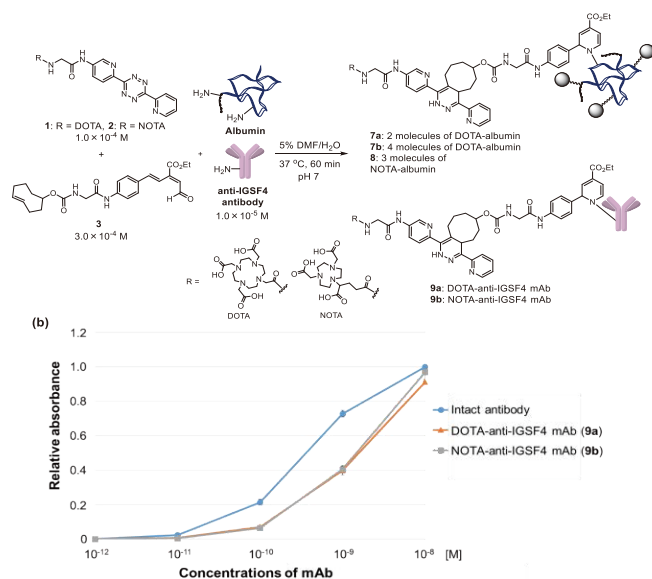
Fig. 1. (a) One-pot three-component click labeling of albumin and anti-IGSF4 antibody as a cancer-targeting agent. (b) Affinities of intact and labeled anti-IGSF4 antibodies to IGSF4 analyzed by ELISA. DMF = N,N-dimethyl formamide, ELISA = enzyme-linked immunosorbent assay.

Table 1. Radiochemical yields (RCY) of ^{67}Cu and ^{65}Zn.

Entry	Chelator-attached biomolecules	Added [^{65}Zn] or [^{67}Cu][a] (Radioactivities)	RCY[b] (%)
1	DOTA-albumin 7b	[^{65}Zn] (300 kBq)	80
2	DOTA-albumin 7b	[^{67}Cu] (11 MBq)	72
3	DOTA-anti-IGSF4 mAb 9a	[^{67}Cu] (11 MBq)	51
4	NOTA-albumin 8	[^{67}Cu] (11 MBq)	19
5	NOTA-anti-IGSF4 mAb 9b	[^{67}Cu] (11 MBq)	7

a) Specific activities of ^{67}Cu and ^{65}Zn were 110 MBq/μg and 125 MBq/μg, respectively.
b) RCY (Radiochemical yield) was obtained from the radioactivity of the purified radiolabeled product against the added [^{65}Zn] or [^{67}Cu].

References
1) M. L. Blackman, M. Royzen, J. M. Fox, J. Am. Chem. Soc. **130**, 13518 (2008).
2) K. Tanaka *et al.*, Angew. Chem. Int. Ed. **47**, 102 (2008).
3) K. Tanaka *et al.*, Angew. Chem. Int. Ed. **49**, 8195 (2010).
4) K. Fukase, K. Tanaka, Curr. Opin. Chem. Biol. **16**, 614 (2012).
5) K. Tanaka *et al.*, J. Org. Chem. **66**, 3099 (2001).
6) K. Tanaka, S. Katsumura, J. Am. Chem. Soc. **124**, 9660 (2002).
7) K. Tanaka *et al.*, J. Org. Chem. **69**, 5906 (2004).
8) K. Fujiki, K. Tanaka, e-EROS Encyclopedia of Reagents for Organic Synthesis (Wiley, 2018) in press.

Cross section measurement to produce ^{99}Mo through alpha-induced reactions on natural Zr

T. Murata,[*1,*2] M. Aikawa,[*2,*3] M. Saito,[*2,*3] N. Ukon,[*2,*4] Y. Komori,[*2] H. Haba,[*2] and S. Takács[*5]

Radiopharmaceuticals containing ^{99m}Tc ($T_{1/2}$ = 6.0 h) produced from the decay of ^{99}Mo ($T_{1/2}$ = 66 h) are used worldwide for imaging in diagnostic nuclear medicine. Although nuclear reactors provide sufficient global supplies of ^{99}Mo, unplanned shutdowns due to technical issues disrupt these supplies. In addition, the nuclear waste created by fission reactions in the nuclear reactors is a problem. Therefore, ^{99}Mo production routes other than neutron-induced fission are needed.

One of the reactions that creates ^{99}Mo is the ^{96}Zr(α,n)^{99}Mo reaction. However, previously obtained experimental cross section data[1,2] and TALYS Evaluated Nuclear Data Library (TENDL)[3] for this reaction exhibit discrepancies in their peak positions. It is very important to provide reliable and consistent cross section data for evaluation of the isotope production yields. Therefore, we performed an experiment to measure the cross sections for this reaction.

The cross sections of the ^{96}Zr(α,n)^{99}Mo reaction were measured using the standard stacked-foil activation method and off-line high-resolution high-purity Germanium (HPGe) γ-ray spectrometry. Natural Zr foils (purity: 99.2%, thickness: 20.3 μm; Nilaco Corp., Japan) having ^{96}Zr isotopic abundance of 2.80% and natural Ti foils (purity: 99.6%, thickness: 5.3 μm; Nilaco Corp., Japan) for the ^{nat}Ti(α,x)^{51}Cr monitor reaction were stacked together as a target. This stacked target was then mounted in a target holder that also served as a Faraday cup, and irradiated by a 51-MeV alpha beam with an average intensity of 203.6 pnA for 2 h at the RIKEN Azimuthally Varying Field (AVF) cyclotron. The alpha particle energy in the i-th foil E_i was derived using the stopping power calculated by Stopping and Range of Ions in Matter (SRIM) software.[4]

After a cooling time of 12 h to reduce the backgrounds, the γ-ray spectra on each foil were measured using high-resolution γ-ray spectrometry with a HPGe detector. The characteristic 739-keV γ-line (I_γ = 12.20%) from the decay of ^{99}Mo in the Zr foils and the 320-keV γ-line (I_γ = 9.91%) from the decay of ^{51}Cr in the Ti foils were measured to derive the cross sections of the ^{96}Zr(α,n)^{99}Mo and ^{nat}Ti(α,x)^{51}Cr re-
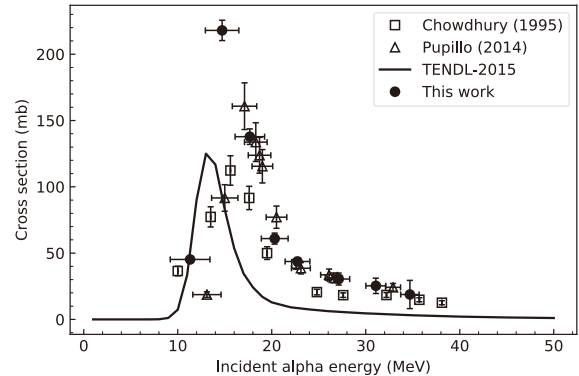
Fig. 1. Experimental cross sections of ^{96}Zr(α,n)^{99}Mo reaction in comparison with previously reported experimental data and TENDL data.

actions, respectively. The distance between the measured foil and detector was optimized to maintain a dead time lower than 10%. To obtain the production cross sections of the assessed radionuclide $\sigma(E_i)$, the well-known activation formula was used.

The measured production cross sections of ^{99}Mo are shown in Fig. 1, along with available previous data[1,2] and the TENDL data.[3] Our result shows that the peak is located in the vicinity of 14 MeV with a cross section value of approximately 210 mb, differing from the results of earlier studies.

In this work, the cross sections of the ^{96}Zr(α,n)^{99}Mo reaction were measured using standard methods, i.e., the stacked target method, activation technique, and high-resolution γ-ray spectrometry. The newly measured cross section data were compared with previously reported experimental data and the TENDL data. The peak of the deduced excitation function was higher than that given by the previous data and was located at approximately 14 MeV. To confirm this excitation function behavior, we will repeat this experiment in detail in the energy range of 10 to 20 MeV.

References
1) D. P. Chowdhury et al., Nucl. Instrum. Methods B **103**, 261 (1995).
2) G. Pupillo et al., J. Radional. Nucl. Chem. **302**, 911 (2014).
3) A. J. Koning et al., Nucl. Data Sheets **113**, 2841 (2012).
4) J. F. Ziegler et al., Nucl. Instrum. Methods B **268**, 1818 (2010).

*1 School of Science, Hokkaido University
*2 RIKEN Nishina Center
*3 Graduate School of Biomedical Science and Engineering, Hokkaido University
*4 Advanced Clinical Research Center, Fukushima Medical University
*5 Institute for Nuclear Research, Hungarian Academy of Sciences (ATOMKI)

Analysis of carbon ion-induced mutations by exome sequencing of an unselected rice population

H. Ichida,[*1] R. Morita,[*1] Y. Shirakawa,[*1] Y. Hayashi,[*1] and T. Abe[*1]

Massively parallel sequencing technology has been utilized in many areas of biology including mutation analysis, by using a large amount of gene and genome sequencing information to achieve a comprehensive and genome-wide analysis. Heavy-ion beams are one of the physical mutagens that are classified as high-LET radiation and are known to induce double strand breaks of DNA in a cell along with its track. The resulting mutations, including deletions, insertions, inversions and base substitutions, that occur on the genome can cause the inactivation and/or temporal change of gene expressions that are necessary for morphogenesis. We have developed a custom-designed oligonucleotide probe library to capture entire exons within the rice genome, which targets a total of 300,746 genomic loci at the same time. We also developed a bioinformatics pipeline to map the sequencing reads to the reference Nipponbare genome sequence and identify reliable mutations in a highly paralleled way by using the "HOKUSAI" parallel computing system operated by the Advanced Center for Computing and Communication, RIKEN. In addition to these previous efforts to make the genome-based mutation detections, we developed a pre-mixed target capture procedure to further reduce the usage of the custom-designed target capture oligonucleotide probes, which takes nearly half of the overall cost in whole exome sequencing, by mixing multiple libraries with different index sequences prior to the target capturing: this reduces the per-sample oligonucleotide probe usage to 1/8th of that of the original protocol.

In the present study, we analyzed a total of 110 independent M_2 lines from carbon-ion beam irradiations ($^{12}C^{6+}$, 135 MeV/u, LET: 30 keV/μm, 150 Gy) to Nipponbare rice seeds, the water content of which was adjusted to 13%. The irradiated seeds were grown in a paddy field, and the M_2 seeds were harvested from each line. In each line, 10 to 15 plants were grown in soil, and an equal amount of leaf blades were collected from each plant and subjected to genomic DNA extraction and sequencing library preparation. As a control, 8 pools of non-irradiated Nipponbare plants were also processed in the same maner. A total of 8 libraries were mixed together prior to the target capturing and then sequenced in a half lane on a HiSeq 4000 instrument. The obtained sequencing dataset was processed using our bioinformatics pipeline described above. As a result, the number of mutations within the target region of whole exome capturing was between 3 and 26 in each line (Fig. 1). The average number of

mutations was 9.06 ± 0.37 (average ± standard error) per line. There were a total of 997 mutations, which consisted of 573 base substitutions, 372 deletions, 36 insertions, 13 substitutions, and 3 inversions, identified from the irradiated M_2 lines. The percentage of deletions and insertions, against all detected mutations, was 40.9%, which was consistent with the previously described characteristics of mutations induced by highly accelerated heavy-ion beams, which often cause nucleotide substitutions and deletions and insertions of less than 100 bp.[1] In contrast, no mutation was identified in non-irradiated Nipponbare pools, indicating that the mutations detected from the carbon-ion-irradiated samples were likely to be induced by the mutagenesis.

Based on an interpolation from the proportion of target exon regions against the entire genome (the total length of the target exon regions is 9.12% of the length of the entire genome), roughly 100 mutations are expected to be induced in the entire genome. This might be an underestimation due to the difference in biological significance between protein-encoding exons and other genomic regions, which are mostly intergenic regions and repetitive elements; however, this estimation was of the same order as our previous results (175 to 549 mutations per genome in the 12 mutants analyzed) obtained from the whole genome sequencing of morphological mutants in rice.[2]
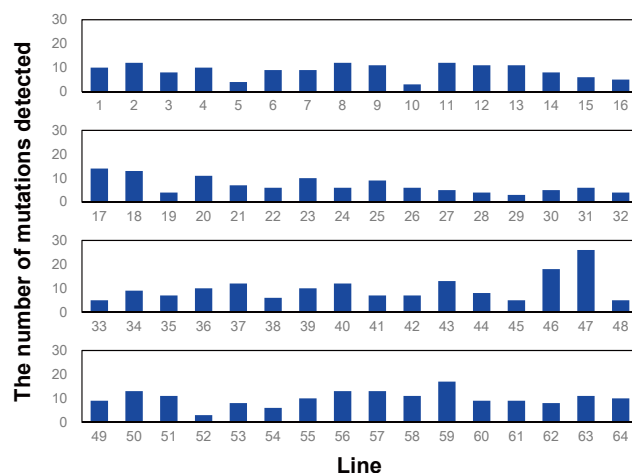
Fig. 1. Number of mutations detected from the carbon-ion irradiated rice M_2 lines (Nos. 1–64).

References
1) Y. Kazama *et al.*, BMC Plant Biol. **11**, 161 (2011).
2) H. Ichida *et al.*, RIKEN Accel. Prog. Rep. **50**, 271 (2017).

*1 RIKEN Nishina Center

Effect of LET on mutational function revealed by whole-genome resequencing of *Arabidopsis* mutants[†]

Y. Kazama,[*1] K. Ishii,[*1] T. Hirano,[*1,*2] T. Wakana,[*1] M. Yamada,[*1] S. Ohbu,[*1] and T. Abe[*1]

Heavy-ion irradiation is a powerful mutagen that possesses high linear energy transfer (LET). Since the value of LET affects DNA lesion formation in several aspects, including the efficiency and density of double-stranded break along the particle path,[1,2] mutations induced after the DNA lesion repair would also be affected by the value of LET. Whole-genome resequencing is an effective way to assess the effect of the value of LET on mutation induction, and provides sufficient number of mutations from each mutant to perform statistical analyses.[3] Here, we investigated the differences in the mutation type induced by irradiation with two representative ions, namely C ions (LET: 30.0 keV/μm) and Ar ions (LET: 290 keV/μm), by whole-genome resequencing of the *Arabidopsis* mutants produced by these irradiations.

Dry seeds of *A. thaliana* were irradiated with C ions (30.0 keV/μm) or Ar ions (290 keV/μm) with doses found to induce 95% survival rates and the highest mutation frequencies.[4] For the C-ion and Ar-ion irradiations, doses of 50 and 400 Gy were adopted, respectively. Eight mutants showing morphological phenotypes were screened in the M_2 generation after each irradiation. Then, the phenotypes of the mutants were confirmed in the M_3 generation. In total, 16 mutants were selected, and DNA pools were extracted from 40 plants of their individual progeny. The extracted DNA was sequenced using the HiSeq 2500 and HiSeq 4000 sequencing systems (Illumina Inc., `https://www.illumina.com`). The obtained reads were input into AMAP, as described previously.[5]

The rearrangements including translocations and large deletions ($\geq$ 100 bp) that were induced by Ar ions were 4.6 times more frequent than those induced by the C ions; the average number of rearrangements in a mutant genome was 10.3 and 2.3 for Ar ions and C ions, respectively (Fig. 1). These differences were statistically significant (P < 0.01; two-sided Welch's t-test). Both Ar and C ions induce rearrangements. However, more complicated rearrangements occurred following Ar-ion irradiation, in which fragments of several hundred kbp to several Mbp were produced and joined with direction or positions different from those of the original ones. Conversely, Ar ions induced small mutations including base substitutions and small indels (< 100 bp), which were 2.3-fold less frequent than C ions: the average number of small mutations in a mutant genome was 18.3 and 41.6 for Ar ions and C ions, respectively. This
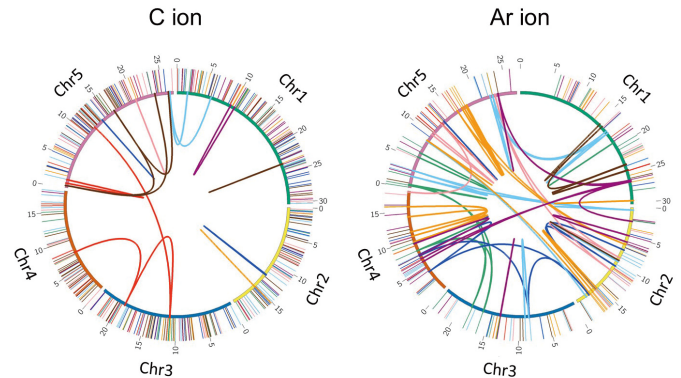
Fig. 1. Mutations in each of the eight mutants induced by C- and Ar-ion irradiation. The rearrangements are plotted as lines on the interior of the circles. Small mutations are indicated by lines on the exterior of the circles. The mutations in each mutant are differently colored.

Table 1. Sum of homozygously mutated genes detected in eight mutants.

	Amino acid changes	Truncation or loss of whole gene	Total
C ion	30	11	41
Ar ion	8	66	74

difference was also statistically significant (P < 0.01; two-sided Student's t-test).

The effects on gene mutations were also different between C-ion and Ar-ion irradiations. The sum of homozygously mutated genes in eight individual mutants after irradiation with Ar and C ions are shown in Table 1. After C-ion irradiation, amino-acid changes were frequently observed, which were caused by small mutations. On the other hand, Ar-ion irradiation frequently induced truncations of genes or losses of whole genes caused by rearrangements.

These data demonstrate that the nature of mutations is significantly different between beams with different LET values. Such a selective irradiation will be a powerful tool for forward genetics as well as studies on chromosomal rearrangements in conjunction with the technics of mutation detection through high-throughput sequencing.

References
1) D. Alloni *et al.*, Radiat. Res. **173**, 263 (2010).
2) N. A. Franken *et al.*, Radiat Oncol. **6**, 64 (2011).
3) K. Shirasawa *et al.*, Plant Biotechnol. J. **14**, 51 (2016).
4) Y. Kazama *et al.*, Plant Biotechnol. **25**, 113 (2008).
5) K Ishii *et al.*, Genes Genet. Syst. **91**, 229 (2016).

II. RESEARCH ACTIVITIES I
(Nuclear, Particle and Astro-Physics)

1. Nuclear Physics

Single-neutron knockout from ^{20}C and the structure of ^{19}C†

J.W. Hwang,[*1,*2] S. Kim,[*1,*2] Y. Satou,[*1] N. A. Orr,[*3] Y. Kondo,[*4,*2] T. Nakamura,[*4,*2] J. Gibelin,[*3]
N. L. Achouri,[*3] T. Aumann,[*5] H. Baba,[*2] F. Delaunay,[*3] P. Doornenbal,[*2] N. Fukuda,[*2] N. Inabe,[*2]
T. Isobe,[*2] D. Kameda,[*2] D. Kanno,[*4,*2] N. Kobayashi,[*4,*2] T. Kobayashi,[*6,*2] T. Kubo,[*2] S. Leblond,[*3]
J. Lee,[*2] F. M. Marques,[*3] R. Minakata,[*4,*2] T. Motobayashi,[*2] D. Murai,[*7] T. Murakami,[*8] K. Muto,[*6]
T. Nakashima,[*4,*2] N. Nakatsuka,[*8] A. Navin,[*9] S. Nishi,[*4,*2] S. Ogoshi,[*4,*2] H. Otsu,[*2] H. Sato,[*2]
Y. Shimizu,[*2] H. Suzuki,[*2] K. Takahashi,[*6] H. Takeda,[*2] S. Takeuchi,[*2] R. Tanaka,[*4,*2] Y. Togano,[*10]
A. G. Tuff,[*11] M. Vandebrouck,[*12] and K. Yoneda[*2]

The unbound states of ^{19}C have been investigated using the one-neutron knockout reaction. ^{19}C has a well established $1n$ halo structure with a weakly bound s-wave neutron. The almost degenerate $0d_{5/2}$ and $1s_{1/2}$ orbitals are expected to govern the low-lying level structure of ^{19}C, comprising $1/2^+$, $3/2^+$, and $5/2^+$ states.[1] Theoretically, while most shell models suggest that these states are closely located below 1 MeV, their ordering has remained uncertain. Experimentally, a few studies have reported the low-lying states including $3/2_1^+$ and $5/2_1^+$. There is an argument of the bound nature of $5/2_1^+$ provided by recent measurements.[2]

The ^{20}C beam of 280 MeV/nucleon at mid-target was produced from BigRIPS with using a 345 MeV/nucleon ^{48}Ca primary beam ($\sim$100 pnA). The secondary beam impinged on a secondary carbon target (1.8 g/cm^2) in front of the SAMURAI spectrometer to produce ^{19}C.[3] The decay products, including ^{18}C and a neutron, were detected using SAMURAI and NEBULA neutron array. Note that the measurement was a part of the first experimental campaign using SAMURAI to study the light neutron-rich nuclei.[4]

Figures 1 show the relative energy ($E_{\rm rel}$) spectrum for the ^{18}C $+ n$ system containing a narrow threshold resonance and two peaks at higher energies. The positions were determined to be at 0.036(1), 0.84(4), and 2.31(3) MeV by fitting analysis with R-matrix lineshapes convoluted with the experimental resolution. The longitudinal momentum distributions for each resonance show clear ℓ characters compared with Glauber model calculation.[5] Such results allow the spin-parity assignment of $5/2_1^+$ and $1/2_1^-$ for the levels
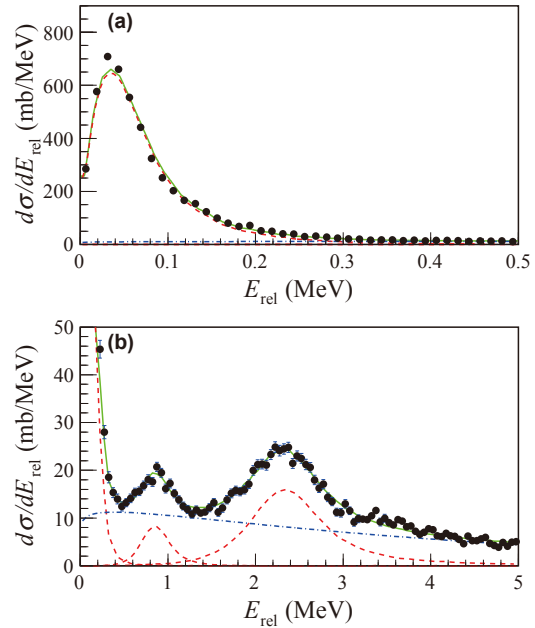
Fig. 1. Relative energy spectrum for the ^{18}C $+ n$ system up to (a) 0.5 MeV and (b) 5 MeV. The solid (green), dashed (red), and dot-dashed (blue) curves represent the lineshapes of the results of the fit, individual resonances, and background, respectively.

at $E_x =$0.62(9) and 2.89(10) MeV with $S_n = 0.58(9)$ MeV. Spectroscopic factors were also found to agree with the shell-model calculations. The valence neutron configuration of the ^{20}C$_{\rm g.s.}$ is thus expected to have a significant $0d_{5/2}^2$ contribution together with the known $1s_{1/2}^2$ component. The level scheme of ^{19}C is well described by the shell model with YSOX interaction based on the monopole-based universal interaction.[6]

References
1) M. Stanoiu *et al.*, Phys. Rev. C **78**, 034315 (2008).
2) N. Kobayashi *et al.*, Phys. Rev. C **86**, 054604 (2012).
3) T. Kobayashi *et al.*, Nucl. Instrum. Methods Phys. Res. Sect. B **317**, 294 (2013).
4) Y. Kondo *et al.*, Phys. Rev. Lett. **116**, 102503 (2016).
5) C. A. Bertulani, A. Gade, Comput. Phys. Commun. **175**, 372 (2006).
6) C. Yuan *et al.*, Phys. Rev. C **85**, 064324 (2012).

† Condensed from the article in Phys. Lett. B **769**, 503-508 (2017)
*1 Department of Physics and Astronomy, Seoul National University
*2 RIKEN Nishina Center
*3 LPC-Caen, ENSICAEN, Université de Caen, CNRS/IN2P3
*4 Department of Physics, Tokyo Institute of Technology
*5 Institut für Kernphysik, Technische Universität Darmstadt
*6 Department of Physics, Tohoku University
*7 Department of Physics, Rikkyo University
*8 Department of Physics, Kyoto University
*9 GANIL, CEA/DSM-CNRS/IN2P3
*10 ExtreMe Matter Institute (EMMI) and Research Division, GSI
*11 Department of Physics, University of York
*12 Institut de Physique Nucléaire, Université Paris-Sud, IN2P3-CNRS

Observation of isoscalar and isovector dipole excitations in ^{20}O[†]

N. Nakatsuka,[*1,*2] H. Baba,[*2] N. Aoi,[*10] T. Aumann,[*3] R. Avigo,[*5,*14] S. R. Banerjee,[*12] A. Bracco,[*5,*14]
C. Caesar,[*3] F. Camera,[*5,*14] S. Ceruti,[*5,*14] S. Chen,[*13,*2] V. Derya,[*4] P. Doornenbal,[*2] A. Giaz,[*5,*14]
A. Horvat,[*3] K. Ieki,[*11] N. Imai,[*7] T. Kawabata,[*1] K. Yoneda,[*2] N. Kobayashi,[*8] Y. Kondo,[*9] S. Koyama,[*8]
M. Kurata-Nishimura,[*2] S. Masuoka,[*7] M. Matsushita,[*7] S. Michimasa,[*7] B. Millon,[*5] T. Motobayashi,[*2]
T. Murakami,[*1] T. Nakamura,[*9] T. Ohnishi,[*2] H. J. Ong,[*10] S. Ota,[*7] H. Otsu,[*2] T. Ozaki,[*9] A. T. Saito,[*9]
H. Sakurai,[*2,*8] H. Scheit,[*3] F. Schindler,[*3] P. Schrock,[*3] Y. Shiga,[*11,*2] M. Shikata,[*9] S. Shimoura,[*7]
D. Steppenbeck,[*2] T. Sumikama,[*6,*2] I. Syndikus,[*3] H. Takeda,[*2] S. Takeuchi,[*2] A. Tamii,[*10] R. Taniuchi,[*8]
Y. Togano,[*9] J. Tscheuschner,[*3] J. Tsubota,[*9] H. Wang,[*2] O. Wieland,[*5] K. Wimmer,[*8,*2] Y. Yamaguchi,[*7]
and J. Zenihiro[*2]

The electric dipole response, or $E1$ response, is one of the most interesting properties of atomic nuclei. In medium to heavy neutron-rich nuclei, the electric dipole excitation is fragmented into a low-energy region around the neutron separation energy, so-called Pygmy dipole resonance.[1,2] Recent experimental studies on ^{40,48}Ca,[6] ^{74}Ge,[7] ^{124}Sn,[8] ^{138}Ba,[9] and ^{140}Ce[9,10] have demonstrated that low-energy dipole excitations exhibit a specific isospin character, sometimes referred to as "isospin splitting." They demonstrated that some dipole excitations, mostly in the low-energy region, were populated by both isoscalar and isovector probes. In this work, the isospin character of low-energy dipole excitations in neutron-rich unstable nucleus ^{20}O was investigated, for the first time in unstable nuclei. The experiment was performed at Radioactive Isotope Beam Factory (RIBF). The ^{20}O beam impinged on two different reaction targets, a 2.45(5) mm gold target as an isovector probe, and a 317(28) mg/cm^2 liquid helium target as an isoscalar probe. The decay γ rays from the excited beam particles were detected with large volume LaBr$_3$ crystals from INFN Milano.[3] Two low-energy dipole states at energies of 5.36(5) MeV (1_1^-) and 6.84(7) MeV (1_2^-), previously known to be populated by the Coulomb excitation,[4,5] were consistently populated both by the isoscalar and isovector probe. The decay scheme of those states were determined by the γ-γ coincidence analysis, and the decay branch via the 2_1^+ state (1.67 MeV) was observed.

In order to extract the cross sections and transition strengths, a distorted-wave Born approximation (DWBA) analysis was performed by using the Ecis97 code.[12] As nuclear potential, we employed the theoretically developed global optical potential described in Refs. 13–15). The transition strengths of the 1^- states were determined in the same manner, by including both the Coulomb and nuclear contributions in either system, with the assumption that the Coulomb potential contributed only to the isovector dipole strength and the nuclear potential contributed only to the isoscalar dipole strength. The Harakeh-Dieperink dipole form factor[11] was employed to determine the isoscalar dipole strength. The strengths were determined so that the experimental cross sections from both the ^{20}O+α and ^{20}O+Au systems were reproduced by the same isoscalar and isovector dipole strengths. The 1_1^- state (5.36(5) MeV) had an isoscalar dipole strength of 2.70(32)% in ISD EWSR, while the 1_2^- state (6.84(7) MeV) had a strength of 0.67(12)% in Isoscalar dipole energy-weighted sum-rule fraction (ISD EWSR). These states, however, have comparable isovector dipole strengths: $B(E1)\uparrow = 3.57(20) \times 10^{-2}$ e^2fm^2 for the 1_1^- state and $B(E1)\uparrow = 3.79(26) \times 10^{-2}$ e^2fm^2 for the 1_2^- state. The results indicate that low-energy dipole excitations in ^{20}O exhibit a dual character. The difference in isoscalar response suggests that these states have different underlying structures.

References
1) A. Bracco et al., Euro. Phys. J. A **51**, 99 (2015).
2) D. Savran et al., Prog. Part. Nucl. Phys. **70**, 210 (2013).
3) A. Giaz et al., Nucl. Instrum. Methods Phys. Res. A **729**, 910 (2013).
4) E. Tryggestad et al., Phys. Lett. B **541**, 52 (2002).
5) E. Tryggestad et al., Phys. Rev. C **67**, 064309 (2003).
6) V. Derya et al., Phys. Lett. B **768**, 387 (2017).
7) D. Negi et al., Phys. Rev. C **94**, 024332 (2016).
8) J. Endres et al., Phys. Rev. Lett. **105**, 212503 (2010).
9) J. Endres et al., Phys. Rev. C **80**, 034302 (2009).
10) D. Savran et al., Phys. Rev. Lett. **97**, 172502 (2006).
11) M. N. Harakeh et al., Phys. Rev. C **23**, 2329 (1981).
12) J. Raynal et al., Phys. Rev. C **23**, 2571 (1981).
13) T. Furumoto et al., Phys. Rev. C **85**, 044607 (2012).
14) T. Furumoto et al., Phys. Rev. C **80**, 044614 (2009).
15) T. Furumoto et al., Phys. Rev. C **78**, 044610 (2008).

† Condensed from the article in Phys. Lett. B **768**, 387 (2017)
*1 Department of Physics, Kyoto University
*2 RIKEN Nishina Center
*3 Institut für Kernphysik, Technische Universität Darmstadt
*4 Institut für Kernphysik, Universität zu Köln
*5 Istituto Nazionale di Fisica Nucleare Milan
*6 Department of Physics, Tohoku University
*7 Center for Nuclear Study, The University of Tokyo
*8 Department of Physics, The University of Tokyo
*9 Department of Physics, Tokyo Institute of Technology
*10 Research Center for Nuclear Physics, Osaka University
*11 Department of Physics, Rikkyo University
*12 Variable Energy Cyclotron Centre, The Indian Department of Atomic Energy
*13 School of Physics, Peking University
*14 University of Milan

Neutron-neutron correlation in Borromean nucleus ^{11}Li via the (p, pn) reaction

Y. Kubota,[*1,*2] A. Corsi,[*3] G. Authelet,[*3] H. Baba,[*2] C. Caesar,[*4] D. Calvet,[*3] A. Delbart,[*3] M. Dozono,[*1]
J. Feng,[*5] F. Flavigny,[*6] J.-M. Gheller,[*3] J. Gibelin,[*7] A. Giganon,[*3] A. Gillibert,[*3] K. Hasegawa,[*8,*2]
T. Isobe,[*2] Y. Kanaya,[*9,*2] S. Kawakami,[*9,*2] D. Kim,[*10,*2] Y. Kiyokawa,[*1] M. Kobayashi,[*1] N. Kobayashi,[*11]
T. Kobayashi,[*8,*2] Y. Kondo,[*12,*2] Z. Korkulu,[*13,*2] S. Koyama,[*11,*2] V. Lapoux,[*3,*2] Y. Maeda,[*9]
F. M. Marqués,[*7] T. Motobayashi,[*2] T. Miyazaki,[*11] T. Nakamura,[*12,*2] N. Nakatsuka,[*14,*2] Y. Nishio,[*15,*2]
A. Obertelli,[*3,*2] A. Ohkura,[*15,*2] N. A. Orr,[*7] S. Ota,[*1] H. Otsu,[*2] T. Ozaki,[*12,*2] V. Panin,[*2] S. Paschalis,[*4]
E. C. Pollacco,[*3] S. Reichert,[*16] J.-Y. Roussé,[*3] A. T. Saito,[*12,*2] S. Sakaguchi,[*15,*2] M. Sako,[*2]
C. Santamaria,[*3,*2] M. Sasano,[*2] H. Sato,[*2] M. Shikata,[*12,*2] Y. Shimizu,[*2] Y. Shindo,[*15,*2] L. Stuhl,[*2]
T. Sumikama,[*8,*2] M. Tabata,[*15,*2] Y. Togano,[*12,*2] J. Tsubota,[*12,*2] T. Uesaka,[*2] Z. H. Yang,[*2]
J. Yasuda,[*15,*2] K. Yoneda,[*2] and J. Zenihiro[*2]

Since a theoretical prediction was made by Migdal,[1] a hypothetical bound state of two neutrons, *dineutron*, has attracted much attention. The neutron-neutron correlation caused by the dineutron is expected to appear in weakly bound systems, such as the Borromean nucleus ^{11}Li. There have been extensive studies to search for such a correlation in ^{11}Li. $E1$ strengths deduced from Coulomb dissociation cross sections have been used by employing the $E1$ cluster sum rule to characterize their correlation.[2] However, the model dependence was not negligible owing to the ^{9}Li core excitation and the final-state interactions.[3] The kinematically complete measurement of the quasi-free (p, pn) reaction was thus performed with Borromean nuclei ^{11}Li, ^{14}Be, and ^{17,19}B at the RIBF so as to determine the neutron momentum distributions that provide more direct information of the ground-state correlation.[4]

The measurement required a high luminosity to have as much statistics as possible. For this purpose, the 15-cm-thick liquid hydrogen target MINOS[5] was introduced. The SAMURAI spectrometer[6] contributed to minimize experimental biases originating from the geometrical acceptance. A missing-mass setup composed of the neutron detector WINDS,[7] the recoil proton detector RPD, and the gamma-ray detector array DALI2[8] was newly configured for realizing the quasi-free (p, pn) measurement.

As a measure of the dineutron correlation in ^{11}Li, the opening angle of two valence neutrons $\cos\theta_Y$ was reconstructed from momentum vectors of all the particles involved in the reaction. The obtained $\cos\theta_Y$ distribution is shown in Fig. 1. The geometrical acceptance of the experimental setup was corrected by performing a Monte-Carlo simulation. The asymmetric distribution indicates an admixture of different parity states and the dineutron correlation in ^{11}Li. The asymmetry obtained in the present work is weaker than that in the previous work employing the neutron removal reaction by using a carbon target.[9] We presume that the dineutron correlation was overestimated in the previous study because of the sensitivity of the probe; the probe used in the previous study is only sensitive to the nuclear surface, where the dineutron correlation is expected to develop.
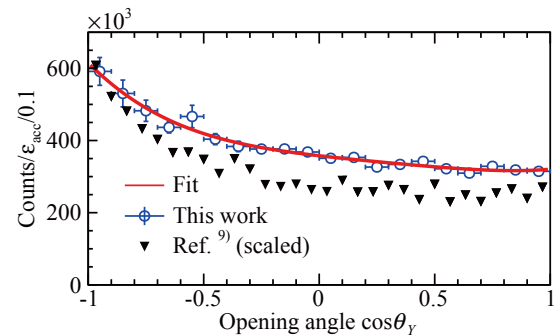
Fig. 1. Opening-angle distribution $\cos\theta_Y$ for ^{11}Li. The blue open and black closed marks represent the data taken in the present and previous works,[9] respectively.

*1　Center for Nuclear Study, University of Tokyo
*2　RIKEN Nishina Center
*3　CEA, Saclay
*4　Department of Physics, Technische Universität Darmstadt
*5　Department of Physics, Peking University
*6　IPN Orsay
*7　LPC Caen
*8　Department of Physics, Tohoku University
*9　Department of Applied Physics, University of Miyazaki
*10　Department of Physics, Ehwa Womans University
*11　Department of Physics, University of Tokyo
*12　Department of Physics, Tokyo Institute of Technology
*13　MTA Atomki
*14　Department of Physics, Kyoto University
*15　Department of Physics, Kyushu University
*16　Department of Physics, Technische Universität München

References
1) A. B. Migdal, Sov. J. Nucl. Phys. **16**, 238 (1973).
2) T. Nakamura *et al.*, Phys. Rev. Lett. **96**, 252502 (2006).
3) Y. Kikuchi *et al.*, Phys. Rev. C **87**, 034606 (2013).
4) Y. Kikuchi *et al.*, Prog. Theor. Exp. Phys. 103D03 (2016).
5) A. Obertelli *et al.*, Eur. Phys. Jour. A **50**, 8 (2014).
6) T. Kobayashi *et al.*, Nucl. Instrum. Methods Phys. Res. B **317**, 294 (2013).
7) J. Yasuda *et al.*, Nucl. Instrum. Methods Phys. Res. B **376**, 393 (2016).
8) S. Takeuchi *et al.*, Nucl. Instrum. Methods Phys. Res. A **763**, 596 (2014).
9) H. Simon *et al.*, Phys. Rev. Lett. **83**, 496 (1999).

Differential cross section of proton elastic scattering from neutron-rich ^{6}He at 200 A MeV and high momentum transfers

S. Chebotaryov,[*1,*2] S. Sakaguchi,[*3] T. Uesaka,[*1] W. Kim[*2]
on behalf of the SAMURAI13 collaboration

Recently, an experiment on p–^{6}He elastic scattering at 200 A MeV was carried out at the RIKEN RI-beam factory (RIBF) by using the SAMURAI spectrometer.[1] Details of the experimental setup and data analysis procedure were described in previous reports.[2,3] In this report, the measured differential cross sections are presented. The main distinguishing feature of the obtained p–^{6}He cross section data is the highest momentum transfer region covered ($q = 1.7$–2.8 fm^{-1}), which makes the present data valuable to deduce ^{6}He density distribution in the interior of the nucleus with high precision.

The measured cross sections of p–^{4}He and p–^{6}He elastic scattering are shown in Fig. 1. The data of p–^{4}He elastic scattering were taken to confirm the validity of the experimental setup and data analysis procedure by comparing them to existing data measured in normal kinematics by Moss et $al.$[4] Good agreement was obtained between the present and existing p–^{4}He data without any normalization. The systematic error was determined to be 9.4% and is the major contribution to the total uncertainty except at the most backward angles, at which statistical error dominates. The slope of the elastic scattering cross section is determined by the matter radius of the probed nucleus. The difference in slopes of the measured p–^{4,6}He cross sections show that the radius of ^{6}He is larger than that of ^{4}He. Such a considerable difference of their magnitudes could also be attributed to the weakly bound nature of the ^{6}He nucleus because scattering at large momentum transfers can easily cause the break-up of ^{6}He, reducing the yield of p–^{6}He elastic scattering events compared to that of p–^{4}He.

Figure 2 shows the obtained data and a summary of theoretical predictions, which were published before the experimental run. The predictions are based on different reaction models and density distributions of ^{6}He. Relativistic impulse approximation (RIA), t- and g-matrix folding models can adequately describe elastic scattering at the incident energy of the present work, making them suitable for the theoretical interpretation of the experimental result. A fit to the present data using one of these reaction models allows us to deduce ^{6}He density, especially in the interior region of the nucleus. The results of such an analysis will be submitted to a journal in the near future.
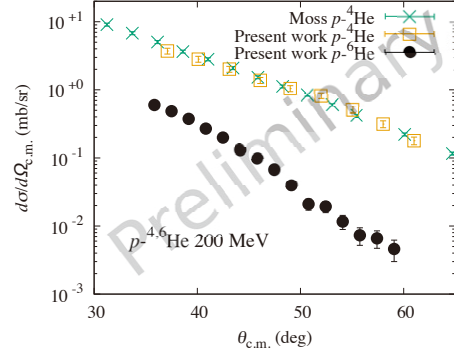
Fig. 1. Measured and existing[4] differential cross sections of p–^{4}He and p–^{6}He elastic scattering.
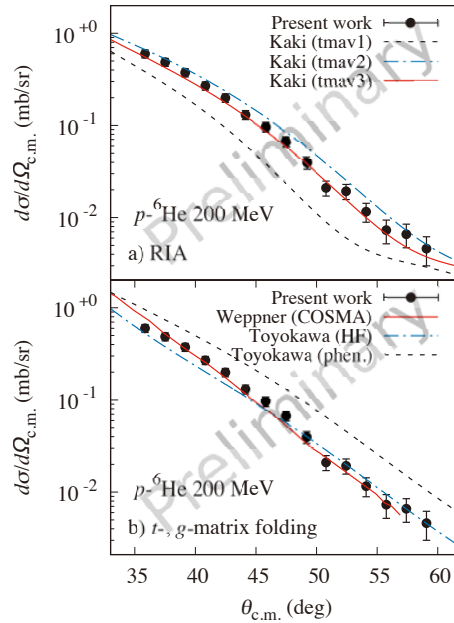
Fig. 2. Comparison of the present experimental result to predictions based on different reaction models.[5–7]

References
1) T. Kobayashi et $al.$, Nucl. Instrum. Methods Phys. Res. B **317**, 294 (2013).
2) S. Sakaguchi et $al.$, RIKEN Accel. Prog. Rep. **50**, 41 (2017).
3) S. Chebotaryov et $al.$, RIKEN Accel. Prog. Rep. **50**, 42 (2017).
4) G. Moss et $al.$, Phys. Rev. C **21**(5), (1980).
5) K. Kaki, Phys. Rev. C **89**(1), 14620 (2014).
6) M. Toyokawa, Phys. Rev. C **88**(5), 1-14 (2013).
7) S. Weppner, C. Elster, Phys. Rev. C **85**(4), 1-13 (2013).

*1　RIKEN Nishina Center
*2　Department of Physics, Kyungpook National University
*3　Department of Physics, Kyushu University

Two methods for invariant mass reconstruction from events with multiple charged particles

S. Koyama[*1,*2] and H. Otsu[*2] for SAMURAI08 collaboration

Invariant mass spectroscopy is one of the techniques to explore unbound states of nuclei. Relative energy (E_r) or the energy above threshold energy is reconstructed from four-momenta of decay particles. Experimental resolution is important since the level density above particle thresholds is higher than that below particle thresholds and unbound states have finite width. Another important aspect is acceptance. These two aspects often compete with each other.

The SAMURAI spectrometer is developed to investigate unbound states of nuclei. In the standard setup with the SAMURAI magnet, we install four multi-wire drift chambers, BDC1, BDC2, FDC1, and FDC2, to measure the four-momentum of a charged particle.[1] FDC1 is placed between the target and the SAMURAI magnet, while FDC2 is placed at the downstream of the magnet. By using positions and angles measured by these detectors, we can deduce the direction vector and the magnetic rigidity of a charged particle, which is converted to the four-momentum. For invariant mass reconstruction from events with multiple charged particles such as α decay into 2 charged particles of α + residue, positions of each charged particle have to be deduced with both FDC1 and FDC2. The positions are separated at FDC2 for particles with different A/Z values, while the positions can be close at FDC1. The cell size of FDC1 is 10 mm, and the requirement of deducing 2 positions with FDC1 can limit the acceptance, especially for a small opening angle corresponding to a low E_r. The four-momenta of charged particles can be deduced only from the reaction point on the target, positions and angles deduced from FDC2, and the magnetic field map of the SAMURAI magnet[2] without FDC1, though the resolution of the direction vector is worse than with FDC1. Therefore, we performed two different methods to deduce E_r, without FDC1 and with FDC1. The former yields a worse resolution but full acceptance, while the latter achieves a better resolution but with biased acceptance for two particles, especially for a small spatial separation at the FDC1 location.

We analyzed the data of the SAMURAI08 experiment[3] in which the α decay of $^{16}\text{C}^*$ is investigated. We used known unbound states of ^{12}B and ^{11}B to compare the two methods. Figure 1 shows E_r spectra of ^{12}B reconstructed from the $^8\text{Li} + \alpha$ decay channel. A clear peak is visible at $E_r = 2.75$ MeV in both spectra, without FDC1 (black line) and with FDC1 (red line). The better resolution with FDC1 allows us to
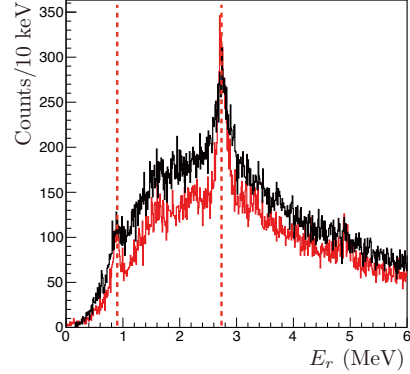
Fig. 1. E_r spectra for $^{12}\text{B}^* \to {}^8\text{Li} + \alpha$. The black line represents the E_r reconstructed without FDC1, while the red line represents that reconstructed with FDC1.

find another peak at $E_r = 0.90$ MeV, while the corresponding peak is not so clear without FDC1. Figure 2 shows E_r spectra of ^{11}B reconstructed from the $^7\text{Li} + \alpha$ decay channel. ^{11}B has doublet unbound states at $E_r = 0.52$ and 0.61 MeV with negligible width. The doublet peaks are not well separated without FDC1, while a dip between the doublet peaks can be seen with FDC1. With FDC1, the resolution (σ) of E_r is approximately $0.04\sqrt{E_r}$ MeV, while the acceptance is approximately 80% of that without FDC1.
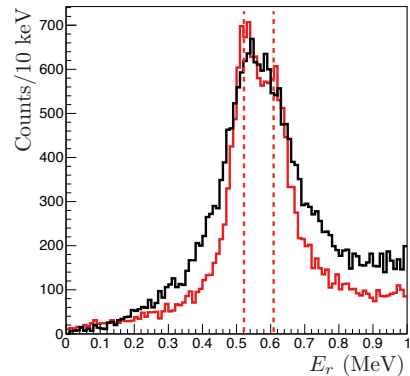
Fig. 2. Same as Fig. 1 but for $^{11}\text{B}^* \to {}^7\text{Li} + \alpha$.

In summary, two methods to reconstruct invariant mass were evaluated. Both methods have advantages and disadvantages. They should be used as per the intended application.

References
1) T. Kobayashi *et al.*, Nucl. Instrum. Methods B **317** (2013).
2) H. Sato *et al.*, IEEE Trans. Appl. Supercond. **23**, 4500308 (2013).
3) H. Otsu *et al.*, RIKEN Accel. Prog. Rep. **47**, highlight page xx (2014).

*1 Department of Physics, University of Tokyo
*2 RIKEN Nishina Center

Electric dipole responses of ^{50}Ca and ^{52}Ca

Y. Togano,[*1,*2] T. Nakamura,[*3,*2] T. Kobayashi,[*4,*2] T. Aumann,[*5,*6] H. Baba,[*2] K. Boretzky,[*6,*2]
A. Bracco,[*7] F. Browne,[*2] F. Camera,[*7] H. Chae,[*8] S. Chen,[*2] N. Chiga,[*2] H. Choi,[*8] L. Cortés,[*2]
F. Delaunay,[*9] D. Dell'Aquila,[*10] Z. Elekes,[*11,*2] Y. Fujino,[*1,*2] I. Gašparić,[*12,*2] J. Gibelin,[*9] K. I. Hahn,[*13]
Z. Halasz,[*11,*2] A. Horvat,[*4] K. Ieki,[*1,*2] T. Inakura,[*14] T. Isobe,[*2] D. Kim,[*13,*2] G. Kim,[*13] H. Ko,[*8]
Y. Kondo,[*3,*2] D. Körper,[*6] S. Koyama,[*15,*2] Y. Kubota,[*2] I. Kuti,[*11] M. Matsumoto,[*3,*2] A. Matta,[*9]
B. Million,[*7] T. Motobayashi,[*2] I. Murray,[*2] N. Nakatsuka,[*16,*2] N. Orr,[*9] H. Otsu,[*2] V. Panin,[*2] S. Y. Park,[*13]
W. Rodriguez,[*17] D. Rossi,[*4] A. T. Saito,[*3,*2] M. Sasano,[*2] H. Sato,[*2] Y. Shimizu,[*2] H. Simon,[*6,*2] L. Stuhl,[*18]
Y. L. Sun,[*19] S. Takeuchi,[*3,*2] T. Tomai,[*3,*2] H. Törnqvist,[*4,*2] T. Uesaka,[*2] V. Vaquero,[*20,*2] O. Wieland,[*7]
K. Wimmer,[*15,*2] H. Yamada,[*3,*2] Z. Yang,[*2] M. Yasuda,[*3,*2] and K. Yoneda[*2]

The electric dipole (E1) strength distributions in ^{50}Ca and ^{52}Ca were measured using relativistic Coulomb excitation.

The equation of state (EOS) of neutron-rich matter is important to understand the properties of neutron-rich nuclei and astrophysical events, such as supernovae and neutron-star mergers. The constraint on the density dependence of the symmetry energy, the isospin-asymmetric part of EOS, is important to evaluate the EOS of neutron-rich matter, while it is not well constrained experimentally.

Recent theoretical work showed that the pygmy dipole resonance (PDR) and the dipole polarizability α_D of nucleus is well correlated to the density dependence of the symmetry energy close to saturation density.[1] PDR is the low-energy E1 mode located at the excitation energies of about 6 to 10 MeV. It is indicated that the PDR strength of Ca isotopes rapidly increases from ^{48}Ca to ^{54}Ca, and the strength in these nuclei is well correlated with the density dependence of the symmetry energy.[2] The dipole polarizability α_D corresponds to the inversely energy weighted sum of E1 strength distribution, and it is pointed out as a less model-dependent observable for the extraction of the symmetry energy parameters.[3] Given that the PDR of neutron-rich Ca isotopes and α_D are correlated to the density dependence of the symmetry energy, the Coulomb excitation of ^{50}Ca and ^{52}Ca was performed to measure their E1 responses.

The experiment was performed using the SAMU-RAI spectrometer[4] at RIBF. The secondary beams of ^{50}Ca and ^{52}Ca were produced via fragmentation of a 345 MeV/nucleon ^{70}Zn beam on a 10-mm thick Be target. The ^{50}Ca and ^{52}Ca beams were separated using the BigRIPS with an Al degrader with a thickness of 5 mm placed at the focal plane F1. For the ^{50}Ca beam, an additional 1-mm thick Al degrader was placed at the focal plane F5 to increase the purity of ^{50}Ca. At the focal planes F3, F5 and F7, 1-mm-thick plastic scintillators are installed. The ^{50}Ca and ^{52}Ca beams were impinged on Pb and C secondary targets. The typical ^{50}Ca and ^{52}Ca intensities were 14 and 1 kHz, respectively.

The ^{50}Ca and ^{52}Ca beams were monitored event-by-event using two 0.2-mm thick plastic scintillators (SBTs), an ionization chamber (ICB), and two drift chambers (BDC1 and BDC2) placed at the upstream of the secondary target. The γ-ray detector CATANA [5] and 8 large-volume LaBr$_3$ detectors were placed to surround the secondary target to measure the de-excitation γ-rays from the reaction residues. The outgoing charged particles were characterized using the detectors located at the entrance and exit of the SAMURAI magnet with 2.7T at the center. Two drift chambers (FDC1 and FDC2) and a plastic scintillator wall (HODF24) were used to identify the charged particles and reconstruct their momenta. The outgoing neutrons were detected by the combination of the NeuLAND demonstrator[6] and NEBULA.

The data analysis is now in progress.

*1 Department of Physics, Rikkyo University
*2 RIKEN Nishina Center
*3 Department of Physics, Tokyo Institute of Technology
*4 Department of Physics, Tohoku University
*5 Institut für Kernphysik, Technische Universität Darmstadt
*6 GSI Helmholtzzentrum für Schwerionenforschung
*7 Instituto Nazionale di Fisica Nucleare sez. di Milano
*8 Department of Physics and Astronomy, Seoul National University
*9 LPC-Caen
*10 IPN Orsay
*11 ATOMKI
*12 Ruđer Bošković Institute
*13 Department of Physics, Ewha Womans University
*14 Department of Physics, Niigata University
*15 Department of Physics, University of Tokyo
*16 Department of Physics, Kyoto University
*17 Universidad Nacional de Colombia
*18 Center for Nuclear Studies (CNS), University of Tokyo
*19 IRFU, CEA, Université Paris-Saclay
*20 Instituto de Estructura de la Materia, CSIC

References
1) J. Piekarewicz, Phys. Rev. C **83**, 034319 (2011).
2) T. Inakura et al., Phys. Rev. C **84**, 921302(R) (2011).
3) P.-G. Reinhard et al., Phys. Rev. C **81**, 051303 (2010).
4) T. Kobayashi et al., Nucl. Instrum. Methods in Phys. Res. Sect. B **317**, 294 (2013).
5) Y. Togano et al., RIKEN Accel. Prog. Rep. **48**, 207 (2015).
6) NeuLAND Technical Design Report, https://edms.cern.ch/document/1865739

Many-neutron systems: search for superheavy ^{7}H and its tetraneutron decay

F. M. Marqués[*1] and Z. Yang[*2] for the SAMURAI34 and R3B-NeuLAND Collaborations

Many-neutron systems represent a fundamental question in Nuclear Physics. Since there is no firm theoretical claim about their existence as a bound or resonant state, their observation would require a deep reconsideration of our understanding of nuclei in general, and the strong force in particular. Two of these systems have attracted most of the attention over the last decades, ^{4}n and ^{7}H (that decays into $t+4n$). However, all the past experiments had in common several issues: they did not measure the four neutrons; the statistics and/or resolution were very low; and some results were in contradiction with each other.

The goal of the NP1512-SAMURAI34 experiment,[1] carried out in July 2017, was to provide the definitive proof of existence of both ^{7}H and ^{4}n, and, in case of a positive answer, their detailed spectroscopy. Concerning the issues noted above, we proposed to obtain very high statistics (several 10^4 complete events) and resolution (about 100 keV) and, by detecting the four neutrons for the first time, have access to the decay properties and correlations within the system. In particular, the fact of measuring the neutrons in the decay $t+4n$ provides a unique opportunity to observe even very broad $4n$ resonances (undetectable using missing mass techniques), since any resonance would be unambiguously identified through the angular anti-correlation between the triton and the neutrons.

We measured the reaction ^{8}He$(p, 2p)^3$H$+4n$ in complete kinematics (see Fig. 1) at the SAMURAI[2] facility of RIBF. The setup was similar to the one of the NP1312-SAMURAI21 experiment.[3] The secondary beam of ^{8}He at 150 MeV/nucleon and 10^5 pps was produced by the fragmentation of an ^{18}O primary beam at 220 MeV/nucleon on a beryllium target, then selected by BigRIPS, and finally sent onto the 15 cm MINOS liquid-hydrogen target.[4] The beam was detected by two plastic scintillators (SBTs) and tracked with two drift chambers (BDC1 and BDC2). The reaction was tagged through the detection of both the target and knocked-out protons with the MINOS TPC (trajectories) and 36 crystals of DALI2 arranged in a cylindrical configuration around the target (energies).

The outgoing triton was tracked by the two drift chambers (FDC0 and FDC2) at the two sides of the SAMURAI dipole magnet, with a 2.4 T field, and detected by the 40 scintillator bars of the extended hodoscope (HODOF+HODOP). The four neutrons were detected with the combination of NEBULA[5] and four double-planes of NeuLAND,[6] with an estimated ef-
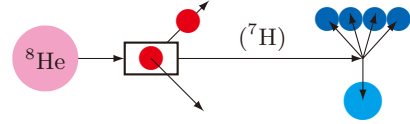
Fig. 1. Schematic view of the ^{8}He$(p, 2p)^3$H$+4n$ reaction on the MINOS target.

ficiency $\varepsilon_{4n} \sim 1\%$. Moreover, since the complete 7-body kinematics are overdetermined, they can be reconstructed from the momenta of only 3 of the neutrons. This method can be crucial if the ground states of ^{7}H and/or ^{4}n were very close to threshold, since at such low energies the $3n$ efficiency can be about 20 times higher than the $4n$ one.

In order to validate the use of DALI2, originally developed as a γ-ray array, for the detection of high-energy protons, a test with an 80 MeV proton beam was done at CYRIC, and before the experiment cosmic runs were undertaken with the crystals placed along their three main directions, with the corresponding energy peaks covering a range of 30–90 MeV. In addition, the elastic scattering of protons was measured during the first hours with a 150 MeV proton beam, leading to clear kinematic lines.

The ^{8}He beam intensity and quality were stable during the 6-day run. The online analysis showed the proper operation of the different multidetectors, as well as of their correlations. The MINOS TPC trajectories and the high-energy hits in DALI2 showed the characteristic p-p back-to-back azimuthal pattern. Tritons were clearly identified in the hodoscope at the predicted location. The neutron multiplicities exhibited the expected distributions for different reaction channels, and a very preliminary analysis of those multiplicities in the ^{8}He$(p, 2p)^3$H channel, including causality conditions, lead to an estimate of several 10^4 complete $2p+t+4n$ events during the whole run, consistent with our proposal goal. The data analysis is in progress.

References
1) K. Kisamori, F. M. Marqués *et al.*, RIKEN-RIBF proposal NP1512-SAMURAI34.
2) T. Kobayashi *et al.*, Nucl. Instrum. Methods B **317**, 294 (2013).
3) Y. Kondo *et al.*, RIKEN Accel. Prog. Rep. **49**, 42 (2016).
4) A. Obertelli *et al.*, Eur. Phys. J. A **50**, 8 (2014).
5) T. Nakamura, Y. Kondo, Nucl. Instrum. Methods B **376**, 1 (2015).
6) https://edms.cern.ch/document/1865739

*1 LPC-Caen, France
*2 RIKEN Nishina Center

Low-energy dipole response of the halo nuclei ^{6,8}He

C. Lehr,[*1,*2] T. Aumann,[*1,*3] T. Nakamura,[*4,*2] A. T. Saito,[*4,*2] N. L. Achouri,[*5] D. Ahn,[*2] H. Baba,[*2]
C. A. Bertulani,[*6] M. Boehmer,[*7] K. Boretzky,[*3,*2] N. Chiga,[*2] A. Corsi,[*5] D. Cortina-Gil,[*8] C. A. Douma,[*9]
F. Dufter,[*7] Z. Elekes,[*10,*2] J. Feng,[*11] U. Forsberg,[*12] N. Fukuda,[*2] I. Gasparic,[*13,*2] Z. Ge,[*2]
R. Gernhäuser,[*7] J. M. Gheller,[*14] J. Gibelin,[*5] A. Gillibert,[*14] Z. Halász,[*10] M. N. Harakeh,[*9]
A. Hirayama,[*4,*2] N. Inabe,[*2] T. Isobe,[*2] J. Kahlbow,[*1,*2] N. Kalantar-Nayestanaki,[*9] D. Kim,[*15,*2]
M. A. Knösel,[*1] T. Kobayashi,[*16] Y. Kondo,[*4,*2] D. Körper,[*3] P. Koseoglou,[*1,*3] Y. Kubota,[*2] P. J. Lee,[*17]
S. Lindberg,[*18,*2] Y. Liu,[*11] F. M. Marques,[*5] S. Masuoka,[*19] M. Matsumoto,[*4,*2] J. Mayer,[*20] H. Miki,[*4,*2]
M. Miwa,[*2] B. Monteagudo,[*21] A. Obertelli,[*1] N. Orr,[*5] H. Otsu,[*2] V. Panin,[*2] S. Y. Park,[*15,*2] M. Parlog,[*5]
S. Paschalis,[*22,*1] P.-M. Potlog,[*23] S. Reichert,[*7] A. Revel,[*21] D. M. Rossi,[*1] M. Sasano,[*2] H. Scheit,[*1]
F. Schindler,[*1] T. Shimada,[*4,*2] S. Shimoura,[*19] H. Simon,[*3] L. Stuhl,[*19] H. Suzuki,[*2] D. Symochko,[*1]
H. Takeda,[*2] S. Takeuchi,[*4,*2] J. Tanaka,[*1] Y. Togano,[*24,*2] T. Tomai,[*4,*2] H. T. Törnqvist,[*1,*2] T. Uesaka,[*2]
V. Wagner,[*1,*2] H. Yamada,[*4,*2] B. Yang,[*11] L. Yang,[*25] Z. H. Yang,[*2] M. Yasuda,[*4,*2] K. Yoneda,[*2]
L. Zanetti,[*1,*2] and J. Zenihiro[*2]

The electromagnetic properties of neutron-rich nuclei provide insight into their structure and dynamics.[1] The low-lying dipole strength of neutron-halo systems is of particular interest. The heaviest bound helium isotopes ^{6}He and ^{8}He are two- and four-neutron halo nuclei with a clear α plus $2n$ and $4n$ structure, respectively. After electromagnetic excitation, they mainly decay *via* two- and four-neutron emission. The ^{6}He breakup has been measured previously by Aumann *et al.*,[2] while *ab initio* calculations have been carried out by Bacca *et al.*[3,4] The existing data cover excitation energies up to 7 MeV, while the full low-energy response predicted by the theory extends up to 20 MeV.[4] Therefore, it is necessary to measure up to higher energies to study the complete region of interest. For ^{8}He, only the $2n$-breakup channel has been measured previously by Meister *et al.*[5] Nothing is known so far about the $4n$-channel, where ^{8}He breaks up into ^{4}He and four neutrons, because of the experimental difficulties of measuring four neutrons in coincidence.

In July 2017, the SAMURAI37 experiment was performed with the purpose of extending the existing data for ^{6}He with better statistics and measuring the breakup of ^{8}He, both up to excitation energies of approximately 15 MeV. The multi-neutron decay of ^{6}He and ^{8}He after heavy-ion-induced electromagnetic excitation has been measured in complete kinematics to study the dipole response of these nuclei. The combination of the neutron detectors NEBULA and R^{3}B-NeuLAND demonstrator at the SAMURAI[6] setup and the high beam intensities available at RIBF made the measurement of the $4n$-breakup channel possible for the first time. A primary ^{18}O beam with an energy of 220 MeV/nucleon was used to produce secondary beams of ^{6}He and ^{8}He with an energy of 180 MeV/nucleon and a beam rate of 100 kHz, which were then guided to the SAMURAI spectrometer.

The experimental method is based on the measurement of the differential cross section $\mathrm{d}\sigma(E1)/\mathrm{d}E$ *via* the invariant-mass method, which allows us to extract the dipole-strength distribution $\mathrm{d}B(E1)/\mathrm{d}E$ and the photo-absorption cross section. To excite ^{6}He and ^{8}He electromagnetically, a Pb target was used. Additionally, a series of targets with increasing Z, namely CH$_2$, C, Ti and Sn, was used to study precisely the nuclear contribution to the cross section. This is especially important in the region of high excitation energy, where the electromagnetic excitation might not be dominant.

The data analysis is in progress.

*1 Institut für Kernphysik, Technische Universität Darmstadt
*2 RIKEN Nishina Center
*3 GSI, Darmstadt
*4 Department of Physics, Tokyo Institute of Technology
*5 Laboratoire de Physique Corpusculaire de Caen
*6 Department of Physics & Astronomy, Texas A&M University-Commerce
*7 Department of Physics, Technische Universität München
*8 Department of Particle Physics, University of Santiago de Compostela
*9 KVI-CART, Univ. of Groningen, Groningen
*10 MTA ATOMKI, Debrecen
*11 School of Physics, Peking University
*12 Department of Physics, Lund University
*13 RBI, Zagreb
*14 CEA, Saclay
*15 Department of Physics, Ewha Womans University, Seoul
*16 Department of Physics, Tohoku University
*17 Department of Physics, The University of Hong Kong
*18 Department of Physics, Chalmers University of Technology, Göteborg
*19 CNS, University of Tokyo
*20 Institut für Kernphysik, Universität zu Köln
*21 GANIL, Caen
*22 Department of Physics, University of York
*23 Institute of Space Sciences, Magurele
*24 Department of Physics, Rikkyo University
*25 Department of Physics, University of Tokyo

References
1) T. Aumann, T. Nakamura, Phys. Scr. **T152**, 014012 (2013).
2) T. Aumann *et al.*, Phys. Rev. C **59**, 1252 (1999).
3) S. Bacca *et al.*, Phys. Rev. Lett. **89**, 052502 (2002).
4) S. Bacca *et al.*, Phys. Rev. C **69**, 057001 (2004).
5) M. Meister *et al.*, Nucl. Phys. A **700**, 3 (2002).
6) T. Kobayashi *et al.*, Nucl. Instr. Meth. Phys. Res. Sect. B **317**, 294 (2013).

Investigation of the tetraneutron by quasi-free α-knockout from ^{8}He

F. Schindler,*1 T. Aumann,*1,*2 S. Paschalis,*3,*1 D. M. Rossi,*1 N. L. Achouri,*4 D. Ahn,*5 H. Baba,*5
C. A. Bertulani,*6 M. Boehmer,*7 K. Boretzky,*2,*5 N. Chiga,*5 A. Corsi,*4 D. Cortina-Gil,*8 C. A. Douma,*9
F. Dufter,*7 Z. Elekes,*10,*5 J. Feng,*11 B. Fernández-Domínguez,*8 U. Forsberg,*12 N. Fukuda,*5
I. Gasparic,*13,*5 Z. Ge,*5 R. Gernhäuser,*7 J. M. Gheller,*14 J. Gibelin,*4 A. Gillibert,*14 Z. Halász,*10
M. N. Harakeh,*9 A. Hirayama,*15,*5 N. Inabe,*5 T. Isobe,*5 J. Kahlbow,*1,*5 N. Kalantar-Nayestanaki,*9
D. Kim,*16,*5 S. Kim,*1 M. A. Knösel,*1 T. Kobayashi,*17 Y. Kondo,*15,*5 D. Körper,*2 P. Koseoglou,*1,*2
Y. Kubota,*5 I. Kuti,*10 P. J. Lee,*18 C. Lehr,*1,*5 S. Lindberg,*19,*5 Y. Liu,*11 F. M. Marqués,*4
S. Masuoka,*20 M. Matsumoto,*15,*5 J. Mayer,*21 B. Monteagudo,*22 T. Nakamura,*15,*5 A. Obertelli,*1
N. Orr,*4 H. Otsu,*5 V. Panin,*5 S. Y. Park,*16,*5 M. Parlog,*4 P.-M. Potlog,*23 S. Reichert,*7 A. Revel,*22
A. T. Saito,*15,*5 M. Sasano,*5 H. Scheit,*1 S. Shimoura,*20 H. Simon,*2 L. Stuhl,*20 H. Suzuki,*5
D. Symochko,*1 H. Takeda,*5 J. Tanaka,*1 Y. Togano,*24,*5 T. Tomai,*15,*5 H. T. Törnqvist,*1,*5 T. Uesaka,*5
V. Wagner,*1,*5 H. Yamada,*15,*5 B. Yang,*11 L. Yang,*25 Z. H. Yang,*5 M. Yasuda,*15,*5 K. Yoneda,*5
L. Zanetti,*1,*5 and J. Zenihiro*5

The possible existence of a four-neutron system as well as its properties has been a long-lasting question in nuclear physics that can be traced back to the mid-1960s.[1] A recent experiment carried out at the SHARAQ spectrometer uncovered 4 candidate events for a ^4n ground-state resonance at $E_{^4n} = 0.83 \pm 0.65\text{(stat)} \pm 1.25\text{(syst)}$ MeV with a 4.9σ significance level generated in a $^4\text{He}(^8\text{He},^8\text{Be})$ reaction.[2] This measurement triggered new enthusiasm for both theoretical and experimental investigations of the tetraneutron system. State-of-the-art *ab initio* theory indeed supports the existence of a low-lying ^4n resonance.[3–5] However, the definite experimental evidence is still pending.

To this end, we have performed an experiment at SAMURAI[6] to investigate the ^4n system *via* a new method, *i.e.*, the measurement of $^8\text{He}(p,p\alpha)^4n$ at large momentum transfer using a secondary ^{8}He beam at an energy of 156 MeV/nucleon impinging on a liquid-hydrogen target of 5 cm thickness from the MINOS

*1 Technische Universität Darmstadt
*2 GSI, Darmstadt
*3 University of York
*4 Laboratoire de Physique Corpusculaire de Caen
*5 RIKEN Nishina Center
*6 Texas A&M University-Commerce
*7 Technische Universität München
*8 University of Santiago de Compostela
*9 KVI-CART, University of Groningen
*10 MTA ATOMKI, Debrecen
*11 Peking University
*12 Lund University
*13 RBI, Zagreb
*14 CEA, Saclay
*15 Tokyo Institute of Technology
*16 Ewha Womans University, Seoul
*17 Tohoku University
*18 Hongkong University
*19 Chalmers University of Technology, Göteborg
*20 CNS, University of Tokyo
*21 Universität zu Köln
*22 GANIL, Caen
*23 Institute of Space Sciences, Magurele
*24 Rikkyo University
*25 University of Tokyo

Fig. 1. Kinematics of the $^8\text{He}(p,p\alpha)^4n$ reaction.

system. The ^{8}He nucleus is expected to be a suitable environment to form the ^4n system in a ground-state resonance and the reaction process described above will allow for its unambiguous identification. As a consequence of the reaction kinematics (see Fig. 1) all outgoing particles are largely separated in momentum space, *i.e.*, final-state interactions are minimized and the reaction products of interest have a clean signature.

The ^4n-energy spectrum will be deduced from the momenta of all charged particles *via* the missing-mass technique to identify the possible resonance and to determine its energy and width. Neutrons have been measured in addition with the combination of the neutron detectors R^{3}B-NeuLAND demonstrator and NEBULA, allowing for a kinematically complete investigation of the reaction and the study of the ^4n decay properties with lower but sufficient statistics. To reduce systematic uncertainties of the missing-mass reconstruction, an invariant-mass measurement for ^{6}He, *i.e.*, $^6\text{He}(p,p\alpha)^2n$ has been carried out for the purpose of calibration. The data analysis is in progress.

References
1) D. R. Tilley *et al.*, Nucl. Phys. **541**, 1104 (1992).
2) K. Kisamori *et al.*, Phys. Rev. Lett. **116**, 052501 (2016).
3) K. Fossez *et al.*, Phys. Rev. Lett. **119**, 032501 (2017).
4) S. Gandolfi *et al.*, Phys. Rev. Lett. **118**, 232501 (2017).
5) A. M. Shirokov *et al.*, Phys. Rev. Lett. **117**, 182502 (2016).
6) T. Kobayashi *et al.*, Nucl. Instrum. Methods Phys. Res. B **317**, 294 (2013).

Shell evolution at $N = 40$ towards ^{60}Ca: Spectroscopy of ^{62}Ti

M. L. Cortés,[*1] W. Rodriguez,[*2,*1] P. Doornenbal,[*1] A. Obertelli,[*3,*4,*1] N. Achouri,[*5] H. Baba,[*1] F. Browne,[*1] D. Calvet,[*4] F. Château,[*4] S. Chen,[*6,*1] N. Chiga,[*1] A. Corsi,[*4] A. Delbart,[*4] J-M. Gheller,[*4] A. Giganon,[*4] A. Gillibert,[*4] C. Hilaire,[*4] T. Isobe,[*1] T. Kobayashi,[*8] Y. Kubota,[*1,*7] V. Lapoux,[*4] H. N. Liu,[*4,*9] T. Motobayashi,[*1] I. Murray,[*10,*1] H. Otsu,[*1] V. Panin,[*1] N. Paul,[*4] H. Sakurai,[*1,*11] M. Sasano,[*1] D. Steppenbeck,[*1] L. Stuhl,[*7] Y. L. Sun,[*4] Y. Togano,[*12,*1] T. Uesaka,[*1] K. Wimmer,[*11,*1] K. Yoneda,[*1] O. Aktas,[*9] T. Aumann,[*3] L. X. Chung,[*13] F. Flavigny,[*10] S. Franchoo,[*10] I. Gasparic,[*14,*1] R.-B. Gerst,[*15] J. Gibelin,[*5] K. I. Hahn,[*16] D. Kim,[*16,*1] T. Koiwai,[*11] Y. Kondo,[*17] P. Koseoglou,[*3,*18] J. Lee,[*19] C. Lehr,[*3] B. D. Linh,[*13] T. Lokotko,[*19] M. MacCormick,[*10] K. Moschner,[*15] T. Nakamura,[*17] S. Y. Park,[*16,*1] D. Rossi,[*18] E. Sahin,[*20] D. Sohler,[*21] P-A. Söderström,[*3] S. Takeuchi,[*17] H. Toernqvist,[*18] V. Vaquero,[*22] V. Wagner,[*3,*1] S. Wang,[*23] V. Werner,[*3] X. Xu,[*19] H. Yamada,[*17] D. Yan,[*23] Z. Yang,[*1] M. Yasuda,[*17] and L. Zanetti[*3]

Experimental evidence collected in the last years show the disappearance of the shell closures at $N = 8$, 20 and 28 in various neutron-rich isotopes, as well as the appearance of new magic numbers, such as $N = 32$ and 34 for Ca isotopes.[1,2] Given that $N = 40$, which corresponds to the filling of the fp neutron shells, is predicted to be a sub-shell closure, the study of the structure of $N = 40$ isotones can provide insight into the mechanism governing shell evolution. A low collectivity is observed in ^{68}Ni, consistent with the magic character of $N = 40$.[3] However, for the Fe and Cr isotopes, a monotonous decrease of the 2^+ energy with increasing neutron number is observed.[4,5] Such a decrease, which extends beyond $N = 40$, indicates a rapid increase of collectivity when removing protons from the $f_{7/2}$ shell. For the case of the Ti isotopes, measurements of the 2^+ energy of ^{58,60}Ti[6,7] do not show an unexpected decrease towards $N = 40$, although it has been suggested that full consideration of the $g_{9/2}$ orbital is required to understand the structure at $N = 40$.[7] To further understand the shell evolution in $N = 40$ isotones towards the supposedly doubly-magic ^{60}Ca, the measurement of the first excited 2^+ state of ^{62}Ti is necessary.

In the third SEASTAR campaign, ^{62}Ti was produced by proton knock-out of ^{63}V at 250 MeV/nucleon on the MINOS liquid hydrogen target.[9] The ^{63}V isotopes were produced by fragmentation of a 345 MeV/nucleon primary beam of ^{70}Zn impinging on a 10-mm Be target and separated using the BigRIPS spectrometer. The average intensity of the Zn beam was 250 pnA, and the average rate of ^{63}V was 3 pps. The MINOS target, of 150 mm length, was placed at the F13 experimental area, in front of the SAMU-RAI magnet. Reaction products were identified on an event-by-event basis using the standard SAMURAI detectors.[8] NEBULA and NeuLAND neutron detectors were also used during the experiment. γ-rays emitted by the reaction products were detected using the upgraded DALI2+ array,[10] consisting of 226 NaI detectors surrounding MINOS. The ongoing data analysis has already provided the incoming particle identification as shown in Fig. 1.
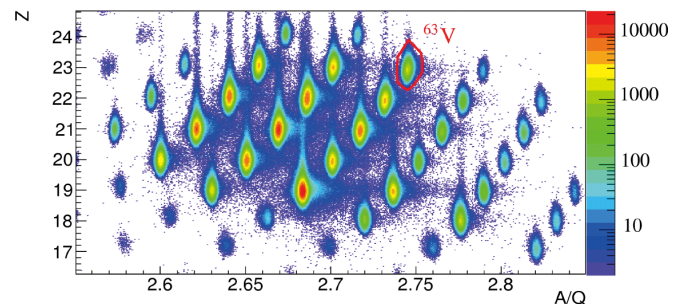
Fig. 1. Incoming particle ID. ^{63}V is labeled in red.

[*1]　RIKEN Nishina Center
[*2]　Departamento de Física, Universidad Nacional de Colombia
[*3]　Institut für Kernphysik, Technische Universität Darmstadt
[*4]　IRFU, CEA, Université Paris-Saclay
[*5]　LPC Caen, ENSICAEN, Université de Caen, CNRS/IN2P3
[*6]　Department of Physics, Peking University
[*7]　Center for Nuclear Study, University of Tokyo
[*8]　Department of Physics, Tohoku University
[*9]　Department of Physics, Royal Institute of Technology
[*10]　IPN Orsay, CNRS, Univ. Paris Sud, Univ. Paris Saclay
[*11]　Department of Physics, University of Tokyo
[*12]　Department of Physics, Rikkyo University
[*13]　Institute for Nuclear Science & Technology, VINATOM
[*14]　Rudjer Boskovic Institute
[*15]　Institut für Kernphysik, Universität zu Köln
[*16]　Ewha Womans University
[*17]　Department of Physics, Tokyo Institute of Technology
[*18]　GSI Helmoltzzentrum für Schwerionenforschung GmbH
[*19]　Department of Physics, The University of Hong Kong
[*20]　Department of Physics, University of Oslo
[*21]　MTA Atomki
[*22]　Instituto de Estructura de la Materia, CSIC
[*23]　Institute of Modern Physics, Chinese Academy of Sciences

References
1) F. Wienholtz et al., Nature (London) 498, 346 (2013).
2) D. Steppenbeck et al., Nature (London) 502, 207 (2013).
3) O. Sorlin et al., Phys. Rev. Lett. 88, 092501 (2002).
4) J. Ljungvall et al., Phys. Rev. C 81, 061301 (2010).
5) A. Gade et al., Phys. Rev. C 81, 051304 (2010).
6) H. Suzuki et al., Phys. Rev. C 88, 024326 (2013).
7) A. Gade et al., Phys. Rev. Lett. 112, 112503 (2014).
8) T. Kobayashi et al., Nucl. Instrum. Methods Phys. Res. B 317, 294 (2013).
9) A. Obertelli et al., Eur. Phys. J. A 50, 8 (2014).
10) I. Murray et al., in this report.

Spectroscopy of Sc isotopes between the $N = 34$ and $N = 40$ subshell closures

P. Koseoglou,[*1,*2] V. Werner,[*1] P.-A. Söderström,[*1,*2] M. Lettmann,[*1] N. Pietralla,[*1] P. Doornenbal,[*3]
A. Obertelli,[*4,*1,*3] N. Achouri,[*4] H. Baba,[*3] F. Browne,[*3] D. Calvet,[*4] F. Château,[*4] S. Chen,[*5,*6,*3]
N. Chiga,[*3] A. Corsi,[*4] M. L. Cortés,[*3] A. Delbart,[*4] J-M. Gheller,[*4] A. Giganon,[*4] A. Gillibert,[*4] C. Hilaire,[*4]
T. Isobe,[*3] T. Kobayashi,[*7] Y. Kubota,[*3,*8] V. Lapoux,[*4] H. Liu,[*4,*9] T. Motobayashi,[*3] I. Murray,[*3,*10]
H. Otsu,[*3] V. Panin,[*3] N. Paul,[*4] W. Rodriguez,[*11,*3] H. Sakurai,[*3,*12] M. Sasano,[*3] D. Steppenbeck,[*3]
L. Stuhl,[*8] Y. L. Sun,[*4] Y. Togano,[*13,*3] T. Uesaka,[*3] K. Wimmer,[*12,*3] K. Yoneda,[*3] O. Aktas,[*9]
T. Aumann,[*1] L. X. Chung,[*14] F. Flavigny,[*10] S. Franchoo,[*10] I. Gasparic,[*3,*15] R.-B. Gerst,[*16] J. Gibelin,[*17]
K. I. Hahn,[*18] D. Kim,[*19] T. Koiwai,[*12] Y. Kondo,[*20] J. Lee,[*6] C. Lehr,[*1] B. D. Linh,[*14] T. Lokotko,[*6]
M. MacCormick,[*10] K. Moschner,[*16] T. Nakamura,[*20] S. Y. Park,[*19] D. Rossi,[*1] E. Sahin,[*21] D. Sohler,[*22]
S. Takeuchi,[*20] H. Toernqvist,[*2] V. Vaquero,[*23] V. Wagner,[*1] S. Wang,[*24] X. Xu,[*6] H. Yamada,[*20] D. Yan,[*24]
Z. Yang,[*3] M. Yasuda,[*20] and L. Zanetti[*1]

Evidence for the existence of a new "magic number," $N = 34$, has been obtained from the level structure of ^{54}Ca[1] while there may not be a corresponding shell gap in Ti[2,3] isotopes. This has created recent interest to study the evolution of neutron-rich scandium isotopes. These nuclei lie between Ca and Ti and the evolution of proton orbitals can reveal the nature of the magic numbers at $N = 34$, recently shown to vanish in ^{55}Sc,[4] and the $N = 40$ pf-shell closure. In this case the valence proton occupies the $\pi f_{7/2}$ orbital, interacting with $\nu f_{5/2}$ orbital in $^{57, 59, 61}$Sc.

The DALI2+ array has been coupled with the wide acceptance SAMURAI spectrometer[5] in the third SEASTAR campaign. This made the measurement of the energies of low-lying states of a large number of isotopes in the previously discussed mass region possible. The radioactive beams were produced by a primary ^{70}Zn beam at 345 MeV/nucleon impinging on a 10-mm-thick ^{9}Be target. The BigRIPS fragment separator[6] was used for the identification and separation
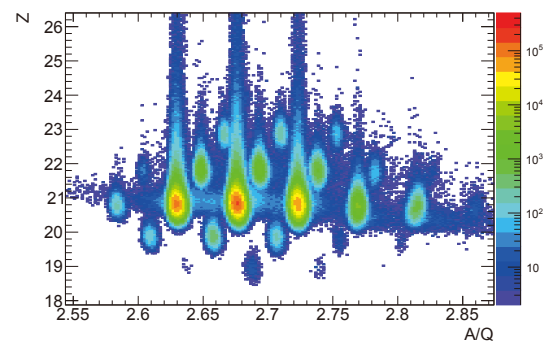
Fig. 1. Particle identification in BigRIPS after gating on $^{55-61}$Sc in SAMURAI.

of the secondary beams. The Sc isotopes of interest were produced by knock-out reactions in MINOS,[7] consisting of a 150-mm-thick LH$_2$ target surrounded by an active TPC. Gamma rays were measured with the DALI2+ array, consisting of 226 NaI(Tl) detectors surrounding MINOS. The reaction products were identfied event-by-event using two drift chambers and a hodoscope plastic-scintillator array after Brho analysis in the SAMURAI magnet. NEBULA and NeuLAND were used in addition for neutron detection. Figure 1 shows all reaction channels producing $^{55-61}$Sc.

In a preliminary analysis, the γ rays reported in Ref. 4) for ^{55}Sc were identified in the data from the neutron knock-out reaction, ^{56}Sc $(p,pn)\,^{55}$Sc. The full analysis of $^{55-61}$Sc is on-going.

*1   Institut für Kernphysik, Technische Universität Darmstadt
*2   GSI Helmoltzzentrum für Schwerionenforschung GmbH
*3   RIKEN Nishina Center
*4   IRFU, CEA, Université Paris-Saclay
*5   School of Physics, Peking University
*6   Department of Physics, The University of Hong Kong
*7   Department of Physics, Tohoku University
*8   Center for Nuclear Study, the University of Tokyo
*9   Department of Physics, Royal Institute of Technology
*10 Institut de Physique Nucléaire Orsay, IN2P3-CNRS
*11 Facultad de Ciencias, Departamento de Física, Sede Bogotá, Universidad Nacional de Colombia
*12 Department of Physics, University of Tokyo
*13 Department of Physics, Rikkyo University
*14 Institute for Nuclear Science & Technology, VINATOM
*15 Rudjer Boskovic Institute, Zagreb
*16 Institut für Kernphysik, Universität zu Köln
*17 LPC Caen, ENSICAEN, Université de Caen
*18 Department of Science Education, Ewha Womans University
*19 Department of Physics, Ewha Womans University
*19 Department of Physics, Tokyo Institute of Technology
*21 Department of Physics, University of Oslo
*22 MTA Atomki
*23 Instituto de Estructura de la Materia, CSIC
*24 Institute of Modern Physics, Chinese Academy of Sciences

References
1) D. Steppenbeck et al., Nature (London) **502**, 207–210 (2013).
2) D.-C. Dinca et al., Phys. Rev. C **71**, 041302(R) (2005).
3) S. N. Liddick et al., Phys. Rev. Lett. **92**, 072502 (2004).
4) D. Steppenbeck et al., Phys. Rev. C **96**, 064310 (2017).
5) T. Kobayashi et al., Nucl. Instrum. Methods B **317**, 294–304 (2013).
6) T. Kubo et al., Prog. Theor. Exp. Phys. **2012**, 03C003 (2012).
7) A. Obertelli et al., Eur. Phys. J. A **50**, 8 (2014).

Production of very neutron-rich nuclei via two-proton knockout reaction with deuterium operation of MINOS

M. Miwa,[*1,*2] T. Uesaka,[*2] Y. Kubota,[*2] H. Wang,[*2] H. Otsu,[*2] P. Doornenbal,[*2] A. Obertelli,[*3,*4,*2]
N. Achouri,[*5] H. Baba,[*2] F. Browne,[*2] D. Calvet,[*4] F. Château,[*4] S. Chen,[*6,*2] N. Chiga,[*2] A. Corsi,[*4]
M. L. Cortés,[*2] A. Delbart,[*4] J.-M. Gheller,[*4] A. Giganon,[*4] A. Gillibert,[*4] C. Hilaire,[*4] T. Isobe,[*2]
T. Kobayashi,[*7] V. Lapoux,[*4] H. N. Liu,[*4,*8] T. Motobayashi,[*2] I. Murray,[*9,*2] V. Panin,[*2] N. Paul,[*4]
W. Rodriguez,[*10,*2] H. Sakurai,[*11,*2] M. Sasano,[*2] D. Steppenbeck,[*2] L. Stuhl,[*12] Y. L. Sun,[*4] Y. Togano,[*13,*2]
K. Wimmer,[*11,*2] K. Yoneda,[*2] O. Aktas,[*8] T. Aumann,[*3] L. X. Chung,[*14] F. Flavigny,[*9] S. Franchoo,[*9]
I. Gasparic,[*15,*2] R.-B. Gerst,[*16] J. Gibelin,[*5] K. I. Hahn,[*17] D. Kim,[*17] T. Koiwai,[*11] Y. Kondo,[*18]
P. Koseoglou,[*3,*19] J. Lee,[*20] C. Lehr,[*3] B. D. Linh,[*14] T. Lokotko,[*20] M. MacCormick,[*9] K. Moschner,[*16]
T. Nakamura,[*18] S. Y. Park,[*17] D. Rossi,[*19] E. Sahin,[*21] D. Sohler,[*22] P.-A. Söderström,[*3] S. Takeuchi,[*18]
H. Törnqvist,[*19] V. Vaquero,[*23] V. Wagner,[*3] S. Wang,[*24] V. Werner,[*3] X. Xu,[*20] H. Yamada,[*18] D. Yan,[*24]
Z. H. Yang,[*2] M. Yasuda,[*18] and L. Zanetti[*3]

The production of neutron-rich nuclei through one-nucleon knockout $(p, 2p)$ reactions has been successfully demonstrated with the MINOS setup.[1] In future RIBF experiments, a method to remove more than one proton with a reasonable rate will be required for the production of more neutron-rich nuclei. At present there is no consensus on the best reaction for two-proton removal. In this work, the performance of the $(d, 3pn)$ reaction with the MINOS setup as a candidate of the two-proton knockout driver in future RIBF experiments is discussed. the results of a recent nuclear transmutation experiment at RIBF[2] show an encouraging indication that the production cross sections of neutron-rich nuclei are larger with a deuteron target than with a proton target. In this report, cross sections of the $(p, 3p)$ and $(d, 3pn)$ reactions on a ^{58}Ti beam are shown and discussed.

The experiment was carried out using the SAMURAI spectrometer after the third SEASTAR campaign[3] in May 2017. A secondary cocktail beam including ^{58}Ti was produced with projectile fragmentation reactions of a primary ^{70}Zn beam at 345 MeV/u impinging on a beryllium target. The experimental setup was the same as that of the SEASTAR experiment, except for the target material. The target was liquid deuterium with a thickness of 2.6 g/cm^2. The ^{58}Ti beam with an initial energy of 240 MeV/u loses its energy by 90 MeV/u in the target. The measured cross section is the one averaged over 150–240 MeV/u. The secondary beam and fragments were identified event by event using the ΔE–TOF–$B\rho$ method.

Figure 1 summarizes preliminary results of the cross-section ratio for a deuteron target to a proton target. The ratio of interaction cross sections is greater than one and less than two. This is due to a well-known eclipse effect proposed by Glauber.[4] The result for two-proton removal cross sections shows a significantly larger value of ~ 3, while that for one-proton removal is not so different from the interaction cross section result. This fact implies possible advantages of a deuteron target to produce neutron-rich nuclei.

Data for other isotopes in the cocktail beam will provide us with a global feature of the cross section ratio and reaction analyses for the data will reveal why a deuteron target is so efficient removing two protons from neutron-rich nuclei.
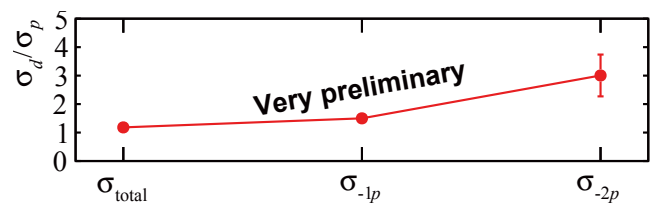
Fig. 1. Ratio of cross sections for a deuteron target to a proton target. σ_{total}: interaction cross section (σ_d/σ_p). σ_{-1p}: one proton removal cross section. σ_{-2p}: two-proton removal cross section.

*1 Department of Physics, Toho University
*2 RIKEN Nishina Center
*3 Institut für Kernphysik, Technische Universität Darmstadt
*4 IRFU, CEA, Université Paris-Saclay
*5 LPC Caen, ENSICAEN, Univeristé de Caen, CNRS/IN2P3
*6 Department of Physics, Peking University
*7 Department of Physics, Tohoku University
*8 Department of Physics, Royal Institute of Technology
*9 IPN Orsay, CNRS, Univ. Paris Sud, Univ. Paris Saclay
*10 Universidad Nacional de Colombia
*11 Department of Physics, The University of Tokyo
*12 Center for Nuclear Study, The University of Tokyo
*13 Department of Physics, Rikkyo University
*14 Institute for Nuclear Science & Technology, VINATOM
*15 Rudjer Boskovic Institute
*16 Institut für Kernphysik, Universität zu Köln
*17 Ewha Womans University
*18 Department of Physics, Tokyo Institute of Technology
*19 GSI Helmholtzzentrum für Schwerionenforschung GmbH
*20 Department of Physics, The University of Hong Kong
*21 Department of Physics, University of Oslo
*22 MTA Atomki
*23 Instituto de Estructura de la Materia, CSIC
*24 Institute of Modern Physics, Chinese Academy of Sciences

References
1) A. Obertelli et al., Eur. Phys. Jour. A **50**, 8 (2014).
2) H. Wang et al., Phys. Lett. B **754**, 104 (2016).
3) P. Doornenbal, A. Obertelli, RIKEN Proposal for Scientific Program (2013).
4) R. J. Glauber, Phys. Rev. **100**, 242 (1955).

Study on the impact parameter dependence on the trigger efficiency for the SπRIT experiment

M. Kaneko,[*1,*2] J. Barney,[*2,*3] G. Cerizza,[*2,*3] J. Estee,[*2,*3] W. G. Lynch,[*3] T. Isobe,[*2] G. Jhang,[*4]
M. Kurata-Nishimura,[*2] P. Lasko,[*5,*2] J. Łukasik,[*5] T. Murakami,[*1,*2] P. Pawłowski,[*5,*2] C. Santamaria,[*2,*3]
M. B. Tsang,[*3] J. W. Lee,[*4,*2] and Y. Zhang[*6,*2] for the SπRIT collaboration

The main objective of the SAMURAI Pion-Reconstruction and Ion-Tracker (SπRIT) project is to place a constraint on the density dependence of the nuclear equation of state (EOS). In particular, the isospin asymmetry term of the EOS, which is called symmetry energy, plays an important role not only in unstable nuclei but also in neutron stars. Currently, the density dependence of symmetry energy is poorly constrained at around twice the saturation density.[1] It is proposed that charged π mesons from heavy-ion (HI) collisions at energies of several hundreds of MeV/nucleon could be a useful probe for the symmetry energy at supra-saturation densities.[2] At intermediate energies, π mesons are produced from the decay of Δ resonance states, which are excited from the nucleon-nucleon (NN) scattering in HI collisions. The π meson production cross-section depends on the NN scattering cross-section, which depends on the impact parameter. Therefore, central collisions will produce higher statistics of π mesons, and will be a region of interest in this experiment.

In the spring of 2016, we performed an experiment at RIBF with collisions between various Sn isotopes at 270 MeV/nucleon.[3] The SπRIT-TPC[4] inside the SAMURAI spectrometer was used to detect the charged particles. To provide a trigger signal focusing on the central collision, a combination of two kinds of detectors—KATANA veto[5] and Kyoto multiplicity array[6]—was utilized. It consisted of an array of plastic paddles and Multi-Pixel Photon Counter for use in the magnetic field of 0.5 T. The KATANA veto was placed downstream from the SπRIT-TPC, enabling us to veto peripheral collisions, which involve high-Z spectator particles. The Kyoto multiplicity array covered both sides of the SπRIT-TPC to detect central collisions by setting a threshold on the sideward-moving charged particle multiplicity. For regular data acquisition runs, the trigger condition required Z less than 20 in the KATANA veto and a multiplicity greater than four in the Kyoto multiplicity array.

The dependece of impact parameter on the trigger efficiency in regular runs has been studied by using Monte Carlo simulation with event generators. As a HI collision generator, JQMD-2.0 in PHITS[7] Ver.

2.880 and UrQMD[8] Ver. 3.4 were used to reproduce $^{132}Sn+^{124}Sn$ reactions at 270 MeV/nucleon. Figure 1 shows the trigger efficiency curve as a function of the impact parameter. For both models, about 100% trigger efficiency was obtained for central collisions with impact parameters of 0–2 fm. However, significant model dependence is found in semi-central collisions with impact parameters of 5–9 fm. For a more proper model parametrization, it would be necessary to compare the experimental observables with further simulations.
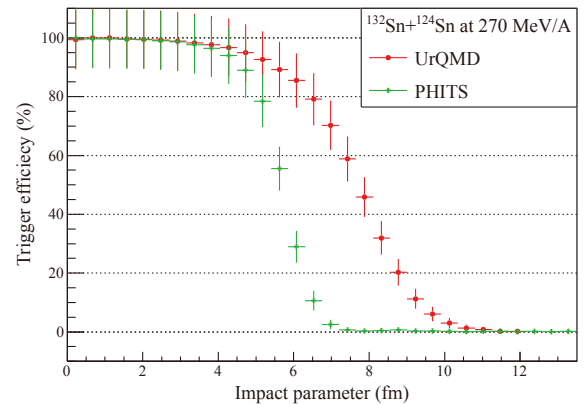
Fig. 1. Trigger efficiency curves as a function of impact parameter in the regular runs.

Further analysis on the impact parameter determination using the reconstructed track in SπRIT-TPC is now under way.

References
1) M. B. Tsang *et al.*, Phys. Rev. C **86**, 015803 (2012).
2) B. A. Li *et al.*, Phys. Rev. C **71**, 014608 (2005).
3) J. Barney *et al.*, RIKEN Accel. Prog. Rep. **50**, 49 (2017).
4) R. Shane *et al.*, Nucl. Instrum. Methods A **784**, 513 (2015).
5) P. Lasko *et al.*, Nucl. Instrum. Methods A **856**, 92 (2017).
6) M. Kaneko *et al.*, RIKEN Accel. Prog. Rep. **49**, 163 (2016).
7) T. Sato *et al.*, J. Nucl. Sci. Technol., (2018).
8) M. Breicher *et al.*, J. Phys. G **25**, 1859 (1999).

*1 Department of Physics, Kyoto University
*2 RIKEN Nishina Center
*3 NSCL and Dept. of Phys. & Ast., Michigan State University
*4 Department of Physics, Korea University
*5 Institute of Nuclear Physics, PAN, Kraków, Poland
*6 Department of Physics, Tsinghua University

Status of collective flow analysis for SπRIT-TPC experiment

M. Kurata-Nishimura,[*1] J. Barney,[2*,1*] G. Cerizza,[2*,1*] J. Estee,[2*,1*] B. Hong,[*3] T. Isobe,[*1] G. Jhang,[3*,1*] M. Kaneko,[4*,1*] H. S. Lee,[*7] J. W. Lee,[3*,1*] J. Łukasik,[*5] W. G. Lynch,[*2] A. B. McIntosh,[*8] T. Murakami,[4*,1*] P. Pawłowski,[5*,1*] K. Pelczar,[*6] H. Sakurai,[*1] C. Santamaria,[2*,1*] R. Shane,[*2] M. B. Tsang,[*2] S. J. Yennello,[*8] and for SπRIT Collaboration

The successful observation of gravitational waves from a neutron star merger[1] highlights the importance of the nuclear Equation of State (EoS). Heavy ion collisions are an appropriate tool to evaluate the nuclear EoS at supra-saturation. In nuclear EoS at a density more than that of normal nuclear matter ($\rho > 2\rho_0$), the isospin symmetry energy term includes large uncertainly in theory, because of the lack of experimental data. In a previous work, the π^-/π^+ production ratio was a super soft EoS;[2] however, the proton and neutron collective flow analysis[3] was inconsistent.

The SAMURAI Pion-Reconstruction and Ion-Tracker-Time-Projection Chamber (SπRIT-TPC) project was proposed to constrain the EoS using different isospin asymmetry systems with ^{132}Sn and ^{108}Sn beams at 270 MeV/u on ^{112}Sn and ^{124}Sn targets at SAMURAI in RIBF. Multiple observations, such as π^-/π^+ production ratio, proton and neutron collective flow, and H^3/He^3 production ratio, will be obtained to study the EoS for heavy ion collisions.

The collective flow of neutron and proton is expected to be sensitive to the isospin symmetry potential because it could minimize the influence of the isoscalar potential.[4] In this paper, recent results for the collective flow analysis will be discussed.

The SπRIT-TPC is described in Ref. 5) NeuLAND was installed 8.8 m downstream from the target to detect neutrons emitted around the mid-rapidity region. Trigger devices, KATANA array[6] and Multiplicity array[7] were installed surrounding the SπRIT-TPC.

The strength of the collective flow is analyzed from the azimuthal distribution with respect to a reaction plane. The reaction plane orientation angle, Ψ, is determined event by event. The azimuthal angle of the reaction plane is defined as the sum of the transverse momentum unit vector.

$$\Psi = \frac{\sum_i^m \omega_i \sin(n\phi_i)}{\sum_i^m \omega_i \cos(n\phi_i)} \qquad (1)$$

$$\Delta\Psi_{sub} = \Psi_A - \Psi_B \qquad (2)$$

The coefficient ω is 1 if rapidity is larger than the center of rapidity, otherwise it is -1.

The geometrical acceptance of the SπRIT-TPC is limited and asymmetric in the azimuthal angle, so it was necessary to apply a flattening correction.[8] Tracks were randomly selected from independent events to create "mixed" events. To check the feasibility of determining the reaction plane with this flattening correction applied, two sub-events of equal multiplicity were formed event by event. The reaction planes Ψ_A and Ψ_B were measured from the sub-events, and the opening angle of two sub-events, $\Delta\Psi_{sub}$, is plotted in Fig. 1. The real events are plotted as red circles, which show an enhancement at $\Delta\Psi_{sub} = 0$ indicating the ability of determining the reaction plane from the measurements. The mixed events are plotted as green circles, which show a flat distribution indicating that the detector bias has been removed. It was confirmed that the reaction plane could be determined using sub-event correlations with SπRIT-TPC. More detailed analysis is on going.
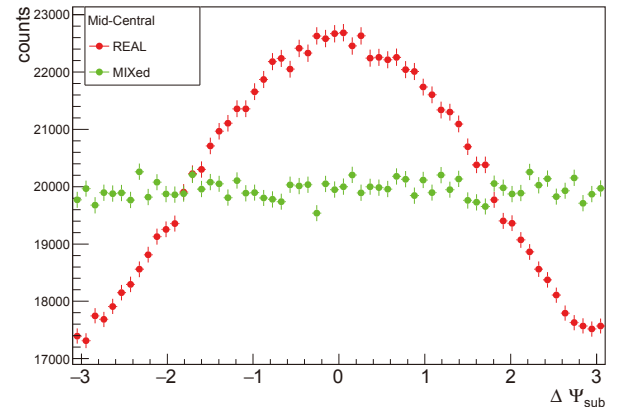
Fig. 1. Opening angle of reaction planes determined by two sub-events Red and green circles show real and mixed events, respectively.

References
1) B. P. Abbot et al., Phys. Rev. Lett. **119**, 161101 (2017).
2) Bao-An Li et al., Phys. Rev. C **71**, 014608 (2005).
3) P. Russotto et al., Phys. Lett. B **471**, (2011).
4) B.-A. Li et al., Phys. Rev. Lett. **85**, 4221 (2000).
5) R. Shane et al., Nucl. Instrum. Methods A **784**, 513 (2015).
6) P. Lasko et al., Accel. Prog. Rep. **50**, 173 (2017).
7) M. Kaneko et al., Accel. Prog. Rep. **50**, 172 (2017).
8) J.-Y. Ollitrault et al., Nucl. Phys. **638**, 195c (1998).

*1　RIKEN Nishina Center
*2　NSCL and Dept. of Phys. & Ast., Michigan State University
*3　Department of Physics, Korea University
*4　Department of Physics, Kyoto University
*5　IFJ PAN, Kraków
*6　Faculty of Physics, Astronomy and Applied Computer Science, Jagiellonian University, Kraków
*7　Rare Isotope Science Project, Institute for Basic Science
*8　Cyclotron Institute, Texas A&M University

Gamma decay of unbound neutron-hole states in ^{133}Sn[†]

V. Vaquero,[*1] A. Jungclaus,[*1] P. Doornenbal,[*2] K. Wimmer,[*2, *3] A. Gargano,[*4] J. A. Tostevin,[*5] S. Chen,[*2, *6]
E. Nácher,[*1] E. Sahin,[*7] Y. Shiga,[*8] D. Steppenbeck,[*2] R. Taniuchi,[*2, *3] Z. Y. Xu,[*9]
and the NP1306-RIBF98R1 collaboration

The region around the doubly magic nucleus ^{132}Sn ($N = 82$ and $Z = 50$) is of particular interest for nuclear structure investigations. Nuclei with a few nucleons outside this closed-shell core provide direct information about the evolution of nucleon-nucleon correlations, quadrupole collectivity and single-particle energies. In this context, the low-lying states in the neutron-rich nucleus ^{133}Sn, which consists of a single neutron coupled to the doubly-magic nucleus ^{132}Sn, provide information about the position of the neutron single-particle orbitals belonging to the $N = 82$–126 major shell. Neutron single-particle energies of 854, 1367, 1561, and 2002 keV for the $2p_{3/2}$, $2p_{1/2}$, $0h_{9/2}$ and $1f_{5/2}$ orbitals, respectively, relative to the $1f_{7/2}$ orbital, have been established combining the information from both β decay and (d, p) neutron-transfer experiments.[1,2] The neutron single-hole states in ^{133}Sn are expected to have excitation energies above $S_n = 2.402(4)$ MeV and to decay via neutron emission mediated by the strong interaction.

In an experiment performed in April 2015 at the RI Beam Factory (RIBF), excited states in the nucleus ^{133}Sn were investigated by in-beam γ-ray spectroscopy. These states in ^{133}Sn were populated knocking out a neutron from a slightly heavier nucleus, ^{134}Sn, at relativistic energies. The exotic nuclei to be investigated were produced by the in-flight fission of a 345 MeV/nucleon ^{238}U beam with an average intensity of 15 pnA, impinging on a 4-mm thick Be target. In the BigRIPS in-flight separator, the $B\rho$-ΔE-$B\rho$ method was used in order to select and identify a secondary beam of ^{134}Sn. The identified ^{134}Sn ions then impinged with a kinetic energy of 165 MeV/nucleon on a 3-mm thick C target. The γ radiation emitted in the decay of excited states was detected using the γ-ray spectrometer DALI2 which was installed surrounding the secondary target. Reaction products from the secondary target were identified using the ZeroDegree spectrometer.[3]

Figure 1 shows the Doppler-corrected γ-ray spec-
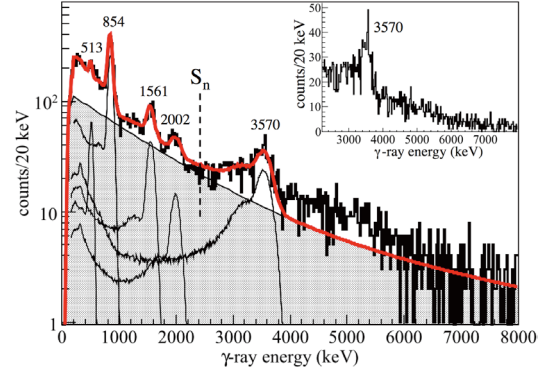
Fig. 1. Doppler-corrected γ-ray spectrum (for γ-ray multiplicity $M_\gamma = 1$ after add back) of ^{133}Sn populated via one-neutron knockout from ^{134}Sn. The response function fit to the experimental spectrum is shown by the thick red line while the individual components are shown as thin black lines. The background is indicated as the gray area. The inset shows the high-energy region of the spectrum on a linear scale.

trum measured in coincidence with ^{134}Sn ions detected in BigRIPS and ^{133}Sn nuclei detected in the ZD spectrometer. Besides the known γ rays emitted in the decay of the single-particle states (transitions at 513, 854, 1561, and 2002 keV), clearly additional γ strength is observed above the neutron separation energy, reaching up to about 5.5 MeV. These excited states are interpreted as neutron-hole states that are populated following the knock-out of a neutron from the closed $N = 50$–82 shell of the ^{134}Sn projectile ion. These neutron-hole states are expected to decay via neutron emission because they are situated far above the neutron separation energy. However, the ability of γ-ray emission to compete with neutron decay is explained taking into account the structure of the initial and final states and the resultant wave-function overlap. Our study raises the question whether, due to nuclear structure effects, the γ-ray emission may play a much more significant role than generally assumed in the decay of highly excited states populated following β decay in the region southeast of ^{132}Sn.

[†] Condensed from the article in Phys. Rev. Lett. **118**, 202502 (2017)
[*1] Instituto de Estructura de la Materia, CSIC
[*2] RIKEN Nishina Center
[*3] Department of Physics, University of Tokyo
[*4] Istituto Nazionale di Fisica Nucleare
[*5] Department of Physics, University of Surrey
[*6] State Key Laboratory of Nuclear Physics and Technology, Peking University
[*7] Department of Physics, University of Oslo
[*8] Department of Physics, Rikkyo University
[*9] Department of Physics, University of Hong Kong

References
1) P. Hoff *et al.*, Phys. Rev. Lett. **77**, 1020 (1996).
2) K. L. Jones *et al.*, Nature (London) **465**, 454 (2010); Phys. Rev. C **84**, 034601 (2011).
3) N. Fukuda *et al.*, Nucl. Instrum. Methods Phys. Res. B **317**, 323 (2013).

Shell evolution beyond $Z = 28$ and $N = 50$: spectroscopy of $^{81-84}$Zn[†]

C. M. Shand,[*1] Zs. Podolyák,[*1] M. Górska,[*2] P. Doornenbal,[*3] A. Obertelli,[*3,*4] F. Nowacki,[*5] T. Otsuka,[*6]
K. Sieja,[*5] J. A. Tostevin,[*1] and Y. Tsunoda[*6] for the SEASTAR collaboration

The Shell Evolution and Search for Two-plus states At the RIBF (SEASTAR) experimental campaigns were conducted at the Radioactive Isotope Beam Factory (RIBF). For the experiments a ^{238}U primary beam was accelerated to 345 MeV/nucleon and subsequently impinged onto a 3 mm thick ^{9}Be production target at the entrance of the BigRIPS separator. Secondary fission beams of interest were then selected within BigRIPS using the $B\rho$-ΔE-$B\rho$ technique. The results presented here on neutron-rich Zn isotopes were obtained from settings centered on ^{79}Cu and ^{85}Ga in the first (2014) and second (2015) SEASTAR campaigns, respectively.
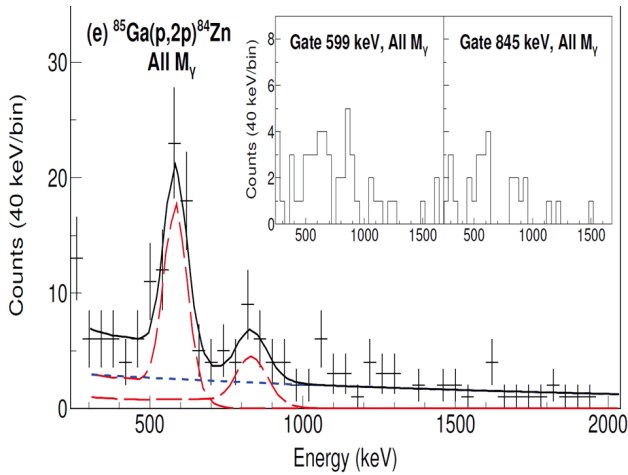
Fig. 1. Doppler corrected γ-ray spectrum of ^{84}Zn.

The incoming ions were impinged on the liquid H$_2$ target of the MINOS device, while the resulting γ rays were detected with the DALI2 high-efficiency NaI(Tl) array. Low-lying excited states in the neutron-rich $^{81-84}$Zn isotopes have been investigated. The 4^+_1 state in ^{82}Zn and the 2^+_1 and 4^+_1 states in ^{84}Zn (see Fig. 1) were observed for the first time. In addition, γ-ray transition were identified in odd-mass ^{81,83}Zn. The main experimental conclusion of the work is that the magicity is confined to neutron number $N = 50$ only, as indicated by the increased $R_{4/2} = E(4^+)/E(2^+)$ ratios in ^{82,84}Zn when compared to than in the neutron-magic ^{80}Zn nucleus.

A magic or semi-magic core can be distorted as valence nucleons are added to a closed shell. The samar-ium isotopes present a typical case. Shape evolution proceeds from a seniority level pattern in $N = 82$ semi-magic ^{144}Sm, to a vibrational pattern at $N = 86$ in ^{148}Sm, and finally a rotational one at $N = 92$ in ^{154}Sm. At $N = 84$ ^{146}Sm provides the transition between the seniority and vibrational schemes. In the case of Zn isotopes, with only two protons outside the $Z = 28$ shell, the situation is rather different. As deduced from the present experiment for the first time, the proton-neutron correlations are strong enough for a rapid change from the semi-magic structure at $N = 50$ to a collective structure at $N = 52$. This is partly due to the weak $Z = 28$ sub-magic structure, which is a consequence of the repulsive nature of the tensor force between the proton $f_{7/2}$ and the fully occupied neutron $g_{9/2}$ orbits.

The experimental results were compared to three state-of-the-art shell-model calculations (see Fig. 2), considering different model spaces. They all correctly predict that the ^{82,84}Zn isotopes exhibit collective-like character. The good agreement between experiment and theory suggests that breaking the ^{78}Ni core provides a significant contribution to low-lying states beyond $Z = 28$ and $N = 50$.
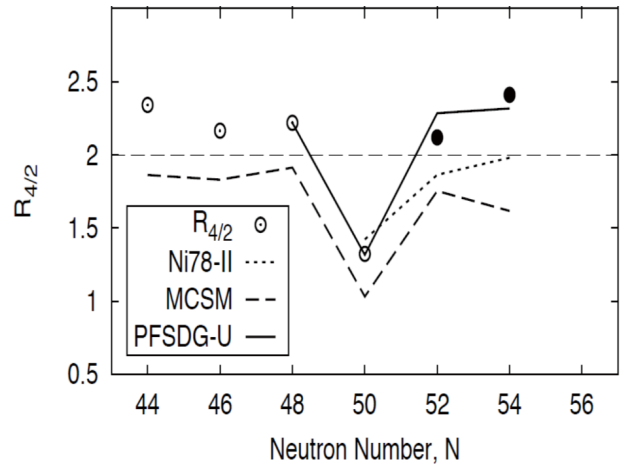
Fig. 2. Systematics of $R_{4/2} = E(4^+)/E(2^+)$ for Zn isotopes. The filled symbols are from this work. The results of the Ni78-II,[1] A3DA-m,[2] and PFSDG-U[3] shell-model calculations are also indicated. The line at $R_{4/2} = 2$ indicates the vibrational limit.

References
1) K. Sieja, T. R. Rodriguez, K. Kolos, D. Verney, Phys. Rev. C **88**, 034327 (2013).
2) Y. Tsunoda, T. Otsuka, N. Shimizu, M. Honma, Y. Utsuno, Phys. Rev. C **89**, 031301 (2014).
3) F. Nowacki, A. Poves, E. Caurier, B. Bounthong, Phys. Rev. Lett. **117**, 272501 (2016).

†　Condensed from the article in Phys. Lett. B **737**, 492 (2017)
*1　Department of Physics, University of Surrey
*2　GSI
*3　RIKEN Nishina Center
*4　IRFU, CEA, Saclay
*5　IPHC, CNRS/IN2P3, Orsay
*6　Center for Nuclear Study, University of Tokyo

Robustness of the $N = 34$ shell closure: First spectroscopy of ^{52}Ar

H. N. Liu,[*1,*2] Y. L. Sun,[*1] A. Obertelli,[*3,*1,*4] P. Doornenbal,[*4] H. Baba,[*4] F. Browne,[*4] D. Calvet,[*1]
F. Château,[*1] S. Chen,[*5,*6,*4] N. Chiga,[*4] A. Corsi,[*1] M. L. Cortés,[*4] A. Delbart,[*1] J-M. Gheller,[*1] A. Giganon,[*1]
A. Gillibert,[*1] C. Hilaire,[*1] T. Isobe,[*4] T. Kobayashi,[*7] Y. Kubota,[*4,*8] V. Lapoux,[*1] T. Motobayashi,[*4]
I. Murray,[*9,*4] H. Otsu,[*4] V. Panin,[*4] N. Paul,[*1] W. Rodriguez,[*10,*4] H. Sakurai,[*4,*12] M. Sasano,[*4]
D. Steppenbeck,[*4] L. Stuhl,[*8] Y. Togano,[*11,*4] T. Uesaka,[*4] K. Wimmer,[*12,*4] K. Yoneda,[*4] N. Achouri,[*13]
O. Aktas,[*2] T. Aumann,[*3] L. X. Chung,[*14] F. Flavigny,[*9] S. Franchoo,[*9] I. Gašparić,[*15,*4] R. -B. Gerst,[*17]
J. Gibelin,[*13] K. I. Hahn,[*18] D. Kim,[*18,*4] T. Koiwai,[*12] Y. Kondo,[*19] P. Koseoglou,[*3,*16] J. Lee,[*6] C. Lehr,[*3]
B. D. Linh,[*14] T. Lokotko,[*6] M. Maccormick,[*9] K. Moschner,[*17] T. Nakamura,[*19] S. Y. Park,[*18,*4] D. Rossi,[*3]
E. Sahin,[*20] D. Sohler,[*21] P-A. Söderström,[*3] S. Takeuchi,[*19] H. Toernqvist,[*16] V. Vaquero,[*22] V. Wagner,[*3,*4]
S. Wang,[*23] V. Werner,[*3] X. Xu,[*6] H. Yamada,[*19] D. Yan,[*23] Z. Yang,[*4] M. Yasuda,[*19] and L. Zanetti[*3]

It is now well known that magic numbers are not universal across the nuclear landscape and that new shell closures may emerge in exotic nuclei. For example, a new subshell closure at $N = 34$ has been predicted for neutron-rich nuclei.[1] On the experimental side, the systematics of the $E(2_1^+)$ of Ti isotopes show no evidence for the existence of the $N = 34$ shell gap.[2] Recently, the $E(2_1^+)$ of ^{54}Ca was measured to be ~ 0.5 MeV smaller than that of ^{52}Ca.[3] This drop was attributed to the larger ground state correlation energy of ^{52}Ca, and the results were interpreted as confirming the $N = 34$ magic number in Ca isotopes. For ^{52}Ar, no spectroscopic information has been measured; however, its $E(2_1^+)$ was predicted to be the highest among Ar isotopes with N > 20.[4] The spectroscopy of ^{52}Ar thus offers a unique chance to explore the robustness of the $N = 34$ subshell closure and pin down the mechanism of its emergence.

The measurement of ^{52}Ar was performed at the RIBF as part of the third campaign of the SEASTAR program. The fast radioactive beam containing ^{53}K, amongst other products, was produced by fragmentation of a ~ 220 pnA ^{70}Zn primary beam at 345 MeV/nucleon on a 10-mm thick Be target. The constituents were identified using the BigRIPS frag-
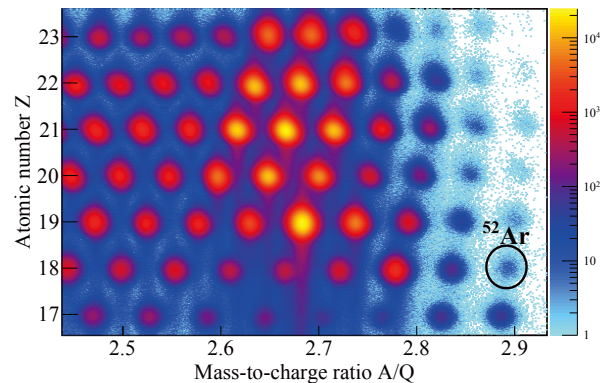
Fig. 1. Particle identification after the secondary target.

ment separator with the ΔE-TOF-$B\rho$ method. The incident beam, magnetically centered on ^{53}K, was impinged on a 150-mm thick MINOS[5] liquid hydrogen target to induce proton-removal reactions. The recoil protons were detected by the MINOS TPC tracker[5] to reconstruct the reaction vertex. The MINOS efficiency was measured to be 90(5)%. The kinematic energy and intensity of the ^{53}K beam in front of the target were ~ 240 MeV/nucleon and 1.0 pps, respectively. The reaction residues passed through the SAMURAI[6] magnet with a central magnetic field of 2.7 T, and were identified by a 24-element plastic hodoscope and two forward drift chambers. Figure 1 shows the particle identification of the reaction residues. The de-excitation γ rays from the reaction residues were measured by the upgraded DALI2+ array,[7] which consists of 226 NaI(Tl) crystals. The preliminary Doppler-corrected γ-ray spectrum of ^{52}Ar was obtained, and a clear $(2_1^+ \rightarrow 0_1^+)$ candidate peak was found. Evidence for other transitions in ^{52}Ar requires further analysis.

*1   IRFU, CEA, Université Paris-Saclay
*2   Department of Physics, KTH
*3   Institut für Kernphysik, TU Darmstadt
*4   RIKEN Nishina Center
*5   Department of Physics, Peking University
*6   Department of Physics, The University of Hong Kong
*7   Department of Physics, Tohoku University
*8   CNS, The University of Tokyo
*9   IPN Orsay, CNRS, Univ. Paris-Sud, Univ. Paris-Saclay
*10 Universidad Nacional de Colombia, Sede Bogotá, Facultad de Ciencias, Departamento de Física
*11 Department of Physics, Rikkyo University
*12 Department of Physics, The University of Tokyo
*13 LPC, Caen
*14 INST Hanoi
*15 Ruđer Bošković Institute, Zagreb
*16 GSI Helmoltzzentrum Darmstadt
*17 Institut für Kernphysik, Universität zu Köln
*18 Department of Physics, Ewha Womans University
*19 Department of Physics, Tokyo Institute of Technology
*20 Department of Physics, University of Oslo
*21 MTA Atomki
*22 Instituto de Estructura de la Materia, CSIC
*23 Institute of Modern Physics, Chinese Academy of Sciences

References
1) T. Otsuka et al., Phys. Rev. Lett. 87, 082502 (2001).
2) S. N. Liddick et al., Phys. Rev. Lett. 92, 072502 (2004).
3) D. Steppenbeck et al., Nature (London) 502, 207 (2013).
4) D. Steppenbeck et al., Phys. Rev. Lett. 114, 252501 (2015).
5) A. Obertelli et al., Eur. Phys. J. A 50, 8 (2014).
6) T. Kobayashi et al., Nucl. Instrum. Methods B 317, 294 (2013).
7) I. Murray et al., in this report.

First Spectroscopic study of ^{56}Ca

S. Chen,[*1,*2,*3] F. Browne,[*3] J. Lee,[*2] P. Doornenbal,[*3] A. Obertelli,[*4,*3,*5] H. Baba,[*3] D. Calvet,[*4]
F. Château,[*4] N. Chiga,[*3] A. Corsi,[*4] M. L. Cortés,[*3] A. Delbart,[*4] J-M. Gheller,[*4] A. Giganon,[*4]
A. Gillibert,[*4] C. Hilaire,[*4] T. Isobe,[*3] T. Kobayashi,[*6] Y. Kubota,[*3,*7] V. Lapoux,[*4] H. N. Liu,[*4,*13]
T. Motobayashi,[*3] I. Murray,[*3,*8] H. Otsu,[*3] V. Panin,[*3] N. Paul,[*4] W. Rodriguez,[*9] H. Sakurai,[*3,*10]
M. Sasano,[*3] D. Steppenbeck,[*3] L. Stuhl,[*7] Y. L. Sun,[*4] Y. Togano,[*11] T. Uesaka,[*3] K. Wimmer,[*10]
K. Yoneda,[*3] N. Achouri,[*12] O. Aktas,[*13] T. Aumann,[*5] L. X. Chung,[*14] F. Flavigny,[*8] S. Franchoo,[*8]
I. Gasparic,[*15] R.-B. Gerst,[*16] J. Gibelin,[*12] K. I. Hahn,[*17] D. Kim,[*17] T. Koiwai,[*10] Y. Kondo,[*18]
P. Koseoglou,[*5,*15] C. Lehr,[*5] B. D. Linh,[*14] T. Lokotko,[*2] M. MacCormick,[*8] K. Moschner,[*16]
T. Nakamura,[*18] S. Y. Park,[*17] D. Rossi,[*15] E. Sahin,[*19] D. Sohler,[*20] P-A. Söderström,[*5] S. Takeuchi,[*18]
H. Toernqvist,[*15] V. Vaquero,[*21] V. Wagner,[*5] S. Wang,[*22] V. Werner,[*5] X. Xu,[*2] H. Yamada,[*18] D. Yan,[*22]
Z. Yang,[*3] M. Yasuda,[*18] and L. Zanetti[*5]

The first measurement of low-lying excited states of ^{56}Ca was performed as part of the third SEASTAR[1] (Shell Evolution And Search for Two-plus energies At the RIBF) campaign in May 2017. In a simple shell-model description, this nucleus has two neutrons in the $f_{5/2}$ orbital outside the closed (sub)-shell nucleus ^{54}Ca.[2] The location of its 2_1^+ energy gives a measurement of the difference between 0^+ and 2^+ two-body matrix elements in $\nu(f_{5/2})^2$, which is of importance to understand the nature of the very neutron-rich, potential closed (sub)-shell nucleus ^{60}Ca. Theoretical predictions of this energy level vary from 0.5 to 2 MeV; therefore, its experimental determination is desirable.

A ^{70}Zn beam accelerated to 345 MeV/nucleon impinged on a 10-mm thick ^{9}Be primary target with an average intensity of $\sim$160 pnA at the entrance of the BigRIPS separator to produce the radioactive secondary beam. BigRIPS was tuned to select and identify particles of interest via the measurement of Bρ, ΔE and ToF by using standard beamline detectors. The particle identification of BigRIPS is shown in Fig. 1. The average production rate of ^{57}Sc nuclei was 13.6 s^{-1}. To induce knock-out reactions populating low-lying states in ^{56}Ca, the secondary beam impinged
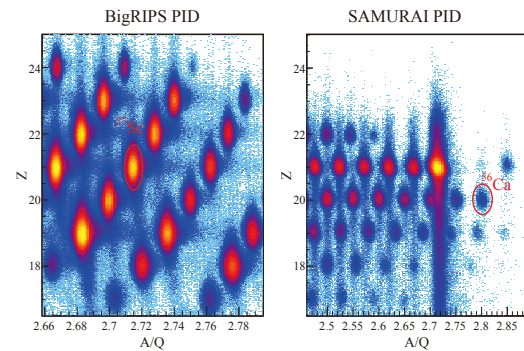
Fig. 1. BigRIPS particle identification (left) and SAMURAI particle identification for ^{57}Sc secondary beam (right). The ^{57}Sc$(p, 2p)^{56}$Ca channel is selected.

on the 150-mm-length LH2 target of the MINOS device.[3] The beam energy in front of the secondary target was measured to be $\sim$250 MeV/nucleon. The upgraded DALI2[4] array, which contains 226 NaI(Tl) detectors, was used to measure gamma rays emitted from the in-flight particles. The reaction residues were identified using the SAMURAI spectrometer.[5] The identification of the residues from the ^{57}Sc secondary beam is also shown in Fig. 1, from which the ^{56}Ca isotopes are selected.

Currently, the gamma-ray spectrum in coincidence with the ^{57}Sc$(p, 2p)^{56}$Ca reaction channel is under analysis. This preliminary energy spectrum shows a candidate peak of the $2_1^+ \rightarrow 0_1^+$ transition observed at an energy consistent with the aforementioned range of theoretical predictions. The spectra coincident with other reaction channels, which produce ^{56}Ca, are also under analysis.

*1   School of Physics, Peking University
*2   Department of Physics, The University of Hong Kong
*3   RIKEN Nishina Center
*4   IRFU, CEA, Université Paris-Saclay
*5   Institut für Kernphysik, Technische Universität Darmstadt
*6   Department of Physics, Tohoku University
*7   Center for Nuclear Study, the University of Tokyo
*8   IPN Orsay, CNRS, Univ. Paris Sud, Univ. Paris Saclay
*9   Universidad Nacional de Colombia
*10 Department of Physics, University of Tokyo
*11 Department of Physics, Rikkyo University
*12 LPC Caen, ENSICAEN, Université de Caen
*13 Department of Physics, Royal Institute of Technology
*14 Institute for Nuclear Science & Technology, VINATOM
*15 GSI Helmholtzzentrum Darmstadt
*16 Institut für Kernphysik, Universität zu Köln
*17 Ewha Womans University
*18 Department of Physics, Tokyo Institute of Technology
*19 Department of Physics, University of Oslo
*20 MTA Atomki
*21 Instituto de Estructura de la Materia, CSIC
*22 Institute of Modern Physics, Chinese Academy of Sciences

References
1) P. Doornenbal, A. Obertelli, RIKEN Proposal for Scientific Program (2013).
2) D. Steppenbeck *et al.*, Nature (London) **502**, 207 (2013).
3) A. Obertelli *et al.*, Eur. Phys. J. A **50**, 8 (2014).
4) I. Murray *et al.*, In this report.
5) T. Kobayashi *et al.*, Nucl. Instrum. Methods B **317**, 294 (2013).

Triaxiality of neutron-rich ^{84,86,88}Ge from low-energy spectra

M. Lettmann,[*1] V. Werner,[*1] N. Pietralla,[*1] P. Doornenbal,[*2] A. Obertelli,[*3,*2,*1] T. R. Rodríguez,[*4]
K. Sieja,[*5] and the SEASTAR 15 collaboration

Spectroscopic measurements of ^{84,86,88}Ge were performed within the SEASTAR campaign in 2015.[1] The spectroscopic results and theoretical predictions inspired intensive discussions of triaxial features for the Ge isotopic chain. Two elementary models, which describe the nucleus as a rigid triaxial rotor or as softly shaped, are competing in this region. Both models describe the breaking of the axial symmetry of the Bohr Hamiltonian[2] by introducing the triaxial deformation parameter γ, which ranges from 0° (prolate shape) to 60° (oblate shape), and the axial elongation β. The maximum of triaxiality is reflected by $\gamma = 30°$. The rigid triaxial rotor model by Davydov and co-workers[3] considers a well-defined minimum for the potential energy surface while the model by Wilets and Jean[4] treats the potential independent of γ, introducing γ-softness. The difference between the soft and rigid cases is manifested in the energy spacing between the odd and even members of the γ band. In the case of a rigid triaxial rotor, the odd-spin levels are located closer to the lower-lying even spin levels, whereas the odd spin levels are located closer to the higher-lying even spin levels in the case of a γ-soft nucleus. This energy difference is referred to as staggering.[5,6]

At the RIBF, a ^{238}U beam with an energy of 345 MeV/u was impinged on a 3-mm-thick ^{9}Be target at the entrance of BigRIPS.[7] The isotopes of interest were identified by BigRIPS and ZeroDegree spectrometer in two different settings. The Ge isotopes were produced by knockout reactions inside the MINOS[8] LH$_2$ target and the emitted γ radiation was detected with DALI2.[9] The TPC of MINOS[8] was used to improve the Doppler correction.

In total, 16 transitions in ^{84,86,88}Ge have been observed, ten of which were so far unknown. For ^{86}Ge and ^{88}Ge, new level schemes are proposed, which are shown in Fig. 1 in red. The experimental results are compared to a shell model calculation and a symmetry-conserving configuration mixing Gogny (SCCM) calculation in Fig. 1. The predicted sequences of states are in good agreement with the experimental results, although both theories overestimate the level energies in all cases. Nevertheless, the predicted $R_{4/2} \approx 2.5$ agrees with the data. Both calculations suggest a low-lying γ band, which indicates some amount of triaxiality in both isotopes. Furthermore, both theories predict a
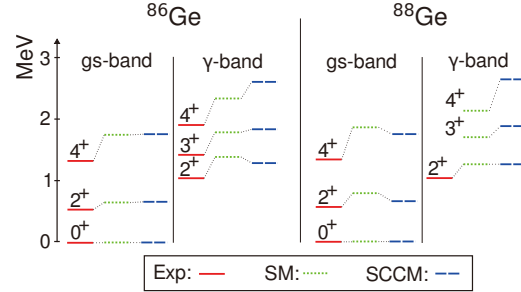
Fig. 1. Systematics of the ^{86,88}Ge level energies from experiment compared to theoretical predictions from shell model (SM) and symmetry-conserving configuration mixing Gogny (SCCM) calculations.

3_1^+ state of ^{86}Ge that is closer to the 2_2^+ state than to the 4_2^+ state of the γ band. A promising candidate for this state is observed through a 380(8)-keV transition of ^{86}Ge, because the strongest decay of the 3_1^+ state is expected to the 2_2^+ state. As highlighted before, the staggering[5,6] in the γ band should take a positive value for a rigid triaxial rotor. This would be the case for a well-deformed rotor with $E(J) \sim J(J+1)$ as well, though in such a case, the γ-band head is at much higher values. So far only one nucleus in the medium-heavy mass region $A < 100$ is known with rigid triaxial features. This nucleus is ^{76}Ge, where a staggering $S(4) = 0.091(2)$ was found.[10] With the level assignments presented in Fig. 1, a value of $S(4) = 0.20(4)$ results for ^{86}Ge, pointing to an even larger degree of triaxiality in the ground state than assigned to ^{76}Ge. This results agrees with the predictions of both theories.

References
1) condensed from M. Lettmann *et al.*, Phys. Rev. C **96**, 011301(R) (2017).
2) A. Bohr, B. Mottelson, Mat. Fys. Medd. Dan. Vid. Selsk. **27** (1958).
3) A. S. Davydov, G. F. Filippov, Nucl. Phys. **8**, 237 (1958).
4) L. Wilets, M. Jean, Phys. Rev. **102**, 788 (1956).
5) N. V. Zamfir, R. F. Casten, Phys. Lett. B **260**, 265 (1991).
6) E. A. McCutchan, D. Bonatsos, N. V. Zamfir, R. F. Casten, Phys. Rev. C **76** 024306(R) (2007).
7) T. Kubo *et al.*, Prog. Theor. Exp. Phys. **2012** 03C003 (2012).
8) A. Obertelli *et al.*, Eur. Phys. J. A **50** 8 (2014).
9) S. Takeuchi *et al.*, Nucl. Instrum. Methods Phys. Res. A **763** 8 (2014).
10) Y. Toh *et al.*, Phys. Rev. C **87** 041304(R) (2013).

[*1] Institut für Kernphysik, Technische Universität Darmstadt
[*2] RIKEN Nishina Center
[*3] CEA, Centre de Saclay
[*4] Departamento de Física Teórica, Universidad Autónoma de Madrid
[*5] IPHC, CNRS/IN2P3 et Université de Strasbourg

Precise measurement of the ^{4}He(^{8}He,^{8}Be) reaction

S. Masuoka,[*1] S. Shimoura,[*1] M. Takaki,[*1] M. Dozono,[*1] C. Iwamoto,[*1] K. Kawata,[*1] N. Kitamura,[*1]
M. Kobayashi,[*1] S. Michimasa,[*1] R. Nakajima,[*1] S. Ota,[*1] H. Tokieda,[*1] R. Yokoyama,[*1] D. S. Ahn,[*2]
H. Baba,[*2] N. Fukuda,[*2] T. Harada,[*3] E. Ideguchi,[*4] N. Imai,[*1] N. Inabe,[*2] Y. Kondo,[*5] T. Kubo,[*2]
Y. Maeda,[*6] F. M. Marqués,[*7] M. Matsushita,[*1] T. Nakamura,[*5] N. Orr,[*7] H. Sakai,[*2] H. Sato,[*2] P. Schrock,[*1]
L. Stuhl,[*1,*2] T. Sumikama,[*2] H. Suzuki,[*2] H. Takeda,[*2] K. Taniue,[*6] T. Uesaka,[*2] K. Wimmer,[*8] K. Yako,[*1]
Y. Yamaguchi,[*1] Y. Yanagisawa,[*2] K. Yoshida,[*2] and J. Zenihiro[*2]

Nuclei composed of only neutrons have been discussed for over a half century. However, their existence has not been confirmed. In 2002, a candidate bound state of the tetra-neutron, which consists of four neutrons, was reported.[1] An *ab-initio* calculation suggested that there might be a tetra-neutron ($4n$) resonance, but a bound $4n$ was not reproduced.[2] An experimental search for the $4n$ resonance state conducted using the exothermic double charge exchange (DCX) ^{4}He(^{8}He,^{8}Be)$4n$ reaction was performed at the SHARAQ spectrometer in RIBF.[3] As a result, four candidate events of the resonance state were found with a 4.9σ significance level, and the excitation energy of $4n$ was determined as $E_{4n} = 0.83 \pm 0.65$ (stat.) $\pm$ 1.25 (syst.) MeV, which is close to the threshold.

To decide that the tetra-neutron state is a bound ($E_{4n} < 0$) or resonance ($E_{4n} > 0$) state, it is necessary to reduce the systematic uncertainty for the excitation energy of $4n$. Then, we performed a new measurement to obtain more statistics than the previous experiment and reduce the uncertainty of the energy of the $4n$ state.

The ^{1}H(^{3}H,^{3}He) reaction with the same magnetic rigidity of the ^{8}He beam (8.3 Tm) was used to determine a missing-mass calibration. Thus, the energy can be calibrated without changing the magnet settings. This is the reason why we do not have to consider the scaling errors of magnetic fields. The accuracy of the excitation energy of $4n$ is evaluated to be approximately 100 keV, which originated from the uncertainty of the energy reference.

In order to obtain more statistics than the previous experiment, the intensity of the ^{8}He secondary beam of 186 MeV/nucleon was approximately twice that in the previous experiment (3.5×10^6 cps at F3 focal plane).[4] At the "F3 (achromatic focus for beam trigger)," "F6 (dispersive focus)," and "S0 (achromatic focus for the secondary target)," low-pressure multi-wired drift chambers (LP-MWDCs) were used for tracking the beam. Events for the physics run were triggered by the S2 plastic scintillator at the focal plane of the SHARAQ spectrometer. Because of the high-rate beam condition, a single event may contain multiple hits at the drift chambers over several beam bunches of 13.7 MHz (RF frequency), considering the maximum drift time for the MWDCs is comparable to the interval of the beam bunch. Hence it is necessary to treat information of the redundant planes and other detectors.

In order to estimate the number of true four-neutron events, a strict cut satisfying the condition that the two clusters at the cathode planes of S2 have consistent energy signals with 2 α particles oeiginating in the ^{8}Be is analyzed. A preliminary analysis shows an similar event pattern in a spectrum as a function of the momenta of ^{8}He and ^{8}Be that is similar to the previous experiment. Considering the analyzed area of the decay cone of ^{8}Be, we expect approximately 2–3 times more statistics than the previous experiment.

A more precise calibration for the missing-mass spectrum taking into account the energy loss and straggling at the detectors and the target to reduce systematic errors will be performed concurrently.

In summary, we are still attempting to purify true events for increasing statistics with careful rejection conditions for the background. In parallel, missing-mass calibration will be tuned up to increase the accuracy of the $4n$ energy. Further analysis is ongoing.

References
1) F. M. Marqués *et al.*, Phys. Rev. C **65**, 044006 (2002).
2) S. C. Pieper, Phys. Rev. Lett. **90**, 252501 (2003).
3) K. Kisamori *et al.*, Phys. Rev. Lett. **116**, 052501 (2016).
4) S. Masuoka *et al.*, RIKEN Accel. Prog. Rep. **50**, 198 (2017).

*1   Center for Nuclear Study, the University of Tokyo
*2   RIKEN Nishina Center
*3   Department of Physics, Toho University
*4   Research Center for Nuclear Physics, Osaka University
*5   Department of Physics, Tokyo Institute of Technology
*6   Faculty of Engineering, Univ. of Miyazaki
*7   Laboratorie de Physique Corpusculaire, IN2P3-CNRS, EN-SICAEN et Université de Caen
*8   Department of Physics, the University of Tokyo

Measurement of ^{77,79}Se(d, p)^{78,80}Se reactions as a surrogate for ^{79}Se(n, γ)^{80}Se reaction

N. Imai,[*1] M. Dozono,[*1] S. Michimasa,[*1] T. Sumikama,[*2] S. Ota,[*1] S. Hayakawa,[*1] K. Iribe,[*3] C. Iwamoto,[*1] S. Kawase,[*4] K. Kawata,[*1,*2] N. Kitamura,[*1] S. Masuoka,[*1] K. Nakano,[*4] P. Schrock,[*1] D. Suzuki,[*2] R. Tsunoda,[*1] K. Wimmer,[*5] D.S. Ahn,[*2] O. Beliuskina,[*1] N. Chiga,[*2] N. Fukuda,[*2] E. Ideguchi,[*6] K. Kusaka,[*2] H. Miki,[*7] H. Miyatake,[*8] D. Nagae,[*2] M. Nakano,[*9] S. Ohmika,[*2] M. Ohtake,[*2] H. Otsu,[*2] H.J Ong,[*6] S. Sato,[*9] H. Shimizu,[*1] Y. Shimizu,[*2] H. Sakurai,[*2,*5] X. Sun,[*2] H. Suzuki,[*2] M. Takaki,[*1] H. Takeda,[*2] S. Takeuchi,[*7] T. Teranishi,[*3] Y. Watanabe,[*4] Y.X. Watanabe,[*8] H. Yamada,[*7] H. Yamaguchi,[*1] L. Yang,[*1] R. Yanagihara,[*6] K. Yoshida,[*2] Y. Yanagisawa,[*2] and S. Shimoura[*1]

To design a facility for decommissioning the spent fuel from nuclear power plants containing long-lived fission products (LLFPs), more nuclear reaction data is needed. Within the ImPACT program, thus far several nuclear reactions of LLFPs produced by Bi-gRIPS impinging on nuclear and proton targets have been measured.[1] Because of the longer mean free path, the transmutation with neutrons can be applied more efficiently. However, since both the neutron and the LLFPs are unstable, the measurement of the neutron-induced cross section requires a neutron facility, in addition to enriched radioactive targets. Instead, the re-action cross-section can be determined in an indirect way employing a surrogate reaction.

It is generally assumed that the (n, γ) cross section separates into two parts: the formation of the compound state and it's subsequent decay. The first term can be calculated using the optical model potentials with global parameters. On the other hand, the theoretical estimates of the second process are uncertain,and need to be validated by experiments.[2] The present work aims to determine the γ emission probability from unbound states of ^{80}Se by using the (d, p) reaction as a surrogate for the ^{79}Se(n, γ)^{80}Se reaction. The method will be tested by measuring the ^{77}Se(d,p)^{78}Se reaction, which is the surrogate for ^{77}Se(n,γ)^{78}Se, which was previously measured.[4]

The ^{77,79}Se beams were produced using the ^{238}U beam impinging on a 3-mm-thick ^{9}Be target. By using this relatively thin primary target and a thick 15-mm Al degrader at F1, a purity of approximately 40% was achieved. Since the total intensity at F3 was approximately 1 MHz, beam particles were identified by the time-of-flight between F3 and F5 measured with diamond detectors alone. The beam energy was further degraded at F5 using a 3.5-mm-thick Al degrader, re-
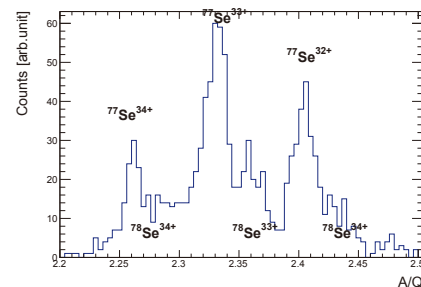
Fig. 1. A/Q spectrum measured at S1 focal plane for the events coincident with the protons detected with TiNA.

sulting in a final value of 26 MeV/nucleon. The OEDO facility[3] was employed to reduce the spatial spread of the beam, resulting in a beam spot of 30 mm FWHM on the secondary target.

The beam from OEDO impinged on a CD_2 target of 4 mg/cm^2 to induce the one-nucleon transfer reaction. The recoiled particles were identified by employing the SSD-CsI(Tl) array, TiNA,[5] which covered 100 to 150° in the laboratory frame. The excitation energies of the state populated in ^{78}Se (^{80}Se) were determined from the measured four-momenta of the protons and the direction of the incident beam.

The outgoing beam-like particles were identified with the dE-E-Bρ method, shown in Fig. 1, using the momentum determined by the horizontal position at the S1 focal plane. This will allow for a determination of the γ-ray emission probability as a function of excitation energy based on the fraction of (N+1,Z) nuclei to (N,Z) residues detected in coincidence with protons in TiNA. Further analysis is ongoing.

*1   Center for Nuclear Study, University of Tokyo
*2   RIKEN Nishina Center
*3   Department of Physics, Kyushu Univ.
*4   Department of Advanced Energy Engineering Science, Kyushu Univ.
*5   Department of Physics, Univ. of Tokyo
*6   RCNP, Osaka University
*7   Department of Physics, Tokyo Insititute of Technology
*8   WNSC, IPNS, KEK
*9   Department of Physics, Rikkyo University

References
1) H. Wang *et al.*, Phys. Lett. **B 754**, 104 (2016).
2) J. E. Escher *et al.*, Rev. Mod. Phys. **84**, 353 (2012).
3) S. Michimasa *et al.*, in this report.
4) S. Kawada, M. Igashira, T. Katabuchi, M. Mizumoto, J. Nucl. Sci. Tech. **47**, 643 (2010).
5) P. Schrock *et al.*, in this report.

Spallation reaction study of ^{136}Xe on proton, deuteron and carbon

X. Sun,[*1] H. Wang,[*1] H. Otsu,[*1] H. Sakurai,[*1] D. S. Ahn,[*1] M. Aikawa,[*2] P. Doornenbal,[*1] N. Fukuda,[*1] T. Isobe,[*1] S. Kawakami,[*3] S. Koyama,[*4] T. Kubo,[*1] S. Kubono,[*1] G. Lorusso,[*1] Y. Maeda,[*3] A. Makinaga,[*5] S. Momiyama,[*4] K. Nakano,[*6] M. Niikura,[*4] Y. Shiga,[*7,*1] P.-A. Söderström,[*1] H. Suzuki,[*1] H. Takeda,[*1] S. Takeuchi,[*1] R. Taniuchi,[*4,*1] Ya. Watanabe,[*1] Yu. Watanabe,[*6] H. Yamasaki,[*4] and K. Yoshida[*1]

Spallation reactions have been attracting considerable interest for their usefulness in the fundamental research to produce unstable nuclei[1] as well as in applications to transmute nuclear waste in accelerator-driven systems (ADS).[2] For these two purposes, it is important to have a comprehensive understanding of the spallation reaction mechanism both experimentally and theoretically. ^{136}Xe is a good candidate for both the fields. For the fundamental research, fragmentation and/or spallation of ^{136}Xe is well known to be one of the power tools to access unstable nuclei. On the other hand, ^{136}Xe is a stable isotope neighboring the long-lived fission product ^{137}Cs, whose spallation reaction has been studied recently for nuclear waste transmutation.[3] The experimental data of ^{136}Xe will be a good benchmark for the theoretical calculations of ^{137}Cs. The comparison between the reaction of ^{136}Xe and ^{137}Cs is critical for checking the validity of the model calculation and clarifying the reaction mechanism. Several experiments have been performed for spallation reactions of ^{136}Xe at reaction energies of 500 AMeV[4] and 1000 AMeV.[5] In the present work, the proton-, deuteron-, and carbon-induced reactions of ^{136}Xe at 168 AMeV have been studied.

The experiment was performed using BigRIPS and ZeroDegree spectrometer. The setup was the same as the one for ^{137}Cs.[3] The average intensity of the ^{136}Xe beams was 2.6×10^3 particles per second.

The isotopic distributions of the cross sections obtained in the present work are plotted in Fig. 1. In general, the cross sections on carbon (σ_C) are similar to the ones on deuteron (σ_d). The Cs isotopes in Fig. 1(a) are produced by charge-exchange reactions ($\Delta Z = +1$). In this channel, both σ_C and σ_d are smaller than the cross sections on proton (σ_p). This behavior of the charge-exchange reaction is consistent with the studies of ^{137}Cs and ^{90}Sr at 185 AMeV.[3] For the Xe isotopes, σ_d is similar to σ_p; both are larger than σ_C. For the I and Te isotopes, σ_d and σ_C becomes larger than σ_p, especially in the neutron-deficient side. Such cross-section differences may be caused by the deposited energy. Deuteron and carbon have more nucleons than proton leading to the deposition of a higher energy relative to proton. This enables a large evaporation of nucleons.

The EPAX[6] calculations are plotted in Fig. 1, in order to compare them with the experimental results. For both carbon and deuteron, EPAX calculations underestimate the cross sections, especially in the neutron-deficient side for the Xe, I, and Te isotopes. In the case of proton, EPAX was found to underestimate the cross sections by for the Xe and I isotopes. For the Te isotopes, EPAX overestimated the cross sections in the neutron-deficient side. For the cross sections on proton, the differences between the EPAX calculations and experimental results are similar to the ones observed in the reactions of ^{137}Cs.[3]
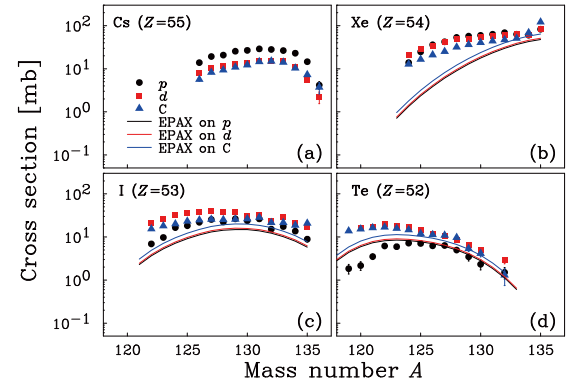
Fig. 1. Isotopic distribution of the cross sections for products from cesium element to tellurium element produced in the reaction ^{136}Xe + p(circle), ^{136}Xe + d(square), and ^{136}Xe + C(triangle) at 168 AMeV. EPAX calculations are displayed for comparison. The error bar shows the statistical uncertainties.

References
1) H. Suzuki *et al.*, Nucl. Instrum. Methods B **317**, 756 (2013).
2) C. D. Bowman *et al.*, Nucl. Instrum. Methods A **320**, 336 (1992).
3) H. Wang *et al.*, Phys. Lett. B **754**, 104 (2016).
4) J. Alcántara-Núñez *et al.*, Phys. Rev. C **92**, 024607 (2015).
5) P. Napolitani *et al.*, Phys. Rev. C **76**, 064609 (2007).
6) K. Sümmerer *et al.*, Phys. Rev. C **61**, 034607 (2000).

*1   RIKEN Nishina Center
*2   Faculty of Science, Hokkaido University
*3   Department of Applied Physics, University of Miyazaki
*4   Department of Physics, University of Tokyo
*5   Graduate School of Medicine, Hokkaido University
*6   Department of Advanced Energy Engineering Science, Kyushu University
*7   Department of Physics, Rikkyo University

Measurements of new beta-delayed neutron emission properties around doubly magic ^{78}Ni

K. Rykaczewski,[*1] N. Brewer,[*1] B. Rasco,[*1] D. Stracener,[*1] R. Yokoyama,[*2] R. Grzywacz,[*2] J. L. Tain,[*3]
J. Agramunt,[*3] A. Tolosa-Delgado,[*3] C. Domingo-Pardo,[*3] A. Algora,[*3] A. I. Morales,[*3] S. Nishimura,[*4]
N. Fukuda,[*4] K. Matsui,[*4] P. Vi,[*4] J. Liu,[*4] H. Baba,[*4] G. Kiss,[*4] S. Go,[*4] S. Kubono,[*4] H. Sakurai,[*4]
A. Tarifeno-Saldivia,[*5] F. Calvino,[*5] I. Dillmann,[*6] R. Caballero-Foch,[*6] T. Davinson,[*7] P. Woods,[*7]
C. Griffin,[*7] A. Estrade,[*8] N. Nepal,[*8] R. Surman,[*9] G. Lorusso,[*10]
and K. Miernik[*11] for the BRIKEN Collaboration

The measurement of new beta-delayed (multi) neutron emission (βxn) properties for nuclei near doubly-magic ^{78}Ni has been performed in May 2017 at RIKEN. Exotic nuclei produced with the 345 MeV/nucleon ^{238}U beam and ^{9}Be target, were studied by means of BigRIPS and using the world-largest array of ^{3}He counters BRIKEN,[1] a highly segmented array of Silicon detectors AIDA[2] and 2 Ge clovers. This hybrid setup has nearly 70% efficiency for detecting one neutron having up to 1 MeV and over 50% for 5 MeV energy. The BigRIPS setting was maximized for the transmission of ^{84}Zn. The isotopes between ^{74}Co-^{78}Co up to ^{97}Kr-^{100}Kr were produced and identified. This 3-day run with 30 to 50 particle-nA beam intensity yielded over 7000 ^{78}Ni ions implanted into AIDA (analysis A. Tolosa-Delgado). The ^{77}Cu test case resulted in β1n branching ratio $P_{1n} = 29(1)\%$ in a good agreement with the known value of 30.3(22)%.[3] The β1n and β2n values for ^{86}Ga decay[4] known as 60(10)% and 20(10)%, respectively, were obtained more precisely as 59(3)% and 16(1)%, see Fig. 1. Over 20 new P_{1n} values have been measured. Predicted β2n decay mode[5,6] has been inspected in over 14 isotopes yielding for the first time P_{2n} values, $e.g.$, for the activities of ^{84}Zn, ^{87}Ga, ^{89}Ge, ^{90}As and ^{91}As. New half-lives ($T_{1/2}$) have been measured using selective time and space correlation between ion, beta, and neutron signals, see ^{87}Ga decay in Fig. 1. New data on the βxn branching ratios together with newly measured half-lives will be used to verify and further develop beta decay modeling,[7] in particular modeling of the competition of the β1n/2n decay modes. Large set of new P_{xn} and $T_{1/2}$ values, obtained near and beyond doubly-magic waiting point nucleus ^{78}Ni, will help to develop further the analysis of heavy nuclei production within the astrophysical r-process, occurring, $e.g.$, at the merging neutron star environment.[8] *Preliminary data analysis was performed by N. Brewer, B. Rasco and R. Yokoyama.*
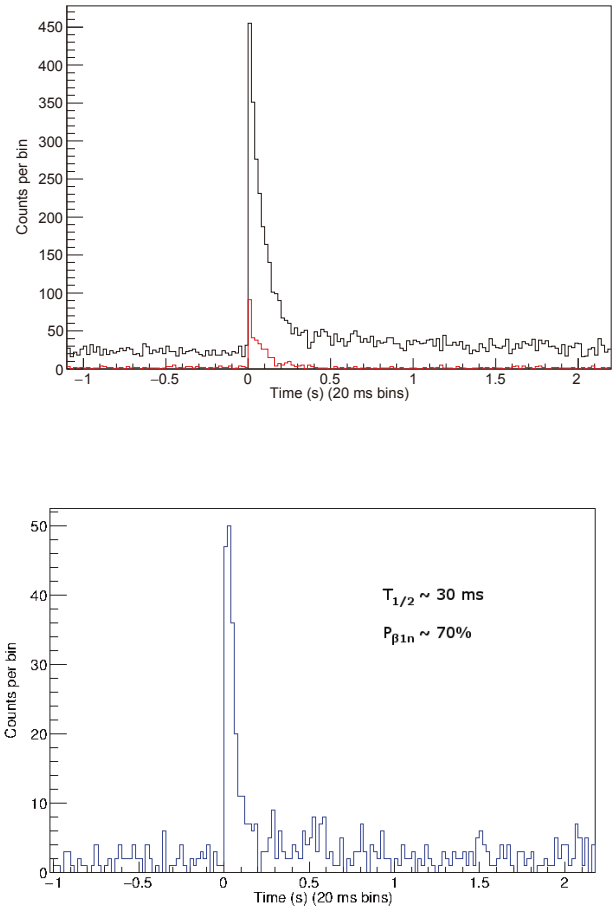
Fig. 1. (upper panel) Decay pattern of 1n (in black) and 2n (in red) events in coincidence with β-emission following identified ^{86}Ga ion implantation into AIDA; (lower panel) decay pattern of β1n events in the decay of identified ^{87}Ga ions in AIDA.

References
1) Tarifeno-Saldivia *et al.*, J. Instrum. **12**, 04006 (2017).
2) Griffin *et al.*, PoS, **NIC-XIII**, 097 (2014).
3) Ilyushkin *et al.*, Phys. Rev. C **80**, 054304 (2009).
4) Miernik *et al.*, Phys. Rev. Lett. **111**, 132502 (2013).
5) Moeller *et al.*, Phys. Rev. C **67**, 055802 (2003). http://t2.lanl.gov/nis/molleretal/publications/tpnff.dat
6) Miernik, Phys. Rev. C **90**, 054306 (2014).
7) Yokoyama *et al.*, in preparation.
8) Abbott *et al.*, Phys. Rev. Lett. **119**, 161101 (2017).

*1　ORNL Physics Division Oak Ridge
*2　Uni. Tennessee Knoxville
*3　IFIC Valencia
*4　RIKEN Nishina Center
*5　UPC Barcelona
*6　TRIUMF Vancouver
*7　Uni. Edinburgh
*8　CMU M. Pleasant
*9　Uni. Notre Dame
*10　NPL Teddington
*11　Uni. Warsaw

Beta-neutron-gamma spectroscopy of beta-delayed neutron emitters around doubly-magic ^{78}Ni

K. Rykaczewski,[*1] N. Brewer,[*1] B. Rasco,[*1] J. M. Allmond,[*1] D. Stracener,[*1] S. Nishimura,[*2] N. Fukuda,[*2]
K. Matsui,[*2] P. Vi,[*2] H. Baba,[*2] J. Liu,[*2] S. Go,[*2] G. Kiss,[*2] S. Kubono,[*2] H. Sakurai,[*2] D. Ahn,[*2]
H. Suzuki,[*2] H. Takeda,[*2] H. Ueno,[*2] R. Yokoyama,[*3] R. Grzywacz,[*3] T. King,[*3] M. Madurga,[*3] M. Singh,[*3]
J. L. Tain,[*4] J. Agramunt,[*4] A. Tolosa-Delgado,[*4] A. Algora,[*4] B. Rubio,[*4] A. Tarifeno-Saldivia,[*5] F. Calvino,[*5]
I. Dillmann,[*6] R. Caballero-Foch,[*6] T. Davinson,[*7] C. Griffin,[*7] A. Estrade,[*8] N. Nepal,[*8] R. Surman,[*9]
G. Lorusso,[*10] A. Korgul,[*11] K. Miernik,[*11] and M. Wolińska-Cichocka[*12] for the BRIKEN Collaboration

The experiment focused on beta-neutron-gamma spectroscopy of βn-emitters nuclei around ^{78}Ni has been performed during 10 days in November 2017 at RIKEN. Exotic nuclei produced with the 345 MeV/nucleon ^{238}U beam reaching nearly 70 particle-nA and ^{9}Be target, were studied by BRIKEN Collaboration[1] by means of BigRIPS. BRIKEN array has been modified in comparison to its first round of experiments, in order to achieve larger gamma efficiency. The AIDA implantation and decay array has been replaced by four smaller double-sided Si-strip counters of WASABI[2] and complemented by a position sensitive detector based on YSO scintillator developed at the UTK. It allowed us to move two Ge clovers of ORNL CLARION array few cm closer to the ion implantation and decay counters increasing gamma counting efficiency. This hybrid setup has kept its high efficiency for detecting beta-delayed neutrons.[1] The BigRIPS setting was maximized for the transmission of ^{82}Cu. Isotopes between ^{61}V–^{69}V up to ^{95}Br–^{97}Br were produced and identified. In comparison to the first run,[3] the counting statistics for most exotic ions was increased by about an order of magnitude, e.g., over 60,000 ^{78}Ni ions were produced and new Co to Ga isotopes were observed in the particle identification plot.[4] The on-line results for the gamma spectra recorded after the implantation of ^{78}Ni fragments are presented in Fig. 1. On should note an intense 283 keV gamma transition observed in the correlation with beta and one neutron signals. It identifies new lowest energy level at 284 keV in ^{77}Cu, not observed through the recent extensive study of ^{77}Ni beta-gamma decay identifying the lowest $(3/2^+)$ state at 293 keV.[5] It points to the discovery potential and selectivity of experiments adding efficient neutron detection to the beta-gamma counting. On-line evaluation pointed to
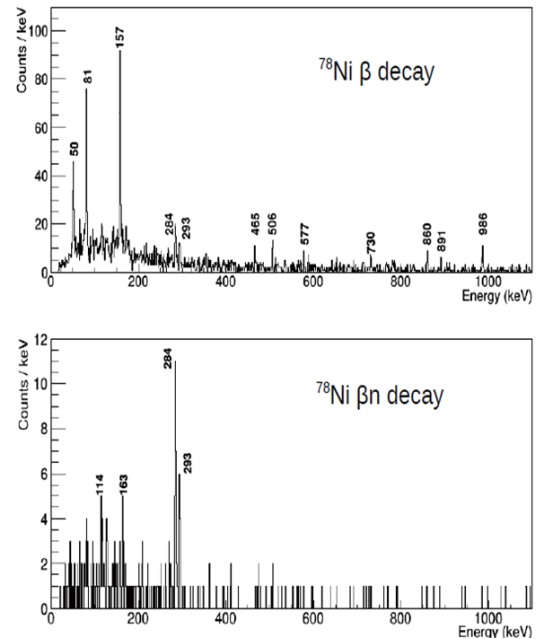
Fig. 1. Low-energy part of gamma spectra following ^{78}Ni decay. Upper part displays beta-gamma data, while lower panel selects beta-1n-gamma correlations (on-line analysis P. Vi and J. Liu).

the evidence for a gamma transition

observed in the decays of ^{81}Cu and ^{82}Cu and interpreted as the de-excitation of the $1/2^+$ state to the $5/2^+$ ground state in the $N = 50$ isotone ^{81}Zn, compare $N = 50$ ^{83}Ge structure[6] studied through ^{83}Ga and ^{84}Ga decays. New data on the observed beta-gamma and beta-xn-gamma correlations together with newly measured half-lives and beta-delayed xn branching ratios will be used to verify and further develop the modeling of nuclear structure evolution and following beta decay properties at and beyond $N = 50$ shell closure.

[*1]　Phys. Div. ORNL Oak Ridge
[*2]　RIKEN Nishina Center
[*3]　Uni. Tennessee Knoxville
[*4]　IFIC Valencia
[*5]　UPC Barcelona
[*6]　TRIUMF Vancouver
[*7]　Uni. Edinburgh
[*8]　CMU Mount Pleasant
[*9]　Uni. Notre Dame
[*10]　NPL Teddington
[*11]　Inst. Exp. Phys. Uni. Warsaw
[*12]　HIL Uni. Warsaw

References
1) A. Tarifeno-Saldivia et al., J. Instrum. 12, 04006 (2017).
2) S. Nishimura, Prog. Theor. Exp. Phys. 2012, 3C006 (2012).
3) R. Rykaczewski et al., in this report.
4) Y. Shimizu et al., in this report.
5) E. Sahin et al., Phys. Rev. Lett. 118, 242502 (2017).
6) J. A. Winger et al., Phys. Rev. C 81, 044303 (2010).

Measuring the β-decay properties of Na-Al species located at the neutron drip line

V. H. Phong,[*1] G. G. Kiss,[*1,*2] S. Nishimura,[*1] I. Dillmann,[*3] D. S. Ahn,[*1] A. Agramunt,[*4] A. Algora,[*2,*4]
H. Baba,[*1] N. T. Brewer,[*5] R. Caballero Folch,[*3] T. Davinson,[*6] A. Estrade,[*7] N. Fukuda,[*1] S. Go,[*1]
R. K. Grzywacz,[*8] C. J. Griffin,[*6] O. Hall,[*6] T. Isobe,[*1] D. Kahl,[*6] S. Kubono,[*1] K. Matsui,[*1] M. Labiche,[*9]
J. Liu,[*1,*10] B. C. Rasco,[*5] K. P. Rykaczewski,[*5] Y. Saito,[*3] H. Sakurai,[*1] Y. Shimizu,[*1] D. W. Stracener,[*5]
T. Sumikama,[*1] H. Suzuki,[*1] J. L. Tain,[*4] H. Takeda,[*1] A. Tarifeno-Saldivia,[*11] and A. Tolosa-Delgado[*4]
on behalf of the BRIKEN collaboration

The β-delayed neutron emission is a process that can occur when the neutron separation energy in the daughter nucleus (S_n) is smaller than the energy window for the β-decay (Q_β). The delayed neutron emission is characterized by the emission probability (P_n) which that yields information on both the β-strength distribution and the level structure of the daughter nucleus.[1]

The existing nuclear structure models approach the delayed neutron emission from different directions, depending on their underlying theoretical bases.[2–5] The difficulties in describing the neutron emission probabilities arise from the need to describe in detail the beta strength of the nucleus, implying an intimate knowledge of its single particle structure.

Of particular importance are the data on multiple neutron emission, as they provide valuable insight into the competition between γ-, one- and multi-neutron emission in highly exotic nuclei. Current models typically assume no competition between the various de-excitation channels, and emit as many neutrons as energetically possible. To improve the predictive powers of macroscopic models and our understanding of nuclear structure in general, more data are required.

The latest atomic mass evaluation lists 2451 isotopes, from which 300/138/58 are energetically allowed delayed 2/3/4 neutron emitters. So far only 23 P_{2n}, 4 P_{3n}, and only 1 P_{4n} values were measured.[6] The beta delayed neutron emission measurements at RIKEN (BRIKEN) project offers a unique opportunity to study this rare decay mode. The BRIKEN[7] setup consists of 140 ^{3}He gas-filled proportional counters embedded in a high-density polyethylene moderator. The neutron detector and two CLARION-type clover HPGe detectors are placed surrounding the AIDA DSSSD array,[8] which contains six layers of highly segmented Si detectors for
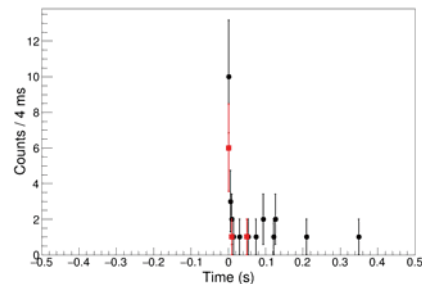
Fig. 1. Time distribution of the β particles emitted after the decay of ^{37}Na. Red and black circles show the data with and without neutron signals in coincidence at the BRIKEN detector, respectively.

the detection of implantations and beta electrons.

In April 2017, the first measurement addressing the multiple neutron emission was conducted in parasitic mode, together with a new isotope search experiment,[9] targeting the very neutron-rich species in the Na-Al region. The secondary beams, produced using a 345-MeV/nucleon energy ^{48}Ca primary beam impinging on a 20-mm thick Be target, were identified and purified using the BigRIPS spectrometer. They were then transported through the ZD spectrometer to reach the decay station located at the F11 focal plane.

The position and time correlations between the implantation and subsequent decay events were used to derive the half-lives of eight (^{35,37}Na, ^{38,40}Mg, ^{40,41,42}Al, and ^{43}Si) isotopes for the first time. Figure 1 shows the time distributions of β and β-n decays ^{37}Na isotope.

A more detailed analysis is in progress. The new data will constrain the theoretical models, and although in some cases the statistics is poor it will be used to optimize the recently accepted NP1712-RIBF159 experiment.

*1   RIKEN Nishina Center
*2   Institute for Nuclear Research (Atomki)
*3   TRIUMF
*4   Instituto de Fisica Corpuscular
*5   Oak Ridge National Laboratory
*6   School of Physics and Astronomy, University of Edinburgh
*7   College of Science and Engineering, Central Michigan University
*8   Department of Physics and Astronomy, University of Tennessee
*9   STFC Daresbury Laboratory
*10   Department of Physics, University of Hong Kong
*11   Institute of Energy Technologies, Universitat Politecnica de Catalunya

References
1) I. N. Borzov, Phys. Rev. C **71**, 065801 (2005).
2) P. Moeller *et al.*, Phys. Rev. C **67**, 055802 (2003).
3) M. Mumpower *et al.*, Phys. Rev. C **94**, 064317 (2016).
4) T. Marketin *et al.*, Phys. Rev. C **93**, 025805 (2016).
5) K. Miernik, Phys. Rev. C **90**, 054306 (2014).
6) M. Birch *et al.*, Nuclear Data Sheets **128**, 131 (2015).
7) A. Tarifeno-Saldivia *et al.*, Jour. of Instr. **12**, P04006 (2016).
8) C. Griffin *et al.*, PoS (NIC-XIII) 097 (2014).
9) S. Ahn *et al.*, DA16-01.

Measurement of β-delayed neutron emission probabilities for progenitors of the $A = 130$ r-process abundance peak

J. Liu,[*1] V. H. Phong,[*2,*3] A. Estrade,[*4] G. Lorusso,[*2,*5] F. Montes,[*6] T. Davinson,[*7] O. Hall,[*7] K. Matsui,[*2] N. Nepal,[*4] S. Nishimura,[*2] J. Agramunt,[*8] D. S. Ahn,[*2] A. Algora,[*8] H. Baba,[*2] N. T. Brewer,[*9] C. Bruno,[*7] R. Caballero-Folch,[*10] F. Calvino,[*11] I. Dillmann,[*10] C. Domingo-Pardo,[*8] S. Go,[*12] C. J. Griffin,[*7] R. Grzywacz,[*9,*12] T. Isobe,[*2] D. Kahl,[*7] G. Kiss,[*2] S. Kubono,[*2] A. I. Morales,[*8] B. C. Rasco,[*9] K. P. Rykaczewski,[*9] H. Sakurai,[*2] Y. Shimizu,[*2] T. Sumikama,[*2] H. Suzuki,[*2] H. Takeda,[*2] J. L. Tain,[*8] A. Tarifeno-Saldivia,[*11] A. Tolosa-Delgado,[*8] P. Woods,[*7] and R. Yokoyama[*12] for the BRIKEN collaboration

The first observation of a merger of two neutron stars,[1] with both gravitational and electromagnetic wave signals, offers tantalizing opportunities to finally identify the astrophysical site of the r-process. The new observations will increase the demand for precise nuclear data necessary to reach a detailed understanding of the r-process mechanism. The r-process abundance peak around $A = 130$ is of particular interest because its shape and position is very sensitive to the the neutron-richness of the astrophysical environment, as its formation reflects the break-out of the reaction flow from the $N = 82$ classical waiting point isotopes. However, the effect on the final r-process abundance is obscured by a numbers of β-delayed neutron emitters along the decay path back to stability. In fact, the β-delayed neutron emission probabilities (P_n values) in the region south-east of ^{132}Sn have a most pronounced effect on the final r-process abundance, according to the recent sensitivity study in Ref. 2).

In June 2017, we have performed an experiment to study the decay properties of the β-delayed neutron emitters in the mass region $A = 130$ near the doubly magic nucleus ^{132}Sn. These neutron-rich isotopes were produced by the projectile fragmentation of a 345 MeV/nucleon ^{238}U beam on a Be target, before being purified and identified by the BigRIPS spectrometer. They were then transported through the Zero-degree spectrometer to reach the decay station located at the F11 focal plane. In the decay station, the active stopper array AIDA[3] was placed at a central position for the implantation of nuclei of interested, and it detected their subsequent β decay. The AIDA detector is a stack of six 8×8 cm^2 DSSDs with 128×128 pixels each. Neutrons emitted from the β decay of ions implanted in AIDA were detected by the BRIKEN neu-
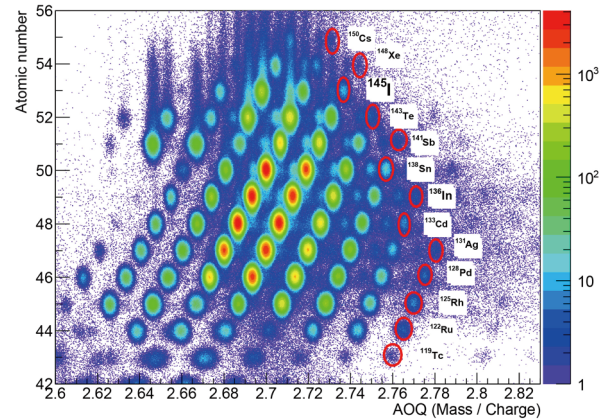
Fig. 1. Particle identification plot for isotopes transported to the decay station at F11, indicating the most neutron-rich isotopes for each element.

tron detector array[4] consisting of 140 gas-filled ^{3}He counters, which were inside a large moderation block made of high-density polyethylene. In addition, two clover-type high-purity Germanium detectors were employed to measure β-delayed and isomeric γ rays.

The particle identification plot combining data of the two settings of the experiment, centered at ^{130}Ag and ^{140}Xe, is shown in Fig. 1. The data analysis is ongoing. Preliminary results indicate that new or improved measurements of P_n values will be obtained for over 40 isotopes, and for 11 isotopes in the case of half-lives. These new measurements would make a significant contribution to the available experimental data for r-process models.

References
1) Abbott *et al.*, Phys. Rev. Lett. **119**, 161101 (2017).
2) M. R. Mumpower, R. Surman, G. C. McLaughlin, A. Aprahamian, Prog. Part. Nucl. Phys. **86**, 86 (2016).
3) C. J. Griffin *et al.*, Proc. XIII Nuclei in the Cosmos **1**, 97 (2014).
4) A. Tarifeño-Saldivia *et al.*, J. Instrum. **12**, 04006 (2017).

[*1] Department of Physics, The University of Hong Kong
[*2] RIKEN Nishina Center
[*3] Faculty of Physics, VNU Hanoi University of Science
[*4] Department of Physics, Central Michigan Univeristy
[*5] National Physics Laboratory(NPL)
[*6] National Superconducting Cyclotron Laboratory
[*7] School of Physics and Astronomy, University of Edinburgh
[*8] Instituto de Fisica Corpuscular, Universidad de Valencia
[*9] Oak Ridge National Laboratory
[*10] TRIUMF
[*14] Universitat Politecnica de Catalunya
[*12] Department of Physics and Astronomy, University of Tennessee

β-delayed neutron emission probabilities for understanding the formation of the r-process rare-earth peak

A. Tarifeño-Saldivia,[*1] G. G. Kiss,[*2,*3] A. I. Morales,[*4] A. Estrade,[*5] S. Nishimura,[*2] C. Domingo-Pardo,[*4]
A. Agramunt,[*4] D. S. Ahn,[*2] A. Algora,[*3,*4] H. Baba,[*2] N. T. Brewer,[*6] R. Caballero Folch,[*7] F. Calvino,[*1]
T. Davinson,[*8] I. Dillmann,[*7] N. Fukuda,[*2] S. Go,[*2] R. K. Grzywacz,[*9] O. Hall,[*8] L. Harkness-Brennan,[*8]
T. Isobe,[*2] C. J. Griffin,[*8] D. Kahl,[*8] A. Korgul,[*10] S. Kubono,[*2] M. Labiche,[*11] J. Liu,[*2] K. Matsui,[*2]
K. Miernik,[*10] N. Nepal,[*5] B. C. Rasco,[*6] K. P. Rykaczewski,[*6] Y. Saito,[*7] H. Sakurai,[*2] Y. Shimizu,[*2]
D.W. Stracener,[*6] T. Sumikama,[*2] H. Suzuki,[*2] J. L. Tain,[*4] H. Takeda,[*2] A. Tolosa,[*4] P. Vi,[*2] P. J. Woods,[*8]
and R. Yokoyama[*9]

The main signatures of the rapid-neutron capture process (so-called r-process) are the three large abundance maxima in the solar-system composition at masses of A∼80, 130, and 195, which are related to the flow of matter through the three neutron shell closures at N=50, 82, and 126. In contrast to these three characteristic peaks, there is a small—but distinct—peak around A∼160, that corresponds to the region of rare-earth elements. From the astrophysics point of view, the most interesting feature of the rare-earth peak (REP) is that, contrary to the three main maxima that form during (n, γ) ↔ (γ, n) equilibrium, the REP originates later, after neutron exhaustion, thus representing a unique opportunity to study the late-time environmental conditions.

Although several different production mechanisms were suggested, most models agree on the fact that β-delayed neutron emission plays a crucial role in the REP formation.[1–3] Recently, the largest and most efficient β-delayed neutron detector[4] was built by the BRIKEN collaboration at the RIKEN Nishina Center to study systematically the decay of very neutron-rich nuclei across the nuclear chart. The so-called BRIKEN neutron detector consists of 140 ³He gas-filled proportional counters embedded in a high-density polyethylene moderator. The neutron detector and two CLARION-type clover HPGe detectors are placed around the AIDA DSSSD array,[5] which contains six layers of highly segmented Si detectors for the detection of implantations and beta electrons.

The NP1612-RIBF148 experiment is focused on the measurement of the β-delayed neutron emitters, which are critical for the formation of the REP in the solar system abundances. In an exploratory run (∼25% total beamtime), performed in June 2017, the β decays of exotic Pr-Gd species were studied at the Radioactive Isotope Beam Factory. A 50-pnA-intensity ²³⁸U beam was
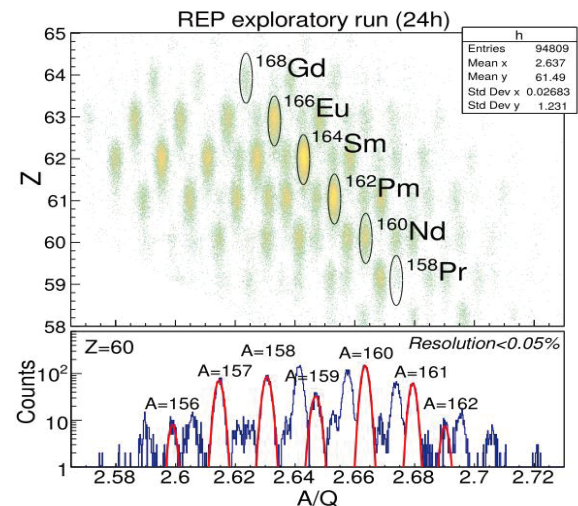
Fig. 1. PID of the exploratory run for the NP1612-RIBF148 experiment.

accelerated up to an energy of 345 MeV/nucleon before it was incident on a 4-mm-thick Be target to produce radioactive secondary beams by in-flight fission. The nuclei of interest were separated and identified in the BigRIPS spectrometer, transported through the Zero-Dregree spectrometer and implanted in the AIDA array. Figure 1 (top) shows the particle identification matrix for the statistics accumulated during the first 24 h. The bottom panel of Fig. 1 shows the projection of the PID matrix on the A/Q axis for the Nd isotopes; the A/Q resolution achieved—less than 0.05%—ensures a good separation of fully- stripped and H-like ions. The results of the exploratory run are promising; for the first time ever, key REP progenitors[3] have become accessible and the study of their beta decay properties will be possible thanks to the use of the state-of-the-art detectors BRIKEN and AIDA. Our intention is to continue the experiment as soon as the ²³⁸U beam is available again.

References
1) R. M. Mumpower, R. Surman, G. C. McLaughlin, A. Aprahamian, Prog. Part. Nucl. Phys. **86**, 86 (2016).
2) A. Arcones, G. Martinez Pinedo, Phys. Rev. C **83**, 045809 (2011).
3) M. Mumpower et al., Prog. Part. Nucl. Phys. **86**, 86 (2016).
4) A. Tarifeno-Saldivia et al., Jour. of Instr. **12**, P04006 (2016).
5) C. Griffin et al., POS (NIC-XIII) 097 (2014).

*1 Universitat Politècnica de Catalunya (UPC)
*2 RIKEN Nishina Center
*3 Institute for Nuclear Research (Atomki)
*4 Instituto de Física Corpuscular
*5 College of Science and Engineering, Central Michigan University
*6 Oak Ridge National Laboratory
*7 TRIUMF
*8 School of Physics and Astronomy, University of Edinburgh
*9 Department of Physics and Astronomy, University of Tennessee
*10 Department of Physics, University of Warsaw
*11 STFC Daresbury Laboratory

Study of the superallowed $0^+ \rightarrow 0^+$ β decay of ^{70}Br[†]

A. I. Morales,[*1] A. Algora,[*1,*2] B. Rubio,[*1] K. Kaneko,[*3] J. Agramunt,[*1] V. Guadilla,[*1] A. Montaner-Pizá,[*1]
S. E. A. Orrigo,[*1] G. de Angelis,[*4] D. Napoli,[*4] F. Recchia,[*5] S. Lenzi,[*5] A. Boso,[*5] S. Nishimura,[*6] G. Kiss,[*6]
V. H. Phong,[*6] J. Wu,[*6] P.-A. Söderström,[*6] T. Sumikama,[*6] H. Suzuki,[*6] H. Takeda,[*6] D. S. Ahn,[*6]
H. Baba,[*6] P. Doornebal,[*6] N. Fukuda,[*6] N. Inabe,[*6] T. Isobe,[*6] T. Kubo,[*6] S. Kubono,[*6] H. Sakurai,[*6]
Y. Shimizu,[*6] C. Sidong,[*6] B. Blank,[*7] P. Ascher,[*7] M. Gerbaux,[*7] T. Goigoux,[*7] J. Giovinazzo,[*7] S. Grévy,[*7]
T. Kurtukián Nieto,[*7] C. Magron,[*7] W. Gelletly,[*1,*8] Zs. Dombrádi,[*7] Y. Fujita,[*9] M. Tanaka,[*9] P. Aguilera,[*10]
F. Molina,[*10] J. Eberth,[*11] F. Diel,[*11] D. Lubos,[*12] C. Borcea,[*13] E. Ganioglu,[*14] D. Nishimura,[*15]
H. Oikawa,[*15] Y. Takei,[*15] S. Yagi,[*15] W. Korten,[*16] G. de France,[*17] P. Davies,[*18] J. Liu,[*19] J. Lee,[*19]
T. Lokotko,[*19] I. Kojouharov,[*20] N. Kurz,[*20] and H. Shaffner[*20]

One of the core concepts of the Electroweak Standard Model (ESM) is the unitarity of the Cabibbo-Kobayashi-Maskawa (CKM) matrix which describes the mixing between the three families of quarks. Increasingly high-precision measurements of the CKM matrix elements are required to set the limits on any possible physics beyond the ESM. The largest matrix element, the up-down term V_{ud}, can be extracted from high-precision measurements of half-lives, masses, and branching ratios of superallowed β transitions between $J^\pi = 0^+$, $T = 1$ analog states starting in $N = Z$ nuclei.[1] In this report we provide the most precise half-life measurement for the $T = 1$ ($J^\pi = 0^+$) ground state of the heavy self-conjugate nucleus ^{70}Br and the first estimate of the total branching fraction decaying through the first 2^+ state in the daughter nucleus, ^{70}Se.

The ^{70}Br nuclei were produced in the fragmentation of a ^{78}Kr primary beam at 345 MeV/nucleon and 38 pnA colliding with a 5-mm thick Be target. After separation and selection in the BigRIPS separator, the nuclei were implanted in the WAS3ABi active stopper, surrounded by the EURICA γ-ray spectrometer.[2]

Standard delayed-coincidence techniques were applied to study the β decay of ^{70}Br, including an exhaustive evaluation of the factors that could influence the half-life measurement.[3] As an example, Fig. 1 shows
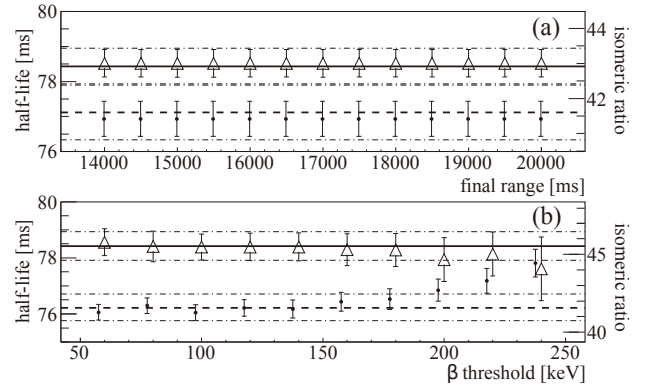
Fig. 1. Measured half-lives for the $T = 1$ ($J^\pi = 0^+$) ground state (empty triangles) and isomeric ratios for the $T = 0$ ($J^\pi = 9^+$) isomer (full dots) in ^{70}Br as a function of the fitting range (a) and the β threshold (b).

the half-life of the $T = 1$ ($J^\pi = 0^+$) ground state as a function of the fitting range (a) and the β threshold (b). The average half-life deduced is shown as a thick continuous line and the total error as dotted-dashed lines. The isomeric ratio of the $T = 0$ ($J^\pi = 9^+$) state is also shown for each lifetime fit and, in thick dashed line, the overall deduced value. The resulting half-lives for the $T = 0$ ($J^\pi = 9^+$) isomer and the $T = 1$ ($J^\pi = 0^+$) ground state, $t_{1/2} = 2157^{+53}_{-49}$ ms and $t_{1/2} = 78.42 \pm 0.51$ ms, respectively, are the most precise values reported hitherto in the literature.

The branching ratio of the superallowed $0^+ \rightarrow 0^+$ transition, $R = 97.94 \pm 1.75\%$, was estimated from the measured γ imbalance of the 2^+_1 level in ^{70}Se, as described in Ref. 3). This has allowed for a first estimate of the $\mathcal{F}t$ value associated with this decay, calling for a new mass measurement of ^{70}Br in order to confirm the Conserved Vector Current hypothesis.[1]

The analyses of the ^{70,71}Kr β and ^{71}Kr isomer decays are in progress.

References

1) J. C. Hardy, I. S. Towner, Phys. Rev. C **91**, 025501 (2015).
2) S. Nishimura, Prog. Theor. Exp. Phys. **03C006** (2012).
3) A. I. Morales *et al.*, Phys. Rev. C **95**, 064327 (2017).

Results on ^{64}As decay measured at BigRIPS

P. Aguilera,[*1,*2] B. Rubio,[*2] F. Molina,[*1] J. Agramunt,[*2] A. Algora,[*2] V. Guadilla,[*2] A. Montaner-Piza,[*2]
A. I. Morales,[*2] S. E. A. Orrigo,[*2] B. Blank,[*3] P. Ascher,[*3] M. Gerbaux,[*3] T. Goigoux,[*3] J. Giovinazzo,[*3]
S. Grévy,[*3] T. Kurtukian Nieto,[*3] C. Magron,[*3] D. Nishimura,[*4] J. Chiba,[*4] H. Oikawa,[*4] Y. Takei,[*4] S. Yagi,[*4]
D. S. Ahn,[*5] P. Doornenbal,[*5] N. Fukuda,[*5] N. Inabe,[*5] G. Kiss,[*5] T. Kubo,[*5] S. Kubono,[*5] S. Nishimura,[*5]
Y. Shimizu,[*5] C. Sidong,[*5] P. A. Söderström,[*5] T. Sumikama,[*5] H. Suzuki,[*5] H. Takeda,[*5] P. Vi,[*5] J. Wu,[*5]
Y. Fujita,[*6] M. Tanaka,[*6] W. Gelletly,[*2,*7] F. Diel,[*8] D. Lubos,[*9] G. de Angelis,[*10] D. Napoli,[*10] C. Borcea,[*11]
A. Boso,[*12] R. B. Cakirli,[*13] E. Ganioglu,[*13] G. de France,[*14] and S. Go[*15]

We have performed an experiment at RIKEN to study the decay of the $Tz= -2$ exotic nucleus ^{64}Se. Some preliminary results have been presented in Refs. 1) and 2). As shown in in Fig. 1 several nuclei are produced in the decay chain of ^{64}Se. This includes the $Tz= -1$ ^{64}As, where little is known and there is no information on the β delayed protons. Fortunately ^{64}As is produced directly in the primary reaction. By placing the implantation condition on ^{64}As we have obtained an improved value for the $T_{1/2}$ and the first experimental information on the β delayed protons.
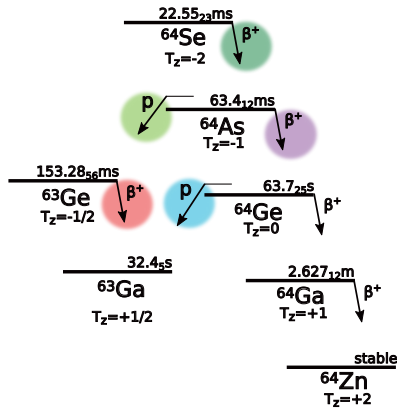
Fig. 1. Scheme showing the full decay chain of ^{64}Se. Pink colour indicates ^{64}As, the nucleus study in the report.

Both ^{64}Se and ^{64}As were produced in the fragmentation of a 345 MeV/u ^{78}Kr beam with typical intensity of 200 pnA on a Be target. The fragments were separated in flight using BigRIPS and implanted in

Fig. 2. Preliminary results on the β delayed protons emitted in the decay of ^{64}As using the implantation condition on ^{64}As (see text).
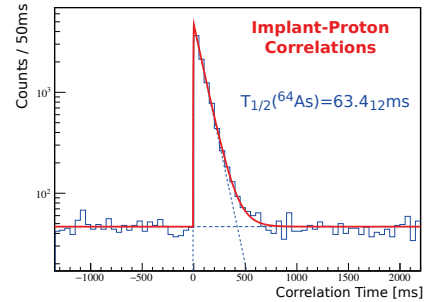
Fig. 3. The half life of ^{64}As based on implant-proton correlations using the implantation condition on ^{64}As.

WAS3ABi double-sided Si strip detectors. The implantation setup was surrounded by the Ge Array (EURICA).

In Figs. 2 and 3 we present the first experimental spectrum of the β delayed protons and the fit of the $T_{1/2}$ of ^{64}As derived from the correlations between the implanted ^{64}As ions in WAS3ABi and the particle decay in the same pixel. The proton spectrum was calibrated as in Ref. 2) and the $T_{1/2}$ analysis is described in Ref. 1). Information on the β delayed γ rays of ^{64}As is presented in a separate contribution to this Accelerator Progress Report.

[*1] Chilean Nuclear Energy Commision
[*2] IFIC, CSIC-Universidad de Valencia
[*3] Centre d'Etudes Nucléaires de Bordeaux-Gradignan
[*4] Department of Physics, Tokyo City University
[*5] RIKEN Nishina Center
[*6] Department of Physics, Osaka University
[*7] Department of Physics, Surrey University
[*8] Institute of Nuclear Physics, Universität zu Köln
[*9] Physics Department E-12, Technische Universität München
[*10] Istituto Nazionale di Fisica Nucleare, Laboratorio Nazionale di Legnaro
[*11] National Institute for Physics and Nuclear Engineering, IFIN-HH
[*12] Istituto Nazionale di Fisica Nucleare, Sezione di Padova
[*13] Department of Physics, Istanbul University
[*14] Grand Accélérateur National d'Ions Lourds
[*15] Department of Physics, Tennessee University

References
1) B. Rubio et al., RIKEN Accel. Prog. Rep. 49, 28 (2015).
2) P. Aguilera et al., RIKEN Accel. Prog. Rep. 50, 33 (2016).

γ rays identified in the decay chain of ⁶⁴Se measured with EURICA

P. Aguilera,[*1,*2] F. Molina,[*1] B. Rubio,[*2] J. Agramunt,[*2] A. Algora,[*2] V. Guadilla,[*2] A. Montaner-Piza,[*2]
A. I. Morales,[*2] S. E. A. Orrigo,[*2] B. Blank,[*3] P. Ascher,[*3] M. Gerbaux,[*3] T. Goigoux,[*3] J. Giovinazzo,[*3]
S. Grévy,[*3] T. Kurtukian Nieto,[*3] C. Magron,[*3] D. Nishimura,[*4] J. Chiba,[*4] H. Oikawa,[*4] Y. Takei,[*4] S. Yagi,[*4]
D. S. Ahn,[*5] P. Doornenbal,[*5] N. Fukuda,[*5] N. Inabe,[*5] G. Kiss,[*5] T. Kubo,[*5] S. Kubono,[*5] S. Nishimura,[*5]
Y. Shimizu,[*5] C. Sidong,[*5] P. A. Söderström,[*5] T. Sumikama,[*5] H. Suzuki,[*5] H. Takeda,[*5] P. Vi,[*5] J. Wu,[*5]
Y. Fujita,[*6] M. Tanaka,[*6] W. Gelletly,[*2,*7] F. Diel,[*8] D. Lubos,[*9] G. de Angelis,[*10] D. Napoli,[*10] C. Borcea,[*11]
A. Boso,[*12] R. B. Cakirli,[*13] E. Ganioglu,[*13] G. de France,[*14] and S. Go[*15]

In a separate contribution to this Accel. Prog. Rep.[1) we have presented the preliminary results for the β delayed proton spectrum of ⁶⁴As decay and its $T_{1/2}$. This was needed in order to fully understand the decay chain following the decay of ⁶⁴Se (see Fig. 1 in the separate contribution). Here we present some γ spectra that will help us to determine the complete decay chain. All of the data for the two contributions come from an experiment performed at RIKEN using the fragmentation of a 345 MeV/nucleon ⁷⁸Kr beam with typical intensity of 200 pnA on a Be target. The fragments were separated in flight using the BigRIPS separator and implanted in three WAS3ABi double-sided Si strip detectors. The implantation setup was surrounded by the EUROBALL-RIKEN Cluster Array (EURICA).[2) It consisted of 12 Euroball IV type HPGe cluster detectors, each consisting of seven tapered, hexagonal HPGe crystals at a nominal distance of 22 cm from the center. We have analysed the γ spectra in prompt coincidence with β signals happening in WAS3ABI in correlation with the implantation signals happening in the same pixel with the conditions set on ⁶⁴Se ($T_{1/2}$ = 22.5 ms), ⁶⁴As ($T_{1/2}$ = 63.4 ms), and ⁶³Ge ($T_{1/2}$ = 153.3 ms). The corresponding γ spectra in "addback" mode (considering the full cluster as a single detector) are shown in Fig. 1. In green are the gamma lines which appear in the spectrum with the condition on ⁶⁴Se implantation and not on the other two. Consequently they are identified as γ rays associated with the beta decay of ⁶⁴Se. Similarly, the lines marked in pink appear with the condition on ⁶⁴Se (as daughter activity) and ⁶⁴As and disappear when the condition is set on ⁶³Ge,
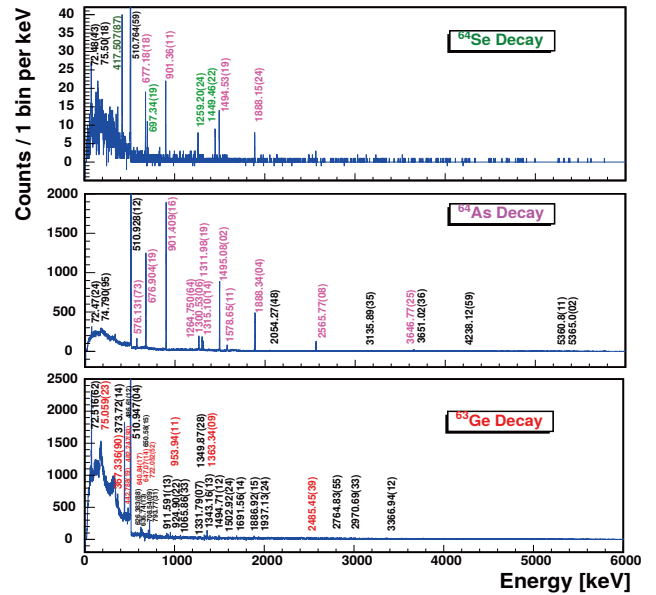
Fig. 1. Spectra showing the γ rays measured with the Ge array EURICA in correlation with implantation signal happening in WASABI with conditions on ⁶⁴Se, ⁶⁴As, and ⁶³Ge implanted ions (see text).

and are consequently associated with the β decay of ⁶⁴As. Finally the γ rays associated with the decay of ⁶³Ge are marked in red. Other possible activities in the decay chain have longer half-lives. No β delayed γ radiation was observed in any of the three cases prior to this work. The corresponding level schemes are in preparation.

References
1) P. Aguilera *et al.*, in this report.
2) P.-A. Söderström *et al.*, Nucl. Instrum. Methods Phys. Res. B **317**, 649–652 (2013).

*1　Chilean Nuclear Energy Commision
*2　IFIC, CSIC-Universidad de Valencia
*3　Centre d'Etudes Nucléaires de Bordeaux-Gradignan
*4　Department of Physics, Tokyo City University
*5　RIKEN Nishina Center
*6　Department of Physics, Osaka University
*7　Department of Physics, Surrey University
*8　Institute of Nuclear Physics, Universität zu Köln
*9　Physics Department E-12, Technische Universität München
*10　Istituto Nazionale di Fisica Nucleare, Laboratorio Nazionale di Legnaro
*11　National Institute for Physics and Nuclear Engineering, IFIN-HH
*12　Istituto Nazionale di Fisica Nucleare, Sezione di Padova
*13　Department of Physics, Istanbul University
*14　Grand Accélérateur National d'Ions Lourds
*15　Department of Physics, Tennessee University

Isomer-decay spectroscopy of ^{67}Fe and reaction-channel dependency of isomeric ratios from interactions in the MINOS proton target

P.-A. Söderström,[*1,*2,*3] L. X. Chung,[*4] A. Gillibert,[*5,*3] B. D. Linh,[*4] A. Obertelli,[*1,*3,*5] P. Doornenbal,[*3] S. Nishimura,[*3] F. Browne,[*6,*3] Z. Patel,[*7] C. Shand,[*7] J. Wu,[*3,*8] G. Authelet,[*5] H. Baba,[*3] D. Calvet,[*5] F. Château,[*5] A. Corsi,[*5,*3] A. Delbart,[*5,*3] Zs. Dombradi,[*9,*3] S. Franchoo,[*10] J.-M. Gheller,[*5,*3] F. Giacoppo,[*11] A. Gottardo,[*10] K. Hadyńska-Klęk,[*11] T. Isobe,[*3] I. Kojouharov,[*2] Z. Korkulu,[*9] S. Koyama,[*3,*12] Y. Kubota,[*3,*13] N. Kurz,[*2] V. Lapoux,[*5,*3] J. Lee,[*14] M. Lettmann,[*1] C. Louchart,[*1] R. Lozeva,[*15] K. Matsui,[*3,*12] M. Matsushita,[*13] T. Miyazaki,[*3,*12] S. Momiyama,[*3,*12] T. Motobayashi,[*3] M. Niikura,[*12,*3] L. Olivier,[*10] S. Ota,[*13] H. Otsu,[*3] C. Péron,[*5] A. Peyaud,[*5] N. Pietralla,[*1] E. C. Pollacco,[*5,*3] J.-Y. Roussé,[*5,*3] E. Sahin,[*11] H. Sakurai,[*3,*12] C. Santamaria,[*3,*5] M. Sasano,[*3] H. Schaffner,[*2] Y. Shiga,[*3,*16] I. G. Stefan,[*10] D. Steppenbeck,[*13,*3] T. Sumikama,[*17,*3] D. Suzuki,[*10] S. Takeuchi,[*3] R. Taniuchi,[*3,*12] T. Uesaka,[*3] Zs. Vajta,[*9] H. Wang,[*3] V. Werner,[*1] K. Yoneda,[*3] and Z. Y. Xu[*14]

In this report, we discuss the properties of the isomeric state in ^{67}Fe. While the existence of this isomer is already well established, its nature is still unknown.

The data were obtained using the EURICA[1,2] setup during the SEASTAR campaign in 2014[3] by fissioning a 345 MeV/u ^{238}U beam on a 3 mm-thick beryllium target. Knockout reactions occured in the liquid hydrogen target of MINOS,[4] installed at the F8 focal plane. At the final focal plane the EURICA array was used for measuring the energy and time between implantation and detection of the γ rays. In this experiment only six EURICA clusters were active. A total of $\sim 3 \times 10^7$ ^{67}Fe nuclei were implanted in a stopper in the center of EURICA. Approximately 96% of these implantation were from unreacted ^{67}Fe secondary beam, the rest were reaction products in MINOS.

Using the BigRIPS and ZeroDegree information the implanted nuclei could be separated into the main reaction channels: ^{68}Co(p, 2p)^{67}Fe, ^{238}U fission, and ^{68}Fe(p, pn)^{67}Fe with isomeric ratios of 56%, 36%, and 28%, respectively. Thus, the isomeric ratio is highest in the proton knock-out channel, but also significant in the other channels. In the Fig. 1, the γ-ray spectra are shown, normalized to the number of incoming ions.

One possible interpretation of the different isomeric ratios is found in the difference in the states of the
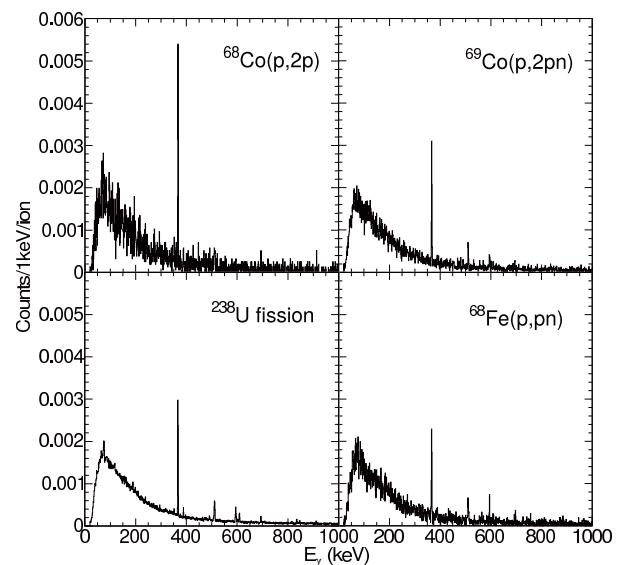
Fig. 1. Spectra of γ rays following isomeric decay separated into the main reaction channels normalised to the respective number of incoming ions.

ternary beam. For ^{68}Co there are two long-lived states that can serve as effective ground state configurations of 1^- and 7^- based on $\pi f_{7/2} \otimes \nu g_{9/2}$. Knocking out a $f_{7/2}$ proton could then leave a $g_{9/2}$ neutron in an excited state, that in turn decays to the isomeric state. With ^{68}Fe in a 0^+ ground state, and no other known long lived configurations, the still relatively high isomeric ratio from neutron knockout can be explained by the breaking of a $\nu g_{9/2}^2$ neutron-pair. In summary, such a picture would be consistent with a $\nu g_{9/2}$-based isomer over a $\nu p_{1/2}$ ground-state.

*1   Institut für Kernphysik, Technische Universität Darmstadt
*2   GSI, Darmstadt
*3   RIKEN Nishina Center
*4   INST, Hanoi
*5   CEA, Saclay
*6   School of Computing, Engineering and Mathematics, University of Brighton
*7   Department of Physics, University of Surrey
*8   School of Physics, Peking University
*9   MTA Atomki, Debrecen
*10   IPN Orsay, Orsay
*11   Department of Physics, University of Oslo
*12   Department of Physics, University of Tokyo
*13   CNS, University of Tokyo
*14   Department of Physics, The University of Hong Kong
*15   ICSNSM, IN2P3/CNRS, Université Paris-Saclay
*16   Department of Physics, Rikkyo University
*17   Department of Physics, Tohoku University

References
1) S. Nishimura, Prog. Theor. Exp. Phys. **2012**, 03C006 (2012).
2) P.-A. Söderström et al., Nucl. Instrum. Methods B **317**, 649 (2013).
3) P. Doornenbal et al., RIKEN Accel. Prog. Rep. **48** 5 (2015).
4) A. Obertelli et al., Eur. Phys. J. A **50**, 8 (2014).

Beta-decay half-lives of ^{78}Kr fragments from Cu to Ge

T. Goigoux,[*1] P. Ascher,[*1] B. Blank,[*1] M. Gerbaux,[*1] J. Giovinazzo,[*1] S. Grévy,[*1] T. Kurtukian Nieto,[*1]
C. Magron,[*1] J. Agramunt,[*2] A. Algora,[*2,*3] V. Guadilla,[*2] A. Montaner-Piza,[*2] A. I. Morales,[*2]
S. E. A. Orrigo,[*2] B. Rubio,[*2] D. S. Ahn,[*4] P. Doornenbal,[*4] N. Fukuda,[*4] N. Inabe,[*4] G. G. Kiss,[*4] T. Kubo,[*4]
S. Kubono,[*4] S. Nishimura,[*4] H. Sakurai,[*4,*5] Y. Shimizu,[*4] C. Sidong,[*4] P.-A. Söderström,[*4] T. Sumikama,[*4]
H. Suzuki,[*4] H. Takeda,[*4] P. Vi,[*4] J. Wu,[*4] Y. Fujita,[*6,*7] M. Tanaka,[*6] W. Gelletly,[*2,*8] P. Aguilera,[*9]
F. Molina,[*9] F. Diel,[*10] D. Lubos,[*11] G. de Angelis,[*12] D. R. Napoli,[*12] C. Borcea,[*13] A. Boso,[*14]
R. B. Cakirli,[*15] E. Ganioglu,[*15] J. Chiba,[*16] D. Nishimura,[*16] H. Oikawa,[*16] Y. Takei,[*16] S. Yagi,[*16]
K. Wimmer,[*3] G. de France,[*17] and S. Go[*18]

The most commonly observed decay process for proton-rich nuclei is β^+ decay. Further away from stability, the Q value of this process increases and the proton separation energy decreases, allowing β-delayed proton (βp) emission. The half-lives and proton branching ratios of nuclei near the proton drip line, especially around $Z = 30 - 40$, are of particular interest for astrophysical rp-process (rapid-proton capture) calculations in X-ray bursts on the surface of accreting neutron stars. The beta and beta-delayed proton decays compete with the rapid-proton capture process.

Nuclei in this mass region were produced and identified with unprecedented statistics at RIBF in 2015 within the RIBF4R1 experiment.[1)] The fragments were produced by fragmentation of a ^{78}Kr beam (350 MeV/A and 150 pnA) on a Be target. After the selection and identification by the BigRIPS fragment separator, the nuclei were implanted in the silicon detectors of the WAS3ABi setup[2)] surrounded by the EURICA γ-detector array.[3)]

The position and time correlations between the implantation and subsequent decay events provide the time distribution used to determine the half-lives of the nuclei of interest. The fit function is composed of the contribution of the parent nucleus, the daughter nuclei for the different decay branches (β and βp decays) and a constant background. The background component of the function is extracted from a fit of negative times between implantation and decay.

More accurate half-lives and proton branching ra-
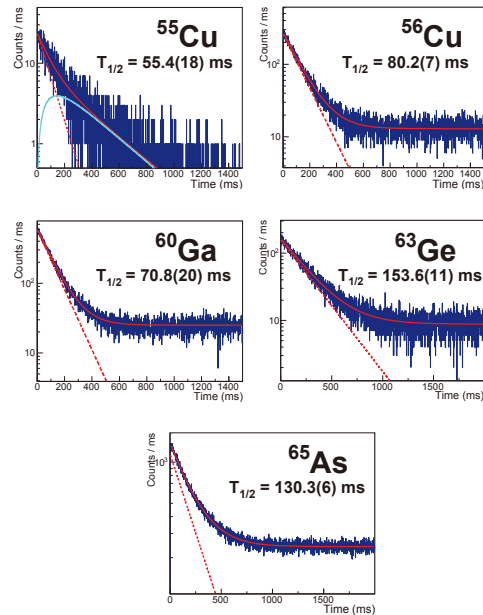
Fig. 1. Time distributions of ^{55}Cu, ^{56}Cu, ^{60}Ga, ^{65}As and ^{63}Ge with their respective β-decay half-lives determined in this work. The dotted red lines are the contributions of the isotopes of interest, whereas the full red lines represent the sums of the decay of interest and a constant background. In the case of ^{55}Cu, the additional light blue line is the contribution of the daughter decay (^{55}Ni), also included in sum line.

tios were obtained from the analysis of the experiment. The values for the βp emitters ^{57}Zn, ^{61}Ge, ^{65}Se, ^{68}Kr and ^{69}Kr were previously reported in Ref. 4). Furthermore, new half-life values of the β emitters ^{55}Cu, ^{56}Cu, ^{60}Ga, ^{65}As and ^{63}Ge were determined. Their fit and time distributions are shown in Fig. 1. Half-life values with a better precision than literature were obtained, providing new inputs to future rp-process calculations.

[*1] CEN Bordeaux Gradignan
[*2] IFIC, CSIC-Universidad de Valencia
[*3] MTA ATOMKI, Debrecen
[*4] RIKEN Nishina Center
[*5] Department of Physics, University of Tokyo
[*6] Department of Physics, Osaka University
[*7] Research Center for Nuclear Physics, Osaka University
[*8] Department of Physics, University of Surrey
[*9] Comisíon Chilena de Energia Nuclear
[*10] Institute of Nuclear Physics, University of Cologne
[*11] Physik Department E12, Technische Universität München
[*12] Laboratori Nazionali di Legnaro dell' INFN
[*13] IFIN-HH
[*14] INFN Sezione di Padova and Dipartimento di Fisica
[*15] Department of Physics, Istanbul University
[*16] Department of Physics, Tokyo University of Science
[*17] Grand Accélérateur National d'Ions Lourds
[*18] Dept. of Physics and Astronomy, University of Tennessee

References
1) B. Blank et al., Phys. Rev. C **93**, 061301(R) (2016).
2) S. Nishimura et al., RIKEN Accel. Prog. Rep. **46**, 182 (2013).
3) P. A. Söderström et al., Nucl. Instrum. Methods B **317**, 649 (2013).
4) T. Goigoux et al., RIKEN Accel. Prog. Rep. **50**, 35 (2017).

Isomer spectroscopy of ^{92,94}Se in the SEASTAR 2015 experiment

C. Lizarazo,[*1,*2] P.-A. Söderström,[*1,*2,*3] V. Werner,[*1] N. Pietralla,[*1] P. Doornenbal,[*3] S. Nishimura,[*3] A. Obertelli,[*1,*3,*4] F. Browne,[*3,*5] C. R. Niţă,[*6] for the SEASTAR and EURICA collaborations

We report on the analysis of the isomer spectroscopy of ^{92,94}Se conducted during the SEASTAR 2015 campaign of experiments.[1] Neutron-rich nuclei were produced via the in-flight fission of a 345-MeV/nucleon ^{238}U primary beam colliding with a ^{9}Be target. The fragments were selected with BigRIPS, previously tuned to produce a radioactive beam centered around ^{95}Br. This secondary beam impinged on a 99(1)-mm LH$_2$ target of the MINOS device placed at F8, producing neutron-rich selenium nuclei via knockout reactions. The ejectiles were transported through the ZeroDegree spectrometer, where particle identification was conducted via the TOF-$B\rho$-ΔE measurement to deduce the mass-to-charge ratio (A/Q) and atomic number (Z). The obtained PID histogram is shown in Fig. 1.

The nuclei were implanted on the silicon layers of the AIDA stopper placed at the end of the ZeroDegree spectrometer. The existence and decay of isomeric states of the implanted ions were studied using the EURICA array comprised of HP Ge detectors.[2,3] The obtained spectra for delayed γ rays are shown in Fig. 2. All the reported transitions for these isotopes[4,5] were observed. For ^{92}Se, new transitions were found at 67, 353 and 1252 keV. For ^{94}Se, the isomeric state was observed for the first time, with new transitions having energies of 495, 822, 752, and 1180 keV.

Several analysis steps such as add-back reconstruction, background subtraction, efficiency and time-walk correction, and $\gamma\gamma$ coincidences have been conducted to identify the γ rays emitted after the isomeric decay and their placement in the level schemes, which have been extended. In both nuclei, a single isomeric state has been found because the half-lives for the individual transitions, measured from their time spectra, are consistent
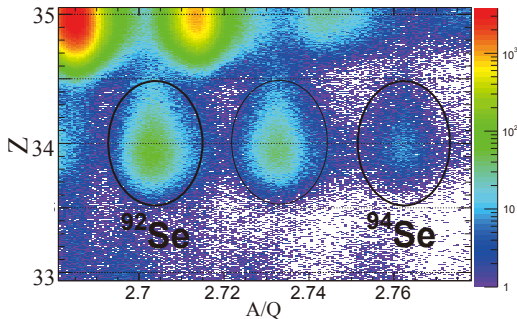
Fig. 1. ZeroDegree PID spectrum and 2D cuts of ^{92,94}Se.

*1 Institut für Kernphysik, Technische Universität Darmstadt
*2 GSI, Darmstadt
*3 RIKEN Nishina Center
*4 CEA, Saclay
*5 School of Computing, Engineering and Mathematics, University of Brighton
*6 IFIN-HH, Bucharest
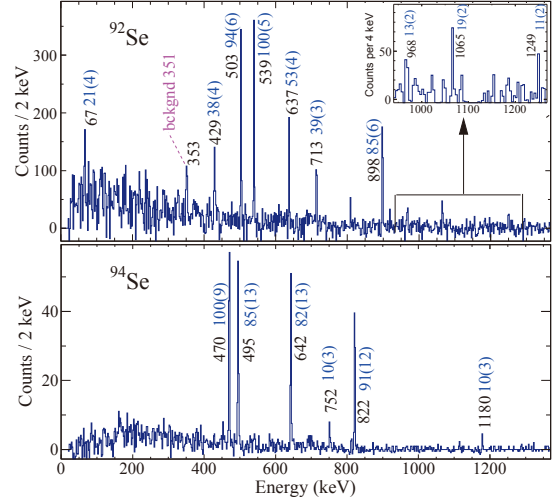
Fig. 2. Delayed γ-rays correlated to ^{92}Se and ^{94}Se. The energy (black) and efficiency-corrected intensity (blue) of the transitions are shown next to the peaks.

with each other. The isomeric half-lives were obtained from the exponential fit of the time spectrum obtained after adding events of individual transitions, leading to $T_{1/2} = 15.7(7)$ μs for ^{92}Se and $T_{1/2} = 0.68(5)$ μs for ^{94}Se.

For ^{92}Se, the isomeric decay occurs because of an E2 67-keV transition with a decay strength of approximately 1 W.u. The comparison between BrICC calculations and experimental intensities allowed the multipolarity assignment. In the context of Nilsson schemes of state-of-the-art beyond mean-field (BMF) theories, the isomeric decay likely corresponds to a $9^-\rightarrow7^-$ transition between two oblate quasi neutron states. For ^{94}Se an oblate K-isomer is suggested, decaying via a $7^-\rightarrow6_1^+$ E1 transition with an energy of 495 keV. The spin quantum numbers were tentatively assigned assuming the simplest high-K quasiparticle couplings near the Fermi surface, in both cases near $\beta\sim-0.24$, involving the $11/2[505]$ level. A prolate-to-oblate transition between $^{90-94}$Se$_{56-60}$ is predicted by BMF theories recently used for the neighbouring ^{98,100}Kr.[6] It seems to be supported by the experimental systematics and the decay pattern between the low-lying levels observed during the isomeric decay.

References
1) P. Doornenbal *et al.*, RIKEN Accel. Prog. Rep. **49**, 35 (2016).
2) P.-A. Söderström *et al.*, Nucl. Instrum. Methods B, **317**, 649 (2013).
3) S. Nishimura *et al.*, Prog. Theor. Exp. Phys. **2012**, 03C006 (2012).
4) S. Chen *et al.*, Phys. Rev. C **95**, 041302(R) (2017).
5) D. Kameda *et al.*, Phys. Rev. C **86**, 054319 (2012).
6) F. Flavigny *et al.*, Phys. Rev. Lett. **118**, 242501 (2017).

γ-decaying isomers and isomeric ratios in the ^{100}Sn region†

J. Park,[*1,*2] R. Krücken,[*1,*2] D. Lubos,[*3,*4,*5] R. Gernhäuser,[*3] M. Lewitowicz,[*6] and S. Nishimura[*4]

for the EURICA Collaboration

The structure of the heaviest $N = Z$ doubly magic nucleus ^{100}Sn and the nuclei in its vicinity has been investigated in depth both experimentally and theoretically.[1] Isomeric states in these exotic isotopes contain valuable experimental information on some of the research topics in this region of nuclides, such as the robustness of the $N = Z = 50$ shells and the role of the proton-neutron interaction in $N \sim Z$ nuclei.

This report contains a summary of results from the EURICA Xe campaign in 2013 on the γ-decaying isomers in the ^{100}Sn region. Proton-rich isotopes in ^{100}Sn region were produced from fragmentation reactions of ^{124}Xe on a ^{9}Be target, and were separated and identified through BigRIPS and the ZeroDegree spectrometer at the RIBF. They were implanted in WAS3ABi,[2] and time-delayed γ rays emitted from the isomers of the implanted nuclei were detected with EURICA[3] for half-life $(T_{1/2})$ measurements.

Several new results were found: the discovery of a (4^+) isomer in ^{92}Rh; the excitation energy of the (15^+) isomer in ^{96}Ag, and the $T_{1/2}$ of the (6^+) isomer in ^{98}Cd. Figure 1 shows the electromagnetic transition strengths derived from half-life measurements of γ-decaying isomers observed in this experiment, as well as the theoretical values from different shell model (SM) calculations. The SLGM interaction[4] uses a model space of proton and neutron $(2p_{1/2}, 1g_{9/2})$ orbitals above the ^{76}Sr core. The other SM approaches are described in the original article. Two sets of proton and neutron effective charges (a) and (b) were employed to gauge and account for core polarization effects. A good agreement between experimental and theoretical transition strengths was found in general. However, the transition strengths were significantly lower than predicted in ^{92,93}Ru. On the other hand, experimental transition strengths of the core-excited (12^+) isomer in ^{98}Cd exceeding SM predictions may be related to the increased proton core polarization in light, even-mass Sn isotopes.[5] Further theoretical efforts are needed to address these discrepancies.

In addition, experimental isomeric ratios of both γ-decaying and β-decaying isomers were determined and compared with the abrasion-ablation model[6,7] coupled to the sharp cutoff model. A good agreement
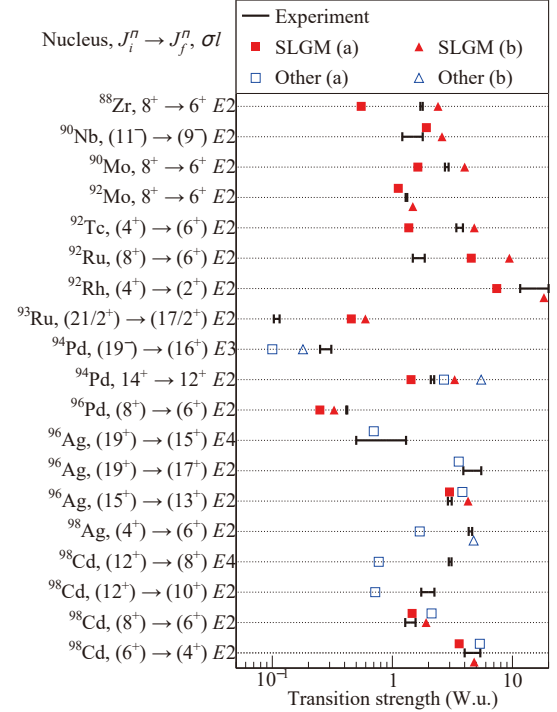
Fig. 1. Experimental electromagnetic transition strengths of isomers measured in this work and shell model calculations. See the text for details on the different models.

between experimental and theoretical values was obtained for positive-parity isomers with $J > 4$.

No experimental signature of an isomer in ^{100}Sn was found, which was hypothesized from SM.[8,9] With assumptions from SM calculations and the theoretical isomeric ratio, limits on the γ-ray energy and $T_{1/2}$ were proposed on the isomer in ^{100}Sn.

References
1) T. Faestermann, M. Górska, H. Grawe, Prog. Part. Nucl. Phys. **69**, 85 (2013).
2) S. Nishimura, Prog. Theor. Exp. Phys. **2012**, 03C006 (2012).
3) P.-A. Söderström et al., Nucl. Instrum. Methods B **317**, 649 (2013).
4) F. J. D. Serduke, R. D. Lawson, D. H. Gloeckner, Nucl. Phys. **256**, 45 (1976).
5) P. Doornenbal et al., Phys. Rev. C **90**, 061302 (2014).
6) J.-J. Gaimard, K.-H. Schmidt, Nucl. Phys. **531**, 709 (1991).
7) M. de Jong, A. V. Ignatuyk, K.-H. Schmidt, Nucl. Phys. **613**, 435 (1997).
8) F. Nowacki, Nucl. Phys. **704**, 223 (2002).
9) V. I. Isakov, K. I. Erokhina, Phys. At. Nucl. **65**, 143 (2002).

† Condensed from the article in Phys. Rev. C **96**, 044311 (2017)
*1 Department of Physics and Astronomy, University of British Columbia
*2 TRIUMF
*3 Physik Department, Technische Universität München
*4 RIKEN Nishina Center
*5 Excellence Cluster Universe, Technische Universität München
*6 Grand Accélérateur National d'Ions Lourds (GANIL)

Coexisting Single-Particle and Collective Structures in ^{137}Sb

J. Keatings,[*1] G. Simpson,[*2,*1] A. Jungclaus,[*3] J. Taprogge,[*4] S. Nishimura,[*5] P. Doornenbal,[*5] G. Lorusso,[*5]
P.-A. Söderström,[*5] T. Sumikama,[*5] J. Wu,[*5] Z. Y. Xu,[*5]
and the EURICA RIBF-85 collaboration[*5]
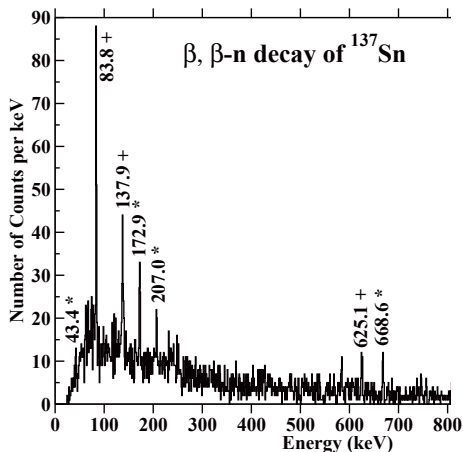
Fig. 1. γ-ray spectrum obtained from the β-decay of ^{137}Sn in the current work.

Fig. 2. Level scheme of ^{137}Sb obtained in the current work.

The structure of the nucleus is governed by a delicate interplay between single-particle and collective states. Currently it is unclear how collective modes develop in nuclei in very neutron-rich regions far from stability, which are difficult to access experimentally. Collectivity occurs when the integrated proton-neutron interaction is able to overcome the pairing force. Experimental measurements have shown that reduced pairing was found to be necessary to correctly describe the structures of ^{136}Sn[1] and ^{72,74}Ni,[2] which possess significant seniority (broken pair) mixing. It is therefore interesting to search for the development of collective modes in nuclei east of ^{132}Sn. The very neutron-rich nucleus ^{137}Sb consists of a single valence proton coupled to ^{136}Sn and its structure is most appropriate for testing the proton–neutron part of shell-model effective interactions. A decay scheme of this nucleus has been constructed via β- and β-n decay spectroscopy data taken at RIBF, RIKEN during the EURICA campaign.

The experimental spectrum obtained is presented in Fig. 1. It was possible to construct a first level scheme using $\gamma - \gamma$ coincidences, along with the β-n decay data of ^{138}Sn, shown in Fig. 2. The ground state spin of the parent ^{137}Sn nucleus was determined from the β-n feeding of known spin (4^-) and (2^-) levels in ^{136}Sb. The ^{137}Sb ground-state spin of $(7/2^+)$ was as-

signed from the β and β-n feeding intensities to levels in ^{136,137}Te. In particular the observed feeding to spin $(2^+) - (6^+)$ levels in ^{136}Te agrees best with a $(7/2^+)$ ground-state spin assignment. It is important to note that the first excited state in ^{137}Sb receives no direct feeding from the β-n decay of ^{138}Sn, allowing a spin of $(5/2^+)$ to be assigned.

The experimental level scheme has been compared to the results obtained from shell-model calculations[3] and level systematics. The calculations predict a set of four low-lying states with spins of $1/2^+, 3/2^+, 5/2^+$, and $7/2^+$ all within an energy range of 0–400 keV, with other states in this spin range at energies >700 keV. As three low-lying states in ^{137}Sb appear to be fed directly from β decay there is considerable unseen population from the γ decay of higher lying levels.

The wavefunctions of the four lowest-lying states of ^{137}Sb are calculated to be different in nature. For example the $7/2^+$ state has a predominantly single-particle character, whereas the $1/2^+$ and $3/2^+$ states are more fragmented, with seniority-3, and higher, couplings making up >70% of the wavefunction. The latter is a sign of the breakdown of independent single-particle behavior and emergening collectivity. Indeed the theoretical results point towards the coexistence of single-particle and weakly collective states near the ground state of ^{137}Sb.

References
1) G. Simpson et al., Phys. Rev. Lett. **113**, 132502 (2014).
2) H. Grawe et al., Nucl. Phys. **704**, 211 (2002).
3) L. Coraggio et al., Phys. Rev. C **87**, 034309 (2013).

*1　School of Engineering, University of the West of Scotland
*2　LPSC, Grenoble
*3　IEM, CSIC Madrid
*4　Departamento de Física Téorica,Universidad Autonoma de Madrid
*5　RIKEN Nishina Center

Investigation of octupole correlations of neutron-rich $Z \sim 56$ isotopes by β-γ spectroscopy

R. Yokoyama,[*1] E. Ideguchi,[*2] G. Simpson,[*3] Mn. Tanaka,[*2] S. Nishimura,[*4] P. Doornenbal,[*4]
P.-A. Söderström,[*4] G. Lorusso,[*4] Z. Y. Xu,[*5] J. Wu,[*4,*6] T. Sumikama,[*7] N. Aoi,[*2] H. Baba,[*4] F. Bello,[*8]
F. Browne,[*9,*4] R. Daido,[*10] Y. Fang,[*10] N. Fukuda,[*4] G. Gey,[*3,*4,*11] S. Go,[*1,*4] N. Inabe,[*4] T. Isobe,[*4]
D. Kameda,[*4] K. Kobayashi,[*12] M. Kobayashi,[*1] T. Komatsubara,[*13] T. Kubo,[*4] I. Kuti,[*14] Z. Li,[*6]
M. Matsushita,[*1] S. Michimasa,[*1] C.-B. Moon,[*15] H. Nishibata,[*10] I. Nishizuka,[*7] A. Odahara,[*10] Z. Patel,[*16,*4]
S. Rice,[*16,*4] E. Sahin,[*8] L. Sinclair,[*17,*4] H. Suzuki,[*4] H. Takeda,[*4] J. Taprogge,[*18,*19] Zs. Vajta,[*14]
H. Watanabe,[*20] and A. Yagi[*10]

Neutron-rich Ba isotopes ($Z = 56$, $N \sim 88$) are expected to have a significant octupole collectivity due to the interactions between orbitals with $\Delta j = \Delta l = 3$ around the Fermi surface. Recently, the reflection-asymmetric shape, octupole deformation, has been reported in ^{144}Ba by Bucher et $al.$[1] The theoretical calculations exhibit different predictions for octupole correlations in this region. For example, the microscopic-macroscopic method[2] predicts some β_3 values, whereas the Hartree-Fock calculation[3] argues that there is no state with a dipole moment relevant to the octupole collectivity. Therefore, experimental studies of more neutron-rich Ba isotopes are required.

We performed the β-γ spectroscopy of the ^{150}Cs decay at RIBF using the in-flight fission of a 345 MeV/nucleon ^{238}U beam bombarding a 3-mm thick Be target. Fission fragments were identified by the TOF-Bρ-ΔE method using BigRIPS.[4] The secondary beam was implanted into an active stopper WAS3ABi,[5] which consists of five layers of double-sided-silicon-strip detectors for ion-β correlation. The γ rays from the implanted nuclei were detected using EURICA,[6] an array of 12-cluster Ge detectors.

The γ-ray energy spectrum of the ^{150}Cs decay is shown in Fig. 1. The ion-β time window was set to 0.2 s considering the previously reported half-life of ^{150}Cs, 0.84(8) ms.[7] Since the peak count was small,
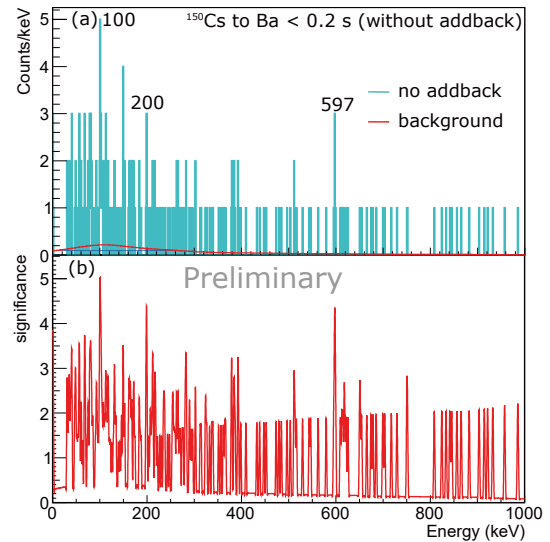
Fig. 1. (a) The preliminary γ-ray energy spectrum of the β decay from ^{150}Cs to ^{150}Ba. The red curve shows the estimated continuum background. (b) The significance spectrum by a likelihood ratio test.

a log-likelihood ratio test was performed for the energy spectrum. The significance spectrum is shown in Fig. 1(b). The background was estimated by smoothing and scaling the energy spectrum with a time window of 2-to-10 s after ion implantation. We requested 4σ as a confidence level to identify significant peaks in the spectrum. There are three significant peaks at energies of 100, 200, and 597 keV. The peak at 200 keV is not assigned to an excited state of ^{150}Ba because it became more pronounced in a spectrum with a longer time window up to 2 s than 0.2 s. Analysis on the 100- and 597-keV γ-ray is in progress.

*1   Center for Nuclear Study, The University of Tokyo
*2   Research Center for Nuclear Physics, Osaka University
*3   LPSC, Université Grenoble-Alpes, CNRS/IN2P3
*4   RIKEN Nishina Center
*5   Department of Physics, The University of Tokyo
*6   Department of Physics, Peking University
*7   Department of Physics, Tohoku University
*8   Department of Physics, University of Oslo
*9   School of Computing Engineering and Mathematics, University of Brighton
*10 Department of Physics, Osaka University
*11 ILL, Grenoble
*12 Department of Physics, Rikkyo University
*13 Department of Physics, University of Tsukuba
*14 MTA Atomki, Hungarian Academy of Science, Hungary
*15 Department of Display Engineering, Hoseo University
*16 Department of Physics, University of Surrey
*17 Department of Physics, University of York
*18 Instituto de Estructura de la Materia, CSIC
*19 Departamento de Física Teórica, Universidad Autónoma de Madrid
*20 Department of Physiscs, Beihang University

References
1) B. Bucher et $al.$, Phys. Rev. Lett. **116**, 112503 (2016).
2) P. A. Butler et $al.$, Nucl. Phys. **533**, 249 (1991).
3) W. Nazarewicz et $al.$, Nucl. Phys. **429**, 269 (1984).
4) N. Fukuda et $al.$, Nucl. Instrum Methods B **317**, 323 (2013).
5) S. Nishimura et $al.$, RIKEN APR **46**, 182 (2013).
6) S. Nishimura, Nucl. Phys. News **22**, No.3, 38 (2012).
7) J. Wu et $al.$, Phys. Rev. Lett. **118**, 072701 (2017).

First result of elastic electron scattering from ^{132}Xe at the SCRIT facility[†]

K. Tsukada,[*1,*2] A. Enokizono,[*2] T. Ohnishi,[*2] K. Adachi,[*3] T. Fujita,[*3] M. Hara,[*2] M. Hori,[*3] T. Hori,[*2]
S. Ichikawa,[*2] K. Kurita,[*3] K. Matsuda,[*1,*2] T. Suda,[*1,*2] T. Tamae,[*1,*2] M. Togasaki,[*3] N. Uchida,[*3]
M. Wakasugi,[*2] M. Watanabe,[*2] and K. Yamada[*3]

For the first time, nuclear charge density distribution was extracted from only 10^8 nuclei target (^{132}Xe) at the SCRIT (Self-Confining Radioactive Isotope Target) electron scattering facility,[1,2)] which has been constructed at RIKEN to realize electron scattering off unstable nuclei. The data were taken in 2016, and reported in the previous report.[3)]

Figures 1(a)–(c) show the reconstructed vertex distributions of scattered electrons along the beam and at vertical positions. The background contributions from residual gases are shown in Figs. 1(a) and (c) as blue histograms. It was found that the target ions were clearly trapped in the SCRIT by the transverse focusing force given by the electron beam itself and the electrostatic potential well provided by both ends of the electrodes.
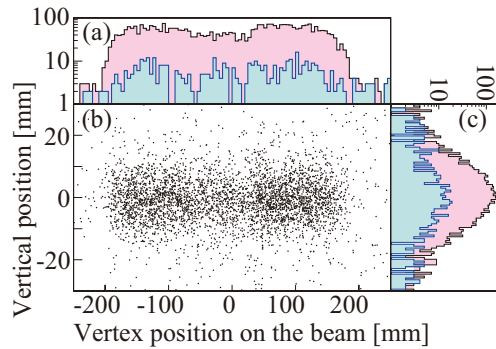
Fig. 1. Reconstructed vertex distributions of scattered electrons. Panels (a) and (c) show the vertex point distributions with and without the target ions. Panel (b) shows the scatter plot of the vertex point distribution with the target ions.

Figure 2 shows the differential cross sections multiplied by luminosity for elastic electron scattering. By changing the electron beam energies, a wide range of momentum transfer can be covered. The lines in Fig. 2 represent the elastic scattering cross sections calculated by a phase shift calculation code DREPHA,[4)] assuming nuclear charge density distributions. In the present analysis, a two-parameter Fermi distribution, $\rho(r) = \rho_0/(1 + \exp(4\ln 3(r - c)/t))$, is assumed to

extract the nuclear charge distribution. The luminosity is also considered as a fitting parameter, because the study of the luminosity monitor (LMon)[5)] to determine the absolute value of luminosity is under way. The achieved luminosity is evaluated to be around 1×10^{27} cm^{-2}s^{-1} on average. From this analysis, the most probable values ($c = 5.42^{+0.11}_{-0.08}$ fm, $t = 2.71^{+0.29}_{-0.38}$ fm, and $\langle r^2 \rangle^{1/2} = 4.79^{+0.12}_{-0.10}$ fm) are obtained.
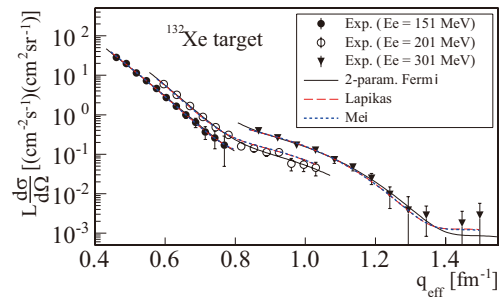
Fig. 2. Differential cross sections multiplied by luminosity, versus effective momentum transfer. The lines represent the results of phase shift calculations assuming nuclear charge density distributions obtained by the two-parameter Fermi distribution (black solid line), the Hartree-Fock + phenomenological calculation (red dashed line),[6)] and the beyond-relativistic-mean-field theory (blue dotted line).[7)] The parameters of the two-parameter Fermi distribution are the best values evaluated in this analysis.

This work demonstrates that the SCRIT technique enables us to perform electron scattering experiment for unstable nuclear targets. The RI production for experiments on unstable nuclei has already started.[2)] Electron scattering off short-lived unstable nuclei will be realized in near future.

References
1) M. Wakasugi et al., Nucl. Instrum. Methods B 317, 668 (2013).
2) T. Ohnishi et al., Physca Scripta, T166 014071 (2015).
3) K. Tsukada et al., RIKEN Accel. Prog. Rep. 50, 11 (2016).
4) B. Drepher et al., a phase-shift calculation code for elastic electron scattering, communicated by J. Friedrich.
5) T. Fujita et al., RIKEN Accel. Prog. Rep. 50, 188 (2016).
6) L. Lapikas, HERMES Internal Report No. 04–41.
7) H. Mei, K. Hagino, private communication.

† Condensed from the article in Phys. Rev. Lett. 118, 262501 (2017)
*1 RIKEN Nishina Center
*2 Research Center for Electron-Photon Science, Tohoku University
*3 Department of Physics, Rikkyo University

Complete set of deuteron analyzing powers from $\vec{d}p$ elastic scattering at 190 MeV/nucleon[†]

K. Sekiguchi,[*1,*2] H. Witała,[*3] T. Akieda,[*1] D. Eto,[*1] H. Kon,[*1] Y. Wada,[*1] A. Watanabe,[*1] S. Chebotaryov,[*4] M. Dozono,[*5] J. Golak,[*3] H. Kamada,[*6] S. Kawakami,[*7] Y. Kubota,[*5] Y. Maeda,[*5] K. Miki,[*1] E. Milman,[*4] A. Ohkura,[*8] H. Sakai,[*2] S. Sakaguchi,[*8] N. Sakamoto,[*2] M. Sasano,[*2] Y. Shindo,[*8] R. Skibiński,[*3] H. Suzuki,[*2] M. Tabata,[*8] T. Uesaka,[*2] T. Wakasa,[*8] K. Yako,[*5] T. Yamamoto,[*7] Y. Yanagisawa,[*2] and J. Yasuda[*8]

All the deuteron analyzing powers, iT_{11}, T_{21}, T_{20} and T_{22}, for elastic deuteron-proton (dp) scattering have been measured with a polarized deuteron beam at 186.6 MeV/nucleon at the angles in the center of mass system of $\theta_{c.m.} = 39°$–$165°$. These data, together with our previously reported deuteron analyzing powers taken at different energies, constitute a solid basis to guide the theoretical investigations of three-nucleon forces (3NFs).

Our new deuteron analyzing powers and the previously measured data at 70 and 135 MeV/nucleon together with the elastic cross section data in the energy region of interest, are compared with the results of 3N Faddeev calculations based on the standard nucleon–nucleon (NN) potentials[1] alone or combined with the TM99 3NF.[2] The AV18 NN potential is also combined with the Urbana IX 3NF.[3] Parts of the data are shown in Figs. 1a), c), and e). Predicted 3NF effects localized at backward angles are supported only partially by the data. The data are also compared to predictions based on locally regularized chiral NN potentials.[4] The N^{4}LO chiral potential predictions are close to the semi-phenomenological NN results for the measured observables. At 190 MeV, the N^{4}LO NN predictions are generally away from the data. This would indicate the effects of 3NF contributions that were neglected in our calculations. An estimation of the theoretical truncation uncertainties in the consecutive orders of chiral expansion (Figs. 1b), d), and f)) suggests that the observed discrepancies between this modern theory and the data could probably be explained by including chiral 3NF's in future calculations.

References
1) R. Machleidt, Phys. Rev. C **63**, 024001 (2001);
   R. B. Wiringa *et al.*, *ibid.* **51**, 38 (1995); V. G. J. Stoks *et al.*, *ibid.* **49**, 2950 (1994).
2) S. A. Coon, H. K. Han, Few Body Syst. **30**, 131 (2001).
3) B. S. Pudliner *et al.*, Phys. Rev. C **56**, 1720 (1997).
4) E. Epelbaum *et al.*, Phys. Rev. Lett. **115**, 122301 (2015).

[†] Condensed from the article in Phys. Rev. C. **96**, 064001 (2017)
[*1] Department of Physics, Tohoku University
[*2] RIKEN Nishina Center
[*3] Jagiellonian University
[*4] Department of Physics, Kyungpook National University
[*5] Center for Nuclear Study, University of Tokyo
[*6] Kyushu Institute of Technology
[*7] Faculty of Engineering, University of Miyazaki
[*8] Department of Physics, Kyushu University
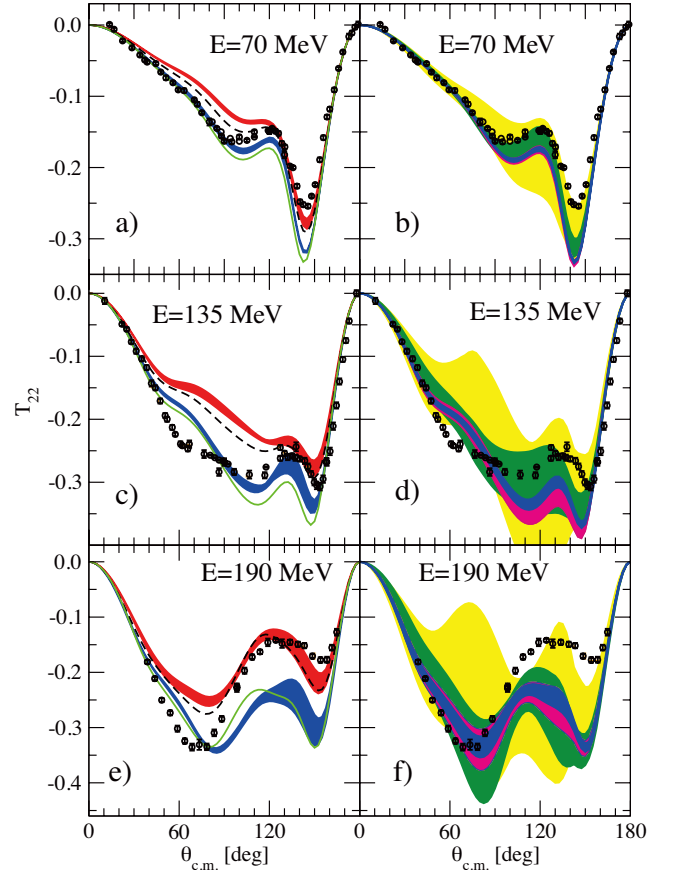
Fig. 1. Elastic dp scattering deuteron tensor analyzing power T_{22} at incoming nucleon laboratory energies of $E = 70$ MeV: a) and b), 135 MeV: c) and d), and 190 MeV: e) and f). In a), c), and e) the blue shaded band indicates predictions of standard NN potentials[1] and the red shaded band indicates predictions when they are combined with the TM99 3NF. The dashed black curve represents the prediction of the AV18+Urbana IX combination. The solid green curve shows prediction of the locally regularized (regulator $R = 0.9$ fm) N^{4}LO chiral potential. In b), d), and f), the estimated theoretical uncertainties at different order of chiral expansion are shown by the bands of increasing width at: N^{4}LO (blue), N^{3}LO (magenta), N^{2}LO (green), and NLO (yellow). The black circles are dp data taken at RIKEN.

Single-particle states and collective modes: magnetic moment of ^{75m}Cu

Y. Ichikawa,[*1] H. Nishibata,[*1,*2] Y. Tsunoda,[*3] A. Takamine,[*1] K. Imamura,[*1,*4] T. Fujita,[*1,*2] T. Sato,[*1,*5]
S. Momiyama,[*6] Y. Shimizu,[*1] D. S. Ahn,[*1] K. Asahi,[*1,*5] H. Baba,[*1] D. L. Balabanski,[*1,*7] F. Boulay,[*1,*8,*9]
J. M. Daugas,[*1,*9] T. Egami,[*10] N. Fukuda,[*1] C. Funayama,[*5] T. Furukawa,[*11] G. Georgiev,[*12]
A. Gladkov,[*1,*13] N. Inabe,[*1] Y. Ishibashi,[*1,*14] T. Kawaguchi,[*10] T. Kawamura,[*2] Y. Kobayashi,[*1,*15]
S. Kojima,[*5] A. Kusoglu,[*7,*12,*16] I. Mukul,[*17] M. Niikura,[*6] T. Nishizaka,[*10] A. Odahara,[*2] Y. Ohtomo,[*1,*5]
T. Otsuka,[*1,*3,*6,*18] D. Ralet,[*12] G. S. Simpson,[*19] T. Sumikama,[*1] H. Suzuki,[*1] H. Takeda,[*1] L. C. Tao,[*1,*20]
Y. Togano,[*1,*5] D. Tominaga,[*10] H. Ueno,[*1] H. Yamazaki,[*1] and X. F. Yang[*18]

Atomic nuclei show dual features, the single-particle shell nature and collective modes, which compete with each other to express the actual nuclear structure. For an attempt to describe the structural variety of unstable nuclei by using unified and general models, it is necessary to understand how the shell evolves in unstable-nuclei regions, and how the shell competes with the collectivity. In the present study, we demonstrate the precision analysis of this competition by focusing on the magnetic moment of an isomeric state of a neutron-rich nucleus ^{75}Cu,[1,2] where an intriguing shell evolution along the Cu isotopic chain has been reported.[3–5]

The experimental magnetic moment measurement was conducted at the BigRIPS at RIBF, taking advantage of a spin-aligned RI beam obtained in a scheme of two-step projectile fragmentation with a technique of momentum-dispersion matching.[6] The ^{75}Cu beam with a spin alignment of 30(5)% was produced by one proton removal from ^{76}Zn, which was a fission product of ^{238}U. The magnetic moment was determined with the time-differential perturbed angular distribution (TDPAD) method. Owing to the high spin alignment realized with the two-step scheme, the oscillation in the TDPAD spectrum was observed with a significance larger than 5σ. The magnetic moment of the 66.2-keV isomer with spin parity $3/2^-$ was determined for the first time to be $\mu = 1.40(6)\mu_N$.
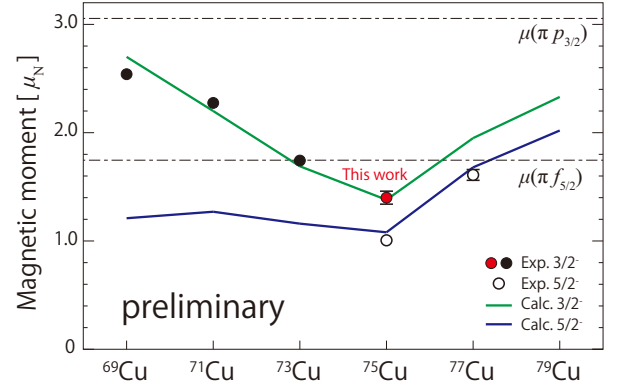
Fig. 1. Systematics of the magnetic moments for odd-A Cu isotopes. Filled and open circles represent experimental data for the $3/2^-$ states and the $5/2^-$ states, respectively. The filled red circle represents the result obtained in this work. The solid green and blue lines represent the MCSM calculations for the $3/2^-$ states and the $5/2^-$ states, respectively, with the $20 \leq (N, Z) \leq 56$ model space.[7] $\mu(\pi p_{3/2})$ and $\mu(\pi f_{5/2})$ denote the proton Schmidt values for $p_{3/2}$ and $f_{5/2}$, respectively.

The magnetic moment, thus obtained, shows a considerable deviation from the Schmidt value, $\mu = 3.05\mu_N$, for the $p_{3/2}$ orbital. Figure 1 shows the systematics of magnetic moments of the $3/2^-$ and $5/2^-$ states, where deviation from the Schmidt values appears to be maximal at ^{75}Cu. The analysis of the magnetic moment with the help of state-of-the-art shell-model calculations[7] reveals that the trend of the deviation corresponds to the effect of the core excitation. Furthermore, it was found that the low-lying states in ^{75}Cu are, to a large extent, of single-particle nature on top of a correlated ^{74}Ni core.

*1   RIKEN Nishina Center
*2   Department of Physics, Osaka University
*3   Center for Nuclear Study, University of Tokyo
*4   Department of Physics, Meiji University
*5   Department of Physics, Tokyo Institute of Technology
*6   Department of Physics, University of Tokyo
*7   ELI-NP, IFIN-HH
*8   GANIL, CEA/DSM-CNRS/IN2P3
*9   CEA, DAM, DIF
*10 Department of Advanced Sciences, Hosei University
*11 Department of Physics, Tokyo Metropolitan University
*12 CSNSM, CNRS/IN2P3, Université Pris-Sud
*13 Department of Physics, Kyungpook National University
*14 Department of Physics, University of Tsukuba
*15 Department of Informatics and Engineering, University of Electro-Communications
*16 Department of Physics, Istanbul University
*17 Department of Particle Physics, Weizmann Institute
*18 Intsituut voor Kern-en Srralingsfysica, K. U. Leuven
*19 LPSC, Université Grenoble Alpes, CNRS/IN2P3
*20 School of Physics, Peking University

References
1) J. M. Daugas *et al.*, Phys. Rev. C **81**, 034304 (2010).
2) C. Petrone *et al.*, Phys. Rev. C **94**, 024319 (2016).
3) T. Otsuka *et al.*, Phys. Rev. Lett. **95**, 232502 (2005).
4) S. Franchoo *et al.*, Phys. Rev. Lett. **81**, 3100 (1998).
5) K. T. Flanagan *et al.*, Phys. Rev. Lett. **103**, 142501 (2009).
6) Y. Ichikawa *et al.*, Nature Phys. **8**, 918 (2012).
7) Y. Tsunoda *et al.*, Phys. Rev. C **89**, 031301(R) (2014).

Track reconstruction of recoil particles in CAT-S at RIBF113: ^{132}Sn(d,d') measurement

S. Ota,[*1] H. Tokieda,[*1] C. Iwamoto,[*1] M. Dozono,[*1] U. Garg,[*2] S. Hayakawa,[*1] K. Kawata,[*1] N. Kitamura,[*1] M. Kobayashi,[*1] S. Masuoka,[*1] S. Michimasa,[*1] A. Obertelli,[*3,*4] D. Suzuki,[*4] R. Yokoyama,[*1] J. Zenihiro,[*4] H. Baba,[*4] O. Beliuskina,[*1] S. Chebotaryov,[*4] P. Egelhof,[*5] T. Harada,[*6] M. N. Harakeh,[*7] K. Howard[*2] N. Imai,[*1] M. Itoh,[*8] Y. Kiyokawa,[*1] C. S. Lee,[*1] Y. Maeda,[*9] Y. Matsuda,[*8] E. Milman,[*4] V. Panin,[*4] H. Sakaguchi,[*10] P. Schrock,[*1] S. Shimoura,[*1] L. Stuhl,[*4] M. Takaki,[*1] K. Taniue,[*9] S. Terashima,[*11] T. Uesaka,[*4] Y. N. Watanabe,[*12] K. Wimmer,[*1,*4,*12] K. Yako,[*1] Y. Yamaguchi,[*1] Z. Yang,[*4] and K. Yoneda[*4]

The equation of state (EoS) of nuclear matter not only governs the femto-scale quantum many-body system, namely nuclei, but also plays an important role in the structure of neutron stars and in supernova phenomena. In particular, the EoS of isospin asymmetric nuclear matter has attracted much interest from the viewpoint of the existence of heavy neutron stars. The asymmetric term of incompressibility, K_τ, can be a benchmark for various EoSs because it can be directly deduced from the energies of the isoscalar giant monopole resonance (ISGMR) measured along an isotopic chain, such as tin isotopes.[1] The present value of K_τ is -550 ± 100 MeV and its error is larger than those of other parameters of the EoS. In order to improve the K_τ value, the measurement on the isotopic chain should be extended to unstable nuclei. A doubly magic tin isotope, ^{132}Sn, has been chosen as a flagship for the measurements of unstable tin isotopes because of its large isospin asymmetry and double magic nature. The measurement of deuterium inelastic scattering off ^{132}Sn was performed at RIBF in RIKEN. The typical intensities of the secondary beam at F3 and F7 were 8.5×10^5 and 3.2×10^5 particles per second, respectively. The main components of the secondary beam were ^{132}Sn, ^{133}Sb, and ^{134}Te with purities of 21%, 46%, and 25% at F7, respectively.

The excitation energy and scattering angle in the center-of-mass frame are extracted by means of missing-mass spectroscopy, for which the range and angle of the low-energy recoil deuteron must be measured. In order to measure such low-energy recoils, a gaseous active target system CAT-S[2] with 0.4-atm deuterium gas has been employed as target and detector simultaneously. In this paper, we report the present status of track reconstruction for recoil particles stopping in CAT-S. Before the track reconstruc-

tion, a cluster of hits as a candidate track is searched for. The detailed procedure of track finding was reported by Tokieda $et\ al.$[3] Here, we focus on the energy calibration of each pad and track reconstruction for the hit cluster found by the track-finding process.

CAT-S has an active are of approximately 10×10-cm^2. Primary electrons produced by energy deposition along the trajectory of the recoil particle drift toward the THGEM and readout pad. The drift velocity is currently assumed to be 1 cm/μs according to the simulation using Garfield for 0.4-atm deuterium gas with an electric field of 1 kV/cm/atm. The lateral diffusion coefficient is assumed to be 0.04 cm$^{1/2}$, which yields a charge spreading of 2 mm in one standard deviation for a drift length of 25 cm. In the procedure of track reconstruction, the charge spreading should be taken into account.

The track reconstruction is performed in a two-fold manner. First, the track in the plane defined by the drift direction (Y) and axis perpendicular to beam (X) is deduced by using a linear fit of position in this plane. The position along the drift direction is calculated from the leading-edge timing multiplied by the drift velocity. The position along the X-axis is the centroid of each pad. Second, the track in the plane defined by the beam axis (Z) and the X-axis is reconstructed by fitting the calculated charges to the measured charges by taking the diffusion and the resolution into account. The second part of track reconstruction requires energy calibration. A set of trial calibration parameters is used to deduce the realistic energy calibration parameter after comparing the measured charge with the one calculated from the best-fit track. The charge resolution can be estimated from the distribution of the difference between the measured and calculated charge. The typical charge resolution after correction is less than 10%. The analyses for particle identification, improvement of track reconstruction using iteration, merging beam particle identification and so on are in progress.

*1　Center for Nuclear Study, the University of Tokyo
*2　Department of Physics, University of Notre Dame
*3　Le Centre CEA de Saclay
*4　RIKEN Nishina Center
*5　GSI Helmholtzzentrum für Schwerionenforschung GmbH
*6　Department of Physics, Toho University
*7　KVI, Center for Advanced Radiation Technology
*8　Cyclotron and Radio Isotope Center, Tohoku University
*9　Department of Applied Physics, University of Miyazaki
*10　Research Center for Nuclear Physics, Osaka University
*11　Dept. of Nucl. Sci. and Tech., Beihang University
*12　Department of Physics, the Univerisity of Tokyo

References

1) T. Li $et\ al.$, Phys. Rev. Lett. **99**, 162503 (2007).
2) S. Ota $et\ al.$, J. Radioanal. Nucl. Chem. **305**, 907–911 (2015).
3) H. Tokieda $et\ al.$, CNS Annual Report 2016, 53 (2018).

Atomic masses of intermediate-mass neutron-deficient nuclei with sub-ppm precision via multireflection time-of-flight mass spectrograph[†]

S. Kimura,[*1,*2] Y. Ito,[*3] D. Kaji,[*2] P. Schury,[*4] M. Wada,[*4,*2] H. Haba,[*2] T. Hashimoto,[*5] Y. Hirayama,[*4] M. MacCormick,[*6] H. Miyatake,[*4] J. Y. Moon,[*5] K. Morimoto,[*2] M. Mukai,[*1,*2] I. Murray,[*6,*2] A. Ozawa,[*1] M. Rosenbusch,[*2] H. Schatz,[*7] A. Takamine,[*2] T. Tanaka,[*8,*2] Y. X. Watanabe,[*4] and H. Wollnik[*9]

Accurate, high-precision nuclear mass data around $N = Z$ line are very important in several fields, e.g., rp–process and unitarity of the CKM matrix. The half lives of their key nuclei are of the order of several tens to several hundreds of milliseconds. The multireflection time-of-flight mass spectrograph (MRTOF-MS)[1] has an advantage in the mass measurements of these short-lived nuclei. However there are no actual results of on-line MRTOF-MS measurements with the required precision, $\delta m/m \lesssim 10^{-8}$, so far.

We demonstrated high-precision mass measurements of ^{63}Cu, $^{64-66}$Zn, $^{65-67}$Ga, $^{65-67}$Ge, ^{67}As, ^{78,81}Br, ^{79}Kr, ^{80,81}Rb, and ^{79,80}Sr utilizing MRTOF-MS combined with the gas-filled recoil ion separator GARIS-II.[2] Two different fusion-evaporation reactions—^{nat}S$(^{36}$Ar$, X)$ and ^{nat}Ti$(^{36}$Ar$, X)$—were used for producing these nuclides. The masses of these nuclides were determined by the single reference method using isobaric references of well-known mass.

The results are summarized in Fig. 1. There are some inconsistencies with the 2016 Atomic Mass Evaluation (AME16) values. In order to understand them, two reliability requirements were imposed on the mass values: (i) there must be no contamination with unresolvable isomers, (ii) there are no undue influences of intense neighboring peaks. Among the masses that were inconsistent with AME16, two were found to meet the reliability criteria, and we propose new mass excess values: ME(^{67}Ge) = −62675.2(46) keV and ME(^{81}Br) = −77955.4(53) keV. These mass values were previously deduced through indirect measurements. This result reinforces the need for direct mass measurements of all nuclides, even for stable isotopes, if their masses were previously evaluated by indirect techniques.

The relative mass precision in the present study spans the range from $\delta m/m = 4.1 \times 10^{-7}$ to 3.5×10^{-8}.

Fig. 1. Differences between the present measurement results and the AME16 values. Purple lines represent the error bands of the AME16 values. The open symbols indicate data derived from spectral peaks insufficiently separated from adjacent spectral peaks.

In the most precise measurement, which was that of ^{65}Ga, a mass uncertainty of 2.1 keV was obtained. This result shows that mass measurements satisfying the requirement of the CKM matrix, $\delta m/m < 5 \times 10^{-8}$, can be achieved with MRTOF-MS, given sufficient statistics.

References
1) P. Schury et al., Nucl. Instrum. Methods B **335**, 39 (2014).
2) D. Kaji et al., Nucl. Instrum. Methods B **317**, 311 (2013).

†   Condensed from the article submitted to IJMS
*1   Institute of Physics, University of Tsukuba
*2   RIKEN Nishina Center
*3   Department of Physics, McGill University
*4   KEK, IPNS, Wako Nuclear Science Center
*5   Institute for Basic Science
*6   Institut de Physique Nucléaire, Orsay
*7   Department of Physics and Astronomy and National Superconducting Cyclotron Laboratory, Michigan State University
*8   Department of Physics, Kyushu University
*9   Department of Chemistry and Biochemistry, New Mexico State University

Decay measurement of ^{283}Cn produced in the ^{238}U(^{48}Ca,3n) reaction using GARIS-II[†]

D. Kaji,[*1] K. Morimoto,[*1] H. Haba,[*1] Y. Wakabayashi,[*1] M. Takeyama,[*1,*2] S. Yamaki,[*1,*3] Y. Komori,[*1] S. Yanou,[*1] S. Goto,[*1,*4] and K. Morita[*1,*5]

A new gas-filled recoil ion separator GARIS-II[1] will be utilized for new superheavy element (SHE) search, precise mass measurement of SHE nuclide, and SHE chemistry and spectroscopy. In this work, the production and decay properties of ^{283}Cn were investigated as the first step towards the identification of SHE beyond $Z = 118$.

The 251.8 MeV ^{48}Ca^{11+} beam was provided by the RIKEN heavy-ion linear accelerator (RILAC). The ^{238}U$_3$O$_8$ targets were prepared on 3-μm Ti backing foils using an electro-deposition technique. On an average, the thickness of the ^{238}U targets was 312 μg/cm^2 as ^{238}U$_3$O$_8$. The sixteen sector-targets with 15-mm width were mounted on a rotating wheel of 300-mm diameter. The target was irradiated by a beam with an average intensity of 0.93 particle μA. The wheel was rotated at 2000 rpm during irradiation. The total beam dose was accumulated to 2.2×10^{18} during the net irradiation time of 4.5 days. The evaporation residues of interest were separated in-flight from the primary beam and other reaction products using GARIS-II. The inside of the separator's chamber was filled with pure helium at a gas pressure of 70 Pa. The magnetic rigidity for measuring ^{283}Cn was set to 2.23 Tm. The focal plane detector (FPD) of GARIS-II consists of double sided Si detectors (DSSD). The DSSD is surrounded by six side Si-detectors (SSDs), which form the DSSD box.

The decay events originating from the products in the reaction ^{48}Ca + ^{238}U were searched using the position correlations between mother and daughter nuclei at the same pixel within 100 s. As a result, two decay chains were found, as shown in Fig. 1. The first chain was an ER-SF, which consisting of 172 MeV (= 167 + 5) two-fold fission, and it was found 14.4 s after the implantation of ER with 12.2 MeV into DSSD. On the other hand, the decay pattern of ER-α-SF in the second chain was different from that of the first one. The 9.45(5) MeV α-decay was observed 5.4 s after the implantation of ER with 11.8 MeV into DSSD. Finally, 154 ms after the α-decay, a two-fold fission event with 179 MeV (= 137 + 42) was detected at the same pixel. During the net irradiation time of 4.5 days, we ob-
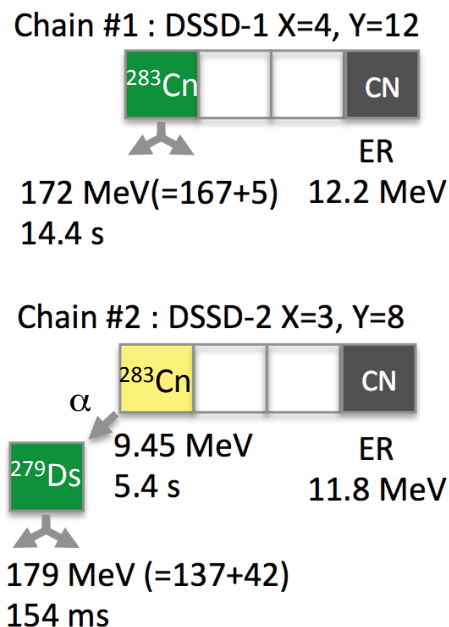
Fig. 1. The two observed decay chains produced in the reaction ^{48}Ca + ^{238}U $\rightarrow$ ^{286}Cn* at a beam energy of 251.8 MeV. The DSSD-ID number, pixel number in the horizontal (X) and vertical (Y) directions, and kinetic energy of ER are given, as well as the decay energy and time for each α-decay and/or SF.

served no other coincidence events between the signals from DSSD and SSD, indicating that our setup has a high sensitivity to SF events. The observed decay energy and time distributions for each generation in the correlated chains indicates good agreement with the reported data on ^{283}Cn and ^{287}Fl, which were studied using recoil separator DGFRS,[2,6] SHIP,[4] and BGS.[5]

The cross-section of $\sigma_{3n} = 2.0^{+2.7}_{-1.3}$ pb obtained in this work was consistent with the reported values of $\sigma_{3n} = 2.5^{+1.8}_{-1.1}$ and $0.72^{+0.58}_{-0.35}$ pb from both DGFRS[3] and SHIP,[4] respectively.

References
1) D. Kaji et al., Nucl. Instrum. Methods Phys. Res. B **317**, 311 (2013).
2) Yu. Ts. Oganessian et al., Phys. Rev. C **70**, 064609 (2004).
3) Yu. Ts. Oganessian, J. Phys. G **34**, R165 (2007).
4) S. Hofmann et al., Eur. Phys. J. A **32**, 251 (2007).
5) L. Stavestra et al., Phys. Rev. Lett. **103**, 132502 (2009).
6) Yu. Ts. Oganessian et al., Phys. Rev. C **74**, 044602 (2004).

Yield development of KEK isotope separation system

Y. X. Watanabe,[*1] Y. Hirayama,[*1] M. Mukai,[*2,*3] Y. Kakiguchi,[*1] H. Miyatake,[*1] M. Oyaizu,[*1] P. Schury,[*1] M. Wada[*1,*2] M. Ahmed,[*1,*3] S. Kimura,[*2,*3] J. Y. Moon,[*4] J. H. Park,[*4] A. Taniguchi,[*5] H. Watanabe,[*2,*6] A. Odahara,[*7] S. Kanaya,[*2,*7] and H. Muhammad[*7]

We have been developing the KEK Isotope Separation System (KISS)[1] for the lifetime measurements of neutron-rich (n-rich) nuclei around $N = 126$, which is relevant to the r-process nucleosynthesis.[2] The multi-nucleon transfer reaction between the ^{136}Xe beam and the ^{198}Pt target is considered as one of the promising candidates for the efficient production of those n-rich nuclei.[3] The reaction products are thermalized and neutralized in a gas cell filled with argon gas. They are transported to the exit of the gas cell by a laminar gas flow, where they are irradiated by lasers to be element-selectively ionized using the laser resonance ionization technique. The extracted ions are mass-separated to be implanted into an aluminized Mylar tape, where β-γ spectroscopy is performed to measure their lifetimes and nuclear structures.

Only the vicinity of the target nucleus could be accessed in the transfer of a few neutrons and protons at the present KISS, because of the limited extraction efficiency and acceptable beam intensity. The yield development is essential for KISS to achieve lifetime measurements of n-rich nuclei around $N = 126$. The GRAZING calculations[4] predict more production yields when using the ^{238}U beam than the ^{136}Xe beam. We performed an R&D experiment using the ^{238}U beam in order to investigate its feasibility.

The doughnut-shaped gas cell[5] was introduced to accept intense beams. A rotating ^{198}Pt target of 12.5 mg/cm^2 thickness was bombarded by a ^{238}U beam that was accelerated up to 10.75 MeV/nucleon by RRC. The beam energy on the target was tuned by rotating energy degraders to approximately 8.9 MeV/nucleon, which is the optimal value in the calculations. The multi-segmented proportional gas counter[6] was used to detect β-rays from the extracted radioactive isotopes in order to identify them by measuring their lifetimes.

The extraction of ^{199,201}Pt, ^{196,197}Ir and ^{196}Os was confirmed in the experiment. Crosses in the upper panel of Fig. 1 show the extraction yields of ^{199}Pt as a function of the ^{238}U beam intensity. They are smaller than those with the ^{136}Xe beam (circles) for all

beam intensities, and the discrepancy becomes larger as the beam intensity increases. The lower panel shows a comparison between the extraction yields of various isotopes with the ^{238}U beam (crosses (26 pnA) and diamonds (36 pnA)) and the ^{136}Xe beam (circles (50 pnA)). The extraction yields with the ^{238}U beam were smaller than those with the ^{136}Xe beam by about one order of magnitude in contrast to the expectations from the GRAZING calculations. The reduction in extraction yields with the ^{238}U beam is supposed to be caused by the re-neutralization of the laser-ionized atoms by the radiation from the dense plasma in the argon gas induced by the scattered ^{238}U beam. We will investigate such a plasma effect systematically using the beam of a lighter nucleus.
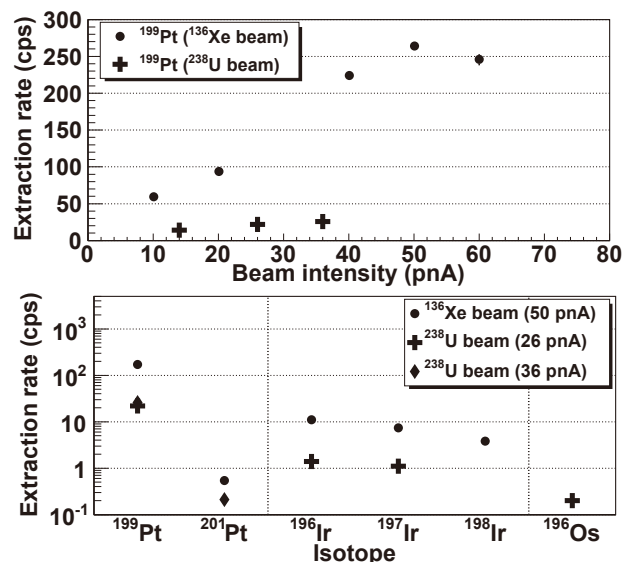
Fig. 1. (Upper) Beam intensity dependence of the measured extraction yields of ^{199}Pt for the ^{136}Xe (circles) and ^{238}U (crosses) beams. (Lower) Extraction yields of various isotopes for the ^{238}U (crosses and diamonds) and ^{136}Xe (circles) beams.

References
1) Y. Hirayama et al., Nucl. Instrum. Methods B **383**, 4 (2015).
2) S. C. Jeong et al., KEK Report **2010-2**, (2010).
3) Y. X. Watanabe et al., Phys. Rev. Lett. **115**, 172503 (2015).
4) A. Winther, Nucl. Phys. A **572**, 191 (1994); **594**, 203 (1995).
5) Y. Hirayama et al., Nucl. Instrum. Methods B **412**, 11 (2017).
6) M. Mukai et al., Nucl. Instrum. Methods A **884**, 1 (2018).

*1　Wako Nuclear Science Center (WNSC), Institute of Particle and Nuclear Studies (IPNS), High Energy Accelerator Research Organization (KEK)
*2　RIKEN Nishina Center
*3　Department of Physics, University of Tsukuba
*4　Institute for Basic Science (IBS)
*5　Research Reactor Institute, Kyoto University
*6　School of Physics and Nuclear Energy Engineering, Beihang University
*7　Department of Physics, Osaka University

The structure and decay of high-K isomers in ^{187}Ta

P. M. Walker,[*1] H. Watanabe,[*2,*3] Y. Hirayama,[*4] Zs. Podolyak,[*1] Yu. A. Litvinov,[*5] F. G. Kondev,[*6]
G. J. Lane,[*7] H. Miyatake,[*4] Y. X. Watanabe,[*4] M. Mukai,[*4] S. Kimura,[*4] A. Murad,[*4] M. Oyaizu,[*4]
Y. Kakiguchi,[*4] and J. H. Park[*8]

High-K isomers in the neutron-rich, mass 180–190 region are predicted to be exceptionally favoured energetically,[1] leading to the expectation of long half-lives that may exceed those of the corresponding ground states. At the same time, a prolate-to-oblate shape transition is predicted to result in prolate high-K isomers co-existing with oblate low-K states.[2] Furthermore, the hexadecapole deformation is predicted to reach a maximum,[3] which will influence both the single-particle states which are close to the neutron and proton Fermi surfaces, and the K-mixing effects. The unique features of this shape-transition/high-K region are related to reinforcing effects, with both the proton and neutron Fermi levels being high in their respective shells. However, experimental investigation is at an early stage on account of the neutron richness, combined with the refractory chemical properties of key elements, which severely limit the experimental opportunities.

Progress in the last decade includes the discovery[4] of long-lived (> 1 s) isomers at MeV excitation energies in ^{183,184,186}Hf ($Z = 72$) and ^{187}Ta ($Z = 73$) in the experimental storage ring at GSI, exploiting projectile fragmentation reactions. Now we report progress with the KISS (KEK Isotope Separation System)[5] facility at RIKEN, giving access to detailed spectroscopic investigation of these high-K isomers, populated using multi-nucleon transfer (MNT) reactions. The technique is complementary to other isomer studies in the neutron-rich rare-earth region at RIKEN, including recent experiments with EURICA (see Ref. 6) for example where the greatest sensitivity is for $T_{1/2} < 1$ s, and projectile-fission reactions have been employed.

The study of long-lived (> 1 s) isomers at KISS[5] makes use of an Ar gas stopping cell that avoids the chemical problems often associated with the $Z = 72$–79 refractory elements. Z selectivity is achieved by laser resonance ionization, and there is mass separation with a dipole magnet. The KISS detection system includes four super-Clover germanium detectors for γ rays, and a multi-segmented proportional gas counter[7] for low-background β particles, X-rays and conversion electrons. There a tape transport system that is synchronized with beam pulsing for half-life selection.
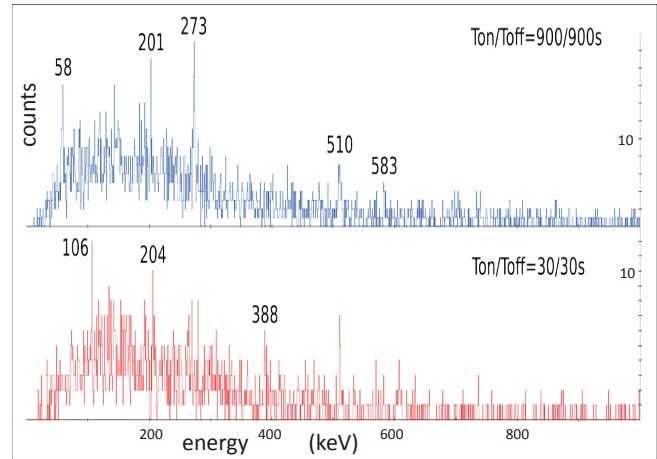
Fig. 1. Gamma rays associated with laser-ionized ^{187}Ta reaction products, measured at the tape-implantation point and with β-counter coincidences. Two different tape-cycle times are illustrated. The longer cycle (900 s beam-on, 900 s beam-off, tape movement) in the upper panel shows γ rays from the ground-state decay ($T_{1/2} = 140$ s) while the shorter cycle (30 s beam-on, 30 s beam-off, tape movement) in the lower panel shows different transitions (e.g. those labelled) which are candidates for the shorter-lived isomeric decay ($T_{1/2} < 22$ s).

In a recent test experiment (July 2017) on neutron-rich Ta isotopes, yields of $^{185g,186m+g,187g}$Ta have been measured following MNT reactions between a ^{136}Xe beam (50 pnA at 7.2 A.MeV) and a natural W target. Under these conditions, β-delayed γ rays from the ^{187}Ta ground state were identified for the first time, and candidate isomeric decays were observed, as illustrated in Fig. 1. Note that the 201 and 273 keV transitions (upper panel) are known transitions from in-beam studies[8] of 187 W, though no previous measurements of ^{187}Ta β-decay to 187 W have been reported. This establishes the capability to produce separated beams of neutron-rich Ta isotopes, and hence the viability of the technique for future spectroscopic studies.

References
1) G. D. Dracoulis, P. M. Walker, F. G. Kondev, Rep. Prog. Phys. **79**, 076301 (2016).
2) H. L. Liu, F. R. Xu, P. M. Walker, C. A. Bertulani, Phys. Rev. C **83**, 067303 (2011).
3) P. Moller *et al.*, At. Data Nucl. Data Tables **109–110**, 1 (2016).
4) M. W. Reed *et al.*, Phys. Rev. Lett. **105**, 172501 (2010).
5) Y. Hirayama *et al.*, Nucl. Instrum. Methods Phys. Res. B **353**, 4 (2015); **376**, 52 (2016); **412**, 11 (2017).
6) H. Watanabe *et al.*, Phys. Lett. B **760**, 641 (2016).
7) M. Mukai *et al.*, Nucl. Instrum. Methods Phys. Res. A **884**, 1 (2018).
8) T. Shizuma *et al.*, Phys. Rev. C **77**, 047303 (2008).

*1　Department of Physics, University of Surrey
*2　RIKEN Nishina Center
*3　International Research Center for Nuclei and Particles in the Cosmos, Beihang University
*4　KEK, WNSC
*5　GSI, Darmstadt
*6　Physics Division, Argonne National Laboratory
*7　Department of Nuclear Physics, Australian National University
*8　IBS

Nuclear spectroscopy of ^{196,197,198}Ir isotopes

M. Mukai,[*1,*2] Y. Hirayama,[*3] Y. X. Watanabe,[*3] P. Schury,[*3] H. Miyatake,[*3] Y. Kakiguchi,[*3] M. Oyaizu,[*3] M. Wada,[*3] M. Ahmed,[*1] S. Kimura,[*1,*2] A. Ozawa,[*1] H. Haba,[*2] H. Ueno,[*2] J. Y. Moon,[*4] J. H. Park,[*4] H. Watanabe,[*5] and S. Kanaya[*6]

For improving the accuracy of theoretical β-decay half-lives ($T_{1/2}$) for the r-process nuclei relevant to the 3rd peak in the r-abundances, a systematic experimental study of nuclear structures around $N = 126$ is required. We performed half-life measurements of ^{196,197,198}Ir ($Z = 77$, $N = 119, 120, 121$) at KISS[1] to extract the refractory elements of the neutron-rich nuclei produced by the multi-nucleon transfer reaction ^{136}Xe + ^{198}Pt.[2] We also measured their hyperfine structure (HFS) to estimate the wave-function from the nuclear electromagnetic moment, spin, and quadrupole deformation parameter.

The extracted ions from KISS are implanted on an aluminized Mylar tape, and then β-rays emitted from the unstable nuclei are detected by the multi-segmented proportional gas-counter.[3] For the half-life measurement, growth and decay curves were measured when the time sequence of the KISS beam on/off = 1.5/4 $T_{1/2}$. After the confirmation of the half-lives and the extraction yields, the HFS spectra of the extracted nuclei were measured by counting the β-rays as a function of the excitation laser wavelength.

The typical time spectrum of the β-decay of ^{198}Ir is shown in Fig. 1. The fitting curve, which consists of one parent nucleus and a constant background, is shown by the red line. The half-lives of ^{196,197,198}Ir were evaluated to be 51(4) s, 6.1(4) min, and 8.9(4) s, respectively. These values are in good agreement with the values in a literature,[4] i.e., 52(1) s, 5.8(5) min, and 8(1) s. The yields of more than 5 pps were high enough to perform the HFS measurements.

The magnetic dipole moment μ and the isotope shift of ^{196,197,198}Ir were deduced from the fittings of the measured HFS spectra. The μ values of odd-A Ir and Au ($Z = 79$) isotopes of $I^\pi = 3/2^{+}$[5] are shown in Fig. 2. The evaluated μ value of ^{197}Ir shows a similar systematic trend in gold isotopes. The μ values of ^{197}Ir and ^{199}Au are about two times larger than the values of the lighter odd-A isotopes, which are close to the Schmidt value 0.12 of the πd3/2 orbit. A larger μ suggests a larger deformation of ^{197}Ir and ^{199}Au.

The HFS also yields the nuclear mean-square charge radius and the quadrupole deformation parameters $|\beta_2|$, as shown in Fig. 3. The variations of $|\beta_2|$ at $A = 196$–198 seem to be consistent with the trend of the theoretical
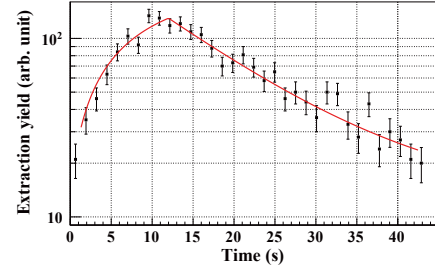
Fig. 1. Measured growth and decay time spectra for ^{198}Ir. The solid line indicates the best fitting curve to the experimental data.
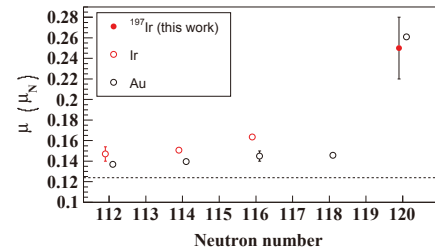
Fig. 2. Magnetic dipole moments of odd-A Ir and Au isotopes of $I^\pi = 3/2^{+}$.[5] The broken line indicates the Schmidt value 0.12 of the πd3/2 orbit.
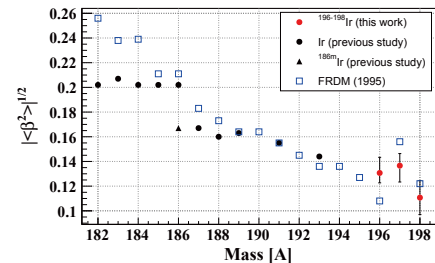
Fig. 3. The experimental β_2 values of iridium isotopes are compared with the theoretical values. The measured $|\beta_2|$ values of the isotopes $A \leq 193$ were taken from Ref. 7).

values given by the FRDM model[6] which predicts the shape transition from a prolate to an oblate shape between $A = 196$ and 197. Further study of the nuclear structures of $^{196–198}$Ir isotopes is in progress for the publication.

References
1) Y. Hirayama et al., Nucl. Instrum. Methods B **383**, 4 (2015).
2) Y. X. Watanabe et al., Phys. Rev. Lett. **115**, 172503 (2015).
3) M. Mukai et al., Nucl. Instrum. Methods A **884**, 1 (2018).
4) http://www.nndc.bnl.gov.
5) N. J. Stone, IAEA Vienna Report No. INDC(NDS)-**0658** (2014).
6) P. Möller, At. Data Nucl. Data Tables **59**, 185 (1995).
7) D. Verney et al., Eur. Phys. J. A **30**, 489 (2006).

*1 Department of Physics, University of Tsukuba
*2 RIKEN Nishina Center
*3 Wako Nuclear Science Center (WNSC), Institute of Particle and Nuclear Studies (IPNS), High Energy Accelerator Research Organization (KEK)
*4 Institute for Basic Science, Rare Isotope Science Project
*5 School of Physics and Nuclear Energy Engineering, Beihang University
*6 Department of Physics, Osaka University

Ground-state electromagnetic moments of ^{21}O

A. Gladkov,[*1,*2] Y. Ishibashi,[*1,*3] H. Yamazaki,[*1] Y. Ichikawa,[*1] A. Takamine,[*1] H. Nishibata,[*1] K. Asahi,[*1]
T. Sato,[*1] W. Y. Kim,[*2] T. Fujita,[*1,*4] L. C. Tao,[*1,*5] T. Egami,[*1,*6] D. Tominaga,[*1,*6] T. Kawaguchi,[*1,*6]
M. Sanjo,[*1,*6] W. Kobayashi,[*1,*6] K. Imamura,[*1,*7] Y. Nakamura,[*1,*7] G. Georgiev,[*8] J. M. Daugas,[*1,*9]
and H. Ueno[*1]

As a continuation of our previous report,[1] here we would like to give an overview of the intermediate results of analysis of the spectra obtained in the ^{21}O β-NMR experiment conducted at RIPS, RIBF. In the experiment, the ^{21}O beam was produced from a ^{22}Ne beam at 69 AMeV on a Be target in a projectile-fragmentation reaction involving one neutron pick-up.

In g-factor measurements, the beta-NMR[2] technique was applied to the ^{21}O ions implanted into the CaO stopper crystal. The Larmor frequency, and hence the g-factor, have been straightforwardly determined from the spectrum obtained with a single-sweep width of 14 kHz (red triangles in Fig. 1) and the value of the ^{21}O magnetic moment $\mu(^{21}O) \approx 1.5~\mu_N$ was preliminary deduced.

In order to measure the electric quadrupole moment, the ^{21}O beam was implanted into a single crystal of TiO$_2$ to provide the electric-field gradient necessary for the β-NQR[3] measurements. The obtained β-NQR spectrum is shown on Fig. 2. Although the statistics does not allow us to directly distinguish the anticipated double-resonance structure of the spectrum,[4] the preliminary result of the least-chi-square fitting with a double-Gaussian function is consistent with the expected double-peak nature of the spectrum. The actual value of the quadrupole moment can be extracted from peak I, which corresponds to the substitutional implantation site in TiO$_2$. From the fitting curve in Fig. 2, $\nu_Q \approx 151.5$ kHz was preliminarily obtained. However, the final analysis and error assignments for both magnetic and quadrupole moments are in progress and will be reported later.

In terms of nuclear structure, at first glance, the neutron-rich ^{21}O appears to be a "normal" nucleus well characterized by a pure $1d_{5/2}$ single particle configuration. However, the theoretical interpretation of these results and the evolution of nuclear structure from ^{19}O to ^{23}O are still under discussion and will be described elsewhere.
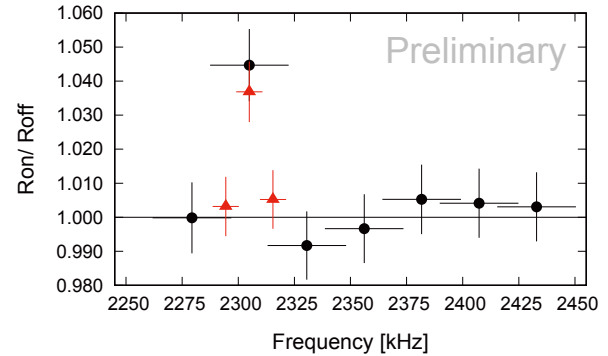
Fig. 1. β-NMR spectrum of ^{21}O in a CaO crystal. The horizontal error bars represent the widths of frequency sweep. Data obtained from two separate runs are shown. The Larmor frequency was determined from the spectrum represented by red triangles.
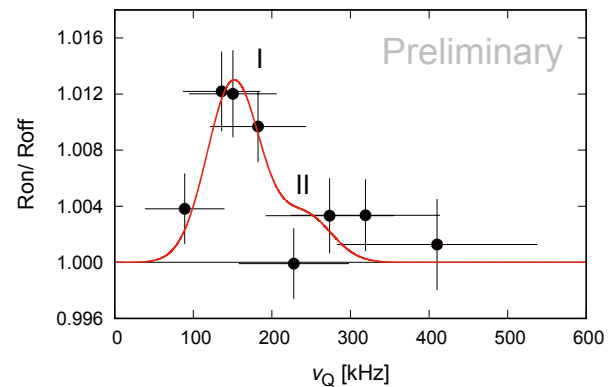
Fig. 2. β-NQR spectrum of ^{21}O in the TiO$_2$ single crystal. The red line represents the least-chi-square fitting with a double-Gaussian function taking into account the physical expectations based on previous works.[4] The interval between the two peaks is a fixed value defined by the ratio between the electric-field gradients of two different implantation sites in TiO2. For the definition of ν_Q, see Ref. 5).

[*1] RIKEN Nishina Center
[*2] Department of Physics, Kyungpook National University
[*3] Cyclotron and Radioisotope Center, Tohoku University
[*4] Department of Physics, Osaka University
[*5] School of Physics, Peking University
[*6] Department of Physics, Hosei University
[*7] Department of Physics, Meiji University
[*8] CSNSM, CNRS/IN2P3, Université Paris-Sud
[*9] CEA, DAM, DIF

References
1) A. Gladkov *et al.*, RIKEN Accel. Prog. Rep. **50**, 74 (2017).
2) K. Sugimoto *et al.*, J. Phys. Soc. Jpn. **21**, 213 (1966).
3) D. Nagae *et al.*, Nucl. Instrum. Methods B **266**, 4612 (2008).
4) T. Minamisono *et al.*, Phys. Lett. B **457**, 9 (1999).
5) H. Izumi *et al.*, Hyperfine Int. **97/98**, 509 (1996).

β-NQR measurement of the ^{23}Ne ground state

H. Nishibata,[*1] A. Gladkov,[*1,*2] T. Kawaguchi,[*3] H. Ueno,[*1] Y. Ichikawa,[*1] A. Takamine,[*1] T. Sato,[*1]
K. Kawata,[*1,*4] H. Yamazaki,[*1] W. Kobayashi,[*3] M. Sanjo,[*3] L. C. Tao,[*5] Y. Namamura,[*3] T. Asakawa,[*3]
Y. Sasaki,[*3] K. Totsuka,[*3] K. Doi,[*3] T. Yada,[*3] K. Asahi,[*1] Y. Ishibashi,[*6] K. Imamura,[*7] T. Fujita,[*8]
G. Georgiev,[*9] and J. M. Daugas[*10]

In this report, we present some results of the experimental program NP1612-RRC47. The aim of this experiment is to search for an appropriate single crystal for the β-NMR measurement of Ne isotopes and to measure its electric field gradient at the sitting site of Ne, as the first step to the nuclear electromagnetic moment measurement of neutron-rich Ne isotopes. In the present study, we applied the β-NQR method[1] to the spin-polarized ^{23}Ne, the ground-state Q moment of which has been well-studied,[2] implanted into the ZnO single crystal.

The experiment was conducted using the RIKEN projectile fragment separator (RIPS). A radioactive ^{23}Ne beam was obtained from the single-neutron pickup reaction of ^{22}Ne at 70 MeV/nucleon on a 0.25-mm thick Be target. In order to produce spin polarization, the primary beam was injected with a tilt angle of 2° with respect to the spectrometer entrance (F0), where the Be target was located. Fragments were accepted at a finite angle $\theta = 1°–3°$ to the primary beam direction, and the center of the momentum distribution ($\Delta p/p \leq |\pm 0.25\%|$) was selected at momentum dispersive focal plane F1. A secondary beam of ^{23}Ne with a purity higher than 90% was separated with a 321-mg/cm^2 thick Al wedge degrader. The intensity of the spin-polarized ^{23}Ne was 5×10^4 pps with a ^{22}Ne beam intensity of 400 pnA.

The spin-polarized ^{23}Ne was implanted in a ZnO single crystal (28 mm × 20 mm × 0.5 mm, inclined at 45° to the horizontal plane), which was located at the center of the β-NMR apparatus. The c-axis of the ZnO single crystal was along the vertical axis. A static magnetic field of 0.5 T was applied to the crystal parallel to its c-axis, and an oscillating magnetic field was applied by a pair of RF coils perpendicular to the static magnetic field. The crystal was cooled to $T \sim$ 50 K to achieve a longer spin-lattice relaxation time than the ^{23}Ne β-decay half-life ($T_{1/2} = 37$ s).

The β rays from the β decay of ^{23}Ne was detected through a vacuum chamber wall, made of 1-mm thick fiber-reinforced plastic, by two β-ray telescopes which were located above and below the crystal. Each telescope consists of a stack of three 1.0-mm thick plastic scintillators. The telescopes cover approximately 50% of the entire solid angle.

In the experiment, we first measured the g-factor of the ^{23}Ne ground state with a NaF polycrystalline stopper by the β-NMR method to confirm the polarization of the ^{23}Ne beam. In this measurement, we observed a nuclear magnetic resonance at 1653.8(5) kHz; thus, a g-factor of $g = 0.43305(14)$ was deduced. The obtained g-factor is consistent with the literature values $g = 0.432(4)$[3] and $0.43268(36)$.[4] The polarization of the ^{23}Ne beam was also determined to be $AP = 5.0(4)\%$.

After measuring the g-factor, we performed the β-NQR measurement of ^{23}Ne by using the ZnO single crystal. Figure 1 shows the obtained β-NQR spectrum of ^{23}Ne in the ZnO single crystal. In the figure, a clear β-ray asymmetry change is found at $\nu_Q (= eqQ/h) = 1.08(5)\times10^3$ kHz. From the obtained ν_Q and the Q moment [$Q = 145(13)$ emb],[2] the electric field gradient q is determined to be $|q| = 31(3)\times10^{19}$ [V/m^2]. Now, we are ready to measure the ground-state electromagnetic moments of neutron-rich Ne isotopes.
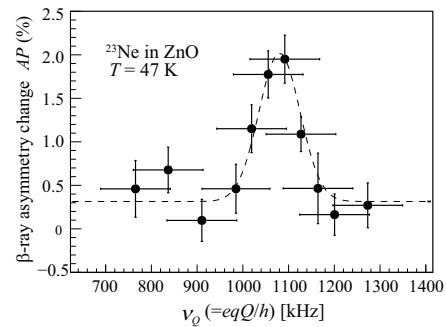
Fig. 1. Beta-NQR spectrum of ^{23}Ne implanted into the ZnO single crystal. The dashed line shows the least chi-square fitting result with a Gaussian function plus a constant. The horizontal error bars indicate the width of the swept frequency ($\Delta\nu_Q = 1.5 \times 10^2$ kHz).

[*1] RIKEN Nishina Center
[*2] Department of Physics, Kyungpook National University
[*3] Department of Physics, Hosei University
[*4] Center for Nuclear Study, University of Tokyo
[*5] School of Physics, Peking University
[*6] Cyclotron and Radioisotope Center, Tohoku University
[*7] Department of Physics, Okayama University
[*8] Department of Physics, Osaka University
[*9] CSNSM, CNRS/IN2P3, Université Paris-Sud
[*10] CEA, DAM, DIF

References
1) D. Nagae *et al.*, Nucl. Instrum. Methods B **266**, 4612 (2008).
2) W. Geithner *et al.*, Phys. Rev. C **71**, 064319 (2005).
3) D. A. Dobson, S. R. Brown, Bull. Am. Phys. Soc. **13** (2), 173, CD3 (1968).
4) R. Matsumiya *et al.*, OULNS Ann. Rept. **2004**, 51 (2005).

^{26m}Al proton resonant elastic scattering with CRIB

D. Kahl,[*1] H. Shimizu,[*2] H. Yamaguchi,[*2] K. Abe,[*2] O. Beliuskina,[*2] S. M. Cha,[*3] K. Y. Chae,[*3] A. A. Chen,[*4]
Z. Ge,[*5] S. Hayakawa,[*2] N. Imai,[*2] N. Iwasa,[*6] A. Kim,[*7] D. H. Kim,[*7] M. J. Kim,[*3] S. Kubono,[*5]
M. S. Kwag,[*3] J. Liang,[*4] J. Y. Moon,[*8,*9] S. Nishimura,[*5] S. Oka,[*10] S. Y. Park,[*7] A. Psaltis,[*4]
T. Teranishi,[*10] Y. Ueno,[*10] and L. Yang[*2]

^{26}Al is known as the first specific radioactivity discovered with extraterrestrial origins.[1] The observed spatial and velocity profiles of galactic ^{26}Al provide insights to nucleosynthesis and galactic chemical evolution. In this context, the stellar nuclear reactions which produce and destroy ^{26}Al should be sufficiently constrained by experimental data when possible, in order to reduce the uncertainties on the ejected mass of ^{26}Al calculated in various stellar models. Knowledge of the reaction rate of radiative proton capture on the low-lying isomeric state ^{26m}Al(p, γ) is still lacking, particularly at higher excitation energies when the two species ^{26g,m}Al are expected to be in thermal equilibrium (> 1 GK).

We performed the first measurement of mixed ^{26g,m}Al proton elastic scattering at the CNS low-energy RI beam separator (CRIB)[2] to search for low-spin states with large Γ_p which may influence the ^{26m}Al(p, γ) rate. Considering the isomer's excitation energy of 228 keV, the typical operating resolution of CRIB ($\frac{\Delta p}{p} \sim 1\%$) is insufficient to distinguish the two ^{26}Al species event by event. To make the measurement tractable, we considered that the ^{26}Mg(p, n)^{26}Al reaction cross section shows anticorrelated yield for ^{26g,m}Al depending on $E_{c.m.}$[3] as well as that the previous measurement of ^{26g}Al(p, p) showed only Rutherford scattering over the measured energy range.[4]

We produced the cocktail beam inflight via the ^{26}Mg(p, n)^{26}Al reaction in inverse kinematics. A primary beam of ^{26}Mg^{8+} was extracted from the Hyper-ECR ion source, accelerated up to 6.65 MeV/u by the AVF cyclotron, and delivered to CRIB with typical intensities of 25–50 pnA. The ^{26}Mg beam impinged on the CRIB cryogenic production target, which contained H$_2$ at 130–290 Torr at an effective temperature of 90 K over 8 cm (0.4 to 0.8 mg cm^{-2}). By varying the H$_2$ gas pressure as well as a removable Havar energy degrader foil upstream of the production target, we could control $E_{c.m.}$ and hence the isomeric purity of the cocktail beam. We regularly monitored the isomeric purity using β-decay measurements in a beam pulsing mode.
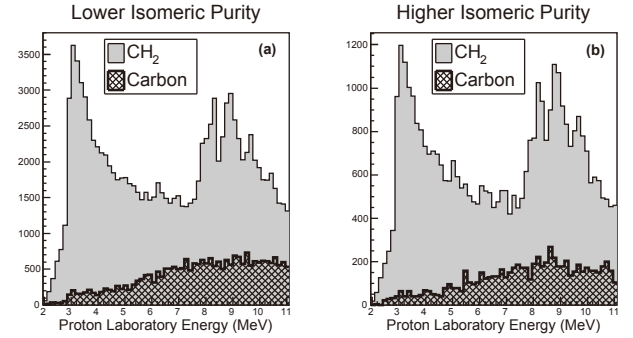
Fig. 1. Example laboratory residual proton energy spectra obtained near 0°. The isomeric purity of (b) is higher than (a).

The decay measurements were interpreted with the assistance of GEANT4 simulations, and we found the isomeric purity was approximately 40–60% depending on the experimental conditions. The ^{26}Al cocktail beams had an average intensity of 1.5×10^5 pps, 93% purity, and on-target energies of 68, 83, and 93 MeV

To measure the physics of interest, the ^{26}Al beam was tracked with two PPACs before fully stopping in a 7.5 mg cm^{-2} CH$_2$ foil which served as a proton target. Scattered protons were measured at forward laboratory angles with ΔE–E silicon telescopes. Background contributions from carbon in the polyethylene target were evaluated by intermittently exchanging the CH$_2$ foil with a 10.6 mg cm^{-2} carbon foil. Examples of the preliminary laboratory proton energy spectra are shown in Fig. 1. The background contribution from carbon (scaled to the number of incident ^{26}Al ions) looks smooth, and hints of some peak-like structures seem to emerge when the isomeric purity is higher. These preliminary results look promising for our future analysis, where we will add all the kinematic conditions including all energy losses to obtain the proton scattering excitation function in the center-of-mass frame. Finally, we plan to extract resonance parameters with an R-matrix analysis.

References
1) W. A. Mahoney, J. C. Ling, A. S. Jacobson, R. E. Lingenfelter, Astrophys. J. **262**, 742 (1982).
2) Y. Yanagisawa *et al.*, Nucl. Instrum. Methods Phys. Res. A **539**, 74 (2005).
3) R. T. Skelton *et al.*, Phys. Rev. C **35**, 45 (1987).
4) S. T. Pittman *et al.*, Phys. Rev. C **85**, 065804 (2012).

*1　School of Physics & Astronomy, University of Edinburgh
*2　Center for Nuclear Study, University of Tokyo
*3　Department of Physics, Sungkyunkwan University
*4　Department of Physics & Astronomy, McMaster University
*5　RIKEN Nishina Center
*6　Department of Physics, Tohoku University
*7　Department of Physics, Ewha Womans University
*8　Institute for Basic Science
*9　Wako Nuclear Science Center
*10　Department of Physics, Kyushu University

Development of a high density ^{7}Be beam at CRIB

A. Inoue,[*1] A. Tamii,[*1] H. Yamaguchi,[*2] K. Abe,[*2] S. Adachi,[*1] S. Hayakawa,[*2] J. Isaak,[*1] N. Kobayashi,[*1] H. Shimizu,[*2] and L. Yang[*2]

The ^{7}Li problem is a discrepancy between the standard Big-Bang Nucleosynthesis (BBN) model and observations. Our research goal is to measure the cross section of the ^{7}Be(d, p) reaction to solve this ^{7}Li problem. A recent theoretical BBN model predicts a primordial ^{7}Li abundance that is 3 times larger than the recent precise observation.[1] This difference is quite large, while the theoretical calculation reproduces the abundance of the other light nuclei well. One possible scenario to solve the problem, which has not been included yet in the BBN model, is that ^{7}Be was destroyed in the nuclear reaction after the Big Bang. The ^{7}Be$(d, p)^8$Be and the ^{7}Be$(n, \alpha)^4$He reactions are two promising processes for destroying ^{7}Be. We are focusing on the ^{7}Be$(d, p)^8$Be reaction since the contribution from ^{7}Be$(d, p)^8$Be is suggested to be larger that from ^{7}Be$(n, \alpha)^4$He.[2,3]

We are developing an unstable ^{7}Be target for high-resolution measurement of the ^{7}Be$(d, p)^8$Be reaction in normal kinematics. This is a big technical challenge since ^{7}Be is an unstable nucleus. We suggested to make the ^{7}Be target by implantation in a host material. This is called the *Implantation method*. The development is ongoing at CRIB, Center for Nuclear Study (CNS), University of Tokyo. The first experiment was performed in June 2016. The primary beam was ^{7}Li^{2+} at 5.6 MeV/nucleon. The secondary beam was produced by the ^{1}H(^{7}Li, ^{7}Be) reaction by employing a cryogenic hydrogen gas target. The gas thickness is 8 cm and the gas pressure was 760 Torr. The secondary beam energy was 4.0 MeV/nucleon. A 10-μm thick gold foil as a host target was irradiated with the ^{7}Be beam after an energy degrader made of gold with a thickness of 15 μm and a collimator with a diameter of 3 mm. We evaluated the amount of the implanted ^{7}Be by detecting 477 keV γ rays with a LaBr$_3$ detector after the implantation. The γ ray is emitted through the electron capture decay of ^{7}Be with a branching ratio of 10.4%. We obtained 1.3×10^{11} (4.3×10^{10}/mm^2) ^{7}Be particles after 19 hours of irradiation. The average beam intensity was 6.3×10^5/mm^2. However, the number of the ^{7}Be particles is almost 10 times smaller than our estimation from the maximum intensity ($\sim 10^6$/mm^2) of CRIB's previous performance. We suspect that the beam spot size and the beam profile at F2 were not fully optimized for the high-intensity ^{7}Be beam downstream of the collimator and not maintained at a fixed position during the long irradiation time since we did not check the ^{7}Be beam profile when the beam intensity was increased. This is because it was not possible to count such a high intensity beam directly.

Based on the result of the experiment in 2016, we performed a development experiment at CRIB to optimize the beam line optics and obtain an intense beam of ^{7}Be, in April 2017. Previously, the beam profile was checked with the PPAC detector at CRIB. However the PPAC detector is not a detector for such a high rate, so we could not count the high intensity beam with the existing detector. To solve this issue, we installed a metal mesh at F1 and a plastic scintillator at F2 to count the beam intensity. This was a new trial at CRIB. The metal mesh was used to reduce the ^{7}Be beam intensity, and hence we could count the ^{7}Be beam intensity directly by the plastic scintillator. In this experiment, we tuned the ion-optical parameters and the steerer on the beam line for the best-positioning and focusing of the secondary ^{7}Be, by counting the intensity with the plastic scintillator. We achieved 6.8×10^6/mm^2 as the average beam intensity after the optimization of the settings of beam-line optics. We obtained 1.2×10^{12} (1.7×10^{11}/mm^2) ^{7}Be particles with 7-hours irradiation. As the next step, we plan to measure the ^{7}Be(d, p) reaction at Japan Atomic Energy Agency, tandem facility. The ^{7}Be target will be produced at CRIB before the (d, p) reaction measurement, planned for 2018. About 8.2×10^{12} (2.6×10^{12}/mm^2) ^{7}Be ions will be implanted in 2 days of irradiation.
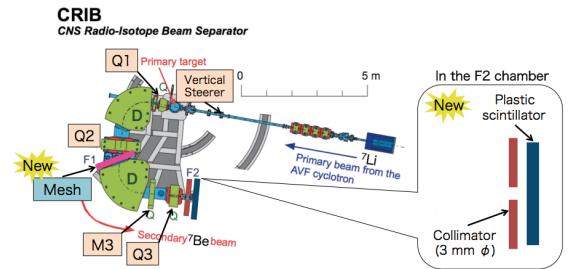
Fig. 1. Plane view of CRIB, where the Q1, Q2, Q3, and M3 magnets and the steerer were optimized in the present work. The installation of the mesh at F1 and the plastic scintillator at F2 was a new trial at CRIB to count the high intensity beam. The ^{7}Be beam was counted after the 3 mm diameter collimator.

References
1) R. H. Cyburt *et al.*, J. Cosmol. Astropart. Phys. **11**, 012 (2008).
2) S. Q. Hou *et al.*, Phys. Rev. C **91**, 055802 (2015).
3) T. Kawabata *et al.*, Phys. Rev. Lett. **118**, 052701 (2017).

*1 Research Center for Nuclear Physics, Osaka University
*2 Center for Nuclear Study, University of Tokyo

Experimental setup of the ^{6}He(p, n) measurement at HIMAC and identification of the charge-exchange (p, n) reaction channel

M. Sasano,[*1] L. Stuhl,[*1,*2] J. Gao,[*1,*3] K. Yako,[*2] Y. Kubota,[*1] Z. Yang,[*1] J. Zenihiro,[*1] V. Panin,[*1] Z. Korkulu,[*1] E. Takada,[*4] H. Baba,[*1] and T. Uesaka[*2]

As reported in another article[1] in this volume, we performed a measurement of the ^{6}He(p, n) reaction in the SB2 course at HIMAC in the winter of 2017 (H391 experiment). In this report, the setup used in the HIMAC experiment is presented with a preliminary result of the analysis to identify the (p, n) reaction channel.
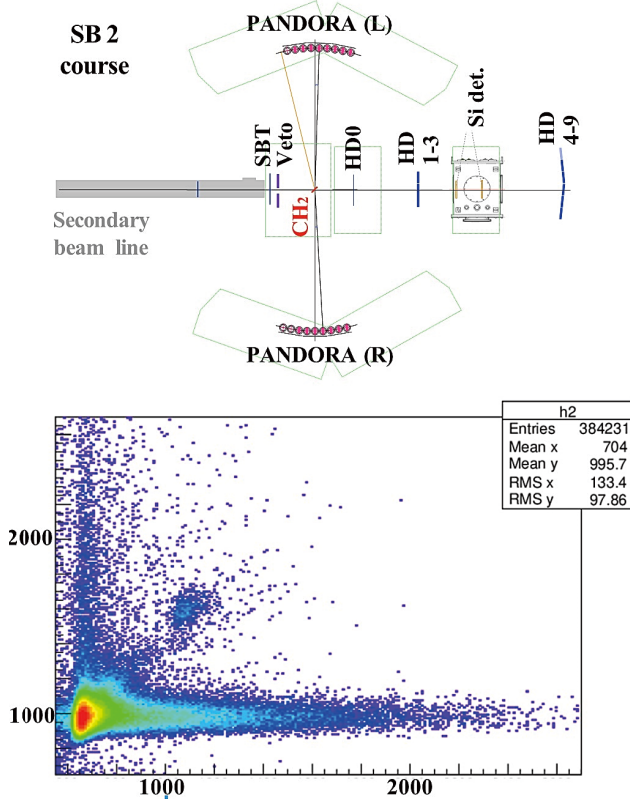
Fig. 1. (top) Layout of the experimental setup used in the HIMAC H391 experiment. (bottom) Particle-identification plot of reaction residues. The vertical and horizontal axes correspond to the energy losses in HD0 and HD1 (E_0 and E_1), respectively. The units are QDC channels.

Figure 1 (top) shows the layout of the experimental setup. In the experiment, a secondary beam of ^{6}He at 123 MeV/nucleon was produced through a fragmentation reaction with a 160 MeV/nucleon primary beam of ^{11}B. The resulting cocktail beam had a total intensity of 2×10^4 particles/s, containing ^{6}He with a purity

of 96%. The particle identification (PID) of the beam particles was performed on an event-by-event basis by using the energy loss information in the SBT plastic scintillator. The secondary beam was impinged on a polyethylene target with a thickness of 7 mm. The recoil neutrons were detected using the PANDORA[2] neutron detectors surrounding the target. The hodoscope bars were placed downstream of the target to identify the reaction residues produced in the (p, n) reaction from the incident ^{6}He particles. Depending on the excitation energy, the daughter nucleus, *i.e.* ^{6}Li, decays into multiple reaction residues of light nuclei such as protons, neutrons, and tritons. With the aim of distinguishing such events, the hodoscope setup consisted of three layers: the first layer was used to identify ^{6}Li only, while the other two layers were segmented so as to detect light nuclei. HD0 (HD1-8) had a plastic scintillator plate with dimensions of $240^W \times 80^H \times 2^D$ mm^3 ($100^W \times 1000^H \times 10^D$ mm^3). HD0 covered the solid angle for ^{6}Li particles emitted at angles up to 7°, which was sufficient to measure the (p, n) reaction at scattering angles up to 15° in the center-of-mass system. As a parasitic setup, the silicon detector setup developed for SAMURAI heavy-ion proton experiments was also installed.

Figure 1 (bottom) shows a PID plot of reaction residues obtained by comparing the charge information in the hodoscope in the first layer (HD0) and that in the second layer immediately behind HD0 (HD2), after selecting events corresponding to ^{6}He beam particles. The data shown here were accumulated within a two hour run. The most intense PID blob corresponds to the events in which the ^{6}He beam particles penetrated both HD0 and HD2 (unreacted events). The blob around $(E_0, E_1) = (1600, 1100)$ is due to the events in which the ^{6}Li beam particles penetrated both HD0 and HD2, corresponding to the (p, n) reaction channel. The ^{6}Li events are clearly separated from the unreacted events in this two-dimensional plot. We have an issue that the energy loss information in HD2 for the unreacted channel has a long tail for higher QDC values. For clarifying the origin of this tail, we are planning to analyze the waveform data of HD2 taken by the CAEN digtizer modules reported in another article[3] in this volume. The analysis is in progress.

References
1) L. Stuhl *et al.*, in this report.
2) L. Stuhl *et al.*, Nucl. Instrum. Methods Phys. Res. A **866**, 164 (2017).
3) J. Gao *et al.*, in this report.

*1　RIKEN Nishina Center
*2　Center for Nuclear Study, University of Tokyo
*3　School of Physics, Peking University
*4　National Institute of Radiological Sciences (NIRS)

RI beam production at BigRIPS in 2017

D. S. Ahn,[*1] N. Fukuda,[*1] H. Suzuki,[*1] Y. Shimizu,[*1] H. Takeda,[*1] T. Sumikama,[*1] N. Inabe,[*1] J. Amano,[*1,*2]
K. Kusaka,[*1] Y. Yanagisawa,[*1] M. Ohtake,[*1] T. Komatsubara,[*1] H. Sato,[*1] K. Yoshida,[*1] and H. Ueno[*1]

The radioactive isotope (RI) beam production at the BigRIPS fragment separator[1] in 2017 is presented here. Table 1 summarizes the experimental programs that involved the use of the BigRIPS separator during this period and the RI beams produced for each experiment.

The spring beam time started with a ^{48}Ca primary beam in March. The experiment was performed to search for the existence of a new ^{39}Na isotope and to determine the neutron dripline of neon isotopes.[2] The parasite BRIKEN experiment was performed to measure the multi-neutron emission probabilities.

Four experiments were conducted in the ^{70}Zn beam campaign that was started in April. The $^{40, 50, 52}$Ca beams were delivered to the SAMURAI spectrometer to measure the electric dipole response of the neutron-rich Ca isotopes. The experiment to search for new neutron-rich isotopes was performed with the BigRIPS separator in the region of ^{60}Ca isotope.[3] A total of 8 new isotopes was identified in the preliminary analysis. The SEASTER experiment was performed with ^{63}V, ^{57}Sc, ^{53}K to understand the evolution of the shell structure towards the dripline.

Seven experiments were conducted in the ^{238}U beam campaign that was started in May. The ^{167}Sm, ^{149}Xe, ^{130}Ag, ^{84}Zn beams were delivered to the ZeroDegree spectrometer for BRIKEN experiments. The ^{200}W beam was produced for neutron-rich nuclei around the $N = 126$ using a projectile-fragmentation of the ^{238}U beam as a machine study.[4] The ^{79}Se and ^{107}Pd beams were produced for OEDO commissioning with the ImPACT program.

The spring beam time ended with an ^{18}O beam campaign, in which three experiments were performed. The ^{1}H and $^{6, 8}$He beams were produced for the SAMURAI experiment.

In the autumn beam time, the ^{238}U beam campaign was started in October with eight experiments. The ^{93}Zr, ^{107}Pd, and $^{77, 79}$Se isotope beams were provided with the ImPACT program. The BRIKEN experiments were performed to measure the multi-neutron emission probabilities and to search for new isotopes.[5] An experiment with two-step reaction scheme was performed to measure the production cross sections of the $^{125-128}$Pd beam from the ^{132}Sn beam using the BigRIPS and the ZeroDegree spectrometer.[6] The

Table 1. List of experimental programs and RI beams produced at the BigRIPS separator in 2017.

Primary beam (Period)	Proposal No.	Course	RI beams
^{48}Ca 345 MeV/nucleon (Mar. 30 – Apr. 2)	DA16-01-01	ZeroDegree	^{39}Na, ^{36}Ne
	PE16-04	ZeroDegree	^{40}Mg, ^{37}Na (parasite experiment)
^{70}Zn 345 MeV/nucleon (Apr. 11 – May 15)	NP1312-SAMURAI9R1-01	SAMURAI	$^{44, 50, 52}$Ca
	NP1406-RIBF44R1-02	BigRIPS	$^{52-54}$Ar, ^{53}Cl, ^{57}K, $^{52, 54, 60}$Ca, ^{50}S
	NP1512-SAMURAI38R1&39R2-01	SAMURAI	^{63}V, ^{57}Sc, ^{53}K
	DA17-01-01	SAMURAI	^{53}K
^{238}U 345 MeV/nucleon (May 30 – Jun. 21)	NP1512-RIBF139-02 NP1406-RIBF127R1-02 NP1406-RIBF128-02 NP1612-RIBF148-01	ZeroDegree	^{167}Sm, ^{149}Xe, ^{130}Ag, ^{84}Zn
	MS-EXP17-02	BigRIPS	^{200}W
	MS-EXP17-04	ZeroDegree	^{238}U (primary beam)
	IMPACT17-01	SHARAQ	^{79}Se, ^{107}Pd
^{18}O 220 MeV/nucleon (Jun. 24 – July 14)	NP1406-SAMURAI19R1-01	SAMURAI	^{1}H, $^{6, 8}$He
	NP1512-SAMURAI37-01	SAMURAI	$^{6, 8}$He
	NP1512-SAMURAI34-01	SAMURAI	^{1}H, ^{8}He
^{238}U 345 MeV/nucleon (Oct. 21 – Nov. 30)	IMPACT17-02-01	SHARAQ	^{93}Zr, ^{107}Pd
	DA17-02-01	ZeroDegree	^{82}Cu
	IMPACT17-02-02	SHARAQ	$^{77, 79}$Se
	MS-EXP17-03	PALIS	^{66}Cu
	NP1512-RIBF139-03 NP1612-RIBF148-02	ZeroDegree	^{100}Br, ^{102}Sr, ^{106}Zr, ^{112}Mo, ^{115}Nb
	NP1306-RIBF102-01	ZeroDegree	$^{126, 128}$Pd, ^{132}Sn
	MS-EXP17-05	Rare-RI Ring	^{78}Ge

*1 RIKEN Nishina Center
*2 Department of Physics, Rikkyo University

Table 2. Number of experiments performed using RI beams in each year.

Year	^{238}U	^{124}Xe	^{86}Kr	^{78}Kr	^{70}Zn	^{48}Ca	^{18}O	^{16}O	^{14}N	^{4}He	^{2}H	Yearly total
2007	4		1									5
2008	2					4						6
2009	3					3			3	1		10
2010						10	1		2		1	14
2011	4	2					2					8
2012	6	3			1	4	6					20
2013	4	2					3					9
2014	11				1	3		1			1	17
2015	15			6		4					1	26
2016	13	1				6	2					22
2017	13				4	2	3					22
Total	75	8	1	6	6	36	17	1	5	1	3	159
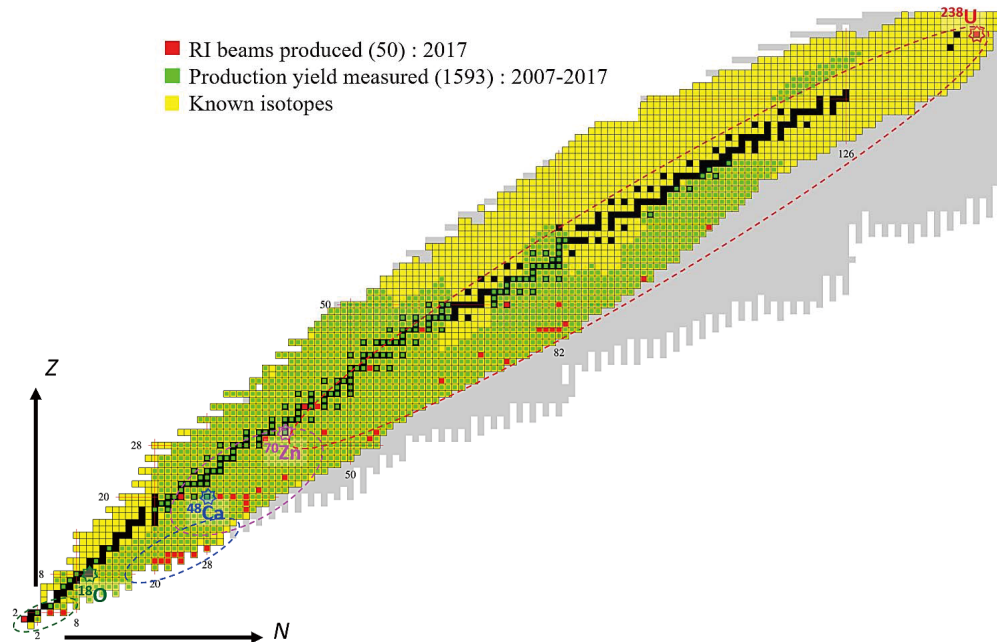
Fig. 1. RI beams produced in 2017 and the production yield measured from March 2007 to December 2017 at the BigRIPS separator.

autumn beam time ended with a machine study of the Rare-RI Ring experiment using the ^{78}Ge beam.

The number of experiments using the RI beams at the BigRIPS separator is summarized in Table 2 for various primary beams in each year. A total of 159 experiments have been performed so far. Figure 1 shows the RI beams produced in 2017 at the BigRIPS separator on the chart of nuclides with red squares. The number of RI beams produced in 2017 is 50. The production yields for 1593 RI beams were measured from March 2007 to December 2017, and they are indicated using green color. The yellow color indicates the known isotopes.

References
1) T. Kubo, Nucl. Instrum. Methods Phys. Res. B **204**, 97 (2003).
2) D. S. Ahn *et al.*, in this report.
3) O. B. Tarasov *et al.*, in this report.
4) N. Fukuda *et al.*, in this report.
5) Y. Shimizu *et al.*, in this report.
6) H. Suzuki *et al.*, in this report.

Observation of new neutron-rich Mn, Fe, Co, Ni, and Cu isotopes in the vicinity of ^{78}Ni[†]

T. Sumikama,[*1,*2] S. Nishimura,[*2] H. Baba,[*2] F. Browne,[*3,*2] P. Doornenbal,[*2] N. Fukuda,[*2] S. Franchoo,[*4]
G. Gey,[*5,*2,*6] N. Inabe,[*2] T. Isobe,[*2] P. R. John,[*7,*8] H. S. Jung,[*9] D. Kameda,[*2] T. Kubo,[*2] Z. Li,[*10]
G. Lorusso,[*2] I. Matea,[*4] K. Matsui,[*11,*2] P. Morfouace,[*4] D. Mengoni,[*12] D. R. Napoli,[*13] M. Niikura,[*11,*2]
H. Nishibata,[*14,*2] A. Odahara,[*14,*2] E. Sahin,[*15] H. Sakurai,[*2,*11] P.-A. Söderström,[*2] G. I. Stefan,[*4]
D. Suzuki,[*4,*2] H. Suzuki,[*2] H. Takeda,[*2] R. Taniuchi,[*11,*2] J. Taprogge,[*16,*17,*2] Zs. Vajta,[*18,*2]
H. Watanabe,[*19,*2] V. Werner,[*20] J. Wu,[*10,*2] Z. Y. Xu,[*11,*2] A. Yagi,[*14,*2] and K. Yoshinaga[*21,*2]

The neutron-rich nucleus ^{78}Ni is expected to be a doubly magic nucleus with the proton magic number 28 and the neutron magic number 50. To study the magicity of ^{78}Ni far from the stability line, the production of new isotopes beyond ^{78}Ni, such as the previous discovery of neutron-rich isotopes at RIBF,[1] is the first step.

In the present study, new isotopes in the vicinity of ^{78}Ni were produced via the in-flight fission reaction of a primary ^{238}U beam with a higher intensity than the previous one.[1] The beam energy was 345 MeV/nucleon and the average intensity was 6.84 particle nA. The fission fragments were purified in the BigRIPS separator and transported to the ZeroDegree spectrometer. For particle identification, the time of flight (TOF) and magnetic rigidities in the second stage of BigRIPS, as well as the energy loss in a multisampling ionization chamber (MUSIC) placed at the end of the ZeroDegree spectrometer, were measured. The atomic number, Z, and the mass-to-charge ratio, A/Q, were deduced as shown in Fig. 1. A significance test using p values was performed for 8 new isotopes ^{73}Mn, ^{76}Fe, ^{77,78}Co, ^{80,81,82}Ni, and ^{83}Cu, as described

† Condensed from the article in Phys. Rev. C **95**, 051601(R) (2017)
*1 Department of Physics, Tohoku University
*2 RIKEN Nishina Center
*3 School of Computing, Engineering and Mathematics, University of Brighton
*4 Institut de Physique Nucléaire (IPN), IN2P3-CNRS
*5 LPSC, CNRS/IN2P3, Institut National Polytechnique de Grenoble
*6 ILL
*7 Dipartimento di Fisica e Astronomia, Università di Padova
*8 Istituto Nazionale di Fisica Nucleare, Sezione di Padova
*9 Department of Physics, University of Notre Dame
*10 Department of Physics, Peking University
*11 Department of Physics, University of Tokyo
*12 Dipartimento di Fisica, Universita di Padova
*13 Institute Nazionale di Fisica Nucleare, Laboratori Nazionali di Legnaro
*14 Department of Physics, Osaka University
*15 Department of Physics, University of Oslo
*16 Departamento de Física Teórica, Universidad Autónoma de Madrid
*17 Instituto de Estructura de la Materia, CSIC
*18 MTA Atomki
*19 International Research Center for Nuclei and Particles in the Cosmos, Beihang University
*20 Wright Nuclear Structure Laboratory, Yale University
*21 Department of Physics, Tokyo University of Science

Fig. 1. Particle-identification plot of Z versus A/Q. Isotopes located on the right side beyond the red line were discovered in the present study.
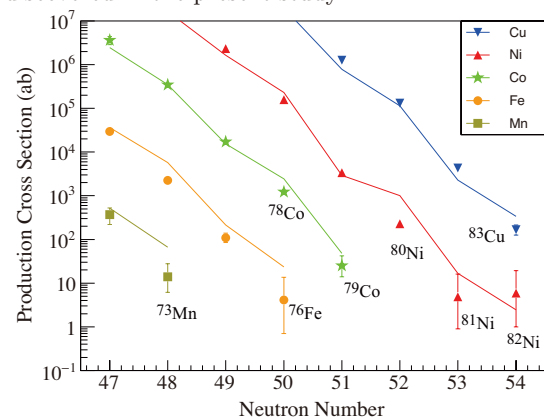
Fig. 2. Production cross section as a function of the neutron number. The lines present model predictions.[2]

in the previous study.[1] The p values, which are all less than 1%, show evidence for these isotopes including the cases of ^{76}Fe, ^{81}Ni, and ^{82}Ni with a single event. The production cross sections, shown in Fig. 2, were also checked and found to be consistent with model predictions.[2]

References
1) T. Ohnishi *et al.*, J. Phys. Soc. Jpn. **79**, 073201 (2010).
2) O. B. Tarasov, D. Bazin, Nucl. Instrum. Methods B **266**, 4657 (2008).

New isotope of ^{39}Na and the neutron dripline of neon isotopes using a 345 MeV/nucleon ^{48}Ca beam

D. S. Ahn,[*1] N. Fukuda,[*1] H. Suzuki,[*1] Y. Shimizu,[*1] H. Takeda,[*1] T. Sumikama,[*1] H. Ueno,[*1] K. Yoshida,[*1] N. Inabe,[*1] H. Sato,[*1] H. Baba,[*1] T. Komatsubara,[*1] Y. Yanagisawa,[*1] K. Kusaka,[*1] M. Ohtake,[*1] H. Otsu,[*1] T. Kubo[*1,*2] O. B. Tarasov,[*1,*2] B. M. Sherrill,[*1,*2] D. J. Morrissey,[*1,*2] D. Bazin,[*1,*2] T. Nakamura,[*1,*3] J. Amano,[*1,*4] N. Iwasa,[*1,*5] S. Ishikawa,[*1,*5] T. Sakakibara,[*1,*5] and H. Geissel[*1,*6]

The neutron dripline drawn between bound and unbound nuclei is important to verify the mass models and to understand nuclear structures. In 2014 experiment,[1] a search for ^{33}F and ^{36}Ne isotopes was performed to determine the neutron dripline. The non-observation for these isotopes indicates that they are unbound.

In April 2017, the experiment (proposal number: DA16-01-01) was carried out, aiming to search the existence of a new ^{39}Na ($Z = 11$, $N = 28$) isotope as shown in Fig. 1 and to determine the neutron dripline for neon isotopes. High statistics data of ^{36}Ne isotope were also obtained to confirm the previous non-observation.
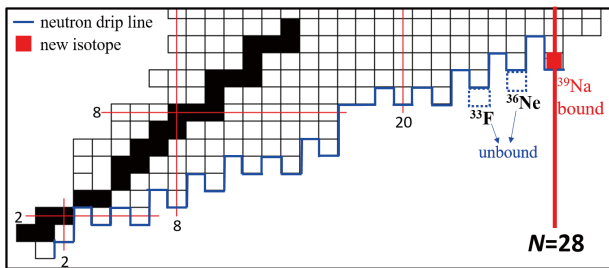
Fig. 1. New isotope of ^{39}Na with the neutron number N=28 and neutron dripline.

The neutron-rich neon and sodium isotopes were produced by the projectile-fragmentation of a ^{48}Ca beam with an energy of 345 MeV/nucleon at RIKEN RIBF. The high-intensity beam made it possible to search the neutron dripline. The magnetic rigidity (Bρ) of the first dipole magent using the BigRIPS[2] separator was tuned for the ^{39}Na isotope. Two wedge-shaped degraders at the F1 and F5 dispersive foci were used to purify the RI beams. A thick collimator[3] made of an SUS material with 50-cm thickness was installed at the F2 focal plane to reject tritons and other light particles. The different Bρ value was tuned for the ^{36}Ne isotope. The experimental conditions for ^{39}Na and ^{36}Ne settings are summarized in Table 1.

The particle identification (PID) was conducted using the TOF-Bρ-ΔE method.[4] Figure 2 shows a pre-liminary PID plot for the ^{39}Na setting. The new isotope of ^{39}Na was clearly observed. The non-observation of any events corresponding to ^{38}Na indicates that it is unbound. In this experiment, we also determined the dripline of neon isotopes with a high confidence level. The detailed data analysis is currently in progress.

Table 1. Experimental conditions.

Settings	^{39}Na	^{36}Ne
Target	Be 20 mm	Be 20 mm
F1 degrader	Al 15 mm	Al 15 mm
F5 degrader	Al 7 mm	Al 7 mm
Bρ	9.155 Tm	9.4077 mm
Momentum acceptance	± 3%	± 3%
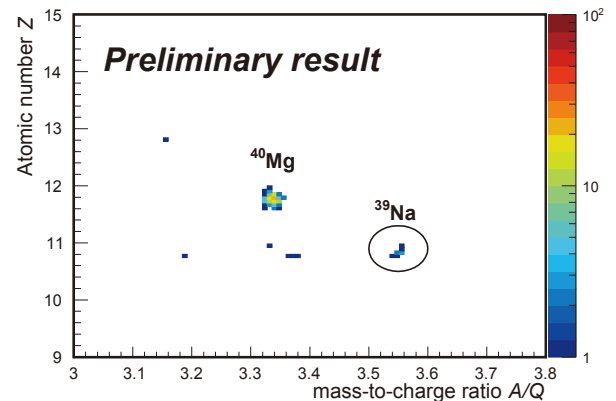
Fig. 2. Preliminary PID plot for the ^{39}Na setting.

References
1) N. Fukuda, T. Kubo *et al.*, to be submitted.
2) T. Kubo *et al.*, Nucl. Instrum. Methods Phys. Res. B **204**, 97 (2003).
3) D. S. Ahn *et al.*, RIKEN Accel. Prog. Rep. 50, 85 (2017).
4) N. Fukuda *et al.*, Nucl. Instrum. Methods Phys. Res. B **317**, 323 (2013).

*1 RIKEN Nishina Center
*2 FRIB/NSCL, Michigan State University
*3 Department of Physics, Tokyo Institute of Technology
*4 Department of Physics, Rikkyo University
*5 Department of Physics, Tohoku University
*6 GSI Helmholtzzentrum für Schwerionenforschung

Exploration of the ^{60}Ca region

O. B. Tarasov,[*1,*2] T. Kubo,[*1,*2] D. Bazin,[*1,*2] D. J. Morrissey,[*1,*2] M. Portillo,[*1,*2] B. M. Sherrill,[*1,*2]
A. Stolz,[*1] M. Thoennessen,[*1] D. S. Ahn,[*2] H. Baba,[*2] N. Fukuda,[*2] N. Inabe,[*2] S. Ishikawa,[*2,*3] N. Iwasa,[*2,*3]
K. Kawata,[*2,*4] T. Komatsubara,[*2] K. Kusaka,[*2] M. Ohtake,[*2] H. Otsu,[*2] T. Sakakibara,[*2,*3] H. Sakurai,[*2]
H. Sato,[*2] Y. Shimizu,[*2] T. Sumikama,[*2] H. Suzuki,[*2] H. Takeda,[*2] H. Ueno,[*2] Y. Yanagisawa,[*2] and
K. Yoshida[*2]

The discovery of new nuclei in the proximity of drip lines is an important benchmark for nuclear mass models, and hence for the understanding of nuclear force and modeling the creation of elements. Recent measurements at the NSCL[1,2] have demonstrated that the fragmentation of ^{76}Ge and ^{82}Se beams can be used to produce new isotopes (NI) in the calcium region. This work was extended at RIKEN using higher energy and intensity in April–May 2017, when the NP1406-RIBF44R1 experiment was carried out.

A 345 MeV/nucleon ^{70}Zn beam with an intensity of 225 pnA, which was accelerated by the RIKEN RIBF accelerator complex, was fragmented in a series of beryllium targets placed at the object position of the BigRIPS fragment separator.[3]

The experimental conditions for the NI production runs are listed in Table 1. These settings were centered on ^{50}S, ^{53}Cl, ^{54}Ar, ^{57}K, and ^{60}Ca based on LISE^{++} calculations.[5] Two aluminum wedge-shaped degraders at the F1 and F5 dispersive planes were used at full BigRIPS momentum acceptance to separate and purify the RI beams.

The particle identification (PID) was conducted using the ToF-$B\rho$-ΔE-TKE method described in the appendix to the previous work.[6] Figure 2 shows the pre-

Table 1. Experimental conditions for NI production runs.

Settings	^{50}S	^{53}Cl	^{54}Ar	^{57}K	^{60}Ca
Target(Be) [mm]	20	15	10	10	15
$B\rho$01 [Tm]	7.35	7.8	8.0	8.0	7.35
F1 degrader [mm]	3	3	3	3	3
F5 degrader [mm]	3	1	1	1	3
Time [h]	8.9	23.5	11.2	17.0	38.9

Fig. 2. PID plot of NI production runs.

liminary Z vs. A/q PID summary plot for all NI production runs. We observed a total of 9 new neutron-rich nuclei during the 100 hours of NI search: ^{47}P, ^{49}S, ^{52}Cl, ^{54}Ar, ^{57,59}K, ^{59,60}Ca, ^{62}Sc.

Production cross sections, secondary reaction contributions, and momentum distributions runs were performed. The data are under analysis.

Fig. 1. The region of the chart of nuclides studied. The solid line is the limit of bound nuclei from the KTUY mass model.[4] The nuclei in the green squares were newly observed in this work.

References
1) O. B. Tarasov *et al.*, Phys. Rev. Lett. **102**, 142501 (2009).
2) O. B. Tarasov *et al.*, Phys. Rev. C **87**, 054612 (2013).
3) T. Kubo *et al.*, Nucl. Instrum. Methods Phys. Res. B **204**, 97 (2003).
4) H. Koura *et al.*, Prog. Theor. Phys. **113**, 305 (2005).
5) O. B. Tarasov *et al.*, Phys. Rev. C **80**, 034609 (2009).
6) O. B. Tarasov, D. Bazin, Nucl. Instrum. Methods Phys. Res. B **266**, 4657 (2008), http://lise.nscl.msu.edu.

*1 NSCL/FRIB, Michigan State University
*2 RIKEN Nishina Center
*3 Department of Physics, Tohoku University
*4 Center for Nuclear Study, University of Tokyo

New isotope search conducted concurrently with BRIKEN campaign

Y. Shimizu,[*1] N. Fukuda,[*1] K. P. Rykaczewski,[*2] R. K. Grzywacz,[*3] J. L. Tain,[*4] I. Dillmann,[*5]
S. Nishimura,[*1] H. Takeda,[*1] H. Suzuki,[*1] D. S. Ahn,[*1] N. Inabe,[*1] K. Yoshida,[*1] H. Ueno,[*1] N. T. Brewer,[*2]
B. C. Rasco,[*2] D. W. Stracener,[*2] and J. M. Allmond[*2] for the BRIKEN collaboration

In order to measure new β-delayed neutron emission properties for near doubly magic nucleus ^{78}Ni using the world-largest array of ^{3}He counters BRIKEN,[1] the experiment was performed at the RIKEN Nishina Center RI Beam Factory (RIBF). The nuclei of interst were produced by the in-flight fission of a 345 MeV/nucleon ^{238}U beam colliding with a 3.87-mm-thick Be target. The primary beam intensity was 56.6 particle nA on average. Fission fragments were separated and identified using the superconducting in-flight separator BigRIPS.[2] In order to separate and purify the RI beams, two wedge-shaped energy degraders were placed at the F1 and F5 dispersive foci. The typical counting rate at the F3 and F7 achromatic foci were 545.4 Hz and 102.4 Hz, respectively. Table 1 summarizes the experimental conditions. The BigRIPS setting in this work included regions of new isotopes on the more neutron rich side. This allowed us to search for new isotopes in parallel with the measurements of the BRIKEN campaign.

Table 1. Summary of the experimental conditions.

Target (mm)	Be 3.87
Bρ ^{a} (Tm)	8.272
Degrader at F1 (mm)	Al 5.01
Degrader at F5 (mm)	Al 3.45
F1 slit (mm)	$+58.0$ / -64.2
F2 slit (mm)	$+20.0$ / -20.0
F5 slit (mm)	$+110.0$ / -110.0
F7 slit (mm)	$+25.0$ / -25.0
Central particle	^{82}Cu
Irradiation time (h)	191.8
Live time of DAQ (%)	95.5
Trigger rate (Hz)	97.8
Total dose	2.44×10^{17}

^{a} The values from the magnetic fields of the first dipole magnet.

Particle identification (PID) was performed using the ΔE-TOF-$B\rho$ method in which the energy loss (ΔE), time of flight (TOF), and magnetic rigidity ($B\rho$) were measured to allow the event-by-event determination of atomic number Z and mass-to-charge ratio A/Q of fragments.[3] The PID was confirmed by measuring the delayed γ-rays emitted from short-lived isomers,

*1 RIKEN Nishina Center
*2 Oak Ridge National Laboratory (ORNL)
*3 Department of Physics and Astronomy, University of Tennessee
*4 Instituto de Física Corpuscular, CSIC-Universidad de Valencia
*5 TRIUMF
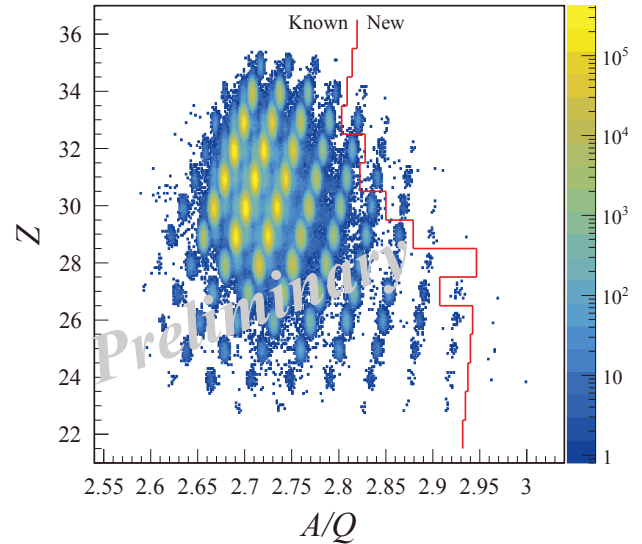
Fig. 1. Two-dimensional PID plot of Z versus A/Q. Red line indicates the limit of known isotopes[5–7] as of January 2018.

such as ^{92}Br and ^{94}Br, by using two clover-type high-purity germanium detectors placed at the F7 achromatic focus; this technique is called isomer tagging.[4]

Figure 1 shows a two-dimensional PID plot of Z versus A/Q. The solid red line indicates the limit of identified isotopes[5–7] as of January 2018. The relative root mean square (rms) Z resolution and the relative rms A/Q resolution were typically 0.61% and 0.081%, respectively. We can see some candidates for new isotopes such as ^{79}Co, ^{84}Cu, ^{86}Zn, and ^{93}As.

Detailed analysis is currently in progress.[8]

References
1) A. Tarifeño-Saldivia et al., J. Instrum. 12, 04006 (2017).
2) T. Kubo, Nucl. Instrum. Methods Phys. Res. B 204, 97 (2003).
3) N. Fukuda et al., Nucl. Instrum. Methods Phys. Res. B 317, 323 (2013).
4) R. K. Grzywacz et al., Phys. Lett. B 355, 439 (1995).
5) M. Bernas et al., Phys. Lett. B 415, 111 (1997).
6) T. Ohnishi et al., J. Phys. Soc. Jpn. 79, 073201 (2010).
7) T. Sumikama et al., Phys. Rev. C 95, 051601R (2017).
8) K. P. Rykaczewski et al., in this report.

Production of neutron-rich nuclei in the vicinity of $N = 126$ by means of projectile fragmentation of 345 MeV/nucleon ^{238}U

N. Fukuda,[*1] Y. Shimizu,[*1] H. Suzuki,[*1] D. S. Ahn,[*1] H. Takeda,[*1] T. Sumikama,[*1] N. Inabe,[*1] K. Yoshida,[*1]
H. Sato,[*1] H. Ueno,[*1] S. Nishimura,[*1] H. Otsu,[*1] D. Suzuki,[*1] M. Sasano,[*1] T. Isobe,[*1] J. Amano,[*2]
H. Miyatake,[*3] Y. X. Watanabe,[*3] and Y. Hirayama[*3]

The neutron-rich nuclei located along the neutron closed shell $N = 126$ are of great importance for investigating the evolution of $N = 126$ shell closure, as well as for understanding the r-process of stellar nucleosynthesis. Experimental information, however, are scarcely available, due to the difficulties in producing these unstable nuclei. Recently, a multi-nucleon transfer reaction with a stable beam was experimentally investigated, and it has proved to be a promising method for producing neutron-rich nuclei around $N = 126$.[1] Another prospective reaction for producing these nuclei is the fragmentation of heavy projectiles such as lead and uranium. The lightest $N = 126$ nucleus so far, ^{202}Os, was produced by the projectile fragmentation of a 1 GeV/nucleon ^{238}U beam.[2]

To access the unexploited region around $N = 126$, we conducted an experiment aimed at producing neutron-rich nuclei around $N = 126$ by means of the projectile fragmentation of a high-intensity 345 MeV/nucleon ^{238}U beam using the BigRIPS in-flight separator[3] at the RIKEN RI Beam Factory.[4] The intensity of the ^{238}U beam was 45 particle nA on average. The production target, which was made of beryllium, was 5 mm thick. The setting of the BigRIPS separator was optimized for the production of ^{200}W, where the magnetic rigidity $B\rho$ settings before and after F3 were tuned for hydrogen-like and helium-like ^{200}W ions with charge state $Q = 73$ and 72, respectively. We employed the two-stage isotope separation mode to sufficiently purify the neutron-rich isotope beams of interest, in which the aluminum degraders

Fig. 1. Particle identification plot of Z vs A/Q for fragments produced in the ^{238}U + Be reaction. The fragments with $Z > 70$ were produced by the projectile fragmentation. The $N = 126$ isotones are expected to be located on the red dotted line. The location of ^{200}W is indicated by the red solid circle, where no events were observed. The blobs in the red dashed circle correspond to the events whose charge states change at F5. The blobs in the red dotted circle correspond to the fission-originated contaminants.

were installed not only at the F1 but also at the F5 foci. The details of experimental conditions are summarized in Table 1. The particle identification (PID) was obtained event by event on the basis of the ΔE-TOF-$B\rho$ method, thus deducing the atomic number Z and the mass-to-charge ratio A/Q of the fragments.[5]

Figure 1 shows the Z vs A/Q PID plot for fragments produced in the ^{238}U+Be reaction. The neutron-rich nuclei around $N = 126$ were produced and identified as shown in the figure, although the resolving power of PID needs to be improved. No events were observed for ^{200}W in the present short-time measurement of 8 h. An elaborate data analysis is currently in progress.

Table 1. Experimental conditions for ^{200}W setting

Production target	Be 5 mm
$B\rho$	6.8000 Tm
Degraders	Al 5 mm at F1, Al 1 mm at F5
Intensity of ^{238}U	45 pnA
Running time	8 hours
F1 slit	± 32 mm ($\pm 1.5\%$ in $\Delta p/p$)
F2 slit	± 10 mm
F5 slit	± 48 mm
F7 slit	± 25 mm
Total rate at F1	$\approx 10^9$ Hz
Total rate at F3	2.5×10^5 Hz
Total rate at F7	30 Hz

References
1) Y. X. Watanabe *et al.*, Phys. Rev. Lett. **115**, 172503 (2015).
2) J. Kurcewicz *et al.*, Phys. Lett. B **717**, 371 (2012).
3) T. Kubo, Nucl. Instrum. Methods Phys. Res. B **204**, 97 (2003).
4) Y. Yano, Nucl. Instrum. Methods Phys. Res. B **261**, 1009 (2007).
5) N. Fukuda *et al.*, Nucl. Instrum. Methods Phys. Res. B **317**, 323 (2013).

*1 RIKEN Nishina Center
*2 Department of Physics, Rikkyo University
*3 KEK

Cross-section measurement of neutron-rich Pd isotopes produced from an RI beam of ^{132}Sn at 280 MeV/nucleon

H. Suzuki,[*1] K. Yoshida,[*1] N. Fukuda,[*1] H. Takeda,[*1] Y. Shimizu,[*1] D. S. Ahn,[*1] T. Sumikama,[*1] N. Inabe,[*1] T. Komatsubara,[*1] H. Sato,[*1] Z. Korkulu,[*1] K. Kusaka,[*1] Y. Yanagisawa,[*1] M. Ohtake,[*1] H. Ueno,[*1] S. Michimasa,[*2] N. Kitamura,[*2] K. Kawata,[*2] N. Imai,[*2] O. B. Tarasov,[*1,*3] T. Kubo,[*1,*3,*4] D. P. Bazin,[*1,*3] J. Nolen,[*1,*5] and W. F. Henning[*1,*5,*6]

We performed an experiment to measure the production cross sections of $^{125-128}$Pd from a radioactive-isotope (RI) beam of ^{132}Sn by using the BigRIPS separator and the ZeroDegree spectrometer at the RIKEN RI Beam Factory (RIBF) in November 2017.

In-flight fission of ^{238}U beam is a useful method for the production of mid-heavy neutron-rich isotopes. At RIBF, approximately 120 new isotopes have been produced from the ^{238}U beam, and various nuclei, such as a double-magic nuclide, ^{132}Sn, are supplied for many experiments. However, the production cross sections decrease drastically for more exotic nuclei. Thus, the nuclei in a very neutron-rich region, such as the ones involved with the rapid process in nucleosynthesis, are difficult to be produced by the in-flight fission of ^{238}U.

Another method of RI-beam production is an ISOL technique, by which greater yields of RIs are produced in the target by a proton beam even at the same beam power as the ^{238}U beam for in-flight fission. However, the extraction efficiency is not good, especially for exotic nuclei with short half-lives.

To solve these problems, a two-step reaction scheme[1] was proposed for the efficient production of very neutron-rich nuclei. First, a long-lived RI such as ^{132}Sn, which has a half-life of 40 s, is produced by an ISOL and reaccelerated by post-accelerators. Then, objective exotic nuclei, such as $^{125-128}$Pd, are produced by fragmentation by impinging on a secondary target. By using this scheme, one may obtain greater yields of neutron-rich nuclei than those obtained by direct production through the in-flight fission of the ^{238}U beam.

Production cross sections up to ^{125}Pd were already measured at GSI;[2] thus, we measured those of more neutron-rich Pd isotopes. A ^{132}Sn beam was produced from a 40-pnA 345-MeV/nucleon ^{238}U^{86+} beam impinging on a 4-mm-thick Be target. Its energy was 280 MeV/nucleon, the intensity was 30 kHz, and the purity was 50%. The neutron-rich Pd isotopes were produced at a 6-mm-thick Be target at F8. The particle identification (PID) of the isotopes was performed by deducing the atomic number, Z, and mass-to-charge ratio, A/Q, of the fragments based on the TOF-
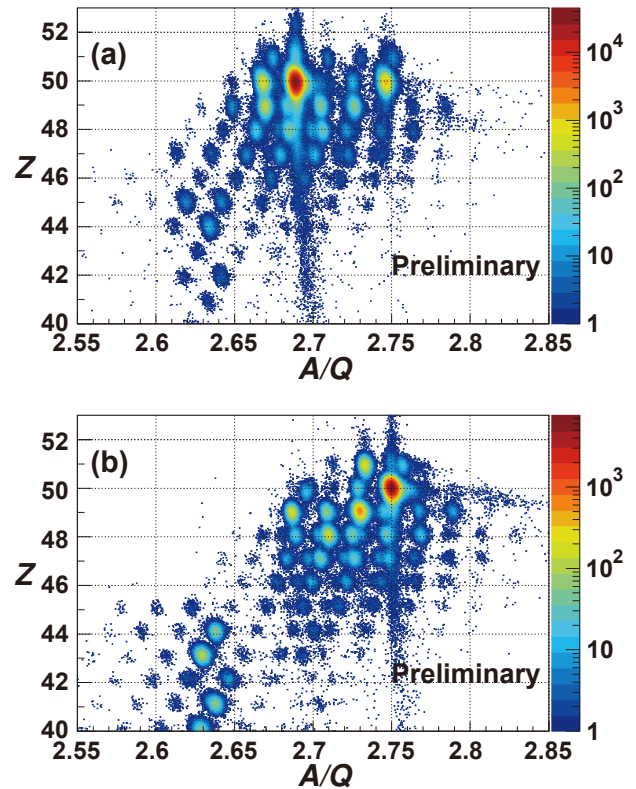
Fig. 1. The Z versus A/Q PID plots in the ZeroDegree spectrometer. (a) The ^{126}Pd setting. (b) The ^{128}Pd setting.

$B\rho$-ΔE method in the ZeroDegree spectrometer, which is essentially the same method as the one in BigRIPS.[3] LaBr$_3$ crystal was installed at F11 for measuring the total kinetic energy. Two ZeroDegree settings—the ^{126}Pd setting and the ^{128}Pd setting—were applied for measuring the cross sections of ^{125,126}Pd and ^{127,128}Pd, respectively.

The Z vs A/Q PID plots for the nuclei produced from the ^{132}Sn beam are shown in Fig. 1. Many isotopes including $^{125-128}$Pd are observed. Further analyses, such as the improvement of the A/Q resolution and the removal of background events, are in progress.

References
1) K. Helariutta *et al.*, Eur. Phys. J. A **17**, 181 (2003).
2) D. Pérez-Loureiro *et al.*, Phys. Lett. B **703**, 552 (2011).
3) N. Fukuda *et al.*, Nucl. Instrum. Methods Phys. Res. B **317**, 323 (2013).

*1 RIKEN Nishina Center
*2 Center for Nuclear Study, University of Tokyo
*3 National Superconducting Cyclotron Laboratory, Michigan State University
*4 Facility for Rare Isotope Beams, Michigan State University
*5 Division of Physics, Argonne National Laboratory
*6 Physik Department, Technische Universität München

2. Nuclear Physics (Theory)

Mesic nuclei with a heavy antiquark [†]

Y. Yamaguchi[*1] and S. Yasui[*2]

Multiflavor nuclei are one of the interesting topics of research in the field of hadron and nuclear physics. Strangeness nuclei such as kaonic and hypernuclei have been extensively studied both experimentally and theoretically.[1] As a new direction, new flavors such as charm and bottom are studied, and nuclei with these flavors have different properties from those of strangeness nuclei.[2] Such multiflavor nuclei are important for studying (i) hadron and nucleon interaction, (ii) the properties of hadrons in a nuclear medium, and (iii) the effect of impurities on nuclear properties. These are related to the fundamental problems in quantum chromodynamics (QCD).

We study the bound and resonant systems of the heavy meson ($P = \bar{D}$ or B) and the nucleus with nucleon number $A = 16, \cdots, 208$, where the $\bar{D}$ (B) meson is a pseudoscalar meson composed of a charm (bottom) antiquark $\bar{c}$ ($\bar{b}$), and a light quark $q = u, d$. The $\bar{D}$ (B) mesons in nuclei have no $q\bar{q}$ annihilation, and therefore the bound state is stable against strong decay. The attraction between the heavy meson and nucleon N, where the $PN - P^*N$ mixing plays an important role, has been discussed. P^* is a vector meson of $\bar{c}q$ or $\bar{b}q$, and the small mass splitting of P and P^* due to the heavy quark spin symmetry[3] enhances the $PN - P^*N$ mixing effect.

We analyze the mesic nuclei as two-body systems of the P meson and the nucleus. The P-nucleus potential is given by the folding potential,

$$V_{fold}(r) = \int V^{PN}(r - r')\rho(r')d^3r', \qquad (1)$$

with the P-nucleon potential $V^{PN}(r)$ and the nucleon number distribution function $\rho(r)$. As for the potential $V^{PN}(r)$, we employ the one pion exchange potential (OPEP). The OPEP is given by the Born term of the pion exchange scattering amplitude described by the effective Lagrangians. Although the $PN - P^*N$ mixing gives coupled-channel potentials, it can be expressed as a single channel potential,

$$V^{PN}(r) = V_{11}(r) + V_{12}(r)\frac{\psi_2^E}{\psi_1^E} + V_{13}(r)\frac{\psi_3^E}{\psi_1^E}, \qquad (2)$$

where $V_{ij}(r)$ is the (i,j) component of the OPEP, and ψ_i^E is i component of the eigenfunction of the PN system.[4,5] Here, we focus on the OPEP in the $I(J^P) = 0(1/2^-)$ state, because it is the most attractive one. The distribution function $\rho(r)$ is given by
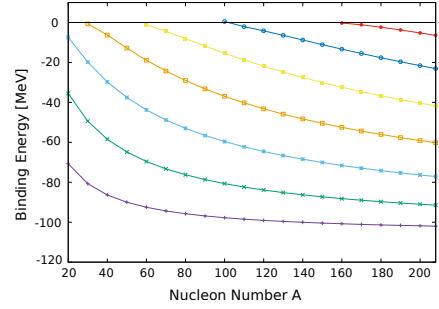
Fig. 1. Energy obtained for the $\bar{D}$-nucleus systems with S-wave for various nucleon numbers A.

$$\rho(r) = \frac{\rho_0}{1 + \exp\left[(r - R)/a\right]}, \qquad (3)$$

where $\rho_0 = 0.17$ fm^{-3}, $a = 0.54$ fm, and R is chosen to satisfy $\int \rho(r)d^3r = A$.[6]

To obtain the bound and resonant states of the two-body P-nucleus system, the Schrödinger equations are solved for the nucleon number $A = 16, \ldots, 208$. As a result, many states are obtained for the P-nucleus systems with S, P, D, and F-waves. Figure 1 shows the energy obtained for the $\bar{D}$-nucleus systems with S-wave. We see that the binding energy increases as the nucleon number A increases. For states with P, D and F-waves, the resonances are also obtained by the centrifugal barrier. We also found many bound and resonant states in the bottom sector. The binding energy and number of bound states of the B-nucleus are larger than those of the $\bar{D}$-nucleus, because small mass splitting between B and B^* mesons enhances the attraction from the OPEP. The information on the energy spectra of mesic nuclei with a heavy antiquark will be useful for future experiments at the Facility for Antiproton and Ion Research (FAIR), the Japan Proton Accelerator Research Complex (J-PARC), the Relativistic Heavy Ion Collider (RHIC), the Large Hadron Collider (LHC), and so forth.

References
1) A. Gal, E. V. Hungerford, D. J. Millener, Rev. Mod. Phys. **88**, 035004 (2016).
2) A. Hosaka, T. Hyodo, K. Sudoh, Y. Yamaguchi, S. Yasui, Prog. Part. Nucl. Phys. **96**, 88 (2017).
3) A. V. Manohar, M. B. Wise, *Heavy Quark Physics* (Cambridge University Press, Cambridge, 2000).
4) S. Yasui, K. Sudoh, Phys. Rev. D **80**, 034008 (2009).
5) Y. Yamaguchi, S. Ohkoda, S. Yasui, A. Hosaka, Phys. Rev. D **84**, 014032 (2011).
6) A. Bohr, B. R. Mottelson, *Nuclear Structure: Single-Particle Motion/Nuclear Deformations* (World Scientific, Singapore, 1998).

Interplay between isoscalar and isovector correlations in neutron-rich nuclei[†]

I. Hamamoto[*1,*2] and H. Sagawa[*1,*3]

The interplay between isoscalar (IS) and isovector (IV) correlations has been an attractive and centrally placed topic in the study of nuclear structure. In the analysis of scattering data by IS particles such as α particles it is often assumed that IS particles excite only IS strength. This assumption is generally incorrect if N≠Z for the target nuclei. For example, in nuclei with neutron excess, IS operators excite IS moments, but the strong neutron-proton forces may tend to maintain the local ratio of neutrons to protons. Then, the presence of neutron excess N>Z implies that IV moments may also be excited by IS particles.[1] The exchange of the above roles of IS and IV excitations in the response is expected to be true as well. That is, IV operators may produce IS moments generally in nuclei with N≠Z except for the case in which the IS moment corresponds to the center of mass motion.

To study this issue, we employ the self-consistent Hartree-Fock (HF) plus the random-phase approximation (RPA) with Skyrme interactions in neuron-rich oxygen isoyopes, simultaneously including both IS and IV interactions. The RPA response function is estimated in coordinate space to properly take into account the continuum effect for the IS compression dipole (ISCD) operator:[2]

$$D_\mu^{\lambda=1,\,\tau=0} = \sum_i \left(r_i^3 - \frac{5}{3}\langle r^2 \rangle r_i \right) Y_{1\mu}(\hat{r}_i). \qquad (1)$$

Figure 1 shows the calculated RPA strength for the ISCD operator. We note the following points. (a) We very often obtain a large portion of ISCD strength in an energy interval several MeV above the threshold. This large strength appearing at an energy much lower than the energy of the ISCD giant resonance (GR), which is recognized as a very broad "resonance" found for Ex>24 MeV in Fig. 1, originates from the possible presence of occupied weakly bound low-ℓ neutron orbits together with the strong r-dependence (r^3) of the ISCD operator. (b) When IV interaction is included on top of IS interaction, the heights of many lower-lying IS peaks become lower and the peak energies may shift to slightly higher energies via the IV components contained in those IS peaks because of the repulsive nature of the IV interaction. (c) There are some peaks denoted by the solid curve, which may not
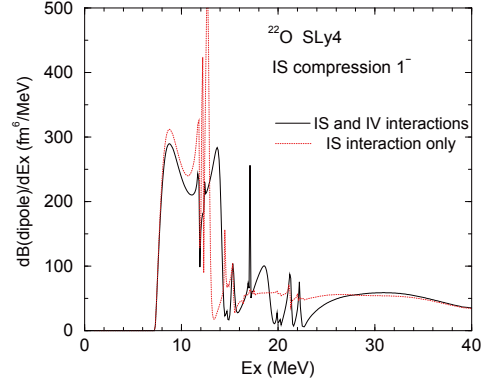
Fig. 1. RPA strength of the isoscalar compression dipole (ISCD) of ^{22}O calculated using the SLy4 interaction as a function of excitation energy (Ex). The solid curve expresses the strength obtained by including both IS and IV interactions in RPA, while the dotted curve expresses the strength obtained by including only the IS interaction.

be understood in the manner above (b). An example is the broad peak around 18.5 MeV in the solid curve. The IS peaks around 14.0 and 18.5 MeVn have no trivial corresponding peaks in the dotted curve. The same behavior is also found in the response for the IV dipole operator interchanging the roles of IV and IS correlations; the IV dipole peak appears at approximately 14 MeV only when both IS and IV interactions are included in the RPA response. We may call the relatively broad peak around Ex = 14 MeV pigmy resonance with both isoScalar and isoVector correlations ("iS-iV pigmy resonance"). The pigmy resonance is interpreted as neither the IS strength induced by a strong IV peak nor the IV strength induced by a strong IS peak, owing to the presence of neutron excess. It is a relatively broad resonance having an energy much lower than the energies of both IVD GR and ISCD GR, but it gathers the collectivity of low-lying IS and IV strengths. The strong neutron-proton interaction can be responsible for controlling the isospin structure of normal modes. In this study, it is explicitly shown that in the scattering by isoscalar (isovector) particles on N≠Z even-even nuclei isovector (isoscalar) strength in addition to isoscalar (isovector) strength may be populated.

References

1) A. Bohr, B. R. Mottelson, *Nuclear Structure* (Benjamin, Reading, MA, 1975).
2) I. Hamamoto, H. Sagawa, X. Z. Zhang, Phys. Rev. C **57**, R1064 (1998).

New interpretation of pairing anti-halo effect[†]

K. Hagino[*1,*2,*3] and H. Sagawa[*4,*5]

The pairing anti-halo effect is a phenomenon by which a pairing correlation suppresses the divergence of nuclear radius, which happens for single-particle states with orbital angular momenta of $l = 0$ and 1 in the limit of vanishing binding energy. This phenomenon was originally proposed based on the Hartree-Fock-Bogoliubov (HFB) theory. Although the HFB method provides a clear mathematical interpretation of the pairing anti-halo effect, its physical mechanism is less transparent. The aim of this paper is to propose a more intuitive idea on the pairing anti-halo effect, using a three-body model. This model is formulated to include many-body correlations beyond the HFB model, providing a complementary opportunity to clarify the concept based on the HFB method. It can be used to test whether the pairing anti-halo effect is specific only to the mean-field treatment or not.

The Hamiltonian for the three-body model reads[1]

$$H = \hat{h}(1) + \hat{h}(2) + v_{\text{pair}}(\vec{r}_1, \vec{r}_2) + \frac{\vec{p}_1 \cdot \vec{p}_2}{m_c}, \quad (1)$$

where $\hat{h}$ is a single-particle (s.p.) Hamiltonian and $v_{\text{pair}}(\vec{r}_1, \vec{r}_2)$ is the pairing interaction between the two valence neutrons. The last term is the two-body part of the recoil kinetic energy of the core nucleus.

The eigen-functions $\psi_{nljm}(\vec{r})$ of $\hat{h}$ is given by

$$\psi_{nljm}(\vec{r}) = \phi_{nlj}(r)\mathcal{Y}_{jlm}(\hat{r}) = \frac{u_{nlj}(r)}{r}\mathcal{Y}_{jlm}(\hat{r}), \quad (2)$$

where $\phi_{nlj}(r)$ and $\mathcal{Y}_{jlm}(\hat{r})$ are the radial and spin angular parts of the s.p. wave function, respectively. Using these eigen-functions, the two-particle wave function for the ground state of the three-body system with spin-parity of $J^\pi = 0^+$ is given as

$$\Psi(\vec{r}_1, \vec{r}_2) = \sum_{n,n',l,j} C_{nn'lj}[\psi_{nlj}(\vec{r}_1)\psi_{n'lj}(\vec{r}_2)]^{J=0}, \quad (3)$$

where the coefficients $C_{nn'lj}$ are calculated by diagonalizing the three-body Hamiltonian (1). The one-particle density constructed with this two-particle wave function is given by

$$\rho(\vec{r}) = \int d\vec{r}' |\Psi(\vec{r}, \vec{r}')|^2 = \frac{1}{4\pi} \sum_{k,l,j} \left| \frac{\tilde{u}_{klj}(r)}{r} \right|^2, \quad (4)$$

where $\tilde{u}_{klj}(r)$ is defined as $\tilde{u}_{klj}(r) \equiv \sum_n C_{nklj} u_{nlj}(r)$.
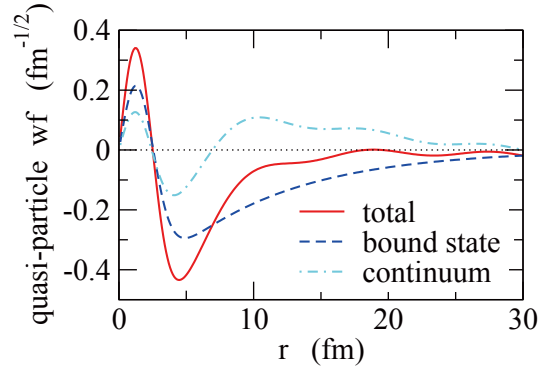
Fig. 1. The radial part of the quasi-particle wave function, $\tilde{u}_{2s_{1/2}}(r)$, defined in Eq. (4), for the weakly bound $2s_{1/2}$ state in ^{24}O. In the uncorrelated case, the two valence neutrons occupy the $2s_{1/2}$ state at $\epsilon = -0.275$ MeV, while the continuum states are also taken into account in the three-body model calculations. A zero-range pairing interaction is employed, which yields a ground state energy of $E_{\text{g.s.}} = -2.46$ MeV. The solid line shows the total wave function, while the dashed and dot-dashed lines denote its bound state and continuum state contributions, respectively.

Note that this is in a similar form as the one-particle density in the HFB approximation, especially if the quasi-particle wave function is expended on the Hartree-Fock basis, u_{nlj}.[2]

The solid line in Fig. 1 shows the radial dependence of the quasi-particle wave function for the weakly-bound $2s_{1/2}$ state; that is, $\tilde{u}_{klj}(r)$ with $(klj) = 2s_{1/2}$ in ^{24}O. The dashed and dot-dashed lines show its decomposition into the bound state and the continuum state contributions, respectively. They are defined as

$$\tilde{u}_{klj}(r) = \tilde{u}_{klj}^{(b)}(r) + \tilde{u}_{klj}^{(c)}(r)$$
$$= \sum_{n=2s_{1/2}} C_{nklj}\, u_{nlj}(r) + \sum_{n=\text{cont.}} C_{nklj}\, u_{nlj}(r). \quad (5)$$

The main feature of this quasi-particle wave function is that the bound state and continuum state contributions largely cancel each other outside the potential while the two components contribute coherently in the inner region. We recognise that the localization due to a coherent superposition of continuum states is the same mechanism as the formation of a localized wave packet. This is an essential ingredient of the pairing anti-halo effect, that is, the formation of a localized wave packet induced by a pairing interaction.

References
1) K. Hagino, H. Sagawa, Phys. Rev. C **72**, 044321 (2005).
2) K. Hagino, H. Sagawa, Phys. Rev. C **71**, 044302 (2005).

Role of deformation in odd-even staggering in reaction cross sections for ^{30,31,32}Ne and ^{36,37,38}Mg isotopes[†]

Y. Urata,[*1] K. Hagino,[*1,*2] and H. Sagawa[*3,*4]

We discuss the role of the pairing anti-halo effect in the observed odd-even staggering in reaction cross sections for ^{30,31,32}Ne and ^{36,37,38}Mg isotopes by taking into account the ground state deformation of these nuclei. We construct the ground state density for the ^{30,31}Ne and ^{36,37}Mg nuclei based on a deformed Woods-Saxon potential, while for the ^{32}Ne and ^{38}Mg nuclei we also take into account the pairing correlation using the Hartree-Fock-Bogoliubov (HFB) method.

We consider the collision of a deformed projectile nucleus with a spherical target nucleus and compute the reaction cross sections, σ_R. To this end, we employ the Glauber theory, which is based on the eikonal approximation and the adiabatic approximation to the rotational motion of a deformed nucleus. That is, we first fix the orientation angle of the deformed nucleus and then take an average of the resultant cross section over all the orientation angles:[1)]

$$\sigma_R = \frac{1}{4\pi} \int d\mathbf{\Omega}\, \sigma_{\mathbf{R}}(\mathbf{\Omega}), \qquad (1)$$

where $\mathbf{\Omega}$ is the angle of the symmetric axis of the deformed nucleus in the laboratory frame, and $\sigma_R(\mathbf{\Omega})$ is the reaction cross section for a fixed $\mathbf{\Omega}$.

We analyze the experimental data at an incident energy $E = 240$ MeV/nucleon with a ^{12}C target. We use the same density for ^{12}C as that given in Ref. 2), while we use the same parameters given in Ref. 3) for the profile function, Γ_{NN} in the Glauber model calculations.

The reaction cross sections for the ^{30,31,32}Ne nuclei evaluated at $S_n(^{31}$Ne$) = 0.3$ MeV are shown in Fig. 1, along with a comparison to the experimental interaction cross sections.[4)] We also show the result of a previous analysis based on the spherical density distributions at a similar one neutron separation energy.[5)] One can see that the odd-even staggering can still be reproduced by taking into account the nuclear deformation. Notice that the degree of the staggering is lower in the present calculation compared to the previous spherical calculation because the valence neutron in ^{31}Ne fully occupies the $1p_{3/2}$ level in the spherical case, while the occupation probability for the $p_{3/2}$ level decreases from unity in the deformed case. We also checked the effect of pairing correlations on the odd-even staggering with
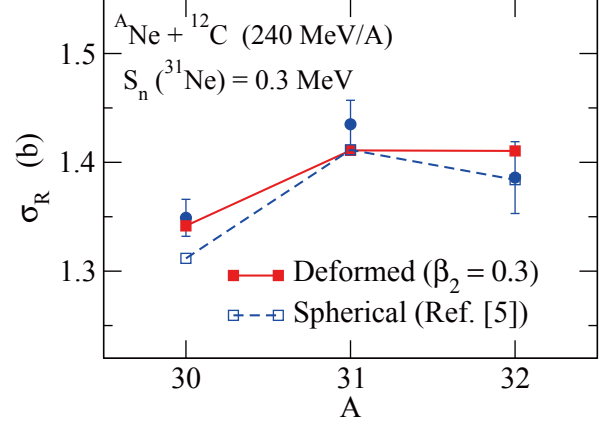
Fig. 1. Reaction cross sections for the ^{30,31,32}Ne $+$ ^{12}C reaction at $E = 240$ MeV/nucleon evaluated at the one neutron separation energy of ^{31}Ne of $S_n = 0.3$ MeV. The filled circles with error bars indicate the experimental interaction cross sections taken from Ref. 4). For comparison, the result of the previous analysis in Ref. 5) based on the spherical density distributions is also shown by the dashed line.

the deformed wave functions. We found that the reaction cross section for ^{32}Ne is not sensitive to the value of the average pairing gap as long as it is large enough.

We have also investigated the role of nuclear deformation in the odd-even staggering observed in reaction cross sections for Mg isotopes. We have shown that the deformation mainly decreases the degree of odd-even staggering, as in the Ne isotopes, because of the admixture of several angular momentum states in a deformed single-particle wave function. Despite this, the odd-even staggering persists even with finite deformation when the one neutron separation energy is small enough. These results strongly indicate that the pairing anti-halo effect indeed contributes to the observed odd-even staggering in reaction cross sections.

References
1) J. A. Christley, J. A. Tostevin, Phys. Rev. C **59**, 2309 (1999); K. Hagino, N. Takigawa, Prog. Theor. Phys. **128**, 1061 (2012).
2) Y. Ogawa, K. Yabana, Y. Suzuki, Nucl. Phys. A **543**, 722 (1992).
3) B. Abu-Ibrahim, W. Horiuchi, A. Kohama, Y. Suzuki, Phys. Rev. C **77**, 034607 (2008).
4) M. Takechi *et al.*, Phys. Lett. B **707**, 357 (2012).
5) K. Hagino, H. Sagawa, Phys. Rev. C **84**, 011303(R) (2011).

†   Condensed from the article in Phys. Rev. C **96**, 064311 (2017)
*1   Department of Physics, Tohoku University
*2   Research Center for Electron Photon Science, Tohoku University
*3   RIKEN Nishina Center
*4   Center for Mathematics and Physics, University of Aizu

Enhancement of pairing fluctuation in neutron-rich Mg isotopes studied by Skyrme QRPA calculation

M. Yamagami [*1]

Nuclei close to the drip line often exhibit novel features that do not appear in stable nuclei. An example is dineutron correlation, which is the strong spatial correlation between two neutrons of a Cooper pair. The pair excitation into continuum states (continuum effect) plays a key role to create the strong correlation. Dineutron correlation has been extensively investigated both experimentally and theoretically in light-mass nuclei such as ^{11}Li. We also expect dineutron correlation in medium-heavy neutron-rich nuclei, for example, around ^{40}Mg,[1] which are accessible in RIKEN RIBF. However, no evidence has been obtained thus far. In this study, we discuss $K^{\pi} = 0^+$ isoscalar quadrupole excitations in neutron-rich Mg isotopes as a probe of dineutron correlation. We emphasize the continuum effect for the collectivity of excitations.

At first, we solve the Hartree-Fock-Bogoliubov (HFB) equation by using the Fourier-series expansion method. The Skyrme SkM* parametrization and the mixed-type density-dependent zero-range pairing force are employed. The pairing correlation is active among single-particle states with the energies ε_k satisfying $|\varepsilon_k - \lambda| < E_{cut}$. Here, λ is the chemical potential and E_{cut} is the cut-off energy. On top of the HFB states, we solve the quasiparticle random phase approximation (QRPA) equation in the matrix form.[2]

The ground states of ^{34,36,38,40}Mg have quadrupole deformations $\beta_2 = 0.243, 0.262, 0.265$, and 0.259, and neutron pairing gaps $\Delta_n = 2.13, 2.05, 2.02$, and 2.04 MeV in our calculation. Figure 1 (upper) shows the excitation energies E of the $K^{\pi} = 0^+$ isoscalar quadrupole excited states $|\nu\rangle$. Figure 2 shows the transition strength of quadruple-pair excitations $B(P_{20}^{(ad)}) = |\langle\nu| P_{20}^{\dagger} |0\rangle|^2$ with the quadrupole-pair additional operator $P_{20}^{\dagger}$. The results with $E_{cut} = 6, 8, 10$, and 12 MeV are compared. Here, $E_{cut} = 6$ is a typical value in stable nuclei. A larger E_{cut} increases the coupling to continuum states. We found the large enhancement of $B(P_{20}^{(ad)})$ as a function of E_{cut} in ^{38,40}Mg, the neutron chemical potentials of which $\lambda_n = -1.57$ and -0.77 MeV satisfy $|\lambda_n| < \Delta_n$. Here, the $B(P_{20}^{(ad)})$ with $E_{cut} = 12$ MeV is small at approximately 10% in ^{40}Mg from the converged value of 215 fm^4 from extrapolation with the exponential-type function of E_{cut}.

Figure 1 (lower) shows the isoscalar transition strength $B(IS2) = |\langle\nu| r^2 Y_{20} |0\rangle|^2$. This vibration of matter density is induced by the fluctuation of neutron-pair occupation among Nilsson orbits with different spatial shapes. In ^{34}Mg, the prolate-type orbits [330]1/2 and [321]3/2 and the oblate-type orbit [202]3/2 are involved. In ^{38,40}Mg, the prolate-type orbits [310]1/2 and [301]1/2 and the oblate-type orbit [303]7/2 are the main contributors. The large pairing fluctuation enhances the $B(IS2)$ around ^{40}Mg. Actually, the ratio of $B(IS2)$ in ^{40}Mg and ^{34}Mg is 1.32 with $E_{cut} = 12$ MeV, while 1.01 with $E_{cut} = 6$ MeV.

In conclusion, we discussed the pairing fluctuation and the induced $B(IS2)$ values of $K^{\pi} = 0^+$ isoscalar quadruple excitations in neutron-rich Mg isotopes. We predicted the enhancement of $B(P_{20}^{(ad)})$ by the continuum effect in ^{38,40}Mg. This phenomenon suggests the presence of dineutron correlation and can be observed by a two-neutron transfer experiment. The $B(IS2)$ values also contain indispensable information about the shell structure and pairing properties.
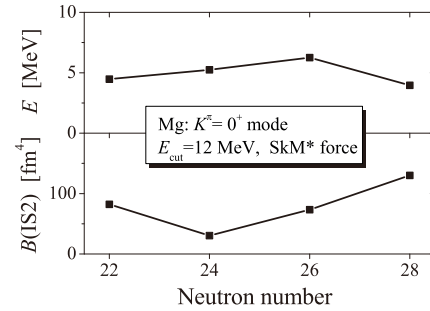
Fig. 1. Excitation energies E and $B(IS2)$ values of the $K^{\pi} = 0^+$ excitations in neutron-rich Mg isotopes.
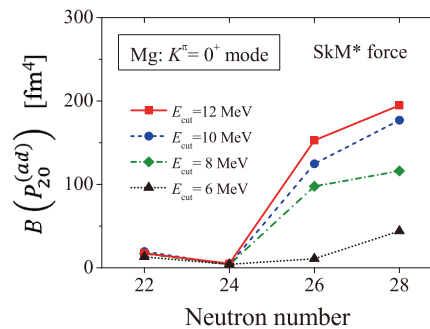
Fig. 2. Transition strength of quadruple-pair excitations $B(P_{20}^{(ad)})$ of the $K^{\pi} = 0^+$ excitations. The results with $E_{cut} = 6, 8, 10$, and 12 MeV are compared.

References
1) M. Yamagami et al., Phys. Rev. C **77**, 064319 (2008).
2) M. Yamagami et al., RIKEN Accel. Prog. Rep. **50**, 92 (2017).

*1　Department of Computer Science and Engineering, University of Aizu

Testing constant-temperature approach for nuclear level density[†]

N. Dinh Dang,[*1] N. Quang Hung,[*2] and L. T. Quynh Huong[*3]

According to thermodynamics, the nuclear temperature is a parameter, which is defined from the nuclear level density (NLD) $\rho(E)$ as

$$T = \left[\frac{\partial \ln \rho(E)}{\partial E}\right]^{-1}. \tag{1}$$

In the first model for NLD proposed by Bethe, the NLD is approximately described as $\exp(2\sqrt{aE^*})$ with the level-density parameter a. The nuclear temperature T, defined from Eq. (1), is then proportional to the square root of the excitation energy E^*, viz $T \simeq \sqrt{E^*/a}$, i.e. it increases with E^*. However this model fails to describe the NLD at low excitation energies below the particle separation threshold. The constant-temperature (CT) model, suggested by Gilbert and Cameron,[1] assumes that the NLD at low excitation energies ($E^* \leq 10$ MeV) can be described by a constant temperature T, namely

$$\rho(E^*) = \frac{1}{T}e^{(E^*-E_0)/T} \equiv B(T)e^{E^*/T} , \tag{2}$$

with $B(T) = [Te^{E_0/T}]^{-1}$, where T and E_0 are obtained by fitting to the experimental NLD. This model has become increasingly popular in the study of NLD in recent years, where it has been suggested that its validity can be extended to much higher excitation energies up to E^* around 20 MeV for ^{60}Ni and ^{60}Co isotopes.[2] Therefore, it is highly desirable to analyze the validity of this phenomenological model by using a microscopic model, which is able to describe the NLD in both low as well as resonance energies. Recently a unified approach has been proposed to simultaneously describe both the NLD and radiative strength function (RSF) based on the solution of exact pairing (EP) problem in combination with the independent-particle model (IPM), which is referred to as EP+IPM hereafter.[4]

In the present work, by using the NLD predicted within the EP+IPM method, which agrees well with the experimental data, the nuclear temperature T is calculated from the derivative of logarithm of NLD (1). This temperature T increases almost linearly with the excitation energy E^*. However this increase is relatively slow so that T can be considered as a constant of around 0.5 MeV at $0 < E^* \leq 10$ MeV. Meanwhile, in ^{60}Ni, the CT model can describe rather well the experimentally extracted NLD with a constant temperature
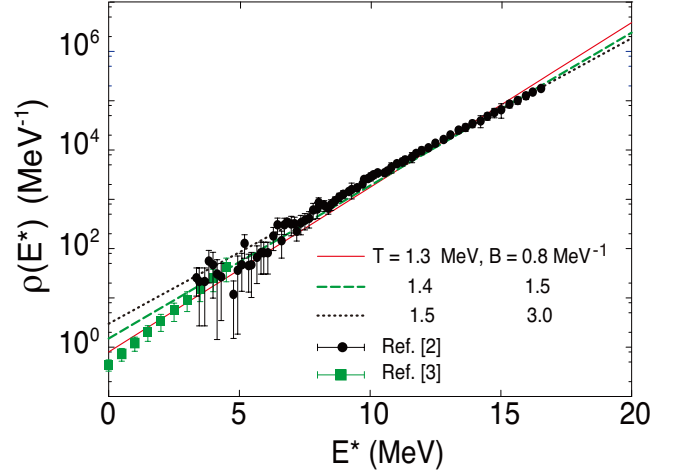
Fig. 1. Comparison of NLDs obtained from the CT model (2) and experimental NLDs for ^{60}Ni.

between $1.3 \leq T \leq 1.5$ MeV up to $E^* = 20$ MeV, i.e. much higher than the particle separation threshold, in excellent agreement with the experimental finding of Ref. 2) (Fig. 1). It is also shown that pairing plays an important role in maintaining this nearly-constant value of temperature at low excitation energy. In this way, the EP+IPM offers a consistent description of the NLD, which goes smoothly from the low-energy region $E^* \leq 5$ MeV to the higher one (up to 20 MeV for Ni isotopes and 10 MeV for Yb isotopes) without the need of matching the CT model at low energy and the Fermi-gas one at high energy, as often done by using the composite level-density formula.[1] Last but not least, the fact that the NLD at low excitation energy, even at $E^* = 0$, can be well described by the CT model at a constant nonzero temperature also supports the suggestion of introducing a ground-state's effective temperature.[5]

References
1) A. Gilbert, A. G. W. Cameron, Can. J. Phys. **43**, 1446 (1965).
2) A. V. Voinov et al., Phys. Rev. C **79**, 031301(R) (2009); EPJ Web of Conferences **21**, 05001 (2012).
3) https://www-nds.iaea.org/RIPL-3/.
4) N. Quang Hung, N. Dinh Dang, L. T. Quynh Huong, Phys. Rev. Lett. **118**, 022502 (2017).
5) V. Zelevisnky, Proc. of 12th Int'l Spring Seminar on Nuclear Physics, Sant'Angelo d'Ischia, May 15-19, 2017 (to be published).

† Condensed from the article in Phys. Rev. C **96**, 054321 (2017)
*1 RIKEN Nishina Center
*2 Institute of Fundamental and Applied Sciences, Duy Tan University
*3 Faculty of Physics and Engineering Physics, Viet Nam National University Ho Chi Minh City

Giant dipole resonance and shape transitions in hot and rotating ^{88}Mo†

A. K. Rhine Kumar,[*1] P. Arumugam,[*2] N. Dinh Dang,[*3] and I. Mazumdar[*4]

The exploration of extremes of nuclear landscape has unraveled several interesting phenomena, leading to a better understanding of the nuclear force. The giant dipole resonance (GDR) has been considered as a unique and powerful tool to investigate the nuclear structure properties at these extreme conditions. The most important experimental observable for the GDR is the cross section (σ) as a function of the photon energy, from which one can extract the centroid energies and the GDR width (Γ). These observables could effectively reflect the structure of the nuclear state on which the GDR is built.

In a recent work,[1] the GDR γ-rays emitted from highly excited ^{88}Mo nucleus which is formed in the reaction ^{48}Ti + ^{40}Ca, and a number of daughter nuclei created along the cooling path of the compound nucleus were measured. The data analysis indicates the possibility of Γ saturation at higher angular momentum (I) values. In this article, we study the GDR properties of the hot and rotating compound nucleus ^{88}Mo at different excitation energies within the thermal shape fluctuation model (TSFM) built on the microscopic-macroscopic approach for the free energy calculations and a macroscopic approach for the GDR calculations.

We calculate the average GDR cross section of a nucleus with a given Z and N at a given average T (T_{ave}) and having a probability distribution for I, as $\sigma_{\mathrm{ave}}(T_{\mathrm{ave}}) = \frac{\sum_i \sigma(T_{\mathrm{ave}}, I_i) C(i)}{\sum_i C(i)}$ where I_i is the spin of the ith step of the statistical decay of the compound nucleus and $C(i)$ are the corresponding spin counts. As the first step, it is very important to analyze, whether the average GDR cross sections $\sigma_{\mathrm{ave}}(T_{\mathrm{ave}})$ of a nucleus obtained by considering the T_{ave} and the probability distribution of I are similar or not, to the GDR cross sections $\sigma(T_{\mathrm{ave}}, I_{\mathrm{ave}})$ of a nucleus obtained with the T_{ave} and average I (I_{ave}) values obtained from the same probability distributions. The I_{ave} is estimated from the probability distribution of I as, $I_{\mathrm{ave}} = \frac{\sum_i I_i C(i)}{\sum_i C(i)}$.

An important conclusion from these analysis is that it is not necessary to calculate the theoretical σ at each value of T and I obtained in the probability distribution with their respective weights, instead the σ ob-
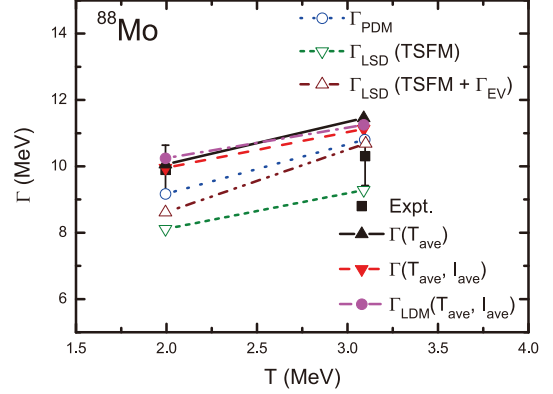
Fig. 1. The GDR width Γ of ^{88}Mo calculated using TSFM at two different excitation energies are plotted as a function of T. The filled upward triangles connected with solid line represent Γ of the final σ [$\Gamma(T_{\mathrm{ave}})$], where σ of the daughter nuclei are obtained by considering the T_{ave} and the angular momentum probability distributions. The filled downward triangles connected with dashed line [$\Gamma(T_{\mathrm{ave}}, I_{\mathrm{ave}})$] and filled circles connected with dash-dotted line [$\Gamma_{\mathrm{LDM}}(T_{\mathrm{ave}}, I_{\mathrm{ave}})$] represent the Γ of the final σ, where σ of the daughter nuclei are obtained by considering the T_{ave} and I_{ave} within the TSFM with free energies obtained from microscopic-macroscopic approach and liquid drop model (LDM), respectively. The experimental results are taken for Ref. 1). The widths obtained within the (Phonon damping model) PDM and Lublin-Strasbourg drop (LSD) model taken from Ref. 1) are also shown with open circles and open triangles. The lines are drawn just to guide the eyes.

tained at the average values of T and I are good enough to compare with the experimental data. In Fig. 1 we compare the Γ of ^{88}Mo calculated using TSFM at two different excitation energies. In the range of $2 \lesssim T \lesssim 3$ MeV, the data suggest a slower increase in the Γ whereas the our results and the PDM suggest a larger increase.

At higher T, as I increases the free energy surfaces shows a gamma-softness before the nucleus undergoes a Jacobi shape transition. Considering the role of enhanced fluctuations at higher T and the Coriolis splitting of GDR components at higher I the GDR width of ^{88}Mo nucleus will not saturate at high T and I.

Reference
1) M. Ciemała et al., Phys. Rev. C 91, 054313 (2015).

---

*1 Department of Physics, Cochin University of Science and Technology
*2 Department of Physics, Indian Institute of Technology Roorkee
*3 RIKEN Nishina Center
*4 Department of Nuclear and Atomic Physics, Tata Institute of Fundamental Research

Level density and thermodynamics in hot rotating ^{96}Tc nucleus†

B. Dey,[*1] D. Pandit,[*2] S. Bhattacharya,[*3] N. Quang Hung,[*4] N. Dinh Dang,[*5] L. Tan Phuc,[*4] D. Mondal,[*2] S. Mukhopadhyay,[*2] S. Pal,[*2] A. De,[*6] and S. R. Banerjee[*2]

One of the basic aims in diverse fields of science (physics, chemistry, and biology) is understanding the small system, which manifests many striking properties due to its tiny dimension. The study of thermodynamic properties of such small system like atomic nucleus, in spite of being an arduous task, is highly imperative as those properties describe how such systems respond to the changes in their environment. In addition, the knowledge of nuclear thermodynamics also enables us to understand the presence of pairing phase transition in the nucleus, whose effect was included in the nuclear theory after the Bardeen-Cooper-Schrieffer (BCS) theory. Thus, the study of nuclear thermodynamics has gained much enthusiasm in the recent past.

Measuring the nuclear level density (NLD) is the starting point to obtain the thermodynamic quantities (TQ) of atomic nuclei. Earlier, the NLD was measured below the particle threshold energy at very low angular momentum J and extrapolated to the higher energy by using the functional form of the Fermi-Gas model to estimate the TQs. But, the knowledge of the NLD functional form is not yet satisfactory due to the lack of experimental data at high E^* and J. Therefore, it would be better if one could measure the NLD below and above the particle threshold, and compare the measured data with a consistent theoretical calculation to investigate TQs of atomic nuclei. In the present work,[1] the angular momentum gated NLDs in the excitation energies range of $E^* \sim 5$–15 MeV are extracted by using the evaporated neutron energy spectra in the ^{4}He+^{93}Nb reaction and compared with the results of different microscopic calculations.

The experimental NLD along with the results of different theoretical calculations for $J = 12$ and $16\ \hbar$ are shown in Fig. 1. It is observed that EP+IPM (exact pairing plus independent particle model) explains rather well the experimental data and thus it was used to extract the thermodynamic properties of ^{96}Tc nucleus. The TQ of ^{96}Tc have been estimated using EP+IPM NLDs for $J = 12$ and $16\ \hbar$ as shown in Fig. 2. It is quite interesting to note that the free energy, entropy, and average energy show the correct trend as that observed in the nearby ^{96}Mo nucleus.[2] However, the bump in the heat capacity (signature of pairing phase transition) of ^{96}Tc is not as pronounced as that seen in ^{96}Mo,[2] in spite of being the same mass. This difference might come from
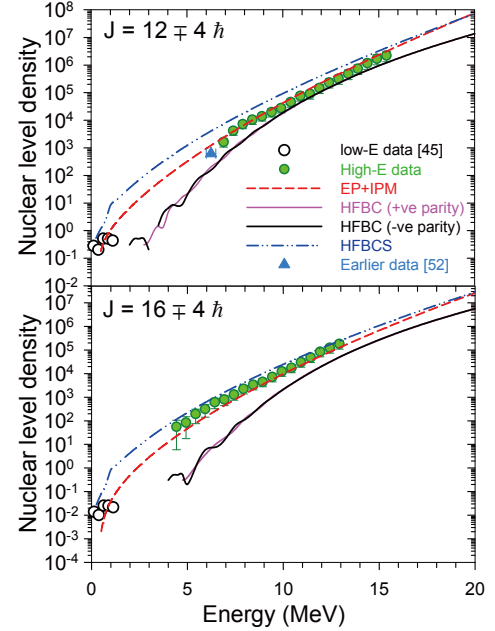
Fig. 1. Angular momentum gated NLD (symbols) along with the results of different theoretical calculations.
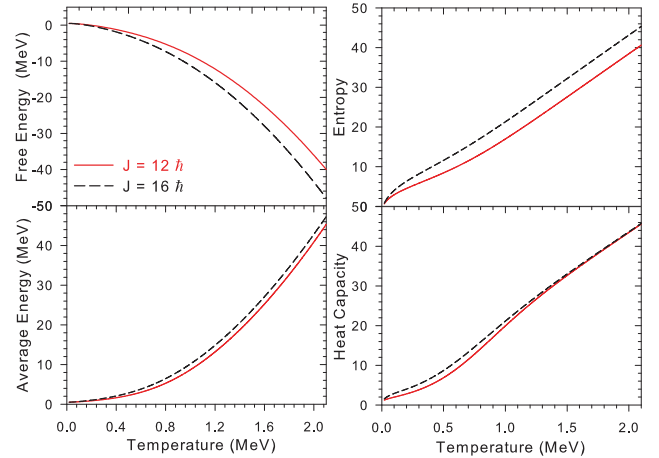
Fig. 2. Angular momentum gated TQs as functions of temperature obtained using EP+IPM level densities.

the pairing property of odd-odd ^{96}Tc nucleus, which is weaker than that in even-even ^{96}Mo. It is also observed that the angular momentum does not have much effect on the nature of the TQs. However, at low T, there is a noticeable change in the heat capcity due to the angular momentum. Therefore, it would be very interesting to study the angular momentum effect on the pairing phase transition in even-even systems in future.

References
1) B. Dey *et al.*, Phys. Rev. C **96**, 054326 (2017).
2) K. Kaneko *et al.*, Phys. Rev. C **74**, 024325 (2006).

Shell-model description of magnetic dipole bands in ^{105}Sn

M. Honma,[*1] T. Otsuka,[*2,*3,*4,*5] T. Mizusaki,[*6] Y. Utsuno,[*7,*8] N. Shimizu,[*8] and M. Hjorth-Jensen[*4,*9,*10]

Because of the well-developed shell closure at N, $Z = 50$, Sn isotopes have often been studied using the shell model by considering only valence neutrons. However, several states have been observed in light Sn isotopes that would be described by the configurations with a broken ^{100}Sn core. One interesting example is the high-spin regular band that decays mainly by M1 transitions.[1] This band has been interpreted by the "shears mechanism" using the tilted-axis cranking model.[2] In this report, we present the results of our trial to describe this magnetic dipole band using the shell model, taking ^{105}Sn as an example.

The adopted model space consists of the proton $(0g_{9/2}, 1d_{5/2}, 0g_{7/2})$ orbits and the neutron $(1d_{5/2}, 0g_{7/2}, 0h_{11/2}, 2s_{1/2}, 1d_{3/2})$ orbits. The effective interaction is prepared by combining the SNBG1[3] interaction as neutron-neutron and proton-proton part, the P1GD5G3[4] interaction for proton-neutron part among the relevant orbits if defined, and for the rest parts the microscopic interaction[5] based on the realistic N^{3}LO interaction.[6] The bare single-particle energies (SPEs) for the neutron orbits are adjusted so as to reproduce the effective SPEs obtained by the SNBG1 interaction at ^{114}Sn. The SPE of the proton $0g_{9/2}$ orbit is taken from the P1GD5G3 interaction, and the rest are deter-

mined so that the effective SPEs agree with those of the neutrons at ^{100}Sn. In order to ensure the computational feasibility, up to 5 nucleons are allowed to excite into the proton $(1d_{5/2}, 0g_{7/2})$ orbits or neutron $(0h_{11/2}, 2s_{1/2}, 1d_{3/2})$ orbits.

The calculated band structure is shown in Fig. 1. One can find reasonable agreement between the experimental data and the shell-model results. The E2 and M1 transition probabilities are calculated by using the effective charge $e_p = 1.6$, $e_n = 0.8$, and the effective spin g-factors $g^{\text{eff}} = 0.74g^{\text{free}}$. The calculated negative parity band $43/2_1^-$-$41/2_1^-$-$39/2_1^-$-$\cdots$ decays mainly by M1 transitions, consistently with the experiment. The typical $B(M1)$ value within the band is $\sim 1\mu_N^2$, while the $B(E2)$ value is at most $0.08e^2b^2$, indicating the M1 dominance. In addition to this band, the shell-model results give a positive-parity M1-dominant band $39/2_2^+$-$37/2_3^+$-$35/2_2^+$-$\cdots$, on top of the $23/2_2^+$ state. The dominant configurations in the calculated wave functions are $\pi(g_{9/2})^{-1}(g_{7/2})^1\nu(g_{7/2}d_{5/2})^4(h_{11/2})^1$ and $\pi(g_{9/2})^{-1}(g_{7/2})^1\nu(g_{7/2}d_{5/2})^5$ relative to the ^{100}Sn closed core for the negative and the positive parity bands, respectively. However, the purity of these configurations is gradually lost for lower spin states, and the feature of the "shears mechanism," *i.e.*, a rapid decrease of $B(M1)$ with increasing spin, is not clear.
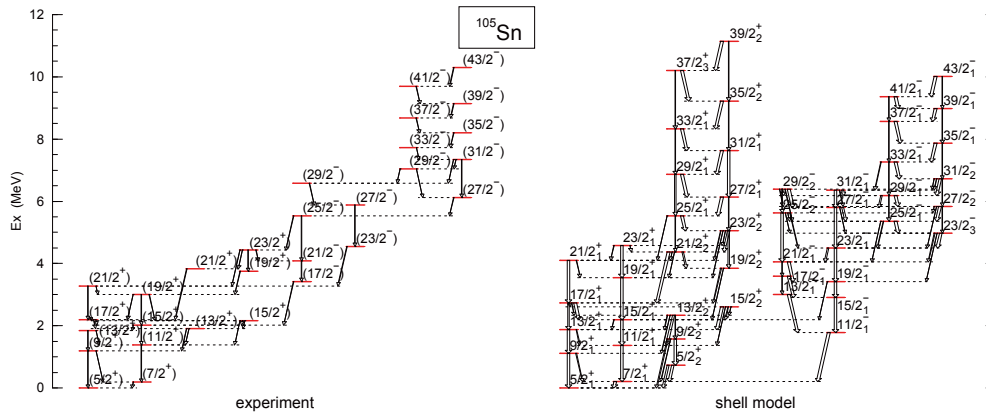
Fig. 1. Energy levels of ^{105}Sn. The experimental data are taken from Refs. 1, 7). The shell-model results are obtained using the code MSHELL64.[8] The width of the arrow drawn in the shell-model results is proportional to the branching ratio.

*1 Center for Mathematical Sciences, University of Aizu
*2 RIKEN Nishina Center
*3 Department of Physics, University of Tokyo
*4 National Superconducting Cyclotron Laboratory, Michigan State University
*5 Instituut voor Kern- en Stralingsfysica, KU Leuven
*6 Institute of Natural Sciences, Senshu University
*7 Advanced Science Research Center, Japan Atomic Energy Agency
*8 Center for Nuclear Study, University of Tokyo
*9 Department of Physics and Astronomy, Michigan State University
*10 Department of Physics, University of Oslo

References
1) G. de Angelis *et al.*, Nucl. Phys. **654**, 659c (1999).
2) S. Frauendorf, Nucl. Phys. **557**, 259c (1993).
3) M. Honma *et al.*, RIKEN Accel. Prog. Rep. **45**, 35 (2012).
4) M. Honma *at al.*, RIKEN Accel. Prog. Rep. **47**, 64 (2014).
5) M. Hjorth-Jensen *et al.*, Phys. Rep. **261**, 125 (1995).
6) D. R. Entem *et al.*, Phys. Rev. C **68**, 041001(R) (2003).
7) Data extracted using the NNDC WorldWideWeb site from the ENSDF database.
8) T. Mizusaki *et al.*, MSHELL64 code (unpublished).

Effect of pairing on the wobbling motion in odd-A nuclei[†]

K. Sugawara-Tanabe[1,2] and K. Tanabe[3]

As an indicator of a triaxial rotor, wobbling motion was proposed by Bohr and Mottelson,[1] and experimental data showing wobbling modes have been reported only in odd-Z nuclei of Lu isotopes,[2] ^{167}Ta,[3] and ^{135}Pr.[4] The wobbling motion is originally defined in classical mechanics[5] as a precessional motion of angular momentum $\vec{I}$ around the axis either with the maximum or the minimum moment of inertia (MoI) of the rotating body. Quantum mechanically, the incremental alignment of $\vec{I}$ along the wobbling axis with the maximum or the minimum MoI is in one unit[1,6,7]. In odd-Z nuclei, we found that in addition to the incremental alignment of $\vec{I}$ along the wobbling axis, the incremental alignment of $\vec{R} = \vec{I} - \vec{j}$ along the same axis is also in one unit (see Fig. 9 and Fig. 15 in Ref. 7)), where $\vec{j}$ is the single-particle angular momentum. Moreover, the D_2 invariance requires that the yrast wobbling band appears for the levels for which $I - j$=odd.

The microscopic theory for nuclear rotational motion includes an important Coriolis anti-pairing (CAP) effect,[8] i.e., the Coriolis force originating from the rotation starts to dissolve the pair in the special high-spin single-particle orbital, and finally the cranking formula for MoI reduces to the rigid (rig) MoI. We have obtained the analytical formula for the I dependence of MoI[9] for both odd- and even-Z nuclei by applying the second-order perturbation approximation to the self-consistent Hartree-Fock-Bogoliubov (HFB) equation under the number and I constraints. To simulate the behavior of the I dependence of MoI, we assume a two-parameter fit for the rigid MoI $\mathcal{J}_0$, $\mathcal{J}_0(I - b)/(I + a)$ for highly excited states as in Lu isotopes,[6] and $\mathcal{J}_0/[1 + \exp\{-(I - b)/a\}]$ for slightly excited states as in ^{135}Pr.[7]

Figure 1 shows the alignments of $\vec{R}$ for the case of the slightly excited states in ^{135}Pr, where the x-axis represents the maximum MoI. The parameter set $\mathcal{J}_0$=25 MeV^{-1}, a=7.5 and b=15.5 for j=11/2 simulates the experimental data quite well (see Figs. 17 and 18 in Ref. 7)). Figure 1 shows that $\langle R_x^2 \rangle_I^{1/2} \sim \langle R_x^2 \rangle_I^{1/2}$ for $I - j$ =even and $\langle R_x^2 \rangle_{I+2}^{1/2} - \langle R_x^2 \rangle_I^{1/2} \sim 2$. Therefore, the difference of $\langle R_x^2 \rangle^{1/2}$ between the solid and dashed lines is almost one, indicating that the incremental alignment of $\langle R_x^2 \rangle^{1/2}$ for $I - j$=odd is less by one unit compared with that for $I - j$=even, which is associated with the excitation of the wobbling motion. A similar behavior is found for $\langle I_x^2 \rangle^{1/2}$ in this I-dependent rig MoI.

Because the wobbling mode is related to the rotational motion of the rotor, the RPA treatment, which is useful for small-amplitude vibrational motion, is not applicable to the wobbling mode.

Fig. 1. Alignments of $\langle R_x^2 \rangle^{1/2}$, $\langle R_y^2 \rangle^{1/2}$, and $\langle R_z^2 \rangle^{1/2}$ for the I-dependent MoI as functions of I. The solid and open circles correspond to $\langle R_x^2 \rangle^{1/2}$ and $\langle R_y^2 \rangle^{1/2}$, while solid and open triangles correspond to $\langle R_z^2 \rangle^{1/2}$. The solid lines are for the levels with $I - j$=even, while the dashed lines for those with $I - j$=odd.

References
1) A. Bohr, B. R. Mottelson, in *Nuclear Structure*, (Benjamin, Reading, MA, 1975), **II**, Chap. 4, pp.190–194.
2) S. W. Ødegård *et al.*, Phys. Rev. Lett. **86**, 5866 (2001).
3) D. J. Hartley *et al.*, Phys. Rev. C **80**, 041304(R) (2009).
4) J. T. Matta, *et al.*, Phys. Rev. Lett. **114**, 082501 (2015).
5) L. D. Landau, E. M. Lifshitz, in *Mechanics*, (Pergamon Press Ltd., Oxford/London, 1960), Sect. 37, pp.116–121.
6) K. Tanabe, K. Sugawara-Tanabe, Phys. Rev. C **77**, 064318 (2008).
7) K. Tanabe, K. Sugawara-Tanabe, Phys. Rev. C **95**, 064315 (2017).
8) B. R. Mottelson, J. G. Valatin, Phys. Rev. Lett. **5**, 511 (1960).
9) K. Tanabe, K. Sugawara-Tanabe, Phys. Rev. C **91**, 034328 (2015).

†   Condensed from the talk in Int. Symp. on "Perspectives of the physics of nuclear structure", Nov. 1-4, The Univ. of Tokyo (2017)
*1   RIKEN Nishina Center
*2   Department of Information Design, Otsuma Women's University
*3   Department of Physics, Saitama University

Application of a Coulomb energy density functional for atomic nuclei: Case studies of local density approximation and generalized gradient approximation[†]

T. Naito,[*1,*2] R. Akashi,[*1] and H. Z. Liang[*2,*1]

The exchange (x) and correlation (c) energy density functionals $E_x[\rho]$ and $E_c[\rho]$ formulated for electron systems are tested in the context of atomic nuclei, respectively. Both the local density approximation (LDA) and generalized gradient approximation (GGA) functionals are investigated. For quantitative calculations, we employed the experimental charge-density distributions ρ_{ch}[1] of the selected nuclei as inputs of ground-state density distributions.

When it is assumed that the energy density ε_i depends only on the density at $\boldsymbol{r}$ locally as

$$E_i[\rho] = \int \varepsilon_i(\rho(\boldsymbol{r})) \, \rho(\boldsymbol{r}) \, d\boldsymbol{r} \qquad (i = x, c), \qquad (1)$$

this approximation is called the LDA. In the GGA, the energy density depends not only on the density distribution ρ but also on its gradient $|\nabla\rho|$ at $\boldsymbol{r}$ locally as

$$E_i[\rho] = \int \varepsilon_i(\rho(\boldsymbol{r}), |\nabla\rho(\boldsymbol{r})|) \, \rho(\boldsymbol{r}) \, d\boldsymbol{r} \qquad (i = x, c). \qquad (2)$$

The GGA exchange energy density weighted with $\rho_{ch}(r)$ for ^{208}Pb is shown in Fig. 1. The LDA result is shown with the long-dashed line, and those given by the GGA functionals B88,[2] PW91,[3] PBE,[4] and PBEsol[5] are shown with the short-dashed, dot-dashed, solid, and dot-dot-dashed lines, respectively. The surface is defined as the region that has a density between 90% and 10% of the maximum density.

For the exchange Coulomb energies, it is found that the deviation between the LDA and GGA,

$$\Delta E_x = \frac{E_x^{GGA} - E_x^{LDA}}{E_x^{GGA}}, \qquad (3)$$

ranges from around 11% in ^{4}He to around 2.2% in ^{208}Pb, by taking the PBE functional as an example of the GGA. From light to heavy nuclei, it is seen that ΔE_x shown in Fig. 2 behaves in a very similar way as the deviation between the Hartree-Fock-Slater approximation and the exact Hartree-Fock given by Le Bloas *et al.*[6] In this sense, the GGA exchange functionals of electron systems can be applied in a straightforward manner with practical accuracy to atomic nuclei. Furthermore, the numerical cost of GGA is $O(N^3)$, whereas that cost of exact Hartree-Fock is $O(N^4)$ for
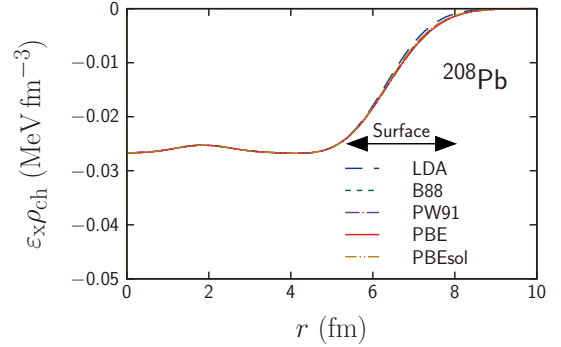
Fig. 1. GGA exchange energy densities weighted with ρ_{ch} for ^{208}Pb as a function of r.
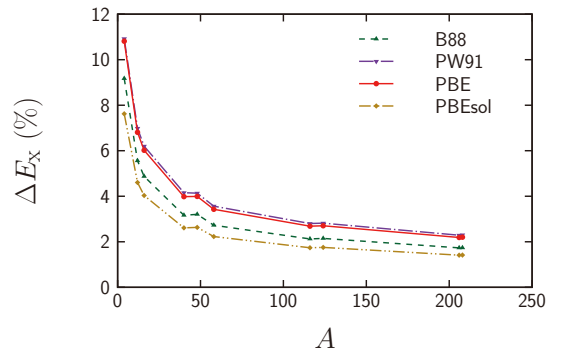
Fig. 2. Deviation between the LDA and GGA in E_x defined as Eq. (3) as a function of A.

self-consistent calculations. In contrast, the correlation Coulomb energy density functionals of electron systems are not applicable for atomic nuclei, because these functionals are not separable and the nuclear interaction determines the properties of atomic nuclei.

References
1) H. De Vries, C. W. De Jager, C. De Vries, At. Data Nucl. Data Tables **36**, 495 (1987).
2) A. D. Becke, Phys. Rev. A **38**, 3098 (1988).
3) J. P. Perdew, J. A. Chevary, S. H. Vosko *et al.*, Phys. Rev. B **46**, 6671 (1992).
4) J. P. Perdew, K. Burke, M. Ernzerhof, Phys. Rev. Lett. **77**, 3865 (1996).
5) J. P. Perdew, A. Ruzsinszky, G. I. Csonka *et al.*, Phys. Rev. Lett. **100**, 136406 (2008).
6) J. Le Bloas, M.-H. Koh, P. Quentin, L. Bonneau, J. I. A. Ithnin, Phys. Rev. C **84**, 014310 (2011).

Joint project for large-scale nuclear structure calculations in 2017

N. Shimizu,[*1] J. Menéndez,[*1] T. Miyagi,[*1] S. Yoshida,[*2] T. Otsuka,[*3,*1,*2] and Y. Utsuno[*4,*1]

We have been promoting a joint project for large-scale nuclear structure calculations since the year 2002 based on a collaboration agreement between the RIKEN Accelerator Research Facility (currently RIKEN Nishina Center) and Center for Nuclear Study, the University of Tokyo. Currently, we maintain 16 PC servers for large-scale nuclear structure calculations. Based on this project, we performed shell-model calculations of the various nuclides that have been measured or are proposed to be measured at the RIKEN RI Beam Factory and other facilities, such as ^{35}Mg,[1] ^{136}Ba, ^{138}Ce, and ^{135}La under various collaborations with many experimentalists. In parallel, we performed several theoretical studies for understanding the nuclear structure. Among them, we briefly show three theoretical achievements: shell-model study of the beta-decay properties of neutron-rich nuclei,[2] the development of an *ab initio* nuclear structure calculation,[3] and the theoretical estimation of nuclear matrix elements that are essential for surveying physics beyond the standard model.[4–6]

In order to discuss the systematic properties of the beta decay of neutron-rich nuclei, we performed large-scale shell-model calculations with $sd + pf + sdg$ model space and evaluated the contributions from both Gamow-Teller and first-forbidden transitions for the 78 nuclei with $13 \leq Z \leq 18$ and $22 \leq N \leq 34$.[2] The obtained beta-decay half-lives and delayed neutron emission rates remarkably agree with experimental data. This indicates the validity of large-scale shell-model calculations for nuclei in the neutron rich region. The shell-model results predict that the first-forbidden transition has a non-negligible contribution to the half-lives in $N > 30$ nuclei. We also discuss the emergence of the Gamow-Teller giant resonance and its origin.

In order to investigate the medium-heavy nuclei based on the underlying nuclear interactions in an *ab initio* way, the unitary-model-operator approach[3] (UMOA) has been developed. In the UMOA, the many-body Hamiltonian is transformed by a unitary transformation such that the one-particle-one-hole and two-particle-two-hole excitations do not occur. We calculated the binding energies and radii of ^{4}He and several oxygen isotopes using the similarity-renormalization-group evolved chiral effective-field-theory interaction consisting of two-nucleon and three-nucleon forces. The resulting binding energies successfully reproduce the experimental data. On the other hand, the calculated radii are underestimated compared to the experimental values. This situation is consistent with the recent studies by the other *ab initio* methods. For a unified description of binding energies and radii, further improvements about the nuclear force are expected.

We performed calculations for determining of the nature of dark matter and neutrinos in experiments using atomic nuclei. On the one hand, we obtained the nuclear matrix element for the interaction of dark matter particles with nuclei via the coupling of nucleons to the Higgs boson.[4] Our results included for the first time the coupling of the Higgs boson to two nucleons via pion-exchange currents. The uncertainty on the matrix element was reduced by roughly an order of magnitude. On the other hand we studied the nuclear matrix elements of neutrinoless double-beta decay, when it is mediated by heavy sterile neutrinos.[5] Contrary to the light-neutrino-exchange channel, different many-body methods agree well when heavy neutrinos are exchanged. This result suggests that long-range nuclear correlations are responsible for the disagreement between matrix elements in the standard light-neutrino-exchange channel. In addition, we investigated the double Gamow-Teller strength distribution of double-beta decay emitters, such as ^{48}Ca. We theoretically predict a linear relation between the nuclear matrix elements of the double Gamow-Teller transition and the $0\nu\beta\beta$ decay.[6]

References
1) S. Momiyama *et al.*, Phys. Rev. C **96**, 034328 (2017).
2) S. Yoshida, Y. Utsuno, N. Shimizu, T. Otsuka, Phys. Rev. C in press.
3) T. Miyagi, T. Abe, R. Okamoto, T. Otsuka, Phys. Rev. C **96**, 054312 (2017).
4) M. Hoferichter, P. Klos, J. Menéndez, A. Schwenk, Phys. Rev. Lett. **119**, 181803 (2017).
5) J. Menéndez, J. Phys. G: Nucl. Part. Phys. **45**, 014003 (2018).
6) N. Shimizu, J. Menéndez, K. Yako, Phys. Rev. Lett. **120**, 142502 (2018).

*1 Center for Nuclear Study, The University of Tokyo
*2 Department of Physics, The University of Tokyo
*3 RIKEN Nishina Center
*4 Japan Atomic Energy Agency

3. Nuclear Data

Proton- and deuteron-induced reactions on ^{107}Pd and ^{93}Zr at 20–30 MeV/nucleon

M. Dozono,[*1] N. Imai,[*1] S. Michimasa,[*1] T. Sumikama,[*2] N. Chiga,[*2] S. Ota,[*1] O. Beliuskina,[*1] S. Hayakawa,[*1] K. Iribe,[*3] C. Iwamoto,[*1] S. Kawase,[*4] K. Kawata,[*1] N. Kitamura,[*1] S. Masuoka,[*1] K. Nakano,[*4] P. Schrock,[*1] D. Suzuki,[*2] R. Tsunoda,[*1] K. Wimmer,[*5] D. S. Ahn,[*2] N. Fukuda,[*2] E. Ideguchi,[*6] K. Kusaka,[*2] H. Miki,[*7] H. Miyatake,[*8] D. Nagae,[*2] M. Nakano,[*9] S. Ohmika,[*2] M. Ohtake,[*2] H. Otsu,[*2] H. J. Ong,[*6] S. Sato,[*9] H. Shimizu,[*1] Y. Shimizu,[*2] H. Sakurai,[*2] X. Sun,[*2] H. Suzuki,[*2] M. Takaki,[*1] H. Takeda,[*2] S. Takeuchi,[*7] T. Teranishi,[*3] H. Wang,[*2] Y. Watanabe,[*4] Y. X. Watanabe,[*8] H. Yamada,[*7] H. Yamaguchi,[*1] R. Yanagihara,[*6] L. Yang,[*1] Y. Yanagisawa,[*2] K. Yoshida,[*2] and S. Shimoura[*1]

The nuclear transmutation of long-lived fission products (LLFPs), which are produced in nuclear reactors, is one of the candidate techniques for the reduction and/or reuse of LLFPs. To design optimum pathways of the transmutation process, several nuclear reactions have been studied by using LLFPs as secondary beams. The studies indicate that proton- and/or deuteron-induced reactions at intermediate energy (100–200 MeV/nucleon) are sufficiently effective for the LLFP transmutation.[1–3)] For a systematic study, we performed an experiment of proton- and deuteron-induced reactions on ^{107}Pd and ^{93}Zr at 20–30 MeV/nucleon by using the OEDO beam line.[4)]

Secondary beams were produced by the in-flight fission of a ^{238}U primary beam at 345 MeV/nucleon on a Be target with a thickness of 3 mm. The beams were degraded and purified by using an Al degrader at F1 and further degraded by using another Al degrader at F5. The beam energies were 32 MeV/nucleon in front of the secondary targets. For ^{107}Pd, another setting was used to study the reaction at a lower beam energy of 26 MeV/nucleon. The beam particles were identified by the time-of-flight (TOF) between F3 and F5 measured with diamond detectors. The OEDO system was used to reduce the beam spot size, and the resulting size was 30 mm in FWHM on the secondary target.

A schematic view of the setup around the secondary target is shown in Fig. 1. The secondary targets, H_2 and D_2, were prepared as high-pressure cooled gas targets. The temperature was 40 K, and the pressure was adjusted to 7.5(15) mg/cm^2 for H_2 (D_2). In order to obtain the background contribution, empty-target measurements were also carried out.

Reaction residues were analyzed by the SHARAQ spectrometer and detected by two PPACs and an ionization chamber located at the focal plane. In order to
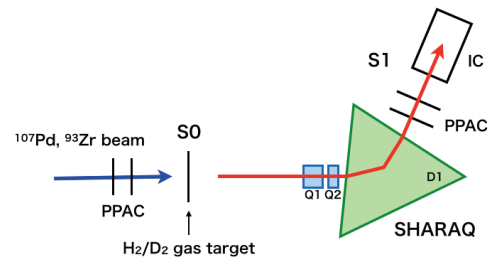
Fig. 1. Schematic view of the experimental setup.
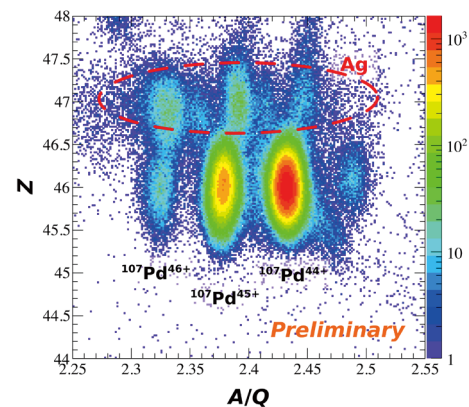
Fig. 2. Correlation of proton number Z and mass-to-charge ratio A/Q of reaction residues produced from a ^{107}Pd beam at 32 MeV/nucleon and a H_2 target.

cover a broad range of reaction products, several different $B\rho$ settings were applied in SHARAQ. The particle identification (PID) was performed with the TOF-$B\rho$-ΔE-E method. An example of the PID is shown in Fig. 2. In addition to the ^{107}Pd beam events, Ag isotope events are seen. Further analysis is ongoing.

References
1) H. Wang et al., Phys. Lett. B **754**, 104 (2016).
2) H. Wang et al., Prog. Theor. Exp. Phys. **2017**, 021D01 (2017).
3) S. Kawase et al., Prog. Theor. Exp. Phys. **2017**, 093D03 (2017).
4) S. Michimasa et al., In this report.

*1　Cener for Nuclear Study, the University of Tokyo
*2　RIKEN Nishina Center
*3　Department of Physics, Kyushu University
*4　Department of Advanced Energy Engineering Science, Kyushu University
*5　Department of Physics, the University of Tokyo
*6　Research Center for Nuclear Physics, Osaka University
*7　Department of Physics, Tokyo Institute of Technology
*8　WNSC, IPNS, KEK
*9　Department of Physics, Rikkyo University

Measurement of isotopic production cross sections of proton- and deuteron-induced spallation reactions on ^{93}Zr at 200 MeV/nucleon

S. Kawase,[*1] Y. Watanabe,[*1] K. Nakano,[*1,*2] J. Suwa,[*1,*2] H. Wang,[*2] N. Chiga,[*2] H. Otsu,[*2] H. Sakurai,[*2]
S. Takeuchi,[*3] and T. Nakamura[*3] for ImPACT-RIBF collaboration

Proton- and deuteron-induced spallation reactions are considered as the candidate processes for the transmutation of long-lived fission products (LLFPs). In our previous study on the proton- and deuteron-induced reactions on LLFP ^{93}Zr at 105 MeV/nucleon,[1] the isotopic production cross sections in few-nucleon removal channels were largely overestimated in the model calculations using PHITS.[2] To improve the reliability of the reaction model calculations, further systematic experimental data are required over a wide range of reaction energies. In this study, the isotopic production cross sections of the proton- and deuteron-induced spallation reactions on ^{93}Zr at 200 MeV/nucleon were measured in an inverse kinematics condition.

The experiment was conducted at the SAMURAI beamline[3] at RIBF. The secondary beam, including ^{93}Zr at 200 MeV/nucleon, was generated via inflight fission of ^{238}U and selected by using BigRIPS. The typical total rate of the beam was 5 kcps, and the purity of ^{93}Zr was 33%. Then, the beam bombarded a liquid hydrogen and a liquid deuterium target.[4] The reaction products were identified by using the SAMURAI spectrometer.[3] The isotopic production cross sections were derived from the number of incident ^{93}Zr beams and that of the generated isotopes.

The isotopic production cross sections of the proton- and deuteron-induced reactions on ^{93}Zr at 200 MeV/nucleon are shown in Fig. 1. The black circles and the red diamonds indicate the proton-induced cross sections (σ_p) and the deuteron-induced cross sections (σ_d), respectively. The error bars indicate only the statistical uncertainties.

Enhancement of the cross sections at ^{90}Zr and ^{89}Y, which have a neutron magic number $N = 50$, was observed as in the case of 105 MeV/nucleon measurement.[1] The effect of shell closure is still important in the interpretation of the spallation reaction cross sections at 200 MeV/nucleon, despite the high reaction energy compared to nucleon separation energies.

In Fig. 1, the experimental results are compared to the model calculations by using the particle and heavy-ion transport code system (PHITS) 2.82.[2] The spallation reactions have been well described as a two-step process composed of the formation of prefragments via
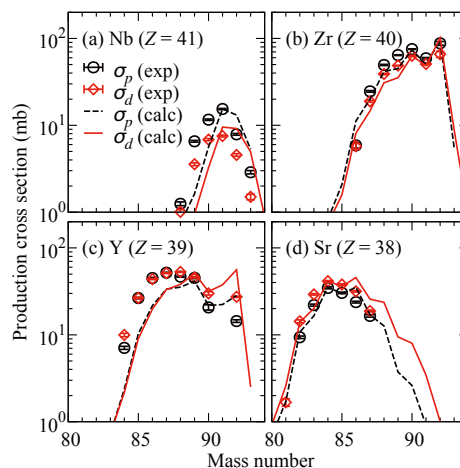
Fig. 1. Isotopic production cross sections of the proton- and deuteron-induced reactions on ^{93}Zr at 200 MeV/nucleon.

an intra-nuclear cascade process and the de-excitation process of the prefragments by evaporation of light particles. In this work, the Liège Intranuclear Cascade model (INCL 4.6)[5] and the generalized evaporation model (GEM)[6] were employed for these processes. The lines in Fig. 1 show the cross sections calculated by using PHITS. The black dashed line and the red solid line correspond to σ_p and σ_d, respectively.

The general behavior of the isotopic production cross sections are apparently well reproduced by the PHITS calculation; however, the mass-number distributions are shifted to heavier isotopes especially in proton-odd isotopes (Nb and Y). The production cross section of ^{92}Y is considerably overestimated in both the proton- and deuteron-induced cases. These can probably be understood by the poor reproduction of the excitation energy of reaction residue after the direct process, which is pointed out in Ref. 1). The models used in PHITS are expected to be improved in near future after close analyses of the spallation reaction data over a wide range of incident energies.

References

1) S. Kawase et al., Prog. Theor. Exp. Phys. **2017**, 093D03 (2017).
2) T. Sato et al., J. Nucl. Sci. Technol., **50**, 913 (2013).
3) T. Kobayashi et al., Nucl. Instrum. Methods B **317**, 294 (2013).
4) H. Ryuto et al., Nucl. Instrum. Methods A **555**, 1 (2005).
5) A. Boudard et al., Phys. Rev. C **87**, 014606 (2013).
6) S. Furihata, Nucl. Instrum. Methods B **171**, 251 (2000).

[*1] Department of Advanced Energy Engineering Science, Kyushu University
[*2] RIKEN Nishina Center
[*3] Graduate School of Science and Engineering, Tokyo Institute of Technology

Measurement of double-differential neutron yields for 345 MeV/nucleon ^{238}U incidence on Cu[†]

K. Sugihara,[*1,*2] N. Shigyo,[*1,*2] A. Akashio,[*1] and K. Tanaka[*1]

The validation of Monte Carlo simulation codes on radiation shielding with a uranium beam is required for future upgrades of RIBF. Experimental data of double-differential neutron thick target yields (TTY) are desired as a neutron source term in the radiation shielding design. We have started to measure neutron energy spectra by the time-of-flight (TOF) method.

The experiment was carried out around the F10 chamber at the ZeroDegree Spectrometer. The experimental arrangement is shown in Fig. 1.

The 345 MeV/nucleon ^{238}U beam which was not pulsed irradiated a Cu target. The bunch width of the beam was less than 1 ns and its repetition rate was about 18 MHz. The thickness of the target was 10 mm, which was longer than the range of the beam ion.

Neutrons produced in the target were measured with two sizes of NE213 liquid organic scintillators. The small scintillator with a length and diameter of 5.08 cm was set at 0°. The large ones with a length and diameter of 12.7 cm were located at 45° and 90°. To determine the threshold level, light outputs of the scintillators were calibrated with γ-ray sources, ^{60}Co, ^{241}Am-Be and ^{244}Cm-^{13}C. A 2 mm thick plastic scintillator was set as a veto detector to distinguish non-charged particle events in front of each neutron detector. Neutron kinetic energy was determined by the TOF method in which the start and stop signal came from the neutron scintillator and the RF signal of the superconducting ring cyclotron. The flight path lengths from the target to the detectors were shown in Fig. 1.

Figure 2 shows the TOF spectrum at 90°. The horizontal axis is the time difference between the RF signal and the neutron detector. The TDC resolution was 0.027 ns/ch. The peak at 1350 ch was the prompt γ-ray
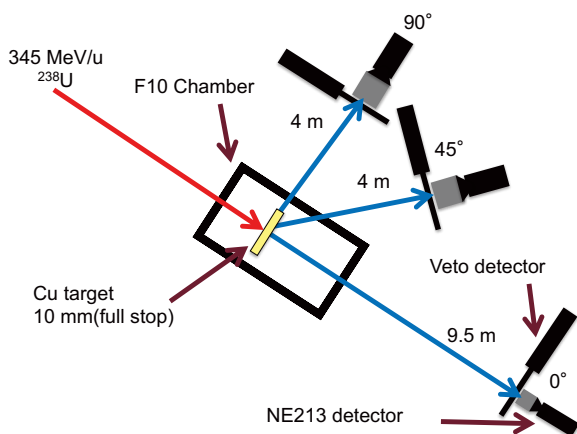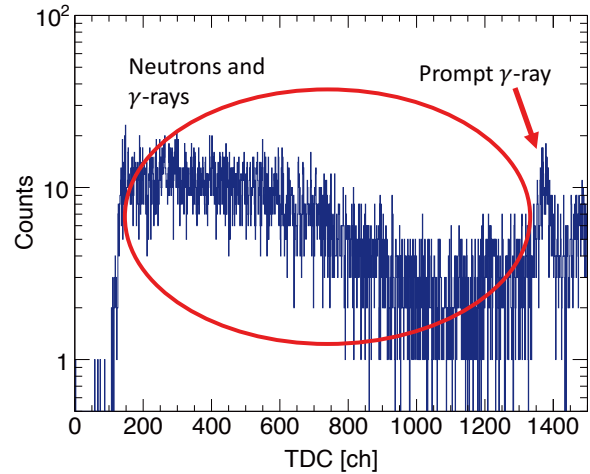
Fig. 2. TOF spectrum.
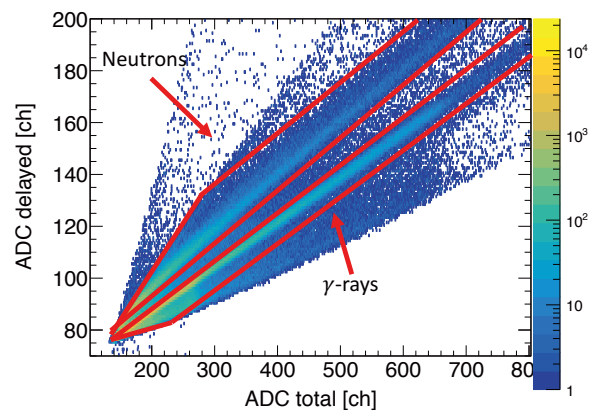
Fig. 3. Separation of neutron and γ-ray events.

from the uranium incident reactions. Neutron energy will be determined with the use of the time difference between each neutron and the prompt γ-ray event. Low-energy neutrons from the preceding beam bunch were overlapped in the TOF gate. The contribution of these neutrons was about 2% at the highest neutron energy point for 0° and substracted from the TOF spectrum.

Neutron events were extracted by using the difference of the decay part of the signal pulse between the neutron and γ-ray[1] because the NE213 scintillator was sensitive to not only neutrons but also γ-rays. Figure 3 illustrates the two-dimensional plot of the total pulse of scintillator light output signal (horizontal axis) and the decay part of it (vertical axis). Neutron and γ-ray events are clearly separated in the low light output region.

The neutron TTY is under analysis and will be compared with calculation results by Monte Carlo codes.

Fig. 1. Experimental arrangement.

[*1] RIKEN Nishina Center
[*2] Department of Engineering, Kyushu University

Reference
1) T. Nakamoto et al., J. Nucl. Sci. Technol. **32**, 827 (1995).

Construction of implantation beam line for the verification test of ^{107}Pd transmutation

Y. Miyake,[*1] N. Ikoma,[*1,*2] N. Chiga,[*1] A. Uchiyama,[*1] A. Takagi,[*1,*3] H. Hasebe,[*1] K. Takahashi,[*1] Y. V. Sahoo,[*1] T. Sasaki,[*1,*2] H. Sakurai,[*1,*4] and H. Okuno[*1,*2]

The nuclear transmutation of long-lived fission products (LLFP) is one of the solutions for the disposal of high-level radioactive waste.[1] It allows LLFP to be converted into stable or short-lived nuclides and rare metals including LLFP to be reused. Palladium is a useful material for industrial use and one of the target nuclides for recycling by nuclear transmutation. To investigate reasonable nuclear reaction paths for ^{107}Pd, an experiment to obtain the cross sections for proton- and deuteron-induced spallation in inverse kinematics was conducted at the RIKEN Radioactive Isotope Beam Factory (RIBF).[2] The experimental results implied ^{107}Pd can be converted into ^{106}Pd by a proton or deuteron. However, considering the actual system, LLFP should be irradiated by ion beams.

In order to investigate the feasibility of this system, we conducted a verification test to transmute ^{107}Pd by deuteron beams produced by the accelerator. To prepare a ^{107}Pd target, we procured ^{107}Pd-condensed material, in which the concentration of ^{107}Pd is 15%. In addition, it is necessary to concentrate ^{107}Pd up to almost 100% in the sample to detect the nuclear transmutation reaction effectively. We constructed the ion-implantation beam line to concentrate ^{107}Pd.

In this paper, the construction of the implantation beam line for the verification test of ^{107}Pd transmutation and some experimental results of the implantation samples are reported.

The implantation beam line consists of an ion source, an 80-cm-radius double-focusing 90° bending magnet, a target chamber, and other components. The ion source is a negative plasma-sputter-type ion source.[3] Negative ions of palladium are produced from the palladium target and extracted with an acceleration voltage of 20 kV. Palladium ion beams are mass-analyzed and focused on the target in the target chamber. A single slit with a diameter of 2, 3, 5, or 10 mm and an electrically suppressed Faraday cup are also placed in it. The beam size on the target was approximately 3 mm with the slit. The target material was a carbon foil with a thickness of approximately 300 μg/cm^2.

The experiment with ^{105}Pd has been conducted prior to that with ^{107}Pd. The typical beam current is between 10 and 20 nA for ^{105}Pd. Two implantation samples were prepared in order to detect the transmutation of ^{105}Pd: one is for the analysis with deuteron irradiation, and the other is for the analysis without the irradiation.
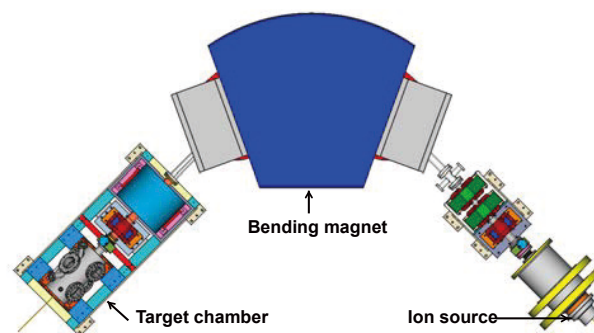
Fig. 1. Implantation beam line for ^{107}Pd concentration.
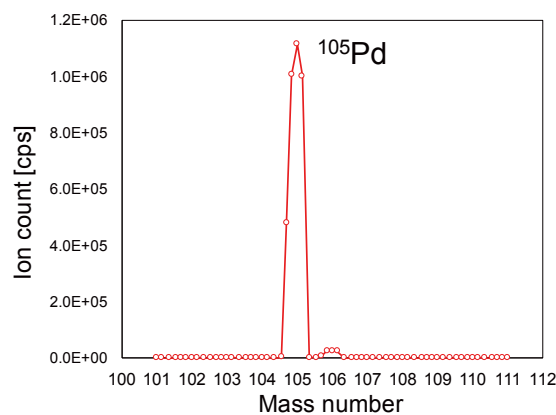
Fig. 2. ICP-MS results of the implantation sample. The vertical axis shows the number of ions detected by ICP-MS, and the horizontal axis shows the mass number of ions.

After the implantation, palladium was extracted from the target foil by reverse aqua regia and perchloric acid, and investigated by ICP-MS. Figure 2 shows the results of ICP-MS. ^{105}Pd was successfully concentrated up to approximately 98% and separated from other palladium isotopes.

Implantation samples will be irradiated by deuteron produced by AVF Ring Cyclotron at RIKEN RIBF in the future and the isotopic ratio of palladium will be measured by thermal ionization mass spectrometry.

References
1) Impulsing Paradigm Change through Disruptive Technologies Program (ImPACT), http://www.jst.go.jp/impact/en/program/08.html, accessed: January 10, 2018.
2) H. Wang *et al.*, Prog. Theor. Exp. Phys. **2017**, 021D01 (2017).
3) Y. Mori, Nucl. Instrum. Methods Phys. Res. A **328** (2017).

*1　RIKEN Nishina Center
*2　Department of Energy and Environment Science, Nagaoka University of Technology
*3　National Laboratory for High Energy Physics (KEK)
*4　Department of Physics, Faculty of Science & Graduate School of Science, The University of Tokyo

A study of additional uncertainties from fit boundaries using a new code for multi-reflection time-of-flight data

M. Rosenbusch,[*1] Y. Ito,[*2] P. Schury,[*3] M. Wada,[*1,*3] D. Kaji,[*1] K. Morimoto,[*1] H. Haba,[*1] S. Kimura,[*1,*4] H. Koura,[*5] M. MacCormick,[*6] H. Miyatake,[*3] J. Y. Moon,[*7] K. Morita,[*1,*8] I. Murray,[*1,*6] T. Niwase,[*8] A. Ozawa,[*4] M. Reponen,[*1] A. Takamine,[*1] T. Tanaka,[*1,*8] and H. Wollnik[*9]

Raw data of the isotopes $^{210-214}$Ra and $^{210-214}$Ac, measured with the RIKEN-KEK multi-reflection time-of-flight mass spectrograph (MRTOF-MS),[1,2] has been analyzed using a new code for mass evaluation. It has been developed to investigate uncertainties of time-of-flight (TOF) fits, which are not covered by the uncertainty provided by the fit routine. Additional effects can occur if the extracted TOF value from the fit depends on the choice of boundary conditions. Such conditions can be the fitting range, and for binned data, the choice of the bin size as well as the choice of bin origin (starting position of the first bin).

The code is a wrapping program around the maximum-likelihood estimator provided by the library ROOT/CERN[3] and enables repeated fits to the TOF data with various bin sizes, bin origins (see bottom of figure), and fitting ranges around the peak center. Due to the change of conditions, every new data fit will converge at a slightly different TOF. However, unless the choice of boundaries is not obviously wrong, as *e.g.*, the fitting range so large that a neighbor peak influences the result, there is no reason to consider any of those choices as incorrect. Such variation of results is not generally covered by the uncertainties obtained from the fitting routine as the optimizer works only with the data and parameter limits given by the user.

For MRTOF-MS spectra recorded over a time span of 20 min up to several hours, another degree of freedom arises when correcting for TOF drifts (temperature and voltage dependent). The data of the reference ions is split into subsets containing a certain number of experimental sweeps, the TOF of the reference ions in each subset is obtained from a fit, and then the data is summed up again with adjusted time origins to eliminate the drifts. However, if not all fluctuation frequencies are resolvable, the variation of the number of sweeps will cause changes in the final mass value, which is not fully predictable. The top of the figure shows the mass results of a selected data set as a function of the number of sweeps for each subset.

*1 RIKEN Nishina Center
*2 Department of Physics, McGill University
*3 Wako Nuclear Science Center (WNSC), IPNS, KEK
*4 Institute of Physics, University of Tsukuba
*5 Advanced Science Research Center, JAEA Ibaraki
*6 Institut de Physique Nucliare, CNRS-IN2P3, Université Paris-Sud, Université Paris-Saclay
*7 Institute for Basic Science
*8 Department of Physics, Kyushu University
*9 Department of Chemistry and Biochemistry, New Mexico State University

Fig. 1. Top: Scattering of the mass result of a selected ^{213}Ac^{2+} data set for various number of sweeps used for the data subsets to perform the TOF drift correction. Bottom: TOF spectrum with 4 ns bin width with two different origins of binning. The time origin of the grey colored spectrum has 2 ns difference from the blue one in the background.

A full analysis with different bin sizes, bin widths, bin origins, and number of sweeps per subset has been performed for all data sets of the measured Ac/Ra isotopes.[4] The result of the full analysis is an additional average scattering, which is covered when multiplying the statistical uncertainty by a factor of about 1.3. This value approaches the Birge ratio of about 1.2 from those isotopes for which a sufficient number of independent data sets could be measured. For low-statistics data, such an evaluation can provide a reasonable estimation of the uncertainty. A thorough future study can give more accurate answer how strong the scattering of mass results can be caused by the choice of the fit boundaries rather than caused by the data itself.

References
1) P. Schury *et al.*, Nucl. Instrum. Methods B **376**, 425 (2015).
2) P. Schury *et al.*, Int. J. Mass Spectrom. **359**, 19 (2014).
3) R. Brun, F. Rademakers, Nucl. Instrum. Methods B **389**, 81 (1997).
4) M. Rosenbusch *et al.*, accepted by PRC (2018).

EXFOR Compilation of RIBF data in 2017

D. Ichinkhorloo,[*1] M. Aikawa,[*1,*2] S. Ebata,[*1] S. Imai,[*3] S. Jagjit,[*1] N. Otuka,[*2,*4] and M. Kimura[*1]

Nuclear reaction data are used in various fields, *e.g.* nuclear physics, engineering and medicine. Accessible databases are therefore required worldwide. One such database open to the public is the EXFOR (EXchange FORmat) library, which is maintained by the International Network of Nuclear Reaction Data Centres (NRDC) under the auspices of the International Atomic Energy Agency (IAEA).[1] The Hokkaido University Nuclear Reaction Data Centre (JCPRG)[2] is a member of NRDC and compiles charged-particle and photon induced nuclear reaction data obtained in the institutes located in Japan. About 10% of charged-particle nuclear reaction data in the EXFOR library is contributed by JCPRG.

Our compilation process involves the following steps. Papers in agreement with the EXFOR scope are basically surveyed in peer-reviewed journals. Information to be compiled includes bibliographic information, experimental setup, physical quantities and numerical data, respectively. The information is retrieved from the papers, formatted and input into the database. During the compilation process, the corresponding authors are contacted for queries over the contents of paper and requests for numerical data.

JCPRG has cooperated with the RIKEN Nishina Center for compilation of data obtained in RIBF since 2010. In this article, we report our activities related to the RIBF data. In 2017, we compiled three new papers including the experiment data of RIBF. Out of the three papers, the corresponding authors of two papers provided us the numerical data for compilation. The compiled data are accessible by the entry numbers listed in Table 1.

Figure 1 shows the number of papers compiled from 2011 and already reserved for compilation in 2018. The number in 2017 is rather small in comparison with the yearly average of 13.7 papers between 2011 and 2016 due to reassignment of compilation staff. Thirteen papers were already reserved for compilation as listed in Table 1. The entries of ten papers among them have been prepared in the EXFOR format and are waiting for transmission to IAEA.

We have established an effective procedure to compile all new publications during the last seven-year collaboration with the RIKEN Nishina Center. Therefore, most of the recent experimental nuclear reaction data are provided by the corresponding authors. This cooperation is valuable and effective, and therefore it is needed to be continued for rapid and reliable compilation.

Table 1. Entry numbers assigned to papers of RIBF data compiled and to be compiled.

Status	Entry number			Total
Compiled	E2506[3]	E2518[4]	E2539[5]	3
Compiling	E2500[6]	E2504[7]	E2507[8]	13
	E2511[9]	E2515[10]	E2516[11]	
	E2522[12]	E2542[13]	E2543[14]	
	E2549[15]	E2553[16]	E2554[17]	
	E2557[18]			
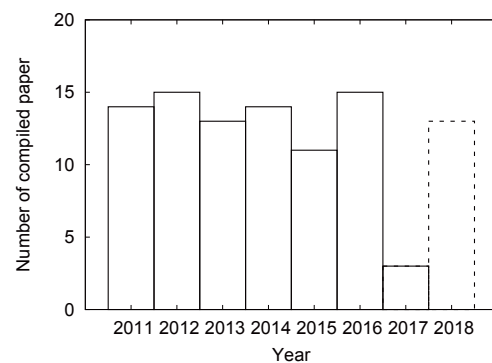
Fig. 1. Number of papers including RIBF data already compiled until 2017 and reserved for compilation in 2018.

References
1) N. Otuka *et al.*, Nucl. Data Sheets **120**, 272 (2014).
2) Hokkaido University Nuclear Reaction Data Centre: http://www.jcprg.org/.
3) S. Cherubini *et al.*, Phys. Rev. C **92**, 015805 (2015).
4) H. Wang *et al.*, Prog. Theor. Exp. Phys. **2017**, 021D01 (2017).
5) S. Kawase *et al.*, Prog. Theor. Exp. Phys. **2017**, 093D03 (2017).
6) K. Kisamori *et al.*, Phys. Rev. Lett. **116**, 052501 (2016).
7) P. Doornenbal *et al.*, Phys. Rev. C **93**, 044306 (2016).
8) I. Čeliković *et al.*, Phys. Rev. Lett. **116**, 162501 (2016).
9) A. R. Usman *et al.*, Appl. Radiat. Isot. **114**, 104 (2016).
10) B. Blank *et al.*, Phys. Rev. C **93**, 061301 (2016).
11) S. Hayakawa *et al.*, Phys. Rev. C **93**, 065802 (2016).
12) Y. Togano *et al.*, Phys. Lett. B **761**, 412 (2016).
13) D. Kaji *et al.*, J. Phys. Soc. Jpn. **86**, 085001 (2017).
14) J. W. Hwang *et al.*, Phys. Lett. B **769**, 503 (2017).
15) T. Sumikama *et al.*, Phys. Rev. C **95**, 051601 (2017).
16) S. Momiyama *et al.*, Phys. Rev. C **96**, 034328 (2017).
17) H. Suzuki *et al.*, Phys. Rev. C **96**, 034604 (2017).
18) V. Vaquero *et al.*, Phys. Rev. Lett. **118**, 202502 (2017).

*1 Faculty of Science, Hokkaido University
*2 RIKEN Nishina Center
*3 Institute for the Advancement of Higher Education, Hokkaido University
*4 NDS, IAEA

Monte-Carlo simulation of transmutation based on experimental nuclear data

S. Ebata,[*1] D. Ichinkhorloo,[*1] and M. Aikawa[*1,*2]

The management of long-lived fission products (LLFPs) in nuclear reactors is one of the most important tasks in nuclear engineering. The transmutation of LLFPs is a promising technology to reduce and reuse high-level radioactive nuclear wastes. Reaction cross sections of the transmutation are fundamental and essential information in nuclear applications. The cross sections of proton- and deuteron-induced reactions on the LLFPs ^{93}Zr and ^{107}Pd were measured using the inverse kinematics technique in RIBF.[1,2]

Furthermore, macroscopic simulations based on a realistic condition are essential for the feasibility study of the transmutation. A Monte-Carlo simulation code PHITS[3] is adopted and used to design the nuclear applications for the transmutation of LLFPs in our project. However the transmutation reaction cross sections calculated using PHITS are partially different from the experiment data.[1,2] To avoid the discrepancies, we need to induce the recent experimental data directly in simulations. A function named Frag Data is implemented in PHITS to use external cross section data. By using this function, we can reflect the experimental data in the macroscopic simulations.

The Frag Data function requires an external data file of cross sections for each reaction system consisting of a target and projectile. The file includes the total, production and double differential cross sections of each outgoing particle for several incident energies. The production cross sections of heavy residual nuclei in a target could be obtained in previous experiments.[1,2] The double differential cross sections of secondary light particles (neutron, proton, deuteron and ^{4}He) are also required because the data are expected to have large effects on the transmutation. The cross sections of such light particles, however, were not measured in the experiments. Therefore, we adopt results for the secondary particles calculated using the default PHITS simulation as inputs of the file.

For the simulation of the proton-induced reaction, the process to prepare the Frag Data input files is as follows. First, simulations for 100- and 200-MeV proton-induced reactions on thin ^{107}Pd and ^{93}Zr targets (5 μm thickness) were performed with the trial number set to 10^6. From the simulations, the double differential cross sections of the secondary light particles were obtained and inserted into the file. Next, the experimental data, *e.g.* production cross section of the residual nuclei (49 isotopes from Ag to Mo for ^{107}Pd and 44 from Nb to Br for ^{93}Zr), were inserted. After the preparation of the Frag Data file, we can perform PHITS simulations of a more realistic situation based on the experimental data.

A simulation using the Frag Data function for proton-induced reactions on a thin ^{107}Pd target was performed for confirmation. The simulation result of production cross sections of Ag isotopes (open squares) is shown in Fig. 1, which is compared with the experimental data (filled squares) and the result without the Frag Data function (filled circles). We can confirm that the result with the Frag Data function reproduces the same result as the experiments.
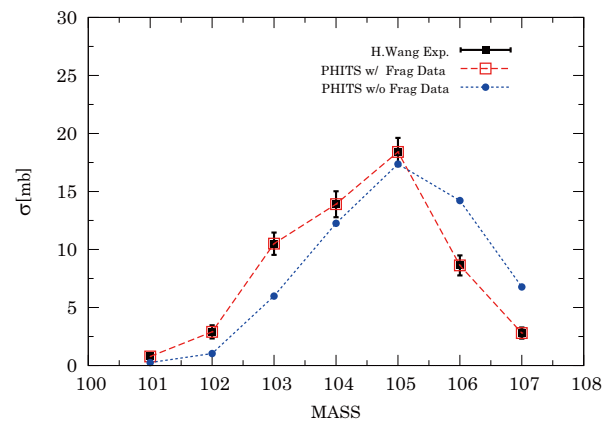
Fig. 1. Production cross sections of Ag isotopes in the ^{107}Pd+p reaction at 200 MeV.

The Frag Data function in PHITS can directly import bare experimental data of cross sections to simulations. We performed simulations of transmutation with the function and then confirmed the reproduction of experimental cross sections. Based on the Frag Data files, we can perform macroscopic simulations with realistic conditions for the feasibility study of transmutation.

References
1) H. Wang *et al.*, Prog. Theor. Exp. Phys. **2017**, 021D01 (2017).
2) S. Kawase *et al.*, Prog. Theor. Exp. Phys. **2017**, 093D03 (2017).
3) T. Sato *et al.*, J. Nucl. Sci. Technol. **50**, 913 (2013).

*1 Faculty of Science, Hokkaido University
*2 RIKEN Nishina Center

4. Hadron Physics

Final result of nuclear dependence on A_N for forward neutron production in polarized p+A collisions at $\sqrt{s_{NN}} = 200$ GeV[†]

M. Kim[*1],[*2] for the PHENIX collaboration

In high-energy hadron collisions, most of the energy goes to the forward region. Yet the particle production mechanism in this region is not well understood, because a small momentum transfer preclude the application of perturbative QCD, and diffractive processes are not well modeled or interpreted. Therefore, measurements of forward particle production may contribute crucially to the theoretical model development. Furthermore the measurement of the transverse-single-spin asymmetry A_N[1] can elucidate processes that are not visible in the cross-section data. In the case of forward neutron production in high-energy $p + p$ collisions, the one-pion exchange (OPE) model had been developed, and it explained cross-section data.[2] However, A_N calculated from this model is approximately an order smaller than that measured in the PHENIX experiment.[1,2] In order to explain these data, an interference between spin-flip π exchange and non-spin-flip a_1-Reggeon exchange amplitudes was introduced.[2]

In 2015, RHIC achieved the world's first high-energy polarized proton-nucleus collisions. In this report, the A_N results of forward neutron production at $\sqrt{s_{NN}} = 200$ GeV $p+p$, $p+$Al, and $p+$Au collisions measured in the PHENIX experiment are presented. Neutrons at $0.3 < \theta < 2.2$ mrad and $x_F > 0.5$ are measured using the zero-degree calorimeter (ZDC), which is a Čerenkov sampling hadron calorimeter with an X-Y hodoscope consisting of plastic strip scintillators. In addition, correlation with charged particle production is measured by two beam-beam counters (BBCs), which are located in the lower pseudorapidity $\pm(3.0$–$3.9)$. The background fraction in $p+p$ collision is not negligible; therefore, background asymmetry was subtracted using the data taken in 2008, when a charge veto counter was installed in front of the ZDC. The smearing of A_N due to the detector resolution is estimated by PYTHIA6 and GEANT3 simulation and then corrected.

The A dependence of A_N is shown in Fig. 1. ZDC inclusive neutrons show a strong A dependence, with a large A_N accompanying a sign change at Au. This result is unexpected from the current π and a_1-Reggeon exchange model in which the possible A dependence is from nuclear absorption.[3] The A dependence is even more drastic when both BBCs are vetoed (ZDC⊗BBC-veto), showing an even larger A_N at Au and a sign change at Al. In contrast, when both BBCs are fired
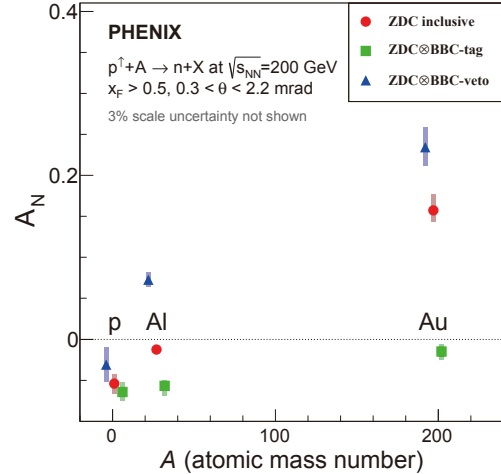
Fig. 1. A_N of forward neutrons in $p + p$, $p + $Al, and $p + $Au collisions for ZDC inclusive, ZDC⊗BBC-tag, and ZDC⊗BBC-veto. Color bars represent systematic uncertainties. Statistical uncertainties are smaller than the marker size.

(ZDC⊗BBC-tag), the A dependence is moderate, and the sign remains negative. This work was announced through a press release by BNL and RIKEN.[4]

In a recently published paper,[5] this A dependence of A_N is explained by the contribution of electromagnetic (EM) processes as follows. In large Z nuclei, neutrons are produced from ultraperipheral collisions (UPC) as well as a decay product of Δ produced from proton excitation by a virtual photon flux from the nucleus. This process is enhanced (suppressed) in ZDC⊗BBC-veto (tag). The A_N^{UPC} is calculated with the virtual photon flux simulated by STARLIGHT and the A_N of $\gamma^* + p^\uparrow \to \pi^+ + n$ obtained from the MAID2007 unitary isobar model. The sum of A_N^{UPC} and A_N^{OPE} reproduced ZDC inclusive A_N.

In order to understand this interesting result even deeper, the measurement of p_T and energy dependence on A_N is ongoing.

References
1) A. Adare *et al.*, Phys. Rev. D **88**, 032006 (2013).
2) B. Z. Kopeliovich, I. K. Potashnikova, I. Schmidt, J. Soffer, Phys. Rev. D **84**, 114012 (2011).
3) B. Z. Kopeliovich, I. K. Potashnikova, I. Schmidt, AIP Conf. Proc., Vol.**1819** (2017), p.050002.
4) The announcement has been reported by multiple media outlets, such as Newsweek online and ScienceAlert.com.
5) G. Mitsuka, Phys. Rev. C **95**, 044908 (2017).

Coulomb-nuclear interference effects on forward π^0 production in polarized-proton–nucleus collisions

G. Mitsuka[*1]

It was reported from the PHENIX experiment at BNL-RHIC that the transverse single spin asymmetry, denoted as A_N, for forward neutrons measured in transversely polarized-proton–nucleus (pA) collisions at $\sqrt{s_{NN}} = 200\,\mathrm{GeV}$ is far different from that in proton–proton (pp) collisions at $\sqrt{s} = 200\,\mathrm{GeV}$.[1]

I presented in Refs. 2–3) that ultra-peripheral pA collisions (UPCs, also known as Primakoff effects) contribute to the measured A_N modestly in pAl collisions and significantly in pAu collisions, and that UPCs together with hadronic interactions successfully explain the PHENIX results. In UPCs, virtual photons (γ^*) emitted from the relativistic nucleus interact with the polarized protons and then produce the neutrons and other particles.

In the Monte Carlo simulations discussed in Refs. 2–3), electromagnetic effects (UPCs) and hadronic effects are taken into account independently. However, the interference between these two effects, called the Coulomb-nuclear interference (CNI) effects, would have nonzero amplitudes in the very small momentum-transfer region. In this report, I present the implementation of the CNI effects for forward π^0s in polarized-proton–nucleus collisions. Forward π^0 production is described by a simpler mechanism than that for forward neutrons. Natural units $\hbar = c = 1$ are used throughout.

The scattering amplitude M for single pion production in the CNI effects is given by

$$M = e^{i\phi} M_C + M_H, \qquad (1)$$

where ϕ is the Coulomb phase, M_C is the Coulomb scattering amplitude, and M_H is the hadronic scattering amplitude. The Coulomb scattering amplitude via a one-photon exchange is expressed as

$$M_C = Ze(p_b + p_2)_\mu \frac{F(q^2)}{q^2} \langle p_1, k | J^\mu | p_a \rangle, \qquad (2)$$

where $\langle p_1, k | J^\mu | p_a \rangle$ is the $\gamma^* + p \to p + \pi^0$ transition current[4] and $F(q^2)$ is the form factor. The kinematic variables are defined in Fig. 1. The hadronic scattering amplitude via a one-Pomeron exchange[5] is obtained by replacing a virtual photon with a Pomeron in Fig. 1:

$$M_H = F_A\, g_{\pi NN}\, F_{\pi N^* N}(p_{1f}^2)\, F_{I\!\!P NN^*}(p_{1f}^2)\, A_{I\!\!P}^{NN}(s, q^2)/2s$$
$$\times\ \bar{u}(p_1) i\gamma_5 S_N(s_1)\gamma^\mu u(p_a)\bar{u}(p_2)\gamma_\mu u(p_b), \qquad (3)$$

where nuclear effects are taken into account in F_A, $g_{\pi NN}$ is the pion-nucleon coupling constant, S_N is the

off-shell nucleon propagator, $F_{\pi N^* N}$ and $F_{I\!\!P NN^*}$ are the form factors at each vertex, $A_{I\!\!P}^{NN}$ is the $I\!\!P NN$ elastic scattering amplitude, $s = (p_a + p_b)^2$, and $s_1 = (p_1 + k)^2$.
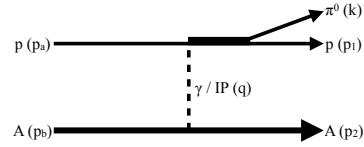
Fig. 1. Diagram of the amplitudes driven by the photon (γ^*) or Pomeron ($I\!\!P$) exchange in proton-nucleus collisions.

The differential cross section for single π^0 production is expressed with the Källén function $\lambda(x, y, z) \equiv x^2 + y^2 + z^2 - 2xy - 2yz - 2zx$ as

$$\frac{d\sigma}{dq^2} = \frac{\pi^2 |M|^2}{8\lambda(s, m_p^2, m_p^2)(2\pi)^5} \int \frac{\lambda(s_1, m_p^2, m_\pi^2)^{1/2}}{s_1} ds_1. \qquad (4)$$

Figure 2 shows the cross section in pAu collisions at $\sqrt{s_{NN}} = 200\,\mathrm{GeV}$. The dominant amplitude transits from Coulomb to hadronic at $q^2 \sim 0.02\,\mathrm{GeV}^2$. This indicates that single spin asymmetries for forward π^0s, most likely produced below $0.1\,\mathrm{GeV}^2$, are significantly modified by the interference between the Coulomb and hadronic interactions.

The estimation of single-spin asymmetries and extension of the presented framework to forward neutrons will be a topic of future investigation.
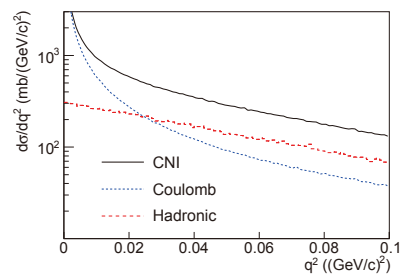
Fig. 2. Differential cross sections for Coulomb (blue dotted), hadronic (red dashed), and CNI effects (black solid).

References
1) C. Aidala *et al.*, (PHENIX Collaboration), Phys. Rev. Lett. **120**, 022001 (2018).
2) G. Mitsuka, Phys. Rev. C **95**, 044908 (2017).
3) G. Mitsuka, RIKEN Accel. Prog. Rep. **50**, 15 (2017).
4) D. Drechsel, S. S. Kamalov, L. Tiator, Eur. Phys. J. A **34**, 64 (2007).
5) P. Lebiedowicz, A. Szczurek, Phys. Rev. D **87**, 074037 (2013).

*1 RIKEN Nishina Center

Preparatory work toward measurement of the azimuthal anisotropy of heavy quark electrons in Au+Au collisions at $\sqrt{s_{NN}} = 200$ GeV

Y. Ueda[*1,*2] for the PHENIX Collaboration

The azimuthal anisotropy (v_2) of heavy (charm and bottom) quarks is a good probe for the study of the quark gluon plasma (QGP). Perturbative QCD (pQCD) calculations can be applied in the production of heavy quark pairs and fragmentation into heavy quark hadrons. It allows a precise comparison of the measured v_2 of heavy quark hadrons, that of their decay electrons, and theoretical models.

In 2007, v_2 of single electrons from c and b hadron decay was measured, without their separation, in Au+Au collisions,[1] leading to an unexpected discovery of substantial v_2. The detailed study of v_2 of heavy quarks, *i.e.* measurement of v_2 with c and b hadron separation, has been recognized to be important; however, it is difficult due to their small yields.

A silicon vertex tracker (VTX) consisting of four layers of silicon detectors was installed in the PHENIX experiment in 2011, in order to separate electrons from c and b hadrons by using the distance of closest approach (DCA) method. The tracks of charged particles in the PHENIX central arm are projected backward from the drift chamber (DC) and associated to hits in the VTX. The DCA is calculated for each associated VTX track, to statistically separate electrons from the semileptonic decays of c and b hadrons, based on the correlation between the DCA and the lifetime of the parent hadron. PHENIX collected about 15 billion minimum bias Au+Au events at $\sqrt{s_{NN}} = 200$ GeV in 2014. The new dataset should be large enough to study c and b hadrons with statistical separation.

For the precise v_2 measurement utilizing the DCA method, it is necessary to understand the background (BG) in the DCA distribution, and to precisely determine the reaction plane (RP), which is defined as the plane containing the beam axis and the impact parameter vector between the two colliding nuclei.

The BG is expected to include the mismatched component (due to mismatching of tracks in DC and VTX, especially in high-multiplicity events), hadrons misidentified as electrons, decay electrons from kaons and quarkonia, and photonic electrons. The study of the mismatched component is described in this review. It is estimated with a method called small angle rotation (SAR) using VTX and DC, where each VTX track is rotated by a small angle. The rotated track is no longer connected to the true DC track, and can only be misconnected randomly to resemble the mismatched component. It has been found through simulation

studies that this BG contains two subcomponents: mis-reconstruction of fake tracks and mis-connection of real tracks. The simulated DCA distribution is shown in Fig. 1 (left), with the mis-reconstruction due to the random association of hits in red with a broad tail, and the mis-connection in blue with a large central peak. The blue subcomponent shows the possibility that a VTX track accidentally matches with another real DC track after the rotation due to the high-multiplicity environment.

The RP resolution is studied as a function of collision centrality. The RP is mainly measured with two forward detectors in PHENIX, the beam beam counters (BBC), and the forward silicon vertex trackers (FVTX), on both sides of the nominal collision point along the beam axis. The observed v_2 needs to be corrected for the RP resolution.[2] The RP resolution has been evaluated for the two detectors using the three sub-event method, from the difference of RPs measured with three different detectors,[2] *i.e.* the north and south side of BBC (or FVTX) and the central arm. The results are shown in Fig. 1 (right), where the larger the parameter is, the better the RP resolution is. The black and red points show the RP resolutions with BBC and FVTX, respectively. The RP resolutions with the two detectors have a similar trend, while that with FVTX is about twice better than that with BBC. The study will be continued with FVTX, which is better suited for the v_2 measurement.
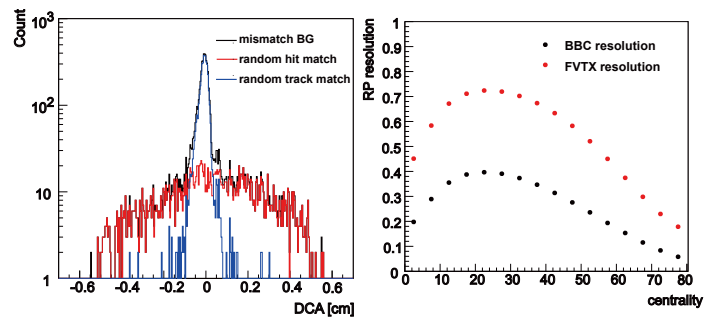
Fig. 1. (Left) Simulated DCA distribution of the mismatched BG component with SAR method. Red histogram shows mis-reconstruction with random hits; blue shows mis-connection of different tracks; black shows the total. (Right) RP resolutions with BBC (black) and FVTX (red).

References
1) A. Adare *et al.*, Phys. Rev. Lett. **98**, 172301 (2007).
2) A. M. Poskanzer, S. A. Voloshin, Phys. Rev. C **58**, 1671 (1998).

---

*1 RIKEN Nishina Center
*2 Department of Physics, Hiroshima University

Study of azimuthal anisotropy of charged particles in Au + Au collisions at $\sqrt{s_{NN}} = 200$ GeV at RHIC-PHENIX

R. Nishitani[*1,*2] for the PHENIX Collaboration

It has been established that the high temperature and high dense matter, quark gluon plasma (QGP), was produced in the gold-gold collision by the relativistic heavy ion collider (RHIC) at the Brookhaven National Laboratory (BNL) in the United States. QGP is a form of matter in which quarks and gluons strongly interact with each other. It was found that it is a "perfect fluid" having almost no viscosity. The quantitative research on the QGP properties is progressing. One of the discoveries that was made at the RHIC is a strong elliptical flow, in which the particles generated by nuclear collision come out with anisotropy, not uniformly with respect to the reaction plane. In this report, we describe the analysis of the azimuthal anisotropy parameter (v_2), which represents the difference in yield between the in and out of planes, in order to investigate the properties of the energy loss mechanism resulting from the different interacting lengths with QGP when high transverse momentum particles are emitted.[1,2]

The parameter v_2 is calculated from the azimuthal angle Φ of the reaction plane using the south and north of the Beam-Beam Counter (BBC) and the azimuthal angle Ψ of the emitted particles. This is called the "reaction plane method."[3] In this method, v_2 is quantified by the Fourier coefficient in the following equation:

$$dN/d(\Phi - \Psi) \propto 1 + 2v_2\cos[2(\Phi - \Psi)] \qquad (1)$$

The angle Φ is determined from the density of the azimuthal angle of the particles detected in the forward and backward BBC for each event. In addition, since the value of $v_2^{measured}$ observed in the experiment is influenced by the detector, we can obtain v_2^{true} from the following formula with the correction factor C_{reso}.

$$v_2^{true} = v_2^{measured}/C_{reso} \qquad (2)$$

The detectors used for the measurement of the plane in this analysis are the south and north of the BBC and Central Arm Detectors (CNT). The resolution of the reaction plane C_{reso} is obtained using the three sub method, which uses these three detectors. The result of the resolution of the reaction plane measured in step of 5% is shown in Fig. 1, which shows that the resolution is at most 20–25%. When the resolution is large, it is possible to measure the reaction plane with good performance. On the other hand, for low centrality (0∼10%), the resolution is small, because the eccentricity of the reaction region is small. For high centrality (30%∼), the resolution decreases due to the reduction in the number of particles.

Fig. 1. Resolution of the reaction plane to centrality.[4]

The following event selections are required for this analysis.

- Collision vertex is within ±10 cm from the origin in the beam axis direction,
- One or more hits in both BBC South and BBC North. In addition, the following track selections are required,
- 5 or 6 hits with Drift Chamber (DC) and Pad Chamber 1,
- Transverse momentum $p_T > 0.5$ GeV/c
- The hit position in the beam axis direction at DC is ±75 cm,
- χ square cut on the tracking
- Position matching cut ($< 3\sigma$)
- E/p cut ($0.2 <$ E/p < 0.8)

I will remove the background even more by turning the above cuts with a detailed study, especially about the E/p cut.

References
1) K. Adcox *et al.*, (PHENIX Collaboration), Nucl. Phys. **757**, 1–2, 8, 184–283 (2005).
2) Y. Akiba, *Physics of Quark Gluon Plasma Recreating Hot Matter in Early Universe in Laboratory* (Kyoritsu Pub. Co., Ltd., Tokyo, 2014, *in Japanese*).
3) S. S. Adler *et al.*, (PHENIX Collaboration), Phys. Rev. Lett. **91**, 182301 (2003).
4) A. Takeda, Master thesis, 2017, Nara Women's University.

*1　RIKEN Nishina Center
*2　Department of Physics, Nara Women's University

Single transverse spin asymmetry (A_{N}) in polarized $p + Au$ collisions at $\sqrt{s_{NN}} = 200$ GeV

J. H. Yoo[*1,*2] for the PHENIX collaboration

A proton is basically composed of many sea quarks and gluons in addition to the three valence quarks. According to the early European Muon Collaboration (EMC) data in the 80 s, the contribution of quarks and antiquarks to the entire proton's spin value (1/2) is less than 30%. As a result, the rest should come from the gluon spin and the orbital motions of quarks, antiquarks and gluons. The detailed spin structure of the proton can be revealed by investigating the longitudinal and transverse components. In particular, the transverse spin structure of the proton can provide some insight into the orbital angular momentum component of the partons (quarks and gluons) in the proton.

Transverse single spin asymmetries (A_{N}) are relevant to the transverse spin structure of the proton. Initially, the A_{N} of hadrons produced in the transversely polarized $p+p$ collision was expected to be small; however, experiments instead measured large asymmetries of up to $A_{\mathrm{N}} \approx 40\%$ in the forward direction. To better describe the large A_{N} measurements, the theoretical framework has been extended to include transverse momentum dependent (TMD) distributions and multiparton dynamics (higher twist effects).[1] At least two TMD effects have been proposed to explain the observed nonzero asymmetries. The first effect, known as the Sivers effect, correlates the proton spin with the partonic transverse momentum k_{T}.[1,2] The second effect, known as the Collins effect, describes the coupling of a transverse quark polarization (transversity) and a transverse spin dependent fragmentation from a struck quark into a hadron.[1,3] A proton + nucleus ($p + A$) collision gives a parton distribution and transverse momentum distribution in the nucleus by comparing it with the nucleon parton distribution function (PDF). Generally accepted cold nuclear matter (CNM) effects are "nuclear shadowing," "gluon saturation," "radiative energy loss," and the "Cronin effect." Nuclear shadowing implies the modification of the parton distribution functions within a nucleus. The gluon saturation signifies the saturation of the gluon distribution function. The radiative energy loss implies the modification of the momentum fraction of partons due to multiple soft scattering. Finally, the Cronin effect implies broadening of the transverse momentum distribution due to multiple scattering of incident partons. Until recently, the transverse spin structure and CNM had been studied separately. The RHIC Run15 exper-
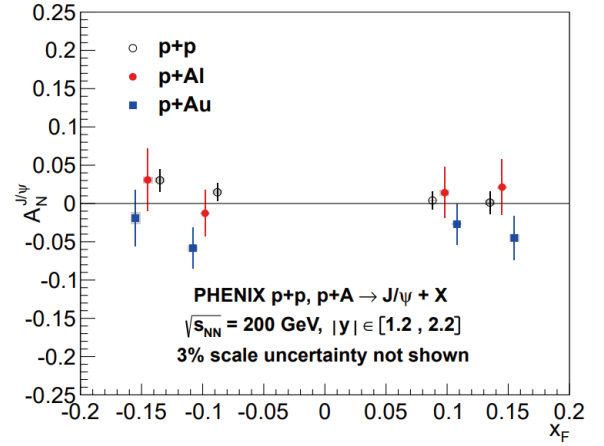
Fig. 1. A_{N} measured at both forward and backward rapidity in $p + p$, $p + Al$ and $p + Au$ collision for J/Ψ mesons.[1]

iment was the first high-energy transversely polarized proton ($p \uparrow$) and nuclear collision in the world. This unique collision experiment allows us to explore the spin degree of freedom in the CNM effects.

The results for A_{N} in forward and backward J/Ψ production in $p \uparrow + p$, $p \uparrow + Al$, $p \uparrow + Au$ collisions is shown in in Fig. 1. These results indicate that the nuclear dependence of A_{N} for J/Ψ production is not small. Compared to the A_{N} of $p \uparrow + p$ collisions, the observed asymmetry in $p \uparrow + Au$ collisions is larger in absolute value and has opposite sign. Moreover, the A_{N} of neutral pions and inclusive charged hadrons in $p \uparrow + p$ have previously been measured with the PHENIX midrapidity spectrometer. These asymmetries have been found to be consistent with zero. In addition to a $p \uparrow + p$ collision, the A_{N} of neutral pions in a $p \uparrow + A$ collision has already been analyzed. The analysis of A_{N} of charged pions in the midrapidity region in a polarized $p + A$ collision is in progress. A_{N} measurements with two species of nuclei (Al and Au) will allow us to study the A dependence of A_{N} and the CNM effects in the system of transversely polarized protons colliding with nuclei.

References
1) PHENIX Collaboration, arXiv:1805.01491v1.
2) D. W. Sivers, Phys. Rev. D **41**, 83 (1990).
3) J. C. Collins, Nucl. Phys. **396**, 161 (1993).

*1 RIKEN Nishina Center
*2 Department of Physics, Korea University

Operation summary of the RHICf experimet

J.S. Park,[*1*2] for the RHICf collaboration

The RHICf forward (RHICf) experiment is an experiment that can provide information about soft QCD physics. One of the measurements in the RHICf experiment is the measurement of energy spectra of forward neutral particles. Another measurement in the RHICf experiment is the measuerment of transeverse single-spin asymmetry (A_N) of forward neutral particles. These measurements are expected to contibute to the determination of Feyman scaling and the production mechanism of forward neutral particles.[1] The main detector in the RHICf experiment is the the LHCf detector that is an electromagnetic calorimeter used in LHCf experiment which is optimized for detecting π^0s.[2] In addition to the RHICf detector, the data from the STAR ZDC, VPD, BBC, and Roman pot were read-out so that a combined analysis could be performed.

The RHICf experiment was performed from 21st June to 26th June in 2017 at STAR IR in RHIC. The RHICf detector was installed immediately in front of the west ZDC.[3] The RHICf detector consists of a large tower and a small tower so that π^0 can be detected more effectively. The RHICf experiment was performed using a horizontally polarized beam (radial polarized beam) and the detector location was adjusted at 3 different heights to extend the transverse momentum (P_T) measurement range:[1] i) the height of the large tower center is the same as the height of the collision point (6 hours), ii) the height of the small tower center is the same as the height of the collision point (12 hous) and iii) the height of the small tower center is 24 mm greater than the height of the collision point (8 hours). The operation was completed with 3 kinds of triggers which enhance single showers, π^0s. and high-energy electromagnetic (EM) showers[4] during 5 RHIC fills and the total run time was approximately 23 hours. Proton-proton collisions proceeded at $\beta^* = 8$ m and $\sqrt{s} = 510$ GeV with the radial polarization $P \sim 0.5$.

During the operation time, the monitoring system achieved stable polarization measurement with satisfactory precision, with a reasonably reconstructed π^0 invariant mass and correlation between STAR ZDC and the RHICf detector.[5] Figure 1 shows the reconstructed invariant mass of photon pair events showing a peak at the rest mass of π^0 from quick offline data analysis in the operation time. The peak location is slightly different from the true π^0 mass because the energy calibration was not perfect in the quick analysis. Figure 2 shows the accumulated number of events during the operation time.

The RHICf experiment was completed successfully under a stable beam condition with STAR detectors and the data showed a reasonable π^0 mass spectrum with sufficiet statistics and correlation with STAR ZDC as expected.
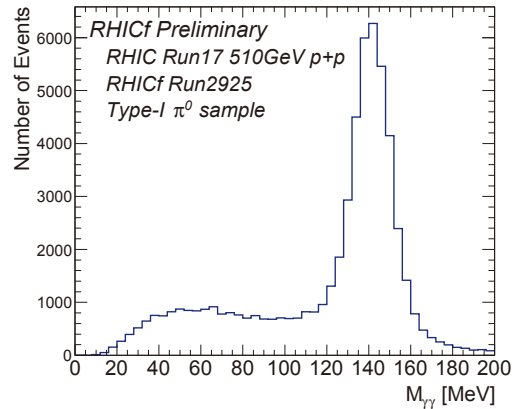
Fig. 1. Reconstructed π^0 mass with data.
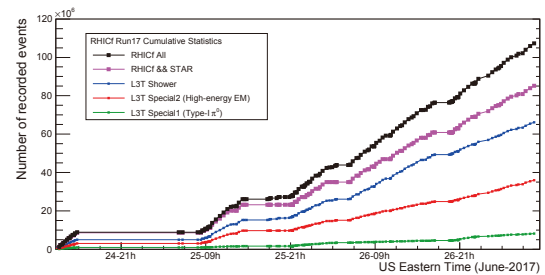
Fig. 2. Black: accumulated events recorded by 3 kinds of triggers, Magenta: accumulated events recorded by coincidence among STAR detector triggers and LHCf triggers, Blue: accumulated events recorded by shower trigger only, Red: accumulated events recorded by π^0 trigger only, Green: accumulated events recorded by high EM trigger only.

References
1) J. S. Park for the RHICf Collaboration, RIKEN Accel. Prog. Rep. **50**, 108 (2017).
2) M.H. Kim for the RHICf Collaboration, RIKEN Accel. Prog. Rep. **50**, 107 (2017).
3) Y. Goto for the RHICf Collaboraccel, Prog. Rep. **48**, 108 (2017).
4) H. Menjo, K. Sato for the RHICf Collaboration, In this report.
5) M. Ueno for the RHICf Collaboration, In this report.

*1 Department of Physics and Astronomy, Seoul National University
*2 RIKEN Nishina Center

RHICf-STAR common operation in $\sqrt{s} = 510$ GeV proton-proton collisions

M. Ueno[*1,*2] for the RHICf collaboration

The RHIC forward (RHICf) experiment[1,2] and the STAR experiment[4] had a joint operation in June 2017.[3] During the RHICf operation, RHICf took about 1.1×10^8 events in total, and 80% of the events were common with STAR. At the RHICf-STAR joint data taking, we recorded the data of the STAR detector, Zero Degree Calorimeter (ZDC),[5] Beam Beam Counter (BBC),[6] and Vertex Position Detector (VPD)[7] together. These common data are useful for the improvement of physics performance. In this report, the improvement of energy resolution for neutrons is discussed.

The RHICf detector has two independent calorimeter towers, which are composed of tungsten plates, 16 layers of GSO scintillators, and 4 X-Y hodoscopes of GSO bar bundles.[1] The thickness of the RHICf detector is 44 radiation length and 1.6 interaction length. The STAR-ZDC detectors were installed on both sides of the STAR IP. The detector was installed 18 m away from the STAR interaction point in front of the west-side STAR ZDC, as shown in Fig. 1. The particle identification between photons and neutrons is performed by using the difference in detector response. The hadronic showers induced by neutrons develop in deeper layers than the electromagnetic showers induced by photons. Because the RHICf detector thickness is not enough to contain hadronic showers, these shower particles leak out from the detector and hit the STAR-ZDC. An MC simulation study by Geant4 shows that the energy resolution for neutrons is expected to be improved from 40% to 20% by combining the RHICf data and ZDC data.

The correlation between the RHICf detected energy and the STAR-ZDC detected energy was confirmed by the data. Figure 2 shows the correlation between the RHICf raw energy and the STAR-ZDC ADC sum when the beam center was set at the RHICf small calorimeter

Fig. 2. Correlation between RHICf detected energy and the STAR-ZDC detected energy. The horizontal axis shows the RHICf raw energy and the vertical axis shows STAR-ZDC ADC sum. The RHICf detector, which consists of two calorimeter towers, was installed at the west side of the STAR interaction point. Only the west side STAR-ZDC ADC sum shows correlation with RHICf raw energy.

tower (TS tower). The upper figures show the results of the west-side STAR ZDC and the lower figures show the results of the east-side STAR ZDC. Figure 2 shows that there is a correlation between the west side STAR-ZDC and RHICf raw data. On the other hand, there is no correlation between the east side STAR-ZDC and RHICf raw data. These results indicate that the event matching between the RHICf and STAR data worked correctly. Analysis of common operation data is on going.

References
1) RHICf Collaboration, Letter of Intent, arXiv:1401.1004.
2) RHICf Collaboration, RHICf proposal, arXiv:1409.4860.
3) J. S. Park for the RHICf Collaboration, in this report.
4) K. H. Ackermann *et al.*, Nucl. Instrum. Methods Phys. Res. A **499**, 624–632 (2003).
5) C. Adler *et al.*, Nucl. Instrum. Methods Phys. Res. A **470**, 488–499 (2001).
6) C. A. Whitten for the STAR Collaboration, AIP Conference Proceedings, 980, 390–396, (2008).
7) W. J. Llope *et al.*, Nucl. Instrum. Methods Phys. Res. A **759**, 23–28 (2014).

Fig. 1. Schematic location view of the RHICf detector (left) and the STAR-ZDC (right).

*1 RIKEN Nishina Center
*2 Institute for Space-Earth Environmental Research, Nagoya University

Beam polarization monitor in $\sqrt{s} = 510$ GeV polarized proton-proton collisions at the RHICf experiment

M. H. Kim[*1,*2] for the RHICf collaboration

A new experiment, RHIC forward[1] (RHICf), has measured the transverse single spin asymmetry, A_N, of very forward particle productions in $\sqrt{s} = 510$ GeV polarized proton-proton collisions at the Relativistic Heavy Ion Collider (RHIC) in June, 2017.[2] A_N is defined as a left-right asymmetry of the production cross section to beam polarization. It plays an important role in the study of the production mechanism of very forward particles, particularly from the view points of diffractive and non-diffractive interactions. The A_N of mainly very forward neutrons, π^0, and γ with a transverse momentum (p_T) up to 1 GeV/c can be studied in detail in the RHICf experiment.

In order to measure the A_N of very forward particles precisely, a new electromagnetic calorimeter (RHICf detector), which had been originally developed for the LHCf experiment at CERN,[3] was installed in front of a hadron calorimeter[4] (ZDC) at STAR to improve the position resolution of the detected particles. The RHICf detector consists of small (TS) and large (TL) towers. Each tower is composed of 17 layers of tungsten plates, 16 layers of GSO plates, and 4 position-sensitive layers of thin GSO bars. ZDC has been used as a polarization monitor by calculating the raw asymmetry (ϵ_N) of neutron-like events using a STAR scaler board. One scaler board is composed of 32 bits, and each bit has a flag of 0 or 1 for every entry depending on whether an event satisfies a specific condition. Finally, it gives the number of counts for each of 2^{32} types of events. However, because the ZDC was screened by the RHICf detector at operation, there was no guarantee that the ZDC monitor works as well as it used to. Owing to the non-negligible interaction length of the RHICf detector, a hadronic shower was expected to be generated in 30% of the neutrons. Therefore, we connected two scaler bits to each tower of the RHICf detector and measured the ϵ_N of each by

$$\epsilon_N = \frac{N^\uparrow - RN^\downarrow}{N^\uparrow + RN^\downarrow} \tag{1}$$

as the second beam-polarization monitor, where $N^\uparrow$ ($N^\downarrow$) is the number of scaler counts with the proton polarized up (down) when a shower is generated at the RHICf detector. Events for which three successive layers at one of the towers were greater than 45 MeV were chosen based on a Monte-Carlo study. This condition is called shower trigger hereafter. R is a correction factor that compensates for the difference in the number of collisions between up and down polarization.
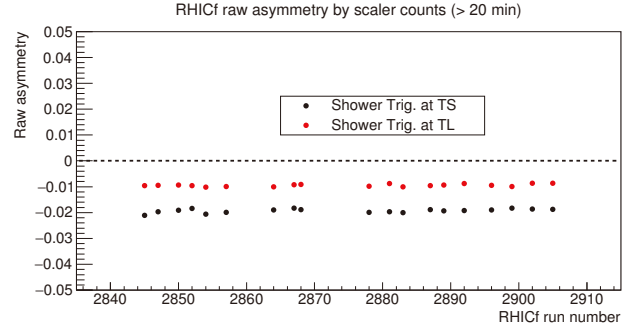
Fig. 1. Measured ϵ_N depending on run number.

Because N is proportional to the production cross section, A_N can be studied using ϵ_N.

Calculated ϵ_N with different run numbers that lasted longer than 20 minutes are described in Fig. 1. We had three types of physics runs depending on the detector positions, and each run lasted 30 minutes if there was no critical issue. This is the result when the beam height is 24 mm below the center of TS. The stability of beam polarization can be confirmed by ϵ_N, which was conserved within 10% error. If the polarization direction was changed or the ratio of polarized beam decreased, the amplitude of ϵ_N would approach to zero. Neutrons are dominant in the shower-triggered events. The signs of ϵ_N show good agreement with the negative sign of A_N for very forward neutron production.[5] ϵ_N at TL is more diluted than at TS because the gamma contamination is more enhanced at TL than at TS.

The production cross-section asymmetry of very forward particles was studied using the RHICf detector with scaler bits. However, because there is a limit in the reconstruction of particle information with it, further issues remain in the detector data analysis.

References
1) RHICf Collaboration: LOI, arXiv:1401.1004; RHICf proposal: arXiv:1409.4860.
2) J. S. Park for the RHICf Collaboration, in this report.
3) LHCf Collaboration, JINST **3**, S08006 (2008).
4) C. Adler *et al.*, Nucl. Instrum. Meth. A **470**, 488 (2001).
5) A. Adare *et al.*, Phys. Rev. D **88**, 032006 (2013).

*1　RIKEN Nishina Center
*2　Department of Physics, Korea University

DAQ performances of the RHICf operation in 2017

H. Menjo[*1,*2] and K. Sato[*2,*3] for the RHICf collaboration

The RHIC forward (RHICf) experiment,[1] measuring very forward neutral particles, photons, neutrons, and π^0 s, produced in 510 GeV proton-proton collisions at RHIC, has successfully completed a 4-day operation in June 2017. The data acquisition (DAQ) system of the RHICf experiment was developed based on the system of the LHCf experiment[2] as well as the detector. The RHICf detector consists of two sampling and imaging calorimeters. Each calorimeter is composed of tungsten plates, 16 layers of GSO scintillators and 4 X-Y hodoscopes of GSO bar bundles. Trigger signals are generated by a logic based on the energy deposit on the scintillator layers, which is implemented on a system with discriminator modules and a field programmable gate array (FPGA) board.[3] In the logic, three trigger modes were implemented as follows;

- **Shower trigger** is implemented for detecting any electromagnetic (EM) showers and hadronic showers induced by photons and neutrons. This trigger is issued when each of any three successive layers has an energy deposit greater than 45 MeV.
- **π^0 trigger** is specialized to detect photon pairs from π^0 decays. This trigger is issued when EM showers are detected in both the calorimeters simultaneously.
- **High-EM trigger** is newly introduced for the RHICf experiment to increase the statistics of high-energy photon events (> 100 GeV). The trigger is issued when the 4th layer in either calorimeter has an energy deposit greater than 500 MeV.

These trigger signals were mixed after being pre-scaled down by factors of 8–30 for shower triggers and 1–4 for high-EM triggers. The rate of π^0 triggers is
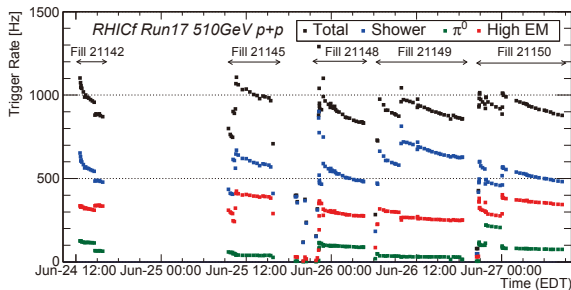
Fig. 2. Spectrum of total visible energy measured by the RHICf calorimeter. Colored lines correspond to spectra obtained from the events triggered by the three modes.

the lowest among the three trigger modes and its pre-scaling factor was always set to 1 (no pre-scaling). The event rates of these triggers strongly depend on the operation conditions such as the detector position with respect to the beam axis. The raw rate of shower triggers was 6–30 kHz, and it was scaled down to approximately 1 kHz after the pre-scaling. These pre-scaling factors were optimized occasionally during the operation to keep the final trigger rate to approximately 1 kHz, which corresponds to the DAQ condition with approximately 50% of the DAQ live fraction. Figure 1 shows the total trigger rate and rates of the three triggers. The rates decreased during an operation period because of the decrease of beam intensity, while the rate suddenly increased in some moments owing to re-optimizations of the pre-scaling factors.

Figure 2 shows the raw spectra of measured total visible energy ΣdE obtained in the EM-shower events. The number of EM showers in the π^0 trigger events is mostly comparable with that in the shower trigger events. The high-EM trigger successfully worked to enrich high-energy EM shower events in the recoded data. The number of photon events in the high-EM-triggered events is larger than that in the shower triggered events by a factor of approximately 10 in the region of $\Sigma dE > 3$ GeV, corresponding to photon energies greater than approximately 100 GeV.

Fig. 1. Trigger rates of the RHICf operation in 2017. The upper arrows indicate the physics operation periods.

*1 Graduate School of Science, Nagoya University
*2 RIKEN Nishina Center
*3 Institute for Space-Earth Environmental Research, Nagoya University

References
1) RHICf Collaboration: Letter of Intent, arXiv:1401.1004; RHICf proposal: arXiv:1409.4860.
2) LHCf Collaboration: TDR, CERN-LHCC-2006-004.
3) H. Menjo *et al.*, RIKEN Accel. Prog. Rep. **50**, 109 (2017).

Fragmentation function measurements in Belle†

R. Seidl,[*1] F. Giordano,[*2] A. Vossen,[*3] H. Li,[*3] W. W. Jacobs,[*3] M. Grosse-Perdekamp,[*2] C. Van Hulse,[*4] and G. Schnell[*4,*5]

Fragmentation functions (FFs) tell us about the transition of asympotically free, nearly massless partons into confined, massive final-state hadrons. They therefore provide important information on some of the main open questions in nuclear physics, confinement and chiral symmetry breaking. Furthermore, FFs can be used as a tool to extract parton distribution functions in semi-inclusive DIS and hadron-hadron collisions. Belle has previously measured polarization dependent interference fragmentation functions,[1] needed to access the quark transversity distribution in a collinear factorization framework. The related unpolarized baseline FF was not available. Recently, inclusive di-hadron cross sections were extracted as a function of invariant mass and fractional energy $z = 2E_{hh}/\sqrt{s}$ for any hadron and charge combination.[2] The di-hadrons had to emerge in the same hemisphere as calculated via the event-shape variable thrust in order to be sensitive to the fragmentation of predominantly one parton into two hadrons, unlike the previous di-hadron publication[3] which focused more on single hadron fragmentation. The cross sections for unlike-sign pion pairs can be seen in Fig. 1 where they are compared to various PYTHIA fragmentation tunes. The overall fractional energy behavior is generally well reproduced in the PYTHIA default tune, while the mass structure above 1 GeV is better described by tunes with larger fragmentation into higher spin states.

Various resonances are visible in the extracted cross sections for opposite-sign pion pairs. Using MC their origin can be resolved as shown in Fig. 2. One can identify various resonances such as the K_S^0 and ρ mesons as well as the Cabbibo-suppressed decay of the D^0 meson. In the data also the $f_0(980)$ is clearly visible while it is not well modeled in the MC. Additionally, di-pions from a common origin, such as from η or ω decays or pions from different levels of the same decay chain can also show up as enhancements. Direct fragmentation with no common ancestors provide the generally smooth and dominant contribution to the mass spectra. Similar figures for other hadron combinations and details on the correction chain leading from raw yields to cross sections can be found in the actual publication. For unlike-sign pion-kaon combinations the K^* and the D^0 decays stand out while for the unlike-sing kaon pairs the ϕ^0 contributes prominently. For all like-sign combinations no resonances exist while some enhancements from common decays are visible.

Fig. 1. Unlike-sign di-pion cross sections as a function of $m_{\pi\pi}$ in bins of z (black circles), compared to various fragmentation tunes in PYTHIA.
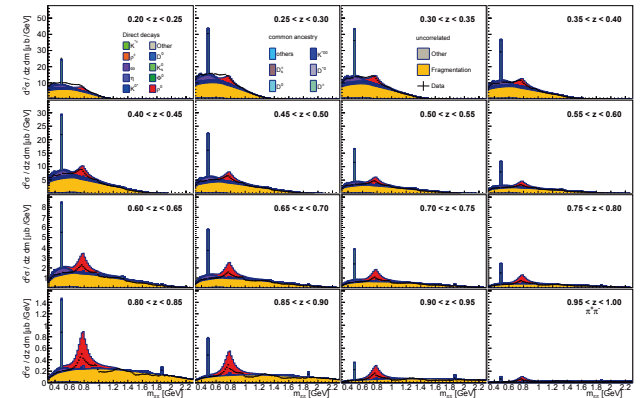
Fig. 2. Comparison of unlike-sign di-pion cross sections (data points) as a function of $m_{\pi\pi}$ in bins of z with the relative contribution from various parents in MC.

Other fragmentation function measurements are currently ongoing such as explicit transverse momentum dependent fragmentation functions, Λ polarizing fragmentation[4] and various spin dependent fragmentation functions.

References
1) A. Vossen *et al.*, [Belle Collaboration], Phys. Rev. Lett. **107**, 072004 (2011).
2) R. Seidl *et al.*, [Belle Collaboration], Phys. Rev. D **96**, 032005 (2017).
3) R. Seidl *et al.*, [Belle Collaboration], Phys. Rev. D **92**, 092007 (2015).
4) A. Abdesselam *et al.*, [Belle Collaboration], e-Print: arXiv:1611.06648

Status of measurements of Drell–Yan process at FNAL SeaQuest

K. Nakano,[*1,*2] Y. Goto,[*2] Y. Miyachi,[*3] K. Nagai,[*1,*4] W. Saito,[*1] S. Sawada,[*2,*5] T.-A. Shibata,[*1,*2] and H. Yamada[*1] for the E906/SeaQuest Collaboration

The partonic structure of the proton is one of the most vital topics in the present study of hadron physics. The SeaQuest experiment is being carried out at Fermi National Accelerator Lab (FNAL) in USA to investigate the partonic structure with the Drell–Yan process. In the Drell–Yan process, a quark in one hadron and an anti-quark in another hadron annihilate into a virtual photon and then decay into a lepton pair as $q + \bar{q} \to \gamma^* \to l^+ + l^-$, as shown in Fig. 1. The cross section at the leading order of α_S is expressed as

$$\frac{d^2\sigma}{dx^{\mathrm{B}}dx^{\mathrm{T}}} = \frac{4\pi\alpha^2}{9x^{\mathrm{B}}x^{\mathrm{T}}}\frac{1}{s}\sum_i e_i{}^2 \cdot$$
$$\left\{ q_i^{\mathrm{B}}(x^{\mathrm{B}})\bar{q}_i^{\mathrm{T}}(x^{\mathrm{T}}) + \bar{q}_i^{\mathrm{B}}(x^{\mathrm{B}})q_i^{\mathrm{T}}(x^{\mathrm{T}}) \right\}, \quad (1)$$

where x is the Bjorken scaling variable, s is the square of the center-of-mass energy of two interacting hadrons, $q_i(x)$ is the parton distribution function of a flavor i, and the superscripts "B" and "T" denote partons in the beam hadron and target hadron, respectively. When the process is measured at forward rapidity as SeaQuest does, the second term $(\bar{q}_i^{\mathrm{B}}(x^{\mathrm{B}})q_i^{\mathrm{T}}(x^{\mathrm{T}}))$ of Eq. (1) becomes negligible since $x_{\mathrm{B}} \gg x_{\mathrm{T}}$ and $\bar{q}(x^{\mathrm{B}}) \sim 0$ at large x^{B}. This implies that a quark mostly originates from the beam with x^{B} and an anti-quark from the target with x^{T}. Therefore, the Drell–Yan process at forward rapidity is directly proportional to the anti-quark distributions, $\bar{q}(x)$.

SeaQuest utilizes the proton beam extracted from the FNAL Main Injector with $E = 120$ GeV as well as several types of targets to cover wide physics topics. Liquid hydrogen (LH$_2$) and deuterium (LD$_2$) targets are used for the measurement of the Drell–Yan processes in $p + p$ and $p + d$ reactions. Carbon, iron, and tungsten targets are also used for the $p + A$ reaction. The SeaQuest spectrometer detects the final-state muon pair of the Drell–Yan process, the details of which were reported in the past.[2] SeaQuest acquired physics data from November 2013 to July 2017 with a summer accelerator shutdown each year. It has recorded 1.4×10^{18} beam protons on targets, and is actively analyzing approximately 40% of the recorded data.

The primary purpose of SeaQuest is to measure the flavor asymmetry of light anti-quarks ($\bar{u}$ and $\bar{d}$) in the proton. Since a large asymmetry has been observed by the NMC, NA51, and E866/NuSea experi-

ments, various theoretical models are being examined to understand the origin of this flavor asymmetry.[1] SeaQuest analyzed high-mass Drell–Yan events in $p+p$ and $p+d$ reactions and obtained a preliminary result of $\bar{d}(x)/\bar{u}(x)$ at $0.10 < x < 0.58$, as reported last year.[3] Further analyses are being performed to improve the statistics and measurement accuracy.

Another purpose of SeaQuest with $p + p$ and $p + d$ reactions is to measure the angular distribution of final-state leptons in the Drell–Yan process. The angular distribution is theoretically predicted to satisfy the Lam-Tung relation but was found by several experiments to violate it. This violation can originate from, for example, QCD higher-order radiation and the Boer-Mulders effect.[4] It can be investigated further with high-precision data from SeaQuest. The angular dependence of the detection efficiency is being studied in detail by tuning detector responses and background distributions in simulation.[5]

SeaQuest also measures the nuclear effect via the Drell–Yan process in $p + A$ reactions. Approximately 1/5 of the beam protons were applied to the carbon, iron and tungsten targets. The nuclear effect is defined as the difference in per-nucleon cross sections between $p+A$ and $p+p$, namely $\frac{\sigma_{p+A}/A}{\sigma_{p+p}} \neq 1$. It involves various physics mechanisms and is widely examined by measurements and theories. SeaQuest is first focusing on the Drell–Yan process in the large-x^T region ($\gtrsim 0.2$) to extract the partonic energy loss in cold nuclear matter.[6] Background events in $p + A$ reactions are being identified in detail, where the rates of all background types are different from those in $p + p$.[7]
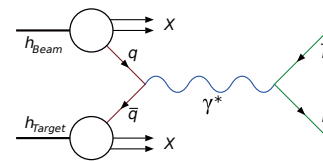
Fig. 1. Feynman diagram of the Drell–Yan process.

References
1) W. C. Chang *et al.*, Prog. Part. Nucl. Phys. **79**, 95 (2014).
2) K. Nagai *et al.*, RIKEN Accel. Prog. Rep. **49**, 114 (2016).
3) K. Nakano *et al.*, RIKEN Accel. Prog. Rep. **50**, 118 (2017).
4) M. Lambertsen *et al.*, Phys. Rev. D **93**, 114013 (2016).
5) B. Ramson, PoS DIS **2016**, 021 (2016).
6) H. Xing *et al.*, Nucl. Phys. A **879**, 77 (2012).
7) P. J. Lin, PoS DIS **2017**, 174 (2017).

*1 School of Science, Tokyo Institute of Technology
*2 RIKEN Nishina Center
*3 Faculty of Science, Yamagata University
*4 Academia Sinica, Taiwan
*5 Institute of Particle and Nuclear Studies, KEK

Design of the innermost layer module of the silicon tracking detector for the sPHENIX experiment

Y. Yamaguchi,[*1] Y. Akiba,[*1] D. Cacace,[*2] E. Desmond,[*2] T. Hachiya,[*1,*3] Y. Kawashima,[*1,*4] E. Mannel,[*2] H. Masuda,[*1,*4] G. Mitsuka,[*1] I. Nakagawa,[*1] R. Nouicer,[*2] R. Pisani,[*2] K. Shiina,[*1,*4] and M. Tsuruta[*1,*4]

High energy heavy ion collisions are the most suitable tool to study the properties of Quark Gluon Plasma (QGP), which is an extreme hot and dense QCD matter where quarks and gluons are free from confinement inside hadrons. The Relativistic Heavy Ion Collider (RHIC) can provide heavy ion collisions with an enough energy to create QGP experimentally. sPHENIX is a new RHIC experiment for QGP study and is scheduled to start data taking from 2021. We are in charge of construction of the intermediate silicon tracking detector (INTT)[1] which plays an important role on charged particle tracking together with the monolithic active pixel sensors (MAPS) and the time projection chamber (TPC). INTT makes a good tracking together with MAPS and TPC and also helps to resolve pile-up events by its excellent timing resolution.

We have designed the innermost INTT layer (L0) sensitive to z-position while the other three layers are ϕ-sensitive. Figure 1 shows the drawings of an L0 single cell and a module consisting of ten cells on one high density interconnect circuit (HDI). One L0 sensor
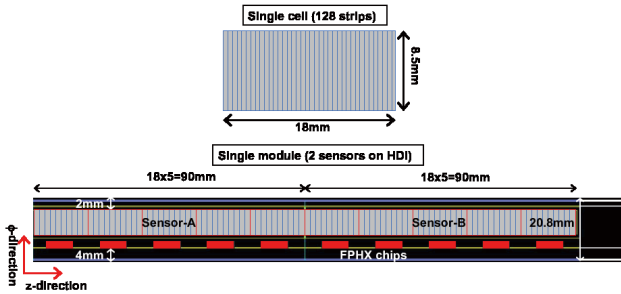
Fig. 1. The drawings of an L0 single cell and a module consisting of ten cells on HDI.

has 5 cells and a FPHX readout chip is wire-bonded to each cell. The z-length of a single cell is 18 mm and it is divided into 128 strips. The width of the cell is optimized through the Geant4 based simulation. Figure 2 shows the simulated L0 acceptance with different ϕ-widths. 1M electron events are simulated within the L0 coverage assuming all electrons are emitted at $z = 0$. Unavoidable 3.2% loss of the acceptance comes from the 2 mm-gap in the z-direction between two modules. 8.5 mm of ϕ-width keeps the maximum acceptance with the minimum occupancy. 48 L0 mod-
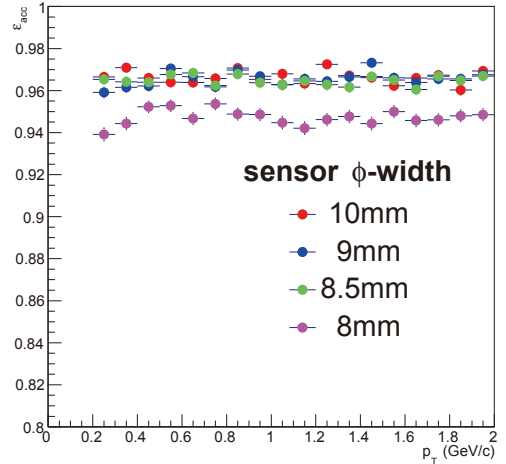
Fig. 2. The simulated L0 acceptance with different ϕ-widths.

ules are integrated into one barrel like rotor blades as shown in Fig. 3. The tilt angle of each module is set to 15° with a 1 mm-gap between neighboring modules for realistic engineering.
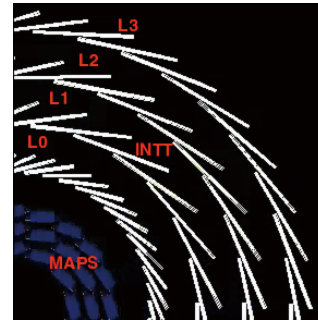
Fig. 3. L0 module alignment from the beam view.

The first prototype sensors and HDIs are being manufactured by HAMAMATSU Photonics K.K. and Yamashita Material Co.+REPIC, respectively. They will be assembled into the first L0 module.

Reference
1) I. Nakagawa *et al.*, in this report.

*1   RIKEN Nishina Center
*2   Brookhaven National Laboratory
*3   Division of Natural Sciences, Nara Women's University
*4   Department of Physics, Rikkyo University

5. Hadron Physics (Theory)

Covariant calculation of quark distribution functions in ρ^+-meson[†]

Y. Ninomiya,[*1] W. Bentz,[*1,*2] and I. C. Cloët[*3]

Spin-1 hadrons are characterized by three elastic form factors (FFs) and four leading-twist parton distribution functions (PDFs). As compared to the familiar spin-1/2 case, the new functions for the spin-1 case are the quadrupole FF and the tensor polarized PDF, both carrying important information on the orbital motion of the constituents. Recent calculations[1] have shown that the quadrupole form factor of the ρ^+ meson is of opposite sign compared to the deuteron. It is then of interest to compare their tensor polarized PDFs as well.

In this work we use the Nambu-Jona-Lasinio (NJL) model as an effective quark theory of QCD to calculate the nine T-even transverse momentum-dependent quark distribution functions (TMDs) of the ρ^+ meson in a completely covariant way. Important effects of quark confinement are included via the use of the proper-time regularization scheme, which avoids unphysical thresholds for the decay of hadrons into free quarks. Integration of the TMDs over the transverse quark momentum components leaves the four PDFs, namely the unpolarized $f(x)$, helicity $g(x)$, transversity $h(x)$, and tensor polarized $f_{LL}(x)$ distribution functions.[2] Our results for these four PDFs are shown in Fig. 1 at the model scale of $Q_0^2 = 0.16$ GeV^2, and in Fig. 2 at the scale $Q^2 = 5$ GeV^2.

Our function $f_{LL}(x)$ is related to the function $b_1(x)$ of Ref. 4) by $b_1(x) = \frac{1}{2} f_{LL}(x)$, and its partonic interpretation at the model scale can be expressed as

$$f_{LL}(x) = q^{(0)}(x) - \frac{1}{2}\left(q^{(1)}(x) + q^{(-1)}(x)\right),$$

where $q^{(\lambda)}(x) = q_\uparrow^{(\lambda)} + q_\downarrow^{(\lambda)}(x)$ is the unpolarized valence quark distribution in a longitudinally polarized ρ^+ meson with spin projection $\lambda = 0$ and $\lambda = \pm 1$. Accordingly, the function $f_{LL}(x)$ satisfies the sum rules

$$\int_0^1 dx\, f_{LL}(x) = \int_0^1 x\, dx\, f_{LL}(x) = 0,$$

which simply mean that the valence quark number and momentum are independent of the hadron's spin state. Our result for the spin sum at the model scale is

$$\int_0^1 dx\, g(x) = 0.56.$$

This means that the total valence quark and antiquark contribution to the spin of the ρ meson is 56%,
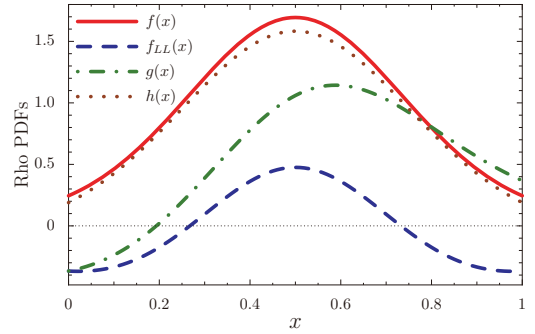
Fig. 1. The unpolarized ($f(x)$), helicity ($g(x)$), transversity ($h(x)$) and tensor polarized ($f_{LL}(x)$) PDFs of the ρ^+ meson at the model scale $Q_0^2 = 0.16$ GeV^2.
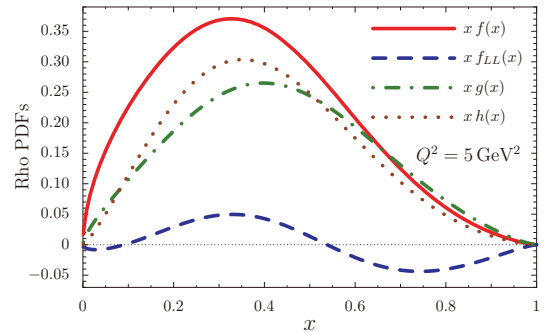
Fig. 2. The four PDFs of the ρ^+ meson, multiplied by x, at the scale $Q^2 = 5$ GeV^2. The NLO non-singlet DGLAP evolution was performed[3] to evolve the PDFs of Fig. 1 from 0.16 GeV^2 to 5 GeV^2.

which implies a substantial contribution of 44% from the quark orbital angular momentum. Our result for the tensor charge is $\int_0^1 dx\, h(x) = 0.94$, which is close to the naive quark model expectation of unity.

In a qualitative comparison between our tensor polarized PDF of the ρ^+ meson and the HERMES Collaboration data for the deuteron[5] we find a similar behavior as functions of x, but the overall sign is opposite and the magnitude is larger for the case of the ρ^+ meson by roughly one order.

References
1) M. E. Carrillo-Serrano, W. Bentz, I. C. Cloët, A. W. Thomas, Phys. Lett. **B 759**, 178 (2016).
2) A. Bacchetta, P. J. Mulders, Phys. Lett. B **518**, 85 (2001).
3) M. Hirai, S. Kumano, M. Miyama, Comput. Phys. Commun. **111**, 150 (1998).
4) P. Hoodbhoy, R. L. Jaffe, A. Manohar, Nucl. Phys. **312**, 571 (1989).
5) A. Airapetian et al., (HERMES), Phys. Rev. Lett. **95**, 242001 (2005).

ΣN and ΛN interactions from $2 + 1$ flavor lattice QCD with almost physical masses

H. Nemura,[*1,*2] S. Aoki,[*2,*3,*4] T. Doi,[*2,*5] S. Gongyo,[*2] T. Hatsuda,[*2,*5] Y. Ikeda,[*1,*2] T. Inoue,[*2,*6] T. Iritani,[*2] N. Ishii,[*1,*2] T. Miyamoto,[*2,*3] and K. Sasaki[*2,*3]

Nuclear force and strangeness nuclear forces provide an important starting point to understand how hypernuclei are bound, in which hyperons (or strange quarks) are embedded in normal nuclei as "impurities." Determining how such a baryon-baryon (BB) interaction is described from a fundamental perspective is a challenging problem in physics. Although a normal nucleus is successfully described by utilizing the high precision nucleon-nucleon (NN) potentials together with a three-nucleon force a quantitatively same-level description of a hypernucleus is still difficult because of the large uncertainties of hyperon-nucleon (YN) and hyperon-hyperon (YY) interactions; those YN and YY potentials are not well constrained from experimental data owing to the short life time of hyperons. A recent experimental study shows a tendency to repulsive Σ-nucleus interaction[1] and only a four-body Σ-hypernucleus ($^4_\Sigma$He) is observed; these results suggest a repulsive nature of the ΣN interaction. Such quantitative understanding is useful to study the properties of hyperonic matter inside neutron stars, where the recent observations of a massive neutron star heavier than $2M_\odot$ might raise a problem of the hyperonic equation of state (EOS) employed in such a study. Furthermore, better understanding of YN and YY is becoming increasingly important owing to the observation of the binary neutron star merger.

During the last decade a new lattice QCD approach to study a hadron-hadron interaction was proposed. In this approach, the interhadron potential is obtained by means of the lattice QCD measurement of the Nambu-Bethe-Salpeter (NBS) wave function. The observables such as the phase shifts and the binding energies are calculated by using the resultant potential. A large scale lattice QCD calculation is now in progress[2] to study the baryon interactions from NN to $\Xi\Xi$ by measuring the NBS wave functions for 52 channels[3] from the $2 + 1$ flavor lattice QCD by employing the almost physical quark masses corresponding to $(m_\pi, m_K) \approx (146, 525)$ MeV and large volume $(La)^4 = (96a)^4 \approx (8.1$ fm$)^4$ with the lattice spacing $a \approx 0.085$ fm.

Figure 1 shows the scattering phase shifts of ΣN system with isospin $I = 3/2$ obtained from the nearly physical point lattice QCD calculation through parametrized analytical functions.[2] The top left panel in the figure shows the scattering phase shift in the $^1S_0$ channel; the
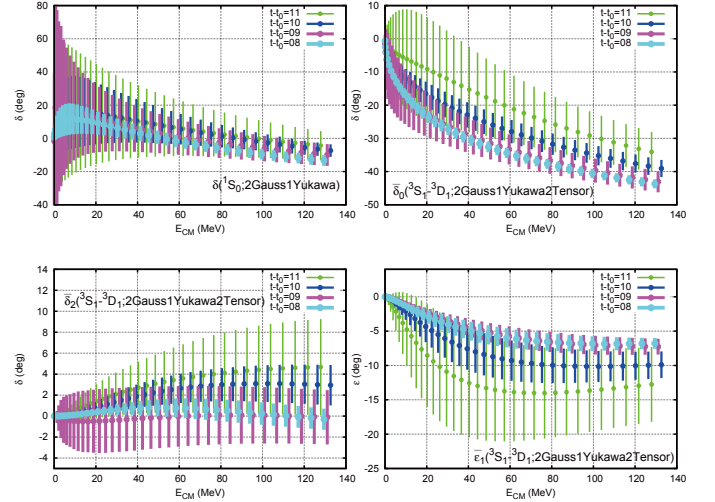
Fig. 1. Scattering (bar-)phase shifts and mixing angle of the $I = 3/2$ ΣN system, $\delta(^1S_0)$ in the $^1S_0$ state (upper left), and $\bar\delta_0$ (upper right), $\bar\delta_2$ (lower left), and $\bar\varepsilon_1$ (lower right) in the $^3S_1 - {}^3D_1$ states, obtained from the nearly physical point lattice QCD calculation on a volume $(96a)^4 \approx (8.1$ fm$)^4$ with the lattice spacing $a \approx 0.085$ fm and $(m_\pi, m_K) \approx (146, 525)$ MeV through parametrized analytical functions.[2]

present result shows that the interaction in the $^1S_0$ channel is attractive on average. The other three panels in Fig. 1 show the bar-phase shifts and mixing angle in the $^3S_1 - {}^3D_1$ states, $\bar\delta_0$ (upper right), $\bar\delta_2$ (lower left), and $\bar\varepsilon_1$ (lower right); the phase shift $\bar\delta_0$ shows the interaction is repulsive while the phase shift $\bar\delta_2$ behaves around almost zero degree. The present results are qualitatively consistent with group theoretical classification based on a quark model which is useful for clarifying the general behavior of various BB interactions in the S-wave; the ΣN $I = 3/2$ $^3S_1 - {}^3D_1$ belongs to **10** which is almost Pauli forbidden while the ΣN $I = 3/2$ $^1S_0$ belongs to **27**, which is the same as NN $^1S_0$. The present S-wave (dominated) phase shifts, the repulsive (attractive) behavior of $\bar\delta_0$ ($\delta(^1S_0)$), augur well for future quantitative conclusions with larger statistics. Further calculations to obtain physical quantities with increased statistics are in progress and will be reported elsewhere.

[*1] Research Center for Nuclear Physics, Osaka University
[*2] RIKEN Nishina Center
[*3] Yukawa Institute for Theoretical Physics, Kyoto University
[*4] Center for Computational Sciences, University of Tsukuba
[*5] iTHEMS Program and iTHES Research Group, RIKEN
[*6] Nihon University, College of Bioresource Sciences

References
1) H. Noumi *et al.*, Phys. Rev. Lett. **89**, 072301 (2002) Erratum: [Phys. Rev. Lett. **90**, 049902 (2003)].
2) H. Nemura *et al.*, arXiv:1711.07003 [hep-lat].
3) H. Nemura, Comput. Phys. Commun. **207**, 91 (2016) [arXiv:1510.00903 [hep-lat]].

P-wave $\pi\pi$ scattering and the ρ resonance from lattice QCD[†]

C. Alexandrou,[*1,*2] L. Leskovec,[*3] S. Meinel,[*3,*4] J. Negele,[*5] S. Paul,[*2] M. Petschlies,[*6] A. Pochinsky,[*5] G. Rendon,[*3] and S. Syritsyn[*7,*4]

The study of hadron-hadron scattering and resonance properties using lattice QCD is a rapidly growing field.[1] There are now many calculations of $I = 1$, P-wave $\pi\pi$ scattering, in which the ρ resonance appears, but a number of questions remain open. For example: Which models best describe the energy-dependence of the phase shift? How large is the nonresonant contribution? How exactly do m_ρ and $g_{\rho\pi\pi}$ depend on the quark masses?

In this work, we have begun to address some of these questions using a high-statistics calculation with $2+1$ flavors of clover fermions at a pion mass of approximately 320 MeV. The lattice size was $32^3 \times 96$ with a lattice spacing of $a \approx 0.114$ fm; we constructed the relevant hadronic correlation functions using a method based on forward, sequential, and stochastic quark propagators, which has a favorable volume scaling compared with the distillation method introduced in Ref. 2). We extracted the lowest two or three energy levels in eight different irreducible representations with total momenta up to $(1,1,1)\frac{2\pi}{L}$, carefully studying systematic uncertainties associated with the choice of fit method and fit range in Euclidean time. The $\pi\pi$ scattering phase shift values obtained from the lattice energy levels using Lüscher's method are shown in Fig. 1.

We performed fits of several different models for the $\sqrt{s}$-dependence of the phase shift: two purely resonant Breit-Wigner models (without or with a Blatt-Weisskopf barrier factor), as well as the combination of these models with three different parameterizations of a nonresonant contribution. The fit results for the nonresonant contribution were consistent with zero. We found that the minimal Breit-Wigner model

$$\delta_\ell(s) = \arctan \frac{\sqrt{s}\,\Gamma(s)}{m_\rho^2 - s}, \qquad \Gamma(s) = \frac{g_{\rho\pi\pi}^2}{6\pi}\frac{k^3}{s}, \qquad (1)$$

which depends only on the two parameters m_ρ and $g_{\rho\pi\pi}$, was sufficient to describe our data. The curve corresponding to this model is also shown in Fig. 1.
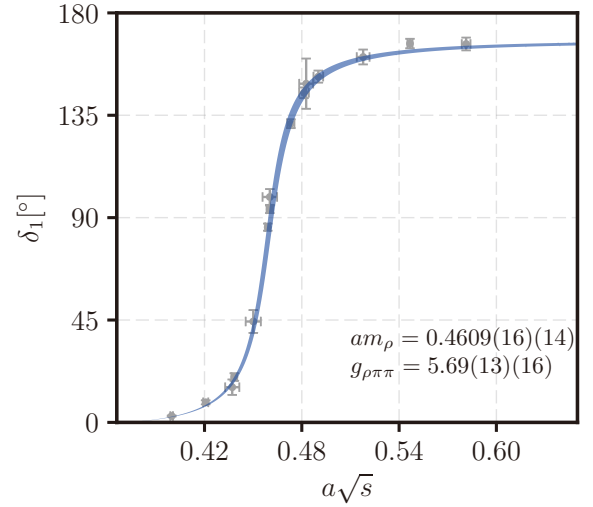
Fig. 1. Lattice QCD results for the $I = 1$, P-wave $\pi\pi$ scattering phase shift as a function of the $\pi\pi$ invariant mass. The data points were obtained by applying Lüscher's method individually to each energy level, while the curve was obtained by fitting the parameters of the minimal Breit-Wigner model directly to the whole energy spectrum.

A comparison of lattice results for m_ρ at several different heavier-than-physical pion masses revealed substantial scale setting ambiguities. It is therefore better to compare dimensionless ratios such as m_ρ/m_N and m_π/m_N, where m_N is the lattice result for the nucleon mass from the same ensemble of gauge configurations. Our calculation gives

$$\frac{m_\rho}{m_N} = 0.7476(38)(23) \quad \text{at} \quad \frac{m_\pi}{m_N} = 0.2968(13), \quad (2)$$

and $g_{\rho\pi\pi} = 5.69(13)(16)$. The most recent lattice results obtained with $2 + 1$ flavors of clover fermions (Refs. 3–5) along with this work) are consistent with a linear dependence of m_ρ/m_N on m_π/m_N, with m_ρ/m_N reaching the experimental value at the physical pion mass.

References
1) R. A. Briceno, J. J. Dudek, R. D. Young, arXiv:1706.06223.
2) M. Peardon et al., (Hadron Spectrum Collaboration), Phys. Rev. D 80, 054506 (2009).
3) J. J. Dudek et al., (Hadron Spectrum Collaboration), Phys. Rev. D 87, 034505 (2013).
4) D. J. Wilson, R. A. Briceno, J. J. Dudek, R. G. Edwards, C. E. Thomas, Phys. Rev. D 92, 094502 (2015).
5) J. Bulava, B. Fahy, B. Hörz, K. J. Juge, C. Morningstar, C. H. Wong, Nucl. Phys. 910, 842 (2016).

Computing the nucleon charge and axial radii directly at $Q^2 = 0$ in lattice QCD[†]

N. Hasan,[*1,*2] J. Green,[*3] S. Meinel,[*4,*5] M. Engelhardt,[*6] S. Krieg,[*1,*2] J. Negele,[*7] A. Pochinsky,[*7] and S. Syritsyn[*4,*8]

The square of the proton electric charge radius is defined as

$$r_E^2 = -6 \left. \frac{dG_E}{dQ^2} \right|_{Q^2=0}, \qquad (1)$$

where G_E is the proton electric form factor and $-Q^2 = (p'-p)^2$ is the square of the four-momentum transfer. In view of the proton radius puzzle,[1] reliable lattice QCD calculations of r_E are needed. The conventional approach involves computing G_E at several discrete values of the momenta allowed by the boundary conditions of the lattice, followed by a fit of the form factor shape that then allows the evaluation of the derivative with respect to Q^2. The fit of the form factor shape may introduce a systematic uncertainty that is difficult to quantify.

In this work, we investigated an alternative approach that allows the lattice computation of r_E^2 and other momentum derivatives of nucleon matrix elements directly at $Q^2 = 0$. In this method, momentum derivatives of quark propagators are taken symbolically at zero momentum[2] before performing the path integral over the gauge fields. We implemented this method to extract the nucleon isovector magnetic moment and charge radius as well as the isovector induced pseudoscalar form factor at $Q^2 = 0$ and the axial radius. For comparison, we also determined these quantities with the conventional approach, using the z-expansion method[3] to fit the form factor shape. The calculation was done at the physical pion mass, on a 64^4 lattice with $2 + 1$ flavors of clover fermions.

Some of our results are shown in Fig. 1 and Table 1. The results from the z expansion and from the derivative method are consistent with each other, which provides a valuable cross-check. Compared to the z expansion, the derivative method suffers from larger statistical uncertainties, especially for the radii, which we obtained from second-order derivatives with respect to **p**.
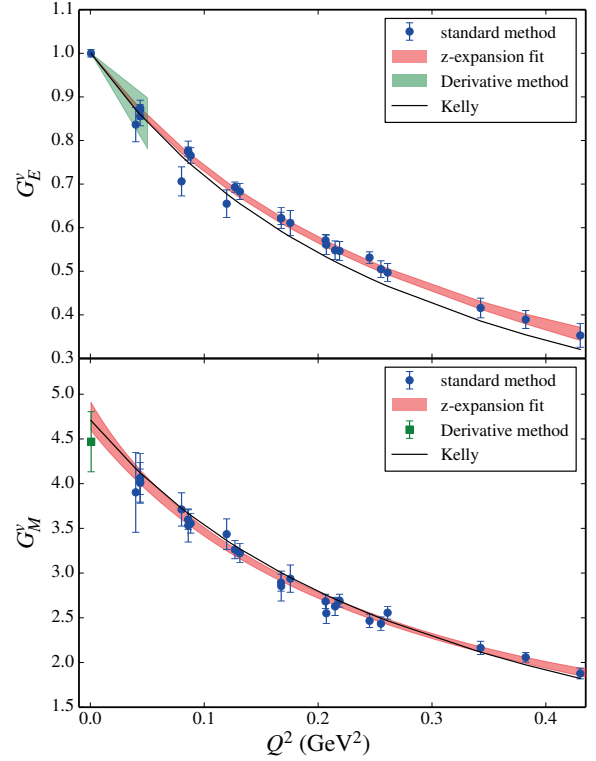
Fig. 1. Results for the nucleon isovector electric and magnetic form factors. The black curve shows a fit to electron-nucleon scattering data.[4]

Table 1. Summary of our results at $Q^2 = 0$.

Quantity		z-expansion	derivative
μ^v	$T/a = 10$	3.899(38)	3.898(54)
	summation	4.75(15)	4.46(33)
$(r_E^2)^v$ [fm^2]	$T/a = 10$	0.608(15)	0.603(29)
	summation	0.787(87)	0.753(273)
$G_P^v(0)$	$T/a = 10$	75(1)	69(1)
	summation	137(7)	137(15)
$(r_A^2)^v$ [fm^2]	$T/a = 10$	0.249(12)	0.288(61)
	summation	0.295(68)	$-0.120(492)$

[†] Condensed from the article in arXiv:1711.11385
[*1] Bergische Universität Wuppertal
[*2] IAS, Jülich Supercomputing Centre, Forschungszentrum Jülich
[*3] NIC, Deutsches Elektronen-Synchroton, Zeuthen
[*4] RIKEN Nishina Center
[*5] Department of Physics, University of Arizona
[*6] Department of Physics, New Mexico State University
[*7] Center for Theoretical Physics, Massachusetts Institute of Technology
[*8] Department of Physics and Astronomy, Stony Brook University

References
1) R. Pohl, R. Gilman, G. A. Miller, K. Pachucki, Ann. Rev. Nucl. Part. Sci. **63**, 175 (2013).
2) G. M. de Divitiis, R. Petronzio, N. Tantalo, Phys. Lett. B **718**, 589 (2012).
3) R. J. Hill, G. Paz, Phys. Rev. D **82**, 113005 (2010).
4) J. J. Kelly, Phys. Rev. C **70**, 068202 (2004).

6. Particle Physics

Phenomenology of $\Lambda_b \to \Lambda_c \tau \bar\nu$ using lattice QCD calculations[†]

A. Datta,[*1,*2] S. Kamali,[*3] S. Meinel,[*3,*4] and A. Rashed[*1,*5]

In the Standard Model, the electroweak interactions are lepton-flavor-universal. Consequently, the ratios of branching fractions

$$R(D) = \frac{\mathcal{B}(B \to D\tau\bar\nu)}{\mathcal{B}(B \to D\ell\bar\nu)}, \tag{1}$$

$$R(D^*) = \frac{\mathcal{B}(B \to D^*\tau\bar\nu)}{\mathcal{B}(B \to D^*\ell\bar\nu)}, \tag{2}$$

where $\ell = e, \mu$, depend only on the lepton and hadron masses and the hadronic form factors. The experimental measurements of $R(D)$ and $R(D^*)$ by the Babar, Belle, and LHCb collaborations exceed the Standard-Model predictions with a combined significance of 4.1σ,[1] hinting at the existence of new fundamental interactions that violate lepton-flavor universality.

The underlying $b \to c\tau\bar\nu$ transition can also be probed with the baryonic decay $\Lambda_b \to \Lambda_c \tau\bar\nu$, in particular by measuring the ratio

$$R(\Lambda_c) = \frac{\mathcal{B}(\Lambda_b \to \Lambda_c \tau\bar\nu)}{\mathcal{B}(\Lambda_b \to \Lambda_c \ell\bar\nu)}. \tag{3}$$

A precise Standard-Model prediction of $R(\Lambda_c)$ using the $\Lambda_b \to \Lambda_c$ vector and axial vector form factors from lattice QCD was given in Ref. 2).

In this work, we studied the effects of several new-physics scenarios that have been proposed to explain the excesses in $R(D^{(*)})$ on the decay $\Lambda_b \to \Lambda_c \tau\bar\nu$. Because some of these scenarios generate tensor couplings, we also determined the $\Lambda_b \to \Lambda_c$ tensor form factors from lattice QCD.

We demonstrated that a future measurement of $R(\Lambda_c)$ can tightly constrain all of the couplings g_L, g_R, g_S, g_P, and g_T in the $b \to c\tau\bar\nu$ effective Hamiltonian. We also analyzed six different leptoquark models, where we constrained the model parameters using the experimental measurements of $R(D)$, $R(D^*)$, the B_c lifetime τ_{B_c}, and the upper limits on $\mathcal{B}(B \to K^{(*)}\nu\bar\nu)$. As an example, Fig. 1 shows the correlations between the predicted values of $R_{\Lambda_c}^{\text{Ratio}} = R(\Lambda_c)/R(\Lambda_c)_{\text{SM}}$ and $R_{D^*}^{\text{Ratio}} = R(D^*)/R(D^*)_{\text{SM}}$ for the $SU(2)$-singlet and $SU(2)$-doublet scalar leptoquarks S_1 and R_2, and for the $SU(2)$-singlet vector leptoquark U_1 (the latter is a particularly attractive model, which can simultaneously explain hints of lepton-flavor-university violation seen in $b \to s\ell^+\ell^-$ decays[3]). Our analyses show that
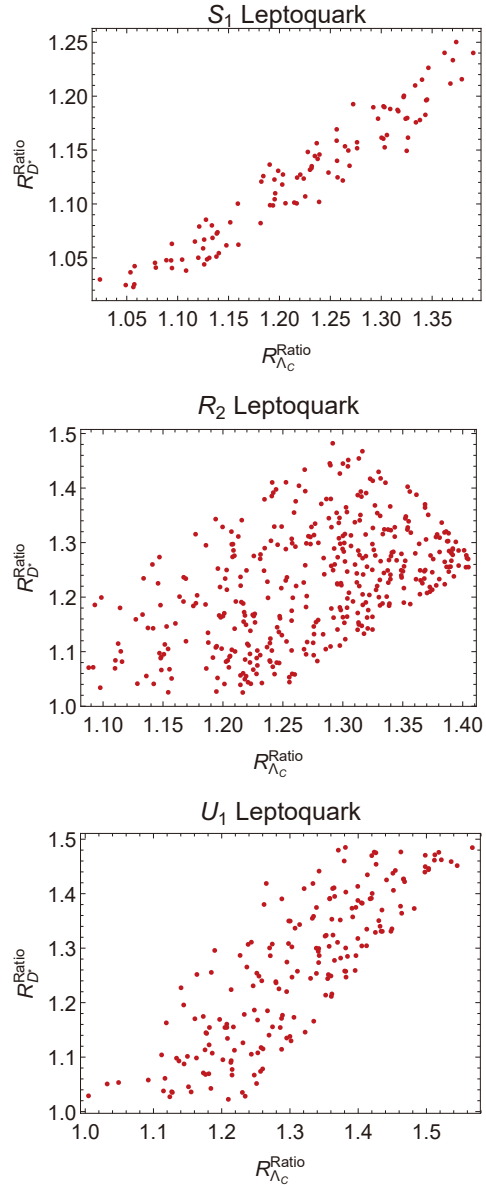
Fig. 1. Correlations between $R_{\Lambda_c}^{\text{Ratio}} = R(\Lambda_c)/R(\Lambda_c)_{\text{SM}}$ and $R_{D^*}^{\text{Ratio}} = R(D^*)/R(D^*)_{\text{SM}}$ in three different leptoquark scenarios. The points sample the region of couplings allowed by experimental measurements of $R(D)$, $R(D^*)$, τ_{B_c}, and $\mathcal{B}(B \to K^{(*)}\nu\bar\nu)$.

a future measurement of $R(\Lambda_c)$ can be helpful in discriminating between the different models.

References
1) Heavy Flavor Averaging Group, http://www.slac.stanford.edu/xorg/hflav/semi/fpcp17/RDRDs.html
2) W. Detmold, C. Lehner, S. Meinel, Phys. Rev. D **92**, 034503 (2015).
3) D. Buttazzo, A. Greljo, G. Isidori, D. Marzocca, J. High Energy Phys. **1711**, 044 (2017).

† Condensed from the article in JHEP **1708**, 131 (2017)
*1 Department of Physics and Astronomy, University of Mississippi
*2 Department of Physics and Astronomy, University of Hawaii
*3 RIKEN Nishina Center
*4 Department of Physics, University of Arizona
*5 Department of Physics, Ain Shams University

A pilot study of proton decay matrix elements at physical quark mass

Y. Aoki,[*1,*2] T. Izubuchi,[*3,*2] Y. Kuramashi,[*4,*5] and E. Shintani[*5]

Proton decay is a smoking-gun signal of the physics beyond the standard model (BSM). Grand unified theory (GUT) is the most natural origin of such an event if observed. Despite no clear signal of the supersymmetry or any BSM phenomena at LHC, the idea of unifying the known fundamental interactions is still attractive. Estimate of the QCD contribution of the proton decay matrix element is needed to test GUTs against the proton lifetime bound obtained in the experiment. Also a reliable estimate of the matrix elements is desirable for planning the future generation proton decay detectors.

The proton decay matrix elements are obtained by numerical computation using lattice QCD. So far, the 2+1 flavor computations have provided the matrix elements with extrapolation to the physical ud quark mass from the results at unphysically large masses. This procedure yields one of the largest systematic uncertainties. Settling this systematics is important[1] and possible using current lattice gauge field ensembles generated at the physical point.

We use gauge field configurations of 2+1 flavor QCD generated with non-perturbatively $O(a)$-improved Wilson fermions by the PACS collaboration.[2] As pointed in the previous works (see e.g.[3]), computations using the three-point functions are mandatory to obtain the matrix elements of a proton decaying into a pseudoscalar (and an anti lepton). Before jumping into the calculation of the three point functions the values of some optimization parameters needs to be fixed. One of them is the smearing function of the quark fields which enter in the interpolation operator of the proton. The smearing parameter is tuned so that the ground state proton reasonably dominates the two point correlation function of the proton operator. As a bi-product of such a computation, the low energy constants of the proton decay can be extracted with almost no additional computational cost.

One of the low energy constants α is defined as

$$\langle 0|(u^T C P_L d)P_R u(0)|p\rangle = \alpha P_R u_p, \tag{1}$$

where u and d in the left hand side are u and d quark operators. $P_{L(R)}$ is left (right) handed projection operator to Dirac spinor. The proton p to vacuum matrix element defines the low energy constant α appearing in the right hand side, where u_p denotes the Dirac spinor of the proton at rest.

Figure 1 shows a ratio of the two point functions
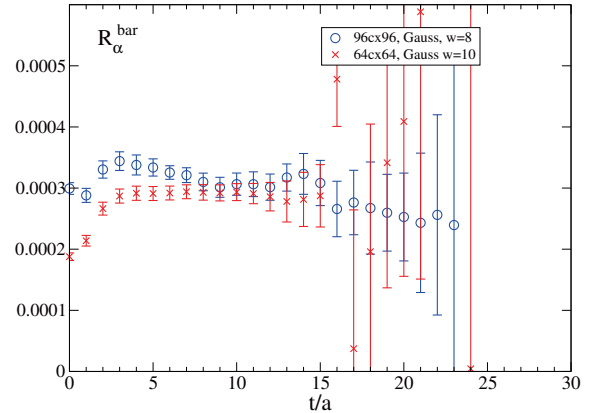
Fig. 1. Local computation $\alpha(t)$ with t being the time separation of the source and sink operators. A low energy constant α is extracted from the asymptotic plateau.

relevant to the computation of α, which is extracted from the asymptotic plateau of this figure. Hokusai supercomputer at RIKEN has been used to obtain the results. The figure compares two different lattice volumes 64^4 and 96^4. It shows a good plateau and show consistency between two different volumes.

We need several further steps to obtain α in the physical unit (GeV^3) and renormalized in a convenient renormalization scheme for phenomenological use. For the renormalization one needs to solve the operator mixing due to an explicit chiral symmetry breaking of the Wilson fermion formulation. The non-perturbative renormalization[4] can be applied to solve the mixing and at the same time to obtain the totally renormalized operator in the $\overline{\text{MS}}$ scheme. Finally the lattice cutoff cubed $1/a^3$ needs to be multiplied.

This pilot study has shown that we have reasonably a good signal for the low energy constant at the physical quark mass. It gives a confidence to obtain a good signal for the relevant matrix element as the signal/noise ratio of the low energy constant and the relevant matrix element are of similar size in the previous computations. We therefore plan to calculate the three point functions for the proton decay matrix elements on Hokusai in next fiscal year.

References
1) A. Martin, G. Stavenga, Phys. Rev. D **85**, 095010 (2012).
2) Y. Kuramashi, talk given at Lattice 2017.
3) Y. Aoki, T. Izubuchi, E. Shintani, A. Soni, Phys. Rev. D **96**, 014506 (2017).
4) Y. Aoki, C. Dawson, J. Noaki, Soni, Phys. Rev. D **75**, 014507 (2007).

[*1]　KEK Theory Center
[*2]　RIKEN Nishina Center
[*3]　Physics Department, BNL
[*4]　CCS, University of Tsukuba
[*5]　RIKEN AICS

Unified scenario for composite right-handed neutrinos and dark matter[†]

H. Davoudiasl,[*1] P. P. Giardino,[*1] E. T. Neil,[*2,*3] and E. Rinaldi[*3]

The Standard Model of particle physics is our most precise theoretical description of Nature and it has been tested to great precision in high energy particle colliders, like LHC. However, we know it represents only a partial description and the most notable missing ingredients are neutrino masses and dark matter, for which there exists a wealth of experimental evidence.

From the theoretical point of view, it is interesting to entertain the possibility that these two physical phenomena are related and emerge from a unified underlying dynamics. In this paper we introduce a new "dark sector" with a confining force, similar to the one of Quantum Chromodynamics (QCD), based on the dark gauge group $SU(3)_D$ and with three dark quarks. This dark sector has small interactions with the Standard Model particles, but more interestingly it contains a large number of composite states (dark mesons, dark baryons etc...) which can be used to successfully construct a low-energy theory with dark matter and right-handed neutrinos.

The construction starts from the dark sector Lagrangian $\mathcal{L}_{\mathrm{DQCD}}$ for the $SU(3)_D$ theory, which is well known and identical to the QCD one with three flavors, and proceeds with the addition of three types of higher-dimensional operators, deriving from different high-energy effective scales Λ_X, such that $\mathcal{L} = \mathcal{L}_{\mathrm{DQCD}} + \mathcal{L}_{\mathrm{eff}}$:

$$\mathcal{L}_{\mathrm{eff}} = \frac{\tilde{H}^* \bar{L}_f \, [\psi_i^3]}{\Lambda_f^3} + \frac{[\psi_i^6]}{\Lambda_N^5} + \frac{\bar{\psi}_i \psi_i H^\dagger H}{\Lambda_H} + \mathrm{H.C.}, \quad (1)$$

where $\tilde{H}^* = \epsilon_{ab} H^{a*}$, with H the Standard Model Higgs doublet, and L_f is a lepton doublet of the Standard Model family $f = 1, 2, 3$. In Eq. (1) $i = 1, 2, 3$ and $[\psi_i^n]$ represents any $SU(3)_D$ singlet and Lorentz invariant combinations of n ψ_i quarks that are $\mathbb{Z}_2$ even. The $\mathbb{Z}_2$ symmetry imposed upon the operators in the theory is necessary to have a stable dark matter candidate.

It is important to note that the nature of the operators in Eq. (1) is determined by confinement of the dark gauge group, giving rise to composite states: *e.g.* the operator $[\psi_i^3]$ will transmute into a dark baryonic-like operator below the confinement scale μ_D such that the first term in Eq. (1) describes the interaction between the Higgs, the leptons and a "dark neutron" state, the second term describes oscillations between "dark neutrons," and the third terms describes masses for the

---

*1 Department of Physics, Brookhaven National Laboratory
*2 Department of Physics, University of Colorato
*3 RIKEN Nishina Center
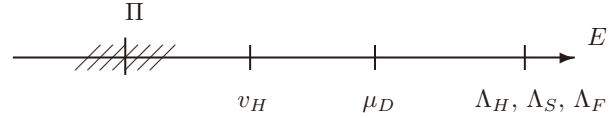
Fig. 1. The figure shows the separation of energy scales.

dark quarks. The dark neutron oscillations are necessary to create neutrino masses: in our framework, dark neutrons are identified with right-handed neutrinos. Hence, the low-energy description in Eq. (1) will give rise to neutrino masses

$$m_\nu \sim \frac{\mu_D^{10} v_H^2}{\Lambda_f^6 \Lambda_N^5}, \quad (2)$$

where $v_H \approx 246$ GeV is the electroweak energy scale. The other scales in Eq. (2) are chosen to reproduce the current known limits for neutrino masses of the order of $m_\nu \lesssim 0.1$ eV: $\mu_D \sim 1$ TeV and $\Lambda_{f,N} \sim 10$ TeV.

The confining nature of the dark sector is also responsible for the presence of a dark matter candidate in the spectrum. Similarly to QCD, the lightest composite particles are dark mesons, states that are made of a pair of dark quark and dark anti-quark. Without loss of generality, we assume that the dark quark masses generated by interactions with the Higgs boson are small and hierarchically distributed $m_1 < m_2 < m_3 \ll \mu_D$. Hence, the octet of lightest mesons comprises the three states

$$P \sim \bar{\psi}_1 \psi_2, \ \kappa \sim \bar{\psi}_1 \psi_3, \ \kappa' \sim \bar{\psi}_2 \psi_3, \quad (3)$$

their antiparticles, and two linear combinations P' and P'' of the flavor-diagonal bilinear $\bar{\psi}_i \psi_i$, analogues of the π^0 and η in QCD.

We will denote these states collectively with the symbol Π, and their masses are compared to the other scales in the theory in Fig. 1. The "dark kaons" κ and κ', containing only one ψ_3, are the only states that are odd under the $\mathbb{Z}_2$ symmetry, because we assume that $\mathbb{Z}_2(\psi_3) = -1 = -\mathbb{Z}_2(\psi_{1,2})$. The dark kaons are the lightest $\mathbb{Z}_2$-odd hadrons and κ will provide a dark matter candidate in this model, since $M_\kappa < M_{\kappa'}$. The mass of κ is related to the confinement scale through a low-energy effective chiral description of the spectrum (similar to QCD) yielding $M_\kappa \sim 10$ GeV. Such a light mass for composite dark matter is very interesting from the experimental point of view, and our scenario can be probed in future experimental setups.

Empirical formulae of the masses of elementary particles

Y. Akiba[*1]

particle	formula	calculated(c)	measured(m)	$|c/m - 1|$
e	$1/(12\pi^2)\epsilon_0^{1/3}(1 + (1/4)(1/(6\pi)^2))^{-1}M_{pl}$	0.511002 MeV	$0.510998946 \pm 0.0000000031$ MeV	5.9×10^{-6}
μ	$3/2\epsilon_0^{1/3}(1 - 1/(2\pi) + 3/(4\pi)^2)^{-1}M_{pl}$	105.6594 MeV	$105.6583745 \pm 0.0000024$ MeV	9.6×10^{-6}
τ	$9\pi\epsilon_0^{1/3}(1 - 1/(8\pi) + (5/4)(1/(6\pi)^2))^{-1}M_{pl}$	1.77684 GeV	1.77686 ± 0.12 GeV	1.9×10^{-5}
t	$8 \times (6\pi)^2\epsilon_0^{1/3}M_{pl}$	172.1 GeV	173.4 ± 0.75 GeV	7.5×10^{-3}
c	$12\epsilon_0^{1/3}M_{pl}$	1.24 GeV	1.28 ± 0.025 GeV($\overline{\text{MS}}$ at m_c)	3.4×10^{-2}
u	$8 \times (6\pi)^{-2}\epsilon_0^{1/3}M_{pl}$	2.07 MeV	2.15 ± 0.15 MeV ($\overline{\text{MS}}$ at 2 GeV)	3.8×10^{-2}
b	$3 \times 2^{-1/12}(6\pi)\epsilon_0^{1/3}M_{pl}$	4.33 GeV	4.18 ± 0.03 GeV($\overline{\text{MS}}$ at m_b)	3.6×10^{-2}
s	$\epsilon_0^{1/3}M_{pl}$	91.8 MeV	93.8 ± 2.4 MeV ($\overline{\text{MS}}$ at 2 GeV)	2.1×10^{-2}
d	$(6\pi)^{-1}\epsilon_0^{1/3}M_{pl}$	4.87 MeV	4.7 ± 0.2 MeV ($\overline{\text{MS}}$ at 2 GeV)	3.6×10^{-2}
Z	$1/(8\pi^2)\epsilon_0^{1/4}(1 + (1/11)(1/(2\pi)^2))^{-1}M_{pl}$	91.1883 GeV	91.1876 ± 0.0021 GeV	7.4×10^{-6}
W	$2^{-1/4}/(8\pi^2)\epsilon_0^{1/4}(1 - (19/11)(1/(2\pi)^2))^{-1}M_{pl}$	80.373 GeV	80.385 ± 0.015 GeV	1.9×10^{-4}
H	$2^{1/2}/(8\pi^2)\epsilon_0^{1/4}(1 + (14/11)(1/(2\pi)^2))^{-1}M_{pl}$	125.22 GeV	125.1 ± 0.2 GeV	1.0×10^{-3}

I report empirical formulae of the masses of charged leptons (e, μ, τ), quarks (t, c, u, b, s, d), gauge bosons (Z, W), and Higgs boson (H). The formulae yield the masses in terms of the Planck mass M_{pl} and a dimensionless constant $\epsilon_0 = 2 \times (6\pi)^{-48}$. There is no adjustable parameter in the formulae.

The mass values calculated using the formulae are compared with measured values. For the calculation, the value of Planck mass from CODATA[1] is used:

$$M_{pl} = 1.220910 \pm 0.000029 \times 10^{19} \text{ GeV}.$$

The measured values of particle masses are taken from PDG2016.[2] The mass of a quark is dependent on the scale and the scheme. In the PDG review, the mass of quarks other than the t quark are given in the $\overline{\text{MS}}$ scheme at $\mu = 2$ GeV for the u, d, s quarks and at $\mu = m_q$ for the b and c quarks. For the t quark, the measured mass is considered to be the pole mass. The formula for a quark is assumed to yield the $\overline{\text{MS}}$ mass at the Z boson mass m_Z. The first-order renormalized group equation (RGE) below is used to correct for the mass value at m_Z to the mass at the scale the PDG uses:

$$\frac{m(t)}{m_0} = \exp\left(-\int \frac{\alpha_s(t)}{\pi} dt\right),$$

where $t = \log\mu^2$ and $\alpha_s(t)$ is the running QCD coupling constant at the scale μ. The value of $\alpha_s(t)$ in the PDG2016 review is used for the calculation.

The formulae, the calculated values (c) using the formulae, the measured values (m), and difference $|c/m - 1|$ are summarized in the table above. The calculation reproduce the measured mass values well. The agreement is within the uncertainty of the measured mass or the Planck mass (2.4×10^{-5}).

There is a pattern in the formulae. The formulae can be summarized as

$$m_l = \frac{1}{2}N_l(6\pi)^{n_l}\epsilon_0^{1/3}(1 + \delta_l)^{-1}M_{pl},$$
$$m_q = 2^{c_q}N_q(6\pi)^{n_q}\epsilon_0^{1/3}M_{pl},$$
$$m_B = \frac{2^{c_B}}{8\pi^2}\epsilon_0^{1/4}(1 + \delta_B)^{-1}M_{pl},$$

where m_l, m_q, and m_B are the masses of charged leptons, quarks, and bosons, respectively. N_l and N_q are small positive integers, n_l and n_q are integers ranging from -2 to 2, and δ_l and δ_B are small real numbers. $c_b = -1/12$ and $c_q = 0$ for all other quarks, and $c_Z = 0$, $c_W = -1/4$, and $c_H = 1/2$. The pattern suggests the existence of a rule that determines the formulae. Note that all fermion masses are order of $(6\pi)^{n_f}\epsilon_0^{1/3}$ with $-2 \leq n_f \leq 2$ and the boson masses are of the order of $1/8\pi^2\epsilon_0^{1/4}$. Presumably, this part is the main part of the mass, and $(1 + \delta_l)$ and $(1 + \delta_B)$ are correction factors due to interactions.

Note that the value of ϵ_0 is consistent with the product of the Hubble constant H_0 and the Planck time $t_{pl} = 1/M_{pl}$:

$$H_0 \times t_{pl} = (1.211 \pm 0.014) \times 10^{-61}$$
$$\epsilon_0 \equiv 2 \times (6\pi)^{-48} = 1.220608 \times 10^{-61}$$

Here, the WMAP 9 year value of H_0 is used. This suggests that the masses of elementary particles are related to the expansion of space-time.

A theoretical model that can explain these formulae is under development.

References
1) Rev. Mod. Phys. **88**, 053009 (2016).
2) Review of Particle Physics, Chin. Phys. C **40**, 100001 (2016).

*1 RIKEN Nishina Center

Exact algebraic separability criterion for two-qubit systems[†]

K. Fujikawa[*1] and C. H. Oh[*2]

A conceptually simpler proof of the separability criterion for two-qubit systems, which is referred to as "Hefei inequality" in literature,[1] is analyzed. This inequality gives a necessary and sufficient separability criterion for any mixed two-qubit system unlike the Bell-CHSH inequality[2,3] which cannot test mixed-states such as the Werner state[4] when regarded as a separability criterion. The original derivation of this inequality[1] emphasized the uncertainty relation of complementary observables; however, we show that the uncertainty relation does not play any role in the actual derivation and that the Peres-Hodrodecki condition[5] is solely responsible for the inequality. Our derivation, which contains technically novel aspects such as an analogy to the Dirac equation, sheds light on this inequality and on the fundamental issue of the to extent to which the uncertainty relation can provide a test of entanglement. This separability criterion is illustrated for an exact treatment of the Werner state.

Our starting point is the fact that the general *pure* two-qubit states are brought to the standard form by the Schmidt decomposition

$$|\Phi\rangle = (u \otimes v)[s_1|+\rangle \otimes |-\rangle - s_2 e^{i\delta}|-\rangle \otimes |+\rangle] \qquad (1)$$

with

$$|+\rangle = \begin{pmatrix} 1 \\ 0 \end{pmatrix}, \quad |-\rangle = \begin{pmatrix} 0 \\ 1 \end{pmatrix}, \qquad (2)$$

and real numbers $s_1^2 + s_2^2 = 1$ and δ. Namely, the states are parametrized by s_1, s_2, δ and two unitary matrices u and v. It is then shown that this system is represented formally in terms of a 4-dimensional Dirac notation.

We then obtain the inequalities (*separability criterion*)

$$\langle P_-\rangle_\rho^2 \geq \langle \gamma_3\gamma_0 P_-\rangle_\rho^2 + \langle \gamma_2\gamma_0 P_-\rangle_\rho^2 + \langle \gamma_1\gamma_0 P_-\rangle_\rho^2,$$
$$\langle P_+\rangle_\rho^2 \geq \langle \gamma_3\gamma_0 P_+\rangle_\rho^2 + \langle \gamma_2\gamma_0 P_-\rangle_\rho^2 + \langle \gamma_1\gamma_0 P_-\rangle_\rho^2, \quad (3)$$

where $P_\pm = (1 \pm \gamma_5)/2$ and

$$\langle \gamma_3\gamma_0 P_\pm\rangle_\rho \equiv \text{Tr}\gamma_3\gamma_0 P_\pm\rho, \qquad (4)$$

for example, using the Peres-Horodecki criterion without referring to the uncertainty relations.

As for the test of the Werner state[4] which is defined by

$$\rho_w = \frac{1}{4}(1 - \beta)\mathbf{1} + \beta|\psi_s\rangle\langle\psi_s| \qquad (5)$$

with the singlet state $|\psi_s\rangle = (1/\sqrt{2})[|+\rangle|-\rangle - |-\rangle|+\rangle]$, we obtain

$$1 \geq \beta + 2\beta. \qquad (6)$$

We thus conclude that the separability condition of the Werner state is equivalent to

$$\beta \leq \frac{1}{3}, \qquad (7)$$

which agrees with the result of a more explicit analysis of ρ_w.[4] This in particular implies that $\beta > \frac{1}{3}$ stands for an *inseparable state.*

We have re-analyzed one of the representative inequalities proposed in Ref. 1) and have shown that the uncertainty relations cannot be alternative to the Peres-Horodecki condition in the analysis of entanglement for general two-qubit systems. The "Hefei inequality," however, stands for a rare algebraic criterion that is applicable to any mixed state that cannot be tested by the Bell-CHSH inequality in general,[2,3] as was illustrated by an exact treatment of the Werner state.

Here, in comparison with the criterions of separability of two-qubit systems, we briefly mention a corresponding test of the separability of systems with two continuous degrees of freedom.[6–8] In the problem of two-party continuum case with two-dimensional continuous phase space freedom (p, q) in each party, it is possible to re-formulate the problem such that[8]

(1) the uncertainty relation leads to a necessary condition for separable two-party systems,
(2) the derived condition is sufficient to prove the separability of two-party Gaussian systems.

Namely, the uncertainty relation *without* referring to the Peres-Horodecki criterion[5] provides a necessary and sufficient separability condition for two-party Gaussian systems.

References
1) S. Yu, J.-W. Pan, Z.-B. Chen, Y.-D. Zhang, Phys. Rev. Lett. **91**, 217903 (2003).
2) Bell J S 1964, Physics, **1**, 195 (1964).
3) J. F. Clauser, M. A. Horne, A. Shimony, R. A. Holt, Phys. Rev. Lett. **23**, 880 (1969).
4) R. F. Werner, Phys. Rev. A **40**, 4277 (1989).
5) A. Peres, Phys. Rev. Lett. **77**, 1413 (1996).
   P. Horodecki, Phys. Lett. A **232**, 333 (1997).
6) R. Simon, Phys. Rev. Lett. **84**, 2726 (2000).
7) L. M. Duan, G. Giedke, J. I. Cirac, P. Zoller, Phys. Rev. Lett. **84**, 2722 (2000).
8) K. Fujikawa, Phys. Rev. A **80**, 012315 (2009).
   K. Fujikawa, Phys. Rev. A **79**, 032334 (2009).

Conformal Quantum Mechanics and Sine-Square Deformation[†]

T. Tada[*1,*2]

In Refs. 1,2), it was shown that sine-square deformation (SSD)[3] for two-dimensional (2D) conformal field theory (CFT)[4] can be understood by introducing a new quantization scheme called "dipolar quantization." The basic idea was generalized in Ref. 5) to incorporate the entanglement Hamiltonian and other interesting deformations of 1D CFT. Here, we examine whether the idea of dipolar quantization is applicable to the one-dimensional (1D) case, which is called conformal quantum mechanics (CQM) and was first studied in the seminal paper by de Alfaro, Fubini, and Furlan.[6]

CQM can be realized by the following Lagrangian:

$$L = \frac{1}{2}(\dot{q}(t))^2 - \frac{g}{2}\frac{1}{q(t)^2}, \tag{1}$$

where t is the 1D "spacetime" coordinate. The Lagrangian Eq. (1) is invariant under the following transformations:

$$t \to t' = \frac{at+b}{ct+d}, \quad ad - bc = 1, \tag{2}$$

$$q(t) \to q'(t') = \frac{1}{ct+d}q(t), \tag{3}$$

which constitute 1D conformal transformations.

The transformation Eq. (2) for t can be conveniently decomposed into the following three components: *Translation*, with $a = d = 1$ and $c = 0$, giving

$$t \to t + b. \tag{4}$$

Dilatation, with $a = 1/d$ and $b = c = 0$, giving

$$t \to a^2 t. \tag{5}$$

Special conformal transformation (SCT), with $a = d = 1$ and $b = 0$, giving

$$t \to \frac{t}{ct+1}. \tag{6}$$

The above transformations are generated by the following operators, respectively:

$$H = P_0 = \frac{1}{2}p(t)^2 + \frac{g}{2}\frac{1}{q(t)^2}, \tag{7}$$

$$D = -\frac{1}{4}\left(p(t)q(t) + q(t)p(t)\right), \tag{8}$$

$$K_0 = \frac{1}{2}q(t)^2. \tag{9}$$

In Ref. 6), de Alfaro, Fubini, and Furlan introduced the new operator

$$R \equiv \frac{1}{2}\left(aP_0 + \frac{1}{a}K_0\right), \tag{10}$$

and proposed to regard it, instead of H, as the time-translation operator, *i.e.*, the Hamiltonian. Here, we introduce another operator

$$\bar{R} \equiv H - K = \frac{1}{2}p(t)^2 + \frac{1}{2}\frac{g}{q(t)^2} - \frac{1}{2}q(t)^2, \tag{11}$$

and showed that it corresponds to the thermal density operator. Therefore, $\bar{R}$ is reminiscent of the entanglement Hamiltonian in 2D CFT case.

$R : c^{(2)} = 1$ $H : c^{(2)} = 0$ $\bar{R} : c^{(2)} = -1$
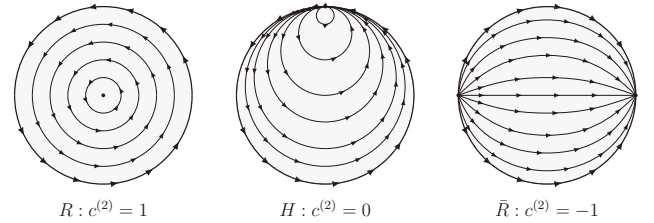
Fig. 1. Time translation on the Poincaré disk. On the boundary of the disk (thick line), "time flow" is uniform without a fixed point for R, while it is limited to the finite region bounded by the two fixed points for $\bar{R}$. H exhibits marginal behavior, and it has one fixed point at infinity. The connection to dipolar quantization is apparent in this depiction.

As for SSD, from the symmetry consideration, we identify the original Hamiltonian $H = P_0$ as the SSD Hamiltonian. Figure 1 depicts the time flow generated by these three operators on the Poincaré disk.

References
1) N. Ishibashi, T. Tada, J. Phys. A **48** (31), 315402 (2015) [arXiv:1504.00138 [hep-th]].
2) N. Ishibashi, T. Tada, Int. J. Mod. Phys. A **31** (32), 1650170 (2016) [arXiv:1602.01190 [hep-th]].
3) A. Gendiar, R. Krcmar, T. Nishino, Prog. Theor. Phys. **122**, 953 (2009); *ibid.* **123**, 393 (2010).
4) H. Katsura, J. Phys. A **45**, 115003 (2012).
5) X. Wen, S. Ryu, A. W. W. Ludwig, Phys. Rev. B **93** (23), 235119 (2016) [arXiv:1604.01085 [cond-mat.str-el]].
6) V. de Alfaro, S. Fubini, G. Furlan, Nuovo Cimento **34**, 569 (1976).

---

†   Condensed from the article in arXiv:1712.09823.
*1   RIKEN Nishina Center
*2   RIKEN iTHEMS

7. Astrophysics and Astro-Glaciology

Measurements of nitric acid formation in humidified air by proton irradiation

Y. Nakai,[*1] S. Tomita,[*2] R. Suganuma,[*2] S. Hattori,[*3] K. Kobayashi,[*3] Y. Shiina,[*2] S. Ishino,[*3] N. Yamamoto,[*2] and K. Sasa[*4]

Gas-phase particle formation by the irradiation of ionizing particles (ionizing radiations) is an important process involving condensable chemical species, such as a water, nitric acid, and sulfuric acid, under conditions of atmospheric pressure and temperature. This phenomenon, the so-called "ion-induced nucleation," has attracted attention as one of the important processes leading to cloud particle formation in the atmosphere.[1,2] Sulfuric and nitric acids are thought to be important chemical species for the nucleation processes in the atmosphere. However, the detailed processes of such acid formations by the irradiation of ionizing particles have not been identified experimentally. Furthermore, large injection of ionizing particles into the atmosphere, such as solar proton events, causes an increase of the atmospheric nitric acid.[3] For understanding the influences of such injection events on the atmospheric environment, laboratory experiments on nitric acid formation by ionizing particle irradiation potentially can provide helpful information. Therefore, we investigated the formation processes of sulfuric and nitric acids by the irradiation of protons. As the first step, we performed experiments for nitric acid formation in humidified air by the irradiation of a proton beam.

The setup for the present experiment consists of a humidified sample-gas generator, an irradiation chamber, a monitor for the sample gas pressure, and a filter-pack holder used for collecting the nitric acid that forms in the sample gas. Wet air was generated by bubbling pure air in ultra-pure water. The sample gas was produced by mixing the wet air with pure dry air. The humidity of the sample gas was adjusted by controlling the flow rates of the wet and dry gases. The total flow rate of the sample gas was maintained at 2.5 SLM (Standard Liters per Minute) using mass flow controllers. The humidity of the sample gas was monitored using a dew-point meter. The sample gas was introduced into the irradiation chamber consisting of a borosilicate glass nipple tube with a length of 25 cm. The 6 MeV proton beam delivered from the 6 MV Pelletron accelerator at Tandem accelerator complex in University of Tsukuba was introduced into the irradiation chamber through a polyimide-film window. The proton beam penetrates along the glass tube, as well as the sample gas flow. After irradiation by protons, the sample gas was transported into the filter holder in which three kinds of
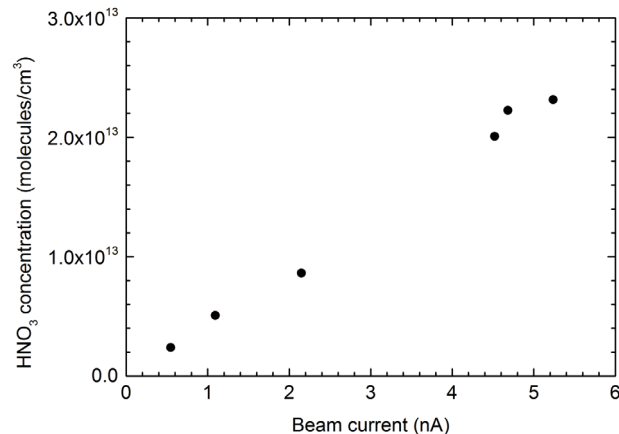
Fig. 1. Concentrations of gas-phase nitric acid in the proton-irradiated gas versus beam intensities (preliminary).

filters were stacked along the gas flow to collect the gas-phase nitric acid and other chemical species in the irradiated gas (Filter-pack method[4]). A polyamide membrane filter was used for collecting the gas-phase nitric acid. The collected nitric acid on the polyamide filter was dissolved in 40 mL ultra-pure water. The amount of nitric anion, NO_3^-, in the solution was measured using ion chromatography analysis. The amount of nitric acid in the irradiated gas was estimated from those of NO_3^- ions in the solution under the assumption that the collection efficiency of the gas-phase nitric acid with the polyamide filter was 100%.

Figure 1 shows the preliminarily results for the concentrations of the gas-phase nitric acid produced in the proton-irradiated gas under the condition of 1 atm pressure, ~42% relative humidity, and ~296 K temperature; the concentration was estimated by dividing the amount of collected nitric acid by the total volume of gas passing through the filters. It is found that the production of nitric acid is almost proportional to the beam intensity. Certain factors, such as collection efficiency of the gas-phase nitric acid, are yet to be considered. Further analysis and consideration are now proceeding.

References
1) J. Curtius, E. R. Lovejoy, K. D. Froyd, Space Sci. Rev. **125**, 159 (2006).
2) F. Arnold, Space Sci. Rev. **137**, 225 (2008).
3) B. Funke et al., Atmos. Chem. Phys. **11**, 9089 (2011).
4) Network Center for EANET, *Technical Manual for Air Concentration Monitoring in East Asia*, (2013).

*1 RIKEN Nishina Center
*2 Institute of Applied Physics, University of Tsukuba
*3 School of Materials and Chemical Technology, Tokyo Institute of Technology
*4 Tandem Accelerator Complex, University of Tsukuba

8. Accelerator

Cooling down test of prototype accelerator system based on SC-QWR

K. Ozeki,[*1] O. Kamigaito,[*1] N. Sakamoto,[*1] K. Suda,[*1] Y. Watanabe,[*1] and K. Yamada[*1]

The construction of a prototype accelerator system based on the superconducting quarter-wavelength resonator (QWR)[1–3] was completed in March 2017. Subsequently, cooling down tests of the system and excitation tests of the QWR were conducted for a number of times. In this contribution, the results of the cooling down tests are reported.

Figure 1 shows an overview of the prototype accelerator system (cryomodule) seen from the beam axis. A thermal shield, which is made of aluminum and enfolded by super insulation, is installed just inside the vacuum vessel. The thermal shield is cooled down using a cryocooler, SHI CH-110L.[4] In order to cut off vibration of the cryocooler, the cryocooler and thermal shield had been connected using thermal contact wires that consist of oxygen-free copper braid wires. A medium such as Apiezon-N or indium had not been applied on the contact faces between the thermal contact wire and the cryocooler or thermal shield.

As a result of the test, liquid helium was filled up to a helium buffer tank, and the excitation of the QWR at a cryogenic temperature was successful. However, we faced a problem in that the temperature of the thermal shield was much higher than expected. While the cryocooler is cooled to below 30 K, the temperature of the bottom of the thermal shield, which was connected directly to the cryocooler via the thermal contact wires, was approximately 70 K. At the design phase of the cryomodule, we had assumed the temperature of the thermal shield to be 40 K. Possible causes for the much higher temperature of the thermal shield are as follows: the thermal contact resistance at the contact faces was too large, or the thermal conduction of the thermal contact wires was too small. At the design phase, these elements had not been estimated sufficiently. The thermal conduction between the cryocooler and the thermal shield must be improved.

In order to obtain information for the improvement, a cooling test of the thermal contact wire was performed. The setup of the test is shown in Fig. 2. An aluminum plate, which simulated the thermal shield, was connected to the cryocooler via a thermal contact wire. A heater was attached to the aluminum plate. By varying the heater power, temperatures at various points were measured with several conditions of the thermal contact faces: no medium, Apiezon-N, and indium.

The application of Apiezon-N showed the best thermal conduction, but it did not show a drastic improvement compared with no medium. More importantly, it was found that the temperature difference between the two ends of the thermal contact wire was very large. This fact suggests that the thermal conduction of the
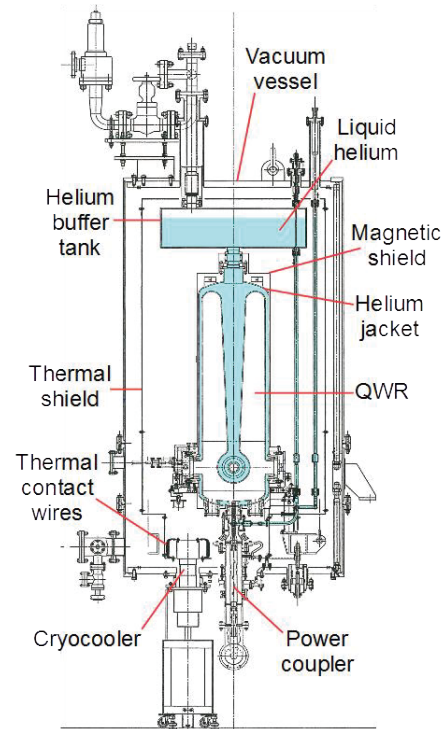
Fig. 1. Overview of the cryomodule.
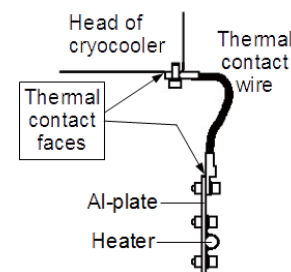
Fig. 2. Setup of the cooling test of the thermal contact wire. The entire system was installed in a vacuum chamber.

thermal contact wire itself is not good. Based on this result, a refinement of the structure and an increase of the number of thermal contact wires are being considered for better thermal conduction.

References
1) N. Sakamoto *et al.*, Proc. SRF2015 (Whistler, Canada 2015), p.976.
2) K. Ozeki *et al.*, Proc. LINAC16 (East Lansing, Michigan, 2016), p.598.
3) K. Yamada *et al.*, Proc. LINAC16 (East Lansing, Michigan, 2016), p.939.
4) http://www.shicryogenics.com/products/specialty-cryocoolers/ch-110-77k-cryocooler-series/

[*1] RIKEN Nishina Center

Transfer of GARIS-II and charge-state multiplier (CSM) cavities

Y. Watanabe,[*1] M. Kase,[*1] E. Ikezawa,[*1] N. Fukunishi,[*1] M. Fujimaki,[*1] O. Kamigaito,[*1] M. Komiyama,[*1] K. Kumagai,[*1] T. Maie,[*1] K. Yamada,[*1] K. Suda,[*1] K. Ozeki,[*1] N. Sakamoto,[*1] A. Uchiyama,[*1] T. Watanabe,[*1] H. Yamasawa,[*1] K. Morimoto,[*1] D. Kaji,[*1] K. Kaneko,[*2] M. Tamura,[*2] T. Ohki,[*2] K. Oyamada,[*2] H. Yamauchi,[*2] A. Yusa,[*2] S. Fukuzawa,[*2] M. Hamanaka,[*2] S. Ishikawa,[*2] K. Kobayashi,[*2] R. Koyama,[*2] T. Nakamura,[*2] M. Nishida,[*2] M. Nishimura,[*2] J. Shibata,[*2] N. Tsukiori,[*2] and K. Yadomi[*2]

An upgrade of the RILAC has been proceeding since FY 2016 to date, as follows: (1) the construction of a stage for the new 28 GHz SC-ECR and the installation of the 28 GHz SC-ECR, (2) the construction of a hot laboratory for RI production, (3) the installation of a superconducting RILAC (sRILAC), and (4) the installation of a helium cooling system for the sRILAC. The RILAC will have an upgrade, which involves replacing the four CSM cavities[1] (A3 - A6) with three superconducting cryomodules. Therefore, these CSM cavities were transferred from the LINAC building in 2017. GARIS-II[2] (including a beam transfer (BT) line) was also transferred from the LINAC building to the Nishina building, to perform experiments with a high-intensity Vanadium (V) beam and to continue experiments during construction. In this paper, we report on the transfer of GARIS-II and the CSM cavities. During the transfer, there were three important points to be considered. First, we had to perform the transfer for approximately four months, because of the beam time, the extension and reconstruction of the LINAC building, and some regular maintenances of the accelerator facilities. Second, we had to keep some temporary storage places for GARIS-II and the CSM cavities, to arrange a period for carrying in. Third, we had to determine a transport route and a method to reverse the top and bottom of the D1 dipole magnet (heaviest magnet, weight: 16 tons) of GARIS-II. This reversal was to change the beam deflection of GARIS-II, because of the interference with a shield door of the E6 room. Table 1 shows the transfer schedule of GARIS-II and the four CSM cavities. A transfer schedule, a transport route, and some temporary storage places were planned by April. In June, the magnets of GARIS-II were carried out from the LINAC building in the following order: Q2, Q3, Q1, D2, BT line, and D1 magnet. Some radioactived chambers and the D1 magnet were temporarily placed in the radiation-controlled area (MB2 floor in front of the SRC room) of the RIBF building, and the other magnets and BT line were placed in the D-crane area (the central machine hatch) of the RIBF building. After GARIS-II was carried out, the two CSM cavities were carried out from the LINAC building in July, in the following order: CSM-A6 and A5. Couplers, tuners, cryopumps, turbo molecular pumps, and cooling water hoses were removed from the CSM cavities in advance. The vertical space in the transport

Table 1. Transfer schedule of GARIS-II and CSM in 2017.

- April	Preparatory works.
June - July	Removal of GARIS-II and CSM cavities.
July - Aug.	Transfer of GARIS-II and CSM-A6 (D6-BEA). Storage of three CSM cavities (A3 - A5).
July - Dec.	Modification of D6-BEA and its BT line. Infrastructure improvement. Set up of GARIS-II, its BT line and D6-BEA
Dec. -	Beam time of GARIS-II

route was insufficient because of an existing BT line and the low shield door. Therefore, the CSM cavities and its stages were carried out separately. Subsequently, the other two CSM cavities (CSM-A3 and A4) were also carried out with their accessories, amplifiers, and control panels from the LINAC building in July. These four radioactive cavities and their accessories were temporarily placed on the MB2 floor, and some amplifiers and control panels were placed in the D-crane area. Here, the D1 dipole magnet was reversed with the C-crane (40 ton) in the BigRIPS room in July, and was divided into the upper yoke and lower yoke in order to transfer it using a 10 ton-crane of the E6 room. The transport route of GARIS-II was from the MB2 floor or the D-crane area to the E6 room, through the machine hatch of the Nishina building and the underground passage. Although the entrance of the E6 room was narrow, the D1 dipole magnet was carefully transferred in July. GARIS-II was installed immediately on some new stages over the D2 magnet of RIPS, and it was checked for vacuum leak after alignment. The old CSM-A6 cavity was used as the new D6-BEA (beam energy adjuster) in the D room. The D6-BEA was transferred from the MB2 floor to the D room, through the D-crane area and the side of the CNS building, in August, and was immediately installed between the QDD61 and QDD62 magnets. it was checked for vacuum leak after alignment. Then, the frequency of the D6-BEA was modified in September. Finally, the three remaining CSM cavities were transferred from the MB2 floor to the E21 room of the RIBF building, through the D-crane area and the north-machine hatch, in August, and were stored on the north side of the SCRIT area. After the transfer, some infrastructure and the BT lines to these infrastucture were installed or modified. The operational checks of GARIS-II and D6-BEA were conducted in December, and the first beam time of GARIS-II with the V beam commenced.

References

1) O. Kamigaito *et al.*, Accel. Prog. Rep. **34**, 322 (2001).
2) D. Kaji *et al.*, Accel. Prog. Rep. **42**, 179 (2009).

*1 RIKEN Nishina Center
*2 SHI Accelerator Service Ltd.

Magnet power supplies for GARIS-II

K. Kumagai,[*1] K. Morimoto,[*1] and D. Kaji[*1]

The superheavy element production team at RIKEN Nishina Center is planning to produce the elements with atomic numbers z = 119 and 120. For early implementation of the project, we planned to relocate GARIS-II[1] from RILAC to the downstream of RRC. The production of new elements will be accelerated by irradiation in parallel with GARIS-III, which will be newly built in RILAC in FY2018. The GARIS-II was relocated to the E6 experimental room. The vanadium beam accelerated by RILAC2 and RRC is guided to GARIS-II after passing through the RIPS-Q6 magnet.

The magnets of GARIS-II consist of two bending magnets and three quadrupole magnets. Two quadrupole magnets and a set of steering magnets were placed upstream of GARIS-II magnets for beam transport. Since the power supplies used in RILAC have been used for GARIS-III, other power supplies had to be prepared. Table 1 summarizes the requested specifications of the power supply for the GARIS-II magnets and their current and voltage specifications. The detectors used in GARIS-II are susceptible to noise. When a power supply using thyristors as a pre-regulator was used for exciting a dipole magnet in GARIS-I, which was installed in RILAC, the noise affected the detectors in some cases. We decided to apply existing power supplies which use a saturable reactor as a pre-regulator as power supplies for five GARIS-II magnets. The four power supplies used for the RIKEN Projectile-fragment Separator (RIPS) and a power supply used in the past for the E2 dipole magnet were used. These supplies are already used not only for RIPS magnets but also for the injection/extraction magnet for the fRC cyclotron and a magnet for beam transport to the E5 experimental room. The connection between the power supply and the magnets for each beam course could be switched using the switching board placed in the E4 experimental room. Since the switching board was able to switch only to two courses (RIPS or fRC/BT), the switching sequence in the board was modified so that it could be switched to three courses (RIPS, fRC/BT and GARIS-II). Figure 1 shows the switching sequence of power supplies.

The maximum current of the power supply connected to GARIS2-D1 is nearly 2 times larger than the allowable current of the magnet. To prevent operational errors, a voltage sensor is planned to be installed in February 2018 on the load terminal to turn off the power when the voltage is higher than the allowable voltage of the magnet. It will be installed.

The power supplies that excite the double quadrupole magnets and a set of steering magnets placed upstream of GARIS-II were switched from the triplet quadrupole (QTD17) and a set of steering magnets (STH16) on the beam transport line to fRC. The switching board was
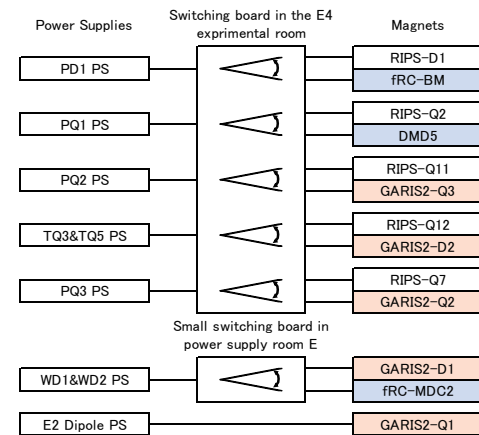
Fig. 1. Switching sequence of the connections of RIPS, fRC/BT and GARIS-II magnets.

Table 1. Specifications of power supplies for GARIS-II magnets.

Region	GARIS-Ⅱ Magnet	Required Specification	Power supply	Max.Current & Voltage
Beam transport line	SH6A0	(10A)[a]	E−S1(E−ST7)	5A−35V
	SV6A0	(10A)[a]	E−S1(E−ST8)	5A−35V
	QD6A1a	(260A)[a]	E−Q1P(E−Q7)	150A−24.3V
	QD6A1b	(260A)[a]	E−Q1P(E−Q8)	150A−32.3V
	Target			
GARIS-Ⅱ	GARIS2−Q1	380A−90V	E2 Dipole	600A−92V
	GARIS2−D1	600A−160V	WD1&WD2−PS	1040A−270V
	GARIS2−Q2	350A−100V	PQ3-PS	330A−95V
	GARIS2−Q3	350A−120V	PQ2-PS	550A−150V
	GARIS2−D2	440A−55V	TQ3&TQ5-PS	450A−80V

[a] Specifications when the magnets were placed in RILAC

relocated from the E4 experimental room, where it was used previously, to a place near the beam transport line in the D room.

After the wiring and the protection interlock test, the current output test for GARIS-II magnets was performed. It is necessary to adjust the power supplies so that stable current can be fed to both magnets on RIPS, fRC and GARIS-II. Most power supplies could feed stable current without matching adjustment of the feedback circuit. For the E2 dipole magnet power supply, the output current was stabilized by replacing the 3-terminal regulator that generate voltage of ± 15 V DC for the error amplifier and the capacitors around it in the feedback loop circuit.

The commissioning of GARIS-II started in December 2017. The power supplies performed satisfactorily. In FY2018, DC current transformers will be installed to measure the precise current of power supplies.

Reference

1) D. Kaji, K. Morimoto, The Japan Society of Nuclear and Radiochemical Sciences 34, 12–23 (2016).

*1 RIKEN Nishina Center

Residual Gas Effect in LEBT on the Transverse Emittance of Multiply-Charged Heavy Ion Beams Extracted from ECRIS[†]

T. Nagatomo,[*1] V. Tzoganis,[*1,*2] J. P. Mira,[*1,*3] T. Nakagawa,[*1] and O. Kamigaito[*1]

When operating the electron cyclotron resonance ion source (ECRIS) with high-intensity beam extraction, we often experience the beam current changing in accordance with the pressure of the low energy beam transport (LEBT). After the LEBT is vented, the beam intensity is sometimes higher than usual, before we evacuate it to the reachable vacuum degree. Space-charge compensation is the one of the possible mechanism that cause the phenomenon as discussed by Toivanen *et al.*,[1] and it should be an advantage when high-intensity ion beams are extracted from the ECRIS. Thus, we investigated the effects of residual gas in the LEBT on the transverse phase space distribution of the ^{40}Ar beam, *e.g.*, correlation between the beam profile and emittance, by using the pepper-pot emittance meter (PPEM).[2]

Figure 1 shows the RIKEN 18-GHz superconducting ECRIS (SC-ECRIS) with the following LEBT. Initially, without the gas injection into the LEBT, the SC-ECRIS was tuned for the Ar^{11+} beam current to be maximum, typically ~ 70 μA, with a 10-kV extraction voltage and a 600-W microwave. The total beam current extracted from the SC-ECRIS was estimated as 0.9 mA from the electric current of the extraction voltage source. The PPEM, by which the four-dimensional transverse phase space distribution was obtained, was positioned before the solenoid lens to avoid the beam-optics complications caused by the helical motion of the beam traveling through the lens. In order to control the residual gas pressure from 10^{-5} to 10^{-3} Pa, we intentionally injected the neutral Ar gas through the variable leak valve
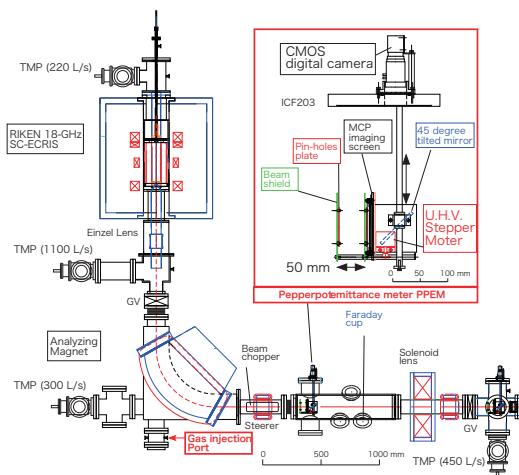
Fig. 1. Schematic of the RIKEN 18-GHz SC-ECRIS, LEBT, and PPEM.
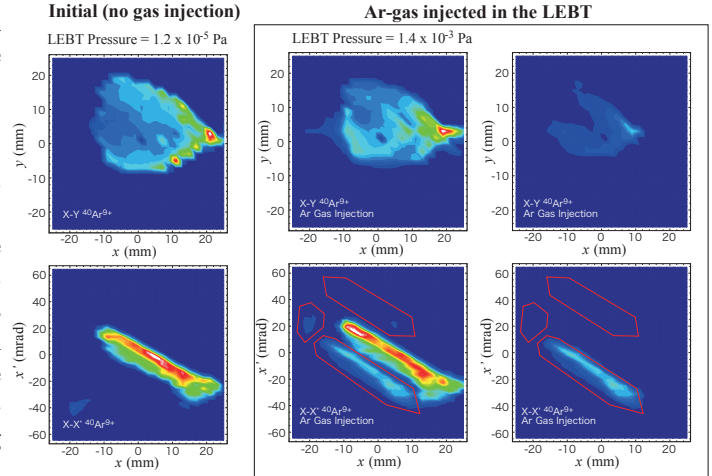
Fig. 2. Obtained beam profile (upper) and horizontal emittance (lower) of ^{40}Ar^{9+} beam by using PPEM.

attached at the gas injection port of the magnet chamber in Fig. 1.

Figure 2 shows the beam profile (x-y plot) and the horizontal emittance (x-x' plot) of ^{40}Ar^{9+} beam at the LEBT pressure of 1.2×10^{-5} Pa (no gas injection) and 1.4×10^{-3} Pa (Ar-gas injection). From Fig. 2, the beam intensity of the central area of the hollow triangle-shaped beam profile appears to increase with Ar-gas injection. However, by selecting a minor component in the emittance plot, a similarly shaped beam profile is clearly separated from the main component. From the systematic studies on the Ar beams from 7+ to 12+, the parasite component is concluded as the Ar beam with other charge that captures an electron before the analyzing magnet. For example, the Ar^{10+} beam, which is extracted as Ar^{11+} from the ECRIS, captures an electron during the travel to the magnet, and is bend by the magnet with the charge of 10+, can mix in the Ar^{9+} beam because of their similar Bρ's. In addition, from the obtained M/Q spectra, the valleys between the Ar peaks become shallower as the LEBT pressure exceeds 10^{-4} Pa by the Ar-injection. Thus, we found that the other charge exchanges and the multiple scatterings with the residual gas are no longer negligible at the LEBT pressure of 10^{-4} Pa. In the case of $\sim 10^{-5}$ Pa, we detected no significant signs of these effects nor the space-charge compensation.

References
1) V. Toivanen *et al.*, Nucl. Instrum. Methods Phys. Res. B **268**, 1508 (2010).
2) V. Tzoganis *et al.*, Proc. 7st Int. Particle Accelerator Conf. (IPAC'16), paper MOPMR048 (Busan, Korea, 2016), p. 361.

An innovative method for $^{12}C^{4+}$ suppression in $^{18}O^{6+}$ beam production in an electron cyclotron resonance ion source[†]

H. Muto,[*1] Y. Ohshiro,[*2] Y. Kotaka,[*2] H. Yamaguchi,[*2] Y. Sakemi,[*2] M. Kase,[*1] S. Kubono,[*1,*2] and S. Shimoura[*1]

It is a major and complex task to accelerate an ion that has the same charge to mass ratio with strong contaminant ions, such as $^{12}C^{4+}$ in the $^{18}O^{6+}$ beam. An innovative method has been developed to suppress the contaminant ions in the Electron Cyclotron Resonance (ECR) ion source by introducing Li vapor. The ion distribution inside the ECR zone was obtained by the optical analysis of ions inside the ECR ion source. The $^{12}C^{4+}$ ions were suppressed as much as by a factor of 10, whereas the $^{18}O^{6+}$ beam changed little with the use of this technique.

A 14 GHz Hyper-Electron Cyclotron Resonance (Hyper-ECR) ion source has been successfully used as an injector for the RIKEN Azimuthal Varying Field (AVF) cyclotron.[1] A grating monochromator was installed at the Hyper-ECR ion source, and the emitted light intensities of gaseous and metal ions were observed during ion beam tuning.[2,3] Recently, the $^{18}O^{6+}$ beam was produced at the Hyper-ECR ion source and injected into the RIKEN AVF cyclotron. After the beam time was started, the users noticed a significant contamination of the $^{18}O^{6+}$ beam with the $^{12}C^{4+}$ ions. The plasma chamber is not hydrocarbon free, and a counter-flow of rotary oil is also suspected for the presence of the carbon atoms. During the beam tuning process, the charge distribution of ions extracted from ECR plasma was measured by a magnetic beam analyzer and a Faraday cup. However, the charge to mass ratio (q/m) of $^{18}O^{6+}$ is 0.33335, and that of $^{12}C^{4+}$ is 0.33333. Even our high-resolution AVF cyclotron ($\Delta m/m = 1/12000$) is unable to separate these two ions.

During the experiment a total beam current of the q/m $=1/3$ ranged from 30 to 50 μA. Although the $^{12}C^{4+}$ beam current contaminating the main beam had to be measured, a direct measurement was impossible. Therefore, we measured the light intensity of the C IV line spectrum during the beam experiment.[4,5] The strength of the light intensity measured by a photomultiplier and a digital voltmeter constantly showed 2.5 mV throughout the experiment. Figure 1 shows the light intensity of the C IV line spectrum from the residual gas plasma as a function of the analyzed $^{12}C^{4+}$ beam intensity. From this result, the 2.5 mV light intensity corresponded to the 12 μA of $^{12}C^{4+}$ beam intensity. Therefore, the contamination ratio of the $^{12}C^{4+}$ ions in the total beam was 24~40%.

When an $^{7}Li^{2+}$ beam was produced and extracted from the Hyper-ECR ion source, there was no C IV light
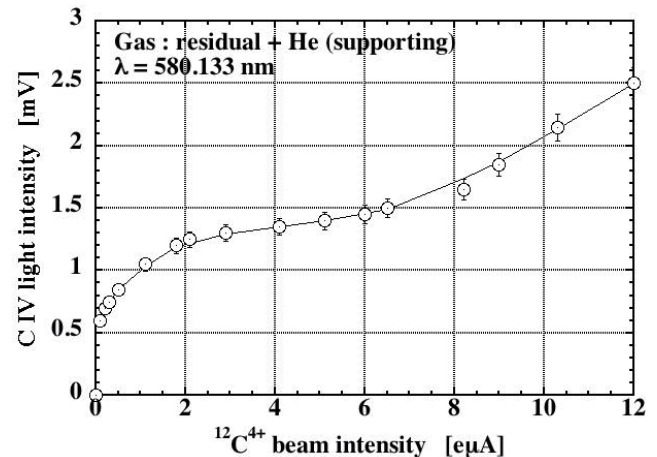
Fig. 1. Light intensity of C IV line spectrum as a function of an analyzed $^{12}C^{4+}$ beam intensity.
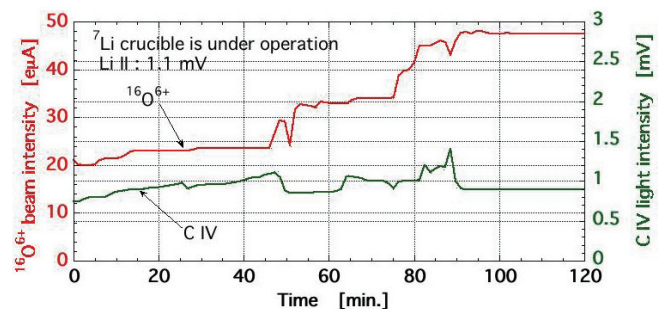
Fig. 2. Time chart of $^{16}O^{6+}$ beam intensity and C IV light intensity with ^{7}Li crucible in operation.

intensity present.

Then, we attempted to tune the $^{16}O^{6+}$ ion beam while vaporizing a small quantity of Li atoms in the plasma chamber. Figure 2 shows a time chart of $^{16}O^{6+}$ ion beam current and C IV light intensity under $^{16}O^{6+}$ ion beam tuning with Li evaporation.

By adjusting the distance between the Li crucible and plasma, the brightness of the Li II light intensity was kept at 1.1 mV. To prevent excessive Li crucible heating, the C IV light intensity was kept at less than 0.9 mV, and the beam current was controlled at 48 μA of $^{16}O^{6+}$. The $^{12}C^{4+}$ beam current became $\sim$1.0 μA when this C IV brightness was converted into the beam current as shown in Fig. 1. The amount of impurities was drastically improved to around 2% from 40% by the Li ion pumping effect.

References
1) Y. Ohshiro et al., Rev. Sci. Instrum. **85**, 02A912 (2014).
2) H. Muto et al., Rev. Sci. Instrum. **84**, 073304 (2013).
3) H. Muto et al., Rev. Sci. Instrum. **85**, 02A905 (2014).
4) H. Muto et al., Rev. Sci. Instrum. **85**, 126107 (2014).
5) NIST Atomic Spectra Database, www.nist.gov/pml/data/asd.cfm.

Renewal of control system and driving mechanism of cavity tuning devices for RILAC Rebuncher

K. Yamada,*1 T. Ohki,*2 K. Oyamada,*2 K. Suda,*1 and N. Sakamoto*1

The RIKEN Linear Accelerator (RILAC) is used as an injector to the RIBF accelerator complex for heavy-ions up to krypton. For example, ^{48}Ca beam is accelerated by a cascade of the RILAC, RIKEN Ring Cyclotron (RRC), Intermediate-stage Ring Cyclotron (IRC), and Superconducting Ring Cyclotron (SRC). The rebuncher called X5-REB and located at the beam transport line from the RILAC to the RRC is required for this operation to adjust the longitudinal bunch length because of the long distance of the beam transport line.[1] The rebuncher system was built approximately 30 years ago[2,3] and showed problems such as low stability of rf voltage and phase because of old low-level (LL) circuits; less reproducibility of the driving mechanism for frequency tuning devices; and insufficient usability of local and remote control. Therefore, the control system as well as the driving mechanism of cavity tuning devices were upgraded to overcome these problems.

We replaced the old control system with a new system using a programmable logic controller (PLC), as shown in Fig. 1. The right side is a controller cabinet including the PLC, and the other side comprises the LL circuits and a transistor wide-band amplifier (WBA). The LL circuits were newly fabricated with rf voltage stability of $\pm 0.1\%$ and phase stability of $\pm 0.1°$. These circuits are compatible with the standard LL circuits of the RIBF. The frequency of the LL circuits ranges are from 36 to 76.4 MHz. The WBA was not new but unused with a maximum output power of 500 W and frequency range of 34–90 MHz. The local operation was performed using a graphical touch panel similar to those used in other rf devices of the RIBF. The remote operation was integrated into the operation terminal of the RILAC2 by using SCADA software of Wanderware InTouch.

A cavity of the X5-REB has five driving devices: two side tuners (L and R) for the coarse tuning of resonant frequency, a shorting plate for the coarse tuning of resonant frequency, a trimmer for the fine tuning of frequency, and an rf power coupler. The old driving mechanism, except for the shorting plate, used a linear actuator with a rack and pinion-geared reversible motor, the amount of rotation and driving speed of which were impossible to control. In addition, the actuator had a large backlash. Thus, we modified the four sets of driving mechanism excluding the shorting plate to use as a stepping motor and a trapezoidal screw. The reversible motor of the shorting plate was

replaced with a new one because of deterioration. Figure 2 shows the cavity and the part of driving devices of the X5-REB after the modification. Tuner L and power coupler cannot be seen in the figure.

Owing to these modifications, the stability of the rf voltage and phase, the reproducibility of position for each tuning device and the usability were greatly improved; this contributed to the stabilization of beam during the RIBF experiment.
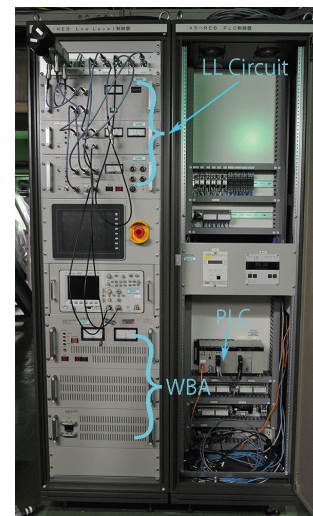
Fig. 1. New control system after the upgrade. Motor drivers are mounted on the backside of the PLC.
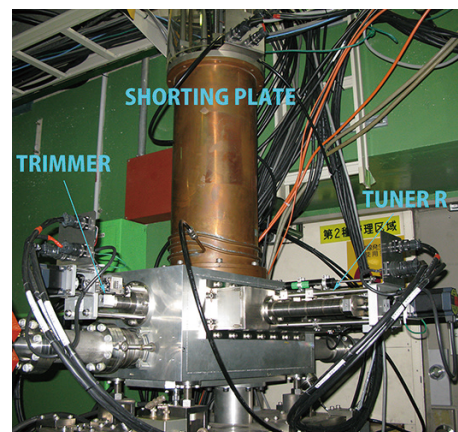
Fig. 2. Cavity and frequency tuning devices of the X5-REB after the modification.

References
1) A. Goto *et al.*, RIKEN Accel. Prog. Rep. **18**, 184 (1984).
2) A. Goto *et al.*, RIKEN Accel. Prog. Rep. **19**, 184 (1985).
3) A. Goto *et al.*, RIKEN Accel. Prog. Rep. **20**, 176 (1986).

*1　RIKEN Nishina Center
*2　SHI Accelerator Service Ltd.

Installation of new central region for energy upgrade at RIKEN AVF cyclotron

J. Ohnishi,[*1] A. Goto,[*1] and Y. Kotaka[*2]

We changed the structure of the central region of the AVF cyclotron to a new one in September 2017. The new structure is the same as the one that was beam-tested in August 2016, except that a part of the inner wall of its RF shield was scraped by hand so that the inflector can be rotated. In the beam test that was conducted in 2016, protons were successfully accelerated to an energy of 30 MeV with harmonic H = 1 acceleration mode. However, the structure was reverted to the previous one because the transmission efficiency of 5-MeV/nucleon $^{56}Fe^{15+}$ beam was 10% and worse than half of the conventional efficiencies.[1] Although the injection acceptance for the original (S1) and new (S2) structures had been calculated in 2016, more detailed simulations including a buncher located at I36 (2.03 m above the median plane of the cyclotron) were executed again in 2017.

Figure 1 shows the injection acceptance sizes of 12-MeV/nucleon deuterons for S1 and S2. The injection acceptance is defined as the phase-space size of the particles accelerated beyond a radius of 180 mm. The abscissa indicates the relative phase angle to the RF at the starting point of the tracking calculation located just above the buncher. Both the dee voltages were 40 kV. The injection acceptances for S1 and S2 were almost the same. The same applies to the other beams. Considering the results of the beam test that was conducted in 2016, the extraction efficiencies for S2 may be worse than those for S1. The reasons for this are not clear because simulations for the extraction efficiencies were not done sufficiently due to the involvement of many adjustable parameters. On the other hand, in the machine time of 9.1-MeV/nucleon $^{12}B^{4+}$ performed in July 2017, only half of the beam current of 300 particle nA that was requested by the experimenters could be supplied. This was due to large beam losses in the first turn for S1, because this beam needed high acceleration voltages. The new structure S2 can reduce the injection beam losses for beams that need high voltages. Therefore, from these two points, we decided to install S2 again and to use it in the machine time for the experiments.

Figure 2 shows a comparison of the transmission efficiencies before and after the installation of S2. The transmission efficiencies are defined as the ratio of the beam currents of Faraday cups FC-I36 and FC-C01 located at the injection and extraction beam lines of the cyclotron. The transmission efficiency of 9.1-MeV/nucleon $^{12}B^{4+}$ beams increased four times and the extracted beam current reached 800 particle nA. Although the transmission efficiencies depend on the kind
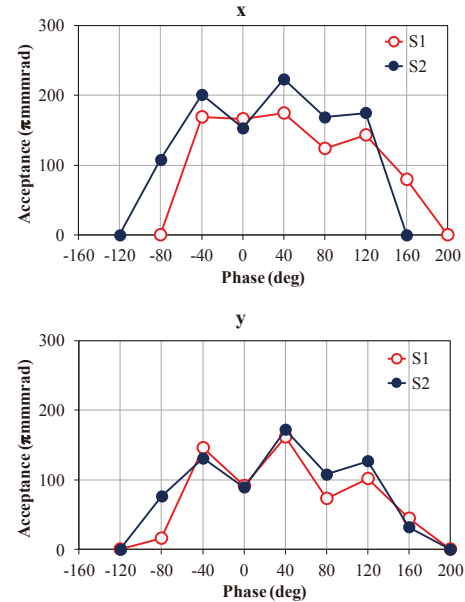
Fig. 1. Injection acceptance sizes for 12-MeV/nucleon deuterons in two orthogonal directions.
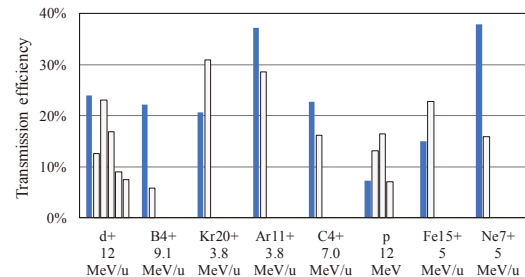
Fig. 2. Transmission efficiencies of the AVF cyclotron after and before the installation of the new structure S2. Filled bars indicate the transmission efficiencies after the installation and empty bars indicate those before the installation.

of beams and the time for operational adjustment of the cyclotron, it seems that the transmission efficiencies for S2 are as good as those for S1 or much better in some cases. Moreover, in the machine study after the installation of S2, we succeeded in accelerating 14-MeV/nucleon deuterons which could not be accelerated before. However, while their injection efficiency was 40–50% as high as other beams, the extraction efficiencies were poor, approximately 10%, which is too low and can supply only weak beams of 1–2 particle μA. Since the increase in the energy of deuterons are strongly requested by experimenters, we plan to do beam simulations and machine study to increase the extraction efficiencies for 14 MeV/nucleon deuterons.

Reference
1) J. Ohnishi *et al.*, RIKEN Accel. Prog. Rep. **50**, 145 (2017).

[*1] RIKEN Nishina Center
[*2] Center for Nuclear Study, the University of Tokyo

Improvement of injection beam-orbit analysis of AVF cyclotron

Y. Kotaka,[*1] Y. Ohshiro,[*1] H. Yamaguchi,[*1] N. Imai,[*1] Y. Sakemi,[*1] T. Nagatomo,[*2] M. Kase,[*2] J. Ohnishi,[*2] A. Goto,[*2] K. Hatanaka,[*3] H. Muto,[*4] and S. Shimoura[*1]

In order to increase the beam intensity of the AVF cyclotron, the injection beam transport system must be improved. As the first step of this improvement, we have developed a calculation method of the beam orbit down to the center of the AVF cyclotron from the ion source by using the 4-dimenssional emittance measured with a pepper-pot emittance monitor[1] (PEM_IH10), as shown in Fig. 1. One feature of our calculation method was the use of the 3D magnetic field calculated with a calculation code to take into account the fringe fields of electromagnets. The other was to implement a space charge effect.[2–4]

As reported previously, the beam-orbit calculation with such magnetic-field distributions of solenoid coils and quadrupole magnets was successful.[2] Therefore, we also renewed the model of the dipole magnet DMI23 shown in Fig. 1 from the hard-edge model of a dipole magnet with a fringing field and pole-face rotations[5] to 3D magnetic-field distributions. The result did not differ from that of the previous model. However, this has helped us to find a practical beam energy by calculating the beam orbit with the 3D dipole magnetic field including the fringing field.

In order to improve the calculation of the space charge effect, we formulated a multistep-ellipse model instead of a single-ellipse model. In the single-ellipse model, the shape and beam-intensity distribution of the beam cross section are approximated by an ellipse and by a uniform distribution, respectively. However, the real beam-intensity distribution is not uniform.[3] Therefore, we increased the number of ellipses that keep the center and give each ellipse the amount of beam elements that exist within it.

To construct the equation of motion (EOM),[4] a standard ellipse must be defined by the combination of the average, standard deviation, and correlation of the beam-intensity distribution. Multistep ellipses are made by evenly dividing the ellipse, the radius of which is 6 times larger than the radius of the standard ellipse, into 30 ellipses.

First, the EOM including the space charge effect for the beam element in the innermost ellipse is constructed. Then, the EOM for the beam element located between the second and first innermost ellipse is constructed from the second ellipse. For the outer ellipses, the EOM is constructed accordingly. The beam elements beyond the outermost ellipse are neglected.

The result of the multistep-ellipse model is shown in
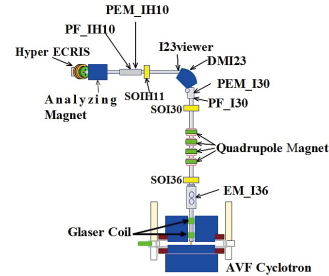
Fig. 1. Injection beam line of the AVF cyclotron.
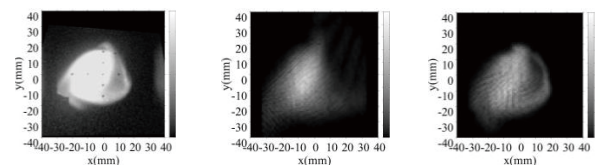
Fig. 2. (Left) Beam-intensity distribution measured with I23viewer. (Middle) Beam-intensity distribution calculated by the single-ellipse model. (Right) Beam-intensity distribution calculated by the multistep-ellipse model. The ion beam is $^4He_2{}^+$ at 15.4 keV and 250 eμA.

Fig. 2. Ion beam measured is $^4He_2{}^+$ at 15.4 keV and 250 eμA. The left of Fig. 2 shows a beam-intensity distribution measured by I23viewer, which is a beam viewer and is shown in Fig. 1. The middle of Fig. 2 shows a beam-intensity distribution calculated using the single-ellipse model. The radius of the single ellipse is 1.8 times larger than the radius of the standard ellipse. The right of Fig. 2 shows a beam-intensity distribution calculated using the multistep-ellipse model. It can be seen that the multistep-ellipse model reproduces the measured distribution better than the single-ellipse model.[6] The reason for this is thought to be that each beam distribution of the cross section on the beam axis is close to the real distribution.

By these improvements, the shapes of the beam deduced from the calculated beam orbit have become close to the measured ones. In addition, we plan to find a method to evaluate these differences of shapes quantitatively. However, the calculated central position and beam angle were not always the same as in the measurement. This is a problem to be improved in the future.

References
1) T. Hoffmann *et al.*, AIP Conf. Proc. **546**, 432 (2000).
2) Y. Kotaka *et al.*, Proc. 13th Annual Meeting of PASJ, (Chiba, 2016), pp. 1072–1075.
3) Y. Kotaka *et al.*, RIKEN Accel. Prog. Rep. **50**, 146 (2017).
4) S. Y. Lee, Accelerator Physics 1st ed. (Singapore, World Scientific, 1999), p. 62.
5) D. C. Carey *et al.*, FERMILAB-Pub-98/310 (1998), p. 131.
6) Y. Kotaka *et al.*, Proc. 14th Annual Meeting of PASJ, (Sapporo, 2017), pp. 1118–1122.

*1 Center for Nuclear Study, University of Tokyo
*2 RIKEN Nishina Center
*3 RCNP, Osaka University
*4 Center of General Education, Tokyo University of Science, Suwa

Radiation monitoring for cycrotrons in RIBF

M. Nakamura,[*1] K. Yamada,[*1] A. Uchiyama,[*1] H. Okuno,[*1] and M. Kase[*1]

Recently, we attempted to monitor the radiation due to beam loss in the RIBF by using ionization chambers (ICs).[1] Usually, we investigate the radiation from the electrostatic diffraction channel (EDC) at RRC and SRC. We would input the alarm signal from these ICs to the beam interlock system (BIS).[2,3] However, in the case of the $^{238}U^{86+}$ beam, for example, RRC, fRC, IRC and SRC are used. Hence, we have installed the ICs near the EDC of fRC and IRC. This time, we attempted to input the alarm signal from the IC near the EDC of IRC to BIS.

We considered the alarm levels of the IC from the signals of the thermocouples (TCs) set at the septum of RRC and SRC.[2,3] According to this method, when the temperature difference between the TC set near the beam-irradiated part of the septum and the temperature of the cooling water of the septum become $10°C$,[4] the alarm signal is input to the BIS. Hence, we compared the temperature difference on the septum with the signal of the IC near the EDC of IRC in the machine time of the $^{238}U^{86+}$ beam. The result is shown in Fig. 1. The data showed little dispersion and the calibration curve in Fig. 1 can be drawn. From this curve, we can recognize that the voltage of the IC became about 8.5 V when the temperature difference on the septum reached to $10°C$, as showed by the red dotted line in Fig. 1.

From October 10 to November 30, the $^{238}U^{86+}$ ion beam was accelerated to 345 MeV/nucleon. The IC signal from 9:00 on 10/19/2017 to 9:00 on 10/20/2017 is shown in Fig. 2(a). The adjustment for high intensity beam was started from about 11:30 on 10/19 and continued to about 9:00 on 10/20. In this figure, we could observe many peaks whose intensities ranged from 3 V to 7 V.

The IC signal from 9:00 on 11/19/2017 to 9:00 on 11/20/2017 is shown in Fig. 2(b). From 9:00 on 11/19 to 9:00 on 11/20, the ion beam current was increased from about 5800 enA to 6000 enA. These ion beam currents reached the maximum values during this machine time of $^{238}U^{86+}$ ion beam. However, in Fig. 2(b), we could observe signals whose intensities were only about 1–3 V and about 3.5 V at maximum.

We performed investigations by inputting the alarm signal to the BIS during the machine time of $^{238}U^{86+}$ ion beam. However, in this term, we could not observe signals stronger than 8.5 V which was the estimated alarm level. Then the BIS from the IC near the EDC of IRC did not act in this term. From these results, we could consider that the operation of the IRC in the machine time of $^{238}U^{86+}$ was completed favorably.

In future, we will investigate the beam loss at the EDC of IRC using other beams in addition to the $^{238}U^{86+}$ beam. In addition, in next time, we will investigate the
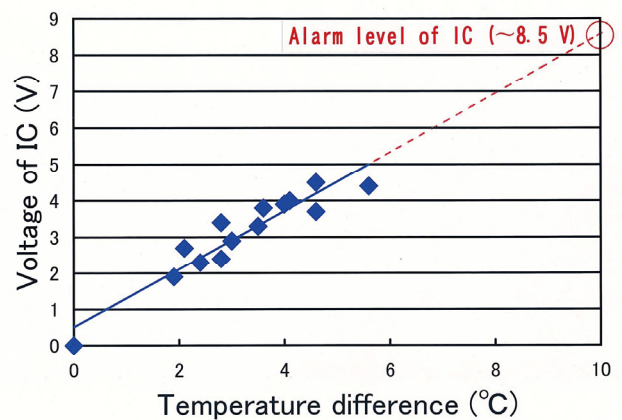
Fig. 1. Correlation of IC voltage and the temperature difference on the septum.
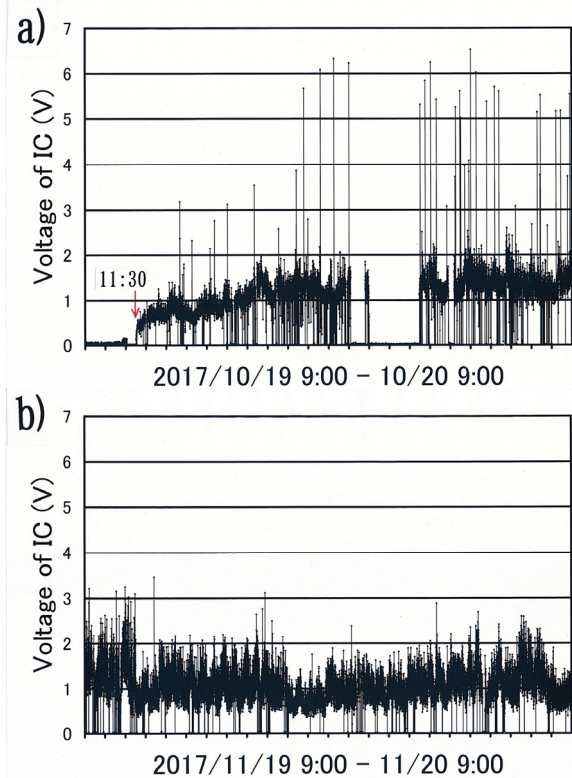
Fig. 2. Signals from the IC installed near the EDC of IRC. a) The signal when the beam was adjusted. b) The signal when the full beam was used.

alarm signal from fRC to BIS.

References
1) M. Nakamura *et al.*, RIKEN Accel. Prog. Rep. **50**, 152 (2017).
2) M. Nakamura *et al.*, RIKEN Accel. Prog. Rep. **49**, 146 (2016).
3) M. Nakamura *et al.*, RIKEN Accel. Prog. Rep. **48**, 237 (2015).
4) K. Yamada *et al.*, RIKEN Accel. Prog. Rep. **48**, 187 (2015).

*1 RIKEN Nishina Center

Update plan of the existing beam interlock system for the RIBF[†]

M. Komiyama,[*1] A. Uchiyama,[*1] M. Fujimaki,[*1] N. Fukunishi,[*1] M. Hamanaka,[*2] and T. Nakamura[*2]

We report on the update plan of the existing beam interlock system (BIS). The BIS is a system that protects the hardware of RIBF accelerators from potential damage caused by accidental irradiation of high-power heavy-ion beams.[1] It was designed to stop beams within 10 ms after receiving an alarm signal from the accelerator and beam transport line components. On receiving an alarm signal, the BIS outputs a signal to one of the beam choppers installed just below the ion source, which deflects the beam immediately. The BIS was developed based on the Melsec-Q series programmable logic controllers (PLCs). The hardware configuration of the BIS is shown in the left part of Fig. 1.

The existing BIS began its operation in 2006, along with the beam commissioning of RIBF. In addition to an increase in the number of input signals to the BIS over 10 years of operation, too much information is shared among all the stations through optical links in the BIS. The response time becomes 15–20 ms, which is greater than its design value. On the other hand, the beam power has exceeded 10 kW recently, and beam operation at the level of several tens of kW is expected in the near future.[2] To handle higher-power beams more safely, a response speed of 10 ms or less is required for the BIS, in order to suppress the hardware damage caused by high-power beams. In addition, a greater number of components than those included in the present BIS have to be carefully monitored because subtler failures can potentially cause severe accidents in the case of very high-power beams. However, there is a limit for the existing BIS to reduce the response speed for the increasing number of associated components. Therefore, we have commenced the development of the next-generation BIS (hereinafter, BIS2), which is designed to have advanced performance and convenience in operation compared to the existing BIS.

The BIS2 implements interlock logic, which is fundamentally equivalent to that of the existing BIS. Based on the operation experience of more than 10 years of the existing BIS, we decided to develop the BIS2 system by ourselves from scratch. Furthermore, we designed it to reduce the amount of data shared between different stations in the BIS2 in order to reduce the response time. In the BIS2, only the output signal status is shared among stations. As a device satisfying the above requirements, we adopted the FA-M3 PLC system. As a prototype of the BIS2, we adopt the two-station configuration; however, there is no technical limit to the number of stations and the number of I/O points included in the BIS2.
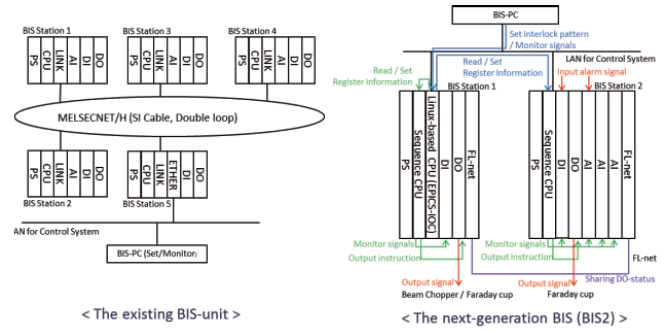
Fig. 1. Hardware configuration of the existing BIS (left) and the BIS2 (right).

The right part of Fig. 1 shows the hardware constitution and the process flow of the BIS2 prototype. The system employs a multi-CPU configuration; the sequence CPU, the Linux-based CPU (hereinafter, F3RP61 CPU), I/O modules, and FL-net module are mounted on one station, and the sequence CPU, I/O modules, and FL-net module are mounted on the other station. We plan to have coupled operation of the BIS2 to the main RIBF control system based on EPICS. Interlock logic is implemented in the sequence CPU, because high-speed processing and high reliability are required. Such high-speed processing is not necessary for setting and monitoring the interlock signal; these functions are implemented in the F3RP61 CPU. We execute EPICS on the F3RP61 CPU and access it from the upper-level PC via Ethernet. The interlock signal information transfer between two stations is performed through FL-net: an open network protocol used for interconnection between controllers.

We plan to apply the BIS2 prototype to the AVF cyclotron and its low-energy experimental facility, as a first step in the RIBF BIS upgrade. By simulating the AVF cyclotron facility, we conducted basic performance tests. First, we verified that the BIS2 prototype outputs signals correctly when the pattern of input signals is changed. Next, we measured the signal transmission speed in the system using an oscilloscope. As a result, the average response time in the same station was found to be 1.4 ms, and when the signal input and output were carried out at different stations, the average response time was 3.8 ms. The measured response speed is better than the specification required in the BIS2 development. Online operation of the BIS2 prototype at the AVF site is scheduled in 2018.

References
1) M. Komiyama et al., RIKEN Accel. Prog. Rep. **39**, 239 (2006).
2) H. Okuno et al., Proc. Cyclotrons2016, p. 1–6.

Upgrade of server systems for RIBF control

A. Uchiyama,*1 M. Komiyama,*1 and N. Fukunishi*1

The RIBF control system is composed of many server for various services. Generally, in order to use them stably without having any serious machine trouble, they should be replaced by new ones appropriately. In this progress report, we will report on the technology used in the upgraded server systems of the RIBF control system. For the accelerator control system, various kinds of data related to the accelerator components and beams accelerated by them, such as vacuum pressures and beam currents, are stored regularly into a data archive system. The archived data is useful for troubleshooting and checking the accelerator condition during daily operations. In the RIBF control system, RIBFCAS has been utilized since 2009.[1] It is a PostgreSQL-based data archive system and the data is acquired from the database and visualized as a GUI chart. NVMe SSD (NVM Express Solid State Drive) was installed as the main storage of the RIBFCAS to realize fast data accessing performance. On the other hand, high redundancy was not available for RIBFCAS. Although RAID 1/5/6/10, which are constructed using multiple physical disk drives, are widely used as the data storage virtualization technology to realize redundant storage systems, RAID was not adopted in the RIBFCAS main storage system, because RAID with NVMe SSD increases the cost and has a finite writing life. Therefore, in the previous system, when a disk failure occurred in the NVMe SSD, the services of RIBFCAS were not available until the NVMe SSD was recovered from the failure. In order to secure redundancy of RIBFCAS with the use of NVMe SSD, we have newly designed a database cluster for RIBFCAS in that we have constructed the PostgreSQL cluster consisting of a master server and a slave server (See Fig. 1). As the main storage of the database, the master server is based on RAID 10 with Serial Attached SCSI disks, and NVMe SSDs manufactured by Memblaze[2] (PBlaze4) are installed in the slave server. Utilizing the replication function, the data stored in the master server is synchronized to the slave server. Since RIBFCAS clients always access the synchronized data of NVMe SSDs in the slave server, it is possible to search and acquire data in a short time. Even when a hardware trouble happens for NVMe SSDs, the RIBFCAS clients can access the archived data stored in the master server by assigning the master server's IP address to the slave server's host name through DNS. As a result, we have succeeded in securing redundancy in RIBFCAS and improving the data response by more than 2 times compared with the previous RIBFCAS.

Since the updating of RIBFCAS has been successfully completed, we have also updated a MyDAQ2[3] system, which is another data archive system based on MySQL and uses a similar technique as that of RIBFCAS with
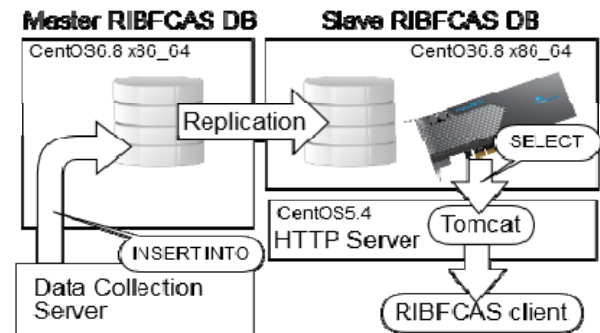
Fig. 1. System chart of the RIBFCAS DB cluster.

NVMe SSDs. The MyDAQ2 system obtains data from each device through an Ethernet and stores them in a MySQL-based database such that users can retrieve the stored data by using an associated Web application. In the case of RIBF control system, the updated MyDAQ2 system adopts MySQL 5.1; it consists of a writing database (master server) and a reading database (slave server), and performs a database replication function similar to that of PostgreSQL for RIBFCAS cluster. The Apache HTTP server is deployed on the same NVMe SSDs as the MyDAQ2 database is stored, and it provides HTTP service. As a result, when 30 days of data is displayed by the MyDAQ2 Web application, the display speed is improved by about two times compared with the conventional system.

We updated the database cluster for RIBFCAS and MyDAQ2 successfully in 2017. We plan to update a cluster of the virtual machines in Apr. 2018. About 40 virtual machines, which are constructed using VMware vSphere, are currently running on three physical servers of the RIBF control system.[4] To manage the image files for the virtual machines, NetApp FAS2240 is adopteda as a network attached storage (NAS) and the physical servers utilize the image file via network file system (NFS). We will upgrade the memory and CPU of the physical server,and also replace the existing FAS2240 with NetApp FAS2620A to further integrate services other than databases. Additionally, since a backup task consumes a large amount of network resources in the RIBF control system, it is difficult to run the task everyday except during maintenance periods each year. In order to solve these inconveniences, we will newly install a 10 Gbps network for backup purposes and shorten the backup time.

References
1) M. Komiyama et al., Proc. ICALEPCS 2011, 90 (2011).
2) http://www.memblaze.com/en/
3) A. Uchiyama et al., Proc. PCaPAC 2016, 35 (2016).
4) A. Uchiyama et al., RIKEN Accel. Prog. Rep. 47, 157 (2014).

*1   RIKEN Nishina Center

Maintenance of vacuum equipment of accelerators

S. Watanabe,[*1] Y. Watanabe,[*1] E. Ikezawa,[*1] N. Sakamoto,[*1] N. Yamada,[*1] M. Kase,[*1] K. Oyamada,[*2]
M. Nishida,[*2] K. Yadomi,[*2] J. Shibata,[*2] and A. Yusa[*2]

This annual report shows the maintenance of vacuum equipment in accelerators in 2017.

First, the maintenance procedure of vacuum equipment in RILAC is described. The worst condition of vacuum in RILAC was in cavity No.5. The pressure of the vacuum in the cavity was 1.0×10^{-3} Pa in February 2017. Vacuum leak points were investigated using a helium leak detector. However, the location of the leak point was not identified because the behavior of the helium gas was complicated. In November 2017, an inner cylinder and a drift tube in cavity No.5 were investigated. The drift tube was placed on the inner cylinder. The space outside the inner cylinder was vacuum and the space inside the cylinder was atmosphere. A gap between the drift tube and inner cylinder was sealed using an O-ring. To find the location of vacuum leak, a dye penetrant inspection material was used. Accordingly, the vacuum leak point was found in the O-ring between the drift tube and inner cylinder. Although the O-ring should be replaced with a new one, it was a special product and there was no spare. An order was thus passed to a supplier (Sumitomo LTD) for an O-ring.

The maintenance of vacuum in cyclotrons was carried out as follows. At AVF, in January 2017, as a compressor of a cryopump did not work so that a turbo molecular pump (TMP) was installed in place of the cryopump, and the AVF was pumped down through the TMP. In February 2017, a vacuum leak was detected at an insulator of RF No.2, and the corresponding O-ring was replaced with a new one. The pressure of the vacuum was thus improved. In August 2017, a broken angle valve connected with a TMP in DTL was replaced with a new one. The RIKEN ring cyclotron (RRC) showed leaks at two locations: one at the bellows connected with RF No.2 and another was due to a pressure increase of 1.2×10^{-5} Pa in N-sector. The leak in the bellows was treated with a sealing agent, however, the location of the leak point was not confirmed. The N-sector was divided into two spaces separated by a membrane with one part in high vacuum and the other in low vacuum. The pressure in the high-vacuum which was in the order of 10^{-5} Pa, could not be decreased. Although the location of the vacuum leak was checked using a helium leak detector, the leak point was not found. If there was no leak outside the N-sector, the space of high vacuum would be connected with that of low vacuum. The helium leak detector was connected to the space of low vacuum. When helium gas was inleted into the space of high vacuum, the leak detector reacted. Thus the connection between the two spaces was confirmed by creating holes in the membrane. As such gas in the low vacuum space flows into the high vacuum space through the holes. However, the condition of the membrane could not be known. To confirm the condition, a Dee of the N-sector was removed in August 2017. The location of the leak point in the bellows and the connection between the spaces of high and low vacuum were investigated. When the Dee was removed, a crack on the surface of the bellows was confirmed. To solve this problem, the bellow should be replaced with a new one. However a large-scale repair work is needed to replace the bellows; this requires a considerable amount of time and a huge budget. Therefore, the vacuum leak at the bellows was tentatively treated with a sealing agent. Moreover, the inside of the Dee or N-sector could be observed after the removal of the Dee. Two holes were confirmed on the membrane. Gas in the low vacuum space flowed into the high vacuum space, and the pressure in the high vacuum space increased. The ion beams were deviated from orbit and hit the membrane, thus creating holes. Therefore, the problem of high pressure in the space of high vacuum must be solved. To decrease the pressure in the high-vacuum space, the pressure in the low vacuum space was reduced. This reduction in the high-vacuum space occurs because inlet flow of gas from the space of low vacuum reduces with pressure reduction. To reduce the pressure in the space of low vacuum, a TMP with a pumping speed of 50 L/s, connected to this space was replaced with a TMP of larger pumping speed of 220 L/s. After replacing the TMP, the pressure in the high-vacuum space was reduced in the order of 4×10^{-6} Pa.

[*1] RIKEN Nishina Center
[*2] SHI Accelerator Service LTD

Operation report 2017 for Nishina and RIBF water-cooling systems

T. Maie,[*1] K. Kusaka,[*1] M. Ohtake,[*1] Y. Watanabe,[*1] E. Ikezawa,[*1] M. Kase,[*1] M. Oshima,[*2] H. Hirai,[*2] K. Kobayashi,[*3] A. Yusa,[*3] and J. Shibata[*3]

1 Operation condition

In FY2017, the Nishina and RIBF water-cooling systems were operated for seven months, respectively. These operation periods correspond to the scheduled beam service time of RIBF, *i.e.*, five months. In addition, the Nishina's water-cooling system was used not only for full RIBF operation but also for AVF standalone and AVF+RRC operations.

2 Trouble report

Fortunately, during FY2017, there was no significant problem that resulted in beam service interruption for both the Nishina and RIBF water-cooling systems. However, they were affected by minor problems.in addition problems such as water leaks, cooling facilities often stopped owing to a blackout and trouble of CGS (cogeneration system) due to thundervolts in FY2017.

3 Periodic maintenance

During the shutdown period of the accelerator, the following activities were carried out as part regular maintenance.

(1) Cleaning of the cooling towers
(2) Inspection and overhauling of the cooling-water pumps
(3) Inspection of the inverter of the RIBF water-cooling pumps
(4) Inspection and overhauling of the air compressor
(5) Replacement of some superannuated hoses, joints and valves used in the system
(6) Cleaning of the strainers and filters used in the deionized water production system
(7) Extension of the sensing wires of the water leakage alarm to floors of new areas
(8) Switching electricity during planned power failure as well as restoration of each device
(9) Securement of minimum power at low load operation of CGS

4 Establishment and improvememt

We relocated the cooling facilities for GARIS 2 because GARIS 2 was moved from the Rilac to the Nishina building this year. As a future will plan , we plan to establish a cooling facility for RILAC RF super-

Fig. 1. Photograph of the RIBF Cooling water pump maintenance.

conducting acceleration cavity Moreover, we a schedule the reinforcement of the RRC cooling system, enhancement of the fRC RF cooling system, and establishment of new Faraday cup G01 cooling facility.

References
1) T. Maie *et al.*, RIKEN Accel. Prog. Rep. **50**, 155 (2016).
2) T. Maie *et al.*, RIKEN Accel. Prog. Rep. **49**, 143 (2015).
3) T. Maie *et al.*, RIKEN Accel. Prog. Rep. **48**, 197 (2014).

*1 RIKEN Nishina Center
*2 Nippon Kucho Service Co., Ltd
*3 SHI Accelerator Service Co., Ltd

Measurement of electron density and temperature in plasma window with diameter of 10 mm

N. Ikoma,[*1,*2] T. Sasaki,[*1,*3] H. Okuno,[*1] S. Namba,[*4] and T. Kikuchi[*5]

The ImPACT Fujita program[1] aims to transmute the LLFP into stable or short-lived nuclei. A scheme utilizing neutrons generated by bombarding deuteron beams on the liquid lithium target has been studied. When the target is irradiated by a high-power beam, lithium vapor is generated. In order to separate the vacuum beam line from the target, the use of plasma window (PW) has been proposed. The original PW[2] has an aperture of 2.36 mm in diameter. However, a beam with a diameter of 100 mm or more is expected in our project. Therefore, we started to test a new PW with a diameter of 10 mm based on the PW developed by Namba et al.,[3] in order to study the possibility of enlargement of the diameter.

In the viscous flow through a circular pipe with a constant diameter, the conductance is obtained from the Hagen-Poiseuille equation.

$$C = \frac{\pi r^4}{8\eta L}\left(\frac{P_1 + P_2}{2}\right) [\text{m}^3/\text{s}] \tag{1}$$

Here, C, r, L, and η are the conductance, radius, length of pipe, and gas viscosity, respectively. P_1 and P_2 are the upstream and downstream pressure, respectively. PW separates the vacuum by high viscosity accompanying the high temperature of the arc plasma.

Figure 1 shows the experimental setup. Helium gas was introduced from the upstream side of the PW. The helium gas was ionized in the PW, and was evacuated by a mechanical booster pump. The flow rate Q was controlled, and the pressures P_1 and P_2 were measured.

Spectroscopic measurement of visible light was also carried out to investigate the plasma characteristics. The light emitted from the plasma was split into two paths, and focused on to two spectrometers. The electron density n_e was determined from the Stark broadening of the H$_\beta$ line. In addition, the electron temperature T_e was determined from the Boltzmann plot by using the transition intensity of He I $2p^3$P-nd^3D.

The results are summarized in Table 1. As the flow rate was increased, the electron density was also increased. On the other hand, the electron temperature was decreased. The electron density was increased with the gas density, while the plasma was cooled by collision with neutral particles.

The pressure P_1 was increased with flow rate. But the contribution of plasma may be greater in the condition of smaller flow rate, because PW exploits its high temperature. We compared the dependency of P_1 on the flow rate under the condition with and without plasma, as shown in Fig. 2. The dotted line shows the fitting result by the power function. P_1 with plasma was 1.43 times larger than that without plasma in the condition of 1 [std L/min]. On the other hand, the factor was 1.38 in the condition of 2 [std L/min]. It was confirmed that the enhancement of P_1 by igniting plasma was slightly high at low flow rate condition. In order to obtain the relation in pressure, diameter, and required input power for a diameter of 100 mm, we plan to carry out the experiment with larger diameter.
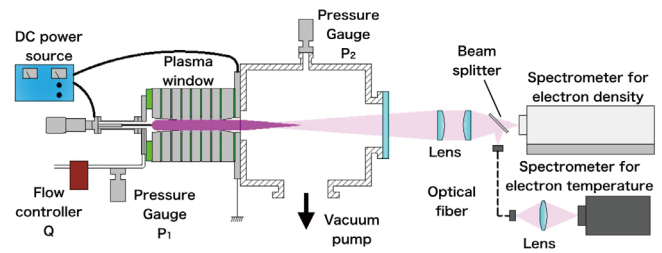
Fig. 1. Experimental setup.

Table 1. Experimental result for PW.

Q [std L/min]	P_1 [kPa]	n_e [1/cm^3]	T_e [eV]
1	8.21	1.94×10^{14}	2.69
2	10.3	2.48×10^{14}	0.192
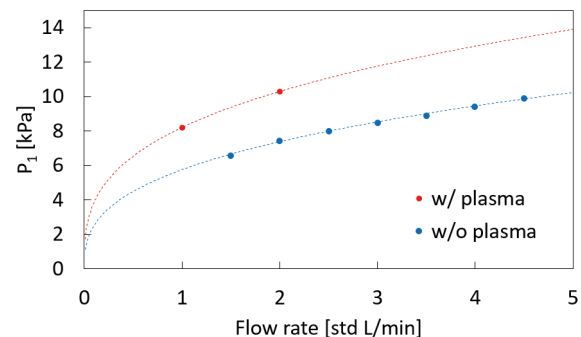
Fig. 2. Dependency of P_1 on flow rate.

References
1) Impulsing Paradigm Change through Disruptive Technologies Program ImPACT, http://www.jst.go.jp/imp-act/en/index.html, accessed: January 6, 2018.
2) A. Hershcovitch, J. Appl. Phys. **78**, 5283 (1995).
3) S. Namba et al., Rev. Sci. Instrum **87**, 083503 (2016).

[*1] RIKEN Nishina Center
[*2] Department of Energy and Environment Science, Nagaoka University of Technology
[*3] Department of Electrical Engineering, Nagaoka University of Technology
[*4] Graduate School of Engineering, Hiroshima University
[*5] Department of Nuclear System Safety Engineering, Nagaoka University of Technology

9. Instrumentation

Pulse-shape data taking with double-sided strip silicon detector

D. Suzuki,[*1] Y. Beaujeault-Taudière,[*2] H. Baba,[*1] and T. Isobe[*1]

A new silicon detector array, TiNA, is currently under development for missing mass spectroscopy using radioactive isotope beams provided by the RIBF. The energy and angle of recoiling ions off the target will be obtained from strip silicon detectors that constitute the array and will be used to deduce excitation energies and differential reaction cross sections. The double sided strip silicon detector type TTT of Micron Semiconductor Ltd, which has 10×10 cm^2 active area divided into 128 strips of 0.7 mm in width, is adopted. The array encompasses four TTT detectors, totaling about 1,000 strips. One challenge in realizing TiNA is the readout electronics system. It should ensure signals from this large number of highly condensed strips to be read out efficiently and without losing the resolution. Given the coupling with γ-ray detectors envisioned in future, compactness to save space around the target area is another key quality of electronics. The capability of pulse-shape analysis, which provides various advantages in noise cancellations or particle identification, is also desirable.

In this study, a TTT detector was tested using the GET (General Electronics for TPCs) system. It is a generic, reconfigurable and comprehensive electronics and data acquisition system for nuclear physics instrumentation of up to 33,792 channels.[1] While developed for large-scale time-projection chambers such as the SπRIT TPC,[2] the GET system is also an attractive option for other gaseous and semiconductor detectors that require the waveform digitizing capability and efficient data taking. A front-end board AsAd of 23×16 cm^2 alone can pulse-shape and digitize a total of 256 signals. Each AsAd board has four application specific integrated circuit chip AGET with a 512-deep circular capacitor array, which records the time-evolution of the input signal at the maximum writing frequency of 100 MHz.

The test was carried out at the GET test bench of the RIBF, which consisted of one AsAd and one concentration board CoBo. For simplicity, only 32 strips on the junction side surface were read out and all other strips were shorted. The junction side was biased to -40 V, while the Ohmic side was grounded. The selected 32 strips were routed through a 1.6-cm-wide flat cable made by the flexible printed circuit board technology. A biasing board and a diode protection circuit board ZAP were added between the feedthrough and the AsAd board. The charge collected from the Ohmic side was fed to a preamplifier to generate an external trigger. A standard ^{241}Am source was measured. We

successfully operated the GET system with different settings in external and internal trigger modes, or in full and partial read out modes, which will help flexibly configure the circuit depending on experiments in future. In the analysis, we realized a common pattern of noise that occured in all connected channels likely due to electromagnetic interferences. This noise was canceled by subtracting the waveform of a strip without a signal (Fig. 1). The energy resolution without any treatment was over 100 keV FWHM, which was improved by this subtraction to about 70 keV FWHM. This resolution is comparable to 50 keV obtained at the same test bench using a NIM-standard spectroscopic amplifier model 671 of ORTEC. The result shows the GET system to be a viable option for silicon detectors.
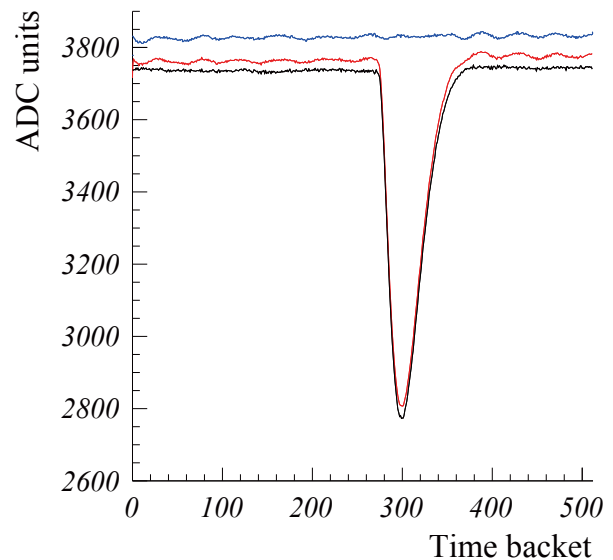
Fig. 1. Example of waveform data with a standard α source using GET electronics. The writing frequency was set to 25 MHz, which corresponds to a full range of 20 μs over 512-deep capacitor array. The pulse shaping was configured with a 1-μs peaking time. The data in red and blue were obtained from two strips with and without a hit of an alpha particle, respectively. A common pattern of noise is seen in both channels. The noise is canceled in the data in black obtained by subtracting the data in blue without a hit.

References
1) E. C. Pollacco et al., Nucl. Instrum. Methods Phys. Res. A 887, 81 (2018).
2) R. Shane et al., Nucl. Instrum. Methods Phys. Phys. Res. A 784, 513 (2015).

*1 RIKEN Nishina Center
*2 NPAC, Université Paris-Sud, Université Paris-Saclay

Stress Test of digital DAQ system for PANDORA

J. Gao,[*1,*2] L. Stuhl,[*2,*3] M. Sasano,[*2] K. Yako,[*3] Y. Kubota,[*2] Z. Yang,[*2] J. Zenihiro,[*2] V. Panin,[*2] Z. Korkulu,[*2] E. Takada,[*4] H. Baba,[*2] and T. Uesaka[*2]

Programable digitizers are employed in the data acquisition (DAQ) system of the PANDORA project.[1] The aim of the PANDORA project is to build a neutron detection system with real-time neutron-gamma discrimination capability for the study of (p,n) reactions. We use a very low energy threshold to avoid loss of neutron events. This increases the background counting rate. For a high beam intensity, this can be a problem. In this work, stress tests were performed to confirm the system works with high trigger rates for future (p,n) experiments.

CAEN 730-series is a family of 14-bit, 500 M Samples/s Flash ADC Waveform Digitizers.[2] According to the manual,[3] the speed of data transfer through an optical fiber from the digitizers to a computer is up to 80 MB/s. The DPP-PSD (digital pulse processing for the pulse shape discrimination) firmware[4] is capable for our purpose. A parameter corresponding to the particle type can be calculated in the firmware and a threshold can be set to filter events.[5] The digitizer can be configured to dump the waveform (waveform mode) or to dump only the time and charge information (list mode). Stress tests were conducted for both modes.

The hardware configuration for the tests is shown in Fig. 1. To suit the experimental situation of acquiring data from at least 15 PANDORA scintilator bars (each has signal on both side) and some auxilliary detectors, we combined two 16-channel modules (V1730B) and one 8-channel module (V1730D) using a daisy chain. Each digitizer was configured to "paired mode," in which one digitizer is triggered only if both channels of a pair, e.g. ch0 and ch1, are triggered. A LUPO(Logic Unit for Programmable Operation) module[6] was used to generate a 62.5 MHz signal to synchronize the three boards. Test input signals were generated from a pulser. We used a software called digiTES developed by CAEN[7] to control the digitizers and to acquire data. Originally, with digiTES, only boards that were of exactly the same model could be used together. We modified the program for using different boards. Other conditions for the stress test is shown in Table 1 along with the results.

For the waveform mode test, we configured the digitizer to acquire waveforms with 300 sampling points for each pulse. In this configuration, the digitizer can work with a low inefficiency up to 10 kHz input pulse frequency. This corresponds to a data transfer rate of 24 MB/s. As some events have already been lost in 10 Hz test, we can assume that the maximum data transfer speed is under 24 MB/s. This is only 30% of the 80 MB/s marked in the manual. We will work around this issue as the waveform can help us improve the charge and time resolution in future applications.

For the list mode test, the digitizers can work fine under a trigger rate of 10 kHz. However, higher rates such as 100 kHz are too much for digitizers. Based on the result of the 100 kHz test, we can expect the maximum inefficiency-free trigger rate for digitizers to be around 36 kHz.
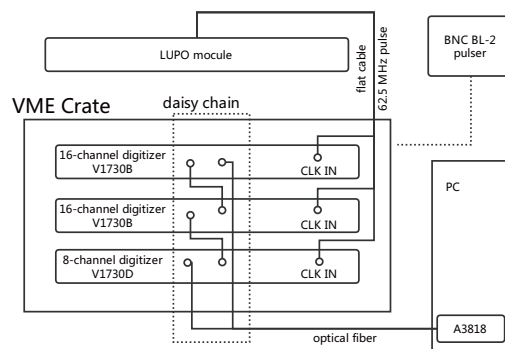
Fig. 1. Hardware diagram for the digitizers stress test.

Table 1. Result of stress testing.

acquiring mode	number of channels	Pulser frequency(kHz)	live time(%)
waveform	4	~ 10	92.3
	4	~ 200	<5
list	40	~ 2	99.9
	40	~ 10	100.0
	40	~ 100	36.0

References
1) L. Stuhl et al., Nucl. Instrum. Methods A **866**, 164 (2017).
2) http://www.caen.it/csite/CaenProd.jsp?idmod=865&parent=62
3) CAEN User Manual UM2792
4) http://www.caen.it/csite/CaenProd.jsp?parent=39&idmod=770
5) L. Stuhl (et al.), In this report.
6) https://ribf.riken.jp/RIBFDAQ/index.php?DAQ/Information/Module/LUPO
7) http://www.caen.it/servlet/checkCaenDocumentFile?Id=11614

*1　School of Physics, Peking University
*2　RIKEN Nishina Center
*3　Center for Nuclear Study, University of Tokyo
*4　National Institute of Radiological Sciences (NIRS)

Development of a high resolution neutron detector HIME

A. T. Saito,[*1,*2] T. Nakamura,[*1,*2] Y. Kondo,[*1,*2] T. Isobe,[*2] S. Takeuchi,[*1,*2] Y. Togano,[*2,*3]
SAMURAI 20, SAMURAI 27, and SAMURAI 36 Collaboration

A high-granularity neutron detector array HIME is newly designed for multiple-neutron detection with good timing and position resolution as well as high efficiency. The high granularity enables us to perform the tracking of recoiled protons produced by (n, p) elastic scattering and knockout reactions such as $^{12}C(n, np)$, cleanly eliminating neutron crosstalk background by using the kinematics and causality of (n, p) elastic scattering. In this report, we show the result of a commissioning experiment aiming at the establishment of a proton tracking method and the evaluation for two-neutron detection with a very low decay energy by simulation.

Figure 1 shows a schematic view of HIME, composed of 48 bars of plastic scintillator modules, each of which has a size of 2 cm(T)×4 cm(V)×100 cm(H). HIME has five layers, and three pieces of thin plastic scintillator modules are equipped to veto charged-particle backgrounds.
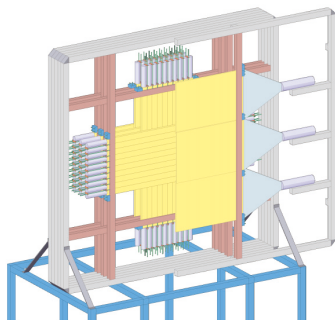
Fig. 1. Schematic view of HIME. Each module of HIME is coupled to two phototubes at both ends to obtain the light-output and timing information. A half of VETO modules is drawn.[1]

The commissioning experiment was carried out as a parasitic run of SAMURAI 20, 27, and 36. Details are described in Ref. 2). Figure 2 shows examples of tracks obtained by the recoil proton tracking analysis. We could successfully establish a proton tracking technique for the first time.

The performance of the proton tracking analysis for eliminating neutron crosstalk background was evaluated by GEANT4 simulation for two-neutron detection in the decay of ^{26}O into $^{24}O + 2n$ ($E_{rel} = 18$ keV[3]). This is one of the most difficult cases because the two neutrons are emitted in a small angle. Figure 3 shows the relative energy spectrum after eliminating neutron

crosstalk background by a conventional method described in Ref. 4) (blue) and by the proton tracking analysis (red). The proton tracking method yields a detection efficiency that is 1.5 times higher than that with the conventional method. The simulated relative energy resolution is 30 keV (FWHM), which is much better than that in a previous experiment ($\Delta E_{rel} = 110$ keV[3]). These results show that the proton tracking analysis of HIME is a powerful method for two-neutron detection, and the proton tracking method can be applied to the detection of more than two neutrons in the future.
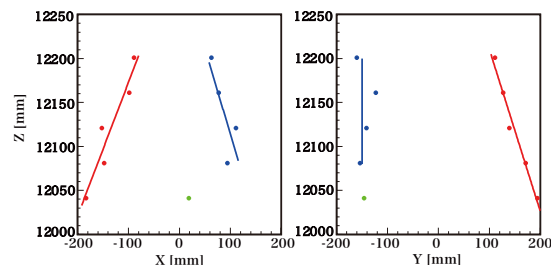
Fig. 2. Examples of recoil proton tracks in which two tracks by two neutrons are observed. The beam is along the Z direction, and X and Y correspond to the hit position in the horizontal and vertical directions, respectively. Each dot corresponds to a hit position. The red and blues dots show each track. The green dot is a hit regarded as background.
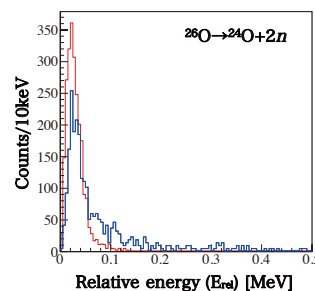
Fig. 3. Relative energy spectrum of ^{26}O. The high-energy tail in the blue histogram originates from the remaining crosstalk, which is not removed by conventional crosstalk analysis.

References
1) R. Tanaka, Master's Thesis (2012).
2) A. T. Saito, Master's Thesis (2017).
3) Y. Kondo *et al.*, Phys. Rev. Lett. **116**, 102503 (2016).
4) T. Nakamura *et al.*, Nucl. Instrum. Methods Phys. Res. B **376**, 156 (2016).

[*1] Department of Physics, Tokyo Institute of Technology
[*2] RIKEN Nishina Center
[*3] Department of Physics, Rikkyo University

Development and test of the dual-gain ASIC preamplifier boards for the GLAST silicon-strip detectors

V. Panin,[*1] Z. Elekes,[*2] Z. Halász,[*2] G. Hegyesi,[*2] C. Dósa,[*2] L. Trache,[*3] A. Chilug,[*3] I. Stefanescu,[*3]
D. Tudor,[*3] M. Sasano,[*1] L. Stuhl,[*1,*4] J. Gao,[*1,*5] K. Yako,[*4] Y. Kubota,[*1] Z. Yang,[*1] Z. Yoneda,[*1]
J. Zenihiro,[*1] Z. Korkulu,[*1] E. Takada,[*6] H. Baba,[*1] and T. Uesaka[*1,*4]

Dual-gain ASIC preamplifier boards have been developed for the GLAST-type silicon trackers aiming at coincident measurements of heavy ions and protons from the breakup reactions in HI-proton experiments at SAMURAI.[1] The dual-gain ASIC chips were successfully tested in the previous HIMAC experiment[2] using a prototype printed-circuit board (PCB) with limited readout capabilities. The new design of the PCB has been developed in MTA Atomki (Hungary) in collaboration with RIKEN Nishina Center based on the previously established ASIC technology.

A single PCB is equipped with two ASIC chips for the instrumentation of 16 strips in total of a silicon-strip detector. Preamplified low-gain and high-gain output signals from the chips are separated on the PCB and sent to the external processing circuit HINP,[3] which implements triggering and amplifier functions for further signal processing. In addition, each PCB is equipped with an auxiliary connector, which distributes the test pulse signal as well as the bias voltage for the chips and silicons sensors. Four PCBs can be assembled into a compact stack-like structure, as shown in the Fig. 1, which can be mounted close to the silicon sensor to enable operation of the preamplifiers inside the vacuum chamber.
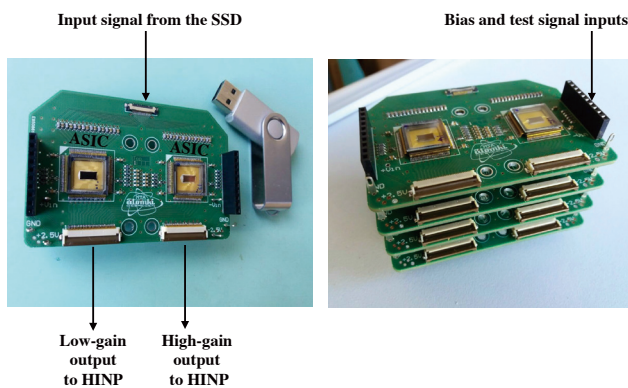
Fig. 1. Preamplifier boards for the GLAST silicon trackers. The left figure shows a single PCB. The right figure shows the assembly of the four PCBs into a compact stack.
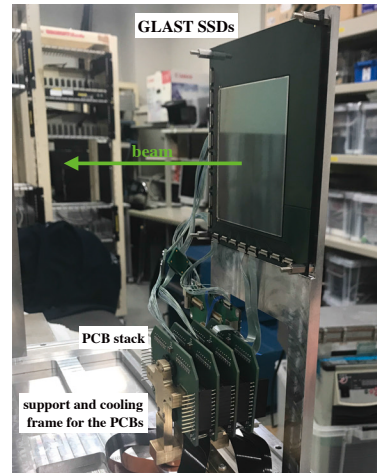
Fig. 2. Arrangement of the GLAST silicon detectors with preamplifier boards for the test experiment in HIMAC.

The four new preamplifier boards were manufactured in MTA Atomki and were sent to RIKEN for the test measurements. The test was carried out in the parasitic mode during the H391 experiment in HIMAC.[4,5] A double layer of the GLAST silicon detectors and the preamplifier PCBs were arranged together inside a vacuum chamber, as shown in Fig. 2. Thirty-two horizontal strips and 32 vertical strips were read-out by the PCBs. The entire structure was exposed to an incident beam consisting primarily of ^{6}He ions with a small contamination of ^{3}H and ^{9}Li particles at an energy of 123 MeV/nucleon and average beam rate of 2×10^4 particles/second. The temperature of the ASIC chips was continuously monitored via a set of thermoelements integrated into the support structure in close proximity to the chips. The temperature stabilized around 36°C throughout the measurements.

The signals from $Z = 1$, 2, and 3 were successfully observed in the measurements, which allowed us to reconstruct the individual particle tracks in the silicon detectors. A detailed analysis of the experimental data is currently in progress.

References
1) V. Panin *et al.*, RIKEN Accel. Prog. Rep. **48**, 53 (2015).
2) V. Panin *et al.*, RIKEN Accel. Prog. Rep. **49**, 164 (2016).
3) G. L. Engel *et al.*, Nucl. Instrum. Methods Phys. Res. A **573**, 418 (2007).
4) M. Sasano *et al.*, in this report.
5) L. Stuhl *et al.*, in this report.

*1　RIKEN Nishina Center
*2　MTA Atomki, Debrecen, Hungary
*3　IFIN-HH, Bucharest-Magurele, Romania
*4　Center for Nuclear Study, University of Tokyo
*5　School of Physics, Peking University
*6　National Institute of Radiological Sciences (NIRS)

A silicon vertex tracker for the ^{8}He$(p, p\alpha)4n$ reaction

F. Dufter,[*1] T. Aumann,[*2,*3] S. Paschalis,[*4,*2] D. M. Rossi,[*2] N. L. Achouri,[*5] D. Ahn,[*6] H. Baba,[*6]
C. A. Bertulani,[*7] M. Boehmer,[*1] K. Boretzky,[*3,*6] N. Chiga,[*6] A. Corsi,[*5] D. Cortina-Gil,[*8] C. A. Douma,[*9]
Z. Elekes,[*10,*6] J. Feng,[*11] B. Fernández-Domínguez,[*8] U. Forsberg,[*12] N. Fukuda,[*6] I. Gasparic,[*13,*6] Z. Ge,[*6]
R. Gernhäuser,[*1] J. M. Gheller,[*14] J. Gibelin,[*5] A. Gillibert,[*14] Z. Halász,[*10,*6] M. N. Harakeh,[*9]
A. Hirayama,[*15,*6] N. Inabe,[*6] T. Isobe,[*6] J. Kahlbow,[*2,*6] N. Kalantar-Nayestanaki,[*9] D. Kim,[*16,*6] S. Kim,[*2]
M. A. Knösel,[*2] T. Kobayashi,[*17] Y. Kondo,[*15,*6] D. Körper,[*3] P. Koseoglou,[*2,*3] Y. Kubota,[*6] I. Kuti,[*10]
P. J. Lee,[*18] C. Lehr,[*2,*6] S. Lindberg,[*19,*6] Y. Liu,[*11] F. M. Marqués,[*5] S. Masuoka,[*20] M. Matsumoto,[*15,*6]
J. Mayer,[*21] B. Monteagudo,[*22] T. Nakamura,[*15,*6] A. Obertelli,[*2,*14,*6] N. Orr,[*5] H. Otsu,[*6] V. Panin,[*6]
S. Y. Park,[*16,*6] M. Parlog,[*5] P.-M. Potlog,[*23] S. Reichert,[*1,*6] A. Revel,[*22] A. T. Saito,[*15,*6] M. Sasano,[*6]
H. Scheit,[*2] S. Shimoura,[*20] F. Schindler,[*2] H. Simon,[*3] L. Stuhl,[*20] H. Suzuki,[*6] D. Symochko,[*2] H. Takeda,[*6]
J. Tanaka,[*2] Y. Togano,[*24,*6] T. Tomai,[*15,*6] H. T. Törnqvist,[*2,*6] T. Uesaka,[*6] V. Wagner,[*2,*6] H. Yamada,[*15,*6]
B. Yang,[*11] L. Yang,[*25] Z. H. Yang,[*6] M. Yasuda,[*15,*6] K. Yoneda,[*6] L. Zanetti,[*2,*6] and J. Zenihiro[*6]

The SAMURAI19[1] experiment at the RIKEN RIBF aimed at producing $4n$ resonances with $(p, p\alpha)$ quasi-free scattering of a 156 AMeV ^{8}He beam at large momentum transfer. A 5 cm thick liquid-hydrogen target (MINOS) with a diameter of 4 cm was used. A luminosity of $\sim 10^{28}$ cm^{-2}s^{-1} was achieved. To obtain the $4n$ energy, the momenta of all outgoing particles were measured with high accuracy and the particle energy loss in the target was determined with essential vertex reconstruction. Reaction vertex positions in the target were determined by a newly developed silicon vertex tracker by TUM and RIKEN, which consists of six single sided silicon detector layers with an active area of $\sim$ 5 x 8 cm^2 and a thickness and pitch size of 100 μm each.[2] As shown in Fig. 1 the detectors are grouped in three units for X and Y determination at distances of 0.6, 12.6 and 24.6 cm with respect to the end of the target container in a vacuum chamber. The target container is thermally shielded from the first detector layer by a 2 um thick aluminized Mylar foil.

All 3708 detector segments are individually read out by the ASIC chip APV25S1.[3] The digital data are collected by a TRB3 board developed by GSI, which can handle trigger rates of up to 50 kHz, and they are time stamped for synchronization with the BABIRL-DAQ used for the other parts of the experiment.

Fig. 1. Installed detectors in the reaction chamber.

With a typical equivalent noise charge of $\sim$ 7 keV, a single channel energy threshold of 38 keV was used to reduce event multiplicities. This is a critical parameter as the average energy loss of the proton from the reaction is $\sim$ 60 keV per detector only. As the ASIC's analogue range is $\sim$ 8 MIPs (Minimum ionizing particle), signals from α-particles may exceed the range. A sophisticated pulse-shape algorithm can separate α-particles from the reaction from the ^{8}He beam particles hitting the detectors at a high rate. From the redundant position measurement of 3 points per track we deduce an average transverse vertex resolution of $\sigma_{x,y} \sim 60$ μm. Owing to the small opening angle of charged reaction residues of interest the resolution along the beam line is $\sigma_z \sim 1$ mm without straggling. As next steps we will further investigate the detection efficiency, the tracking towards the SAMURAI detectors, hit multiplicities and transverse momenta.

*1 Technische Universität München
*2 Technische Universität Darmstadt
*3 GSI, Darmstadt
*4 University of York
*5 Laboratoire de Physique Corpusculaire de Caen
*6 RIKEN, Nishina Center
*7 Texas A&M University-Commerce
*8 University of Santiago de Compostela
*9 KVI-CART, University of Groningen
*10 MTA ATOMKI, Debrecen
*11 Peking University
*12 Lund University
*13 RBI, Zagreb
*14 IRFU, CEA, Université Paris-Saclay
*15 Tokyo Institute of Technology
*16 Ewha Womans University, Seoul
*17 Tohoku University
*18 Hongkong University
*19 Chalmers University of Technology, Göteborg
*20 CNS, University of Tokyo
*21 Universität zu Köln
*22 GANIL, Caen
*23 Institute of Space Sciences, Magurele
*24 Rikkyo University
*25 University of Tokyo

References
1) S. Paschalis, S. Shimoura et al., RIBF Proposal NP1406-SAMURAI19.
2) S. Reichert et al., RIKEN Accel. Prog. Rep. **49**, 167 (2016).
3) M. J. French et al., Nucl. Instrm. Methods Phys. Res. A **466**, 359 (2001).

First implementation of the new segmented implantation detector for decay studies with BRIKEN array

R. Grzywacz,*1*2 M. Singh,*1 T. King,*1 R. Yokoyama,*1 J. Agramunt,*3 N. Brewer,*2 S. Go,*4
J. Heideman,*1 A. Keeler,*1 J. Liu,*4 S. Nishimura,*4 V. Phong,*4*5 M. Rajabali,*6 B. Rasco,*2
K. Rykaczewski,*2 D. Stracener,*2 J. L. Tain,*3 A. Tolosa-Delgade,*3 M. Wolinska-Cichocka,*7
and the BRIKEN collaboration

A new implantation detector was developed at the University of Tennessee and implemented for the first time during the October 2017 BRIKEN[1] campaign. The detector is an evolved version of the array proposed previously[2] but uses YSO instead of a plastic scintillator. The developments were driven primarily by the need to have a fast trigger detector for the neutron time-of-flight array VANDLE.[3,4] The benefits of using an inorganic-crystal scintillator such as YSO are its high effective atomic number ($Z = 35$) and density (4.4 g/cm^3) which result in a short range of beta particles. Both properties should enable a very high detection efficiency and good spatial correlation between ions and decay, thereby providing a good alternative to DSSDs. The YSO scintillator is also very fast and radiation hard, and therefore, it can be used with high rates. The disadvantage of using this high-Z material is its relatively high absorption for the γ-rays, which has to be considered with measurements at energies below $E_\gamma = 100$ keV. The detector unit consisted of a segmented YSO crystal and flat-panel multi-anode photomultiplier (Hamamatsu H8500 or H12700 series). The readout from the photomultiplier used a resistive-network scheme for event position determination. The signals were digitized and integrated with the BRIKEN digital data acquisition system. The YSO crystal was 5-mm thick and was assembled from 1×1 mm^2 segments arranged in a 48×48 array, as shown in Fig. 1. The isolation among segments of the detector, the cover of the detector face, and the sides used ESR (3M) reflector material. The YSO array was attached to the photomultiplier with a 2-mm quartz diffuser glass. The detector unit was enclosed in a 3D printed light-tight enclosure with a thin front window. It was placed inside the BRIKEN matrix directly behind the WAS3ABI[5] detector array with the YSO crystal centered between two clover detectors. During the DA17-02 experiment ions with $Z < 30$ were partially implanted in the YSO detector enabling the ability to test the ion-implantation correlation performance of the detectors. Light yield for heavy ions in the YSO is unknown. It was critical to establish exper-

imentally the optimum operating voltage that avoids the saturation of the photomultiplier and enables the detection of signals induced by ions and betas. The explored range of voltages was from 550 V to 1200 V. The electronic signals from the Anger logic and common dynode were split into two electronic tracks. One set of signals was dedicated to measuring heavy ions and was fed directly into electronics; the other signals used fast amplifiers and were needed to record beta particles. Owing to a very high light yield and very efficient light collection, the system had to be operated at a relatively low voltage of 575 V during the experiment. Despite the resulting small amplification, we were able to detect signals induced by beta particles with a very high efficiency of at least 65%. We observed moderate distortion of the image which will be corrected by the selection of a more appropriate voltage divider. The detector operation was very stable throughout the experiment. The advantages of the simplicity of operation of this new detector were clearly demonstrated.
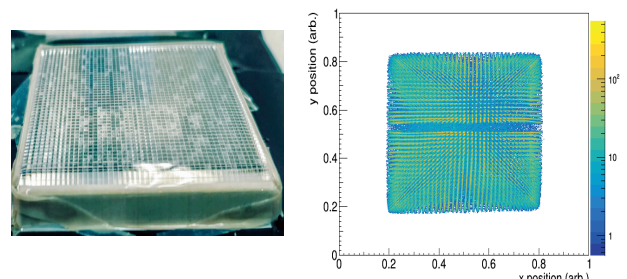
Fig. 1. (Left) Segmented YSO scintillator before coupling to the photomultiplier. (Right) Implantation profile recorded by the segmented YSO detector.

References
1) A. Tarifeno-Saldivia et al., J. of Instrum 12, 1 (2017).
2) M. Alsudifat et al., Physics Procedia 66, 445 (2015).
3) W.A. Peters et al., Nucl. Instrum. Methods A 836, 122 (2016).
4) M. Madurga et al., Phys. Rev. Lett. 117, 092502 (2016).
5) S. Nishimura et al., RIKEN Accel. Prog. Rep. 46, 182 (2013).

*1　University of Tennessee
*2　Oak Ridge National Laboratory (ORNL)
*3　Instituto de Fisica Corpuscular, Valencia
*4　RIKEN Nishina Center
*5　VNU Hanoi University of Science
*6　Tennessee Technological University
*7　HIL University of Warsaw

Preparation of the VANDLE array for beta decay studies at RIBF

S. Go,[*1] R. Grzywacz,[*2] J. Bundgaard,[*2] J. Heideman,[*2] T. King,[*2] M. Madurga,[*2] M. M. Rajabali,[*3] M. Singh,[*2] and R. Yokoyama[*2] for the VANDLE collaboration

Owing to the recent developments of RIBF beams to produce neutron-rich nuclei, the frontier of decay spectroscopy reached nuclei far from stability where delayed neutron emission dominates beta decay. The energy measurements of neutrons provides the beta-decay strength distribution above the neutron separation energy. The strength distribution reflects the nuclear structure and allows to predict the decay properties of even more exotic nuclei. One of the experimental techniques to determine the energy of delayed neutrons is the neutron-time-of-flight measurement.

The Versatile Array of Neutron Detectors at Low Energy (VANDLE)[1] has been constructed at the University of Tennessee. We recently reported strong beta-delayed neutron emissions in ^{83,84}Ga decay[2] from Holifield Radioactive Ion Beam Facility at Oak Ridge National Laboratory with the array. Part of the array is recently being moved to RIKEN RIBF. The modules of plastic scintillators with dimensions of $3 \times 6 \times 120$ cm^3. Both sides of the scintillator are made of Eljen EJ-200[3] or Bicron BC408[4] coupled with PMTs and the time for each left and right signal is averaged to get the position independent time. The detectors cover about 20% of the solid angle around the decay station with a 1 m TOF base. The use of digital data acquisition is essential to achieve good timing resolution. Pixie-16 digitizing modules from XIA LLC allow the digitizing of the signals from detectors sampled at 250 MS/s.

During the BRIKEN experiment[6] in November 2017, we tested our data acquisition system, in particular, we tested the time stamping capability needed for synchronization with BigRIPS.

While the VANLDE array provides good timing resolution for neutron detection, it is also important to develop an implantation detector to give the start timing with good timing resolution. We developed a new, fast timing implantation detector that uses various types of inorganic scintillators and position-sensitive photomultiplier.[5] The implantation detector which was developed for the experiment at RIBF consists of a segmented YSO scintillator coupled with position-sensitive PMT. The performance of the detector was confirmed during the BRIKEN experiment.[7] Combining the fast-timing implantation detector and the VANDLE array will provide sufficient timing resolution for neutron-time-of flight measurement. The construction process for the full VANDLE array for experiments will be completed in the beginning of 2018.

References
1) W. A. Peters et al., Nucl. Instrum. Methods A **836**, 122 (2016).
2) M. Madurga et al., Phys. Rev. Lett. **117**, 092502 (2016).
3) Eljen Technology, 1300 W. Broadway, Sweetwater, TX 79556, USA, www.eljentechnology.com.
4) Saint-Gobain Crystals and Detectors, Scintillation Products, 12345 Kinsman Rd., Newbury, OH 44065, USA, www.crystals.saint-gobain.com.
5) M. Alsudifat et al., Physics Procedia **66**, 445 (2015).
6) K. P. Rykaczewski et al., in the report.
7) R. Grzywacz et al., in the report.

Fig. 1. Part of the VANDLE array setup at RIBF B3F. The delayed neutron will be detected by the array and the time-of-flight provides neutron energy.

*1 RIKEN Nishina Center
*2 Department of Physics and Astronomy, University of Tennessee
*3 Tennessee Technological University

Timing performance of a mirror-type MCP detector use for mass measurements at the Rare RI Ring

Z. Ge,[*1,*2,*5] S. Naimi,[*1] D. Nagae,[*1] Y. Abe,[*1] S. Omika,[*1,*2] F. Suzaki,[*1] H. F. Li,[*1,*5] T. Uesaka,[*1]
Y. Yamaguchi,[*1] M. Wakasugi,[*1] T. Yamaguchi,[*1,*2,*3] N. Tadano,[*2] K. Wakayama,[*2] A. Ozawa,[*1,*3]
S. Suzuki,[*3] T. Moriguchi,[*1,*3] H. Arakawa,[*2] K. Inomata,[*2] T. Kobayashi,[*2] G. Lorusso,[*4] and Y. Yano[*1]

High resolution time-of-flight (TOF) measurements are crucial for mass measurements via TOF methods such as in-ring isochronous TOF or beam-line Bϱ-TOF. To characterize and optimize the timing resolution of a mirror-type micro-channel plate (MCP) detector[1] with a timing anode, an experiment aimed at studying the performance of the detector was conducted at HIMAC (Heavy Ion Medical Accelerator in Chiba). We demonstrate preliminary online results of the timing detector which can be used for the revolution time measurement inside the Rare RI Ring[2] (R3), start TOF of the total TOF for in-ring circulation, beam-line TOF measurement for beam-line mass determination and velocity reconstruction for in-ring mass correction.

To investigate the properties of the detector, a primary beam of $^{84}Kr^{36+}$ at the energy of 200 MeV/nucleon is used. The experimental setup is shown in Fig. 1(a). The setup consisted of two parallel plate avalanche chambers (PPACs) for beam tracking, one electrostatic MCP detector, two plastic scintillators for intrinsic timing resolution deduction of the mirror detector. The MCP with a diameter of 40 mm is mounted on a triangular detector structure as shown in Fig. 1(b). The conversion foil is made of mylar (2 μm) coated with aluminium. The accelerating grid consisting of gold-plated tungsten (W+Au) wires (40 μm in diameter) possesses a distance of 8 mm from the conversion foil with a 1 mm pitch, and wires (W+Au) for the inner and outer mirror grids are arranged with a 3 mm pitch. During the experiment, the high voltage (HV) potential of the MCP, accelerating grid and inner mirror were set at 2.5 kV and the accelerating HV of the foil and outer mirror grid were varied. The timing resolution for isochronous and non-isochronous condition[3] has both been studied by the experiment and simulation performed via SIMION[4] as shown in Figs. 1(c) and (d). The distance between the outer mirror and inner mirror is 20 mm for isochronous condition, while it is 8 mm for the non-isochronous condition. As demonstrated from Figs. 1(c) and (d), when the accelerating HV is increased, the timing resolution improves for both configurations with the corresponding settings.

As can be seen from Figs. 1(c) and (d), the trends of timing resolution (only statistical errors included) as a function of the accelerating HV for the simulation and experimental results are consistent with each other. Simulation results show that a timing resolution of less than 20 ps could be achieved. However, the experimental results could not be achieved and seem to be saturated around 40 ps for both conditions. One possibility could be systematic error from the data acquisition electronics. The detection efficiency reaches ~ 96% by suitable arrangement of the MCP position on the support plate of the triangular structure from the theoretical calculation of the electromagnetic motion of the secondary electrons inside the detector.
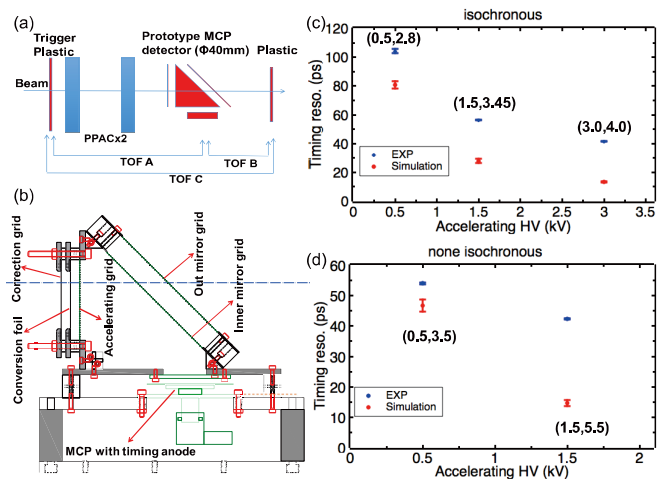
Fig. 1. (a) Schematic diagram of the setup for HIMAC experiment. (b) The side view of the MCP detector structure. (c) and (d) depict the timing resolution (in σ) as function of the accelerating HV potential (the HV difference between the accelerating grid and conversion foil) for isochronous and non-isochronous condition, respectively. The red points are simulation results and the blue points display the experimental results. The HV values described in this report are all negative and in the unit of kV, and values in brackets correspond to (accelerating HV, outer mirror HV).

References
1) Y. Abe *et al.*, RIKEN Accel. Prog. Rep. **47**, 200 (2014).
2) A. Ozawa *et al.*, Prog. Theor. Exp. Phys. **2012**, 03C009 (2012).
3) Z. Ge *et al.*, RIKEN Accel. Prog. Rep. **50**, 187 (2017).
4) http://www.simion.com.

*1   RIKEN Nishina Center
*2   Department of Physics, Saitama University
*3   Institute of Physics, University of Tsukuba
*4   Department of Physics, University of Surrey
*5   Institute of Modern Physics, Chinese Academy of Sciences

Delay-line Anode for MCP-based Position Sensitive Detector at Rare RI Ring

H. F. Li,[*1],[*2],[*3],[*4] Z. Ge,[*1],[*5] S. Naimi,[*1] D. Nagae,[*1] Y. Abe,[*1] T. Uesaka,[*1] T. Yamaguchi,[*1],[*5],[*6] F. Suzaki,[*1] Y. Yamaguchi,[*1] M. Wakasugi,[*1] S. Omika, [*1],[*5] K. Wakayama,[*5] H. Arakawa,[*5] A. Ozawa,[*1],[*6] S. Suzuki,[*1],[*6] and T. Moriguchi[*1],[*6]

Rare RI Ring[1] (R3) is a newly developed mass spectrometer for the measurement of exotic nuclei with a high precision of 10^{-6}. In order to achieve this goal, beam diagnostics need to be on the beam line (including BigRIPS, SHARAQ, and R3 injection)[1] for several reasons: (1) velocity measurement with a precision of 10^{-4} is needed for mass determination;[2] (2) in order to improve the transport efficiency, emittance matching should be applied, which requires emittance measurement before the ring.[3,4] To achieve a precision of 10^{-4} for the velocity measurement, new position sensitive detectors with energy loss as low as 10^{-5} are needed, which cannot be achieved by conventional PPAC. High position resolution (< 1 mm) and high efficiency ($\sim 100\%$) are also needed. For these detectors, it is very important to use position sensitive anodes for collecting the secondary electrons. To achieve high position resolution, we chose 2D delay-line anode for Micro-Channel-Plate (MCP) based detectors. The result of the calibration and position resolution of the anode is shown in this report.

A mask with several holes (the size of the holes were 1 mm and 0.5 mm in diameter) was placed on the MCP, whose active area had a diameter of 120 mm, as illustrated in Fig. 1. We used the vacuum gauge as
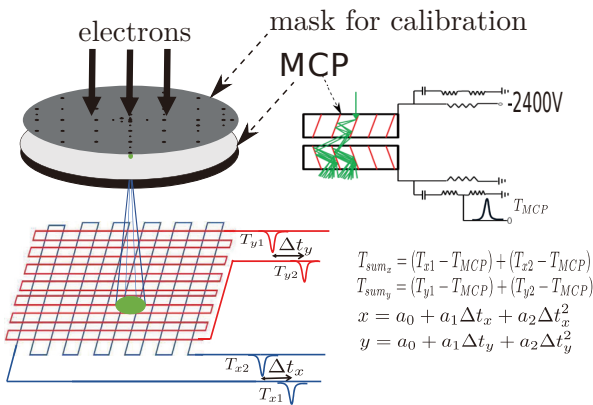
Fig. 2. (a) Image produced by the electrons that pass through the mask's holes and hit the MCP; (b), (c) Accuracy of the points in slice I and II in (a) by using linear and quadratic functions; the error bar represents the σ of the peak.

the source of electrons to calibrate the position of the anode. For each dimension of the delay-line anode, the sum of the times from the two ends, T_{sum}, should be constant, see Fig. 1. We chose 3σ of T_{sum} as a gate to cut the noise signal in both dimensions. The time information of each hole was obtained by projecting the points in the X axis and Y axis, and by fitting it using the Gauss function. It is not possible to use a linear function to calibrate the relationship between the time and position. Therefore, a quadratic function is chosen since it has a higher accuracy as shown in Fig. 2(b)(c). The position information of the holes after calibration is shown in Fig. 2(a). For holes with a diameter of 1 mm, the resolution in both the x and y directions is smaller than 0.6 mm in σ, which is required for high-resolution position sensitive detector.

An MCP with a delay-line anode that has a resolution smaller than 0.6 mm in σ is adequate for a position sensitive detector. One detector has already been developed and is under testing.[5] In the coming years, other position sensitive detectors with the same delay-line anode will be developed.

Fig. 1. Principle of the MCP with 2-D delay line anode; the MCP was placed in vacuum (3.5×10^{-3} Pa).

$$T_{sum_x} = (T_{x1} - T_{MCP}) + (T_{x2} - T_{MCP})$$
$$T_{sum_y} = (T_{y1} - T_{MCP}) + (T_{y2} - T_{MCP})$$
$$x = a_0 + a_1 \Delta t_x + a_2 \Delta t_x^2$$
$$y = a_0 + a_1 \Delta t_y + a_2 \Delta t_y^2$$

References
1) A. Ozawa et al., Prog. Theor. Exp. Phys. **2012**, 03C009 (2012).
2) D. Nagae et al., in this report.
3) Y. Yamaguchi et al., in this report.
4) S. Naimi et al., in this report.
5) Z. Ge et al., Accel. Prog. Rep. **50**, 187 (2017).

*1　RIKEN Nishina Center, RIKEN
*2　Institute of Modern Physics, Chinese Academy of Sciences
*3　School of Nuclear Science and Technology, Lanzhou University
*4　University of Chinese Academy of Sciences
*5　Department of Physics, Saitama University
*6　Institute of Physics, University of Tsukuba

Improvement of detection efficiency of time-of-flight detector with large effective area

S. Ishizawa,[*1,*2] K. Morimoto,[*1] D. Kaji,[*1] and F. Tokanai[*3]

A time-of-flight (TOF) detector was developed in a large entrance foil of 140 mm in diameter for GARIS-II.[1] One of the important characteristics of the TOF detector is the detection efficiency for charged particles passing through the TOF detector. The TOF detector consists of an entrance foil, three wire grids for the formation of electric fields, two side panels, and a micro-channel plate (MCP), as shown in Fig. 1.
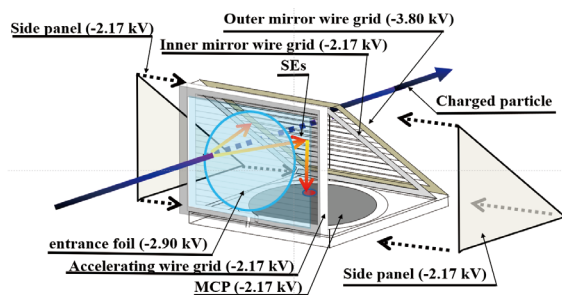
Fig. 1. Schematic view of the TOF detector and typical applied voltage. When the charged particles pass through the TOF detector, secondary electrons (SEs) are emitted from the entrance foil and guided to the MCP along the electrostatic field.

In previous work,[2] it was found that the detection efficiency decreased in the horizontal space of a region more than ±30 mm away from the center of the entrance foil. This is because there are cases where the SEs emitted from edge of the entrance foil are not collected at the MCP.

In order to improve this problem, correction voltages were newly applied to the side panels of the TOF detector for the modification of electric field in the horizontal space. The detection efficiency was checked by impinging alpha particles from an ^{241}Am standard source on the entrance foil. Nine Si detectors were set with suitable intervals behind the TOF detector and operated in coincidence mode. Thus, the position dependence of the detection efficiency was obtained as shown in Fig. 2. The detection efficiency was defined as the ratio N_{TOF}/N_{Si}, where N_{TOF} and N_{Si} are the number of alpha particles detected by the TOF and that detected by Si detectors, respectively. The correction voltages for the side panels were -350 V lower than the applied voltage for the upper surface of the MCP, the accelerating wire grid, and the inner mirror

wire grid.

As a result, we improved of the detection efficiency up to 99% at the edge region of the entrance foil with the correction voltage. The improvement can be verified by comparison with the trajectories of the electrons using an ion optics simulation program (SIMION 3D),[3] as shown in Fig. 3.
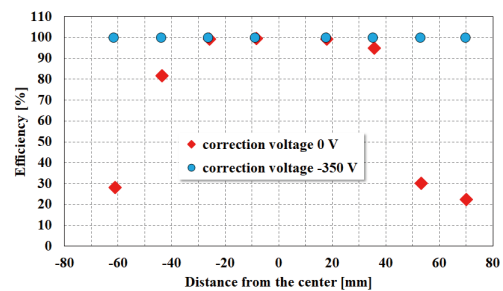
Fig. 2. Measured detection efficiency at the entrance foil in the horizontal space. The horizontal axis indicates the incident position of alpha particles.
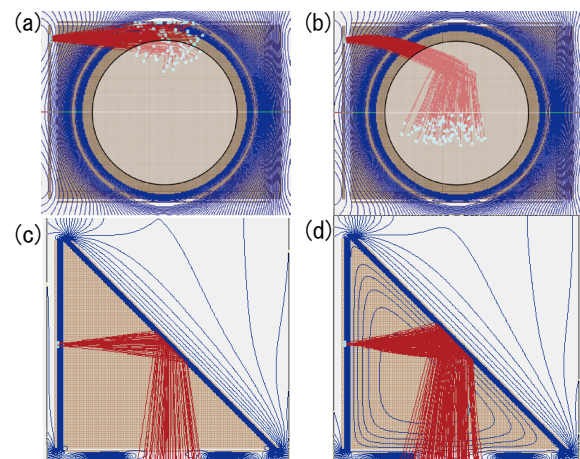
Fig. 3. Simulation results of trajectories of SEs obtained using SIMION 3D. The equipotential lines (blue) and the electronic tracks (red) are calculated with an correction voltage of 0 V (a, c) and -350 V (b, d). MCP is indicated by the white region (a, b).

References
1) D. Kaji *et al.*, Nucl. Instr. Methods Phys. Res. B **317**, 311 (2013).
2) K. Morimoto *et al.*, RIKEN Accel. Prog. Rep. **46**, 191 (2013).
3) D. A. Dahl, SIMION 3D; http://www.simion.com

*1 RIKEN Nishina Center
*2 Graduate School of Science and Engineering, Yamagata University
*3 Department of Physics, Yamagata University

Performance test of low-pressure MWDC
for missing mass spectroscopy at BigRIPS

T. Nishi,[*1] S.Y. Matsumoto,[*2] H. Fujioka,[*2,*1] K. Itahashi,[*1] T. Kawabata,[*2,*1] Y. Matsuda,[*3,*1] K. Miki,[*4]
M. Miwa,[5,*1] M. Takaki,[*6] Y.K Tanaka,[*7,*1] T. Uesaka,[*1] Y.N. Watanabe,[*8,*1] K. Yako[*6] and J. Zenihiro[*1]

In December 2017, we conducted a performance test for a new low-pressure multi-wire drift chamber (MWDC) using proton beams to evaluate tracking resolution and efficiency, as well as their stability under a high-rate beam condition. In this paper, we report the online results of the test experiment.

The MWDC is developed as a tracking detector at the F5 focal plane in BigRIPS, mainly for two experiments of missing mass spectroscopy: a precise measurement of deeply bound pionic atoms via the $(d, {}^3\text{He})$ reaction[1] (piAF) and a search for double Gamow-Teller giant resonance (DGTGR) via the $({}^{12}\text{C}, {}^{12}\text{Be})$ reaction.[2] In these experiments, the tracking detector is required for (1) the detection of light ions under a high-rate background condition (an order of MHz triton in the DGTGR experiment and proton in the piAF experiment) and (2) operation in vacuum to avoid multiple scattering from a vacuum window. For these experiments, we designed and constructed the new low-pressure MWDCs.[3]

The test experiment was conducted in 1.5 days at CYRIC, Tohoku University, by using primary proton beams of 30 MeV/u. The beam energy was selected to simulate the energy loss of the signal ^{3}He of 120 MeV/u in the pionic atom experiment. The beam was detected and identified by two plastic scintillators at the upstream and downstream of the MWDCs as shown in Fig. 1. MWDC consists of 9 planes (XX'X"(0°), UU'U"(+30°), VV'V"(−30°)), and is operated with pure isobutane gas at 13.3 kPa. Figure 2 shows the evaluated detection efficiency as a function of the voltage applied to cathode planes and potential wires. As shown in the figure, the single-plane efficiency is greater than 98% with a voltage of higher than −1300 V. The plane resolution and stability under the high-rate condition are also evaluated with voltage of −1350 V. Though the precise evaluation is still in progress, the position resolution is apparently better than 0.5 mm (FWHM), which satisfies the experimental requirement. The stability test of the MWDC was performed with ≃ 100 kHz proton beams. The condition is comparable with the expected high-rate background in BigRIPS in terms of the space charge effect. Under this severe condition, we confirmed that the detection efficiency does not change by more than a few percent.

From the above results, we found that the MWDC shows satisfactory performance for the experiments at BigRIPS. The precise analysis is ongoing.
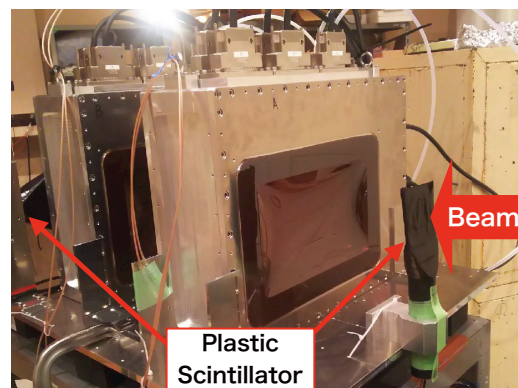
Fig. 1. New constructed MWDCs and plastic scintillators placed on the beam line at CYRIC.
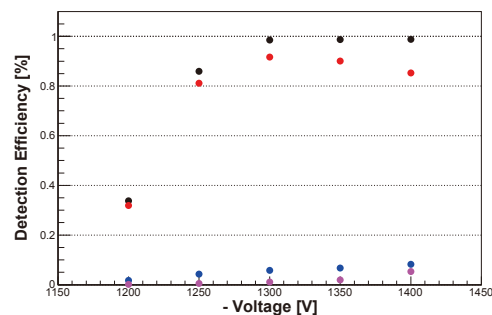
Fig. 2. Evaluated detection efficiency of the single plane as a function of voltage for cathode planes and potential wires. The red, blue, and magenta colors correspond to the multiplicity (≡ number of fired wires par plane) is one, two, and more than three in one event, and the black shows the overall efficiency of the plane.

---

*1 RIKEN, Nishina Center
*2 Department of Physics, Kyoto University
*3 CYRIC, Tohoku University
*4 Department of Physics, Tohoku University
*5 Department of Physics, Toho University
*6 Center for Nuclear Study, University of Tokyo
*7 GSI Helmholtzzentrum für Schwerionenforschung GmbH
*8 Department of Physics, University of Tokyo

References
1) K. Itahashi *et al.*, RIBF Proposal **135**, (2015).
2) T. Uesaka *et al.*, RIBF Proposal **141**, (2015).
3) S. Y. Matsumoto *et al.*, RIKEN Accel. Prog. Rep. **50**, 205 (2017).

Development of the gaseous Xe scintillation detector

J. Zenihiro,*1 T. Harada,*1,*6 S. Terashima,*1,*2 Y. Matsuda,*1,*3 S. Ota,*4 H. Sakaguchi,*1,*5 K. Kawata,*4 S. Ishida,*1,*3 Y. Kasamatsu,*1,*3 and E. Takada*7

RIBF can provide very intense RI beams, but we cannot fully utilize this ability because of the radiation damages of the existing detectors for particle identification. We need a new detector with a good radiation hardness as well as a good energy and/or timing resolution.

For this purpose, we proposed a Xe gas scintillation detector. Xe gas has a small work function (~ 20 eV), its time response for the scintillation process is relatively fast, and the wavelength of the scintillation photons is approximately 175 nm.[1] The performance of the Xe gas scintillation for high-energy heavy-ion particles has not been fully measured so far.

The detector consists of an Al chamber filled with high-pressure ($1 \sim 5$ atm) and pure (99.999%) Xe gas, two 5-mm-thick and 80-mm-ϕ synthetic silica glass windows, and two PMTs (Hamamatsu, R6041-406). Scintillation photons produced in the Xe gas go through the two silica glass windows on both sides of the chamber and finally reach the photo-cathode of the PMTs.

To study the performance of this new detector, we carried out a test experiment at HIMAC in November 2017 (H390). A secondary beam with a mass-to-charge ratio A/Z of approximately 2.28 at 300 MeV/nucleon was produced by the fragmentation of a primary ^{132}Xe beam at 400 MeV/nucleon with a 9-mm-thick Be target. The cocktail beam (1 k ~ 100 k particles/spill) was delivered to the Xe detector through the SB2 beam line.[2] In addition to the Xe detector, a 100-μm-thick plastic scintillator and a 300-μm-thick Si detector were used for reference.

Figure 1 shows the raw signals of the left (yellow) and right (green) PMTs from the Xe detector at 1 and 4 atm in the upper and lower panels, respectively. Two com-

Fig. 2. Particle identification plot of the secondary beam. The x and y axes correspond to the energy loss for 4-atm Xe in QDC channels and the time of flight in TDC channels, respectively.
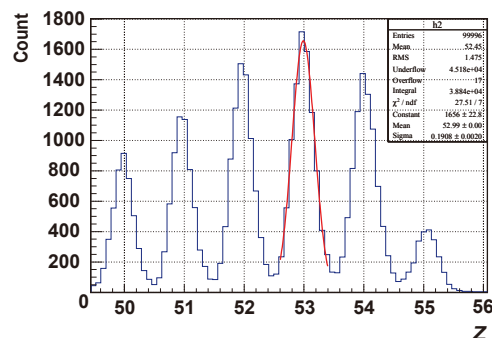
Fig. 3. Atomic number spectrum around 50 deduced from the energy-loss information of the Xe detector.

ponents were found in the scintillation process. We also checked the signals at 2, 3, and 5 atm, which shows that the ratio of the slow component decreases as a function of pressure.

The energy resolutions at 1 and 4 atm for the ^{132}Xe primary beam are approximately 1.2% and 0.8%, respectivley. The timing resolution is approximately 100 ps in sigma and does not change between 1 and 4 atm. In Fig. 2, the correlation between the mean QDC value of the Xe detector at 4 atm and the time of flight is plotted. The secondary beam particles with Z up to 55 are clearly identified. The Z spectrum around 50 was deduced from the energy-loss information of the Xe detector, as shown in Fig. 3. The root-mean-square resolution of $\Delta Z = 0.2$ (5σ separation) is achieved.

These results are very promising for the high-intensity and heavy RI-beam experiments. A more detailed analysis is in progress.

Fig. 1. Raw signals of the Xe detector monitored by an oscilloscope. The left panel shows the signals when the Xe gas pressure is 1 atm, while the right shows that at 4 atm. One division of the horizontal axis is 100 ns, and that of the vertical axis is 50 mV for the left and 200 mV for the right.

---

*1　RIKEN Nishina Center
*2　School of Physics and Nuclear Energy Engineering, Beihang University
*3　CYRIC, Tohoku University
*4　Center for Nuclear Study, University of Tokyo
*5　RCNP, Osaka University
*6　Department of Physics, Toho University
*7　National Institute of Radiological Science

References
1) M. Mimura et al., Jpn. J. Appl. Phys. **48**, 076501 (2009).
2) M. Kanazawa et al., Nucl. Phys. **746**, 393c (2004).

Development of α-ToF detector for correlation measurement of atomic masses and decay properties of superheavy nuclides

T. Niwase,[*1,*2] M. Wada,[*3,*1] P. Schury,[*3] Y. Ito,[*1,*6] M. Rosenbusch,[*1] D. Kaji,[*1] K. Morimoto,[*1] H. Haba,[*1] S. Ishizawa,[*1,*4] K. Morita,[*1,*2] and H. Wollnik[*5]

The atomic mass is a unique quantity for each nucleus. Precise mass measurement allows us to identify the atomic number as well as the mass number of a nucleus. Recently, we measured the masses of fusion-evaporation products[1–4] provided from GARIS-II[5] by using an MRTOF mass spectrograph.[6] We plan to measure the masses of hot-fusion superheavy nuclei (SHN) to identify the nuclides. The expected event rate is of the order of one event per day. We should accurately distinguish a true event from a large number of background events which might have originated from scattered ions or molecular ions. For this purpose, we have developed an α-ToF detector. The time correlation between a time-of-flight (ToF) signal and successive α-decay signals can discriminate such background events.
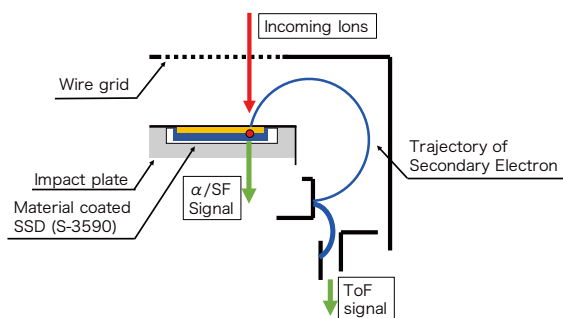
Fig. 1. Schematic of the α-ToF detector. The impact plate is appoximately 3 mm thick.

The α-ToF detector is made of a commercial MagneToF detector (ETP 14DM572) and a Si PIN diode (Hamamatsu S-3590), as shown in Fig. 1. When a heavy ion is incident on the impact plate of the MagneToF, secondary electrons are emitted from the impact plate and the electrons are isochronously transported by a magnetic field and amplified by an electron multiplier to provide a timing signal of the ion. We replaced the impact plate with an Au+MgO-or Au+Al_2O_3-coated Si PIN diode.

We tested the detector by using an ^{241}Am alpha source, and results are shown in Fig. 2. The upper panel shows the count-rate ratio of the coincident timing signal to the α-ray signal. The efficiency of the tim-

ing signal was greater than 90% for 5-MeV α-particles with both coating materials when -2100 V was applied to the impact plate. The lower panel of Fig. 2 shows the correlation mapping of ToF and α-ray energy. The start signal of ToF was made by the triangle roof ToF detector[7] and the stop signal was the timing signal of the α-ToF. The vertical axis indicates the α-ray energy measured by the α-ToF. The distance between the triangle-roof ToF and the α-ToF was 27 cm.

We confirmed that the correlation between the timing signal and the decay energy can be measured using the α-ToF. We will use the α-ToF for the mass-measurement experiment of SHN using the GARIS-II+MRTOF setup, which is scheduled for FY2018-2019.
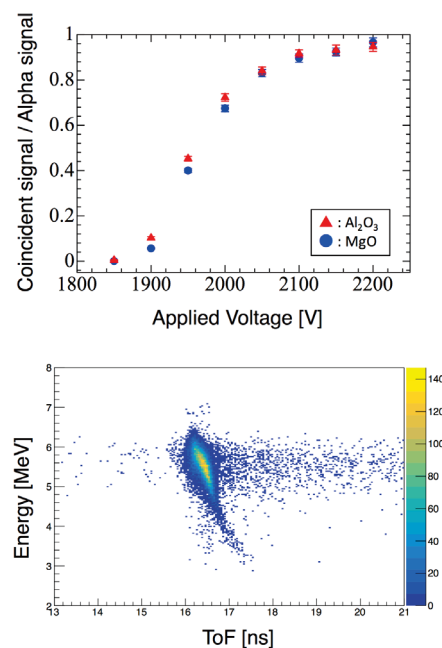
Fig. 2. Count-rate ratio of timing signals coincident with the α-ray signal (upper panel). Correlation mapping of ToF and energy (lower panel).

References
1) P. Schury *et al.*, Phys. Rev. C **95**, 011305(R) (2017).
2) S. Kimura *et al.*, arXiv: 1706.00186.
3) Y. Ito *et al.*, Phys. Rev. Lett. **120**, 152501 (2018).
4) M. Rosenbusch *et al.*, arXiv: 1801.02823.
5) D. Kaji *et al.*, Nucl. Instrum. Methods Phys. Res. B **317**, 311 (2013).
6) P. Schury *et al.*, Nucl. Instrum. Methods Phys. Res. B **335**, 39 (2014).
7) K. Morimoto *et al.*, RIKEN Accel. Prog. Rep. **46**, 191 (2013).

[*1] RIKEN Nishina Center
[*2] Department of Physics, Kyushu University
[*3] KEK, Wako Nuclear Science Center
[*4] Department of Physics, Yamagata University
[*5] Department of Chemistry and Biochemistry, New Mexico State University
[*6] Department of Physics, McGill University

DALI2+ at the RIKEN Nishina Center RIBF

I. Murray,[*1,*2] F. Browne,[*2] S. Chen,[*3,*2] M. L. Cortés,[*2] P. Doornenbal,[*2] H. Sakurai,[*2,*7] J. Lee,[*4]
M. MacCormick,[*1] W. Rodriguez,[*5] V. Vaquero,[*6] D. Steppenback,[*2] and K. Wimmer[*7]

The utilization of large arrays of sensitive γ-ray detectors in combination with fast beams and a reaction target, is a powerful approach to interrogate nuclear structure.[1] This technique, known as in-beam γ ray spectroscopy and often in association with additional particle detectors, permits access to observables such as excited state energies, transition probabilities, exclusive and differential cross-sections, deformation lengths and parameters, state lifetimes and exclusive parallel momentum distributions. Highlights of RIKEN in-beam γ ray spectroscopy results can be found in the references.[2–4]

The Detector Array for Low Intensity Radiation (DALI) was constructed in 1995 for observing nuclear reactions with a low yield.[5] DALI originally consisted of 60 $6 \times 6 \times 12$ cm^3 thallium-doped sodium iodide (NaI(Tl)) scintillators arranged around a reaction target to cover a large solid angle. The granularity of the detector array permitted a correction to the Doppler shifted γ-rays at RI beam velocities of $v/c \sim 0.3$.

DALI was supplemented with additional NaI(Tl) detectors up to a total of 186 in 2002[6] and renamed DALI2. With the opening of the RIBF facility, where the RI beam velocities are $v/c \sim 0.6$, DALI2's greater angular resolution and detection efficiency was integral to its continuing success.

In the spring of 2017, DALI2 was further upgraded to DALI2+ by the inclusion of additional new detectors to the array, bringing the total to 226. Poorly performing older detectors were substituted. A rendering of the new arrangement is shown in Fig. 1. Additional support structures were fabricated to accommodate the new detectors. The simulated full-energy-peak efficiency (FEP) and inherent energy resolution of the DALI2 and DALI2+ configurations for various photon energies (in a centre-of-mass (CM) frame) are listed in Table 1. The beam pipe, shield, target thickness, beam velocity distribution and individual detector resolutions are not included in the simulations. The γ-rays are emitted isotropically in the CM frame and Doppler corrected. The small reduction in FEP efficiency of the DALI2+ configuration is a consequence of the reduced angular coverage. The smaller opening angles of the detectors lead to an increase in inherent energy resolution because of Doppler correction.

DALI2+ was employed for the first time for the third SEASTAR campaign.[7–9] It surrounded the liquid hy-
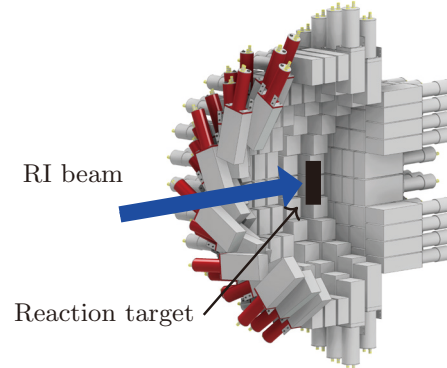
Fig. 1. A 3D rendering of the half sector of DALI2+.

Table 1. GEANT4 simulated FEP efficiencies and inherent energy resolution of the DALI2 and DALI2+ arrays. (without add-back / with 15 cm radius add-back[6])

	$v/c = 0$	$v/c = 0.6$	
E_γ (MeV)	eff. (%)	eff. (%)	FWHM (keV)
DALI2 & standard target position			
0.5	41/48	42/51	38/43
1.0	25/33	25/36	76/85
2.0	14/20	15/25	150/161
DALI2+ & standard target position			
0.5	37/43	40/48	38/43
1.0	22/29	24/34	76/85
2.0	13/19	15/23	139/155
DALI2+ & MINOS target position			
0.5	36/42	39/48	36/41
1.0	22/29	24/34	72/80
2.0	12/18	14/23	138/146

drogen target of MINOS[10] which was situated between BigRIPS[11] and SAMURAI[12] spectrometers.

References
1) P. Doornenbal, Prog. Theor. Exp. Phys. **2012**, 1 (2012).
2) D. Steppenbeck *et al.*, Nature (London) **502**, 7470 (2013).
3) T. Nakamura *et al.*, Phys. Rev. Lett. **96**, 25 (2006).
4) T. Motobayashi *et al.*, Phys. Lett. B **346**, 1 (1995).
5) T. Nishio *et al.*, RIKEN Accel. Prog. Rep. **29**, 184 (1996).
6) S. Takeuchi *et al.*, Nucl. Instrum. Methods Phys. Res. A **763** (2014).
7) S. Chen *et al.*, in this report.
8) M. L. Cortés *et al.*, in this report.
9) H. N. Liu *et al.*, in this report.
10) A. Obertelli *et al.*, Eur. Phys. J. A **50**, 8 (2014).
11) T. Kubo *et al.*, PTEP **2012**, 1 (2012).
12) T. Kobayashi *et al.*, Nucl. Instrum. Methods B Phys. Res. **317B** (2013).

*1　IPNO, CNRS, Univ. Paris-Sud, Univ. Paris-Saclay
*2　RIKEN Nishina Center
*3　Department of Physics, Peking University
*4　Department of Physics, The University of Hong Kong
*5　Universidad Nacional de Colombia
*6　Instituto de Estructura de la Materia, CSIC
*7　Department of Physics, University of Tokyo

Improvement of the maintenance environment for Ge detectors

H. Sato,[*1] T. Komatsubara,[*1] N. Chiga,[*1] H. Takeda,[*1] T. Koike,[*1,*2] and K. Yoshida[*1]

During the delivery of the secondary beams at the BigRIPS separator, we usually confirm and calibrate the particle identification by detecting delayed γ rays emitted from known isomers by using two clover-type germanium (Ge) detectors placed at F7.[1,2] We mainly use ORTEC GMX-clover-S Ge detectors, which are tagged as ORTEC#1, #2, #3, and #4. Each clover Ge detector consists of four pure Ge crystals, each with its own output channel. Radiative backgrounds (such as fast neutrons) could damage the detectors, leading to a reduction in energy resolution during usage. In addition, a good vacuum is required for low temperature operation with liquid nitrogen (LN$_2$). Therefore, periodic annealing and vacuum pumping should be applied to the detectors. For this purpose, we have started the maintenance of the clover Ge detectors since 2016.

First of all, preparation room No.1 on B2F at the Nishina building was cleaned up. At first, when we checked each detector, channels 2, 3 and 4 of OR-TEC#4 did not output any signals. The FETs and hybrid-ICs on the preamplifiers were replaced, and then the signal outputs for each channel were recovered. Next, we prepared a new vacuum pumping system (dry pump: 250 L/min, and TMP: 51 L/s), which has three ports for parallel pumping operation. We also designed and produced a vacuum valve operator, which is used when pumping the detector, at much lower cost than the commercially available ones. The ORTEC Ge detector does not have a heater inside the detector cryostat. Therefore a rod heater and a temperature controller were designed and produced for annealing. The rod heater is inserted into an LN$_2$ dewar from the top port and the bottom of the dewar is heated. The crystals are heated indirectly via a cold finger (a copper rod) connecting the crystals and the bottom of the dewar. A photo of this vacuum pumping and annealing system is shown in Fig. 1.

In the annealing process, the vacuum is typically kept at 10^{-6} to 10^{-7} Torr. The end cap is wrapped by a ribbon heater and aluminum foils to help the heating of the crystals. We tried a few annealing conditions, and found out that typically, annealing at 80°C for 3 to 4 weeks is suitable for our case. The cooling time to reach room temperature ($\sim$22°C) is typically 30 hours. The example of the effect of the annealing process is shown in Fig. 2. Figure 2(a) shows the spectrum of ^{60}Co taken before using the Ge detector in the experiments. Figure 2(b) shows the spectrum taken after usage from 2017.4.3 to 2017.5.7 (primary beam was ^{70}Zn in this period). By annealing over a 35 day pe-

riod, with initial temperature of 22°C, maximum temperature of 80°C, and final temperature of 22°C, the resolution was recovered as shown in Fig. 2(c). As the next step, we will try to tune and modify the electrical components including preamplifiers since annealing alone did not completely recover the intrinsic energy resolution (several keV).
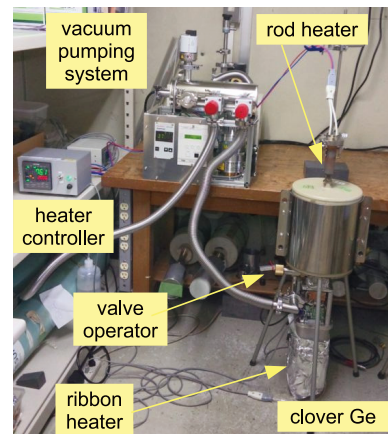
Fig. 1. The pumping and annealing system.
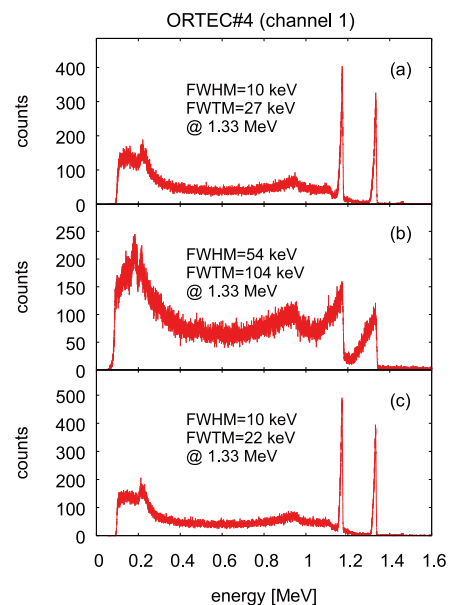
Fig. 2. Example of ^{60}Co spectrum: (a) before MT, (b) after MT, (c) after annealing process.

References
1) N. Fukuda *et al.*, Nucl. Instrum. Methods Phys. Res. B **317**, 323 (2013).
2) http://ribf.riken.jp/BigRIPSInfo/chamber/f7.html

*1 RIKEN Nishina Center
*2 Global Leadership Center, Tohoku University

Overview of silicon strip sensor detector development for sPHENIX experiment

I. Nakagawa,[*1] Y. Akiba,[*1] D. Cacace,[*2] E. Desmond,[*2] T. Hachiya,[*2,*3] Y. Kawashima,[*1,*4] E. Mannel,[*2]
H. Masuda,[*1,*4] G. Mitsuka,[*1] R. Nouicer,[*2] R. Pisani,[*2] K. Shiina,[*1,*4] M. Tsuruta,[*1,*4] and Y. Yamaguchi[*1]

The intermediate tracker (INTT)[1,2] is a barrel type tracker to be implemented outside of another tracking device MVTX detector near the beam pipe and covering central rapidity region of the sPHENIX collision point as shown in Fig. 1. The development of INTT is now in the second generation prototype testing stage. Shown in Fig. 2 is the INTT ladder prototype for layers 1 to 3. Various response tests have been executed and resulting performances are found to be satisfactory.[3] Further tests will be performed using cosmic rays in the test bench. An external trigger using scintillators is under development for the measurement.[4] These prototypes are to be tested with a beam at Fermilab in March, 2018. A three-layer telescope setup is under preparation for the beam test. In parallel, the third generation silicon sensors for the layers 1 to 3 are already under manufacture and they are expected to be the pre-production version.

Fig. 2. The INTT ladder prototype for layers 1 to 3. The ladder consisted of silicon sensors, FPHX readout chips used for former silicon detector in the PHENIX experiment, a high density interconnect (HDI) readout cable and a support structure.

Fig. 3. R&D schedule of INTT.

Fig. 1. Layout of inner tracking systems of the sPHENIX experiment. The beam pipe is lapped with 3 layers of MVTX and 4 layers of INTT detectors.

The study was made to optimize the design of the layer-0.[7] Due to the closest distance from the collision point, the layer-0 is designed to reduce its channel occupancy of the detector by charged particles as much as possible. As shown in Fig. 3, the first prototype for the layer-0 silicon and the high density interconnect (HDI) readout cable have been manufactured and to be tested in spring of 2018. The HDI of layer-0 is designed to be narrower than that of layers 1 to 3 since number of signal lines are fewer.

The biggest technical challenge in the R&D process of the INTT is a design of its bus extender cable. Due to the requirement of long signal transmission (~ 1.3 m) within a limited space, standard flat flexible cables can not be used. A development of a high density multi-layered flexible cable have started effectively in spring of 2017.[5] One of key developments is to make the differential signal line width as narrow as possible and achieve the higher density in order to satisfy the compactness of the cable. We are about to get to the latest technology limit of the line width for 1.3 m distance.

References
1) I. Nakagawa *et al.*, Accel. Prog. Rep. **48**, (2015).
2) I. Nakagawa *et al.*, Accel. Prog. Rep. **49**, 106 (2016).
3) H. Masuda, in this report.
4) K. Shiina, in this report.
5) T. Hachiya, in this report.
6) M. Tsuruta, in this report.
7) Y. Yamaguchi, in this report.

*1 RIKEN Nishina Center
*2 Brookhaven National Laboratory
*3 Nara Woman's University
*4 Department of Physics, Rikkyo University

Development of long multi-layered flexible cable of silicon sensor detector for sPHENIX experiment

M. Tsuruta,[*1,*2] Y. Akiba,[*1] D. Cacace,[*5] E. Desmond,[*5] T. Hachiya,[*1,*3] Y. Kawashima,[*1,*2] T. Kondo[*4]
E. Mannel,[*5] H. Masuda,[*1,*2] G. Mitsuka,[*1] I. Nakagawa,[*1] R. Nouicer,[*5] R. Pisani,[*5] K. Shiina,[*1,*2] and
Y. Yamaguchi[*1]

The progress in the new development of the bus extender[1] for the sPHENIX intermediate tracker (INTT) is reported. The INTT composed of silicon strip sensors. Due to a tight space budget around the collision area, the space to run signal cables for INTT is strictly limited. Thus, high density signal transfer cables are required to send signals from silicon sensors to the front-end readout electronics by 1.3 m. The additional requirements to the cable are flexibility and the impedance matching with circuits to be connected to. As defined in the Eqs. (1) and (2), one of the key essences is the signal line width and pitch.

$$Z_{\rm dif} = 2 \times Z_0 \exp\left(1 - 0.374 e^{-2.9\frac{S}{D}}\right) \qquad (1)$$

$$Z_0 = \frac{60}{\sqrt{\epsilon_r}} \ln\left(\frac{4D}{0.67\pi(0.8W + d)}\right) \qquad (2)$$

Here, $Z_{\rm dif}$ and Z_0 are differential and characteristic impedance, and ϵ_r is the relative dielectric constant. For given impedance, the narrower the line width, the thinner the cable can be. Thus we need to design the signal line width as narrow as possible for the cable to be flexible.

In order to judge the technological limit of a finest width and pitch of the signal line of long flexible print cables (FPCs), we measured a 1.3-m long sample FPC, as
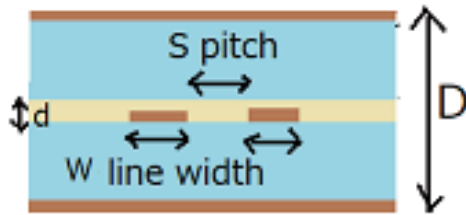
Fig. 1. Cross section of differential signal lines. S and W are line width and pitch, respectively. D and d are thickness between ground planes and thickness of signal layer, respectively.

Fig. 2. Sample FPC

*1 RIKEN Nishina Center
*2 Department of Physics, Rikkyo University
*3 Division of Natural Sciences, Nara Womens University
*4 Tokyo Metropolitan Industrial Technology Research Institute
*5 Brookhaven National Laboratory
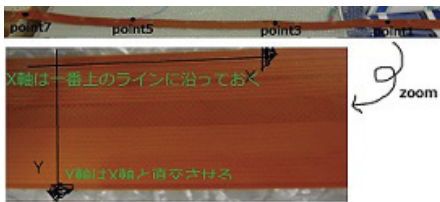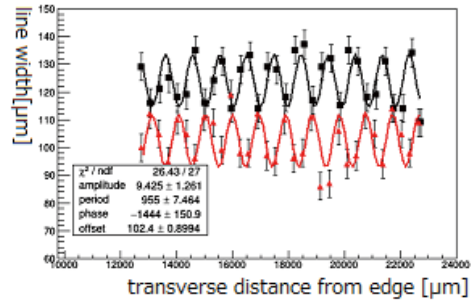
Fig. 3. Observed line width (y-axis) of the sample FPC (black) and its mask(red). The x-axis is the transverse distance from the edge of the sample FPC.
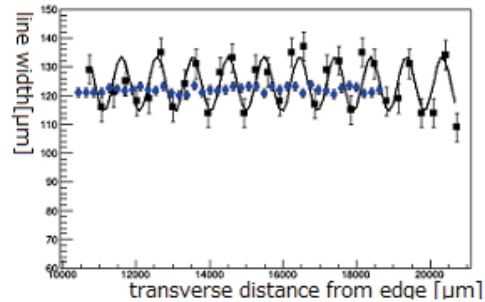
Fig. 4. Observed line widths of the new prototype FPC (blue) superimposed on these of the sample FPC.

shown in Fig. 2, manufactured by the Print-Electronics Laboratory. The measurement was conducted for 32 signal lines whose width were designed to be 120 μm.

The observed line widths are plotted in Fig. 3 (black symbols). As can be guided by the curve showing a sine function fitting, the observed line-width oscillates by 10 μm with a constant ($<$ 1 mm) repetition. Most likely, the origin is propagated from the mask itself used at an exposure process. As shown by black symbols, almost exact pattern was observed in the mask. Therefore, we employed a higher precision mask printer to produce the next-round prototype FPC. The resulting line-width data are superimposed in Fig. 4 on top of previous measurements of the sample FPC. As is apparent from the Fig. 4, the new mask successfully provided much better precision (3 μm) of the line width. There found 10 μm offset in the line width between the FPC and the mask. This offset can be diminished by design the line width 10 μm narrower for the mask on purpose.

References
1) T. Hachiya *et al.*, in this report.
2) I. Nakagawa *et al.*, in this report.

Research and development of very long and dense data bus for sPHENIX INTT detector

T. Hachiya,[*1,*2] Y. Akiba,[*1] Y. Kawashima,[*1,*3] T. Kondo,[*4] E. Mannel,[*5] H. Masuda,[*1,*3] G. Mitsuka,[*1]
I. Nakagawa,[*1] R. Nouicer,[*5] K. Shiina,[*1,*3] M. Tsuruta,[*1,*3] and Y. Yamaguchi[*1]

sPHENIX is a major upgrade project of the PHENIX experiment at RHIC.[1] The aim of sPHENIX is to explore the properties of the quark-gluon medium created in high energy heavy ion collisions by using the jets and bottom quarkonia as probes. sPHENIX consists of a tracking detector system followed by electromagnetic and hadron calorimeters with a superconducting solenoid magnet. INTT is an intermediate tracker, which is a silicon detector sandwiched between the MAPS silicon detector and the time projection chamber, as shown in Fig. 1.[2,3] The space available for INTT is small, and the readout electronics (ROC) needs to be placed at least 105 cm away from the detector. INTT is also designed to have a good timing resolution to resolve the collision timing in some beam crossings. In addition, we reuse the ROC of the PHENIX forward silicon vertex detector for INTT. Thus, the interface for the electronics is also pre-defined. This indicates that the data bus for INTT must satisfy the following requirements:

- at least 120-cm long,
- flexible form to fit the tight space,
- a data rate of 200 mega bits per second,
- 100-ohm differential impedance, Z_{diff}, of LVDS data transfer,
- 62 (124) differential pairs (signal lines) for one ladder.

It is challenging to meet all the requirements for the data bus because a long data bus and high-speed transfer of the signal are contradictory. There is no commercial data bus in the market. We carried out research and development of the data bus through an electromagnetic field simulation and by making prototypes.

First, we designed a data bus made from a flexible printed circuit board (FPC) because FPC is capable of establishing a high-density data line with impedance control. We studied the signal integrity by simulation with the realistic layer structure of the FPC, which has a line width (l) and space (s) between lines of 150 μm as shown in Fig. 2. Here, Z_{diff} is calculated based on the intrinsic impedance Z_0 and the space between the pair.[4] From the result, we found that the thickness (w) of FPC should be 400 μm to make Z_{diff} 100 ohm. A thick FPC is usually made by gluing some thin sheets of FPC to each other. However the adhesive to glue the FPC causes a significant loss of signal for the long data bus
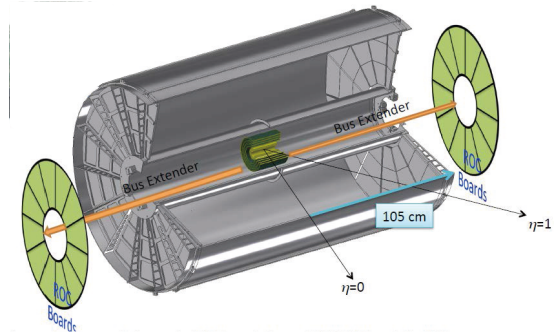
Fig. 1. INTT detector in the sPHENIX tracking system.
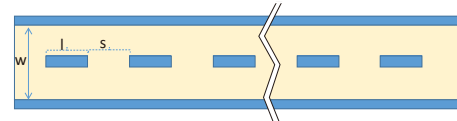
Fig. 2. Cross-sectional view of the FPC.

because of a large dielectric tangent of the adhesive. To solve this problem, we need a thick FPC material with a small dielectric tangent. A liquid crystal polymer (LCP) is a material. Thick LCP sheets (100 μm) with a small dielectric tangent are available in the market.

Second, we studied the uniformity of line and space which is key to keep the impedance for the long data bus. The widths of the signal lines and spaces between the signal lines for the 120-cm-long FPC are measured to examine how accurately the manufacturer produces the FPC.[4] We found that the line width changed periodically depending on the position of the FPC. After further investigation, we pinned down the cause of the problem as the printed circuit on the mask film for the FPC production.

Third, we produced the first version of the prototype FPC to verify our solutions. The prototype FPC has a strip-line structure with 72 signal lines. We are now measuring the line and spaces of the prototype and studying the electrical properties such as impedance, signal loss, and signal distortion.

We plan to make the second and third versions of the prototype in 2018 to ensure that the data bus for INTT meets all the requirements, and mass production will be performed in 2019.

References
1) A. Adare *et al.*, arXiv:1207.6378 [nucl-ex].
2) I. Nakagawa *et al.*, in this report.
3) Y. Yamaguchi *et al.*, in this report.
4) M. Tsuruta *et al.*, in this report.

*1　RIKEN Nishina Center
*2　Division of Natural Sciences, Nara Womens University
*3　Department of Physics, Rikkyo University
*4　Tokyo Metropolitan Industrial Technology Research Institute
*5　Brookhaven National Laboratory

Commissioning of the OEDO beamline

S. Michimasa,[*1] S. Shimoura,[*1] K. Yamada,[*2] S. Ota,[*1] M. Dozono,[*1] N. Imai,[*1] J. W. Hwang,[*1]
M. Matsushita,[*1] K. Yoshida,[*2] Y. Yanagisawa,[*2] K. Kusaka,[*2] M. Ohtake,[*2] D. S. Ahn,[*2] O. Beliuskina,[*1]
N. Chiga,[*2] K. Chikaato,[*3] N. Fukuda,[*2] S. Hayakawa,[*1] E. Ideguchi,[*4] K. Iribe,[*5] C. Iwamoto,[*1] S. Kawase,[*6]
K. Kawata,[*1] N. Kitamura,[*1] S. Masuoka,[*1] H. Miyatake,[*7] D. Nagae,[*2] S. Naimi,[*2] R. Nakajima,[*1]
T. Nakamura,[*8] K. Nakano,[*6] M. Nakano,[*9] S. Ohmika,[*2] H. Otsu,[*2] H. Sakurai,[*2,*10] S. Sato,[*9] P. Schrock,[*1]
H. Shimizu,[*1] Y. Shimizu,[*2] T. Sumikama,[*2] X. Sun,[*2] D. Suzuki,[*2] H. Suzuki,[*2] M. Takaki,[*1] M. Takechi,[*3]
H. Takeda,[*2] S. Takeuchi,[*8] T. Teranishi,[*5] R. Tsunoda,[*1] H. Wang,[*2] Y. Watanabe,[*6] Y. X. Watanabe,[*7]
K. Wimmer,[*10,*2] K. Yako,[*1] H. Yamaguchi,[*1] L. Yang,[*1] and H. Yoshida[*5]

The OEDO system was proposed to produce focused slow-down radioactive-ion (RI) beams in RIBF[1] and has been installed in the High-Resolution Beamline (HRB) in the end of fiscal year 2016.[2] The commissioning of the OEDO beamline has been performed in June 15–21, 2017.

A schematic view of the OEDO beamline and detector setup is shown in Fig. 1. The main components of the OEDO system are a radio-frequency deflector (RFD) synchronized with the cyclotron's RF and 2 sets of superconducting triplet quadrupole (STQ) magnets. For matching to the ion optics of the OEDO system, the momentum dispersion from the BigRIPS to FE9 was tuned to be 13 mm/% at FE9. An Al degrader at FE9 slows down RIs to less than 50 MeV/nucleon. The inset of Fig. 1 shows calculated ion trajectories of the OEDO system on the horizontal plane. The first STQ in the figure provides point-to-parallel transport, resulting in a strong correlation between the angular and time components of the beam. The second STQ works as inverse transformation of the first one. The RFD periodically changes the RI's horizontal angles in order to align them in parallel. The aligned RIs focus at FE11 through the central trajectory in the second half of the OEDO system.

In the commissioning run, long-lived fission prod-

ucts ^{79}Se and ^{107}Pd were produced from a 345-MeV/nucleon ^{238}U beam. The beam energy of ^{79}Se (^{107}Pd) was tuned to be 170 (180) MeV/nucleon in BigRIPS and 45 ± 2 (33 ± 0.5) MeV/nucleon at FE11 after energy reduction by degraders and detectors.

Figure 2 displays correlations between the arrival timing at FE10 and the horizontal hit position at FE11, where Figs. 2(a) and (b) show those without and with RFD operation, respectively. The figures demonstrate that the RFD focuses the ^{79}Se beam and can adjust the beam position. The FE11 horizontal beam spot size was reduced from 25 mm to 15 mm in FWHM, as shown in Fig. 3.
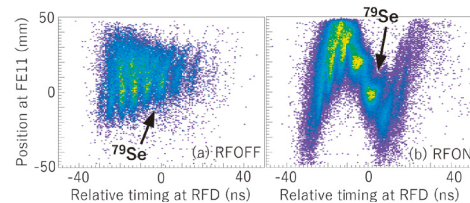
Fig. 2. Ion-optical effect of RFD for beam focusing.
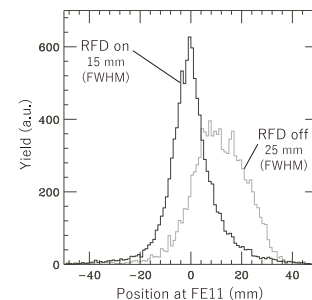
Fig. 3. Beam focusing of ^{79}Se at FE11 with and without RFD.

The OEDO beamline was successfully launched. Further data analysis is ongoing to improve the transmission of the beamline and to develop an effective tuning procedure for upcoming physics experiments.

Fig. 1. Schematic view of the OEDO beamline. The ion optics in the OEDO system are also shown.

[*1] Center for Nuclear Study, the University of Tokyo
[*2] RIKEN Nishina Center
[*3] Dept. of Physics, Niigata University
[*4] RCNP, Osaka University
[*5] Dept. of Physics, Kyushu University
[*6] Dept. of Advanced Energy Eng. Sci., Kyushu University
[*7] Wako Nuclear Science Center, KEK
[*8] Dept. of Physics, Tokyo Institute Technology
[*9] Dept. of Physics, Rikkyo University
[*10] Dept. of Physics, The University of Tokyo

References
1) S. Shimoura et al., CNS-REP-93, 56 (2015).
2) S. Michimasa et al., RIKEN Accel. Prog. Rep. 50, 19 (2017).

Optimization of sextupole magnets in the BigRIPS fragment separator for a high-purity RI beam

T. Sumikama,[*1] H. Suzuki,[*1] D. S. Ahn,[*1] N. Fukuda,[*1] Y. Shimizu,[*1] H. Takeda,[*1] K. Kusaka,[*1] Y. Yanagisawa,[*1] M. Ohtake,[*1] and K. Yoshida[*1]

The purification of radioactive-isotope (RI) beams is one of the most important issues especially for nuclear reaction studies with the intensity of 10^5 particles per second or more, to reduce the total beam rate at beam-line detectors, which are used for the particle identification of RI beams. The reaction studies for the long-lived fission products at a low energy of 20 or 50 MeV/nucleon are typical examples.[1] The first stage of the BigRIPS fragment separator is used for the separation of RI beams.[2] Higher-order aberrations of the ion optics in the separator have negative influences on not only the beam size and transmission efficiency but also the separation from contaminants. Sextupole magnets have been employed to reduce the higher-order aberrations of one given isotope in standard optics. For the contaminants, however, the higher-order aberrations remained. In the present study, the sextupole magnets were optimized for the separation of contaminants to obtain high-purity RI beams.

One of the largest aberrations is the focus shift as a function of the momentum. It is given by the $(x|a\delta_{B\rho})$ term of the ion optical matrix elements, where a is the beam angle in the x direction, and $\delta_{B\rho} = (B\rho - B\rho_0)/B\rho_0$. The magnetic rigidity, $B\rho$, is used instead of the momentum to consider both the given isotope and other contaminants. The aberration of $(x|a\delta_{B\rho})$ was removed by two sextupole magnets between two dipole magnets, D1 and D2, in the first stage. However, extra aberrations appeared. The aberrations were compensated by two more sextupole magnets with the opposite polarity in standard optics.

The magnetic rigidity of the contaminants is changed by a wedge-shaped degrader placed between D1 and D2. The focus shift of contaminants can be removed by the forth sextupole magnet after D2, but in standard optics, the shift increased because of the opposite polarity. To reduce the aberrations not only for the given isotope but also for the contaminants, the polarity of the forth sextupole magnet was inverted, and the first one before D1 was not used, for simplicity in the present study. Figure 1 shows the third order calculation of the ion optics of the first stage of BigRIPS by using the COSY INFINITY code.[3]

A ^{93}Zr beam was used to test this optimization. A 4-mm-thick Al wedge degrader was used for the isotope separation. The dependece of a and $\delta_{B\rho}$ on x at F2 were measured for ^{93}Zr and neighboring isotopes. The sextupole magnets were tuned so as to cancel out the a and $\delta_{B\rho}$ dependences. Figure 2 shows the a versus
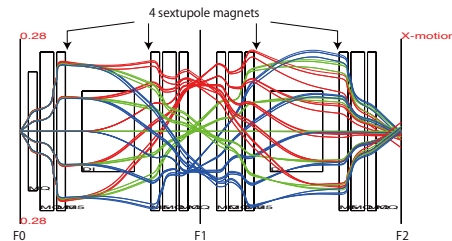
Fig. 1. Third-order ion optics of the BigRIPS first stage with the modified optimization of the sextupole magnets (SXs). The polarity of the forth SX is inverted from standard optics. The red and blue lines are -3% and $+3\%$ from the central momentum, respectively.
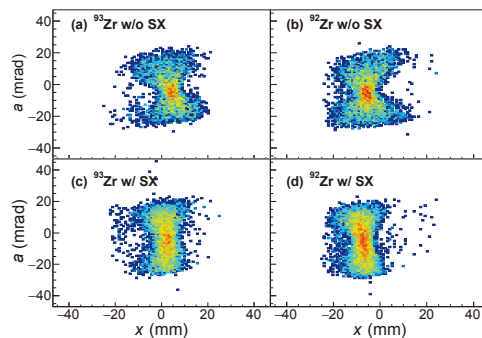
Fig. 2. Angle versus position distributions in the lateral direction at F2 for (a) ^{93}Zr without SX, (b) ^{92}Zr without SX, (c) ^{93}Zr with SX, and (d) ^{92}Zr with SX. The momentum distribution was $\pm 3\%$.

x plot for ^{93}Zr with and without the sextupole magnets. The blur at the large a region in Fig. 2(a) was reduced by applying the sextupole magnets as shown in Fig. 2(c). The distribution obtained for ^{92}Zr was similar to that for ^{93}Zr, as shown in Fig. 2(d). The separation between these isotopes was improved from 1.7σ to 2.5σ.

References
1) T. Sumikama et al., RIKEN Accel. Prog. Rep. **50**, 165 (2017).
2) T. Kubo et al., Prog. Theor. Exp. Phys. **2012**, 03C003 (2012).
3) K. Makino, M. Berz, Nucl. Instrum. Methods A **558**, 346 (2006).

*1　RIKEN Nishina Center

Improvement of transmission efficiency for the rare-RI ring

Y. Yamaguchi,[*1] S. Naimi,[*1] Y. Abe,[*1] D. Nagae,[*1] S. Omika,[*1,*2] A. Ozawa,[*1,*3] F. Suzaki,[*1] T. Uesaka,[*1] M. Wakasugi,[*1] and T. Yamaguchi[*1,*2] for the Rare RI Ring collaboration

The injection and extraction efficiency of the rare-RI ring (R3) is one of the main factors used to determine the feasibility of experiments. Based on the triggered events for injection that are generated at the F3 focal plane of BigRIPS, the required extraction efficiency from R3 is 1% or more for the region where the production rate is 0.1 cps. However, the extraction efficiency in the third machine study,[1] where unstable nuclei were successfully extracted for the first time, was less than 0.2% for the reference particle of ^{78}Ge. This is insufficient to conduct an experiment within a reasonable beamtime period using R3. This report describes the improvement of transmission efficiency obtained in the fourth machine study using new beam injection optics.

The particles produced and identified in the first stage of BigRIPS are transported to R3 through a long beam line including the SHARAQ spectrometer. Recently, the OEDO system[2] was completed on the long beam line by installing new magnets and rearranging the existing magnets as shown in Fig. 1. Because the standard OEDO optics is not suited for our injection, we recalculated the injection optics from F3 of BigRIPS to R3. Achromatic (F-E9, S0) and momentum-dispersive (F4, F5, F6, and F-E7) focal planes were arranged in the long beam line to ensure that the transmission efficiency from F3 to S0 is close to 100%. The section from S0 is very important when considering the injection optics. It is necessary to consider dispersion matching in the horizontal direction while paying attention not to diverge in the vertical direction, because after the SHARAQ spectrometer, the apertures of the beam ducts are narrower compared with the for-

Fig. 2. Transmission efficiency of ^{78}Ge. The ILC2 is located just before the injection septa of R3. The RMD4 and ELC are located in the next straight section of the kicker and the region after extraction, respectively. The achieved extraction efficiency was larger than 1% as indicated by the red circle in the ELC column.

mer stage. In the fourth machine study, we carefully performed emittance matching between the injection beam emittance and the acceptance of R3. This is because, emittance mismatch was the main cause of the poor extraction efficiency of the third machine study.[3] The matching point is the kicker center; however, there was no position detector there. Therefore, two PPACs at ILC2 were used to adjust the beam emittance.

Figure 2 shows the result of the transmission efficiency of ^{78}Ge. There is no emittance gate at F3. The excitation timing and magnetic field strength of the kicker are optimized. The circulation time at R3 is about 700 μs. The injection efficiency is better than the previous one as indicated in the RMD4 column. The extraction efficiency is also improved by more than 10 times as indicated in the ELC column.

Experiments using R3 are now ready to be conducted for regions where sufficient statistics could be obtained. Because further improvement in transmission efficiency is very useful when conducting experiments at extremely rare-RI regions in the near future, we aim for a measurement efficiency of 20%.

Fig. 1. Long beam transport line from BigRIPS to R3 with OEDO system.

References

1) D. Nagae et al., RIKEN Accel. Prog. Rep. **50**, 18 (2017).
2) S. Michimasa et al., RIKEN Accel. Prog. Rep. **50**, 19 (2017).
3) S. Naimi et al., in this report.

*1   RIKEN Nishina Center
*2   Department of Physics, Saitama University
*3   Institute of Physics, University of Tsukuba

Investigation of transmission efficiency loss at Rare-RI Ring

S. Naimi,[*1] Y. Yamaguchi,[*1] Y. Abe,[*1] D. Nagae,[*1] S. Omika,[*1,*2] A. Ozawa,[*3] F. Suzaki,[*1] T. Uesaka,[*1] M. Wakasugi,[*1] and T. Yamaguchi[*2] for the Rare RI Ring collaboration

We have conducted a test experiment at the Rare-RI Ring (Fig. 1) using Rare Isotopes (RIs) produced from ^{238}U beam on Be target at RIBF.[1] The aim was to demonstrate the mass measurement principle of Rare Isotopes using the Rare-RI Ring.[1,2] In this experiment, the total transmission efficiency at the extraction (ELC) was very low (0.14%), which is not suited for mass measurement of RIs with very low yield. To investigate the origin of the efficiency loss, we have conducted simulation using MOCADI. As it can be seen from Fig. 2, the transmission efficiency loss is dominated by loss at the injection (between ILC2 and Kicker) and extraction (between Kicker and ELC). In order to investigate the reason for such large drop in efficiency, we examined the emittance evolution at the injection. Since it was not possible to measure the emittance during the experiment, we deduce the emittance from elements matrix calculated in COSY
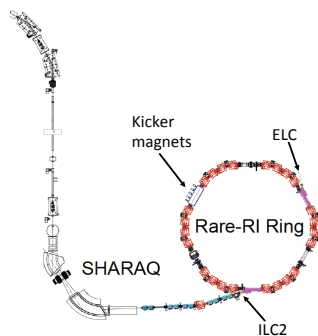
Fig. 1. Overview of the Rare-RI Ring (R3).
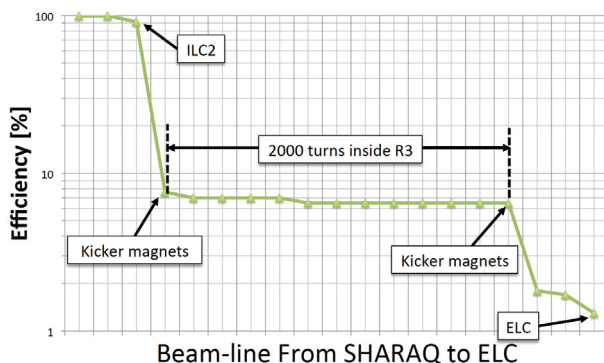
Fig. 2. MOCADI simulation of transmission efficiency.
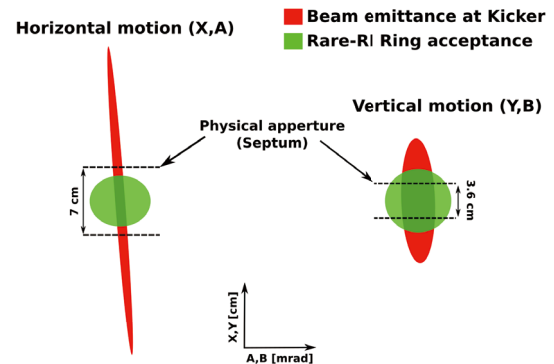
Fig. 3. Horizontal and vertical beam emittance at the Kicker compared to Rare-RI Ring acceptance. Typical beam emittance was around $50 \sim 80 \ mm \cdot mrad$.

Infinity based on the initial experimental emittance. We compared the emittance at Kicker magnets to the Rare-RI Ring acceptance in Fig. 3. It is clear that there is a mismatch between the beam emittance and the storage ring acceptance, especially in the horizontal direction, since the dispersion matching condition should be also satisfied for a stable particle motion in the ring.[3] The total transmission in Fig. 2 is overestimated by simulation (experimental value 0.14%). We believe this is due to observed vertical and horizontal shift of the beam, which is still under investigation.

We can also evaluate the efficiency from the intersection of the beam emittance and the storage ring acceptance taking into account the physical aperture of the injection septum located at the ring entrance. The evaluated efficiency after the Kicker is consistent with experimental efficiency of about 2% measured behind the Kicker. From this result, we conclude that the loss in transmission efficiency is mainly due to emittance mismatch between the beam emittance and the Rare-RI Ring acceptance. A compromise between dispersion matching and emittance matching should be found in order to increase the transmission efficiency. For this purpose, we designed a new injection optics, which was tested end of November 2017. We have improved the over all transmission efficiency by 13 times. Details of the simulation and results are discussed in details in Ref. 4).

References
1) D. Nagae et al., Accel. Prog. Rep. **50**, 18 (2017).
2) D. Nagae et al., in this report.
3) A. Ozawa et al., Prog. Theor. Exp. Phys. **2012**, 03C009 (2012).
4) Y. Yamaguchi et al., in this report.

---

*1　RIKEN Nishina Center
*2　Department of Physics, Saitama University
*3　Institute of Physics, University of Tsukuba

Isochronous condition in Rare RI Ring

Y. Abe,[*1] Y. Yamaguchi,[*1] M. Wakasugi,[*1] D. Nagae,[*1] S. Naimi,[*1] S. Omika,[*1,*3] A. Ozawa,[*1,*2] F. Suzaki,[*1] T. Uesaka,[*1] T. Yamaguchi,[*1,*2,*3] and for the Rare RI Ring collaboration

The Rare RI Ring (R3) is an isochronous storage ring used to measure masses of short-lived rare nuclei. The expected precision of the measured masses is of the order of 10^{-6}. The precision of the isochronism is one of the key issues regarding R3, because it directly determines the precision in mass determination for poor statistics, which are expected for rarely produced exotic nuclei. Two magnets at both ends of each sector are additionally equipped with ten trim coils to form the isochronous magnetic field with a precision of 1 ppm over a wide range of momentum values. The isochronism of the order of 1 ppm is realized by adjusting the currents of the trim coils.

In the third machine study, we used secondary beams around ^{78}Ge nuclei, and the isochronous condition was tuned to ^{78}Ge. Figure 1(a) shows the two-dimensional plot of events for ^{78}Ge, and the histogram of the revolution time (b). The isochronism was achieved as 5.4×10^{-6} in σ, within the momentum range of $\pm 0.3\%$.[1)] The obtained isochronism has not yet reached to the target value of 1 ppm. As can be seen in Fig. 1(a), the revolution time is still slightly correlated to the momentum due to imperfections in the isochronous conditions.

We performed a fourth machine study in November by using the same secondary beams to improve the isochronism. Figure 2 shows the results obtained after fine tuning the trim coils in this experiment. The isochronism was improved, and was achieved as 3.7×10^{-6} in σ. This seems to come from the instability of the main magnetic field in R3 caused by the instability of the power supply. In fact, the magnetic field measured using an NMR probe fluctuated within

Fig. 2. Present result of isochronism. (a) Correlation(s) between revolution time and the momentum difference for ^{78}Ge. (b) Distribution of revolution time of ^{78}Ge with Gaussian fitting (broken line).
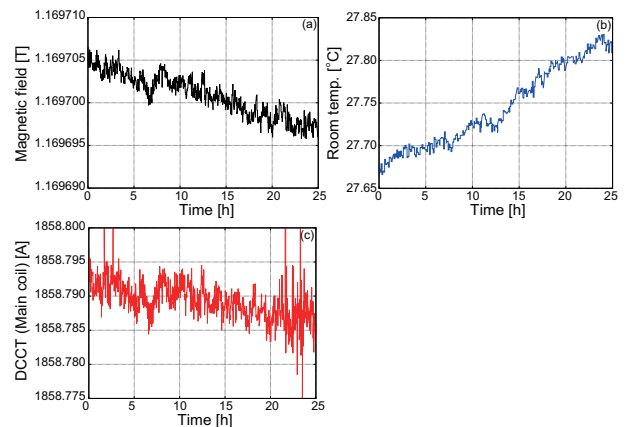
Fig. 3. Trend graphs obtained in one day; (a) Magnetic field measured by NMR probe. (b) Room temperature. (c) DCCT value of main power supply.

8.5×10^{-6} of the full width during the measurements. We cannot see a strong correlation between the revolution time and the magnetic field; however, it would be necessary to reduce the fluctuation of the magnetic field to further improve the isochronism.

The above measurement time was about one hour. However, a longer time, such as several days, is necessary for mass measurements of exotic nuclei. Figure 3 shows the trends of the magnetic field, room temperature, and DCCT value of the main power supply during one day. These data were obtained four days after the magnets were excited. In order to measure the masses of exotic nuclei with high precision, it may be necessary to introduce technology to reduce the effect of this drift in the near future.

Fig. 1. Result of isochronism measurements in the third machine study. (a) Correlation(s) between revolution time and the momentum difference for ^{78}Ge. (b) Distribution of revolution time of ^{78}Ge with Gaussian fitting (broken line).

Reference
1) Y. Yamaguchi et al., RIKEN Accel. Prog. Rep. **50**, 183 (2017).

[*1] RIKEN Nishina Center
[*2] Institute of Physics, University of Tsukuba
[*3] Department of Physics, Saitama University

Present status of data analysis of commissioning experiment using exotic nuclei

D. Nagae,[*1] S. Omika,[*1,*2] Y. Abe,[*1] Y. Yamaguchi,[*1] F. Suzaki,[*1] K. Wakayama,[*2] N. Tadano,[*2]
R. Igosawa,[*2] K. Inomata,[*2] H. Arakawa,[*2] K. Nishimuro,[*2] T. Fujii,[*2] T. Mitsui,[*2] T. Yamaguchi,[*2,*3]
T. Suzuki,[*2] S. Suzuki,[*3] T. Moriguchi,[*3] M. Amano,[*3] D. Kamioka,[*3] A. Ozawa,[*3] S. Naimi,[*1] Z. Ge,[*1,*2]
Y. Yanagisawa,[*1] H. Suzuki,[*1] H. Baba,[*1] S. Michimasa,[*4] S. Ota,[*4] G. Lorusso,[*5] Yu.A. Litvinov,[*6]
M. Wakasugi,[*1] T. Uesaka,[*1] and Y. Yano[*1]

The Rare RI Ring[1] is an isochronous storage ring constructed to measure the masses of short-lived rare nuclei using the time-of-flight (TOF) measurement method. In 2016, we performed a commissioning experiment using exotic nuclei with well-known masses[2] to confirm the feasibility and principle of mass determination using the following equation:

$$\frac{m_1}{q} = \frac{m_0}{q}\frac{T_1}{T_0}\sqrt{\frac{1-\beta_1^2}{1-\left(\frac{T_1}{T_0}\beta_1\right)^2}},\tag{1}$$

where $m_{0,1}/q$ denote the mass-to-charge ratio of the reference particle and particle of interest, respectively; $T_{0,1}$ are the revolution times of these particles; and β_1 is the velocity of the particle of interest. Because the isochronous condition is adjusted for the reference particle, isochronism is not fulfilled for the particles of interest. To evaluate masses of nuclei with non-isochronism, we correct their revolution time T_1 by the velocity measured upstream.

Exotic nuclei around ^{78}Ge were produced by in-flight fission of a 345 MeV/nucleon primary beam of ^{238}U on a 10-mm thick ^{9}Be target. We identified these nuclei before the F3 achromatic focus of BigRIPS. These nuclei were injected into the ring using the individual injection method with the fast kicker system.[3] The isochronous magnetic field in the ring was adjusted for the reference particle ^{78}Ge with a precision of 5.4 ppm for a momentum spread of $\pm$ 0.3%.[4] The exotic nuclei ^{79}As, ^{77}Ga, ^{76}Zn, and ^{75}Cu were successfully stored for about 0.7 ms and extracted from the ring. These particles, ^{79}As, ^{78}Ge, ^{77}Ga, ^{76}Zn, and ^{75}Cu, were circulated 1904 turns, 1880 turns, 1855 turns, 1828 turns, and 1801 turns, respectively. $T_{0,1}$ for each nuclei were deduced from the TOF between the S0 achromatic focus of SHARAQ and the ring exit ELC, and the turn number. β_1 was deduced from $B\rho$ and the TOF between the F3 achromatic focus of BigRIPS and S0.

Figure 1 shows the deviations of experimental m/q from their literature values listed in AME2016[5] as a function of m/q. The mass accuracies prelimi-

nary obtained for ^{79}As, ^{77}Ga, ^{76}Zn, and ^{75}Cu were -2.2×10^{-5}, 1.9×10^{-5}, 2.5×10^{-5}, and 3.5×10^{-5}, respectively. The statistical uncertainty that is taken into account comes from measurements of T_0 ($\sim 10^{-6}$) and T_1 ($\sim 10^{-6\sim-5}$). Systematic uncertainty coming from β determination is of the order of about 10^{-5}.

A notable difference is observed between the experimental m/q and their literature values. The disagreement comes from the difference between the measured β_1 and in-ring β_1, which is due to the position-sensitive detector PPAC that was used at F6 for momentum tagging. Further analysis for correction of this effect is in progress. For future experiments, a position-sensitive detector with thin foil is needed to reduced the disagreement. Such a detector is now under development.[6,7]
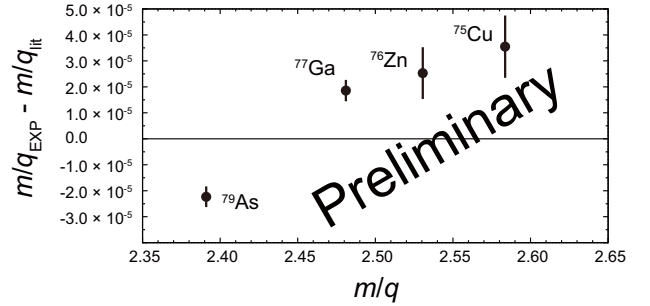
Fig. 1. Differences between the m/q values obtained in this analysis and the corresponding values from the literature.[5] The error bars that are shown contain only statistical contributions.

References
1) A. Ozawa *et al.*, Prog. Theor. Exp. Phys. **2012**, 03C009 (2012).
2) D. Nagae *et al.*, RIKEN Accel. Prog. Rep. **50**, 18 (2017).
3) H. Miura *et al.*, RIKEN Accel. Prog. Rep. **49**, 154 (2017).
4) Y. Yamaguchi *et al.*, RIKEN Accel. Prog. Rep. **50**, 183 (2017).
5) M. Wang *et al.*, Chin. Phys. C **41**, 030003 (2017).
6) Z. Ge *et al.*, In this report.
7) H. Li *et al.*, In this report.

[*1] RIKEN Nishina Center
[*2] Department of Physics, Saitama University
[*3] Institute of Physics, University of Tsukuba
[*4] Center for Nuclear Study, University of Tokyo
[*5] Department of Physics, University of Surrey
[*6] GSI Helmholtzzentrum für Schwerionenforschung

The progress of on-line commissioning study on parasitic production of low-energy RI-beam system (PALIS) at BigRIPS

T. Sonoda,[*1] M. Wada,[*2] M. Reponen,[*3] I. Katayama,[*1] V. Sonnenschein,[*4] M. Oohashi,[*4] H. Tomita,[*4]
S. Nishimura,[*1] H. Iimura,[*5] T. M. Kojima,[*1] A. Deuk Soon,[*1] N. Fukuda,[*1] T. Kubo,[*1] K. Kusaka,[*1]
N. Inabe,[*1] Y. Shimizu,[*1] H. Suzuki,[*1] H. Takeda,[*1] Y. Yanagisawa,[*1] K. Yoshida,[*1] F. Arai,[*1] S. Arai,[*1]
Y. Ito,[*1] M. Rosenbusch,[*1] K. Okada,[*6] P. Schury,[*2] and H. Wollnik[*7]

The progress of the on-line commissioning study on parasitic production of low-energy RI-beam system (PALIS)[1] is reported. The beam time was dedicated for 24 hours in FY2017. Although PALIS can operate in a parasitic manner during the BigRIPS main experiment, the present commissioning study was used a main beam. The main aim of this experiment, which is the confirmation of photo-ionized RI-ions after thermalization in the gas cell, was not achieved in this limited experimental period. However, the ion extraction behaviors in terms of the degrader thickness and laser wavelength were investigated during RI-beam implantation to the gas cell.

The main beam was chosen from Cu isotopes such as ^{66}Cu (5×10^4 pps/pnA primary beam) and ^{68}Cu (2×10^4 pps/pnA primary beam), other isotope beams such as ^{67}Ni (5×10^2 pps/pnA primary beam) were also included. We adjusted the primary beam intensity from 0.01 pnA to 10 pnA. The RI-beams were first decelerated by a copper degrader, where the energy was reduced from around 280 to 10 MeV/nucleon, and then thermalized in the gas cell. A part of the RI-beams are stopped within the finite gas cell. In the case of ^{68}Cu, we estimated a stopping efficiency of about 10% by LISE calculation, when the gas cell pressure is set at one atmosphere of argon gas. When the high energy RI-beams enter the gas cell, gas ionization occurs by the beam itself. These ions comprise of mainly argon ions, and impurity ions included in the gas. We detected these ions in the high-vacuum region, after the ions were extracted from the gas cell and transported to the ion detector via SPIG and QMS in the differential pumping region. Figure 1 shows the ion intensity around mass 68 (a.m.u) when the degrader thickness was varied (circle points scaled by the left vertical axis). We remark that the behavior of this ion signal is consistent with the calculated estimation from the stopping efficiency (square points scaled by the right vertical axis). We confirmed that the number of ions produced by RI-beams is maximum, when the stopping efficiency is maximum.

As we could not find the photo-ionized radioac-
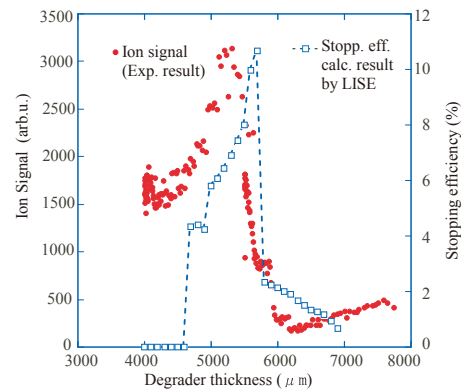
Fig. 1. The extracted ion signal (circle points scaled by the left vertical axis) and the calculated stopping efficiency (square points scaled by the right vertical axis) versus the degrader thickness.

tive Cu ion signal, we confirmed the performance of the laser ionization, extraction and ion transportation by using stable copper atoms that were evaporated from a filament. As shown in Fig. 2, photo-ionized $^{63-65}$Cu ions were observed even when RI-beams were implanted into the gas cell. In the next beam time, we will further investigate the stopping efficiency, optimum size of the gas cell and space charge effect.
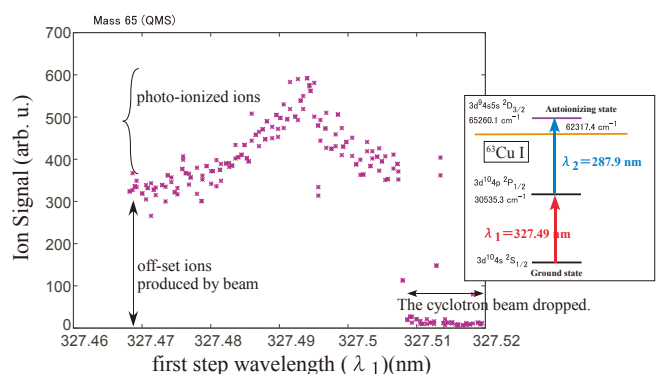
Fig. 2. The wavelength scan for the first-step laser versus the photo-ionized Cu ions, when the RI-beams enter the gas cell and Cu atoms are evaporated by a filament.

Reference
1) T. Sonoda *et al.*, AIP Conf. Proc. **1104**, 132 (2009).

*1 RIKEN Nishina Center
*2 High Energy Accelerator Research Organization (KEK)
*3 Department of Physics, University of Jyvaskyla
*4 Faculty of Engineering, Nagoya University
*5 Japan Atomic Energy Agency
*6 Department of Physics, Sophia University
*7 Department of Physics, New Mexico State University

Improved wide bandwidth mass analysis with MRTOF-MS

P. Schury,[*1] M. Wada,[*1,*2] M. Rosenbusch,[*2] Y. Ito,[*2] H. Haba,[*2] Y. Hirayama[*1] D. Kaji,[*2] S. Kimura,[*1,*2,*3] H. Koura,[*4] H. Miyatake,[*1] J. Y. Moon,[*7,*1] K. Morimoto,[*2] K. Morita,[*2,*5] A. Ozawa,[*2,*3] M. Rosenbusch,[*2] M. Reponen,[*2] A. Takamine,[*2] T. Tanaka,[*2,*5] Y. X. Watanabe,[*1] and H. Wollnik[*6]

In recent studies of fusion-evaporation reactions using GARIS-II,[1] higher order evaporation channel (pxn, αxn, etc.) products were observed with the multi-reflection time-of-flight mass spectrograph[2] (MRTOF-MS). As exemplified in Fig. 1, in many cases, such products had A/q sufficiently different from the neutron evaporation products of primary interest as to make a different number of laps within the MRTOF. As a result, they have a different flight path than the reference ions, which complicates the mass analysis.

We have previously[3] developed an analytic framework for making use of such wide mass bandwidth spectra. However, the technique was only accurate on the few-ppm level—sufficient for identification, but insufficient for the precision mass analysis we desire. While the earlier technique was useful at identification of ions within a large mass bandwidth, it was also complicated and required at least two measurements be performed in series under substantially similar conditions, making it prone to errors from e.g. slight voltage drifts. Utilizing our presently unique ion preparation trap geometry, we have been able to modify the operation of the MRTOF to allow two measurements to be made nearly in parallel, a scheme we call "concomitant referencing." This in turn has allowed for development of an improved method to determine the masses of ions within a large mass bandwidth.

In the present implementation of concomitant referencing, the measurement cycle is split into two subcycles. Reference ions making different number of laps in each of the sub-cycles are utilized to precisely determine the circulation period, T_{ref}, of the reference ions during the measurement. We then use the original wide mass bandwidth analysis method to determine the number of laps analyte ions made in the MRTOF, and to determine their m/q with sufficient accuracy for identification . Once the number of laps are known, the measured T_{ref} is used to adjust the reference ion ToF, t_{ref}, to match the flight path of the analyte ion:

$$t'_{ref} = t_{ref} - \Delta n \cdot T_{ref}, \qquad (1)$$

where Δn is the difference in laps between reference and analyte. Finally, t'_{ref} is used in the single-reference analysis methodology[5] to determine the analyte ion's
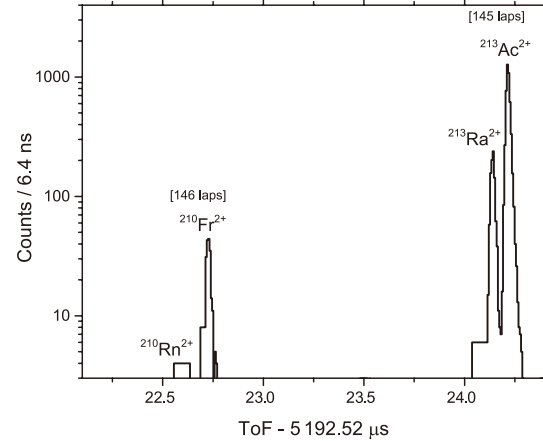
Fig. 1. Portion of online time-of-flight spectrum observed in the study of ^{169}Tm(^{48}Ca, X) reaction. The A=213 isotopes performed 145 laps in the MRTOF, as did the reference ions. The A=210 isotopes performed 146 laps in the MRTOF, complicating the mass analysis.

mass-to-charge ratio:

$$m_{analyte} = m_{ref} \left(\frac{t_{analyte} - t_0}{t'_{ref} - t_0} \right)^2, \qquad (2)$$

where t_0 is an inherent delay between the ions leaving the flat ion trap and the start of the TDC, previously[4] determined to be t_0=45(5) ns.

Offline tests with ^{85,87}Rb have demonstrated an accurate relative mass accuracy of $\frac{\delta m}{m} \sim 10^{-7}$ up to Δn=4. This makes MRTOF mass spectrometry highly-competitive with storage rings[6–8] in terms of mass accuracy and bandwidth.

References
1) D. Kaji et al., Nucl. Instrum. Methods Phys. Res. B **317**, 311 (2013).
2) P. Schury et al., Nucl. Instrum. Methods Phys. Res B **335**, 39 (2014).
3) P. Schury et al., Int. J. Mass Spectrom. **359**, 19 (2013).
4) P. Schury et al., Phys. Rev. C **95**, 251 (2017).
5) Y. Ito et al., Phys. Rev. C **88**, 011306(R) (2013).
6) F. Bosch, Yu. A. Litvinov, Int. J. Mass Spectrom. **349**, 151 (2013).
7) J. W. Xia et al., Nucl. Instrum. Methods Phys. Res. A **488**, 11 (2002).
8) M. Wakasugi, Rare RI Ring Collaborations, JPS Conf. Proc. 6 010020 (2015).

*1   KEK Wako Nuclear Science Center (WNSC)
*2   RIKEN Nishina Center
*3   Institute of Physics, University of Tsukuba
*4   Advanced Science Research Center, JAEA
*5   Dept. Physics, Kyushu University
*6   Dept. Chem. and BioChem., New Mexico State University
*7   Institute for Basic Science

Surface temperature measurements of the high power beam dump of the BigRIPS separator

K. Yoshida,[*1] Y. Yanagisawa,[*1] Z. Korkulu,[*1] H. Takeda,[*1] K. Kusaka,[*1] N. Fukuda,[*1] and T. Kubo[*1,*2]

The surface temperatures of the high-power beam dump[1,2] of the BigRIPS separator were measured during the irradiation of the ^{48}Ca beam with a beam power of 8.3 kW in order to evaluate the cooling power of the beam dump. The beam dump consists of the side dump and the exit dump. The two exit beam dumps with 1 mm and 3 mm wall thicknesses were designed to handle various ion beams up to ^{238}U with intensities of up to 1 pμA.[2] The exit beam dump with 3 mm wall thickness and the side dump were constructed in 2007. Since then, they have been successfully operated with various beams. The design of the beam dumps was based on the sophisticated thermal model simulation;[1,2] however, its validity has not been well verified because of the limitation of available beam intensity. With the intense ^{48}Ca beam, which recently became available, temperatures of the inner-side exit beam dump were measured by using the thermocouples mounted on the dump.[3] The observed temperatures were consistent with the thermal model simulations, indicating that the beam dump has the expected cooling power. However, the results have some ambiguity. The highest temperature in the beam dump is expected at the beam impinging surface, but the thermocouples measure temperatures 3 mm behind the dump surface. In order to obtain clearer results, measurements of the surface temperature are highly desired.

The surface temperature of the outer-side exit dump was measured with the compact thermo-viewer camera IP160 manufactured by OPTRIS. The camera was placed at the side window of the beam dump chamber, as shown in Fig. 1. A vacuum window made out of BaF$_2$ was used to observe the infrared image of the dump surface, which was irradiated with the ^{48}Ca beam having an energy of 345 MeV/n and intensity of 500 pnA. The beam size on the dump surface was estimated to be 20 mm (X) and 30 mm (Y) from the separately measured beam emittance. A BaF$_2$ crystal with a thickness of 13 cm was placed between the vacuum window and the camera to reduce radiations (γ-rays and neutrons) from the beam dump. For further reduction of radiations, 20 cm thick concrete shielding blocks surrounded the camera. Cooled water, with a temperature of 13°C, pressure of 1.0 MPa, and flow speed of 10 m/s, were supplied to the dump as the coolant. The temperatures were also measured by using a thermocouple (TC) mounted on the dump 3 mm behind the dump surface.

The observed thermal image is shown in Fig. 2. The beam hitting portion of the beam dump is seen as a hot spot. Its size is about 30 mm (X) × 10 mm (Y), and the
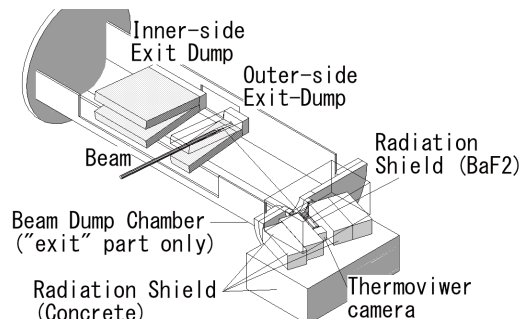
Fig. 1. Setup for the surface temperature measurement of the beam dump.

Fig. 2. Thermal image of the beam dump with 8.3 kW ^{48}Ca beam irradiation.

temperatures are 62 and 23°C according to the beam on and off. The temperatures of the TC are 15.4 and 13.6°C. The temperatures observed by the camera need to be corrected for the emissivity and the attenuation of the vacuum window and the BaF$_2$ crystal. The calibration data was taken by changing the temperatures of the cooling water in off-line condition. The observed temperatures varied from 23 to 32°C when temperatures of the dump varied from 15 to 45°C. With the assumption of the linear relation between both the temperatures, the observed temperature 65°C corresponds to an actual temperature of 147°C.

ANSYS[4] simulation for this condition shows that the spot temperature is 170°C and the temperature at TC is 46°C. Both temperatures are higher than the observed ones. The observed temperatures can be reproduced by modifying the beam size to 30 mm (X) and 22 mm (Y) and shifting the center of the beam 0.6 mm downward (this corresponds to 6 mm shift on the dump surface). The observed spot size is also reproduced by the modification.

References

1) N. Fukuda *et al.*, RIKEN Accel. Prog. Rep. **41**, 119 (2008).
2) K. Yoshida *et al.*, Nucl. Instrum. Methods B **317**, 373 (2013).
3) K. Yoshida *et al.*, RIKEN Accel. Prog. Rep. **49**, 159 (2016).
4) ANSYS Inc. Product Release 18.0, USA.

*1　RIKEN Nishina Center
*2　FRIB/NSCL, Michigan State University

Thermo-mechanical calculations of the high power beam dump of the BigRIPS separator

Z. Korkulu,[*1] K. Yoshida,[*1] Y. Yanagisawa,[*1] and T. Kubo[*1,*2,*3]

The beam dump is a critical component for the in-flight fragment separator that uses high-power primary beams at the RI Beam Factory (RIBF). The exit beam dump and side dump of the BigRIPS fragment separator were designed and constructed in 2007. The maximum beam power is planned to be 82 kW for ^{238}U at 345 MeV/nucleon, and most of the beam power is dissipated to a target and a beam dump. The beam dump system has been successfully operated so far, although the available beam power is still less than the goal power value. The temperature of the beam dump was measured and the observed temperature was compared with the value calculated by the finite element analysis (FEA).[1] An important aspect in high-power beam dump design is to limit the maximal temperature due to beam energy loss in the material. Controlling this absorbed power is a key challenge. The technical challenges include overheating and excessive thermo-mechanical stress load variations caused by the high beam intensity. Since the available beam intensity is lower than the goal value, the finite element thermal analysis code, ANSYS,[2] was used to study these technical issues for 1 particle μA which corresponds to a beam power of 82 kW in the case of ^{238}U. Steady state structural FEA was performed to estimate the static stress around the exit beam dump.

To perform the thermo-mechanical simulation a 3D solid model of the exit beam dump was considered and meshed with high-order tetrahedral elements, which is shown in Fig. 1. The exit dump is a V-shaped CuCrZr plate equipped with screw tubes (M8 1.25-pitch screw formed every 14 mm) as cooling channels.[3] Cooled water with a temperature of 13°C, a pressure of 1.0 MPa, and a flow speed of 10 m/s was supplied to the dump as the coolant. The heat transfer coefficient of the screw tube was calculated (using JAERI formula[4]) and used in the simulation. The mechanical temperature-dependent properties of the CuCrZr for the FEA are taken from similar work.[5] The literature results show that the CuCrZr alloy exhibits good strength and plasticity simultaneously between room temperature and 350°C. The value of the ultimate tensile strength is 308±15 MPa at 350°C. This ensures that the CuCrZr alloy has enough strength to be applied under the high temperature condition.

Figure 1 shows the solid model of the exit beam dump and the result of the equivalent stress on the
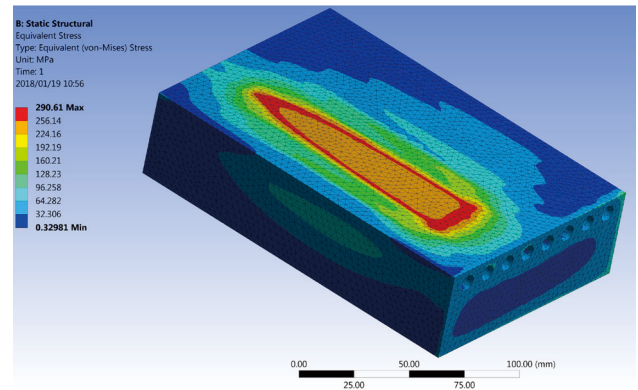
Fig. 1. Calculated equvialent (von-Misses) stress on the exit beam dump.

exit beam dump by the static structural analysis. The beam size at the stopping location was estimated from the first-order optics calculation of the BigRIPS separator with respect to the primary beam trajectory. In the calculation, the input power was given as the heat generation, which is approximately 49 W/mm^3. The maximum temperature of the beam center is approximately 355°C and the maximum von-Misses stress is 291 MPa under the above mentioned conditions.

The simulation results showed that the maximum temperature exceeds the critical limit (350°C) to avoid creep and softening under irradiation for the CuCrZr alloy while the maximum stress is found at the limit of the ultimate tensile strength. The thermal creep effect needs to be considered at a temperature more than 350°C. When the thermal and thermo-mechanical data can be measured, the beam dump should be tested with a high intensity beam in order to understand and characterize the thermo-mechanical challenges and validate simulation results.

References
1) K. Yoshida *et al.*, RIKEN Accel. Prog. Rep. **49**, 159 (2016).
2) ANSYS, Inc. Product Release 16.0, USA.
3) K. Yoshida *et al.*, Nucl. Instrum. Methods B **317**, 373 (2013).
4) J. Boscary *et al.*, Fusion Eng. Des. **43**, 147 (1998).
5) D. Zhu *et al.*, J. Nucl. Mater. **455**, 185 (2014).

---

*1　RIKEN Nishina Center
*2　National Superconducting Cyclotron Laboratory, Michigan State University
*3　Facility for Rare Isotope Beams, Michigan State University

Present status of the beam transport line from SRC to BigRIPS

K. Kusaka,[*1] K. Yoshida,[*1] M. Ohtake,[*1] and Y. Yanagisawa[*1]

The beam transport line that delivers a primary beam extracted from SRC to the BigRIPS target has been operated since 2007 and is called the "T-course" beam line. The T-course beam line consists of three bending magnets and 17 quadrupoles.[1,2] All of them are of the resistive type, and the maximum magnetic rigidity of the beam line is 8.0 Tm. Two identical 50° bending magnets DMT2 and DMT3 in the T-course are "2-Tesla" room-temperature dipoles, the maximum current of which is 650 A. Here we report the incident we faced in 2017 at the DMT3 magnet.

Since the DMT2 and DMT3 magnets are designed as high-field resistive-type magnets with sufficiently uniform field distribution, saddle-shaped correction coils are installed in the gap of the magnet in addition to the main coils. The main and correction coils are excited in series with one power supply. As shown in Fig. 1, the 12-layer main coil consists of 6 double pancakes in which a 13.5×13.5 mm hollow conductor is wound 6 times in each layer. For the correction coils, a 14×10 mm rectangular hollow conductor of is wound 6 times in each layer, forming a 2-layer double pancake. The correction coil end is located between the main coil and the pole end.

At the beginning of the uranium beam time in October 2017, we found that one of the correction coils in the DMT3 magnet was damaged. Figure 2 shows the excitation voltage at each pancake of the DMT3 coils logged on October 14. The voltage of the lower correction coil was unstable and much lower than that of upper correction coil. We concluded that the layer isolation of the lower correction coil was damaged. We then investigated the lower correction coil by inserting a fiberscope CCD camera into the space between the main coils of the DMT3 magnet. Damage to the epoxy isolation between the coil layers was found at many places on the outer circumference of the lower correction coil (Fig. 3).

In order to proceed with the scheduled beam time, we have isolated the lower correction coil from the excitation circuit, and the DMT3 magnet was re-excited after increasing the flow rate of the cooling water for the coils. After beam-time suspension for 5 days, a uranium beam was transported from SRC to the BigRIPS target and scheduled experiments were performed. The excitation current of the DMT3 magnet during the beam time was approximately 647 A, which is close to the maximum current of 650 A. The temperature and excitation voltage of the DMT3 coils were carefully monitored during the beam time.

A new correction coil is being fabricated at Toshiba, and the disassembly of the DMT3 magnet and installation of the new coil is scheduled for March 2018. The origin of the incident is under investigation.
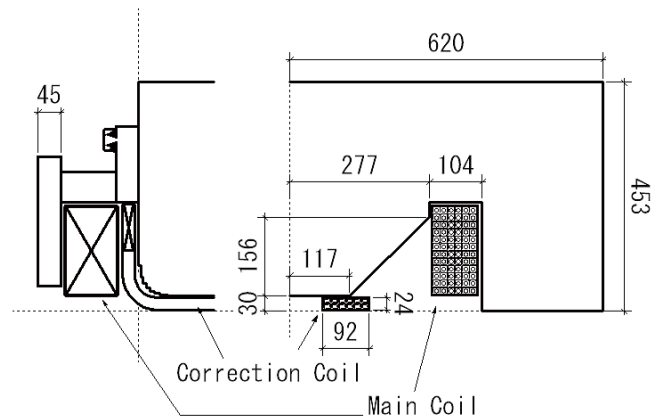
Fig. 1. Schematic of the upper-half cross section of the DMT3 magnet.
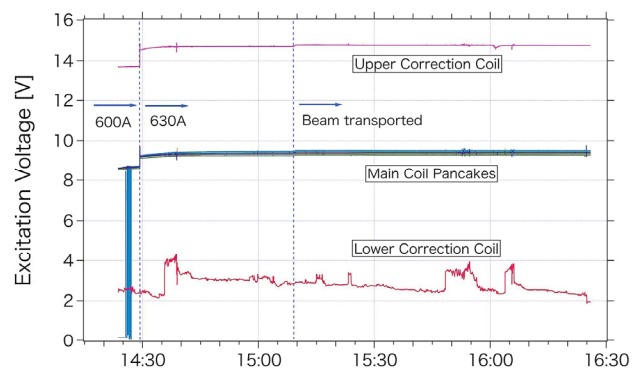
Fig. 2. Excitation voltage at each pancake of the DMT3 coils.

Fig. 3. Damaged correction coil of the DMT3 magnet.

References
1) K. Kusaka *et al.*, RIKEN Accel. Prog. Rep. **39**, 259 (2006).
2) K. Kusaka *et al.*, IEEE Trans. Appl. Supercond. **18**, 318 (2008), and references therein.

[*1] RIKEN Nishina Center

Present status of ERIS at the SCRIT electron scattering facility

T. Ohnishi,[*1] S. Ichikawa,[*1] and M. Wakasugi[*1]

The Electron-beam-driven RI separator for SCRIT (ERIS)[1] at the SCRIT electron scattering facility[2] is an online isotope separator system used to produce low-energy RI beams for electron scattering experiments of unstable nuclei. Recently, ion stacking and pulse extraction were performed at ERIS in order to inject RI beams into a dc-to-pulse converter named fringing-RF-field activated dc-to-pulse converter (FRAC).[3] The results were reported in Ref. 4). In the present year, we modified the ionization chamber to increase the intensity of ion beams. In this paper, we report the results and present status of ERIS.

Figure 1 shows a schematic of the new ionization chamber of ERIS. The new ionization chamber consists of a curved cathode, an ionization chamber (anode), and entrance and exit grids. The entrance grid is a curved tungsten-wire mesh. The wire diameter of the mesh is 30 μm, and the mesh pitch is 0.85 mm. The entrance and exit grids are connected to the ionization chamber through an insulator. Ion stacking and extraction are controlled by switching the voltage of the exit grid. Neutral atoms enter the ionization chamber, passing through the cathode. They are ionized by collision with thermionic electrons emitted from the cathode, which is maintained at approximately 2000°C.

Though ionization occurs everywhere inside the ionization chamber, ions located near the exit hole are mainly extracted, because the potential is low enough for ion extraction only around the exit hole owing to its small diameter of 2.5 mm. To increase the number of ions near the exit hole, the focusing of electron beams on the exit hole is proposed using a new curved cathode and a curved entrance grid, as shown in Fig. 1. The bending of the cathode and entrance grid was determined based on the electron track simulation using the SIMION code.[5]

The properties of the new ionization chamber were studied using 10-keV ^{132}Xe ion beams. The voltages of the cathode and anode were set to 0 and 180 V, respectively. The exit-grid voltages at the stacking and extraction points were 185 and 0 V, respectively. The entrance-grid voltage needed to prevent the escape of ions from the entrance grid was 200 V. This voltage is higher than the voltage in the case of the non-curved entrance grid, 182 V,[4] which indicates the large difference of potential distribution between the curved and non-curved electrodes. Under the same condition for the anode current, ~20 mA, the ion beam currents with the curved and non-curved electrodes were approximately 2 and 6 nA, respectively. Pulse shapes measured at the exit of ERIS with the curved and non-curved electrodes

are shown in Fig. 2. The stacking time was 10 ms, and the extraction period was 300 μs. These pulse shapes are plotted as the ratio of the pulse beam current to the continuous beam current. With the curved electrodes, it takes almost 1.5 ms to extract all of the stacked ions. In the case of the non-curved electrodes, the stacked ions are extracted within 0.5 ms. These results show that the ionization with the curved electrodes occurs mainly far from the exit hole contrary to the calculated results. More detailed calculation including the effect of the space charge and other effects is needed in order to understand the obtained results.

In summary, we tested the new ionization chamber with the curved electrodes at ERIS. The expected improvement of the ion beam intensity was not observed. More detailed study and developments are in process.
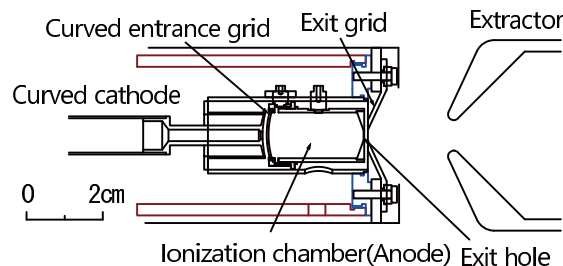
Fig. 1. Schematic of the new ionization chamber of ERIS.
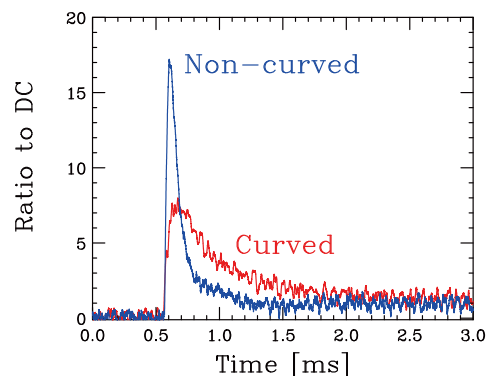
Fig. 2. Pulse shapes extracted from ERIS after the stacking. The pulse shape is plotted as the ratio of the pulse beam current to the continuous beam current. The red and blue shapes are measured with the curved and non-curved electrodes, respectively.

References
1) T. Ohnishi *et al.*, Nucl. Instrum. Methods Phys. Res. B **317**, 357 (2013).
2) M. Wakasugi *et al.*, Nucl. Instrum. Methods Phys. Res. B **317**, 668 (2013).
3) M. Wakasugi *et al.*, in this report.
4) T. Ohnishi *et al.*, Accel. Prog. Rep. **50**, 192 (2017).
5) SIMION, http://simion.com/

---

*1 RIKEN Nishina Center

Progress in the dc-to-pulse converter FRAC

M. Wakasugi,[*1] M. Togasaki,[*1] T. Ohnishi,[*1] K. Kurita,[*2] R. Toba,[*3] M. Watanabe,[*1] and K. Yamada[*2]

An appropriate dc-to-pulse converter is required at the SCRIT electron scattering facility,[1,2] where a continuous radioactive ion beam from the ISOL, called ERIS,[3] has to be converted to a pulsed beam with a duration of 300–500 μs to inject target ions into the SCRIT device. We developed a new type of a dc-to-pule converter, named fringing-Rf-field activated dc-to-pule Converter (FRAC), by utilizing the fringing RF field at both ends of RFQ rods. It is based on an RFQ linear trap technique and works under an ultra-high-vacuum condition. Ions continuously injected into FRAC are decelerated by the alternating longitudinal electric field produced in the distorted RF field appearing around both ends of the RFQ rods. They are accumulated in FRAC for a significantly long time, stacked during the FRAC operation period, and consequently ejected as a high-intensity pulsed beam. This edge effect notably appears only when the energy of incoming ions is less than several eV at the injection barrier and the energy spread is considerably small.

There are barrier electrodes with an aperture 6 mm in diameter at both ends of the RFQ rods. A slightly lower voltage, V_{BI}, compared to the ion beam energy is applied to the injection barrier electrode to accept the continuously incoming beam, and the beam is decelerated to a few eV at the injection barrier. The dc voltage, V_{RFQ}, which is lower than that at the injection barrier by typically 20 V, is applied to the RFQ rods to form a longitudinal potential well for ion confinement, and the ejection barrier voltage is set to be higher than the ion energy. The "basic operation mode" in which the continuous ion beam is injected into FRAC with the fixed DC potential structure as mentioned above, successfully contributed to the first electron scattering experiment for the ^{132}Xe iosotope.[4]

We attempted other operation modes to enhance the dc-to-pulse conversion efficiency toward the experiments for radioactive isotopes. They are two-step stacking, in which the pre-pulsed beams produced by the grid switching at the ion source are injected into FRAC and stacked again in FRAC for 1 s. The pre-pulsed beam has a duration of 200 μs, repetition rate of 500 Hz, and the duty of 0.1. The injection barrier potential is synchronously switched between open and close with the pre-pulsed beam arrival. This is a "synchronous pulse injection (SPI) mode" Since we found the energy spread of the pre-pulsed beam is doubled relative to that of the dc beam owing to the shift of the most-probable energy with time, we suppressed the energy-to-time correlation by modulating V_{BI} and V_{RFQ} to trace the energy shift when the beam is injected. This is an advancement of the SPI mode, and it is called the "modulated injection barrier (MIB) mode." Another operation mode is a "ramped RFQ voltage (RRV) mode," in which V_{RFQ} is ramped down during a FRAC operation period with a rate of 10 V/s. This procedure expands the longitudinal phase volume for the ion stacking, adiabatically moves the formerly stacked ions to a lower energy region, and provides free space for the later incoming ions. Although the energy spread of the output pulsed beam becomes wider, a higher dc-to-pulse conversion efficiency is expected.

The waveforms of the output pulsed beams in these operation modes are shown in Fig. 1. The output pulsed beam intensity was enhanced by a factor of 2.5 for the SPI mode, a factor of 4.5 for the MIB mode, and a factor of 10 for the RRV mode relative to the basic operation mode. The dc-to-pulse conversion efficiencies at an operation frequency of 1 Hz are, for instance, 0.8% in the basic operation mode, 2.1% in the SPI mode, 3.4% in the MIB mode, and 5.6% in the RRV mode. While the dc ion beam intensity was practically 4.6 nA, in this measurement, a high-intensity pulsed beam containing 1.6×10^9 ions was obtained at 1 Hz.
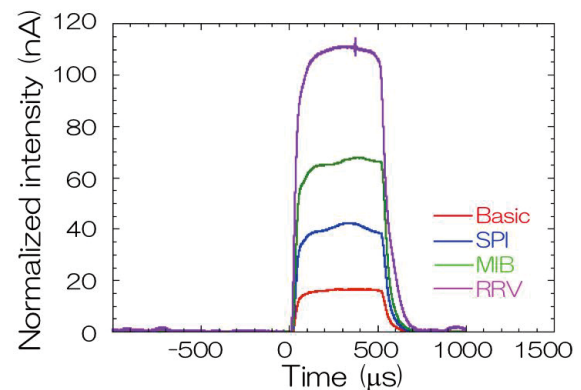
Fig. 1. Waveforms of the output pulsed beam obtained in four operation modes.

References
1) M. Wakasugi *et al.*, Nucl. Instrum. Methods B **317**, 668 (2013).
2) T. Ohnishi *et al.*, Physca Scripta T **166**, 014071 (2015).
3) T. Ohnishi *et al.*, Nucl. Instrum. Methods B **317**, 357 (2013).
4) K. Tsukada *et al.*, Phys. Rev. Lett. **118**, 262501 (2017).

*1 RIKEN Nishina Center
*2 Department of Physics, Rikkyo University
*3 Department of Electrical Engineering, Nagaoka University of Thchnology

Improvements on the racetrack microtron at SCRIT

A. Enokizono,[*1] T. Hori,[*1] M. Wakasugi,[*1] and M. Watanabe[*1]

The SCRIT group has successfully performed its first physics experiment using stable ^{132}Xe target[1]) and opened a new window to the research of unstable nuclei by means of electron scattering. An upgrade of the SCRIT facility is currently in progress, aiming at the world's first electron scattering experiment using short-lived RI targets.

For the SCRIT experiment, a racetrack microtron (RTM; Fig. 1) was used to inject the electron beam not only into a storage ring but also into the Electron-beam-driven RI separator for SCRIT (ERIS) to irradiate a uranium target to generate RIs.[2]) A typical output power of the electron beam is currently ∼20 W (with 20 Hz operation), but 1 kW is required to generate a sufficient number of ^{132}Sn to achieve the luminosity of more than 10^{26} cm^{-2}s^{-1}. As such a high power RTM needs massive modifications, $e.g.$, a new modulator power supply, we decided to improve the 20 W beam power up to 50 W by using the current RTM configuration with several minor upgrades before the future 1 kW upgrade. For example, a study of a gun-grid-pulsing device and its upgrade plan was reported by Watanabe $et\ al.$[3]) In addition to the upgrade, the cause of electron-beam instabilities must be determined out and fixed. The RTM device is already 20 years old, and some of its components are becoming the source of the instabilities. We found that a surface of a ceramic RF coupler was carbonized and blackened, as shown in Fig. 1 (inset). As such a carbonized coupler is known to be easily discharged at a high power input, we carefully polished the surface. Further, we found that the charge-up of a ceramic duct coupler for the CT monitor located at the exit of the electron gun causes beam instability, and the shape of the beam
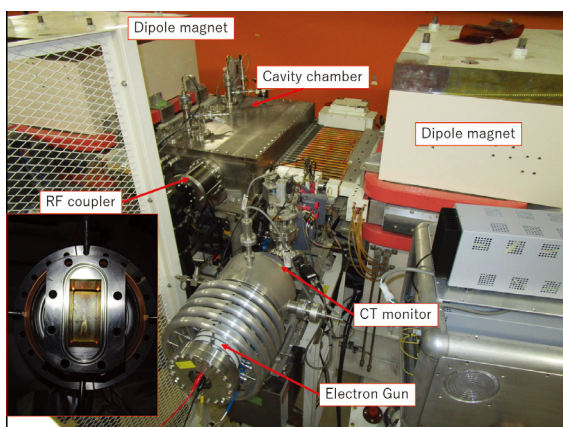
Fig. 1. Overview of SCRIT RTM device.

*1 RIKEN Nishina Center
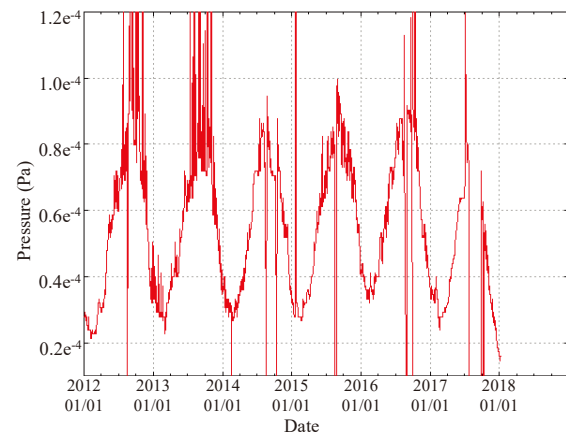
Fig. 2. Trend of the vacuum at RTM cavity in the past six years. TMPs were upgraded in August 2017.

profile monitored by a camera installed after the CT monitor was observed to change. After installing an additional SUS pipe to hide the ceramic part from the electron beam, the beam profile stabilized. We are also attempting to stabilize the RF power input, $e.g.$, the klystron module and the power variator, in the waveguide.

The RTM operation is also frequently disrupted by arc detections especially at higher RF power inputs, and it unfortunately reduces the duty factor of the experiment time. This issue is considered to be caused partly by the discharge inside a cavity chamber, and in such a case, the vacuum improvement of the chamber could be helpful. A better vacuum is also important for a stable operation and longer lifetime of RF components. The two (400 L + 300 L) TMPs attached to the chamber were replaced with two larger (520 L + 520 L) TMPs. A typical vacuum range during the RTM operation was 2–8×10^{-5} Pa, as shown in Fig. 2, and with the TMP upgrade, the vacuum was improved by more than 20%. Note that the seasonal dependence, which presumably originates from the temperature in the RTM room, results in a difference in the vacuum by a factor of 3–4. Therefore, it is also important to control the room temperature or develop a new cooling system for the cavity chamber.

In summary, the improvements of the RTM at SCRIT are in progress to achieve a stable operation at ∼50 W. This work must be successfully completed before the future RTM upgrade to 1 kW operation.

References
1) K. Tsukada $et\ al.$, Phys. Rev. Lett. **118**, 262501 (2017).
2) T. Ohnishi $et\ al.$, PoS (INPC2016) 088.
3) M. Watanabe $et\ al.$, in this report.

Electron energy stabilization at the electron gun in RTM

M. Watanabe,[*1] A. Enokizono,[*1] T. Hori,[*1,*2] and M. Wakasugi[*1]

We have been upgrading[1] a racetrack microtron[2] (RTM) as an electron injector for the electron storage ring SR2 and ISOL-type nuclei source, ERIS[3] (electron-beam-driven RI separator for SCRIT), at the SCRIT facility.[4] For both the apparatuses, a stable electron beam in two specifications of current and energy is important to accomplish reliable and continuous measurement of electron scattering in unstable nuclei. In addition to stability, a high power beam is necessary to maintain a good signal-to-noise ratio in the electron scattering measurement results.

The electron beam energy of 150 MeV from the RTM is determined by the mechanical design and magnetic field of the dipole magnets of the RTM. If the electron acceleration by the RF cavities is insufficient or unstable, the beam at the middle points in the RTM do not reach the designed energy and fail to exit the RTM. In order to accelerate the electron beam up to the designed energy, the RF power for the acceleration and electron beam current from the DC electron gun should be balanced at a certain ratio. Therefore, the stability of the DC electron gun with a maximum energy of 80 keV is important for the RTM and all of the facility.

We measured the stability of the DC electron gun of the RTM. The black line in Fig. 1 shows the time dependence of the voltage of the electron gun cathode, which corresponds to the electron beam energy at a test voltage of 1.45 kV, extractor-grid voltage of 200 V, cathode filament voltage of 6.1 V, and grid pulse width of 5 μs without any special treatment for stability. The voltage drop is 20 to 40 V during the grid pulse, except for the pulse switching noise. This voltage drop directly corresponds to the drop in energy of the electron beam, which results in different electron beam passes in the transport line and finally changes the beam current going into the RF cavities of the RTM. As a consequence, the outgoing 150 MeV electron beam becomes unstable

Simple solutions to reduce the instability include the installation of a high-current power supply as the DC voltage source of the gun, or the installation of a capacitor with high capacitance at the cathode to maintain the voltage. We tested the effects of the capacitances. The blue line and red line in Fig. 1 show the results of installing the 8.4 nF ceramic capacitor and 100 nF oil capacitor, respectively. The voltage drops were apparently reduced by these capacitors. The 8.4 nF ceramic capacitor reduces the voltage drop by half, while the 100 nF oil capacitor reduces it by more than 10 times. In general, the oil capacitor is not good at high-speed time ranges; however the result shows that it still works sufficiently in the microsecond time range.
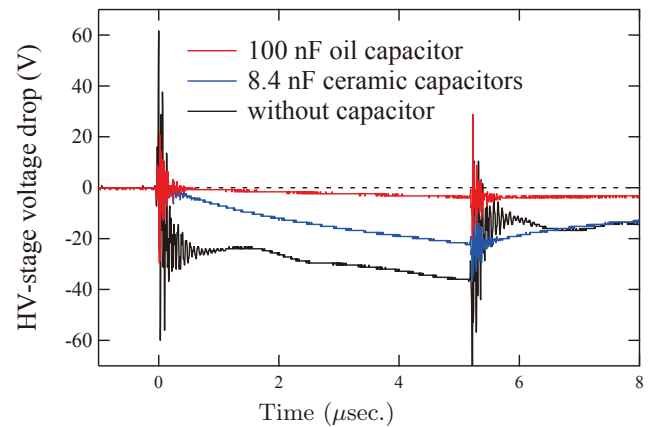
Fig. 1. Voltage drop of the H.V. stage of the electron gun in the time range of the grid pulse of 5 μs.
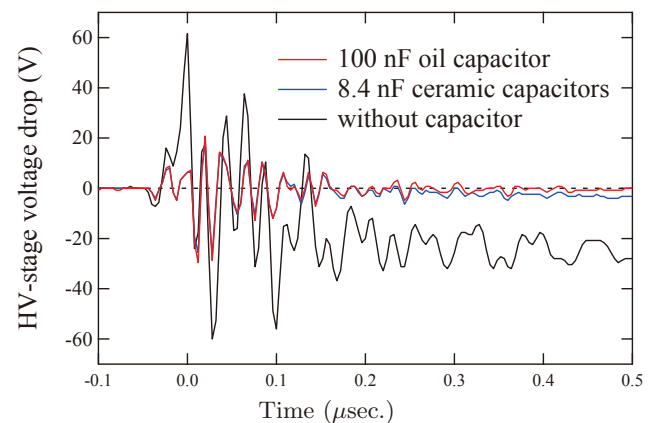
Fig. 2. Voltage drop of the H.V. stage in a short time range around the switching noise of the grid pulse.

In Fig. 2, the same data shown in Fig. 1 are shown for a different time range of 600 ns. The high speed oscillations of the data originate from the switching electronic circuit of the grid pulse. Compared to the black line, both the 8.4 nF ceramic and 100 nF oil capacitors reduce the high speed noise of more than 10 MHz by similar amounts. This means that the ceramic capacitors are good in the speed range of 10 MHz.

This result shows that the installation of a capacitor at the electron gun cathode electrode stabilizes the electron beam voltage of the RTM. Therefore, we are planning to install a larger oil capacitor of 500 nF at the electron gun cathode.

References
1) M. Watanabe *et al.*, RIKEN Accel. Prog. Rep. **49**, 188 (2015) and **50**, 190 (2016).
2) T. Hori, Doctor thesis (2002).
3) T. Ohnishi *et al.*, Nucl. Instrum. Methods B **317**, 357 (2013).
4) M. Wakasugi *et al.*, Nucl. Instrum. Methods B **317**, 668 (2013).

*1 RIKEN Nishina Center
*2 Department of Physics, Hiroshima Univ.

High pressure cold gas target system with large capacity for low-energy beam at RIBF

R. Nakajima,*1 S. Koyama,*2 M. Kurata-Nishimura,*3 N. Chiga,*3 H. Otsu,*3 and X. Sun*3

The use of low-energy beams (20 to 50 MeV/nucleon) with large atomic numbers ($Z > 40$) in experiments at RIBF has been attracting attention in recent years. We are developing hydrogen and deuterium targets for cross-section measurements at a low beam energy. For the cross-section measurements, the uniformity of the target thickness is very important. Polyethylene and deuterated polyethylene films are often used as hydrogen and deuterium targets since it is easy to produce those targets with good uniformity. However, the carbon nuclei in such polyethylene targets create a background signal in the cross-section measurement. In RIBF, a cryogenic proton and alpha target system (CRYPTA) has been developed and used in experiments with high-energy beams.[1] Since CRYPTA uses thin harbor foils as the target window, the background from carbon nuclei is lower than in the conventional film targets. However, it is difficult to realize a thin and uniform-thickness target cell with a liquid target system, owing to the bulging of the window. The non-uniformity becomes considerably large especially in a thin target for low-energy beams. The current liquid target system does not satisfy the requirements of the cross-section measurement with low-energy beams. In order to reduce the non-uniformity, a high-pressure cold gas target was employed instead of the liquid target. Since the density of the hydrogen in the gas phase is much lower than that in the liquid phase, we can make the length of the target longer than that of the liquid target with the same substantial thickness. Owing to the high length of the target, the effect of the bulging becomes small and the non-uniformity is reduced. We developed a high-pressure cold gas target system with large capacity by modifying CRYPTA. The stability of this system during a cross-section measurement with a low-energy beam was studied.

There were mainly three improvements made to CRYPTA for the gas target: (1) Total power of the heating system was increased from 10 W to 25 W by adding three heaters. (2) New target cells for a high-pressure gas with large capacity were built. The length of the target cells are 50 mm and 70 mm. A heat shield from radiant heat was attached to the cell with 50-mm length. The heat shield was not attached to the 70 mm cells owing to the geometrical limitation. (3) The tar-
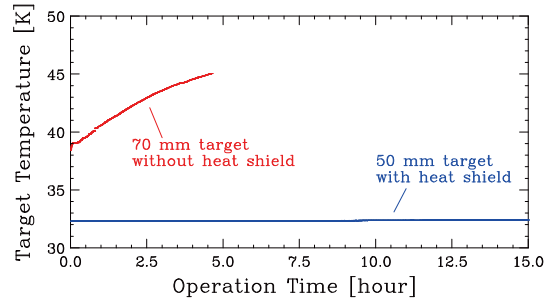
Fig. 1. Correlation with operation time and temperature change during the experiment.

get windows were also replaced with new ones with a Harvar foil of 10-μm thickness and 36 mm diameter in oder to endure the high pressure. A thermometer was installed at the target cell and the lowest temperature of the system. The error of the thermometer is 0.01 K. To keep the target thickness constant, we isolated the target cell. We applied feedback to the lowest temperature in the system so that the gas did not transform into the liquid phase. In order for the gas target to be stable, it is required that the changes of target temperature and pressure are small and that the pressure is not more than 5.0×10^5 Pa, at which the target has never been tested.

Figure 1 shows the change of temperature at the target cells during the experiment. The temperature of the target cell with 50-mm thickness was stable, while that of the 70-mm cell increased by 1.28 K/h. Because the 70-mm target cell was not covered with the heat shield, molecules floating in a circumference of the chamber were attracted to the surface of the cold cell, which is expected to be a source of heat. The conditions of operation are summarized in Table 1. Because the pressure change becomes 4.3×10^5 Pa or less even in the two weeks of operation, this is very useful for experiments in RIBF. In conclusion, high-pressure and large-capacity cold gas target systems were constructed for cross-section measurement at a low beam energy at RIBF. By using this system with a heat shield, we confirmed its stability.

Reference
1) M. Kurata-Nishimura *et al.*, RIKEN Accel. Prog. Rep. **46**, 165 (2013).

Table 1. Summary of the operation of the new target cells

Gas	Target Length	Temperature	Pressure	Target Thickness	Heat Shield	Operating Time	Rate of Temperature
H_2	70 mm	39.25 K	4.03×10^5 Pa	18.78 mg/cm^2	×	4.4 h	1.28 K/h
H_2	50 mm	32.29 K	4.04×10^5 Pa	17.23 mg/cm^2	○	90.5 h	0.13 K/day
D_2	50 mm	35.99 K	4.01×10^5 Pa	28.63 mg/cm^2	○	60.5 h	−0.01 K/day

*1　Center for Nuclear Study, University of Tokyo
*2　Department of Physics, University of Tokyo
*3　RIKEN Nishina Center

Resonance ionization spectroscopy of Nb utilizing a narrowband injection-locked Titanium:Sapphire laser

M. Reponen,[*1,*3] V. Sonnenschein,[*2] T. Sonoda,[*1] H. Tomita,[*2] M. Oohashi,[*2] D. Matsui,[*2] and M. Wada[*1,*4]

Hyperfine structures and isotope shifts in electronic transitions contain readily available model-free information on the single-particle and bulk properties of exotic nuclei, namely the nuclear spin, magnetic dipole and electric quadrupole moments as well as changes in root-mean-square charge radii.[1]

Recently, the implementation of resonance ionization spectroscopy (RIS) in a low-temperature supersonic gas jet[2] utilizing a narrowband first step excitation has gained considerable interest.[3] An optimal solution to combine high pulse powers required for efficient ionization with a narrow bandwidth is the pulsed amplification of a narrow-band continuous wave (CW) laser. While for high-gain dye lasers a single pass amplification is sufficient, the lower gain Titanium:Sapphire gain medium requires a different approach. In a regenerative amplifier, the cavity length is locked to a multiple of the seed wavelength allowing Titanium:Sapphire -based lasers to reach a final output power of several kW (during the pulse) from the few mW of CW input.

In this work, we present a pulsed injection-locked Titanium:Sapphire laser for the PALIS laser laboratory[4] based on a design presented in Ref. 5). Numerous advancements over the previous iterations have been included into the design to improve stability and usability. These include design choices such as mounting the cavity mirrors directly on the baseplate and positioning the laser feet to minimize the vibration sensitivity. Furthermore, the laser was designed to accept the seed laser via a fiber input thus improving reproducibility when, for example, modifying the Master laser setup.

The laser cavity was designed for flexibility. It can be reconfigured to two different round-trip lengths and crystal locations in order to operate the laser with different pulse width and gain modes. The longer cavity round-trip configuration allows us to extend the tuning range using birefringent plates and has a intracavity second harmonic generation option. The latter option can lead to increased second harmonic power and, more importantly, to high-quality beams required by the long laser transport path at PALIS.

The laser has been shown to perform as designed with a tuning range across the whole Master laser range, with a 30% slope efficiency. Importantly, the laser was applied to hyperfine spectroscopy of ^{93}Nb (See Fig. 1). These measurements yielded a total
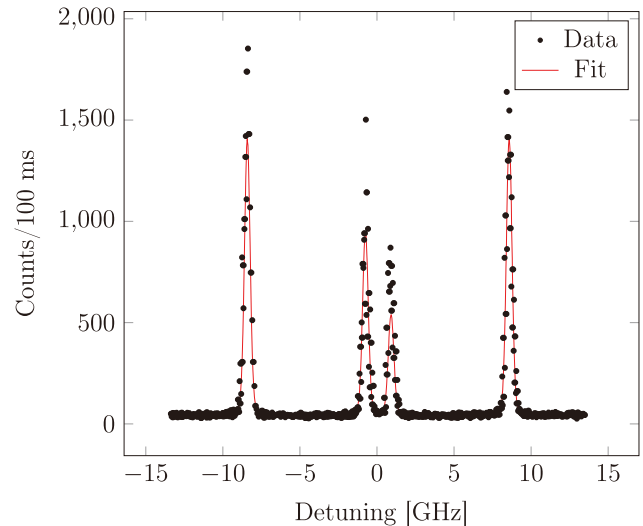
Fig. 1. An example hyperfine spectra for transition $4d^45s$ a $^6D^0_{1/2} \rightarrow 4d^35s5p$ y $^6D_{1/2}$ in ^{93}Nb.

FWHM of ~ 400 MHz and hyperfine A coefficient of 1866 ± 8 MHz for the ground state and 1536 ± 7 MHz for the first excited state in a good agreement with the literature values.[6] Possible future goals for niobium include the determination of the efficiency of the newly developed ionization scheme and its application for RIS of radioactive niobium isotopes, as well as studying the possibility to separate the ^{93m}Nb isomer from the ground state for the application in integrated fast neutron dosimetry.[7] In conclusions, the injection-locked Titanium:Sapphire laser system has been demonstrated to be ready for high-resolution in-gas-jet spectroscopy at the PALIS facility in the near future.

References
1) P. Campbell, I. D. Moore, M. R. Pearson, Prog. Part. Nucl. Phys. **86**, 127–180, 2016.
2) T. Sonoda et al., Nucl. Instrum. Methods Phys. Res. B **267**, 17, 2918–2926 (2009).
3) Yu. Kudryavtsev et al., Nucl. Instrum. Methods Phys. Res. B **297**, 7–22, (2013).
4) T. Sonoda et al., Nucl. Instrum. Methods Phys. Res. A **877**, 118–123 (2018).
5) V Sonnenschein et al., Las. Phys. **27**, 8, 085701 (2017).
6) A. Bouzed et al., Euro. Phys. J. D **23**, 1, 57–62 (2003).
7) H. M. Lauranto et al., Appl. Phys. B **50**, 4, 323–329 (1990).

*1 RIKEN Nishina Center
*2 Department of Energy Engineering, Nagoya University
*3 Department of Physics, University of Jyväskylä
*4 Wako Nuclear Science Center (WNSC), IPNS, KEK

Development of co-located ¹²⁹Xe and ¹³¹Xe nuclear spin masers with external feedback scheme[†]

T. Sato,[*1,*2] Y. Ichikawa,[*1,*2] S. Kojima,[*2] C. Funayama,[*2] S. Tanaka,[*2] T. Inoue,[*3,*4,*1] A. Uchiyama,[*4,*1]
A. Gladkov,[*1,*5] A. Takamine,[*1] Y. Sakamoto,[*2] Y. Ohtomo,[*2] C. Hirao,[*2] M. Chikamori,[*2] E. Hikota,[*2]
T. Suzuki,[*2] M. Tsuchiya,[*2] T. Furukawa,[*6] A. Yoshimi,[*7,*1] C. P. Bidinosti,[*8] T. Ino,[*9] H. Ueno,[*1]
Y. Matsuo,[*10,*1] T. Fukuyama,[*11] N. Yoshinaga,[*12] Y. Sakemi,[*13,*4] and K. Asahi[*1,*2]

Precision measurement of the frequency of a nuclear spin is important in fundamental physics experiments such as searches for an electric dipole moment. To achieve high precision, we have developed a nuclear spin maser with an external feedback framework,[1–3] which enables us to extend the spin precession far beyond the transverse relaxation time. In our previous works on ¹²⁹Xe, the frequency precision was found to be limited by the changes in the environmental magnetic field and the effective magnetic field due to the Fermi contact interaction between a Xe atom and a Rb atom. In order to eliminate the sources of uncertainty, we newly introduced a ¹³¹Xe maser as a comagnetometer for the ¹²⁹Xe experiment. In addition to the frequency drift caused by the change in environmental fields, the system of ¹²⁹Xe and ¹³¹Xe co-located in a common cell can eliminate the frequency instability that stems from the change in the effective magnetic field, because the interaction strengths between ¹²⁹Xe-Rb and ¹³¹Xe-Rb[4] are almost the same. Thus, comagnetometry using ¹³¹Xe may provide more efficient cancellation of uncertainties for the ¹²⁹Xe experiments, as compared to that using ³He, which has been widely used in this field. The shortened measurement time due to quadrupole relaxation, which is one of the difficulties for the ¹³¹Xe comagnetometer, can be overcome by introducing the maser scheme.

In order to investigate the long-term stability of the masers, frequency responses (i.e., susceptibilities) to operational parameters of the experiment (magnetic field, cell temperature, power and frequency of laser lights) were measured. By combining the obtained susceptibilities and the measured instabilities of the individual parameters, the maser frequency instabilities caused by the parameters were evaluated. Fig-

ure 1 shows the standard deviation of the maser frequency evaluated from the drifts in the cell temperature (which leads to change in the Rb number density, and hence change in the effective magnetic field) and environmental magnetic fields as a function of the averaging time. It was found that frequency drifts due to the magnetic effects on ¹²⁹Xe were reduced by two orders of magnitude by applying the appropriate correction based on the measured ¹³¹Xe spin precession frequency. This result indicates the efficient performance of the proposed comagnetometry using ¹³¹Xe co-located with ¹²⁹Xe. Because of the enhanced stability of masers, the frequency drifts at a level of μHz associated with the drifts in the power of the laser lights were also revealed. Experimental investigation of the origin of this instability and its reduction are subjects of our ongoing work.
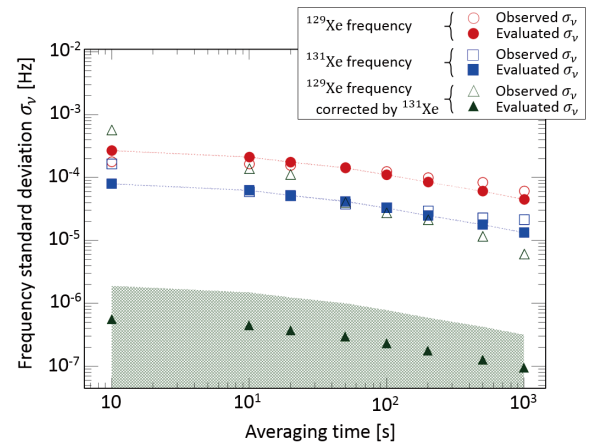
Fig. 1. Long-term stability of masers and the evaluated contribution from the instabilities of magnetic effects. Closed symbols represent the evaluated contributions from the frequency instabilities due to magnetic effects for frequency of masers. Hatched band represents the error associated with the evaluated standard deviation of maser frequency σ_ν. Open symbols represent the measured standard deviations of the frequency of masers.

References
1) A. Yoshimi et al., Phys. Lett. A **304**, 13 (2002).
2) A. Yoshimi et al., Phys. Lett. A **376**, 1924 (2012).
3) T. Inoue et al., Eur. Phys. J. D **70**, 129 (2016).
4) M. Bulatowicz et al., Phys. Rev. Lett. **111**, 102001 (2013).

[*1] RIKEN Nishina Center
[*2] Department of Physics, Tokyo Institute of Technology
[*3] FRIS, Tohoku University
[*4] CYRIC, Tohoku University
[*5] Department of Physics, Kyungpook National University
[*6] Department of Physics, Tokyo Metropolitan University
[*7] RIIS, Okayama University
[*8] Department of Physics, University of Winnipeg
[*9] Institute of Material Structure Science, KEK
[*10] Department of Advanced Sciences, Hosei University
[*11] RCNP, Osaka University
[*12] Department of Physics, Saitama University
[*13] CNS, University of Tokyo

Searching optimum measurement conditions of the laser-microwave double resonance for the atoms stopped in superfluid helium

M. Sanjo,[*1,*2] K. Imamura,[*2,*3] A. Takamine,[*2] T. Fujita,[*2,*4] T. Egami,[*1,*2] D. Tominaga,[*1,*2]
W. Kobayashi,[*1,*2] Y. Nakamura,[*2,*3] T. Wakui,[*2,*5] T. Furukawa,[*2,*6] H. Ueno,[*2] and Y. Matsuo[*1,*2]

We have developed a laser spectroscopic method named OROCHI (Optical RI-atoms Observation in Condensed Helium as Ion catcher) aiming at nuclear structure studies of unstable nuclei with low production yields and short lifetimes. In OROCHI, highly energetic ion beams are efficiently caught as neutralized atoms in superfluid helium (He II) owing to its high density. In addition, the absorption wavelength of atoms in He II is significantly blue-shifted due to the effect of surrounding He atoms while the emission wavelength is almost the same as that in vacuum. This enables us to detect photons emitted from the atoms with low background by removing the excitation-laser stray light. Consequently, we can measure Zeeman and hyperfine structure (HFS) splittings with a high sensitivity by applying laser-RF and laser-microwave (MW) double resonance methods to the atoms in He II.

So far, we have succeeded in observing the laser MW double resonance (LMDR) signals for 10^4 particles per second (pps) Rb ion beams with an energy of 66 A MeV.[1,2)] However, the LMDR signal intensities were insufficient to realize measurements of the HFS splitting for lower intensity ion beams of less than 10^3 pps. In general, it is expected that the higher-power laser and MW irradiations lead to higher resonance peak heights in LMDR spectroscopy. In order to estimate the optimum measurement conditions, it is necessary to experimentally and quantitatively investigate the laser and MW power dependence of LMDR signal intensities. As a pilot study, we measured the laser power dependence of LMDR signal intensities for different MW powers using a glass cell containing Rb vapor with He buffer gas ("Rb cell").

We irradiated the Rb atoms in the cell with a circularly polarized laser light (wavelength: 794 nm), and applied a magnetic field to the atoms, parallel to the laser axis, in order to generate and maintain spin polarization. On scanning the MW frequency, we observed a resonant peak at the MW frequency corresponding to the HFS splitting in the ground state of ^{85}Rb. We measured the LMDR signal intensities (defined as resonant peak heights in LMDR – background) for different laser powers when the MW powers were 6.0 W, 3.5 W, 1.9 W, and 0.15 W.

Figure 1 shows the laser power dependence of LMDR intensities for different MW powers with two different Rb cells containing 1.3×10^4 Pa and 1.0×10^5 Pa He buffer gas. The stronger the laser and MW we applied, the higher the LMDR intensities we observed. However, the intensities were saturated at a certain laser power. The higher He buffer gas pressure case required higher laser power for saturation. This means that the laser excitation cross section was decreased because of the effect of pressure broadening. The absorption spectral line width in 1.3×10^4 Pa He gas is of the order of 1 GHz and that in He II is of the order of 1 THz. Therefore, the laser excitation probability is estimated to decrease by the order of 10^3 in He II similar that in to Ref. 3). We can roughly estimate that the saturation of LMDR signal intensities needs 10^3 times more laser power density in He II compared to that in He gas. In the previous online experiment, we performed the experiment with 100 mW laser power (diameter: 2 mm), which corresponds to a laser excitation probability of 1.68×10^3 s^{-1}. Our present result implies that this value was too low to saturate the LMDR signal intensities, and that it was in a linearly increasing region at a low laser power, as depicted in Fig. 1.

The laser power can be increased without increasing the laser stray light by using the newly developed detection system.[4)] Now, we can irradiate atoms with up to 1 W laser by using a Ti:Sa laser. By using a laser power of 1 W, the LMDR intensities are expected to be increased by a factor of 10.
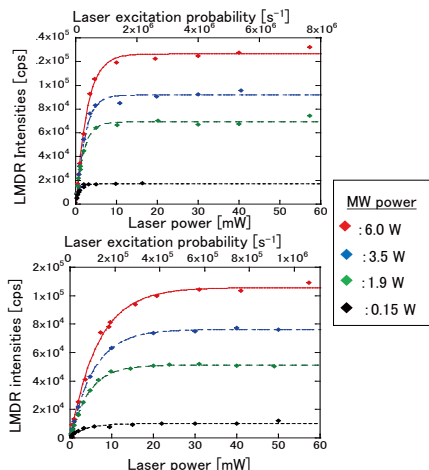
Fig. 1. Laser power dependence of LMDR intensities for different MW powers. The upper and lower figures show the result using Rb cells containing He buffer gas of 1.3×10^4 Pa and 1.0×10^5 Pa, respectively.

*1 Department of Advanced Science, Hosei University
*2 RIKEN Nishina Center
*3 Department of Physics, Meiji University
*4 Department of Physics, Osaka University
*5 QST
*6 Department of Physics, Tokyo Metropolitan University

References
1) X. F. Yang et al., Phys. Rev. A **90**, 052516 (2014).
2) K. Imamura et al., JPS Conf. Proc. **6**, 030115 (2015).
3) S. I. Kanorsky et al., Phys. Rev. B **49**, 3645 (1994).
4) W. Kobayashi et al., RIKEN Accel. Prog. Rep. **50**, 198 (2017).

Optimizing the conditions to measure the hyperfine splitting in the μp ground state

A. Vacchi,[*1,*2,*3] K. Ishida,[*1] E. Mocchiutti,[*3] and E. Furlanetto[*2,*3] on behalf of the FAMU collaboration

Experimental studies were performed during 2017 at Port 1 of the RIKEN RAL facility, in preparation for the measurement of the hyperfine splitting in the 1S state of muonic hydrogen $\Delta E_{hfs}(\mu - p)_{1S}$, to allow the choice of the final layout and confirm the details of the foreseen methodology.[1–6] By measuring the transition $\Delta E_{hfs}(\mu - p)_{1S}$ in μp with a precision of $< 10^{-5}$, the experiment will provide the Zemach radius of the proton $\mathbf{r_Z}$ with high precision, allowing diesntanglement of the discordant theoretical values. The level of discrepancy between the values of $\mathbf{r_Z}$ as extracted from the normal and muonic hydrogen atoms will be quantified, a result that is also important for the not yet explained anomalies on the charge $\mathbf{r_{ch}}$ radius of the proton. The physical process behind this experiment is as follows: μp are formed in a mixture of hydrogen and a higher-Z gas. When a photon is absorbed at resonance-energy $\Delta E_{hfs} \approx 0.182$ eV, in subsequent collisions with the surrounding H_2 molecules, the μp is quickly de-excited and and accelerated by $\sim$2/3 of the excitation energy. The observable is the time distribution of the K X-rays emitted from the μZ formed by muon transfer $(\mu p) + Z \to (\mu Z)^* + p$, a reaction whose rate depends on the μp kinetic energy. The maximal response, to the tuned laser wavelength, of the time distribution of K X-ray from the $(\mu Z)^*$ cascade indicates the resonance.

During 2017, using the set of beam-hodoscopes[7] developed for this purpose, it has been possible to show the adaptability of the beam to our layout and to verify its shape and position. Figure 1 shows the total charge deposited in the hodoscope, an increase of about 10% indicates that by tuning the beam optics a muon beam intensity increase was obtained.

Subsequently, as an addition to the previously performed measurements (in 2016) of the muon transfer rate to oxygen at different temperatures, the same FAMU cryogenic gas target[8] was used to perform a detailed study of the shape of the background underneath the peaks of the x-rays characterizing the delayed transition
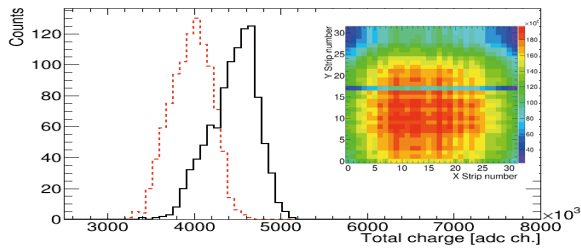
Fig. 1. Total charge detected by the hodoscope before (red dashed line) and after (black solid line) the tuning of the magnets and, in the insert, the two dimensional beam profile of 1 mm per strip.
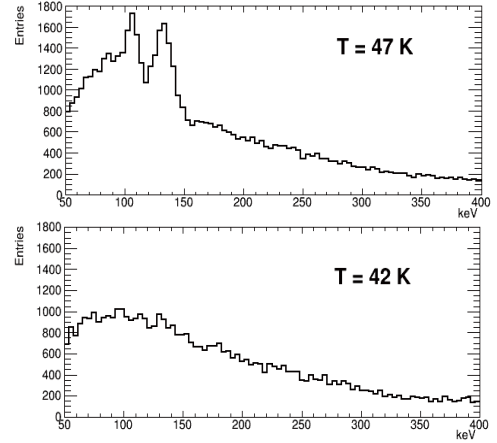
Fig. 2. Upper panel, shows the delayed nitrogen X-rays lines at a temperature of 47 K. In the lower panel the same spectrum is shown at a temperature of 42 K.

of the muon from μp to oxygen. The target loaded with high purity hydrogen was exposed to the 57 MeV/c muon beam, the x-ray spectra was detected with LaBr fast detectors.[9]

During the following phase, dedicated to extending the temperature range of the 2016 transfer rate measurements, it was discovered with great disappointment that the custom delivered gas mixture was badly polluted with nitrogen. Since it was impossible to obtain a new delivery on time, by virtue of necessity and to obtain useful data, we investigated the condensation temperature limits of the heavy elements in the available mixture. Under the assumption of perfect gases and the Dalton law, we can calculate that the gas condensation on the internal vessel surface occur at 54 K for oxygen and 46 K for nitrogen, however in our experimental conditions of pressurized gas mixture, this needs to be verified experimentally.

The delayed nitrogen X-rays lines, at the temperature of 47 K, is shown in the upper panel of Fig. 2. At 42 K the nitrogen lines disappear and pure hydrogen background distribution remains visible in the lower panel. The equipment used in the 2017 experiments performed as expected except for the gas contamination. This has restricted our program especially the possibility to extend the study of transfer rate to oxygen at higher temperatures.

References
1) A. Adamczak, et al., Nucl. Instrum. Methods Phys. Res B **281**, 72–76 (2012).
2) D. Bakalov et al., Hyp. Int. **233**, 97–101 (2015).
3) D. Bakalov et al., Phys. Lett. A **379**, 151–156 (2015).
4) A. Adamczak et al., J. of Inst. **11**, P05007 (2016).
5) E. Mocchiutti et al., arXiv:1708.03172 [physics] (2017).
6) A. Vacchi et al., RIKEN Accel. Prog. Rep. **49**, 230 (2016).
7) M. Bonesini et al., J. of Inst. **12**, C03035 (2017).
8) A. Vacchi et al., RIKEN Accel. Prog. Rep. **50**, 24 (2017).
9) G. Baldazzi, et al., J. of Inst. **12**, C03067 (2017).

*1　RIKEN Nishina Center
*2　Department Math, Info, Physics, University of Udine
*3　INFN Trieste

Neutron spin filter with dynamic nuclear polarization using photo-excited triplet electron for T-violation search in a compound nucleus

S. Takada,[*1,*2] K. Tateishi,[*1] Y. Wakabayashi,[*3] Y. Ikeda,[*3] Y. Otake,[*3] T. Yoshioka,[*2] and T. Uesaka[*1]

In a compound nucleus (*e.g.* ^{139}La+n, ^{81}Br+n), parity violation is enhanced due to the interference between s-wave and p-wave amplitudes. It is theoretically predicted that time reversal (T-) violation can be also enhanced by the same mechanism.[1] We are planning an experiment for sensitive T-violation search using a polarized neutron beam. The p-wave resonances of the candidate nuclei are observed in the energy range of 0.1–100 eV. For this purpose, we need a neutron spin filter that is suitable for the energy region.

A neutron spin filter can polarize the neutron beam by passing it through a spin-polarized media, for example ^{1}H or ^{3}He because their cross-sections have a large helicity dependence. In particular, ^{1}H has flat cross-section of 20 barn in the wide energy range mentioned above. Therefore, we selected neutron spin filter using ^{1}H media.

A solid-state of ^{1}H doped media is often polarized by Dynamic Nuclear Polarization (DNP). DNP is a technique of transferring spin polarization from electrons to nuclei with microwave irradiation. We applied DNP with photo-exited triplet electron spin (Triplet-DNP)[2] because it can be used at a relatively high temperature (> 77 K) and in a low magnetic field (< 1 T) compared to the conventional DNP method. The neutron spin filter with Triplet-DNP was first developed at the Paul Scherrer Institut (PSI) in Switzerland. They achieved ^{1}H polarization of 70% using a naphthalene crystal with the size of $5 \times 5 \times 5$ mm^3 in 0.36 T and at 25 K,[3,4] and evaluated its performance using a polarized neutron beam in the meV region.

The neutron spin filter is characterized with a neutron transmittance T, a neutron polarization $P_{\rm n}$, and a figure of merit (FOM) which is defined as follows:

$$T = \exp\left(-(n\sigma_0 + n'\sigma_0')d\right)\cosh\left(P_{1{\rm H}}n\Delta\sigma d\right), \quad (1)$$

$$P_{\rm n} = \tanh\left(P_{1{\rm H}}n\Delta\sigma d\right), \quad (2)$$

$$\text{FOM} = P_{\rm n}^2 T, \quad (3)$$

where σ_0 and $\Delta\sigma$ are the spin-independent and spin-dependent cross section of ^{1}H, respectively. σ_0' is the spin-independent cross section of other nuclei. n and n' are the density of ^{1}H and other nuclei. d and $P_{1{\rm H}}$ are the thickness and polarization of the filter. Here, the naphthalene crystal ($C_{10}H_8$) is assumed as a filter media. Based on the expression, a 15 mm thickness of the neutron spin filter can conform to the wide en-

ergy range. In addition, we need large acceptance of the spin filter to obtain high statistics. Therefore, we develop $\phi15 \times 15$ mm^3 of the spin filter.

A setup of the neutron spin filter with Triplet-DNP is shown in Fig. 1. Triplet-DNP is carried out at 0.3 T and 100 K. A single crystal of naphthalene doped with deuterated pentacene with a size of $\phi15 \times 15$ mm^3 is used as a filter. To polarize such a huge crystal, a high-power laser was implemented.
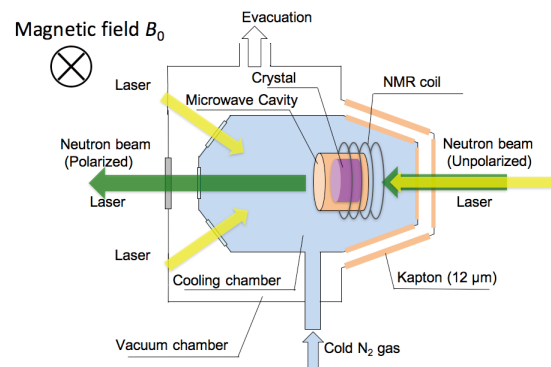
Fig. 1. Setup of the neutron polarization system using Triplet-DNP.

We are planning to check the performance of the neutron spin filter at RIKEN Accelerator-driven compact Neutron source (RANS) next year. We will measure the position dependence of polarization in the spin filter. In November and December 2017, we carried the existing polarization system to RANS and measured the position resolution to check whether performance measurement is possible. Since the position resolution was about 2 mm, it is possible to sufficiently measure the position dependence of the polarization and the transmittance of the spin filter.

References
1) V. P. Gudkov, Phys. Rep. **212**, 77 (1992).
2) A. Henstra, P. Dirksen, W. Th. Wenckebach, Phys. Lett. A **134**, 134 (1988).
3) M. Haag, B. van den Brandt, T. R. Eichhorn, P. Hautle, W. Th. Wenckebach, Nucl. Instrum. Methods Phys. Res. A **678**, 91 (2012).
4) T. R. Eichhorn, N. Niketic, B. van den Brandt, U. Filges, T. Panzner, E. Rantsiou, W. Th. Wenckebach, P. Hautle, Nucl. Instrum. Methods Phys. Res. A **754**, 10 (2014).

*1 RIKEN Nishina Center
*2 Department of Physics, Kyushu University
*3 RIKEN Center for Advanced Photonics

Trigger selector system for BigRIPS DAQ

H. Baba,[*1] T. Ichihara,[*1] T. Isobe,[*1] T. Ohnishi,[*1] K. Yoshida,[*1] Y. Watanabe,[*1] S. Ota,[*2] S. Shimoura,[*2] S. Takeuchi,[*1,*3] D. S. Ahn,[*1] N. Fukuda,[*1] Y. Shimizu,[*1] H. Suzuki,[*1] and H. Takeda[*1]

A new trigger selector system has been introduced for the BigRIPS data acquisition (DAQ) system. One of the advantages of this system is that trigger signals could be switched by a web-interface controller without physically chaining connections between trigger-related circuits. This function will help the RI-beam tuning in BigRIPS because the trigger for the BigRIPS DAQ is frequently switched to obtain profiles of RI beams at each focal plane. In addition, it is possible to configure a complex trigger condition by applying logic gates of AND, OR, and NOT for triggers from each focal plane.

The new system consists of five Generic Trigger Operator[1] (GTO) modules and a web-interface controller coded in the PHP language. A connection diagram of the system is shown in Fig. 1. This system is divided into three sections: the focal plane section, trigger logic section, and trigger output section. The trigger signal for the measurement is hierarchically selected by these three sections. GTO modules with selector firmware[2] (SELGTO) are used for the focal plane and trigger output sections. To configure complex trigger conditions in the trigger logic section, new firmware for the logic unit has been developed and implemented in the GTO module (LUGTO). LUGTO has 20 input channels and 8 output channels. Up to 8 logic conditions, a combination circuit of input signals with AND, OR, and NOT logic gates can be configured in LUGTO.

In the focal plane section, the signals from plastic scintillators and PPACs at the F1–F12 focal planes are separately connected to three SELGTO modules. Here, signals named as F1–F12 Beam are produced and sent to the trigger logic section. For example, the F2 Beam signal is defined from the selection of signals from F2Plastic, F2PPAC1, and F2PPAC2 detectors. By using LUGTO in the trigger logic section, coincidence triggers named as BigRIPS, ZeroDegree, and dE can be configured by signals labeled as F1–F7 Beam, F8–F11 Beam and F3–F7dE (energy-loss gate at each focal plane), respectively. For example, the BigRIPS (ZeroDegree) trigger can be defined as F3Beam×F7Beam (F8Beam×F11Beam). Finally, the trigger output is determined by choosing signals of BigRIPS, down-scaled BigRIPS (BigRIPS(1/n)), ZeroDegree, dE, etc. in the trigger output section.

The trigger configuration is selected from the web-interface controller as shown in Fig. 2. The settings in GTO modules are updated on pushing the "Save" button. However, these settings will be lost when a power cycle occurs. The "EEPWrite" button is used to keep configurations permanently in GTO modules. Compo-
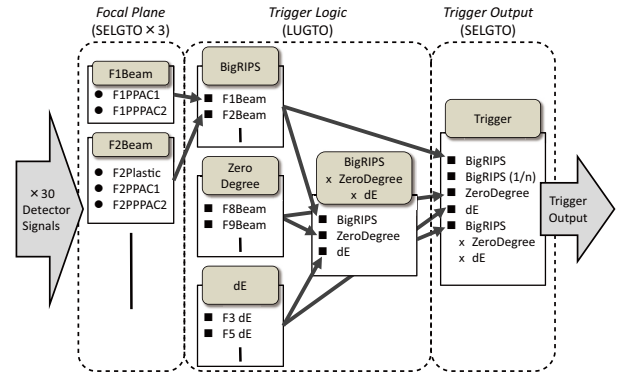
Fig. 1. Diagram of signal connections.
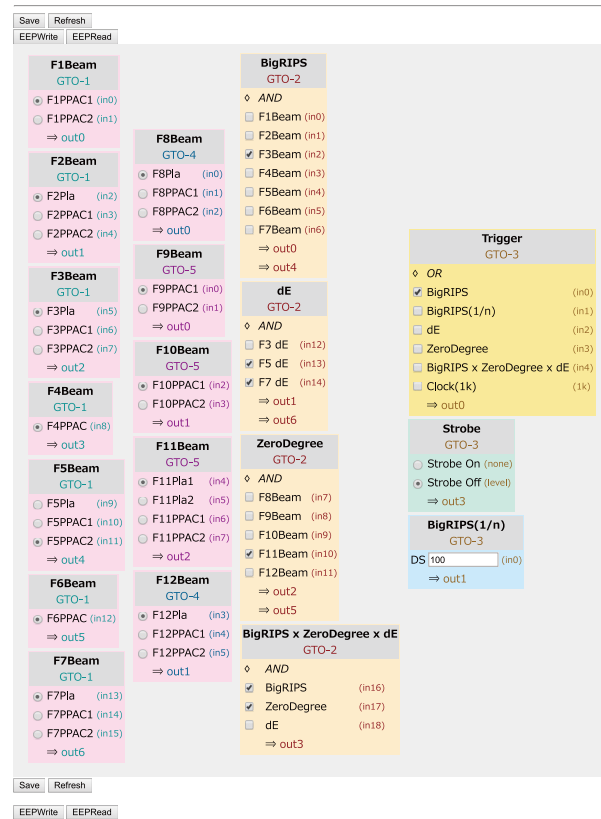
Fig. 2. Screenshot of the web-interface controller.

nents of the web-interface contoller can be customized by a text setting file to facilitate the modification of trigger connections.

This trigger selector system for the BigRIPS DAQ has been in operation since from April 2018, enabling us to perform RI-beam tuning efficiently.

References
1) H. Baba et al., RIKEN Acc. Prog. Rep. **46**, 213 (2013).
2) H. Baba et al., RIKEN Acc. Prog. Rep. **49**, 201 (2016).

*1   RIKEN Nishina Center
*2   Center for Nuclear Study, University of Tokyo
*3   Department of Physics, Tokyo Institute of Technology

Beam preparation for industrial utilization of Ar, Kr, Xe, and Au beams

A. Yoshida[*1] and T. Kambara[*1]

Through the fee-based industrial utilization of RIBF facilities, a space-use semiconductor company has been using Ar and Kr beams at the E5A beam line[1] a few times in a year. The client irradiates semiconductor devices in the air to test the radiation tolerance of single event effects (SEEs).

Figure 1 shows the configuration for the irradiation. A uniform beam-flux distribution is achieved[2] with wobbler magnets and a beam scattering foil placed 4.5 m upstream of a vacuum separation window. Downstream of the window, an air-ionization chamber (IC1) that consists of a stack of 24 μm-thick Al-Mylar foils is used as a total beam intensity monitor for all beams. To monitor beam intensity below 1 M cps, a thin plastic scintillator (PL) covered by a 48-μm-thick Al-Mylar foil is used. An adjustable energy degrader follows to control the LET, where the beam energy is adjusted by inserting up to ten Al foils with thickness ranging from 5 to 975 μm. At the sample irradiation position, the range value of the beam is measured using a small air-ionization chamber (IC2), and the beam energy is measured with a replaceable Si-detector stack (SSDs) 2 mm in total thickness.

As a next step, the client plans to use heavier beams with a higher linear energy transfer (LET) for the SEE test. Therefore, we have studied the characteristics of ^{136}Xe and ^{197}Au beams in the air. In Table 1, the measurement results and the irradiation parameters for the Xe and Au beams are summarized and compared with those of Ar and Kr beams. Since the Xe and Au beams are slow, we minimized the thickness of materials in the beam line. The vacuum separation window was replaced with a 25-μm thick Kapton foil. For the Xe beam, we used a 100-μm-thick PL scintillator, while for the Au beam, we did not use a PL scintillator or a beam scattering foil. The air path lengths Lair1 and Lair2 indicated in Fig. 1 were minimized as well.

We first measured the range of the beams in Al at the exit of the energy degrader. On increasing the degrader thickness, the IC2 current increased until the Bragg peak and dropped at the range of the ions. From this measured range of values, we obtained the maximum beam energy on a sample placed in the air by referring to the thickness-energy relation from SRIM[3] calculations. In the same manner, the SSDs were energy-calibrated by changing the degrader thickness.

From the measured energy spectra of SSDs, the LET peak value and its 1σ width in a Si sample were calculated. The corresponding range of values of the beam in Si is listed. According to the client, a beam range of 50–100 μm is indispensable for the SEE test of usual semiconductor devices. A high-LET condition near the
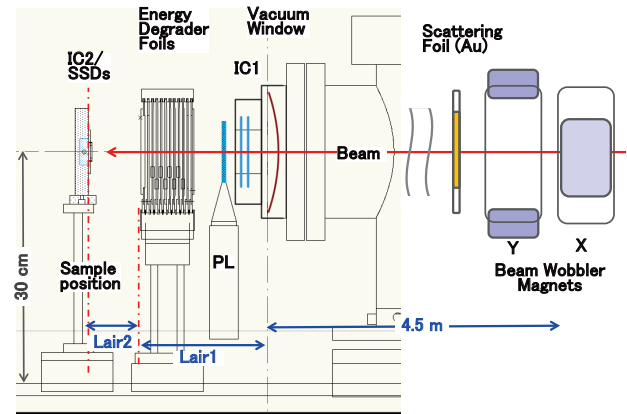
Fig. 1. Irradiation setup at the E5-A beam line.

Table 1. Summary of irradiation parameters.

Beam	40Ar	84Kr	136Xe	197Au	
Accelerators	AVF +RRC	AVF +RRC	RILAC1 +RRC	RILAC1 +RRC	
E in vacuum	95.0	70.0	39.0	18.4	A.MeV
Scattering foil : Au	75	50	20	0	μm
Vacuum foil: Kapton (diameter)	75 (Φ6)	75 (Φ6)	25 (Φ5)	25 (Φ5)	μm (Φcm)
PL scintillator	500	500	100	0	μm
Air path: Lair1	14.5	14.5	14.5	10.5	cm
Lair2	16.0	16.0	2.0	2.0	cm
* Exp.Range in Al	3260	715	175	60	μm
without energy degrader Al–foil; *max. E on sample surface*					
* E on sample	81.19	41.82	17.34	4.62	A.MeV
* σE on sample	8.4	18.0	32.7	41.8	MeV
Range (σR) in sample: Si	3567.0 (16.5)	722.7 (6.3)	180.2 (4.4)	56.6 (1.7)	μm
corresponding LET (σLET) in Si	2.21 (0.03)	13.48 (0.07)	47.19 (0.32)	94.09 (0.11)	MeV/ (mg/cm2)
maximum LET in Si at Bragg peak	18.7	41.0	70.0	95.0	MeV/ (mg/cm2)
with energy degrader Al–foil ; *near to the Bragg peak*					
Degrader foil: Al	3124.8	586.8	113.6	15.7	μm
* E on sample	6.78	5.90	6.01	2.50	A.MeV
* σE on sample	48.2	49.8	52.2	22.6	MeV
Range (σR) in sample: Si	77.8 (14.6)	59.6 (6.3)	61.9 (3.4)	37.5 (1.2)	μm
corresponding LET (σLET) in Si	11.69 (0.93)	37.10 (0.96)	66.50 (0.67)	91.35 (0.70)	MeV/ (mg/cm2)

*) measured value

Bragg peak was also measured by controlling the thickness of the degrader.

From this result, the ^{136}Xe beam is available for the SEE test with a LET value ranging from 47 to 67 MeV/(mg/cm^2). On the other hand, the maximum energy of the ^{197}Au beam in the air corresponds to its maximum LET at the Bragg peak. More detailed information on the E5A beam line is provided in our home page[4].

References
1) T. Kambara, RIKEN Accel. Prog. Rep. **48**, 239 (2015).
2) T. Kambara, RIKEN Accel. Prog. Rep. **49**, 193 (2016).
3) J. F. Zeigler, http://www.srim.org/
4) http://ribf.riken.jp/sisetu-kyoyo/equipments/e5a.html.

*1   RIKEN Nishina Center

Evaluation of radioactivity in semiconductor samples by Kr-ion beam irradiation

T. Kambara[*1] and A. Yoshida[*1]

On the basis of a fee-based facility-sharing program, RIKEN provides heavy-ion beams from RIKEN Ring Cyclotron (RRC) to private companies for the irradiation of semiconductor devices to be used in satellites. By using the accelerated heavy ions, the clients simulate the single-event effects (SEEs) of the devices caused by heavy-element components of cosmic rays. The samples are irradiated at the E5A beamline[1] in the atmosphere, and the linear energy transfer (LET) of the beam can be adjusted with an energy-degrader system. During the irradiation, the samples become radioactive through two processes: (1) nuclear reactions in the sample induced by the beam and (2) the injection of secondary nuclides produced in upstream materials. The secondary nuclides contaminate the beam and affect the LET distribution, while the nuclear reactions in the sample may contribute to SEEs. To assess the beam contamination and to understand the irradiation effects in industrial utilization, we studied the radionuclides in the irradiated samples by employing a radiochemical method.

In March 2017, during beam preparation and characterization for a client's beam utilization, we irradiated test samples with a ^{84}Kr beam under the same condition as the client's irradiations. A 70-MeV/nucleon ^{84}Kr beam from the RRC passed through a 50-μm-thick Au foil as a scatterer, a Kapton window separating vacuum and the atmosphere, an ionization chamber, a 0.1-mm-thick plastic scintillator, an energy degrader consisting of a 586-μm-thick aluminum layer, and an approximately 305-mm-thick atmosphere, following which it impinged a test sample of Si wafers (100-mm diameter and 0.5-mm thickness) or acrylic plates (75 mm × 80 mm, 1-mm thickness), where two identical plates were stacked for each material. The Si test sample was selected to simulate the clients' sample of semiconductor devices, and the acrylic resin was used to distinguish different activation processes. The yield of the secondary nuclides from the upstream materials should be independent of the sample materials, whereas that of the reaction products in the samples should be dependent. The number of the ions was approximately 4.5×10^{10} for the Si wafers and 5.5×10^{10} for the acrylic plates during irradiation for 10 min. According to SRIM calculation,[2] the ions impinged the sample at 25 MeV/nucleon, which corresponded to an LET of approximately 19 MeV/(mg/cm^2) in Si, and the primary ^{84}Kr ions stopped in the first plate of the stack. In the following, we report the analyses of the first plate, which had most of the radioactivity.

We measured the gamma rays from the irradiated samples with Ge detectors; for the Si wafer, we performed measurements 9 times from 7 min to 91 days after the irradiation, and for the acrylic plate, we performed measurements 9 times from 10 min to 106 days. We analyzed the observed gamma-ray peaks according to the transition energies, lifetimes, and branching ratios, and we identified 61 radionuclides from ^{24}Na to ^{104}Ag in the Si wafer and 49 nuclides from ^{24}Na to ^{93m}Mo in the acrylic plate. Subsequently, we extrapolated the decay curves of radioactivity to the end of the irradiation time to obtain the production rates of the nuclides and deduced their production probabilities normalized to one incident ^{84}Kr ion.

Figure 1 shows some of the obtained nuclide-production probabilities. Nuclides with atomic number $Z \leq 36$ have similar production probabilities between the Si and acrylic samples, except for a few small-Z nuclides, which indicates that these consist mainly of secondary nuclides produced in the upstream materials. The production probabilities of nuclides with $37 \leq Z \leq 42$ are similar or higher in the acrylic sample compared with the Si sample; in particular, those of ^{83}Rb and ^{84}Rb are three to four times higher. Nuclides with $Z > 42$ are found only in the Si sample, which indicates that these nuclides are only produced by nuclear reactions in the Si sample.
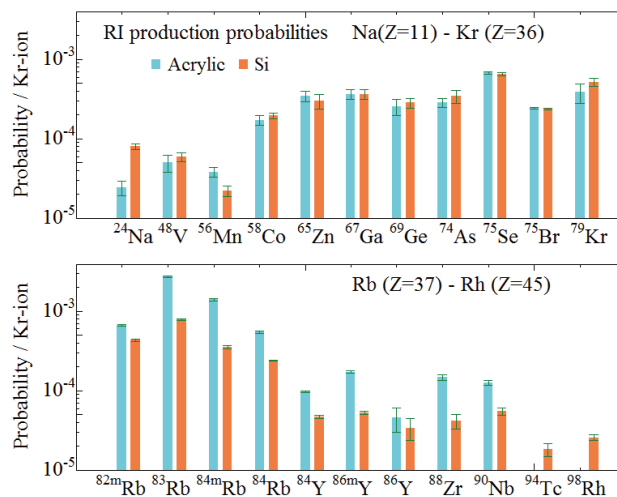
Fig. 1. Production probabilities of nuclides from ^{24}Na to ^{98}Rh obtained by the gamma-ray measurements.

References
1) T. Kambara, A. Yoshida, RIKEN Accel. Prog. Rep. **48**, 239 (2015).
2) J. F. Ziegler, http://www.srim.org.

*1　RIKEN Nishina Center

Computing and network environment at the RIKEN Nishina Center

T. Ichihara,[*1] Y. Watanabe,[*1] and H. Baba[*1]

We are operating Linux cluster systems[1,2] at the RIKEN Nishina Center (RNC).

Figure 1 shows the current configuration of the Linux servers at the RNC. The major part of the systems is installed in the 1F server room of the RIBF building that is equipped with emergency power supply and UPS systems, which ensure the non-stop operation of the computing system, even during power outages. We replaced the UPS systems (20 kVA) in December 2017, which were installed in 2005.

The host *RIBF.RIKEN.JP* is used as the mail server, NFS server of the user home directory, and the NIS master server. This is the core server for the RIBF Linux cluster with approximately 700 registered user accounts. Because six years had passed since the installation of this server, we replaced it with a new server, HP-DL380G9 with SL7.4 OS in January 2018. At the same time, the RAID for user home directory /rarf/u/ was replaced.

Fig. 2. Mail trends:message categories in 2017.

We installed three RAID units for *RIBFDATA02* and *RIBFDATA03* in 2012 for data analysis and raw data storage of RIBF experiments, as shown in Fig. 2. Each RAID consists of 24 units of 3 TB Hard Disk Drives(HDD), Seagate ST33000650SS. Suddenly after October 2017, we encountered frequent failures of HDDs of these RAIDs. Because of the redundancy of the RAID6 system, RAID volume is healthy up to the simultaneous failure of two HDDs. However, we encountered successive failures of three HDDs, resulting in volume failure of the RAID. After the investigation, we noticed that the Seagate 3 TB HDD used in the RAID is very fragile.[3] Therefore, we decided to replace all the HDDs (72 units) of these RAIDs with reliable HGST 6 TB HDDs. This will be done by March 2018. After the replacement, the capacity of the RAID will double and reliability will increase.

The hosts *RIBFSMTP1/2* are the mail gateway, which are used for tagging spam mails and isolating virus-infected mails. The latest version of Sophos Email Protection-Advanced (PMX 6.4.1) has been installed. Figure 2 shows the mail trends in 2017. Approximately 39% of the incoming mails were blocked by PMX ip-blocker.

An anonymous ftp server, *FTP.RIKEN.JP*, is managed and operated at the RNC. Major Linux distributions, including Scientific Linux, Ubuntu, and CentOS, are mirrored daily for the convenience of their users and for facilitating high-speed access. An HP-DL380G6 server was installed in 2009, and it was replaced by HP-DL380G9 with SL7.4 OS in June 2017.

Fig. 1. Configuration of the RIBF Linux cluster.

References
1) https://ribf.riken.jp/comp/
2) T. Ichihara *et al.*, RIKEN Accel. Prog. Rep. **50**, 226 (2017).
3) https://www.backblaze.com/blog/hard-drive-reliability-stats-for-q2-2015/

*1 RIKEN Nishina Center

CCJ operations in 2017

S. Yokkaichi,[*1] H. En'yo,[*1] T. Ichihara,[*1] and Y. Watanabe[*1]

1 Overview

The RIKEN Computing Center in Japan (CCJ)[1] commenced operations in June 2000 as the largest off-site computing center for the PHENIX[2] experiment being conducted at RHIC. Since then, CCJ has been providing numerous services as a regional computing center in Asia. We have transferred several hundred TBs of raw data files and nDST[a] files from the RHIC Computing Facility (RCF)[3] to CCJ.

Many analysis and simulation projects are being carried out at CCJ, and these projects are listed on the web page `http://ccjsun.riken.go.jp/ccj/proposals/`. As of December 2017, CCJ has contributed to 43 published papers and 42 doctoral theses.

2 Computing hardware and software

The network configuration and the computing hardware (nodes) and software (OS, batch queuing systems, database engine, etc.) are almost same as described in the previous APR.[1] We had 28 computing nodes, of which 18 nodes were purchased in Mar. 2009 and 10 nodes were purchased in Mar. 2011. In 2017, two old nodes out of these were retired. Thus, in total, 368 ($=8\times16$ nodes $+ 24\times10$ nodes) jobs can be processed simultaneously by these computing nodes using a batch queuing system LSF.[4] The version of LSF is 9.1, which was upgraded from 8.0.0 in Mar. 2016.[b]

One database (postgreSQL[5]) server and one AFS[6] server are operated in order to share the PHENIX computing environment. Now, only the SL5[7] environment is shared by the computing nodes, which have approximately 0.9 TB of library files. We have two data-transfer servers, on which the grid environment[8] is installed for the data transfer to/from RCF. Two new data-transfer servers will be delivered in Jan. and Mar. in 2018. After the deployment of the two, the current two servers will be retired. Data transfer of the order of 100 TB from J-PARC and BNL will be performed in the future.

Moreover, two login servers, one main server (users' home directory, NIS, DNS, NTP), and two disk servers are operated. In July 2017, a disk server machine was replaced by HP DL180 Gen9, which has 25.5 TB of SATA RAID6. In August 2017, a login server machine was replaced by HP DL20 server with SL7.4.

Table 1 lists the number of malfunctioning SATA or SAS disks in the HP servers, namely, computing nodes and NFS/AFS servers.

The current total power of the four UPSs is 40 KVA, in which one 10-KVA UPS will require an exchange of batteries soon. Downsizing of the machine rooms (258/260 in Main Bldg.) was planned in 2017, but it has been postponed.

3 Joint operation with ACCC/HOKUSAI

CCJ and the RIKEN Integrated Cluster of Clusters (RICC) have been jointly operated since July 2009. In April 2015, a new system named "HOKUSAI Greatwave" was launched by RIKEN ACCC[9] and the joint operation with CCJ has been continued, including a new hierarchical archive system in which approximately 900 TB of CCJ data are stored. The dedicated usage of 10 nodes, a legacy of old RICC, was also continued and ended in June 2017, at the time of deployment of the new cluster system "HOKUSAI BigWaterFall" by ACCC.

The usage of BigWaterFall, which has 840 nodes/33600 CPU cores, by CCJ has not been started yet. It is planned to use one of the "container technologies" (such as "Docker"[10]) to share the computing environment of PHENIX, in place of NFS, which was used in the old "dedicated" system. When NFS is not used, the nodes can also be used by other users of Hokusai, which results in more efficient usage of Hokusai's CPUs.

Table 1. Number of malfunctioning HDDs in HP servers (calculation nodes and NFS/AFS servers) in 2011–2017, including nodes retired in 2017.

Type (Size)	total	2017	'16	'15	'14	'13	'12	'11
SATA (1 TB)	192	18	8	14	11	16	20	9
SATA (2 TB)	120	10	2	10	0	2	5	4
SATA (4 TB)	10	-	-	-	-	-	-	-
SAS(146 GB)	38	1	5	3	2	0	1	1
SAS (300 GB)	26	1	0	1	1	0	0	1

References
1) S. Yokkaichi *et al.*, RIKEN Accel. Prog. Rep. **50**, 225 (2017).
2) `http://www.phenix.bnl.gov/`
3) `https://www.racf.bnl.gov/`
4) `http://www-03.ibm.com/systems/technicalcomputing/platformcomputing/products/lsf/index.html`
5) `http://www.postgresql.org/`
6) `http://www.openafs.org/`
7) `http://www.scientificlinux.org/`
8) `http://www.globus.org/toolkit/docs/latest-stable/gridftp/`
9) `http://accc.riken.jp/`
10) `https://www.docker.com/`

[*1] RIKEN Nishina Center
[a] term for a type of summary data files in PHENIX
[b] It was performed in 2016 and should be written in the previous APR.[1]

III. RESEARCH ACTIVITIES II
(Material Science and Biology)

1. Atomic and Solid State Physics (Ion)

Anomalous peak effect in 122-type iron-based superconductors

T. Tamegai,[*1] N. Ito,[*1] S. Pyon,[*1] A. Ichinose,[*2] A. Yoshida,[*3] and T. Kambara[*3]

Iron-based superconductors (IBSs) have attracted considerable attention due to their potential for high-field applications. In such applications, the critical current density, J_c, has to be reasonably large even under strong magnetic field. Introduction of artificial pinning centers in terms of heavy-ion irradiation, which creates columnar defects (CDs), is one of the promising ways to enhance J_c.[1] The effects of heavy-ion irradiation have been studied in 122-type IBSs.[2–4] The first attempt to create CDs in Ba(Fe,Co)$_2$As$_2$ made its J_c more than five times larger compared with unirradiated crystals.[2] J_c has been enhanced to $\sim$15 MA/cm^2 in (Ba,K)Fe$_2$As$_2$ by irradiating various kinds of heavy ions.[3] Theoretically, it is predicted that further enhancement of J_c is possible by dispersing the direction of CDs, thereby suppressing the motion of kinks and promoting flux entanglements. In fact, we have confirmed that J_c in (Ba,K)Fe$_2$As$_2$ can be enhanced by $\sim$30% by dispersing the direction of CDs.[5] In the course of such studies, we discovered an anomalous peak effect in (Ba,K)Fe$_2$As$_2$ when CDs are introduced at angles of $\theta_{CD} = 15°$ or more.[5] The peak of J_c as a function of magnetic field appears at about 1/3 of the matching field B_Φ ($= n\Phi_0$, n: density of CDs, Φ_0: flux quantum).

In the present experiment, we studied how the anomalous peak effect shows up in another IBSs, Ba(Fe$_{0.93}$Co$_{0.07}$)$_2$As$_2$ ($T_c \sim$ 24 K). U ion irradiation of 2.6 GeV has been performed at the RI Beam Factory at RIKEN Nishina Center at a total dose of $B_\Phi = 8$ T. U ions are irradiated from two directions at $\pm\theta_{CD}$ with $\theta_{CD} = 0°$ to 30°. J_c is evaluated by measuring the magnetization of the sample with the help of the extended Beam model.

Figure 1(a) shows the magnetic field dependence of J_c at 25 K in (Ba$_{0.6}$K$_{0.4}$)Fe$_2$As$_2$ ($\theta_{CD} = \pm15°$) for the field angle from the c-axis, θ_H, from 0° to 20.6°. As we have mentioned above, an anomalous peak effect shows up at around $H \sim 1/3B_\Phi$. It should be noted that the anomalous peak is strongly suppressed when the direction of the magnetic field is away from the average direction of CDs. The magnetic field dependence of J_c in Ba(Fe$_{0.93}$Co$_{0.07}$)$_2$As$_2$ ($\theta_{CD} = \pm15°$) from $T = 2$ K to 20 K with the field parallel to the c-axis is shown in Fig. 1(b). Unlike the case of (Ba$_{0.6}$K$_{0.4}$)Fe$_2$As$_2$, no anomalous peaks are observed at $H \sim 1/3B_\Phi$ at any temperature. The weak anomalies observed below 5 kOe are due to the self-field effect as we have discussed in Ref. 4). In order to reveal the origin of the difference in the J_c behavior between the two materials, scanning transmission electron microscopy (STEM) observations
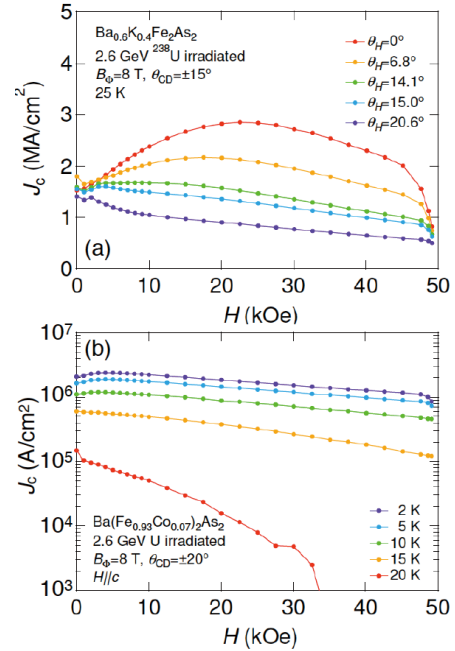
Fig. 1. Magnetic field dependence of J_c in (a) (Ba$_{0.6}$K$_{0.4}$)Fe$_2$As$_2$ ($T = 25$ K, $B_\Phi = 8$ T, $\theta_{CD} = \pm15°$) and (b) Ba(Fe$_{0.93}$Co$_{0.07}$)$_2$As$_2$ ($B_\Phi = 8$ T, $\theta_H = 0°$, $\theta_{CD} = \pm20°$).
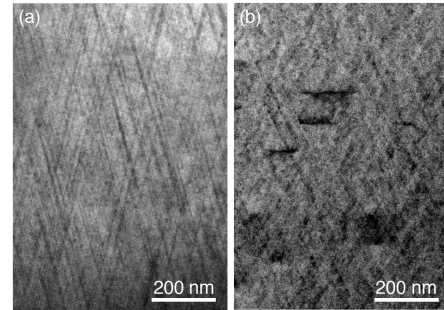
Fig. 2. STEM images of CDs created by 2.6 GeV U irradiation ($B_\Phi = 8$ T) in (a) (Ba$_{0.6}$K$_{0.4}$)Fe$_2$As$_2$ ($\theta_{CD} = \pm20°$) and in (b) Ba(Fe$_{0.93}$Co$_{0.07}$)$_2$As$_2$ ($\theta_{CD} = \pm30°$).

have been made. Figures 2(a) and (b) show STEM images for (Ba$_{0.6}$K$_{0.4}$)Fe$_2$As$_2$ and Ba(Fe$_{0.93}$Co$_{0.07}$)$_2$As$_2$. The defects created by 2.6 GeV U irradiation are almost continuous CDs in the case of (Ba$_{0.6}$K$_{0.4}$)Fe$_2$As$_2$, while they are strongly discontinuous in Ba(Fe$_{0.93}$Co$_{0.07}$)$_2$As$_2$. Such discontinuity of CDs are believed to make the effect of splay insignificant in Ba(Fe$_{0.93}$Co$_{0.07}$)$_2$As$_2$, leading to the suppression of the anomalous peak effect.

References
1) L. Civale *et al.*, Phys. Rev. Lett. **81**, 45 (1991).
2) Y. Nakajima *et al.*, Phy. Rev. B **80**, 012510 (2009).
3) F. Ohtake *et al.*, Physica (Utrecht) **518**, 47 (2015).
4) T. Tamegai *et al.*, Supercond. Sci. Technol. **25**, 084008 (2012).
5) A. Park *et al.*, Phy. Rev. B **97**, 064516 (2018).

*1 Department of Applied Physics, The University of Tokyo
*2 Central Research Institute of Electric Power Industry, Electric Power Engineering Research Laboratory
*3 RIKEN Nishina Center

Evolution of Kr precipitates in Kr-implanted Al as observed by the channelling method[†]

E. Yagi[*1] and S. Takagi[*2]

It was discovered that heavy inert gases (Ar, Kr, and Xe) implanted into metals at room temperature precipitate in bubbles into a solid phase (solid precipitates) in the high-pressure state. It became possible to produce inert gas solids at room temperature by a rather simple technique, *i.e.*, ion implantation, without applying a high-pressure technique, and transmission electron microscopy (TEM) became feasible. Since then, the structure of inert gas solids, which are the simplest atomic solids, and the process from nucleation to formation of inert gas solids have been extensively studied mainly by TEM. TEM is very useful for investigating visible-sized bubbles and a lot of data on their structure and behaviour have been obtained. For invisible small-sized defects such as those in the initial stage of nucleation, channelling analysis is particularly useful, because it can provide direct information on the lattice location of implanted atoms.

In this study, processes from nucleation to formation of solid Kr precipitates in Al implanted with Kr atoms at room temperature are discussed. In previous studies, experiments were performed for four different implantation doses, 1, 4, 10×10^{14}, and 1×10^{16} Kr/cm^2, by the channelling method and/or TEM. By the channelling method, it was suggested that at low implantation doses, Kr atoms interact strongly with vacancies introduced during Kr-implantation to form various types of Kr-vacancy (V) complexes and they act as nucleation centres for the Kr precipitates. According to the TEM, at a dose of 1×10^{15} Kr/cm^2, a number of cavities were observed, while, at a dose of 1×10^{16} Kr/cm^2, the presence of epitaxially aligned fcc solid Kr precipitates with a 1.3 times larger lattice parameter than that of Al was observed. Between the stages of nucleation and formation of solid Kr precipitates, the initial stage of growth of Kr precipitates to bubbles and a key process towards the epitaxial alignment of solid Kr precipitates remain unclear. The objectives of this study are to elucidate such unresolved processes through a change in the site occupancy of Kr atoms with dose and to discuss the evolution of Kr precipitates from nucleation to formation of solid Kr precipitates. Therefore, the channelling experiment is extended to the specimens implanted with four higher doses from 2×10^{15} to 8×10^{15} Kr/cm^2 at intervals of 2×10^{15} Kr/cm^2.

Kr-implantation was carried out at room temperature at 50 keV into Al single crystal slices. Channelling angular scan was performed at room temperature by Rutherford backscattering spectroscopy (RBS) with a

He$^+$ beam of 1.02 MeV accelerated by a tandem accelerator.

In the range of dose up to 2×10^{15} Kr/cm^2, Kr atoms are distributed over substitutional (S), tetrahedral (T), octahedral (O), and random (R) sites. With increasing dose, the fractions of T and S site occupancies decrease, while those of O and R sites increase. The T and O site occupancies are a result of the formation of Kr-V complexes; a Kr atom traps four vacancies (KrV_4) or six vacancies (KrV_6) to take configuration similar to trivacancy or pentavacancy, and is displaced to a T or an O site, respectively. The R site occupancy is attributed to Kr atoms associated with larger vacancy clusters. At low implantation doses, a Kr atom interacts with vacancies in its vicinity in the displacement cascade produced by the implantation of the Kr atom itself, because the overlapping of cascades is not significant. Such Kr-V complexes act as nucleation centres for the growth to Kr precipitates. With increasing dose, the overlapping of cascades becomes significant. In the initial stage of growth of Kr precipitates, not only existing Kr atoms at S sites but also additionally implanted Kr atoms migrate to Kr-V complexes, especially Kr associated large vacancy clusters, to be trapped, being assisted by mobile vacancies created by additional implantation (radiation-enhanced diffusion of Kr atoms). Thus, the fraction of Kr atoms associated with large vacancy clusters increases, resulting in Kr bubbles, which are in the fluid state. The fraction of the T site occupancy also decreases, while that of the O site occupancy increases.

At doses higher than 2×10^{15} Kr/cm^2, the fraction of the T site occupancy disappears, and that of the O site occupancy decreases. Instead, the displaced O (dis-O) site occupancy newly appears. This is interpreted as follows: small clusters of Kr atoms located at O and dis-O sites, the latter of which are displaced from O sites by about 0.4 Å in the $\langle 112 \rangle$ or $\langle 110 \rangle$ direction, are formed on the planes parallel to $\{111\}$ planes at the bubble-matrix interface. They are precursors for the two dimensional growth of Kr layers in parallel to $\{111\}$ planes with ordered arrangement of Kr atoms in the layers at higher implantation doses. With increasing dose to 8×10^{15} Kr/cm^2, bubbles, in which the pressure reaches the threshold value for solidification, solidify into an epitaxially aligned fcc structure. The ordered Kr layers act as a trigger for the formation of epitaxially aligned solid Kr precipitates. In the solidification, the increase in the internal pressure of bubbles by absorbing interstitials introduced during Kr implantation is important, as reported in previous channelling studies.[1]

Reference
1) E. Yagi, Phys. Rev. Lett. **67**, 3804 (1991).

Magnetism of the antiferromagnetic spin-3/2 dimer compound CrVMoO₇ having an antiferromagnetically ordered state[†]

M. Hase,[*1] Y. Ebukuro,[*2] H. Kuroe,[*2] M. Matsumoto,[*3] A. Matsuo,[*4] K. Kindo,[*4] J. R. Hester,[*5] T. J. Sato,[*6] and H. Yamazaki[*7]

In a magnetically ordered state, two types of magnetic excitations exist: gapless transverse-mode (Nambu-Goldstone mode) and gapped longitudinal-mode (amplitude Higgs mode) excitations. The former is well known as spin wave excitation. The longitudinal-mode (L-mode) was observed by inelastic neutron scattering experiments in the pressure-induced magnetically ordered state of TlCuCl₃, which is a three-dimensional (3D) interacting antiferromagnetic (AF) spin-1/2 dimer compound.[1–3] While the L-mode has weak intensity and spontaneously decays into a pair of transverse-modes, it is well defined in the ordered state in the vicinity of the quantum critical point for 3D systems.[4]

As for low-dimensional systems, it is difficult to observe the L-mode in longitudinal susceptibility by inelastic neutron scattering, since the longitudinal susceptibility exhibits an infrared singularity that can obscure the amplitude peak at a finite energy. In terms of scalar susceptibility, however, the L-mode can be well defined both in 2D and 3D systems. In magnetic systems, the L-mode was actually observed by Raman scattering experiments (which can measure the scalar susceptibility) in the pressure-induced ordered state of KCuCl₃ and in the magnetic-field-induced ordered state of TlCuCl₃.[5–7]

According to the results of theoretical investigations on interacting AF spin-cluster compounds, the L-mode excitations can be observed in the antiferromagnetically ordered state that appears on cooling under atmospheric pressure and zero magnetic field.[8] A shrinkage of the ordered magnetic moments by quantum fluctuations leads to a large intensity of the L-mode excitations. If the ground state of the isolated spin cluster is a spin-singlet state, the shrinkage of ordered moments can be expected in an ordered state that is generated by introducing intercluster interactions. We expect that an interacting AF spin-3/2 dimer model can be applied to the compound CrVMoO₇, judging from its crystal structure (Fig. 1).[9,10]

We studied the magnetic properties of CrVMoO₇ in powder form, using magnetization, specific heat, electron spin resonance, neutron diffraction, and inelastic
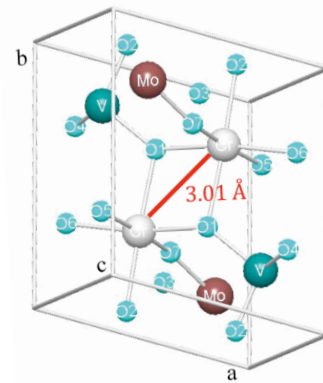
Fig. 1. The unit cell of CrVMoO₇. An AF spin-3/2 dimer is formed by two neighboring Cr³⁺ ions with a distance of 3.01 Å.

neutron scattering measurements. An antiferromagnetically ordered state appeared below $T_N = 26.5 \pm 0.8$ K. The magnetic susceptibility at high temperatures was close to that calculated for the isolated AF spin-3/2 dimer with an intradimer interaction of $J = 25 \pm 1$ K and $g = 1.92 \pm 0.02$. We were able to explain the magnetization curves on the basis of the interacting AF spin-3/2 dimer model with an effective interdimer interaction of $J_{eff} = 8.8 \pm 1$ K. The magnitude of the ordered moment was $0.73(2)\mu_B$, which is much smaller than the classical value of $\sim 3\mu_B$. Using inelastic neutron scattering measurements, the magnetic excitations were observed, and the results were qualitatively explained on the basis of the interacting AF spin-3/2 dimer model.

In conclusion, CrVMoO₇ is a rare spin-dimer compound that shows an antiferromagnetically ordered state under atmospheric pressure and zero magnetic field. Though we could not confirm the L-mode in this study, the magnetic excitations of L-mode would be observable in *single crystalline* CrVMoO₇.

References
1) Ch. Rüegg *et al.*, Phys. Rev. Lett. **100**, 205701 (2008).
2) P. Merchant *et al.*, Nat. Phys. **10**, 373 (2014).
3) M. Matsumoto *et al.*, Phys. Rev. B **69**, 054423 (2004).
4) I. Affleck, G. Wellman, Phys. Rev. B **46**, 8934 (1992).
5) H. Kuroe *et al.*, J. Phys.: Conf. Ser. **400**, 032042 (2012).
6) M. Matsumoto *et al.*, J. Phys. Soc. Jpn. **77**, 033702 (2008).
7) H. Kuroe *et al.*, Phys. Rev. B **77**, 134420 (2008).
8) M. Matsumoto *et al.*, J. Phys. Soc. Jpn. **79**, 084703 (2010).
9) X. Wang *et al.*, Inorg. Chem. **37**, 3252 (1998).
10) K. Knorr *et al.*, Eur. J. Solid State Inorg. Chem. **35**, 161 (1998).

†　Condensed from the article in Phys. Rev. B **95**, 144429 (2017)
*1　Research Center for Advanced Measurement and Characterization, NIMS
*2　Department of Physics, Sophia University
*3　Department of Physics, Shizuoka University
*4　ISSP, The University of Tokyo
*5　Australian Center for Neutron Scattering, ANSTO
*6　IMRAM, Tohoku University
*7　RIKEN Nishina Center

Investigation of single-event effect observed in GaN-HEMT

Y. Nakada,[*1] E. Mizuta,[*1] S. Kuboyama,[*1] and H. Shindou[*1]

Wide bandgap semiconductor devices, such as GaN and SiC, are attractive for next-generation satellites to reduce the energy losses in high-power and high-frequency systems. Although Si is still the dominant material used in space systems, there is a strong demand for new more efficient new devices. For GaN-HEMTs, the single event effects (SEEs) for tele-communication or radar components have already been evaluated. However, there are few reports for power-handling applications. For use in satellite power applications, it is necessary to resolve SEE mechanisms and take some appropriate steps.

In this study, we report the results of evaluating SEE on GaN-HEMT for power-handling applications. Table 1 lists the details of ions that were used for the evaluation in this study. Figure 1 shows device structures. The GaN-HEMT in this study is a commercial off-the-shelf 600 V device.

Typical experiment results are shown in Fig. 2. Figure 2(a) shows the change of I_{DS} during irradiation as a function of Xe fluence at $V_{GS}=0$ V. Devices were irradiated sequentially in steps of 20 V. Figure 2(b) shows I_{DS} and IGS at the end of each irradiation run as a function VDS. Therefore, the curves indicate the increase of leakage current induced by the heavy ions. For Xe ions, the leakage current increased continuously as the fluence increased in the range of 300–360 V, and finally the device was destroyed at 380 V because of excessive current. The continuous behavior suggests that the damages occur at localized damage sites introduced by each ion strike. For tests with Kr ions that at $V_{GS}=0$ V, the leakage current does not increase up to 500 V, and the device was suddenly destroyed at 520 V because of excessive current. On the other hand, for a test at $V_{GS}=+0.95$ V, device destruction did not occur until the rated voltage of the device. It is assumed that the reason why the device was not broken at $V_{GS}=+0.95$ V was the voltage drop between the drain and source due to the current flowing between the drain and source. The difference of behaviors between Xe and Kr ions might be attributable to the difference of LETs to create the damage sites. From Fig. 2, it can be seen that a large current flow between the drain and source. However, because the source pad of this device was connected to the substrate, to distinguish the current pass, a detailed electrical measurement was performed after cutting the connection between the source and substrate. Figure 3 shows the leak current between the drain and substrate after irradiation. Clearly, a conduction pass was observed between the drain and substrate.

To confirm the electrical pass between the drain and substrate, charge collection measurements with Kr ions

were performed before breakdown. In the measurements, the sample device works as a solid-state detector (SSD) for the particle-energy analyzing system, and the collected charge spectra are shown in Fig. 4. The figure also shows that charges flow between the drain and substrate. Moreover, the peak corresponds to the charge collected in the entire geometric active area on the Si substrate. Additionally, the collected charge is enhanced at a higher bias voltage. However, the maximum collected charge is approximately 1.0 pC, which is much less than the charge deposited in the Si substrate, approximately 70 pC. The active layer and Si substrate are electrically connected by a charge column generated by an ion, but the conductivity disappears while a small portion of the charge deposited in the Si substrate is collected.

In this experiment, the SEE in GaN-HEMT was observed. It is assumed that one failure mode of this GaN-HEMT is the electrical connection between the active layer and Si substrate due to ion incidence. On the other hand, this phenomenon might depend on the angle of ion incidence or portions on which ions are incident. In future work, it is necessary to change these parameters and to investigate another failure mode.

Table 1. Characteristics of the ion species.

Ion	^{86}Kr	^{136}Xe
Energy [MeV]	1600	2567
Range [um]	0.951	98.3
LET (GaN surface) [MeV·cm^2/mg]	18.0	36.2
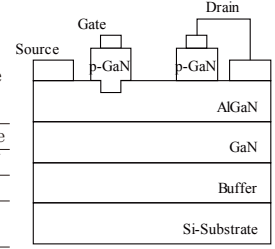
Fig. 1. Device structure.
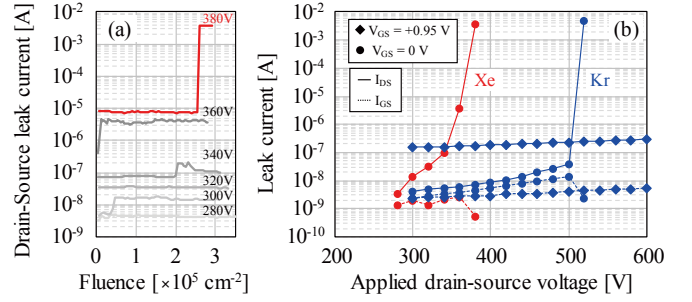
Fig. 2. Irradiation experiment results of GaN-HEMT.
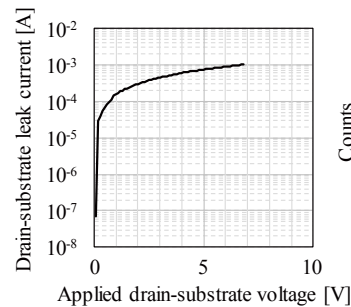
Fig. 3. Drain-substrate leak current after irradiation.
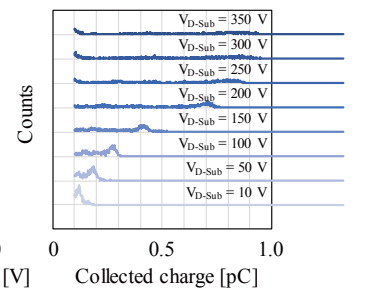
Fig. 4. Collected charge spectra.

*1 Research and Development Directorate, Japan Aerospace Exploration Agency

Profile measurements of laser beam for the aiming system of ion microbeam irradiation with glass capillaries

K. Hirose,[*1,*2] T. Ikeda,[*1,*2] K. Sato,[*1,*2] M. Matsubara,[*2] T. Masuyama,[*2] T. Minowa,[*2] and W.-G. Jin[*2]

Ion beam irradiation on biological objects has played an important role in applications such as cancer therapy, mutation induction in plants, etc., which are based on DNA damaging. The mechanism of DNA repair can be investigated by performing microbeam irradiation to a small area of the nucleus in order to artificially induce accumulation of proteins for repairing. One of the methods for producing the microbeams for irradiation on cell nuclei involves the use of tapered glass capillary optics whose beam inlet and outlet diameters are ∼1 mm and several micrometer, respectively. A microbeam irradiation system employing a glass capillary and MeV H/He ions generated by Pelletron accelerator has been developed at RIKEN.[1] So far, irradiation experiments have been performed on HeLa cells,[2] *E-coli.* cells,[3] and medaka embryos. To maintain a high accuracy while shooting the targets, we introduce an aiming system that utilizes laser μm-spot for a cell and sub-mm-spot for insects. The laser spotlight is generated by the glass capillary, which is also used to produce the ion microbeam, because the capillary can transmit both ions and laser at the same time. In the case of the aiming system, the transmitted laser is used to spotlight the target prior to ion irradiation. When the wavelength of the laser is selected as the excitation energy of a specific fluorescent protein or fluorescent dye, only the labeled target to be irradiated will be recognized.

The laser transmission experiments have been carried out with tapered glass capillary optics in Toho University. The transmission characteristic was studied by comparing the transmitted laser powers of the experimental and simulated results. The simulation, including the real capillary shape, showed good agreement with the experimental data.[4] In order to apply this technique to the aiming system for a sub-mm-sized target on the surface of a small live insect in air, profile measurements of the laser spot should be performed to define the spot size as the area having a power density larger than the threshold density to detect the fluorescence from the target. In this case, the irradiation distance will be several millimeter.

The profiles of the laser beams extracted from the glass capillaries were measured at Quantum Electronics Lab. in Toho Univ. The laser beam from an Ar$^+$ laser source (wavelength = 488 nm, CW power = 15 mW) was introduced into an aperture having a diameter of 1 mm, followed by a tapered glass capillary. The glass capillaries with a beam inlet of 1.8 mm in diameter were fabricated by the authors so that the outlet sizes range from 5.7 to 21.5 μm. The capillary entrance surface was
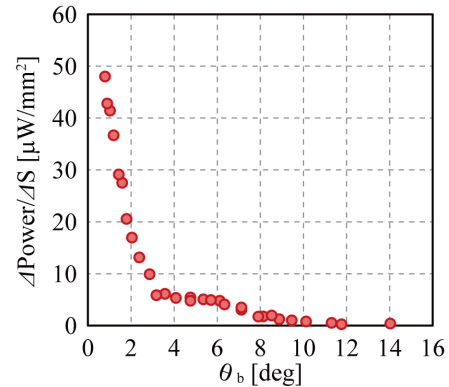
Fig. 1. Extracted laser profile. The vertical axis represents the power density when the target is located 14 mm downstream of the capillary outlet whose diameter is 21.5 μm.

covered with silver paste to prevent the laser from transmitting through the glass wall. Due to refraction, some fraction of the laser beam in the capillary penetrates the inner wall and travels outside toward the downstream, which forms a serious background in the power measurement of the beam extracted only from the capillary outlet. To avoid the background, the bottle shaped region of the capillary, which has the maximum taper angle, is also covered with the silver paste. The power of the extracted beam was measured using a power meter based on a photodiode.

For the first time, the power densities of the developed aiming laser at the 21.5 and 11.7 μm capillary outlets were obtained as 0.40 and 1.26 μW/μm^2, respectively, which were 104 and 327 times larger than those at the inlets, where the input power was measured to be 9.8 mW. Figure 1 shows the laser microbeam profile for the capillary outlet with a diameter of 21.5 μm, employing apertures of various sizes to cut the beam profile. The horizontal axis represents the angle with respect to the capillary direction, and the vertical axis represents the power density when the target is located 14 mm downstream of the capillary outlet. The density map was measured, also for the first time, to estimate the spot size at the target in terms of sufficient excitation light area. The plot shows that the effective spot area is limited to within about 3° with respect to the spot center. The calibration measurement of the center position difference between the ion microbeam and the laser spot using the Pelletron accelerator is in progress.

References
1) V. Mäckel *et al.*, Rev. Sci. Instrum. **85**, 014302 (2014).
2) Y. Iwai *et al.*, Appl. Phys. Lett. **92**, 023509 (2008).
3) M. Kato *et al.*, Appl. Phys. Lett. **100**, 193702 (2012).
4) W.-G. Jin *et al.*, J. Phys. Soc. Jpn **84**, 114301 (2015).

*1　RIKEN Nishina Center
*2　Department of Physics, Toho University

2. Atomic and Solid State Physics (Muon)

First measurement of magnetic correlations in T*-214 cuprate

K. M. Suzuki,[*1] S. Asano,[*1] I. Watanabe,[*2] and M. Fujita[*1]

Superconductivity in copper oxides is considered to appear with either hole- or electron-doping into an antiferromagnetic Mott insulator. However, the appearance of superconductivity in a parent compound has been recently reported for R_2CuO_4 (R = Pr, Nd, Sm, Eu) with the Nd_2CuO_4-type structure.[1] An ab-initio calculation supports the fact that the T' structured compound with CuO_4 coplanar coordination has a rather metallic ground state, in contrast to the Mott insulating state of T structured compound with CuO_6 octahedra.[2] These results suggest the dominant role of Cu coordination in determining the physical properties of CuO_2 plane.

There is another 214 system, namely, T*-structured copper oxide which has the intermediate crystal structure between the T and T' structures with CuO_5 pyramid coordination. T*-structured $Nd_{2-x-y}Ce_xSr_yCuO_4$ is known to exhibit superconductivity below $T_c \sim 32$ K after heat treatment under high oxygen pressures.[3] Although the T* compound is suitable for a study of the relation between the Cu coordination and the physical properties, only little is known about the magnetism of the T*-structured compound.

We performed muon spin rotation/relaxation (μSR) measurements to investigate the magnetism of the T* compound. We chose $La_{1-x/2}Eu_{1-x/2}Sr_xCuO_4$ (LESCO) as a target substance because magnetic rare earth ions are absent and thereby μSR data can be simply analyzed as the intrinsic signal from Cu^{2+} spins. The pelletized polycrystals were fired at 1050°C in air. Subsequently, the as-sintered samples were annealed under high oxygen pressure of 400 atm at 500°C for 60 h to obtain superconducting (SC) samples with T_c = 20–30 K. The heat treatment was performed in the Koike Laboratory in Tohoku University. Zero-field μSR measurements were performed on both as-sintered and annealed samples using the spectrometer CHRONUS installed at Port 4, RIKEN-RAL.

Figure 1 shows the zero-field μSR time spectra for the as-sintered LESCO with x = 0.16. A slow Gaussian-type decay can be observed in the time spectra at high temperatures above 30 K. Upon cooling, the muon spin relaxation changes gradually and an exponential-type decay component appears below 10 K, suggesting the development of electronic magnetic correlations. No evidence of oscillatory behavior down to the lowest temperature of 5.0 K indicates the absence of long range magnetic order in this compound. In the as-sintered LESCO, the temperature

below which the muon spin relaxation begins to develop, tends to decrease with hole doping from $\sim$30 K (x = 0.14) to $\sim$ 15 K (x = 0.24). This is basically the same trend as the doping evolution of magnetic correlations in $La_{2-x}Sr_xCuO_4$ (LSCO) and $YBa_2Cu_3O_{7-\delta}$. Compared to as-sintered T' compounds in which the long-range magnetic order is formed at low temperatures, spin correlation is rather weak in the T* compound. The in-plane defects possibly cut off the superexchange paths between the neighboring Cu and O ions in the T* compounds, resulting in the degradation of spin correlations, while partially existing apical oxygens do not directly break the superexchange coupling in the T* compound.

The SC samples of LESCO with x = 0.14 and 0.18 do not show any indication of the development of muon spin relaxation down to 2 K. Therefore, it was revealed that the oxygen annealing weakens the magnetic correlations in the $T^\star$-214 copper oxides. Furthermore, the absence of magnetic order in the SC LESCO with x = 0.14 and 0.18 is consistent with the result for LSCO with hole concentrations comparable to those of LESCO. To elucidate the universality of magnetism in the T and T* compounds, further measurements on underdoped LESCO are needed. Further investigation of the precise crystal structures before and after the oxygen annealing is also necessary to understand the physical properties of the T*-structured system and thier relation to local structures.
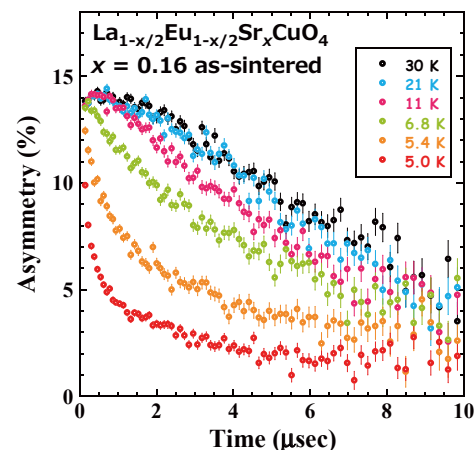
Fig. 1. The μSR time spectra for as-sintered and non-SC $La_{1-x/2}Eu_{1-x/2}Sr_xCuO_4$ with x = 0.16.

References
1) M. Naito et al., Physica (Utrecht) **523**, 28 (2016).
2) C. Weber et al., Nat. Phys. **6**, 574 (2010).
3) J. Akimitsu et al., Jpn. J. Appl. Phys. **27**, L1859 (1988).

*1 Institute for Materials Research, Tohoku University
*2 RIKEN Nishina Center

Nano-size effect on Néel temperature and magnetic ordering of La$_2$CuO$_4$

S. Winarsih,[*1,*2] F. Budiman,[*3] H. Tanaka,[*3] and I. Watanabe[*1,*2,*4]

Finite-size effects of antiferromagnetic materials, which refer to the reduction in particle size of antiferromagnetic materials until they become nanoscale sized, have received much attention in recent years.[1,2] As predicted by Néel, there will be uncompensated spin from the surface due to the reduction in particle size of antiferromagnetic materials until they become nanoscale sized. Because of this, antiferromagnetic nanoparticles exhibit superparamagnetic properties, and the physical properties of antiferromagnetic nanoparticles will change.[3]

La$_2$CuO$_4$ (LCO) is chosen because it is one of the typical Mott insulating systems and is the parental compound of the superconducting high-T_c cuprate; therefore, this work can provide the basic knowledge for studying the size effect on Mott insulating systems.[4] Prof. Tanaka's group as our collaborator the grain size can be controlled to be in the nanoscale range. As far as we know, there has been no similar research on high-T_c cuprates so far.

A previous measurement, which investigated other nanoparticle systems, proved that dc magnetic susceptibility cannot measure the T_N value of an antiferromagnetic material.[5] The transition temperature obtained by this measurement is the blocking temperature or freezing temperature of the antiferromagnetic material, and not T_N.[5] In this case, muon spin relaxation (μSR) was used to investigate the magnetic ordering of this material. Prof. Tanaka's group has already performed the dc susceptibility measurement of LCO 96 nm.[6] Therefore, we can compare and analyze the results from susceptibility measurement and μSR measurement.

Zero-Field (ZF) μSR measurement at RAL, UK, using single pulsed muon beam, was carried out in order to detect the muon spin precession of the material. The ZF-μSR time spectrum at various temperatures is shown in Fig. 1. The muon spin precession can be clearly seen to start from 35 K, indicating that antiferromagnetic (AF) ordering starts at this temperature; however, the precession disappears at 100 K. This suggests that the Néel temperature T_N of this material is between 35 K and 100 K. The value of T_N is significantly reduced compared to bulk LCO, which has $T_N = 240 \pm 10$ K.[4]

Figure 2(a) depicts the temperature dependence of the internal field, H_{int}. H_{int} is zero at 100 K, since no muon precession is observed at this temperature; it increases with a decrease in temperature and reaches a saturated internal field of 400 G. The same tendency of H_{int} dependence on temperature and the same saturated internal

field value is observed for LCO bulk material. However, in the bulk material, H_{int} is zero at 250 K. It means that although T_N decreases with reduction in particle size, the average magnetic moment and magnetic interaction are still the same.

The damping rate of muon spin precession, which is caused by the static and dynamic field dependence of this material on temperature, is demonstrated in Fig. 2. The damping rate seems to increase for temperatures below 100 K, achieve a maximum value at 35 K, and then decrease for temperatures below 35 K. The muon spin depolarization dependence of this material on temperature, which is shown in Fig. 2(c), also has the same tendency. It is indicated that below 35 K, the spin fluctuation slows down and there is an alignment of the magnetic moments of Cu^{2+}; this means that long range ordering starts at temperatures below 35 K.

We plan to complete ZF data between 35 K and 100 K in order to evaluate the T_N, and we are going to analyze the internal field of this material to find out whether it is coming from the static or dynamic spin fluctuation by measuring the Longitudinal Field (LF)-μSR. Besides, we plan to measure the other LCO nanoparticle whose particle size is different from that of this material. Hence, the analysis on the nano-size effect on Néel temperature and magnetic properties can be confirmed.
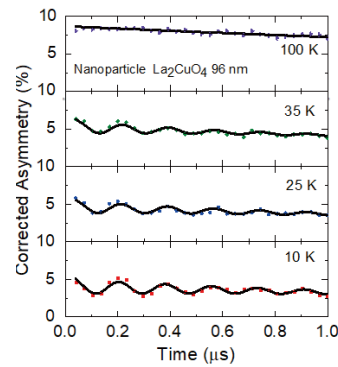
Fig. 1. ZF-μSR time spectrum of La$_2$CuO$_4$ with particle size of 96 nm.
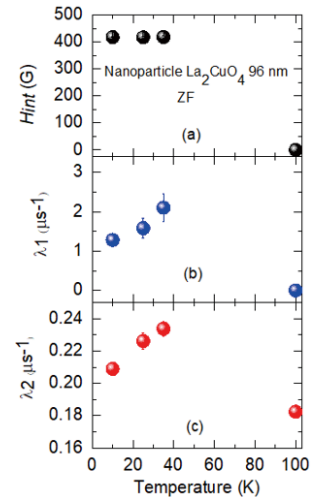
Fig. 2. Temperature dependence of (a) the internal field at the muon site; (b) the damping rate of muon spin precession; and (c) muon spin depolarization rate of La$_2$CuO$_4$ 96 nm.

References
1) M. M. Ibrahim *et al.*, Phys. Rev. B **51**, 2955 (1995).
2) S. Gider *et al.*, Science **268**, 77 (1955).
3) L. Néel, in *Low Temperature Physics*, (New York, 1962).
4) Budnick *et al.*, Phys. Lett. A **124**, 1, 2 (1987).
5) Tang *et al.*, Phys. Rev. B **67**, 054408 (2003).
6) H. Tanaka *et al.*, (in preparation).

*1　Department of Physics, Universitas Indonesia
*2　RIKEN Nishina Center
*3　Department of Human Intelligence Systems, Kyushu Institute of Technology
*4　Department of Physics, Hokkaido University

Effect of Supercell Calculation on Muon Sites in La$_2$CuO$_4$

M. R. Ramadhan,[*1,*3] M. I. Mohamed-Ibrahim,[*2] S. Sulaiman,[*2] and Watanabe[*1,*2,*3]

The muon spin relaxation (μSR) is a powerful tool for investigating the electronic states of Cu-based high-T_c superconducting oxides. It is important to understand the μSR data of the base material, La$_2$CuO$_4$ (LCO), especially in the magnetically ordered states, as it provides an insight to the other phases of this material. Although the μSR data can provide information on the local magnetic fields at the muon site, it is not so easy to obtain the details of the electronic structure surrounding the muons, which is the origin of the local fields at the muon site. This is because, we need to have the exact information on where the muon is located inside the material. Several attempts have been made to tackle this problem in the past.[1–3] However, a unified method to obtain the muon positions inside the material has not yet been established.

In this study, the effect of supercell calculation on muon sites inside La$_2$CuO$_4$ system were investigated. DFT method was applied to determine possible muon sites in LCO. To account for the correlation energy of the strongly localized copper $3d$ orbitals, we employed Hubbard correction within our calculations (DFT + U) with the Hubbard parameter $U = 10$ eV, which opens the gap in the Fermi level of the system (2.6 eV) showing an insulating nature as predicted in the experiments. Three minimum potentials were found at positions near the apical and planar oxygens, which correspond well to the μSR experimental results shown in Fig. 1. These three positions (M1, M2, and M3) were set to be the initial muon positions on a $4 \times 2 \times 4$ LCO supercell for subsequent calculations in order to include the effect of local deformations caused by the presence of muons inside the material, as the inclusion of lattice deformations were found to be important to simulate the muon presence in the system realistically. The local deformations induced by muons on each site is shown in Fig. 2. From our current results, it was observed that M1 and M3 relaxation will affect the position of Cu inside the octahedra and the nearest planar oxygen. M2 relaxation only affects the nearest planar oxygen in the system without shifting the Cu atoms. It was also observed from our calculation that the magnetic moment on the nearest Cu atom is changed by the presence of a muon. The initial value of 0.7 μ_B in the case without the muon system is slightly lowered by the presence of muon. However, these local deformations do not change the insulating and antiferromagnetic nature for our material.
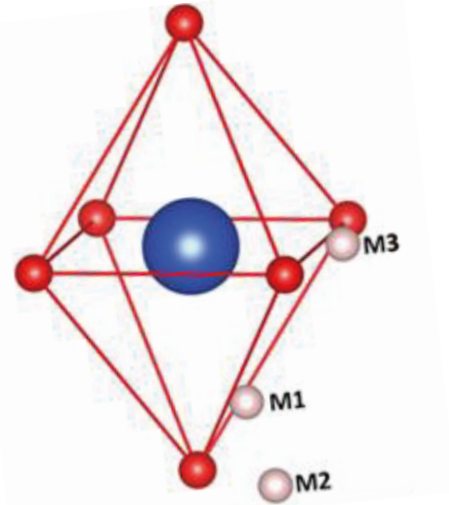
Fig. 1. Three minimum positions observed by the DFT method (muon positions are enlarged for clarity).
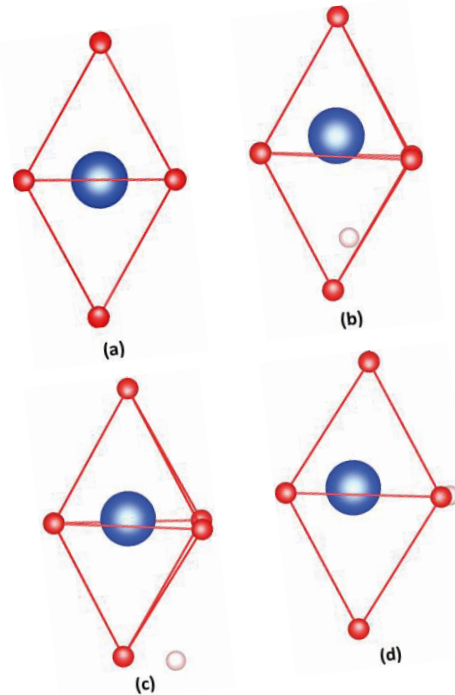
Fig. 2. Comparison of CuO$_6$ octahedra after relaxation (a) Without muon (b) M1 (c) M2 (d) M3.

References
1) R. Saito, *et al.*, Physica (Utrecht) C **185–189**, 1217 (1991).
2) S. B. Sulaiman, *et al.*, Phys. Rev. B **49**, 9879 (1994).
3) H. U. Suter, *et al.*, Physica (Utrecht) B **326**, 329 (2003).

*1　Department of Physics, Universitas Indonesia
*2　School of Distance Education, Universiti Sains Malaysia
*3　RIKEN Nishina Center

Modulated Kubo-Toyabe functions to study fluctuated weak magnetism and muon diffusion at pseudogap state of underdoped $La_{2-x}Sr_xCuO_4$

M. D. Umar[*1,*2] and I. Watanabe[*1,*2]

One of the interesting puzzles for understanding the nature state of the pseudogap at the cuprate-based high-temperature superconductor is the discrepancy between neutron scattering and muon spin relaxation experiments in the detection of spontaneous magnetic order by, for instance, orbital (loop) current or intra-unit-cell (IUC) magnetic order. A neutron scattering experiment on YBCO[1] has shown the presence of an ordered magnetic state preserving the translational symmetry of the underlying lattice, indicating the orbital current model. This result was also supported earlier by an angle-resolved photoemission spectroscopy (ARPES) experiment, which confirmed time-reversal-symmetry breaking (TRSB) at the pseudogap state of Bi-2212.[2] Contrary to Neutron scattering and ARPES results, μSR has confirmed the absence of TRSB associated with the spontaneous ordered magnetic state in the single crystal of LSCO.[3] However, using a pulse-μSR experiment, Watanabe *et al.*[4] strongly indicated the presence of weak magnetism at the pseudogap state in a polycrystalline LSCO sample.

A theoretical study[5] on the effect of screening charge density on a muon (point charge) has been proposed to explain the discrepancy. To confirm the presence of weak magnetism associated with the orbital current model or IUC magnetic order due to the screening process, by applying the Kubo-Golden Formula, we have extended known Kubo-Toyabe functions (muon spin relaxation functions) for four scenarios of the internal field distribution of nuclear moments on muon sites broadened by a comparable weak magnetism. The scenarios of two independent sources include a Gaussian distribution (nuclear moments) broadened by a delta-function distribution (ordered magnetic state in a polycrystalline sample), Lorentzian distribution, and Voigtian distribution. Another possibility for nuclear moments belonging to a Voigtian distribution broadened by weak sources with a Lorentzian distribution has been developed.

Since muon diffusion and the dynamic behavior of weak magnetism in the dependence of temperature and doping concentration can also possibly occur in a μSR experiment, we have extended muon spin relaxation functions for dynamic cases (modulated Kubo-Toyabe functions). The dynamic cases are constructed by applying a strong collision model with a modulated internal field on muon sites treated as a Markovian process. The equations of the modulated Kubo-Toyabe function for the developed scenarios exist in the Volterra integral equation, and they can be solved numerically. In our
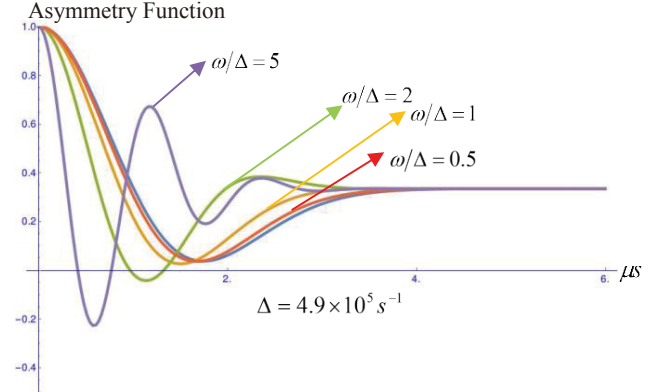
Fig. 1. Line shapes of the muon spin relaxation function for the summation of internal fields from the ordered magnetic state of a polycrystalline sample and nuclear moments in the zero-field condition plotted for different ratios of the field from the ordered magnetic state ($\omega = \gamma_\mu B$) to the width of the dipole nuclear field (Δ).
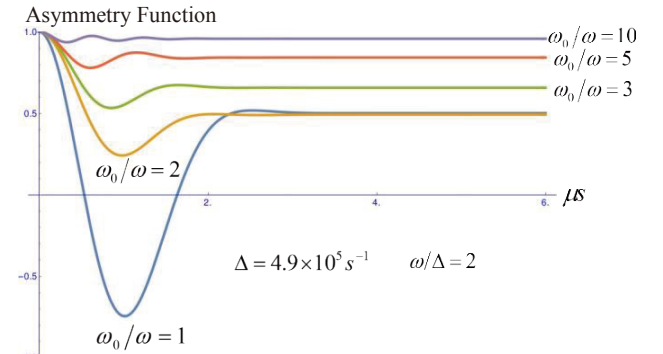
Fig. 2. Line shapes of muon spin relaxation function for the summation of internal fields from the ordered magnetic state of a polycrystalline sample and nuclear moments in the longitudinal-field (LF) condition plotted for different ratios of the applied longitudinal field ($\omega_0 = \gamma_\mu B_{LF}$) to the field from the ordered magnetic state ($\omega = \gamma_\mu B$).

ongoing research, we have been implementing the numerical solution of Volterra integral equation in Mathematica software with the trapezoidal method, in which every area of the partitioned integration interval is approached as a trapezoid.

References
1) B. Fauque *et al.*, Phys. Rev. Lett. **96**, 197001 (2006).
2) A. Kamiski *et al.*, Nature (London), **416**, 610 (2002).
3) G. J. MacDougall *et al.*, Phys. Rev. Lett. **101**, 017001 (2008).
4) I. Watabe *et al.*, J. Phys. Soc. Jpn. **73**, 2232 (2008).
5) A. Shekhter *et al.*, Phys. Rev. Lett. **101**, 227004 (2008).

*1　RIKEN Nishina Center
*2　Department of Physics, Hokkaido University

Study of Implanted Muons in YBa$_2$Cu$_3$O$_6$

I. Ramli,[*1,*2] S. S. Mohd-Tajudin,[*3] S. Sulaiman,[*3] M. I. Mohamed-Ismail,[*3] and I. Watanabe[*1,*2]

Since the discovery of cuprate-based high-Tc superconductivity, enormous efforts in both experimental and theoretical studies have invested to understand its superconductivity mechanism. However, this mechanism is still unclear and debatable. YBa$_2$Cu$_3$O$_6$ (YBCO$_6$) is one of the mother compunds of cuprate-based high-Tc superconductors. This system shows antiferromagnetic (AF) ordering with T$_N$ = 350 K.[1] The AF ordering of this system disappears by doping, YBa$_2$Cu$_3$O$_{6+x}$, and superconductivity appears.[2] We study the magnetic and electronic properties of YBCO$_6$ by using the muon-spin resonance (μSR) technique. This technique is extremely sensitive to probe local magnetism but has a limitation, because muon sites in the lattice and perturbation by muons to the host system are unknown.[3]

Therefore, we have been developing the method to estimate muon sites in YBCO$_6$ by using density functional theory (DFT) which is implemented in *Vienna Ab-initio Simulation Package* (VASP). Based on the μSR experimental data of YBCO$_6$ below T$_N$, three muon-spin precession components are observed, indicating the presence of three different kinds of muon sites in this system.

We first calculate the density of state and the band structure to confirm the insulator state in this system. Considering strong electron correlation among cuprate ions in this system, we optimize the exchange-correlation function and the value of Hubbard parameter (U). The second step is to calculate the potentials in this system under the same condition as that in the first step. In the calculation of the potential, the pseudopotential for hydrogen is used, because a muon is considered to be a light isotope of a proton. As a muon has a positive charge, it prefers to be located at sites of the local minimum of the potential. Thus the local minimum site can be regarded as the initial muon site. We found three kinds of muon sites (marked M1-M3) in YBCO$_6$ as shown in Fig. 1.

To investigate the effect of the presence of a muon in the system, we performed calculation by placing a muon at the initial site in the 4x4x2 supercell and allowing the lattice to be relaxed. Then, we got the final site of the muon, the change of local electronic states and spatial spin distributions.

We are also developing the program to calculate internal fields at the muon stopping sites. In this program, we considered zero point energy (ZPE) vibration of a muon because the muon is a light particle.
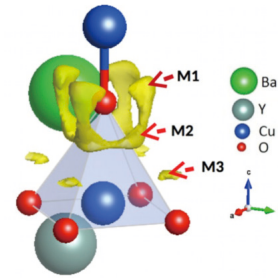
Fig. 1. Possible muon sites in YBCO$_6$ estimated from our DFT calculations. Yellow area indicates the isosurface at 500 meV.

The density distribution of the muon extends over the amplitude of the ZPE vibration. The density distribution of muon was calculated by solving the Schrödinger equation for the wave function of muon around the local minimum of potential in the range up to 1.5 angstrom. By taking all those results into account, we calculated the internal fields at each kind of muon site to be 116 G for the M1, 335 G for the M2, and 446 G for the M3 sites.

From previous μSR measurements for the antiferomagnetic phase of YBCO, Brewer *et al.* found one muon spin precession frequency in YBCO$_{6.2}$ which corresponds to the internal field 300 G[4] and Nishida *et al.* found two additional muon spin precession frequencies which correspond to the internal fields of 100–150 G and 1.8 kG. The amplitude of muon spin precession for the 1.8 kG is less than 1%.[5] The calculated values on the internal fields for the M1 and M2 sites are compatible with the experimental results, 100–150 G and 300 G, respectively. However, the calculated value for the M3 site is not compatible. To clarify the origin of this discrepancy in the values for the M3 site, the μSR measurement for the high-quality YBCO single crystal and further checking the calculation for the M3 site are still ongoing

References
1) N. Nishida *et al.*, Jpn. J. Appl. Phys. **26**, L1856 (1987).
2) Y. Koike *et al.*, J. Phys. Soc. Jpn. **85**, 091006 (2016).
3) P. Bonfa *et al.*, J. Phys. Soc. Jpn. **85**, 091014 (2016).
4) J. W. Brewer *et al.*, Phys. Rev. Lett. **60**, 1073 (1988).
5) N. Nishida *et al.*, Hypefine Interaction **63**, 183–197 (1990).

*1 RIKEN Nishina Center
*2 Department of Condensed Matter Physics, Hokkaido University
*3 School of Distance Education, University Sains Malaysia

μSR study of FeSe$_{1-x}$S$_x$ around nematic critical point

Y. Tanabe,[*1] R. Asih,[*2,*3,*4] I. Watanabe,[*2,*3] A. Takimoto,[*1] T. Urata,[*1] and K. Tanigaki[*1,*5]

Iron-based superconductors (FeSCs) provide an intriguing platform where the spin and orbital degree of freedom can contribute to the emergence of exotic phenomena including high temperature superconductivity. Superconductivity was usually observed in most FeSCs when antiferromagnetism in the parent materials was suppressed by chemical doping, indicating the competition between superconductivity and antiferromagnetism.[1] On the other hand, another electronic state called electronic nematicity was clarified where the lattice C_4 symmetry is spontaneously broken by some electronic origin.[2] The relation between superconductivity and electronic nematicity is one of key piece to understand the complex phase diagram. The recent nonmagnetic nematic states in FeSe may provide an opportunity to clarify this key piece. By sulfur doping on the selenium site, electronic nematicity was suppressed and superconductivity tended to be enhanced around the nematic critical point.[3] This may indicate a competitive relationship between superconductivity and electronic nematicity, whereas the magnetic phase diagram is still controversial in the FeSe$_{1-x}$S$_x$ system. In this report, we studied the magnetic phase diagram of FeSe$_{1-x}$S$_x$ ($0.09 \leq x \leq 0.15$) from the view of electrical transport and muon spin relaxation.

From electrical transports, the electronic phase diagram of FeSe$_{1-x}$S$_x$ was still unclear below the superconducting transition temperatures. Figure 1(b)–(d) shows the temperature dependence of the electrical resistivity in FeSe$_{1-x}$S$_x$ single crystals under various magnetic fields (Bs). At zero magnetic fields, the resistivity curves showed a kink due to the tetragonal to the orthorhombic structural transition at temperature ranges from 30–60 K in the present sulfur doping range. At low temperatures, superconducting transitions were observed at around 10 K. Both the superconducting transition temperature (T_c) and the structural transition temperature (T_s) were summarized in Fig. 1(a). By sulfur doping, T_s continuously decreased and disappeared around $x = 0.16$ together with the broad maximum of T_c around 0.125. Since the electronic nematic phase were previously clarified below $x = 0.15$ in the orthorhombic phase, the normal state resistivity curves unveiled by high magnetic fields would provide further information about the relationship between superconductivity and electronic nematicity. Under the magnetic fields, the resistivity curves showed a suppression
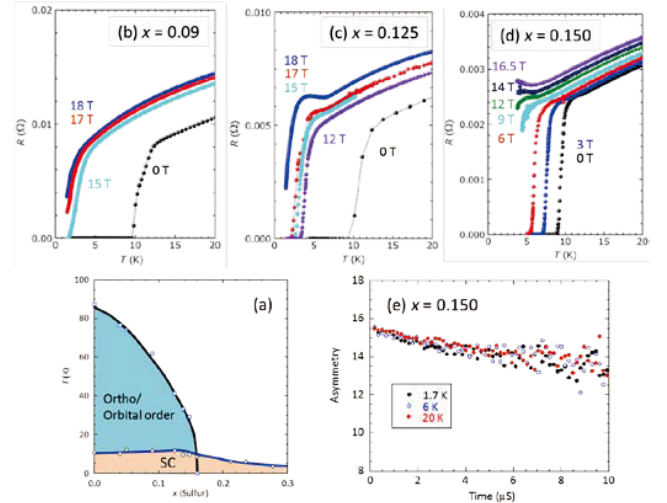
Fig. 1. (a) Electrical phase diagram of FeSe$_{1-x}$S$_x$. (b)–(d) Electrical resistivity curves for $x = 0.09 - 0.15$ under various magnetic fields. (e) μSR time spectra for $x = 0.15$ from 1.7 K to 20 K.

of T_c with an increase in B. For $x = 0.125 - 0.15$, other kink structures tended to be developed around 5 K, which resemble resistivity curves for the pressure induced antiferromagnetic transition in FeSe.[4] To clarify the hidden magnetic phase below T_c, we carried out the zero field (ZF) μSR measurements in FeSe$_{1-x}$S$_x$ as shown in Fig. 1(e). ZF-μSR showed the relatively exponential-like time spectra from 1.7 K to 20 K, being similar with those of the FeSe single crystal. All spectra considerably overlapped. These demonstrated no development of magnetism where anomalies were detected in the resistivity curves under high magnetic fields.

For $x = 0.125$–0.15, resistivity anomalies under high magnetic fields suggested a development of another new phase at low temperatures whereas no development of magnetism was detected by the ZF-μSR measurements. An origin of resistivity anomaly is still unclear in the present states. Since the nonmagnetic nematic quantum critical point (QCP) would be a key to understand the mechanism of the superconductivity from the comparison to the magnetic QCP, further studies clarifying an origin of low temperature anomalies in resistivity curves may be important to understand the relationship between superconductivity, magnetism and electronic nematicity.

References
1) H. Hosono, K. Kuroki, Physica (Utrecht) **514**, 399 (2015).
2) R. M. Fernandes *et al.*, Nat. Phys. **10**, 97 (2014).
3) S. Hosoi *et al.*, Proc. Nat. Acad. Sci. USA **113**, 8139 (2016).
4) J. P. Sun *et al.*, Nat. Commun. **7**, 12146 (2016).

*1 Department of Physics, Tohoku University
*2 RIKEN Nishina Center
*3 Department of Physics,Graduate School of Science, Osaka University
*4 Department of Physics, Faculty of Mathematics and Natural Science, Institut Teknologi Sepuluh Nopember
*5 WPI-AIMR, Tohoku University

Caged-type superconductor $Sc_5Ru_6Sn_{18}$ probed by μSR

Dinesh Kumar,[*1] C. N. Kuo,[*1] F. Astuti,[*2,*3] M. K. Lee,[*1] C. S. Lue,[*1] I. Watanabe,[*2,*3] and L. J. Chang[*1,*4]

Superconductors with caged-type structures have attracted considerable attention among researchers because of their fascinating characteristics, such as heavy fermion superconductivity and exciton-mediated superconductivity. These compounds crystallize in the tetragonal structure having space group $I4_1/acd$ and consist of three-dimensional skeletons that surround large atomic cages, in which small atoms are situated. One such type of caged compound is $R_5Rh_6Sn_{18}$ (R = Sc, Y, Lu), which exhibits superconductivity at 5 K (Sc), 3 K (Y) and 4 K (Lu),[1] where R occupies sites of different symmetry.[2] Superconducting gap structures and ZF-μSR have been studied in $Lu_5Rh_6Sn_{18}$ and $Y_5Rh_6Sn_{18}$,[3,4] where the time-reversal-symmetry-broken phenomenon has been observed below T_c in both compounds. However, $Lu_5Rh_6Sn_{18}$ is a strong-coupling s-wave superconductor with isotropic gap; while $Y_5Rh_6Sn_{18}$ reveals an anisotropic superconducting gap with a point node. These experimental results in sharp contrast motivate us to study the time-reversal-symmetry-broken mechanism in the $R_5M_6Sn_{18}$ (R = Sc, Y, Lu; M = Co, Rh, Ru, and Ir) family. $Sc_5Ru_6Sn_{18}$ is the first compound for our studies. $Sc_5Ru_6Sn_{18}$ has $T_c \approx 3.5$ K. The T^3 dependence of electronic heat capacity (C_e) below T_c at zero field clearly indicates that $Sc_5Ru_6Sn_{18}$ has an anisotropic superconducting gap with a point node.

In the ZF-μSR measurement, the sample temperature was changed in the ZF condition from approximately 30 K ($> T_C$) down to 1.6 K ($< T_C$). The sample was cooled down using a helium-flow cryostat in the He exchange gas, maintaining good temperature homogeneity. The time dependence of $A(t)$, which is called the μSR time spectrum, was measured. Figure 1(a) shows the μSR time spectrum measured at various temperatures crossing T_c. Time spectra were analyzed by using the function $A(T) = A_0 G_{KT} \times \exp(-\lambda t)$, subtracting the background signals coming from the sample holder. Here, A_0 is the initial asymmetry at $t = 0$. G_{KT} is the static Gaussian Kubo-Toyabe function to describe static internal fields, which come from surrounding nuclear moments, and are randomly distributed at a muon site. This term can be treated as a temperature-independent parameter from the viewpoint of the μSR time window.[5] λ is the muon-spin depolarization rate, which is considered related to the dynamic spin fluctuation of surrounding electronic spins around the muon. The solid lines are the best-fit results obtained by using this analytical function. Fig-
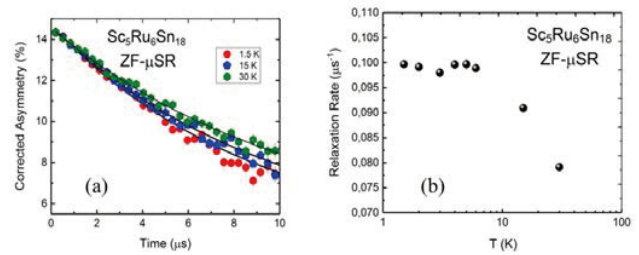
Fig. 1. (a) ZF-μSR time spectra of $Sc_5Ru_6Sn_{18}$ measured at various temperatures. The solid lines are the best-fit results obtained by using the analysis function, $A(T) = A_0 G_{KT} \times \exp(-\lambda t)$. (b) Temperature dependence of the muon-spin relaxation rate obtained from the analysis by using the function $A(T) = A_0 G_{KT} \times \exp(-\lambda t)$.

ure 1(b) shows the fitting of time spectra. λ increases with decreasing temperature, which was obtained from temperatures above T_c. This would mean that some electronic spins remain in the sample, causing this muon-spin depolarization behavior.

An important observation in this ZF-μSR measurement is the temperature-independent behavior of λ below approximately 10 K, even crossing T_c. No change in λ means that the time spectrum does not change any more below 10 K even in the superconducting phase. In the case of the conventional superconducting state with the BCS type s-wave Cooper pair symmetry, there is no change in the time spectrum and we do not see any effect on the ZF-μSR data from the superconducting electronic state. On the other hand, the ZF-μSR time spectrum is modified by the appearance of a spontaneous internal magnetic field below T_c when the time reversal symmetry (TRS) is broken. Such a case can occur in the case of the p-wave Cooper pair symmetry, as has been proved in the case of Sr_2RuO_4.[6] As shown in Fig. 1(b), the time spectrum does not show any changes in its shape within statistical errors; we can conclude that the TRS breaking of the superconducting state is unlikely in this system, even though the appearance of point-node structures on the superconducting gap state is suggested from the heat capacity measurement. This result would restrict the discussion of the model of the superconducting mechanism by excluding the possibility of the formation of the p-wave symmetry.

References
1) M. Koga *et al.*, J. Phys. Soc. Jpn **75**, 014709 (2006).
2) S. Miraglia *et al.*, Acta Crystallogr., Sect. B **43**, 76 (1987).
3) A. Bhattacharyya *et al.*, Phys. Rev. B **91**, 060503(R) (2015).
4) A. Bhattacharyya *et al.*, Sci. Rep **5**, 12926 (2015).
5) Y. J. Uemura *et al.*, Phys. Rev. B **31**, 546 (1985).
6) G. M. Luke *et al.*, Nature (London) **394**, 558 (1998).

*1　Department of Physics, National Cheng Kung University
*2　RIKEN Nishina Center
*3　Department of Physics, Hokkaido University
*4　ASRC., JAEA

Spin fragmentation in $Nd_2Ir_2O_7$ and its carrier-doped dependence

R. Asih,[*1,*2] J. Angel,[*1,*3] K. Matsuhira,[*4] T. Nakano,[*2] Y. Nozue,[*2] and I. Watanabe[*1,*2,*3]

Pyrochlore iridates, $R_2Ir_2O_7$ ($R227$, R is a rare-earth element), provide an ideal platform of strongly frustrated systems to study the interplay between electron-electron correlation (U) and spin-orbit interaction (SOI) given from $5d$ electrons of Ir^{4+}.[1] Among $R227$, Nd227 stands out as a fascinating system because of the additional interesting properties. Nd227 exhibits metallic behavior and undergoes metal-insulator transition (MIT) at T_{MI}= 33 K.[2] μSR and neutron-scattering studies on Nd227 showed the appearance of a long-range magnetic ordering (LRO) of Ir^{4+} moments below T_{MI} followed by an additional LRO of Nd^{3+} moments below 10 K.[3–5] With such progressive reports, however, the sizes of the magnetic ordered moments remain debatable. A reduction in the Nd^{3+} moments was found in the recent neutron study[6] compared with those estimated from the previous study[3] and crystal electric field (CEF) analysis,[7] which is argued to be attributed to a strong quantum fluctuation. This argument was also indicated from μSR results on Nd227, which show an appreciable reduction on the internal field at the muon site (H_{int}) compared with other $R227$ compounds.[4,5] These results signify a possible magnetic fragmentation in Nd227, where ordered and fluctuating phases occur simultaneously. The onset of magnetic ordering on Nd227 was also reported to be suppressed by hole doping via Ca^{2+} substitution on the Nd^{3+} site, and T_{MI} was found to gradually decrease by increasing the Ca concentration.[8] In this study, we investigated the existence of magnetic fragmentation in Nd227 and Ca-doped Nd227, $(Nd_{1-x}Ca_x)_2Ir_2O_7$.

Longitudinal-field (LF-μSR) measurements were performed to confirm the emergence of fluctuations in the ordered phase of the compounds. Figure 1 displays the temperature dependence of the relaxation rate λ of $(Nd_{1-x}Ca_x)_2Ir_2O_7$ for $x = 0.00, 0.05, 0.07$ and 0.10 under an applied field of 3.6 T. An appreciable peak in λ was observed at higher temperatures compared with ordered and meta-transition temperatures. For $x = 0.07$ and 0.10, a clear peak was observed at about 20 K despite the fact that neither muon-spin precession nor a slowing-down behavior was observed under the zero-field (ZF) condition at this temperature. These results may indicate that Nd and/or Ir have low-lying spin fluctuations, which can be easily changed by temperatures and magnetic fields. Figure 2 shows the field dependence of the relaxation rate measured in Nd227 at 50 K (paramagnetic state), 15 K (ordered state of Ir moments), and 1.5 K (ordered state of Ir and Nd moments). λ increases
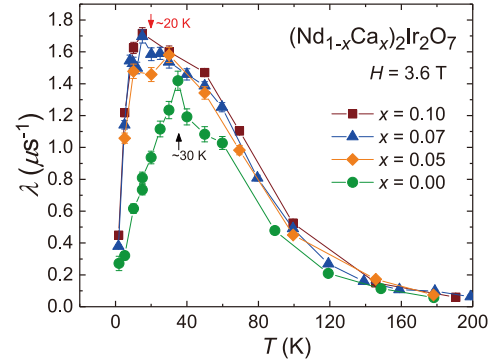
Fig. 1. Temperature dependence of the relaxation rate λ of $(Nd_{1-x}Ca_x)_2Ir_2O_7$ for $x = 0.00, 0.05, 0.07,$ and 0.10 under the applied field of 3.6 T.
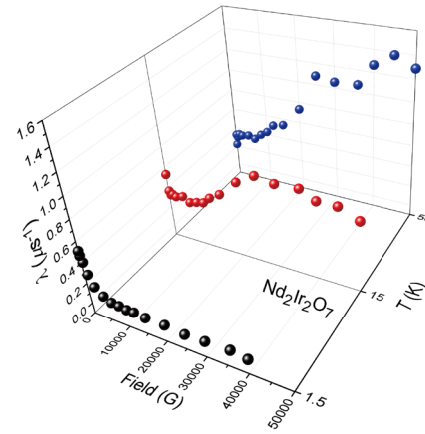
Fig. 2. Field dependence of the relaxation rate λ of $Nd_2Ir_2O_7$ at 1.5 K, 15 K, and 50 K.

with an increase in the applied field at 50 K and shows a peak around 2.5 T at 15 K, which signifies that the spectrum density of the spin fluctuations shifts down to the lower frequency side with decreasing temperature followed by the change in the dynamics of spins. At 1.5 K, λ remains about 0.6 μs^{-1} in the ZF condition, and then, it decreases exponentially with an increasing field showing Redfield-like behavior, which indicates the maintenance of the spin fluctuation even in the ordered state, *i.e.*, a magnetic-fragmentation is realized in Nd227. To further discuss the scheme of spin-fluctuations in these compounds, it is necessary to collect more data points at different temperatures and applied fields.

References
1) X. Wan *et al.*, Phys. Rev. B **83**, 205101 (2011).
2) K. Matsuhira *et al.*, J. Phys. Soc. Jpn. **80**, 094701 (2011).
3) K. Tomiyasu *et al.*, J. Phys. Soc. Jpn. **81**, 034709 (2012).
4) H. Guo *et al.*, Phys. Rev. B **88**, 060411(R) (2013).
5) R. Asih *et al.*, J. Phys. Soc. Jpn. **86**, 024705 (2017).
6) H. Guo *et al.*, Phys. Rev. B **94**, 161102(R) (2016).
7) M. Watahiki *et al.*, J. Phys. Conf. Ser. **320**, 012080 (2011).
8) R. Asih *et al.*, RIKEN Accel. Prog. Rep. **50**, 23 (2017).

*1   RIKEN Nishina Center
*2   Department of Physics, Osaka University
*3   Department of Condense Matter Physics, Hokkaido University
*4   Graduate School of Engineering, Kyushu Institute of Technology

Spin dynamics in the $S = 1/2$ zigzag spin chain magnets $K_2CuCl_2SO_4$ and $Na_2CuCl_2SO_4$

M. Fujihala,[*1] S. Mitsuda,[*1] and I. Watanabe[*2]

The $S = 1/2$ Heisenberg chain is an outstanding and versatile model system in quantum many-body physics. The cuprate is known to exhibit magnetic properties of the quantum spin chain, thus providing access to the experimental study of spin chains with various perturbations. Among these are frustrated intrachain exchange interactions, staggered g tensors, staggered Dzyaloshinskii-Moriya (DM) interactions, or disorder.

We recently succeeded in synthesizing the pure-phase of a new compound $Na_2CuCl_2SO_4$. This compound has the same crystal structure as $K_2CuCl_2SO_4$ and $K_2CuBr_2SO_4$.[1] On first inspection, the ferromagnetic nearest-neighbor interaction J_1 and the antiferromagnetic next-nearest-neighbor interaction J_2 through the Cu-Cl(Br)-Cu path seem to compete, however, it was reported that the linear spin chains along the a-axis are formed by the exchange interaction J through the Cu-Cl(Br)-Cl(Br)-Cu path in $K_2CuCl_2SO_4$ and $K_2CuBr_2SO_4$. In addition, from the crystal structure information, these two compounds feature substantial DM interactions that are uniform within each chain, but are anti-parallel in adjacent chains. Therefore, we consider that $Na_2CuCl_2SO_4$ has the unique spin frustration induced by the DM interaction.

Further, we succeeded to grow large single crystals ($\sim$10 mm^3). Therefore, $Na_2CuCl_2SO_4$ is suitable for observing the spin dynamics along and perpendicular to the spin chain by both muon spin rotation and relaxation (μSR) and inelastic neutron scattering. The temperature dependence of the total specific heat divided by temperature C/T and the magnetic susceptibility are shown in Figs. 1(a) and (b). Short-range correlation is developed around 5 K, and the long-range magnetic ordering is observed at $T_N = 0.5$ K. The INS data measured at 1.5 K in the $(h, 1.5, 0)$ scattering plane reveals a spinon continuum, indicating that the Tomonaga-Luttinger liquid state is realized in $Na_2CuCl_2SO_4$ above T_N. Then, in order to investigate the spin fluctuations in $Na_2CuCl_2SO_4$, we performed μSR measurements at the RIKEN-RAL Muon facility at the Rutherford-Appleton Laboratory, UK.

The crystal orientations were determined by Laue X-ray diffraction. The crystal was cut into slices along the bc-plane with a homogeneous thickness of 3 mm, and it was mounted on a silver sample holder. Powder sample of $Na_2CuCl_2SO_4$ was prepared by milling single crystals.

A clear oscillation indicative of the long-range magnetic order was observed at 0.3 K in zero field (Fig. 2(a)). The weak LF asymmetries for $T > 0.6$ K
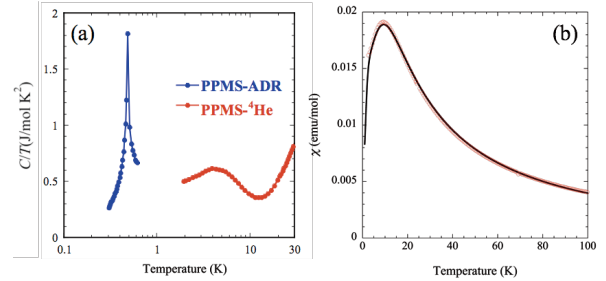
Fig. 1. (a) Temperature dependence of the total specific heat divided by temperature C/T. (b) Temperature dependence of magnetic susceptibility measured at 1 T (open red circles). The grey solid line represents the theoretical curve of the linear spin chain model with a AFM interaction $J = 15.5$ K.
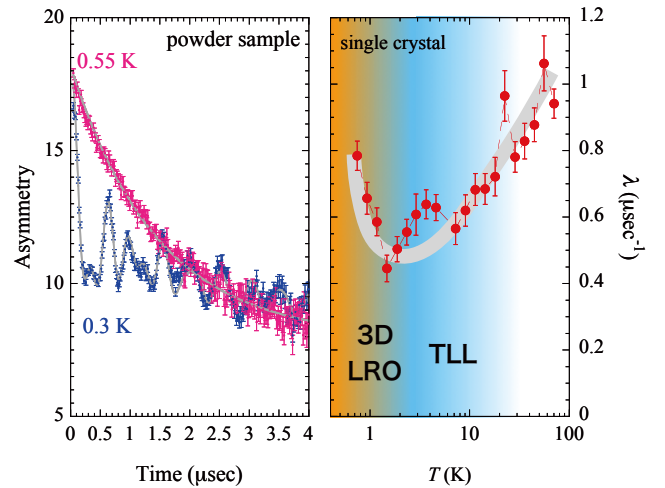
Fig. 2. (a) Selected ZF-μSR signals (asymmetry vs time). The gray lines are the corresponding fits to the data. (b) Temperature dependence of the muon spin relaxation rate in $Na_2CuCl_2SO_4$ measured in longitudinal field 50 G.

are fitted by the stretched exponential function $a(t) = a_1 \exp[-(\lambda t)^\beta] + a_{BG}$, where a_1 is an intrinsic asymmetry, a_{BG} is a constant background, λ is the muon spin relaxation rate, and β is the stretching exponent. We observe a decrease in the λ with increasing temperature above 1 K in the full time window, 0–20 μs as shown in Fig. 2(b). This behavior is expected in the TLL system; they have been seen in other spin-liquid candidates.[2] Further the analyses of our μSR spectrum measured in both the single crystal and the powder sample are now in progress.

References
1) M. Hälg *et al.*, Phys. Rev. B **90**, 174413 (2014).
2) F. L. Pratt *et al.*, Phys. Rev. B **96**, 247203 (2006).

*1　Department of Physics, Tokyo University of Science
*2　RIKEN Nishina Center

Study of Magnetic Ordering by p-orbital in RbO$_2$ using μSR

F. Astuti,[*1,*2] M. Miyajima,[*3] R. Asih,[*2,*4] I. Watanabe,[*1,*4] and T. Kambe[*3]

Alkali metal superoxides AO$_2$ (A= Na, K, Rb, Cs) present an interesting example of magnetic materials based on p-elements. This become the first example of an inorganic quantum spin system with unpaired π-electrons.[1] Alkalimetal superoxides adopt the rocksalt-type crystal structure and two oxygen atoms form a dumbbell shaped structure sharing one excess electron, O$_2^-$, which is known as the "superoxide" anion. This leads to one unpaired spin (S=1/2) in a pair of degenerate π^* (antibonding) molecular orbitals. The magnetic ordering of KO$_2$, RbO$_2$, and CsO$_2$ have been observed at temperatures of 7 K, 15 K, and 9.6 K, respectively by using specific heat measurement.[2] The Tomonaga Luttinger Liquid (TLL) model suggested for CsO$_2$ is supposed to present a field-induced magnetic order related to the TLL state.[3]

Therefore, detailed investigation on the magnetic properties near or in the zero-field (ZF) condition is strongly required to describe the magnetically ordered state appearing in CsO$_2$ and other alkali metal superoxides. Last year, we have carried out μSR measurements in RbO$_2$ at the RIKEN-RAL muon facility by using the pulsed muon beam. At that time, we felt that the sample quality was not so good. For that reason, in the next beam time, we improved the sample quality and measured the new batch of RbO$_2$ samples.

No clear muon-spin precession was seen at any temperature (Fig. 1), however the decrease in the initial asymmetry around the suggested T$_N$ was clearly observed. The anomaly was also observed at ∼15 K as shown in Fig. 2(a).

The asymmetry parameter can represent the magnetic volume fraction. By comparing the asymmetry parameters in Fig. 2(b), it seems that the new sample has bigger magnetic volume fraction than the old sample. It means that we succesfully improved the sample quality.

The decrease in the initial asymmetry possibly means that the magnetically ordered state appears causing the depolarization behavior faster than the observable limit of the pulsed muon facility. This ordered state might accomodate the fast muon-spin precession. Therefore, it is indispensable to test RbO$_2$ by using the continuous muon beam in order to detect clear evidence of the appearance of magnetically ordered states. As we expected, the result of μSR measurement at PSI, Switzerland, by using continuous muon beam showed clear-muon spin precession at the temperature ∼15 K,
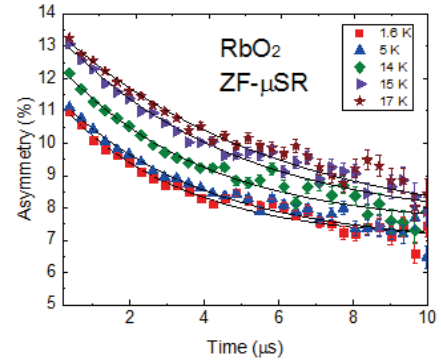
Fig. 1. ZF-μSR time spectrum for RbO$_2$ for the first 10 microsecond from 17 K down to base temperature.
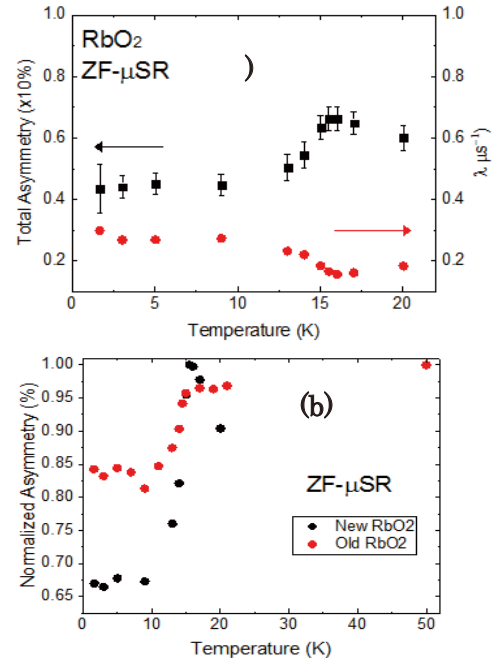
Fig. 2. (a) Temperature dependence of the initial asymmetry and relaxation rate of the ZF-μSR time spectrum measured at the RIKEN-RAL Muon Facility. The anomaly in the μSR measurement is observed at 15 K around the suggested T$_N$. (b) Comparison between the new and old RbO$_2$ samples. The result of the old sample has been reported in RIKEN APR 2016 Vol.50.

indicating long-range magnetic ordered state (the result is not shown in this report).

*1　Department of Condensed Matter Physics, Hokkaido University
*2　RIKEN Nishina Center
*3　Department of Physics, Okayama University
*4　Department of Physics, Osaka University

References
1) S. Riyadi et al., Phys. Rev. Lett. **108**, 217206 (2012).
2) A. Zumsteg et al., Phys. Cond. Matter, 267–291 (1974).
3) M. Klanjsek et al., Phys. Rev. Lett. **115**, 057205 (2015).

Muon spin relaxation study on the new organic spin liquid material λ-(STF)$_2$GaCl$_4$

T. Minamidate,[*1] D. P. Sari,[*2,*3] N. Matsunaga,[*1] and I. Watanabe[*2]

Research on quantum spin liquid (QSL) states in frustrated quantum magnetism is a critical issue in the field of condensed matter physics. In recent research, some candidate QSL materials have been found in molecular-based organic systems, such as κ-(ET)$_2$Cu$_2$(CN)$_3$[1] and EtMe$_3$Sb[Pd(dmit)$_2$]$_2$.[2] The spin systems in these salts have been well described as an antiferromagnetic (AF) spin system with a nearly equilateral regular triangular lattice. Recently, we found a new candidate QSL material, λ-(STF)$_2$GaCl$_4$, which is related to the organic superconductor λ-(BETS)$_2$GaCl$_4$. As shown in Fig. 1, down to 2 K, the static susceptibility of λ-(STF)$_2$GaCl$_4$ is very well described by the AF Heisenberg model with a regular triangular lattice, which is the typical behavior of the QSL system.[3] In contrast to the good agreement of the susceptibility behavior, the calculated geometry of the spin interaction in λ-(STF)$_2$GaCl$_4$ is quite distorted from the regular triangle. Therefore, it can be the key material to investigate the stabilization mechanism of the QSL state.
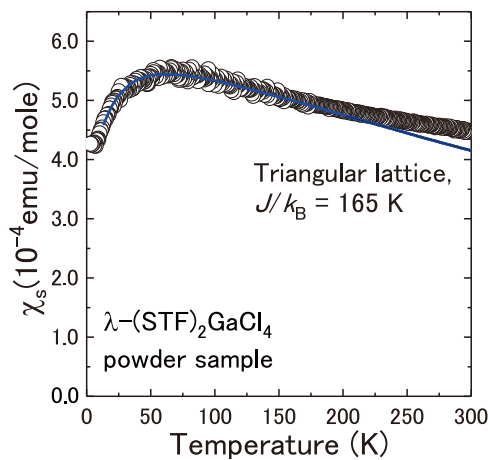
Fig. 1. Temperature dependence of the static susceptibility of λ-(STF)$_2$GaCl$_4$. The solid line is the susceptibility curve calculated for the $S = 1/2$ AF Heisenberg model in a triangular lattice with an exchange coupling constant $J/k_B = -165$ K.[3]

We succeeded in synthesizing a high-quality sample of λ-(STF)$_2$GaCl$_4$ with the total mass ∼ 75 mg and conducted ZF-μSR measurement down to 0.3 K. Figure 2 shows the μSR time spectra measured at 0.3 K in ZF and under an LF of 100 G. The ZF-μSR time

spectrum is well described by the simple exponential function. Since the μSR time spectrum is well decoupled by applying LF of 100 G, there is no static internal field due to AF long-range ordering. On the other hand, we can see a slow relaxation behavior even at 0.3 K under an LF of 100 G. This implies that there are some effects of fluctuating internal fields originating from surrounding electronic spins, and the sample does not show the long-range AF ordering although it has a strong AF interaction $J/k_B \sim -165$ K, at least down to 0.3 K.

This behavior is similar to that observed in the μSR measurement for the first organic QSL salt, κ-(ET)$_2$Cu$_2$(CN)$_3$.[4] Additionally, the authors of Ref. 4) found that the LF-μSR time spectrum is described by a two-component exponential function and pointed out that the system undergoes phase separation into paramagnetic islands and a singlet phase at a low temperature. Therefore, we are now planning an additional experiment for λ-(STF)$_2$GaCl$_4$ to observe the spin behavior in the range between ZF and an LF of 100 G. With the progress of this research, the microscopic spin dynamics in the QSL state and the stabilization mechanism of the QSL state in a distorted lattice system can probably be clarified.
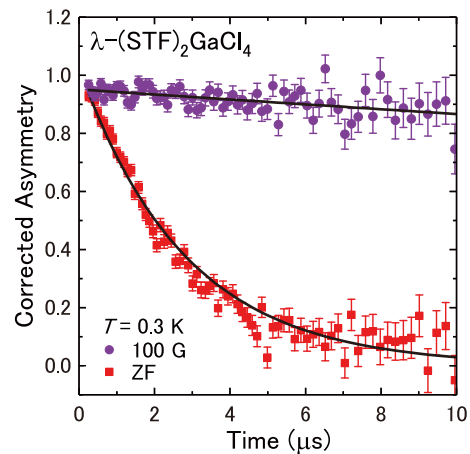
Fig. 2. Muon spin depolarization curves of λ-(STF)$_2$GaCl$_4$ at 0.3 K under zero field and a longitudinal field of 100 G.

References
1) Y. Shimizu *et al.*, Phys. Rev. B **91**, 107001 (2003).
2) T. Itou *et al.*, Phys. Rev. B **77**, 104413 (2008).
3) T. Minamidate *et al.*, J. Phys. Soc. Jpn. **84**, 063704 (2015).
4) S. Nakajima *et al.*, J. Phys. Soc. Jpn. **81**, 063706 (2012).

*1   Department of Physics, Hokkaido University
*2   RIKEN Nishina Center
*3   Department of Physics, Osaka University

Superconducting gap symmetry in organic superconductor λ-(BETS)₂GaCl₄ studied by μSR with DFT

D. P. Sari,[*1,*2] H. Aizawa,[*3] T. Koretsune,[*4] H. Seo,[*5] and I. Watanabe[*2]

The superconducting gap symmetry determination in λ-(BETS)₂GaCl₄ has been intriguing, since the superconducting state of this organic superconductor may be linked to that of the isostructural compound, λ-(BETS)₂FeCl₄, showing a field-induced superconductivity in the fields > 17 T.[1] We have performed transverse field μSR in fields of 150 Oe down to 0.3 K at ISIS Muon Facility in the UK. The temperature dependence of superfluid density was best described by the s+d-wave with a dominant s-wave component.[2] Motivated by the μSR result, we have performed the first-principles electronic structure calculations with the generalized-gradient approximation on the basis of the density functional theory (DFT). The VASP software package adopting the plane-wave basis set with cutoff energies of 500 meV was used. The ground state charge densities were computed using $4 \times 4 \times 4$ k-point sampling and crystal structure information from Ref. 3) was used. Furthermore, we constructed maximally localized Wannier orbitals on BETS dimers to make the tight-binding energy band (dimer model) reproduce the band structure of DFT based on the experimental crystal data. The calculation was done by using the HOKUSAI RIKEN supercomputer.

Figure 1 shows the DFT band energy of λ-(BETS)₂GaCl₄. Since the system has four BETS molecules or two BETS dimers, contributing to the electronic properties, in one unit cell, there exist two bands close to the Fermi level. Those two bands were well reproduced by the dimer model with the parameter transfer integral, in the unit of meV, as follows: $t_c = 64$, $t_{d1} = 52$, $t_{d2} = 13$, $t_{d3} = 76$, $t_{d4} = 64$, $t_e = -17$. Accordingly, the Fermi surface was consisting of an open sheet and a closed pocket as shown in the bottom right panel of Fig. 1.

The superconducting gap was then calculated by using the Random Phase Approximation (RPA) method following the extended Hubbard model,

$$H = \sum_{\langle i,j \rangle} t_{ij} c_{i\sigma}^{\dagger} c_{j\sigma} + \sum_{i} U n_{i\uparrow} n_{i\downarrow} + \sum_{\langle i,j \rangle, \sigma, \sigma'} V_{ij} n_{i\sigma} n_{j\sigma}, \quad (1)$$

where t is the transfer integral, and U and V are intra- and inter-dimer interactions. We assumed a spin-fluctuation-mediated superconductor in the spin singlet channel. $U = 0.2$ eV was introduced in the calculation in order to investigate the low-energy interaction on the BETS dimer.[4] The result is shown in Fig. 2 showing that the red colored area is the result from RPA. More-
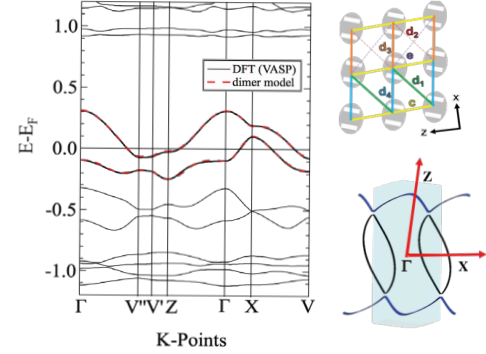
Fig. 1. DFT band structures of λ-(BETS)₂GaCl₄. The tight-binding band structure using a dimer model with parameter inter-dimer transfer integral $t_c - t_e$ is shown as a broken line. The upper right panel shows a 2×2 molecular arrangement of the a-c conducting plane. The grey ellipse represents a BETS dimer and c–e represents inter-dimer transfer integral. The bottom right panel is the Fermi surface.
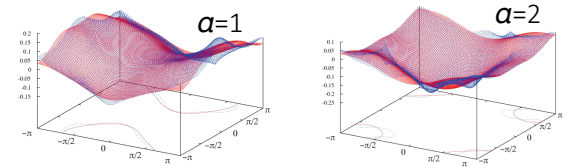
Fig. 2. Superconducting gap function from the band indexes 1 and 2, which are bands from the open sheet and closed pocket Fermi surface, respectively. The red and blue colored areas denote the RPA result and fitting result, respectively.

over, the pairing symmetry from RPA was then fitted to a linear combination of defined pairing symmetries in the k-space, with the basis functions as follows:

isotropic s-wave: $f_{s0}(k_x, k_y) = 1$
extended s-wave: $f_{s1}(k_x, k_y) = 2[\cos(k_x) + \cos(k_y)]$
$d_{x^2-y^2}$-wave: $f_{d_{x^2-y^2}}(k_x, k_y) = 2[\cos(k_x) - \cos(k_y)]$. (2)

The fitting result is shown in the blue-colored area of Fig. 2. We found that there exists a finite $d_{x^2-y^2}$-wave component in conjunction with s-wave components from the contribution of two bands mentioned above. However, this mixture symmetry of $s + d_{x^2-y^2}$ indicates only one order parameter since the superconducting gap looks almost continuous along the Fermi surface, as shown in Fig. 2. Thus, from the μSR and DFT calculation we assign a new type of superconducting gap symmetry in λ-(BETS)₂GaCl₄, $s + d$-wave.

References
1) S. Uji et al., Syn. Met. 133–134, 481–483 (2003).
2) D. P. Sari et al., to be submitted.
3) H. Tanaka et al., J. Am. Chem. Soc. 121, 760–768 (1999).
4) C. Hotta, H. Fukuyama, J. Phys. Soc. Jpn. 69, 2577 (2000).

*1 Department of Regional Environment Systems, Shibaura Inst. of Tech.
*2 RIKEN Nishina Center
*3 Institute of Physics, Kanagawa University
*4 Department of Physics, Tohoku University
*5 Condensed Matter Theory Laboratory, RIKEN

Effect of light irradiation on charge carrier dynamics in active layer hybrid solar cells

L. Safriani,[*1] Risdiana,[*1] Fitrilawati,[*1] A. Bahtiar,[*1] A. Aprilia,[*1] D. Puspita Sari,[*2] J. Angel,[*2] and I. Watanabe[*2]

Solar power generation is a key method for generating electronic power. Several researchers have attempted to achieve higher performance of the solar cells and more effective materials for use in cells. The discovery of conjugated polymers, such as Polythiophene (PT) and its derivatives, attracted much attention owing to their chemical and thermal stability as well as their potential use as an absorbing solar spectrum material (active layer) in solar cells. The most necessary property of these active layers is their ability to transfer the charge carrier resulting from the absorption of solar spectrum. In particular, Poly(3-hexylthiophene)/P3HT has considerable research interest, because it shows the highest hole mobility among the series of Poly(3-alkylthiophene).[1] In our previous muon Spin Relaxation (μSR) study, the charge carrier mobility in P3HT was found to change from one-dimensional to a three-dimensional model, which is strongly dependent on their molecular structure and temperature.[2,3]

Recently, the so-called hybrid (organic-inorganic) solar cell was developed owing to the combined advantage between organic material (P3HT) and inorganic material such as ZnO, which ensures better performance for practical application. ZnO is inorganic material with high electron mobility and can be easily prepared as electron acceptor to dissociate excitons formed in conjugated polymer as the active material of solar cells. ZnO can be prepared as a nanoparticle that can resolve the problem of small diffusion range of P3HT.[4] The existence of ZnO in active layer will support charge transfer from P3HT to electrode of solar cell because the conduction band of ZnO is lower than that of low unoccupied molecular orbital (LUMO) of P3HT.

We studied the microscopic intrinsic charge carrier dynamics in active material of P3HT:ZnO along and perpendicular to the chain by using the longitudinal field (LF) μSR method. We found that the charge carrier mobility changes from intrachain to interchain diffusion above 25 K for P3HT:ZnO. We also have measured charge carrier dynamics of P3HT:ZnO with light irradiation. Figure 1 shows the asymmetry data of P3HT:ZnO at 10, 15, 25, and 300 K for various longitudinal magnetic field values with (red data) and without (black data) light irradiation. We found small changes of asymmetry when light irradiation on condition and off condition, however we cannot observe significant effect probably due to low intensity of light irradiation.

Figure 2 show the longitudinal-field dependence of relaxation rate λ_1 of P3HT:ZnO nanoparticles at 10, 15, 25, and 300 K. Without light irradiation, for the low-
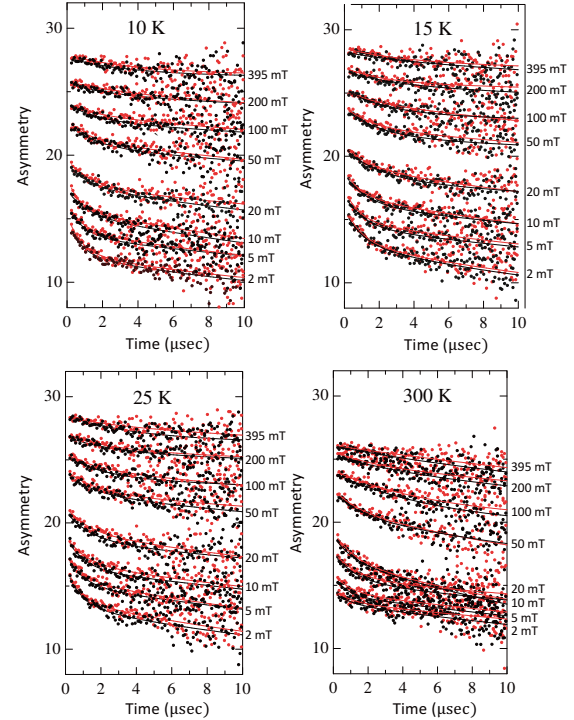
Fig. 1. The asymmetry data of P3HT:ZnO at 10, 15, 25, and 300 K for various longitudinal magnetic field values.
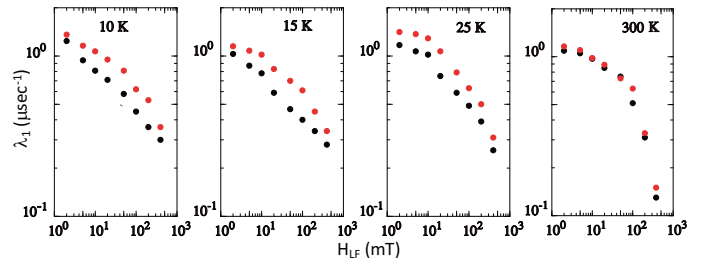
Fig. 2. The longitudinal-field H_{LF} dependence of relaxation rate λ_1 of P3HT:ZnO nanoparticles at 10, 15, 25, and 300 K.

est temperature of 10 K, $\lambda \sim H^{-0.5}$ is clearly displayed indicating one-dimensional intra-chain diffusion. In contrast, for the same temperature, light irradiation displayed $\lambda \sim C - H^{0.5}$ curve, indicating three-dimensional inter-chain diffusion. Thus, it is clearly seen that with light irradiation, temperature crossover occurred from one-dimensional to three-dimensional at the lower temperature of 10 K compared to that in a previous result at 25 K.[5]

References
1) A. Babel et al., Synth. Met. **148**, 169 (2005).
2) Risdiana et al., Journal of Physics Conf. Series **200**, 052024 (2010).
3) Risdiana et al., Physica B **405**, S381 (2010).
4) L. W. Ji et al., J. Matter Sci. **45**, 3266 (2010).
5) L. Safriani et al., AMR **896**, 477 (2014).

*1　Department of Physics, Padjadjdaran University
*2　RIKEN Nishina Center

Electron Transport Studies in Biological Molecules with respect to Ageing Science

H. Rozak,[*1] W. Zaharim,[*2] F. Astuti,[*1,*3] R. Asih,[*1,*4] R. Samian,[*2] S. Samsudin,[*2] S. N. Abu Bakar,[*2] N. Ismail,[*2] I. Watanabe,[*1,*3,*4] M. I. Mohamed-Ibrahim,[*2] and S. Sulaiman[*2]

The electron transport process in deoxyribonucleic acid (DNA) is a very important biological phenomenon but the process itself is not fully understood at the microscopic level. DNA is the molecule that stores genetic information in a living cell and the structure of DNA consists of four bases. These four bases are guanine (G), adenine (A), cytosine (C) and thymine (T).[1] Damages in DNA can lead to various types of diseases such as cancers and neurological disorders. There is a direct relationship between the damages in DNA and ageing. We hypothesize that damages in the DNA would alter the behavior of electron transfer since DNA is well known as a good electron conductor. If there are some defects in DNA, the electron transfer in it will be disturbed, thus changing the electron motion. However, the degree and type of alterations are yet unknown at the microscopic level. In order to understand this phenomenon, systematic studies on the alteration of electron transfer in DNA are needed and μSR is known to be useful in this respect as has been demonstrated in the past on one-dimensional organic molecules.[2–4]

In this project, we used simple model molecules of DNA where the sequence is less than 12 bases, which would make it easier to interpret the results.

Experiments on the μ^+ relaxation in guanine and adenine have been conducted using an intense pulsed beam μ^+ at the RIKENRAL Muon Facility. All measurements were conducted on the powder sample and the weight of each sample was 50 mg. We measured the muon-spin relaxation rate under various longitudinal magnetic fields in the range between 0 T and 0.3 T and the temperatures that we used to carry out our experiment were at 100 K and 300 K. The observed relaxation functions, $G(t)$, were fitted to the Risch-Kher function.

Based on the curve in Fig. 1, at temperatures 100 K, the μ^+ relaxation function was found to depend on the external field, where the initial asymmetry was increased as the external magnetic field increased. Unfortunately, the muon spin precession did not show clearly in this curve due to the limitation of the pulse muon source at RAL. Therefore, it is better to repeat the experiment involving guanine at PSI by using a continuous beam to confirm the existence of the diamagnetic muon components which are strongly bound
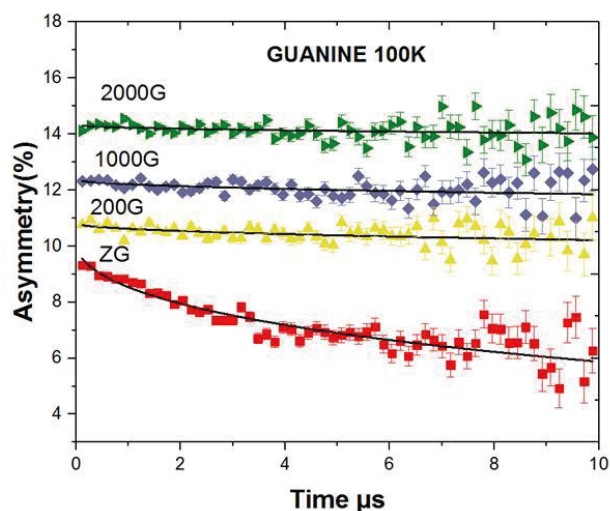
Fig. 1. μSR Time spectra in Guanine at 100 K under external longitudinal fields of 0, 200, 1000 and 2000 G.
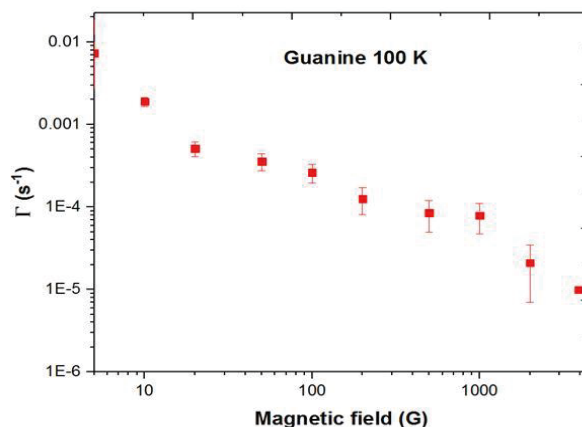
Fig. 2. Relaxation parameter versus an external longitudinal magnetic field for μ^+ in guanine at a temperatures of 100 K.

to the molecules. For the curve in Fig. 2, the relation parameter (Γ) was found to take an inverse-field dependence in guanine above 50 G, thus suggesting existence of a quasi-1D rapid diffusion of electron in DNA strands It is clear that the electron-transfer process at the microscopic level was directly detected in the present experiments as shown in Fig. 2.

References
1) S. P. Jackson et al., Nature (London) **461**, 1071 (2009).
2) K. Ishida et al., Phys. Rev. Lett. **55**, 2009 (1985).
3) K. Nagamine et al., Phys. Rev. Lett. **53**, 1763 (1984).
4) E. Torikai et al., Hyperfine Interact. **138**, 509 (2001).

[*1] RIKEN Nishina Center
[*2] School of Distance Education, Universiti Sains Malaysia
[*3] Department of Physics, Hokaido University
[*4] Department of Physics, Osaka University

Approach to determination of muon stopping sites in proteins

Y. Sugawara,[*1] T. Fujita,[*1] A. D. Pant,[*2] E. Torikai,[*3,*4] K. Ishida,[*5] W. Higemoto,[*4,*6] K. Shimomura,[*2] F. L. Pratt,[*7] and K. Nagamine[*2]

In order to explore the electron-transfer process in life sciences, we have been carrying out μSR studies using the electron labeling method on cytochrome c, a protein which is a member of the respiratory chain in mitochondria.[1–3)] In order to deepen the understanding of the μSR data, we intend to determine the muon stopping sites and the electronic structure. In addition, our LF μSR data showed a level crossing resonance (LCR) signature for cytochrome c indicating that some portion of the muons have a strong energy transfer at a specific LF to the surrounding species at the stopping site (Fig. 1(b)). The observed LCR data around 20 G was similar to that of polyglycine (Fig. 1(c)) (F. L. Pratt, private communication). Proteins are made of amino acids, which are linked by peptide bonds, and polyglycine is the simplest polypeptide made of aliphatic ($-CH_2-$) parts, peptide bonds ($-CONH-$), terminal $-COOH$ (or $-COO^-$), and $-NH_2$ (or $-NH_3^+$) groups. The candidates of muon stopping sites are peptide bonds ($-CONH-$) and terminal $-COOH$ or $-NH_2$ (Fig. 1(a)).

Under such a background, we carried out μSR measurements of triglycine, tetraglycine, and N-methylacetamide ($CH_3CONHCH_3$), which is the simplest molecule containing a peptide bond, and compared the characteristics of the μSR data with those of glycine, glycylglycine, and polyglycine.

The low LF μSR data of glycine were fitted well using the product of Kubo-Toyabe and Lorentzian functions. LCR was not detected around 20 G, contrary to the cases of cytochrome c and polyglycine. On the other hand, the low LF μSR data of glycylglycine, triglycine and tetraglycine were approximately fitted with the Lorentzian function, and the LCR was observed (Fig. 1(d)). In addition, the missing fraction of the initial asymmetry of oligoglycine under zero magnetic field was approximately 20% of the full asymmetry, and larger than that of glycine (approximately 10%). A similar tendency was observed in the μSR data of N-methylacetamede at 10 K, although the quality of the data was inferior because the sample melted during the treatment (melting point: 300 K), and a cavity appeared in the sample cell. Taking the results of theoretical calculations into account,[4)] muon would stop at $-COOH$ (or $-COO^-$) moiety in glycine, and at
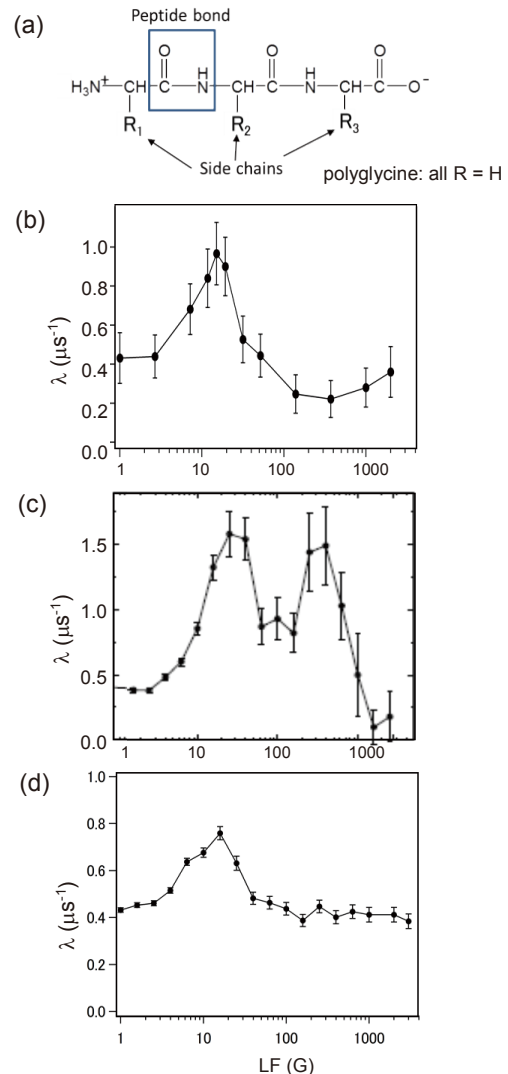
Fig. 1. Schematic structure of protein (a) and longitudinal field dependence of relaxation rates (λ) of cytochrome c (18 K) (b), polyglycine (5 K) (c) and tetraglycine (16 K) (d).

CO moiety of peptide bonds in oligoglycine.

The results indicate that the LCR data of cytochrome c originates from the muon stopping at peptide bonds.

References
1) K. Nagamine et al., Physica (Utrecht), **289–290**, 631 (2000).
2) K. Nagamine, E. Torikai, J. Phys. Condensed Matter **16**, S4797 (2004).
3) A. D. Pant et al., JPS Conference Proceedings **8**, 033007-1-5 (2015).
4) A. D. Pant et al., JPS Conference Proceedings **21**, 011038-1-4 (2018).

[*1] School of Science, Kitasato University
[*2] IMSS, KEK
[*3] Graduate Faculty of Interdisciplinary Research, University of Yamanashi
[*4] ASRC, JAEA
[*5] RIKEN Nishina Center
[*6] School of Science Tokyo Institute of Technology
[*7] ISIS Science and Technology Facilities Council

Time dependence of dipole width obtained by zero-field μSR for Al and Al-0.5 at.%Si

K. Nishimura,[*1,*2] K. Matsuda,[*1,*2] T. Namiki,[*1] S. Lee,[*1] N. Nunomura,[*1] I. Watanabe,[*2] M. A. Jaward,[*2] and T. Matsuzaki[*2]

Al-Mg-Si aluminum alloys are widely used for vehicles, buildings, home appliances, *etc.*, because of their low weight, excellent formability and age hardenability. The mechanical strength (hardness) of the alloy depends on the density, size and structure of precipitates consisting of Mg and Si atoms; dense nano-size Mg_2Si precipitates make the alloys harder.[1–5] From various studies on Al-Mg-Si alloys, vacancy behavior is considered to play an important role in the aging process, stimulating the diffusion of solute Mg and Si atoms and the nucleation of Mg/Si/vacancy clusters. Positron annihilation spectroscopy (PAS)[3,4] and muon spin relaxation spectroscopy (μSR)[6,7] have been successfully used to investigate the behavior of vacancies and solute atoms in their clustering in Al-Mg-Si alloys. Taking advantage of high beam intensity and a high counting rate of muons at the ARGUS line, we have observed the time dependence of the dipole width (Δ) via zero-field muon spin relaxation spectroscopy in a pure (99.99%) aluminum and an Al-0.5at.%Si alloy to understand the details of the clustering process of solute atoms in Al-Mg-Si alloys.

All samples underwent heat treatment at 848 K for 1 h and subsequent quenching in ice water (STQ). Approximately 10 min after STQ, the sample was inserted into the ARGUS muon spectrometer, and then zero-field μSR measurement was started at a constant temperature. Typical spin relaxation spectra obtained for pure Al are shown in Fig. 1, in which the relaxation rate obviously decreases with time; the relaxation rate observed at 16 min after STQ (black circle) is larger than that at 378 min (blue square). The observed spin relaxation spectra were fit with the Kubo-Toyabe function using the WIMDA program,[8] and the dipole widths (Δ) deduced at three different temperatures are plotted in Fig. 2. Surprisingly, they appear to decrease linearly with time. The reduction of Δ is most likely ascribed to the annihilation of vacancies that are the main trapping sites of muons at these temperatures. The reason for the linear variation of Δ vs. t is unclear.

Figure 3 shows the time dependence of Δ in Al-0.5 at.%Si (described as Al-Si) obtained at 280 K, which seems to change on a logarithmic scale. On the Δ variation, there is obviously an effect of Si solutes that can bind vacancies. It is also noticeable that there is a change in the slope on the Δ vs. $\log(t)$ curve at ap-

proximately 300 min. For a comparison, the time dependence of Δ in the Al-1.6 at.%Mg_2Si (described as Al-Mg_2Si), which was previously reported,[9] is shown in Fig. 4. The similar change in the slope on the Δ vs. $\log(t)$ curve existed at approximately 150 min, which takes place earlier than in Al-Si. The magnitude of change of Δ in Al-Mg_2Si, however, is about one half of that in Al-Si in the same time range. The difference of the solute elements and the concentrations possibly affects the time dependence of Δ in Al-Si and Al-Mg_2Si.
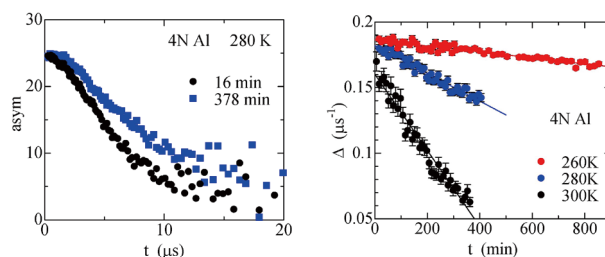
Fig. 1. (left) Zero-field muon spin relaxation spectra obtained for the pure Al sample at 280 K.

Fig. 2. (right) Time dependencies of dipole width in pure Al at 260, 280, and 300 K.
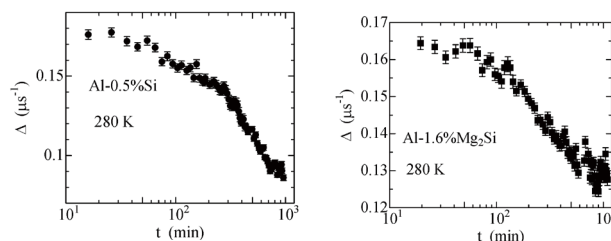
Fig. 3. (left) Time dependencies of dipole width in the Al-0.5 at.%Si alloy at 280 K.

Fig. 4. (right) Time dependencies of dipole width in the Al-1.6 at.%Mg_2Si alloy at 280 K.[9]

References
1) S. Pogatscher *et al.*, Acta Mater. **59**, 3352 (2011).
2) H. Seyedrezai *et al.*, Mater. Sci. Eng. A **525**, 186 (2009).
3) J. Banhart *et al.*, Phys. Rev. B **83**, 014101 (2011).
4) A. Somoza *et al.*, Phys. Rev. B **61**, 14454 (2000).
5) S. Pogatscher *et al.*, Phy. Rev. Lett. **112**, 225701 (2014).
6) S. Wenner *et al.*, Phys. Rev. B **86**, 104201 (2012).
7) S. Wenner *et al.*, Acta Mater. **61**, 6082 (2013).
8) F. L. Pratt, Physica (Utrecht) B **289**, 710 (2000).
9) K. Nishimura *et al.*, RIKEN Accel. Prog. Rep. **50**, 242 (2017).

[*1] Department of Materials Science and Engineering, U. Toyama
[*2] RIKEN Nishina Center

μSR investigation of atomic structure and photocatalytic properties of defects in rutile TiO₂ crystal

H. Ariga-Miwa,[*1,*2] H. Konno,[*1] K. Shimomura,[*3] K. Ishida,[*2] W. Higemoto,[*4] A. D. Pant,[*3] E. Torikai,[*4] K. Nagamine,[*3,*5] and K. Asakura[*1]

Photocatalysis is a promising process to solve the environmental pollution problem and energy crisis, resulting in a sustainable society. TiO₂ is the most widely used material for high efficiency photocatalysis. Since the discovery of the Honda-Fujishima effect,[1] many researches have been carried out to understand the key factor for the photocatalytic activities. Since photocatalysis systems are complex, their nature is strongly affected by the crystal structure, surface area, number of surface hydroxyls, defect sites, and so on. Defect sites are one of the most significant factors that determine the photocatalytic activities. However, the characterization of defect sites has not been established yet, since in most cases several types of defect sites coexist in photocatalysts. For example, the pump-and-probe spectroscopy by the femto-second laser for TiO₂ nanocrystals suggested that defect sites affect the electron-hole pair recombination process, which depress the photocatalytic reaction by extinguishing 90% of the excited electrons.[2] On the other hand, X. Chen et al. showed that a reduction of TiO₂ nanocrystals enhances solar-driven photocatalytic activities.[3] These results suggest that defects with different properties coexist in the TiO₂ nanocrystal catalysts. The best way to clarify photocatalytic properties is to identify each defect site and track the electronic properties during photocatalysis.

Our recent zero field μSR measurements of a reduced rutile TiO₂ single crystal at RIKEN-RAL showed atomic structure around the defect sites. The μ-H complex in oxygen vacancy was observed, which corresponds to two hydrogens stabilized at the oxygen vacancy. The origin of hydrogen is not clear yet. The purpose of the present work is to clarify the origin of hydrogen by comparing two types of rutile TiO₂, prepared by Vernoulli method (TiO₂-H) and Floating Zone method (TiO₂-noH). It is known that TiO₂-H includes hydrogen as impurity while TiO₂-noH does not.

The μSR measurements were performed at the RIKEN-RAL Muon Facility. Mirror-polished rutile TiO₂ single crystals ($25 \times 25 \times 0.5$ mm³, Crystal Base) oriented to the (110) plane were used. The oxygen vacancy was generated by performing reduction at 1173 K for 2 hr under an ultra-high vacuum (0.5×10^{-8} Pa). The sample was irradiated with flash lamp light from the opposite side of the muon through a quartz glass

by utilizing the sample cell developed by Prof. Torikai's group.

The ZF μSR spectra before and after reduction were obtained for TiO₂-H and TiO₂-noH, respectively, at various temperatures from 4 K to room temperature. The muon stabilized site for the TiO₂ without oxygen vacancy, whose spectra are shown in Fig. 1(a), has been reported by Shimomura et al.[4] The site is next to the lattice oxygen with which the muon bonds. Characteristic oscillations for both the spectra suggest the existence of an isotropic magnetic field. The frequency was 0.8 MHz, corresponding to 5.9 mT at the muon site. The possible origin for the isotropic magnetic field is Ti³⁺, which exists at the second neighbor site of the muon.[4] Clear differences were observed after the reduction, which generated oxygen vacancies as shown in Fig. 1(b). The oscillation in the TiO₂-H spectra is attributed to the interaction with hydrogen in the oxygen vacancy, similar to what same as we previously found. The small Lorentzian type relaxation observed for TiO₂-noH could be explained by the magnetic interaction with nuclear spins of Ti (^{47}Ti and ^{49}Ti) (<0.2 mT), which suggests that no μ-H interaction exists. The present study strongly supports the existence of μ-H complex in oxygen vacancy by interacting with the existing H in TiO₂-H.

In addition, the photocatalytic properties of μ-H complex were examined by pump-and-probe measurements. The details are still under analysis.
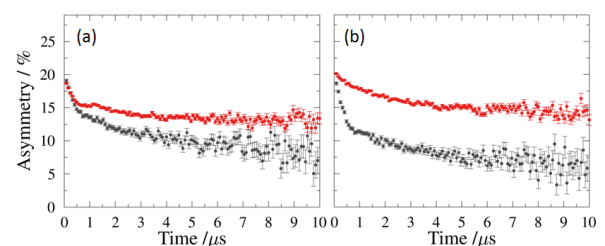
Fig. 1. Zero field μSR spectrum of rutile TiO₂ (a) before and (b) after reduction. Black and red dots correspond to TiO₂-H (6 K) and TiO₂-noH (5 K).

References
1) A. Fujishima, K. Honda, Nature (London) **238**, 37 (1972).
2) K. Ikeda, N. Sugiyama, S. Murakami, H. Kominami, Y. Kera, H. Noguchi, Y. Uosaki, T. Torimoto, B. Ohtani, Phys. Chem. Chem. Phys **5**, 778. (2003).
3) X. B. Chen, L. Liu, P. Y. Yu, S. S. Mao, Science **331**, 746 (2011).
4) K. Shimomura, R. Kadono, A. Koda, K. Nishiyama, M. Mihara, Phys. Rev. B **92**, 075203 (2015).

*1   Institute of Catalysis, Hokkaido University
*2   RIKEN Nishina Center
*3   Insittue of Material Structure Science, KEK.
*4   Advanced Science Research Center, Japan Atomic Energy Agency
*5   Department of Physics & Astronomy, University of California, Riverside

Observation of Li in graphite by muonic x-rays

I. Umegaki,[*1] Y. Higuchi,[*1] K. Ninomiya,[*2] M. K. Kubo,[*3] Y. Kondo,[*1] H. Nozaki,[*1] K. Ishida,[*4]
and J. Sugiyama[*1]

In a Li-ion battery, Li reversely intercalates (deinterrcalates) into (from) electrodes as follows:

$$\begin{cases} \text{cathode}: \text{Li}MO_2 \Leftrightarrow MO_2 + \text{Li}^+ + e^- & (1) \\ \text{anode}: 6\text{C} + \text{Li}^+ + e^- \Leftrightarrow \text{C}_6\text{Li}, & (2) \end{cases}$$
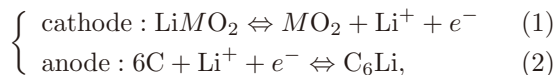
where M is a transition metal ion, such as Co, Ni, and/or Mn. For safety and high efficiency, these reactions should proceed homogeneously in both electrodes. An inhomogeneous distribution or the segregation of Li may cause overcharged states or a short circuit in a battery. Therefore, it is important to know how these reactions proceed in a Li-ion battery.

However, in order to study the distribution of Li during the reactions, we need a non-destructive compositional analysis technique. Elemental analysis with muonic x-rays (μXEA)[1,2] is a suitable technique for such a purpose. We succeeded in obtaining muonic x-ray spectra of a cathode in J-PARC,[3] where an intense negative muon beam with low momentum is available.[4,5] In order to trace the movement of Li between electrodes in a Li-ion battery in the near future, we attempted to observe Li in the anode of a Li-ion battery as the next step by using a graphite anode sheet.

The graphite anode sheet consists of a mixture of graphite and a binder on a Cu foil. A Li-intercalated graphite sheet was prepared by discharging a pouch cell with an electrochemical analyzer. The composition of the anode was confirmed as C_6Li by inductively coupled plasma optical emission spectrometry (ICP-OES). The C_6Li sheet was retrieved from the pouch cell and was covered by Al laminate in an Al holder. The sample was set against the incident beam, and a detector was arranged at an angle of $45°$ to the beam on port 4 at RIKEN RAL.

The muonic x-rays were detected by a Ge semiconductor detector (Canberra), synchronizing with muon pulses at a frequency of 50 Hz in ISIS. As a reference, we also measured a graphite plate with 1 mm thickness.

All signals observed as peaks for the C_6Li sheet were assigned to the muonic x-rays of Li, C, Cu, and Al [Fig. 1(b)]. Since energy difference between C-Lβ and Li-Kα is only 300 eV, it was difficult to distinguish these two signals. It is found that the intensity of the signal C-Lβ (18.4 keV) is $(19.4\pm1.4)\%$ of that of the
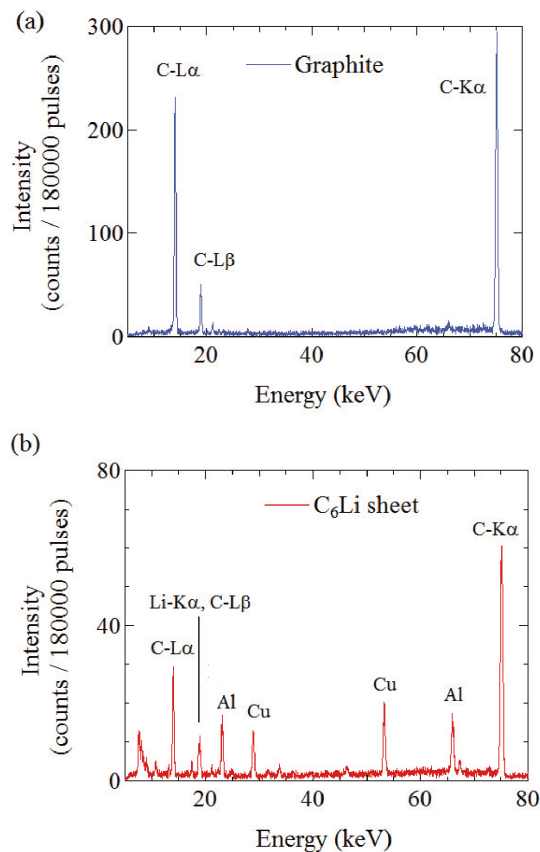
Fig. 1. Muonic x-ray spectra for (a) a graphite plate and (b) a C_6Li sheet. Intensity is represented as the number of counts per 180,000 pulses, corresponding to an hour.

signal C-Lα (14 keV) in the spectra obtained from the graphite plate [Fig. 1(a)]. Assuming the same ratio in C_6Li, we subtracted the contribution from C-Lβ in the peak observed around 18 keV. The intensity of the signal Li-Kα is deduced as $(8.6 \pm 0.8)\%$ of that of the signal C-Lα.

We concluded that μXEA can also detect Li in the Li-intercalated graphite anode of a Li-ion battery. This result may lead to further development of μXEA as a non-destructive compositional analysis technique for Li-ion batteries.

References
1) H. Daniel, Nucl. Instrm. Methods B **3**, 65 (1984).
2) M. K. Kubo *et al.*, J. Radioanal. Nucl. Chem. **278**, 777 (2008).
3) I. Umegaki *et al.*, J. Phys. Soc. Conf. Ser. **21**, 011041 (2018).
4) Y. Miyake *et al.*, Nucl. Instrum. Methods Phys. Rev. A **600**, 22 (2009).
5) M. Tampo *et al.*, J. Phys. Soc. Conf. Proc. **8**, 036016 (2015).

*1   Toyota Central Research & Development Labs., Inc.
*2   Department of Chemistry, Graduate School of Science, Osaka University
*3   Division of Arts & Science, College of Liberal Arts, International Christian University
*4   RIKEN Nishina Center

Development of the in-situ electronic-field-application μSR technique and test application to multiferroic systems

R. Asih,[*1,*2] Y. Taniguchi,[*3] Y. Tokunaga,[*3] T. Nakano,[*2] Y. Nozue,[*2] and I. Watanabe[*1,*2]

One advantage of the pulsed muon facility is that it can be used to carry out *in-situ* measurements with external conditions applied from outside a sample, which optimizes the timing of the application with the arrival of the injected pulsed muon. One of the important systems for external conditions is the *in-situ* electric-field-application system, which is needed to carry out μSR studies on some multiferroic systems. Since the repetition rate of the pulsed muon beam at the ISIS is 50 Hz and the life of the muon itself is less than approximately 20 μs, there is no need to apply the external electric field continuously for more than 30 μs. These conditions can decrease the duty factor. It is well known that the magnetic properties in the multiferroic systems can be controlled by the electric field and vice-versa. These systems are promising candidates for industrial applications such as storage devices and sensors. The new data acquisition (DAQ) system called DAE-III is now available in the RIKEN-RAL Muon Facility, which consequently supports the development of the electric-field-application condition.

In this study, we intend to apply this in-situ electric-field-application system to investigate the spin dynamics of multiferroic systems. We designed a simple sample holder for the in-situ electric-field-application system, as shown in Fig. 1(b). The sample holder was installed on the sample stick of JANIS cryostat, which can reach the lowest temperature of 1.6 K. A single-crystal sample of $Dy_{0.75}Gd_{0.25}FeO_3$ arranged along the c-direction [Fig. 1(a)] was placed between Ag foils (thickness of 12.5 μm) and then flanked by two Al rings. For electric insulation, Mylar sheets were inserted between the sample holder and metal backing plate of JANIS. In the test experiment, an electric field of approximately 300 V, which is generated from the High Voltage Switching Unit (HVSU) device, was applied between the sample and backing plate. By using this designed sample holder, we aim to apply electric fields up to approximately 300–500 V with a pulse length of approximately 30 μs without any discharges in the He exchange gas.

$GdFeO_3$ is a typical system showing significant multiferroic behavior. This system has been synthesized in 1956,[1] but its multiferroicity has been recently confirmed.[2] The spin system enters the static ferromagnetically ordered state below $T_C = 2.5$ K, and its spin direction can be changed by the application of an electric field of approximately 2 kV/cm.[2] The mutiferroic
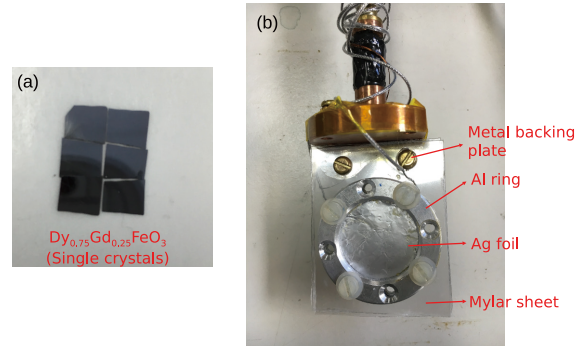
Fig. 1. (a) Six pieces of the single crystal $Dy_{0.75}Gd_{0.25}FeO_3$. (b) The designed sample holder for the *in-situ* electric-field-application μSR at RIKEN-RAL Muon Facility.
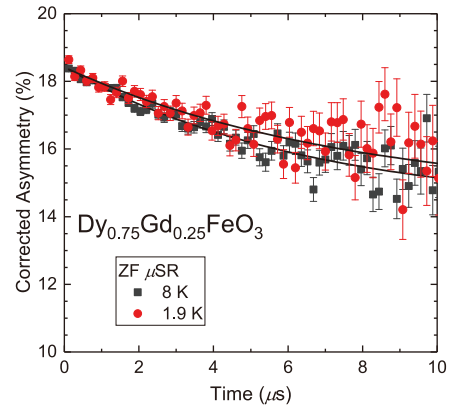
Fig. 2. Time spectra of $Dy_{0.75}Gd_{0.25}FeO_3$ at 8 K and 1.9 K. Solid lines are fitting results as described in the text.

behavior of this system can be tuned by the substitution of Dy for Gd.[3] We first performed the measurement under the zero-field condition to check the time spectra of muon polarization. We found that there is no significant difference in the time spectra above and below T_C, as shown in Fig. 2. The spectra were well fitted by a single exponential function, $A(t) = A \exp(-\lambda t)$, where A is the initial asymmetry and λ is the relaxation rate. The absence of spontaneous muon-spin precession below T_C is expected owing to a large magnetic moment of Fe moments in the sample, which therefore cannot be detected using a pulsed muon source. Further test application on multiferroic compounds with a relatively small moment, such as organic multiferroics, is needed to check the in-situ electric-field-application system at RIKEN-RAL Muon Facility.

References
1) S. Geller *et al.*, J. Chem. Phys. **24**, 1236 (1956).
2) Y. Tokunaga *et al.*, Nature Matt. **8**, 558 (2009).
3) Y. Tokunaga *et al.*, Nature Phys. **8**, 838 (2012).

[*1] RIKEN Nishina Center
[*2] Department of Physics, Osaka University
[*3] Center of Emergence Material Science, RIKEN

Development of an intense mid-infrared coherent light source for muonic hydrogen spectroscopy

S. Kanda,[*1] S. Aikawa,[*2] K. Ishida,[*1] M. Iwasaki,[*1] Y. Ma,[*1] Y. Matsuda,[*3] K. Midorikawa,[*4] Y. Oishi,[*5] S. Okada,[*6] N. Saito,[*4] M. Sato,[*5] A. Takamine,[*1] K. S. Tanaka,[*7] H. Ueno,[*1] S. Wada,[*4] and M. Yumoto[*4]

The proton is a fundamental constituent of the matter. However, its internal structure is complicated and perplexing. The internal structure of a proton is described by the electric and magnetic form factors. These form factors appear in the charge radius which has been measured by using electron-proton scattering and spectroscopy of hydrogen-like atoms. Since the proton charge radius was determined by the spectroscopy of Lamb shift in muonic hydrogen at PSI,[1] there has been a significant discrepancy between the electronic and muonic measurement results of the charge radius.[2] Both the experiments have been validated; however, the discrepancy was reproduced.[3,4]

Alternatively, the proton structure is expressed by the Zemach radius, which is defined by a convolution of the charge distribution with the magnetic moment distribution. The Zemach radius can be extracted from the hyperfine splitting (HFS) of muonic hydrogen as a contribution arising from the finite volume effect of the proton. We aim to determine the proton Zemach radius via laser spectroscopy of the ground-state hyperfine splitting in muonic hydrogen. The HFS energy of muonic hydrogen is 183 meV, and it corresponds to a light having the wavelength of 6.8 μm. The hyperfine transition is E1-forbidden, and an intense mid-infrared coherent light source is essential to the experiment.

In order to perform precision spectroscopy of muonic hydrogen HFS, a pulse energy of 20 mJ and a spectral width of 100 MHz are required for the transition laser. The coherent light with a wavelength of 6.8 μm is generated by an optical parametric oscillator (OPO) using a ZnGeP$_2$ (ZGP) nonlinear optical crystal. The OPO is pumped with a Tm^{3+}, Ho^{3+} co-doped YAG ceramic laser. A quantum cascade laser (QCL) is adopted as a narrowband seeder. The output beam of the OPO is amplified by the ZGP optical parametric amplifiers (OPAs). Figure 1 illustrates a diagram of the proposed laser system.

As a first step to develop the laser system, the Tm,Ho:YAG ceramic laser was developed. A YAG ceramic rod was pumped by laser diodes and a quasi-continuous light output was pulsated by an acousto-optic Q-switch. A pulse energy of 20 mJ or higher and

a pulse width of 150 ns or less are required for the output beam of Tm,Ho:YAG ceramic laser. Figure 2 shows the measured pulse energy and pulse width of the laser beam as a function of the current applied to the laser diodes. A TEM$_{00}$ mode beam profile was obtained, and the beam radius was 1 mm. Sufficient performance of the light source was achieved by alignment optimization of each optical component.

Since the development of pumping light source was successful, the OPO pumped with the Tm,Ho:YAG ceramic laser will be demonstrated as the next step. The QCL as a seeder is under development and needs to be tested.
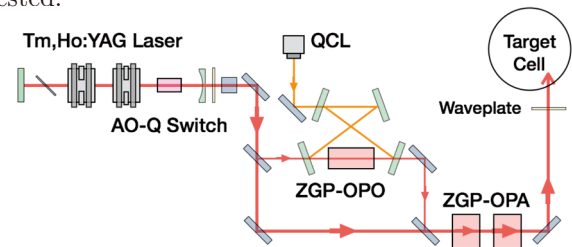
Fig. 1. Diagram of the laser system. The system comprises of three stages: the Tm,Ho:YAG ceramic laser; the QCL-seeded ZGP-OPO; and the ZGP-OPAs. A quarter-waveplate is placed after the OPA to obtain a circularly polarized light. In the spectroscopy experiment, two sets of the laser system will be employed for a total energy of 20 mJ.
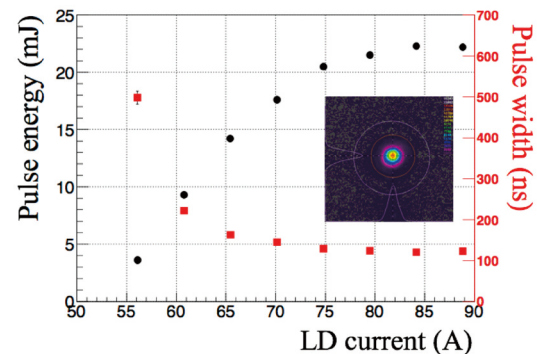
Fig. 2. Output characteristics of the Tm,Ho:YAG ceramic laser. The black circles correspond to the pulse energy, which refers to the left ordinate. The red squares correspond to the pulse width, which refers to the right ordinate. The inset represents the beam profile.

References
1) R. Pohl *et al.*, Nature (London) **466**, 213 (2010).
2) P. J. Mohr, B. N. Taylor, D. B. Newell, Rev. Mod. Phys. **84**, 1527 (2012).
3) A. Antognini *et al.*, Science **339**, 417 (2013).
4) J. C. Bernauer *et al.*, Phys. Rev. C **90**, 015206 (2014).

*1　RIKEN Nishina Center
*2　Department of Physics, Tokyo Institute of Technology
*3　Graduate School of Arts and Sciences, The University of Tokyo
*4　Photonics Control Technology Team, RIKEN
*5　High Energy Accelerator Research Organization (KEK)
*6　Atomic, Molecular, and Optical Physics Laboratory, RIKEN
*7　Cyclotron and Radioisotope Center, Tohoku University

3. Radiochemistry and Nuclear Chemistry

Solid-liquid extraction of Mo and W by Aliquat 336 from HCl solutions toward extraction chromatography experiments of Sg[†]

Y. Komori,[*1,*2] T. Yokokita,[*1,*2] Y. Kasamatsu,[*2] H. Haba,[*1] A. Toyoshima,[*3] K. Toyomura,[*1] K. Nakamura,[*1] J. Kaneya,[*2] M. Huang,[*2] Y. Kudou,[*2] N. Takahashi,[*1] and A. Shinohara[*1]

Chemical characterization of transactinide elements with atomic number $\geq$ 104 is an attractive and challenging subject in the field of radiochemistry. Two decades ago, Schädel $et\ al.$ performed the pioneering cation-exchange experiment of seaborgium (Sg) in 5×10^{-4} M HF/0.1 M HNO$_3$[1)] and 0.1 M HNO$_3$[2)] using an automated rapid chemistry apparatus (ARCA). In the literature, it was reported that the fluoride complexation of Sg was similar to that of its lighter homologs, Mo and W. In their experiment, however, Schädel $et\ al.$ observed only four time-correlated events from the daughters and granddaughters of ^{265}Sg^{a,b}[1,2)] produced in the ^{248}Cm(^{22}Ne, $5n$)^{265}Sg^{a,b} reaction because of the time-consuming α-sample preparation. One of the possible methods of unambiguous identification through detection of α-correlations from ^{265}Sg^{a,b} and its descendants is to adopt liquid scintillation counting for the physically pre-separated ^{265}Sg^{a,b} with GARIS.[3)] This approach has high detection efficiency and the sample preparation time is short. In parallel with the development of the measurement apparatus, it is also necessary to search for experimental conditions applicable to ^{265}Sg^{a,b}. In this study, we examined solid-liquid extraction of Mo and W in the Aliquat 336/HCl system as a model experiment for Sg.

^{90}Mo ($T_{1/2}$ = 5.7 h) and ^{173}W ($T_{1/2}$ = 7.6 min) were simultaneously produced via the ^{nat}Ge(^{22}Ne, xn)^{90}Mo and ^{nat}Gd(^{22}Ne, xn)^{173}W reactions, respectively, using Gd/Ge targets at the RIKEN K70 AVF cyclotron. Reaction products recoiling out of the targets were continuously transported to the chemistry laboratory using a He/KCl gas-jet method. The transported products were deposited on the ARCA collection site for 5 min. The products were then dissolved in HCl and subsequently fed into a microcolumn (1.0 mm i.d. and 3.5 mm) filled with 52-wt.% Aliquat 336/CHP20Y resin at a flow rate of 1 mL/min. The effluents were collected in polypropylene (PP) tubes for every 50- or 80-μL fraction. Then, the remaining products in the column were stripped with 400–500 μL of 6 M HNO$_3$/0.01 M HF and collected in another PP tube. These samples were assayed through γ-ray spectrometry with Ge detectors. We also performed batch experiments with ^{93m}Mo and ^{181}W using the Aliquat 336/CHP20Y resin in HCl solutions.
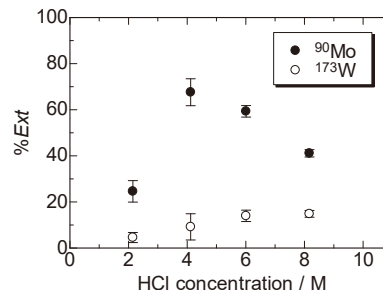
Fig. 1. Variation of %Ext values of ^{90}Mo and ^{173}W on 52-wt. % Aliquat 336/CHP20Y column (1.0 mm i.d. and 3.5 mm) as a function of HCl concentration.

In the experiments involving the transactinide elements and performed using the ARCA, chromatographic separation was conducted with approximately 200 μL of the eluent (first fraction) and the remaining radioactivities in the column were eluted by a stripping solution as the second fraction.[4)] To evaluate the extraction behaviors of Mo and W by this method, the percent extraction (%Ext) on the resin was defined as

$$\%Ext = \frac{100A_2}{A_1 + A_2} \tag{1}$$

where A_1 indicates the amount of radioactivity eluted with 200 μL of the effluent and A_2 is that remaining in the column with the effluent. The variation of the %Ext values as a function of HCl concentration are shown in Fig. 1.

In the figure, the %Ext values of Mo increase to 70% in 2–4 M HCl and then decrease in 4–6 M, while those of W are less than 20% for all examined concentrations. The trend of the %Ext values, Mo > W, is qualitatively consistent with the results of the batch experiments performed with ^{93m}Mo and ^{181}W. This indicates that the extraction behaviors of Mo and W obtained with ARCA reflect the chloride complex formation of these elements, $i.e.$, formation of the anionic oxochloro complexes [MO$_2$Cl$_3$]$^-$ (M = Mo and W) in 1–6 M HCl.[5,6)] Under the present conditions, therefore, it is expected that information on the chloride complexation of Sg can be obtained by comparing its %Ext values with those of Mo and W using our developed systems.

References
1) M. Schädel $et\ al.$, Radiochim. Acta **77**, 149 (1997).
2) M. Schädel $et\ al.$, Radiochim. Acta **83**, 163 (1998).
3) H. Haba $et\ al.$, Phys. Rev. C **85**, 024611, (2012).
4) H. Haba $et\ al.$, Radiochim. Acta **95**, 1 (2007).
5) C. Heinter-Wirguin, R. Cohen, J. Inorg. Nucl. Chem. **27**, 1989 (1965).
6) T. Sato, K. Sato, Hydrometallurgy **37**, 253 (1995).

† Condensed from J. Radioanal. Nucl. Chem. **303**, 1385 (2015).
*1 Graduate School of Science, Osaka University
*2 RIKEN Nishina Center
*3 Advanced Science Research Center, Japan Atomic Energy Agency

Reversed-phase chromatography for element 105, Db
with Aliquat 336 resin from 2.7 M and 27 M HF solutions

D. Sato,[*1,*2] M. Murakami,[*1] S. Goto,[*1] K. Ooe,[*1] R. Motoyama,[*1] K. Shirai,[*1] R. Yamada,[*1] S. Tsuchiya,[*5]
T. Moriyama,[*5] H. Haba,[*2] Y. Komori,[*2] S. Yano,[*2] A. Toyoshima,[*3] A. Mitsukai,[*3] K. Tsukada,[*3]
H. Kikunaga,[*4] and H. Kudo[*5]

Elements with atomic number ≥ 104 are called superheavy elements. As aqueous chemical studies for element 105, Db, an anion-exchange experiment was performed in 13.9 M hydrofluoric acid solution.[1] However, the chemical species of Db in HF solution is not still clear. We have been studying a liquid-liquid and a solid-liquid extraction of Nb and Ta which are lighter homologues of Db with Aliquat 336 in solutions of various concentration of HF.[2,3] In the liquid-liquid extraction, univalent anionic complex of Nb and Ta were extracted, and it was implied that the extracted species were $[NbOF_4]^-$ or $[NbF_6]$ and $[TaF_6]^-$.[2] On the other hand, the results of solid-liquid extraction with 52 wt% Aliquat 336 resin lead indicated that the distribution coefficients, K_d, of ^{95g}Nb has the minimum value at 10 M HF, while those of ^{179}Ta gradually decrease with increasing HF concentration.[3] Because the adsorption behaviors of Nb and Ta differed clearly, similarity with the homologues of the character of Db could be clear by measuring the dependence of K_d values of Db on HF concentration. Because the results of Nb and Ta of on-line experiment were good agreement with those of batch experiment in 2.7 M and 27 M HF, it is suggested that the chemical formation of Nb and Ta of on-line experiment is same with that of batch experiment.[3] Therefore, 2.7 M and 27 M HF were decided as the condition of Db experiment. In this study, we performed experiments of a reversed-phase chromatography experiment of Db with 2.7 M and 27 M HF.

The isotope ^{262}Db was produced in the $^{248}Cm(^{19}F, 5n)^{262}Db$ reaction at the RIKEN K70 AVF cyclotron. The small amount of ^{nat}Gd was induced in the Cm target in order to monitor the state of the experiment by measuring ^{170}Ta which was produced in the $^{nat}Gd(^{19}F, xn)^{170}Ta$ reaction. The reaction products transported by the He/KCl gas-jet system were deposited on the collection part in Automated Rapid Chemical Apparatus (ARCA) for 60 s. Then, the products were dissolved in 2.7 M or 27 M HF solution and loaded on a small chromatographic column (1.6 mm $i.d. \times$ 7.0 mm height) filled with the 52 wt% Aliquat 336 resin at a flow rate of 1.0 mL/min. The effluent was collected into a Ta disk as a primary fraction. The adsorbed species on the column were stripped
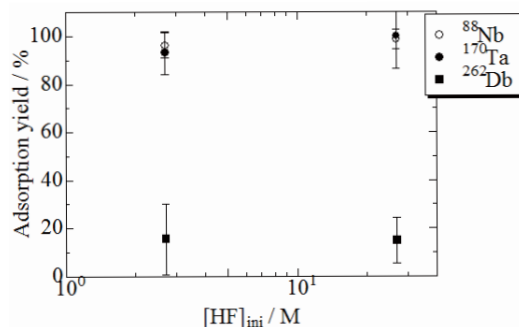
Fig. 1. The dependences of the adsorption yields of Nb, Ta, Db on $[HF]_{ini}$ with 52 wt% Aliquat 336 resin.

with 6 M HNO_3/0.015 M HF solution at a flow rate of 1.0 mL/min. The effluents was collected another Ta disk as a secondary fraction. The both quantity of the primary and the secondary fraction was 150 μL. These Ta disks were heated to dry the solution by halogen lamp, then they were picked up into the automated rapid α/SF detection system, RIDER, by robot arm to measure their radioactivities. The Db experiments were performed for 596 times in 2.7 M HF and for 950 times in 27 M HF. The average chemical yields of ^{170}Ta were about 22% in 2.7 M HF and 18% in 27 M HF, respectively.

From the obtained α-spectra, the number of events corresponding to ^{262}Db ($E_\alpha = $ 8420–8740 keV)[4] in 2.7 M HF were 10 in the 1st fraction and 2 in the 2nd fraction. In 27 M HF, 24 events in 1st fraction and 3 events in 2nd fraction were observed. Considering the contamination, the distribution of decay time and the background, the adsorption yields on the 52 wt% Aliquat 336 resin which were estimated by radioactivity ratio were 15.4% in 2.7 M HF and 14.8% in 27 M HF, respectively. In Fig. 1, it was found that the adsorption yields of Nb and Ta are almost 100% in the both cases of 2.7 M and 27 M HF, while those of Db are very smaller than those of homologues. In addition, the adsorption yields of Db are almost constant to $[HF]_{ini}$. Therefore, if the K_d values of Db are estimated from the adsorption yield, the dependence of K_d values of Db on $[HF]_{ini}$ is also constant. Because the K_d values of Ta are decreased with increasing $[HF]_{ini}$,[3] the extraction behavior of Db would not be like Ta at least. Therefore, it was suggested that the fluoride complex formation of Db is not similar to that of Ta.

*1 Graduate School of Science and Technology, Niigata University
*2 RIKEN Nishina Center
*3 Japan Atomic Energy Agency
*4 Research Center for Electron Photon Science, Tohoku University
*5 Department of Chemistry, Faculty of Science, Niigata University

References
1) K. Tsukada et al., Radiochim. Acta. 97, 83 (2009).
2) D. Sato et al., RIKEN Accel. Prog. Rep. 47, 247 (2014).
3) D. Sato et al., JNRS, sorc 61, 3B09 (2017).
4) M. Murakami, Dr. thesis, Niigata Univ. (2015).

Solvent extraction of Rf in the Aliquat 336/HCl system using flow-type extraction apparatus

N. Kondo,[*1] Y. Kasamatsu,[*1] H. Haba,[*2] M. Nagase,[*3] Y. Yasuda,[*1] Y. Shigekawa,[*1] H. Ninomiya,[*1] E. Watanabe,[*3] A. Kanda,[*1] K. Ouchi,[*1] Y. Kuboki,[*2] Y. Komori,[*2] S. Yano,[*2] N. Sato,[*2] T. Yokokita,[*2] and A. Shinohara[*1]

Superheavy elements (SHEs) with $Z \geq 104$ are synthesized by heavy-ion-induced nuclear reactions. It is very difficult to investigate the chemical properties of SHEs because of the low production rates and short half-lives of these nuclides.[1] In the solution chemistry of SHEs, ion-exchange and extraction experiments were so far performed for mainly element 104, Rf and 105, Db. Especially for fluoride complexation, various interesting data were obtained.[1] To deepen the understanding of the halide complexation of Rf, we aim at investigating the chloride complexation of Rf. In our previous studies, we investigated the solid-liquid extraction behavior of Rf using Aliquat 336 as an extractant by confirming the extraction reaction equilibrium for the first time.[2,3] The distribution coefficient (K_d) of Rf was acquired. In the results, the variation of the K_d value of Rf with HCl concentration showed a slightly different tendency from those of Zr and Hf, and the sequence of the K_d values was different from that for fluoride complexation. In this study, we developed an online solvent extraction apparatus and performed solvent extraction experiments of Zr, Hf, and Rf in the Aliquat 336/HCl system for further investigation of the chloride complexation of Rf.

We first investigated the dependence of the distribution ratios (D) of Zr and Hf on Aliquat 336 concentration ([Aliquat 336]) by a batch method to determine the net charge of the extracted anionic chloride complexes. We used 7.8–11.2 M HCl as the aqueous phase and $CHCl_3$ or CCl_4 as the organic phase, and we used carrier-free radiotracers of ^{88}Zr ($T_{1/2} = 83.4$ d) and ^{175}Hf ($T_{1/2} = 70$ d).

Consequently, the slopes in the $\log D$ versus $\log$ [Aliquat 336] plots of Zr and Hf were both 1.9 in $CHCl_3$ as shown in Fig. 1, suggesting that the bivalent chloride complex is extracted. On the other hand, the slopes in CCl_4 were 1.2 for both Zr and Hf, which suggests that the monovalent chloride complex is dominantly extracted. These results imply that different chloride complexes (net charge) would be extracted for different organic solvents: $CHCl_3$ and CCl_4.

A flow-type solvent extraction apparatus called the flow Injection Solvent Extraction apparatus (ISE), which is suitable for online extraction experiments with short-lived isotopes of SHEs, was developed and its performance was checked by solvent extraction with Zr and Hf. Subsequently, as a model experiment of Rf, the online liquid-liquid extraction using ISE was performed with the AVF cyclotron in the Research Center for Nu-
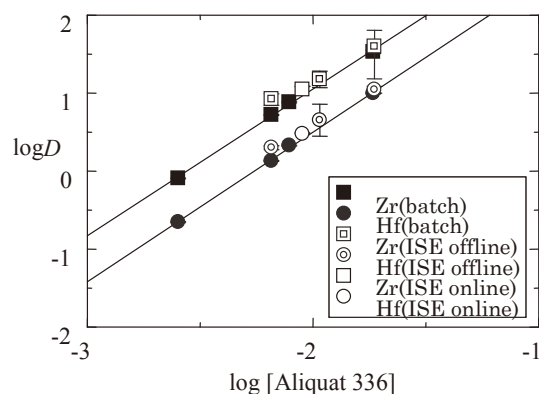
Fig. 1. Dependence of the D values of Zr and Hf on Aliquat 336 concentration in $CHCl_3$ at 11.2 M HCl.

clear Physics, Osaka University (RCNP) by using ^{89m}Zr ($T_{1/2} = 4.18$ min) and ^{173}Hf ($T_{1/2} = 23.4$ h) produced in the $^{nat}Sr(\alpha, xn)$ and $^{nat}Yb(\alpha, xn)$ reactions, respectively. The D values acquired with ISE in 9.3–11.2 M HCl were in good agreement with those acquired by the batch method as shown in Fig. 1, suggesting applicability of the present method to the Rf experiment.

Recently, we produced ^{261}Rf ($T_{1/2} = 68$ s) and ^{169}Hf ($T_{1/2} = 3.24$ min) in the $^{248}Cm(^{18}O, 5n)^{261}Rf$ and $^{nat}Gd(^{18}O, xn)^{169}Hf$ reactions, respectively, by using the RIKEN AVF cyclotron, and carried out the solvent extraction of Rf in the Aliquat 336/HCl system (the organic solvent is $CHCl_3$ or CCl_4). The reaction products were transported by a He/KCl gas-jet system to the chemistry room and dissolved in 9.3 M HCl with a dissolution apparatus.[3] The solution was injected to ISE. After phase separation by ISE, we collected the two phases on different Ta plates and the samples were assayed by alpha-particle measurement by the automated rapid α/SF detection system. After alpha particle measurement, we measured γ-ray activities of ^{169}Hf in the samples with Ge detectors.

We carried out 667 extraction cycles. We observed good reproducibility for the D values of Hf and the average D values of Hf are equivalent to the values obtained in the batch experiment. The chemical yield including dissolution efficiency was approximately 40%. In the alpha-particle measurement, we detected 118 counts of ^{261}Rf and ^{257}No, and the D values of Rf are now under analysis.

References
1) M. Schädel, Radiochim. Acta **100**, 579 (2012).
2) T. Yokokita *et al.*, Dalton Trans. **45**, 18827 (2016).
3) Y. Kasamatsu *et al.*, Radiochim. Acta **103**, 513 (2015).

*1 Graduate School of Science, Osaka University
*2 RIKEN Nishina Center
*3 Faculty of Science, Osaka University

Anion and cation exchanges of Zr, Hf, and Th in H₂SO₄ for chemical study of Rf

for chemical study of Rf

T. Yokokita,[*1] S. Yano,[*1] Y. Komori,[*1] and H. Haba[*1]

Clarifying the chemical properties of superheavy elements with atomic number $Z \geq 104$ is an intriguing and important subject. These elements are produced at accelerators using heavy-ion-induced nuclear reactions. The production rates of these elements are low, and their half-lives are short ($T_{1/2} \leq 1$ min). Thus, chemical studies on these elements are conducted on a single-atom basis.[1]

The solution chemistry of superheavy elements has been studied mainly for element 104, Rf. In these studies, experiments on Rf and homologous elements have been carried out under the same conditions, but for even homologous elements, equilibrated data were obtained in few conditions. Particularly, it was reported that the chemical reaction kinetics between Zr and Hf are different in H₂SO₄.[2] Thus, the observation of equilibration and the equilibrated distribution data are very important to characterize the sulfate complex formation of Rf. In this work, we performed anion and cation exchange of Zr, Hf, and Th by using ion-exchange resin and fiber to search the rapid reaction system for the chemical study of Rf.

We produced ⁸⁸Zr and ¹⁷⁵Hf in the ⁸⁹Y($d, 3n$) and ^{nat}Lu(d, xn)¹⁷⁵Hf reactions (nat = natural isotopic abundance), respectively, by using the RIKEN AVF cyclotron. ²³⁴Th was obtained as an α-decay daughter nuclide of ²³⁸U. These radiotracers were purified by an anion-exchange method.

The ion-exchange experiments of Zr, Hf, and Th were performed by the batch method using 0.1–36.3 mg of the ion exchanger (anion-exchange resin (Mitsubishi Chemical, MCI GEL AC08Y), anion-exchange fiber (Nichibi, IEF-BrA-SA), cation-exchange resin (Mitsubishi Chemical, MCI GEL CK08Y), or cation-exchange fiber (Nichibi, IEF-MR-SC)) and 0.25 mL of 0.12–1.0 M H₂SO₄. We also performed control experiments without the resin. The distribution ratio (Q_d) was obtained according to $Q_d = (A_c - A_s)V/A_s w$, where A_c and A_s denote the radioactivities in the control and extracted solutions, respectively; V is the volume of the solution; and w is the weight of the ion exchanger.

The dependence of the Q_d values of Zr, Hf, and Th on the shaking time is shown in Figs. 1(a), (b), and (c), respectively. When using the anion-exchange resin, the Q_d values of Zr, Hf, and Th are constant in the entire time range studied. When using the anion-exchange fiber, the Q_d values of Zr, Hf, and Th become constant after 1 h, 2 h, and 10 s for Zr, Hf, and Th, respectively. When using the cation-exchange resin, the Q_d values become constant after 10 min for Zr and Hf and after 10 s for Th. When using the cation-exchange fiber, the Q_d values of
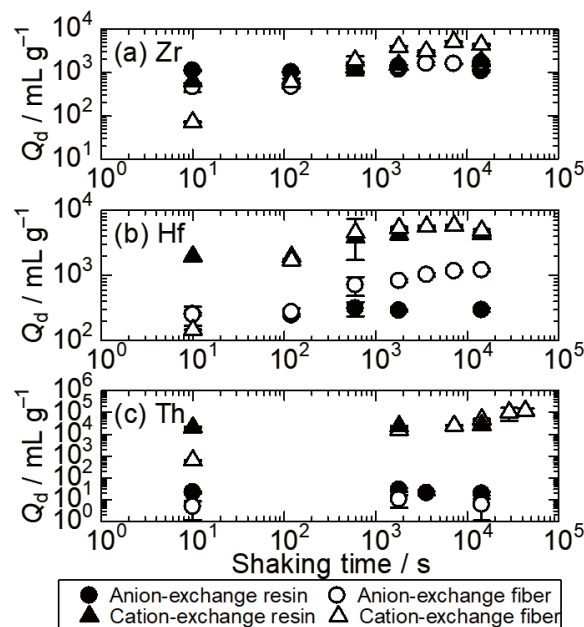
Fig. 1. Variations of the Q_d values of (a) ⁸⁸Zr, (b) ¹⁷⁵Hf, and (c) ²³⁴Th on the shaking time in 0.1 M H₂SO₄.

Zr, Hf, and Th become constant after 2 h, 10 min, and 4 h, respectively. These results suggest that the anion-exchange reaction reaches equilibrium within 10 s when using the anion-exchange resin, and this reaction system would be applicable for ²⁶¹Rf ($T_{1/2} = 68$ s). On the other hand, the time required to reach equilibria in the ion-exchange reaction with the other ion exchangers used in this work are relatively long compared to that with the short-lived ²⁶¹Rf. We found that the time required to reach the equilibrium with the ion-exchange resin is shorter than that with the fiber for both anion and cation exchange. We concluded that the ion-exchange fibers are unavailable for experiments with the short-lived ²⁶¹Rf.

We also studied the variations of the distribution coefficients (Q_d values in equilibrium condition) of Zr, Hf, and Th on the anion-exchange resin to obtain comparison data and to determine the appropriate experimental condition for Rf experiment. We would like to perform a similar experiment on Rf experiments by using AMBER,[3] to observe the equilibration of the anion-exchange reaction, and to investigate the chemical properties of the sulfate complex of Rf.

References
1) A. Turler, V. Pershina, Chem. Rev. **113**, 1273 (2013).
2) Z. J. Li *et al.*, Radiochim. Acta **100**, 157 (2012).
3) Y. Kasamatsu *et al.*, Radiochim. Acta **103**, 513 (2015).

*1 RIKEN Nishina Center

Solvent extraction behavior of Zr and Hf with 2-furoyltrifluoroacetone as model experiments for rutherfordium (element 104)

K. Ooe,[*1,*2] S. Kusakari,[*1] S. Goto,[*1] H. Haba,[*3] Y. Komori,[*3] and H. Kudo[*4]

Our group has been investigating the solvent extraction behavior of zirconium (Zr) and hafnium (Hf) with chelating agents such as 2-thenoyltrifluoroacetone (HTTA) and di-2-ethylhexylphosphoric acid (HDEHP) as model experiments for the heavier homolog, rutherfordium (Rf).[1–3] In our previous study, we extracted Zr and Hf (extractant: HDEHP) with a rapid extraction apparatus by using a flow injection analysis (FIA) technique.[3] Although the distribution ratio (D) of Zr and Hf increased more rapidly than those in the batch method, it took more than several minutes to reach the extraction equilibrium of Zr and Hf with the apparatus. An experiment with HTTA using the apparatus showed almost the same result; therefore, we planned to employ another chelate extractant having faster extraction kinetics for the short-lived Rf experiment. In this study, we used 2-furoyltrifluoroacetone (HFTA), which is a β-diketone like HTTA, for extraction experiments of Zr and Hf. This extractant has lower distribution constant (K_d) and acid dissociation constant (pK_a) values than HTTA.[4] Because lower K_d and pK_a values lead to a higher concentration of the coordinating anion, FTA^-, in the aqueous phase, HFTA may show faster kinetics than HTTA. The extraction kinetics and mechanism for Zr and Hf with HFTA were investigated by the batch method. In addition, an extraction experiment using the FIA apparatus was conducted.

Long-lived radionuclides of ^{88}Zr ($T_{1/2} = 83.4$ d) and ^{175}Hf ($T_{1/2} = 70$ d) were produced in the ^{89}Y$(d, 3n)^{88}$Zr and ^{nat}Lu$(d, xn)^{175}$Hf reactions, respectively, by using the RIKEN K70 AVF cyclotron. These produced radiotracers were separated and purified by an anion exchange and a solvent extraction method. In the batch extraction experiment, 600 μL of 1 M HNO_3 solution containing ^{88}Zr and ^{175}Hf tracers was mixed with the same volume of 0.008–0.021 M HFTA/toluene solution. The mixture was mechanically shaken at 25°C and then centrifuged. After the separation of each phase, the samples of aqueous and organic phases were subjected to γ-ray spectrometry using a Ge detector. In the FIA experiment, aqueous (1 M HNO_3) and organic (0.018 M HFTA/toluene) phases were pumped with syringe pumps at the same flow rate of 30–100 μL/min. These two phases were mixed in an extraction coil (Teflon capillary) with an inner diameter of 0.17 mm and a length of 1–10 m. The aqueous and organic solutions eluting from the extraction coil were collected in a sample tube. After centrifugation, both phases were
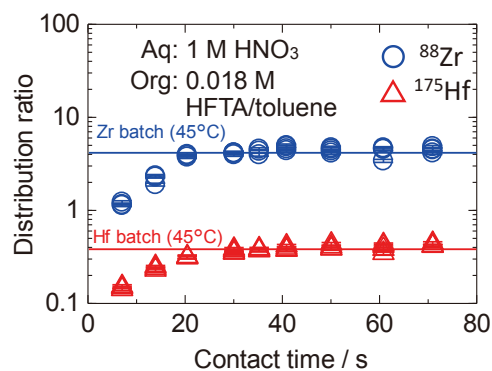
Fig. 1. Dependence of the D values of Zr and Hf on contact time in the extraction coil (inner diameter: 0.017 mm) of the FIA apparatus at 45°C.

separated by pipetting into other sample tubes. The samples were then subjected to γ-ray spectrometry using a Ge detector. The D values of Zr and Hf were calculated from the following equation:

$$D = A_o/A_a,$$

where A denotes the radioactivity of either ^{88}Zr or ^{175}Hf and the subscripts a and o refer to the aqueous and organic phase, respectively.

In the batch extraction experiment, the extraction equilibrium of Zr and Hf with HFTA was attained in 3–4 min, showing faster kinetics than HTTA which required approximately 1 h for attaining equilibrium.[5] The plots of $\log D$ of Zr and Hf against $\log[\text{HFTA}]$ showed linear relations with slopes of approximately 4 for both Zr and Hf. The slope indicates the number of HFTA molecules involved in the extraction reaction, and therefore, the extracted species would be $Zr(FTA)_4$ and $Hf(FTA)_4$.

Figure 1 shows the dependence of the D values of Zr and Hf on contact time in the extraction coil of the FIA apparatus. The experiment in Fig. 1 was conducted at an increased temperature (45°C) because the acceleration of the extraction reaction by using the FIA apparatus at 25°C was insufficient. The result showed that the extraction equilibrium of Zr and Hf with HFTA using the FIA apparatus was attained in 30–40 s. This is a promising result for the extraction experiment of the short-lived ^{261}Rf ($T_{1/2} = 68$ s) isotope. In the future, an on-line extraction experiment of Zr and Hf with the FIA apparatus coupled to a gas-jet transport system will be conducted.

References
1) A. Tanaka *et al.*, RIKEN Accel. Prog. Rep. **48**, 288 (2015).
2) R. Yamada *et al.*, RIKEN Accel. Prog. Rep. **49**, 241 (2016).
3) R. Yamada *et al.*, RIKEN Accel. Prog. Rep. **50**, 251 (2017).
4) T. Sekine *et al.*, J. Inorg. Nucl. Chem. **35**, 3968 (1973).
5) K. Ooe *et al.*, the 61st Symposium on Radiochemistry, (Tsukuba, Ibaraki, Japan, 2017), p. 31.

[*1] Institute of Science and Technology, Niigata University
[*2] Department of Nuclear Medicine and Tracer Kinetics, Osaka University Graduate School of Medicine
[*3] RIKEN Nishina Center
[*4] Faculty of Science, Niigata University

Activation cross sections of α-induced reactions on ^{nat}In for ^{117m}Sn production

M. Aikawa,[*1,*2] M. Saito,[*1,*2] Y. Komori,[*2] and H. Haba[*2]

The radioisotope (RI) ^{117m}Sn ($T_{1/2}$ = 13.76 d) decays with emission of both conversion electrons (126.82, 129.369, and 151.56 keV) and γ rays (158.56 keV). Further, this RI can be used as a bone pain palliation agent, because the electrons and γ rays are appropriate for therapy and imaging, respectively. The production reactions of this RI have previously been investigated and discussed; however, their production in adequate quantities remains of much concern.[1] In this study, we focused on one of the reactions, i.e., the ^{115}In(α,x)^{117m}Sn reaction, the cross sections of which have exhibited large discrepancies in previous studies.[2–4] Another experiment measuring the cross sections of the reactions is, therefore, valuable.

The experiment was performed at the Azimuthally Varying Field cyclotron of the RIKEN RI Beam Factory using well-established methods, e.g., the stacked foil technique, activation method, and high-resolution γ-ray spectrometry. Natural In foils (purity: 99.99%; Nilaco, Japan) were stacked with natural Ti monitor foils (purity: 99.6%; Nilaco, Japan). The thicknesses of the In and Ti foils were estimated from the measured areas and weights of large foils (50 × 50 mm^2) and found to be 16.60 and 2.44 mg/cm^2, respectively. The stacked target consisted of 11 sets of In-In-Ti-Ti foils (8 × 8 mm^2) cut from the large foils. The first foils on the downstream side of the beam were measured to compensate for the losses of the recoil products. However, the In foils were melted because of their low melting point at 156.6°C and could not be separated after α beam irradiation. Each set of In foils was therefore considered as one foil of 33.3 mg/cm^2. Irradiation with a 51.6-MeV α beam with an average intensity of 202.1 nA was performed for 2 h. The intensity and beam energy were measured by a Faraday-cup-like target holder and the time-of-flight method using a plastic scintillator monitor.[5] The γ rays emitted from the irradiated foils were measured by a high-resolution high-purity Germanium detector.

The decay data[6,7] are summarized in Table 1. Measurement of the 156.02-keV γ-line (I_γ = 2.113%) from the ^{117m}Sn decay was performed after a cooling time of approximately 45 h. The cooling time was set to be sufficiently long for decay of the parent nuclei, ^{117}Sb ($T_{1/2}$ = 2.80 h), ^{117g}In ($T_{1/2}$ = 43.2 min), and ^{117m}In ($T_{1/2}$ = 116.2 min). The γ-line at 158.56 keV (I_γ = 86.4%) was not selected to avoid the overlapped contribution of the 159.377-keV γ-line (I_γ = 68.3%)

Table 1. Decay data for ^{117m}Sn and related nuclei

Nuclide	$T_{1/2}$	E_γ (keV)	I_γ (%)
^{117m}Sn	13.76 d	156.02	2.113
		158.56	86.4
^{47}Sc	3.3492 d	159.381	68.3
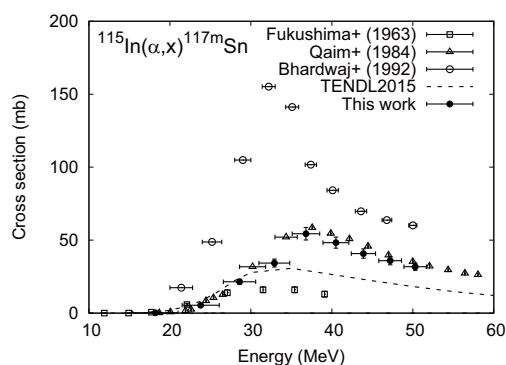
Fig. 1. Excitation function of ^{115}In(α,x)^{117m}Sn reaction. The result is compared with previous experimental data[2–4] and TENDL-2015.[8]

from the ^{47}Sc ($T_{1/2}$ = 3.3492 d) in the Ti catcher foils. The ^{115}In(α,x)^{117m}Sn reaction cross sections estimated from the ^{115}In abundance (95.71%) are shown in Fig. 1, together with the previous experimental data (open symbols)[2–4] and the TENDL-2015 data (dashed line).[8] Among the three sets of experimental data, the present result (filled symbols) is consistent with Qaim et al. (1984).[3] More detailed analysis regarding ^{117m}Sn and other RIs is currently being performed.

References
1) T. Das, S. Banerjee, Clin. Exp. Metastasis **34**, 1 (2017).
2) S. Fukushima et al., Bull. Chem. Soc. Jpn. **36**, 1225 (1963).
3) S. M. Qaim, H. Döhler, Int. J. Appl. Radiat. Isot. **35**, 645, (1984).
4) M. K. Bhardwaj et al., Int. J. Mod. Phys. E **1**, 389 (1992).
5) T. Watanabe et al., Proc. 5th Int. Part. Accel. Conf. (IPAC2014), (2014), p.3566.
6) National Nuclear Data Center, The NuDat 2 database, http://www.nndc.bnl.gov/nudat2/.
7) S. Y. F. Chu et al., The Lund/LBNL nuclear data search, http://nucleardata.nuclear.lu.se/toi/.
8) A. J. Koning et al., TENDL-2015: TALYS-based evaluated nuclear data library.

*1　Graduate School of Biomedical Science and Engineering, Hokkaido University
*2　RIKEN Nishina Center

Prodution cross sections of ^{169}Yb and ^{167,168,170}Tm isotopes in deuteron-induced reactions on ^{169}Tm[†]

M. Saito,[*1,*2] M. Aikawa,[*1,*2] Y. Komori,[*2] H. Haba,[*2] and S. Takács[*3]

The ^{169}Yb (T$_{1/2}$ = 32.018 d, EC = 100%) radionuclide is an Auger electron and X-ray emitter, making it suitable for brachytherapy.[1,2] Previously measured experimental cross-section data suggest that the deuteron-induced reaction on ^{169}Tm[3–5] is one of the best candidates for the production of high-specific-activity ^{169}Yb owing to the large cross sections of the (d,2n) reaction and 100% natural abundance of the target ^{169}Tm. However, the available experimental cross-section data of the ^{169}Tm(d,2n)^{169}Yb reaction have relatively large uncertainties and are scattered; therefore, the excitation function is not defined properly. We report cross-section data of the ^{169}Tm(d,2n)^{169}Yb reaction using pure, thin metallic thulium foils as the target material to reduce the uncertainty of the experimental data.

The excitation functions of the deuteron-induced reactions on ^{169}Tm were measured by using the stacked-foil activation method and high-resolution γ-ray spectrometry of the irradiated target foils. The ^{169}Tm metallic target foils (purity: 99%, Goodfellow, UK) were stacked with ^{nat}Ti (purity: 99.9%, Goodfellow, UK) and ^{27}Al foils (purity: >99.95%, Nilaco, Japan) for monitoring the beam parameters and for degrading the beam energy. The average thicknesses of Tm, Ti, and Al foils were determined by measuring the surface area and the weight of larger pieces of the foils and were found to be 28.65, 4.95, and 13.44 mg/cm^2, respectively. The irradiation was performed at the AVF cyclotron of the RIKEN RI Beam Factory. The stacked target was irradiated for 75 min with a 24.36-MeV deuteron beam having an average intensity of 135.6 nA, which was measured by a Faraday cup. The incident beam energy was measured by the time-of-flight method using plastic scintillator monitors.[6] The beam-energy degradation in the stacked target was calculated using the SRIM code available online.[7] The γ-ray spectra of the activated foils were measured by HPGe detectors. Nuclear decay data were taken from the online NuDat 2.7 database.[8]

The excitation function of the ^{169}Tm(d,2n)^{169}Yb reaction was derived from the γ-line at 177.21-keV (22.28%), as shown in Fig. 1, together with the previously measured experimental data,[3–5] and the result of the TALYS calculation.[9] Our peak energy is in good agreement with the previous data[3–5] although
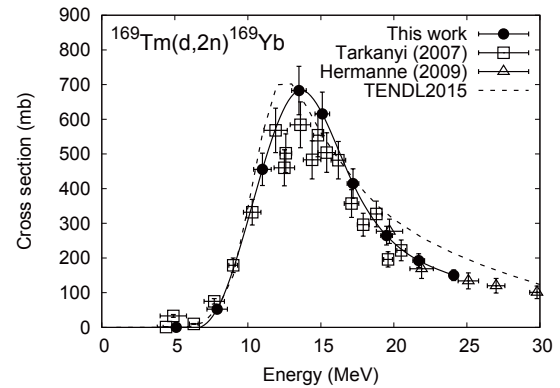
Fig. 1. Excitation function of the ^{169}Tm(d,2n)^{169}Yb reaction. The solid curve shows a spline fit over the experimental data. The result is compared with the previous experimental data[3–5] and TENDL-2015.[9]

the cross sections are slightly higher. In addition to ^{169}Yb, we have measured the production cross sections of ^{167,168,170}Tm. The measured data of Tm isotopes are not included in this report owing to the space limitation, but all data are available in Appl. Radiat. Isot. 125, 23 (2017). The present results for the Tm isotope production show good agreements with the previous data in general.

In summary, we determined the cross sections of the deuteron-induced reactions on ^{169}Tm to produce ^{169}Yb and ^{167,168,170}Tm by using the stacked-foil activation method and γ-ray spectrometry. The thin metallic Tm foils with Ti and Al foils were irradiated by a 24.36-MeV deuteron beam. The obtained excitation functions were compared with previous experimental data, and good agreements were found in general. The excitation function of the ^{169}Tm(d,p)^{170}Tm reaction is reported for the first time.

References
1) F.H. DeLand et al., J. Nucl. Med. 12, 683 (1971).
2) G. Lymperopoulou et al., Med. Phys. 33, 4583 (2006).
3) F. Tárkányi et al., Appl. Radiat. Isot. 65, 663 (2007).
4) A. Hermanne et al., Nucl. Instrum. Methods B 267, 727 (2009).
5) A. Hermanne et al., Nucl. Instrum. Methods B 383, 81 (2016).
6) T. Watanabe et al., Proc. 5th Int. Part. Accel. Conf. (IPAC2014), (2014), p.3566.
7) SRIM: the Stopping and Range of Ions in Matter, http://www.srim.org/.
8) National Nuclear Data Center: the NuDat 2 database, http://www.nndc.bnl.gov/nudat2/.
9) A. J. Koning et al., Nucl. Data Sheets 113, 2841 (2012).

† Condensed from the article in Appl. Radiat. Isot. 125, 23 (2017)
*1 Graduate School of Science, Hokkaido University
*2 RIKEN Nishina Center
*3 MTA ATOMKI, Hungarian Academy of Sciences

Production cross sections of ^{177g}Lu in α-induced reactions on ^{nat}Yb

M. Saito,[*1,*2] M. Aikawa,[*1,*2] T. Murata,[*2,*3] N. Ukon,[*2,*4] Y. Komori,[*2] H. Haba,[*2] and S. Takács[*5]

Radioisotopes (RI) are used for therapy and diagnosis in nuclear medicine. The combination of both therapy and diagnosis (Theranostics) is one of the hot topics in the field. One of the candidate isotopes suitable for theranostics is ^{177g}Lu ($T_{1/2} = 6.6$ d).[1] It emits β particles ($E_{mean} = 134.2$ keV) and γ rays ($E_\gamma = 112.95$ keV ($I_\gamma = 6.17\%$) and 208.37 keV (10.36%)), which are suitable for therapy and diagnosis, respectively.

There are many possible reactions to produce ^{177g}Lu, e.g., neutron-induced reaction on ^{176}Lu and charged-particle-induced reactions on ^{174,176}Yb. Cross section data of such reactions are required to find the best production route of ^{177g}Lu. Among them, we focused on the cross sections of ^{177g}Lu in α-induced reactions on ^{nat}Yb, because we could find only one data set for this reaction up to 40 MeV[2] in a literature survey. Therefore, we performed an experiment to measure the excitation function of the reaction up to 50 MeV.

The experiment was performed at the AVF cyclotron of the RIKEN RI Beam Factory by using a stacked-foil activation method and high-resolution γ-ray spectrometry. Thin metallic foils of ^{nat}Yb (purity: 99%, Goodfellow Co., Ltd., UK) and ^{nat}Ti (purity: 99.6 %, Goodfellow Co., Ltd., UK) for the monitor ^{nat}Ti$(\alpha,x)^{51}$Cr reaction were stacked together as a target. The average thicknesses of the Yb and Ti foils were determined by measuring the surface area and weight of the larger pieces, three Yb foils (25×25 mm^2) and one Ti foil (50×100 mm^2). Their average thicknesses were found to be 16.43, 16.15, 16.93, and 2.40 mg/cm^2, respectively. The target foils (8×8 mm^2) were cut from the measured foils. The stacked target was irradiated by a 50-MeV α beam with an average intensity of 207 particle nA for 2 hours. The initial beam energy was determined by using time of flight measurement,[3] and the energy degradation in the target was calculated by using the SRIM code available online.[4] The initial uncertainty of the α-beam energy was estimated to be ±0.1 MeV, and it increased to ±1.1 MeV at the last Yb foil. Nuclear decay data of ^{177g}Lu and ^{51}Cr were taken from the online NuDat 2.7 database.[5]

Cross sections of the monitor ^{nat}Ti$(\alpha,x)^{51}$Cr reaction were derived from the γ line of $E_\gamma = 320.08$ keV ($I_\gamma = 9.91\%$) and compared with the IAEA recommended values[6] to assess the beam parameters. Our
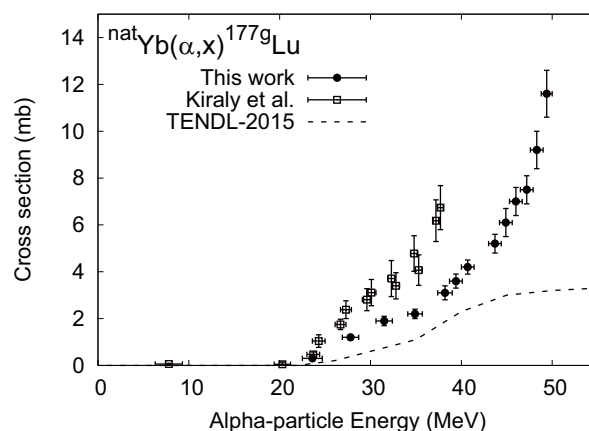
Fig. 1. Cross sections of the ^{nat}Yb$(\alpha,x)^{177g}$Lu reaction in comparison with the previous data[2] and TENDL-2015 data.[7]

result shows a good agreement with the recommended values, and suggests that no adjustment is necessary for the beam parameters. Cross sections of the ^{nat}Yb$(\alpha,x)^{177g}$Lu reaction were also derived from the γ line at $E_\gamma = 208.37$ keV ($I_\gamma = 10.36\%$). The preliminary result is shown in Fig. 1, together with the previous data[2] and the TENDL-2015 data.[7] Our result shows a smooth and monotonical increase, indicating disagreements with the other data.

In summary, we performed an experiment on the α-induced reactions on ^{nat}Yb to produce ^{177g}Lu by using a stacked-foil activation method. Thin metallic ^{nat}Yb foils were irradiated by a 50-MeV α beam. Cross section values were determined from the activity of the produced radioisotopes by using high-resolution γ-ray spectrometry. The result was compared with the previous data and the TENDL-2015 data. We found that there are disagreements with the other data. A more detailed analysis is required to finalize the cross sections and confirm this deviation.

References
1) K. Rahbar *et al.*, J. Nucl. Med. **58**, 85 (2017).
2) B. Király *et al.*, Nucl. Instrum. Methods Phys. Res. B. **266**, 3919 (2008).
3) T. Watanabe *et al.*, Proc. 5th Int. Part. Accel. Conf. (IPAC2014), (2014), p.3566.
4) J. F. Ziegler *et al.*, SRIM: the Stopping and Range of Ions in Matter, http://www.srim.org/.
5) National Nuclear Data Center: the NuDat 2 database, http://www.nndc.bnl.gov/nudat2/.
6) Tárkányi *et al.*, IAEA-TECDOC-1211 (2007).
7) A. J. Koning *et al.*, Nucl. Data Sheets **113**, 2841 (2012).

*1 Graduate School of Biomedical Science and Engineering, Hokkaido University
*2 RIKEN Nishina Center
*3 School of Science, Hokkaido University
*4 Advanced Clinical Research Center, Fukushima Medical University
*5 MTA ATOMKI, Hangarian Academy of Sciences

Activation cross sections of alpha-induced reactions on natural tungsten for ^{186}Re and ^{188}Re production

N. Ukon,[*1,*2] M. Aikawa,[*2,*3] M. Saito,[*2,*3] T. Murata,[*2,*4] Y. Komori,[*2] H. Haba,[*2] and S. Takacs[*5]

Radioisotopes (RI) are used for diagnosis and therapy in nuclear medicine. ^{186}Re is a β emitter with a half-life of 3.72 days, a maximum β energy of 1.07 MeV, average penetration ranges of 1.1 mm in soft tissue and 0.5 mm in bone, and a 9.47% γ-ray emission at 137 keV. ^{188}Re is a β emitter with a half-life of 17 hours, maximum β energy of 2.12 MeV, and 15.61% γ-ray emission at 155 keV.[1,2] Both isotopes can be used for theranostics (therapy and diagnosis).

We focused on a process to produce ^{186,188}Re through alpha-induced reactions of natural tungsten because we could find data for only one 43 MeV.[3] Therefore, we measured the excitation function of the $^{nat}W(\alpha, x)^{186,188}$Re reactions up to 51 MeV.

The excitation functions of the $^{nat}W(\alpha, x)^{186,188}$Re reaction were measured by the stacked-foil method, activation method and high-resolution γ-ray spectroscopy. ^{nat}W foils (purity: 99%, Goodfellow Co., Ltd., UK) were stacked with ^{nat}Ti foils (purity: 99%, Goodfellow Co., Ltd., UK) for monitoring the beam parameters and degrading the beam energy. The thicknesses of the W and Ti foils were 15.03 and 2.23 mg/cm^2, respectively.

The irradiation was performed at the RIKEN AVF cyclotron. A 51 MeV alpha beam with an average intensity of 209.7 pnA was irradiated on the target for 2 h. The incident beam energy was measured by the time-of-flight method using plastic scintillator monitors.[4] The beam energy degraded in the stacked target was calculated using the SRIM code available online.[5] The γ-ray spectra of the activated foils were measured by an HPGe detector. Nuclear decay data were taken from the online NuDat 2.7 database.[6]

From the net peak areas of the 137.16- and 155.04-keV γ-rays, the activation cross sections for the $^{nat}W(\alpha, x)^{186,188}$Re reaction were deduced using the standard activation formula

$$\sigma = \frac{T_\gamma \lambda}{\varepsilon_d \varepsilon_\gamma \varepsilon_t N_t N_b (1 - e^{-\lambda t_b}) e^{-\lambda t_c} (1 - e^{-\lambda t_m})}$$

where N_t denotes the surface density of target atoms; N_b the number of bombarding particles per unit time; T_γ the number of counts in the photo-peak; ε_d the detector efficiency; ε_γ the γ-ray abundances; ε_t the

Fig. 1. Excitation functions of the $^{nat}W(\alpha, x)^{186,188}$Re reactions. The result is compared with a previous study[3] and TENDL-2015.[7]

measurement dead time, which is the ratio of live time to real time; λ the decay constant; t_b the bombarding time; t_c the cooling time; and t_m the acquisition time.

We found that our $^{nat}W(\alpha, x)^{186}$Re result is in good agreement with previous data obtained by NE. Scott *et al.*[3] and the theoretical calculation (TENDL-2015).[7]

On the other hand, the $^{nat}W(\alpha, x)^{188}$Re result shows disagreements with the other data. TENDL-2015[7] underestimates the cross section at all energies.

References
1) A. M. Denis-Bacelar *et al.*, Eur. J. Nucl. Med. Mol. Imaging. **44**, 620 (2017).
2) I. G. Finlay *et al.*, Lancet Oncol. **6**, 392 (2005).
3) N. E. Scott *et al.*, Nucl. Phys. **119**, 131 (1968).
4) T. Watanabe *et al.*, Proc. 5th Int. Part. Accel. Conf. (IPAC2014), (2014), 3566.
5) J. F. Ziegler *et al.*, SRIM: the Stopping and Range of Ions in Matter, http://www.srim.org/.
6) National Nuclear Data Center: the NuDat 2 database, http://www.nndc.bnl.gov/nudat2/.
7) A. J. Koning *et al.*, TENDL-2015: TALYS-based evaluated nuclear data library.

*1 Advanced Clinical Research Center, Fukushima Medical University
*2 RIKEN Nishina Center
*3 Graduate School of Biomedical Science and Engineering, Hokkaido University
*4 School of Science, Hokkaido University
*5 Institute for Nuclear Research, Hungarian Academy of Sciences (ATOMKI)

Measurement of excitation functions of the $^{206/207/208}$Pb(^{11}B, x)^{212}Fr reactions

Y. Komori,[*1] T. Yokokita,[*1] S. Yano,[*1] and H. Haba[*1]

Francium (Fr) is the heaviest alkali metal with the atomic number 87. It is one of the least-studied elements among the naturally occurring elements because all its isotopes are short-lived; the half-life of its longest-lived isotope, ^{223}Fr, is only $T_{1/2} = 21.8$ min. Owing to experimental difficulties, the chemical properties of Fr have not been studied in detail so far. It is considered that the chemical properties of Fr are similar to those of its lighter homolog, Cs. However, the chemical properties of Fr cannot be simply deduced from the extrapolation from the lighter homologs because relativistic effects come into play in such a heavy atom as Fr.[1] Therefore, it is of great interest and importance to clarify the chemical properties of Fr and to elucidate the influence of relativistic effects on the chemical properties of Fr. Recently, Haverlock et al reported on the complex formation of Fr$^+$ with calix[4]arene-bis(benzocrown-6) (BC6B).[2] They reported that Fr$^+$ is more effectively extracted with BC6B than Cs$^+$; however, the reason for the selectivity is unclear. We plan to investigate the stability of the complex formation of Fr with crown ethers by systematically varying their cavity size and substituent group to understand their influences on the selectivity in the complex formation and solvent extraction of Fr. In this study, we will use the long-lived isotope ^{212}Fr ($T_{1/2} = 20$ min), which can be produced in the $^{206/207/208}$Pb(^{11}B, x)^{212}Fr reactions. Because no experimental excitation functions are available for these reactions, we measured the excitation functions of the $^{206/207/208}$Pb(^{11}B, x)^{212}Fr reactions to optimize the production conditions of ^{212}Fr.

The excitation functions were measured using the stacked-foil technique. The $^{206/207/208}$Pb targets were prepared by vapor deposition on 3.1-μm Al foils ($> 99\%$ chemical purity). The size of all foils was 10×10 mm^2. The target stacks consist of 20 sets of ^{206}Pb (99.51%-enrichment, 791-μg/cm^2 thickness), ^{207}Pb (99.40%-enrichment, 851-μg/cm^2 thickness), or ^{208}Pb (99.59%-enrichment, 642 μg/cm^2 thickness). The 3.1-μm Al foils were inserted between the $^{206/207/208}$Pb targets to catch ^{212}Fr atoms that recoiled out of the targets. Each stack was irradiated for 10 min with a 100.9-MeV ^{11}B beam supplied from the RIKEN AVF cyclotron. The incident beam energy was determined by time-of-flight measurement.[3] The average beam current was measured with a Faraday cup and found to be 48.6, 48.8, and 50.0 pnA for the ^{206}Pb, ^{207}Pb, and ^{208}Pb stacks, respectively. After the irradiation, each foil was subjected to γ-ray spectrometry with Ge detectors.

The radioactivity of ^{212}Fr was determined from its 227.72-keV (γ-ray intensity $I_\gamma = 42.6\%$) γ line. Figure 1
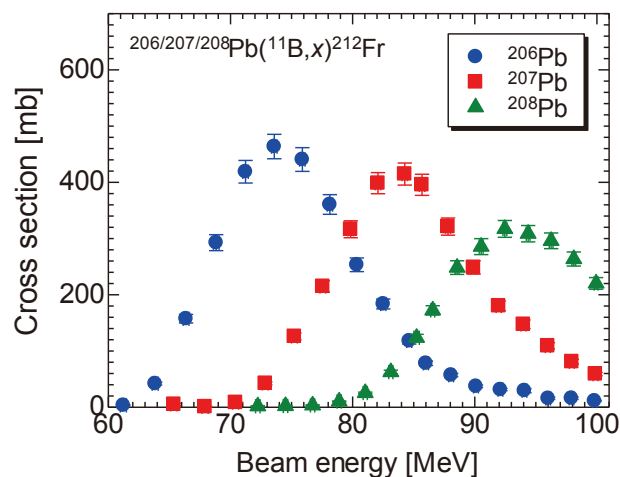
Fig. 1. Excitation functions of the $^{206/207/208}$Pb(^{11}B, x)^{212}Fr reactions.

shows the excitation functions measured for the first time for the ^{206}Pb(^{11}B, $5n$)^{212}Fr, ^{207}Pb(^{11}B, $6n$)^{212}Fr, and ^{208}Pb(^{11}B, $7n$)^{212}Fr reactions. The maximum cross section for the production of ^{212}Fr is available in the ^{206}Pb(^{11}B, $5n$)^{212}Fr reaction around 73.6 MeV.

Based on the measured excitation functions, we will optimize the production condition of ^{212}Fr in the ^{206}Pb(^{11}B, $5n$)^{212}Fr reaction for future chemistry studies of Fr using the multitarget He/KCl-jet transport system.[4] In this system, 4 sets of an 864-μg/cm^2 ^{206}Pb target on a 10-μm Be foil are placed in 12-mm-spacing in 129-kPa He and are irradiated with a ^{11}B beam at an energy of 86 MeV. The beam energies on the four ^{206}Pb targets are calculated to be in the range of 70–79 MeV, which covers the peak region of the excitation function of the ^{206}Pb(^{11}B, $5n$)^{212}Fr reaction. The ^{212}Fr atoms that recoiled out of the ^{206}Pb target are thermalized in the He gas, attached to KCl aerosol particles, and transported through a Teflon capillary to a chemistry laboratory, where the solvent extraction of ^{212}Fr will be performed. 60 kBq ^{212}Fr, which is sufficient radioactivity to study its solvent extraction behavior, is available after the 1-min aerosol collection by assuming a beam intensity of 300 particle nA, recoil efficiency of 48%, and gas-jet efficiency of 50%.

References
1) V. Pershina *et al.*, Chem. Phys. **395**, 87 (2012).
2) T. J. Haverlock *et al.*, J. Am. Chem. Soc. **125**, 1126 (2003).
3) T. Watanabe *et al.*, Proc. 5th Int. Part. Accel. Conf. (IPAC2014), (2014), 3566.
4) H. Haba *et al.*, Advances in Nuclear and Radiochemistry. Extended abstracts, 333 (2004).

*1 RIKEN Nishina Center

Improved method for preparation of no-carrier added ^{28}Mg tracer

H. Kikunaga,[*1,*2] H. Haba,[*2] Y. Komori,[*2] and S. Yano[*2]

Magnesium is involved in important physiological activities such as many enzymatic reactions. The isotope ^{28}Mg, which has the longest half-life (21.6 h[1]) among radioactive magnesium isotopes, is useful in biological sciences as a radioactive tracer.[2,3] We plan to provide a no-carrier added ^{28}Mg tracer produced in the ^{27}Al$(\alpha, 3p)$ reaction to applicants through, for example the Supply Platform of Short-lived Radioisotopes for Fundamental Research. In a precious paper,[4] we attempted to separate ^{28}Mg from an Al target, focusing on reducing waste radioactive materials. However, there was an unwanted problem that the obtained tracer contained nuclide ^{7}Be. In this work, we report an improved method for the preparation of no-carrier-added ^{28}Mg tracer in addition to the procedure of beryllium elimination.

Magnesium-28 was produced at either the RIKEN K70 AVF Cyclotron or the AVF Cyclotron at CYRIC, Tohoku University. The target stack of 7 Al foils (99.9% pure) with a thickness of 100 μm was irradiated with an α-particle beam with a beam energy of 50 MeV and a mean current of approximately 3 μA.

First, the conditions for the separation of ^{28}Mg from ^{7}Be were searched for. The irradiated Al targets were dissolved in 12 M (mol/dm^3) HCl. A portion of it, containing 0.1 mmol of Al and trace amounts of ^{7}Be, ^{24}Na, and ^{28}Mg, was heated to dryness and adjusted to 0.5 M oxalic acid. The solution was passed through a cation exchange column (Muromac 50 W×8, 100–200 mesh, 1 mL), which adsorbs Al(III), ^{7}Be,^{24}Na, and ^{28}Mg ions, following which the resin was washed with 7 mL of 0.5 M oxalic acid to eliminate Al(III) and 5 mL of 0.2 M HF. The elution curves of the cation-exchange separation is shown in Fig. 1. The ^{7}Be ions are eluted completely within 5 mL of 0.2 M HF, whereas the ^{24}Na and ^{28}Mg ions are retained onto the column.

Next, the procedure to eliminate ^{7}Be was incorporated into the previous procedure.[4] The improved chemical scheme is shown in Fig. 2. The irradiated Al targets were dissolved in 9 M HCl and then diluted with water to 15 mL. The ^{28}Mg isotopes were co-precipitated with iron hydroxide by adding 2 mg of Fe(III) and 15 mL of 6 M NaOH and separated from Al, Na, and Be ions. The precipitation of iron hydroxide was dissolved in 9 M HCl. The solution was passed through an anion exchange resin column (Muromac 1×8, 100–200 mesh, 1 mL), which adsorbs Fe(III) ions, and the resin was washed with additional 9 M HCl. The eluate was heated to dryness and adjusted to 0.5 M oxalic acid. The solution was passed through a cation exchange resin column (Muromac 50W×8, 100–200 mesh, 1 mL) to adsorb ^{28}Mg isotopes. The resin was washed with 0.2 M HF for Be elimination, 0.5 M oxalic acid for Al elimination, and 0.5 M HCl for Na elimination. The ^{28}Mg isotopes were eluted from the column with 2 M HCl.

The chemical yield of the separation procedure, determined by γ-spectrometry of ^{28}Mg, was approximately 85% and radioactivity other than ^{28}Mg was not detected in the Mg fraction.
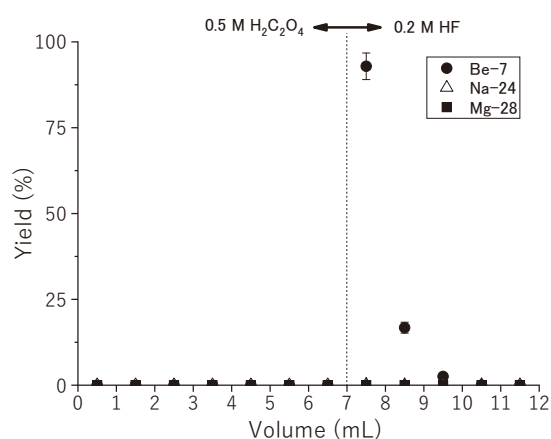
Fig. 1. Elution curves for the cation exchange separation of Be, Na, and Mg.
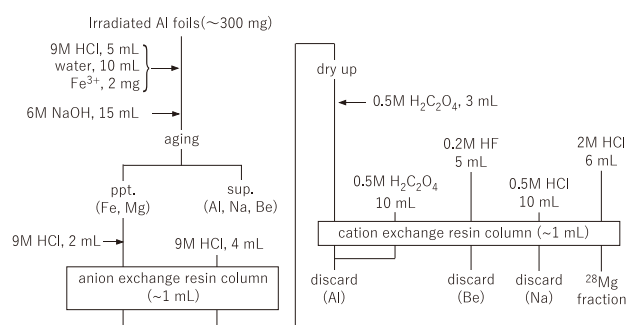
Fig. 2. Chemical procedure for the preparation of no-carrier added ^{28}Mg tracer.

References

1) R. B. Firestone, V. S. Shirley, *Table of Isotopes*, 8th ed. (John Wiley and Sons, New York, 1996).
2) C. Schimansky, J. Plant Nutr. **8**, 467 (1985).
3) K. Tanoi *et al.*, Plant Soil **384**, 69 (2014).
4) H. Kikunaga *et al.*, RIKEN Accel. Prog. Rep. **50**, 260 (2017).

*1 Research Center for Electron Photon Science, Tohoku University
*2 RIKEN Nishina Center

Production of no-carrier-added barium tracer of ^{135m}Ba

S. Yano,[*1] H. Haba,[*1] Y. Komori,[*1] T. Yokokita,[*1] and K. Takahashi[*1]

The long-lived ^{133}Ba isotope (half-life $T_{1/2} = 10.51$ y) is the only Ba isotope commercially available from Japan Radioisotope Association. Since ^{133}Ba is produced at a nuclear reactor, its specific radioactivity is low with a typical value of approximately 0.5 MBqμg^{-1}. Barium-135m with $T_{1/2} = 28.7$ h can be produced from the ^{133}Cs$(\alpha, x)^{135m}$Ba reaction by using a cyclotron. Barium-135m emits a single 268.2-keV γ-ray, which would be useful for radiotracer studies of Ba, especially for single- photon-emission computed tomography (SPECT).[1] In this work, we investigated a procedure to produce ^{135m}Ba of high specific radioactivity by using the ^{133}Cs$(\alpha, x)^{135m}$Ba reaction and no-carrier-added chemical separation.

CsCl powder (Sigma-Aldrich; chemical purity $>$ 99.999%) was pressed into a disk of 10-mm diameter and 240-mg cm^{-2} thickness at a pressure of 2×10^3 kg cm^{-2} for 3 min. The CsCl pellet covered with a 10-μm Al foil (chemical purity $>$ 99.99%) was placed on a target holder. The target was irradiated for 30 min with a 50-MeV alpha beam having an intensity of 3.0 μA at the RIKEN AVF cyclotron. During the beam irradiation, the target was cooled with circulating helium gas (30 L min^{-1}) and water (1.5 L min^{-1}). The beam axis was continuously rotated in a circle of diameter approximately equal to 2 mm at 2 Hz to avoid local heating of the target by using electromagnets on the beam line of the RIKEN AVF cyclotron. After the irradiation, ^{135m}Ba was chemically separated from the target material and by-products such as ^{135}La and ^{132}Cs by using a chromatography column filled with the Eichrom Sr resin[2] (Fig. 1). The radioactivity and radionuclidic purity of the purified ^{135m}Ba were determined by γ-ray spectrometry using a Ge detector. The chemical purity and specific radioactivity were evaluated by chemical analysis using an inductively coupled plasma mass spectrometer (ICP-MS). The γ-ray spectrum of the purified ^{135m}Ba is shown in Fig. 2. Only Ba isotopes of ^{131}Ba, ^{133}Ba, ^{133m}Ba, and ^{135m}Ba were identified. The radioactivity of ^{135m}Ba was determined to be 2.25 MBq at the end of bombardment (EOB). The chemical yield of ^{135m}Ba was greater than 96%. Decontamination factors of ^{135}La and ^{132}Cs from ^{135m}Ba were evaluated to be 10^3 and 10^5, respectively. The radionuclidic purity of ^{135m}Ba was approximately 68% at the EOB. The major radionuclidic impurity was ^{133m}Ba ($T_{1/2} = 38.9$ h) which was produced in the ^{133}Cs$(\alpha, x)^{133m}$Ba reaction. Referring to the excitation functions for the ^{133}Cs$(\alpha, x)^{135m}$Ba and ^{133}Cs$(\alpha, x)^{133m}$Ba reactions in the TENDL-2015 library,[3] it is expected that the radionuclidic purity of ^{135m}Ba can be increased at lower beam energies. In the ICP-MS analysis, only Cu (1280 ng), U (160 ng), Zn (140 ng), and Ba (100 ng)
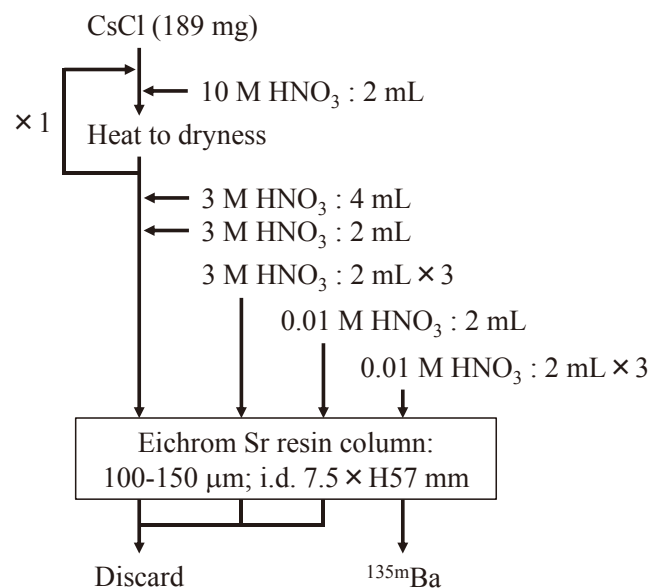
Fig. 1. Chemical separation procedure of ^{135m}Ba from the CsCl target.
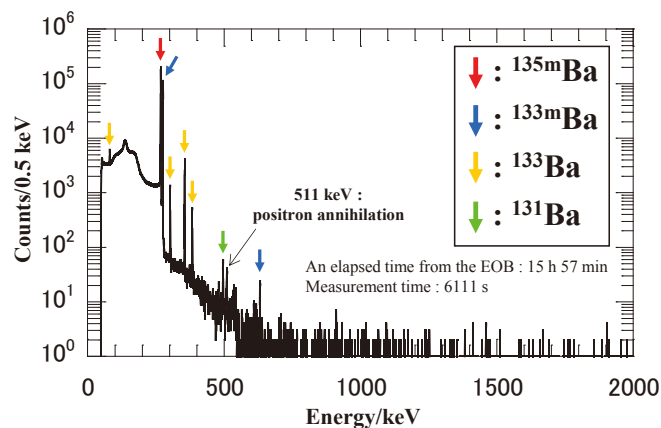
Fig. 2. γ-ray spectrum of purified ^{135m}Ba.

were detected among the elements having atomic number $Z \geq 20$ in the purified ^{135m}Ba with a contamination level $>$ 100 ng. The specific radioactivity of ^{135m}Ba was then 23 MBq μg^{-1} at the EOB. This specific radioactivity is two orders of magnitude larger than that of the commercial ^{133}Ba.

Based on the present results, we estimate that approximately 80 MBq of the no-carrier-added ^{135m}Ba could be produced after 24-h irradiation of the 240-mg cm^{-2} CsCl target with the 50-MeV and 3-μA alpha beam. The expected specific radioactivity is approximately 830 MBq μg^{-1}.

References
1) R. P. Spencer *et al.*, J. Nucl. Med. **12**, 216 (1971).
2) E. P. Horwitz *et al.*, Solvent Extr. Ion Exc. **10**, 313 (1992).
3) A. J. Koning, D. Rockman, Nucl. Data Sheets **113**, 2841 (2012).

*1 RIKEN Nishina Center

Trial of astatine separation using column chromatography

H. Ikeda,[*1,*2,*3] H. Kikunaga,[*2,*3] Y. Komori,[*3] S. Yano,[*3] T. Yokokita,[*3] H. Haba,[*3] and H. Watabe[*1]

Astatine (At) is one of the nuclides expected to be applied for targeted α-particle therapy (TAT). Several methods for At separation are known, but mainly two methods (dry distillation[1]) and wet extraction[2,3]) are used. Dry distillation can obtain yield a pure solution of At, however complicated apparatus must be constructed.[1]) On the other hand, although wet extraction is a simple method, the aqueous solution is contaminated with an organic solvent after back extraction. In order to apply At for TAT, the separation method has be improved further. In this work, column chromatography was attempted as one of the improved methods.

We produced ^{211}At at RIKEN Nishina Center using the ^{209}Bi$(\alpha, 2n)^{211}$At reaction (29 MeV, 250 particle nA, 30 min) and ^{210}At at Cyclotron and Radioisotope Center (CYRIC), Tohoku University using the ^{209}Bi$(\alpha, 3n)^{210}$At reaction (50 MeV, 100 particle nA, 30 seconds). A bismuth oxide (Bi_2O_3) pellet was used as the target. The irradiated target was dissolved in 2 mL of 4 M HCl containing 1 M $NaHSO_3$, and 6 mL of 0.84 M EDTA·2Na solution was added (stock solution).

Batch experiments of 5 fillers (anion-exchange resin, cation exchange resin, activated carbon, alumina, and cellulose) were conducted, in which 0.1 mL of fillers were added to 1 mL of stock solution. These mixtures were shaken for 5 min and centrifuged for 10 min. The fillers and supernatant was separated and their radioactivity were measured (Table 1). A significant amount of At was adsorbed on anion exchange resin and activated carbon, however little At was adsorbed on the other fillers.

We attempted column chromatography using anion-exchange resin and activated carbon. 1 mL of stock solution was charged into a filler (5 mmϕ × 4 mm), and the column was eluted. In both cases, almost all At was trapped in the column. Trapped At was not eluted by concentrated HCl. However, At on the activated carbon column was eluted by 10 M NaOH solution. Thus we optimized the separation method (Fig. 1) and drew the elution curve (Fig. 2). In the experiment, 85% of charged At was eluted by 10 column volumes of 10 M NaOH solution. It is suggested that At is oxidized to AtO(OH) at pH 14 which is the condition of the eluent.[4]) This result suggested that AtO(OH) do not adsorbed on activated carbon. We could harvest high yield At easily.

However, the At solution was strongly alkaline.

Table 1. Results of batch experiment (ratio of At%).

	Absorbed	Supernatant
Anion-Exchange Resin	73.4 ± 1.4	0.95 ± 0.14
Cation-Exchange Resin	8.4 ± 0.3	78.8 ± 0.5
Activated Carbon	85.1 ± 1.3	1.3 ± 0.2
Alumina	15.5 ± 0.5	66.4 ± 1.3
Cellulose	11.8 ± 0.4	68.3 ± 2.5
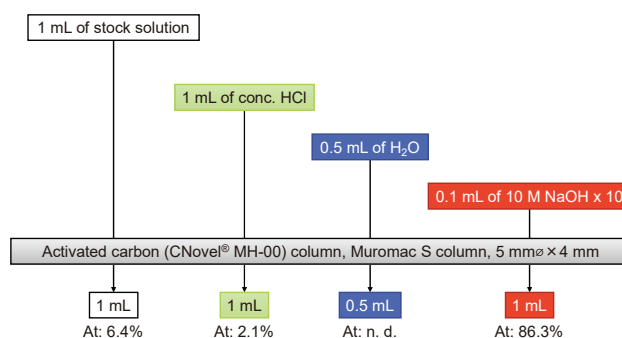
Fig. 1. Separation method of At using column chromatography (filler: activated carbon).
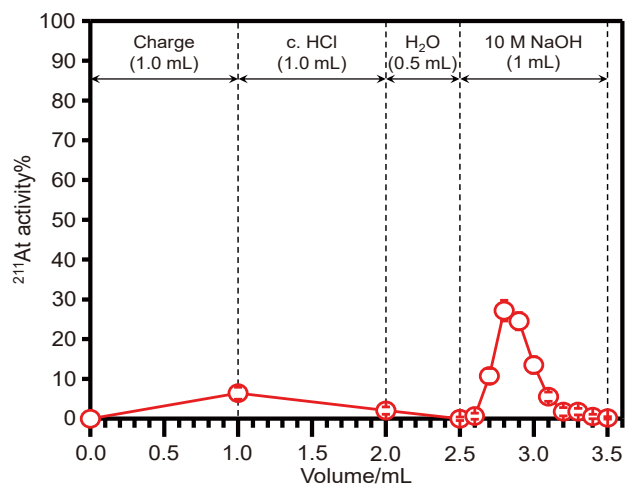
Fig. 2. Elution curve of At from activated carbon column.

Therefore, it is not possible to use this solution for biological research (pre-clinical and clinical research). In the future, we plan to test the removal method of concentrated cations, consider another target dissolution method, and apply other fillers.

References
1) S. Lindegren *et al.*, Appl. Radiat. Isot. **55**, 157 (2001).
2) M. S. Sultana *et al.*, J. Radioanal. Nucl. Chem. **243**, 631 (2000).
3) C. Zona *et al.*, J. Radioanal. Nucl. Chem. **276**, 819 (2008).
4) J. Champion *et al.*, Inorg. Chim. Acta. **362**, 2654 (2009).

*1 Cyclotron and Radioisotope Center, Tohoku University
*2 Research Center for Electron Photon Science, Tohoku University
*3 RIKEN Nishina Center

Wet chemistry processes utilized in development of ^{211}Rn/^{211}At generator for targeted alpha therapy

Y. Shin,[*1] K. Kawasaki,[*2] N. Yamada,[*1]
K. Washiyama,[*3] A. Yokoyama,[*2] I. Nishinaka,[*4] S. Yanou,[*5] and H. Haba[*5]

The short path length and high linear energy transfer of alpha particles are expected to facilitate targeted alpha therapy in tumor treatment. One of the promising nuclides among the various alpha emitters is ^{211}At, which has a half-life of 7.21 h. This nuclide attracts much attention because of its suitable half life and the expected chemical properties of the element, and this has motivated a large number of preclinical studies on At chemistry.[1–3] As regards improvement of the ^{211}At availability, development of a 14.6-h ^{211}Rn generator, where ^{211}Rn is a parent nuclide of ^{211}At, can potentially provide nuclides in a wider range of locations distant from the accelerator facilities in which they are produced. However, At chemistry has not been well studied in relation to Rn decay and further knowledge is needed to control its behaviors in the required successive chemical processes.[4] The aim of this study was to investigate the wet chemistry processes of At so as to realize a ^{211}Rn/^{211}At generator that may facilitate a prevalent technology.

Radon-211 was produced through irradiation of a stack of Bi targets with 60-MeV ^{7}Li^{3+} beams from the Japan Atomic Energy Agency (JAEA) tandem accelerator via the ^{209}Bi(^{7}Li, 5n) ^{211}Rn nuclear reaction. After the irradiation, the Bi target was dissolved in nitric acid solution and diluted with distilled water. Then, the produced ^{211}Rn was transferred to an organic phase, $i.e.$, dodecane, through solvent extraction. The trapped ^{211}Rn was then allowed to stand for over half a day to generate ^{211}At. Back-extraction of ^{211}At was performed using alcohol with an oxidizing agent.

In this study, to obtain the ^{211}At distribution ratios between the dodecane and ethanol (EtOH) solution with an oxidizing agent, the Bi target, which was irradiated at the RIKEN Azimuthally Variable Field (AVF) cyclotron, was delivered to Kanazawa University, dissolved in nitric acid, and diluted to a 1 M solution in acid concentration. The dodecane solution, into which At species were extracted from the nitric acid solution, was subjected to extraction experiments with and without an oxidization agent, $i.e.$,
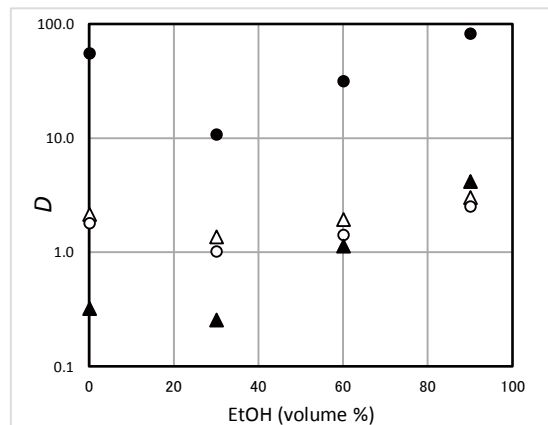
Fig. 1. Distribution values of ^{131}I (open symbols) and ^{211}At (closed symbols) for extraction with (circles) and without (triangles) an oxidizing agent.

N-Bromosuccinimide. The results were compared with those of the same experiments performed with a commercially available I-131 isotope.

After the back extraction to the EtOH solution, each phase was subjected to measurements with a liquid scintillation counter, to determine the back extraction distribution, D, of ^{211}At. Hence, we found that only At exhibit a notable effect of oxidation, as shown in Fig. 1. Here, the distributions were obtained from the ratios of the radioactivity in the EtOH solution to that in the dodecane. We also aimed to control the extraction behavior of the At from the nitric acid solution by using an ionic liquid with a crown ether. For the combination of 1-butyl-3-methylimidazolium Bis (trifluoromethanesulfonyl) imide and 18-crown-6, the extraction system was found to be promising because an extraction rate of up to 90% was attained at low acid concentrations.

References
1) F. Guérard, J-F. Gestin, M. W. Brechbiel, Cancer Biother. Radiopharm. **28**, 1 (2013).
2) D. S. Wilbur, Nat. Chem. **5**, 246 (2013).
3) M. R. Zalutsky, M. Pruszyński, Curr. Radiopharm. **4**, 177 (2011).
4) E. Maeda, A. Yokoyama, T. Taniguchi, K. Washiyama, I. Nishinaka, J. Radioanal, Nucl. Chem. **303**(2), 1465 (2015).

[*1] Institute and College of Science and Engineering, Kanazawa University
[*2] Graduate School of Natural Science and Technology, Kanazawa University
[*3] Fukushima Global Medical Science Center, Fukushima Medical Unversity
[*4] Quantum Beam Science Research Directorate, National Institutes for Quantum and Radiological Science and Technology
[*5] RIKEN Nishina Center

Development of Np standard material for accelerator mass spectrometry

A. Yokoyama,[*1] A. Sakaguchi,[*2] K. Yamamori,[*3] Y. Hayakawa,[*1] J. Sekiguchi,[*2] S. Yanou,[*4] Y. Komori,[*4] T. Yokokita,[*4] and H. Haba[*4]

Recently, there has been a rapid development in the techniques of highly sensitive mass spectrometry. Several elements or nuclides that were not supposed to be applicable in that technique are now quantitatively analyzed. Especially for long-lived actinide elements, the techniques are becoming more and more important as a promising alternative for radioactivity measurements. The tracer nuclide for chemical recovery determination, which has to be non-existent in nature and should not be contained in target samples, is absolutely necessary for that purpose. Tracers for several elements are available now; however, the tracer for neptunium has not been developed, yet. We are searching for an appropriate method for the production of Np-236 in the ground state with a half life of 1.54×10^5 y as a candidate of the tracer nuclide, from the viewpoints of both purity and production rate.

In the present study, we perform Np tracer production through the reaction of ^{232}Th + ^{7}Li and aim to apply Np contamination in environmental samples.

For the irradiation of ^{7}Li beam, two types of target stacks were prepared. One includes several targets of electrodeposited Th of ca. 1 mg/cm^2 on Al foils, as shown in Fig. 1. The other includes a thick target disc of 100 mg/cm^2 Th as shown at the bottom of the same figure. The former stack was utilized to check the production rate and interfering products depending on the projectile energy dumped in the stacking targets, and the latter was used to conduct a trial for the thick target production. Silver foils of natural abundance were also used to monitor the beam intensity calculated from the produced radioactivity of ^{111}In during the irradiation of ^{7}Li as well as for monitoring the current with a Faraday cup in the beam course.

We performed irradiation with ^{7}Li ions of 42 MeV from the RIKEN AVF cyclotron on the stack of thin targets for 8.5 h at 0.6 pμA and on the thick target for 14 h 21 min at 0.2 pμA on average. In order to isolate Np atoms from the irradiated targets, the chemical procedures were performed as follows. The target material was dissolved in 3M HNO$_3$ with Np-237 tracer for checking the chemical recoveries and was dried by heating. Then, the process of dissolving the residue in conc. HNO$_3$ and drying up was repeated three times. Finally, the sample was dissolved again in conc. HCl,
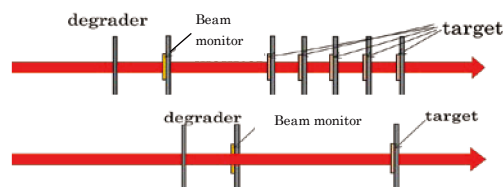
Fig. 1. Schematic illustration of target stacks for the reaction of ^{232}Th with ^{7}Li ions.
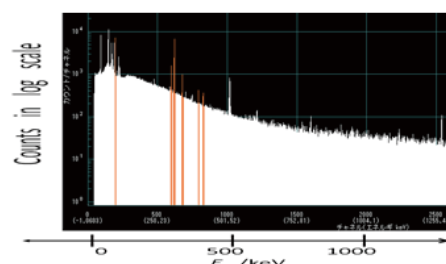
Fig. 2. An example of γ spectrum of isolated Np solution sample. Colored regions correspond to the most prominent emission of U-X ray and γ emissions from Pa-233.

and adjusted to the 10 M HCl solution of 4 mL. The solution was subjected to the separation procedure using a TEVA resin column and treated with 10 M HCl, followed by 3 M HNO$_3$, for purification, and finally 0.1 M HCl for elution of Np.

The purified samples of Np were subjected to γ spectrometry and α spectrometry to check the radiation emitted from the by-products.

As a preliminary result, an example of γ spectrum of the purified solution from one of the stacked targets is shown in Fig. 2. Li ions were projected onto the target at 17.3 MeV. The spectrum shows that the final solution from the sample was still contaminated by protactinium products. The intensities of uranium X-rays following decay of Np-236m with a half life of 22.5 h suggest that the production rate of Np-236g is greater than 5×10^9 atoms/g-Th/h/pμA, assuming an isomeric ratio of products, m/g, of ca. 5. The ratio was estimated from the production data of the same nuclides in the proton induced reaction of ^{238}U.[1] Analysis of the results is still in progress and additional experiments are under planning at present.

Reference
1) J. Aaltonen *et al.*, Phys. Rev. C **41**, 513 (1990).

*1 Institute and College of Science and Engineering, Kanazawa University
*2 Center for Research in Isotopes and Environmental Dynamics, University of Tsukuba
*3 Graduate School of Natural Science and Technology, Kanazawa University
*4 RIKEN Nishina Center

^{99}Ru Mössbauer spectroscopy of Na-ion batteries of Na$_2$RuO$_3$ (IV)

K. Takahashi,[*1] Y. Kobayashi,[*1,*2] H. Haba,[*2] and H. Ueno[*2]

Na$_2$RuO$_3$ with a two-dimensional layered structure of [RuO$_3$]2$^-$ is expected as an electrode material for next-generation Na-ion batteries.[1–3)] Until now, we have studied the crystal structures and oxidation states of Ru ions in Na$_2$RuO$_3$ and Na-Ru oxides with different ratios of Na/Ru using X-ray diffraction patterns and ^{99}Ru Mössbauer spectroscopy. It was revealed that the structures changed from two-dimensional to three-dimensional properties with Na deficiencies. In this paper, we report the result of the chemical states of Ru ion in Na$_2$RuO$_3$ observed before and after a charging experiment. A sample of Na$_2$RuO$_3$ was prepared through a solid-state reaction. A mixture of RuO$_2$ and NaHCO$_3$ was pressed and sintered at 850 °C for 12 h in Ar atmosphere. 95 wt% of Na$_2$RuO$_3$ was mixed with 5 wt% of amorphous carbon powder, and pressed to create a pellet for electrochemical measurements. The pellet sample and carbon rod were used as a cathode and an anode, respectively. 1 mol/L NaPF$_6$ in ethylene carbonate and diethyl carbonate (1:1 by volume) was used as an electrolyte. The charging experiment, which was an anodic process (Na$^+$ de-intercalation), was conducted at 20 mA/g and 4.0 V for 0.5 h and 2.0 h in an Ar-filled glove box. After the charging experiment, the Na$_2$RuO$_3$ electrode was washed with anhydrous dimethyl carbonates and then dried in a vacuum desiccator. For ^{99}Ru Mössbauer spectroscopy, the ^{99}Rh ($T_{1/2}$ = 15.0 d) of the source nuclide was produced by the ^{99}Ru$(p, n)^{99}$Rh reaction in an AVF cyclotron. ^{99}Ru Mössbauer spectra were obtained by employing a conventional arrangement with the source and absorber maintained at 4.2 K in a liquid He cryostat.[4,5)] The XRD pattern of Na$_2$RuO$_3$ after the charging experiment showed that interlayer distance was significantly decreased from 5.45(1) Å to 5.18(3) Å. It was indicated that Na$^+$ ions were extracted from the [Na$_{1/3}$Ru$_{2/3}$]O$_2$ layers. The ^{99}Ru Mössbauer spectrum of Na$_2$RuO$_3$ after charging for 0.5 h showed two doublet peaks, as shown in Fig. 1. The spectrum was analyzed by D1 with an isomer shift (δ) of $-0.32(1)$ mm/s and a quadrupole splitting ($\Delta E_{\rm Q}$) of 0.28(2) mm/s and D2 with δ = $+0.20(5)$ mm/s and $\Delta E_{\rm Q}$ = 1.52(8) mm/s. The ratio of absorption intensities was D1:D2 = 85:15. The isomer shift of D2 is a typical value of Ru^{5+}, for example, $+0.19$ mm/s for Ca$_2$EuRuO$_6$ and $+0.11$ mm/s for Na$_3$RuO$_4$. It was found that the de-intercalation of Na$^+$ ions increased the oxidation state of the Ru ion from Ru^{4+} to Ru^{5+} and significantly distorted the octahedron of RuO$_6$. Further details of the electronic structure of Ru ions

in Na$_2$RuO$_3$ for the electrochemical procedure will be discussed with density functional calculations.
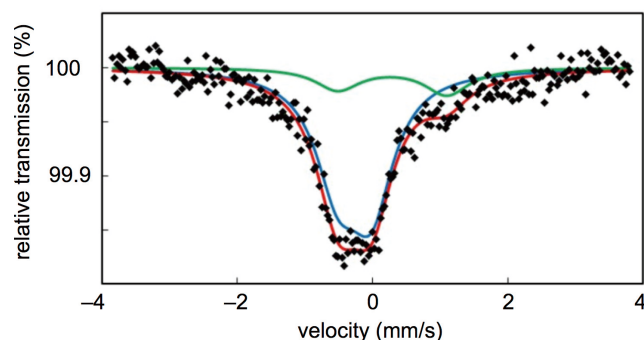
Fig. 1. ^{99}Ru Mössbauer spectrum of Na$_2$RuO$_3$ used as a cathode after charging (20 mA/g, 4.0 V) for 0.5 h. The blue and green lines correspond to components of D1 and D2, respectively. The spectrum was measured at 5.0 K.

References
1) K. M. Mogare *et al.*, Z. Anorg. Allg. Chem. **630**, 547 (2004).
2) M. Tamaru *et al.*, Electrochem. Commun. **33**, 23 (2013).
3) B. M. de Boisse *et al.*, Nat. Commun. **7**, 11397, 10.1038/ncomms11397 (2016).
4) K. Takahashi *et al.*, RIKEN Accel. Prog. Rep. **49**, 242 (2015).
5) Y. Kobayashi *et al.*, J. Phys. **217**, 012023 (2010).

[*1] Dep. of Eng. Sci., University of Electro-Commun.
[*2] RIKEN Nishina Center

Fractionation of Zr-Hf in ferromanganese crusts

J. Inagaki,[*1] A. Sakaguchi,[*1] H. Haba,[*2] Y. Komori,[*2] and S. Yano[*2]

Ferromanganese crusts (FMCs) are abyssobenthic chemical sediments that consist mainly of Fe and Mn oxide and hydroxide minerals, and are enriched with trace and precious metals.[1] As a result of their similar physicochemical properties, the elements zirconium (Zr) and hafnium (Hf), which are concentrated in FMCs, have a theoretically uniform ratio (Zr/Hf), and this ratio is found in numerous systems. However, recent developments in analytical techniques have allowed observation of significant fractionation of these elements between seawater (Zr/Hf~45–350)[2] and FMCs (Zr/Hf~57–88).[1] In this study, we conducted adsorption experiments to clarify the concentrations and fractionation mechanisms of Zr-Hf in FMCs using synthesized minerals (ferrihydrite and δ-MnO$_2$) and radio-Zr and Hf tracers.

Radiotracers of ^{88}Zr (T$_{1/2}$ = 83.4 d), ^{89}Zr (T$_{1/2}$ = 78.4 h), and ^{175}Hf (T$_{1/2}$ = 70.0 d) were produced in ^{89}Y(d, 3n)^{88}Zr, ^{89}Y(p, n)^{89}Zr, ^{175}Lu(d, 2n)^{175}Hf, and ^{175}Lu(p, n)^{175}Hf rections using the RIKEN Azimuthally Varying Field cyclotron. The ^{88}Zr, ^{89}Zr, and ^{175}Hf were radiochemically purified following Haba *et al.* (2001),[3] and mixed with stable Zr or Hf in 1-M HCl solutions.

Appropriate amounts of these solutions were added to 5 mL/0.7 M NaCl solutions containing organic chelate desferrioxamine B (DFOB) to obtain 0 μM, 5 μM, 1 μM, 100 nM, 10 nM and 1 nM solutions. The pH values of these solutions were all adjusted to 8. DFOB, a kind of siderophore present in the environment, has been reported to affect the fractionation of Zr-Hf between crustal rock and seawater.[4] The speciations of these elements in the solutions were confirmed as [Zr(DFOB)]$^+$ and [Hf(DFOB)]$^+$ via electron spray ionization time-of-flight mass spectrometry. The activities of ^{88}Zr, ^{89}Zr, and ^{175}Hf were measured using a Ge detector after stirring for 1 h. Synthesized ferrihydrite or δ-MnO$_2$ (2.50 mg) was added to the solutions and stirred for 3 h at a pH of 8. Note that this stirring time was previously confirmed to be sufficient to achieve the equilibrium condition required for the adsorption reactions. The activities of the ^{88}Zr, ^{89}Zr, and ^{175}Hf in the filtered solutions were measured using a Ge detector. The adsorption amounts to the solid phase were calculated using the differences in the solution radioactivity before and after filtration.

The Zr and Hf adsorption amounts are shown in Fig. 1. Hf to δ-MnO$_2$ yielded the largest adsorption rate, with Zr to δ-MnO$_2$, Hf to ferrihydrite, and Zr to ferrihydrite following in order. The partition coefficients (K_D values) were calculated using the Zr and Hf concentration ranges of in seawater, and it was clear that the
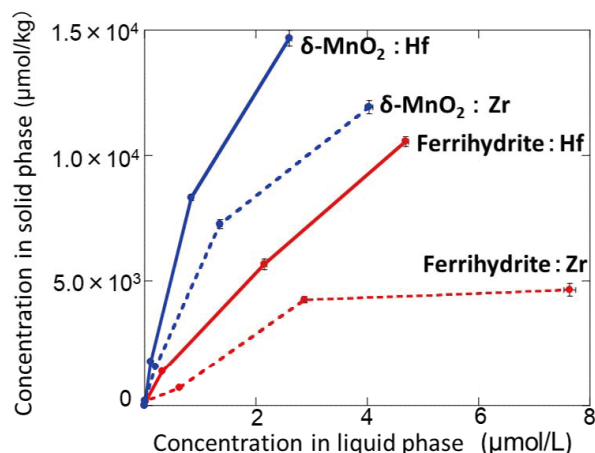
Fig. 1. Adsorption behavior of Zr (dashed line) and Hf (solid line) on ferrihydrite (red) and δ-MnO$_2$ (blue).

Table 1. Partition coefficients K_D for Zr and Hf.

Elements	Minerals	Partition coefficients K_D
Zr	Ferrihydrite	5.73×10^4
	δ-MnO$_2$	1.83×10^5
Hf	Ferrihydrite	2.75×10^5
	δ-MnO$_2$	5.01×10^5

Hf underwent greater adsorption on both minerals than the Zr, and that the Zr and Hf had greater adsorption on δ-MnO$_2$ than ferrihydrite, as apparent from Table 1.

Even though the complexation rates estimated through radioactive isotope thin-layer chromatography (87% for Zr and 79% for Hf) were considered, the adsorption behaviors of these experiments did not change. Furthermore, the ferrihydrite (232 m^2/g) and δ-MnO$_2$ (135 m^2/g) surface areas obtained from Brunauer-Emmett-Teller measurements did not affect the results. It is predicted that the fractionation of Zr and Hf can be caused by differences in the stabilities of the adsorption processes. The binding energy differences between these elements and DFOB/minerals are now being calculated using density functional theory to observe their adsorption stabilities. This knowledge will allow us to discuss the results of Zr-Hf fractionation results obtained from our experimental systems.

References
1) K. Schmidt *et al.*, Geochem. Cosmochim. Acta. **140**, 468 (2014).
2) M. L. Firdaus *et al.*, Nat. Geosci. **4**, 227 (2011).
3) H. Haba *et al.*, Radiochim. Acta. **89**, 733 (2001).
4) D. Kraemer *et al.*, Geochem. Cosmochim. Acta. **165**, 263 (2015).

*1 Graduate School of Pure and Applied Sciences, University of Tsukuba
*2 RIKEN Nishina Center

Desorption of ^{88}Zr from soil with artificial digestive juices

T. Kubota,[*1,*2] K. Iwata,[*1] S. Fukutani,[*1] T. Takahashi,[*1] S. Yanou,[*2] S. Shibata,[*2] H. Haba,[*2] and S. Takahashi[*1]

Some fission products in high-level radioactive waste are planned to be recovered for reusing of valuable materials and reducing waste volume. Zirconium is one of such materials; however, the reuse of radioactive nuclides in public requires safety assessment, clearance level, and internal exposure assessment because ^{93}Zr including fission products has a long half-life $(1.61 \times 10^6$ y). The careful and reasonable evaluation of the internal exposure, in particular, is of importance for reuse in public.

Internal-exposure experiments on animals should be conducted with materials that provide an easy measurement and have no chemical toxicity. Zirconium-88 is the one of suitable zirconium isotopes for the experiments because it is a gamma-emitting nuclide with an adequately long half-life (83.4 d) and can be produced as carrier-free isotopes from yttrium.

Although internal exposure is evaluated from the migration of radio isotopes inside a living body, as a preliminary experiment in this report, we have investigated the desorption property of ^{88}Zr from contaminated soil samples with digestive juices in vitro before using animals.

Zirconium-88 was produced by the bombardment of yttrium metal with deuterons at the RIKEN AVF cyclotron and then purified by solvent extraction at Kyoto University Research Reactor Institute (KURRI).[1] The resulting solution of c.HCl was evaporated once and prepared in 1 M HNO$_3$ with a specific activity of 9.8×10^4 Bq/mL as the initial solution.

Contaminated soil samples were prepared by the following methods. Soil collected from a farm field in KURRI was dried at room temperature, ground to pieces, and then sieved through 0.25 mm. An aliquot of 1 g of the soil was immersed into a zirconium solution, which was prepared by mixing 0.2 mL of the initial ^{88}Zr solution and ultra-pure water immediately before immersion at a solid-to-solution ratio of 0.1 g/mL and shaking reciprocally at 120 rpm for 48 h. Subsequently, the soil was completely dried at 40°C to obtain the initial contaminated soil.

The desorption of ^{88}Zr from soil was investigated based on methods described elsewhere.[2,3] The contaminated soil was treated with the following four eluent solutions: ultra-pure water, simple artificial gastric acid (pH 1),[4] artificial gastric juice (pH 1),[3] and artificial gastrointestinal juice (pH 8).[3] An aliquot of 0.2 g of contaminated soil was added into 20 mL of each eluent, except artificial gastrointestinal juice, and

Table 1. Desorption ratio of ^{88}Zr from soil samples.

Eluent	Desorption ratio
Ultra-pure water	0.09 ± 0.02
Simple artificial gastric juice	0.17 ± 0.02
Artificial gastric juice	0.17 ± 0.02
Artificial gastrointestinal juice	0.22 ± 0.02

the mixture was agitated at 120 rpm at 37°C for 2 h. As artificial gastrointestinal juice, an aliquot of 0.2 g of contaminated soil first added into 5.45 mL of artificial gastric juice was agitated at 120 rpm at 37°C for 2 h, following which the mixture was added with 14.55 mL of artificial gastrointestinal juice and agitated under the same condition. After agitation, the mixture was centrifuged at 3000 rpm for 10 min. The comparison of the specific activity to the initial activity yielded the desorption ratio of ^{88}Zr from contaminated soil.

The results of the desorption of ^{88}Zr are listed in Table 1. The desorption ratios were relatively low with every eluent, and the difference between gastric and gastrointestinal juices was almost negligible, which showed that the adsorption of zirconium was strong and independent of pH. Most of zirconium adsorbed onto soil was directly excreted without desorption. Furthermore, taking account of the history of soil in the environment, soil washed out by rain, for example, would provide lesser desorption and, consequently, lower inner exposure. Based on these results, internal exposure experiments using animals will be conducted in future work.

References
1) T. Kubota *et al.*, RIKEN Accel. Prog. Rep. **50**, 254 (2017).
2) Assessment of human exposure from ingestion of soil and soil material (ISO/TS (Technical Speciation) 17924).
3) Sips *et al.*, RIVM report 711701012 (2001).
4) The Japanese Pharmacopoeia, Sixteenth Edition, 1st Fluid for disintegration test (2010).

*1　Kyoto University Research Reactor Institute
*2　RIKEN Nishina Center

4. Radiation Chemistry and Biology

Recruitment of Rad51 and phosphorylated DNA-PKcs after heavy-ion irradiation of human normal fibroblast

M. Izumi[*1] and T. Abe[*1]

DNA double-strand breaks (DSBs) caused by exposure to ionizing radiation are the most lethal type of damage because an accumulation of misrepaired or unrepaired DSBs can lead to a loss of genetic information and cell death. Accelerated heavy-ion particles with a high linear energy transfer (LET) induce complex clustered DNA damage including DSBs, which is considered to be an obstacle to efficient repair. DSBs are repaired primarily by non-homologous end joining (NHEJ) or homologous recombination (HR) in mammalian cells.[1] Our previous studies using the wild-type CHO cell and two CHO mutant lines deficient in HR or NHEJ suggest that HR is essential for survival after exposure to high-LET ionizing radiation.[2] However, several lines of evidence suggest that NHEJ is also involved in the repair of DSBs caused by high-LET ionizing radiation,[3,4] and the repair mechanism remains controversial in higher eukaryotes.

In this study, we investigated the foci formation of Rad51 and phosphorylated DNA-PKcs (catalytic subunit of DNA-dependent protein kinase), which are involved in HR and NHEJ, respectively (Fig. 1). We used human normal fibroblast NB1RGB cells since immortal cell lines often lose genetic stability or checkpoint control. The number of Rad51 foci and the percentage of Rad51foci-positive cells were maximized 3 h after X-ray irradiation (Figs. 1A, B). On the other hand, the number of Rad51 foci was almost maximized at 1 h after C (LET = 80 keV/μm) or Ar-ion (LET = 300 keV/μm) irradiation (Fig. 1A), suggesting that high LET radiation stimulates HR. In NB1RGB cells synchronized at a quiescent state (at the G0 phase) by serum starvation, the formation of Rad51 foci was not observed after X-ray, C-ion, or Ar-ion irradiation since HR is dependent on DNA replication. The number of Rad51 foci and the percentage of Rad51 positive cells gradually decreased as time proceeded after both X-ray and heavy-ion irradiation (Figs. 1A, B).

The number of phosphorylated DNA-PKcs foci in quiescent NB1RGB cells was twice that in logarithmically growing NB1RGB cells 1 h after X-ray irradiation (Fig. 1C), suggesting that NHEJ and HR work competitively. In contrast, the number of phosphorylated DNA-PKcs foci in quiescent cells was almost the same as that in logarithmically growing cells after C or Ar-ion irradiation. These results suggest that NHEJ does not recognize the fraction of DSBs caused by heavy-ion irradiation, which is consistent with the previous reports that HR is more relevant in the repair of complex DNA damage.[5,6] In addition, the number
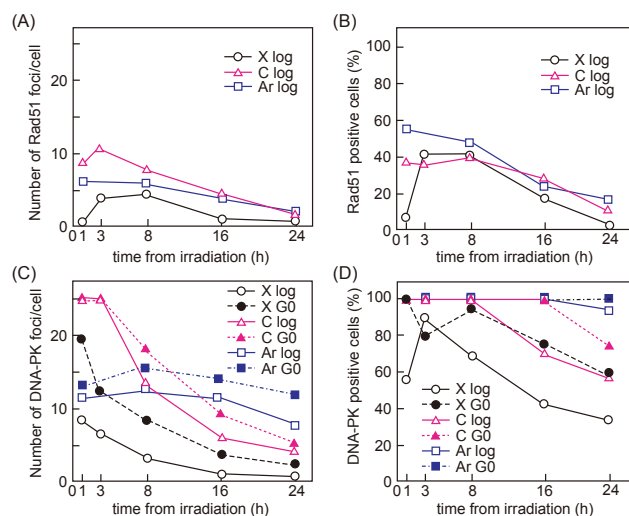
Fig. 1. Kinetics of the foci formation of Rad51 (A, B) and phosphorylated DNA-PKcs (C, D) in logarithmically growing NB1RGB cells (log) or synchronized cells at a quiescent state (G0). Cells were irradiated by 5 Gy of X-rays (circles), carbon-ions (triangles), and argon-ions (squares), and foci were detected by indirect immunofluorescent staining 1–24 h post irradiation.

of phosphorylated DNA-PKcs foci and the percentage of foci-positive cells decreased gradually as time proceeded after both X-ray and C-ion irradiation, whereas the number of phorphorylated DNA-PKcs foci persisted 24 h after Ar-ion irradiation in quiescent cells (Figs. 1C, D), suggesting that NHEJ does not efficiently repair DSBs after Ar-ion irradiation. We observed that 53BP1 and Rif1, which facilitate NHEJ, were co-localized with phosphorylated DNA-PKcs after the Ar-ion and X-ray irradiation (data not shown). Therefore, even though the components for the initial step of NHEJ were recruited to DSBs and DNA-PKcs was activated, NHEJ was impaired at a later step after Ar-ion irradiation.

References
1) L. S. Symington, J. Gautier, Annu. Rev. Genet. **45**, 247–271 (2011).
2) M. Izumi, T. Abe, RIKEN Accel. Prog. Rep. **47**, 253 (2014).
3) A. Takahashi et al., Radiat. Res. **182**, 338–344 (2014).
4) H. Ma et al., Radiat, Oncol. **10**, 225 (2015).
5) H. Yajima et al., DNA repair **12**, 936–946 (2012).
6) A. Gerelchuluun et al., Radiat. Res. **183**, 345–356 (2015).

*1 RIKEN Nishina Center

Low-dose high-LET heavy ion-induced bystander signaling (IV)

M. Tomita,[*1,*2] T. Tsukada,[*2] and M. Izumi[*2]

Radiation-induced bystander response (RIBR) is a cellular response induced in non-irradiated cells that received bystander signals from directly irradiated cells within an irradiated cell population.[1] RIBR induced by low doses of high-LET radiation is an important issue for the health of astronauts and in hadrontherapy. Here, we investigated the underlying molecular mechanisms and biological implications of RIBR induced by such low doses of high-LET radiation.

We found that normal human fibroblasts cultured confluent, which were harvested 16–24 h after exposure to high-LET (1000 keV/μm) iron (Fe) ions, showed the cell killing effect at low doses (≤ 0.2 Gy) higher than that estimated by a linear extrapolation from high doses. This enhanced cell killing effect could not be observed in the cells harvested immediately after irradiation.[2] At 0.1 Gy, the average number of Fe-ion traversals per cell nucleus was 0.11; however, the surviving fraction was 0.84.[3] These results suggested that the enhanced cell killing effect at low doses was at least partly caused by the induction of bystander responses. In addition, we established an optimal system to assess the low doses of high-LET radiation-induced bystander cell killing, and reported that gap-junction intercellular communication (GJIC), cyclooxygenase-2 (COX-2), and nitric oxide (NO) were involved in its signal transfer.[3]

In our previous study using high-LET heavy-ion microbeam and broadbeam,[4] we showed that DNA double-strand breaks (DSBs) and reproductive cell death were induced by NO-mediated bystander response in normal human fibroblasts. In addition, the activation of NF-κB, Akt, and COX-2 by bystander signaling depended on incubation time after irradiation and presence of NO. In this study, we investigated phosphorylation and accumulation of these bystander signaling related molecules in the cells irradiated with low doses of high-LET radiation.

Figure 1 shows phosphorylation and accumulation of bystander signaling related molecules in normal human fibroblasts, WI-38, irradiated with 0.1 Gy of 90 MeV/u Fe ions (1000 keV/μm). WI-38 cells were cultured on 25 cm^2 plastic flasks for 1 week to form confluent monolayers and were pretreated with or without a scavenger of NO, c-PTIO, (20 μM) 2 h before irradiation with 0.1 Gy of Fe ions. Cells were harvested 3 and 6 h after irradiation followed by immunoblotting. Phosphorylation of Akt at Ser473 and NF-κB p65 at Ser536 and accumulation of COX-2 were observed in

the cell 3 h after irradiation and were efficiently inhibited by pretreatment with c-PTIO. Phosphorylated histone H2AX at Ser139 is widely used as a surrogate marker of DSBs. Phosphorylated histone H2AX was observed at 3 and 6 h after irradiation. Prolonged phosphorylation of H2AX at 6 h after irradiation was inhibited by c-PTIO, although phosphorylation at 3 h was not suppressed. NO-mediated prolonged phosphorylation of H2AX also indicated the induction of bystander responses. These results suggest that NF-κB/COX-2/prostaglandin E2 and NF-κB/iNOS/NO pathways[1,5] are activated in the cells irradiated with low doses of high-LET radiation.
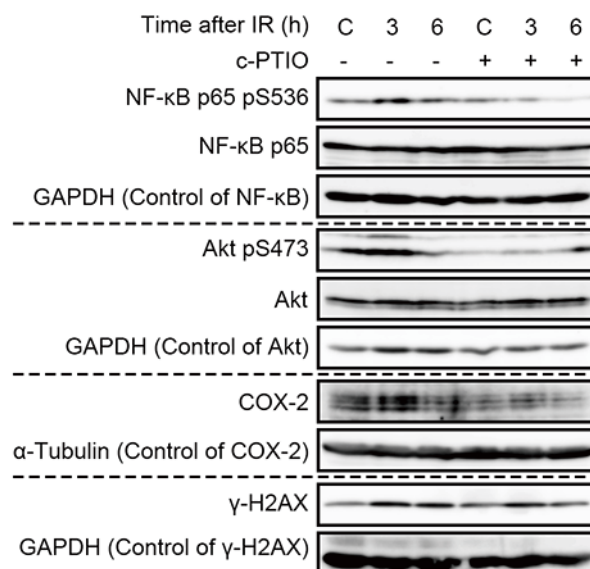
Fig. 1. Phosphorylation and accumulation of bystander signaling related molecules. Normal human fibroblasts, WI-38, were pretreated with or without c-PTIO (20 μM) 2 h before irradiation with 0.1 Gy of 90 MeV/u Fe ions (1000 keV/μm). Cells were harvested 3 and 6 h after irradiation followed by immunoblotting.

References
1) M. Tomita, M. Maeda, J. Radiat. Res. **56**, 205 (2015).
2) M. Tomita et al., RIKEN Accel. Prog. Rep. **48**, 302 (2015).
3) M. Tomita et al., RIKEN Accel. Prog. Rep. **50**, 266 (2017).
4) M. Tomita et al., Life Sci. Space Res. **6**, 36 (2015).
5) T. K. Hei et al., Curr. Mol. Pharmacol. **4**, 96 (2011).

[*1] Radiation Safety Research Center, Central Research Institute of Electric Power Industry
[*2] RIKEN Nishina Center

Results of whole-genome analysis of *mahogany* mutant

K. Tsuneizumi,[*1] H. Ichida,[*1] R. Morita,[*1] and T. Abe[*1]

Heavy-ion-beam mutagenesis is generally recognized as an effective method for mutation breeding.[1,2] Although this method was greatly successful with plants, its application is limited for animals. Therefore, we plan to acquire more basic data to set up optimal conditions for the heavy-ion-beam irradiation system by using *Drosophila melanogaster* (fruit fly) as the model.

In our previous study, we determined the suitable condition for the large-scale screening of mutant lines of heavy-ion-beam mutagenesis.[3] To elucidate the biological effect of heavy-ion-beam irradiation on the genome, we established several mutants that expressed typical phenotypes on eyes, wings, bodies, and bristles by a carbon-ion beam irradiation.

In this report, we show the analysis of data obtained from the whole-genome sequence of the *mahogany* (*mah*) mutant. The mutant eye color is darker than that of the wild type (Figs. 1a, b). This mutant line was established by the condition with 50 keV/μm linear energy transfer at 10 Gy dose level. Whole genome analysis revealed that the causal mutation of *mah* was a large deletion (Fig. 1c). An open reading frame of *mah* is 1,581 bp and a 387 bp deletion was observed in the first exon of a *mah* gene (Fig. 1c). An in-frame deletion produces a mutated Mahogany protein from which 129 amino acid residues were removed (Fig. 1c).

The role of the Mahogany protein (Mah) has an unknown function. InterPro is a freely available database
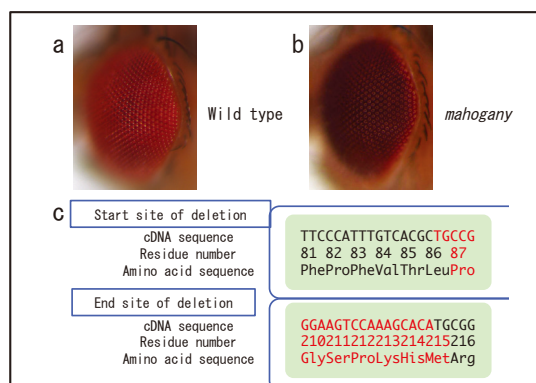
Fig. 1. Phenotype of the *mahogany* mutant and the result of whole-genome analysis.
  a) Wild type eye color is vivid red. b) The mutant eye color becomes darker than that of the wild type. c) The alignments of genome and protein sequences at start and end sites of the deletion. The top line indicates the cDNA sequence. The middle line indicates the numbers of amino acid residues. The bottom line indicates amino acid sequence. The red texts represent deleted regions.

*1 RIKEN Nishina Center
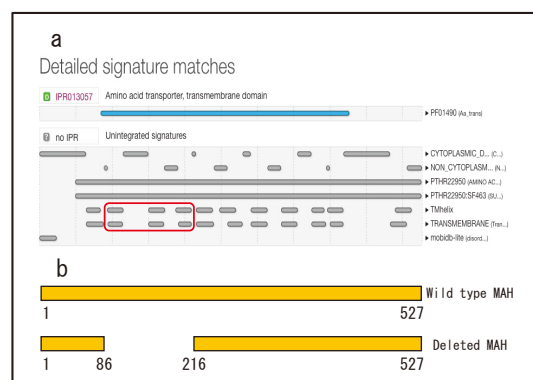
Fig. 2. Diagrams of protein domain analysis using InterPro and deleted Mahogany protein.
  a) A result data of domain analysis of Mahogany protein using InterPro database. The red box highlights the deleted three transmembrane domains. b) A diagram of wild type and deleted proteins of Mahogany. Full length Mahogany protein consist of 527 amino acid residues. The numbers indicate the numbers of amino acid residues of the proteins. The deleted protein lacks 129 amino acid residues (87–215).

used to classify protein sequences into families and to predict the presence of important domains and sites.[4] InterPro analysis of the predicted protein Mah identified 11 transmembrane helices and a conserved domain found in amino acid transporters (Fig. 2a). The deleted protein lacks three putative transmembrane domains (Figs. 2a, b). Both the amounts of ommochrome pigments and pteridine pigments are decreased in classical *mah* mutants.[5] These results indicate that Mah function is related to both pigments transport in eye ommatidia.

Chemical mutagen mostly introduces point mutations into genomic DNA. In this report, we confirmed that heavy-ion-beam mutagenesis has diverse mutations, for example small insertions, point mutations, small deletions, and large deletions, in the animal genome. Currently, we are analyzing other mutants. The data will be helpful for the elucidation of the biological effect of heavy-ion-beam irradiation to the animal genome.

References
1) T. Abe *et al.*, in *Plant Mutation Breeding and Biotechnology*, edited by Q. Y. Shu *et al.*, (CABI, Oxfordshire, 2012), pp. 99.
2) A. Tanaka *et al.*, J. Radiat. Res. **51**, 223 (2010).
3) K. Tsuneizumi *et al.*, RIKEN Accel. Prog. Rep. **49**, 253 (2016).
4) A. Mitchell *et al.*, Nucleic Acids Res. **43**, D213 (2015).
5) J. Ferre *et al.*, Biochem. Genet. **24**, 545 (1986).

Chromosomal rearrangement induced by high-LET heavy-ion-beam irradiation in *Parachlorella kessleri*

K. Ishii,[*1] M. Asano,[*2] Y. Kazama,[*1] T. Abe,[*1] and S. Kawano[*2]

Heavy-ion beams are used as an effective mutagen that induces localized mutations owing to their high linear energy transfer (LET).[1] Breeding with heavy-ion beams has been attempted often on land plants and recently on microalgae. *Parachlorella kessleri* (Chlorellales, Trebouxiophyceae, Chlorophyta) is a type of unicellular green algae that has received much attention as a biological resource for biomass production. A *P. kessleri* mutant with high oil production has been produced by heavy-ion-beam irradiation.[2] Recently, in a land plant *Arabidopsis thaliana*, it has been reported that an Ar ion beam (LET: 290 keV/μm) significantly induced chromosomal rearrangements more frequently than a C ion beam (LET: 30.0 keV/μm).[3] In this study, we produced *P. kessleri* mutants in which chromosomes were fragmented by Ar-ion-beam and Fe-ion-beam (LET: 640 keV/μm) irradiations. We performed mutation analysis on those mutants to characterize the nature of mutations induced by the high-LET heavy-ion beams.

P. kessleri was irradiated with the Ar-and Fe-ion beams with a dose of 75 Gy and cultured for 16–20 h in a TAP medium at 23°C under the continuous light condition. For microscopic observation, both irradiated and unirradiated cells were fixed by glutaraldehyde and stained by SYBR Green I. A typical karyotype of the wild type indicates that *P. kessleri* has seven chromosomes (Fig. 1A). On the other hand, chromosome fragmentation was observed in the irradiated cells (Fig. 1B–C). Irradiated cell lines were established by single colony isolation. Though some of these fragmented chromosomes were not inherited by descendant cells, the two established lines (Fe75-1-3H and Ar75-1-3H) were confirmed to stably possess fragmented chromosomes by pulsed field gel electrophoresis (data not shown).

The two established lines (Fe75-1-3H and Ar75-1-3H) and the wild-type line were resequenced by the MiSeq sequencing system (Illumina Inc., https://www.illumina.com). Mutation analysis was conducted by the mutation analysis pipeline AMAP as described previously[4] with some modifications: we modified AMAP to utilize the draft genome sequence (consisting of 400 scaffolds and 60 Mb in total) and the gene structure information (in the GTF format) of *P. kessleri*. As rearrangements defined previously[3] as including indels more than 100 bp and chromosomal rearrangements, one inversion was detected in Ar75-1-2C. In Fe75-1-3H, two inversions and three translocations were detected. All of the three translocations were localized in a region of approximately 2 kb of the genome, which

Fig. 1. Karyotypes of *P. kessleri*. (A) Typical karyotype of the wild type. (B–C) Typical karyotypes of cells after irradiation with Ar- (B) and Fe-ion beams (C), indicating that chromosomes were fragmented into 17 and 39 parts, respectively.
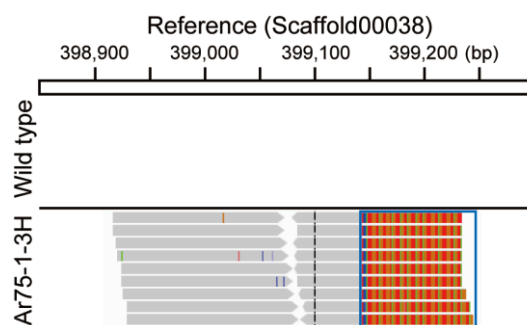
Fig. 2. Mapped read sequences including only telomeric repeats. The gray bars indicate read sequences. The colored lines on read sequences indicate single nucleotide polymorphisms. The blue box indicates telomeric repeats.

may reflect the dense ionization produced by the high-LET heavy-ion beam. To detect chromosome rearrangements involving chromosome ends, reads that only include continuous (more than three units) telomeric repeat (TTTAGGG) were extracted from the resequenced data and mapped to the draft genome sequence by Burrows-Wheeler Aligner. One newly formed junction with telomeric repeats in Ar75-1-2C was found (Fig. 2). This junction possibly explains the stability of some of the fragmented chromosomes. Alternatively, it was possibly the junction with internal telomere sequences. Fluorescence *in situ* hybridization that utilizes the genomic sequence near the junction as a probe will provide information based on which a hypothesis would be plausible.

In this study, it was revealed that the Ar and Fe ion beams induced chromosome fragmentations in *P. kessleri*. Mutation analysis suggested that the fragmentations were caused by localized DNA double-strand breaks and that chromosome ends of stable fragmented chromosomes possessed telomeric repeats. The complete genome sequence will provide clearer information on the nature of mutations induced by the high-LET heavy-ion beam.

References
1) T. Hirano *et al.*, Mutat. Res. **735**, 19 (2012).
2) S. Ota *et al.*, Bioresour. Technol. **149**, 432 (2013).
3) Y. Kazama *et al.*, Plant J. **92**, 1020 (2017).
4) K. Ishii *et al.*, Genes Genet. Syst. **91**, 229 (2016).

*1 RIKEN Nishina Center
*2 Future Center Initiative, The University of Tokyo

Trials of mutation detection programs to detect structural variations induced by heavy-ion beams in rice

R. Morita,[*1] H. Ichida,[*1] Y. Shirakawa,[*1] and T. Abe[*1]

We screened rice mutants generated by heavy-ion-beam irradiation and identified mutations using whole-genome sequencing (WGS). A heavy-ion beam induces both small mutations (single-nucleotide variants and small insertions/deletions) and structural variations (SVs) such as large deletions, inversions, and translocations.[1] The detection of SVs using short-read WGS data is a challenging task compared with the detection of small mutations.[2] We used the Pindel[3] software to detect SVs. Pindel can detect break points of large deletions (< 10 kb) and small-size insertions (1–20 bp).[3] However, the heavy-ion beam can generate deletions with lengths of over 10 kb.[1] Therefore, besides Pindel, another program is needed to detect the SVs induced by the heavy-ion-beam irradiation.

In the present study, we tested two programs, Delly[4] and Manta,[5] for detecting the SVs induced by heavy-ion irradiation. We used a high-performance bioinformatics pipeline[6] incorporated with Delly and Manta. The candidate mutations were visually confirmed by using Integrated Genomics Viewer (IGV). We analyzed WGS data of 11 rice mutants induced by carbon ion irradiations ($^{12}C^{6+}$, 50–175 Gy, LET: 30 keVμm^{-1}). In the present study, we ignored the candidates of heterozygous mutations detected by Delly and Manta because all heterozygous mutations were false-positives in our initial experiment (Data not shown).

In the 11 mutants, there were 10 and 19 homozygous candidates detected by Delly and Manta, respectively. Of the 10 and 19 candidates detected by Delly and Manta, 8 and 9 were positive mutations, respectively. These data suggest that both programs detected positive mutations induced by carbon ions. Of the 8 and 9 positive mutations detected by Delly and Manta, 4 and 2 were also detected by Pindel. In other words, both 4 mutations detected by Delly and 7 mutations detected by Manta were not detected by Pindel. In total, 8 independent mutations that were not detected by Pindel were identified (Table 1), *i.e.* one mutation (No. 1) was detected by Delly only, 4 mutations (No. 2, 5, 7, and 8) were detected by Manta only, and 3 mutations (No. 3, 4, and 6) were detected by both programs. Using IGV, we determined the types of each mutation. One mutation (No. 1) was determined to be a deletion (Table 1). The remaining mutations (No. 2, 3, 4, 5, 6, 7, and 8) were estimated to be translocations (Table 1). We tried to design primer pairs around the breakpoints of each mutation to confirm the existence of mutation by PCR analysis. Around the mutation

*1 RIKEN Nishina Center
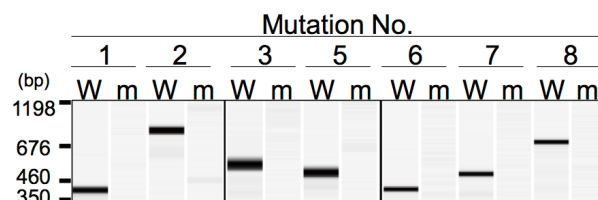
Fig. 1. PCR confirmation of 7 mutations. W indicates the result of using wild-type DNA as the template, and m indicates the result of using mutant DNA as the template. The PCR pruducts are analyzed using MultiNA MCE-202 (Shimadzu). DNA size markers are shown on the left side.

Table 1. Structural variations detected by Delly and Manta.

No.	Program	Types of mutation	Position of structural variation breakpoints
1	Delly	deletion	chr06: 19711627 ~ chr06: 20041214
2	Manta	translocation	chr10: 4549172 ~ ND
3	Both	translocation	chr01: 4662084 ~ chr08: 25179978
4	Both	translocation	chr08: 25179965 ~ chr01: 5523529
5	Manta	translocation	chr01: 5523529 ~ chr08: 25179965
6	Both	translocation	chr03: 964315 ~ chr02: 627397
7	Manta	translocation	chr02: 627397 ~ chr03: 964315
8	Manta	translocation	chr03: 5844008 ~ ND

ND, not determined by

No. 4, a primer pair specific to the wild-type allele could not be designed. When we performed PCR with the 7 primer pairs using wild-type genomic DNA as a template, each band was detected (Fig. 1, lane W). However, no band was

detected when we used mutant genomic DNA as a template (Fig. 1, lane m), indicating that the wild-type alleles do not exist in these mutants. Our present study indicated that both Delly and Manta are useful programs to detect SVs in rice mutants induced by heavy-ion irradiation.

References
1) T. Hirano *et al.*, Plant J. **82**, 93 (2015).
2) K. Ye *et al.*, Next Generat. Sequenc. & Applic. **S1**, 007 (2016).
3) K. Ye *et al.*, Bioinformatics **25**, 2865 (2009).
4) T. Rausch *et al.*, Bioinformatics **28**, 1333 (2012).
5) X. Chen *et al.*, Bioinformatics **32**, 1220 (2016).
6) H. Ichida *et al.*, RIKEN Accel. Prog. Rep. **49**, 254 (2016).

Comparison of LET effect of heavy-ion beam irradiation in rice

Y. Hayashi,[*1] K. Ichinose,[*1] Y. Shirakawa,[*1] S. Ohbu,[*1] H. Tokairin,[*1] T. Sato,[*1,*2] and T. Abe[*1]

Linear energy transfer (LET) is a contributing factor in heavy-ion mutagenesis. Our previous study revealed a LET-dependent effect in *Arabidopsis thaliana*. A LET of 30 keV/μm is the most effective for inducing mutation.[1] Although a high LET of heavier ions such as Ar and Fe resulted in a lower mutation frequency, they can easily cause larger deletions and complex mutations.[2–5] In 2015, a new high-energy beam line called the WACAME line was constructed, which enables the irradiation of heavier ions with a longer range.[6] The choice of LET values for biological samples was extended by using this beam line. Knowledge about the LET effect in model plants can be applied for other plants and is useful for efficient mutagenesis. In this study, we examined the effect of a higher LET of heavy-ion beam irradiation in rice as another model plant.

Dry seeds of rice (*Oryza sativa* L. cv. Nipponbare) with a water content of 13% were used for the experiment. The seeds were placed into a plastic bag without overlapping and vacuum-packed for irradiation treatment. The seeds were irradiated with Ar (184 keV/μm, 289 keV/μm) and Fe (650 keV/μm). Ar (184 keV/μm) is a high-energy beam produced using the WACAME line. The doses of Ar ions and Fe ion were 10 to 50 Gy, 7.5 to 40 Gy, and 10 to 50 Gy, respectively. Survival rates were estimated by counting plants surviving four weeks after sowing. Figure 1 shows the survival curve after irradiation. A decrease of survival rate was observed for a dose greater than 20 Gy with Ar (289 keV/μm) irradiation. On the other hand, a decrease of survival rate was observed for a dose greater than 30 Gy with Ar (184 keV/μm) and Fe (650 keV/μm) irradiation. M_1 plants from the irradiation with a high survival rate were grown in a paddy field. M_2 seeds were obtained individually from each M_1 plant. The fertility was evaluated using the number of fertile spikelets in the main panicle of the M_1 plant. Figure 2 shows the percentage of fertility in M_1 plants. The mean value of the number of fertile spikelets per panicle in control Nipponbare was 105.7 ± 16.24. The percentage of low-fertility plants increased with the increase of dose at any LET value.

Chlorophyll-deficient mutants (CDM) were observed in two-weeks-old M_2 seedlings grown in a greenhouse. Mutation rates were calculated based on the numbers of M_1 lines, which showed CDM in M_2 generation. The highest frequency of CDM was observed at 20–30 Gy of Ar (184 keV/μm) irradiation (Table 1). Furthermore, there was no severe decrease of fertility at a dose of 20 Gy. This result suggests the possibility of high efficiency of the Ar-ion beam produced using the WACAME line. We will conduct the genome sequencing of isolated mutants to characterize the mutations irradiated at 184,
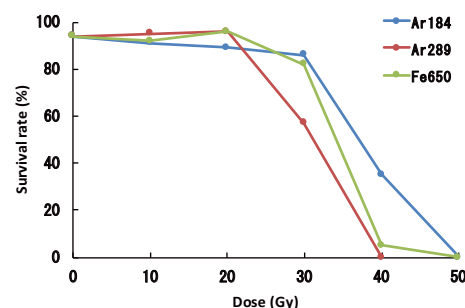
Fig. 1. Effect of LET on survival rate in rice.
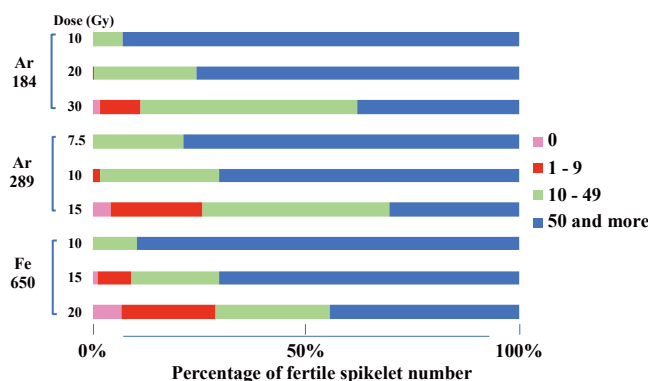
Fig. 2. Comparison of the number of fertile spikelets per panicle.

Table 1. Effect of High-LET ion-beam irradiation on mutation induction.

Ion	LET (keV/μm)	Dose (Gy)	Mutation rate (%)	Albino	Pale green	Stripe	Yellow	Others
					Number of CDM			
Ar	184	10	10.28	16	7	1	0	5
		20	11.63	12	10	5	0	3
		30	11.98	16	4	4	0	5
Ar	289	7.5	6.28	8	5	1	0	1
		10	8.37	9	5	2	0	4
		15	9.28	11	7	2	0	2
Fe	650	10	4.18	3	3	2	0	2
		15	4.66	6	1	0	1	3
		20	10.17	11	8	3	1	1

289, and 650 keV/μm and compare the mutagenic effects of higher-LET irradiation in rice.

References
1) Y. Kazama *et al.*, Plant Biotech. **25**, 113 (2008).
2) T. Hirano *et al.*, Mutat. Res. **735**, 19 (2012).
3) Y. Kazama *et al.*, Genes Genet. Syst. **88**, 189 (2013).
4) T. Hirano *et al.*, Plant J. **82**, 93 (2015).
5) Y. Kazama *et al.*, Plant J. **92**, 1020 (2017).
6) N. Fukunishi *et al.*, Proc. 13th Int. Conf. on Heavy Ion Accel. Tech. (2015), p. 42.

*1　RIKEN Nishina Center
*2　Graduate School of Agricultural Science, Tohoku University

Relationship between early-flowering mutation and LET-Gy combination of ion beam irradiation in durum wheat

K. Murai,[*1] Y. Kazama,[*2] and T. Abe[*2]

Durum wheat (*Triticum turgidum* ssp. *durum*) is a tetraploid species with the genome constitution AABB derived from two wild diploid ancestral species: the A genome from *T. urartu* and the B genome from *Aegilops speltoides* or another species classified in the Sitopsis section. Therefore, the tetraploid durum wheat genome contains duplicated homoeologous genes, and this characteristic may increase the difficulty of screening for mutants in durum wheat. To avoid this problem, we have chosen the use of cultivated diploid einkorn wheat (*T. monococcum*) with the A^m genome, similar to the A genome in bread wheat, for developing a large-scale mutant panel.[1] and screened and analyzed several mutants from the mutant panel.[2] However, durum wheat is an important crop species for making pasta, and we have started to make a mutant panel of durum wheat by heavy-ion beam irradiation.

To avoid the rainy season for harvesting, early maturing is one of the important properties of bread wheat in East Asia, including Japan. Therefore, we focused on identifying early-flowering mutations in the screening of the mutant panel.

Dry seeds of the durum wheat cultivar "Langdon" were irradiated with 15, 30, or 50 Gy of $^{12}C^{6+}$ ions at LET values of 30, 50, or 70 keV μm^{-1}, or 2.5, 5.0, 7.5, 10, or 20 Gy of $^{40}Ar^{17+}$ ions (290 keV μm^{-1}) to determine the optimal conditions for mutant generation by using the E5 beam line of the Ring Cyclotron (RRC) in the RIKEN RI-beam factory. The M_1 seedlings were planted in the field in October 2014. The viability rate for the Ar ion beam was reduced to less than 60% with a dose greater than 7.5 Gy, and all plants died when the dose was 10 or 20 Gy. The harvested seeds from each individual M_1 plant were used to produce the next generation (M_2) lines. 77–134 M_2 lines (1068 lines in total) for each LET-Gy combination were sown in October 2015 in the fields; ten seeds of each M_2 line were sown. The frequency of lines with albino plant(s) among the ten plants was determined to assess the comparative mutation ratio of the different irradiation conditions. The frequency of albino plants in the M_2 generation was different for different LET-Gy combinations (data not shown). The highest ratio (>2.0%) was observed for the LET50-30Gy treatment condition. On the other hand, the data of survival ratio
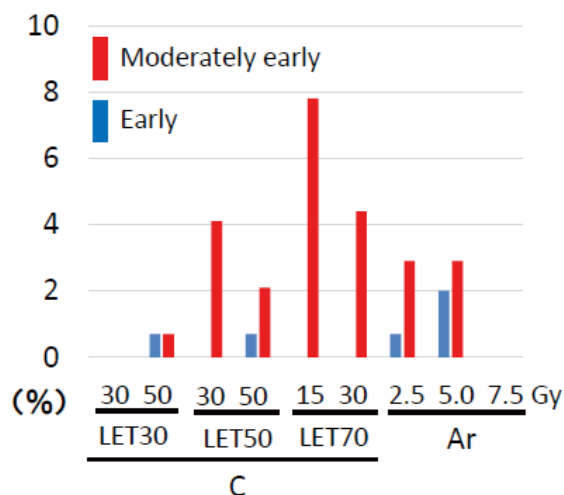
Fig. 1. Appearance of early-flowering mutant plants in M_2 generation. Percentages (%) of M_2 lines segregating mutant plants are shown in each LET-Gy combination of ion-beam irradiation. Red and blue bars indicate moderately early-flowering and early-flowering mutants, respectively.

suggests that LET70-15Gy treatment was the optimal condition for durum wheat.[3]

In the mutant screening in 2016, we observed moderately early-flowering mutation within a few days and early-flowering mutation before four days, compared with the wild-type. Figure 1 shows the percentages of the M_2 lines segregating early-flowering mutant(s). The moderately early-flowering mutants were obtained under relatively moderate treatment condition of LET70-15Gy with C, whereas early-flowering mutants were mainly obtained under harsher treatment condition of 5.0 Gy with Ar.

Durum wheat cultivars are usually late-heading and not suitable for cultivation in Japan, because we have a rainy season from June to July. All known cultivars of durum wheat show pre-harvest sprouting when subjected to prolonged rainfall before harvest. Furthermore, durum wheat cultivars are susceptible to the Fusarium head blight disease. To develop durum wheat cultivars suitable for wide cultivation in Japan, we are focusing on identifying mutations of early-heading, short culm, and resistance against pre-harvest sprouting and Fusarium head blight in durum wheat by using heavy-ion beam mutagenesis.

References
1) K. Murai *et al.*, Nucl. Instrum. Methods Phys. Res. B **314**, 59 (2013).
2) A. Nishiura *et al.*, Breed. Sci. **64**, 213 (2014).
3) K. Murai *et al.*, RIKEN Accel. Prog. Rep. **50** (2017).

Analysis of DNA damage response in *Cyrtanthus* pollen after Ar-ion beam irradiation

T. Hirano,[*1,*2] A. Hanada,[*1] Y. Hayashi,[*2] T. Abe,[*2] and H. Kunitake[*1]

Heavy-ion-beam mutagenesis has been applied for various plant materials, and many mutants have successfully been obtained through the screening process. As one of the plant materials for the irradiation, pollen was used for mutant induction.[1,2] This implies that the DNA damage induced by a heavy-ion beam would be repaired during the double-fertilization process, and the genomic information including mutations would be transmitted to the next generation. DNA damage response (DDR) in male gametes of *Cyrtanthus mackenii* after C-ion beam (22.5 keV/μm) irradiation has been reported, and the male gametes repaired the DNA lesions during the pollen tube growth.[3] In the present study, we irradiated mature pollen of *C. mackenii* with an Ar-ion beam, which has a higher linear energy transfer (LET) than the C-ion beam, and analyzed the DDR in the male gametes. Moreover, we compared the DDR after irradiation with Ar-ion and C-ion beams.

Anthers of *C. mackenii* in 0.2-mL tubes were irradiated with Ar ions (280 keV/μm) at a dose of 2.5–40 Gy and then stored at $-20°$C. Pollen grains from the anthers were cultured in 2 mL of liquid pollen culture medium at 25°C in the dark.[4] Sperm cell formation in the pollen tube was observed after 4′,6-diamidino-2-phenylindole staining of the pollen tube. Immunocytochemical analysis for the evaluation of DDR in male gametes was performed according to a protocol described previously.[3]

When the germination rate of the pollen grains and pollen tube length were measured after 24 h of *in vitro* culture, the germination rate and pollen tube length in irradiated pollen showed no decrease compared to non-irradiated pollen. These results were similar to those for C-ion irradiation.[3] Since *C. mackenii* forms bicellular pollen, sperm cells are divided from a generative cell in the pollen tube. Although the sperm cell formation rate was not decreased up to 10-Gy irradiation, sperm-cell formation was inhibited by high-dose irradiation of 20 and 40 Gy (Fig. 1). In the C-ion-beam irradiation, the sperm-cell formation rates were decreased to approximately 70% at 40 Gy and 30% at 80 Gy.[3] Thus, it is interpreted that the Ar-ion beam has a greater effect of inhibition of sperm-cell formation compared to the C-ion beam.

To investigate the cause of inhibition of sperm-cell formation, male gametes were isolated from pollen tubes and immunostained by using anti-α-tubulin antibody for cell-cycle confirmation and by using anti-
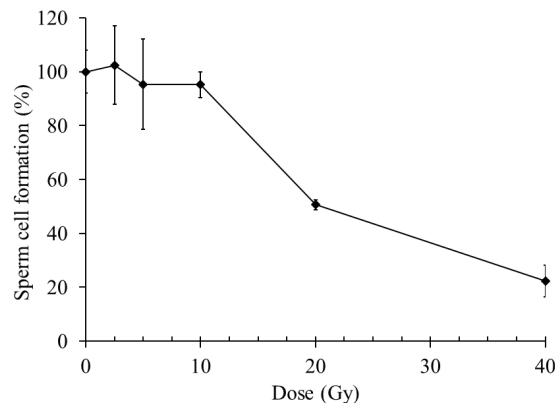
Fig. 1. Sperm cell formation after Ar-ion beam irradiation. Values ± SD are expressed relative to the unirradiated control (value set at 100%).

phosphorylated histone H2AX (γH2AX) for the detection of DNA double-strand breaks (DSBs) in the chromosome. After 40-Gy irradiation, the cell cycle in a part of the generative cells was arrested at the metaphase in pollen mitosis II (PMII) at 24 h of culture. In the male gametes, proportions of metaphase cells were 0% at 0 Gy, 1% at 10 Gy, and 35% at 40 Gy, suggesting that cell-cycle arrest was induced by the high-dose irradiation. The proportions of metaphase cells at 24 h of culture after the C-ion-beam irradiation were approximately 8% at 10 Gy and 11% at 40 Gy.[3] These results indicated that one of the causes of the inhibition of sperm-cell formation is the cell cycle arrest. Approximately half of the metaphase cells with 40-Gy Ar-ion irradiation showed γH2AX foci in the chromosomes, indicating that unrepaired DSBs remained in the genome. Therefore, a spindle assembly checkpoint in the metaphase would be activated by chromosomal lesions including the DSBs and arrested in the cell cycle progression.

In the C-ion-beam irradiation, chromosomal bridges were formed between the sperm cells, and generative-cell-like sperm cells, which are defined as cells with generative-cell-like nuclei and sperm-cell-like microtubule arrays that completed PMII but failed in chromosome separation, were also formed.[3] We also analyzed the male gametes that completed PMII in the Ar-ion-beam irradiation, and those data will be useful for understanding the effects of heavy-ion-beam irradiation on male gametes.

References
1) K. Naito *et al.*, Genet. **169**, 881 (2005).
2) Y. Kazama *et al.*, Sci. Rep. **6**, 18917 (2016).
3) T. Hirano *et al.*, AoB Plants **5**, plt004 (2011).
4) T. Hirano, Y. Hoshino, J. Plant Res. **122**, 225 (2009).

[*1] Faculty of Agriculture, University of Miyazaki
[*2] RIKEN Nishina Center

Isolation of C$_4$ *Flaveria bidentis* mutants with reduced quenching of chlorophyll fluorescence from heavy-ion-beam-mutagenized M$_2$ population

T. Ogawa,[*1] M. Yamane,[*1] Y. Taniguchi,[*1] T. Furumoto,[*2] T. Abe,[*3] and Y. N. Munekage[*1]

Plants using C$_4$ photosynthesis exhibit higher CO$_2$ assimilation rates than plants using C$_3$ photosynthesis under low CO$_2$ conditions. This C$_4$ photosynthesis (except for single-cell C$_4$ photosynthesis) is usually achieved by the operation of the C$_4$ metabolic cycle between mesophyll (M) and bundle-sheath (BS) cells, which concentrates CO$_2$ at the site of ribulose 1,5-bisphosphate carboxylase/oxygenase (RuBisCO) in BS cells.[1] With an aim to analyze the regulation of light-energy conversion and metabolic cycle between two cells, we screened mutants with a reduced quenching of chlorophyll fluorescence from a heavy-ion-beam-mutagenized M$_2$ population of C$_4$ *Flaveria bidentis* (*Asteraceae*) which carries NADP-malic enzyme-type C$_4$ photosynthesis.

We first investigated the survival ratio of mutagenized seedlings to evaluate the optimum condition for mutagenesis by the irradiation of a carbon-ion beam. *F. bidentis* seeds were irradiated at different dose levels ranging from 25 to 300 Gy with a linear energy transfer (LET) value of 30 keV/μm (Table 1). The Number of seedlings forming true leaves/total number of seedlings (true leaf formation ratio), average true leaf length in 13-days-old seedlings, and survival ratio 1 month after germination decreased with the increase of dose level. Although the true leaf formation ratio was only slightly affected at 50 Gy, the survival ratio was lower at 50 Gy than at 25 Gy. Therefore, we determined 25 Gy as an optical condition for mutagenesis. A large number of seeds were mutagenized with a 25 Gy carbon-ion beam (M$_1$) and grown in a green house, and the next population of seeds (M$_2$) was corrected for screening.

Table 1. Survival ratio in *F. bidentis* M$_1$ population at different dose levels. Average $\pm$SD is shown for the true leaf length. $*P < 0.01$.

Dose level, Gy	True leaf formation ratio, % (n=50-70)	True leaf length, mm (n=25)	Survival ratio, % (n=50-70)
Non-irradiation	100	3.4 ± 2.2	100
25	97	2.4 ± 1.8 *	94
50	97	3.4 ± 1.8	83
100	59	1.4 ± 3.1 *	10
150	62	1.3 ± 2.0 *	4
200	58	1.4 ± 2.2 *	0
300	3.9	0.3 ± 0.8 *	0

We used a chlorophyll fluorescence imaging system, Maxi-Imaging-PAM (Walz, Germany), for screening mutants. Chlorophyll fluorescence emitted from photosystem II reflects the photosynthetic electron transport
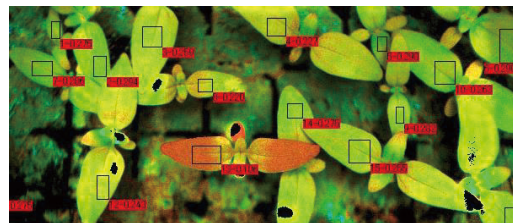
Fig. 1. Chlorophyll fluorescence imaging after exposure to blue light of 500 μmol photons m^{-2} s^{-1} for 1 min. Orange shows lower NPQ levels than green.
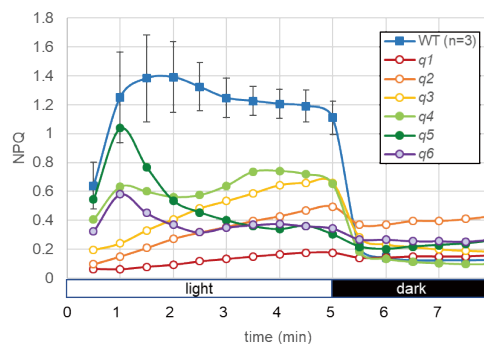
Fig. 2. Time courses of NPQ induction in white-light illumination at 270 μmol photons m^{-2} s^{-1} and relaxation of NPQ in 3 min in dark.

state and light energy dissipation induced by the luminal acidification of the thylakoid membrane, which is monitored as nonphotochemical quenching (NPQ) of chlorophyll fluorescence.[2] In the imaging system, the majority of detected chlorophyll fluorescence was assumed to be derived from chloroplasts in palisade M cells and a minority was assumed to be derived from BS chloroplast because BS cells surround the vasculature immediately beneath the palisade cells within leaves and contain chloroplasts with reduced grana and PSII activity.

Six mutants named *q1*~*q6* with reduced NPQ were isolated from a population of 860 M$_2$ plants, which were obtained from 180 M$_1$ parents (Figs. 1 and 2). *q1*~*q3* or *q4* and *q5* can possess identical mutation because those were derived from the same parental batch, but at least 3 independent mutants were isolated from this screening system. *q1* and *q4* showed lower CO$_2$ assimilation rates than the wild type (data not shown). Since coordinated metabolism in M and BS cells is required for C$_4$ photosynthesis, mutants isolated with this screening method are expected to include defects in not only genes directly related to NPQ induction but also genes related to the regulation of C$_4$ photosynthesis.

References
1) M. D. Hatch, Biochim. Biophys. Acta **895**, 81 (1987).
2) T. Shikanai *et al.*, Plant Cell Physiol. **40**, 1134 (1999).

[*1] School of Science and Technology, Kwansei Gakuin University
[*2] Faculty of Agriculture, Ryukoku University
[*3] RIKEN Nishina Center

Development of flower color mutations from the light-yellow mutant of spray-mum 'Southern Chelsea' by heavy-ion beam re-irradiation

M. Tamari,[*1] G. Watanabe,[*1] F. Tojima,[*1] Y. Hayashi,[*2] and T. Abe[*2]

Heavy ion beam irradiation induces plant mutation effectively, and is used for plant breeding.[1] In Kagoshima prefecture, we induced flower color mutation on a pink-colored spray-mum cultivar 'Southern Chelsea' (Registration number: 17847), using heavy ion beam or soft X-ray irradiation. As a result, a yellow flower 'Southern Chelsea Yellow' (Registration number: 26523) was developed from the pink-colored flower color. However, pure white mutants have not been obtained from previous mutagenesis experiments. We also reported that stem segments are more suitable for producing 'Southern Chelsea' mutants using Ar-ion beam irradiation.[2] In this report, we describe the flower color variation that appeared due to the re-irradiation of heavy ion beam on the in-vitro cultured stem of the light-yellow mutant (B25CL-16) obtained from 'Southern Chelsea.'

Cultured stem segments of 'B25CL-16' with an axillary bud were irradiated with Ar-ion beam (LET: 280 keV/ μm) or C-ion beam (LET: 23 keV/μm) at doses from 0.5 to 3 Gy, and each treatment was carried out with 40 stems. After irradiation, the stems of each treatment were cultured using in vitro propagation. One month later, the elongated shoots of these tissues were subcultured with the axillary bud sections to separate the chimeric mutant sectors, and this was repeated twice. The plantlets grown from subcultured nodes were transferred to a greenhouse to investigate the flower color mutation in August flowering cultivation.

The numbers of flower-color mutants obtained by Ar-ion or C-ion beam irradiation were 89 out of 316 and 26 out of 275, respectively (Table 1, Fig. 1). In the mutation induction of 'B25CL-16,' the mutants in which the yellowish-white of flower petal were observed also included the non-irradiated group. In the cultivated chrysanthemum, the yellow pigment of the flower petal is almost carotenoid, and the white flower color is known to be obtained by the expression of the gene encoding carotenoid cleavage dioxygenase 4a (CmCCD4a).[3] The yellow color mutants were thought to be decreased expression of CmCCD4a. The mutants of yellowish-white colors needs to be investigated with regard to the petal pigment in order to clarify the relationship between the gene and secondary metabolite.

The present study was supported by the Council for Science, Technology and Innovation (CSTI), Cross-ministerial Strategic Innovation Promotion Program

Table 1. Flower-color mutation induced by heavy-ion beam irradiation.

Variation source			Number of plants [1]	Number of Flower-color mutants			Number of mutants	Mutation rate(%)
Line class	LET (KeV/ μm)	Dose (Gy)		Yellowish -white	Yellow	Yellowish- white streak		
Ar	280	0.5	95	1		13	14	14.7
		1	94	14	1	5	20	21.3
		2	89	15	19	4	38	42.7
		3	38	17			17	44.7
		Total	316	47	20	22	89	28.2
		0	36	3			3	8.3
C	23	1	96	2		12	14	14.6
		2	95			4	4	4.2
		3	84	5		3	8	9.5
		Total	275	7		19	26	9.5
		0	36	1		3	4	11.1

1)Regenerated and flowered plants after irradiation
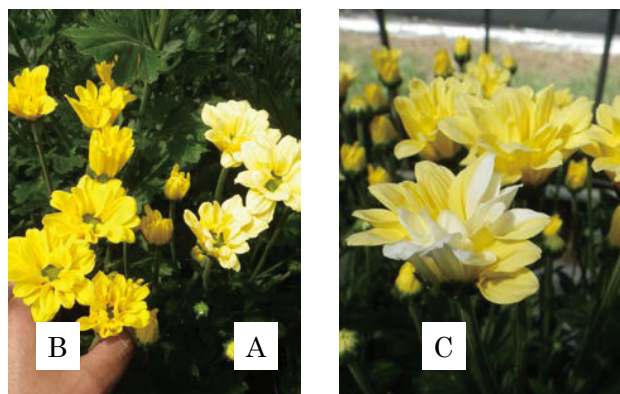
Fig. 1. 'B25CL-16'(A) and flower color mutation B: Yellow C: Yellowish-white steak.

References
1) T. Abe *et al.*, Breed. Res. **16**, 67 (2014).
2) M. Tamari *et al.*, RIKEN Accel. Prog. Rep. **50**, 274 (2017).
3) A. Ohmiya, Agriculture and Horticulture, **82**, 11, 1153–1160 (2007).

[*1] Kagoshima Prefectural Institute for Agricultural Development
[*2] RIKEN Nishina Center

Effects of heavy-ion-beam irradiation on survival in Eisenia arborea

H. Yamada,[*1] Y. Hayashi,[*2] and T. Abe[*2]

Along the coast of Hainan on the west coast of Suruga Bay in Shizuoka prefecture, there once existed a kelp forest of species such as *Eisenia arborea* (Fig. 1). This kelp forest was a good fishing ground for shellfish such as abalone. In addition, *E. arborea* was caught as edible seaweed. However, the kelp forest disappeared, along with shellfish, and fishery suffered serious economic damage. Although measures to restore the kelp forest have been taken subsequently, *E. arborea* has not recovered. Therefore, we investigated survival in *E. arborea* after irradiation with a heavy-ion beam and examined the optimum dose for creating useful properties in *E. arborea* such as high growth and to contribute to the recovery of the kelp forest.

Gametophytes of *E. arborea* were irradiated with an Ar-ion beam (184 keVμm) at a dose range of 0.625–20 Gy and with a C-ion beam (23 keVμm) at a dose range of 5–100 Gy. After the irradiation, batches of 48 female and 48 male gametophytes (approximately 100 μm in length) were incubated at 20°C with 12-h photoperiods and a light intensity of 30 μmol m^{-2} s^{-1}. After 3 weeks of culture, they were measured with a microscope, and gametophytes not growing were deemed to have died. Furthermore, to confirm the survival again, gametophytes visually confirmed to be alive after 8–9 months of culture were regarded as surviving individuals, and the survival rates were obtained.

Sporophytes of *E. arborea* (approximately 3 mm in length) were irradiated with an Ar-ion beam at a dose range of 1.25–10 Gy and with a C-ion beam at a dose range of 10–100 Gy. After the irradiation, batches of 50 sporophytes were incubated at 20°C with 12-h photoperiods and a light intensity of 80 μmol m^{-2} s^{-1}. The survival rates were measured after 4 weeks of culture.

The survival rates after 3 weeks of gametophytes irradiated with the Ar-ion beam showed a tendency to decrease beyond a dose of 10 Gy in both male and female samples (Fig. 2). The survival rates after 3 weeks of gametophytes irradiated with the C-ion beam decreased from 80 Gy in male samples and 100 Gy in female samples (Fig. 3). The survival rates after 8–9 months of culture decreased and abruptly decreased for Ar-ion-beam irradiation at 10 Gy and C-ion-beam irradiation at 80 Gy, respectively (Table 1), which almost agreed with the results after 3 weeks of culture. The survival rates of the sporophytes sharply decreased for Ar-ion-beam irradiation at 7.5 Gy and C-ion-beam irradiation at 20 Gy, respectively (Fig. 2, 3). Susceptibility to heavy-ion beams was higher in sporophytes than in gametophytes.

Based on the above results, the optimum doses were

Fig. 1. *Eisenia arborea*.
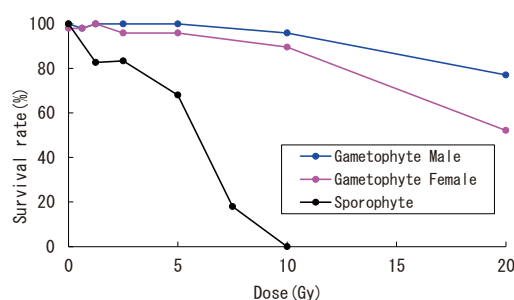
Fig. 2. Survival rates of male and female gametophytes and sporophytes 3 and 4 weeks after irradiation with an Ar-ion beam, respectively.
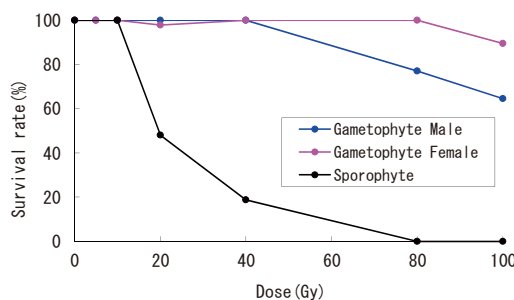
Fig. 3. Survival rates of male and female gametophytes and sporophytes 3 and 4 weeks after irradiation with a C-ion beam, respectively.

Table 1. Survival rates of male and female gametophytes 8–9 months after irradiation with Ar and C-ion beams.

	Ar		C	
	control	10Gy	control	80Gy
Male	100%	71%	100%	17%
Female	50%	29%	94%	8%

estimated as 2.5 and 5 Gy for gametophytes and sporophytes irradiated with an Ar-ion beam, respectively; 20 and 40 Gy for gametophytes irradiated with a C-ion beam; and 10 and 20 Gy for sporophytes irradiated with C-ion beam. In the future, we will perform mutant screening of the sporophytes in the M$_2$ generations.

[*1] Shizuoka Prefectural Research Institute of Fishery
[*2] RIKEN Nishina Center

Aargon-ion-beam mutagenesis of the plant-symbiotic edible mushroom *Tricholoma matsutake*[†]

H. Murata,[*1] T. Abe,[*2] H. Ichida,[*2] Y. Hayashi,[*2] T. Yamanaka,[*1] T. Shimokawa,[*1] and K. Tahara[*1]

Tricholoma matsutake is a filamentous fungus that produces prized mushrooms "matsutake" in association with conifers.[1,2] Currently, no cultivars allow the fungus to fruit artificially, unlike commercially available edible mushrooms. Developing cultivars that are suitable for spawn cultivation will greatly contribute to the artificial cultivation of the plant-symbiotic mushrooms. We hypothesized that irradiation breeding could help produce *T. matsutake* cultivars for fruiting during spawn cultivation. In the present study, as a prerequisite for generating *T. matsutake* mutants, we analyzed the lethality of an argon-ion beam ($^{40}Ar^{17+}$, 95 MeV/u) and generated mutants; this nuclide was used because it has an LET of 280 keV/μm with a theoretical penetrating range in water of 8 mm, which should be sufficient to penetrate the fungal mycelial colony on an agar plate.

An argon-ion beam (0–300 Gy) was irradiated on *T. matsutake* mycelia on agar plates, after which hyphae at the edge of the colony were picked and transferred onto fresh agars, conferring a lethality rate proportional to the radiation dose (Fig. 1). Irradiation with 100–150 Gy accelerated the killing, and that with 300 Gy exterminated the fungi (Fig. 1). *Tricholoma matsutake* strain NBRC 33136, which had fewer aerial hyphae, was more sensitive to the radiation, while NBRC 108262 and NBRC 112911 with more aerial hyphae were somewhat resistant (Fig. 1). No putative mutants were obtained based on mycelial morphology during the lethality experiment. Therefore, we irradiated NBRC 33136 mycelia on agar plates at a dose of 500 Gy and picked pieces from an internal portion of the mycelia, rather than hyphae at the edge of the colony; we hypothesized that with such a high dose, the hyphae in less populated areas would be killed completely, while mutants might occur in densely populated areas.

The protocol conferred some putative mutants with colony morphologies different from that of the wild-type strain. Compared with the wild-type strain (Fig. 2a), most of the putative mutants exhibited abnormal traits at the first screening, including thin mycelial colonies (Fig. 2b), increased numbers of aerial hyphae (Fig. 2c), hyphae that were bundled and grew rather straight (Fig. 2d), and hyphae that were erect (Fig. 2e); however, they generally reverted to the wild-type phenotype during the second screening. Despite such a problem, we isolated one relatively stable mu-
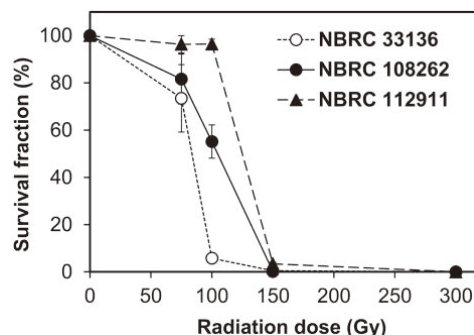
Fig. 1. Lethality of argon-ion beam on *T. matsutake* (*n*=3).
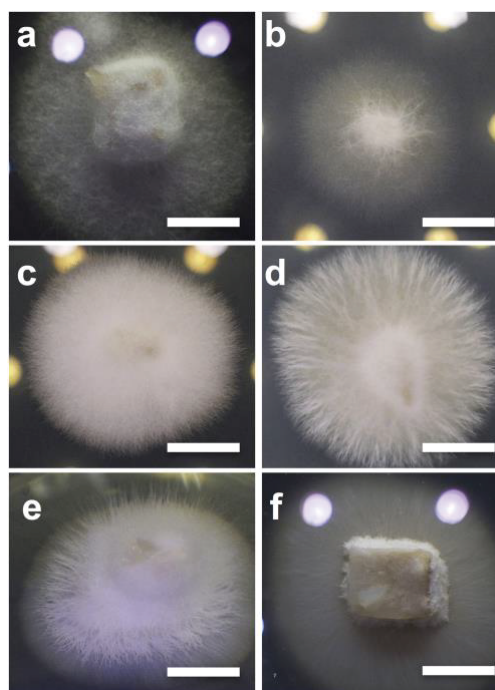
Fig. 2. Mycelial morphology on agar plates of putative *T. matsutake* mutants. **a** The wild-type NBRC 33136. **b**–**e** Putative mutants whose phenotypes reverted to that of the wild-type after a culture transfer. **f** Putative mutant whose phenotype is relatively stable. Scale bar: 5 mm.

tant, which had much fewer aerial hyphae and grew solely in a planar manner on MMN+V8 agar plates (Fig. 2f). While heavy-ion beams may be useful for isolating mutants of *T. matsutake*, maintaining mutants requires precautions to prevent given traits from reverting after repetitively culturing their mycelia.

References
1) L. Vaario *et al.*, Mycorrhiza **20**, 511 (2010).
2) A. Yamada *et al.*, Mycoscience **55**, 27 (2014).

†　Condensed from the article in Mycorrhiza **28**, 171 (2018)
*1　Forestry and Forest Products Research Institute
*2　RIKEN Nishina Center

Current status of development of ion microbeam device with tapered glass capillary for biological use

T. Ikeda,[*1] M. Hamagaki,[*1] K. Sato,[*1,*2] K. Hirose,[*1,*2] M. Miwa,[*1,*2] H. Sato,[*1] and T. Abe[*1]

A microbeam irradiation system based on single tapered glass capillary optics with thin end-window has been developed at a beam line of the Pelletron tandem accelerator in the Nishina R&D Building. The microbeam is extracted through a several-μm diameter outlet. The previous system (FY2006-2015) was used to investigate only the cellular response to ion microbeam hitting.[1–4] The new system will irradiate samples of not only (1) cells (transparent target), but also (2) the surfaces of small insects (not transparent). The corresponding aims are (1) investigation of the mechanism of repair of DNA by microbeam irradiation to a small area in the nucleus to artificially induce accumulation of proteins for the repairing, and (2) search for a specific gene that corresponds to an active organ (horn, wing *etc.*) to develop its structure or shape. The system will employ H^+ ions of up to 3 MeV and He^{2+} ions of up to 4.5 MeV, whose ranges after the end-window are approximately 130 μm and 20 μm in water, respectively. For the irradiation of cells, the ion energy is selected such that the ion can be stopped inside the nucleus or can penetrate the cell. For the irradiation of an insect that is alive in air, the distance from the capillary outlet is several mm for both H^+ and He^{2+} beams, since air is about 1000 times thinner than water. One can select the ion species according to their linear energy transfer (LET) of up to about 80 and 230 keV/μm for H^+ and He^{2+} in the target, respectively. This means that single ion hitting can cause a serious damage in the DNA. This year, the following parts were installed or are in progress:

(a) Laser alignment system for capillary axis: a green (wavelength = 532 nm, 1 mW max. for output) laser source is positioned at the counter part of the capillary beam line on the analyzing magnet so that the ion beam axis can be visualized as the laser beam. The laser is transmitted through the capillary optics. The system allows users to reduce the alignment time from a few hours to a few minutes. The inset photo in Fig. 1 shows a diffraction ring pattern that is obtained when a capillary is aligned precisely. The capillary is seen at the bottom left part as a shining cone by the green laser.

(b) Prototype of vertically bending magnet of MeV ion beams using neodymium magnets located in the vacuum chamber: the magnetic field in the gap was measured to be 6.4 kGauss. The gap will be tuned so that the optimum bending angle of the ion beam will be obtained.

(c) Capillary holder with a remote-control tilt system (Fig. 2): the actuators (SGSP-13ACTR-B0, SIG-MAKOKI Co., LTD) for the horizontal and vertical tilting are controlled by Windows Tablet PCs through Eth-
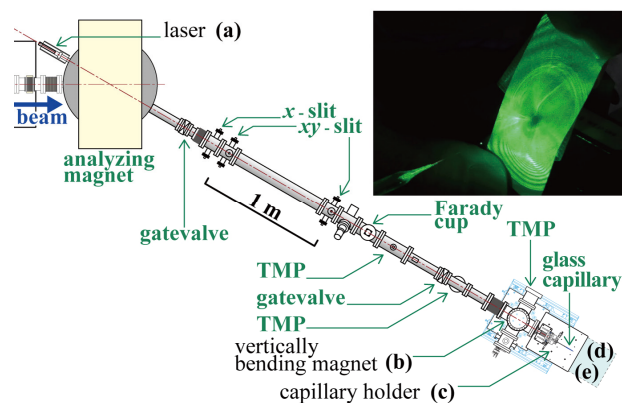
Fig. 1. The beam line of the new microbeam system. The symbols (a)–(e) are explained in the text. The degree of vacuum level is kept better than 10^{-5} Pa.
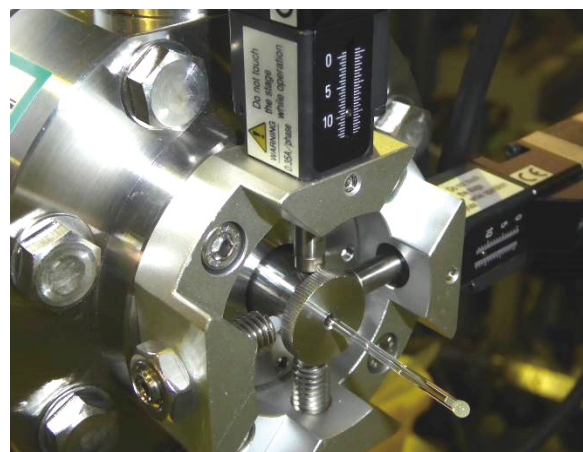
Fig. 2. Capillary holder with a remote tilt system controlled through Ethernet. The glass tube will be replaced with a tapered glass capillary optics to produce microbeams.

ernet.

(d) Ion counting system to estimate the dose for the irradiation: PIN photodiode sensor (S3590-09, Hamamatsu) is connected to a charge-sensitive pre-amplifier whose output signals are processed by NIM modules.

(e) An inverted microscope (IX73, OLYMPUS) and a motorized XY stage system (BIOS-225T-OL, SIGMAKOKI Co., LTD) were purchased. The working distances of the stage are 110 and 75 mm for the X (left-right) and Y directions, respectively, with a position resolution of 0.1 μm.

The next step is the irradiation to biological target for the aims mentioned in the introduction section.

References
1) Y. Iwai *et al.*, Appl. Phys. Lett. **92**, 023509 (2008).
2) M. Kato *et al.*, Appl. Phys. Lett. **100**, 193702 (2012).
3) V. Mackel *et al.*, Rev. Sci. Instrum. **85**, 014302 (2014).
4) T. Ikeda *et al.*, RIKEN Accel. Prog. Rep. **48**, 315 (2015).

*1 RIKEN Nishina Center
*2 Department of Physics, Toho University

IV. OPERATION RECORDS

Program Advisory Committee meetings for nuclear physics and for materials and life experiments

K. Yoneda,[*1] K. Ishida,[*1] H. Yamazaki,[*1] N. Imai,[*2] Y. X. Watanabe,[*3] K. Yako,[*2] H. Miyatake,[*3] M. Iwasaki,[*1] H. Ueno,[*1] and H. Sakai[*1]

The Program Advisory Committees (PAC) are in charge of reviewing the scientific proposals submitted for the use of the accelerator facility of RIKEN Nishina Center (RNC). Three PAC meetings were held in fiscal year 2017; one for the proposals of nuclear physics (NP-PAC), and two for the proposals of materials and life experiments (ML-PAC). The NP-PAC reviewed experimental proposals at RIBF, whereas the ML-PAC reviewed proposals at Rutherford Appleton Laboratory (RAL) and RIBF.

NP-PAC

The 18th NP-PAC meeting was held from December 7–9, 2017,[1] with attendance of 16 PAC members including 8 new members. In this meeting, the experimental proposals that utilize OEDO were called for the first time.

In the 18th NP-PAC meeting, 36 proposals were reviewed, and 25 proposals were approved as grade S or A. The outcome of the NP-PAC meeting is summarized in Table 1.

The 18th NP-PAC members are as follows: A. Bracco (INFN, the chair), D. Ackermann (GANIL), A. Andreyev (University of York), I. Hamamoto (University of Lund/RNC), R. V. F. Janssens (University of North Carolina at Chapel Hill), A. O. Macchiavelli (LBNL), D. J. Morrissey (MSU), T. Nagae (Kyoto University), H. Nakada (Chiba University), K. Ogata (RCNP, Osaka University), T. Rauscher (University of Hertfordshire), K. Sekiguchi (Tohoku University), H. Simon (GSI), P. Van Duppen (KU Leuven), Y. -H. Zhang (IMP). Angela Bracco from INFN became a new chairperson of the meeting.

ML-PAC

The 14th and 15th ML-PAC meetings were held on July 3, 2017, and January 11, 2018, respectively.[2] The proposal review was performed using only submitted documents, i.e., no presentation was given by proponents, as was done for the first time in the 13th ML-PAC meeting. The outcome of the meeting is summarized in Table 2.

The 14th and 15th ML-PAC members are as follows:

Table 1. Summary of the outcome of the 18th NP-PAC meeting. The proposals ranked as S and A are treated as the "approved" proposals.

18th NP-PAC (December 7–9, 2017)		
	requested proposals (days)	approved proposals (days)
GARIS (RILAC)	2 (57)	2 (53.5)
CRIB (AVF)	5 (38.5)	3 (17)
RIPS	1 (6)	1 (3)
KISS	3 (23.5)	3 (16.5)
BigRIPS/ZD	19 (133.5)	12 (50.5)
SHARAQ/OEDO	2 (16.5)	1 (10.5)
Rare RI Ring	1 (15)	1 (10.5)
SAMURAI	3 (27)	2 (15.5)
Total	36 (317)	25 (173.5)

Table 2. Summary of the outcome of the 14th and 15th ML-PAC meetings. The RIBF proposals ranked as A are treated as the "approved" proposals.

14th ML-PAC (July 3, 2017)		
	requested proposals (days)	approved proposals (days)
RAL	12 (52)	8 (26)
RIBF	3 (18.5)	2 (8)
Total	15 (70.5)	10 (34)
15th ML-PAC (January 11, 2018)		
	requested proposals (days)	approved proposals (days)
RAL	21 (87)	17 (47)
RIBF	1 (6.5)	1 (6.5)
Total	30 (199)	22 (82)

A. Hiller (ISIS, RAL, the chair), T. Azuma (RIKEN), R. Kadono (KEK), A. Kawamoto (Hokkaido University), N. Kojima (Toyota RIKEN), K. Kubo (ICU), P. Mendels (University of Paris), A. Shinohara (Osaka University), S. Sulaiman (Universiti Sains Malaysia), H. Yamase (NIMS), S. Yoshida (Thera Projects Associates), and X. G. Zheng (Saga University).

References
1) http://www.nishina.riken.jp/RIBF/NP-PAC/index.html
2) http://www.nishina.riken.jp/RIBF/ML-PAC/index.html

*1 RIKEN Nishina Center
*2 Center for Nuclear Study, the University of Tokyo
*3 Wako Nulcear Science Center, Institute of Particle and Nuclear Studies, KEK

Beam-time statistics of RIBF experiments

K. Yoneda [*1] and H. Sakai[*1]

This report describes the statistics of the beam times (BTs) at the RIBF facility in fiscal year (FY) 2017. The BTs are categorized into the following two groups: high-energy-mode and low-energy-mode BTs. In the former mode, the beams are delivered in the acceleration scheme of AVF, RILAC, or RILAC2 $\rightarrow$ RRC $\rightarrow$ (fRC $\rightarrow$ IRC $\rightarrow$) SRC, where the accelerators in parentheses can be skipped in cascade acceleration depending on the beam species used. In the latter mode, the acceleration scheme is AVF or RILAC ($\rightarrow$ RRC).

The BTs in the high-energy mode were scheduled from April to July and from October to November 2017, considering the restriction of utility-power use, budgetary constraints, the maintenance schedule of the accelerator system and co-generation system, etc. In the series of experiments performed in spring, the primary beams of ^{70}Zn, ^{238}U, and ^{18}O were provided to users, and the ^{238}U primary beam was provided in autumn. Eleven experiments approved by the RIBF Program Advisory Committees[1] with an approved BT of 64.5 days were conducted. The facility development programs used 4.5 days of BT; these are defined as machine study (MS) experiments. In addition, three nuclear transmutation experiments and two director discretionary expreiments were conducted as the Nishina Center mission programs.

The summary of the high-energy-mode BTs in FY2017 is given in Fig. 1 as a bar chart. User time decreased compared to the BT in FY2016; this indicates a relatively longer Nishina Center mission BT. The total length of the MS is almost as short as the length in FY2016. Even though there remain only few newly-introduced facility device requiring beam tests, the opportunities of machine studies should be promoted as an investment for expanding the potential capability and availability of the facility.

The summary of the low-energy mode is shown in Fig. 2. Here, the BTs are classified based on the accelerator operation modes, *i.e.*, AVF standalone, RILAC standalone, and RRC. In FY2017, the total BT length of the low-energy mode reduced compare to that in FY2016 because of the RILAC shutdown started in the middle of June 2017 for accelerator upgrade. The relatively longer RRC time is mainly due to the start of the long runs for superheavy element search in December 2017. It is anticipated that RRC will be mostly used for the superheavy element search experiments until RILAC becomes available again in 2019.
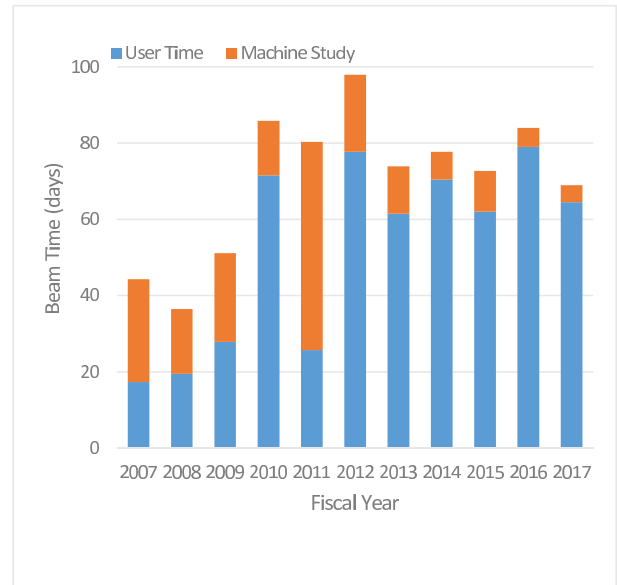
Fig. 1. Bar chart showing the BT statistics for high-energy-mode experiments from FY2007 to FY2017. The accelerator tuning time and Nishina Center mission time are not included.
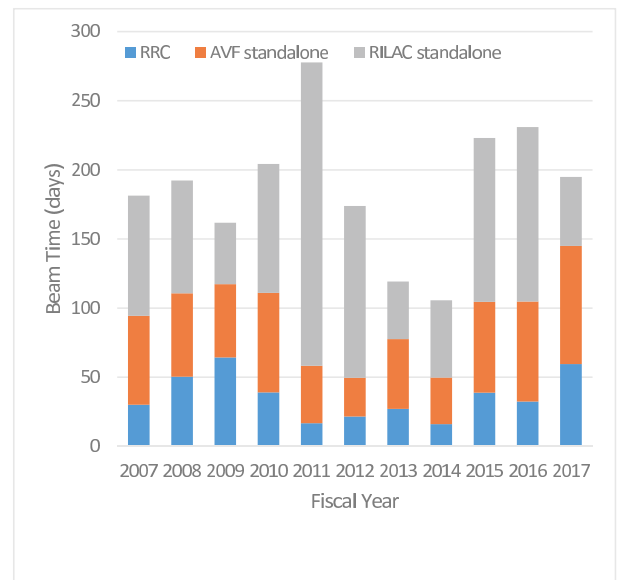
Fig. 2. Bar chart showing the BT statistics for low-energy-mode experiments from FY2007 to FY2017.

References
1) K. Yoneda, K. Ishida, H. Yamazaki, N. Imai, Y. Watanabe, K. Yako, H. Miyatake, H. Ueno, H. Sakai, Elsewhere in this report.

---

*1   RIKEN Nishina Center

Electric power condition of Wako campus in 2017

E. Ikezawa,[*1] M. Kato,[*2] H. Yamasawa,[*3] and M. Kase[*1]

The monthly electrical power consumption data for the RIKEN Wako campus (Wako) and RIKEN Nishina Center (RNC) and the energy supply by the cogeneration systems (CGSs) in 2017 are shown in Fig. 1. The average hourly electrical power consumption in each day for RNC in 2017 is shown in Fig. 2. The annual data of the electrical power consumption and energy supply in 2017 are listed in Table 1. The total electrical power consumption of Wako in 2017 was 153,800 MWh, which is 4% lower than that in 2016. The total electrical power consumption of RNC in 2017 was 73,694 MWh, which is 5% lower than that in 2016. When RI Beam Factory (RIBF) experiments using an uranium (^{238}U) beam were conducted, the maximum electrical power supply to Wako from the Tokyo electric power corporation (TEPCO) reached 20.7 MW with a CGS output of 6.5 MW on June 1, 2017, and the maximum electrical power consumption of RNC reached 17.6 MW on June 2, 2017.

A complete overhaul of the gas turbine of CGS #1 after 4,000 hours of operation was performed from 28 August to 31 August, 2017.

A complete overhaul of the gas turbine of CGS #1 after 48,000 hours of operation is from 16 December, 2017 in progress, and is scheduled to be completed by 23 March, 2018.
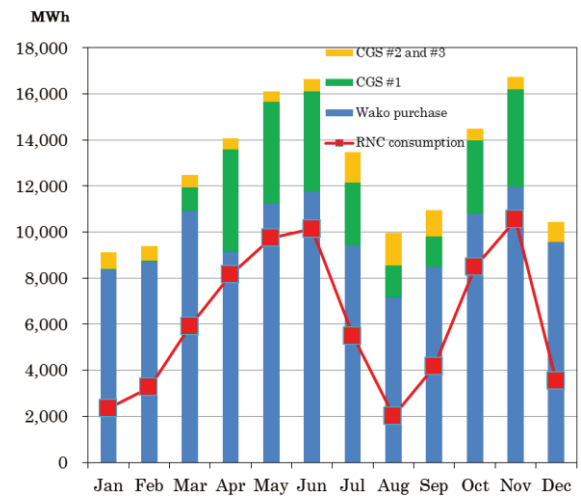
Fig. 1. Monthly electrical power consumption and energy.

Fig. 2. Average hourly electrical power consumption in each day for RNC in 2017.

Table 1. Annual data of electrical power consumption and energy supply in 2017.

	Total (MWh)	Note	Percentage change form 2016
Wako purchase	117,524	Total electrical power supply to Wako from TEPCO	93%
Wako consumption	153,800	Wako electrical power consumption (CGSs + TEPCO)	96%
RNC purchase	46,570	Total electrical power supply to RNC from TEPCO	85%
CGS #1	27,124	CGS #1 total electrical power output	118%
CGS #2 and #3	9,152	CGS #2 and #3 total electrical power output	96%
RNC consumption	73,694	RNC total electrical power consumption	95%

*1 RIKEN Nishina Center

Operation report on the ring cyclotrons in the RIBF accelerator complex

M. Nishimura,[*1] K. Ozeki,[*2] T. Dantsuka,[*2] M. Fujimaki,[*2] T. Fujinawa,[*2] N. Fukunishi,[*2] S. Fukuzawa,[*1]
M. Hamanaka,[*1] H. Hasebe,[*2] Y. Higurashi,[*2] E. Ikezawa,[*2] H. Imao,[*2] S. Ishikawa,[*1] O. Kamigaito,[*2]
Y. Kanai,[*2] M. Kase,[*2] M. Kidera,[*2] K. Kobayashi,[*1] M. Komiyama,[*2] R. Koyama,[*1] K. Kumagai,[*2] T. Maie,[*2]
M. Nagase,[*2] T. Nagatomo,[*2] T. Nakagawa,[*2] M. Nakamura,[*2] T. Nakamura,[*1] M. Nishida,[*1] J. Ohnishi,[*2]
H. Okuno,[*2] N. Sakamoto,[*2] J. Shibata,[*1] K. Suda,[*2] N. Tsukiori,[*1] A. Uchiyama,[*2] S. Watanabe,[*2]
T. Watanabe,[*2] Y. Watanabe,[*2] K. Yamada,[*2] K. Yadomi,[*1] and H. Yamasawa[*2]

In this report, the operation of the ring cyclotrons in the RIBF accelerator complex from Jan. to Dec. 2017 is presented. Table 1 presents a summary of the beams accelerated by these cyclotrons. The "availability" in the table represents the ratio of the actual beam time to the scheduled beam time. For the old facility, multiple experiments supplying identical beams are shown as a block. For the new facility, each experiment is shown separately because each operation is long-running.

In the old facility, the actual beam time was 870.5 h, and the availability was 96.0%. Stable beams were supplied as usual. In the RIBF, six machine times were carried out. The total beam supply time was 2546.8 h, and the availability was 91.3%.

The beam supply of ^{48}Ca was started 1.5 days ahead of schedule. The down time caused by the accelerator was 4.5 h, which was spent to replace the charge stripper foils.

The beam supply of ^{70}Zn (1st) was started about 1 day later than scheduled, was stopped for three days due to the vacuum leakage at the bellows in the injection beam line to the SRC, and was aborted due to the vacuum leakage at a plastic insulation pipe used for the ion source.

The maximum beam intensity of ^{70}Zn (2nd), 250 particle nA, was about twice higher than ever before. This intensity was achieved by changing the acceleration mode from the variable-frequency mode to the fixed-frequency mode using RILAC2. Because of a malfunc-

tion of the fRC RF-W, the beam supply was stopped temporarily for beam tuning.

The averaged beam intensity of ^{238}U (1st) over a week, in which a high-intensity and stable beam was supplied, was 52 particle nA. In order to repair the failed fRC RF-W and fRC-EDC, the schedule for beam tuning was readjusted and the beam time was extended for 0.5 day.

During the beam supply of ^{18}O, a voltage breakdown of the AVF spiral inflector took place. Therefore, the maintenance of the insulator was carried out. The cryogenic pumps for the SRC valley box and the RRC RF#2 failed, possibly caused by radiation.

For the beam supply of ^{238}U (2nd), the transmission efficiency down to the A02 gas stripper was improved, owing to the refinement of the RRC tuning and the introduction of N_2 gas-jet system to the gas stripper. The supply of uranium vapor from the oven used in the ion source was greatly reduced five times because of the blockade in its ejection hole.

For the synthesis of the 119th element, the beam supply of ^{51}V using RILAC2-RRC acceleration was started. For the experiment, the beam energy adjuster (D6-BEA) was installed in the D-room. In the experiment conducted in Dec. 2017, beams decelerated to 4.50–4.87 MeV/nucleon using both D6-BEA and rotating charge strippers with various thicknesses were also supplied. These beams were used for the experiment system check.

Table 1. Summary of the accelerated beams in 2017.

Beam particle	Energy (MeV/nucleon)	Acceleration mode	Beam course	Beam intensity (particle nA)		Beam time (h)		Down time (h)	Availability (%)
				Requested	Actual	Scheduled	Actual		
^{56}Fe	90		E5B (Biology)	1	1.2	21.0	28.9	0	100.0
^{22}Ne	70		E6 (RIPS)	> 200	220.0	122.0	121.9	0.4	99.9
^{12}C	135	AVF-RRC	E5B (Biology)	1	200.0	28.5	22.2	0	100.0
^{40}Ar	95		E5B (Biology)	1	77.6	13.0	8.3	0	100.0
^{84}Kr	70		E5A (Industry)	0.1	5.7	72.0	77.3	0	107.3
^{86}Kr	66		E3A (JAXA)	1	4.0	24.0	23.5	0	98.0
^{197}Au	18.4		E5A (Industry)	0.1	2.1	3.0	2.2	0	72.2
^{197}Au	18.4	RILAC-RRC	E3A (JAXA)	1	0.8	8.0	11.8	0	147.9
^{136}Xe	39		E3A (JAXA/Industry)	1	1.4	24.0	6.8	0	39.7
^{136}Xe	39		E5A (Industry)	0.1	0.8	3.0	3.8	0	125.6
^{136}Xe	10.75		E2B (KEK/KISS)	250	214.3	147.0	146.1	0	99.4
^{136}Xe	7.2		E2B (KEK/KISS)	250	55.0	48.0	46.1	0	96.0
^{51}V	6	RILAC2-RRC	D18/M11 (MS)	4000	3083.0	78.0	81.9	0	105.0
^{51}V	6		E6 (GARIS2)	N/A	1923.1	324.0	206.3	1.1	63.7
^{238}U	10.75		E2B (KEK/KISS)	140	342.9	48.0	47.6	0.2	98.6
^{238}U	10.75		E5A (Material)	2	34.3	24.0	25.3	0	105.3
^{40}Ar	160	AVF-RRC-IRC	E5B (Biology)	1	17.2	10.5	10.5	5.0	74.0
^{48}Ca	345	RILAC-RRC-IRC-SRC	BigRIPS/ZDS	> 530	493.0	96.0	120.0	12.0	125.0
^{18}O	220	AVF-RRC-SRC	SAMURAI	> 300	550.0	492.0	474.6	17.5	96.5
^{70}Zn (1st)	345		BigRIPS/ZDS/SAMURAI	as much as possible	193.0	228.0	94.4	133.6	41.4
^{70}Zn (2nd)	345	RILAC2-RRC-fRC-IRC-SRC	BigRIPS/SAMURAI	as much as possible	250.0	432.0	435.2	44.8	100.7
^{238}U (1st)	345		BigRIPS/ZDS/PALIS/SHARAQ	> 50	58.0	570.7	502.7	68.0	88.1
^{238}U (2nd)	345		BigRIPS/ZDS/PALIS/SHARAQ/Rare-RI Ring	> 50	71.0	960.0	919.9	220.1	95.8
			Total			3776.7	3417.3	502.7	92.5

*1 SHI Accelerator Service Ltd.
*2 RIKEN Nishina Center

RILAC operation

E. Ikezawa,[*1] T. Ohki,[*2] M. Kase,[*1] T. Nakagawa,[*1] N. Sakamoto,[*1] H. Okuno,[*1] N. Fukunishi,[*1]
M. Komiyama,[*1] A. Uchiyama,[*1] T. Maie,[*1] M. Nagase,[*1] M. Fujimaki,[*1] T. Watanabe,[*1] H. Hasebe,[*1]
H. Imao,[*1] K. Ozeki,[*1] K. Suda,[*1] Y. Higurashi,[*1] K. Yamada,[*1] Y. Watanabe,[*1] S. Watanabe,[*1] M. Kidera,[*1]
T. Nagatomo,[*1] H. Yamauchi,[*2] K. Oyamada,[*2] M. Tamura,[*2] A. Yusa,[*2] K. Kaneko,[*2] and O. Kamigaito[*1]

The RIKEN heavy-ion linac (RILAC) has been operated throughout the reporting period and it has supplied various ion beams for different experiments. Some statistics regarding the operation of RILAC from January 1 to December 31, 2017 are presented in Table 1. The total beam service time of the RILAC accounted for 77.6% of its operation time. The two operation modes of the RILAC, namely the standalone mode and the injection mode, in which the beam is injected into the RIKEN Ring Cyclotron (RRC), accounted for 77.7% and 22.3% of the total beam service time of the RILAC, respectively. For experiments, a 2.675-MeV/nucleon ^{48}Ca-ion beam accelerated by the RILAC was injected into the RRC from March 25 to April 2. Table 2 lists the beam service times in the standalone mode of the RILAC, which were allotted to the e2 and e3 beam courses in target room no. 1 in 2017. The e2 beam course was used in experiments with GARIS2. The e3 beam course was used in experiments with GARIS. Table 3 lists the operation time of the 18-GHz ECR ion source in 2017.

We performed the following overhauls during the reporting period.

(1) In the RF systems, the DC high-voltage power supplies were subjected to annual inspection. The major components with mechanical parts were subjected to simple inspection.
(2) All the cooling towers were subjected to monthly inspection and annual cleaning.
(3) All the turbomolecular pumps were subjected to annual inspection.

We faced the following mechanical problems during the reporting period.

(1) Water was found to have splashed in the end drift tube of the Charge-State Multiplier (CSM) A3 and in the trimmer of the CSM A3 cavities because of leakage from each cooling pipe. As a stopgap measure, we repaired the pipes with a repair material.
(2) The RILAC no. 5 cavity had a vacuum leak because of a deteriorated O-ring. We will replace the O-rings of the cavities in 2018.

Table 1. Statistics of RILAC operation from January 1 to December 31, 2017.

Operation time of RILAC	1592.2	h
Mechanical problems	190.9	h
Standalone RILAC	959.9	h
Injection into RRC	275.9	h
Total beam service time of RILAC	1235.8	h

Table 2. Beam service time of the standalone RILAC allotted to each beam course in target room no. 1 in 2017.

Beam course	Total time (h)	%
e2	794.9	82.8
e3	165.0	17.2
Total	959.9	100.0

Table 3. Operation time of the 18-GHz ECR ion source in 2017.

Ion	Mass	Charge state	Total time (h)
O	18	5	74.7
F	19	6	117.3
Ne	22	6	61.9
Mg	26	7	48.3
Si	30	8	57.4
S	34	10	58.1
Ar	40	11	120.0
Ca	48	10,11	296.8
Ti	50	11, 12, 13	1090.0
Xe	136	26	96.0
Au	197	28	72.0
Total			2092.5

*1 RIKEN Nishina Center
*2 SHI Accelerator Service Ltd.

Operation report on the RIKEN AVF cyclotron for 2017

R. Koyama,[*1] K. Suda,[*2] A. Goto,[*2] J. Ohnishi,[*2] Y. Ohshiro,[*3] T. Watanabe,[*2]
M. Fujimaki,[*2] N. Fukunishi,[*2] S. Fukuzawa,[*1] M. Hamanaka,[*1] H. Hasebe,[*2] Y. Higurashi,[*2]
E. Ikezawa,[*2] H. Imao,[*2] S. Ishikawa,[*1] O. Kamigaito,[*2] K. Kaneko,[*1] M. Kase,[*2] M. Kidera,[*2]
K. Kobayashi,[*1] M. Komiyama,[*2] Y. Kotaka,[*3] K. Kumagai,[*2] T. Maie,[*2] M. Nagase,[*2] T. Nagatomo,[*2]
T. Nakagawa,[*2] T. Nakamura,[*1] M. Nishida,[*1] M. Nishimura,[*1] H. Okuno,[*2] K. Oyamada,[*1] K. Ozeki,[*2]
N. Sakamoto,[*2] J. Shibata,[*1] M. Tamura,[*1] N. Tsukiori,[*1] A. Uchiyama,[*2] S. Watanabe,[*2] Y. Watanabe,[*2]
K. Yadomi,[*1] K. Yamada,[*2] and A. Yusa[*1]

The yearly report on the operation of the RIKEN AVF cyclotron (denoted as AVF hereinafter) for the period January–December 2017, is presented.

AVF has been used not only as an injector for the RIKEN ring cyclotron RRC but also to supply various ion beams directly to three beam courses (C03 for RI production, E7A for nuclear experiment with CRIB, and E7B for general-purpose) in its stand-alone operations, as schematically shown in Fig. 1. In the machine studies performed in 2017, accelerated beams were observed with a Faraday-cup at C01.
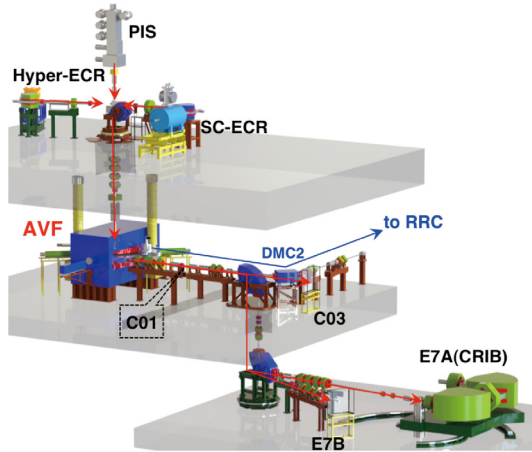
Fig. 1. Overview of the AVF cyclotron with three ion sources, three experimental courses, and beam transport line to RIKEN ring cyclotron RRC.

The yearly operation statistics and accelerated beams of AVF are summarized in Tables 1 and 2, respectively. The operation status was very fine and the total operation time was 3951 h, of which only 13 h involved temporary suspension due to the minor accelerator troubles.

For more details of AVF and RRC operations and others, refer to Refs. 1) and 2).

References
1) R. Koyama *et al.*, Proc. of PASJ14, Sapporo, Japan, August 2017, FSP027, pp.1390–1394.
2) M. Nishinura *et al.*, Proc. of PASJ14, Sapporo, Japan, August 2017, FSP028, pp.1395–1399.

*1　SHI Accelerator Service Ltd.
*2　RIKEN Nishina Center
*3　Center for Nuclear Study, the University of Tokyo

Table 1. AVF operation statistics. Statistics in 2016 are also shown.

AVF operation statistics	2016 [h]	2017 [h]
Total	3365	3951
Stand-alone operation		
Tuning of AVF	576	742
Fault of AVF	5	4
C01 machine study	0	32
C03 experiment	562	1113
E7A experiment	686	245
E7B experiment	73	597
Sub total	1897	2697
Operation as injector of RRC		
Tuning of AVF	213	141
Fault of AVF	0	9
RRC-RARF experiment	842	564
RRC-RIBF experiment	414	549
Sub total	1468	1254

Table 2. Accelerated beams of AVF in 2017.

Particle	Energy [MeV/u]	Course
Stand-alone operation		
p	12.0	C03, E7B
d	12.0	C01, C03, E7B
d	14.0	C01
α	6.50	E7B
α	7.18	C03, E7B
α	7.25	C03
α	12.5	C03, E7B
^{7}Li	5.60	C03
^{7}Li	6.00	C03
^{11}B	7.82	C03
^{11}B	9.10	C01, C03
^{18}O	6.07	C03
^{18}O	6.07	C03
^{19}F	6.77	C03
^{26}Mg	6.60	E7A
Operation as injector of RRC		
^{12}C	7.00	RRC-RARF
^{18}O	4.51	RRC-RIBF
^{22}Ne	3.97	RRC-RARF
^{40}Ar	3.75	RRC-RARF
^{40}Ar	3.75	RRC-IRC-RARF
^{40}Ar	5.19	RRC-RARF
^{56}Fe	5.00	RRC-RARF
^{84}Kr	3.97	RRC-RARF
^{86}Kr	3.78	RRC-RARF

Present status of the liquid-helium supply and recovery system

T. Dantsuka,[*1] H. Okuno,[*1] M. Nakamura,[*1] M. Kase,[*1] S. Tsuruma,[*1] M. Ohshima,[*2] H. Miura,[*2] H. Shiraki,[*2] H. Hirai,[*2] and H. Hazama[*2]

The liquid-helium supply and recovery system,[1)] which can produce liquid helium at a liquefaction rate of 200 L/h from pure helium gas, has been under stable operation since the beginning of April 2001. The volumes of liquid helium supplied each year from 2001 to 2016 are shown in Fig. 1. During the period from 2001 to 2013, there was a gradual increase in the supplied volume, with two declines in 2009 and 2011. In 2014, the supplied volume decreased because of a malfunction of the system; however, in 2015, the supplied volume returned to its original value. In 2016, the supplied volume decreased.

The purity of helium gas recovered from the laboratories gradually improved after the construction of the system was completed. At present, the impurity concentration in the recovered gas rarely exceeds 200 ppm. The volume of helium gas recovered from each building in the Wako campus as well as the volume transported to the liquid helium supply and recovery system were measured. The recovery efficiency, which is defined as the ratio of the amount of recovered helium gas to the amount of supplied liquid helium, was calculated.

The recovery efficiency for the buildings on the south side of the Wako campus, namely the Cooperation Center building of the Advanced Device Laboratory, Chemistry and Material Physics building, and Nanoscience Joint Laboratory building, increased to more than 85%.

Reference
1) K. Ikegami *et al.*, RIKEN Accel. Prog. Rep. **34**, 349 (2001).
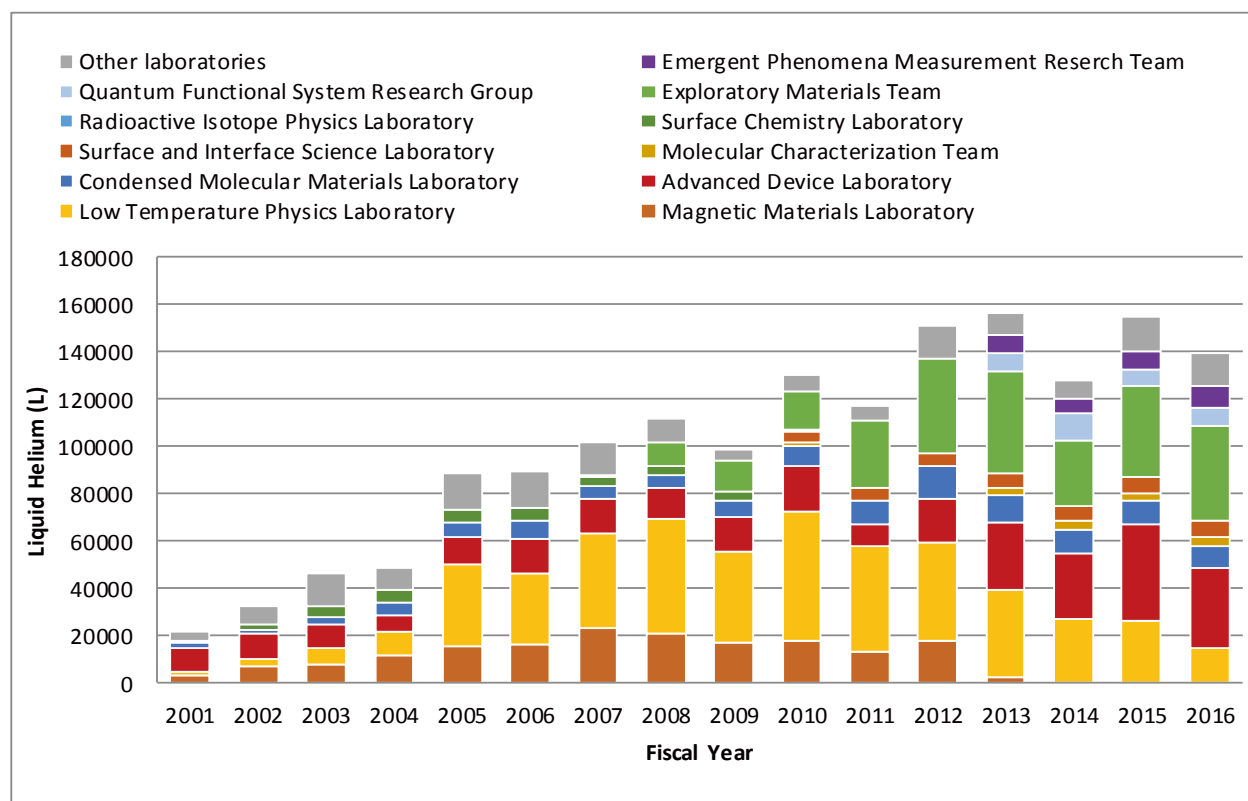
Fig. 1. Volumes of liquid helium supplied to the various laboratories for each fiscal year from 2001 to 2016.

*1 RIKEN Nishina Center
*2 Nippon Air Conditioning Service K.K

Operation of the BigRIPS cryogenic plant

K. Kusaka,[*1] M. Ohtake,[*1] K. Yoshida,[*1] M. Ohshima,[*2] A. Mikami,[*2] H. Hazama,[*2] H. Miura,[*2] H. Shiraki,[*2] H. Hirai,[*2] M. Haneda,[*2] R. Sasaki,[*2] K. Kimura,[*2] M. Noguchi,[*3] and N. Suzuki[*3]

Based on the RIBF beam time schedule, we performed two continuous operations of the BigRIPS cryogenic plant in 2017. The first operation period was from Feb. 28 to July 21 and the second was from Sept. 16 to Dec. 15 after the summer maintenance. The total operation time of the compressor unit was 64,869 h.

At the beginning of the second operation, we had a significant incident. When we started the refrigerator after the purification operation, the interlock system stopped the rotation of the expansion turbines. The reason was poor cooling water flow caused by impurities in the cooling water system. We found that the water pipelines for the refrigerator system were badly blocked up by muddy impurities and the pipes had rusted away (Fig. 1). After flushing the water channels of the turbine system, we started the refrigerator using the independent chiller unit of ORION RKE3750A, and this temporary cooling system worked well for 2 months of the second operation period. We will replace the entire piping of the cooling water system for the BigRIPS cryogenic plant in March 2018.

Except for the incident stated above, we operated the cryogenic system without any trouble. Figure 2 shows the vibration acceleration in the vertical and horizontal directions as a function of the total operation time. We have regularly measured the vibrations of the main compressor unit both at the high-pressure and low-pressure sides since 2015. After the replacement of the damaged baring unit in Dec. 2016, which corresponds to the operation time of 59,218 h, the vibration acceleration stayed less than 8 m/s^2 and the compressor unit worked well during the entire operation period in 2017.

Another important observation for the cryogenic system is the low oil contamination in helium gas. By measuring the operation interval of the drain valves of the coalescer vessels in the compressor unit, the oil contamination level of the coalescer vessels was evaluated.[1] Figure 3 shows an estimate of the oil contamination level at the entrance of the third coalescer vessel as a function of the coalescer filter operation time. The navy blue, green, and yellow diamonds represent the estimates for the 2008–2009, 2010–2011, and 2012–2013 operations, respectively. The coalescer filters used in these periods were discontinued.[2] The estimate for the 2014–2015 and 2016–2016 operations with the new coalescer filters are shown with pink and red diamonds, respectively. The oil contamination values measured using the oil check kit are also shown. The open triangles, squares, and circles represent the results for the 2008–2009, 2010–2011, and 2012–2013 operations. The results with new coalescer

Fig. 1. Blocked cooling water piping for the turbines.
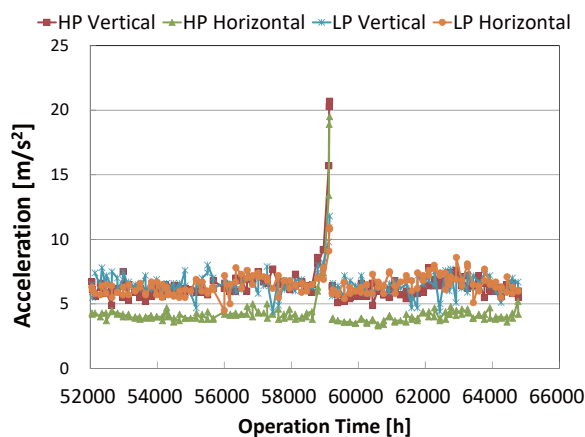
Fig. 2. Vibration acceleration of the compressor unit.
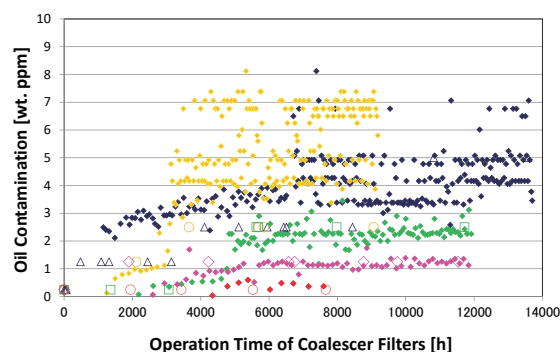
Fig. 3. Oil contamination at the entrance of the third coalescer vessel.

filters for the 2014–2015, and, 2016–2017 operations are indicated by the open diamonds and circles, respectively. Both estimates of the oil contamination level are consistent with each other, and the performance efficiency of the new filter elements seems to be better than that of the discontinued ones.

References
1) K. Kusaka *et al.*, RIKEN Accel. Prog. Rep. **41**, 309 (2010).
2) K. Kusaka *et al.*, RIKEN Accel. Prog. Rep. **50**, 285 (2017).

[*1]　RIKEN Nishina Center
[*2]　Nippon Kucho Service Co., Ltd.
[*3]　Mayekawa Mfg. Co., Ltd.

Radiation safety management at RIBF

K. Tanaka,[*1] Y. Uwamino,[*1] H. Sakamoto,[*1] R. Hirunuma-Higurashi,[*1] H. Mukai,[*2] A. Akashio,[*1]
T. Okayasu,[*1] R. Suzuki,[*3] M. Takekoshi,[*3] Y. Yamauchi,[*3] S. Fujita,[*1] H. Aiso,[*1] K. Igarashi,[*1] S. Iizuka,[*1]
N. Usudate,[*1] and Y. Shioda[*1]

The results of radiation monitoring at RIBF, carried out at the border of the facility and the radiation-controlled area are reported. The residual doses along the accelerator setups are also presented. In 2017, ^{238}U beam of about 345 MeV/u was provided at an intensity of 50 particle nA during May, June, October, and November. A ^{48}Ca beam of 500 particle nA was used in April, a ^{70}Zn beam of 300 particle nA was used in April and May, and a ^{18}O beam of 1000 particle nA was used in June and July.

The dose rates at the boundary of the radiation-controlled area were monitored. Neutron and γ-ray monitors were used at three locations: roofs of the RRC, IRC, and BigRIPS. Figure 1 shows the annual neutron dose at these positions. In 2017, even the highest annual dose of 51 μSv/y at the IRC roof was lower than the legal limit of 5.2 mSv/y.

The dose rates at the site boundary, where the legal limit is 1 mSv/y, were monitored. Neutron and γ-ray monitors were used, and the annual dose in 2017 was found to be lower than the detection limit after the background correction. The detection limit of the neutron monitor is 2 μSv/y and that of the γ-ray monitor is 8 μSv/y. Therefore, it was inferred that the annual dose at the boundary was less than 10 μSv/y, which is considerably lower than the legal limit.

The residual radioactivity at the deflectors of the cyclotrons was measured just before the maintenance work.

The residual dose depends on factors such as the beam intensity, accelerator operation time, and cooling time. The dose rates from 1986 are shown in Fig. 2. The dose rates for FRC, IRC, and SRC are shown for years after 2006, when the RIBF operation started. For AVF, the dose rate increased in 2006 because the radioisotope production was started and the beam intensity increased.

The residual radioactivity along the beam lines was measured after almost every experiment. Figure 3 shows the locations of measurement points where high residual doses were observed. Table 1 lists the dose rates, beam conditions, and cooling time at the measurement points. The maximum dose was 29 mSv/h at point 14, which is in the vicinity of the G01 faraday cup.

The radioactivity in the closed cooling system at BigRIPS was measured. The water for the F0 target, the
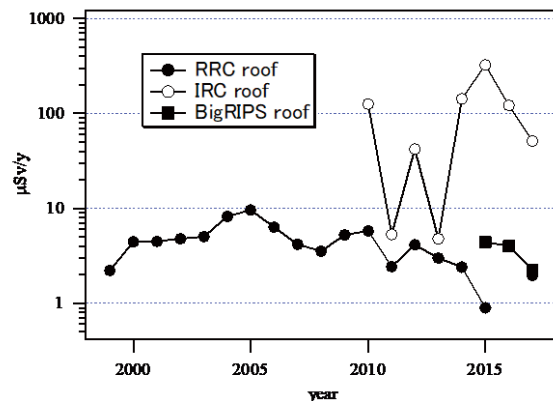
Fig. 1. Radiation dose at the boundary of the radiation-controlled area.
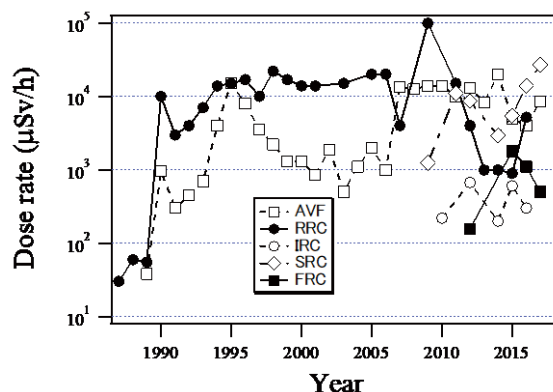
Fig. 2. Dose rates of residual radioactivity at the deflectors of 5 cyclotrons.

exit beam dump, and the sidewall dump were sampled in August. The water in the closed cooling systems was replaced in August 2016; therefore, the detected radioisotopes were generated during one year of operation in RIBF. The results are shown in Table 2. A liquid scintillation counter was used for the low energy β ray of 18 keV from H-3 nuclide. A Ge detector was also used for γ rays emitted from other radionuclides. The radionuclides, except for H-3, were already filtered by an ion exchange resin in the closed cooling systems. Although the overall value of contamination was less than the legal limit for drain water, as shown in Table 2, the water from the closed cooling system will be dumped into the drain tank before the next operation to prevent contamination in the room in case of a water leakage.

---

*1　RIKEN Nishina Center
*2　Japan Environment Research Corporation
*3　Daiwa Atomic Engineering Corporation

The E-learning module, which can be accessed anytime and from anywhere (even from the outside RIKEN), has been used for the re-training to the radiation workers at RIBF. About 660 radiation workers have completed the training in 2017.
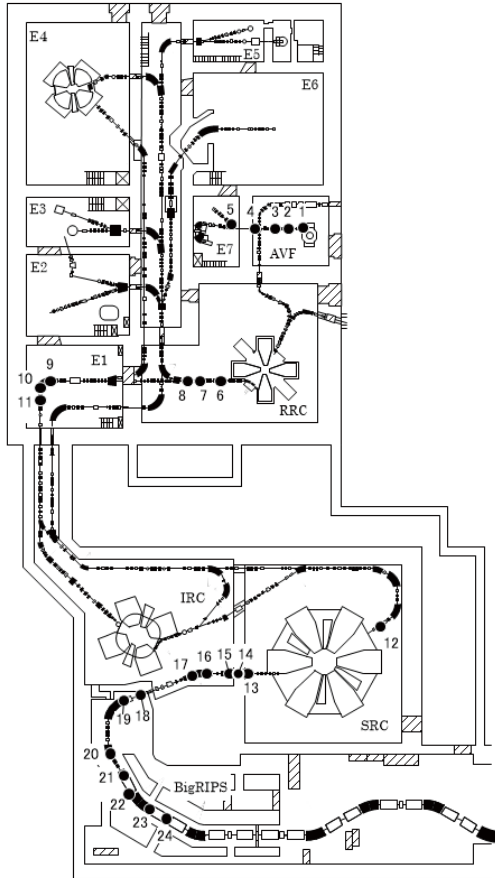
Fig. 3. Layout of the beam lines at RIBF. The measurement locations listed in Table 1 are indicated.

Table 1. Dose rates measured at beam lines in 2017. Points 1–24 indicate the locations where measurements were taken as shown in Fig. 3.

Point	Dose rate (μSv/h)	Date (M/D)	Particle	Energy (MeV/u)	Intensity (pnA)	Cooling time (h)
1	1000	8/4	d	12	10000	97
2	450	8/4	d	12	10000	97
3	500	8/4	d	12	10000	97
4	500	8/4	d	12	10000	97
5	280	12/12	α	6.5	10	291
6	800	8/4	C-12	135	1	186
7	400	8/4	C-12	135	1	186
8	200	12/12	U-238	10.75	1657	283
9	4000	12/12	U-238	50	390	282
10	3000	12/12	U-238	50	390	282
11	400	12/12	U-238	50	390	282
12	170	8/4	O-18	220	550	497
13	8600	8/4	O-18	220	550	497
14	29000	12/8	U-238	345	71	183
15	950	12/8	U-238	345	71	183
16	250	12/8	U-238	345	71	183
17	950	8/4	O-18	220	550	496
18	450	12/8	U-238	345	71	183
19	830	12/8	U-238	345	71	183
20	450	8/8	O-18	220	550	589
21	1780	8/8	O-18	220	550	589
22	1850	8/8	O-18	220	550	589
23	25000	12/8	U-238	345	71	183
24	189	8/8	O-18	220	550	589

Table 2. Concentrations of radionuclide in the cooling water at BigRIPS, the allowable legal limits for drain water, and the ratios of concentration to the allowable limit.

Cooling water	Nuclide	Concentration[a] (Bq/cm^3)	Limit[b] (Bq/cm^3)	Ratio to limit [a/b]
BigRIPS F0 target	H-3	6.	60	0.11
			summation	0.11
BigRIPS exit beam dump	H-3	22.	60	0.37
	Be-7	9.4e-3[1]	30	3.1e-4
	Co-57	8.1e-4	4	2.0e-4
	Co-58	6.4e-4	1	6.4e-4
	Mn-54	1.4e-3	1	1.4e-3
			summation	0.37
BigRIPS side-wall beam dump	H-3	47.	60	0.79
			summation	0.79

1) read as 9.4×10^{-3}

Operation of the Pelletron tandem accelerator

T. Ikeda,[*1] M. Hamagaki,[*2] and H. Sato[*1]

The tandem accelerator (Pelletron 5SDH-2, 1.7 MV max.) with two ion sources in the Nishina R&D Building (Fig. 1) is managed by the Detector Team of RNC. The accelerator has three beam lines for (1) Rutherford backscattering (RBS) spectrometry/elastic recoil detection analysis (ERDA), (2) a microbeam port, and (3) multi-purpose use. The RF charge-exchange ion source, called Alphatross, is mainly used for the extraction of He$^-$ ions. Another source is the Source of Negative Ions by Cesium Sputtering (SNICS). Almost all other ions can be extracted from SNICS as negative ions, such as H$^-$ and C$^-$. Thus far, ion species of H, He, Li, B, C, N, O, Si, Ti, Ni, Cu, and Au have been accelerated with the two ion sources. The range of the ion beams is several 10 μm at most for water (density = 1 g/cm^3). Only H$^+$ can have ranges greater than 100 μm for water. All experiments except for microbeam irradiation with tapered glass capillaries should be performed in vacuum chambers. However, heavy ions of several MeV, such as Au ions, can provide stopping powers greater than 200 keV/μm at only the surface layer of samples or detector-sensitive areas. Since the experimental area is approved as a second-class radiation-controlled area, users for all measurements can access their setup even during the beam irradiation time. The users are free from any setup for remote control utilities. These are advantages of the use of the Pelletron accelerator.

During the annual reporting period from Jan. 1 to Dec. 31, 2017, the total machine time including machine studies was 24 days, where the condition check of the ion sources is not counted. The experiments in the machine time and details of maintenance are described in this report.

The ion species accelerated in this year were H$^+$, He$^+$, He^{2+}, C^{2+}, C^{3+}, and C^{4+}, with energies ranging from 1.0 to 7.2 MeV, as summarized in Table 1. Experimental studies on the following subjects were performed.

(1) Ion irradiation on thin layers for the modification and creation of micro-particles (4 days)
(2) Machine study of a proton microbeam using tapered glass capillaries (6 days)
(3) Test of microbeam irradiation on single cells (8 days)
(4) ERDA experiments using carbon ions (3 days)
(5) Educational experiment of proton capture by a carbon nucleus for Nishina School (3 days)
(6) Analyses using elastic scattering (RBS/ERDA) as Wako joint-use equipment (0 days = no user)

In this year, the He ion source (Alphatross) was repaired because there was no machine time using the He ion beam owing to the extremely low intensity of He$^-$
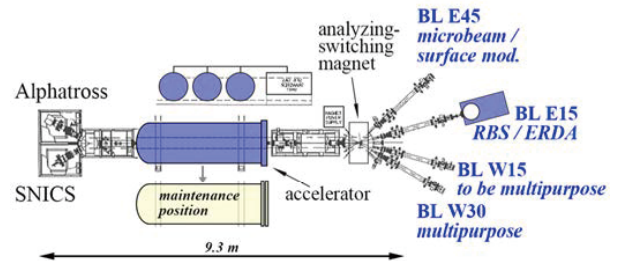
Fig. 1. Pelletron tandem accelerator and beamlines in the Nishina R&D Building. The tank colored blue is the position of operation, and the white one is for maintenance.
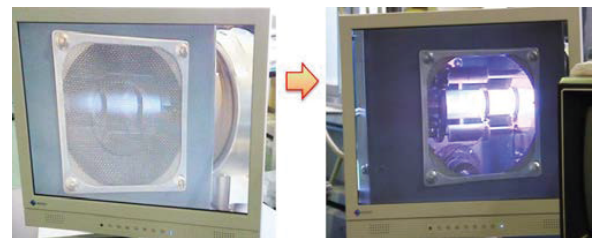
Fig. 2. Improvement of He plasma density to provide He ion beams with sufficient intensities.

Table 1. Beam conditions and experiments conducted in the tandem accelerator.

Ion	Energy [MeV]	Beam current [nA]	Experiment	Operation time [days]
^{1}H$^+$	1.0–3.0	0.01–50	Irradiation	9
^{4}He$^{+, 2+}$	1.5–4.5	1–50 [pnA]	Irradiation	13
^{12}C$^{2, 3, 4+}$	up to 7.2	0.01–1	Irradiation	2

ions in the previous year. The reason for the low intensity was found to be the aged deterioration of the power supply for the confinement magnetic field and the RF supply tubes. Figure 2 shows the change of the He plasma densities between before and after the renewal (Left and Right, respectively). Precise alignment of the position of the source was also performed. The final intensity of the He^{2+} beam at an irradiation port was increased back to 50 particle nA.

For accurate positioning in the microbeam irradiation, a laser beam alignment system was tested at BL-E45. Glass capillary optics providing micrometer-sized ion beams needs axis orientation with respect to the initial beam with accuracy of the order of mrad. The alignment time was successfully reduced from a few hours down to a few minutes.

*1   RIKEN Nishina Center

Operation of fee-based activities by the industrial cooperation team

A. Yoshida,[*1] T. Kambara,[*1] H. Haba,[*1] and S. Yano[*1]

The fee-based activities operated by the industrial cooperation team in 2017, which are the utilization of heavy-ion beams in the industry and the distribution of radioisotopes, are summarized below.

RIKEN Nishina Center allows the use of the AVF cyclotron, RILAC, and RIKEN Ring Cyclotron (RRC) by private companies in Japan for a fee.[1] In 2017, three clients successfully used fee-based beamtimes to test space-use semiconductor devices. In February, one client used a 39-MeV/A ^{136}Xe beam at the E3A beamline of the RRC for approximately 8 h, and in March, two clients used a 70-MeV/A ^{84}Kr beam at the E5A beamline for approximately 60 h in total.

Since 2007, RIKEN has distributed radioisotopes (RIs) to users in Japan for a fee in collaboration with the Japan Radioisotope Association[2] (JRIA). The nuclides are ^{65}Zn ($T_{1/2} = 244$ days), ^{109}Cd ($T_{1/2} = 463$ days), ^{88}Y ($T_{1/2} = 107$ days), and ^{85}Sr ($T_{1/2} = 65$ days), produced by the RI Applications Team at the AVF cyclotron. According to a material transfer agreement (MTA) drawn between JRIA and RIKEN, JRIA mediates the transaction of the RIs and distributes them to users. ^{65}Zn and ^{109}Cd are delivered approximately two weeks after the acceptance of an order. ^{85}Sr and ^{88}Y, which have shorter half-lives, are not stocked like ^{65}Zn and ^{109}Cd but are rather produced in a scheduled beamtime after an order is accepted. Therefore, they are delivered two months or more after the acceptance of an order. Details can be found in the online ordering system J-RAM[3] of JRIA.

In 2017, we delivered no ^{109}Cd, two shipments of ^{65}Zn with a total activity of 5.5 MBq, two shipments of ^{88}Y with a total activity of 2 MBq, and a shipment of ^{85}Sr with an activity of 3.7 MBq. The final recipients of the RIs were three universities and one medical research center.

Figure 1 shows the yearly trends in the number of orders and the amounts of distributed RIs. Compared with 2016, the amount of distributed ^{65}Zn decreased by 4, that of ^{88}Y remained same, and that of ^{85}Sr increased by 3.7.

We are preparing to start the distribution of a new RI ^{67}Cu ($T_{1/2} = 61.8$ h) in spring 2018. Since its half-life is very short, it will be produced in a scheduled beamtime after an order is accepted. Details will be announced in J-RAM.
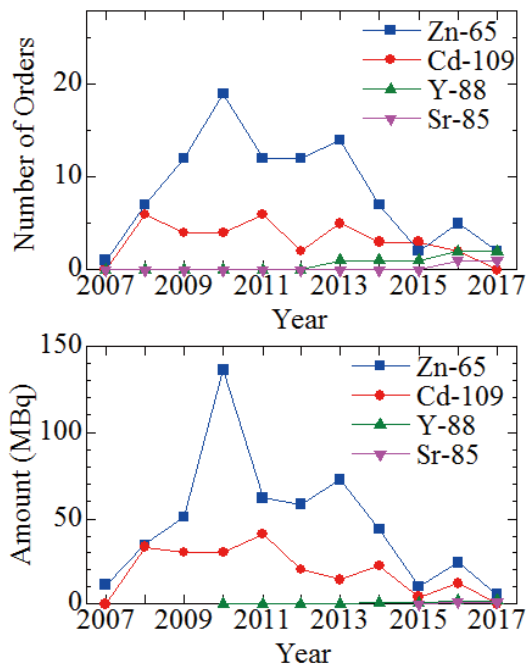
Fig. 1. Number of orders (upper) and amount (lower) of the RIs distributed yearly from 2007 to 2017. The distribution of ^{88}Y started in 2010 and that of ^{85}Sr in 2015.

References
1) http://ribf.riken.jp/sisetu-kyoyo/ (Japanese).
2) http://www.jrias.or.jp/ (Japanese),
   http://www.jrias.or.jp/e/ (English).
3) https://www.j-ram.net/jram/DispatchTopPage.do (Japanese).

*1 RIKEN Nishina Center

V. EVENTS

ImPACT-OEDO workshop

H. Otsu,[*1] N. Imai,[*2] S. Michimasa,[*2] T. Sumikama,[*1] D. Suzuki,[*1] K. Washiyama,[*3] Y. Watanabe,[*4] and
Y. X. Watanabe[*5]

The ImPACT-OEDO workshop[1] was held on July 13 and 14, 2017 at the RIKEN Wako campus. The workshop was jointly organized by the RIKEN Nishina Center and the Center for Nuclear Study, the University of Tokyo. A total of 70 participants with physics or engineering backgrounds gathered from institutions throughout Japan.

The project "Reduction and Resource Recycling of High-level Radioactive Wastes through Nuclear Transmutation" is one of the selected programs of the ImPACT (Impulsing Paradigm Change through Disruptive Technologies) program under the initiative of the Cabinet Office. The project has been in operation since 2014 under the collaboration of a number of major research institutes in Japan, including the RIKEN Nshina Center. Its mission is to develop a new method to transmutate long-lived fission products (LLFP) that would otherwise remain highly toxic and to pave a realistic path toward a sustainable society. At the RIBF and other facilities, the collaboration has been conducting a number of measurements of reaction rates of nuclei identified as LLFPs. In parallel, theoretical studies have been widely and actively carried out to interpret the experimental results and extract nuclear data that can be incorporated into state-of-the-art simulation codes. In addition, FY2017 is marked by the inauguration of the OEDO beam line at the RIBF. This new beam line is capable of decelerating fast radioactive isotope beams of the RIBF down to energies below 50 MeV/nucleon. With the OEDO beam line, the RIBF will enable reaction measurements of LLFPs over a wide range of energies.

The ImPACT-OEDO workshop was organized to overview and discuss a wide range of activities related to nuclear data of LLFPs that have been carried out in the ImPACT project. Another important goal is to stimulate discussions on future experiments that will be conducted at the OEDO beam line.

The two-day workshop started with an overview of the ImPACT program by H. Sakurai (Nishina Center), which was followed by another overview of the subworking group for nuclear data by S. Shimoura (Center for Nuclear Study). A total of 29 speakers orally presented their activities and future plans in six sessions. Four sessions were dedicated to recent or on-going studies, and the remaining two were focused on future experiments at the OEDO beam line.

The experiments reported include a series of reaction studies of LLFPs at the RIBF using a beam of LLFPs produced from the fission of a ^{238}U beam. The reaction products from spallation or Coulomb breakup reactions of ^{107}Pd or ^{93}Zr were measured in flight. The deduced cross sections to transmuate LLFPs into stable nuclei or the inclusive total reaction cross sections were presented. Another transmutation method under study uses muon capture. Recent measurements of muon capture rates and decay branches in the RCNP or in the RIKEN-RAL facility were presented. These newly aquired data were discussed in several reports on theoretical studies. One major topic is related to the integration of the measured data into widely-used nuclear reaction simulation codes such as PHITS.[2] It was discussed how the nuclear data should be extracted from the measured data and be inputted into the code, in addition to how the results will improve the applicability of the simulation to LLFPs. Another direction in theoretical activities is to further our understanding of nuclear reactions within the framework of modern nuclear theory, such as the effective-mean-field and direct-reaction formalisms, so that more reliable predictions of nuclear data can be made. In addition to these experimental and theoretical studies, a few engineering activities were reported. The talks on the development of a new isotope separation method to chemically isolate LLFPs and on a new superconducting cavity as a key device for realizing intense beam acceleration highlighted the interdisciplinary nature of this project.

The completion of the OEDO beam line was appreciated by the audience. The development history and successful in-beam commissioning were presented. The plan of the first physics experiments was discussed. One envisioned experiment is to extract neutron capture cross sections of the LLFP ^{79}Se from (d, p) reaction cross sections using the so-called surrogate method. The reaction mechanism behind this method was also discussed. The other is to measure excitation functions of proton- and deuteron-induced reactions of ^{107}Pd. The participants also had animated discussions on future experiments using energy-degraded RI beams that will be provided by the OEDO beam line.

[*1] RIKEN Nishina Center
[*2] Center for Nuclear Study, University of Tokyo
[*3] Department of Physics, Tsukuba University
[*4] Department of Advanced Energy Enginnering Science, Kyushu University
[*5] Wako Nuclear Science Center, KEK

References
1) Workshop website: `https://indico2.riken.jp/event/2534`
2) K. Niita *et al.*, Radiat. Meas. **41**, 1080 (2006).

Nishina School 2017

T. Motobayashi[*1] and H. Ueno[*2]

The 11th Nishina School was held from July 24 to August 4, 2017. The school aims at guiding Asian undergraduate students who are deciding their future field of study. A photograph taken at the beginning of the school is shown in Fig. 1. Students and supervisors from Peking University (PKU) and the University of Hong Kong (HKU) joined this 11th School. High-school students from Phillips Exeter Academy, USA, along with their teachers, participated in most of the School programs.

Fig. 1. Photograph of Nishina School 2017 participants.

The 11th School began with self-introductions by the students of PKU and HKU, followed by welcome addresses by Hideto En'yo, Nishina Center Director and Shunichiro Itakura, RIKEN's Executive Director. The first week is dedicated mostly to lectures and training on a few subjects related to the nuclear reaction experiment performed in the second week of the school.

The lectures were on a few basic topics for research, including overviews of nuclear physics and nuclear astrophysics, the function of particle accelerators, and methods of radiation measurements. Other lectures were devoted to radiation safety, paper writing and oral presentation, and issues that researchers may encounter in their future. The subjects of training were electronic-pulse propagation and radiation detection. The detectors, electronics, and data acquisition systems to be used in the experiment in the following week were employed in the training.

The second-week program was focused on the reaction experiment using proton beams from the Pelletron accelerator at RIKEN Nishina Center. The students were divided into four teams, which were in charge of four different types of measurements. They designed the experiment by first evaluating the feasibility of measurements, then set the detectors around the reaction target, and determined the conditions of beam exposure based on their considerations. After the experiment, they analyzed the experimental data obtained,

and finally made presentations on their results. The reaction they studied was the radiative proton capture by the ^{12}C nucleus, which is relevant to the CNO cycle hydrogen burning in stars.

Fig. 2. Experimental setup. Proton beams from the Pelletron accelerator hit a carbon target in the small vacuum chamber, and γ rays were measured by the NaI(Tl) scintillator seen in the center of the photograph.

Figure 2 shows the experimental setup. Proton beams with 1 MeV or 2 MeV energy bombarded a carbon target, which stopped the protons to provide a so-called thick target yield of the ^{12}C(p,γ)^{13}N reaction. Two methods were employed for determination of the resonance yield: detection of "in-beam" γ rays emitted during the collision of the beam with the carbon target, and measurement of ^{13}N activities by detecting positron-annihilation photons or the 511-keV γ line, known as the "activation" technique.

An example of the γ ray spectrum is shown in Fig. 3. It is for the "in-beam" measurement with 2 MeV proton beams. Two distinct peaks, which are of relevance in the experiment, are clearly seen. The four teams could finally extract the capture cross sections for the two resonances in ^{13}N.
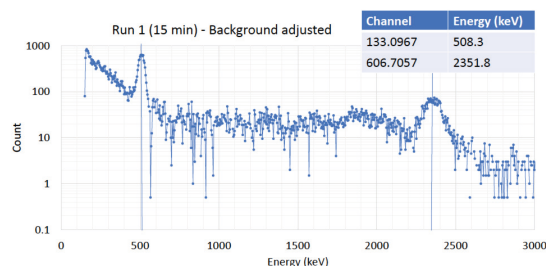
Fig. 3. An example of the γ ray spectra obtained for the "in-beam" measurement for the ^{12}C(p,γ)^{13}N reaction with 2 MeV proton beams. The two γ ray peaks correspond respectively to the two low-lying resonances in ^{13}N.

We thank all the staff members of the Nishina Center who participated and helped the Nishina School 2017.

[*1]   School Master
[*2]   Chair, Nishina School Steering Committee

IUPAP Meetings and Nuclear Science Symposium at Nihon-Bashi

H. En'yo[*1]

IUPAP Commission 12 (C.12) and Working Group 9 (WG.9) meetings were held at the RIKEN Tokyo office in Nihon-Bashi, Tokyo on August 29–30, 2017. Nihon-Bashi means Japan-Bridge, and the 113th element nihonium is named after Nihon (Japan or Nippon). As the name of the place suggests, the office is in a very posh central district of Tokyo and in the same building as Bank of America and Merrill Lynch.

Every two years, the meetings are organized together with the Nuclear Science Symposium (NSS), in which recent progress in nuclear physics and related developments are reviewed and discussed in the presence of invited representatives from national funding agencies worldwide. This year, representatives from South Africa, Canada, France, Italy, Australia, USA, UK, Japan, France, and China participated in the symposium.

During the symposium, special in-camera meetings were held for the representatives of funding agencies. These meetings are meant for representatives to share the progress in nuclear science and exchange the status of research in their countries, as well as to see how their efforts fit into an international framework. The agenda and slides from the symposium can be found at `http://www.triumf.info/hosted/iupap/icnp/nss2017.html`.

Shoji Nagamiya, who chaired the in-camera meetings, presented the following briefing at the end of the IUPAP WG.9 annual general meeting:

(1) The participants of the in-camera meetings recognized that an unprecedented era of nuclear science will be realized, especially with the next-generation of rare isotope beam facilities around the world.

(2) They expressed concerns regarding the effect of open-access policies on large nuclear science laboratories and the implementation of user fees.

(3) They recommended that IUPAP WG.9 may take a more explicit role in international cooperation for large-scale nuclear science projects.

(4) They recommend that IUPAP WG.9 may positively consider as an "international project" a project in which the share of responsibilities is discussed in IUPAP WG.9 from the beginning of the project by including all the stakeholder countries.

(5) They also stressed the importance of small-scale university-based nuclear science laboratories because these are essential training grounds for young scientists.

Similar discussions were also made at the IUPAP WG.9 annual general meeting. Shigeo Koyasu, the executive director of RIKEN, described the future plans for operations of the Rare Isotope Beam Facility at RIKEN. He suggested the possibility of asking the users to bear the cost (collaboration fee) not for electricity, but rather for miscellaneous expenses from the common fund for experiments.

There was a wide-ranging discussion of such user fees in the meeting. A general concern is that, if one facility implements such charges, other facilities would then be forced by their funding agencies to follow suit. This could have serious implications on the scientific productivity and mobility of the international community. Some opinions generally supported by the members were as follows: (1) Beam time should be granted based on scientific excellence. Any payment for beam time contradicts this general principle. (2) There is an established tradition among the user community to share some of the operating costs, but such sharing is not related to beam time. (3) The host institute must be very clear about what these user fees can cover. The funding agencies may prohibit the use of grant funds to pay these, which might cut off a facility's access to talented scientists around the world.

Other issues discussed in IUPAP WG.9 include reports from the Asian Nuclear Physics Association, the US Nuclear Science Advisory Committee, the Five Year Plan for TRIUMF in Canada, the Nuclear Physics European Collaboration Committee, the Latin-America Community, and the South-African Isotope Facility.

[*1] RIKEN Nishina Center

International conference on nuclear physics at storage rings (STORI2017)

M. Wakasugi[*1]

The 10th international conference on nuclear physics at storage rings (STORI2017) was held at Kanazawa from November 13 to 18, 2017. The venue was the Kanazawa theatre (Kageki-za), which is located in the vicinity of the Kanazawa castle. The conference was hosted by RIKEN Nishina center and sponsored by Kanazawa city and Ishikawa prefecture.

(1) Participants and presentations

We had 73 participants in total, and the number of country-specific participants are listed in Table 1. We had 61 presentations in total, and the breakdown of the presentations are as follows: 27 invited talks, 15 oral talks, and 19 poster presentations. Figure 1 shows a conference photograph taken at the Kanazawa castle during the excursion.

(2) Presented topics

The conference started on 0ct. 14th (Tue.), and we had many active discussions during the week. A wide range of topics relevant to storage rings and traps were presented. On Tuesday, M. Steck presented the status of GSI and the rather new facility for decelerated RI beam, including the newly installed CRYRING, and B. Juardo presented the topics on neutron induced reaction at CRYRING. The topics that were presented on physics experiments at ESR/GSI included nuclear reactions such as a proton scattering using EXL and laser spectroscopy. There were four talks on the research going on at CERN, namely the status of the ELENA project, the anti-matter subject at the AD, the anti-proton annihilation experiment in the PANDA project, and the ISOLTRAP equipped by a MRTOF. The current status of the mass measurements using TI-TAN at TRIUMF was reported. The mass measurements at CSRe/IMP-CAS and the status of the new project HIAF were presented as ongoing projects in China. The other mass measurements for exotic nuclei and some related detector developments at R3/RIKEN and MRTOF/RIKEN were presented. The RIKEN RIBF facility and the achievements since its construction were overviewed by H. Sakurai, and the recent results at the SCRIT facility was reported. The status of the NICA project at JINR/Dubna was reported by E. Syresin. Atomic physics topics related to the cryogenic electrostatic storage rings at RIKEN and Max Plank were presented. The high intensity light source for nuclear physics in Romania and the muon $g-2$ experiment at Fermi Lab. were also interesting topics. Experiments on fundamental physics problems such as EDM and CP violation going on at COSY and RIKEN were presented. Finally, two theorists, A. Surzhykov and P. Indelicato, presented the capability of the QED test in a storage ring.

(3) Poster presentation

We had 19 poster presentations on Friday afternoon, and the international advisory committee gave poster awards to L. Varga (GSI), B. Wu (IMP), and H. Arakawa (Saitama U.).

(4) Excursion

In the excursion on Thursday afternoon, we conducted a tour of the Kanazawa castle and the adjacent old town, and organized an experience-based tour on gold leaf craftwork, which is a traditional speciality in Kanazawa. The participants enjoyed and learned the history of Kanazawa and the traditional culture of Japan.

(5) Next STORI2020

In this conference, the international advisory committee decided that the IPM-CSA will host the next STORI conference, which will be held in 2020 at Huizhon in China, where there is a planed cite of HIAF.

(6) Acknowledgment

We would like to specially thank the staffs of Kanazawa Convention Bureau for their great help in organizing the conference.

Table 1. Number of country-specific participants.

Country	Participants	Country	Participants
Japan	37	Canada	1
Germany	15	Romania	1
China	10	Russia	1
Italy	2	U.K.	1
Switzerland	2	Korea	1
France	2	Total	73

*1　RIKEN Nishina Center

Fig. 1. Conference photograph taken at Kanazawa castle.

International symposium on RI beam physics in the 21st century: 10th anniversary of RIBF

T. Isobe,[*1,*2] Y.X. Watanabe,[*1,*6] S. Ota,[*1,*3] N. Aoi,[*4] N. Imai,[*3] T. Suda,[*5] T. Uesaka,[*2] D. Suzuki,[*2] Y. Ichikawa,[*2] T. Nakamura,[*1,*7] K. Yoshida,[*1,*8] and K. Yoneda[*2]

The "International symposium on RI beam physics in the 21st century: 10th anniversary of RIBF" (jointly hosted by the RIBF User Executive Committee and RIKEN Nishina Center) was held on 4th and 5th December, 2017. The RI Beam Factory celebrated its 10th anniversary in 2017. Since it started the delivery of RI beams in 2007, the RIBF has successfully produced a lot of rare isotopes, and completed many in nuclear physics. In the symposium, recent progress in the physics of unstable nuclei, novel technologies in RI-beam experiments, and future activities at RIBF and other RI-beam facilities were discussed.

Fig. 1. Group photo of the symposium. The symposium was held at the large conference room of the RIBF building at RIKEN.

The number of participants was about 120. Figure 1 shows a group photo of the symposium. The program mainly consisted of four physics categories: Nuclear Structure, Equation of State, Nuclear Astrophysics, and Superheavy elements. Four theorists were invited to give review talks about the progress and perspectives of nuclear structure, nuclear astrophysics, light nuclear reactions and heavy nuclear reactions based on the physics outputs from experimental studies curried out in last decade. Further, presentations about the future the RI experimental facility were given: FRIB in USA, NuStar at FAIR in Germany, HIAF in China, and RISP in Korea. Owing to the condensed topics and presentations, the discussion regarding future RI

beam physics was very stimulated in the symposium. The details of the symposium program can be found in Ref. 1).

Finally, as a special session by the RIBF user executive committee, a ceremony to present the RIBF thesis award to two winners was conducted, as shown in Fig. 2, along with a special talk by the recipients. The awards honor the achievements of Dr. Kazuyuki Sekizawa (Faculty of Physics, Warsaw University of Technology) and Dr. Jin Wu (Argonne National Laboratory) for the Ph.D theses titled "Multinucleon Transfer Reactions and Quasifission Processes in Time-Dependent Hartree-Fock Theory" (University of Tsukuba in 2015) and "Beta-Decay Spectroscopy of $Z = 55$–67 Neutron-Rich Nuclei" (Peking University in 2016), respectively. The RIBF Thesis Award was co-hosted by UEC and Nishina Center.

Fig. 2. Ceremony for RIBF theses award 2017. It was presented to Dr. Jin Wu (left) and Dr. Kazuyuki Sekizawa (right). Certificates and plates were given to winners.

References
1) https://indico2.riken.jp/event/2541/.

---

*1   RIBF User Group Executive Committee
*2   RIKEN Nishina Center
*3   Center for Nuclear Study, The University of Tokyo
*4   Research Center for Nuclear Physics, Osaka University
*5   Research Center for Electron-Photon Science, Tohoku University
*6   Wako Nuclear Science Center, Institute of Particle and Nuclear Studies, KEK
*7   Department of Physics, Tokyo Institute of Technology
*8   Department of Physics, Kyoto University

VI. ORGANIZATION AND ACTIVITIES OF RIKEN NISHINA CENTER

(Activities, Members, Publications & Presentations)

1. Organization

1.1 Organization Chartas of March 31, 2018 （End of FY2017）

Theoretical Research Division
- Quantum Hadron Physics Laboratory — Tetsuo Hatsuda
- Strangeness Nuclear Physics Laboratory — Emiko Hiyama

Sub Nuclear System Research Division
- Radiation Laboratory — Hideto En'yo
- Advanced Meson Science Laboratory — Masahiko Iwasaki
- RIKEN BNL Research Center — Hideto En'yo, Deputy Director: Robert Pisarski
  - Theory Group — Kharzeev Dmitri E.
  - Computing Group — Taku Izubuchi
  - Experimental Group — Yasuyuki Akiba
- RIKEN Facility Office at RAL — Philip King

RIBF Research Division
- Radioactive Isotope Physics Laboratory — Hiroyoshi Sakurai
- Spin isospin Laboratory — Tomohiro Uesaka
- Nuclear Spectroscopy Laboratory — Hideki Ueno
- High Energy Astrophysics Laboratory — Toru Tamagawa
- Astro-Glaciology Research Unit — Yuko Motizuki
- Research Group for Superheavy Element — Kosuke Morita
  - Superheavy Element Production Team — Kosuke Morita
  - Superheavy Element Device Development Team — Kouji Morimoto
- Nuclear Transmutation Data Research Group — Hiroyoshi Sakurai
  - Fast RI Data Team — Hideaki Otsu
  - Slow RI Data Team — Toshiyuki Sumikama
  - Muon Data Team — Teiichiro Matsuzaki
- High-Intensity Accelerator R&D Group — Osamu Kamigaito
  - High-Gradient Cavity R&D Team — Naruhiko Sakamoto
  - High-Power Target R&D Team — Hiroki Okuno
- Accelerator Group — Osamu Kamigaito, Deputy Director: Hiroki OKUNO (Intensity Upgrade), Nobuhisa FUKUNISHI (Stable Operation), Masayuki KASE (Energy-Efficiency Management)
  - Accelerator R&D Team — Hiroki Okuno
  - Ion Source Team — Takahide Nakagawa
  - RILAC Team — Eiji Ikezawa
  - Cyclotron Team — Naruhiko Sakamoto
  - Beam Dynamics & Diagnostics Team — Nobuhisa Fukunishi
  - Cryogenic Technology Team — Hiroki Okuno
  - Infrastructure Management Team — Masayuki Kase
- Instrumentation Development Group — Masanori Wakasugi
  - SLOWRI Team — Michiharu Wada
  - Rare RI-ring Team — Masanori Wakasugi
  - SCRIT Team — Masanori Wakasugi
- Research Instruments Group — Hideki Ueno
  - BigRIPS Team — Koichi Yoshida
  - SAMURAI Team — Hideaki Otsu
  - Computing and Network Team — Takashi Ichihara
  - Detector Team — Hiromi Sato
- Accelerator Applications Research Group — Tomoko Abe
  - Ion Beam Breeding Team — Tomoko Abe
  - RI Applications Team — Hiromitsu Haba
- User Liaison and Industrial Cooperation Group — Hideyuki Sakai
  - RIBF User Liaison Team — Ken-ichiro Yoneda
  - Industrial Cooperation Team — Atsushi Yoshida
- Safety Management Group — Yoshitomo Uwamino

President RIKEN — Hiroshi Matsumoto
- Nishina Center Advisory Council
- RBRC Scientific Review Committee (SRC)
- International Advisory Committee for the RIKEN-RAL Muon Facility
- RBRC Management Steering Committee (MSC)

Nishina Center Planning Office

Nishina Center for Accelerator-Based Science — Hideto En'yo
Deputy Director: Hiroyoshi Sakurai
Senior Advisor: Walter F. Henning
Senior Advisor: Yasushige Yano
Senior Advisor: Tohru Motobayashi

- Scientific Policy Committee
- Program Advisory Committee
- Coordination Committee
- Safety Review Committee
- Machine Time Committee
- Public Relations Committee

1.2 Topics in FY2017

In fiscal year 2017, RNC discovered 73 new isotopes. The total number of new isotopes discovered at the RIBF from 2010 will reach about 194 in the near future.

With regard to Superheavy Element Research, RNC succeeded in creating copernicium using GARIS-II which is suitable for hot fusion. It was RNC's first step on the road to search for more new superheavy elements such as element 119.

Having developed new technology to produce a large amount of At-211, RNC has distributed radioisotopes of At-211 to several universities and institutes engaged in radionuclide therapy research.

Year	Date	Topics in Management
2017	Apr. 1	Newly appointed: Director of the RIKEN BNL Research Center: Hideto En'yo
	Aug. 4	Review of the Safety Management Group
	Oct. 30	Review of the Accelerator Applications Research Group
	Nov. 2	Review of the Instrumentation Development Group, the Research Instruments Group and the User Liaison and Industrial Cooperation Group

2. Finances

A transition of the RNC budget for the past five years is shown in following graph.

Million Yen

Year	2013	2014	2015	2016	2017
Million Yen	3,005	2,986	2,800	3,060	3,199
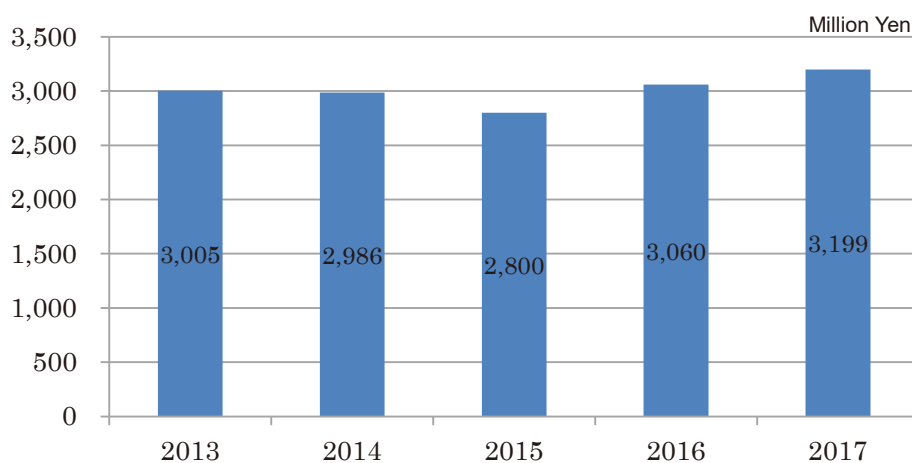
3. Staffing

At the start of FY 2017, there were 165 personnel affiliated with RNC and 392 researchers visiting RNC for research purpose. The following graphs show a breakdown of personnel into six categories as of April 1, 2017, and a transition of the number of each category.

Permanent Researcher
Contract Researcher
Technical staff
Special Postdoctoral Researcher
Junior Research Associate
External researcher

FY2017
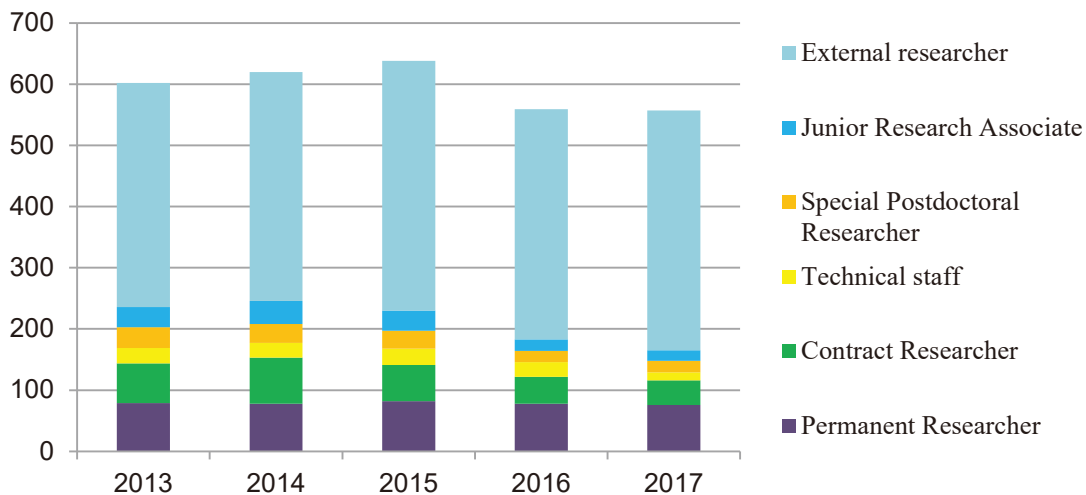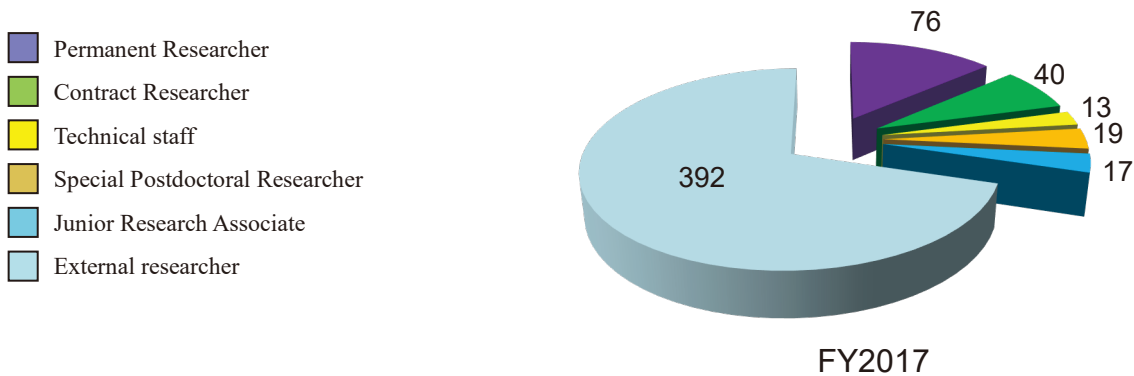
4. Research publication

The number of papers published annually from RNC is shown graphically using the data obtained from Thomson Reuters' Web of Science Documents.
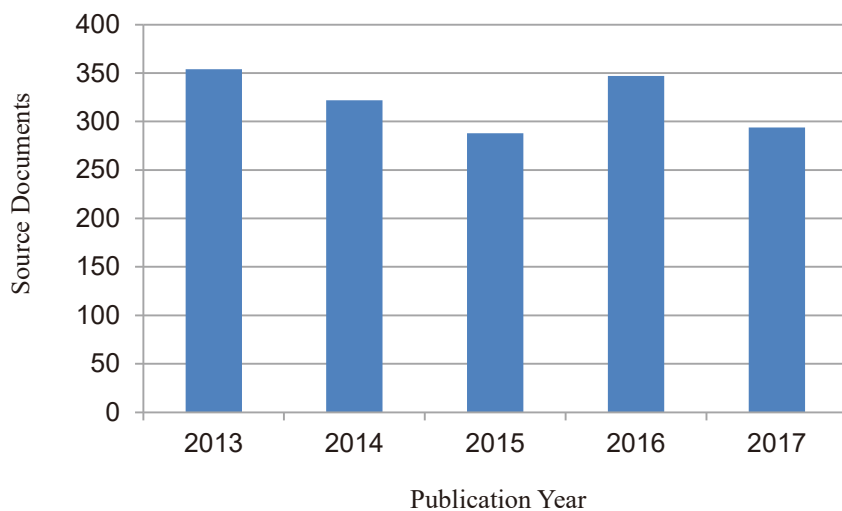
Citation analysis for the past five years

As of April, 2018

Year / Indicators	2013	2014	2015	2016	2017
Total number of papers	354	322	288	347	294
Total number of citations	5250	4503	2866	2329	797
Number of papers in top 10%	58	69	56	51	39
Percentage of papers in top 10%	16.4	21.4	19.4	14.7	13.4
Number of papers in top 1%	7	6	3	3	9
Percentage of papers in top 1%	1.98	1.86	1.04	0.86	3.09

5. Management

Headed by the RNC Director Hideto En'yo, the RIKEN Nishina Center for Accelerator-Based Science (RNC) consists of:

- 8 Laboratories
- 1 Research unit
- 9 Groups with 25 Teams
- 2 overseas research centers with 3 Groups

as of the latter half of FY2017. There are also three 'Partner Institutes' which conduct research in the laboratories set up in RNC. RNC is managed by its Director who takes into consideration the majority decision of the RNC Coordination Committee. The Nishina Center Planning Office under the auspices of President of RIKEN is responsible for administrative matters of RNC. The management of RNC is supported by the following committees:

- Scientific Policy Committee
- Program Advisory Committee
- RIBF Machine-Time Committee
- Public Relations Committee

There are also committees to support the President of RIKEN and/or the Director of RNC such as:

- Scientific Policy Committee
- Nishina Center Advisory Council with three subcommittees
- RBRC Scientific Review Committee (SRC)
- International Advisory Committee for the RIKEN-RAL Muon Facility
- RBRC Management Steering Committee (MSC)

Nishina Center for Accelerator-based Science

Executive Members (as of March 31, 2018)

Hideto EN'YO	Director RNC, Chief Scientist, Director of Radiation Laboratory
Hiroyoshi SAKURAI	Deputy Director (RIBF Research), RNC, Chief Scientist, Radioactive Isotope Physics Laboratory, Group Director, Nuclear Transmutation Data Research Group
Walter F. HENNING	Senior Advisor
Yasushige YANO	Senior Advisor
Tohru MOTOBAYASHI	Senior Advisor

RNC Coordination Committee

The following subjects relevant to the RNC management are deliberated under the chairmanship of the RNC Director:

- Establishment of the new organization or reorganization in RNC

- Personnel management of RNC researchers
- Research themes and research budget
- Approval of the Partner Institutes
- Evaluation of the management of RNC and the response to the recommendations by external evaluation

The RNC Coordination Committee is held monthly.

Members (as of March 31, 2018)

Hideto EN'YO	Director, RNC, Chief Scientist, Radiation Laboratory
Hiroyoshi SAKURAI	Deputy Director, RNC, Chief Scientist, Radioactive Isotope Physics Laboratory, Group Director, Nuclear Transmutation Data Research Group
Walter F. HENNING	Senior Advisor, RNC
Yasushige YANO	Senior Advisor, RNC
Tohru MOTOBAYASHI	Senior Advisor, RNC
Tetsuo HATSUDA	Chief Scientist, Quantum Hadron Physics Laboratory
Masahiko IWASAKI	Chief Scientist, Advanced Meson Science Laboratory
Tomohiro UESAKA	Chief Scientist, Spin isospin Laboratory
Hideki UENO	Chief Scientist, Nuclear Spectroscopy Laboratory, Group Director, Research Instruments Group
Toru TAMAGAWA	Chief Scientist, High Energy Astrophysics Laboratory
Emiko HIYAMA	Chief Scientist, Strangeness Nuclear Physics Laboratory
Kosuke MORITA	Group Director, Research Group for Superheavy Element, Team Leader, Superheavy Element Production Team
Osamu KAMIGAITO	Group Director, Accelerator Group, Group Director, High-Intensity Accelerator R&D Group
Hideyuki SAKAI	Group Director, User Liaison and Industrial Cooperation Group
Hiroki OKUNO	Deputy Group Director, Accelerator Group, Team Leader, Accelerator R&D Team, Team Leader, Cryogenic Technology Team, Team Leader, High-Power Target R&D Team
Nobuhisa FUKUNISHI	Deputy Group Director, Accelerator Group, Team Leader, Beam Dynamics & Diagnostics Team
Masayuki KASE	Deputy Group Director, Accelerator Group, Team Leader, Infrastructure Management Team
Tomoko ABE	Group Director, Accelerator Applications Research Group, Team Leader, Ion Beam Breeding Team
Yoshitomo UWAMINO	Group Director, Safety Management Group
Masanori WAKASUGI	Group Director, Instrumentation Development Group, Team Leader, Rare RI-ring Team, Team Leader, SCRIT Team
Yuko MOTIZUKI	Research Unit Leader, Astro-Glaciology Research Unit
Eiji IKEZAWA	Team Leader, RILAC Team
Takashi ICHIHARA	Vice Chief Scientist, Radioactive Isotope Physics Laboratory, Team Leader, Computing and Network Team
Hideaki OTSU	Team Leader, SAMURAI Team, Team Leader, Fast RI Data Team
Naruhiko SAKAMOTO	Team Leader, Cyclotron Team, Team Leader, High-Gradient Cavity R&D Team
Hiromi SATO	Team Leader, Detector Team
Toshiyuki SUMIKAMA	Team Leader, Slow RI Data Team
Takahide NAKAGAWA	Team Leader, Ion Source Team
Hiromitsu HABA	Team Leader, RI Applications Team
Teiichiro MATSUZAKI	Team Leader, Muon Data Team
Koji MORIMOTO	Team Leader, Superheavy Element Device Development Team
Atsushi YOSHIDA	Team Leader, Industrial Cooperation Team
Koichi YOSHIDA	Team Leader, BigRIPS Team
Ken-ichiro YONEDA	Team Leader, RIBF User Liasison Team
Michiharu WADA	Team Leader, SLOWRI Team
Yasuyuki AKIBA	Vice Chief Scientist, Radiation Laboratory, Group Leader, Experimental Group, RIKEN BNL Research Center
Katsuhiko ISHIDA	Vice Chief Scientist, Advanced Meson Science Laboratory
Tsukasa TADA	Vice Chief Scientist, Quantum Hadron Physics Laboratory
Kanenobu TANAKA	Deputy Group Director, Safety Management Group
Yasushi WATANABE	Deputy Team Leader, RIBF User Liaison Team
Noriko SHIOMITSU	Director, Nishina Center Planning Office

Nishina Center Planning Office

The Nishina Center Planning Office is responsible for the following issues:

- Planning and coordination of RNC's research program and system
- Planning and management of RNC's use of budget
- Public relations activities

Members (as of March 31, 2018)

Noriko SHIOMITSU	Director, Nishina Center Planning Office
Kazunori MABUCHI	Manager, Nishina Center Planning Office, Administration Manager, RBRC, Administration Manager, RIKEN Facility Office at RAL
Keiko IWANO	Deputy Manager, Nishina Center Planning Office
Hiroshi ITO	Deputy Manager, Nishina Center Planning Office, Deputy Administration Manager, RBRC

Yukari ONISHI	Chief, Nishina Center Planning Office
Kumiko SUGITA	Chief, Nishina Center Planning Office
Yuko OKADA	Task-Specific Employee
Aiko KAWAMURA	Task-Specific Employee
Miyoko NAITO	Task-Specific Employee
Rie KUWANA	Temporary Staff

Scientific Policy Committee

The Scientific Policy Committee deliberates on the following issues:

- Research measures and policies of RNC
- Administration of research facilities under RNC's management

The Committee members are selected among professionals within and outside RNC. The members were not chosen nor the Committee held in FY2017.

Program Advisory Committee

The Program Advisory Committee reviews experimental proposals submitted by researchers and reports the approval/disapproval of the proposals to the RNC Director. The Committee also reports to the RNC Director the available days of operation at RIBF or the Muon Facility at RAL allocated to researchers. The Committee is divided into three categories according to the research field.

- Nuclear Physics Experiments at RIBF (NP-PAC): academic research in nuclear physics
- Materials and Life Science Researches at RNC (ML-PAC): academic research in materials science and life science
- Industrial Program Advisory Committee (In-PAC): non-academic research

Program Advisory Committee for Nuclear Physics Experiments at RI Beam Factory (NP-PAC)

The 18th NP-PAC was held on December 7−9, 2017 at RIBF.

Members (as of March 31, 2018)

Angela BRACCO (Chair)	INFN
Dieter ACKERMANN	GANIL
Andrei ANDREYEV	University of York
Ikuko HAMAMOTO	Lund University
Robert V.F. JANSSENS	University of North Carolina at Chapel Hill
Augusto O. MACCHIAVELLI	Lawrence Berkeley National Laboratory
David J. MORRISSEY	Michigan State University
Tomofumi NAGAE	Kyoto University
Hitoshi NAKADA	Chiba University
Alexandre OBERTELLI	Technische Universität Darmstadt
Kazuyuki OGATA	RCNP, Osaka University
Tomas RAUSCHER	University of Basel
Kimiko SEKIGUCHI	Tohoku University
Haik SIMON	GSI
Piet VAN DUPPEN	K.U.Leuven
Yuhu ZHANG	Institute of Modern Physics, CAS

Program Advisory Committee for Materials and Life Science Researches at RIKEN Nishina Center (ML-PAC)

The 15th ML-PAC was held on January 11−12, 2018 at RIBF.

Members (as of March 31, 2018)

Adrian HILLIER (Chair)	ISIS, RAL(UK)
Toshiyuki AZUMA	RIKEN
Ryosuke KADONO	Institute of Materials Structure Science(KEK)
Atsushi KAWAMOTO	Hokkaido University
Norimichi KOJIMA	Toyota RIKEN
Kenya KUBO	ICU
Philippe MENDELS	Universite Paris-SUD(France)
Atsushi SHINOHARA	Osaka University
Shukri SULAIMAN	Universiti Sains Malaysia (Malaysia)
Hiroyuki YAMASE	NIMS
Shigeo YOSHIDA	Thera-Projects
Xu-Guang ZHENG	Saga University

Industrial Program Advisory Committee (In-PAC)

The 7th In-PAC was held on January 19, 2018 at RNC.

Members (as of March 31, 2018)

Akihiro IWASE (Chair)	Osaka Prefecture University
Toshiyuki AZUMA	RIKEN
Kenya KUBO	International Christian University
Hitoshi NAKAGAWA	National Agriclture and Food Research Organization.
Nobuhiko NISHIDA	Toyota Physical and Chemical Research Institute
Yasushi AOKI	Sumitomo Heavy Industries, Ltd

Safety Review Committee

The Safety Review Committee is composed of two sub committees, the Safety Review Committee for Accelerator Experiments and the Hot-Lab Safety Review Committee. These Committees review the safety regarding the usage of radiation generating equipment based on the proposal submitted to the RNC Director from the spokesperson of the approved experiment.

Safety Review Committee for Accelerator Experiments

Members (as of March 31, 2018)

Hiromi SATO (Chair)	Team Leader, Detector Team
Kouji MORIMOTO	Team Leader, Superheavy Element Device Development Team
Eiji IKEZAWA	Team Leader, RILAC Team
Hiromitsu HABA	Team Leader, RI Applications Team
Shinichiro MICHIMASA	Assistant Prof., Center for Nuclear Study, University of Tokyo
Hidetoshi YAMAGUCHI	Lecturer, Center for Nuclear Study, University of Tokyo
Yutaka WATANABE	Associate Professor, High Energy Accelerataor Reserch Organization, KEK
Atsushi YOSHIDA	Team Leader, Industrial Cooperation Team
Koichi YOSHIDA	Team Leader, BigRIPS Team
Naoki FUKUDA	Nishina Center Research Scientist, BigRIPS Team
Naruhiko SAKAMOTO	Team Leader, Cyclotron Team
Daisuke SUZUKI	Research Scientist, Radioactive Isotope Physics Laboratory
Juzo ZENIHIRO	Research Scientist, Spin Isospin Laboratory
Yuichi ICHIKAWA	Research Scientist, Nuclear Spectroscopy Laboratory

Ex officio members

Yoshitomo UWAMINO	Group Director, Safety Management Group
Kanenobu TANAKA	Deputy Group Director, Management Group
Hisao SAKAMOTO	Nishina Center Technical Scientist, Safety Management Group

Hot-Lab Safety Review Committee

Members (as of March 31, 2017)

Masako IZUMI (Chair)	Senior Research Scientist, Ion Beam Breeding Team
Yoshitomo UWAMINO	Group Director, Safety Management Group
Hisao SAKAMOTO	Nishina Center Technical Scientist, Safety Management Group
Hiroki MUKAI	Assigned Employee, Safety Management Group
Kanenobu TANAKA	Deputy Group Director, Safety Management Group
Hiromitsu HABA	Team Leader, RI Applications Team

RIBF Machine Time Committee

Upon request of the RNC Director, the RIBF Machine Time Committee deliberates on the machine time schedule of RIBF, and reports the results to him.

Members (as of March 31, 2018)

Hideyuki SAKAI (Chair)	Group Director, User Liaison and Industrial Cooperation Group
Tomoko ABE	Group Director, Accelerator Applications Research Group
Nobuhisa FUKUNISHI	Deputy Group Director for Stable and Efficient Operation, Accelerator Group
Osamu KAMIGAITO	Group Director, Accelerator Group
Masayuki KASE	Deputy Group Director for Energy -Effciency Management, Accelerator Group
Kouji MORIMOTO	Team Leader, Superheavy Element Research Device Development Team
Hiroki OKUNO	Deputy Group Director for Intensity Upgrade, Accelerator Group

Hiroyoshi SAKURAI   Chief Scientist, Radioactive Isotope Physics Laboratory
Hideki UENO   Chief Scientist, Nuclear Spectroscopy Laboratory, Group Director, Research Instruments Group
Tomohiro UESAKA   Chief Scientist, Spin Isospin Laboratory
Yoshitomo UWAMINO   Group Director, Safety Management Group
Masanori WAKASUGI   Group Director, Instrumentation Development Group
Koichi YOSHIDA   Team Leader, BigRIPS Team
Ken-ichiro YONEDA   Team Leader, RIBF User Liasion Team

External members

Kentaro YAKO   Associate Professor, Center for Nuclear Study, University of Tokyo
Hidetoshi YAMAGUCHI   Lecturer, Center for Nuclear Study, University of Tokyo
Michiharu WADA   Professor, High Energy Accelerataor Reserch Organization, KEK

Observers

Hideto EN'YO   Director, RNC
Susumu SHIMOURA   Director, Center for Nuclear Study, University of Tokyo
Hiroari MIYATAKE   Director, KEK Wako Nuclear Science Center
Hiromitsu HABA   Team Leader, RI Applications Team
Kosuke MORITA   Group Director, Research Group for Superheavy Element
Tohru MOTOBAYASHI   Senior Advisor, RNC
Hideaki OTSU   Team Leader, SAMURAI Team
Atsushi YOSHIDA   Team Leader, Industrial Cooperation Team
Kanenobu TANAKA   Deputy Group Director, Safety Management Group
Tadaaki ISOBE   Senior Reserch Scientist, Radioactive Isotope Physics Laboratory
Kazunori MABUCHI   Manager, Nishina Center Planning Office

Public Relations Committee

Upon request of the RNC Director, the Public Relations Committee deliberates and coordinates the following matters:

- Creating public relations system for RNC
- Prioritization of the public relations activities for RNC
- Other general and important matters concerning the public relations of RNC

Members (as of March 31, 2018)

Noriko SHIOMITSU (Chair)   Director, Nishina Center Planning Office
Hiroyoshi SAKURAI   Deputy Director, RNC, Chief Scientist, Radioactive Isotope Physics Laboratory
Tetsuo HATSUDA   Chief Scientist, Quantum Hadron Physics Laboratory
Tohru MOTOBAYASHI   Senior Advisor
Walter F. HENNING   Senior Advisor
Yasushige YANO   Senior Advisor
Masahiko IWASAKI   Chief Scientist, Advanced Meson Science Laboratory
Tomohiro UESAKA   Chief Scientist, Spin isospin Laboratory
Hideki UENO   Chief Scientist, Nuclear Spectroscopy Laboratory, Group Director, Research Instruments Group
Toru TAMAGAWA   Chief Scientist, High Energy Astrophysics Laboratory
Emiko HIYAMA   Chief Scientist, Strangeness Nuclear Physics Laboratory
Kosuke MORITA   Group Director, Research Group for Superheavy Element
Osamu KAMIGAITO   Group Director, Accelerator Group
Hideyuki SAKAI   Group Director, User Liaison and Industrial Cooperation Group

RBRC Management Steering Committee (MSC)

RBRC MSC is set up according to the Memorandum of Understanding between RIKEN and BNL concerning the collaboration on the Spin Physics Program at the Relativistic Heavy Ion Collider (RHIC). The 23rd MSC was held on June 15, 2017.

Members (as of June 15, 2017)

Yoichiro MATSUMOTO   Executive Director, RIKEN
Shoji NAGAMIYA   Science Advisor, RIKEN
Tetsuo HATSUDA   Program Director, RIKEN Interdisciplinary Theoretical and Mathematical Sciences Program
Berndt MUELLER   Associate Laboratory Director for Nuclear and Particle Physics, BNL
Satoshi OZAKI   Senior Scientist Emeritus, BNL
David LISSAUER   Deputy Chair, Physics Department, BNL

6. International Collaboration

Country	Partner Institute	Objects	RNC contact person
Austria	Stefan Meyer Institute for Subatomic Physics	Experimental and theoretical hadron physics, especially in exotic hadronic atoms and meson and baryon nuclear bound states	Masahiko IWASAKI, Chief Scientist, Advanced Meson Science Laboratory
China	China Nuclear Physics Society	Creation of the council for China -Japan research collaboration on nuclear physics	Hiroyoshi SAKURAI, Deputy Director, RNC, Chief Scientist, Radioactive Isotope Physics Laboratory
	Peking University	Nuclear Science	Hiroyoshi SAKURAI, Deputy Director, RNC, Chief Scientist, Radioactive Isotope Physics Laboratory
	Institute of Modern Physics, Chinese Academy of Science	Physics of heavy ions	Hiroyoshi SAKURAI, Deputy Director, RNC, Chief Scientist, Radioactive Isotope Physics Laboratory
	School of Nuclear Science and Technology, Lanzhou University	Framework	Yue MA, Senior Research Scientist, Advanced Meson Science Laboratory
	School of Physics, Nanjing University	Framework	Emiko HIYAMA, Chief Scientist, Strangeness Nuclear Physics Laboratory
	Department of Physics, Faculty of Science, The Univ. of Hong Kong	Experimental and educational research collaboration in the area of experimental nuclear physics	Hiroyoshi SAKURAI, Deputy Director, RNC, Chief Scientist, Radioactive Isotope Physics Laboratory
	School of physics, Nankai University	Framework	Emiko HIYAMA, Chief Scientist, Strangeness Nuclear Physics Laboratory
Finland	University of Jyvaskyla	Basic nuclear physics and related instrumentation	Michiharu WADA, Team Leader, SLOWRI Team
France	National Institute of Nuclear Physics and Particle Physics (IN2P3)	Physics of heavy ions	Tohru MOTOBAYASHI, Senior Advisor, RNC
	CNRS, CEA,GANIL, Université Paris Sud, etc.	Creation of an International Associated Laboratory (LIA) French-Japanese International Associated Laboratory for Nuclear Structure Problems	Tomohiro UESAKA, Chief Scientist, Spin Isospin Laboratory
	CEA-DSM	The use of MINOS device at RIKEN	Tomohiro UESAKA, Chief Scientist, Spin Isospin Laboratory
	SIMEM Graduate School, Department of Physics, Caen University	Framework	Tohru MOTOBAYASHI, Senior Advisor, RNC
	Centre National de la Rocherche Scientifique（CSRS） Commissariat A L'Energie Atomique Et Aux Energies Alternatives (CEA)	Research Collaboration in EXPAND （Exploration Across the Neutron Dripline) project	Tomohiro UESAKA, Chief Scientist, Spin Isospin Laboratory
Germany	Technische Universität München	Nuclear physics, hadron physics, nuclear astrophysics	Emiko HIYAMA, Chief Scientist, Strangeness Nuclear Physics Laboratory
	GSI	Physics of heavey ions and accelerator	Hiroyoshi SAKURAI, Deputy Director, RNC, Chief Scientist, Radioactive Isotope Physics Laboratory
	Department of Physics, Technische Universität Darmstadt	Framework	Emiko HIYAMA, Chief Scientist, Strangeness Nuclear Physics Laboratory
Hungary	The Institute of Nuclear Research of the Hungarian Academy of Sciences (ATOMKI)	Nuclear physics, Atomic Physics	Tomohiro UESAKA, Chief Scientist, Spin Isospin Laboratory
Indonesia	ITB, UNPAD, ITS, UGM, UI	Material science using muons at the RIKEN-RAL muon facility	Masahiko IWASAKI, Chief Scientist, Advanced Meson Science Laboratoy
	Universitas Hasanuddin	Agricultural science and related fields involving heavy-ion beam mutagenesis using Indonesian crops	Tomoko ABE, Group Director, Accelerator Applications Research Group
Italy	Applied Physics Division, National Institute for New Technologies, Energy and Environment (ENEA)	Framework	Tohru MOTOBAYASHI, Senior Advisor, RNC
	European Center for Theoretical Studies in Nuclear Physics and Related Areas (ECT*)	Theoretical physics	Tetsuo HATSUDA, Chief Scientist, Quantum Hadron Physics Laboratory

Country	Partner Institute	Objects	RNC contact person
Korea	Seoul National University	Nishina School	Hiroyoshi SAKURAI, Deputy Director, Chief Scientist, Radioactive Isotope Physics Laboratory
	Department of Physics, Kyungpook National University	Framework	Tomohiro UESAKA, Chief Scientist, Spin Isospin Laboratory
	College of Science, Yonsei University	Framework	Tomohiro UESAKA, Chief Scientist, Spin Isospin Laboratory
	Department of Physics, Korea University	Framework	Hideto EN'YO, Chief Scientist, Radiation Laboratory
	College of Natural Science, Ewha Women's University	Framework	Tomohiro UESAKA, Chief Scientist, Spin Isospin Laboratory
	College of Natural Sciences, INHA Univ.	Framework	Emiko HIYAMA, Chief Scientist, Strangeness Nuclear Physics Laboratory
Malaysia	Universiti Sains Malaysia	Muon Science	Isao WATANABE, Senior Research Scientist, Advanced Meson Science Laboratoy
Poland	the Henryk Niewodniczanski Institute of Nuclear Physics, Polish Academy of Sciences(IFPAN)	Framework	Hiroyoshi SAKURAI, Deputy Director, RNC, Chief Scientist, Radioactive Isotope Pfysicis Laboratory
Romania	"Horia Hulubei" National Institute of Physics and Nuclear Engineering Bucharest-Magurele, Romania	Framework	Tomohiro UESAKA, Chief Scientist, Spin Isospin Laboratory
Russia	Joint Institute for Nuclear Research (JINR)	Framework	Tomohiro UESAKA, Chief Scientist, Spin Isospin Laboratory
	Russian Research Center "Kurchatov Institute"	Framework	Hiroyoshi SAKURAI, Tomohiro UESAKA, Osamu KAMIGAITO, Masanori WAKASUGI
Switzerland	Paul Scherrer Institute	Improve the performance and reliability of accelerator systems	Osamu KAMIGAITO, Director, Accelerator Group
	CERN	RD-51 R&D programme for micro-pattern gas detectors (MPGD)	Hideto EN'YO, Chief Scientist, Radiation Laboratory
	CERN	Collaboration in the ALICE Experiment as an Associate Member	Hideto EN'YO, Chief Scientist, Radiation Laboratory
UK	The Science and Technology Facilities Council	Muon science using the ISIS Facility at the Rutherford Appleton Laboratory	Philip KING, Director of RIKEN-RAL muon facility
	University of Surrey	Theoretical physics	Tetsuo HATSUDA, Chief Scientist, Quantum Hadron Physics Laboratory
USA	BNL	The Spin Physics Program at the Relativistic Heavy Ion Collider (RHIC)	Hideto EN'YO, Chief Scientist, Radiation Laboratory
	Columbia University	The development of QCDCQ	Taku IZUBUCHI, Group Leader, Computing Group, RBRC
	Michigan State University	Comprehensive The use of TPC (Time Projection Chamber)	Tomohiro UESAKA, Chief Scientist, Spin Isospin Laboratory Hiroyoshi SAKURAI, Deputy Director, RNC Chief Scientist, Radioactive Isotope Physics Laboratory, Tadaaki ISOBE, Senior Research Scientist, Radioactive Isotope Physics Laboratory
Vietnam	Vietnam Atomic Energy Commission	Framework	Tohru MOTOBAYASHI, Senior Advisor, RNC
	Institute of Physics, Vietnam Academy of Science and Technology	Framework	Hiroyoshi SAKURAI, Deputy Director, RNC, Chief Scientist, Radioactive Isotope Physics Laboratory
Europe	European Nuclear Science and Application Research2	Framework	Tomohiro UESAKA, Chief Scientist, Spin Isospin Laboratory

7. Awards

Awardee, Laboratory / Team	Award	Organization	Date
The Research Group for Superheavy Element	HAPPY NEWS 2016	The Japan Newspaper Publishers & Editors Association	Apr. 8
The Element 113 Research Group	The 2017 48th Seiun Awards Non-Section category	The Japan Science Fiction Convention	Aug. 26
Yusuke KAZAMA, Contract Researcher at the Ion Breeding Team	BSJ Encouragement Prize	The Botanical Society of Japan(BSJ)	Sep. 9
Naoki KIMURA, Student Trainee at the SLOWRI Team	The Young Scientist Award	The Atomic Collision Society of Japan	Oct. 11
Rachid NOUICER, Visiting Scientist at the Experiment Group of the RIKEN BNL Research Center	APS Fellow	The Atomic Collision Society of Japan	Oct. 12
Kosuke MORITA, Group Director of the Research Group for Superheavy Element	The 76th Western Japan Culture Award	Nishi Nihon Shimbunsha	Nov. 13
Taiki TANAKA, Junior Research Associate at the Superheavy Element Production Team, the members of the Research Group for Superheavy Element	Papers of Editors' Choice	The Physical Society of Japan	Dec. 14
Hiroshi SUZUKI, Visiting Scientist at Quantum Hadron Physics Laboratory	The 2017 Yukawa-Kimura Prize	Yukawa Institute for Theoretical Physics, Kyoto University	Nov. 16
Hiromitsu HABA, Team Leader at the RI Applications Team	The BRAVE Prize and the Cosmo Bio Awar	Cosmo Bio	Mar. 5
Yukari MATSUO, Senior Visiting Scientist at Nuclear Spectroscopy Laboratory	The 8th Promotion and Nurturing of Female Researchers Contribution Award (Kodate Kashiko Award)	The Japan Society of Applied Physics (JSAP)	Mar. 17
Naoki KIMURA, Student Trainee at the SLOWRI Team	The 6th Student Presentation Award	The Physical Society of Japan	Mar. 23
Sohtaro KANDA, Special Postdoctoral Researcher at the Advanced Meson Science Laboratory	The 4th Student Encouragement Award for FY2017	The Society of Muon and Meson Science of Japan	Mar. 23
Sohtaro KANDA, Special Postdoctoral Researcher at the Advanced Meson Science Laboratory	The 12th (2018) Young Scientist Award	The Physical Society of Japan	Mar. 23
Hajime TOGASHI, Special Postdoctoral Researcher at the Strangeness Nuclear Physics Laboratory	The 12th (2018) Young Scientist Award	The Physical Society of Japan	Mar. 23
Gaku MITSUKA, RBRC Researcher at the Experiment Group of the RIKEN BNL Research Center	The 12th (2018) Young Scientist Award	The Physical Society of Japan	Mar. 23

8. Brief overview of the RI Beam Factory

Intensity of Primary Beams

Achieved beam intensities (as of March 2018)

^{238}U	70 pnA (345 MeV/nucleon, Nov. 2017)
^{124}Xe	102 pnA (345 MeV/nucleon, Apr. 2016)
^{86}Kr	30 pnA (345 MeV/nucleon, Nov. 2007)
^{78}Kr	486 pnA (345 MeV/nucleon, May 2015)
^{70}Zn	250 pnA (345 MeV/nucleon, May 2017)
^{48}Ca	730 pnA (345 MeV/nucleon, Nov. 2016)
^{18}O	1000 pnA (345 MeV/nucleon, Jun. 2010)
^{14}N	400 pnA (250 MeV/nucleon, Oct. 2010)
^{4}He	1000 pnA (250 MeV/nucleon, Oct. 2009)
d	1000 pnA (250 MeV/nucleon, Oct. 2010)
pol. d	120 pnA, $P{\sim}80\%$ (250 MeV/nucleon, May 2015)

History of Beam Intensity Upgrade
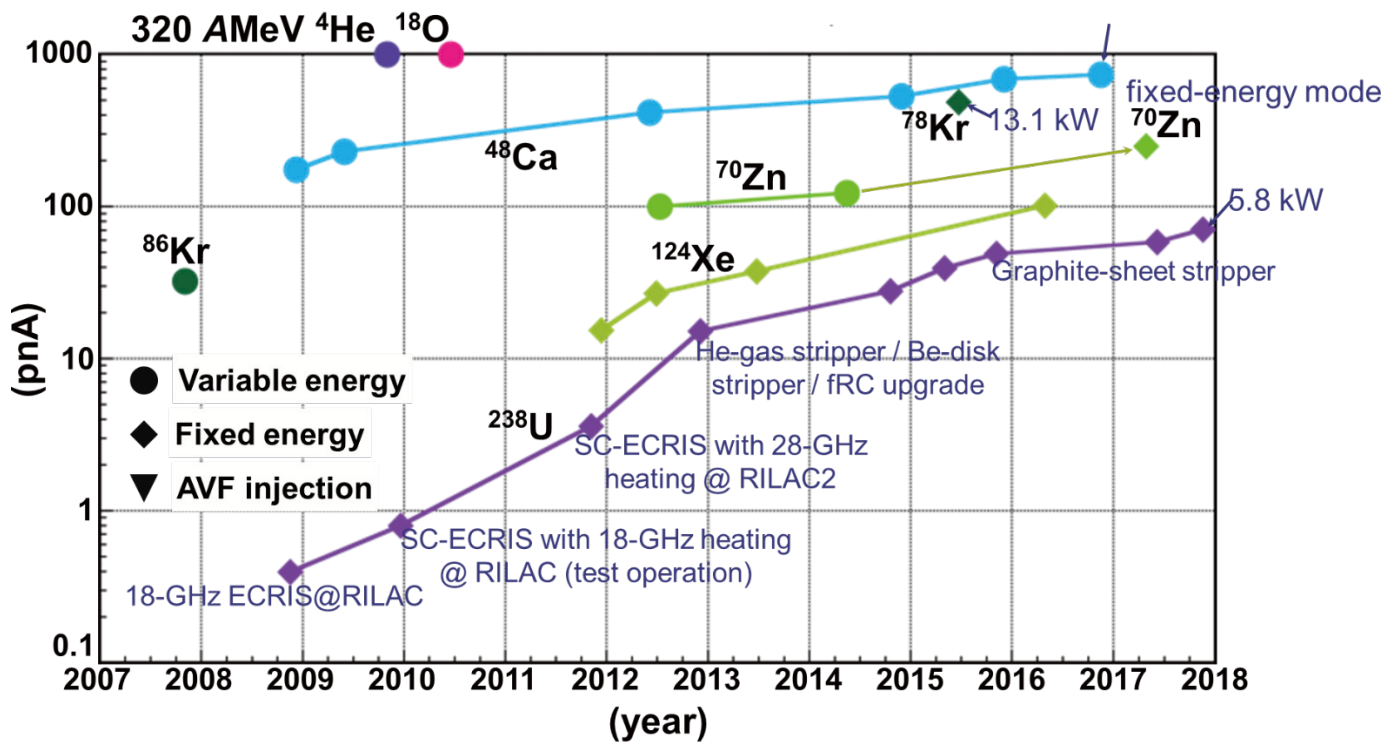
Beam energies are 345 AMeV if it is not explicitly written.

Total beam time for experiments
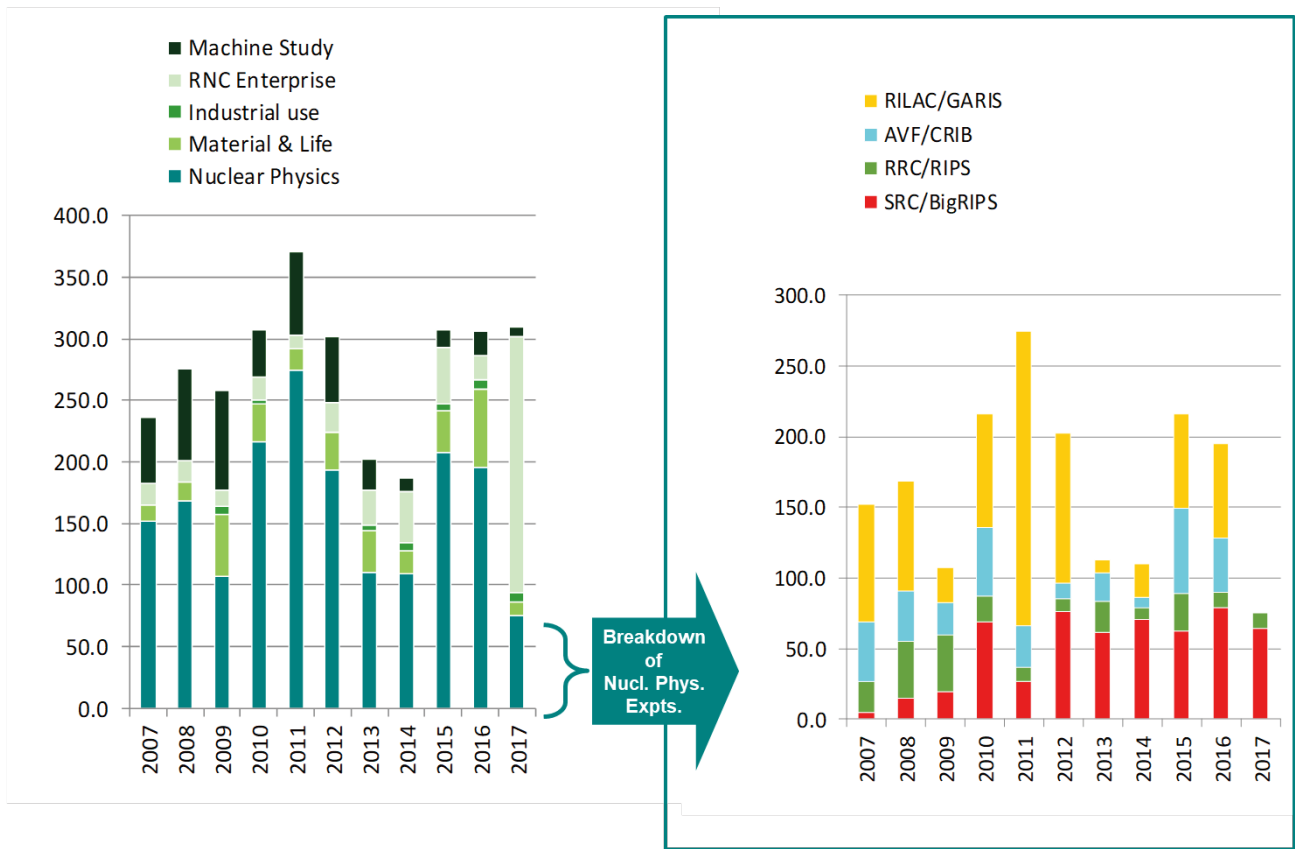
Total beam time allocated to BigRIPS experiments
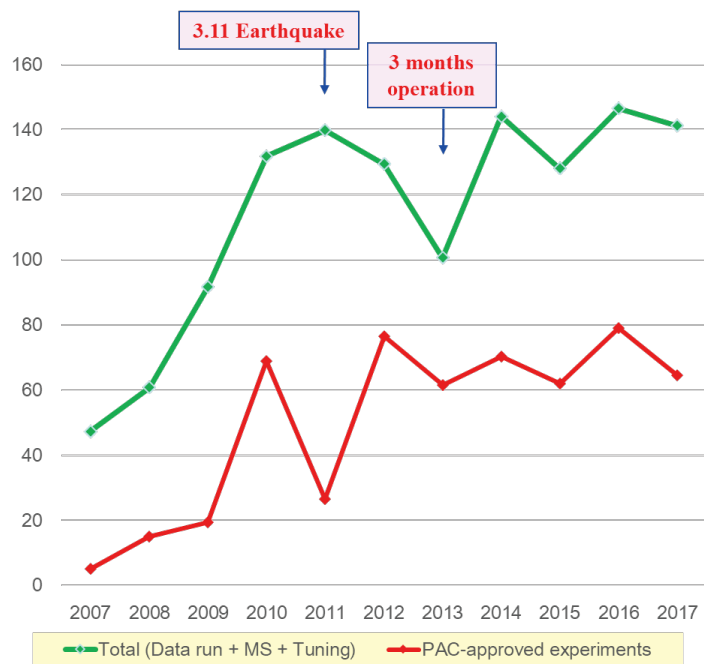
Theoretical Research Division
Quantum Hadron Physics Laboratory

1. Abstract

Atomic nuclei are made of protons and neutrons bound by the exchange of pion and other mesons. Also, protons and neutrons are made of quarks bound by the exchange of gluons. These strong interactions are governed by the non-Abelian gauge theory called the quantum chromodynamics (QCD). On the basis of theoretical and numerical analyses of QCD, we study the interactions between the nucleons, properties of the dense quark matter realized at the center of neutron stars, and properties of the hot quark-gluon plasma realized in the early Universe. Strong correlations common in QCD and cold atoms are also studied theoretically to unravel the universal features of the strongly interacting many-body systems. Developing perturbative and non-perturbative techniques in quantum field theory and string theory are of great importance not only to solve gauge theories such as QED and QCD, but also to find the theories beyond the standard model of elementary particles. Various theoretical approaches along this line have been attempted.

2. Major Research Subjects

(1) Perturbative and non-perturbative methods in quantum field theories
(2) Theory of spontaneous symmetry breaking
(3) Lattice gauge theory
(4) QCD under extreme conditions
(5) Nuclear and atomic many-body problems

3. Summary of Research Activity

(1) Perturbative and non-perturbative methods in quantum field theories
(1-1) 10th order QED calculation and the lepton anomalous magnetic moments
First preliminary value of the tenth-order QED contribution to the electron anomalous magnetic moment $a_e = (g−2)/2$ was reported by us in 2012. Since then, we have been improving and establishing its accuracy: We reevaluated the most difficult and large set of the Feynman diagrams by using advanced techniques of numerical calculation especially suitable to RIKEN's supercomputer. As a result, we have obtained precise values for the eighth- and tenth-order terms. Assuming the validity of the standard model, it leads to the world-best value of the fine-structure constant $\alpha^{-1}(a_e) = 137.035\ 999\ 1570(29)(27)(18)(331)$, where uncertainties are from the eighth-order term, tenth-order term, hadronic and electroweak terms, and the experimental measurement of a_e. This is the most precise value of α available at present in the world and provides a stringent constraint on possible theories beyond the standard model.

(1-2) Picard–Lefschetz theory and the sign problem
Understanding strongly-correlated quantum field theories and many-body systems has been one of the ultimate goals in contemporary physics. Exact diagonalization of a Hamiltonian provides us with complete information on the system; however, it usually requires the huge computational cost and is limited to small systems. For large systems, numerical simulation on discretized spacetime lattice with quantum Monte Carlo method is a powerful ab initio tool based on the importance sampling. In many quantum systems of great interest, however, it suffers from the so-called sign problem; large cancellation occurs between positive and negative quantities to obtain physical signals, so that the computational time grows exponentially with the system size. So far, many attempts have been proposed overcome the sign problem, which include the two promising candidates, the complex Langevin method and the Lefschetz-thimble method. In particular, the Lefschetz-thimble approach is a generalization of the steepest descent method for multiple oscillatory integrals. In the past few years, we have studied extensively the mathematical basis of the Lefschetz-thimble method as well as its practical applications to quantum systems such as the real-time path integral for quantum tunneling, zero-dimensional bosonic and fermionic models, the one-site Hubbard model, and Polyakov-loop effective models for QCD. We have shown that the interference among multiple Lefschetz thimbles is important to reproduce the general non-analytic behavior of the observables as a function of the external parameter. Such an interference is a key to understand the sign problem of finite-density QCD.

(1-3) Functional renormalization group
• 　　BEC-BCS crossover in cold fermionic atoms
We have developed a fermionic functional renormalization group (FRG) and applied this method to describe the superfluid phase transition of the two-component fermionic system with an attractive contact interaction. The connection between the fermionic FRG approach and the conventional Bardeen-Cooper-Schrieffer (BCS) theory with Gorkov and Melik-Barkhudarov (GMB) correction was clarified in the weak coupling region by using the renormalization group flow of the fermionic four-point vertex with particle-particle and particle-hole scatterings. To go beyond the BCS+GMB theory, coupled FRG flow equations of the fermion self-energy and the four-point vertex are studied under an Ansatz concerning their frequency/momentum dependence. We found that the fermion self-energy turns out to be substantial even in the weak coupling regime, and the frequency dependence of the four-point vertex is essential to obtain the correct asymptotic-ultraviolet behavior of the flow for the self-energy. The superfluid transition temperature and the associated chemical potential were evaluated in the region of negative scattering lengths.
• 　　Tricritical point of the superconducting transition
The order of the phase transition in the Abelian Higgs model with complex scalar fields became of interest because of the analyses of the spontaneous symmetry breaking due to radiative corrections in 3+1 dimensions, and of a superconductor near the critical point with the dimensionally reduced Ginzburg-Landau theory. Indeed, the fluctuations of the gauge field were of great importance and may even turn the second-order transition to first-order at least for strongly type-I superconductors. We analyzed the order of the superconducting phase transition via the functional renormalization group approach: We derived for the first time fully analytic expressions for the β functions of the charge and the self-coupling in the Abelian Higgs model with N-component scalar field in $d = 3$ dimensions. The result supports the existence of two charged fixed-points: an infrared (IR) stable fixed point describing a second-order phase transition and a tricritical fixed

point controlling the region of the parameter space that is attracted by the former one. It was found that the region separating first and second-order transitions can be uniquely characterized by the critical Ginzburg-Landau parameter, $\kappa_c \approx 0.62/\sqrt{2}$ for N=1.

- Chiral dynamics under strong magnetic field

The magnetic field is not only interesting as a theoretical probe to the dynamics of QCD, but also important in cosmology and astrophysics: A class of neutron stars called magnetars has a strong surface magnetic field of order 10^{10} T while the primordial magnetic field in early Universe is estimated to be even as large as $\sim 10^{19}$ T. In non-central heavy-ion collisions at RHIC and LHC, a magnetic field of the strength $\sim 10^{15}$ T perpendicular to the reaction plane could be produced and can have impact on the thermodynamics and transport properties of the quark-gluon plasma. We investigated the quark-meson model in a magnetic field using the functional renormalization group equation beyond the local-potential approximation. We considered anisotropic wave function renormalization for mesons in the effective action, which allows us to investigate how the magnetic field distorts the propagation of neutral mesons. We found that the transverse velocity of mesons decreases with the magnetic field at all temperatures. Also, the constituent quark mass is found to increase with magnetic field, resulting in the crossover temperature that increases monotonically with the magnetic field.

(1-4) Emergent spacetime

In quantum field theories, symmetry plays an essential and exceptional role. Focusing on some proper symmetry and delving into its meaning have been proven to be one of the most fruitful strategies. A recent example is the SO(2, 4) symmetry in AdS/CFT correspondence which leads to unexpected connection between gravity and gauge theory defined in different dimensions. We offer another example of quantum field theory where symmetry plays a central role and reveals interesting phenomena: Our focal point is the global conformal symmetry in two dimensional conformal field theory (2d CFT), which is homomorphic to SL(2, R). We have shown that 2d CFT admits a novel quantization which we call dipolar quantization. Usually the study of the quantum field theory starts by defining the spacetime where the field is situated. On the other hand, in our case, we first obtain quantum system and then the nature of spacetime emerges. This is in accordance with the general ideas of emergent spacetime such as those discussed in matrix models.

(2) Theory of spontaneous symmetry breaking

(2-1) Dispersion relations of Nambu-Goldstone modes at finite temperature and density

We clarified the dispersion relations of Nambu-Goldstone (NG) modes associated with spontaneous breaking of internal symmetries at finite temperature and/or density. We showed that the dispersion relations of type-A and type-B NG modes are linear and quadratic in momentum, whose imaginary parts are quadratic and quartic, respectively. In both cases, the real parts of the dispersion relations are larger than the imaginary parts when the momentum is small, so that the NG modes can propagate for long distances. We derived the gap formula for NG modes in the presence of explicit symmetry breaking. We also discussed the gapped partners of type-B NG modes, when type-A and type-B NG modes coexist.

(2-2) Effective field theory for spacetime symmetry breaking

We studied the effective field theory for spacetime symmetry breaking from the local symmetry point of view. By gauging spacetime symmetries, the identification of Nambu-Goldstone (NG) fields and the construction of the effective action were performed based on the breaking pattern of diffeomorphism, local Lorentz, and isotropic Weyl symmetries as well as the internal symmetries including possible central extensions in nonrelativistic systems. Such a local picture provides a correct identification of the physical NG fields, while the standard coset construction based on global symmetry breaking does not. We also revisited the coset construction for spacetime symmetry breaking: Based on the relation between the Maurer-Cartan one-form and connections for spacetime symmetries, we classified the physical meanings of the inverse Higgs constraints by the coordinate dimension of broken symmetries. Inverse Higgs constraints for spacetime symmetries with a higher dimension remove the redundant NG fields, whereas those for dimensionless symmetries can be further classified by the local symmetry breaking pattern.

(2-3) Nambu-Goldstone modes in dissipative systems

Spontaneous symmetry breaking (SSB) in Hamiltonian systems is a universal and widely observed phenomena in nature, e.g., the electroweak and chiral symmetry breakings, superconductors, ferromagnets, solid crystals, and so on. It is also known that the SSB occurs even in dissipative systems such as reaction diffusion system and active matters. The translational symmetry in the reaction diffusion system is spontaneously broken by a spatial pattern formation such as the Turing pattern in biology. The rotational symmetry is spontaneously broken in the active hydrodynamics which describes collective motion of biological organisms. We found that there exist two types of NG modes in dissipative systems corresponding to type-A and type-B NG modes in Hamiltonian systems. By taking the O(N) scalar model obeying a Fokker-Planck equation as an example, we have shown that the type-A NG modes in the dissipative system are diffusive modes, while they are propagating modes in Hamiltonian systems. We pointed out that this difference is caused by the existence of two types of Noether charges, Q^α_R and Q^α_A : Q^α_R are symmetry generators of Hamiltonian systems, which are not generally conserved in dissipative systems. Q^α_A are symmetry generators of dissipative systems described by the Fokker-Planck equation and are conserved. We found that the NG modes are propagating modes if Q^α_R are conserved, while those are diffusive modes if they are not conserved.

(3) Lattice gauge theory

(3-1) Hadron interactions from lattice QCD

One of the most important goals in nuclear physics is to determine baryon-baryon interactions directly from QCD. To achieve this goal, the HAL QCD Collaboration has been developing a novel lattice QCD formulation (HAL QCD method) and performing first-principles numerical simulations. We have calculated the spin-orbit forces for the first time from QCD by the HAL QCD method, and have observed the attraction in the $^3P_2$ channel related to the P-wave neutron superfluidity in neutron star cores. Our calculation of the N-Ω interaction shows that this system is bound in the $^5S_2$ channel. We have shown that the Ω-Ω interaction in the spin-singlet channel is in the unitary region where the scattering length becomes large. Three-nucleon forces have been calculated for several heavy quark masses. Our lattice calculations was extended to the heavy quark systems, e.g. the exotic tetraquark, T_{cc} and T_{cs}. Properties of the light and medium-heavy nuclei (^{4}He, ^{16}O, ^{40}Ca) have been calculated by combining the nuclear many-body techniques and the nuclear forces obtained from lattice QCD. Also, we have theoretically and numerically shown that the Luscher's method traditionally used in studying the hadron-hadron interactions does not lead to physical results for baryon-baryon interactions unless the lattice volume is unrealistically large, so that the HAL QCD method is the only reliable approach to link QCD to nuclear physics.

As a part of the High Performance Computing Infrastructure (HPCI) Project 5, we have completed the generation of (2+1)-flavor full QCD configurations with a large box, $V = (8 \text{ fm})^3$, and with nearly physical pion mass, 145 MeV, on the 10 Pflops super computer "K". We are currently in the process of calculations of baryon-baryon interactions using these configurations.

(3-2) Momenta and Angular Momenta of Quarks and Gluons inside the Nucleon

Determining the quark and gluon contributions to the spin of the nucleon is one of the most challenging problems in QCD both experimentally and theoretically. Since the quark spin is found to be small (~ 25% of the total proton spin) from the global analysis of deep inelastic scattering data, it is expected that the rest should come from the gluon spin and the orbital angular momenta of quarks and gluons. We made state-of-the-art calculations (with both connected and disconnected insertions) of the momenta and the angular momenta of quarks and gluons inside the proton. The u and d quark momentum/angular momentum fraction extrapolated to the physical point is found to be 0.64(5)/0.70(5), while the strange quark momentum/angular momentum fraction is 0.024(6)/0.023(7), and that of the gluon is 0.33(6)/0.28(8). This implies that the quark spin carries a fraction of 0.25(12) of the proton spin. Also, we found that the quark orbital angular momentum, which turned out to be dominated by the disconnected insertions, constitutes 0.47(13) of the proton spin.

(4) QCD under extreme conditions

(4-1) Production and Elliptic Flow of Dileptons and Photons in the semi-Quark Gluon Plasma

A notable property of peripheral heavy-ion collisions at RHIC and LHC is the elliptic flow which is a measure of the transfer of initial spatial anisotropy to momentum anisotropy. Both the PHENIX experiment at RHIC and the ALICE experiment at LHC have announced a puzzling observation; a large elliptic flow for photons, comparable to that of hadrons. We considered the thermal production of dileptons and photons at temperatures above the QCD critical temperature (T_c) on the basis of semi-QGP, a theoretical model for describing the quark-gluon plasma (QGP) near T_c. With realistic hydrodynamic simulations, we have shown that the strong suppression of photons in semi-QGP due to the inhibition of colored excitations tends to bias the elliptical flow of photons to that generated in the hadronic phase. This increases the total elliptic flow for thermal photons significantly towards the experimental data.

(4-2) Deriving relativistic hydrodynamics from quantum field theory

Hydrodynamics describes the spacetime evolution of conserved quantities, such the energy, the momentum, and the particle number. It does not depend on microscopic details of the system, so that it can be applied to many branches of physics from condensed matter to high-energy physics. One of the illuminating examples is the recent success of relativistic hydrodynamics in describing the evolution of QGP created in heavy-ion collisions. Inspired by the phenomenological success of relativistic hydrodynamics in describing QGP, theoretical derivations of the relativistic hydrodynamics have been attempted on the basis of the kinetic theory, the fluid/gravity correspondence, the non-equilibrium thermodynamics, and the projection operator method. In our study, a most microscopic and non-perturbative derivation of the relativistic hydrodynamics from quantum field theory was given on basis of the density operator with local Gibbs distribution at initial time. Performing the path-integral formulation of the local Gibbs distribution, we derived the generating functional for the non-dissipative hydrodynamics microscopically. Moreover, we formulated a procedure to evaluate dissipative corrections.

(4-3) Hadron-quark crossover in cold and hot neutron stars

We studied bulk properties of cold and hot neutron stars (NS) on the basis of the hadron-quark crossover picture where a smooth transition from the hadronic phase to the quark phase takes place at finite baryon density. By using a phenomenological equation of state (EOS) "CRover" which interpolates the two phases at around 3 times the nuclear matter density (ρ_0), it is found that the cold NSs with the gravitational mass larger than two solar mass can be sustained. This is in sharp contrast to the case of the first-order hadron-quark transition. The radii of the cold NSs with the CRover EOS are in the narrow range (12.5±0.5) km which is insensitive to the NS masses. Due to the stiffening of the EOS induced by the hadron-quark crossover, the central density of the NSs is at most 4 ρ_0 and the hyperon-mixing barely occurs inside the NS core. This constitutes a solution of the long-standing hyperon puzzle first pointed out by Takatsuka et al. The effect of color superconductivity (CSC) on the NS structures was also examined with the hadron-quark crossover picture. For the typical strength of the diquark attraction, a slight softening of the EOS due to two-flavor CSC takes place and the maximum mass is reduced by about 0.2 solar mass. The CRover EOS is generalized to the supernova matter at finite temperature to describe the hot NSs at birth. The hadron-quark crossover was found to decrease the central temperature of the hot NSs under isentropic condition. The gravitational energy release and the spin-up rate during the contraction from the hot NS to the cold NS were also estimated.

(5) Nuclear and atomic many-body problems

(5-1) Giant dipole resonance in hot nuclei

Over the last several decades, extensive experimental and theoretical works have been done on the giant dipole resonance (GDR) in excited nuclei covering a wide range of temperature (T), angular momentum (J) and nuclear mass. A reasonable stability of the GDR centroid energy and an increase of the GDR width with T (in the range ~ 1−3 MeV) and J are the two well-established results. Some experiments have indicated the saturation of the GDR width at high T: The gradual disappearance of the GDR vibration at much higher T has been observed. Experiments on the Jacobi transition and the GDR built on superdeformed shapes at high rotational frequencies have been reported in a few cases. We have demonstrated that thermal pairing included in the phonon damping model (PDM) is responsible for the nearly constant width of GDR at low temperature $T < 1$ MeV. We have also shown that the enhancement observed in the recent experimentally extracted nuclear level densities in ^{104}Pd at low excitation energy and various angular momenta is the first experimental evidence of the pairing reentrance in finite (hot rotating) nuclei. The results of calculations within the PDM were found in excellent agreement with the latest experimental data of GDR in the compound nucleus ^{88}Mo.

(5-2) Hidden pseudospin symmetries and their origins in atomic nuclei

The quasi-degeneracy between single-particle orbitals, (n, l, $j = l+1/2$) and ($n-1$, $l+2$, $j = l+3/2$), indicates a hidden symmetry in atomic nuclei, the so-called pseudospin symmetry (PSS). Since the introduction of the concept of PSS in atomic nuclei, there have been comprehensive efforts to understand its origin. Both splittings of spin doublets and pseudospin doublets play critical roles in the evolution of magic numbers in exotic nuclei discovered by modern spectroscopic studies with radioactive ion beam facilities. Since the PSS was recognized as a relativistic symmetry in 1990s, many special features, including the spin symmetry (SS) for anti-nucleon, and other new concepts have been introduced. We have published a comprehensive review article (Liang et al., Phys. Rept. 2015) on the PSS and SS in various systems, including extensions of the PSS study from stable to exotic nuclei, from non-confining to confining potentials, from local to non-local potentials, from central to tensor potentials, from bound to resonant states, from nucleon to anti-nucleon spectra, from nucleon to hyperon spectra, and from spherical

to deformed nuclei. We also summarized open issues in this field, including the perturbative nature, the supersymmetric representation with similarity renormalization group, and the puzzle of intruder states.

(5-3) Efimov Physics in cold atoms

For ultra-cold atoms and atomic nuclei, the pairwise interaction can be resonant. Then, universal few-body phenomena such as the Efimov effect may take place. We carried out an exploratory study suggesting that the Efimov effect can induce stable many-body ground states whose building blocks are universal clusters. We identified a range of parameters in a mass and density imbalanced two-species fermionic mixture for which the ground state is a gas of Efimov-related universal trimers. An explicit calculation of the trimer-trimer interaction reveals that the trimer phase is an SU(3) Fermi liquid stable against recombination losses. We proposed to experimentally observe this phase in a fermionic mixture of ^{6}Li-^{53}Cr atoms. We have also written a comprehensive review article on theoretical and experimental advances in Efimov physics.

(5-4) Supersymmetric Bose-Fermi mixtures

Some special Bose-Fermi mixtures of cold atoms and molecules in optical lattices could be prepared in such a way as they exhibit approximate supersymmetry under the interchange of bosons and fermions. Since supersymmetry is broken at finite temperature and/or density, an analog of the Nambu-Goldstone excitation, dubbed the "Goldstino", should appear. We evaluated the spectral properties of the Goldstino in a Bose-Fermi mixture of cold atoms and molecules. We derived model independent results from sum rules obeyed by the spectral function. Also, by carrying out specific calculations with random phase approximation, analytic formula for the dispersion relation of Goldstino at small momentum was obtained.

Members

Chief Scientist (Lab. Head)
Tetsuo HATSUDA

Vice Chief Scientist
Tsukasa TADA

Research & Technical Scientists
Takumi DOI (Senior Research Scientist)   Yoshimasa HIDAKA (Senior Research Scientist)
Pascal Raphaël Gabriel NAIDON (Senior Research Scientist)   Haozhao LIANG (Senior Research Scientist)

Nishina Center Research Scientists
Makiko NIO   Dang NGUYEN DINH

Special Postdoctoral Researchers
Noriaki OGAWA   Takahiro DOI
Shinya GONGYO   Matthias Wilhelm Georg BERWEIN

Foreign Postdoctoral Researcher
Di-Lun YANG

Postdoctoral Researcher
Takumi IRITANI

International Program Associate
Shihang SHEN (Peking University)

Visiting Researcher
Hiroyuki TAJIMA (JSPS Fellow)

Senior Visiting Scientist
Koichi YAZAKI (Univ. of Tokyo)

Visiting Scientists
Noriyoshi ISHII (Osaka Univ.)   Norisuke SAKAI (Keio Univ.)
Motoi TACHIBANA (Saga Univ.)   Masaki MURATA (Univ. of Tokyo Hospital)
Masashi HAYAKAWA (Nagoya Univ.)   Tatsuyuki TAKATSUKA (Iwate Univ.)
Kenji SASAKI (Kyoto Univ.)   Arata YAMAMOTO (Univ. of Tokyo)
Tatsumi AOYAMA (Kyoto Univ.)   Kanabu NAWA (Univ. of Tokyo Hospital)
Shinya AOKI (Kyoto Univ.)   Tomoya HAYATA (JSPS Fellow)
Hiroshi SUZUKI (Kyushu Univ.)   Gergely FEJOS (Osaka Univ.)
Atsushi NAKAMURA (Hiroshima Univ.)   Takashi SANO (AIST)
Takeo INAMI (Sungkyunkwan Univ.)   Takashi INOUE (Nihon Univ.)
Hung NGUYEN (Duy Tan University)   Sachiko TAKEUCHI (Japan College of Social Work)
Koji HASHIMOTO (Osaka Univ.)   Shinsuke YOSHIDA (Los Alamos National Laboratory)
Keiko MURANO (Osaka Univ.)   Toshifumi NOUMI (Kobe Univ.)
Daisuke KADOH (Keio Univ.)   Takayuki MATSUKI (Tokyo Kasei Univ.)
Minoru ETO (Yamagata Univ.)   Rhine Kumar Arayakkandi Keechiprath (Cochin Univ. of Sci.
Yoichi IKEDA (Osaka Univ.)   and Tech.)

Shinya GONGYO (Centre national de la recherche scientifique)
Yoichi KAZAMA (Univ. of Tokyo)
Yoji OHASHI (Keio Univ.)
Hiroshi TOKI (Osaka Univ.)

Tetsuo MATSUI (The Open Univ. of Japan)
Makoto TAKIZAWA (Showa Pharm. Univ.)
Shoichi SASAKI (Tohoku Univ.)
Kazuo FUJIKAWA (Univ. of Tokyo)

Student Trainees
Shoichiro TSUTSUI (Kyoto Univ.)
Takaya MIYAMOTO (Kyoto Univ.)
Tan Phuc LE (Univ. of Sci., Vietnam National Univ.)

Asahi CHIKAOKA (Univ. of Tokyo)
Daisuke OHASHI (Univ. of Tokyo)
Tomoya NAITO (Univ. of Tokyo)

Theoretical Research Division
Strangeness Nuclear Physics Laboratory

1. Abstract

We proposed accurate calculation method called 'Gaussian Expansion Method using infinitesimally shifted Gaussian lobe basis function'. When one proceeds to four-body systems, calculation of the Hamiltonian matrix elements becomes much laborious. In order to make the four-body calculation tractable even for complicated interactions, the infinitesimally-shifted Gaussian lobe basis function has been proposed. The GEM with the technique of infinitesimally-shifted Gaussians has been applied to various three-, four- and five-body calculations in hypernuclei, the four-nucleon systems, and cold-atom systems. As results, we succeeded in extracting new understandings in various fields.

2. Major Research Subjects

(1) Hypernuclear structure from the view point of few-body problem
(2) Structure of exotic hadron system
(3) quantum atomic system and ultra cold atomic system
(4) Equation of state for neutron star

3. Summary of Research Activity

(1) Recently, at RIBF, they observed tetra neutron system to be bound or resonant state. Theoretically, it is requested to study this system theoretically.   We performed four-body calculation using NN realistic force and a phenomenological three-body force. We found that we need unrealistically strong three-body force to describe 4n system.

(2) We investigate the effects of the odd-state part of bare $\Lambda\Lambda$ interactions on the structure of neutron stars by constructing equations of state (EOSs) for uniform nuclear matter containing Λ and Σ^- hyperons with use of the cluster variational method. The EOS obtained for NS matter becomes stiffer as the odd-state $\Lambda\Lambda$ interaction becomes more repulsive, and correspondingly the maximum mass of NSs increases.

(3) We calculate the universal spectrum of trimer and tetramer states in heteronuclear mixture of ultracold atoms with different masses in the vicinity of the heavy-light dimer threshold. We find that trimer and tetramer cross into the heavy-light dimer threshold at the same point and that as the mass ratio M/m decreases, the distance between the thresholds for trimer and tetramer states become smaller.

Members

Chief Scientist (Lab. Head)
Emiko HIYAMA

Research Scientist
Hiroya SUNO (Research Scientist, concurrent: Strangeness
Nuclear Physics Laboratory, Main: Field Theory Research Team)

Special Postdoctoral Researchers
Hajime TOGASHI   Shin WATANABE
Yasuhiro YAMAGUCHI   Kadir Utku CAN

Postdoctoral Researcher
Dalibor SKOUPIL

Research Consultants
Toshio MOTOBA (Osaka Elec.-Com. Univ.)   Tomokazu FUKUDA(Osaka Elec.-Com. Univ.)

Junior Research Associates
Saori MAEDA (Tokyo Tech.)   Tetsuya YOSHIDA (Tokyo Tech.)
Jehee LEE (Tokyo Tech.)

International Program Associate
Qian WU (Nanjing Univ.)

Visiting Scientists
Masayuki ASAKAWA (Osaka Univ.)   Daisuke JIDO (Tokyo Met. Univ.)
Takayuki MYO (Osaka Inst. of Tech.)   Soichi ISHIKAWA (Hosei Univ.)
Taiichi YAMADA (Kanto Gakuin Univ.)   Atsushi HOSAKA (Osaka Univ.)
Yasuo YAMAMOTO (Tsuru Univ.)   Akinobu DOTE (KEK)
Atsushi UMEYA (Nihon Inst. of Tech.)   Yasuro FUNAKI (Kanto Gakuin Univ.)

Hidekatsu NEMURA (Osaka Univ.)　　　　　　　　　　　　Shin WATANABE (National Inst. of Tech., Gifu College)
Takenori FURUMOTO (Yokohama National Univ.)　　　　　Jiwei CUI (Xidian Univ.)
Makoto OKA (Tokyo Tech.)　　　　　　　　　　　　　　　Satoshi NAKAMURA (Tohoku Univ.)
Tetsuo HYODO (Kyoto Univ.)　　　　　　　　　　　　　　Tomokazu FUKUDA (Osaka Elec.-Com. Univ.)
Yoichi IKEDA (Osaka Univ.)　　　　　　　　　　　　　　Toru SATO (Osaka Univ.)
Thomas Adriaan RIJKEN (Radboud Univ. Nijmegen)　　　　Jinniu HU (Nankai Univ.)
Shoji SHINMURA (Gifu Univ.)　　　　　　　　　　　　　Wolfram WEISE (TUM)
Kazuma NAKAZAWA (Gifu Univ.)　　　　　　　　　　　　Masahiro ISAKA (JSPS)
Ying ZHANG (Tianjin Univ.)　　　　　　　　　　　　　　Javier ROCAMAZA (Univ. of Milan)
Shimpei ENDO (Monash Univ.)　　　　　　　　　　　　　Xian-Rong ZHOU (East China Normal Univ.)
Philipp GUBLER (Keio Univ.)　　　　　　　　　　　　　Kei KOTAKE (Fukuoka Univ.)
Toshio MOTOBA (Osaka Elec.-Com. Univ.)　　　　　　　　Jean-Marc RICHARD (Lyon Univ.)
Shuichi GOJUKI (SGI Japan Ltd.)　　　　　　　　　　　　Ulugbek YAKHSHIEV (Inha Univ.)
Hyun-Chul KIM (Inha Univ.)　　　　　　　　　　　　　　Jirina STONE (Univ. of Tennessee Knoxville)
Petr VESELY (Academy of Science of Czech Rep.)　　　　　Chengjun XIA (Zhejiang Univ.)
Hans-Josef SCHULZE (INFN)　　　　　　　　　　　　　　Satoru HIRENZAKI (Nara Women's Univ.)
Tingting SUN (Zhengzhou Univ.)　　　　　　　　　　　　Kiyomi IKEDA (Niigata Univ.)

Student Trainees
Saori MAEDA (Tokyo Tech.)　　　　　　　　　　　　　　Christiane SCHMICKLER (TU Darmstadt)

List of Publications & Presentations

Publications
[Journal]
(Original Papers) *Subject to Peer Review

S. Furusawa, H. Togashi, H. Nagakura, K. Sumiyoshi, S. Yamada, H. Suzuki and M. Takano, "A new equation of state for core-collapse supernovae based on realistic nuclear forces and including a full nuclear ensemble," J. Phys. G **44**, 094001 (2017).

Y. Yamamoto, H. Togashi, T. Tamagawa, T. Furumoto, N. Yasutake and Th. A. Rijken, "Neutron-star radii based on realistic nuclear interactions," Phys. Rev. C **96**, 065804 (2017).

K. Nakazato, H. Suzuki and H. Togashi, "Heavy nuclei as thermal insulation for proto-neutron stars," Phys. Rev. C **97** (2018) 035804.

富樫甫「現実的核力に基づく超新星物質状態方程式の構築」，原子核研究 Vol. **62** No. 2, 2018 年, pp. 28–40.

Y. Yamaguchi and E. Santopinto, "Hidden-charm pentaquarks as a meson-baryon molecule with coupled channels for $\overline{D}^{(*)}\Lambda_c$ and $\overline{D}^{(*)}\Sigma_c^{(*)}$," Phy. Rev. D **96**, 014018 (2017).*

A. Hosaka, T. Hyodo, K. Sudoh, Y. Yamaguchi and S. Yasui, "Heavy Hadrons in Nuclear Matter," Prog. Part. Nucl. Phys. **96**, 88–153 (2017).*

Y. Yamaguchi and S. Yasui, "Mesic nuclei with a heavy antiquark," Prog. Theor. Exp. Phys. **2017**, 093D02 (2017).*

Y. Yamaguchi, A. Giachino, A. Hosaka, E. Santopinto, S. Takeuchi and M. Takizawa, "Hidden-charm and bottom meson-baryon molecules coupled with five-quark states," Phy. Rev. D **96**, 114031 (2017).*

P. Achenbach, D. Skoupi *et al.*, "Beam helicity asymmetries in $K^+\Lambda$ electroproduction off the proton at low Q^2," Eur. Phys. J. A **53**, 198(2017).

D. Skoupil, P. Bydžovský, "Photo- and electroproduction of $K^+\Lambda$ with a unitarity-restored isobar model," Phys. Rev. C **97**, 025202 (2018).

H. Bahtiyar, K.U. Can, G. Erkol, M. Oka, T.T. Takahashi, "$\Xi_c\gamma \to \Xi_c'$ transition in Lattice QCD," Phys. Lett. B **772**, 121–126 (2017).

K.U. Can, G. Erkol, M. Oka, T.T. Takahashi, "$\Lambda_c\Sigma_c\pi$ coupling and $\Sigma_c\to\Lambda_c\pi$ decay in Lattice QCD," Phys. Lett. B **768**, 309–316 (2017).

[Proceedings]
(Original Papers) *Subject to Peer Review

H. Togashi, E. Hiyama and M. Takano, "Variational approach to neutron star matter with hyperons," JPS Conf. Proc. **17**, 102002 (2017).

H. Togashi, E. Hiyama and M. Takano, "Equation of state of hyperonic nuclear matter at zero and finite temperatures with the variational method," JPS Conf. Proc. **18**, 011028 (2017).

H. Togashi, K. Nakazato, Y. Takehara, S. Yamamuro, H. Suzuki and M. Takano, "New table of supernova equation of state using a variational method and its application to astrophysical compact objects," JPS Conf. Proc. **20**, 011021 (2018).

Oral Presentations
[International Conference etc.]

E. Hiyama, "Structure of few-body light Λ hypernuclei," The 7th Asia-Pacific Conference on Few-Body Problems in Physics, Guilin, China, August, 2017.

E. Hiyama, "Structure of Ξ hypernuclei and ΞN interaction," XVII international Conference on Hadron Spectroscopy and structure, Salamanca, Spain, September, 2017.

E. Hiyama, "Structure of light hypernuclei," Workshop on anti-matter, hyper-matter and exotica production at the LHC, Turin, Italy, November, 2017.

E. Hiyama, "Gaussian Expansion Method and its application to resonant states hadron ohysics," Multiparticle resonances in hadrons, nuclei and ultracold gases, Hirschegg, Austria, January, 2018.

E. Hiyama, "Five-body calculation of heavy pentaquark system," French-Japanese workshop on Hadrons and Nuclear Physics met ultracold atoms, Paris, France, January, 2018.

H. Togashi, E. Hiyama and M. Takano, "Variational calculation for nuclear equation of state and hyperon mixing in "Nuclear equation of state with realistic nuclear forces," ECT* Workshop "New perspectives on Neutron Star Interiors," Trento, Italy, October, 2017.

H. Togashi, E. Hiyama and M. Takano, "Variational calculation for nuclear equation of state and hyperon mixing in the supernova core," ECT* Workshop "ASTRA: Advances and open problems in low-energy nuclear and hadronic STRAngeness physics," Trento, Italy, October, 2017.

H. Togashi, M. Takano, K. Nakazato, Y. Takehara, S. Yamamuro, H. Suzuki, K. Sumiyoshi and E. Hiyama, "Variational approach to hot and dense matter in compact stars," International Workshop on Hadron and Nuclear Physics 2017 (HNP2017), Wako, Japan, December, 2017. (invited talk)

H. Togashi, M. Takano, K. Nakazato, Y. Takehara, S. Yamamuro, H. Suzuki and K. Sumiyoshi, "Properties of a variational equation of state in core-collapse supernovae," PACIFIC 2018, Yoichi-gun, Japan, February, 2018. (invited talk)

H. Togashi, M. Takano, K. Nakazato, Y. Takehara, S. Yamamuro, H. Suzuki, K. Sumiyoshi and E. Hiyama, "Supernova equation of state with realistic nuclear interactions and hyperon mixing in hot dense matter," International conference on "Physics of core-collapse supernovae and compact star formations," Tokyo, Japan, March, 2018.

Y. Yamaguchi, "Hidden-charm meson-baryon molecules with a short-range attraction from five quark states," 9th Workshop on Hadron physics in China and Opportunities Worldwide, Nanjing, China, July, 2017.

Y. Yamaguchi, "Hidden-charm meson-baryon molecules with a short-range attraction from five quark states," The 7th Asia-Pacific Conference on Few-Body Problems in Physics (APFB 2017), Guilin, China, August, 2017.

Y. Yamaguchi, "Hidden-charm meson-baryon molecules coupled with five-quark states," Tokyo Tech - Uppsala University Joint Symposium, Tokyo, Japan, November, 2017.

Y. Yamaguchi, A. Giachino, A. Hosaka, E. Santopinto, S. Takeuchi and M. Takizawa, "Hidden-charm meson-baryon molecules coupled with five-quark states," International workshop on Hadron and Nuclear Physics 2017 (HNP2017), Wako, Japan, December, 2018.

Y. Yamaguchi, A. Giachino, A. Hosaka, E. Santopinto, S. Takeuchi and M. Takizawa, "Hadronic molecules with a short-range force by a Quark model," Hadrons and Nuclear Physics meet ultracold atoms: a French Japanese workshop, Paris, France, January, 2018.

D. Skoupil, "Photoproduction of $K^+\Lambda$," The 7th Asia-Pacific Conference on Few-Body Problems in Physics, Guilin, China, August, 2017.

D. Skoupil, "$K^+\Lambda$Photo- and Electroproduction off Proton, " International Workshop on Hadron and Nuclear Physics 2017, (HNP2017), Wako, Japan, December, 2017.

K.U. Can, "Omega_c spectrum in Lattice QCD − a progress report," International workshop on Hadron and Nuclear Physics 2017, Wako, Japan, December, 2017.

K.U. Can, "Charmed baryon spectrum in Lattice QCD - a status update," Workshop on Structure of Heavy Quark Hadrons and Exotic Hadrons, Tokai, Japan, March, 2018.

[Domestic Conference]

肥山詠美子, "Five-body structure of heavy pentaquark system," 日本物理学会第 73 回年次大会, 野田市, 3 月, 2018.

富樫甫,「現実的核力に基づく核物質状態方程式の研究と今後の展望」, RIBF 理論若手放談会：エキゾチック核物理の広がり, 神戸市, 8 月, 2017 年 (招待講演).

富樫甫,「現実的核力に基づく核物質状態方程式とハイペロン混合系への拡張」, 新学術領域「中性子星核物質」理論班主催研究会, 熱海市, 2 月, 2018.

富樫甫,「現実的核力に基づく超新星物質状態方程式の構築」日本物理学会第 73 回年次大会, 野田市, 3 月, 2018. (招待講演)

山口康宏,「ハドロン分子における 5 クォーク状態が作る近距離引力」, RCNP 研究会「核子・ストレンジネス多体系におけるクラスター現象」, 大阪市, 8 月, 2017.

山口康宏,「ハドロン分子における 5 クォーク状態が作る近距離引力」, French-Japanese workshop on Hadrons and Nuclear Physics met ultracold atoms, 日本物理学会 2017 年秋季大会, 宇都宮市, 9 月, 2017.

山口康宏,「反ヘビークォークを含むメソン原子核系の解析」, 日本物理学会 2017 年秋季大会, 宇都宮市, 9 月, 2017.

山口康宏,「ハドロン分子におけるコンパクトな 5 クォーク状態が作る近距離引力」, KEK 理論センター研究会「ハドロン・原子核物理の理論研究最前線 2017」, つくば市, 11 月, 2017.

山口康宏, 安倍幸大, 福川賢治, 保坂淳,「クォーク交換による $D\bar{D}^*$-$J/\psi\pi$ ポテンシャル」, 研究会「ヘビークォークハドロンとエキゾチックハドロンの構造」, つくば市, 3 月, 2018.

安倍幸大, 福川賢治, 保坂淳, 山口康宏,「クォーク交換で記述する $D\bar{D}^*$-$J/\psi\pi$ ポテンシャル」, 日本物理学会第 73 回年次大会, 野田市, 3 月, 2018.

Sub Nuclear System Research Division
Radiation Laboratory

1. Abstract

Nucleons, such as protons and neutrons, are a bound state of constituent quarks glued together with gluons. The detail structure of nucleons, however, is not well understood yet. Especially the mechanism to build up the spin of proton, which is 1/2, is a major problem in physics of the strong force. The research goal of Radiation Laboratory is to solve this fundamental question using the world first polarized-proton collider, realized at RHIC in Brookhaven National Laboratory (BNL) in USA. RHIC stands for Relativistic Heavy Ion Collider, aiming also to create Quark Gluon Plasma, the state of Universe just after the Big Bang, and study its property. RIKEN-BNL Research Center (RBRC) carries our core team at BNL for those exciting researches using the PHENIX detector. We have observed that the proton spin carried by gluons is finite and indeed sizable. We also identified W bosons in the electron/positron decay channel and in the muon decay channel, with which we are about to conclude how much anti-quarks carry the proton spin. Other than the activities at RHIC we are preparing and starting new experiments at J-PARC and Fermilab to study the nature of hadron. We are also performing technical developments such as novel ion sources, fine-pitch silicon pixel detectors and high-performance trigger electronics.

2. Major Research Subjects

1) Spin physics with relativistic polarized-proton collisions at RHIC
2) Study of nuclear matter at high temperature and/or at high density
3) Technical developments on radiation detectors and accelerators

3. Summary of Research Activity

(1)　Experimental study of spin structure of proton using RHIC polarized proton collider

[See also RIKEN-BNL Research Center Experimental Group for the activities at BNL]

The previously published central neutral pion double spin asymmetries at the highest collision energies at RHIC of 510 GeV have been augmented with the release of charged pion double spin asymmetries in 2017 by PHENIX. The ordering of the three pion asymmetries allows a direct determination of the sign of the gluon polarization which has been found to be nonzero. The precision of the charged pion asymmetries is slightly limited due to the trigger capabilities in PHENIX but the results are consistent with a dominant, positive gluon contribution to the nucleon spin. With the valence quark spin contribution already reasonably well known, the contributions from sea quarks and orbital angular momenta remain to be understood. PHENIX has collected data to access the sea quark polarizations via leptonic decays of W bosons. Preliminary results have been obtained using all the data taken so far. The central rapidity electron decay channel results have been published while the forward muon decay channel results have been finalized and are submitted for publication.

While orbital angular momentum cannot be directly accessed at RHIC, several transverse spin phenomena have been observed which relate to orbital angular momentum and the three-dimensional structure of the nucleon. These phenomena by themselves have become a major field of research as the dynamics of the strong interaction. During the 2015 RHIC operation, collisions of transversely polarized protons with Au and Al nuclei were provided for the first time. Two rather surprising results have been discovered here. First, the single transverse spin asymmetries for J/ψ particles which are found to be consistent with zero to even higher precisions, show distinctly nonzero asymmetries in proton-Au collisions at the lowest transverse momenta both if detected at slightly forward or backward regions with respect to the polarized beam. The mechanism for such a behavior is not known and the publication will initiate substantial theoretical discussions to resolve this. Also charged hadron single spin asymmetries have been observed in all three colliding systems. While a previously known nonzero forward asymmetry for positive hadrons was confirmed, a substantial reduction of these asymmetries for $p+$Al and $p+$Au collisions was observed. Such a reduction was predicted by several theoretical models describing the non-linear effects of high gluon densities in nuclei suggested by the so-called color-glass-condensate.

In June of 2017, we installed an electro-magnetic calorimeter in the most forward area of the STAR experiment and took polarized proton collision data for neutral particle production (neutron, photon, neutral pion). The cross section measurement will give us new inputs to develop high-energy particle-collision models which are essential to understand air-shower from ultra-high energy cosmic rays. The asymmetry measurement will enable us to understand the hadron collision mechanism based on QCD. Some of us are participating in the Fermilab SeaQuest experiment as a pilot measurement of muon pairs from Drell-Yan process using a 120-GeV unpolarized proton at Fermilab. After finishing unpolarized measurements in 2017 to study the quark spin-orbit effect, a new measurement with a polarized proton target will start in 2018 to study the sea-quark orbit effect of the polarized proton in the target. For many jet related measurements fragmentation functions are necessary to gain spin and or flavor sensitivity. Those are currently extracted by some of us using the Belle data. In addition to using the fragmentation results with RHIC measurements, they will also provide the basis of several of the key measurements to be performed at the electron-ion collider.

(2)　Experimental study of quark-gluon plasma using RHIC heavy ion collider

[See also RIKEN-BNL Research Center Experimental Group for the activities at BNL]

We have completed several key measurements in the study of quark-gluon plasma at RHIC. As the top of them, we lead the analysis of the first thermal photon measurement in heavy ion collisions. The measurement indicates that the initial temperature reached in the central Au+Au collision at 200 GeV is about 350MeV, far above the expected transition temperature $T_c \sim 170$MeV, from hadronic phase to quark-gluon plasma. This work was rewarded by Nishina Memorial Prize given to Y. Akiba in 2011. We also measured direct photons in $d+$Au and direct photon flow strength v_2 and v_3 in Au+Au.

We lead measurement of heavy quark (charm and bottom) using VTX, a 4 layer silicon vertex tracker which we jointly constructed

with US DOE. The detector was installed in PHENIX in 2011. Analysis of heavy quark using the silicon vertex detector is ongoing. The final results of the 2011 run was published in Physical Review C (Phys. Rev. C **93**, 034904 (2016)). This is the first publication from VTX. The result showed that the electrons from bottom quark decay is suppressed for $p_T > 4$ GeV/c, but the suppression factor is smaller than that of charm decay electrons for $3 < p_T < 4$ GeV/c. This is the first observation of bottom electron suppression in heavy ion collisions, and the first result that shows the bottom and charm suppression is different. PHENIX recorded approximately 10 times more data of Au+Au collisions in the 2014 run than the 2011 run. We report preliminary results of about 1/4 of the 2014 data in QM2017 conference, confirming the published results with 3 times of statistics. PHENIX recorded high statistics $p+p$ and $p+A$ data in 2015, and the doubled the Au+Au in 2016. PHENIX concluded its data taking in the 2016 run.

We have completed several key measurements in the study of quark-gluon plasma at RHIC. As the top of them, we lead the analysis of the first thermal photon measurement in heavy ion collisions. The measurement indicates that the initial temperature reached in the central Au+Au collision at 200 GeV is about 350 MeV, far above the expected transition temperature $T_c \sim 170$MeV, from hadronic phase to quark-gluon plasma. This work was rewarded by Nishina Memorial Prize given to Y. Akiba in 2011. We also measured direct photons in $d+Au$ and direct photon flow strength v_2 and v_3 in Au+Au.

We lead measurement of heavy quark (charm and bottom) using VTX, a 4 layer silicon vertex tracker which we jointly constructed with US DOE. The detector was installed in PHENIX in 2011. Analysis of heavy quark using the silicon vertex detector is ongoing. The final results of the 2011 run was published in Physical Review C (PRC93, 034904 (2016). This is the first publication from VTX. The result showed that the electrons from bottom quark decay is suppressed for $p_T > 4$ GeV/c, but the suppression factor is smaller than that of charm decay electrons for $3 < p_T < 4$ GeV/c. This is the first observation of bottom electron suppression in heavy ion collisions, and the first result that shows the bottom and charm suppression is different. PHENIX recorded approximately 10 times more data of Au+Au collisions than the 2011 run in each of the 2014 and 2016 run. PHENIX recorded high statistics $p+p$ and $p+A$ data in 2015.

PHENIX concluded its data taking in the 2016 run. We are now working on the data analysis of the high statistics data recorded in 2014 to 2016 runs.

In Wako we are operating a cluster computer system (CCJ) specialized to analyze huge data sets taken with the PHENIX detector. It consists of 28 nodes (18 old nodes and 10 new nodes) each of which has two CPUs and 10 sets of local disk for data repository (old node: quad-core CPU, 1TB disk, new node: six-core CPU, 2TB disk). There are 264 CPU cores and 380 TB disks in total. This configuration ensures the fastest disk I/O when each job is assigned to the node where the required data sets are stored. It is also important that this scheme doesn't require an expensive RAID system and network. Through this development we have established a fast and cost-effective solution in analyzing massive data.

0.9 PB of data for the PHENIX experiment is stored in a hierarchical storage system which is a part of HOKUSAI GreatWave supercomputer system operated by the Advanced Center for Computing and Communication (ACCC). ACCC also provides 10 dedicated PC nodes for CCJ.

(3)   Study of properties of mesons and exotic hadrons with domestic accelerators

Preparation of the experiment E16 at J-PARC Hadron experimental facility is underway with several Grant-in-Aids. This experiment aims to perform a systematic study of the spectral modification of low-mass vector mesons in nuclei to explore the physics of chiral symmetry breaking and restoration in dense nuclear matter, namely, the mechanism proposed by Nambu to generate most of hadron masses.

The Gas Electron Multiplier (GEM) technology is adopted for the two key detectors, GEM Tracker (GTR) and Hadron-blind Cherenkov detector (HBD). We have joined the CERN-RD51 collaboration to acquire the read out technology for GEM. To improve electron-identification performance, lead-glass calorimeters (LG) are used in combination with HBD. The development phase of those detectors is over and we are in the production phase. The parts for six modules of GTR and two modules of HBD are delivered and their assembly processes have started. Read-out electronics and trigger logic modules were also developed and necessary parts are almost delivered. Amongst all the electronics, only the HBD trigger ASIC is still under development. Development of firmware on the trigger logic modules is also on-going.

Due to the budgetary limitation, we aim to install a part of detectors at the beginning of experiment, eight modules of GTR/HBD/LG out of 26 modules in the full installation. The yield of phi mesons and sensitivity to the possible spectral modification with the eight-module configuration under the expected high-rate environment was evaluated by the Geant4 simulation taking into account the expected performance of the detectors and by using a newly-developed GEM-signal simulator. Based on this study, J-PARC PAC gave us a stage-2 approval on Jul. 2017, to the commissioning run (Run 0), which will be performed when the beam line is completed. Although with a significant delay from originally planned March 2016, the construction of the beam line by KEK will be completed in 2019 in order to realize experiments with the stage-2 approval. We are preparing the spectrometer toward the Run 0, which is scheduled on Oct. 2019.

(4)   Detector development for PHENIX experiment

The PHENIX experiment proposes substantial detector upgrades to go along the expected accelerator improvements, including the future electron-ion collider "eRHIC". The present PHENIX detector is repurposed to the sPHENIX (super PHENIX) detector replacing the present magnet with the Babar solenoid magnet at SLAC, and will be covered by the hadronic calorimeter which was absent in present RHIC experiment. The sPHENIX project is now funded by DOE, and RIKEN will participate in the construction of the inner silicon tracker (INTT). The R&D of the INTT has been in progress since 2015 and the 2nd generation prototype successfully demonstrated a designed performance as a result of the beam test executed at Fermilab in March 2018.

We have been developing a plan to build a forward spectrometer to be added to the sPHENIX detector. With this addition, the fsPHENIX detector will have both hadronic and electromagnetic calorimetry as well as tracking in the forward rapidity region. This upgrade makes it possible to study forward jets and hadrons in jets which are of vital importance for the cold QCD program in polarized $p+p$ and $p+A$ collisions at RHIC. The fsPHENIX detector can be further upgraded to the ePHENIX detector to be used for electron-ion

collisions at eRHIC. We are preparing test bench to perform R&D for the forward hadron calorimeter.

Members

Chief Scientist (Lab. Head)
Hideto EN'YO (Director, RNC)

Vice Chief Scientist
Yasuyuki AKIBA

Research & Technical Scientists
Yasushi WATANABE (Senior Research Scientist)
Yuji GOTO (Senior Research Scientist)
Itaru NAKAGAWA (Senior Research Scientist)
Satoshi YOKKAICHI (Senior Research Scientist)

Ralf SEIDL (Senior Research Scientist)
Hiroaki ONISHI (Senior Research Scientist, concurrent;
 Advanced Meson Science Lab.)

Junior Research Associates
Kohei TERASAKI (Univ. of Tokyo)

International Program Associates
Minjung KIM (Seoul Nat'l Univ.)
Minho KIM (Korea Univ.)
Junsang PARK (Seoul Nat'l Univ.)

Se Young HAN (Ewha Womans Univ.)
Jaehee YOO (Korea University)

Senior Visiting Scientists
Toshiaki SHIBATA (Tokyo Tech.)

Takashi NAKANO (Osaka Univ.)

Visiting Scientists
Kyoichiro OZAWA (KEK)
Susumu SATO (JAEA)
Megumi NARUKI (Kyoto Univ.)
Yoshinori FUKAO (KEK)
Kiyoshi TANIDA (JAEA)
Hirotsugu KASHIWAGI (National Institute for
Quantum and Radiological Science and Technology)
Taku GUNJI (Univ. of Tokyo)
Junpei TAKANO (KEK)
Kazuya AOKI (KEK)
Masashi KANETA (Tohoku Univ.)
Munehisa OHTANI (Kyorin Univ.)
Kenichi NAKANO (Tokyo Tech.)
Maya SHIMOMURA (Nara Women's Univ.)
Noriyosu HAYASHIZAKI (Tokyo Tech.)
Hiroaki MENJO (Nagoya Univ.)

Yuhei MORINO (KEK)
Kenji FUKUSHIMA (Univ. of Tokyo)
Tomohiro NISHITANI (Nagoya Univ.)
Tomonori TAKAHASHI (Osaka Univ.)
Tsutomu MIBE (KEK)
Makoto KUWAHARA (Nagoya Univ.)
Masahiro OKAMURA (BNL)
Shunzo KUMANO (KEK)
Bentz WOLFGANG (Tokai Univ.)
Alexander BAZILEVSKY (BNL)
Shin-ya SAWADA (KEK)
Kenta SHIGAKI (Hiroshima Univ.)
Sanghwa PARK (Stony Brook University)
Robert JAMESON (Goethe Universitat Frankfurt)
Takuya SUZUKI (Waseda Univ.)

Student Trainees
Shoichiro NISHIMURA (Univ. of Tokyo)
Yuki OBARA (Univ. of Tokyo)
Mana UENO (Nagoya Univ.)
Qidong Zhou (Nagoya Univ.)
Seiya MIYATA (Univ. of Tokyo)
Sakiko ASHIKAGA (Kyoto Univ.)
Yuri ITO (Nara Woman's Univ.)
Tomoko SAKAMOTO (Nara Woman's Univ.)
Risa NISHITANI (Nara Woman's Univ.)
Hiroki KATO (Tsukuba Univ.)

Kazuki SATO (Tsukuba Univ.)
Kazuya NAKAGAWA (Tsukuba Univ.)
Jaehee YOO (Korea University)
Yosuke UEDA (Hiroshima Univ.)
Key NAGAI (Tokyo Tech.)
Koji IGARASHI (Tokyo Tech)
Kenta SATO (Nagoya Univ.)
Kazuya NAGASHIMA (Hiroshima Univ.)
Kenichiro SHIINA (Rikkyo Univ.)
Masato TSURUTA (Rikkyo Univ.)

Interns
Junsang PARK (Seoul Nat'l Univ.)
Daisuke NEMOTO (Rikkyo Univ.)
Ryota KAWASHIMA (Rikkyo Univ.)

Kazuki SUZUKI (Kyoto Univ.)
Masato TSURUTA (Rikkyo Univ.)
Minjung KIM (Seoul Nat'l Univ.)

Masaya ICHIKAWA (Kyoto Univ.)
Kenichiro SHIINA (Rikkyo Univ.)

Taebong MOON (Yonsei Univ.)

Part-time Workers
Wataru NAKAI (Univ. of Tokyo)
Hidekazu MASUDA (Rikkyo Univ.)
Koki KANNO (Univ. of Tokyo)

Michiko SEKIMOTO
Ryota KAWASHIMA (Rikkyo Univ.)

Assistant
Keiko SUZUKI

List of Publications & Presentations

Publications

[Journal]

(Original Papers) *Subject to Peer Review

Y. Komatsu *et al*., "Measurement of the vector meson spectral modification in the nuclear medium at J-PARC," JPS Conf. Proc. **13**, 020005 (2017).

A. Adare *et al*. (PHENIX Collaboration), "Angular decay coefficients of J/ψ mesons at forward rapidity from $p+p$ collisions at $\sqrt{s}$ = 510 GeV," Phys. Rev. D **95**, 092003 (2017).

A. Adare *et al*. (PHENIX Collaboration), "Measurement of the relative yields of ψ(2S) to ψ(1S) mesons produced at forward and backward rapidity in $p+p$, $p+$Al, $p+$Au, and ^{3}He$+$Au collisions at $\sqrt{s_{NN}}$ = 200 GeV," Phys. Rev. C **95**, 034904 (2017).

A. Adare *et al*. (PHENIX Collaboration), "Nonperturbative-transverse-momentum effects and evolution in dihadron and direct photon-hadron angular correlations in $p+p$ collisions at $\sqrt{s}$ = 510 GeV," Phys. Rev. D **95**, 072002 (2017).

C. Aidala *et al*., "Measurement of long-range angular correlations and azimuthal anisotropies in high-multiplicity $p+$Au collisions at $\sqrt{s_{NN}}$ = 200 GeV," Phys. Rev. C **95**, 034910 (2017).

A. Adare *et al*. (PHENIX Collaboration), "Measurements of double-helicity asymmetries in inclusive J/ψ production in longitudinally polarized $p+p$ collisions at $\sqrt{s}$ = 510 GeV," Phys. Rev. D **94**, 112008 (2016).

R. Arnaldi et al. (NA60 Collaboration), "Precision study of the $\eta \rightarrow \mu^+ \mu^- \gamma$ and $\omega \rightarrow \mu^+ \mu^- \pi^0$ electromagnetic transition form-factors and of the $\rho \rightarrow \mu^+ \mu^-$ line shape in NA60," Phys. Lett. B **757**, 437−444 (2016).

A. Adare *et al*. (PHENIX Collaboration), Inclusive cross section and double-helicity asymmetry for π^0 production at midrapidity in $p+p$ collisions at $\sqrt{s}$ = 510 GeV," Phys. Rev. D **93**, 011501 (2016).

A. Adare *et al*. (PHENIX Collaboration), "Azimuthally anisotropic emission of low-momentum direct photons in Au$+$Au collisions at $\sqrt{s_{NN}}$ = 200 GeV," Phys. Rev. C **94**, 064901 (2016).

A. Adare *et al*. (PHENIX Collaboration), "Scaling properties of fractional momentum loss of high-p_{T} hadrons in nucleus-nucleus collisions at $\sqrt{s_{NN}}$ from 62.4 GeV to 2.76 TeV," Phys. Rev. C **93**, 024911 (2016).

A. Adare *et al*. (PHENIX Collaboration), "Transverse energy production and charged-particle multiplicity at midrapidity in various systems from $\sqrt{s_{NN}}$ = 7.7 to 200 GeV," Phys. Rev. C **93**, 024901 (2016).

A. Adare *et al*. (PHENIX Collaboration), "φ meson production in the forward/backward rapidity region in Cu$+$Au collisions at $\sqrt{s_{NN}}$ = 200 GeV," Phys. Rev. C **93**, 024904 (2016).

A. Adare *et al*. (PHENIX Collaboration), "Centrality-dependent modification of jet-production rates in deuteron-gold collisions at $\sqrt{s_{NN}}$ = 200 GeV," Phys. Rev. Lett. **116**, 122301 (2016).

A. Adare *et al*. (PHENIX Collaboration), "Measurement of higher cumulants of net-charge multiplicity distributions in Au$+$Au collisions at $\sqrt{s_{NN}}$ = 7.7−200 GeV," Phys. Rev. C **93**, 011901 (2016).

A. Adare *et al*. (PHENIX Collaboration), "Measurement of parity-violating spin asymmetries in W^{+-} production at midrapidity in longitudinally polarized $p + p$ collisions," Phys. Rev. D **93**, 051103 (2016).

M. Okamura *et al*., "Performance of the low charge state laser ion source in BNL," 10.18429/JACoW-HIAT2015-THM1C03.

S. Ikeda *et al*., "Control of laser ablation plasma by pulsed magnetic field for heavy ion beam production," 10.18429/JACoW-HIAT2015-WEPB28.

K. Kanno *et al*., "Development of a hadron blind detector using a finely segmented pad readout," Nucl. Instrum. Methods Phys. Res. A **819**, 20−24 (2016).

[Proceedings]

(Original Papers) *Subject to Peer Review

Y. Goto (PHENIX Collaboration), "Polarized nucleon-structure physics at RHIC-PHENIX," PoS **Hadron2013**, 155 (2014).

Y. Goto (RHICf collaboration), "Cross section and asymmetry measurement of very forward neutral particle production at RHIC," Int. J. Mod. Phys. Conf. Ser. **40**, 1660110 (2016).

R. Seidl, "Spin physics," PoS **DIS2016**, 007 (2016).

R. Seidl and T. Moon, "Measurement of double helicity asymmetries (A_{LL}) at mid- and forward rapidities in longitudinally polarized $p+p$ collisions at $\sqrt{s}$ = 510 GeV with PHENIX experiment," PoS **DIS2016**, 230 (2016).

I. Nakagawa., "Recent highlights from spin structure study of proton in PHENIX experiment at RHIC," The European Physical Society Conference on High Energy Physics, Venice, Italy, July 2017, PoS **EPS-HEP2017**, 391 (2018).

Oral Presentations

[International Conference etc.] [Domestic Conference]

S. Yokkaichi (JPARC E16 collaboration), "Systematic study of the vector meson spectral modification in the nuclear medium at J-PARC," MENU2016, Kyoto, Japan, July 27, 2016.

S. Yokkaichi (JPARC E16 collaboration), "Measurements of spectral change of vector mesons in nuclear matter," HINT2016, Tokai, Japan, Dec 05, 2016.

Y. Goto, "GPDs and TMDs at Electron-Ion Collider" in Hadron Tomography at J-PARC and KEKB," Tsukuba, Japan, Jan. 6, 2017.

R. Seidl, "Spin physics" in 24th International Workshop on Deep-Inelastic Scattering and Related Subjects, Hamburg, Germany, Apr. 11 2016.

R. Seidl, "Measurement of double helicity asymmetries (A_{LL}) in π^0 and π^{+-} production at mid-rapidity in longitudinally polarized $p + p$ collisions at $\sqrt{s} =$ 510 GeV with PHENIX experiment," 24th International Workshop on Deep-Inelastic Scattering and Related Subjects, Hamburg, Germany, Apr. 13, 2016.

R. Seidl, "RHIC spin and Belle," Workshop on hadron tomography, Kyoto, Japan, July 31, 2016.

R. Seidl, "The fragmentation function program at Belle," 22th International Spin Symposium, Urbana-Champaign, IL, USA, Sep. 28, 2016.

R. Seidl, "Fragmentation function measurements in Belle," KEK Hadron and Nuclear Physics Workshop, Tsukuba, Japan, Jan. 7.

I. Nakagawa, "The role of nucleon resonance via Primakoff effect in the very forward neutron asymmetry in high energy polarized proton-nucleus collision," Bled, Slovenia, July 2017.

[Domestic Conference]

Y. Goto (RHICf collaboration), "RHICf experiment: Very forward measurement of particle production at RHIC" Japan Physical Society Meeting, Sendai, Japan, March 20, 2016.

Y. Goto (PHENIX Collaboration), "Double-helicity asymmetry measurement of J/ψ production in $\sqrt{s} =$ 510 GeV polarized $p + p$ collisions at PHENIX," Japan Physical Society Meeting, Miyazaki, Japan, Sep. 23, 2016.

R. Seidl, "Fragmentation function measurements in Belle," JPS Fall Meeting, Miyazaki, Japan, Sep. 23, 2016.

I. Nakagawa (sPHENIX collaboration), "Development of silicon strip detector for the RHIC-sPHENIX experiment," Japan Physical Society Meeting, Utsunomiya University, Japan, September 14, 2017.

I. Nakagawa (RHICf collaboration), "Preparation for polarized proton scattering at very forward region at RHIC-Run17," Japan Physical Society Meeting, Osaka, Japan, March 17, 2017.

Sub Nuclear System Research Division
Advanced Meson Science Laboratory

1. Abstract

Particles like muons, pions, and kaons have finite life times, so they do not exist in natural nuclei or matters. By implanting these particles into nuclei/matters, exotic phenomena in various objects can be studied from new point of view.

Kaon is the second lightest meson, which has strange quark as a constituent quark. It is expected that if one embed mesons into nuclei, the sizes of the nuclei become smaller and one can form a high-density object beyond the normal nuclear density. Study of this object could lead to better understanding of the origin of the mass of the matter, and may reveal the quark degree of freedom beyond the quark-confinement. The other example is the weak interaction in nuclear matter. It can only be studied by the weak decay of hypernuclei, which have Lambda particle in the nuclei.

Muon provides even wider scope of studies, covering condensed matter physics as well as nuclear and atomic physics, and we are trying to extend the application field further into chemical and biological studies. For instance, stopping positively charged muon in a material, we obtain information on the magnetic properties or the local field at the muon trapped site (μSR). Injecting negatively charged muon to hydrogen gas, muonic hydrogen atom (μp) is formed. We are planning to measure μp hyperfine splitting energy to measure proton magnetic radius, which is complementary quantity to the proton charge radius and its puzzle lately attracts strong interest. We are also interested in precision measurement of muon property itself, such as muon anomalous magnetic moment ($g-2$).

In our research, we introduce different kind of impurities into nuclei / matters, and study new states of matter, new phenomena, or the object properties.

2. Major Research Subjects

(1) Study of meson property and interaction in nuclei
(2) Origin of matter mass / quark degree of freedom in nuclei
(3) Condensed matter and material studies with muon
(4) Nuclear and particle physics studies via muonic hydrogen
(5) Development of ultra cold muon beam, and its application from material science to particle physics

3. Summary of Research Activity

(1) Hadron physics at J-PARC, RIKEN-RIBF, GSI and SPring-8

Kaon and pion will shed a new insight to the nuclear physics. The recent discovery of deeply bound pionic atom enables us to investigate the properties of mesons in nuclear matter. At RIKEN-RIBF, we are preparing precise experimental study of the pionic atom. We have also started next generation kaon experiments (E15 and E31) at J-PARC. In these experiments, we are aiming to determine the $\overline{K}N$ interaction precisely, clarify the nature of kaon in nuclei, and $\Lambda(1405)$ that could be K^-p bound state. At Spring-8 and at GSI, we are also aiming to study omega and eta' nuclei. By these experiments, we aim to be a world-leading scientific research group using these light meta-stable particles.

(1-A) Deeply bound kaonic nuclei

We have performed experimental exploration of theoretically predicted deeply bound kaonic nuclear states, such as the K^-pp bound state. One of the most interesting features of the kaonic nucleus is the strong attraction of the $\overline{K}NN$ interaction. Because of this strong attraction, the kaon in nucleus will attract surrounding nucleons resulting in extremely high-density object, which is several times larger than normal nuclear density. Measurement of the kaon properties at such high energy density will provide precious information on the origin of hadron masses and the chiral symmetry breaking and its partial restoration.

The experiment J-PARC E15 aims to identify the nature of the K^-pp bound state by the in-flight ${}^3\text{He}(K^-, n)$ reaction, which allows us to investigate such state both in the formation via the missing-mass spectroscopy using the emitted neutron, and in its decay via the invariant-mass spectroscopy by detecting decay particles from K^-pp. For the experiment, we constructed a dedicated spectrometer system at the secondary beam-line, K1.8BR, in the hadron hall of J-PARC.

The first physics data-taking was carried out in March and May, 2013 with 6×10^9 kaons on ${}^3\text{He}$ target, corresponding to a ~1% of the approved proposal. We successfully obtained semi-inclusive ${}^3\text{He}(K^-, n)\text{X}$ missing-mass spectrum, and found a tail structure just below the mass threshold of $(K^- + p + p)$ which cannot be explained by well-known processes and backgrounds. We also demonstrated an exclusive analysis by reconstructing ${}^3\text{He}(K^-, \Lambda p)n$ events. To derive more information on the $\overline{K}NN$ interaction by the exclusive measurement, we carried out the second physics data-taking in November-December, 2015 with 43×10^9 kaons on ${}^3\text{He}$ target, in which 7 times more data was accumulated. We have been analyzing the new data set focusing on the ${}^3\text{He}(K^-, \Lambda p)n$ channel, and a significant bump structure below the $(K^- + p + p)$ mass threshold has been observed in the Λp invariant-mass spectrum. In addition, we have successfully observed $\Lambda(1405)pn$ final state in $K^- + {}^3\text{He}$ reactions by reconstructing $\pi^{\pm}\Sigma^{\mp}pn$ events, which is of special importance to understand the production mechanism of the $\langle K^-\text{pp}\rangle$ state via theoretically predicted $\Lambda(1405)p \rightarrow K^-pp$ doorway process. To confirm whether or not the observed structure is the K^-pp bound state, further analysis is currently in progress.

(1-B) Precision X-ray measurement of kaonic atom

Simultaneously with the above experiment (1-A), we have performed an X-ray spectroscopy of atomic $3d \rightarrow 2p$ transition of negatively charged K-mesons captured by helium atoms. However, the energy resolution of the conventional semiconductor spectrometers is insufficient to see the K^--nucleus potential observed by atomic levels at zero energy. This is closely related to the problem on the existence of deeply bound kaonic states in nuclei, well below the atomic levels, and this is one of the biggest problems in strangeness nuclear physics. Aiming to provide a breakthrough from atomic level observation, we will perform high-resolution X-ray spectroscopy of kaonic atoms at a J-PARC hadron beam line using a novel cryogenic X-ray spectrometer: an array of superconducting transition-edge-sensor (TES) micro-calorimeters.

The spectrometer offers unprecedented energy resolution, which is about two orders of magnitude better than that of conventional semiconductor detectors. A spectrometer array of 240 pixels will have an effective area of about 20 mm^2. In 2014, we have performed a proof-of-principle experiment by measuring pionic-atom X rays with a TES array at the πM1 beam line at the Paul Scherrer Institut (PSI), and successfully demonstrated the feasibility of TES-based exotic-atom x-ray spectroscopy in a hadron-beam environment. Based on the results, the kaonic-atom experiment at J-PARC was proposed in 2015 and will be conducted as the physics run in June 2018.

Another important X-ray measurement of kaonic atom would be $2p \rightarrow 1s$ transition of kaonic deuteron. We have measured same transition of kaonic hydrogen, but the width and shift from electro-magnetic (EM) value reflect only isospin average of the $\bar{K}NN$ interaction. We can resolve isospin dependence of the strong interaction by the measurement. We are presently preparing a proposal to J-PARC PAC to measure kaonic deuteron X-ray.

(1-C) Deeply bound pionic atoms and η' mesonic nuclei

We have been working on precision spectroscopy of pionic atoms systematically, that leads to understanding of hidden non-trivial structure of the vacuum and origin of hadron masses. The precision data set stringent constraints on the chiral condensate at nuclear medium. We are presently preparing for the systematic high precision measurement of pionic tin isotopes at RIBF. A pilot experiment was performed in 2010, and showed a very good performance of the system. A main experiment was performed in 2014 and we achieved unprecedented resolution with much reduced systematic errors. A new experiment is being prepared with an improved setup.

We are also working on spectroscopy of η' mesonic nuclei in GSI/FAIR. Theoretically, peculiarly large mass of η' is attributed to UA(1) symmetry and chiral symmetry breaking. As a result, large binding energy is expected for η' meson bound states in nuclei (η'-mesonic nuclei). First experiment was conducted in 2014 in GSI. We accumulated very high quality data in terms of the spectral resolution and the statistics and set constraints in the η'-nucleus interaction. A next generation experiment aims at improving the signal-to-background ratio and is in preparation.

(1-D) Hadron physics at SPring-8/LEPS2

Photo production of meson in nuclei is known to be a powerful tool to investigate property of the hadron in nuclear media. For this study, we started a new experimental project named LEPS2 (Laser Electron Photon at SPring-8 II) in this RIKEN Mid-term. The experimental hutch for LEPS2 at SPring-8 was constructed in March 2011, lead by RIKEN. The Large solenoid spectrometer magnet (2.96 m inner diameter × 2.22 m length) was successfully transported from BNL (US) to SPring-8 and installed into LEPS2 hutch in 2011.

One of the first physics programs is photo-production of η' in nuclei. Especially (γ, p) is most important reaction channel, where we can perform missing mass spectroscopy by detecting forward going proton. One of the big advantages of photo-production reaction is that the initial reaction is expected to be much cleaner than the hadron channel.

Detector construction for the first physics program is in progress. The 4π Electro-Magnetic calorimeter has been constructed and proton counter to detect forward going proton produced via (γ, p) reaction was partially installed in November 2013. Engineering run for the first experiment was performed in December 2013 to confirm performance of our detector system. Detector construction have been completed and 1st physics data taking was starting since 2014. Based on data collected, detail analysis to extract signal of η'-mesic nucleus, photoproduction of η etc are in progress.

(2) Muon science at RIKEN-RAL branch

The research area ranges over particle physics, condensed matter studies, chemistry and life science. Our core activities are based on the RIKEN-RAL Muon Facility located at the Rutherford-Appleton Laboratory (UK), which provides intense pulsed-muon beams. We have variety of important research activities such as particle / nuclear physics studies with muon's spin and condensed matter physics by muon spin rotation / relaxation / resonance (μSR).

(2-A) Condensed matter/materials studies with μSR

Two μSR spectrometer named CHRONUS and ARGUS are working together with ISIS standard data acquisition system, DAEII, with the front-end control system, SECI. Running a pulse-kicker system, we can perform two independent μSR experiments on CHRONUS and ARGUS at the same time, splitting double-pulse to share beam between the two.

Among our scientific activities on μSR studies from year 2017 to 2018, following five subjects of material sciences are most important achievements at the RIKEN-RAL muon facility:

    1) Novel superconducting state having partial nodal gaps in the two-dimensional organic superconductor λ-[BETS]$_2$GaCl$_4$.

    2) Tiny magnetic moments and spin structures of Ir^{4+}, Nd^{3+} in carrier doped pyrochlore iridates (Y$_{1-x}$Ca$_x$)$_2$Ir$_2$O$_7$.

    3) Magnetism and spin dynamics in superoxides CsO$_2$, NaO$_2$ and RbO$_2$.

    4) Magnetic properties of the nano-cluster gold in the border of macro- and micro-scale

    5) Effects of the spatial distributions of magnetic moments and muon positions estimated from density functional theory
      (DFT) and dipole-field calculations.

(2-B) Nuclear and particle physics studies via ultra cold muon beam and muonic atoms

If we can improve muon beam emittance, timing and energy dispersion (*so-called* "ultra-slow muon"), then the capability of μSR study will be drastically improved. The ultra-slow muon beam can stop in thin foil, multi-layered materials and artificial lattices, so one can apply the μSR techniques to surface and interface science. The development of ultra-slow muon beam is also very important as the source of ultra-cold (pencil-like small emittance) muon beam for muon $g - 2$ measurement. Therefore, we have been working on R&D study.

We have been working on the "ultra-slow muon" generation by laser ionization of muonium atoms in vacuum (bound system of μ^+ and electron) emitted after stopping "surface muon beam" in a material. In this mid-term, we are developing two key components, namely, high efficiency muonium generator at room temperature and high intensity ionization laser. The study of muonium generator has been done in collaboration with TRIUMF and KEK. In 2013, we demonstrated at least 10 times increase of the muonium emission efficiency by fabricating fine laser drill-holes on the surface of silica aerogel. In 2017, we further studied in detail which surface structure most contributes to the high yield. We also developed a high power Lyman-α laser based on novel laser crystal Nd:YGAG in collaboration with laser group at RIKEN. We are working on the growth of large laser amplifying crystal to further increase the Lyman-α power. In order to fully apply these new

developments to slow muon generation, we installed a new ultra-slow muon source chamber dedicated for silica aerogel in Port-3 with new features such as spin manipulation. We also plan measurement of the muonium emission rate by using μSR method, which should have sensitivity even to the muonium staying very close to the surface where the ionizing laser will be shot.

Concerning the muonic atom, we are planning a new precise measurement of proton radius. A large discrepancy was found recently in the proton charge radius between the new precise value from muonic hydrogen atom at PSI and those from normal hydrogen spectroscopy and e-p scattering. We propose a precise measurement of Zemach radius (with charge and magnetic distributions combined) using the laser spectroscopy of hyperfine splitting energy in the muonic hydrogen atom. Preparation of the hydrogen target, mid-infrared laser and muon spin polarization detectors is in progress. This year, we started a measurement of the lifetime of the μp triplet state, for which there has been no measured value but only theoretical calculations. Keeping the triplet state is essential for the measurement of polarization caused by resonant laser excitation.

Members

Chief Scientist (Lab. Head)
Masahiko IWASAKI

Vice Chief Scientist
Katsuhiko ISHIDA

Research & Technical Scientists
Isao WATANABE (Senior Research Scientist)   Hiroaki OHNISHI (Senior Research Scientist)
Kenta ITAHASHI (Senior Research Scientist)   Fuminori SAKUMA (Senior Research Scientist)
Haruhiko OUTA (Senior Research Scientist)   Yue MA (Senior Research Scientist)

Special Postdoctoral Researchers
Tadashi HASHIMOTO   Sohtaro KANDA
Hidemitsu ASANO

Research Consultants
Yoshinori AKAISHI   Masayasu KAMIMURA
Hironari MIYAZAWA   Eiichi YAGI

Junior Research Associates
Takuya SHIBUKAWA (Univ. of Tokyo)   Retno ASIH (Osaka Univ.)
Nam TRAN (Osaka Univ.)   Shu AIKAWA (Tokyo Tech.)
Fahmi ASTUTI (Hokkaido Univ.)   Shintaro TANAKA (Osaka Univ.)
Dita PUSPITA SARI (Osaka Univ.)   Juila ANGEL (Hokkaido Univ.)

International Program Associates
Noraina ADAM(Universiti Sains Malaysia)   Harison Binti ROZAK (UTM)
Sungwon YOON (Catholic Univ. of Korea)   Suci WINARSIH (Universitas Indonesia)
Saidah Sakinah Mohd Tajudin (Universiti Sains Malaysia)   Redo Muhammad RAMADHAN (Universitas Indonesia)

Senior Visiting Scientist
Kazuhiro TANAKA (KEK)

Visiting Scientists
Toshimitsu YAMAZAKI (Univ. of Tokyo)   Hiroyuki FUJIOKA (Kyoto Univ.)
Mototsugu MIHARA (Osaka Univ.)   Takayuki KAWAMATA (Tohoku Univ.)
Donald George FLEMING (Univ. of British Columbia) Helmut WEICK (GSI)
Yasuo NOZUE (Osaka Univ.)   Agustinus NUGROHO (ITB)
Takehito NAKANO (Osaka Univ.)   Yuta SADA (Osaka Univ.)
Tadashi ADACHI (Sophia Univ.)   Ichiro SHIRAKI (Univ. of Yamanashi)
Zyun Francis EZAWA (Tohoku Univ.)   Kensuke SUZUKI (Tohoku Univ.)
Yasuyuki ISHII (Shibaura Inst. of Tech.)   Kyosuke ISODA (Kagawa Univ.)
Johann ZMESKAL (SMI)   Tadashi HASHIMOTO (JAEA)
Risdiana (UNPAD)   Ken SUZUKI (SMI)
Takao SUZUKI (Shibaura Inst. of Tech.)   Irwan DHARMAWAN (UNPAD)
Georg Peter BERG (Univ. of Notre Dame)   Catalina Oana Curceanu(INFN)
Takayuki GOTO (Sophia Univ.)   Maryam Hassanvand(IUT)
Masaya ENOMOTO (Tokyo Univ. of Sci.)   Kazuki UENO (KEK)

    Lusy SAFRIANI (UNPAD)

    Hiroyuki NOUMI (Osaka Univ.)

    Zhuan XU (Zhejiang Univ.)

    Hiroshi TANIDA (Hiroshima Univ.)

    Atsushi OKAZAWA (Univ. of Tokyo)

    Hiroko MIWA (Hokkaido Univ.)

    Yoshiki TANAKA(GSI)

    Katsuhiko NISHIMURA (Univ. of Toyama)

    Kenji MATSUDA (Univ. of Toyama)

    Hexi SHI (LNF)

    Mohamed Ismail MOHAMED IBRAHIM (USM)

    Shukri SULAIMAN (USM)

    Eberhard WIDMANN(SMI)

    Koichi ICHIMURA (Hokkaido Univ.)

    KwangYong CHOI (Chung-Ang Univ.)

    Hideyuki TATSUNO (Lund Univ.)

    Emma HAETTNER (GSI)

    Andrea VACCHI (INFN)

    Takahiro NAMIKI (Univ. of Toyama)

    Naohito SAITO (KEK)

    Kouichirou SHIMOMURA (KEK)

    Ryousuke KADONO (KEK)

    Wataru HIGEMOTO (JAEA)

    Yoji KOIKE (Tohoku Univ.)

    Kazuhiko SATOH (Saitama Univ.)

    Masaru YOSOI (Osaka Univ.)

    Dai TOMONO (Osaka Univ.)

    Kazuki OHISHI (Comprehensive Res. Org. for Sci. and Soc.)

    Yasuhiro MIYAKE (KEK)

    Yu OISHI (KEK)

    Seiko KAWAMURA(JAEA)

Research Fellows

    Yuta SADA (Osaka Univ.)

    Yuki NOZAWA (Osaka Univ.)

Student Trainees

    Sohtaro KANDA (Univ. of Tokyo)

    Hiroyuki YAMADA (Univ. of Tokyo)

    Yuni WATANABE (Univ. of Tokyo)

    Xingliang Xu (Saga Univ.)

    Ryo KITAMURA(Univ. of Tokyo)

    Kim Taehyung (Tokyo Tech.)

    Kazuki MATSUI (Sophia Univ.)

    Ainul Fauzeeha Binti ROZLAN (Univ. Saints Malaysia)

    Sungwon YOON (Catholic Univ. of Korea)

    Koshi KURASHIMA (Tohoku Univ.)

    Takuro FUJIMAKI (Yamanashi Univ.)

    Govinda KHANAL (Yamanashi Univ.)

    Akane SAKAUE (Kyoto Univ.)

    Muhamad UMAR (Hokkaido Univ.)

    Irwan RAMLI (Hokkaido Univ.)

    Harison Binti ROZAK (UTM)

    Suci WINARSIH (Universitas Indonesia)

    Redo Muhammad RAMADHAN (Universitas Indonesia)

    Noraina ADAM(Universiti Sains Malaysia)

Part-time Workers

    Irwan RAMLI (Hokkaido Univ.)

Assistants

    Mitsue YAMAMOTO

    Noriko ASAKAWA

    Tokomo IWANAMI

List of Publications & Presentations

Publications

[Journal]

(Original Papers) *Subject to Peer Review

X.L. Xu *et al.*, "Utilizing Muon-spin-relaxation to probe ferroelectric transition in hydroxyl salt $Co_2(OD)_3Cl$," Ferroelectrics **505**, 1255131-1-6 (2016).*

E. Mocchiutti, *et al.*, "First FAMU observation of muon transfer from μp atoms to higher-Z elements," J. Instrum. **13**, 02019 (2018).*

R. Asih *et al.*, "Magnetic moments and ordered states in pyrochlore irridates $Nd_2Ir_2O_7$ and $Sm_2Ir_2O_7$ studied by muon spin relaxation," J. Phys. Soc. Jpn. **86**, 024705-1-7 (2017).*

M. Miyajima *et al.*, "Magnetism and high-magnetic field magnetization in alkali superoxide CsO_2," J. Phys. Soc. Jpn. **87**, 063704-1-4 (2018).*

K.L. Brown, C.P.J. Stockdale, H. Luo, X. Zhao, J.- H. Li, D. Viehland, G. Xu, P.M. Gehring, K. Ishida, A.D. Hillier and C. Stock, "Depth dependent element analysis of $PbMg_{1/3}Nb_{2/3}O_3$ using muonic X-rays," J. Phys. Condens. Matt. **30**, 125703 (2018).*

A. Taufiq *et al.*, "Studies on nanostructure and magnetic behaviors of Mn-doped black iron oxide magnetic fluids synthesized from iron sand," Nano **12**, 1750110-1-11 (2017).*

K. Wang *et al.*, "Temporal mapping of electrophilic photochemical reactions and excitonic processes with carbon specificity," Nat. Mat. **16**, 467−473 (2017).*

E. Spurayoga *et al.*, "3D long-range magnetic ordering in $(C_2H_5NH_3)_2CuCl_4$ compound revealed by internal magnetic field from muon spin rotation and first principal calculation," Physica B **545,** 76−79 (2018).*

S. Bae *et al.*, "First muon acceleration using a radio frequency accelerator," Phys. Rev. Accel. Beams **21**, 050101 (2018).*

X.L. Xu *et al.*, "Critical slowing of quantum atomic H/D with features of multiferroicity in geometrically frustrated system $Co_2(OD)_3Cl/Co_2(OH)_3Cl$," Phys. Rev. B **95**, 024111-1-10 (2017).*

A. Glamazda *et al.*, "Quantum criticality in the coupled two-leg spin ladder Ba_2CuTeO_{6}"," Phys. Rev. B **95**, 184430 (2017).*

R. Takagi *et al.*, "Antiferromagnetic Mott insulating state in the single-component molecular material Pd(tmdt)$_2$," Phys. Rev. B **96**, 214432 (2017).*

K. Mizutani *et al.*, "φ photoproduction on the proton at $E_\gamma = 1.5-2.9$ GeV," Phys. Rev. C **96**, 062201(R) (2017).*

Y.K. Tanaka, K. Itahashi *et al.*, "Missing-mass spectroscopy of the ^{12}C(p, d) reaction near the η'-meson production threshold," Phys. Rev. C **97**, 015202 (2018).*

H. Kohri *et al.*, "Differential cross section and photon-beam asymmetry for the $\gamma p \to \pi^+ n$ reaction at forward π^+ angles at $E_\gamma = 1.5-2.95$ GeV," Phys. Rev. C **97**, 015205 (2018).*

S.H. Shiu *et al.*, "Photoproduction of Λ and Σ^0 hyperons off protons with linearly polarized photons at $E_\gamma = 1.5-3.0$ GeV," Phys. Rev. C **97**, 015208 (2018).*

T. Hiraiwa *et al.*, "First measurement of coherent φ-meson photoproduction from ^{4}He near threshold," Phys. Rev. C **97**, 035208 (2018).*

[Proceedings]
(Original Papers) *Subject to Peer Review

Y.K. Tanaka *et al.*, "First results on the experimental search for η'-mesic nuclei with the ^{12}C(p, d) Reaction," Acta Phys. Pol. B **48**, 1813−1818 (2017).*

K. Itahashi, "Precision spectroscopy of pionic atoms and chiral symmetry in nuclei," EPJ Web Conf. **130**, 01017 (2016).*

T. Hashimoto *et al.*, "Beamline test of a transition-edge-sensor spectrometer in preparation for kaonic-atom measurements," IEEE Trans. Appl. Supercond. **27**(4), 1–5, 10.1109/TASC.2016.2646374, (2017)*

K. Takao *et al.*, "Paramagnetic-to-nonmagnetic transition in antiperovskite nitride Cr$_3$GeNi studied by ^{14}N-NMR and μSR," J. Phys. Conf. Ser. **868**, 012021-1-4 (2017).*

Risdiana *et al.*, "Zn-induced development of the Cu-spin correlation in electron-doped superconducting cuprates of Eu$_{2-x}$Ce$_x$CuO$_4$," J. Phys. Conf. Ser. **1013**, 012180-1-5 (2018).*

F. Sakuma *et al.*, "$\bar{K}NN$ Bound State Search at J-PARC," Proceedings of the 14th International Conference on Meson-Nucleon Physics and the Structure of the Nucleon (MENU2016), JPS Conf. Proc. **13** (2017) 010002. *

K. Itahashi, "Excitation Spectra of Carbon Nuclei near η' Emission Threshold," JPS Conf. Proc. **13**, 020030 (2017).

T. Hashimoto *et al.*, "Kaonic-atom X-ray spectroscopy with superconducting microcalorimeters," JPS Conf. Proc. **17**, 072001, 10.7566/JPSCP.17.072001, (2017).*

K. Itahashi, "Search for η' mesic nuclei in GSI/FAIR," JPS Conf. Proc. **17**, 082008 (2017).*

T. Sumura *et al.*, "Reduction effect on the Cu-spin correlation in the electron-doped T'-cuprate Pr$_{1.3-x}$La$_{0.7}$Ce$_x$CuO$_{4+\delta}$ ($x = 0.10$)," J. Phys. Conf. Proc. **21**, 011027-1-5 (2018).*

A. Hillier *et al.*, "Element specific imaging using muonic x-rays," JPS Conf. Proc. **21**, 011042 (2018).*

D.P. Sari *et al.*, "μSR Study of organic superconductor λ-(BETS)$_2$GaCl$_4$," Mater. Sci. Eng. **196**, 012047-1-6 (2017) *

I. Watanabe *et al.*, "The RIKEN-RAL Muon Facility and the application of muons for studies of magnetic properties of nano-materials," Mater. Sci. Forum **901**, 37−43 (2017).*

S. Kanda *et al.*, "Precision laser spectroscopy of the ground state hyperfine splitting in muonic hydrogen," Proceedings of Science, PoS, **NuFACT2017**, 122 (2018).*

Oral Presentations

[International Conference etc.]

M. Niiyama, "Hadron physics at LEPS/LEPS II and Belle", ETC*2017 "Space-like and time-like electromagnetic baryonic transitions," Trento, Italy, May 2017.

K. Ishida, "MuP HFS measurement with spin polarization," FAMU meeting, Trieste, Italy, May 2017.

K. Itahashi, "Status and plans of pionic atoms spectroscopy at RIBF," 2nd Jagiellonian symposium on fundamental and applied subatomic physics, Krakow, Poland, June 2017.

T. Hashimoto et al., "TES application to kaonic atom X-ray spectroscopy in a charged-particle beamline," 17th International Workshop on Low Temperature Detectors 2017 (LTD17), Fukuoka, July 2017.

S.Y. Ryu, "Exotic baryon systems from photoproduction and beam commissioning of the LEPS2 solenoid spectrometer," APFB2017, Guilin, China, August 2017.

H. Kohri, "PhotoProduction of π-Δ^{++}, $\pi+\Delta^0$, and $\pi^+ n$ on the proton at $E\gamma = 1.5-3.0$ GeV at LEPS/SPring-8," NSTAR2017, Columbia, USA, August 2017.

K. Ishida, "Muon Facility at RIKEN-RAL," International Workshop on Organic Molecule Systems, Penang, Malaysia, August 2017.

H. Kohri, "PhotoProduction of π-Δ^{++} and $\pi^+\Delta^0$ on the proton for the comparison of $\bar{u}u$ and $\bar{d}d$ productions," XVII International conference on hadron spectroscopy and structure (HADRON2017), Salamanca, Spain, September 2017.

M.Iwasaki, "Search for the simplest kaonic bound state K^-pp via ^{3}He(K^-, n) reaction at J-PARC2," XVII International conference on hadron spectroscopy and structure (HADRON2017), Salamanca, Spain, September 2017.

K. Itahashi, "Meson-nucleus bound states," XVII International conference on hadron spectroscopy and structure (HADRON2017), Salamanca, Spain, September 2017.

T. Nishi, "Precision spectroscopy of pionic $^{121, 116}$Sn atoms at RI Beam Factory," International Conference on Exotic Atoms and Related Topics (EXA2017), Vienna, Austria, September 2017.

S. Okada et al., "X-ray spectroscopy of kaonic atoms with cryogenic detectors," International Conference on Exotic Atoms and Related Topics (EXA2017), Vienna, Austria, September 2017.

K. Ishida for J-PARC muon $g-2$/EDM collaboration, "Muon $g-2$/EDM experiment at J-PARC," The 19th international workshop on neutrinos from accelerators (NUFACT2017), Uppsala, Sweden, September 2017.

Y. Yanai, "Development of polarized HD target for SPring-8/LEPS experiment," PSTP2017, Daejeon, Korea, October 2017.

F. Sakuma, "$\bar{K}NN$ bound state search at J-PARC E15," ASTRA: Advances and open problems in low-energy nuclear and hadronic STRAngeness physics, ECT, Trento, Italy, October 2017.

M. Iwasaki, "Search for Kaonic Bound States at JPARC," 3rd Resonance Workshop in Bergamo, Camera di Commercio, Bergamo, Italy, October 2017.

S. Kanda, "Precision laser spectroscopy of the ground state hyperfine splitting in muonic hydrogen," NuFACT2017, Uppsala, Sweden, October 2017.

K. Ishida, "Nuclear physics experiments using muons," CSNS Seminar, Dongguan, China, December 2017.

S. Kanda "Precision laser spectroscopy of the ground-state hyperfine splitting in muonic hydrogen atom," FPUA2018, Nagoya, January 2018.

K. Ishida, "Proton radius measurement from studies in muonic hydrogen," International Symposium on Nucleon Structure, Yamagata, March 2018.

[Domestic Conference]

時安敦史,「LEPS 実験［γ-indeced］と LEPS2 での後続実験」, 第 1 回「ストレンジネス核物理を考える会」, 和光, 4 月(2017).

石田勝彦,「ミューオン水素分光ー陽子半径の決定」, 核物理の将来　基礎物理班勉強会, 4 月(2017).

石田勝彦,「ミュオン水素原子の超微細構造エネルギー測定による陽子 Zemach 半径決定」, 電子光理学研究センターセミナー, 仙台, 8 月(2017).

時安敦史,「Λ(1405) photoproduction at LEPS/LEPS2」, 第 5 回「ストレンジネス核物理を考える会」, 和光, 9 月(2017).

川﨑新吾,「J-PARC K1.8BR ビームラインにおける $d(K^-,\mathrm{n})$反応による Λ(1405)粒子の精密分光実験の $\pi^0\Sigma^0$ 終状態に関する解析状況(2) 」, 日本物理学会 2017 年秋季大会, 宇都宮大学, 9 月(2017).

井上謙太郎,「J-PARC K1.8BR ビームラインにおける $d(K^-, N)\pi\Sigma$ 反応を用いた Λ(1405)の精密分光実験の解析状況」, 日本物理学会 2017 年秋季大会, 宇都宮大学, 9 月(2017).

神田聡太郎,「ミュオン水素原子の精密レーザー分光」, 日本物理学会 2017 年秋季大会, 宇都宮大, 9 月(2017).

佐久間史典, "The latest results from J-PARC E15," 新学術領域研究「実験と観測で解き明かす中性子星の核物質」第 6 回「中性子 星核物質」研究会, RIKEN, 和光, 12 月(2017).

石田勝彦,「理研 RAL ミュオン施設」, 第 8 回 Muon 科学と加速器研究, つくば, 1 月(2018).

神田聡太郎, "Laser spectroscopy of the hyperfine splitting in ground-state of muonic hydrogen atom," 第 8 回 Muon 科学と加速器研究, つくば, 1 月(2018).

神田聡太郎,「超伝導計測のミューオン実験への応用」, TIA かけはし事業「簡単・便利な超伝導計測」研究会, 和光, 1 月(2018 年).

佐久間史典, "Recent results of the $\bar{K}NN$ search at J-PARC," 2017 年度 KEK 理論センターJ-PARC 分室活動 総括研究会, J-PARC, 2 月(2018).

岩崎雅彦,「K 中間子と原子核 (K-meson and nuclei)－Based on E15: Search for kaonic nuclear bound state」, KEK 理論センターJ-PARC 分室/JAEA 先端基礎研究センター共催研究会　「ヘビークォークハドロンとエキゾチックハドロンの構造」, J-PARC, 3 月(2018).

橋本直,「J-PARC E15 実験における前方核子を用いた$\bar{K}NN$束縛状態の研究」, 日本物理学会第 73 回年次大会, 東京理科大, 野田, 3 月(2018).

佐久間史典,「J-PARC E15 実験における $\pi\Sigma N$ 崩壊チャンネルを用いた $\bar{K}NN$ 束縛状態の研究」, 日本物理学会第 73 回年次大会, 東京理科大, 野田, 3 月(2018).

山我拓巳,「Λpn 終状態における$\bar{K}NN$束縛状態の研究」, 日本物理学会第 73 回年次大会, 東京理科大, 野田, 3 月(2018).

岩崎雅彦,「J-PARC E15 実験の解析の進展と今後の展望」, 日本物理学会第 73 回年次大会, 東京理科大, 野田, 3 月(2018).

Omar Zhadyra, "Toward a study of Λ(1405) via the $d(K^-, \Sigma\pi)$ reaction," 日本物理学会第 73 回年次大会, 東京理科大, 野田, 3 月(2018).

川﨑新吾,「J-PARC K1.8BR ビームラインにおける $d(K^-, n)$反応による Λ(1405)粒子の精密分光実験の $\pi^0\Sigma^0$ 終状態に関する解析状況 (3)」, 日本物理学会第 73 回年次大会, 東京理科大, 野田, 3 月(2018).

井上謙太郎,「J-PARC K1.8BR ビームラインにおける $d(K^-, N)\pi\Sigma$ 反応を用いた Λ(1405)の精密分光実験の解析結果」, 日本物理学会第 73 回年次大会, 東京理科大, 野田, 3 月(2018).

石田勝彦,「陽子パズルに挑むミュオン水素原子超微細構造分光」, 日本物理学会第 73 回年次大会, 東京理科大, 野田, 3 月(2018).

神田聡太郎, "Direct measurement of muonium ground state hyperfine splitting with high-intensity pulsed muon beam," 日本物理学会第 73 回年次大会, 東京理科大, 野田, 3 月(2018).

神田聡太郎,「ミュオン水素原子分光実験のための中赤外光源の開発」, 日本物理学会第 73 回年次大会, 東京理科大, 野田, 3 月(2018).

Sub Nuclear System Research Division
RIKEN BNL Research Center

1. Abstract

The RIKEN BNL Research Center was established in April 1997 at Brookhaven National Laboratory with Professor T. D. Lee of Columbia University as its initial Director. It is funded by the Rikagaku Kenkyusho (RIKEN, The Institute of Physical and Chemical Research) of Japan. The Center is dedicated to the study of strong interactions, including spin physics, lattice QCD and RHIC physics through the nurturing of a new generation of young physicists. Professor Lee was succeeded by BNL Distinguished Scientist, N. P. Samios, who served until 2013. Dr. S. H. Aronson led the Center from 2013. After strong and significant leadership for 4 years, S. Aronson stepped down from Director in March 31st 2017. Hideto En'yo succeeds from JFY 2017.Support for RBRC was initially for five years and has been renewed four times, and presently extends to 2023. The Center is located in the BNL Physics Department. The RBRC Theory Group activities are closely and intimately related to those of the Nuclear Theory, High Energy Theory, and Lattice Gauge Theory Groups at BNL. The RBRC Experimental Group works closely with Radiation Laboratory at RIKEN, Wako, the RHIC Spin Group at BNL, the RHIC Spin Physics community, and the PHENIX collaboration. BNL provides office space, management, and administrative support. In addition, the Computational Science Initiative (CSI) and Information Technology Division (ITD) at BNL provide support for computing, particularly the operation and technical support for the RBRC 400 Teraflop QCDCQ (QCD Chiral Quark) lattice gauge theory computer. The Deputy Director of RBRC is R. Pisarski (BNL). D. Kharzeev (Stony Brook/BNL) is leader of the Theory Group. Y. Akiba (RIKEN) is Experimental Group leader with A. Deshpande (Stony Brook) deputy. T. Izubuchi (BNL) is Computing Group leader.

2. Major Research Subjects

Major research subjects of the theory group are
  (1)   Heavy Ion Collision
  (2)   Perturbative QCD
  (3)   Phenomenological QCD
Major research subjects of the computing group are
  (1)   Search for new law of physics through tests for Standard Model of particle and nuclear physics
  (2)   Dynamics of QCD and related theories
  (3)   Theoretical and algorithmic development for lattice field theories, QCD machine design
Major research subject of the experimental group are
  (1)   Experimental Studies of the Spin Structure of the Nucleon
  (2)   Study of Quark-Gluon Plasma at RHIC
  (3)   sPHENIX detector construction

3. Summary of Research Activity

Summary of Research Activities of the three groups of the Center are given in the sections of each group.

Members

Director
Hideto En'yo (concurrent: Director, Nishina Center for Accelerator-Based Science)

Deputy Director
Robert PISARSKI

Administrative Staff
Kazunori Mabuchi (Administration Manager, Nishina Center Planning Office)

Yasutaka AKAI (Deputy Administration Manager, Nishina Center Planning Office)

Hiroshi ITO (Deputy Administration Manager, Nishina Center Planning Office)

Colleen MICHAEL (Administrative Assistant)

Pamela ESPOSITO (Administrative Assistant)

Maureen McNeill-Shea (Administrative Assistant)

Sub Nuclear System Research Division
RIKEN BNL Research Center
Theory Group

1. Abstract

The efforts of the RBRC theory group are concentrated on the major topics of interest in High Energy Nuclear Physics and strongly interacting Chiral Matter. This includes: understanding of the Quark-Gluon Plasma; the nature of dense quark matter; the initial state in high energy collisions, the Color Glass Condensate; its evolution through a Glasma; spin physics, as is relevant for polarized hadronic collisions; physics relevant to electron-hadron collisions and the Electron-Ion Collider; quantum transport and the Chiral Magnetic Effect.

Theory Group hosted many joint tenure track positions with universities in U.S. and Japan.

2. Major Research Subjects

(1) Heavy Ion Collisions
(2) Perturbative Quantum Chromo-Dynamics (QCD)
(3) Phenomenological QCD
(4) Chiral Matter

3. Summary of Research Activity

(1) Phase diagram of QCD

The heavy ion program at Relativistic Heavy Ion Collider (RHIC) at BNL is focused on the study of the properties of QCD matter at high energy densities and high temperatures. The RBRC Theory group performs research that supports and guides the experimental program at RHIC. In the past year, RBRC researchers had identified the possibility for the higher-order phase transitions in QCD (H. Nishimura, R. Pisarski, V. Skokov) by using the novel approach based on the matrix models.

The first-principle studies of QCD phase diagram at finite baryon density using the lattice Monte Carlo approach are very difficult because of the so-called "sign problem." The work by H. Nishimura and Y. Tanizaki, in collaboration with J. Verbaarschot of Stony Brook Nuclear Theory group, has proposed a new kind of the gradient flow method that can be used to alleviate this problem.

An important feature of strongly interacting matter at finite baryon density is the liquid-gas phase transition. The paper by H. Nishimura (in collaboration with M. Ogilvie and K. Pangeni) develops a field-theoretic approach to the liquid-gas phase transition based on an effective 3D field theory.

Quantum anomalies play an important role in QCD phase transitions. Y. Tanizaki, Y. Kikuchi (who will join the RBRC Theory group in 2018) and collaborators utilized the method of "anomaly matching" to obtain important constraints on the dynamics of deconfinement and chiral restoration phase transitions in QCD. They also used this method to study the vacuum structure of QCD at finite theta-angle.

(2) QCD Matter at High Energy Density and at small x

The RHIC experimental heavy ion program is designed to study the properties of matter at energy densities much greater than that of atomic nuclei. This includes the initial state of nucleus-nucleus collisions, the Color Glass Condensate, the intermediate state to which it evolves, the Glasma, and lastly the thermal state to which it evolves, the Quark-Gluon Plasma. Theorists at the RBRC have made important contributions to all of these subjects.

During the past year, V. Skokov (in collaboration with Y. Kovchegov, A. Dumitru, and others) investigated the role of classical gluon fields at small Bjorken x in generating the azimuthal anisotropy of hadrons produced in AA and pA collisions at RHIC. It has been found that the correlations inside the small x distributions effectively generate odd azimuthal harmonics in hadron distributions, with a long-range separation in rapidity. In collaboration with A. Kovner and M. Lublinsky, V. Skokov also investigated the possible effect of quark-gluon correlations at small x on the studies of the Chiral Magnetic Effect in pA collisions at RHIC. D. Kharzeev, in collaboration with W. Li and Z. Tu, investigated the role of fluctuating proton size on the CME studies in pA collisions, and found that these fluctuations induce a significant correlation between the direction of magnetic field and the reaction plane, enabling the observation of CME.

The ongoing Isobar run at RHIC (made possible due to the RIKEN scientists working on Zr source) will establish or rule out the existence of the Chiral Magnetic Effect (originally proposed by RBRC theorists) in the quark-gluon plasma. During the past year, D. Kharzeev and H.-U. Yee, in collaboration with Y. Hirono, M. Mace and others have developed the Chiral Magneto-Hydodynamics (CMHD) approach to the Chiral Magnetic Effect (CME) in quark-gluon plasma. The first numerical results of CMHD have become available due to the collaboration of RBRC with the ECHO-QGP group. H.U. Yee and collaborators investigated dynamical instabilities in CMHD. D. Kharzeev and H.U. Yee, in collaboration with M. Stephanov, solved a long-standing puzzle of the apparent discrepancy between the field theory and the kinetic theory on the magnitude of the CME current at finite frequency. D. Kharzeev, with Y. Hirono and A. Sadofyev, proposed a new "chiral propulsion effect" for the chiral solitons on vortices in chiral media.

The activity of RBRC members described above bridges the gap between fundamental theory and phenomenology of heavy ion collisions. This includes the lattice QCD studies, the analytical work on the dynamics of phase transitions, the development of hydrodynamical and kinetic theory approaches incorporating quantum anomalies, and phenomenology. Much of the current work in the field is based on the ideas originally developed by the RBRC theorists.

(3) Chiral Matter

Much of the work done at the RBRC Theory group has broad implications beyond the domain of Nuclear and High Energy physics. One example is the Chiral Magnetic Effect, originally proposed to occur in quark-gluon plasma, but discovered recently in condensed matter systems, so-called Dirac and Weyl semimetals (the original experimental observation of CME was made at BNL in $ZrTe_5$ in a paper co-authored by D. Kharzeev). It has become clear that RBRC can make a very substantial impact also on condensed matter physics, where the methods developed at RBRC can be applied to a new set of problems. Vice versa, some of the new theoretical developments in condensed matter physics can be utilized for the study of QCD matter. Because of this, the RBRC developed a new initiative on Chiral Matter focusing on the studies of quantum behavior in strongly interacting matter containing chiral fermions – this includes the quark-gluon plasma, electroweak plasma, Dirac and Weyl semimetals, and topological insulators.

In the past year, the RBRC members within this new initiative obtained a number of new results. Some of them, with a direct relevance for the quark-gluon plasma, have been already described above; other results are of direct relevance for condensed matter physics. D. Kharzeev, Y. Tanizaki and Y. Kikuchi (a postdoc who will join RBRC in 2018), in collaboration with R. Meyer, found that asymmetric Weyl semimetals support a giant photocurrent as a result of chiral anomaly. D. Kharzeev, Y. Kikuchi and R. Meyer also proposed a new kind of dynamical CME in asymmetric Weyl semimetals that does not require an external source of chirality, and proposed an experiment to test their prediction. D. Kharzeev with his Stony Brook student S. Kaushik have identified a new type of quantum oscillations in the CME conductivity at finite doping.

The Chiral Matter initiative has already broadened the impact of RBRC beyond the traditional domain of high-energy nuclear physics, and has extended the RBRC research into a new and extremely active area.

Members

Group Leader (Lab. Head)
Dmitri KHARZEEV

Deputy Group Leader
Robert PISARSKI

RBRC Researchers

Ho-Ung YEE (RHIC Physics Fellow)

Yuya TANIZAKI (Special Postdoctoral Researcher)

Hiromichi NISHIMURA (Special Postdoctoral Researcher)

Vladimir SKOKOV (Special Postdoctoral Researcher)

Sub Nuclear System Research Division
RIKEN BNL Research Center
Computing Group

1. Abstract

The computing group founded in 2011 as a part of the RIKEN BNL Research Center established at Brookhaven National Laboratory in New York, USA, and dedicated to conduct researches and developments for large-scale physics computations important for particle and nuclear physics. The group was forked from the RBRC Theory Group.

The main mission of the group is to provide important numerical information that is indispensable for theoretical interpretation of experimental data from the first principle theories of particle and nuclear physics. Their primary area of research is lattice quantum chromodynamics (QCD), which describes the sub-atomic structures of hadrons, which allow us the ab-initio investigation for strongly interacting quantum field theories beyond perturbative analysis.

The RBRC group and its collaborators have emphasized the necessity and importance of precision calculations, which will precisely check the current understandings of nature, and will have a potential to find a physics beyond the current standard model of fundamental physics. We have therefore adopted techniques that aim to control and reduce any systematic errors. This approach has yielded many reliable results.

The areas of the major activities are R&D for high performance computers, developments for computing algorithms, and researches of particle, nuclear, and lattice theories. Since the inception of RBRC, many breakthroughs and pioneering works has carried out in computational forefronts. These are the use of the domain-wall fermions, which preserve chiral symmetry, a key symmetry for understanding nature of particle nuclear physics, the three generations of QCD devoted supercomputers, pioneering works for QCD calculation for Cabibbo-Kobayashi-Maskawa theory, QCD + QED simulation for isospin breaking, novel algorithm for error reduction in general lattice calculation. Now the chiral quark simulation is performed at the physical up, down quark mass, the precision for many basic quantities reached to accuracy of sub-percent, and the group is aiming for further important and challenging calculations, such as the full and complete calculation of CP violating K $\to \pi\pi$ decay and ε'/ε, or hadronic contributions to muon's anomalous magnetic moment $g - 2$. Another focus area is the nucleon's shape, structures, and the motion of quarks and gluon inside nucleon called parton distribution, which provide theoretical guidance to physics for future Electron Ion Collider (EIC), Hyper Kamiokande, DUNE, or the origin of the current matter rich universe (rather than anti-matter). Some of members carry out interesting research on strong gauge dynamics other than QCD to get hints for the true nature of the Higgs particle or the Dark Matter, or even quantum gravity.

2. Major Research Subjects

(1) Search for new law of physics through tests for Standard Model of particle and nuclear physics, especially in the framework of the Cabibbo–Kobayashi–Maskawa (CKM), hadronic contributions to the muon's anomalous magnetic moment $(g - 2)$ for FNAL and J-PARC's experiments, as well as B physics at Belle II and LHCb.

(2) Nuclear Physics and dynamics of QCD or related theories, including study for the structures of nucleons related to physics for Electron Ion Collider (EIC or eRHIC), Hyper Kamiokande, T2K, DUNE.

(3) Theoretical and algorithmic development for lattice field theories, QCD machine (co-)design and code optimization.

3. Summary of Research Activity

In 2011, QCD with Chiral Quarks (QCDCQ), a third-generation lattice QCD computer that is a pre-commercial version of IBM's Blue Gene/Q, was installed as an in-house computing resource at the RBRC. The computer was developed by collaboration among RBRC, Columbia University, the University of Edinburgh, and IBM. Two racks of QCDCQ having a peak computing power of 2×200 TFLOPS are in operation at the RBRC. In addition to the RBRC machine, one rack of QCDCQ is owned by BNL for wider use for scientific computing. In 2013, 1/2 rack of Blue Gene/Q is also installed by US-wide lattice QCD collaboration, USQCD. The group has also used the IBM Blue Gene supercomputers located at Argonne National Laboratory and BNL (NY Blue), and Hokusai and RICC, the super computers at RIKEN (Japan), Fermi National Accelerator Laboratory, the Jefferson Lab, and others. From 2016, the group started to use the institutional cluster both GPU and Intel Knight Landing (KNL) clusters installed at BNL and University of Tokyo extensively.

Such computing power enables the group to perform precise calculations using up, down, and strange quark flavors with proper handling of the important symmetry, called chiral symmetry, that quarks have. The group and its collaborators carried out the first calculation for the direct breaking of CP (Charge Parity) symmetry in the hadronic K meson decay (K $\to \pi\pi$) amplitudes, ε'/ε, which provide a new information to CKM paradigm and its beyond. They also provide the hadronic contribution in muon's anomalous magnetic moment $(g - 2)_\mu$. These calculation for ε'/ε, hadronic light-by-light of $(g - 2)$, are long waited calculation in theoretical physics delivered for the first time by the group. The K $\to \pi\pi$ result in terms of ε'/ε currently has a large error, and deviates from experimental results by 2.1 σ. To collect more information to decide whether this deviation is from the unknown new physics or not, the group continues to improve the calculation in various way to reduce their error. Hadronic light-by-light contribution to $(g - 2)_\mu$ is improved by more than two order of magnitudes compared to our previous results. As of 2018 summer, their calculation provide the most precise determination for the $g - 2$ hadronic vacuum polarization (HVP), and only one calculation in the world for the hadronic light-by-light (HLbL) contribution. Other projects including flavor physics in the framework of the CKM theory for kaons and B mesons that include the new calculation of b-baryon decay, $\Lambda b \to p$; the electromagnetic properties of hadrons; the proton's and neutron's form factors and structure function including electric dipole moments; proton decay; nucleon form factors, which are related to the proton spin problem or neutrino-nucleon interaction;

Neutron-antineutron oscillations; inclusive hadronic decay of τ leptons; nonperturbative studies for beyond standard model such composite Higgs or dark matter models from strong strongly interacting gauge theories; a few-body nuclear physics and their electromagnetic properties; and QCD thermodynamics in finite temperature/density systems such as those produced in heavy-ion collisions at the Relativistic Heavy Ion Collider.
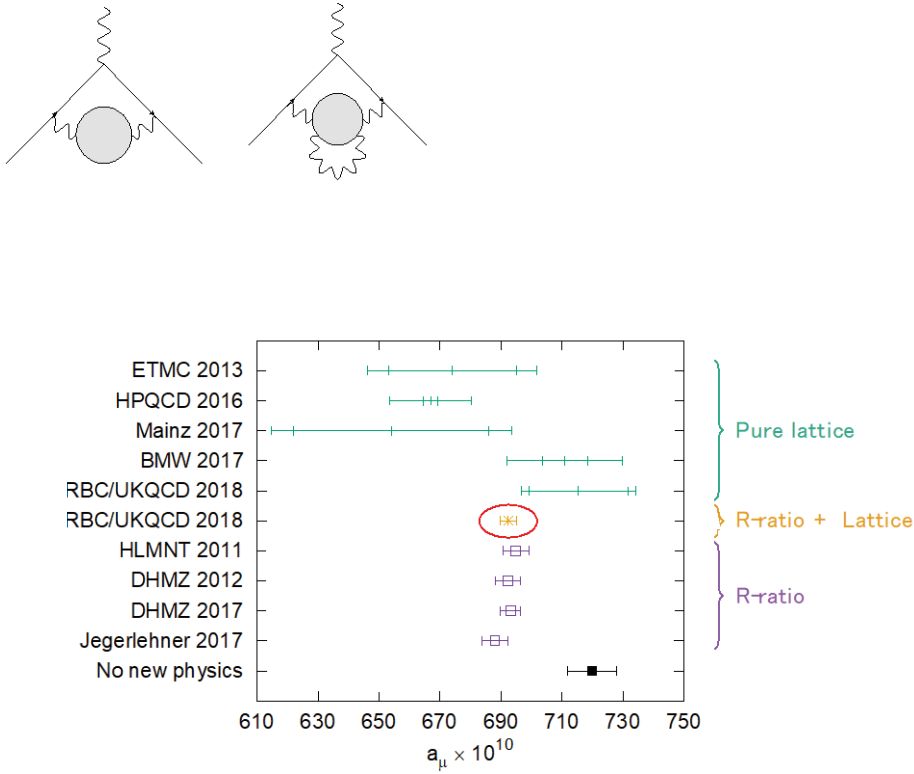
Figure: The botT. plot is the overview of the Hadronic Vacuum Polarization (HVP) to muon anomalous magnetic moment shown at top-left. Our result (RBC/UKQCD 2018) is the first calculation to include QED and the strong isospin breaking (top-right). Our combined method of lattice QCD and R-ratio (circled) validates and improves the precision. From arXiv: 1801.07224.

Theme	Significant Outcomes	Expected Impacts & Extensions
(a) DWF QCD ensemble generation and measurements of basic quantities	Hadron spectrum, f_π, f_K, K_{l3}, B_K, and accurate ChPT Low Energy Constants (LECs)	Basis of physical observables
(b) Operator Renormalization	Precise matrix elements, bag parameters quark masses, and coupling constants	Reduced systematic error in e.g. $K \to \pi\pi$ amplitudes
(c) Computational Algorithms, Software, and Machines	Fast and Cost-Effective Computing All Mode Averaging (AMA) PhySyHCAl	Unprecedented precision and new physical quantities
(d) K physics	$K_{l3}, \Delta I = 1/2, 3/2, K \to \pi\pi$ amplitudes, ε'/ε $K_L - K_S$ Mass Difference, ε_K^{LD}	New tests of the SM
(e) B physics	Matrix elements for (semi-)leptonic decays and $B^0 - \overline{B^0}$ oscillations	CKM matrix, e.g., V_{ub}, V_{ts}, V_{td} and R-ratios for LUV tests .
(f) QED and Isospin breaking effects	Better determination of quark masses Proton-Neutron Mass Difference	A step towards sub-% precision groundwork for $(g-2)_\mu$
(g) Muon Anomalous Magnetic Moment $(g-2)_\mu$	Hadronic Vacuum Polarization contribution Light-by-Light contribution	$(g-2)_\mu$ experiments at BNL, FNAL, J-PARC
(h) Nucleon calculations for HEP	Vector/Axial form factors of nucleon Proton decay matrix element Nucleon EDM and $F_3(q^2)$ from vacuum angle θ and quark's (Chromo) EDM Parton Distribution Function	DUNE, Super-K, T2K GUT EDM experiments incl. ORNL, LANL Origin of matter in Universe LHC, Electron-Ion Colliders

Table: Summery of current physics program and their impacts
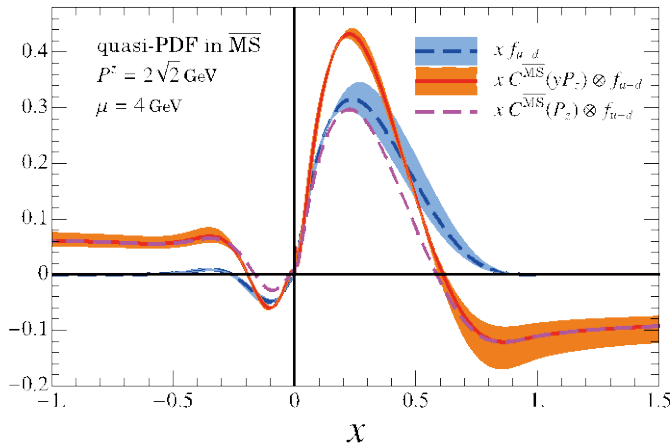
Figure: Parton distribution function (blue) and the corresponding quasi-PDF in MSbar renormalization with the correct Kernel (red) and that from the original formula (purple) from arXiv:1801.03917.

The RBRC group and its collaborators have emphasized the necessity and importance of precision calculations, which will provide stringent checks for the current understandings of nature, and will have a potential to find physics beyond the current standard model of fundamental physics. We have therefore adopted techniques that aim to control and reduce any systematic errors. This approach has yielded many reliable results, many of basic quantities are now computed within sub-percent accuracies.

The group also delivers several algorithmic breakthroughs, which speed up generic lattice gauge theory computation. These novel technique divides the whole calculation into frequent approximated calculations, and infrequent expensive and accurate calculation using lattice symmetries called All Mode Averaging (AMA), or a compression for memory needs by exploiting the local-coherence of QCD dynamics. Together with another formalism, zMobius fermion, which approximate chiral lattice quark action efficiently, the typical calculation is now improved by a couple of orders of magnitudes, and more than an order of magnitude less memory needs compared to the traditional methods. RBRC group and its collaborators also provide very efficient and generic code optimized to the state-of-arts CPU or GPU, and also improve how to efficiently generate QCD ensemble.

Members

Group Leader (Lab. Head)
T. IZUBUCHI

RBRC Researcher
Y. AOKI (RIKEN BNL Fellow, KEK)
E. NEIL (RHIC Physics Fellow)
S. MEINEL (RHIC Physics Fellow)

S. SYRITSYN (RHIC Physics Fellow)
E. RINALDI (Special Postdoctoral Researcher)
L. Jin (RHIC Physics Fellow)

Visiting Scientists
T. BLUM (Univ. of Connecticut)
Chulwoo JUNG (BNL)
C. LEHNER (BNL)
Meifeng LIN (BNL)
Robert MAWHINNEY (Columbia Univ.)
Shigemi OHTA (KEK)

Tomomi ISHIKAWA (Shanghai Jiao-Tong Univ.)
H. Oki (Nara Women's Univ.)
Takeshi Yamazaki (Tsukuba Univ.)
Christopher Kelly (Columbia Univ.)

List of Publications & Presentations

Publications

[Journal]

(Original Papers) [* Currently subject to peer review]

T. Blum, P. A. Boyle, V. Gülpers, T. Izubuchi, L. Jin, C. Jung, A. Jüttner, C. Lehner, A. Portelli, and J. T. Tsang, "Calculation of the hadronic vacuum polarization contribution to the muon anomalous magnetic moment," arXiv: 1801.07224 (selected as Editors' Suggestion of PRL).*

T. Izubuchi, Y. Kuramashi, C. Lehner, E. Shintani (PACS collaboration), "Finite-volume correction on the hadronic vacuum polarization contribution to muon $g - 2$ in lattice QCD," arXiv: 1805.04250.*

P. Boyle, R. J. Hudspith, T. Izubuchi, A. Jüttner, C. Lehner, R. Lewis, K. Maltman, H. Ohki, A. Portelli, M. Spraggs, "Novel $|V_{us}|$ determination using inclusive strange T decay and lattice HVPs," arXiv: 1803.07228.*

T. Blum, P.A. Boyle, V. Guelpers, T. Izubuchi, L. Jin, C. Jung, A. Jüttner, C. Lehner, A. Portelli, J.T. Tsang, "Calculation of the hadronic vacuum polarization contribution to the muon anomalous magnetic moment," arXiv:1801.07224.*

T. Izubuchi, X. Ji, L. Jin, I. W. Stewart, Y. Zhao, "Factorization theorem relating euclidean and light-cone parton distributions," arXiv: 1801.03917.*

Y. Aoki, T. Izubuchi, E. Shintani, A. Soni, "Improved lattice computation of proton decay matrix elements," Phys. Rev. D **96**, 014506 (2017), 1705.01338.

T. Blum, N. Christ, M. Hayakawa, T. Izubuchi, L. Jin, C. Jung, C. Lehner, "Using infinite volume, continuum QED and lattice QCD for the hadronic light-by-light contribution to the muon anomalous magnetic moment," Phys. Rev. D **96**, 034515 (2017), 1705.01067.

M. Abramczyk, S. Aoki, T. Blum, T. Izubuchi, H. Ohki, S. Syritsyn, "Lattice Calculation of Electric Dipole Moments and Form Factors of the Nucleon," Phys. Rev. D **96**, 014501 (2017), 1701.07792(Editors' Suggestion).

M. Bruno, C. Lehner, A.Soni, "Towards a nonperturbative calculation of weak Hamiltonian Wilson coefficients," Phys. Rev. D **97**, 074509 (2017), arXiv:1711.05768.*

P. Boyle, M. Chuvelev, G. Cossu, C. Kelly, C. Lehner, L. Meadows, "Accelerating HPC codes on Intel(R) Omni-Path Architecture networks: From particle physics to Machine Learning," arXiv: 1711.04883.*

P. A. Boyle, N. Garron, R. J. Hudspith, C. Lehner, and A. T. Lytle, "Neutral kaon mixing beyond the Standard Model with $n_f = 2 + 1$ chiral fermions. Part 2: non perturbative renormalisation of the $\Delta F = 2$ four-quark operators," JHEP **10**, 054 (2017), 1708.03552.*

P. Boyle, V. Gülpers, J. Harrison, A. Jüttner, C. Lehner, A. Portelli, and C.T. Sachrajda, "Isospin breaking corrections to meson masses and the hadronic vacuum polarization: a comparative study," JHEP **09**, 153 (2017), 1706.05293.

A. Carosso, A. Hasenfratz, E. T. Neil, "Non-perturbative renormalization of operators in near-conformal systems using gradient flow," arXiv: 1806.01385.*

V. Ayyar, T. DeGrand, D. C. Hackett, W. I. Jay, E. T. Neil, Y. Shamir, B. Svetitsky,"Finite-temperature phase structure of SU(4) gauge theory with multiple fermion representations," Phys. Rev. D **97**, 114502 (2018).

Fermilab Lattice and MILC and TUMQCD Collaborations (A. Bazavov, E. Neil *et al*.), "Up-, down-, strange-, charm-, and bottom-quark masses from four-flavor lattice QCD," arXiv: 1802.04248.*

V. Ayyar, T. DeGrand, D. C. Hackett, W. I. Jay, E. T. Neil, Y. Shamir, B. Svetitsky, "Baryon spectrum of SU(4) composite Higgs theory with two distinct fermion representations," Phys. Rev. D **97**, 114505 (2018).

A. Bazavov, E. Neil *et al*., "B- and D- meson leptonic decay constants from four-flavor lattice QCD," arXiv: 1712.09262.*

Fermilab Lattice and LATTICE-HPQCD and MILC Collaborations (B. Chakraborty, E. Neil *et al*.), "Strong-isospin-breaking correction to the muon anomalous magnetic moment from lattice QCD at the physical point," Phys. Rev. Lett. **120**, 152001 (2018).

V. Ayyar, T. DeGrand, M. Golterman, D. C. Hackett, W. I. Jay, E. T. Neil, Y. Shamir, B. Svetitsky, "Spectroscopy of SU(4) composite Higgs theory with two distinct fermion representations," Phys. Rev. D **97**, 074505 (2018).

H. Davoudiasl, P. P. Giardino, E. T. Neil, E. Rinaldi, "Unified scenario for composite right-handed neutrinos and dark matter," Phys. Rev. D **96**, 115003 (2017).

A. Bazavov, E. Neil *et al*., "Short-distance matrix elements for D^0-meson mixing for $N_f = 2+1$ lattice QCD," Phys. Rev. D **97**, 034513 (2018).

S. Meinel, "$\Lambda_c \to N$ form factors from lattice QCD and phenomenology of $\Lambda_c \to n\ell^+\nu_\ell$ and $\Lambda_c \to pu^+\mu^-$ decays," Phys. Rev. D **97**, 034511 (2018).

N. Hasan, J. Green, S. Meinel, M. Engelhardt, S. Krieg, J. Negele, A. Pochinsky, S. Syritsyn, "Computing the nucleon charge and axial radii directly at $Q^2 = 0$ in lattice QCD," Phys. Rev. D **97**, 034504 (2018).

C. Alexandrou, S. Meinel, "P-wave $\pi\pi$ scattering and the ρ resonance from lattice QCD," Phys. Rev. D **96**, 034525 (2017).

C. Rohrhofer, Y. Aoki, G. Cossu, H. Fukaya, L. Ya. Glozman, S. Hashimoto, C. B. Lang, S. Prelovsek, "Approximate degeneracy of $J = 1$ spatial correlators in high temperature QCD," Phys. Rev. D **96**, 094501 (2017).

Y. Aoki, T. Izubuchi, E. Shintani, A. Soni, "Improved lattice computation of proton decay matrix elements," Phys. Rev. D **96**, 014506 (2017).

C. C. Chang, E. Rinaldi *et al.*, "Nucleon axial coupling from Lattice QCD," EPJ Web Conf. **175**, 01008 (2018).

E. Rinaldi, E. Berkowitz, M. Hanada, J. Maltz, P. Vranas, "Toward Holographic Reconstruction of Bulk Geometry from Lattice Simulations," JHEP **1802**, 042 (2018).

HotQCD Collaboration (A. Bazavov, E. Rinaldi *et al.*), "Skewness and kurtosis of net baryon-number distributions at small values of the baryon chemical potential," Phys. Rev. D **96**, 074510 (2017).

E. Berkowitz, E. Rinaldi *et al.*, "Möbius domain-wall fermions on gradient-flowed dynamical HISQ ensembles," Phys. Rev. D **96**, 054513 (2017).

B. Yoon, S. Syritsyn *et al.*, "Nucleon transverse momentum-dependent parton distributions in lattice QCD: Renormalization patterns and discretization effects," Phys. Rev. D **96**, 094508 (2017).

J.-W. Chen, L. Jin, H.-W. Lin, Y.-S. Liu, A. Schäfer, Y.-B. Yang, J.-H. Zhang, Y. Zhao, "First direct lattice-QCD calculation of the x-dependence of the pion parton distribution function," arXiv: 1804.01483.*

J.-W. Chen, L. Jin, H.-W. Lin, Y.-S. Liu, Y.-B. Yang, J.-H. Zhang, Y. Zhao, "Lattice Calculation of Parton Distribution Function from LaMET at Physical Pion Mass with Large Nucleon Momentum," arXiv: 1803.04393.*

J.-W. Chen, L. Jin *et al.*, "Kaon Distribution Amplitude from Lattice QCD and the Flavor SU(3) Symmetry," arXiv:1712.10025.*

J.-W. Chen, Tomomi Ishikawa, L. Jin, H.-W. Lin, A. Schäfer, Y.-B. Yang, J.-H. Zhang, Y. Zhao, "Gaussian-weighted Parton Quasi-distribution," arXiv: 1711.07858.*

J.-W. Chen, Tomomi Ishikawa, L. Jin, H.-W. Lin, Y.-B. Yang, J.-H. Zhang, Y. Zhao, "Operator classification for nonlocal quark bilinear on lattice," arXiv:1710.01089.*

J.-W. Chen, Tomomi Ishikawa, L. Jin, H.-W. Lin, Y.-B. Yang, J.-H. Zhang, Y. Zhao, "Parton distribution function with nonperturbative renormalization from lattice QCD," Phys. Rev. D **97**, 014505 (2018).

[Proceedings]
(Original Papers)

S. Hashimoto, B. Colquhoun, T. Izubuchi, T. Kaneko and H. Ohki, "Inclusive B decay calculations with analytic continuation," EPJ Web Conf. **175**, 13006 (2018) .

M. Abramczyk, Sinya Aoki, T. Blum, T. Izubuchi, H. Ohki and S. Syritsyn, "Computing nucleon EDM on a lattice," EPJ Web Conf. **175**, 06027 (2018).

T. Izubuchi, Y. Kuramashi, C. Lehner and E. Shintani, "Lattice study of finite volume effect in HVP for muon $g-2$," EPJ Web Conf. **175**, 06020 (2018) .

P. Boyle, R. J. Hudspith, T. Izubuchi, A. Jüttner, C. Lehner, R. Lewis, K. Maltman, H. Ohki, A. Portelli, M. Spraggs, "$|V_{us}|$ determination from inclusive strange tau decay and lattice HVP," EPJ Web Conf. **175**, 13011 (2018) .

K. Maltman, R. Hudspith, T. Izubuchi, R. Lewis, H. Ohki, J. Zanotti, "The inclusive flavor-breaking τ-based sum rule determination of V_{us}," Nucl. Part. Phys. Proc. **287–288**, 25–28 (2017) .

K. Maltman, R. Hudspith, T. Izubuchi, R. Lewis, H. Ohki, J. Zanotti, "$|V_{us}|$ from T decays in theory," PoS **CKM2016**, 030 (2017) .

T. Izubuchi, M. Abramczyk, T. Blum, H. Ohki, S. Syritsyn, "Calculation of nucleon electric dipole moments induced by quark chromo-electric dipole moments," PoS **LATTICE2016**, 398 (2017) .

P. Boyle, V. Gülpers, J. Harrison, A. Jüttner, C. Lehner, A. Portelli, and C. Sachrajda, "Isospin Breaking Corrections to the HVP with Domain Wall Fermions," EPJ Web Conf. **175**, 06024 (2017), 1710.07190.

M. A. Clark, C. Jung, and C. Lehner, "Multi-Grid Lanczos," EPJ Web Conf. **175**, 14023 (2017), 1710.06884.

C. Lehner, "A precise determination of the HVP contribution to the muon anomalous magnetic moment from lattice QCD," EPJ Web Conf. **175**, 01024 (2017), 1710.06874.

V. Ayyar, D. C. Hackett, W. I. Jay, E. T. Neil, "Automated lattice data generation," arXiv:1802.00851, EPJ Web Conf. **175**, 09009 (2018).

Fermilab Lattice and MILC Collaborations (Y. Liu, E. Neil *et al.*), "$B_s \to K\ell\nu$ Form Factors with 2 + 1 Flavors," EPJ Web Conf. **175**, 13008 (2018).

V. Ayyar, D. Hackett, W. Jay, E. Neil, "Confinement study of an SU(4) gauge theory with fermions in multiple representations," EPJ Web Conf. **175**, 08025 (2018) .

V. Ayyar, T. DeGrand, D. C. Hackett, W. I. Jay, E. T. Neil, Y. Shamir, B. Svetitsky, "Chiral transition of SU(4) gauge theory with fermions in multiple representations," EPJ Web Conf. **175**, 08026 (2018) .

S. Paul, S. Meinel *et al.*, "$\pi\pi$ P-wave resonant scattering from lattice QCD," EPJ Web Conf. **175**, 05022 (2018).

JLQCD Collaboration (K. Suzuki, Y.Aoki *et al.*), "Axial U(1) symmetry at high temperature in 2-flavor lattice QCD," EPJ Web Conf. **175**, 07025 (2018).

JLQCD Collaboration (Sinya Aoki, Y.Aoki *et al.*), "Topological Susceptibility in $N_f = 2$ QCD at Finite Temperature," EPJ Web Conf. **175**, 07024 (2018).

Christian Rohrhofer, Y. Aoki, Guido Cossu, Hidenori Fukaya, Leonid Glozman, S. Hashimoto, Christian B.Lang, Sasa Prelovsek, "Degeneracy of vector-channel spatial correlators in high temperature QCD," EPJ Web Conf. **175**, 07029 (2018).

Y. Aoki *et al.*, "Flavor-singlet spectrum in multi-flavor QCD," EPJ Web Conf. **175**, 08023 (2018).

E. Berkowitz, E. Rinaldi *et al.*, Calm Multi-Baryon Operators," EPJ Web Conf. **175**, 05029 (2018).

Oral Presentations

[International Conference etc.]

T. Izubuchi, "Hadronic contributions to muon $g-2$ – LQCD confronting the most precise experiments," invited seminar at Department of Theoretical

Physics (DTP)Tata Institute of Fundamental Research (TIFR), Mumbai, India, April 26, 2018.

T. Izubuchi, "Leading disconnected diagram and other disconnected diagrams," Invited presentation at Muon $g-2$ Theory Initiative Hadronic Light-by-Light working group workshop, University of Connecticut, Storrs, CT March 12–14, 2018.

T. Izubuchi, "Hadronic contributions to muon $g-2$ and inclusive tau decay," Invited seminar for Lattice Theory group, DESY, Zeuthen, June 26, 2017.

T. Izubuchi, "Finite volume study for muon $g-2$ light-by-light contribution," Contribution talk at Lattice 2017, Granada, Spain, 18–24 June, 2017.

T. Izubuchi, "Interplay between R-ratio and Lattice for the muon $g-2$ HVP," Invited talk at First Workshop of the Muon $g-2$ Theory Initiative, June 4, 2017, Q center, St. Charles, IL, USA.

E. Neil, "Lattice Insights for Composite BSM Models," High Energy/Cosmology Seminar, University of Wisconsin, Madison, WI. March 2017.

E. Neil, "Lattice study of gauge theory with multiple fermion representations.," RIKEN Lunch Seminar, Brookhaven National Laboratory, Upton, NY. May 2017.

E. Neil, "Light composite scalars from lattice gauge theory beyond QCD.," Particle Theory Seminar, Fermi National Accelerator Laboratory, Batavia, IL. September 2017.

E. Neil, "Light composite scalar from $N_f = 8$ lattice gauge theory," Invited presentation, workshop on Continuum and Lattice Approaches to the Infrared Behavior of Conformal and Quasi-Conformal Gauge Theories, Simons Center for Geometry and Physics, Stony Brook, NY, January 2018.

S. Meinel, "Charm baryon semileptonic decays with lattice QCD," The 35th International Symposium on Lattice Field Theory, Granada, Spain, June 2017.

S. Meinel, "Weak decays of heavy mesons to multi-hadron final states," Lattice QCD Workshop, Santa Fe, NM, August 2017.

S. Meinel, "Flavor physics with charm and bottom baryons," Theory Seminar, Jefferson Lab, Newport News, VA, September 2017.

S. Meinel, "Hints for physics beyond the Standard Model in decays of beauty quarks," Physics Department Colloquium, Old Dominion University, Norfolk, VA, September 2017.

S. Meinel, "Heavy baryon decay form factors from lattice QCD," Lattice Meets Continuum Workshop, Siegen, Germany, September 2017.

S. Meinel, "$\Lambda_b \to \Lambda_c^{(*)}$ form factors from lattice QCD," Challenges in Semileptonic B Decays, Mainz, Germany, April 2018.

S. Meinel, "Opportunities for lattice QCD in quark and lepton flavor physics," USQCD All Hands Meeting, Fermilab, Batavia, IL, April 2018.

S. Meinel, "Flavor physics with charm and bottom baryons," Cosmology Seminar, Arizona State University, Tempe, AZ, May 2018.

S. Meinel, "Form factors for b hadron decays from lattice QCD," Frontiers in Lattice Quantum Field Theory, Madrid, Spain, May 2018.

Y. Aoki, "Topological susceptibility in $N_f = 2$ QCD at finite temperature," Lattice 2017, Granada, Spain, June 19, 2017.

Y. Aoki, "Spectral properties and S parameter of $N_f = 8$ QCD," Brookhaven Forum, BNL, Oct. 11, 2017.

Y. Aoki, "Lattice QCD and hadron structure," plenary talk at DIS 2018, Kobe Japan, Apr. 16, 2018.

Y. Aoki, "Fate of axial U(1) symmetry at two flavor chiral limit of QCD in finite temperature," invited talk at XQCD 2018, FIAS, Frankfurt, Germany, May 21, 2018.

L. Jin., "Pion Transition Form Factor (TFF) on Lattice: RBC results," Second Plenary Workshop of the Muon $g-2$ Theory Initiative, elmholtz-Institut Mainz, Mainz, Germany, June 18, 2018.

L. Jin., "Operator product expansion analysis of Quasi-PDF." ITP seminar, Peking University, Beijing, China, May 10, 2018.

L. Jin., "HLbL contribution to the muon $g-2$ on the lattice.," Physics Seminar, University of Kentucky, Lexington, KY, April 12, 2018.

L. Jin., "OPE analysis of quasi-PDFs." Lattice PDF Workshop, University of Maryland, College Park, MD, April 6, 2018.

L. Jin., "HLbL contribution to the muon g − 2 on the lattice: overall strategy," Muon $g-2$ Theory Initiative HLbL Working Group Workshop, University of Connecticut, Storrs, CT, March 12, 2018.

L. Jin., "Hadronic light-by-light contribution to muon $g-2$ with lattice QCD and infinite volume, continuum QED," Theory Seminar, Jefferson Lab, Newport News, VA, January 8, 2018.

L. Jin., "The muon anomalous magnetic moment." SANTA FE WORKSHOP ON LATTICE QCD, Santa Fe, NM, August 29, 2017.

E. Rinaldi, "Composite dark matter." Invited Talk at the conference CIPANP18, Palm Springs, CA, USA, June 2018.

E. Rinaldi, "How to test the gauge/gravity duality with lattice simulations." Invited seminar at New York University, New York, NY, USA, May 2018.

E. Rinaldi, "High-precision tests of the gauge/gravity duality and future applications." Invited Talk at the workshop LBSM18 "Lattice for Beyond the Standard Model Physics," University of Colorado, Boulder, CO, USA, April 2018

E. Rinaldi, "What lattice gauge theory can do for dark matter searches?" Invited seminar at Stony Brook University, Stony Brook, NY, USA, February 2018.

E. Rinaldi, "The nucleon axial charge from Lattice QCD" Invited seminar at Lawrence Livermore National Laboratory, Livermore, CA, USA, January 2018.

E. Rinaldi, "Exploring signals of conformality in theories with many flavors: a LatKMI report" Invited talk at the workshop "Continuum and Lattice Approaches to the Infrared Behavior of Conformal and Quasi-Conformal Gauge Theories," Stony Brook University, Simons Center for Geometry and Physics, Stony Brook, NY, USA, January 2018.

E. Rinaldi, "Dark interactions and supercomputers," Talk at "Brookhaven forum 2017: in search of new paradigms," Brookhaven National Laboratory, Upton NY, USA, October 2017.

E. Rinaldi, "Petaflops computing for the search of New Physics" Invited Talk at the inter-institutional meeting ITCPS2017 "Interdisciplinary Theoretical and Computational Physical Sciences," Tokyo Institute of Technology, Tokyo, Japan, October 2017.

E. Rinaldi, "The nucleon axial coupling from Lattice QCD" Seminar at RIKEN Nishina Center, Wako, Japan, October 2017.

E. Rinaldi, "Lattice Field Theory results on new strong dynamics" Invited Talk at the workshop LFC17 "Old and new strong interactions from LHC to future colliders," ECT*, Trento, Italy, September 2017.

E. Rinaldi, "Flavor-singlet spectrum in multi-flavor QCD, SU(3) with $N_f = 4$, 8 and 12" Talk at Lattice 2017, Granada, Spain, June 2017.

E. Rinaldi, "How to test the gauge/gravity duality with lattice simulations" Invited seminar at University of Oregon, Eugene, US, May 2017.

E. Rinaldi, "The nucleon axial charge from lattice QCD" Seminar at RIKEN, BNL, Upton, US, May 2017.

E. Rinaldi, "Many-flavor theories on the lattice" Invited talk at the workshop "Lattice for Beyond the Standard Model Physics," Boston University,

Boston, USA, April 2017.

E. Rinaldi, "How to test the gauge/gravity duality with lattice simulations," Invited talk at the workshop "Quantum gravity, string theory and holography," YITP, Kyoto, Japan, April 2017.

E. Rinaldi, "Beyond the Standard Model physics with lattice simulations," Invited seminar at Università di Roma 2, Tor Vergata, Roma, Italy, March 2017.

E. Rinaldi, "What lattice gauge theory can do for Dark Matter searches," Invited seminar at Università di Roma 1, La Sapienza, Roma, Italy, February 2017.

H. Ohki, "Nucleon Electric dipole moments from lattice QCD," The 7th KIAS Workshop on Particle Physics and Cosmopology and The 2nd KEK-NCTS-KIAS Workshop on Particle Physics Phenomenology, KIAS, Soul, Korea, November 10, 2017.

H. Ohki, "|Vus| determination from inclusive strange tau decay and lattice HVP," Lattice 2017, Granada, Spain, June 23, 2017, [Domestic Conference]

T. Izubuchi, "Hadronic contributions to muon $g-2$ – LQCD confronting the most precise experiments," invited seminar at Department of Theoretical Physics (DTP) Tata Institute of Fundamental Research (TIFR), Mumbai, India, April 26, 2018.

T. Izubuchi, "Leading disconnected diagram and other disconnected diagrams," Invited presentation at Muon $g-2$ Theory Initiative Hadronic Light-by-Light working group workshop, University of Connecticut, Storrs, CT March 12-14, 2018.

T. Izubuchi, "Hadronic contributions to muon $g-2$ and inclusive tau decay," Invited seminar for Lattice Theory group, DESY, Zeuthen, June 26, 2017.

T. Izubuchi, "Finite volume study for muon $g-2$ light-by-light contribution," Contribution talk at Lattice 2017, Granada, Spain, 18–24 June, 2017.

T. Izubuchi, "Interplay between R-ratio and Lattice for the muon $g-2$ HVP," Invited talk at First Workshop of the Muon $g-2$ Theory Initiative, June 4, 2017, Q center, St. Charles, IL, USA.

Y. Aoki,「QCD の有限温度相転移とトポロジー −サブ課題 A「QCD 相転移」−」, 素粒子・原子核・宇宙「京からポスト京に向けて」シンポジウム, 筑波大学東京キャンパス（東京都）, Feb 17, 2017.

Y. Aoki,「有限温度 2 フレーバーQCD のトポロジカル感受率」, 日本物理学会第 72 回年次大会, 大阪大学, Mar. 18, 2017.

Y. Aoki,「QCD の有限温度相転移とトポロジー −サブ課題 A「QCD 相転移」−」, ポスト「京」重点課題 9 研究報告会(5/31), 筑波大学 CCS, May 31, 2017.

Y. Aoki, "Topology and axial U(1) symmetry at hight temperature in $N_f = 2$ QCD," AICS seminar, Kobe RIKEN AICS, Jan. 15, 2018.

Y. Aoki,「有限温度 2 フレーバーOCD のトポロジカル感受率」, 日本物理学会 2017 年秋期大会, 宇都宮大学, Sep. 12, 2017.

H. Ohki,「New Inclusive Decay Analysis with Lattice QCD," poster presentation at FY 2017 SPDR and FPR Research Report Session, RIKEN, Wako, Japan, January 31, 2018.

H. Ohki, "Nucleon Electric Dipole Moments from Lattice QCD," 10th International Workshop on Fundamental Physics Using Atoms (FPUA), Nagoya University, Nagoya, Japan, January 8, 2018.

H. Ohki,「格子 QCD による核子構造の研究と標準模型を越えた物理 (Lattie QCD study of nucleon EDM and physics beyond the standard model)」, 2017 JPS Autumn meeting, Utsunomiya University, Utsunomiya, Japan, September 14, 2017.

H. Ohki,「核子(chromo)EDM 演算子の格子 QCD 計算 (Lattice calculation of the nucleon chromo-EDM)」, 2017 JPS Annual Meeting, Osaka University, Toyonaka, Japan, March 19, 2017.

Sub Nuclear System Research Division
RIKEN BNL Research Center
Experimental Group

1. Abstract

RIKEN BNL Research Center (RBRC) Experimental Group studies the strong interactions (QCD) using RHIC accelerator at Brookhaven National Laboratory, the world first heavy ion collider and polarized $p + p$ collider. We have three major activities: Spin Physics at RHIC, Heavy ion physics at RHIC, and detector upgrades of PHENIX experiment at RHIC.

We study the spin structure of the proton using the polarized proton-proton collisions at RHIC. This program has been promoted by RIKEN's leadership. The first focus of the research is to measure the gluon spin contribution to the proton spin. Recent results from PHENIX π^0 measurement and STAR jet measurement has shown that gluons in the proton carry about 30% of the proton spin. This is a major milestone of RHIC spin program. The second goal of the spin program is to measure the polarization of anti-quarks in the proton using $W \rightarrow e$ and $W \rightarrow \mu$ decays. The results of $W \rightarrow e$ measurement was published. The final results of $W \rightarrow \mu$ as submitted for publication.

The aim of Heavy ion physics at RHIC is to re-create Quark Gluon Plasma (QGP), the state of Universe just after the Big Bang. Two important discoveries, jet quenching effect and strong elliptic flows, have established that new state of dense matter is indeed produced in heavy ion collisions at RHIC. We are now studying the property of the matter. Recently, we have measured direct photons in Au + Au collisions for $1 < p_T < 3$ GeV/c, where thermal radiation from hot QGP is expected to dominate. The comparison between the data and theory calculations indicates that the initial temperature of 300 MeV to 600 MeV is achieved. These values are well above the transition temperature to QGP, which is calculated to be approximately 160 MeV by lattice QCD calculations.

We had major roles in detector upgrades of PHENIX experiment, namely, the silicon vertex tracker (VTX) and muon trigger upgrades. Both of the upgrade is now complete. The VTX is the main device to measure heavy quark (charm and bottom) production and the muon trigger is essential for $W \rightarrow \mu$ measurement. The results from the first run with VTX detector in 2011 was published. The results show that electrons from bottom quark decay is strongly suppressed at high p_T, but the suppression is weaker than that of charm decay electron for $3 < p_T < 4$ GeV/c. We have recorded 10 times as much Au + Au collisions data in each of the 2014 run and 2016 run. The large dataset will produce definitive results on heavy quark production at RHIC.

PHENIX completed its data taking in 2016. We are now working on R&D of intermediate silicon tracker INTT for sPHENIX, a new experiment at RHIC that will be installed in the PHENIX IR.

2. Major Research Subjects

(1) Experimental Studies of the Spin Structure of the Nucleon
(2) Study of Quark-Gluon Plasma at RHIC
(3) PHENIX detector upgrades

3. Summary of Research Activity

We study the strong interactions (QCD) using the RHIC accelerator at Brookhaven National Laboratory, the world first heavy ion collider and polarized $p + p$ collider. We have three major activities: Spin Physics at RHIC, Heavy ion physics at RHIC, and detector upgrades of PHENIX experiment.

(1) Experimental study of spin structure of proton using RHIC polarized proton collider

How is the spin of proton formed with 3 quarks and gluons? This is a very fundamental question in Quantum Chromodynamics (QCD), the theory of the strong nuclear forces. The RHIC Spin Project has been established as an international collaboration between RIKEN and Brookhaven National Laboratory (BNL) to solve this problem by colliding two polarized protons for the first time in history. This project also has extended the physics capabilities of RHIC.

The first goal of the Spin Physics program at RHIC is to determine the gluon contribution to proton spin. It is known that the spin of quark accounts for only 25% of proton spin. The remaining 75% should be carried either by the spin of gluons or the orbital angular momentum of quarks and gluons. One of the main goals of the RHIC spin program has been to determine the gluon spin contribution. Before the start of RHIC, there was little experimental constraint on the gluon polarization, ΔG.

PHENIX measures the double helicity asymmetry (A_{LL}) of π^0 production to determine the gluon polarization. Our most recent publication of π^0 A_{LL} measurement at 510 GeV shows non-zero value of A_{LL}, indicating that gluons in the proton is polarized. Global analysis shows that approximately 30% of proton spin is carried by gluons.

RHIC achieved polarized $p + p$ collisions at 500 GeV in 2009. The collision energy increased to 510 GeV in 2012 and 2013. The main goal of these high energy $p + p$ run is to measure anti-quark polarization via single spin asymmetry A_L of the W production. We upgraded the muon trigger system to measure $W \rightarrow \mu$ decays in the forward direction. With the measurement of $W \rightarrow e$ and $W \rightarrow \mu$, we can cover a wide kinematic range in anti-quark polarization measurement. The 2013 run is the main spin run at 510 GeV. PHENIX has recorded more than 150/pb of data in the run. The final results of the A_L measurement in $W \rightarrow e$ channel in combined data of 2011 to 2013 was published. The high statistics results give strong constraints on the polarization of anti-quarks in the proton. The paper on the final results of $W \rightarrow \mu$ was submitted for publication.

RHIC has the first polarized proton nucleus collision run in 2015. In this run, we discovered a surprisingly large nuclear dependence of single spin asymmetry of very forward neutron. The paper of this discovery was published in Physical Review Letters.
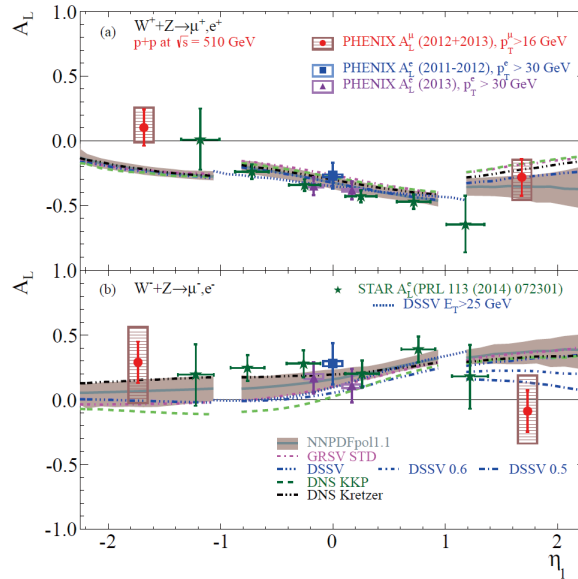
Figure 1. Single spin asymmetry A_L of electrons from W and Z decays. The A_L is sensitive to the polarization of anti-quarks in the proton. The curves and the shaded region show theoretical calculations based on various polarized parton distribution (PDF) sets. The mid-rapidity points are published in Phys. Rev. D **93**, 051103(R) (2016). From arXiv: 1804.04181 (submitted to Physical Review D)
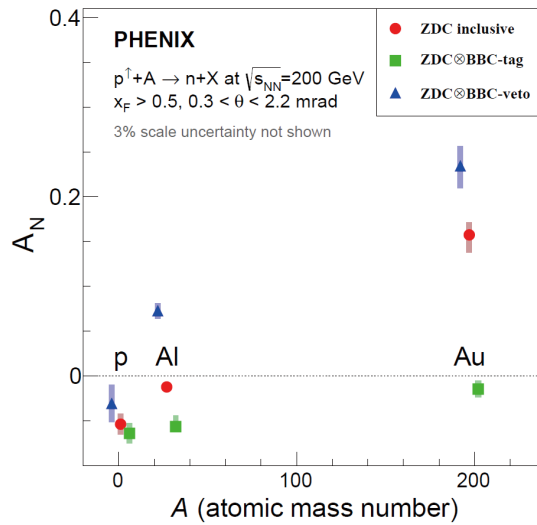
Figure 2. Single spin asymmetry A_N of very forward neutron in $p + p$, $p + Al$, and $p + Au$ collision. Published in Phys. Rev. Lett. **120**, 022001 (2018).

(2) Experimental study of Quark-Gluon Plasma using RHIC heavy-ion collider

The goal of high energy heavy ion physics at RHIC is study of QCD in extreme conditions i.e. at very high temperature and at very high energy density. Experimental results from RHIC have established that dense partonic matter is formed in Au + Au collisions at RHIC. The matter is very dense and opaque, and it has almost no viscosity and behaves like a perfect fluid. These conclusions are primarily based on the following two discoveries:

- Strong suppression of high transverse momentum hadrons in central Au + Au collisions (jet quenching)
- Strong elliptic flow

These results are summarized in PHENIX White paper, which has approximately 2500 citations to date.

The focus of the research in heavy ion physics at RHIC is now to investigate the properties of the matter. RBRC have played the leading roles in some of the most important results from PHENIX in the study of the matter properties. These include (1) measurements of heavy quark production from the single electrons from heavy flavor decay (2) measurements of J/ψ production (3) measurements of di-electron continuum and (4) measurements of direct photons.

The most important recent result is the measurement of direct photons for $1 < p_T < 5$ GeV/c in $p + p$ and Au + Au through their internal conversion to e^+e^- pairs. If the dense partonic matter formed at RHIC is thermalized, it should emit thermal photons. Observation of thermal photon is direct evidence of early thermalization, and we can determine the initial temperature of the matter. It is predicted that thermal photons from QGP phase is the dominant source of direct photons for $1 < p_T < 3$ GeV/c at the RHIC energy. We measured the direct photon in this p_T region from measurements of quasi-real virtual photons that decays into low-mass e^+e^- pairs. Strong enhancement of direct photon yield in Au + Au over the scaled $p + p$ data has been observed. Several hydrodynamical models can reproduce the central Au + A data within a factor of two. These models assume formation of a hot system with initial temperature of $T_{init} = 300$ MeV to 600 MeV. This is the first measurement of initial temperature of quark gluon plasma formed at RHIC. These results are recently published in Physical Review Letters. Y. Akiba is the leading person of the analysis and the main author of the paper. **He received 2011 Nishina memorial Prize mainly based on this work.**

(3) Detector upgrade

The group had major roles in several PHENIX detector upgrades, namely, the silicon vertex tracker (VTX) and muon trigger upgrades. VTX is a high precision charged particle tracker made of 4 layers of silicon detectors. It is jointly funded by RIKEN and the US DOE. The inner two layers are silicon pixel detectors and the outer two layers are silicon strip detectors. Y. Akiba is the project manager and A. Deshpande is the strip system manager. The VTX detector was completed in November 2010 and subsequently installed in PHENIX. The detector started taking data in the 2011 run. With the new detector, we measure heavy quark (charm and bottom) production in $p + p$, A + A collisions to study the properties of quark-gluon plasma. The final result of the 2011 run was published. The result show that single electrons from bottom quark decay is suppressed, but not as strong as that from charm decay in low p_T region ($3 < p_T < 4$ GeV/c). This is the first measurement of suppression of bottom decay electrons at RHIC and the first observation that bottom suppression is smaller than charm. We have recorded 10 times as much Au + Au collisions data in each of the 2014 run and 2016 run. The large dataset will produce definitive results on heavy quark production at RHIC. A preliminary results on the elliptic flow strength v_2 of $b \rightarrow e$ and $c \rightarrow e$ has been presented in Quark Matter 2018 conference.
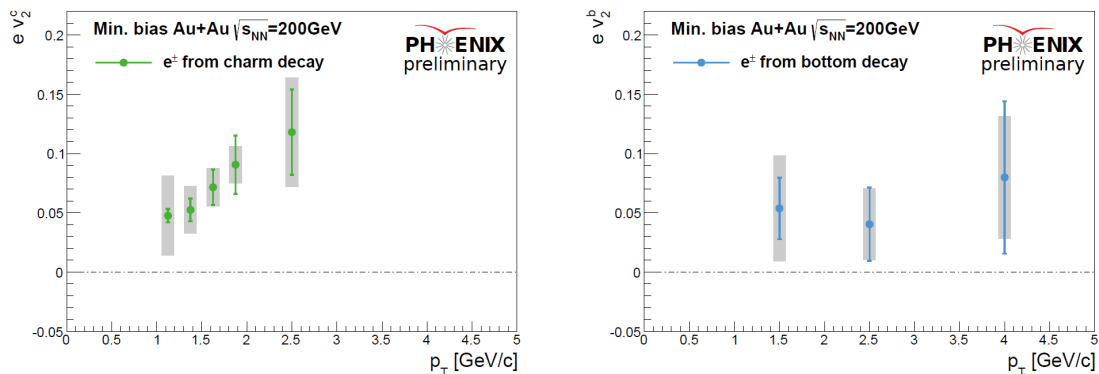
Figure 3. Preliminary results of the elliptic flow strength v_2 of single electrons from charm and bottom decays.

PHENIX completed its data taking in 2016. We are now working on R&D of intermediate silicon tracker INTT for sPHENIX, a new experiment at RHIC that will be installed in the PHENIX IR. A three ladder telescope of INTT prototype modules was tested in a beam test at FNAL. The prototype detector worked very well during the test.
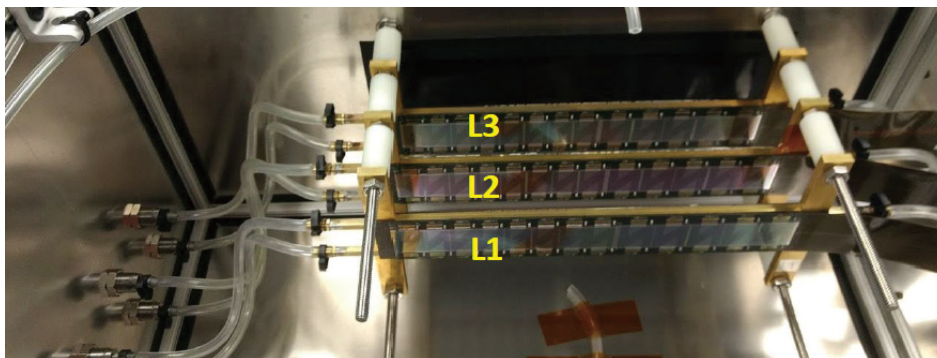
Figure 4. Three ladder telescope made from INTT silicon tracker prototype. The prototype detector was tested in a beam test at FNAL in February 2018.

Members

Group Leader (Lab. Head)
Yasuyuki AKIBA (Deputy Chief Scientist)

Deputy Group Leader
Abhay DESHPANDE

RBRC Researcher
Xiaorong WANG (RHIC Physics Fellow)

Takashi HACHIYA (RIKEN BNL Fellow, Nara Women's University)

Yorito YAMAGUCHI

Gaku MITSUKA

Takahito TODOROKI

Megan CONORS (RHIC Physics Fellow)

Marta VERWEIJ (RHIC Physics Fellow)

Yasushi WATANABE (RIKEN Spin Program Researcher, concurrent: Radiation Lab.)

Yuji GOTO (RIKEN Spin Program Researcher, concurrent: Radiation Lab.)

Itaru NAKAGAWA (RIKEN Spin Program Researcher, concurrent: Radiation Lab.)

Takashi ICHIHARA (RIKEN Spin Program Researcher, concurrent: RI Physics Lab.)

Atsushi TAKETANI (RIKEN Spin Program Researcher, concurrent: Neutoron Beam Technology Team, Advanced Photonics Technology development Group, RAP)

Satoshi YOKKAICHI (RIKEN Spin Program Researcher, concurrent: Radiation Lab.)

Ralf SEIDL (RIKEN Spin Program Researcher, concurrent: Radiation Lab.)

Visiting Scientists
Stefan BATHE (Baruch College University of New York)

Rachid NOUICER (BNL)

Masahiro OKAMURA (BNL)

Takao SAKAGUCHI (BNL)

Takashi SAKO (Nagoya University)

Hiroaki MENJO (Nagoya University)

List of Publications & Presentations

Publications
[Journal]

(Original Papers)

G. Mitsuka, "Recently measured large A_N for forward neutron in $p^{\uparrow}A$ collisions at $\sqrt{s_{NN}} = 200$ GeV explained through simulations of ultraperipheral collisions and hadronic interactions," Phys. Rev. C **95**, 044908 (2017).

Oral Presentations
[International Conference etc.]

T. Hachiya, "Recent results on open and closed heavy flavor from PHENIX at RHIC," ICHEP2016.

T. Hachiya, "Recent heavy flavor measurements from PHENIX at RHIC," ISMD2016.

T. Hachiya, "Recent results on heavy flavor production at RHIC-PHENIX," INPC2016.

G. Mitsuka, "Disentangling transverse single spin asymmetry for very forward neutrons in polarized pA collisions using ultra-peripheral collisions," 25th International Workshop of Deep Inelastic Scattering (DIS2017).

T. Hachiya, "Nuclear modification factor and flow of charm and bottom quarks in Au + Au collisions at $\sqrt{s_{NN}} = 200$ GeV by the PHENIX Experiment," (Quark Matter 2018).

[Domestic Conference]

G. Mitsuka, 「RHIC 単スピン非対称測定に対する ultra-peripheral collision の影響」，日本物理学会 第 72 回年次大会.

Poster Presentations
[International Conference etc.]

G. Mitsuka, "sPHENIX Intermediate silicon tracker INTT," Quark Matter 2017.

Sub Nuclear System Research Division
RIKEN Facility Office at RAL

1. Abstract

Our core activities are based on the RIKEN-RAL Muon Facility located at the Rutherford Appleton Laboratory (UK), which provides intense pulsed-muon beams. Muons have their own spins with 100% polarization, and can detect local magnetic fields and their fluctuations at muon stopping sites very precisely. The method to study characteristics of materials by observing time dependent changes of muon spin polarization is called "Muon Spin Rotation, Relaxation and Resonance (μSR method), and is applied to study electro-magnetic properties of insulating, metallic, magnetic and superconducting systems. Muons reveal static and dynamic properties of the electronic state of materials in the zero-field condition, which is the ideal magnetic condition for research on magnetism. We have carried out μSR investigations on frustrated pyrochlore systems, which have a variety of exotic ground states of magnetic spins, so the magnetism study of this system using muons is quite unique.

The ultra-slow muon beam can be stopped in thin foil, multi-layered materials and artificial lattices, which enables us to apply the μSR techniques to surface and interface science. The development of an ultra-slow muon beam is also very important as a source of ultra-cold (pencil-like small emittance) muon beam for muon $g - 2$/EDM measurement. We have been developing muonium generators to create more muonium atoms in vacuum even at room temperature to improve beam quality compared with the conventional hot-tungsten muonium generator. We demonstrated a tremendous increase of the muonium emission efficiency by fabricating fine laser drill-holes on the surface of silica aerogel. We also developed a high power Lyman-alpha laser in collaboration with the Advanced Photonics group at RIKEN. The new laser will ionize muonium atoms 100 times more efficiently for slow muon beam generation.

We are planning a major refurbishment of the muon facility, since the major part of the facility was built around 1994. The plan was discussed in 2017 and the areas and components that need refurbishment were identified. RIKEN and STFC/RAL also agreed on extension of the collaboration for another five years starting 2018. RAL will take over the facility ownershp and will be responsible for its operation and maintenance, while RIKEN will keep access to the facility with access charge to conduct its science program.

2. Major Research Subjects

(1) Materials science by muon-spin-relaxation method
(2) Hyperfine interactions at muon sites studied by the computation science
(3) Nuclear and particle physics studies via muonic atoms and ultra-cold muon beam

3. Summary of Research Activity

(1) Material Science at the RIKEN-RAL Muon Facility

Muons have their own spins with 100% polarization, and can detect local magnetic fields and their fluctuations at muon stopping sites very precisely. The μSR method is applied to studies of newly fabricated materials. Muons enable us to conduct (1) material studies under external zero-field condition, (2) magnetism studies with samples without nuclear spins, and (3) measurements of muon spin relaxation changes over a wide temperature range with same detection sensitivity. The detection time range of local field fluctuations by μSR is 10^{-6} to 10^{-11} second, which is an intermediate region between neutron scattering methods ($10^{-10}–10^{-12}$ second) and Nuclear Magnetic Resonance (NMR) (longer than 10^{-6} second). At Port-2 and 4 of the RIKEN-RAL Muon Facility, we have been performing μSR research on strong correlated-electron systems, organic molecules and biological samples to study electron structures, superconductivity, magnetism, molecular structures and crystal structures.

In the period from 2017 to 2018, we have obtained excellent results, and the highlights are listed in the following,

1) The superconducting gap state of λ-[BETS]$_2$GaCl$_4$ has both the s- and d-wave characters.
2) A static ordering in the Ca-doped pyrochlore iridate; $(Y_{1−x}Ca_x)_2Ir_2O_7$ is strongly suppressed by the carrier doping.
3) A long-range magnetic ordering is observed in alkari-metal superoxides of CsO$_2$ and RbO$_2$ but not in NaO$_2$.
4) Missing of a static ordering is confirmed in both Au25 nano-clusters.
5) The quantum spatial distribution of the muon by the zero-point vibration energy is clarified by density functional theory calculations by using the RIKEN supercomputing system. HOKUSAI.

Result-1) One dimensional organic superconductor, λ-[BETS]$_2$GaCl$_4$, has a unique Fermi-surface structure with the four-fold nodal points. The estimation of the superconducting gap from computational analysis of μSR experimental data indicates a unique view of the supeconducting gap to be a mixed state of the major s-wave component and the minor d-wave one. Result-2) Static orderings of Ir magnetic spins are strongly suppressed by the carrier doping. A quantum critical change to the non-magnetic ground state is expected around $x = 0.20$ being accompanied by changes in the transport properties. Result-3) The π electrons which are widely distributed on the O$_2$ dumbbell in superoxides CsO$_2$ and RbO$_2$ are found to form static long-range orderings. The magnetic moment is quantitatively estimated in conjunction with density functional theory calculations and confirmed to shrink to less than a half in the magnetically ordered state. Result-4) Ground states of nano-cluster of Au with 25 atoms are concluded to be still nonmagnetic down to 0.3 K from the magnetic susceptibility, NMR and μSR measurements although those systems have been argued to show some static magnetic states. Result-5) The muon trapped in materials is confirmed to be spatially distributed around the local minimum potential position by the zero-point vibration energy, which is due to the muon's physics character as a light particle. This quantum spatial distribution is now taken into account for the μSR data analysis with the similar quantum spatial distribution of magnetic moments.

We are developing international collaborations on the muon science with Asian groups in order to organize new μSR experimental research themes and to develop muon-site calculation activities using computational method. We renewed MOU's with Indonesian and Malaysian universities to enhance collaborative researches on the muon science at the RIKEN-RAL Muon Facility. We formed a new MOU

with Universitus Indonesia (UI) as a new partner to work on the muon science and student education. We are developing new collaborations in μSR experiments on strongly correlated systems with researchers from China, Taiwan and Korea including graduate students.

(2) Ultra Slow (low energy) Muon Beam Generation and Applications

A positive muon beam with thermal energy has been produced by laser ionization of muonium atoms (bound system of μ^+ and electron) emitted from hot tungsten surface with stopping surface muon beam at Port-3. The method generates a positive muon beam with acceleration energy from several 100 eV to several 10 keV, small beam size (a few mm) and good time resolution (less than 8 nsec). By stopping the ultra-slow muon beam in thin foil, multi-layered materials and artificial lattices, we can precisely measure local magnetic field in the materials, and apply the μSR techniques to surface and interface science. Since there has been no appropriate probe to study magnetism at surface and interface, the ultra-slow muon beam will open a new area of these research fields. In addition, the development of ultra-slow muon beam is very important as the source of ultra-cold (pencil-like small emittance) muon beam for muon $g-2$/EDM measurement. It is essential to increase the slow muon beam production efficiency by 100 times for these applications. There are three key techniques in ultra-slow muon generation: production of thermal muonium, high intensity Lyman-alpha laser and the ultra-slow muon beam line.

We have developed a high power Lyman-alpha laser in collaboration with the Advanced Photonics group at RIKEN. This development was funded mostly by the Grant-in-Aid for Scientific Research on Innovative Areas "Frontier in Materials, Life and Particle Science Explored by Ultra Slow Muon Microscope". The new laser system was installed to J-PARC slow muon beam line and is being used for the generation of ultra-slow muons. In this development, we succeeded in synthesizing a novel ceramic-based Nd:YGAG crystal. We already achieved 10 times increase in Lyman-alpha intensity and are waiting the growth of a large crystal to achieve the goal of 100 times increase. This crystal can also be applicable to the flash-lamp based Lyman-alpha laser system of RIKEN-RAL to realize substantial improvement of the laser power at a much reduced cost.

We also aimed to realize drastic improvements on the ultra-slow muon source with much reduced emittance. We have been developing muonium generators to create more muoniums in vacuum even at room temperature. In 2013, we demonstrated at least 10 times increase of the muonium emission efficiency in one of the silica aerogel samples with fine holes fabricated on the surface. The measurement was carried out at TRIUMF in collaboration with J-PARC muon $g-2$/EDM group. In 2017, we carried out systematic study of muonium emission under various target conditions at TRIUMF in collaboration with Canadian collaborators who developed the method of stable production of various laser drill-holes.

We are planning to feed these new techniques to RIKEN-RAL ultra-slow muon beam line to realize further improvement of ultra-slow muon technology. The muonium production target section, which had been designed with hot tungsten, was completely redesigned and rebuilt to use advantages of the new room temperature silica aerogel target, such as no need of thermal shielding and spin control by applying weak magnetic field, etc. In test experiment, we demonstrated a new powerful method of the muon stopping optimization in silica aerogel using muonium spin rotation.

(3) New Proposal for Fundamental Physics

We proposed the measurement of the proton radius by using the hyperfine splitting of the 1S states of muonic hydrogen. Recent measurement of the proton radius using muonic hydrogen at PSI revealed that the proton radius is surprisingly smaller than the radius so far measured using normal hydrogen spectroscopy and *e-p* scattering by more than 5 times their experimental precision. In contrast to the conventional measurement by means of electron, measurement with muonic hydrogen has larger sensitivity to the proton radius because the negative muon orbits closer to the proton, although there is no reason why these measurements can yield inconsistent results. The cause of the discrepancy is not understood yet, thus a new measurement with independent method is much anticipated.

There are two independent experimental proposals to RIKEN-RAL PAC to measure the hyperfine splitting energy of the 1S energy levels by laser excitation from singlet ground state to triplet state. This energy splitting is sensitive to the Zemach radius, which is a convolution of charge and magnetic distributions inside proton. Both commonly search resonant excitation from singlet 1S ($F=0$) to triplet 1S ($F=1$) using high intensity 6.7 μm excitation laser, but different schemes are proposed to detect the resonance. One is to detect muon transfer to the surrounding impurity atom by x-ray (European group), and the other is to detect the muon decay asymmetry recovery along the circularly polarized excitation laser, which selectively excites one of the $F=1$ states and regenerates the muon spin polarization (RIKEN group). RIKEN-RAL PAC accepted both proposals for feasibility studies.

RIKEN laser group made basic design of the laser system, based on their recent success on mid-infared (6 μm) high-power pulse laser system. There is no direct way to produce 6.7 μm lasers, so we started to test the wavelength conversion efficiency of the laser key components. Concerning the target, we need to stop muons in extremely low-density hydrogen target to substantially reduce the polarization quenching effect due to atomic collision. All the muons stopped in the material other than the target can be a background source. Thus, we carried out the measurement of long-life background level, and confirmed that the background dies out quickly before the laser is introduced. We also started the optimizaiton of the muon stopping in low-density gas target.

(4) Other topics

There were many demands for the use of negative muons for the non-destructive elements analysis using muonic x-rays. Especially its good depth sensitivity was clearly demonstrated. The applied objects so far are archaeological coins, sword, ship models, oxygen concentration measurement in levers, movement of Li concentration in batteries, etc. Several papers on this work have already been published both on the technique's development and potential capabilities. Techniques developments such as new data aquisition system, pixel detector for imaging, and 3D imaging with rotating samples are in progress.

Members

Director
Philip KING

Research & Technical Scientist
Isao WATANABE (concurrent: Advanced Meson Science Lab.)

Administration Manager
Kazunori MABUCHI (concurrent: Nishina Center Planning Office)

List of Publications & Presentations

Publications
[Journal]

(Original Papers) *Subject to Peer Review

X.L. Xu *et al.*, "Utilizing muon-spin-relaxation to probe ferroelectric transition in hydroxyl salt $Co_2(OD)_3Cl$," Ferroelectrics **505,** 1255131-1-6 (2016).*

E. Mocchiutti, *et al.*, "First FAMU observation of muon transfer from mup atoms to higher-Z elements," J. Instrum. **13**, 02019 (2018).*

R. Asih *et al.*, "Magnetic moments and ordered states in pyrochlore irridates $Nd_2Ir_2O_7$ and $Sm_2Ir_2O_7$ studied by muon spin relaxation," J. Phys. Soc. Jpn. **86**, 024705-1-7 (2017).*

M. Miyajima *et al.*, "Magnetism and high-magnetic field magnetization in alkali superoxide CsO_2," J. Phys. Soc. Jpn. **87**, 063704-1-4 (2018).*

K.L. Brown, C.P.J. Stockdale, H. Luo, X. Zhao, J.- H. Li, D. Viehland, G. Xu, P.M. Gehring, K. Ishida, A.D. Hillier and C. Stock, "Depth dependent element analysis of $PbMg_{1/3}Nb_{2/3}O_3$ using muonic X-rays," Journal of Physics: Condensed Matter **30**, 125703 (2018).*

A. Taufiq *et al.*, "Studies on nanostructure and magnetic behaviors of Mn-doped black iron oxide magnetic fluids synthesized from iron sand," Nano **12**, 1750110-1-11 (2017).*

K. Wang *et al.*, "Temporal mapping of electrophilic photochemical reactions and excitonic processes with carbon specificity," Nat. Mater. **16**, 467-473 (2017).*

S. Bae *et al.*, "First muon acceleration using a radio frequency accelerator," accepted publication in Phys. Rev. Accel. Beams (2018).*

E. Spurayoga *et al.*, "3D Long-range magnetic ordering in $(C_2H_5NH_3)_2CuCl_4$ compound revealed by internal magnetic field from muon spin rotation and first principal calculation," Physica B **545**, 76−79 (2018).*

X.L. Xu *et al.*, "Critical slowing of quantum atomic H/D with features of multiferroicity in geometrically frustrated system, $Co_2(OD)_3Cl/Co_2(OH)_3Cl$," Phys. Rev. B **95**, 024111-1-10 (2017).*

A. Glamazda *et al.*, "Quantum criticality in the coupled two-leg spin ladder Ba_2CuTeO_6," Phys. Rev. B **95**, 184430 (2017).*

R. Takagi *et al.*, "Antiferromagnetic Mott insulating state in the single-component molecular material $Pd(tmdt)_2$," Phys. Rev. B **96**, 214432 (2017).*

[Proceedings]

(Original Papers) *Subject to Peer Review

I. Watanabe *et al.*, "The RIKEN-RAL Muon Facility and the application of muons for studies of magnetic properties of nano-materials," Mater. Sci. Forum **901**, 37−43 (2017).

Risdiana *et al.*, "Zn-induced development of the Cu-spin correlation in electron-doped superconducting cuprates of $Eu_{2−x}Ce_xCuO_4$," J. Phys. Conf. Ser. **1013**, 012180-1-5 (2018).

K. Takao *et al.*, "Paramagnetic-to-nonmagnetic transition in antiperovskite nitride Cr_3GeNi studied by ^{14}N-NMR and μSR," J. Phys. Conf. Ser. **868**, 012021-1-4 (2017).

T. Sumura *et al.*, "Reduction effect on the Cu-spin correlation in the electron-doped T'-cuprate $Pr_{1.3-x}La_{0.7}Ce_xCuO_{4+δ}$ ($x = 0.10$)," JPS. Conf. Proc. **21,** 011027-1-5 (2018).

A. Hillier, K. Ishida, P. Seller, M. C. Veale and M. D. Wilson, "Element specific imaging using muonic x-rays," JPS Conf. Proc. **21**, 011042 (2018).*

D.P. Sari *et al.*, "μSR study of organic superconductor λ-$(BETS)_2GaCl_4$," Mater. Sci. Eng. **196**, 012047-1-6 (2017).

S. Kanda *et al.*, "Precision laser spectroscopy of the ground state hyperfine splitting in muonic hydrogen," Proceedings of Science, PoS, **NuFACT2017**, 122 (2018).

Oral Presentations
[International Conference etc.]

K. Ishida, "MuP HFS measurement with spin polarization," FAMU meeting, Trieste, May 2017.

K. Ishida, "Muon Facility at RIKEN-RAL," International Workshop on Organic Molecule Systems, Penang, Malaysia, August 2017.

K. Ishida for J-PARC muon $g − 2$/EDM collaboration, "Muon $g − 2$/EDM experiment at J-PARC," The 19th international workshop on neutrinos from accelerators (NUFACT2017), Uppsala, Sweden, September 2017.

S. Kanda, "Precision laser spectroscopy of the ground state hyperfine splitting in muonic hydrogen," The 19th international workshop on neutrinos from accelerators (NUFACT2017), Uppsala, Sweden, September. 2017.

K. Ishida, "Nuclear physics experiments using muons," CSNS Seminar, Dongguan, China, December 2017.

S. Kanda, "Precision laser spectroscopy of the ground-state hyperfine splitting in muonic hydrogen atom," FPUA2018, Nagoya, January 2018.

K. Ishida, "Proton radius measurement from studies in muonic hydrogen," International Symposium on Nucleon Structure, Yamagata, March 2018.

[Domestic Conference]

石田勝彦,「ミューオン水素分光－陽子半径の決定」，核物理の将来　基礎物理班勉強会, 2017 年 4 月.

石田勝彦,「ミュオン水素原子の超微細構造エネルギー測定による陽子 Zemach 半径決定」，電子光理学研究センターセミナー、仙台、2017 年 8 月.

神田聡太郎,「ミュオン水素原子の精密レーザー分光」，日本物理学会 2017 年秋季大会, 宇都宮, 2017 年 9 月.

神田聡太郎, "Laser spectroscopy of the hyperfine splitting in ground-state of muonic hydrogen atom," 第 8 回 Muon 科学と加速器研究, つくば, 2018 年 1 月.

石田勝彦,「理研 RAL ミュオン施設」，第 8 回 Muon 科学と加速器研究, つくば, 2018 年 1 月.

神田聡太郎,「超伝導計測のミューオン実験への応用」，TIA かけはし事業「簡単・便利な超伝導計測」研究会, 和光, 2018 年 1 月.

神田聡太郎, "Direct measurement of muonium ground state hyperfine splitting with high-intensity pulsed muon beam," 日本物理学会第 73 回年次大会, 野田, 2018 年 3 月.

神田聡太郎,「ミュオン水素原子分光実験のための中赤外光源の開発」，日本物理学会第 73 回年次大会, 野田, 2018 年 3 月.

石田勝彦,「陽子パズルに挑むミュオン水素原子超微細構造分光」，日本物理学会第 73 回年次大会, 野田, 2018 年 3 月.

RIBF Research Division
Radioactive Isotope Physics Laboratory

1. Abstract

This Laboratory works as one of core research groups conducting programs at the world-premiere heavy-ion accelerator facility of RIKEN "RI Beam Factory (RIBF)." The Laboratory explores exotic nuclear structures and dynamics in exotic nuclei that have never been investigated before, such as those with largely imbalanced proton and neutron numbers. Our aim is to develop new experimental techniques utilizing fast radioactive isotope (RI) beams at RIBF, to discover new phenomena and properties in exotic nuclei. The Laboratory is focusing three major subjects; shell evolution of very neutron-rich nuclei, the r-process path and equation-of-state in asymmetric nuclear matter. The Laboratory has initiated international collaborations for in-beam gamma spectroscopy, decay spectroscopy and heavy-ion induced reactions, and has formed a discussion forum for next generation gamma detectors.

2. Major Research Subjects

(1) Study of structure and dynamics of exotic nuclei through developments of new tools in terms of reaction- and technique-based methodology
(2) Research on EOS in asymmetric nuclear matter via heavy-ion induced reactions
(3) Detector developments for spectroscopy and reaction studies

3. Summary of Research Activity

(1) In-beam gamma spectroscopy

In the medium and heavy mass region explored at RIBF, collective natures of nuclei are one of important subjects, which are obtained through production and observation of high excited and high spin states. To populate such states, heavy-ion induced reactions such as fragmentation, fission are useful. So far, we have developed two-step fragmentation method as an efficient method to identify and populate excited states, and lifetime measurements to deduce transition strength.

Devices utilized for the in-beam gamma spectroscopy are ZeroDegree Spectrometer (ZDS) and a NaI array DALI2. Since the end of 2008, the first spectroscopy on nuclei island-of-inversion region was performed, we have explored step-by-step new and unknown regions in the nuclear chart. The second campaign in 2009 was organized to study background components originating from atomic processes in a heavy target. Neutron-rich nuclei at $N = 20$ to 28 were studied in 2010. In 2011−2013, we conducted experiment programs for Ca-54, Ni-78, neutron-rich nuclei at $N = 82$ and neutron-deficient nuclei at $Z = 50$.

A multitude of data obtained with inelastic, nucleon knock-out, fragmentation channels have been analyzed and published. In 2011−2013, collective natures of Mg-36, 38 and Si-42 were both published in PRL. Excited states firstly observed in Ca-54 were reported in Nature to demonstrate a new nuclear magic number of 34. Fragmentation reaction has been found efficient for nuclei with $A > 100$ and low-lying excited state in Pd-126 has been successfully observed and reported in PRC.

To further strengthen the in-beam gamma spectroscopy at RIBF, we have proposed a new setup of MINOS + DALI2 to search for the 1st excited states in even-even neutron-rich nuclei with $Z \sim 20$ to 40. The program was submitted to the PAC 2013 as a new category "proposal for scientific program" and was S-ranked. A dedicated collaboration "SEASTAR" has been established as a subset of in-beam gamma collaboration "SUNFLOWER." The two campaigns were organized in 2014 and 2015 to study very neutron-rich isotopes. In 2017, the third campaign was organized at the SAMURAI spectrometer, and bunch of structure data was obtained for very exotic nuclei at $Z \sim 20$.

Concerning a next generation detector, a discussion forum has been established to write up a white paper on tracking germanium detectors and high-efficient crystal detectors such as $LaBr_3$ and GAGG.

(2) Decay spectroscopy

Beta- and isomer-spectroscopy is an efficient method for studying nuclear structure, especially for non-yrast levels. We had accumulated experimental techniques at the RIPS facility to investigate nuclear structure in light mass region via beta-gamma and beta-p coincidence. Concerning the medium and heavy mass region available at RIBF, we have developed two position-sensitive active-stoppers, strip-silicon detectors and a cylindrical active stopper called CAITEN, to achieve a low-background measurement by taking correlation between heavy ion stop position and beta-ray emission position. A site of decay-spectroscopy at the new facility of RIBF is the final focal plane of ZDS, where high precision of TOF in particle identification is obtained due to a long flight path from BigRIPS to ZDS.

At the end of 2009, the first decay spectroscopy was organized with a minimum setup of four clover gamma detectors and silicon strip detectors, to study neutron-rich nuclei with $A \sim 110$. The first campaign was found successful and efficient to publish four letter articles in 2011, two PRL's and two PLB's. One of the PRL papers is associated to the r-process path where half-lives for 18 neutron-rich nuclei were determined for the first time. The other PRL paper reported a finding of deformed magic number 64 in the Zr isotopes.

The success of the first decay-spectroscopy campaign stimulated to form a new large-scale collaboration "EURICA," where a twelve Euroball cluster array is coupled with the silicon-strip detectors to enhance gamma efficiency by a factor of 10. A construction proposal of "EURICA" was approved in the PAC 2011, and the commissioning was successfully organized in spring 2012. Since then, physics runs have been conducted for programs approved to survey nuclei of interest as many as possible, such as Ni-78, Pd-128, Sn-100. So far, 44 papers including 12 PRL's and 10 PLB's were published. One of the highlights is discovery of a seniority isomer in Pd-128, of which cascade gamma decay gives the energy of 1st excited state and robustness of $N = 82$ magic number, and the other is a half-life measurement for 110 neutron-rich nuclei across the $N = 82$ shell gap, which shows implications for the mechanism and universality of the r-process path. The EURICA collaboration finished its physics programs in summer 2016.

Beta-delayed neutron emission probability of medium and heavy neutron-rich nuclei is important to understand nuclear structure and the r-process path. In 2013, a new collaboration "BRIKEN" has been established to form a He-3 detector array. A present design of the array

has neutron efficiency as high as 70% up to 3 MeV. The array was coupled with the AIDA silicon strip system. A construction proposal was approved at the PAC 2013 and three physics proposals have been approved. The commissioning run was conducted in autumn 2016. The major physics runs were conducted in 2017.

The CAITEN detector was successfully tested with fragments produced with a Ca-48 beam in 2010.

(3) Equation-of-state via heavy-ion central collisions

Equation-of-state in asymmetric nuclear matter is one of major subjects in physics of exotic nuclei. Pi-plus and pi-minus yields in central heavy ion collisions at the RIBF energy are considered as one of EOS sensitive observables at the RIBF energy. To observe charged pions, a TPC for the SAMURAI spectrometer is being constructed under an international collaboration "SπRIT." Construction proposal was submitted at the PAC 2012, and physics proposals were approved at the PAC 2012 and 2013. The physics runs were successfully conducted in spring 2016. The data analysis is in progress to produce the first physics results.

An international symposium "NuSYM" on nuclear symmetry energy was organized at RIKEN July 2010 to invite researchers in three sub-fields, nuclear structure, nuclear reaction and nuclear astrophysics, and to discuss nuclear symmetry energy together. Since then, the symposium series have been held every year and been useful to encourage theoretical works and to strengthen the collaboration.

(4) Nucleon correlation and cluster in nuclei

Nucleon correlation and cluster in nuclei are matters of central focus in a "beyond mean-field" picture. The relevant programs with in-beam gamma and missing-mass techniques are to depict nucleon condensations and correlations in nuclear media as a function of density as well as temperature. Neutron-halo and –skin nuclei are objects to study dilute neutron matter at the surface. By changing excitation energies in neutron-rich nuclei, clustering phenomena and role of neutrons are to be investigated.

In 2013, two programs were conducted at the SAMURAI spectrometer. One is related to proton-neutron correlation in the C-12 nucleus via p-n knockout reaction with a carbon target. The other is to search for a cluster state in C-16, which was populated via inelastic alpha scattering. The data is in preparation.

A new project based on missing mass spectroscopy was launched to investigate an exotic cluster state in a very proton-rich nucleus. The experiment will be organized at GANIL with combination of RIKEN liquid hydrogen target CRYPTA and the MUST2 detector array in 2018.

Members

Chief Scientist (Lab. Head)
Hiroyoshi SAKURAI (Deputy Director, RNC)

Vice Chief Scientist
Takashi ICHIHARA

Research & Technical Scientists
Yoichi NAKAI (Senior Research Scientist)   Tadaaki ISOBE (Senior Research Scientist)
Akihisa KOHAMA (Senior Research Scientist)   Pieter Christiaan DOORNENBAL (Research Scientist)
Shunji NISHIMURA (Senior Research Scientist)   Daisuke SUZUKI (Research Scientist)

Contract Researchers
David STEPPENBECK   Mizuki NISHIMURA

Research Consultants
Masayasu ISHIHARA   Hiroyuki MURAKAMI
Akitsu IKEDA   Kenji TANABE
Kenichi MATSUYANAGI

Special Postdoctoral Researcher
Shintaro GO   Browne FRANK

Foreign Postdoctoral Researchers
He WANG

Junior Research Associate
Noritsugu NAKATSUKA (Kyoto Univ.)   Masanori KANEKO (Kyoto Univ.)
Keishi MATSUI (Univ. of Tokyo)

International Program Associates
Ian MURRAY (Univ. Paris Sud)   Phong VI (Hanoi University of Science)
Sidong CHEN (Peking Univ.)   Longchun TAO (Peking University)
Xiaohui SUN (Peking Univ.)   Jiajian LIU (Univ. of Hong Kong)

Visiting Researchers

Gabor KISS (JSPS Fellow)

Martha Liliana CORTES SUA (JSPS Fellow)

David STEPPENBECK (JSPS Fellow)

Frank BROWNE (JSPS Fellow)

Senior Visiting Scientists

Kengo OGAWA (Chiba Univ.)

Koichiro ASAHI (TIT)

Shigeru KUBONO (Univ. of Tokyo)

Visiting Scientists

Hooi Jing ONG (RCNP)

Megumi NIIKURA (Univ. of Tokyo)

Silivio CHERUBINI (Univ. of Catania)

Daiki NISHIMURA (Tokyo Univ. of Sci.)

Takashi KISHIDA (Aoyama Univ.)

Naohiko OTSUKA (Intl. Atomic Energy Agency, Austria)

Giuseppe LORUSSO (National Physics Lab., UK)

Hiu Ching LEE (Univ. of Hong Kong)

Zhengyu XU (Univ. of Hong Kong)

Byungsik HONG (Korea Univ.)

Alan MCINTOSH (Texas A & M Univ.)

Thomas DAVINSON (Univ. of Edinburgh)

Yassid AYYAD (Osaka Univ.)

Kathrin WIMMER (Univ. of Tokyo)

Tetsuya MURAKAMI (Kyoto Univ.)

Kazuo IEKI (Rikkyo Univ.)

Mitsunori FUKUDA (Osaka Univ.)

Nori AOI (RCNP)

Khiem Hong LE (Vietnam Academy of Sci. and Tech.)

Evgueni NIKOLSKI (RRC Kurchatov Inst.)

Alexey OGLOBLIN (RRC Kurchatov Inst.)

Hiroshi WATANABE (Beihang Univ.)

Akira ONO (Tohoku Univ.)

Kazuhiro OYAMATSU (Aichi Shukutoku University)

Clementine SANTAMARIA (Michigan State University)

Kei IIDA (Kochi University)

Natsumi IKENO (Tottori Univ.)

Giordano CERIZZA (NSCL)

Marisa GULINO (Universita di Enna Kore Italy)

Satoshi TAKEUCHI (TIT)

Gabor KISS (MTA Atomki)

Paer-Anders SOEDERSTROEM (T.U.Darmstadt)

JinWU (ANL)

Jin-hee CHANG (MSU)

Yoshiharu MORI (Kyoto univ.)

Visiting Technicians

Ivan KOJOUHAROV (GSI)

Jorge AGRAMUNT ROS (Valencia City Hall)

Student Trainees

Ayumi YAGI (Osaka Univ.)

Ryo TANIUCHI (Univ. of Tokyo)

Akira HOMMA (Niigata Univ.)

Satoru MOMIYAMA (Univ. of Tokyo)

Kouta WATANABE (Osaka Univ.)

Justin ESTEE (Michigan State University)

MasanoriKANEKO (Kyoto Univ.)

JungWoo LEE (Korea University)

Takashi ANDO (Univ. of Tokyo)

Shunpei KOYAMA (Univ. of Tokyo)

Hang DU (Osaka Univ.)

Yuutaro TANAKA (Osaka Univ.)

Jonathan BARNEY (Michigan State University)

Hiroyuki OIKAWA (Tokyo Univ. of Science)

Shinnosuke KANAYA (Osaka Univ.)

Shunsuke NAGAMINE (Univ. of Tokyo)

TakeshiSAITO (Univ. of Tokyo)

Eri MIYATA (Niigata Univ.)

Shoichi YAGI (Osaka Univ.)

KousukeONISHI (Osaka Univ.)

Takanobu SUGIHARA (Osaka Univ.)

Chun Yuen TSANG (CUHK)

Kosuke MAEBA (Rikkyo Univ.)

Ryunosuke BANNAI (Rikkyo Univ.)

Sakiko ASHIKAGA (Kyoto Univ.)

Kento INABA (Kyoto Univ.)

Ken WATANABE (Kyoto Univ.)

Yu TAKAHASHI (Kyoto Univ.)

Ami KOSHIKAWA (Kyoto Univ.)

Taku KUMON (Univ. of Tokyo)

Takuma KOIWAI (Univ. of Tokyo)

Yuma SHIMIZU (Univ. of Tokyo)

Taichi HORI (Osaka Univ.)

Shoken NAKAMURA (Osaka Univ.)

Rikuto YANAGIHARA (Osaka Univ.)

Naoto KANDA (Niigata Univ.)

Suharu HOSHINO (Niigata Univ.)

Ryohei HOSODA (Niigata Univ.)

Masaki SHIOTA (Niigata Univ.)

Taro WADA (Niigata Univ.)

Toshiki MOCHIZUKI (Univ. of Tokyo)

Tomoaki KASUGA (Univ. of Tokyo)

Ryohei ITO (Univ. of Tokyo)

Herrera Wilmar RODRIGUEZ (Univ.Nacional de Colombia)

Yusuke FUJINO (Rikkyo Univ.)

Interns

Beaujeault-Taud, YANN (Univrsite Paris SUD)

Part-time Workers

Ryo TANIUCHI (Univ.of Tokyo)

Keishi, MATSUI (Univ. of Tokyo)

List of Publications & Presentations

Publications

[Journal]

(Original Papers) *Subject to Peer Review

E. Teruya, N. Yoshinaga, K. Higashiyama, and K. Asahi, "Effects of particle-hole excitations to nuclear Schiff moments in Xe isotopes," Phys. Rev. C **96**, 015501(10 pages), 10.1103/PhysRevC.96.015501 (2017).

T. Sato, Y. Ichikawa, S. Kojima, C. Funayama, S. Tanaka, T. Inoue, A. Uchiyama, A. Gladkov, A. Takamine, Y. Sakamoto, Y. Ohtomo, C. Hirao, M. Chikamori, E. Hikota, T. Suzuki, M. Tsuchiya, T. Furukawa, A. Yoshimi, C. P. Bidinosti, T. Ino, H. Ueno, Y. Matsuo, T. Fukuyama, N. Yoshinaga, Y. Sakemi and K. Asahi, "Development of co-located ^{129}Xe and ^{131}Xe nuclear spin masers with external feedback scheme," Phys. Lett. A **382**, 588−594 (2018).

N. Yamanaka, B. K. Sahoo, N. Yoshinaga, T. Sato, K. Asahi and B. P. Das, "Probing exotic phenomena at the interface of nuclear and particle physics with the electric dipole moments of diamagnetic atoms: A unique window to hadronic and semi-leptonic CP violation," Eur. Phys. J. A **53**, 54 (49 pages) (2017).

J. Wu, S. Nishimura, G. Lorusso, P. Möller, E. Ideguchi, P. -H. Regan, G. S. Simpson, P. -A. Söderström, P. M. Walker, H. Watanabe, Z. Y. Xu, H. Baba, F. Browne, R. Daido, P. Doornenbal, Y. F. Fang, G. Gey, T. Isobe, P. S. Lee, J. J. Liu, Z. Li, Z. Korkulu, Z. Patel, V. Phong, S. Rice, H. Sakurai, L. Sinclair, T. Sumikama, M. Tanaka, A. Yagi, Y. L. Ye, R. Yokoyama, G. X. Zhang, T. Alharbi, N. Aoi, F. L. Bello Garrote, G. Benzoni, A. M. Bruce, R. J. Carroll, K. Y. Chae, Z. Dombradi, A. Estrade, A. Gottardo, C. J. Griffin, H. Kanaoka, I. Kojouharov, F. G. Kondev, S. Kubono, N. Kurz, I. Kuti, S. Lalkovski, G. J. Lane, E. J. Lee, T. Lokotko, G. Lotay, C. -B. Moon, H. Nishibata, I. Nishizuka, C. R. Nita, A. Odahara, Zs. Podoly´ak, O. J. Roberts, H. Schaffner, C. Shand, J. Taprogge, S. Terashima, Z. Vajta, and S. Yoshida, "94-Decay half-lives of neutron-rich ^{55}Cs to ^{67}Ho: Experimental of the r-process rare-earth peak formation," Phys. Rev. Lett. **118**, 072701-7 (2017).

P. Zhang, X. Xu, P. Shuai, R. J. Chen, X. L. Yan, Y. H. Zhang, M. Wang, Yu. A. Litvinovc, K. Blaum, H. S. Xu, T. Bao, X. C. Chen, H. Chena, C. Y. Fua, J. J. He, S. Kubono, Y. H. Lam, D. W. Liua, R. S. Mao, X. W. Ma, M. Z. Suna, X. L. Tu, Y. M. Xing, J. C. Yang, Y. J. Yuan, Q. Zenga, X. Zhoua, X. H. Zhou, W. L. Zhan, S. Litvinov, G. Audi, T. Uesaka, Y. Yamaguchi, T. Yamaguchi, A. Ozawa, B. H. Sun, Y. Sun, F. R. Xu, "High-precision QEC values of super-allowed $0^+ \rightarrow 0^+$ β-emitters ^{46}Cr, ^{50}Fe and ^{54}Ni," Phys. Lett. B **767**, 20, 10.1016/j.physletb.2017.01.039 (2017).

T. Kawabata, Y. Fujikawa, T. Furuno, T. Goto, T. Hashimoto, M. Ichikawa, M. Itoh, N. Iwasa, Y. Kanada-En'yo, A. Koshikawa, S. Kubono, E. Miyawaki, M. Mizuno, K. Mizutani, T. Morimoto, M. Murata, T. Nanamura, S. Nishimura, S. Okamoto, Y. Sakaguchi, I. Sakata, A. Sakaue, R. Sawada, Y. Shikata, Y. Takahashi, D. Takechi, T. Takeda, C. Takimoto, M. Tsumura, K. Watanabe, and S. Yoshida, "Time-reversal measurement of the p-wave cross sections of the ^{7}Be(n, α)^{4}He reaction for the cosmological Li problem," Phys. Rev. Lett. **118**, 052701-5, 10.1103/PhysRevLett.118.052701 (2017) .

H. Wang, H. Otsu, H. Sakurai, D. Ahn, M. Aikawa, T. Ando, S. Araki, S. Chen, N. Chiga, P. Doornenbal, N. Fukuda, T. Isobe, S. Kawakami, S. Kawase, T. Kin, Y. Kondo, S. Koyama, S. Kubono, Y. Maeda, A. Makinaga, M. Matsushita, T. Matsuzaki, S. Michimasa, S. Momiyama, S. Nagamine, T. Nakamura, K. Nakano, M. Niikura, T. Ozaki, A. Saito, T. Saito, Y. Shiga, M. Shikata, Y. Shimizu, S. Shimoura, T. Sumikama, P. -A. Söderström, H. Suzuki, H. Takeda, S. Takeuchi, R. Taniuchi, Y. Togano, J. Tsubota, M. Uesaka Y. Watanabe, Y. Watanabe, K. Wimmer, T. Yamamoto, K. Yoshida, "Spallation reaction study for the long-lived fission product ^{107}Pd," Prog. Theor. Exp. Phys. **2017**, 021D01(10 pages), 10.1093/ptep/ptw187 (2017).

A. I. Morales, A. Algora, B. Rubio, K. Kaneko, S. Nishimura, P. Aguilera, S. E. A. Orrigo, F. Molina, G. de Angelis, F. Recchia, G. Kiss, V. H. Phong, J. Wu, D. Nishimura, H. Oikawa, T. Goigoux, J. Giovinazzo, P. Ascher, J. Agramunt, D. S. Ahn, H. Baba, B. Blank, C. Borcea, A. Boso, P. Davies, F. Diel, Zs. Dombrádi, P. Doornenbal, J. Eberth, G. de France, Y. Fujita, N. Fukuda, E. Ganioglu, W. Gelletly, M. Gerbaux, S. Grévy, V. Guadilla, N. Inabe, T. Isobe, I. Kojouharov, W. Korten, T. Kubo, S. Kubono, T. Kurtukián Nieto, N. Kurz, J. Lee, S. Lenzi, J. Liu, T. Lokotko, D. Lubos, C. Magron, A. Montaner-Pizá, D. R. Napoli, H. Sakurai, H. Schaffner, Y. Shimizu, C. Sidong, P. -A. Söderström, T. Sumikama, H. Suzuki, H. Takeda, Y. Takei, M. Tanaka, and S. Yagi, "Simultaneous investigation of the $T = 1$ ($J^\pi = 0^+$) and $T = 0$ ($J^\pi = 9^+$) β decays in ^{70}Br," Phys. Rev. C **95**, 064327, 10.1103/PhysRevC.95.064327 (2017).

S. Kawase, K. Nakano, Y. Watanabe, H. Wang, H. Otsu, H. Sakurai, D. S. Ahn, M. Aikawa, T. Ando, S. Araki, S. Chen, N. Chiga, P. Doornenbal, N. Fukuda, T. Isobe, S. Kawakami, T. Kin, Y. Kondo, S. Koyama, S. Kubono, Y. Maeda, A. Makinaga, M. Matsushita, T. Matsuzaki, S. Michimasa, S. Momiyama, S. Nagamine, T. Nakamura, M. Niikura, T. Ozaki, A. Saito, T. Saito, Y. Shiga, M. Shikata, Y. Shimizu, S. Shimoura, T. Sumikama, P. A. Söderström, H. Suzuki, H. Takeda, S. Takeuchi, R. Taniuchi, Y. Togano, J. Tsubota, M. Uesaka, Y. Watanabe, K. Wimmer, T. Yamamoto, and K. Yoshida, "Study of proton- and deuteron-induced spallation reactions on the long-lived fission product ^{93}Zr at 105 MeV/nucleon in inverse kinematics," Prog. Theor. Exp. Phys. **2017**, 093D03(10 pages), 10.1093/ptep/ptx110 (2017).

H. Suzuki, L. Sinclair, P. -A. Söderström, G. Lorusso, P. Davies, L. S. Ferreira, E. Maglione, R. Wadsworth, J. Wu, Z. Y. Xu, S. Nishimura, P. Doornenbal, D. S. Ahn, F. Browne, N. Fukuda, N. Inabe, T. Kubo, D. Lubos, Z. Patel, S. Rice, Y. Shimizu, H. Takeda, H. Baba, A. Estrade, Y. Fang, J. Henderson, T. Isobe, D. Jenkins, S. Kubono, Z. Li, I. Nishizuka, H. Sakurai, P. Schury, T. Sumikama, H. Watanabe, and V. Werner, "Discovery of ^{72}Rb: A nuclear sandbank beyond the proton drip line," Phys. Rev. Lett. **119**, 192503(6), 10.1103/PhysRevLett.119.192503 (2017).

D. Kahl, H. Yamaguchi, S. Kubono, A. A. Chen, A. Parikh, D. N. Binh, J. Chen, S. Cherubini, N. N. Duy, T. Hashimoto, S. Hayakawa, N. Iwasa, H. S. Jung, S. Kato, Y. K. Kwon, S. Nishimura, S. Ota, K. Setoodehnia, T. Teranishi, H. Tokieda, T. Yamada, C. C. Yun, and L. Y. Zhang, "First measurement of ^{30}S + α resonant elastic scattering for the ^{30}S(α, p) reaction rate" Phys. Rev. C **97**, 015802(16), 10.1103/PhysRevC.97.015802 (2018).

H. Muto, Y. Ohshiro, Y. Kotaka, H. Yamaguchi, Y. Sakemi, K. Kobayashi, M. Nishimura, M. Oyaizu, S. Kubono, M. Kase, T. Hattori, and S. Shimoura, "Note: An innovative method for ^{12}C^{4+} suppression in ^{18}O^{6+} beam production in an electron cyclotron resonance ion source (selected as the editor's pick)," Rev. Sci. Instrum. **89**, 016103(3), 10.1063/1.5000426 (2018).

Y. M. Xing, K. A. Li, Y. H. Zhang, X. H. Zhou, M. Wang, Yu. A. Litvinov, K. Blaum, S. Wanajo, S. Kubono, G. Martínez-Pinedo, A. Sieverding, R. J. Chen, P. Shuai, C. Y. Fu, X. L. Yan, W. J. Huang, X. Xu, X. D. Tang, H. S. Xu, T. Bao, X. C. Chen, B. S. Gao, J. J. He, Y. H. Lam, H. F. Li, J. H. Liu,

X. W. Ma, R. S. Mao, M. Si, M. Z. Sun, X. L. Tu, Q. Wang, J. C. Yang, Y. J. Yuan, Q. Zeng, P. Zhang, X. Zhou, W. L. Zhan, S. Litvinov, G. Audi, T. Uesaka, Y. Yamaguchi, T. Yamaguchi, A. Ozawa, C. Fröhlich, T. Rauscher, F. -K. Thielemann, B. H. Sun, Y. Sun, A. C. Dai, F. R. Xu "Mass measurements of neutron-deficient Y, Zr, and Nb Isotopes and their impact on rp and vp nucleosynthesis processes," Phys. Lett. B **781**, 358–363, 10.1016/j.physletb.2018.04.009 (2018).

N. Lalović, D. Rudolph, Zs. Podolyák, L. G. Sarmiento, E. C. Simpson, T. Alexander, M. L. Cortés, J. Gerl, P. Golubev, F. Ameil, T. Arici, Ch. Bauer, D. Bazzacco, M. A. Bentley, P. Boutachkov, M. Bowry, C. Fahlander, A. Gadea, J. Gellanki, A. Givechev, N. Goel, M. Górska, A. Gottardo, E. Gregor, G. Guastalla, T. Habermann, M. Hackstein, A. Jungclaus, I. Kojouharov, R. Kumar, N. Kurz, M. Lettmann, C. Lizarazo, C. Louchart, E. Merchán, C. Michelagnoli, Th. Moeller, K. Moschner, Z. Patel, N. Pietralla, S. Pietri, D. Ralet, M. Reese, P. H. Regan, P. Reiter, H. Schaffner, P. Singh, C. Stahl, R. Stegmann, O. Stezowski, J. Taprogge, P. Thöle, A. Wendt, O. Wieland, E. Wilson, R. Wood, H. -J. Wollersheim, B. Birkenbach, B. Bruyneel, I. Burrows, E. Clément, P. Désesquelles, C. Domingo-Pardo, J. Eberth, V. González, H. Hess, J. Jolie, D. S. Judson, R. Menegazzo, D. Mengoni, D. R. Napoli, A. Pullia, B. Quintana, G. Rainovski, M. D. Salsac, E. Sanchis, J. Simpson, J. J. Valiente-Dóbon and the AGATA Collaboration, "Study of isomeric states in 198, 200, 202, 206Pb and 206Hg populated in fragmentation reactions," J. Phys. G: Nucl. Part. Phys. **45**, 035105 (2018).

D. Kocheva, G. Rainovski, J. Jolie, N. Pietralla, A. Blazhev, A. Astier, R. Altenkirch, S. Ansari, Th. Braunroth, M. L. Cortés, A. Dewald, F. Diel, M. Djongolov, C. Fransen, K. Gladnishki, A. Hennig, V. Karayonchev, J. M. Keatings, E. Kluge, J. Litzinger, C. Müller-Gatermann, P. Petkov. M. Rudigier, M. Scheck, Ph. Scholz, P. Spagnoletti, M. Spieker, C. Stahl, R. Stegmann, M. Stoyanova, P. Thöle, V. Warr, V. Werner, W. Witt, D. Wölk, K. O. Zell, P. Van Isacker, V. Yu. Ponomarev, "A revised B(E2; $2_1^+ \rightarrow 0_1^+$) value in the semi-magic nucleus 210Po," Eur. Phys. J. A **53**, 1752017 (2017).

Ch. Lorenz, L. G. Sarmiento, D. Rudolph, D. E. Ward, M. Block, F. P. Heßberger, D. Ackermann, L. -L. Andersson, M. L. Cortés, C. Droese, M. Dworschak, M. Eibach, U. Forsberg, P. Golubev, R. Hoischen, I. Kojouharov, J. Khuyagbaatar, D. Nesterenko, I. Ragnarsson, H. Schaffner, L. Schweikhard, S. Stolze, and J. Wenzl, "Quantum-state-selective decay spectroscopy of 213Ra," Phys. Rev. C **96**, 034315 (2017).

F. Flavigny, P. Doornenbal, A. Obertelli, J. -P. Delaroche, M. Girod, J. Libert, T. R. Rodriguez, G. Authelet, H. Baba, D. Calvet, F. Château, S. Chen, A. Corsi, A. Delbart, J. -M. Gheller, A. Giganon, A. Gillibert, V. Lapoux, T. Motobayashi, M. Niikura, N. Paul, J. -Y. Roussé, H. Sakurai, C. Santamaria, D. Steppenbeck, R. Taniuchi, T. Uesaka, T. Ando, T. Arici, A. Blazhev, F. Browne, A. Bruce, R. Carroll, L. X. Chung, M. L. Cortés, M. Dewald, B. Ding, S. Franchoo, M. Górska, A. Gottardo, A. Jungclaus, J. Lee, M. Lettmann, B. D. Linh, J. Liu, Z. Liu, C. Lizarazo, S. Momiyama, K. Moschner, S. Nagamine, N. Nakatsuka, C. Nita, C. R. Nobs, L. Olivier, R. Orlandi, Z. Patel, Zs. Podolyák, M. Rudigier, T. Saito, C. Shand, P. A. Söderström, I. Stefan, V. Vaquero, V. Werner, K. Wimmer, and Z. Xu1, "Shape evolution in neutron-rich krypton isotopes beyond $N = 60$: First spectroscopy of 98, 100Kr," Phys. Rev. Lett. **118**, 242501 (2017).

M. Lettmann, V. Werner, N. Pietralla, P. Doornenbal, A. Obertelli, T. R. Rodríguez, K. Sieja, G. Authelet, H. Baba, D. Calvet, F. Château, S. Chen, A. Corsi, A. Delbart, J. -M. Gheller, A. Giganon, A. Gillibert, V. Lapoux, T. Motobayashi, M. Niikura, N. Paul, J. -Y. Roussé, H. Sakurai, C. Santamaria, D. Steppenbeck, R. Taniuchi, T. Uesaka, T. Ando, T. Arici, A. Blazhev, F. Browne, A. Bruce, R. J. Caroll, L. X. Chung, M. L. Cortés, M. Dewald, B. Ding, F. Flavigny, S. Franchoo, M. Górska, A. Gottardo, A. Jungclaus, J. Lee, B. D. Linh, J. Liu, Z. Liu, C. Lizarazo, S. Momiyama, K. Moschner, S. Nagamine, N. Nakatsuka, C. Nita, C. R. Nobs, L. Olivier, Z. Patel, Zs. Podolyák, M. Rudigier, T. Saito, C. Shand, P. -A. Söderström, I. Stefan, V. Vaquero, K. Wimmer, and Z. Xu, "Triaxiality of neutron-rich 84, 86, 88Ge from low-energy nuclear spectra," Phys. Rev. C **96**, 011301 (2017).

C. M. Shand, Zs. Podolyák, M. Górska, P. Doornenbal, A. Obertelli, F. Nowacki, T. Otsuka, K. Sieja, J. A. Tostevin, Y. Tsunoda, G. Authelet, H. Baba, D. Calvet, A. Château, S. Chen, A. Corsi, A. Delbart, J. M. Gheller, A. Giganon, A. Gillibert, T. Isobe, V. Lapoux, M. Matsushita, S. Momiyama, T. Motobayashi, M. Niikura, H. Otsu, N. Paul, C. Péron, A. Peyaud, E. C. Pollacco, J. -Y. Roussé, H. Sakurai, C. Santamaria, M. Sasano, Y. Shiga, D. Steppenbeck, S. Takeuchi, R. Taniuchi, T. Uesaka, H. Wang, K. Yoneda, T. Ando, T. Arici, A. Blazhev, F. Browne, A. M. Bruce, R. J. Carroll, L. X. Chung, M. L. Cortés, M. Dewald, B. Ding, Zs. Dombrádi, F. Flavigny, S. Franchoo, F. Giacoppo, A. Gottardo, K. Hadyńska-Klęk, A. Jungclaus, Z. Korkulu, S. Koyama, Y. Kubota, J. Lee, M. Lettmann, B. D. Linh, J. Liu, Z. Liu, C. Lizarazo, C. Louchart, R. Lozeva, K. Matsui, T. Miyazaki, K. Moschner, M. Nagamine, N. Nakatsuka, S. Nishimura, C. R. Nita, C. R. Nobs, L. Olivier, S. Ota, R. Orlandi, Z. Patel, P. H. Regan, M. Rudigier, E. Şahin, T. Saito, P. -A. Söderström, I. Stefan, T. Sumikama, D. Suzuki, Zs. Vajta, V. Vaquero, V. Werner, K. Wimmer, J. Wu, Z. Y. Xu, "Shell evolution beyond $Z = 28$ and $N = 50$: Spectroscopy of 81, 82, 83, 84Zn," Phys. Lett. B **773**, 492−497 (2017).

B. Moon, C. -B. Moon, P. -A. Soderstrom, A. Odahara, R. Lozeva, B. Hong, F. Browne, H. S. Jung, P. Lee, C. S. Lee, A. Yagi, C. Yuan, S. Nishimura, P. Doornenbal, G. Lorusso, T. Sumikama, H. Watanabe, I. Kojouharov, T. Isobe, H. Baba, H. Sakurai, R. Daido, Y. Fang, H. Nishibata, Z. Patel, S. Rice, L. Sinclair, J. Wu, Z. Y. Xu, R. Yokoyama, T. Kubo, N. Inabe, H. Suzuki, N. Fukuda, D. Kameda, H. Takeda, D. S. Ahn, Y. Shimizu, D. Murai, F. L. Bello Garrote, J. M. Daugas, F. Didierjean, E. Ideguchi, T. Ishigaki, S. Morimoto, M. Niikura, I. Nishizuka, T. Komatsubara, Y. K. Kwon, K. Tshoo, "Nuclear structure and beta-decay schemes for Te nuclides beyond $N = 82$," Phys. Rev. C **95**, 044322, 10.1103/PhysRevC.95.044322 (2017).

T. Sumikama, S. Nishimura, H. Baba, F. Browne, P. Doornenbal, N. Fukuda, S. Franchoo, G. Gey, N. Inabe, T. Isobe, P. R. John, H. S. Jung, D. Kameda, T. Kubo, Z. Li, G. Lorusso, I. Matea, K. Matsui, P. Morfouace, D. Mengoni, D. R. Napoli, M. Niikura, H. Nishibata, A. Odahara, E. Sahin, H. Sakurai, P. -A. Soderstrom, G. I. Stefan, D. Suzuki, H. Suzuki, H. Takeda, R. Taniuchi, J. Taprogge, Zs. Vajta, H. Watanabe, V. Werner, J. Wu, Z. Y. Xu, A. Yagi, K. Yoshinaga, "Observation of new neutron-rich Mn, Fe, Co, Ni, and Cu isotopes in the vicinity of 78Ni," Phys. Rev. C **95**, 05160(R) (2017).

E. Sahin, F. L. Bello Garrote, Y. Tsunoda, T. Otsuka, G. de Angelis, A. Gorgen, M. Niikura, S. Nishimura, Z. Y. Xu, H. Baba, F. Browne, M. -C. Delattre, P. Doornenbal, S. Franchoo, G. Gey, K. Hadynska-Klek, T. Isobe, P. R. John, H. S. Jung, I. Kojouharov, T. Kubo, N. Kurz, Z. Li, G. Lorusso, I. Matea, K. Matsui, D. Mengoni, P. Morfouace, D. R. Napoli, F. Naqvi, H. Nishibata, A. Odahara, H. Sakurai, H. Schaffner, P. -A. Soderstrom, D. Sohler, I. G. Stefan, T. Sumikama, D. Suzuki, R. Taniuchi, J. Taprogge, Z. Vajta, H. Watanabe, V. Werner, J. Wu, A. Yagi, M. Yalcinkaya, K. Yoshinaga, "Shell evolution towards 78Ni: Low-lying states in 77Cu," Phys. Rev. Lett. **118**, 242502, 10.1103/PhysRevLett.118.242502 (2017).

B. Moon, C. -B. Moon, A. Odahara, R. Lozeva, P. -A. Soderstrom, F. Browne, C. Yuan, A. Yagi, B. Hong, H. S. Jung, P. Lee, C. S. Lee, S. Nishimura, P. Doornenbal, G. Lorusso, T. Sumikama, H. Watanabe, I. Kojouharov, T. Isobe, H. Baba, H. Sakurai, R. Daido, Y. Fang, H. Nishibata, Z. Patel, S. Rice, L. Sinclair, J. Wu, Z. Y. Xu, R. Yokoyama, T. Kubo, N. Inabe, H. Suzuki, N. Fukuda, D. Kameda, H. Takeda, D. S. Ahn, Y. Shimizu, D. Murai, F. L. Bello Garrote, J. M. Daugas, F. Didierjean, E. Ideguchi, T. Ishigaki, S. Morimoto, M. Niikura, I. Nishizuka, T. Komatsubara, Y. K. Kwon, K. Tshoo, "β-decay scheme of 140Te to 140I: Suppression of Gamow-Teller transitions between the neutron $h_{9/2}$ and proton $h_{11/2}$ partner orbitals," Phys. Rev. C **96**, 014325, 10.1103/PhysRevC.96.014325 (2017).

F. Browne, A. M. Bruce, T. Sumikama, I. Nishizuka, S. Nishimura, P. Doornenbal, G. Lorusso, P. -A. Soderstrom, H. Watanabe, R. Daido, Z. Patel, S. Rice,

L. Sinclair, J. Wu, Z. Y. Xu, A. Yagi, H. Baba, N. Chiga, R. Carroll, F. Didierjean, Y. Fang, N. Fukuda, G. Gey, E. Ideguchi, N. Inabe, T. Isobe, D. Kameda, I. Kojouharov, N. Kurz, T. Kubo, S. Lalkovski, Z. Li, R. Lozeva, N. Nishibata, A. Odahara, Zs. Podolyak, P. H. Regan, O. J. Roberts, H. Sakurai, H. Schaffner, G. S. Simpson, H. Suzuki, H. Takeda, M. Tanaka, J. Taprogge, V. Werner, O. Wieland, "K selection in the decay of the ($\nu 5/2[53\otimes 3/2[411]$) 4^- isomeric state in ^{102}Zr," Phys. Rev. C **96**, 024309, 10.1103/PhysRevC.96.024309 (2017).

Z. Patel, P. M. Walker, Zs. Podolyak, P. H. Regan, T. A. Berry, P. -A. Soderstrom, H. Watanabe, E. Ideguchi, G. S. Simpson, S. Nishimura, Q. Wu, F. R. Xu, F. Browne, P. Doornenbal, G. Lorusso, S. Rice, L. Sinclair, T. Sumikama, J. Wu, Z. Y. Xu, N. Aoi, H. Baba, F. L. Bello Garrote, G. Benzoni, R. Daido, Zs. Dombradi, Y. Fang, N. Fukuda, G. Gey, S. Go, A. Gottardo, N. Inabe, T. Isobe, D. Kameda, K. Kobayashi, M. Kobayashi, T. Komatsubara, I. Kojouharov, T. Kubo, N. Kurz, I. Kuti, Z. Li, M. Matsushita, S. Michimasa, C. -B. Moon, H. Nishibata, I. Nishizuka, A. Odahara, E. Sahin, H. Sakurai, H. Schaffner, H. Suzuki, H. Takeda, M. Tanaka, J. Taprogge, Zs. Vajta, A. Yagi, R. Yokoyama, "Isomer-delayed γ-ray spectroscopy of $A = 159-164$ midshell nuclei and the variation of K-forbidden E1 transition hindrance factors," Phys. Rev. C **96**, 034305, 10.1103/PhysRevC.96.034305 (2017).

A. Jungclaus, H. Grawe, S. Nishimura, P. Doornenbal, G. Lorusso, G. S. Simpson, P. -A. Soderstrom, T. Sumikama, J. Taprogge, Z. Y. Xu, H. Baba, F. Browne, N. Fukuda, R. Gernhauser, G. Gey, N. Inabe, T. Isobe, H. S. Jung, D. Kameda, G. D. Kim, Y. -K. Kim, I. Kojouharov, T. Kubo, N. Kurz, Y. K. Kwon, Z. Li, H. Sakurai, H. Schaffner, Y. Shimizu, K. Steiger, H. Suzuki, H. Takeda, Zs. Vajta, H. Watanabe, J. Wu, A. Yagi, K. Yoshinaga, G. Benzoni, S. Bonig, K. Y. Chae, L. Coraggio, J. -M. Daugas, F. Drouet, A. Gadea, A. Gargano, S. Ilieva, N. Itaco, F. G. Kondev, T. Kroll, G. J. Lane, A. Montaner-Piza, K. Moschner, D. Mucher, F. Naqvi, M. Niikura, H. Nishibata, A. Odahara, R. Orlandi, Z. Patel, Zs. Podolyak, A. Wendt, "Observation of a γ decaying millisecond isomeric state in ^{128}Cd$_{80}$," Phys. Lett. B **772**, 483−488, 10.1016/j.physletb.2017.07.006 (2017).

J. Park, R. Krucken, D. Lubos, R. Gernhauser, M. Lewitowicz, S. Nishimura, D. S. Ahn, H. Baba, B. Blank, A. Blazhev, P. Boutachkov, F. Browne, I. Celikovic, G. de France, P. Doornenbal, T. Faestermann, Y. Fang, N. Fukuda, J. Giovinazzo, N. Goel, M. Gorska, H. Grawe, S. Ilieva, N. Inabe, T. Isobe, A. Jungclaus, D. Kameda, G. D. Kim, Y. -K. Kim, I. Kojouharov, T. Kubo, N. Kurz, G. Lorusso, K. Moschner, D. Murai, I. Nishizuka, Z. Patel, M. M. Rajabali, S. Rice, H. Sakurai, H. Schaffner, Y. Shimizu, L. Sinclair, P. -A. Soderstrom, K. Steiger, T. Sumikama, H. Suzuki, H. Takeda, Z. Wang, H. Watanabe, J. Wu, Z. Y. Xu, "Properties of γ-decaying isomers and isomeric ratios in the ^{100}Sn region," Phys. Rev. C **96**, 044311, 10.1103/PhysRevC.96.044311 (2017).

L. Olivier, S. Franchoo, M. Niikura, Z. Vajta, D. Sohler, P. Doornenbal, A. Obertelli, Y. Tsunoda, T. Otsuka, G. Authelet, H. Baba, D. Calvet, F. Chateau, A. Corsi, A. Delbart, J. -M. Gheller, A. Gillibert, T. Isobe, V. Lapoux, M. Matsushita, S. Momiyama, T. Motobayashi, H. Otsu, C. Peron, A. Peyaud, E. C. Pollacco, J. -Y. Rousse, H. Sakurai, C. Santamaria, S. Sasano, Y. Shiga, S. Takeuchi, R. Taniuchi, T. Uesaka, H. Wang, K. Yoneda, F. Browne, L. X. Chung, Z. Dombradi, F. Flavigny, F. Giacoppo, A. Gottardo, K. Hadynska-Klek, Z. Korkulu, S. Koyama, Y. Kubota, J. Lee, M. Lettmann, C. Louchart, R. Lozeva, K. Matsui, T. Miyazaki, S. Nishimura, K. Ogata, S. Ota, Z. Patel, E. Sahin, C. Shand, P. -A. Soderstrom, I. Stefan, D. Steppenbeck, T. Sumikama, D. Suzuki, V. Werner, J. Wu, Z. Xu, "Persistence of the $Z = 28$ shell gap around ^{78}Ni: First spectroscopy of ^{79}Cu," Phys. Rev. Lett. **119**, 192501, 10.1103/PhysRevLett.119.192501 (2017).

Y. Shimizu, T. Kubo, N. Fukuda, N. Inabe, D. Kameda, H. Sato, H. Suzuki, H. Takeda, K. Yoshida, G. Lorusso, H. Watanabe, G. S. Simpson, A. Jungclaus, H. Baba, F. Browne, P. Doornenbal, G. Gey, T. Isobe, Z. Li, S. Nishimura, P. -A. Soderstrom, T. Sumikama, J. Taprogge, Z. Vajta, J. Wu, Z. Xu, A. Odahara, A. Yagi, H. Nishibata, R. Lozeva, C. Moon, H. S. Jung, "Observation of New Neutron-rich isotopes among fission fragments from in-flight fission of 345 MeV/nucleon ^{238}U: Search for new isotopes conducted concurrently with decay measurement campaigns," J. Phys. Soc. Jpn. **87**, 014203, 10.7566/JPSJ.87.014203 (2018).

P. Davies, H. Grawe, K. Moschner, A. Blazhev, R. Wadsworth, P. Boutachkov, F. Ameil, A. Yagid, H. Baba, T. Back, M. Dewald, P. Doornenbal, T. Faestermann, A. Gengelbach, J. Gerl, R. Gernhaeuser, S. Go, M. Gorska, E. Gregor, T. Isobe, D. G. Jenkins, H. Hotaka, J. Jolie, I. Kojouharov, N. Kurz, M. Lewitowicz, G. Lorusso, L. Maier, E. Merchan, F. Naqvi, H. NishibataDC, D. Nishimura, S. Nishimura, F. Nowacki, N. Pietralla, H. Schaffner, P. -A. Söderström, H. S. Jung, K. Steiger, T. Sumikama, J. Taprogge, P. Thole, N. Warr, H. Watanabe, V. Werner, Z. Y. Xu, K. Yoshinaga, Y. Zhu, "The role of core excitations in the structure and decay of the 16$^+$ spin-gap isomer in ^{96}Cd," Phys. Lett. B **767**, 474–479 (2017).

D. Verney, D. Testov, F. Ibrahim, Yu. Penionzhkevich, B. Roussiere, V. Smirnov, F. Didierjean, K. Flanagan, S. Franchoo, E. Kuznetsova, R. Li, B. Marsh, I. Matea, H. Pai, E. Sokol, I. Stefan, D. Suzuki, "Pygmy Gamow-Teller resonance in the $N = 50$ region: New evidence from staggering of β-delayed neutron-emission probabilities," Phys. Rev. C **95**, 054320, 10.1103/PhysRevC.95.054320 (2017).

T. Konstantinopoulos, P. Petkov, A. Goasduff, T. Arici, A. Astier, L. Atanasova, M. Axiotis, D. Bonatsos, P. Detistov, A. Dewald, M. J. Eller, V. Foteinou, A. Gargano, G. Georgiev, K. Gladnishki, A. Gottardo, S. Harissopulos, H. Hess, S. Kaim, D. Kocheva, A. Kusoglu, A. Lagoyannis, J. Ljungvall, R. Lutter, I. Matea, B. Melon, T. J. Mertzimekis, A. Nannini, C. M. Petrache, A. Petrovici, G. Provatas, P. Reiter, M. Rocchini, S. Roccia, M. Seidlitz, B. Siebeck, D. Suzuki, N. Warr, H. De Witte, T. Zerrouki, "Lifetime measurements in ^{100}Ru," Phys. Rev. C **95**, 014309, 10.1103/PhysRevC.95.014309 (2017).

S. Chen, P. Doornenbal, A. Obertelli, T. R. Rodriguez, G. Authelet, H. Baba, D. Calvet, F. Chateau, A. Corsi, A. Delbart, J. -M. Gheller, A. Giganon, A. Gillibert, V. Lapoux, T. Motobayashi, M. Niikura, N. Paul, J. -Y. Rousse, H. Sakurai, C. Santamaria, D. Steppenbeck, R. Taniuchi, T. Uesaka, T. Ando, T. Arici, A. Blazhev, F. Browne, A. M. Bruce, R. Caroll, L. X. Chung, M. L. Cortes, M. Dewald, B. Ding, F. Flavigny, S. Franchoo, M. Gorska, A. Gottardo, A. Jungclaus, J. Lee, M. Lettmann, B. D. Linh, J. Liu, Z. Liu, C. Lizarazo, S. Momiyama, K. Moschner, S. Nagamine, S. Nakatsuka, C. R. Nita, C. Nobs, L. Olivier, R. Orlandi, Z. Patel, Zs. Podolyak, M. Rudigier, T. Saito, C. Shand, P. -A. Soderstrom, I. Stefan, V. Vaquero, V. Werner, K. Wimmer, Z. Xu, "Low-lying structure and shape evolution in neutron-rich Se isotopes," Phys. Rev. C **95**, 041302 (2017).

P. Doornenbal, H. Scheit, S. Takeuchi, Y. Utsuno, N. Aoi, K. Li, M. Matsushita, D. Steppenbeck, H. Wang, H. Baba, E. Ideguchi, N. Kobayashi, Y. Kondo, J. Lee, S. Michimasa, T. Motobayashi, T. Otsuka, H. Sakurai, M. Takechi, Y. Togano, K. Yoneda, "Low-Z shore of the 'island of inversion' and the reduced neutron magicity toward ^{28}O," Phys. Rev. C **95**, 041301 (2017).

H. N. Liu, J. Lee, P. Doornenbal, H. Scheit, S. Takeuchi, N. Aoi, K. A. Li, M. Matsushita, D. Steppenbeck, H. Wang, H. Baba, E. Ideguchi, N. Kobayashi, Y. Kondo, G. Lee, S. Michimasa, T. Motobayashi, A. Poves, H. Sakurai, M. Takechi, Y. Togano, J. A. Tostevin, Y. Utsuno "Intruder configurations in the ground state of ^{30}Ne," Phys. Lett. B **767**, 58 (2017).

S. Momiyama, P. Doornenbal, H. Scheit, S. Takeuchi, M. Niikura, N. Aoi, K. Li, M. Matsushita, D. Steppenbeck, H. Wang, H. Baba, E. Ideguchi, M. Kimura, N. Kobayashi, Y. Kondo, J. Lee, S. Michimasa, T. Motobayashi, N. Shimizu, M. Takechi, Y. Togano, Y. Utsuno, K. Yoneda, H. Sakurai, "In-beam gamma-ray spectroscopy of ^{35}Mg via knockout reactions at intermediate energies," Phys. Rev. C **96**, 034328 (2017).

N. Nakatsuka, H. Baba, T. Aumann, R. Avigo, S. R. Banerjee, A. Bracco, C. Caesar, F. Camera, S. Ceruti, S. Chen, V. Derya, P. Doornenbal, A. Giaz, A.

Horvat, K. Ieki, T. Inakura, N. Imai, T. Kawabata, N. Kobayashi, Y. Kondo, S. Koyama, M. Kurata-Nishimura, S. Masuoka, M. Matsushita, S. Michimasa, B. Million, T. Motobayashi, T. Murakami, T. Nakamura, T. Ohnishi, H. J. Ong, S. Ota, H. Otsu, T. Ozaki, A. Saito, H. Sakurai, H. Scheit, F. Schindler, P. Schrock, Y. Shiga, M. Shikata, S. Shimoura, D. Steppenbeck, T. Sumikama, I. Syndikus, H. Takeda, S. Takeuchi, A. Tamii, R. Taniuchi, Y. Togano, J. Tscheuschner, J. Tsubota, H. Wang, O. Wieland, K. Wimmer, Y. Yamaguchi, K. Yoneda, J. Zenihiro, "Observation of isoscalar and isovector dipole excitations in neutron-rich ^{20}O," Phys. Lett. B **768**, 387 (2017).

T. Nakamura, H. Sakurai, H. Watanabe, "Exotic nuclei explored at in-flight separators," Prog. Part. Nucl. Phys. **97**, 53 (2017).

D. Steppenbeck, S. Takeuchi, N. Aoi, P. Doornenbal, M. Matsushita, H. Wang, H. Baba, S. Go, J. D. Holt, J. Lee, K. Matsui, S. Michimasa, T. Motobayashi, D. Nishimura, T. Otsuka, H. Sakurai, Y. Shiga, P. -A. Soderstrom, S. R. Stroberg, T. Sumikama, R. Taniuchi, J. A. Tostevin, Y. Utsuno, J. J. Valiente-Dobon, K. Yoneda, "Structure of ^{55}Sc and development of the $N = 34$ subshell closure," Phys. Rev. C **96**, 064310 (2017).

V. Vaquero, A. Jungclaus, P. Doornenbal, K. Wimmer, A. Gargano, J. A. Tostevin, S. Chen, E. Nacher, E. Sahin, Y. Shiga, D. Steppenbeck, R. Taniuchi, Z. Y. Xu, T. Ando, H. Baba, F. L. Bello Garrote, S. Franchoo, K. Hadynska-Klek, A. Kusoglu, J. Liu, T. Lokotko, S. Momiyama, T. Motobayashi, S. Nagamine, N. Nakatsuka, M. Niikura, R. Orlandi, T. Saito, H. Sakurai, P. A. Soderstrom, G. M. Tveten, Zs. Vajta, M. Yalcinkaya, "Gamma decay of unbound neutron-hole states in ^{133}Sn," Phys. Rev. Lett. **118**, 202502 (2017).

P. Lasko *et al*., "KATANA – a charge-sensitive triggering system for the SπRIT experiment," Nucl. Instrum. Methods Phys. Res. A **856**, 92 (2017).

M. B. Tsang J. Estee, H. Setiawan, W. G. Lynch, J. Barney, M. B. Chen, G. Cerizza, P. Danielewicz, J. Hong, P. Morfouace, R. Shane, S. Tangwancharoen, K. Zhu, T. Isobe, M. Kurata-Nishimura, J. Lukasik, T. Murakami, Z. Chajecki, and SπRIT Collaboration, "Pion production in rare isotope collisions," Phys. Rev. C **95** 044614 (2017).

E. C. Pollacco *et al*., "GET: A generic electronics system for TPCs and nuclear physics instrumentation," Nucl. Instrum. Methods Phys. Res. A **887**, 81 (2018).

A. Tarifeno-Saldivia, J. L. Tain, C. Domingo-Pardo, F. Calvino, G. Cortes, V. H. Phong, A. Riego, J. Agramunt, A. Algora, N. Brewer, R. Caballero-Folch, P. J. Coleman-Smith, T. Davinson, I. Dillmann, A. Estrade, C. J. Griffin, R. Grzywacz, L. J. Harkness-Brennan, G. G. Kiss, M. Kogimtzis, M. Labiche, I. H. Lazarus, G. Lorusso, K. Matsui, K. Miernik, F. Montes, A. I. Morales, S. Nishimura, R. D. Page, Z. S. Podolyak, V. F. E. Pucknell, B. C. Rasco, P. Regan, B. Rubio, K. P. Rykaczewski, Y. Saito, H. Sakurai, J. Simpson, E. Sokol, R. Surman, A. Svirkhin, S. L. Thomas, A. Tolosa and P. Woods, "Conceptual design of a hybrid neutron-gamma detector for study of β-delayed neutrons at the RIB facility of RIKEN," J. Instrum. **12**, P04006, 10.1088/1748-0221/12/04/P04006 (2017).

[Proceedings]

(Original Papers) *Subject to Peer Review

H. Yamaguchi, D. Kahl, S. Hayakawa, Y. Sakaguchi, K. Abe, H. Shimuzu, Y. Wakabayashi, T. Hashimoto, S. Cherubini, M. Gulino, C. Spitaleri, G. G. Rapisarda, L. La Cognata, L. Lamia, S. Romano, S. Kubono, N. Iwasa, T. Teranishi, T. Kawabata, Y. K. Kwon, D. N. Binh, L. H. Khiem, N. N. Duy, S. Kato, T. Komatsubara, A. Coc, N. de Sereville, F. Hammache, G. Kiss, and S. Bishop (invited), "1) Experimental studies of light-ion nuclear reactions using low-energy RI beams," The Proceedings of the 14th International Symposium on Nuclei in the Cosmos, Niigata, June 19−24, 2016, JPS Conference Proc. **14**, 010503, 10.7566/JPSCP.14.010503 (2017).

T. Takeda, T. Kawabata, T. Furono, M. Ichikawa, N. Iwasa, Y. Kanada-En'yo, A. Koshikawa, S. Kubono, E. Miyawaki, T. Morimoto, M. Murata, T. Nanamura, S. Nishimura, Y. Shikata, Y. Takahashi, M. Tsumura, and K. Watanabe, "The first measurement of cross section for the ^{7}Be(n, α)^{4}He reaction at the cosmological energy," The Proceedings of the 14th International Symposium on Nuclei in the Cosmos, Niigata, June 19−24, 2016, JPS Conference Proc. **14**, 010103, 10.7566/JPSCP.14.010103 (2017).

H. Wang *et al*., "[1] Spallation reaction study for fission products in nuclear waste: Cross section measurements for ^{137}Cs, ^{90}Sr and ^{107}Pd on proton and deuteron," EPJ Web Conf. **146**, 09022 (2017).

H. Wang *et al*., "[2] Spallation reaction study for the long-lived fission products in nuclear waste: Cross section measurements for ^{137}Cs, ^{90}Sr and ^{107}Pd using inverse kinematics method," Energy Procedia **131**, 127 (2017).

L. A. Gurgi, P. H. Regan, P. -A. Söderström, H. Watanabe, P. M. Walker, Zs. Podolyák, S. Nishimura, T. A. Berry, P. Doornenbal, G. Lorusso, T. Isobe, H. Baba, Z. Y. Xu, H. Sakurai, T. Sumikama, W. N. Catford, A. M. Bruce, F. Browne, G. J. Lane, F. G. Kondev, A. Odahara, J. Wu, H. L. Liu, F. R. Xu, Z. Korkulu, P. Lee, J. J. Liu, V. H. Phong, A. Yagi, G. X. Zhang, T. Alharbi, R. J. Carroll, K. Y. Chae, Zs. Dombradi, A. Estrade, N. Fukuda, C. Griffin, E. Ideguchi, N. Inabe, H. Kanaoka, I. Kojouharov, T. Kubo, S. Kubono, N. Kurz, I. Kuti, S. Lalkovski, E. J. Lee, C. S. Lee, G. Lotay, C. B. Moon, I. Nishizuka, C. R. Nita, Z. Patel, O. J. Roberts, H. Schaffner, C. M. Shand, H. Suzuki, H. Takeda, S. Terashima, Zs. Vajta, S. Kanaya and J. J. Valiente-Dobòn, "Isomer-delayed gamma-ray spectroscopy of neutron-rich ^{166}Tb," EPJ Web Conf. **146**, 10009, 10.1051/epjconf/201714610009 (2017).

L. A. Gurgi, P. H. Regan, P. -A. Söderström, H. Watanabe, P. M. Walker, Zs. Podolyák, S. Nishimura, T. A. Berry, P. Doornenbal, G. Lorusso, T. Isobe, H. Baba, Z. Y. Xu, H. Sakurai, T. Sumikama, W. N. Catford, A. M. Bruce, F. Browne, G. J. Lane, F. G. Kondev, A. Odahara, J. Wu, H. L. Liu, F. R. Xu, Z. Korkulu, P. Lee, J. J. Liu, V. H. Phong, A. Yagi, G. X. Zhang, T. Alharbi, R. J. Carroll, K. Y. Chae, Zs. Dombradi, A. Estrade, N. Fukuda, C. Griffin, E. Ideguchi, N. Inabe, H. Kanaoka, I. Kojouharov, T. Kubo, S. Kubono, N. Kurz, I. Kuti, S. Lalkovski, E. J. Lee, C. S. Lee, G. Lotay, C. B. Moon, I. Nishizuka, C. R. Nita, Z. Patel, O. J. Roberts, H. Schaffner, C. M. Shand, H. Suzuki, H. Takeda, S. Terashima, Zs. Vajta, S. Kanaya and J. J. Valiente-Dobòn, "Isomer spectroscopy of neutron-rich ^{168}Tb$_{103}$," Rad. Phys. Chem. **140**, 493−496, 10.1016/j.radphyschem.2016.12.011 (2017).

J. L. Tain, S. Nishimura *et al*., "The BRIKEN project: Extensive measurements of β-delayed neutron emitters for the astrophysical r-process,"Acta Phys. Pol. B **49**, 417−428 (2018).

B. Moon, C. -B. Moon, R. Lozeva, P. -A. Söderström, S. Nishimura *et al*., "Gamow-Teller transitions between proton $h_{11/2}$ and neutron $h_{9/2}$ partner orbitals in ^{140}I," AIP Conf. Proc. **1947**, 030002 (2018).

S. Kawase, Y. Watanabe, H. Wang, H. Otsu, H. Sakurai, S. Takeuchi, Y. Togano, T. Nakamura, Y. Maeda, D. S. Ahn, M. Aikawa, S. Araki, S. Chen, N. Chiga, P. Doornenbal, N. Fukuda, T. Ichihara, T. Isobe, S. Kawakami, T. Kin, Y. Kondo, S. Koyama, T. Kubo, S. Kubono, M. Kurokawa, A. Makinaga, M. Matsushita, T. Matsuzaki, S. Michimasa, S. Momiyama, S. Nagamine, K. Nakano, M. Niikura, T. Ozaki, A. Saito, T. Saito, Y. Shiga, M. Shikata, Y. Shimizu, S. Shimoura, T. Sumikama, P. -A. Soderstrom, H. Suzuki, H. Takeda, R. Taniuchi, J. Tsubota, Y. Watanabe, K. Wimmer, T. Yamamoto, K. Yoshida, "Cross section measurement of residues produced in proton- and deuteron-induced spallation reactions on ^{93}Zr at 105 MeV/u using the inverse

kinematics method," Proc. Intern. Conf. Nuclear Data for Science and Technology (ND2016), Bruges, Belgium, September 11−16, 2016, Eds. A. Plompen *et al*, EPJ Web Conf. **146**, 03012 (2017).

T. Isobe *et al*. (SPiRIT Collaboration), "Constraint on nuclear symmetry energy through heavy RI collision experiment by using SπRIT device at RIBF-SAMURAI," JPS Conf. Proc. **14**, 010803 (2017).

[Others]

The Proceedings of the 14th International Symposium on Nuclei in the Cosmos NIC2016 (Niigata, 19-24 June, 2016), Eds. S. Kubono, T. Kajino, S. Nishimura, T. Isobe, S. Nagataki, T. Shima, and Y. Takeda, JPS Conf. Proc. **14**, (2017).

櫻井博儀, 「2 重に魔法数をもったニッケル-78」, パリティ, 2016 年 12 月号.

櫻井博儀, 「百年の計」, Isotope News（特別号 No. 1）, 2017 年 1 月号.

本林透、櫻井博儀, 「魔法数の帰趨をめぐって」, 原子核研究第 61 巻 2 号 1 (2017).

I. Dillmann, A. Tarifeno-Saldivia, "The beta-delayed neutrons at RIKEN project (BRIKEN): Conquering the most exotic beta-delayed neutron-emitters," Nucl. Phys. News **28**, 28−31 (2018).

西村俊二, 「世界最高水準の核分光研究プロジェクト「EURICA」440 種の希少原子核崩壊データ収集完了」, Isotope News **752**, 26−29, 2017 年 8 月号.

櫻井博儀, 「不安定核ビームを利用した核構造研究」, 原子核研究、2018 年 1 月.

T. Isobe *et al*., "Operation of GET system as main readout device for SπRIT experiment at 2016 spring campaign," RIKEN Accel. Prog. Rep. **50**, 167 (2017).

Oral Presentations

[International Conference etc.]

K. Asahi, "Spin precession − Listening to the whisper of a spin about fundamental physics," Physics Colloquium, Department of Physics, Kyungpook National University, Daegu, South Korea, September 21, 2017.

S. Kubono, T. Kawabata, S. Q. Hou, and J. J. He (invited), "1) Experimental challenge to the big-bang nucleosynthesis − Cosmological ^{7}Li problem in BBN," The 14th International Symposium on Origin of Matter and Evolution of Galaxies, Daejeon, Korea, June 2017.

S. Kubono (invited), "The ^{7}Li cosmological problem in big bang model," Beihang University International workshop, November 2017.

S. Kubono (invited), "High-temperature hydrogen burning in neutron stars and core-cpllpse supernovae," International symposium on unstable nuclei, September, 2017.

S. Kubono (invited), "Experimental approach to explosive H-burning in X-ray bursts and SNeII," Experimental nuclea astrophysics summer school, Santa Tecla, Italy, September 2017.

S. Kubono (invited), "U and Th problem in nuclear astrophysics," International JAEA workshop on Es Campaign, Tokai, Ibaraki, Nov. 2017.

S. Chen, "In-beam gamma-ray spectroscopy of ^{56}Ca," 6th SUNFLOWER Workshop, Oslo, Norway, Sep. 12th, 2017.

M. L. Cortés, "Shell evolution for $N = 40$ isotones towards ^{60}Ca: First spectroscopy of ^{62}Ti," 6th SUNFLOWER Workshop, The University of Oslo, Norway, Sep. 12, 2017.

M. L. Cortés, "Coulomb excitation of ^{102}Sn," 6th SUNFLOWER Workshop, The University of Oslo, Norway, Sep. 12, 2017.

M. L. Cortés, "Shell evolution for $N = 40$ isotones towards ^{60}Ca: First spectroscopy of ^{62}Ti," The International Symposium on Physics of Unstable Nuclei 2017 (ISPUN17), Halong City, Vietnam, Sep. 29, 2017.

M. L. Cortés, "Shell evolution at $N = 40$ on the pathway towards ^{60}Ca: Spectroscopy of ^{62}Ti," Perspectives of the physics of nuclear structure, The University of Tokyo, Nov. 2, 2017.

F. Browne (Invited), "The lifetimes of the first-excited 2^+ states in ^{104}Zr and ^{106}Zr: the first measurement using a fast-timing array at a fast-fragmentation facility," Institute of Physics Nuclear Physics General Meeting, University of Birmingham, UK, Apr. 5, 2017.

F. Browne, "Detailed spectroscopy of ^{54}Ca," 6th SUNFLOWER Workshop, The University of Oslo, Norway, Sep. 12, 2017.

F. Browne, "Coulomb excitation of ^{136}Sn," 6th SUNFLOWER Workshop, The University of Oslo, Norway, Sep. 12, 2017.

F. Browne, "In-beam γ-ray spectroscopy of ^{54}Ca," International Workshop on Physics Opportunities using CAGRA and RCNP tracking Ge detector (CAGRA17), Osaka Univ. , Oct. 10, 2017.

F. Browne (Invited), "Isomerism of ^{115}Mo (and $^{109-113}$Mo)," Collaboration workshop on RI and heavy-ion sciences, Ewha Womans University, Republic of Korea, Oct. 19, 2017.

F. Browne, "In-beam γ-ray spectroscopy of $^{54,\,56}$Ca: Probing the tensor and three body force," Perspectives of the physics of nuclear structure, The University of Tokyo, Nov. 2, 2017.

F. Browne, "NP1712-RIBF163: Coulomb excitation of ^{136}Sn at intermediate energies," The 18th Program Advisory Committee (PAC) Meeting for Nuclear-Physics Experiments at RI Beam Factory, RIKEN, Dec. 8, 2017.

F. Browne, "In-beam γ-ray spectroscopy of $^{54,\,56}$Ca," IVth Topical Workshop on Modern Aspects in Nuclear Structure, Bormio, Italy, Feb. 22, 2018.

S. Nishimura (Invited), "Origin of heavy elements in the universe: r-Process nucleosynthesis," Inaugural Synposium TCHoU, Tsukuba, March 26−27, 2018.

S. Nishimura (Invited), "Experimental challenges ar RIBF: nuclear properties and nucleosynthesis," International symposium on RI beam physics in the 21st century: 10th anniversary of RIBF, RIKEN, Dec. 4−5, 2017.

S. Nishimura (Invited), "Collective flow and equation of state in heavy-ion collisions," REIMEI Workshop, Tokai, Dec. 11−14, 2017.

S. Nishimura (Invited), "Highlights of decay spectroscopy experiments at RIBF," Ito International Research Center (IIRC) symposium "Perspectives of the physics of nuclear structure," The Univ. Tokyo, Nov. 1−4, 2017.

S. Nishimura (Invited), "RIB and explosive nucleosynthesis (Concluding Remarks)," The 9th European Summer School on Experimental Nuclear Astrophysics Santa Tecla, Italy, Sep. 17−24, 2017.

S. Nishimura (Invited), "Experimental challenges relevant to r-process nucleosynthesis," China-Japan collaboration Workshop on "Nuclear mass and life for unravelling myesteries of r-process," Tsukuba, June 26−28, 2017.

D. Suzuki, "GET electronics for missing mass spectroscopy at RIBF," Workshop on Active Targets and Time Projection Chambers for High-intensity and

Heavy-ion beams in Nuclear Physics, Santiago de Compostela, January 17−19, 2018.

H. Sakurai, "Recent highlights and future projects for the nuclear structure study at RIBF,"16th International Symposium on Capture Gamma-ray Spectroscopy and Related Topics, Shanghai, China, Sept. 2017.

H. Sakurai, "Decay spectroscopy at RIBF past and future," Collaboration workshop on RI and heavy-ion sciences, Seoul, Korea, Oct. 2017.

H. Sakurai, "RIBF -recent activities and highlights," STORI'17 10th International Conference on Nuclear Physics at Storage Rings, 2017.

T. Isobe, "Study of density dependent symmetry energy by using heavy ion collision at RIBF," Collaboration workshop on RI and heavy-ion sciences, Ewha Womens University, Seoul Korea, Oct. 2017.

T. Isobe, "Analysis of SπRIT experimental data: measurement of charged particles and neutrons in heavy RI collisions," NuSYM 2017, invited talk, GANIL CAEN France, Sep. 2017.

T. Isobe (Invited), "Performance of SπRIT-TPC with GET readout system for heavy ion collision experiment," Workshop on Active Targets and Time Projection Chambers for High-intensity and Heavy-ion beams in Nuclear Physics, Univ. of Santiago de Compostela, Jan. 2018.

R. Taniuchi, "Level structure of ^{78}Ni," 6th SUNFLOWER Workshop, Oslo, Norway, September 11, 2017.

G. Kiss (Invited), "Beta-delayed neutron emission probability measurements for r process studies at RIKEN RIBF," Nuclear Physics in Astrophysics VIII International conference, Catania, Italy, June 18−23, 2017.

G. Kiss (Invited), "β-decay studies for r-process nucleosynthesis," Workshop on Nuclear Astrophysics at the Dresden Felsenkeller, Dresden, Germany, June 26−28, 2017.

[Domestic Conference]

S. Kubono (invited), 「X-線バースト、超新星初期の爆発的水素燃焼過程の実験的アプローチ」, UKAKUREN workshop, RIKEN, July 2017

H. Wang, "Systematic study for the spallation reaction of ^{107}Pd at different energies," ImPACT-OEDO workshop, Center for Nuclear Study, University of Tokyo, Wako-shi, Saitama, Japan, July 13−14, 2017.

M. L. Cortés, "Development of a new scintillation detector based spectrometer at the RIBF," Physics Opportunities using CAGRA and RCNP tracking Ge detector (CAGRA17), Osaka Univ. , Oct. , 12, 2017.

S. Nishimura (Invited), "Low-energy (α, n) reactions in mass $A \sim 100$ and r-process," ImPACT-OEDO workshop 2017, CNS, Univ. Tokyo, July 13−14, 2017.

西村俊二, 「非等方的集団運動から探る高密度物質の状態方程式の研究」, 平成 28 年度 HIMAC 共同利用研究成果発表会, 千葉市, 4 月 17−18 日.

D. Suzuki, "One neutron transfer (d, p) reactions," ImPACT-OEDO workshop 2017, RIKEN Wako Campus, July 13 and 14, 2017.

櫻井博儀, 「不安定核ビームを利用した核構造研究」, 原子核三者若手夏の学校, 国立オリンピック記念青少年総合センター, 2017 年 8 月.

X. Sun, "Reaction study of ^{136}Xe on proton, deuteron and carbon at 168 AMeV," Impact-OEDO Workshop, Center for Nuclear Study, University of Tokyo, Wako-shi, Saitama, Japan, July 13−14, 2017.

磯部忠昭, 「RIBF-SπRIT 実験システムの開発」, 計測システム研究会, 函館アリーナ, 2017 年 10 月.

磯部忠昭, 「仮想計算機環境技術 docker を用いた、大規模汎用クラスタにおける物理解析環境の開発」, 日本物理学会年次大会, 東京理科大学, 2018 年 3 月.

Posters Presentations

[International Conference etc.]

Y. Nakai, N. Watanabe, Y. Oba, "Hydrogenation of C_{60} deposited on a substrate under low temperature condition," The 30th International Conference on Photonic, Electronic and Atomic Collisions, Cairns Australia, August 2017.

[Domestic Conference]

X. Sun, "Reaction study of ^{136}Xe on proton, deuteron and carbon at 168 AMeV," 2017 Symposium on Nuclear Data, Nuclear Data Division, Atomic Energy Society of Japan, Advanced Science Research Center, Japan Atomic Energy Agency, November 16−17, 2017.

RIBF Research Division
Spin isospin Laboratory

1. Abstract

The Spin Isospin Laboratory pursues research activities putting primary focus on interplay of spin and isospin in exotic nuclei. Understanding nucleosyntheses in the universe, especially those in r- and rp-processes is another big goal of our laboratory.

Investigations on isospin dependences of nuclear equation of state, spin-isospin responses of exotic nuclei, occurrence of various correlations at low-densities, evolution of spin-orbit coupling are main subjects along the line. We are leading a mass measurement project with the Rare RI Ring project, too. Through the experimental studies, we will be able to elucidate a variety of nuclear phenomena in terms of interplay of spin and isospin, which will in turn, lead us to better understanding of our universe.

2. Major Research Subjects

(1) Direct reaction studies of neutron-matter equation of state
(2) Study of spin-isospin responses with RI-beams
(3) R-process nucleosynthesis study with heavy-ion storage ring
(4) Application of spin-polarization technique to RI-beam experiments and other fields
(5) Development of special targets for RI-beam experiments

3. Summary of Research Activity

(1) Direct reaction studies of neutron matter equation of state

Direct reactions induced by light-ions serve as powerful tools to investigate various aspects of nuclei. We are advancing experimental programs to explore equation of state of neutron matter, via light-ion induced reactions with RI-beams.

(1-a) Determination of a neutron skin thickness by proton elastic scattering

A neutron skin thickness is known to have strong relevance to asymmetry terms of nuclear equation of state, especially to a term proportional to density. The ESPRI project aims at determining density distributions in exotic nuclei precisely by proton elastic scattering at $200-300$ MeV/nucleon. An experiment for ^{132}Sn that is a flagship in this project has been successfully performed.

(1-b) Asymmetry terms in nuclear incompressibility

Nuclear incompressibility represents stiffness of nuclear matter. Incompressibility of symmetric nuclear matter is determined to be 230 ± 20 MeV, but its isospin dependence still has a large uncertainty at present. A direct approach to the incompressibility of asymmetric nuclear matter is an experimental determination of energies of isoscalar giant monopole resonances (GMR) in heavy nuclei. We have developed, in close collaboration with Center for Nuclear Study (CNS) of University of Tokyo, an active gas target for deuteron inelastic scattering experiments to determine GMR energies. The active gas target has been already tested with oxygen and xenon beams at HIMAC and finally has been applied to a ^{132}Sn experiment at RIBF.

(1-c) Multi-neutron and α-cluster correlations at low densities

Occurrences of multi-neutron and α-cluster correlations are other interesting aspects of nuclear matter and define its low-density behavior. The multi-neutron and α-cluster correlations can be investigated with the large-acceptance SAMURAI spectrometer. The SAMURAI has been already applied to experiments to explore light neutron-rich nuclei close to the dripline. We plan to reinforce experimental capabilities of the SAMURAI by introducing advanced devices such as MINOS (Saclay) and NeuLAND (GSI).

(1-d) Fission barrier heights in neutron-rich heavy nuclei

The symmetry energy has a strong influence on fission barrier heights in neutron-rich nuclei. Knowledge on the fission barrier heights, which is quite poor at present, is quite important for our proper understanding on termination of the r-process. We are planning to perform, in collaboration with the TU Munich group, $(p, 2p)$-delayed fission experiments at the SAMURAI to determine the fission barrier heights in neutron-rich nuclei in Pb region.

(2) Study of spin-isospin responses with RI-beams

The study of spin-isospin responses in nuclei forms one of the important cores of nuclear physics. A variety of collective states, for example isovector giant dipole resonances, isobaric analogue states, Gamow-Teller resonances, have been extensively studied by use of electromagnetic and hadronic reactions from stable targets.

The research opportunities can be largely enhanced with light of availabilities of radioactive isotope (RI) beams and of physics of unstable nuclei. There are three possible directions to proceed. The first direction is studies of spin-isospin responses of unstable nuclei via inverse-kinematics charge exchange reactions. A neutron-detector array WINDS has been constructed, under a collaboration of CNS, Tokyo and RIKEN, for inverse kinematics (p, n) experiments at the RI Beam Factory. We have already applied WINDS to the (p, n) experiments for ^{12}Be, ^{132}Sn and plan to extend this kind of study to other exotic nuclei.

The second direction is studies with RI-beam induced charge exchange reaction. RI-beam induced reactions have unique properties which are missing in stable-beam induced reactions and can be used to reach the yet-to-be-discovered states. We have constructed the SHARAQ spectrometer and the high-resolution beam-line at the RI Beam Factory to pursue the capabilities of RI-beam induced reactions as new probes to nuclei. One of the highlights is an observation of β^+ type isovector spin monopole resonances (IVSMR) in ^{208}Pb and ^{90}Zr via

the (t, ^{3}He) reaction at 300 MeV/nucleon.

The third direction is studies of neutron- and proton-rich nuclei via stable-beam induced charge exchange reactions, which is conducted under collaboration with Research Center for Nuclear Physics (RCNP), Osaka University. We have performed the double charge exchange ^{12}C(^{18}O, ^{18}Ne)^{12}Be reaction at 80 MeV/nucleon to investigate structure of a neutron-rich ^{12}Be nucleus. Peaks corresponding to ground and excited levels in ^{12}Be have been clearly observed. Another double charge exchange reaction, (^{12}C, ^{12}Be(0_2^+)) are being used to search for double Gamow-Teller resonances.

(3) R-process nucleosynthesis study with heavy-ion storage ring

Most of the r-process nuclei become within reach of experimental studies for the first time at RI Beam Factory at RIKEN. The Rare RI Ring at RIBF is the unique facility with which we can perform mass measurements of r-process nuclei. Construction of the Rare RI Ring started in FY2012 in collaboration with Tsukuba and Saitama Universities. A major part of the ring has been completed and the commissioning run is planned in FY2014.

We are planning to start precise mass measurements of r-process nuclei soon. A series of experiments will start with nuclei in the A=80 region and will be extended to heavier region.

(4) Application of spin-polarization technique to RI-beam experiments and other fields

A technique to produce nuclear polarization by means of electron polarization in photo-excited triplet states of aromatic molecules can open new applications. The technique is called "Tripletd-DNP". A distinguished feature of Triplet-DNP is that it works under a low magnetic field of 0.1−0.7 T and temperature higher than 100 K, which exhibits a striking contrast to standard dynamic nuclear polarization (DNP) techniques working in extreme conditions of several Tesla and sub-Kelvin.

We have constructed a polarized proton target system for use in RI-beam experiments. Recent experimental and theoretical studies have revealed that spin degrees of freedom play a vital role in exotic nuclei. Tensor force effects on the evolution of shell and possible occurrence of p-n pairing in the proton-rich region are good examples of manifestations of spin degrees of freedom. Experiments with the target system allow us to explore the spin effects in exotic nuclei. It should be noted that we have recently achieved a proton polarization of 40% at room temperature in a pentacene-d$_{14}$ doped p-terphenyl crystal.

Another interesting application of Triplet-DNP is sensitivity enhancement in NMR spectroscopy of biomolecules. We started a new project to apply the Triplet-DNP technique to study protein-protein interaction via two-dimensional NMR spectroscopy, in close collaboration with biologists and chemists.

(5) Development of special targets for RI-beam experiments

For the research activities shown above, we are developing and hosting special targets for RI-beam experiments listed below:

a) Polarized proton target (described in (4))
b) Thin solid hydrogen target
c) MINOS (developed at Saclay and hosted by the Spin Isospin Laboratory)

Members

Chief Scientist (Lab. Head)
Tomohiro UESAKA

Research & Technical Scientists
Masaki SASANO (Research Scientist)   Sarah NAIMI (Research Scientist)
Juzo ZENIHIRO (Research Scientist)

Contract Researcher
Daisuke NAGAE

Special Postdoctoral Researchers
Kenichiro TATEISHI   Yuki KUBOTA

Foreign Postdoctoral Researchers
Zaihong YANG

Postdoctoral Researchers
Valerii PANIN   Takahiro NISHI
Fumi SUZAKI

Research Associate
Masami SAKO   Tsz Leung TANG
Kenichiro TATEISHI

Junior Research Associates
Shunichiro OMIKA (Saitama Univ.)   Shusuke TAKADA (Kyushu Univ.)

International Program Associates
Sergey CHEBOTARYOV (Kyungpook Nat'l Univ.)   Alexandra-Ionela CHILUG
Jian GAO (Peking Univ.)   Zhuang GE (Institute of Modern Physics Chinese Academy of
                                                     Sciences,)

Research Consultant
Harutaka SAKAGUCHI   Kazuko TANABE

Senior Visiting Scientists
Hiroyuki SAGAWA (Aizu Univ.)

Visiting Scientists
Didier BEAUMEL (IPN)   Takashi WAKUI (Tohoku Univ.)
Yasuyuki SUZUKI (Niigata Univ.)   Kimiko SEKIGUCHI (Tohoku Univ.)
Yosuke KONDO (Tokyo Tech.)   Dorottya KUNNE SOHLER (Institute of Nuclear Research
Zoltan ELEKES (ATOMKI)   Hungarian Academy of Sciences (ATOMKI))
Hidetoshi AKIMUNE (Konan Univ.)   Satoru TERASHIMA (Beihang University)
Yohei MATSUDA (Osaka Univ.)   Valdir GUIMARAES (Instituto de Fisica da Universidade de Sao
Yasuhiro TOGANO (Tokyo Tech.)   Paulo)
Satoshi SAKAGUCHI (Kyusyu Univ.)   Yasutaka TANIGUCHI (Nihon Institute of Medical Science)
Kenjiro MIKI (TU Darmstadt)   Tetsuaki MORIGUCHI (Univ. of Tsukuba)
Valerie LAPOUX (CEA Saclay)   Kazuyuki OGATA (Osaka Univ.)
Alexandre OBERTELLI (CEA Saclay)   Shinji SUZUKI (Univ. of Tsukuba)
Alain GILLIBERT (CEA Saclay)   Zsolt VAJTA (Institute of Nuclear Research Hungarian Academy
Emanuel POLLACCO (CEA Saclay)   of Sciences (ATOMKI))
Anna CORSI (CEA Saclay)   Istvan KUTI (Institute of Nuclear Research Hungarian Academy of
Dennis MUECHER (TUM)   Sciences (ATOMKI))
Yuma KIKUCHI (Osaka City Univ.)   Makoto NEGORO (Osaka Univ.)
Yury LITVINOV (GSI)   Konstanze BORETZKY (GSI)
Yuhu ZHANG (CAS)   Zsolt FULOP (Institute of Nuclear Research Hungarian Academy
Igor GASPARIC (Ruder Boskovic Inst. Zagreb Croatia) of Sciences (ATOMKI))
Hans Toshihide TOERNQVIST (TU Darmstadt)   Zsolt DOMBRADI (Institute of Nuclear Research Hungarian
Christoph CAESAR (GSI)   Academy of Sciences (ATOMKI))
Haik SIMON (GSI)   Akinori KAGAWA (Osaka Univ.)
Matthias HOLL (TU Darmstadt)   Baohua SUN (Beihang Univ.)
Takayuki YAMAGUCHI (Saitama Univ.)   Leyla ATAR (TU Darmstadt)
Takashi NAKAMURA (Tokyo Tech.)   Zoltan HALASZ (ATOMKI)
Atsushi TAMII (Osaka Univ.)   Li-Gang CAO (North China Electric Power Univ.)
Attila KRASZNAHORKAY (ATOMKI)   Kaori KAKI (Shizuoka Univ.)

Visiting Technicians
Tomomi KAWAHARA (Toho Univ.)   Alain DELBART (CEA Saclay)
Gilles AUTHELET (CEA Saclay)   Frederic CHATEAU (CEA Saclay)
Jean-Marc GHELLER (CEA Saclay)   Caroline LAHONDE-HAMDOUN (CEA Saclay)
Cedric PERON (CEA Saclay)   Arnaud GIGANON (CEA Saclay)
Jean-Yves ROUSSE (CEA Saclay)   Daniel KOERPER (GSI)
Denis CALVET (CEA Saclay)   Clement HILAIRE (CEA Saclay)
Alan PEYAUD (CEA Saclay)

Student Trainees
Yasunori WADA (Tohoku Univ.)   Motoki MURATA (Kyoto Univ.)
Tatsuya FURUNO (Kyoto Univ.)   Syunsuke KAWAKAMI (Miyazaki Univ.)
Miho TSUMURA (Kyoto Univ.)   Daijiro ETO (Tohoku Univ.)
Jumpei YASUDA (Kyushu Univ.)   Junki TANAKA (Osaka Univ.)
Mizuki SHIKATA (Tokyo Tech.)   Sebastian Benedikt REICHERT (TU Munchen)
Junichi TSUBOTA (Tokyo Tech.)   Tomoyuki OZAKI (Tokyo Tech.)
Yuuki TAKEUCHI (Saitama Univ.)   Atsumi SAITO (Tokyo Tech.)
Syunichirou OHMIKA (Saitama Univ.)   Yusuke SHINDO (Kyushu Univ.)
Hiroshi MIURA (Saitama Univ.)   Munemi TABATA (Kyushu Univ.)
Takuma NISHIMURA (Saitama Univ.)   Atomu WATANABE (Tohoku Univ.)

Ayaka OHKURA (Kyushu Univ.)
Yukina ICHIKAWA (Univ. of Tsukuba)
Kotaro YAMADA (Toho Univ.)
Tomoaki KANEKO (Toho Univ.)
Julian KAHLBOW (TU Darmstadt)
Taras LOKOTKO (Univ. of Hong Kong)
Dahee KIM (Ewha Womans Univ.)
Natsuki TADANO (Saitama Univ.)
Ikuma KATO (Saitama Univ.)
Tomomi AKIEDA (Tohoku Univ.)
Hiroshi KON (Tohoku Univ.)
Tomoyuki MUKAI (Tohoku Univ.)
Shinnosuke NAKAI (Tohoku Univ.)
Takato TOMAI (Tokyo Tech.)
Akihiro HIRAYAMA (Tokyo Tech.)
Yoshiyuki TAJIRI (Univ. of Tsukuba)
Kentaro HIRAISHI (Univ. of Tsukuba)
Simon LINDBERG (Chalmers University of Technology)
Masamichi AMANO (Univ. of Tsukuba)
Daisuke SAKAE (Kyushu Univ.)
Yasuaki NORIMATSU (Kyushu Univ.)
Takahiro FUKUTA (Kyushu Univ.)
Youhei AKIYAMA (Kyushu Univ.)
Kiyoshi WAKAYAMA (Saitama Univ.)

Han Hagen MAYER (University of Cologne)
Takahiro MORIMOTO (Kyoto Univ.)
Katsuyoshi HEGURI (Konan Univ.)
Takuya MATSUMOTO (Univ. of Tsukuba)
Tomoya HARADA (Toho Univ.)
Kosei TANIUE (Univ. of Miyazaki)
Masahiro YASUDA (Tokyo Tech.)
Hiroki YAMADA (Tokyo Tech)
Jun OKAMOTO (Tohoku Univ.)
Yu NASU (Tohoku Univ.)
Shota MATSUMOTO (Kyoto Univ.)
Simon GIRAUD (Université de Nantes)
Yu ANDO (Kyungpook National Univ.)
Sonja STORCK (TU Darmstadt)
Ina Josephine SYNDIKUS (TU Darmstadt)
Mayuko MATSUMOTO (Tokyo Tech.)
Daiki KAMIOKA (Univ. of Tsukuba)
Christopher LEHR (TU Darmstadt)
Tomoya FUJII (Saitama Univ.)
Kunimitsu NISHIMURO (Saitama Univ.)
Ryo IGOSAWA (Saitama Univ.)
Kumi INOMATA (Saitama Univ.)
Hiroki ARAKAWA (Saitama Univ.)
Jan Daniel STEINHAUSER (Tokyo Tech.)

Interns
Howard Bradley Kevin

Part-time Worker
Kotaro YAMADA

Assistants
Emiko ISOGAI   Noriko KIYAMA
Yuri TSUBURAI

List of Publications & Presentations

Publications

[Journal]

(Original Papers) *Subject to Peer Review

L. Stuhl, M. Sasano, K. Yako, J. Yasuda, H. Baba, S. Ota, T. Uesaka, "PANDORA, a large volume low-energy neutron detector with real-time neutron–gamma discrimination," Nucl. Instrum. Methods Phys. Res. A **866**, 164−171 (2017).

J.C. Zamora, T. Aumann, S. Bagchi, S. Bönig, M. Csatlós, I. Dillmann, C. Dimopoulou, P. Egelhof, V. Eremin, T. Furuno, H. Geissel, R. Gernhäuser, M.N. Harakeh, A.L. Hartig, S. Ilieva, N. Kalantar-Nayestanaki, O. Kiselev, H. Kollmus, C. Kozhuharov, A. Krasznahorkay, Th. Kröll, M. Kuilman, S. Litvinov, Yu. A. Litvinov, M. Mahjour-Shafiei, M. Mutterer, D. Nagae, M.A. Najafi, C. Nociforo, F. Nolden, U. Popp, C. Rigollet, S. Roy, C. Scheidenberger, M. von Schmid, M. Steck, B. Streicher, L. Stuhl, M. Thürauf, T. Uesaka, H. Weick, J.S. Winfield, D. Winters, P.J. Woods, T. Yamaguchi, K. Yue, J. Zenihiro, "Nuclear-matter radius studies from ^{58}Ni(α, α) experiments at the GSI Experimental Storage Ring with the EXL facility," Phys. Rev. C **96**, 03461 (2017).

K. Sekiguchi, H. Witała, T. Akieda, D. Eto, H. Kon, Y. Wada, A. Watanabe, S. Chebotaryov, M. Dozono, J. Golak, H. Kamada, S. Kawakami, Y. Kubota, Y. Maeda, K. Miki, E. Milman, A. Ohkura, H. Sakai, S. Sakaguchi, N. Sakamoto, M. Sasano, Y. Shindo, R. Skibiński, H. Suzuki, M. Tabata, T. Uesaka, T. Wakasa, K. Yako, T. Yamamoto, Y. Yanagisawa, J. Yasuda, "Complete set of deuteron analyzing powers from $\vec{d}p$ elastic scattering at 190 MeV/nucleon," Phys. Rev. C **96**, 064001 (2017).

S. Adachi, T. Kawabata, K. Minomo, T. Kadoya, N. Yokota, H. Akimune, T. Baba, H. Fujimura, M. Fujiwara, Y. Funaki, T. Furuno, T. Hashimoto, K. Hatanaka, K. Inaba, Y. Ishii, M. Itoh, C. Iwamoto, K. Kawase, Y. Maeda, H. Matsubara, Y. Matsuda, H. Matsuno, T. Morimoto, H. Morita, M. Murata, T. Nanamura, I. Ou, S. Sakaguchi, Y. Sasamoto, R. Sawada, Y. Shimizu, K. Suda, A. Tamii, Y. Tameshige, M. Tsumura, M. Uchida, T. Uesaka, H.P. Yoshida, S. Yoshida, "Systematic analysis of inelastic α scattering off self-conjugate $A = 4n$ nuclei," Phys. Rev. C **97**, 014601 (2018).

S. Kawase *et al.*, "Exclusive quasi-free proton knockout from oxygen isotopes at intermediate energies," Prog. Theor. Exp. Phys. **2018**, 021D01 (2018).

S. Chebotaryov, S. Sakaguchi, T. Uesaka, T. Akieda, Y. Ando, M. Assie, D. Beaumel, N. Chiga, M. Dozono, A. Galindo-Uribarri, B. Heffron, A. Hirayama, T. Isobe, K. Kaki, S. Kawase, W. Kim, T. Kobayashi, H. Kon, Y. Kondo, Y. Kubota, S. Leblond1, H. Lee1, T. Lokotko, Y. Maeda, Y. Matsuda, K. Miki, E. Milman, T. Motobayashi, T. Mukai, S. Nakai, T. Nakamura, A. Ni, T. Noro, S. Ota, H. Otsu, T. Ozaki, V. Panin, S. Park, A. Saito, H. Sakai, M. Sasano, H. Sato, K. Sekiguchi, Y. Shimizu, I. Stefan, L. Stuhl, M. Takaki, K. Taniue, K. Tateishi, S. Terashima, Y. Togano, T. Tomai, Y. Wada, T. Wakasa, T. Wakui, A. Watanab4, H. Yamada, Zh. Yang, M. Yasuda, J. Yasuda, K. Yoneda, and J. Zenihiro, "Proton elastic scattering at 200 A MeV and high

momentum transfers of 1.7−2.7 fm^{-1} as a probe of the nuclear matter density of ^{6}He," Prog. Theor. Exp. Phys. **2018**, 053D01 (2018).

L. Atar, S. Paschalis, C. Barbieri, C. A. Bertulani, P. Daz Fernndez, M. Holl, M. A. Najafi, V. Panin, H. Alvarez-Pol, T. Aumann, V. Avdeichikov, S. Beceiro-Novo, D. Bemmerer, J. Benlliure, J. M. Boillos, K. Boretzky, M. J. G. Borge, M. Caamao, C. Caesar, E. Casarejos, W. Catford, J. Cederkall, M. Chartier, L. Chulkov, D. Cortina-Gil, E. Cravo, R. Crespo, I. Dillmann, Z. Elekes, J. Enders, O. Ershova, A. Estrade, F. Farinon, L. M. Fraile, M. Freer, D. Galaviz Redondo, H. Geissel, R. Gernhuser, P. Golubev, K. Gbel, J. Hagdahl, T. Heftrich, M. Heil, M. Heine, A. Heinz, A. Henriques, A. Hufnagel, A. Ignatov, H. T. Johansson, B. Jonson, J. Kahlbow, N. Kalantar-Nayestanaki, R. Kanungo, A. Kelic-Heil, A. Knyazev, T. Krll, N. Kurz, M. Labiche, C. Langer, T. Le Bleis, R. Lemmon, S. Lindberg, J. Machado, J. Marganiec-Gazka, A. Movsesyan, E. Nacher, E. Y. Nikolskii, T. Nilsson, C. Nociforo, A. Perea, M. Petri, S. Pietri, R. Plag, R. Reifarth, G. Ribeiro, C. Rigollet, D. M. Rossi, M. Rder, D. Savran, H. Scheit, H. Simon, O. Sorlin, I. Syndikus, J. T. Taylor, O. Tengblad, R. Thies, Y. Togano, M. Vandebrouck, P. Velho, V. Volkov, A. Wagner, F. Wamers, H. Weick, C. Wheldon, G. L. Wilson, J. S. Winfield, P. Woods, D. Yakorev, M. Zhukov, A. Zilges, and K. Zuber, "Quasifree (p, 2p) reactions on oxygen isotopes: observation of isospin independence of the reduced single-particle strength," Phys. Rev. Lett. **120**, 052501 (2018).

G. Audi, F.G. Kondev, M. Wang, W.J. Huang, S. Naimi, "The NUBASE2016 evaluation of nuclear properties," Chin. Phys. C **41**, 030001 (2017).

J. Kahlbow, C. Caesar, T. Aumanna, V. Panin, S. Paschalis, H. Scheit, H. Simon, "Neutron radioactivity—Lifetime measurements of neutron-unbound states," Nucl. Instrum. Methods Phys. Res. A **866**, 265−271 (2017).

W.J. Huang, G. Audi, F.G. Kondev, M. Wang, S. Naimi, X. Xu, "The AME2016 atomic mass evaluation (I). Evaluation of input data; and adjustment procedures," Chin. Phys. C **41**, 030002 (2017).

M. Wang, G. Audi, F.G. Kondev, W.J. Huang, S. Naimi, X. Xu, "The AME2016 atomic mass evaluation (II). Tables, graphs and references," Chin. Phys. C **41**, 030003 (2017).

Y. Urata, K. Hagino and H. Sagawa, "Role of deformation in odd-even staggering in reaction cross sections for ^{30,31,32}Ne and ^{36,37,38}Mg isotopes," Phys. Rev. C **96**, 064311 (2017).

I. Hamamoto and H. Sagawa, Interplay between isoscalar and isovector correlations in neutron-rich nuclei, Phys. Rev. C **96**, 064312 (2017).

Eunja Ha, Myung-Ki Cheoun and H. Sagawa, "Spin singlet and spin triplet pairing correlations on shape evolution in sd-shell $N = Z$ nuclei," Phys. Rev. C **97**, 024320 (2018).

Y. Ayyad, J. Lee, A. Tamii, J.A. Lay, A.O. Macchiavelli, N. Aoi, B.A. Brown, H. Fujita, Y. Fujita, E. Ganioglu, K. Hatanaka, T. Hashimoto, T. Ito, T. Kawabata, Z. Li, H. Liu, H. Matsubara, K. Miki, H.J. Ong, G. Potel, I. Sugai, G. Susoy, A. Vitturi, H.D. Watanabe, N. Yokota, J. Zenihiro, "Investigating neutron-proton pairing in sd-shell nuclei via (p, ^{3}He) and (^{3}He, p) transfer reactions," Phys. Rev. C **96**, 021303 (2017).

N. Nakatsuka, H. Baba, T. Aumann, R. Avigo, S.R. Banerjee, A. Bracco, C. Caesar, F. Camera, S. Ceruti, S. Chen, V. Derya, P. Doornenbal, A. Giaz, A. Horvat, K. Ieki, T. Inakura, N. Imai, T. Kawabata, N. Kobayashi, Y. Kondo, S. Koyama, M. Kurata-Nishimura, S. Masuoka, M. Matsushita, S. Michimasa, B. Million, T. Motobayashi, T. Murakami, T. Nakamura, T. Ohnishi, H.J. Ong, S. Ota, H. Otsu, T. Ozaki, A. Saito, H. Sakurai, H. Scheit, F. Schindler, P. Schrock, Y. Shiga, M. Shikata, S. Shimoura, D. Steppenbeck, T. Sumikama, I. Syndikus, H. Takeda, S. Takeuchi, A. Tamii, R. Taniuchi, Y. Togano, J. Tscheuschner, J. Tsubota, H. Wang, O. Wieland, K. Wimmer, Y. Yamaguchi, K. Yoneda, J. Zenihiro, "Observation of isoscalar and isovector dipole excitations in neutron-rich ^{20}O," Phys. Lett. B **768**, 387−392 (2017).

H. Sakaguchi and J. Zenihiro, " Proton elastic scattering from stable and unstable nuclei — Extraction of nuclear densities," Prog. Part. Nucl. Phys. **97**, 1−52 (2017).

[Proceedings]
(Original Papers) *Subject to Peer Review

T. Uesaka, "Studies of neutron-rich nuclei at RIBF — From tetraneutron to fission," Proceedings of the Sixth International Conference on ICFN6, Fission and Properties of Neutron-Rich Nuclei: pp. 47−47 (2017).

H. Sagawa and K. Hagino, "Thee-body model for nuclei near and beyond drip line," Acta Phys. Pol. B **10**, 211−224 (2017).

Y. Niu, G. Colo, E. Vigezzi, C. L. Bai and H. Sagawa, "Beyond mean-field description of Gamow-Teller resonances and beta-decay," J. Phys. Conf. Ser. **966**, 012046 (2018).

T. Furuno, T. Kawabata, M. Murata, S. Adachi, Y. Ayyad, H. Baba, T. Baba, M. Cavallaro, T. Hashimoto, Y. Ishii, R. Kobayakawa, Y. Matsuda, Y. Matsuoka, T. Morimoto, T. Nanamura, S. Beceilo-Novo, H.J. Ong, A. Sakaue, J. Tanaka, I. Tanihata, D.T. Trong, M. Tsumura, H.D. Watanabe. "Active target MAIKo to investigate cluster structures in unstable nuclei," 11th International Conference on Clustering Aspects of Nuclear Structure and Dynamics, J. Phys. Conf. Ser. **863**, 012076 (2017).

M. Tsumura, T. Kawabata, T. Furuno, A. Koshikawa, M. Murata, T. Morimoto, S. Adachi, A. Tamii, K. Hatanaka, T. Ito, J. Zenihiro, S. Kubono, M. Itoh, Y. Matsuda, Y. Maeda, S. Sakaguchi, H. Akimune, H. Fujimura, I. Ou, T. Hashimoto, C. Iwamoto, "Search for the rare γ-decay mode in ^{12}C," 11th International Conference on Clustering Aspects of Nuclear Structure and Dynamics, J. Phys. Conf. Ser. **863**, 012075 (2017).

Oral Presentations
[International Conference etc.]

V. Panin, "Dissociation of proton-rich nuclei at SAMURAI as a method to study the most critical (p, γ) reaction rates in stellar nucleosynthesi," KPS 2017 meeting, Daejeon, South Korea, April 20, 2017.

S. Naimi, "Rare-RI Ring (R3) at RIBF/RIKEN: Mass measurement of r-process nuclei," Workshop on Nuclear Astrophysics at Rings and Recoil Separators, GSI Darmstadt, Germany, March 13–15, 2018.

S. Naimi," The Rare-RI Ring Ready to Explore Terra Incognita," International Conference on Advances in Radioactive Isotope Science, ARIS 2017, Colorado, USA, May 28–June 2, 2017.

H. Sagawa, "Spin and spin-isospin responses and isoscalar spin-triplet pairing," Int. Symp. on Physics of Unstable Nuclei (ISPUN) 2017, Ha Long Bay, Vietnam, September 25–30, 2017.

H. Sagawa, "Three-body model for nuclei near and beyond drip line," Ischia Nuclear Structure workshop, Ischia, Italy, May 15–19, 2017.

H. Sagawa, "Three-body model for nuclei near and beyond drip line," 25th KAU mini-workshop, Korea Aerospace University, Seoul, April 17, 2017.

H. Sagawa, "Three-body model for nuclei near and beyond drip line," Complex decays and the splicing of reactions and structure, Kyungpook Nat. University, Daegu, Korea, April 14, 2017.

D. Nagae, "Mass measurements of exotic nuclei using Rare-RI Ring," The 10th International Conference on Nuclear Physics at Storage Rings (STORI'17), Kanazawa, Japan, Nov. 13–18, 2017.

D. Nagae, "First mass measurement using Rare-RI Ring," The 3ed International Conference on Advances in Radioactive Isotope Science (ARIS2017), Keystone, USA, May 28–Jun. 2, 2017.

Y. Kubota, "Probing neutron-neutron correlation in 11Li via the quasi-free (p, pn) reaction," Hadrons and Nuclear Physics meet ultracold atoms: a French Japanese workshop, Paris, France, January 29–February 2, 2018.

Y. Kubota, "Probing neutron-neutron correlation in ^{11}Li through the quasi-free (p, pn) reaction," The 244th RIKEN RIBF Nuclear Physics Seminar, Saitama, Japan, December 19, 2017.

Y. Kubota, "Neutron-neutron correlation in Borromean nucleus ^{11}Li," SAMURAI International Collaboration Workshop 2017, Darmstadt, Germany, August 8–11, 2017.

Y. Kubota, "Dineutron correlation in Borromean nuclei," 3rd International Workshop on Quasi-Free Scattering with Radioactive-Ion Beams: QFS-RB 17, York, United Kingdom, July 24–27, 2017.

Z. H. Yang, "Studies of multi-neutron systems with (p, $2p$) reactio," SAMURAI International Collaboration Workshop 2017, Darmstadt, Germany, August 2017.

[Domestic Conference]

H. Sagawa, "Spin and spin-isospin responses in $N = Z$ nuclei and isoscalar spin-triplet pairing," Interdisciplinary symposium on modern density functional theory, RIKEN, June 19–23, 2017.

H. Sagawa, "The nuclear symmetry energy and the breaking of isospin symmetry," Workshop on "Nuclear matter in neutron stars," RIKEN, December 1–3, 2017.

H. Sagawa, "Microscopic models for spin, isospin and spin-isospin responses," Yukawa Institute of Theoretical Physics (YITP) school "Recent Progress of Nuclear Structure and Reaction Physics", Kyoto, December 18–22, 2017.

Z . H. Yang, "Neutrons in extremely many-neutron systems," Workshop on Nuclear Cluster Physics 2017, Sapporo, Japan, 2017.

松田洋平,「炭素 14 偏極陽子弾性散乱測定の現状」, 日本物理学会第 73 回年次大会, 2018 年 3 月 22–25 日.

松田洋平,「偏極陽子弾性散乱実験のための炭素 14 標的の開発」, 日本物理学会 2017 年秋季大会, 2017 年 9 月 12–15 日.

原田知也,「大強度イオンビーム用の Xe ガスシンチレーション検出器の開発」, 日本物理学会第 73 回年次大会, 2018 年 3 月 22–25 日.

松本翔汰,「BigRIPS における高精度パイ中間子原子分光・二重 Gamow-Teller 巨大共鳴探索実験に向けた新検出器システムの性能評価(ii)」, 日本物理学会第 73 回年次大会, 2018 年 3 月 22–25 日.

高橋祐羽,「パラ水素を用いた薄型自己保持固体水素標的の開発」, 日本物理学会 2017 年秋季大会, 2017 年 9 月 12–15 日.

Poster Presentations

[International Conference etc.]

Z. Ge, "Development of Mirror-type MCP Detectors for Mass Measurements at the Rare-RI Ring," The 10th International Conference on Nuclear Physics at Storage Rings (STORI'17), Kanazawa, Japan, Nov. 13–18, 2017.

RIBF Research Division
Nuclear Spectroscopy Laboratory

1. Abstract

The research group has conducted nuclear-physics studies utilizing stopped/slowed-down radioactive-isotope (RI) beams mainly at the RIBF facility. These studies are based on the technique of nuclear spectroscopy such as β-ray-detected NMR, γ-PAD (Perturbed Angular Distribution), laser, and Mössbauer among other methods that takes advantage of intrinsic nuclear properties such as nuclear spins, electromagnetic moments, and decay modes. In particular, techniques and devices for the production of spin-controlled RI beams have been developed and combined to the spectroscopic studies, which enable high-sensitivity measurements of spin precessions/resonances through a change in the angular distribution of radiations. Anomalous nuclear structures and properties of far unstable nuclei are investigated from thus determined spin-related observables. The group also aims to apply such techniques to interdisciplinary fields such as fundamental physics and materials science by exploiting nuclear probes.

2. Major Research Subjects

(1) Nuclear spectroscopy with spin-oriented RI beams
(2) R&D studies for laser spectroscopy of stopped/slowed-down RI beams
(3) Application of RI probes
(4) Fundamental physics: Study of symmetry

3. Summary of Research Activity

(1) Nuclear spectroscopy with spin-oriented RI beams

Measurements of static electromagnetic nuclear moments over a substantial region of the nuclear chart have been conducted for structure studies on the nuclei far from the β-decay stability. Utilizing nuclear spin orientation phenomena of RIs created in the projectile-fragmentation reaction, ground- and excited-state nuclear moments of nuclei far from the stability have been determined by means of the β-ray-detected nuclear magnetic resonance (β-NMR) and the γ-ray time differential perturbed angular distribution (γ-TDPAD) methods. To extend these observations to extremely rare RIs, development of a new apparatus to produce highly spin-polarized RI beams will be conducted by extending the atomic beam resonance method to fragmentation-based RI beams.

(2) R&D studies for laser spectroscopy of stopped/slowed-down RI beams

For the measurement of electromagnetic nuclear properties such as spin, isotope shift, and electromagnetic nuclear moments at RIBF, we have been conducting R&D studies on nuclear laser spectroscopy. One is development of a new laser-spectroscopy system utilizing superfluid helium (He II) as a stopping medium of energetic RI beams, where characteristic atomic properties of ions surrounded by liquid helium enable us to perform unique nuclear laser spectroscopy. The other is a system for collinear laser spectroscopy for a large variety of elements using slowed-down RI beams produced via projectile-fragmentation reaction at RIBF, which can be achieved only by a universal low-energy RI-beam delivery system SLOWRI.

(3) Application of RI probes

The application of RI and heavy ion beams as a probe for condensed matter studies is also conducted by the group. The microscopic material dynamics and properties have been investigated through the deduced internal local fields and the spin relaxation of RI probes based on various spectroscopies utilizing RI probes such as the β-NMR/nuclear quadrupole resonance (NQR) methods, in-beam Mössbauer spectroscopy and the γ-ray time differential perturbed angular correlation (γ-TDPAC) spectroscopy.

(4) Fundamental physics: Study of symmetry

The nuclear spins of stable and unstable isotopes sometimes play important roles in fundamental physics research. New experimental methods and devices have been developed for studies of the violation of time reversal symmetry (T-violation) using spin-polarized nuclei. These experiments aim to detect the small frequency shift in the spin precession arising from new mechanisms beyond the Standard Model.

Members

Chief Scientist (Lab. Head)
Hideki UENO

Research & Technical Scientists
Hiroki YAMAZAKI (Senior Research Scientist)　　　　　　　　Yuichi ICHIKAWA (Senior Research Scientist)
Aiko TAKAMINE (Research Scientist)

Research Consultant
Takuya OKADA

Special Postdoctoral Researcher
Tomoya SATO

Postdoctoral Researcher
Minori TAJIMA

Junior Research Associates
Tomomi FUJITA (Osaka University)   Keita KAWATA (University of Tokyo)

International Program Associates
Ian MURRAY (University Paris Sud)   Aleksey GLADKOV (Kyungpook National University)

Part-time Worker
Momo MUKAI

Senior Visiting Scientists
Yukari MATSUO (Hosei University)   Takaharu OTSUKA (University of Tokyo)

Visiting Researcher
Hiroki NISHIBATA (JSPS Fellow)

Visiting Scientists
Wataru SATO (Kanazawa University)   Kenya KUBO (International Christian University)
Kensaku MATSUTA (Osaka University)   Akihiro YOSHIMI (Okayama University)
Jin NAKAMURA (University of Elec.-Com.)   Dimiter Loukanov BALABANSKI (IHIN)
Atsushi HATAKEYAMA (Tokyo Univ. of Agric. and Tech.)   Naoki NISHIDA (Tokyo University of Science)
Takeshi FURUKAWA (Tokyo Met. University)   Boulay FLORENT (CNRS GANIL)
Satoshi TSUTSUI (JASRI)   Takeshi INOUE (Tohoku University)
Takamasa MOMOSE (University of British Columbia)   Yoko ISHIBASHI (Tohoku University)
Jean-Michel DAUGAS (CEA)   Kei IMAMURA (Okayama University)
Yoshio KOBAYASHI (Univ. of Elec.-Com.)   Takashi ABE (University of Tokyo)
Jiro MURATA (Rikkyo University)   Xiaofei YANG (CERN)
Jun MIYAZAKI (Hokuriku University)   Deyan Todorov YORDANOV (IPN Orsay)
Yasuhiro YAMADA (Tokyo University of Science)

Student Trainees
Masaomi TANAKA (Osaka University)   Ippei KUBONO (Tokyo Univ. of Sci.)
Daiki TOMINAGA (Hosei University)   Shota AMAGASA (Tokyo Univ. of Sci.)
Tsuyoshi EGAMI (Hosei University)   Masanari SEKI (Tokyo Univ. of Science)
Takafumi KAWAGUCHI (Hosei University)   Honami ITO (Tokyo Univ. of Science)
Makoto SANJO (Hosei University)   Sayato NOGUCHI (Tokyo Univ. of Science)
Wataru KOBAYASHI (Hosei Univ.)   Fuminori HATAYAMA (Tokyo Univ. of Science)
Haruka GONDA (Hosei University)   Kazuki HAMAZAKI (Tokyo Univ. of Science)
Mari IIJIMA (Hosei University)   Takumi FUNABASHI (Tokyo Univ. of Science)
Yosuke BABA (Hosei University)   Kenya TAKAHASHI (Univ. of Elec.-Com.)
Rio NAKAZATO (Hosei University)   Masato SUZUKI (Univ. of Elec.-Com.)
Yasuharu TAKEUCHI (Hosei University)   Kyosuke KAMEYAMA (Univ. of Elec.-Com.)
Tomoaki YADA (Hosei University)   Yutaro NAKAMURA (Meiji University)
Katsumi TOZUKA (Hosei University)   Takayuki KAWAMURA (Osaka Univ.)
Takumi ASAKAWA (Hosei University)   Fumiya GOTO (Nagoya University)
Kazuho DOI (Hosei University)   Takatoshi MAEKAWA (International Christian University)
Yusuke SASAKI (Hosei University)   Aiko UCHIYAMA (Tohoku University)

Interns
Jie LIN (Peking University)   Kin Ming FUNG (University Hong Kong)
Fangzhou LIU (Peking University)   Chi_Ho LAU (University Hong Kong)
Yidi CHEN (Peking University)   Samantha Y S YU (University Hong Kong)
Sixuan LI (Peking University)   ChiKin TAM (University Hong Kong)
Qingyuan LIU (Peking University)   Chi En TEH (University Hong Kong)
Kai MA (Peking University)   Kwok Lung FAN (University Hong Kong)

Temporary Staffing
Yuka TAGUCHI

List of Publications & Presentations

Publications

[Journal]

(Original Papers) *Subject to Peer Review

H. Nishibata, T. Shimoda, A. Odahara, S. Morimoto, S. Kanaya, A. Yagi, H. Kanaoka, M. R. Pearson, C. D. P. Levy, M. Kimura, "Shape coexistence in the $N = 19$ neutron-rich nucleus ^{31}Mg explored by β-γ spectroscopy of spin-polarized ^{31}Na," Phys. Lett. B **767**, 81–85 (2017).*

M. Hase, Y. Ebukuro, H. Kuroe, M. Matsumoto, A. Matsuo, K. Kindo, J. R. Hester, T. J. Sato, and H. Yamazaki, "Magnetism of the antiferromagnetic spin-3/2 dimer compound CrVMoO$_7$ having an antiferromagnetically ordered state," Phys. Rev. B **95**, 144429 (2017).*

M. Mukai, Y. Hirayama, Y. X. Watanabe, P. Schury, H. S. Jung, M. Ahmed, H. Haba, H. Ishiyama, S. C. Jeong, Y. Kakiguchi, S. Kimura, J.Y. Moon, M. Oyaizu, A. Ozawa, J. H. Park, H. Ueno, M. Wada, H. Miyatake, "High-efficiency and low-background multi-segmented proportional gas counter for β-decay spectroscopy," Nucl. Instrum. Methods Phys. Res. A **884**, 1–10 (2018).*

T. Sato, Y. Ichikawa, S. Kojima*, C. Funayama, S. Tanaka, T. Inoue, A. Uchiyama, A. Gladkov, A. Takamine, Y. Sakamoto, Y. Ohtomo, C. Hirao, M. Chikamori, E. Hikota, T. Suzuki, M. Tsuchiya, T. Furukawa, A. Yoshimi, C. P. Bidinosti, T. Ino, H. Ueno, Y. Matsuo, T. Fukuyama, N. Yoshinaga, Y. Sakemi, K. Asahi, "Development of co-located ^{129}Xe and ^{131}Xe nuclear spin masers with external feedback scheme," Phys. Lett. A **382**, 588 (2018).*

(Review)

N. Yamanaka, B. K. Saoo, N. Yoshinaga, T. Sato, K. Asahi, B. P. Das, "Probing exotic phenomena at the interface of nuclear and particle physics with the electric dipole moments of diamagnetic atoms: A unique window of hadronic and semi-leptonic CP violation," Eur. Phys. J. A **53**, 54 (2017).*

[Proceedings]

(Original Papers) *Subject to Peer Review

S. Kinbara, H. Ekawa, T. Fujita, S. Hayakawa, S.H. Hwang, Y. Ichikawa, K. Imamura, H. Itoh, H. Kobayashi, R. Murai, K. Nakazawa, M.K. Soe, A. Takamine, A.M.M. Theint, H. Ueno, J. Yoshida, "Development of PID method in nuclear emulsion," JPS Conf. Proc. **17**, 032002 (2017).*

Oral Presentations

[International Conference etc.]

T. Otsuka, "Quantum self-organization and nuclear collectivities," 12th International Spring Seminar on Nuclear Physics Current Problems and Prospects for Nuclear Structure, Sant'Angelo d'Ischia, Italy, May 15–19, 2017.

Y. Ichikawa, "Magnetic moment measurement of isomeric state of ^{75}Cu using spin-aligned RI beam at RIBF," Advances in Radioactive Isotope Science (ARIS) 2017, Keystone, USA, May 28–June 2, 2017.

H. Nishibata, T. Shimoda, A. Odahara, S. Morimoto, S. Kanaya, A. Yagi, H. Kanaoka, M. R. Pearson, C. D. P. Levy, M. Kimura, "Shape coexistence in neutron-rich ^{31}Mg investigated by beta-gamma spectroscopy of spin-polarized ^{31}Na," Advances in Radioactive Isotope Science (ARIS) 2017, Keystone, USA, May 28–June 2, 2017.

T. Otsuka, "Quantum self-organization and nuclear shapes," Advances in Radioactive Isotope Science (ARIS) 2017, Keystone, USA, May 28–June 2, 2017.

T. Otsuka, "Impact to shell model, impact of shell model," Probing fundamental interactions by low energy excitations – Advences in theoretical nuclear physics, Stockholm, Sweden, June 5–9, 2017.

T. Otsuka, "Shell-model challenges to gamma-ray spectroscopy," NUSPIN 2017, Darmstadt, Germany, June 26–29, 2017.

T. Otsuka, "Recent developments in shell model studies of atomic nuclei," International School of Physics "Enrico Fermi," Varenna, Italy, July 14–19, 2017.

W. Kobayashi, K. Imamura, T. Egami, T. Nishizaka, A. Takamine, M. Sanjo, T. Fujita, D. Tominaga, Y. Nakamura, Y. Ichikawa, T. Sato, H. Nishibata, A. Gladkov, L.C. Tao, T. Kawaguchi, T. Wakui, T. Furukawa, H. Ueno, Y. Matsuo, "Development of a new fluorescence detection system for a small amount of atoms in superfluid helium," The 24th Congress of the International Commission for Optics (ICO-24), Tokyo, Japan, August 21–25, 2017.

T. Otsuka, "Beauty and quantum," Pre-Workshop "AE Section on Physics and Engineering Sciences," Joint Annual Conference of Academia Europaea and ALLEA, Budapest, Hungary, September 3, 2017.

T. Otsuka, "Single-particle states vs. collective modes: friends or enemies?" 16th International Symposium on Capture Gamma-Ray Spectroscopy and Related Topics (CGS16), Changhai, China, September 18–22, 2017.

T. Otsuka, "Quantum self-organization and the structure evolution of heavy exotic nuclei," The International Symposium on Physics of Unstable Nuclei 2017 (ISPUN17), Halong City, Vietnam, September 25–30, 2017.

A. Gladkov, Y. Ishibashi, H. Yamazaki, Y. Ichikawa, A. Takamine, H. Nishibata, K. Asahi, T. Sato, W. Y. Kim, T. Fujita, L. C. Tao, T. Egami, D. Tominaga, T. Kawaguchi, M. Sanjo, W. Kobayashi, K. Imamura, Y. Nakamura, G. Georgiev, J. M. Daugas, H. Ueno, "Ground-state electromagnetic nuclear moments of ^{21}O," The 2017 International Workshop on Polarized Sources, Targets & Polarimetry, Daejeon, South Korea, October 16–20, 2017.

T. Otsuka, "Shape coexistence and quantum phase transition in the Monte-Carlo shell model," ESNT workshop Shape Coexistence and Electric Monopole Transitions in Atomic Nuclei," Paris, France, October 23–27, 2017.

T. Otsuka, "Alpha clustering in nuclei viewed from an ab initio shell model," Workshop on Nuclear Cluster Physics (WCNP2017), Sapporo, Japan, October 25–27, 2017.

H. Ueno, "Nuclear moment and shell model," Ito International Research Center (IIRC) Symposium – Perspective of the physics of nuclear structure-, Tokyo, Japan, November 1–4, 2017.

T. Otsuka, "Twenty years ago, twenty years later," Ito International Research Center (IIRC) Symposium – Perspective of the physics of nuclear structure-, Tokyo, Japan, November 1–4.

Y. Ichikawa, "Nuclear moment measurements using spin-aligned RI beam at RIBF," ANL Seminar, Lemont, USA, November 8, 2017.

T. Otsuka, "Single-particle states vs. collective modes: friends or enemies," Shapes and Symmetries in Nuclei: from Experiment to Theory (SSNET'17), Orsay, France, November 6–10, 2017.

Y. Ichikawa, "Nuclear moment measurement using spin-oriented RI beam at RIBF," International Symposium on RI Beam Physics in the 21st Century:

10th Anniversary of RIBF, Wako, Japan, December 4–5, 2017.

T. Otsuka, "Bogdan and quest for Copernican turn," The 60th Anniversary seminar of Bogdan Fornal, Krakow, Poland, December 13, 2017.

T. Otsuka, "Quantum self-organization in atomic nuclei," The COPIGAL Meeting on recent results and future projects involving PARIS, AGATA, NEDA, and FAZIA detectors, Krakow, Poland, December 13–15, 2017.

T. Otsuka, "Quantum self-organization and nuclear collectivity," IVth Topical Workshop on Modern Aspects in Nuclear Structure, Bolmio, Italy, February 19–25, 2018.

T. Otsuka, "Suppression of double beta decay and quadrupole pairing correlation," INT program INT-18-1a Nuclear ab initio Theories and Neutrino Physics, Seattle, USA, February 26–March 30, 2018.

T. Otsuka, "Perspectives of the shell model on and beyond monopole," First Workshop on Nuclear Shell Model Development and Applications in Eastern Asia (NuSEA-2018), Shanghai, China, March 30–31, 2018.

[Domestic Conference]

伊藤由太, 和田道治, P. Schury, 加治大哉, 森本幸司, 羽場宏光, I. Murray, M. Rosenbusch, 木村創大, 高峰愛子, 宮武宇也, 山木さやか, 新井郁也, H. Wollnik,「MRTOF 質量分析器による八重極変形核 ^{223,224}Th の精密原子質量測定」, 日本物理学会第 72 回年次大会, 大阪, 2017 年 3 月 17–20 日.

高峰愛子,「原子スペクトルの精密分光による超変形原子核探索」, 物質階層原理第一回春合宿, 御殿場, 2017 年 5 月 12–13 日.

大塚孝治,「核力と原子核の基本的性質」, 軽井沢研究会「原子核多体問題の進展と展望」, 軽井沢, 2017 年 6 月 11 日.

Y. Honda, N. Sasao, M. Yoshimura, K. Yoshimura, A. Yoshimi, S. Uetake, T. Masuda, Y. Miyamoto, H. Hara, T. Hiraki, K. Yokoya, M. Yoshida, O. Kamigaito, T. Nakagawa, Y. Kanai, Y. Ichikawa, T. Nagatomo, K. Sakaue,「相対論的量子イオンビームによる高強度ガンマ線源」, 日本加速器学会第１４回年会, 札幌, 2017 年 8 月 1–3 日.

佐藤智哉, 市川雄一, 井上壮志, 内山愛子. A. Gladkov, 高峰愛子, 小島修一郎, 舟山智歌子, 田中俊也, 坂本雄, 大友祐一, 平尾千佳, 近森正敏, 彦田絵里, 古川武, 吉見彰洋, C.P. Bidinosti, 猪野隆, 上野秀樹, 松尾由賀利, 福山武志, 吉永尚孝, 酒見泰寛, 旭耕一郎,「間欠帰還型能動核スピンメーザーの動作特性と環境応答」, 日本物理学会 2017 年秋季大会, 宇都宮, 2017 年 9 月 11–14 日.

神田聡太郎, 石田勝彦, 岩崎雅彦, 上野秀樹, 大石裕, 岡田信二, 斎藤徳人, 佐藤将春, 高峰愛子, 松崎禎市郎, 馬越, 緑川克美, 湯本正樹, 和田智之, 相川脩, 田中香津生, 松田恭幸,「ミュオン水素原子の精密レーザー分光」, 日本物理学会 2017 年秋季大会, 宇都宮, 2017 年 9 月 11–14 日.

平山賀一, 向井もも, 渡辺裕, M. Ahmed, S.C. Jeong, H.S. Jung, 垣口豊, 金谷晋之介, 木村創大, J.Y. Moon, 中務孝, 小柳津充広, J.H. Park, P. Schury, 谷口秋洋, 和田道治, 鷲山広平, 渡邉寛, 宮武宇也,「KISS I : ^{199}Pt のレーザー共鳴イオン化核分光」, 日本物理学会 2017 年秋季大会, 宇都宮, 2017 年 9 月 11–14 日.

向井もも, 平山賀一, 渡辺裕, P. Schury, H.S. Jung, M. Ahmed, 羽場宏光, S.C. Jeong, 垣口豊, 金谷晋之介, 木村創大, 宮武宇也, J.Y. Moon, 小沢顕, 小柳津充広, J.H. Park, 谷口秋弘, 上野秀樹, 和田道治 ^{A}, 渡邉寛,「KISS II : $^{196-198}$Ir のレーザー共鳴イオン化核分光」, 日本物理学会 2017 年秋季大会, 宇都宮, 2017 年 9 月 11–14 日.

岩本ちひろ, 大田晋輔, 時枝紘史, 小嶋玲子, 李清秀, 溝井浩, 郡司卓, 山口英斉, 鈴木大介, 早川勢也, 今井伸明, 岡本潤, 銭廣十三, 堂園昌伯, 中島亮, O. Beliuskina, 松田洋平, 道正新一郎, 矢向謙太郎, 横山輪, 磯部忠昭, 川田敬太, 村上哲也, 武田栄一,「ガスアクティブ標的 CAT の大型化に向けた二重増幅率制御型多層 THGEM の開発」, 日本物理学会 2017 年秋季大会, 宇都宮, 2017 年 9 月 11–14 日.

川田敬太, 矢向謙太郎, 大田晋輔, 堂園昌伯, 銭廣十三, 岩本ちひろ, 北村徳隆, 小林幹, 酒井英行, 笹野匡紀, 高木基伸, 増岡翔一朗, 道正新一郎, 横山輪, L. Stuhl,「^{58}Ni の入射核破砕反応による高スピンアイソマービームの生成」, 日本物理学会 2017 年秋季大会, 宇都宮, 2017 年 9 月 11–14 日.

角田直文, 大塚孝治, 清水則孝, 高柳和雄, Morten Hjorth-Jensen,「pf+sdg shell 領域の中性子過剰核の核力に基づいた研究」, 日本物理学会 2017 年秋季大会, 宇都宮, 2017 年 9 月 11–14 日.

富樫智章, 角田佑介, 大塚孝治, 清水則孝,「Zr 同位体近傍における形の量子相転移のモンテカルロ殻模型による研究」, 日本物理学会 2017 年秋季大会, 宇都宮, 2017 年 9 月 11–14 日.

王惠仁, D.T. Tran, G. Hagen, 青井考, 寺嶋知, 延與佳子, 鈴木俊夫, L.S. Geng, 谷畑勇夫, T.T. Nguyen, Y.Ayyad, P.Y. Chan, 福田光順, H. Geissel, M.N. Harakeh, 橋本尚志, T.H. Hoang, 井手口栄治, 井上梓, R. Kanungo, 川畑貴裕, L.H. Khiem, W.P. Lin, 松多健策, 三原基嗣, 百田佐多生, 長江大輔, N.D. Nguyen, 西村太樹, 大塚孝治, 小沢顕, P.P. Ren, 坂口治隆, C. Scheidenberger, 田中純貴, 武智麻耶, R. Wada, 山本哲也,「中性子過剰な炭素同位体における陽子魔法数について」, 日本物理学会 2017 年秋季大会, 宇都宮, 2017 年 9 月 11–14 日.

吉田聡太, 宇都野穣, 清水則孝, 大塚孝治,「質量数 40 領域の中性子過剰核におけるベータ崩壊の系統的記述」, 日本物理学会 2017 年秋季大会, 宇都宮, 2017 年 9 月 11–14 日.

清水則孝, 大塚孝治, 角田佑介, 宇都野穣,「ボゴリューボフ準粒子基底によるモンテカルロ殻模型」, 日本物理学会 2017 年秋季大会, 宇都宮, 2017 年 9 月 11–14 日.

角田佑介, 大塚孝治, 清水則孝, 富樫智章,「モンテカルロ殻模型による Sm 同位体の形状変化の研究」, 日本物理学会 2017 年秋季大会, 宇都宮, 2017 年 9 月 11–14 日.

富樫智章, 清水則孝, 大塚孝治, 宇都野穣,「大規模殻模型計算による中性子過剰 $N = 82$ 近傍の半減期の計算」, 日本物理学会 2017 年秋季大会, 宇都宮, 2017 年 9 月 11–14 日.

宮城宇志, 阿部喬, 河野通郎, P. Navratil, 岡本良治, 大塚孝治, 清水則孝, S.R. Stroberg,「3 体力効果を取り込んだ UMOA 計算」, 日本物理学会 2017 年秋季大会, 宇都宮, 2017 年 9 月 11–14 日.

A. Gladkov, Y. Ishibashi, H. Yamazaki, Y. Ichikawa, A. Takamine, H. Nishibata, K. Asahi, T. Sato, W. Y. Kim, T. Fujita, L. C. Tao, T. Egami, D.Tominaga, T. Kawaguchi, M. Sanjo, W. Kobayashi, K. Imamura, Y. Nakamura, G. Georgiev, J. M. Daugas, H. Ueno, "Ground-state quadrupole moment of ^{21}O," 日本物理学会 2017 年秋季大会, 宇都宮, 2017 年 9 月 11–14 日.

川口高史, 上野秀樹, 西畑洸希, Aleksey Gladkov, 市川雄一, 高峰愛子, 佐藤智哉, 川田敬太, 山崎展樹, Tao Longchun, 中村祐太郎, 小林航, 三條真, 浅河拓光, 佐々木悠輔, 戸塚克, 土井一歩, 矢田智昭, G. Georgiev, 松尾由賀利,「中性子過剰核の構造研究に向けた β 線検出型核磁気共鳴法における新型 RF 磁場制御系の開発」, 日本物理学会第 73 回年次大会, 野田, 2018 年 3 月 22–25 日.

石橋陽子, A. Gladkov, 西畑洸希, 山崎展樹, 旭耕一郎, J. -M. Daugas, 江上魁, 藤田朋美, G. Georgiev, 市川雄一, 今村慧, 川口高史, W.Y. Kim, 小林航, L. Tao, 中村祐太郎, 三條真, 佐藤智哉, 高峰愛子, 富永大樹, 上野秀樹,「中性子過剰核 ^{21}O の核磁気モーメント測定」, 日本物理学会第 73 回年次大会, 野田, 2018 年 3 月 22–25 日.

西畑洸希, A. Gladkov, 川口高史, 上野秀樹, 市川雄一, 高峰愛子, 佐藤智哉, 川田敬太, 山崎展樹, 小林航, 三條真, L.C. Tao, 中村祐太郎, 浅河拓光, 佐々木悠輔, 戸塚克, 土井一歩, 矢田智昭, 旭耕一郎, 石橋陽子, 今村慧, 藤田朋美, G. Georgiev, J.M. Daugas,「スピン偏極 ^{23}Ne ビームを用いた単結晶電場勾配測定；中性子過剰 Ne 基底状態電磁気モーメント測定に向けて」, 日本物理学会第 73 回年次大会, 野田, 2018 年 3 月 22–25 日.

藤枝亮, 笹尾登, 吉村太彦, 吉村浩司, 吉見彰洋, 植竹智, 宮本祐樹, 増田孝彦, 原秀明, 今村慧, 上垣外修一, 中川孝秀, 金井保之, 市川雄一, 長友傑, 本田洋介, 坂上和之,「量子イオンビーム (QIB) へ向けた Ba イオン源の開発」, 日本物理学会第 73 回年次大会, 野田, 2018 年 3 月 22–25 日.

福田直樹, 清水陽平, 鈴木宏, AHN DeukSoon, 竹田浩之, 炭竈聡之, 宮武宇也, 渡辺裕, 稲辺尚人, 西村俊二, 大津秀暁, 吉田光一, 上野秀樹, 佐藤広海, 鈴木大介, 笹野匡紀, 磯部忠昭, 平山賀一, 家城和夫, 天野順貴,「^{238}U の入射核破砕反応を用いた $N = 126$ 近傍の中性子過剰核の生成」, 日本物理学会第 73 回年次大会, 野田, 2018 年 3 月 22–25 日.

神田聡太郎, 石田勝彦, 岩崎雅彦, 上野秀樹, 大石裕, 岡田信二, 斎藤徳人, 佐藤将春, 高峰愛子, 松崎禎市郎, 馬越, 緑川克美, 湯本正樹, 和田智之, 相川脩, 田中香津生, 松田恭幸,「ミュオン水素原子分光実験のための中赤外光源の開発」, 日本物理学会第 73 回年次大会, 野田, 2018 年 3 月 22–25 日.

川田敬太, 大田晋輔, 堂薗昌伯, 銭廣十三, 岩本ちひろ, 北村徳隆, 小林幹, 酒井英行, 笹野匡紀, 高木基伸, 増岡翔一朗, 道正新一郎, 横山輪, 矢向謙太郎, Laszlo STUHL, 坂口治隆, 原田知也, 寺嶋知, 西畑洸希, 角田理恵子, 今井伸明,「^{59}Co の入射核破砕反応による高スピンアイソマービームの生成」, 日本物理学会第 73 回年次大会, 野田, 2018 年 3 月 22–25 日.

角田佑介, 大塚孝治, 清水則孝, 富樫智章,「Sm 同位体の形状変化のモンテカルロ殻模型による研究」, 日本物理学会第 73 回年次大会, 野田, 2018 年 3 月 22–25 日.

吉田聡太, 清水則孝, 富樫智章, 大塚孝治,「ベイズ推定に基づく殻模型有効相互作用の解析」, 日本物理学会第 73 回年次大会, 野田, 2018 年 3 月 22–25 日.

富樫智章, 角田佑介, 大塚孝治, 清水則孝,「モンテカルロ殻模型による Sn 同位体の系統的研究」, 日本物理学会第 73 回年次大会, 野田, 2018 年 3 月 22–25 日.

Poster Presentations

[International Conference etc.]

A. Gladkov, Y. Ishibashi, H. Yamazaki, Y. Ichikawa, A. Takamine, H. Nishibata, K. Asahi, T. Sato, W. Y. Kim, T. Fujita, L. C. Tao, T. Egami, D.Tominaga, T. Kawaguchi, M. Sanjo, W. Kobayashi, K. Imamura, Y. Nakamura, G. Georgiev, J. M. Daugas, H. Ueno, "Ground-state electromagnetic nuclear moments of ^{21}O," Advances in Radipactive Isotope Science (ARIS), Keystone, USA, May 28–June 2, 2017.

W. Kobayashi, K. Imamura, T. Nishizaka, A. Takamine, M. Sanjo, T. Fujita, D. Tominaga, Y. Nakamura, Y. Ichikawa, T. Sato, H. Nishibata, A. Gladkov, L.C. Tao, T. Kawaguchi, T. Wakui, T. Furukawa, H. Ueno, Y. Matsuo, "Development of a low-background detection system for the laser-induced fluorescence from the atoms injected into superfluid helium," Keystone, USA, May 28–June 2, 2017.

[Domestic Conference]

小林航, 今村慧, 江上魁, 西坂太志, 三條真, 藤田朋美, 富永大樹, 中村祐太郎, 高峰愛子, 涌井崇志, 古川武, 上野秀樹, 松尾由賀利,「低収量不安定原子核の核構造研究に向けた超流動ヘリウム中原子からのレーザー誘起蛍光の低バックグラウンド検出系の開発」, 第 14 回原子・分子・光科学（AMO）討論会, 調布, 2017 年 6 月 30 日–7 月 1 日.

向井もも, 平山賀一, 渡辺裕, Schury Peter, 鷲山広平, Ahmed Murad, 垣口豊, 木村創大, 小沢顕, 小柳津充宏, Park Jinhyung, Moon Junyoung, 上野秀樹, 和田道治, 宮武宇也,「Laser resonance isonization spectroscopy of $^{196-198}$Ir」, KEK Student Day, 2017 年 10 月 24 日.

土井一歩, 戸塚克, 小林航, 今村慧, 藤田朋美, 三條真, 矢田智昭, 高峰愛子, 涌井崇志, 古川武, 上野秀樹, 松尾由賀利,「超流動ヘリウム (He II) 中の低収量核原子の核構造研究に向けた光学クライオスタットの改良」, 日本物理学会第 73 回年次大会, 野田, 2018 年 3 月 22–25 日.

RIBF Research Division
High Energy Astrophysics Laboratory

1. Abstract

Immediately after the Big Bang, the beginning of our universe, only hydrogen and helium existed. However, nuclear fusion in the interior of stars and the explosion of supernovae in the universe over the course of 13.8 billion years led to the evolution of a world brimming with the many different elements we have today. By using man-made satellites to observe X-rays and gamma-rays emitted from celestial objects, we are observing the synthesis of the elements at their actual source. Our goal is to comprehensively elucidate the scenarios for the formation of the elements in the universe, together with our research on sub-atomic physics using an accelerator.

2. Major Research Subjects

(1) Connect missing links of nucleosynthesis in our universe
(2) Reveal the particle acceleration mechanism in astronomical objects, planets and inter-planetary space
(3) Discover new physics in extremely strong magnetic and gravitational environment
(4) Research and development of innovative X-ray and gamma-ray detectors

3. Summary of Research Activity

We have performed data analysis of Japanese X-ray satellite Hitomi, which was lost by an accident one month after the launch in 2016, and obtained many new research achievements on neutron stars, supernova remnants, galaxies, and cluster of galaxies. Some of them are verification of solar abundance of Perseus cluster, and non-detection of dark matter signal at 3.5 keV. We have contributed to the new X-ray polarimeter mission IXPE (Imaging X-ray Polarimeter Explorer) and provided gas electron multiplier foils. We have studied particle acceleration around Jupiter with Hisaki/Juno/Hubble space telescope, and pursued the gamma-ray emission mechanism of thundercloud.

Members

Chief Scientist (Lab. Head)
Toru TAMAGAWA

Contract Researchers

Yuki OKURA	Takao KITAGUCHI
Asami HAYATO	

Special Postdoctoral Researchers

Tomoki KIMURA	Toshio NAKANO
Hirokazu ODAKA	Liyi GU

Junior Research Associate
Yuuki WADA (Univ.of Tokyo)

Part-time Workers

Yuki OKURA	Sonoe ODA
Kazuki NISHIDA	Yuanhui ZHOU
Naoto MURATA	

Visiting Researcher
Asami HAYATO (JSPS Fellow)

Visiting Scientists

Yukikatsu TERADA (Saitama Univ.)	Shin'ya YAMADA (Tokyo Metropolitan Univ.)
Motohide KOKUBUN (JAXA)	Takao KITAGUCHI (Hiroshima Univ.)
Masaki WAKABAYASHI (Jakulin Commercial Company LC)	Teruaki ENOTO (Kyoto Univ.)
Aya BAMBA (Aoyama Gakuin Univ.)	Kazuki KOMIYA (TIRI)
Naohisa INADA (National Institute of Tech., Nara College)	Hirofumi NODA (Tohoku Univ.)
Rohta TAKAHASHI (Tomakomai Nat'l College of Tech.)	Yuki OKURA (NAOJ)
Toru MISAWA (Shinshu Univ.)	Yuzuru Tawara (Nagoya Univ.)
Yoko TAKEUCHI (TIRI)	Ikuyuki Mitsuishi (Nagoya Univ.)
Satoru KATSUDA (Chuo Univ.)	Harufumi TSUCHIYA (JAEA)

Student Trainees

Megu KUBOTA (Tokyo Univ. of Sci.)	Kazuki NISHIDA (Tokyo Univ. of Sci.)

Sonoe ODA (Tokyo Univ. of Sci.)
Naoto MURATA (Tokyo Univ. of Sci.)
Yuanhui ZHOU (Tokyo Univ. of Sci.)

Miho OKUBO (Tokyo Univ. of Sci.)
Takaya WAKAMATSU (Tokyo Univ. of Sci.)

List of Publications & Presentations
[Journal]
(Original Papers) * Subject to Peer Review

The Hitomi collaboration, "Glimpse of the highly obscured HMXB IGR J16318-4848 with Hitomi," Publ. Astron. Soc. Jpn. **70**, 17 (2018).*

The Hitomi collaboration, "Hitomi observations of the LMC SNR N 132 D: Highly redshifted X-ray emission from iron ejecta," Publ. Astron. Soc. Jpn. **70**, 16 (2018).*

The Hitomi collaboration, "Hitomi X-ray studies of giant radio pulses from the Crab pulsar," Publ. Astron. Soc. Jpn. **70**, 15 (2018).*

The Hitomi collaboration, "Search for thermal X-ray features from the Crab nebula with the Hitomi soft X-ray spectrometer," Publ. Astron. Soc. Jpn. **70**, 14 (2018).*

The Hitomi collaboration, "Hitomi observation of radio galaxy NGC 1275: The first X-ray microcalorimeter spectroscopy of Fe-K α line emission from an active galactic nucleus," Publ. Astron. Soc. Jpn. **70**, 13 (2018).*

The Hitomi collaboration, "Atomic data and spectral modeling constraints from high-resolution X-ray observations of the Perseus cluster with Hitomi," Publ. Astron. Soc. Jpn. **70**, 12 (2018).*

The Hitomi collaboration, "Temperature structure in the Perseus cluster core observed with Hitomi," Publ. Astron. Soc. Jpn. **70**, 11 (2018).*

The Hitomi collaboration, "Measurements of resonant scattering in the Perseus Cluster core with Hitomi SXS," Publ. Astron. Soc. Jpn. **70**, 10 (2018).*

The Hitomi collaboration, "Atmospheric gas dynamics in the Perseus cluster observed with Hitomi," Publ. Astron. Soc. Jpn. **70**, 9 (2018).*

R. Fujimoto et al., "Performance of the helium dewar and the cryocoolers of the Hitomi soft x-ray spectrometer," J. Astron. Telesc. Instrum. Syst. **4**, 011208 (2018).*

M. Tsujimoto et al., "In-orbit operation of the soft x-ray spectrometer onboard the Hitomi satellite." J. Astron. Telesc. Instrum. Syst. **4**, 011205 (2018).*

Y. Yamamoto, H. Togashi, T. Tamagawa, T. Furumoto, N. Yasutake, Th. A. Rijken, "Neutron-star radii based on realistic nuclear interactions," Phys. Rev. C **96**, 065804 (2017).*

The Hitomi collaboration, "Solar abundance ratios of the iron-peak elements in the Perseus cluster," Nature **551**, 478–480, (2017).*

The Hitomi collaboration, "Hitomi Constraints on the 3.5 keV Line in the Perseus Galaxy Cluster," Astrophys. J. **837**, L15–23 (2017).*

T. Hayashi, T. Kitaguchi, M. Ishida, "X-ray reflection from cold white dwarfs in magnetic cataclysmic variables," Mon. Not. R. Astron Soc. **474**, 1810–1825 (2017).*

K. Miyaoka et al., "Multiwavelength study of X-ray luminous clusters in the Hyper Suprime-Cam Subaru Strategic Program S16A field," Publ. Astron. Soc. Jpn. **70**, S22 (2017).*

T. Enoto, S. Shibata, T. Kitaguchi, Y. Suwa, T. Uchide, H, Nishioka, S. Kisaka, T. Nakano, H. Murakami, K. Makishima, "Magnetar Broadband X-Ray Spectra correlated with Magnetic Fields: Suzaku Archive of SGRs and AXPs Combined with NuSTAR, Swift, and RXTE," Astrophys. J. Suppl. Ser. **231**, 8 (2017).*

F. M. Fornasini et al., "The NuSTAR Hard X-Ray Survey of the Norma Arm Region," Astrophys. J. Suppl. Ser. **229**, 33 (2017).*

I. Yoshikawa, F. Suzuki, R. Hikida, K. Yoshioka, G. Murakami, F. Tsuchiya, C. Tao, A. Yamazaki, T. Kimura, H. Kita, H. Nozawa, M. Fujimoto, "Volcanic activity on Io and its influence on the dynamics of the Jovian magnetosphere observed by EXCEED/Hisaki in 2015," Earth Planets Space **69**, 110 (2017).*

R. Koga et al., "The time variation of atomic oxygen emission around Io during a volcanic event observed with Hisaki/EXCEED," Icarus, **299**, 300–307 (2017).*

J. Kinrade et al., "An isolated, bright cusp aurora at Saturn," J. Geophys. Res. **122**, 6121−6138 (2017).*

J. D. Nichols et al., "Response of Jupiter's auroras to conditions in the interplanetary medium as measured by the Hubble Space Telescope and Juno," Geophys. Res. Lett. **44**, 7643−7652 (2017).*

M. Kuwabara, K. Yoshioka, G. Murakami, F. Tsuchiya, T. Kimura, A. Yamazaki, I. Yoshikawa, "The geocoronal responses to the geomagnetic disturbances," J. Geophys. Res. **122**, 1269–1276 (2017).*

K. Yoshioka et al., "Radial variation of sulfur and oxygen ions in the Io plasma torus as deduced from remote observations by Hisaki," J. Geophys. Res. Space Physics **122**, 2999-3012 (2017).*

K. Masunaga et al., "Dawn-dusk difference of periodic oxygen EUV dayglow variations at Venus observed by Hisaki," Icarus **292**, 102–110 (2017).*

B. W. Grefenstette, V. C. Bhalerao, W. Rick, F. A. Harrison, T. Kitaguchi, K. K. Madsen, P. H. Mao, H. Miyasaka, V. Rana, "Ground calibration of the spatial response and quantum efficiency of the CdZnTe hard X-ray detectors for NuSTAR," Proceedings of the SPIE, **10392**, 1039207 (2017).

[Oral Presentations]
(International Conference etc.)

T. Tamagawa, "Coincident observation and localization of GW counterparts in X-ray band," LSST Detection of Optical Counterparts of Gravitational Waves, New York, USA, May 2017.

T. Tamagawa, "X-ray observations of neutron stars," Hadron and Nuclear Physics 2017, Wako, Japan, December 2017.

T. Kimura, et al., "Transient brightening of Jupiter's aurora observed by the Hisaki satellite and Hubble Space Telescope during approach phase of the Juno spacecraft," American Geophysical Union Fall meeting 2017, New Orleans, USA, December 2017.

T. Kimura, "Multi-wavelength observations of Jupiter's aurora during Juno's cruise phase," Planetary Space Weather Meeting, Toulouse, France, October 2017.

T. Kimura, "Development of virtual observatory database for Hisaki, planetary space weather meeting," Toulouse, France, October 2017.

T. Kimura, "Transient brightening of Jupiter's aurora observed by the Hisaki satellite and Hubble Space Telescope during approach phase of the Juno spacecraft," National Astronomical Observatory of Japan Solar Seminar, October 2017.

T. Kimura, "Transient brightening of Jupiter's aurora observed by the Hisaki satellite and Hubble Space Telescope during approach phase of the Juno spacecraft," Magnetospheres of Outer Planets 2017, Swedish Institute of Space Physics, Uppsala, Sweden, June 2017.

T. Kimura, "Status report of Hisaki meta-database development," JSPS Sakura project meeting, Paris Observatory, France, September 2017.

T. Kimura et al., "Transient brightening of Jupiter's aurora observed by the Hisaki satellite and Hubble Space Telescope during approach phase of the Juno spacecraft," International Space Science Institute, Bern, Switzerland, September 2017.

T. Kimura et al., "Transient brightening of Jupiter's aurora observed by the Hisaki satellite and Hubble Space Telescope during approach phase of the Juno spacecraft," European Planetary Science Congress, Latvia, September 2017.

T. Kimura et al., "Auroral explosion at Jupiter observed by the Hisaki satellite and Hubble Space Telescope during approaching phase of the Juno spacecraft," Japan Geoscience Union Meeting 2017, Makuhari, Japan, May 2017.

(Domestic Conference)

勝田哲, A. Fabio, 冨永望, 福井康雄, 平賀純子, 小山勝二, S. -H. Lee, 森浩二, 長瀧重博, 大平豊, P. Robert, 佐野栄俊, 武内陽子, 玉川徹, 辻直美, 常深博, 内山泰伸,「超新星残骸 RX J1713.7-3946 からの熱的X線放射の発見」,日本天文学会 2017 年秋季年会, 北海道大学, 2017 年 9 月.

玉川徹 ほか IXPE-J team,「X 線偏光観測衛星 IXPE への緊急参加」, 日本天文学会 2017 年秋季年会, 北海道大学, 2017 年 9 月.

周圓輝, 村田直人, 窪田恵, 小田苑会, 大久保美穂, 若松孝也, 玉川徹, 中野俊男, 早藤麻美, 岩切渉, 北口貴雄, 榎戸輝揚,「偏光観測衛星 IXPE 搭載用 GEM の画像処理を用いた品質検査法の開発」,日本天文学会 2017 年秋季年会, 北海道大学, 2017 年 9 月.

早藤麻美, 中野俊男, 玉川徹, 岩切渉, 北口貴雄, 榎戸輝揚, 窪田恵,「高エネルギー X 線を検出するマイクロパターン TPC 型 X 線偏光計の開発」, 日本天文学会 2017 年秋季年会, 北海道大学, 2017 年 9 月.

北口貴雄, 深沢泰司, 水野恒史, 玉川徹, 早藤麻美, 岩切渉, 中野俊男, 榎戸輝揚,「光電子追跡型X線偏光計の機械学習による偏光応答モデルの開発」, 日本天文学会 2017 年秋季年会, 北海道大学, 2017 年 9 月.

中野俊男, 玉川徹, 早藤麻美, 岩切渉, 北口貴雄, 榎戸輝揚, 窪田恵,「Time Projection Chamber とフーリエ合成による撮像偏光計の基礎研究」, 日本天文学会 2017 年秋季年会, 北海道大学, 2017 年 9 月.

石崎欣尚 ほか XARM Resolve チーム ,「X 線天文衛星代替機(XARM)搭載の軟 X 線分光器 Resolve の検討状況」, 日本天文学会 2017 年秋季年会, 北海道大学, 2017 年 9 月.

宮岡敬太, 岡部信広, 北口貴雄, 深澤泰司, 大栗真宗, HSC Cluster Members,「Subaru/HSC サーベイ領域にある重量級銀河団の X 線観測による質量推定 III」, 日本天文学会 2017 年秋季年会, 北海道大学, 2017 年 9 月.

大野雅功ほか「ひとみ」HXI/SGD チーム ,「『ひとみ (ASTRO-H)』搭載軟ガンマ線検出器における軌道上バックグラウンドの理解」, 日本天文学会 2017 年秋季年会, 北海道大学, 2017 年 9 月.

和田有希, 湯浅孝行, 中澤知洋, 牧島一夫, 林多佳由, 石田学,「矮新星 GK Persei の X 線スペクトル解析による白色矮星質量の推定」, 日本天文学会 2017 年秋季年会, 北海道大学 , 2017 年 9 月.

山本安夫, 玉川徹, 安武伸俊,「中性子星半径の観測とハイペロン混合」, 日本物理学会 2017 年秋季大会, 宇都宮大学, 9 月 (2017).

楳本大悟, 土屋晴文, 中澤知洋, 湯浅孝行, 榎戸輝揚, 牧島一夫, 古田禄大, 玉川徹, 伊藤伸泰 ,「GROWTH 実験 2014 年度データを用いた雷雲ガンマ線のイベント探索法の改善」, 日本物理学会 2017 年秋季大会, 宇都宮大学, 2017 年 9 月.

古田禄大, 中澤知洋, 和田有希, 楳本大悟, 榎戸輝揚, 湯浅孝行, 土屋晴文, 牧島一夫 ほか GROWTH コラボレーション,「モンテカルロシミュレーションによる雷雲ガンマ線放射モデルの構築」, 日本物理学会 2017 年秋季大会, 宇都宮大学, 9 月 (2017).

中澤知洋 ほか GROWTH コラボレーション ,「雷雲ガンマ線の地上観測の現状と 2017 年の GROWTH 実験計画」, 日本物理学会 2017 年秋季大会, 宇都宮大学, 2017 年 9 月.

玉川徹, 三石郁之, 郡司修一, 水野恒史, 早藤麻美, 北口貴雄, 中野俊男, 岩切渉, 榎戸輝揚, 深沢泰司, 林田清 ,「X 線偏光観測衛星 IXPE への国際協力 」, 第 18 回宇宙科学シンポジウム, 宇宙科学研究所/JAXA, 2018 年 1 月.

玉川徹, 早藤麻美, 北口貴雄, 岩切渉, 中野俊男, 三石郁之, 郡司修一, 深沢泰司, 水野恒史, 榎戸輝揚, 林田清 ほか IXPE-J チーム ,「X 線偏光観測衛星 IXPE への参加現状」, 日本天文学会 2018 年春季年会, 千葉大学, 2018 年 3 月.

三石郁之, 二村泰介, 清水貞行, 田原譲, 立花一志, 大西崇文, 玉川徹 ,「X 線偏光観測衛星 IXPE 搭載 X 線望遠鏡用受動型熱制御素子サーマルシールドの開発 (2) 」, 日本天文学会 2018 年春季年会, 千葉大学, 2018 年 3 月.

二村泰介, 清水貞行, 田原譲, 三石郁之, 立花一志, 大西崇文, 立花健二, 玉川徹 ,「IXPE 搭載 X 線望遠鏡用サーマルシールドの開発における環境試験 (2) 」, 日本天文学会 2018 年春季年会, 千葉大学, 2018 年 3 月.

若松孝也, 大久保美穂, 窪田恵, 周圓輝, 小田苑会, 早藤麻美, 中野俊男, 北口貴雄, 岩切渉, 玉川徹, 榎戸輝揚,「高エネルギー X 線の偏光を検出するマイクロパターン TPC 型偏光計の開発」, 日本天文学会 2018 年春季年会, 千葉大学, 2018 年 3 月.

石原雅士, 三石郁之, 中野慎也, 田村啓輔, 宮田喜久子, 立花一志, 西田和樹, 玉川徹, 岩切渉, Philip Kaaret,「軟 X 線全天観測超小型衛星 HaloSat の性能評価とサイエンス検討 (2) 」, 日本天文学会 2018 年春季年会, 千葉大学, 2018 年 3 月.

内田悠介 ほか SGD チーム,「ひとみ」コラボレーション,「X 線天文衛星「ひとみ」搭載 SGD によるかに星雲からの偏光ガンマ線の観測」, 日本天文学会 2018 年春季年会, 千葉大学, 2018 年 3 月.

楊冲, 深沢泰司, 岡部信広, 宮岡敬太, 北口貴雄 ,「XMM 衛星データを用いた MCXC J0157.4-0550 の 2 次元温度密度構造の解析」, 日本天文学会 2018 年春季年会, 千葉大学, 2018 年 3 月.

寺田幸功,「X 線衛星代替機 XARM における科学運用計画 」, 日本天文学会 2018 年春季年会, 千葉大学, 2018 年 3 月.

真貝寿明, 玉川徹, 野田篤司, 香取秀俊, 牧野淳一郎, 戎崎俊一,「光格子時計を用いた重力波検出法の提案」, 日本物理学会第 73 回年次大会, 東京理科大学, 2018 年 3 月.

武内陽子, 小宮一毅, 玉川徹 ,「放電抑制を目指した LTCC- GEM の開発 」, 日本物理学会第 73 回年次大会, 東京理科大学, 2018 年 3 月.

和田有希, 古田禄大, 榎戸輝揚, 中澤知洋, 湯浅孝行, 奥田和史, 牧島一夫, 佐藤光輝, 佐藤陽祐, 中野俊男, 鈴木寛大, �本大悟, 土屋晴文 ,「落雷による光核反応の発見：地上観測による中性子と陽電子の検出 」, 日本物理学会第 73 回年次大会, 東京理科大学, 2018 年 3 月.

古田禄大, 和田有希, 榎戸輝揚, 中澤知洋, 湯浅孝行, 奥田和史, 牧島一夫, 佐藤光輝, 佐藤陽祐, 中野俊男, �本大悟, 土屋晴文 ,「落雷による光核反応の発見：シミュレーションによるデータ解釈」, 日本物理学会第 73 回年次大会, 東京理科大学, 2018 年 3 月.

榎戸輝揚, 和田有希, 古田禄大, 中澤知洋, 湯浅孝行, 奥田和史, 牧島一夫, 佐藤光輝, 佐藤陽祐, 中野俊男, �本大悟, 土屋晴文 , 「雷雲ガンマ線の観測プロジェクトと雷での光核反応の検出」, 日本物理学会第 73 回年次大会, 東京理科大学, 2018 年 3 月.

北口貴雄,「光電子追跡型 X 線偏光計の機械学習による偏光応答モデルの構築」, 第 14 回 MPGD 研究会, 岩手, 2017 年 12 月.

北口貴雄,「X 線偏光計の光電子トラッキングへの機械学習の応用」, ASTRO-AI 研究会, 仙台, 2017 年 9 月).

中野俊男,「超新星残骸の観測と中性子星の磁場進化」, 日本 SKA パルサー・突発天体研究会, 茨城, 2018 年 1 月.

木村智樹,「リモートセンシングと探査機その場観測の連携で取り組む回転惑星磁気圏のリコネクションと粒子加速」, 磁気リコネクション・粒子加速勉強会, 東京大学, 2017 年 6 月.

木村智樹 ほか, "Brightening of Jupiter's aurora observed by the Hisaki satellite and Hubble Space Telescope during Juno's approach phase," 地球電磁気・地球惑星圏学会第 142 回総会, 京都大学, 2017 年 10 月.

木村智樹 ほか,「ひさき衛星による木星磁気圏観測とグローバル MHD シミュレーションの連携解析の概要」, 地球電磁気・地球惑星圏学会第 142 回総会, 京都大学, 2017 年 10 月.

玉川 徹,「ガス電子増幅フォイルの X 線検出器ならびに X 線発生装置への応用 」, 学振 186 委員会・第 24 回研究会, 東京大学, 2017 年 7 月.

RIBF Research Division
Astro-Glaciology Research Unit

Summary of Research Activities

Our Astro-Glaciology Research Unit promotes both experimental and theoretical studies to open up the new interdisciplinary research field of astro-glaciology, which combines astrophysics and glaciology.

On the experimental side, we analyze ice cores drilled at the Dome Fuji station, in Antarctica, in collaboration with the National Institute of Polar Research (NIPR, Tokyo). These ice cores are time capsules. In particular, the ice cores obtained at Dome Fuji are known to be unique because they contain much more information on conditions in the stratosphere than any other ice cores recovered from other locations in either hemisphere. This means that there are significant advantages in using Dome Fuji ice cores if we wish to study astronomical phenomena of the past. Since gamma-rays and high-energy protons that are emitted in certain astronomical processes affect the chemical and isotopic compositions in the stratosphere but not those in the troposphere, we have been measuring:

(1) Variations in the nitrate ion (NO_3^-) concentrations in the ice cores, in an effort to establish a new proxy for supernova explosions in our own galaxy as well as past solar activity.

(2) Variations in the water isotopes (^{18}O and ^2H) in the ice cores, in order to construct in more detail records of past changes in the temperature of the surface of the earth; and

(3) Variations in the nitrogen isotope (^{15}N) in the nitrates contained in the ice cores, in order to investigate the possibility of utilizing ^{15}N as a new and more stable proxy for galactic supernovae explosions and past solar activity.

In the case of items (1), (2), and (3), our analyses of Dome Fuji ice cores cover the most recent 2000 years. The temporal resolution of the results of our research is currently 12 months. We intend to compare the results obtained in item (1) with those in item (2), in order to understand better the relationships between solar activity and long-term changes in the temperature of the earth. The underlying assumptions in item (2) are already well accepted in glaciology. Item (3) refers to one of the very first measurements of ^{15}N concentrations in ice cores.

On the theoretical side, we are simulating numerically:

(4) Changes in the chemical composition of the stratosphere induced by gamma-rays and/or high-energy particles emitted from explosive astronomical phenomena, such as galactic supernovae and solar proton events; and

(5) The explosive nucleosynthesis (including the r-process, the rapid neutron capture process, which creates elements heavier than iron) that arises in the environment of core-collapse supernova explosions.

Items (4) and (5) in our list, the chemical composition of the stratosphere and explosive nucleosynthesis, are very important in solar–terrestrial research and nuclear astrophysics; furthermore, these simulations provide a theoretical support when considering the characteristics of supernova explosions and solar activity, as seen in our ice core data. These studies are also important because it is necessary to discount the effects of the meteorological noise.

It is noteworthy that the as yet not fully understood frequency of supernova explosions in our galaxy is crucial to an understanding of the r-process nucleosynthesis. The results obtained from items (1) and (3) are expected to reveal the average rate of supernova explosions in our galaxy during the past million years of ice deposition.

Members

Research Unit Leader (Lab. Head)
Yuko MOTIZUKI

Research & Technical Scientists
Kazuya TAKAHASHI (Senior Research Scientist)   Yoichi NAKAI (Senior Research Scientist)

Senior Visiting Scientist
Yasushige YANO (Nishina Memorial Foundation)

Visiting Scientists
Hideharu AKIYOSHI (Nat 'l Inst. for Environ. Studies)   Akira HORI (Kitami Inst. of Tech.)
Hideki MADOKORO (Mitsubishi Heavy Ind., Ltd.)   Kenji TANABE (Okayama Univ. of Sci.)

Part-time Workers
Yuma HASEBE   Satomi NEGISHI

Student Trainees
Yuma HASEBE (Saitama Univ.)

List of Publications & Presentations

Publications
[Journal]
(Original Papers) *Subject to Peer Review
E. Tsantini, T. Minami, K. Takahashi, and M. A. C. Ontiveros, "Analysis of sulfur isotopes to identify the origin of cinnabar in the Roman wall paintings from Badalona (Spain)," J. Arcaeological Science, **18**, 300−307 (2018).*

Y. Nakai, S. Tomita, R. Suganuma, S. Hattori, K. Kobayashi, Y. Shiina, S. Ishino, N. Yamamoto and K. Sasa, "Measurements for nitric acid formation in a humidified air by proton irradiation," RIKEN Accel. Prog. Rep. **51**, in press.*

M. Maruyama, M. Yumoto, K. Kase, K. Takahashi, Y. Nakai, S. Wada, Y. Yano and Y. Motizuki, "A prototype novel laser-melting sampler for analyzing ice cores with high depth resolution and high throughput," RIKEN Accel. Prog. Rep. **51**, in press.*

Kenji Tanabe and Yuko Motizuki, "R Aquarii and Gamma Ray Astronomy," Proceedings of Science (PoS), in press.*

Y. Motizuki, H. Motoyama, Y. Nakai, K. Suzuki, Y. Iizuka and K. Takahashi, "Overview of the chemical composition and characteristics of Na^+ and Cl^- distributions in shallow samples from Antarctic ice core DF01 (Dome Fuji) drilled in 2001," Geochemical J. **51**, 3, 293−298 (2017), doi:10.2343/geochemj.2.0458 (Open Access article).*

Y. Nakai, Y. Motizuki, M. Maruyama, Y. Hasebe, H. Akiyoshi, T. Imamura, "Box-model simulation for influence of solar proton events on the middle atmosphere," RIKEN Accel. Prog. Rep. **50**, 143 (2017).*

Y. Motizuki, H. Motoyama, Y. Nakai, K. Suzuki, Y. Iizuka and K. Takahashi, "Characteristics of Na^+ and Cl^- distributions in shallow samples from an Antarctic ice core DF01 (Dome Fuji) drilled in 2001: Result of strong atmospheric high-pressure blocking events?" RIKEN Accel. Prog. Rep. **50**, 144 (2017).*

Y. Motizuki, K. Takahashi, Y. Nakai, Y. Iizuka, K. Suzuki, H. Motoyama, "Overview of the chemical composition and characteristics of Na^+ and Cl^- distributions in samples from Antarctic ice core DF01 (Dome Fuji) drilled in 2001," RIKEN Accel. Prog. Rep. **49**, 133 (2017).*

Y. Nakai, Y. Motizuki, M. Maruyama, H. Akiyoshi, T. Imamura, "Box-model simulation for variation of atmospheric chemical composition caused by solar energetic particles," RIKEN Accel. Prog. Rep. **49**, 132 (2017).*

Y. Hasebe, Y. Motizuki, Y. Nakai, K. Takahashi, "Diagnose oscillation properties observed in an annual ice-core oxygen isotope record obtained from Dronning Maud Land, Antarctica," RIKEN Accel. Prog. Rep. **49**, 131 (2017).*

[Book]
(Original Papers) *Subject to Peer Review
望月優子, 佐藤勝彦, 『シリーズ現代の天文学第1巻　人類の住む宇宙　第2版』, pp. 99–144 (「第3章　元素の起源」), 岡村定矩他編, 日本評論社, 2017年3月.*

望月優子, 『Newtonライト　周期表』（協力）, ニュートンプレス, 2017年12月.

望月優子, 「ナイスステップな研究者から見た変化の新潮流」, 文部科学省機関紙STI Horizon, 2017年第3巻1号, pp. 17–20.*

Y. Motizuki, "Six Years of cross-disciplinary studies at the Astro-Glaciology Research Unit: Astronomical signatures in polar ice cores," RIKEN Accel. Prog. Rep. **50**, S-80 (2017).

Oral Presentations
[International Conference etc.]
(Invited talk) S. Hayashi and Y. Motizuki, "Mighty minority of women in Astronomy in Japan," IMU-led, ICSU-sponsored Workshop on "Gender gap in mathematical and other natural sciences", Taipeh, Taiwan, Nov. 7–8, 2017.

(Invited talk) K. Tanabe and Y. Motizuki, "Symbiotic Binary R Aquarii and Gamma-ray Astronomy," PALERMO WORKSHOP 2017 "The Golden Age of Cataclysmic Variables and Related Objects – Ⅳ," Palermo, Italy, Sep. 11–16, 2017.

(Invited talk) Yuko Motizuki, "Supernova signatures in polar ice cores," International Symposium on Origin of Matter and Evolution of Galaxies 2017 (OMEG 2017), Daejeon, Korea, June 27–30, 2017.

T. Minami, E. Tsantini, and K. Takahashi, "Effect of Gypsum on Sulfur Isotope Ratio of Vermilion Painted on Gypsum Wall," the Colloquium Spectroscopicum Internationale XL, Pisa, Italy, June, 2017.

(Invited talk) H. Akiyoshi, Y. Nakai, Y. Motizuki, T. Imamura, Y. Yamashita, "A preliminary result of NOx and ozone change simulation for a solar proton event using a nudged CCM and box chemistry model," Int. Workshop on Solar Cycle Activity and Impact on Climate for The 2nd PSTEP International symposium (PSTEP-2) , Kyoto, March 22, 2017.

[Domestic Conference]
（招待講演）秋吉英治, 中井陽一, 望月優子, 今村隆史, 山下陽介, 「化学気候モデルを用いた太陽プロトンイベントのオゾンと気候に及ぼす影響に関する研究 – 化学ボックスモデル＋3次元化学輸送モデルによるシミュレーション – 」, 名古屋, PSTEP報告会, 2018年3月29–30日.

高橋和也, 望月優子, 中井陽一, 「アイスコア詳細解析を見据えた硫黄同位体比分析の高感度化の試み」, 国立極地研究所研究集会「南極ドームふじ氷床深層アイスコアの解析による気候・環境変動の研究の新展開」, 立川, 2018年3月28–29日.

（招待講演）望月優子, 「アイスコアからさぐる天文・宇宙のサイエンス – 過去の超新星爆発と太陽活動, 地球への影響 – 」, 埼玉大学理学部物理量子力学特別講義, さいたま, 2018年1月22日.

（招待講演）望月優子, 「南極アイスコアからひもとく私たちの宇宙と地球の歴史」, 日本天文学会秋季年会公開講演会, 札幌, 2017年9月10日.

高橋和也,「同位体分析法から見た墳墓出土朱の産地変遷 – 大和政権による朱の政治的利用 – 」，日本分析化学会第77回分析化学討論会，京都市, 2017年5月.

（招待講演）望月優子,「宇宙と生命とのつながり〜生命と元素、星、宇宙のリズム〜」，理化学研究所 和光地区一般公開サイエンスレクチャー，和光, 2017 年 4 月 22 日.

望月優子,「日本天文学会における女性理事・委員の割合と今後について – 日本天文学会及び IAU における女性研究者割合の推移も含めて – 」，女性天文研究者の会，日本天文学会春季年会，福岡, 2017 年 3 月 18 日.

望月優子, 中井陽一, 高橋和也, ほかドームふじ氷床コア解析チーム,「南極氷床コアに刻まれた超新星カシオペアA の爆発年代」，日本天文学会春季年会，福岡, 2017年3月17日.

(招待講演) 望月優子, 埼玉大学理学部物理量子力学特別講義「アイスコアからさぐる天文・宇宙のサイエンス – 過去の超新星爆発と太陽活動、地球への影響 – 」，さいたま, 2017年1月23日.

(招待講演) 中井陽一, 第36回北海道大学低温科学研究所セミナー「太陽プロトン現象に誘起される地球中層大気の微量成分濃度変化 – ボックスモデルシミュレーションによるイオン化学反応の影響の研究 – 」，札幌, 2017年1月19日.

Poster Presentations

[International Conference etc.]

K. Takahashi, "New method for comprehensive detection of trace elements in environmental or biochemical materials using an electron-cyclotron-resonance ion-source mass spectrometer"(A poster paper), the 4th World Congress on Mass Spectrometry, London, UK, June 2017.

Y. Nakai, N. Watanabe, Y. Oba, "Hydrogenation of C_{60} deposited on a substrate under low temperature condition" (A poster paper), The 30th International Conference on Photonic, Electronic and Atomic Collisions, Cairns Australia, August 2017.

RIBF Research Division
Research Group for Superheavy Element

1. Abstract

The elements with their atomic number $Z > 103$ are called as trans-actinide or superheavy elements. The chemical properties of those elements have not yet been studied in detail. Those elements do not exist in nature. Therefore, they must be produced by artificially for the scientific study of those elements. In our laboratory, we have been studying the physical and chemical properties of the superheavy elements utilizing the accelerators in RIKEN and various methods of efficient production of the superheavy elements.

2. Major Research Subjects

(1) Search for new superheavy elements
(2) Decay spectroscopy of the heaviest nuclei
(3) Study of the chemical properties of the heaviest elements
(4) Study of the reaction mechanism of the fusion process (theory)

3. Summary of Research Activity

(1) Searching for new elements

To expand the periodic table of elements and the nuclear chart, we will search for new elements.

(2) Spectroscopic study of the nucleus of heavy elements

Using the high sensitivity system for detecting the heaviest element, we plan to perform a spectroscopic study of nuclei of the heavy elements.

(3) Chemistry of superheavy elements

Study of chemistry of the trans-actinide (superheavy element) has just started world-wide, making it a new frontier in the field of chemistry. Relativistic effects in chemical property are predicted by many theoretical studies. We will try to develop this new field.

(4) Study of a reaction mechanism for fusion process

Superheavy elements have been produced by complete fusion reaction of two heavy nuclei. However, the reaction mechanism of the fusion process is still not well understood theoretically. When we design an experiment to synthesize nuclei of the superheavy elements, we need to determine a beam-target combination and the most appropriate reaction energy. This is when the theory becomes important. We will try to develop a reaction theory useful in designing an experiment by collaborating with the theorists.

(5) Research Highlight

The discovery of a new element is one of the exciting topics both for nuclear physicists and nuclear chemists. The elements with their atomic number $Z > 103$ are called as trans-actinides or superheavy elements. The chemical properties of those elements have not yet been studied in detail. Since those elements do not exist in nature, they must be produced by artificially, by using nuclear reactions for the study of those elements. Because the production rate of atoms of those elements is extremely small, an efficient production and collection are key issues of the superheavy research. In our laboratory, we have been trying to produce new elements, studying the physical and chemical properties of the superheavy elements utilizing the accelerators in RIKEN.

Although the Research Group for Superheavy element has started at April 2013, the Group is a renewal of the Superheay Element Laboratory started at April 2006, based on a research group which belonged to the RIKEN accelerator research facility (RARF), and had studied the productions of the heaviest elements. The main experimental apparatus is a gas-filled recoil ion separator GARIS. The heaviest elements with their atomic numbers, 107 (Bohrium), 108 (Hassium), 109 (Meitnerium), 110 (Darmstadtium), 111 (Roentogenium), and 112 (Copernicium) were discovered as new elements at Helmholtzzentrum für Schwerionenforschung GmbH (GSI), Germany by using ^{208}Pb or ^{209}Bi based complete fusion reactions, so called "cold fusion" reactions. We have made independent confirmations of the productions of isotopes of 108th, 110th, 111th, and 112th elements by using the same reactions performed at GSI. After these work, we observed an isotope of the 113th element, ^{278}113, in July 2004, in April, 2005, and in August 2012. The isotope, ^{278}113, has both the largest atomic number, ($Z = 113$) and atomic mass number ($A = 278$) which have determined experimentally among the isotopes which have been produced by cold fusion reactions. We could show the world highest sensitivity for production and detection of the superheavy elements by these observations. Our results that related to ^{278}113 has been recognized as a discovery of new element by a Joint Working Party of the International Union of Pure and Applied Chemistry (IUPAC) and International Union of Pure and Applied Physics (IUPAP). Finally, we named the 113th element as "Nihonium".

We decided to make one more recoil separator GARIS-II, which has an acceptance twice as large as existing GARIS, in order to realize higher sensitivity. The design of GARIS-II has finished in 2008. All fabrication of the separator will be finished at the end of fiscal year 2008. It has been ready for operation after some commissioning works.

Preparatory work for the study of the chemical properties of the superheavy elements has started by using the gas-jet transport system coupled to GARIS. The experiment was quite successful. The background radioactivity of unwanted reaction products has been highly suppressed. Without using the recoil separator upstream the gas-jet transport system, large amount of unwanted radioactivity strongly prevents the unique identification of the event of our interest. This new technique makes clean and clear studies of chemistry of the heaviest elements promising.

The spectroscopic study of the heaviest elements has started by using alpha spectrometry. New isotope, ^{263}Hs ($Z = 108$), which has the smallest atomic mass number ever observed among the Hassium isotopes, had discovered in the study. New spectroscopic information for ^{264}Hs and its daughters have obtained also. The spectroscopic study of Rutherfordium isotope ^{261}Rf ($Z = 104$) has done and 1.9-s isomeric state has directly produced for the first time.

Preparatory works for the study of the new superheavy elements with atomic number 119 and 120 have started in 2013. We measured the reaction products of the ^{248}Cm (^{48}Ca, xn) $^{296-x}$Lv ($Z = 116$) previously studied by Frelov Laboratory of Nuclear Reaction, Russia, and GSI. We observed 5 isotopes in total which tentatively assigned to ^{293}Lv, and ^{292}Lv.

Members

Group Director
Kosuke MORITA

Visiting Scientist
Kunihiro FUJITA (Kyushu Univ.)

Student Trainees
Yuki YAMANO (Kyushu Univ.)   Kenyu WATANABE (Kyushu Univ.)

Publications
[Journal]

T. Tanaka, Y. Narikiyo, K. Morita, K. Fujita, D. Kaji, K. Morimoto, S. Yamaki, Y. Wakabayashi, K.Tanaka,M. Takeyama, A. Yoneda, H. Haba, Y. Komori, S. Yanou, B.J. Gall, Z. Asfari, H. Faure, H. Hasebe, M. Huang, J. Kanaya, M. Murakami, A. Yoshida, T. Yamaguchi, F. Tokanai, T. Yoshida, S. Yamamoto, Y. Yamano, K. Watanabe, S. Ishizawa, M. Asai, R. Aono, S. Goto, K. Katori, and K. Hagino, "Determination of fusion barrier distributions from quasielastic scattering cross sections towards superheavy nuclei synthesis," J. Phys. Soc. Jpn. **87**, 014201 (2018).

D. Kaji, K. Morimoto, H. Haba, Y. Wakabayashi, M. Takeyama, S. Yamaki, Y. Komori, S. Yanou, S. Goto, and K. Morita, "Decay measurement of ^{283}Cn produced in the ^{238}U(^{48}Ca, 3n) reaction using GARIS-II," J. Phys. Soc. Jpn. **86**, 085001 (2017).

D. Kaji, K. Morita, K. Morimoto, H. Haba, M. Asai, K. Fujita, Z. Gan, H. Geissel, H. Hasebe, S. Hofmann, M. Huang, Y. Komori, L. Ma, J. Maurer, M. Murakami, M. Takeyama, F. Tokanai, T. Tanaka, Y. Wakabayashi, T. Yamaguchi, S. Yamaki, and A. Yoshida, "Study of the Reaction ^{48}Ca + ^{248}Cm → ^{296}Lv* at RIKEN-GARIS," J. Phys. Soc. Jpn. **86**, 034201 (2017).

[和文]

森本幸司,「新元素『ニホニウム』の発見と意義」, 繊維学会誌 pp. 83 第 74 巻 3 号, 2018 年 3 月.

Oral Presentations
[International Conference etc.]

K. Morimoto, "Status and future plan of SHE experiment at RIKEN," 3rd International Symposium on Super-Heavy Elements (SHE2017), Poland, September 10, 2017.

K. Morimoto, "Discovery of new element 'Nihonium'," International Symposium on Radiation Detectors and Their Uses (ISRD2018), Tsukuba Univ., January 23, 2018.

D. Kaji, "Hot fusion study using a new separator GARIS-II," 3rd International Symposium on Super-Heavy Elements (SHE2017), Poland, September 10, 2017.

[Domestic Conference]

T. Niwase, M. Wada, P. Schury, Y. Ito, S. Kimura, M. Rosenbusch, D. Kaji, K. Morimoto, H. Haba, S. Yamaki, T. Tanaka, K. Morita, A. Takamine, H. Miyatake, Y. Hirayama, Y. Watanabe, J. Y. Moon, M. Mukai, H. Wollnik, "High-precision mass measurements of short-lived nuclei with MRTOF+GARIS-II, " 第 61 回放射化学討論会, Tsukuba University Japan, September 6–8 2017.

T. Niwase, M. Wada, P. Schury, Y. Ito, M. Rosenbusch, D. Kaji, K. Morimoto, H. Haba, S. Ishizawa, K. Morita, H. Wollnik "Development of Alpha-ToF detector for mass measurements of superheavy nuclides," 123th Annual Meeting of Kyushu Branch of JPS, Kagoshima University Japan, December 6 2017.

T. Niwase, M. Wada, P. Schury, Y. Ito, M. Rosenbusch, D. Kaji, K. Morimoto, H. Haba, S. Ishizawa, K. Morita, H. Wollnik, "Development Alpha-ToF detector for high precision mass spectrometry of superheavy nuclei," JPS 73th Annual Meeting (2018), Tokyo University of Science Japan, March 22–25 2018.

森本幸司, 「日本初、新元素 "ニホニウム" の発見」, 繊維学会年次大会, 江戸川区タワーホール船堀, 2017 年 6 月 7 日.

森本幸司, 「新元素ニホニウムはいかにして発見されたのか」, 第 34 回物理教育研究大会, 甲南大学, 2017 年 8 月 11 日.

加治大哉, 「スパッタ法による厚い金属ウラン標的の調整と照射試験」第 61 回放射化学討論会, 2017 年 9 月 6 日.

[Others]

森本幸司, 「サイエンスアゴラ in KOBE 〜科学って本当に大事？〜新元素『ニホニウム』の発見」神戸大学統合研究拠点コンベンションホール, 神戸, 2017 年 10 月 14 日.

森本幸司, 「ニホニウム 113 番元素の発見」, 図書館まつり, 和光市立図書, 2017 年 10 月 28 日.

森本幸司, 「新元素にニホニウムはいかにして検出されたのか」, 放射線科学とその応用第 186 委員会, 東北大学片平ホール, 2018 年 1 月 11 日.

森本幸司, 「新元素"ニホニウムの発見"」, 滋賀大学教育学部, 2018 年 2 月 28 日.

K. Morimoto, "Discovery of new chemical element Nihonium," The 112th ISAS Space Science Colloquim, Sagamihara, ISAS/JAXA, March 28, 2018.

森田浩介,「新元素の探索」, 別府市鶴見丘高等学校, 2017 年 9 月 2 日.
森田浩介,「新元素の探索」, 日本甲状腺学会特別講演, 別府市, 2017 年 10 月 7 日.
森田浩介,「新元素の探索」, アカデミックフェスティバル, 九州大学椎木講堂, 2017 年 10 月 21 日.

RIBF Research Division
Research Group for Superheavy Element
Superheavy Element Production Team

1. Abstract

The elements with their atomic number $Z > 103$ are called as trans-actinide or superheavy elements. The chemical properties of those elements have not yet been studied in detail. Those elements do not exist in nature. Therefore, they must be produced by artificially for the scientific study of those elements. In our laboratory, we have been studying the physical and chemical properties of the superheavy elements utilizing the accelerators in RIKEN and various methods of efficient production of the superheavy elements.

2. Major Research Subjects

(1) Search for new supreheavy elements
(2) Decay spectroscopy of the heaviest nuclei
(3) Study of the chemical properties of the heaviest elements
(4) Study of the reaction mechanism of the fusion process (theory)

Summary of Research Activity

(1) Searching for new elements

To expand the periodic table of elements and the nuclear chart, we will search for new elements.

(2) Spectroscopic study of the nucleus of heavy elements

Using the high sensitivity system for detecting the heaviest element, we plan to perform a spectroscopic study of nuclei of the heavy elements.

(3) Chemistry of superheavy elements

Study of chemistry of the trans-actinide (superheavy element) has just started world-wide, making it a new frontier in the field of chemistry. Relativistic effects in chemical property are predicted by many theoretical studies. We will try to develop this new field.

(4) Study of a reaction mechanism for fusion process

Superheavy elements have been produced by complete fusion reaction of two heavy nuclei. However, the reaction mechanism of the fusion process is still not well understood theoretically. When we design an experiment to synthesize nuclei of the superheavy elements, we need to determine a beam-target combination and the most appropriate reaction energy. This is when the theory becomes important. We will try to develop a reaction theory useful in designing an experiment by collaborating with the theorists.

Members

Team Leader

Kosuke MORITA (concurrent; Group Director, Research Group for Superheavy Element)

Research & Technical Scientist

Kouji MORIMOTO (Senior Research Scientist, concurrent; Team Leader, Superheavy Element Device Development Team)

Nishina Center Research Scientist

Daiya KAJI (concurrent; Superheavy Element Device Development Team)

Nishina Center Technical Scientist-Consultant

Akira YONEDA

Research Consultant

Kenji KATORI

Junior Research Associate

Taiki TANAKA(Kyushu Univ.)

Visiting Scientists

Hiroyuki KOURA (JAEA)
Benoit Jean-Paul GALL (Strasbourg Univ.)
Olivier DORVOUX (Strasbourg Univ.)

Marc ASFARI (Institut Pluridisciplinaire Hubert Curien)
Mirei TAKEYAMA (Yamagata Univ.)

Student Trainees

Toshitaka NIWASE (Kyushu Univ.)　　　　　　　　　　　　Shun MITSUOKA(Kyushu Univ.)

Takeshi HIRANO (Kyushu Univ.)　　　　　　　　　　　　　Pierre BRIONNET (Strasbourg University)

Publications

[Journal]

T. Tanaka, Y. Narikiyo, K. Morita, K. Fujita, D. Kaji, K. Morimoto, S. Yamaki, Y. Wakabayashi, K.Tanaka,M. Takeyama, A. Yoneda, H. Haba, Y. Komori, S. Yanou, B.J. Gall, Z. Asfari, H. Faure, H. Hasebe, M. Huang, J. Kanaya, M. Murakami, A. Yoshida, T. Yamaguchi, F. Tokanai, T. Yoshida, S. Yamamoto, Y. Yamano, K. Watanabe, S. Ishizawa, M. Asai, R. Aono, S. Goto, K. Katori, and K. Hagino, "Determination of fusion barrier distributions from quasielastic scattering cross sections towards superheavy nuclei synthesis," J. Phys. Soc. Jpn. **87**, 014201 (2018).

D. Kaji, K. Morimoto, H. Haba, Y. Wakabayashi, M. Takeyama, S. Yamaki, Y. Komori, S. Yanou, S. Goto, and K. Morita, "Decay Measurement of ^{283}Cn Produced in the ^{238}U(^{48}Ca, 3n) Reaction Using GARIS-II," J. Phys. Soc. Jpn. **86**, p.085001 (2017).

D. Kaji, K. Morita, K. Morimoto, H. Haba, M. Asai, K. Fujita, Z. Gan, H. Geissel, H. Hasebe, S. Hofmann, M. Huang, Y. Komori, L. Ma, J. Maurer, M. Murakami, M. Takeyama, F. Tokanai, T. Tanaka, Y. Wakabayashi, T. Yamaguchi, S. Yamaki, and A. Yoshida, "Study of the reaction ^{48}Ca + ^{248}Cm → ^{296}Lv* at RIKEN-GARIS," J. Phys. Soc. Jpn. **86**, 034201 (2017).

[和文]

森本幸司,「元素『ニホニウム』の発見と意義」, 維学会誌 pp. 83 第 74 巻 3 号, 2018 年 3 月.

Oral Presentations

[International Conference etc.]

K. Morimoto, "Status and future plan of SHE experiment at RIKEN," 3rd International Symposium on Super-Heavy Elements (SHE2017), Poland, September 10, 2017.

K. Morimoto, "Discovery of new element 'Nihonium'," International Symposium on Radiation Detectors and Their Uses (ISRD2018), Tsukuba Univ., January 23, 2018.

D. Kaji, "Hot fusion study using a new separator GARIS-II," 3rd International Symposium on Super-Heavy Elements (SHE2017), Poland, September 10, 2017.

[Domestic Conference]

T. Niwase, M. Wada, P. Schury, Y. Ito, S. Kimura, M. Rosenbusch, D. Kaji, K. Morimoto, H. Haba, S. Yamaki, T. Tanaka, K. Morita, A. Takamine, H. Miyatake, Y. Hirayama, Y. Watanabe, J. Y. Moon, M. Mukai, H. Wollnik, "High-precision mass measurements of short-lived nuclei with MRTOF+GARIS-II, " 第 61 回放射化学討論会, Tsukuba University Japan, September 6–8 2017.

T. Niwase, M. Wada, P. Schury, Y. Ito, M. Rosenbusch, D. Kaji, K. Morimoto, H. Haba, S. Ishizawa, K. Morita, H. Wollnik, "Development of Alpha-ToF detector for mass measurements of superheavy nuclides," 123th Annual Meeting of Kyushu Branch of JPS, Kagoshima University Japan, December 6 2017.

T. Niwase, M. Wada, P. Schury, Y. Ito, M. Rosenbusch, D. Kaji, K. Morimoto, H. Haba, S. Ishizawa, K. Morita, H. Wollnik, "Development Alpha-ToF detector for high precision mass spectrometry of superheavy nuclei," JPS 73th Annual Meeting (2018), Tokyo University of Science Japan, March 22–25 2018.

森本幸司,「日本初、新元素 "ニホニウム" の発見」, 繊維学会年次大会, 江戸川区タワーホール船堀, 2017 年 6 月 7 日.

森本幸司,「新元素ニホニウムはいかにして発見されたのか」, 第 34 回物理教育研究大会, 甲南大学, 2017 年 8 月 11 日.

加治大哉,「スパッタ法による厚い金属ウラン標的の調整と照射試験」第 61 回放射化学討論会, 2017 年 9 月 6 日.

[Others]

森本幸司,「サイエンスアゴラ in KOBE ～科学って本当に大事？～新元素『ニホニウム』の発見」, 神戸大学統合研究拠点コンベンションホール, 神戸, 2017 年 10 月 14 日.

森本幸司,「ニホニウム 113 番元素の発見」図書館まつり, 和光市立図書館, 2017 年 10 月 28 日.

森本幸司,「新元素にニホニウムはいかにして検出されたのか」放射線科学とその応用第 186 委員会, 東北大学片平ホール, 2018 年 1 月 11 日.

森本幸司,「新元素"ニホニウムの発見"」, 滋賀大学教育学部, 2018 年 2 月 28 日.

K. Morimoto, "Discovery of new chemical element Nihonium," The 112th ISAS Space Science Colloquim, Sagamihara, ISAS/JAXA, March 28, 2018.

森田浩介,「新元素の探索」, 別府市鶴見丘高等学校, 2017 年 9 月 2 日.

森田浩介,「新元素の探索」, 日本甲状腺学会特別講演, 別府市, 2017 年 10 月 7 日.

森田浩介,「新元素の探索」, アカデミックフェスティバル, 九州大学椎木講堂, 2017 年 10 月 21 日.

RIBF Research Division
Research Group for Superheavy Element
Superheavy Element Device Development Team

1. Abstract

A gas-filled recoil ion separator has been used as a main experimental device for the study of superheavy elements. This team is in charge of maintain, improve, develop and operate the separators and related devices. There are two gas-filled recoil ion separators installed at RILAC experimental hall. One is GARIS that is designed for symmetric reaction such as cold-fusion reaction, and the other is newly developed GARIS-II that is designed for an asymmetric reaction such as hot-fusion reaction. New elements ^{278}Nh were produced by ^{70}Zn + ^{209}Bi reaction using GARIS. Further the new element search $Z > 118$ are preparing by using GARIS-II.

2. Major Research Subjects

(1) Maintenance of GARIS and development of new gas-filled recoil ion separator GARIS-II.
(2) Maintenance and development of detector and DAQ system for GARIS and GARIS-II.
(3) Maintenance and development of target system for GARIS and GARIS-II.

3. Summary of Research Activity

The GARIS-II is newly developed which has an acceptance twice as large as existing GARIS, in order to realize higher sensitivity for asymmetric reaction such as a hot fusion reaction. After some commissioning works, the GARIS-II has been ready for new element research. We will also offer user-support if a researcher wishes to use the devices for his/her own research program.

Members

Team Leader
Kouji MORIMOTO

Nishina Center Research Scientist
Daiya KAJI

Fixed-term Employee
Yuta ITO

Junior Research Associate
Sayaka YAMAKI (Saitama Univ.)

Visiting Scientists
Fuyuki TOKANAI (Yamagata Univ.)   Katsuhisa NISHIO (JAEA)
Eiji IDEGUCHI (Osaka Univ. RCNP)   Yuta ITO (McGill University)

Student Trainees
Satoshi ISHIZAWA (Yamagata Univ.)   Keigo BANDO(Kyushu Univ.)
Ryutaro ITO (Yamagata Univ.)   Takao SAITO (Kyushu Univ.)
Yuichiro INOMATA (Yamagata Univ.)   Kenta MANABE (Kyushu Univ.)

Publications

[Journal]

T. Tanaka, Y. Narikiyo, K. Morita, K. Fujita, D. Kaji, K. Morimoto, S. Yamaki, Y. Wakabayashi, K.Tanaka,M. Takeyama, A. Yoneda, H. Haba, Y. Komori, S. Yanou, B.J. Gall, Z. Asfari, H. Faure, H. Hasebe, M. Huang, J. Kanaya, M. Murakami, A. Yoshida, T. Yamaguchi, F. Tokanai, T. Yoshida, S. Yamamoto, Y. Yamano, K. Watanabe, S. Ishizawa, M. Asai, R. Aono, S. Goto, K. Katori, and K. Hagino, "Determination of fusion barrier distributions from quasielastic scattering cross sections towards superheavy nuclei synthesis," J. Phys. Soc. Jpn. **87**, 014201 (2018).

D. Kaji, K. Morimoto, H. Haba, Y. Wakabayashi, M. Takeyama, S. Yamaki, Y. Komori, S. Yanou, S. Goto, and K. Morita, "Decay measurement of ^{283}Cn Produced in the ^{238}U(^{48}Ca, 3n) reaction using GARIS-II," J. Phys. Soc. Jpn. **86**, 085001 (2017).

D. Kaji, K. Morita, K. Morimoto, H. Haba, M. Asai, K. Fujita, Z. Gan, H. Geissel, H. Hasebe, S. Hofmann, M. Huang, Y. Komori, L. Ma, J. Maurer, M. Murakami, M. Takeyama, F. Tokanai, T. Tanaka, Y. Wakabayashi, T. Yamaguchi, S. Yamaki, and A. Yoshida, "Study of the reaction ^{48}Ca + ^{248}Cm → ^{296}Lv* at RIKEN-GARIS," J. Phys. Soc. Jpn. **86**, 034201 (2017).

[和文]

森本幸司,「元素『ニホニウム』の発見と意義」, 維学会誌 pp. 83 第 74 巻 3 号, 2018 年 3 月.

Oral Presentations

[International Conference etc.]

K. Morimoto, "Status and future plan of SHE experiment at RIKEN," 3rd International Symposium on Super-Heavy Elements (SHE2017), Poland, September 10, 2017.

K. Morimoto, "Discovery of new element 'Nihonium'," International Symposium on Radiation Detectors and Their Uses (ISRD2018), Tsukuba Univ., January 23, 2018.

D. Kaji, "Hot fusion study using a new separator GARIS-II," 3rd International Symposium on Super-Heavy Elements (SHE2017), Poland, September 10, 2017.

[Domestic Conference]

T. Niwase, M. Wada, P. Schury, Y. Ito, S. Kimura, M. Rosenbusch, D. Kaji, K. Morimoto, H. Haba, S. Yamaki, T. Tanaka, K. Morita, A. Takamine, H. Miyatake, Y. Hirayama, Y. Watanabe, J. Y. Moon, M. Mukai, H. Wollnik, "High-precision mass measurements of short-lived nuclei with MRTOF+GARIS-II," 第 61 回放射化学討論会, Tsukuba University Japan, September 6–8 2017.

T. Niwase, M. Wada, P. Schury, Y. Ito, M. Rosenbusch, D. Kaji, K. Morimoto, H. Haba, S. Ishizawa, K. Morita, H. Wollnik, "Development of Alpha-ToF detector for mass measurements of superheavy nuclides," 123th Annual Meeting of Kyushu Branch of JPS, Kagoshima University Japan, December 6 2017.

T. Niwase, M. Wada, P. Schury, Y. Ito, M. Rosenbusch, D. Kaji, K. Morimoto, H. Haba, S. Ishizawa, K. Morita, H. Wollnik, "Development Alpha-ToF detector for high precision mass spectrometry of superheavy nuclei," JPS 73th Annual Meeting (2018), Tokyo University of Science Japan, March 22–25 2018.

森本幸司,「日本初、新元素 "ニホニウム" の発見」, 繊維学会年次大会, 江戸川区タワーホール船堀, 2017 年 6 月 7 日.

森本幸司,「新元素ニホニウムはいかにして発見されたのか」, 第 34 回物理教育研究大会, 甲南大学, 2017 年 8 月 11 日.

加治大哉,「スパッタ法による厚い金属ウラン標的の調整と照射試験」第 61 回放射化学討論会, 2017 年 9 月 6 日.

[Others]

森本幸司,「サイエンスアゴラ in KOBE 〜科学って本当に大事？〜新元素『ニホニウム』の発見」, 神戸大学統合研究拠点コンベンションホール, 神戸, 2017 年 10 月 14 日.

森本幸司,「ニホニウム 113 番元素の発見」図書館まつり, 和光市立図書館, 2017 年 10 月 28 日.

森本幸司,「新元素にニホニウムはいかにして検出されたのか」放射線科学とその応用第 186 委員会, 東北大学片平ホール, 2018 年 1 月 11 日.

森本幸司,「新元素"ニホニウムの発見"」, 滋賀大学教育学部, 2018 年 2 月 28 日.

K. Morimoto, "Discovery of new chemical element Nihonium," The 112th ISAS Space Science Colloquim, Sagamihara, ISAS/JAXA, March 28, 2018.

森田浩介,「新元素の探索」, 別府市鶴見丘高等学校, 2017 年 9 月 2 日.

森田浩介,「新元素の探索」, 日本甲状腺学会特別講演, 別府市, 2017 年 10 月 7 日.

森田浩介,「新元素の探索」, アカデミックフェスティバル, 九州大学椎木講堂, 2017 年 10 月 21 日.

RIBF Research Division
Nuclear Transmutation Data Research Group

1. Abstract

The disposal of high-level radioactive wastes from nuclear power plants is a problem considered to be one of the most important issues at both national and international levels. As a fundamental solution to the problem, the establishment of nuclear transmutation technology where long-lived nuclides can be changed to short-lived or stable ones will be vital. Progress in R & D in the transmutation of long-lived fission products (LLFP) in the nuclear wastes however, has been slow. Our group aims to obtain reaction data of LLFP at RIBF and other facilities which may lead to a new discovery and invention for peaceful use of nuclear power and the welfare of humanity.

2. Major Research Subjects

The Group is formed by three research teams. The first two Teams, "Fast RI Data Team" and "Slow RI Data Team," are in charge of proton- and deuteron-induced reaction data for LLFP in inverse kinematics at RIBF. The third Team "Muon Data Team" is to obtain muon capture data of LLFP at muon facilities. All the teams are focusing to obtain high-quality data which are essentially necessary to establish reliable reaction models. Each team has its own subjects and promotes LLFP reaction programs based on their large experiences, techniques and skills.

3. Summary of Research Activity

In 2014, all the teams polished up experimental strategies, formed collaboration and prepared experiments. Physics runs for spallation reaction and Coulomb breakup reaction with the beams at 100−200 MeV/nucleon were successfully organized by using the ZeroDegree and SAMURAI spectrometers at RIBF in 2015−2016. In 2017, a physics run with an energy-decelerated radioactive beam was conducted under collaboration with CNS, Univ. of Tokyo. The muon program started at J-PARC and RCNP (Osaka University) in spring 2016. A neutron detection array was newly developed to measure evaporation neutrons after muon capture process, and was utilized at an experiment at RCNP in February 2017. In 2017 and 2018, experiments were organized at both RAL and RCNP to have complete sets of the muon data for a specific LLFP nuclide.

Members

Group Director
Hiroyoshi SAKURAI (concurrent: Chief Scientist, RI Physics Lab.)

Assitant
Izumi YOSHIDA
Asako TAKAHASHI

List of Publications & Presentations

[Others]
櫻井博儀,「核廃棄物の核変換処理と核反応率」, パリティ, 2018 年 1 月.

Oral Presentations
[International Conference etc.]
H. Sakurai, "Reduction and resource recycling of high-level radioactive wastes through nuclear transmutation – Accelerator transmutation system and related developments for element technology," Global 2017 International Nuclear Fuel Cycle Conference, Seoul, Korea, Sept. 2017.
H. Sakurai, "Nuclear data of long-living products," Korea-Japan Workshop on P&T for Long-living Products, Wako, Japan, January 2018.
H. Sakurai, "Nuclear reactions with LLFP in high level radioactive waste," The 7the Yamada Workshop on RI Science Evolution 2018 (RISE18), Osaka, Japan, March 2018.

[Domestic Conference]
櫻井博儀, "Overview of ImPACT Program," ImPACT-OEDO Workshop, Wako, Japan, July 13, 2017.
櫻井博儀,「LLFP 安定核種化・短寿命化のための核変換法の開発 (9) 負ミュオン捕獲反応」, 日本原子力学会, 札幌, 2017 年 9 月 13 日.
櫻井博儀,「LLFP 核変換のための基礎データ取得結果紹介」, ImPACT 加速器検討ワークショップ, 市ケ谷, 2018 年 1 月.
櫻井博儀,「核変換－放射性物質を高効率で短寿命・無害化する」, ImPACT 公開シンポジウム, 市ケ谷, 2018 年 3 月.

[報道]
日経産業新聞, 先端技術, 2017 年 11 月 21 日, 朝刊 6 面.
日経産業新聞, 解剖　先端拠点, 2018 年 2 月 21 日, 朝刊 7 面.

RIBF Research Division
Nuclear Transmutation Data Research Group
Fast RI Data Team

1. Abstract

Fast RI team aims at obtaining and accumulating the cross section data for long lived fission products (LLFPs) in order to explore the possibility of using accelerator for nuclear transmutation.

LLFPs as nuclear waste have been generated continuously in nuclear power plants for wealth for human lives, while people noticed the way of disposal has not necessarily been established, especially after the Fukushima Daiichi power plant disaster. One of the ways to reduce the amount of LLFP or to recover them as recycled resources is nuclear transmutation technique.

RIBF facility has a property to generate such LLFP as a secondary beam and the beam species are identified by event by event. Utilizing the property, absolute values of the cross section of various reactions on LLFPs are measured and accumulated as database.

2. Major Research Subjects

1) Measurement of reaction products by the interaction of LLFPs with proton, deuteron, and photon to explore candidate reactions for transmutation of LLFPs.
2) Evaluation of the cross section data for the neutron induced reactions from the obtained data.

3. Summary of Research Activity

1) Acting as collaboration hub on many groups which plan to take data using fast RI beam in RIBF facility.
2) Concentrating on take data for proton and deuteron induced spallation reactions with inverse kinematics.
3) Accumulating the cross section data and evaluating them as evaluated nuclear data.
4) Evaluating cross section of neutron induced reaction on LLFP by collaborating with the nuclear model calculation and evaluation group.

Members

Team Leader
　Hideaki OTSU (Concurrent: Team Leader, SAMURAI Team)

Technical Staff I
　Nobuyuki CHIGA

Visiting Scientists
　Takashi TERANISHI (Kyushu Univ.)

Student Trainees

Keita NAKANO (Kyushu Univ.)	Akira HOMMA (Niigata Univ.)
Ayaka IKEDA (Niigata Univ.)	Naoto KANDA (Niigata Univ.)
Kazuya CHIKAATO (Niigata Univ.)	Tatsuya YAMAMOTO (Miyazaki Univ.)
Shouhei ARAKI (Kyushu Univ.)	Kotaro IRIBE (Kyushu Univ.)
Kenji NISHIZUKA (Niigata Univ.)	Hiroya YOSHIDA (Kyushu Univ.)
Junki SUWA (Kyushu Univ.)	
Yoshiki SOUDO（Miyazaki Univ.）	

List of Publications & Presentations

Publications

[Journal]
(Original Papers)

S. Kawase, K. Nakano, Y. Watanabe, H. Wang, H. Otsu, H. Sakurai (other 43 members)，"Study of proton- and deuteron-induced spallation reactions on the long-lived fission product ^{93}Zr at 105 MeV/nucleon in inverse kinematics," Prog. Theor. Exp. Phys. **2017**, 093D03 (2017).

(Proceedings)

H. Wang, H. Otsu, H. Sakurai *et al*., "Spallation reaction study for fission products in nuclear waste: Cross section measurements for ^{137}Cs, ^{90}Sr and ^{107}Pd on proton and deuteron," EPJ Web of Conf. **146**, 09022 (2017).

H. Wang, H. Otsu, H. Sakurai *et al*., "Spallation reaction study for the long-lived fission products in nuclear waste: Cross section measurements for ^{137}Cs, ^{90}Sr and ^{107}Pd using inverse kinematics method," Energy Procedia **131**, 127 (2017).

X. Sun, H. Wang, H. Otsu *et al*., "Reaction study of ^{136}Xe on proton, deuteron and carbon at 168 AMeV," Proceeding of ND2017, November, 2017.

S. Kawase, Y. Watanabe, H. Wang, H. Otsu, H. Sakurai *et al*., "Cross section measurement of residues produced in proton- and deuteron-induced spallation reactions on ^{93}Zr at 105 MeV/u using the inverse kinematics method," EPJ Web of Conf. **146**, 10.1051/epjconf/201714611046, 11046 (2017).

Oral Presentations

[International Conference]

H. Otsu (Invited), "Nuclear reaction data of long-lived fission product," Ito International Research Center (IIRC) Symposium "Perspectives of the Physics of Nuclear Structure," Tokyo, Japan, November, 2017.

S. Kawase, Y. Watanabe, K. Nakano, H. Wang, H. Otsu, H. Sakura, S. Takeuchi, T. Nakamura, "Reduction and resource recycling of high-level radioactive wastes through nuclear transmutation − Proton- and deuteron-induced spallation reactions on long-lived fission products," International Nuclear Fuel Cycle Conference (GLOBAL2017), September 2017.

[Domestic Conference]

H, Wang (Invited), "Systematic study for the spallation reaction of ^{107}Pd at different energies," ImPACT-OEDO Workshop, Wako, Saitama, Japan, July 2017.

X. Sun, "Reaction study of ^{136}Xe on proton, deuteron and carbon at 168 AMeV," ImPACT-OEDO Workshop, Wako, Saitama, Japan, July 2017.

武内聡,「$^{79,\,80}$Se, $^{93,\,94}$Zr, $^{107,\,108}$Pd のクーロン分解反応実験」, ImPACT-OEDO workshop, Wako, Saitama, Japan, July 2017.

親跡和弥, 武智麻耶 他 29 名,「^{90}Sr および ^{89}Rb, ^{88}Kr, ^{91}Y の相互作用断面積測定」, 日本物理学会秋季大会, 宇都宮, 2017 年 9 月.

平山晃大, 中村隆司 他 12 名, ImPACT-RIBF Collaboration,「^{79}Se,^{80}Se のクーロン分解反応断面積」, 日本物理学会秋季大会, 宇都宮, 2017 年 9 月.

大津秀暁 他 3 名,「理研 RIBF での LLFP 断面積測定」, 日本原子力学会秋の大会, 札幌, 2017 年 9 月.

川瀬頌一郎 他 9 名,「^{93}Zr に対する 200 MeV/u 陽子・重陽子入射同位体生成反応の断面積測定」, 日本原子力学会秋の大会, 札幌, 2017 年 9 月.

中野敬太 他 9 名,「^{93}Zr に対する 50 MeV/u 陽子・重陽子入射同位体生成反応の断面積測定」, 日本原子力学会秋の大会, 札幌, 2017 年 9 月.

武内聡 他 5 名,「^{79,80}Se および ^{93,94}Zr のクーロン分解反応による光吸収断面積の導出」, 日本原子力学会秋の大会, 札幌, 2017 年 9 月.

武内聡 他 6 名, ImPACT-RIBF Collaboration,「クーロン分解反応による ^{79,80}Se および ^{93,94}Zr の光吸収断面積導出」, 日本物理学会第 73 回年次大会, 野田, 2018 年 3 月.

道正新一郎 他 8 名, ImPACT-RIBF Collaboration,「OEDO ビームラインの開発および 2017 年度実験」, 日本原子力学会年会, 大阪, 2018 年 3 月.

堂園昌伯 他 8 名, ImPACT-RIBF Collaboration,「低速 RI ビームを用いた ^{107}Pd, ^{93}Zr の陽子および重陽子誘起反応測定」, 日本原子力学会年会, 大阪, 2018 年 3 月.

武内聡 他 5 名,「$^{79,\,80}$Se および, $^{93,\,94}$Zr のクーロン分解反応断面積の統計崩壊モデルを使った解析」, 日本原子力学会年会, 大阪, 2018 年 3 月.

諏訪純貴 他 9 名,「Y, Zr, Nb 同位体に対する 100 MeV/u 陽子・重陽子入射反応の同位体生成断面積測定」, 日本原子力学会年会, 大阪, 2018 年 3 月.

千賀信幸,「低エネルギー中重核用イオンチェンバーの設計・製作」, 平成 29 年度核融合科学研究所技術研究会, 岐阜, 2018 年 3 月.

Poster Presentations

[International Conference]

K. Nakano, "Measurement of isotopic production cross sections of proton- and deuteron-induced reactions on 93Zr at 50 MeV/nucleon in inverse kinematics," The 9th Korea-Japan Joint Summer School on Accelerator and Beam Science, Nuclear Data, Radiation Engineering and Reactor Physics, Daejeon, Korea, Aug. 2017.

[Domestic Conference]

X. Sun, "Reaction study of ^{136}Xe on proton, deuteron and carbon at 168 AMeV," Symposium on Nuclear Data, Nuclear Data Division, Atomic Energy Society of Japan, Ibaragi, Japan, November 2017.

三木晴瑠,「^{238}U の飛行核分裂反応における低速 ^{107}Pd および ^{77}Se のアイソマー比の測定」, 日本物理学会第 73 回年次大会, 野田, 2018 年 3 月.

Master Thesis

諏訪純貴,「陽子・重陽子に対する ^{93}Zr 入射核破砕反応による核種生成実験データの予備解析」, 九州大学大学院総合理工学府先端エネルギー理工学専攻.

平山晃大,「^{79,80}Se のクーロン分解反応断面積測定」, 東京工業大学理学院物理学系.

Bachelor Thesis

三木晴瑠,「^{238}U の飛行核分裂反応における低速 ^{77}Se および ^{107}Pd のアイソマー比測定」, 東京工業大学.

受賞

H. Wang, 9th RIKEN Research Incentive Awards, 2017.

川瀬頌一郎,「^{93}Zr に対する 200 MeV/u 陽子・重陽子入射反応による同位体生成断面積測定」, 2017 年核データ研究会 最優秀ポスター賞.

中野敬太, 日本原子力学会 2017 年春の年会 原子力・放射線分野を学び修めた学業優秀な学生に対する表彰 フェロー賞.

中野敬太,「長寿命核分裂生成物 Zr-93 の短寿命化・再資源化に向けた核反応データ測定」, 九州大学エネルギーウィーク 2018 優秀賞.

RIBF Research Division
Nuclear Transmutation Data Research Group
Slow RI Data Team

1. Abstract

This team is in charge of the development of low-energy RI beams of long-lived fission fragments (LLFP) from the ^{238}U by means of degrading the energy of beams produced by the BigRIPS fragment separator.

2. Major Research Subjects

Studies of the slowing down and purification of RI beams are the main subjects of the team. Developments of devices used for the slowing down of RI beams are also an important subject.

3. Summary of Research Activity

1) Study and development of the slowed-down methods for LLFP.
2) Development of the devices used for the slowing down.
3) Operation of the BigRIPS separator and supply the low energy LLFP beam to the experiment in which the cross sections of LLFP are measured at the low energy.

Members

Team Leader
Toshiyuki SUMIKAMA

List of Publications & Presentations

Publications

[Journal]

(Original Papers) *Subject to Peer Review

T. Sumikama, S. Nishimura, H. Baba, F. Browne, P. Doornenbal *et al.*, "Observation of new neutron-rich Mn, Fe, Co, Ni, and Cu isotopes in the vicinity of ^{78}Ni," Phys Rev C **95**, 051601(R) (2017). *

F. Browne, A. M. Bruce, T. Sumikama, *et al.*, "K selection in the decay of the (ν5/2[532]⊗3/2 [411]) 4⁻ isomeric state in ^{102}Zr," Phys. Rev. C **96**, 024309 (2017).*

Oral Presentations

[International Conference etc.]

T. Sumikama *et al.*, "Pioneering work on low energy RI beams at RIBF," ImPACT-OEDO Workshop 2017, Wako, July 13−14, 2017.

T. Sumikama *et al.*, "Towards lower beam energy at RIBF," ImPACT-OEDO Workshop 2017, Wako, July 13−14, 2017.

RIBF Research Division
Nuclear Transmutation Data Research Group
Muon Data Team

1. Abstract

Dr. Yoshio Nishina observed muons in cosmic rays in 1937. The muon is an elementary particle similar to electron and classified to lepton group. The muon has positive or negative electric charge, and the lifetime is 2.2 μsec. The negative muon (μ⁻) is 207 times heavier than the electron and behaves as a "heavy electron" in materials. The negative muon is captured by atomic orbits of nuclei to form the muonic atom and cascades down to the 1s orbit to make muon nuclear capture. The muon is combined with a proton in the nucleus to convert to a neutron and a neutrino. The muon nuclear capture reaction on a nucleus ($^A_Z N$) with the atomic number Z and mass number A generates the isotopes of $^{A-x}_{Z-1}N$ ($x = 0, 1, 2, 3, 4$) by emitting some neutrons in the reaction. The phenomenon is called "muon nuclear transmutation". The reaction branching ratio of $^A_Z N(\mu^-, x n\nu)^{A-x}_{Z-1}N$ reactions ($x = 0, 1, 2, 3, 4$) is one of important factors toward various applications with nuclear transmutation technique. From a viewpoint of the nuclear physic, the muon nuclear capture reaction is very unique and interesting. High energy is suddenly introduced in the nuclei associated with a conversion of proton to neutron and neutrino. Many experimental results have been so far reported, but the reaction mechanism itself is not well clarified. The research team aims at obtaining the experimental data to understand the reaction mechanism of muon nuclear capture, and also at establishing the nuclear reaction theory.

2. Major Research Subjects

(1) Experimental clarification on the reaction mechanism of nuclear muon capture
(2) Establishment of the reaction theory on nuclear muon capture
(3) Interdisciplinary applications with nuclear transmutation technique

3. Summary of Research Activity

There are two experimental methods to study the muon nuclear capture reaction. The first one is "muon in-beam spectroscopy method". The neutron and γ-ray emissions from the excited states of $^{A-x}_{Z-1}N$ nuclei are prompt events and are observed by the "muon in-beam spectroscopy method" with a DC muon beam. The reaction branching ratio is directly determined by measuring the neutron multiplicity in the reaction. The DC muon beam is available at the MuSIC (Muon Science Innovative Channel) muon facility in the Research Center for Nuclear Physics (RCNP) at Osaka University. The second one is "muon activation method" with the pulsed muon beam. The produced unstable nuclei $^{A-x}_{Z-1}N$ make $\beta^{+/-}$ decays. The γ-rays associated with $\beta^{+/-}$ decays to the daughter nuclei are observed in the experiment. The build-up curve of γ-ray yield at muon beam-on and the decay curve at beam-off are measured. Since the half-lives and decay branching ratios of $\beta^{+/-}$-γ decays are known, the reaction branching ratios to the $^{A-x}_{Z-1}N$ nuclei are determined by the γ-ray yield curves. The pulsed muon beam is available at the RIKEN-RAL Muon Facility in the UK and J-PARC muon facility.

Muon nuclear capture reactions are studied on five isotope-enriched palladium targets (¹⁰⁴, ¹⁰⁵, ¹⁰⁶, ¹⁰⁸, ¹¹⁰Pd) employing two experimental methods. By obtaining the experimental data on the Pd targets, the reaction mechanism is investigated experimentally, and the results are compared with appropriate theoretical calculations. The ¹⁰⁷Pd is classified to a long-lived fission product (LLFP) and is contained in a spent nuclear fuel. The study of muon nuclear capture on the Pd targets is aiming at exploring a possible reaction path to make the nuclear transmutation of the Pd metal extracted from the spent nuclear fuel without an isotope separation process. This research was funded by the ImPACT Fujita Program of Council for Science, Technology and Innovation (Cabinet Office, Government of Japan).

3.1 Experiments with "muon in-beam spectroscopy method"

Muon nuclear capture reactions were investigated on five isotope-enriched palladium targets (¹⁰⁴,¹⁰⁵,¹⁰⁶,¹⁰⁸,¹¹⁰Pd) by employing the DC muon beam at MuSIC. The γ-ray and neutron in the muon nuclear capture reaction were measured with the time information relative to muon beam arrival. The measured neutron multiplicity directly gives the reaction branching ratio of $^A_{46}Pd(\mu^-, x n\nu)^{A-x}_{45}Rh$ reactions, where A = 104, 105, 106, 108, 110 and x = 0, 1, 2, 3, 4.

Employing a newly built neutron spectrometer, the neutron was measured to obtain the reaction branching ratios of muon capture reactions on the ¹⁰⁴, ¹⁰⁵, ¹⁰⁶, ¹⁰⁸, ¹¹⁰Pd targets. We have constructed a neutron spectrometer named "Seamine": **S**cintillator **E**nclosure **A**rray for **M**uon **I**nduced **N**eutron **E**mission. The spectrometer consists of 21 liquid scintillation counters, 2 Ge γ-ray detectors, 7 BaF₂ counters. The Pd target, muon beam counters and muon degraders are placed at the center of spectrometer. The neutron counter is a BC-501A liquid scintillation counter with 20 cm diameter and 5 cm depth and is connected to a 5" photo multiplication tube (H4144-01). The total neuron detection efficiency is estimated 5%, where the distance is 4 cm from the target to neutron counters. The Ge γ-ray detectors are placed at 10 cm form the target, and the typical detection efficiency is 0.5% for 200 keV γ-ray. The BaF₂ counters are located beneath the target to detect fast γ-rays emitted from the compound nucleus formed in the reactions. Signals from the liquid scintillation counters are processed in a CAEN V1730B waveform digitizer (16 channel, 14 bit, 500M samplings/sec.). The neuron-γ discrimination is performed on-line during the experiment, and the detailed data analysis is conducted off-line after the experiment. The neutron energy spectrum is constructed in the digitizer. Signals from Ge detectors are also processed in the digitizer to obtain the energy and time spectrum of γ-rays associated with the reaction. Signals from the BaF₂ counters and muon beam counters are sent to the digitizer to make the fast timing signals.

We have established the muon in-beam spectroscopy method employing the "Seamine" spectrometer. The neutron data analysis is in progress to obtain the multiplicity, the energy and the TOF spectrum using start signals given by γ-rays detected in the BaF₂ counters. The γ-ray data gives the energy spectrum of prompt γ-rays and muonic X-rays originated from the ¹⁰⁴, ¹⁰⁵, ¹⁰⁶, ¹⁰⁸, ¹¹⁰Pd targets.

3.2 Experiments with "muon activation method" at the RIKEN-RAL Muon Facility

We conducted the experiments on the muon nuclear capture employing the muon activation method at the RIKEN-RAL Muon Facility in the UK. The pulsed muon beam was irradiated on the $^{104,\,105,\,106,\,108,\,110}$Pd targets. The γ-rays were detected by a Ge detector located at the downstream of the Pd targets to maximize the detection efficiency. The build-up and decay curves of γ-ray intensities were measured associated with $\beta^{+/-}$ decays of produced unstable nuclei to daughter nuclei. The γ-ray-yield curves give the absolute radiation activity produced by the reaction, and the reaction branching ratios are determined for $^{A}_{46}$Pd(μ^{-}, xnν)$^{A-x}_{45}$Rh reactions. The decay curves of γ-rays from the produced nuclei with long half-lives were measured under low γ-ray background at an experimental apparatus built in a separated room.

3.3 Experiments with "muon activation method" at J-PARC muon facility

The experiments employing the muon activation method were performed at J-PARC muon facility. The five isotope-enriched Pd targets ($^{104,\,105,\,106,\,108,\,110}$Pd) were irradiated by the pulsed muon beam, and the build-up and decay curves of γ-ray intensities were measured.

In addition to the Pd targets, the experiments on five isotope-enriched Zr target ($^{90,\,91,\,92,\,94,\,96}$Zr) were conducted to obtain the reaction branching ratios of $^{A}_{40}$Zr(μ^{-}, xnν)$^{A-x}_{39}$Y reactions, where A = 90, 91, 92, 94, 96. The obtained reaction branching ratios on the Pd and Zr targets are important to understand the reaction mechanism of muon nuclear capture. The ^{93}Zr is one of the LLFP and is contained in a spent nuclear fuel. The experiment on the Zr targets is to explore a possibility to realize the nuclear transmutation of the Zr metal extracted from the spent nuclear fuel.

In order to obtain the reaction branching ratio of $^{107}_{46}$Pd(μ^{-}, xnν)$^{107-x}_{45}$Rh reactions, the muon activation experiment was performed employing a Pd target containing ^{107}Pd of 15.3%. The γ-ray intensities associated with $\beta^{+/-}$ decays of produced unstable nuclei were measured to obtain the build-up and decay curves. Once the branching ratios of the reactions on the $^{104,\,105,\,106,\,108,\,110}$Pd targets are obtained, these contributions are extracted from the branching ratio measured for the Pd target with ^{107}Pd. The reaction branching ratio of $^{107}_{46}$Pd(μ^{-}, xnν)$^{107-x}_{45}$Rh reactions is finally determined. The detailed data analysis is in progress.

3.4 Comparison with theory

The muon activation method gives the reaction branching ratios. The muon in-beam method gives the neutron multiplicity and the neutron energy spectrum. These experimental results are important to investigate the compound nuclear state and neutron emission mechanism. The reaction branching ratios obtained by the muon activation method are compared with the measured neutron multiplicity. The neutron energy spectrum is considered to be reflected by the energy distribution of compound nuclear state and neutron emission mechanism. The experimental results are compared with the results by the appropriate calculations employing the neutron emission mechanisms with an evaporation, a cascade and a direct emission processes under an assumption of the energy distribution at compound nuclear state.

Members

Team Leader
Teiichiro MATSUZAKI

List of Publications & Presentations

Oral Presentations
[Domestic Conference]
齋藤岳志,「ミュオン原子 X 線を用いた Pd 同位体の核荷電半径の測定」, 日本物理学会 第 73 回年次大会（2018 年）東京理科大学（野田キャンパス）（千葉県野田市）, 2018 年 3 月 22 日.
新倉潤,「Muon Nuclear Capture Reaction」, 第 8 回 Muon 科学と加速器研究, 高エネルギー加速器研究機構（茨城県つくば市）,2018 年 1 月 11 日.
齋藤岳志,「ミュオン原子 X 線から求める原子核荷電半径」, 第 8 回 Muon 科学と加速器研究, 高エネルギー加速器研究機構（茨城県つくば市）, 2018 年 1 月 11 日.
新倉潤,「Pd 同位体のミュオン原子核捕獲反応」, ImPACT-OEDO Workshop 2017, 理化学研究所 仁科加速器研究センター（埼玉県和光市）, 2017 年 7 月 13 日.

[特許出願]
国際特許公開：「ミュオン照射による放射性物質の製造方法およびその製造物質」, 国際出願番号：JP2017/003226, 出願人：理化学研究所, 国際出願日：2017 年 1 月 30 日, 発明者：松崎禎市郎, 櫻井博儀, 国際公開番号：WO2017/135196 A1, 国際公開日：2017 年 8 月 10 日.

RIBF Research Division
High-Intensity Accelerator R&D Group

1. Abstract

The R&D group, consisting of two teams, develops elemental technology of high-power accelerators and high-power targets, aiming at future applications to nuclear transmutations of long-lived fission product into short-lived nuclides. The research subjects are superconducting rf cavities for low-velocity ions, design of high-power accelerators, high-power target systems and related technologies.

2. Major Research Subjects

(1) R&D of elemental technology of high-power accelerators and high-power targets

3. Summary of Research Activity

(1) Based on the discussion with other research groups, R&D study of various accelerator components and elements is under progress.

Members

Group Director

Osamu KAMIGAITO (concurrent: Chief Scientist, Group Director, Accelerator Gr.)

RIBF Research Division
High-Intensity Accelerator R&D Group
High-Gradient Cavity R&D Team

1. Abstract
　　We develop new components for accelerators dedicated for low-beta-ions with very high intensity. Specifically, we are designing and constructing a cryomodule for superconducting linac efficient for acceleration of low-beta-ions. In parallel, we try to optimize an rf acceleration system by making computer simulations for acceleration of very high intensity beams.

2. Major Research Subjects
　　-Development of high-gradient cavites for low beta ions
　　-Development of power saving cryomodules

3. Summary of Research Activity
　　Development of highly efficient superconducting accelerator modules

Members

Team Leader
　　Naruhiko SAKAMOTO (concurrent: Cyclotron Team)

Research & Technical Scientists
　　Kazunari YAMADA (concurrent: Senior Technical Scientist, Beam Dynamics & Diagnostics Team)
　　Kazutaka OZEKI (concurrent: Technical Scientist, Cyclotron Team)

　　Yutaka WATANABE (concurrent: Senior Technical Scientist, RILAC team)

Nishina Center Research Scientist
　　Kenji SUDA (concurrent: Cyclotron Team)

Postdoctoral Researchers
　　Xingguang LIU

List of Publications & Presentations

Oral Presentations
[International Conference etc.]
　　N. Sakamoto, O. Kamigaito, H. Okuno, K. Ozeki, K. Suda, Y. Watanabe, K. Yamada, H. Hara, K. Sennyu, T. Yanagisawa, K. Okihara, E. Kako, H. Nakai, K. Umemori, "Construction and Performance Tests of Prototype Quarter-wave Resonator and its Cryomodule at RIKEN," International Conference on RF Superconductivity, Lanzhou, China, July 17–21, 2107.

[Domestic Conference]
　　山田一成，上垣外修一，大関和貴，坂本成彦，須田健嗣，渡邉裕，加古永治，仲井浩孝，梅森健成，宮本明啓，仙入克也，柳澤剛，「重イオン線形加速器用 λ/4 型超伝導加速空洞共振器プロトタイプシステムの開発」，第 14 回日本加速器学会年会，北海道大学，札幌市，2018 年 8 月 1–3 日.
　　山田一成，上垣外修一，大関和貴，坂本成彦，須田健嗣，渡邉裕，加古永治，仲井浩孝，梅森健成，宮本明啓，仙入克也，柳澤剛，「核変換による高レベル放射性廃棄物の大幅な提言・資源化（加速器技術）(1) 超伝導用 λ/4 型共振器プロトタイプシステムの開発」，日本原子力学会 2017 年秋の年会，北海道大学，札幌市，2017年9月13–15 日.

Poster Presentations
[International Conference etc.]
　　X. Liu, O. Kamigaito, N. Sakamoto, K. Yamada, "Preliminary design of a high-intensity continuous-wave deuteron RFQ", 8th International Particle Accelerator Conference, Copenhagen, Denmark, 14–19 May 2017.

Publications
[Proceedings]
　　X. Liu, O. Kamigaito, N. Sakamoto, K. Yamada, "Preliminary design of a high-intensity continuous-wave deuteron RFQ", 8th International Particle Accelerator Conference, Copenhagen, Denmark, May 14−19, 2017, pp. 2287.
　　N. Sakamoto, O. Kamigaito, H. Okuno, K. Ozeki, K. Suda, Y. Watanabe, K. Yamada, H. Hara, K. Sennyu, T. Yanagisawa, K. Okihara, E. Kako, H. Nakai, K. Umemori, "Construction and Performance Tests of Prototype Quarter-wave Resonator and its Cryomodule at RIKEN", International Conference on

RF Superconductivity,Lanzhou, China, July 17−21, 2107, pp. 681.

山田一成, 上垣外修一, 大関和貴, 坂本成彦, 須田健嗣, 渡邉裕, 加古永治, 仲井浩孝, 梅森健成, 宮本明啓, 仙入克也, 柳澤剛,「重イオン線形加速器用 λ/4 型超伝導加速空洞共振器プロトタイプシステムの開発」, 第 14 回日本加速器学会年会 2018年8月1–3日, 北海道大学, 札幌市, pp. 1395.

RIBF Research Division
High-Intensity Accelerator R&D Group
High-Power Target R&D Team

1. Abstract

The subjects of this team cover R&D studies with respect to target technology for the transmutation of the LLFPs. Furthermore this team works for the demonstration test of the transmutation of ^{107}Pd.

2. Major Research Subjects

(1) Liquid lithium target for production of neutron or muon
(2) Beam window without solid structure
(3) Ion implantation and TIMS for the demonstration of the transmutation of ^{107}Pd

3. Summary of Research Activity

(1) Liquid lithium target for production of neutron or muon
    (H. Okuno, M. Takahashi)
(2) Beam window with solid structure
    (H. Okuno)
(3) Ion plantation and TIMS of ^{107}Pd
    (Y. Miyake, Y. Sahoo)

Members

Team Leader
Hiroki OKUNO (concurrent: Deputy Group Director, Accelerator
  Gr.)

Research and Technical Scientist
Yasuto MIYAKE (Postdoctoral Researcher)

Part-time Worker
Akira TAKAGI   YuVin SAHOO

RIBF Research Division
Accelerator Group

1. Abstract

The accelerator group, consisting of seven teams, pursues various upgrade programs of the world-leading heavy-ion accelerator facility, RI-Beam Factory (RIBF), to enhance the accelerator performance and operation efficiency. The programs include the R&D of superconducting ECR ion source, charge stripping systems, beam diagnostic devices, radiofrequency systems, control systems, and beam simulation studies. We are also maintaining the large infrastructure to realize effective operation of the RIBF, and are actively promoting the applications of the facility to a variety of research fields.

Our primary mission is to supply intense, stable heavy-ion beams for the users through effective operation, maintenance, and upgrade of the RIBF accelerators and related infrastructure. The director members shown below govern the development programs that are not dealt with by a single group, such as intensity upgrade and effective operation. We also promote the future plans of the RIBF accelerators along with other laboratories belonging to the RIBF research division.

2. Major Research Subjects

(1) Intensity upgrade of RIBF accelerators (Okuno)
(2) Effective and stable operation of RIBF accelerators (Fukunishi)
(3) Operation and maintenance of infrastructures for RIBF (Kase)
(4) Promotion of the future plan (Kamigaito, Fukunishi, Okuno)

3. Summary of Activity

(1) The maximum intensity of the uranium beam reached 71 pnA at 345 MeV/nucleon, which corresponds to 5.8 kW.
(2) The maximum intensity of the zinc beams reached 240 pnA at 345 MeV/nucleon, by using the fixed-energy mode of acceleration.
(3) An intense vanadium beam has been successfully developed at the 28-GHz ECRIS and accelerated through RRC.
(4) The overall beam availability for the RIBF experiments has been kept above 90 % since 2014.
(5) The large infrastructure was properly maintained based on a well-organized cooperation among the related sections.

Members

Group Director
Osamu KAMIGAITO

Deputy Group Directors
Hiroki OKUNO (Intensity upgrade)   Masayuki KASE (Energy-efficiency management)
Nobuhisa FUKUNISHI (Stable and efficient operation)

Postdoctoral Researcher
Joele Paulus MIRA

Junior Research Associates
Takahiro KARINO (Utsunomiya Univ.)

Part-time Worker
Akira GOTO

Research Consultant
Tadashi FUJINAWA

Visiting Scientists
Toshiyuki HATTORI (TIT)   Hirotaka NAKAI (KEK)
Kensei UMEMORI (KEK)   Eiji KAKO (KEK)
Robert JAMESON (IAP Frankfurt)   Noboru SASAO (Okayama Univ.)

Student Trainee
Akira FUJIEDA (Okayama Univ.)

Assistant
Karen SAKUMA

RIBF Research Division
Accelerator Group
Accelerator R&D Team

1. Abstract

We are developing the key hardware in upgrading the RIBF accelerator complex. Our primary focus and research is charge stripper which plays an essential role in the RIBF accelerator complex. Charge strippers remove many electrons in ions and realize efficient acceleration of heavy ions by greatly enhancing charge state. The intensity of uranium beams is limited by the lifetime of the carbon foil stripper conventionally installed in the acceleration chain. The improvement of stripper lifetimes is essential to increase beam power towards the final goal of RIBF in the future. We are developing the low-Z gas stripper. In general gas stripper is free from the lifetime related problems but gives low equilibrium charge state because of the lack of density effect. Low-Z gas stripper, however, can give as high equilibrium charge state as that in carbon foil because of the suppression of the electron capture process. Another our focus is the upgrade of the world's first superconducting ring cyclotron.

2. Major Research Subjects

(1) Development of charge strippers for high power beams (foil, low-Z gas)
(2) Upgrade of the superconducting ring cyclotron
(3) Maintenance and R&D of the electrostatic deflection/inflection channels for the beam extraction/injection

3. Summary of Research Activity

(1) Development of charge strippers for high power beams (foil, low-Z gas)
(H. Hasebe, H. Imao, H. Okuno)
We are developing the charge strippers for high intensity heavy ion beams. We are focusing on the developments on carbon or berrilium foils and gas strippers including He gas stripper.

(2) Upgrade of the superconducting ring cyclotron
(J. Ohnishi, H. Okuno)
We are focusing on the upgrade of the superconducting ring cyclotron.

(3) Maintenance and R&D of the electrostatic deflection/inflection channels for the beam extraction/injection
(J. Ohnishi, H. Okuno)
We are developing high-performance electrostatic channels for high power beam injection and extraction.

Members

Team Leader
Hiroki OKUNO (concurrent: Deputy Group Director, Accelerator
Gr.)

Research & Technical Scientists
Hiroshi IMAO (Senior Research Scientist)   Jun-ichi OHNISHI (Senior Technical Scientist)

Nishina Center Technical Scientist
Hiroo HASEBE

Visiting Scientists
Andreas ADELMANN (PSI)   Noriyosu HAYASHIZAKI (TIT.)
Hironori KUBOKI (KEK)

Junior Research Associate
Naoya IKOMA (Nagaoka Univ. of Technology)

List of Publications & Presentations

Publications
[Journal]
(Original Papers) *Subject to Peer Review
H. Hasebe, H. Okuno, H. Kuboki, H. Imao, N. Fukunishi, M. Kase, O. Kamigaito, "Development of rotating beryllium disk stripper," J. Radioanal. Nucl. Chem. **305**, 825 (2015).

[Proceedings]
 (Original Papers) *Subject to Peer Review
　H. Hasebe, H. Okuno, H. Kuboki, H. Imao, N. Fukunishi, M. Kase, O. Kamigaito, "History of solid disk improvement for rotating charge stripper,"
　　Proceeding of HIAT2015, MOA1C01, Yokohama, Japan (2015).

Oral Presentation
 [International Conference etc.]
　H. Hasebe, H. Okuno, H. Kuboki, H. Imao, N. Fukunishi, M. Kase, O. Kamigaito, "History of solid disk improvement for rotating charge stripper,"
　　HIAT2015, MOA1C01, Yokohama, Japan (2015).

Poster Presentation
 [International Conference etc.]
　H. Imao, H. Kuboki, H. Hasebe, O. Kamigaito, M. Kase, H. Okuno, "Operation of gas strippers at RIBF ; Thining effect of high-intensity very heavy ion
　　beams," HIAT2015, MOPA32, Yokohama, Japan (2015).

RIBF Research Division
Accelerator Group
Ion Source Team
- 362 -

1. Abstract

Our aim is to operate and develop the ECR ion sources for the accelerator-complex system of the RI Beam Factory. We focus on further upgrading the performance of the RI Beam Factory through the design and fabrication of a superconducting ECR ion source for production of high-intensity heavy ions.

2. Major Research Subjects

(1)　Operation and development of the ECR ion sources
(2)　Development of a superconducting ECR heavy-ion source for production of high-intensity heavy ion beams

3. Summary of Research Activity

(1) Operation and development of ECR ion sources
　(T. Nakagawa, M. Kidera, Y. Higurashi, T. Nagatomo, Y. Kanai and H. Haba)

We routinely produce and supply various kinds of heavy ions such as zinc and calcium ions for the super-heavy element search experiment as well as uranium ions for RIBF experiments. We also perform R&D's to meet the requirements for stable supply of high-intensity heavy ion beams.

(2) Development of a superconducting ECR ion source for use in production of a high-intensity heavy ion beam
　(T. Nakagawa, J. Ohnishi, M. Kidera, Y. Higurashi, and T. Nagatomo)

The RIBF is required to supply heavy ion beams with very high intensity so as to produce RI's and for super-heavy element search experiment. We have designed and are fabricating an ECR ion source with high magnetic field and high microwave- frequency, since the existing ECR ion sources have their limits in beam intensity. The coils of this ion source are designed to be superconducting for the production of high magnetic field. We are also designing the low-energy beam transport line of the superconducting ECR ion source.

Members

Team Leader
　Takahide NAKAGAWA

Research & Technical Scientist
　Takashi NAGATOMO (Technical Scientist)

Nishina Center Research Scientists
　Masanori KIDERA　　　　　　　　　　　　　　　　　　Yoshihide HIGURASHI

Special temporal employee
　Yasuyuki KANAI

List of Publications & Presentations

Publications
　[Proceedings]
　(Original Papers) *Subject to Peer Review
　T. Nagatomo, V. Tzoganis, J. P. Mira, T. Nakagawa and O. Kamigaito, "Residual gas effect in LEBT on transverse emittance of multiply-charged heavy ion beams extracted from ECR ion source," Proceedings of 17th International Conference on Ion Sources, ICIS17, Geneva, Switzerland, Oct. 15–20, 2017 (accepted).

Oral Presentations
　[International Conference etc.]
　T. Nagatomo, "Residual gas effect in LEBT on transverse emittance of multiply-charged heavy ion beams extracted from ECR ion source," ICIS2017, Geneva, Switzerland, Oct. 15−20, 2017.

RIBF Research Division
Accelerator Group
RILAC Team

1. Abstract

The operation and maintenance of the RIKEN Heavy-ion Linac (RILAC) have been carried out. There are two operation modes: one is the stand-alone mode operation and the other is the injection mode operation. The RILAC has been used especially as an injector for the RIKEN RI- Beam Factory accelerator complex. The RILAC is composed of the ECR ion source, the frequency-variable RFQ linac, six frequency-variable main linac cavities, and six energy booster cavities (CSM).

2. Major Research Subjects

(1) The long term high stability of the RILAC operation.
(2) Improvement of high efficiency of the RILAC operation.

3. Summary of Research Activity

The RILAC was started to supply ion beams for experiments in 1981. Thousands hours are spent in a year for delivering many kinds of heavy-ion beams to various experiments.

The RILAC has two operation modes: one is the stand-alone mode operation delivering low-energy beams directly to experiments and the other is the injection mode operation injecting beams into the RRC. In the first mode, the RILAC supplies a very important beam to the nuclear physics experiment of "the research of super heavy elements". In the second mode, the RILAC plays a very important role as upstream end of the RIBF accelerator complex.

The maintenance of these devices is extremely important in order to keep the log-term high stability and high efficiency of the RILAC beams. Therefore, improvements are always carried out for the purpose of more stable and more efficient operation.

Members

Team Leader
Eiji IKEZAWA

Research & Technical Scientist
Yutaka WATANABE (Senior Technical Scientist)

Research Consultants
Masatake HEMMI

List of Publications & Presentations

Publications
[Proceedings]
A. Yusa, E. Ikezawa, T. Ohki, H. Yamauchi, K. Oyamada, M. Tamura, K. Kaneko, Y. Watanabe, K. Suda, K. Ozeki, K. Yamada, N. Sakamoto, M. Kase, O. Kamigaito, "Present Status of RILAC," Proceedings of the 14th Annual Meeting of Particle Accelerator Society of Japan, 1400−1403 (2017).

Poster Presentations
[Domestic Conference]
A. Yusa, E. Ikezawa, T. Ohki, H. Yamauchi, K. Oyamada, M. Tamura, K. Kaneko, Y. Watanabe, K. Suda, K. Ozeki, K. Yamada, N. Sakamoto, M. Kase, O. Kamigaito, "Present Status of RILAC," The 14th Annual Meeting of Particle Accelerator Society of Japan, Sapporo, Japan, August 1−3, 2017.

RIBF Research Division
Accelerator Group
Cyclotron Team

1. Abstract

Together with other teams of Nishina Center accelerator division, maintaining and improving the RIBF cyclotron complex. The accelerator provides high intensity heavy ions. Our mission is to have stable operation of cyclotrons for high power beam operation. Recently stabilization of the rf system is a key issue to provide 10 kW heavy ion beam.

2. Major Research Subjects

(1) RF technology for Cyclotrons
(2) Operation of RIBF cyclotron complex
(3) Maintenance and improvement of RIBF cyclotrons
(4) Single turn operation for polarized deuteron beams
(5) Development of superconducting cavity

3. Summary of Research Activity

・Development of the rf system for a reliable operation
・Development of highly stabilized low level rf system
・Development of superconducting cavity
・Development of the intermediate-energy polarized deuteron beams.

Members

Team Leader
Naruhiko SAKAMOTO

Research & Technical Scientist
Kazutaka OZEKI

Nishina Center Research Scientist
Kenji SUDA

List of Publications & Presentations

Oral Presentations
[International Conference]
N. Sakamoto, O. Kamigaito, H. Okuno, K. Ozeki, K. Suda, Y. Watanabe, K. Yamada, H. Hara, K. Sennyu, T. Yanagisawa, K. Okihara, E. Kako, H. Nakai, K. Umemori, "Construction and Performance Tests of Prototype Quarter-wave Resonator and its Cryomodule at RIKEN," International Conference on RF Superconductivity, Lanzhou, China, July17−21, 2107.

Publications
[Proceedings]
N. Sakamoto, O. Kamigaito, H. Okuno, K. Ozeki, K. Suda, Y. Watanabe, K. Yamada, H. Hara, K. Sennyu, T. Yanagisawa, K. Okihara, E. Kako, H. Nakai, K. Umemori, "Construction and Performance Tests of Prototype Quarter-wave Resonator and its Cryomodule at RIKEN," International Conference on RF Superconductivity, Lanzhou, China, July17−21, pp. 681 (2107).
小山亮児, 福澤聖児, 濱仲誠, 石川盛, 小林清志, 仲村武志, 西田稔, 西村誠, 柴田順翔, 月居憲俊, 矢冨一慎, 須田健嗣, 藤巻正樹, 福西暢尚, 後藤彰, 長谷部裕雄, 日暮祥英, 今尾浩士, 加瀬昌之, 上垣外修一, 木寺正憲, 込山美咲, 熊谷桂子, 真家武士, 長瀬誠, 長友傑, 中川孝秀, 大西純一, 奥野広樹, 大関和貴, 坂本成彦, 内山暁仁, 渡部秀, 渡邉環, 渡邉裕, 山田一成, 小高康照, 大城幸光,「理研AVFサイクロトロン運転の現状報告」, 第 14 回日本加速器学会年会 2018 年 8 月 1−3 日, 北海道大学, 札幌市, pp. 1395.
西村誠, 福澤聖児, 濱仲誠, 石川盛, 小林清志, 小山亮児, 仲村武志, 西田稔, 柴田順翔, 月居憲俊, 矢冨一慎, 須田健嗣, 藤巻正樹, 福西暢尚, 後藤彰, 長谷部裕雄, 日暮祥英, 今尾浩士, 加瀬昌之, 上垣外修一, 木寺正憲, 込山美咲, 熊谷桂子, 真家武士, 長瀬誠, 長友傑, 中川孝秀, 大西純一, 奥野広樹, 大関和貴, 坂本成彦, 内山暁仁, 渡部秀, 渡邉環, 渡邉裕, 山田一成, 山澤秀行,「理研 RIBF におけるリングサイクロトロン運転の現状報告」, 第 14 回日本加速器学会年会 2018 年 8 月 1−3 日, 北海道大学, 札幌市.

Poster Presentations
[Domestic Conference]

小山亮，福澤聖児，濱仲誠，石川盛，小林清志，仲村武志，西田稔，西村誠，柴田順翔，月居憲俊，矢冨一慎，須田健嗣，藤巻正樹，福西暢尚，後藤彰，長谷部裕雄，日暮祥英，今尾浩士，加瀬昌之，上垣外修一，木寺正憲，込山美咲，熊谷桂子，真家武士，長瀬誠，長友傑，中川孝秀，大西純一，奥野広樹，大関和貴，坂本成彦，内山暁仁，渡部秀，渡邉環，渡邉裕，山田一成，小高康照，大城幸光，「理研AVFサイクロトロン運転の現状報告」，第 14 回日本加速器学会年会 2018 年 8 月 1–3 日，北海道大学，札幌市, pp. 1395.

西村誠，福澤聖児，濱仲誠，石川盛，小林清志，小山亮，仲村武志，西田稔，柴田順翔，月居憲俊，矢冨一慎，須田健嗣，藤巻正樹，福西暢尚，後藤彰，長谷部裕雄，日暮祥英，今尾浩士，加瀬昌之，上垣外修一，木寺正憲，込山美咲，熊谷桂子，真家武士，長瀬誠，長友傑，中川孝秀，大西純一，奥野広樹，大関和貴，坂本成彦，内山暁仁，渡部秀，渡邉環，渡邉裕，山田一成，山澤秀行，「理研 RIBF におけるリングサイクロトロン運転の現状報告」，第 14 回日本加速器学会年会 2018 年 8 月 1–3 日，北海道大学，札幌市.

RIBF Research Division
Accelerator Group
Beam Dynamics & Diagnostics Team

1. Abstract

The cascaded cyclotron system at RIKEN RI Beam Factory (RIBF) requires not only strict matching of operation parameters but also high stability of all the accelerator components in order to establish stable operation of the world's most intense heavy-ion beams. Beam Dynamics and Diagnostics Team is responsible for power supplies, beam instrumentation, computer control and beam dynamic of the RIBF accelerator complex and strongly contributes to the performance upgrade of the RIBF.

2. Major Research Subjects

(1) Extracting the best performance of the RIBF accelerator complex based on the precise beam dynamics study.
(2) Maintenance and developments of the beam instrumentation, especially non-destructive monitors.
(3) Upgrade of the computer control system of the RIBF accelerator complex.
(4) Maintenance and improvements of the magnets and their power supplies.
(5) Upgrade of the existing beam interlock system for higher-intensity beams.

3. Summary of Research Activity

(1) High-intensity heavy-ion beams including 70-pnA uranium, 102-pnA xenon, 486-pnA krypton, and 740-pnA calcium beams have been obtained.
(2) The world-first high-T_c SQUID beam current monitor has been developed.
(3) The bending power of the fixed-frequency Ring Cyclotron has been upgraded to 700 MeV. It enables us to accelerate $^{238}U^{64+}$ ions obtained by the helium gas stripper.
(4) An EPICS-based control system and a homemade beam interlock system have been stably operated. Replacements of the existing legacy control system used in the old half of our facility is ongoing. Construction of the new control system for the new injector RILAC2 was successfully completed, where the embedded EPICS system running on F3RP61-2L CPU module, developed by KEK and RIKEN control group, was used.
(5) We replaced some dated power supplies of RIKEN Ring Cyclotron by new ones, which have better long-term stability than the old ones. The other existing power supplies (~900) are stably operated owing to elaborate maintenance work.
(6) We have contributed to RILAC2 construction, especially in its beam diagnosis, control system, magnet power supplies, vacuum system, high-energy beam transport system etc.

Members

Team Leader
Nobuhisa FUKUNISHI (concurrent; Deputy Group Director, Accelerator Gr.)

Research & Technical Scientists
Masaki FUJIMAKI (Senior Technical Scientist)   Tamaki WATANABE (Senior Technical Scientist)
Keiko KUMAGAI (Senior Technical Scientist)   Kazunari YAMADA (Senior Technical Scientist)

Nishina Center Technical Scientists
Misaki KOMIYAMA   Akito UCHIYAMA

Part-time Workers
Makoto NAGASE

Visiting Scientists
Kenichi ISHIKAWA (Univ. of Tokyo)   Hiromichi RYUTO (Kyoto Univ.)
Shin-ichiro HAYASHI (Hiroshima Int'l Univ.)   Takuya MAEYAMA (Kitasato Univ.)

Visiting Technician
Jun-ichi ODAGIRI (KEK)

List of Publications & Presentations

Publications

[Journal]

(Original Papers) *Subject to Peer Review

T. Maeyama, Y. Ishida, Y. Kudo, K. Fukasaku, K. L. Ishikawa, N. Fukunishi, "Polymer gel dosimeter with AQUAJOINT as hydrogel matrix," Radiat. Phys. Chem. **146**, pp. 121–125, doi:0.10216/j.radphyschem.2018.01.014 (2018).

T. Maeyema, N. Fukunishi, K.L. Ishikawa, K. Fukasaku, S. Fukuda, "Organic-gelatin-free nanocomposite Fricke gel dosimeter," J. Phys. Chem. B, **2017**, 121 (16), pp. 4238−4246, doi:10.1021/acs.jpcb.6b11936 (2017).

Oral Presentations

[International Conference etc.]

A. Uchiyama, M. Komiyama, N. Fukunishi, "Implementation of web-based operational log system at RIBF," The 16th Int. Conf. on Accelerator and Large Experimental Control System (ICALEPCS2017), Barcelona, Spain, October 2017, THAPL01, doidoi:10.18429/JaCOW-ICALEPCS2017-THAPL01 (2017).

Poster Presentations

[International Conference etc.]

M. Komiyama, M. Fujimaki, N. Fukunishi, A. Uchiyama, M. Hamanaka, T. Nakamura, "Recent update of the RIKEN RI beam factory control system," The 16th Int. Conf. on Accelerator and Large Experimental Control System (ICALEPCS2017), Barcelona, Spain, October 2017, TUPHA028, doi:10.18429/JaCOW-ICALEPCS2017-TUPHA028 (2017).

[Domestic Conference]

T. Watanabe, N. Fukunishi, M. Fujimaki, R. Koyama, T. Toyama, T. Miyao, A. Miura, "Development of beam energy and position monitor system at RIBF," 14th Annual Meeting of Particle Accelerator Society of Japan, August 2017, Sapporo, Japan, pp. 1112−1117 (2017).

A. Uchiyama, M. Komiyama, "Improvement of data archive system at RIBF," 14th Annual Meeting of Particle Accelerator Society of Japan, August 2017, Sapporo, Japan, pp. 644−647 (2017).

RIBF Research Division
Accelerator Group
Cryogenic Technology Team

- 368 -

1. Abstract

We are operating the cryogenic system for the superconducting ring cyclotron in RIBF. We are operating the helium cryogenic system in the south area of RIKEN Wako campus and delivering the liquid helium to users in RIKEN. We are trying to collect efficiently gas helium after usage of liquid helium.

2. Major Research Subjects

(1)   Operation of the cryogenic system for the superconducting ring cyclotron in RIBF
(2)   Operation of the helium cryogenic plant in the south area of Wako campus and delivering the liquid helium to users in Wako campus.

3. Summary of Research Activity

(1)   Operation of the cryogenic system for the superconducting ring cyclotron in RIBF
         (H. Okuno, T. Dantsuka, M. Nakamura, T. Maie)
(2)   Operation of the helium cryogenic plant in the south area of Wako campus and delivering the liquid helium to users in Wako campus.
         (T. Dantsuka, S. Tsuruma, H. Okuno).

Members

Team Leader
   Hiroki OKUNO (concurrent: Deputy Group Director, Accelerator
      Gr.)

Research & Technical Scientist
   Masato NAKAMURA (Senior Technical Scientist)

Nishina Center Technical Scientist
   Takeshi MAIE

Technical Staff I
   Tomoyuki DANTSUKA

Part-time Worker
   Shizuho TSURUMA   Mayumi KUROIWA

RIBF Research Division
Accelerator Group
Infrastructure Management Team

1. Abstract

The RIBF facility is consisting of many accelerators and its infrastructure is very important in order to make an efficient operation of RIBF project. We are maintaining the infrastructure of the whole system and to support the accelerator operation with high performance. We are also concerning the contracts of gas- and electricity-supply companies according to the annual operation plan. The contracts should be reasonable and also flexible against a possible change of operations. And we are searching the sources of inefficiency in the operation and trying to solve them for the high-stable machine operation.

2. Major Research Subjects

(1) Operation and maintenance of infrastructure for RIBF accelerators.
(2) Renewal of the old equipment for the efficient operation.
(3) Support of accelerator operations.

Members

Team Leader
    Masayuki KASE (concurrent; Deputy Group Director, Accelerator Gr.)

Research & Technical Scientists
    Shu WATANABE (Senior Technical Scientist)

Research Consultant
    Hideyuki YAMASAWA

Visiting Scientist
    Hideshi MUTO (Tokyo Univ. of Sci. Suwa)

RIBF Research Division
Instrumentation Development Group

1. Abstract

This group develops core experimental installations at the RI Beam factory. They are a slow-RI beam facility (SLOWRI), and highly program specific facilities of SCRIT and Rare-RI Ring (R3). All were designed to maximize the research potential of the world's most intense RI beams, made possible by the exclusive equipment available at the RI Beam Factory. While SLOWRI is under preparation for commissioning, physics experiments conducted in storage rings have been just started at SCRIT and R3 facilities. Beam manipulation techniques, such as a beam accumulation and a beam cooling, will be able to provide opportunities of new experimental challenges and the foundation for future developments of RIBF.

2. Major Research Subjects

(1) SCRIT Project
(2) SLOWRI Project
(3) Rear RI Ring Project

3. Summary of Research Activity

We are developing beam manipulation technology in carrying out above listed project. They are the high-quality slow RI beam production (SCRIT and SLOWRI), the beam cooling and stopping (SCRIT and SLOWRI), and the beam accumulation technology (SCRIT and R3). The technological knowhow accumulated in our projects will play a significant role in the next generation RIBF. Status and future plan for each project is described in subsections. SCRIT is now under test experimental phase in which the angular distribution of scattered electrons from ^{132}Xe isotopes has been successfully measured and the nuclear charge density distribution has been obtained. Electron scattering off unstable nuclei is now under preparation for the first experiment in 2018. Rare RI Ring was commissioned in four-times machine-study experiments, and we have demonstrated that the ring has an ability for precision mass measurement with the accuracy of better than 10 ppm. We will be able to try to measure masses of nuclei $^{74\text{-}76}$Ni in 2018 and continuously make improvement in the accuracy. Construction of the SLOWRI system is now in tuning phase and it will be commissioned in 2018. PALIS device was commissioned in 2015 and 2016, and basic functions such as the RI-beam stopping in argon gas cell and the extraction with the gas flow were confirmed. Other devices are now under setting up for the first commissioning.

Members

Group Director
Masanori WAKASUGI

Visiting Scientist
Akira OZAWA (Univ. of Tsukuba)

Student Trainees
So SATO (Rikkyo Univ.)   Moe NAKANO (Rikkyo Univ.)

List of Publications & Presentations

Publications and presentations for each project team are listed in subsections.

RIBF Research Division
Instrumentation Development Group
SLOWRI Team

1. Abstract

SLOWRI is a universal low-energy RI-beam facility at RIBF that provides a wide variety of short-lived nuclei as high-purity and low-emittance ion beams or stored ions in a trap, including a parasitic operation mode. The SLOWRI team develops and manages the facility and performs high-precision spectroscopy experiments. The construction of the SLOWRI facility began in FY2013 and commissioning work is ongoing. Two major online prototype setups have been successfully tested. The first was a large room-temperature gas cell with an RF-carpet structure. With this setup, the hyperfine structure constants of all odd Be isotopes were precisely measured by laser-microwave double resonance spectroscopy of trapped Be ions, following which the first online mass measurement with a multi-reflection time-of-flight mass spectrograph (MRTOF) was performed on ^{8}Li$^+$ ions. The second prototype is a medium-sized cryogenic RF carpet gas cell for the SHE-Mass project that aims to measure the masses of trans-uranium elements at the GARIS-II facility. This prototype showed that a traveling-wave RF-carpet works fine and the cryogenic gas cell dominantly provides doubly charged ions even for Fr isotopes. Using the SHE-Mass setup, more than 80 nuclear masses have been measured including the first mass measurements of Md and Es isotopes.

2. Major Research Subjects

(1) Construction of the stopped and low-energy RI-beam facility, SLOWRI.
(2) Laser spectroscopy of trapped radioactive beryllium isotopes.
(3) Development of a multi-reflection time-of-flight mass spectrograph for precision mass measurements of short-lived nuclei.
(4) Development of collinear laser spectroscopy apparatus.
(5) Development of a parasitic slow RI-beam production method using resonance laser ionization.
(6) Development of highly charged ion trap for fundamental physics

3. Summary of Research Activity

(1) Construction of stopped and low-energy RI-beam facility (SLOWRI)

Installation of SLOWRI began in FY2013. It consists of two gas catchers (RF Carpet gas cell and PALIS gas cell), magnetic mass separators, a 50-m beam transport line, a beam cooler-buncher, an isobar separator, and a laser system. The RF Carpet gas cell will be installed at the exit of the D5 dipole magnet of BigRIPS. This gas catcher comprises a large cryogenic He gas cell with a large traveling wave RF carpet. It will convert main beams of BigRIPS to low-energy, low-emittance beams without any restrictions from the chemical properties of the elements. The PALIS gas cell will be installed in the vicinity of the second focal plane slit of BigRIPS. It will provide parasitic RI beams from the ions normally lost in the slits during other experiments. In this gas catcher, thermalized RIs quickly become neutralized and will be selectively re-ionized by resonant laser radiations. These gas catchers have been tested off-line. The 50 m beam transport line consists of four dipole magnets (SD1 to SD4), two focal plane chambers, 62 electrostatic quadrupole singlets, 11 electrostatic quadrupole quartets (EQQ1 to EQQ11) and 7 beam profile monitors (BPMs). SD1 and SD2, located immediately after the gas catchers, will be used for isotope separation. After eliminating contaminant ions at the focal plane chamber, the low energy beam will be transported by a FODO lattice structure with phase space matching using EQQs. The EQQs have multipole elements made of 16 rods on which various potentials can be applied to produce 6-pole and 8-pole fields simultaneously to compensate for ion optical aberrations. This multipole element can also produce dipole fields for steering and scanning the beam. The BPMs have a classical cross-wire beam monitor as well as a channel electron multiplier with a pinhole collimator. Combining the scanning capability of the EQQs and the pinhole detector, we can observe a beam profile even for very-low-intensity RI beams. Off- and on-line commissioning is underway.

Based on test experiments with the prototype setups, the large RF-carpet gas cell contains a three-stage RF-carpet structure: a gutter RF carpet for the collection of thermal ions in the cell into a small slit, a narrow ($\approx$10 mm) traveling-wave RF carpet for the collection of ions from the gutter carpet and for transporting the ions toward the exit, and a small RF carpet for extraction from the gas cell. An off-line test of the gutter structure has shown a high collection efficiency of ions in the gas cell.

(2) Laser spectroscopy of trapped radioactive beryllium isotope ions

As the first application of the prototype SLOWRI setup, we applied hyperfine structure spectroscopy on beryllium isotopes to determine, in particular, the anomalous radius of the valence neutron of the neutron halo nucleus ^{11}Be, and to determine the charge radii of these beryllium isotopes through laser-laser double resonance spectroscopy of laser-cooled ions. Laser cooling is an essential prerequisite for these planned experiments. The first laser spectroscopy experiments for beryllium isotopes were performed to measure the resonance frequencies of the 2s ^{2}S$_{1/2}$ - 2p ^{2}P$_{3/2}$ transition in ^{7}Be+, ^{9}Be+, ^{10}Be$^+$ and ^{10}Be+ ions and the nuclear charge radii of these isotopes were determined. The hyperfine structures of ^{11}Be$^+$ and ^{7}Be$^+$ ions were also determined using laser-microwave double resonance spectroscopy and the magnetic hyperfine constants of ^{7}Be$^+$ and ^{11}Be$^+$ ions were determined with accuracies better than 10^{-7}. A new combined-trap setup for high-precision determination of nuclear g-factors of the odd Be isotopes using a superconducting Helmholtz magnet is under preparation at the SLOWRI experimental area in collaboration with the Ueno nuclear spectroscopy laboratory.

(3) Development of a multi-reflection TOF mass spectrograph for short-lived nuclei

The atomic mass is one of the most important quantities of a nucleus and has been studied by various methods since the early days of modern physics. From among many methods we have chosen a multi-reflection time-of-flight (MR-TOF) mass spectrometer. Slow RI beams extracted from the RF ion guide are bunched and injected into the spectrometer with a repetition rate of ~100 Hz. The spectrometer

consists of two electrostatic mirrors between which the ions travel back and forth repeatedly. These mirrors are designed such that energy isochrononicity in the flight time is guaranteed during the multiple reflections, while the flight time varies with the masses of ions. A mass-resolving power of 170,000 has been obtained within a 2-ms flight time for the $^{40}K^+$ and $^{40}Ca^+$ isobaric doublet. This mass-resolving power should allow determination of ion masses with an accuracy of $\leq 10^{-7}$. On-line mass measurement for the radioactive isotope ^8Li has been performed with the prototype SLOWRI setup.

The MR-TOF mass spectrograph has been placed under the GARIS-II separator with the goal of direct mass measurements of trans-uranium elements. A cryogenic gas catcher cell was placed at the focal plane box of GARIS-II and bunched low-energy heavy ion beams were transported to the trap of MR-TOF. In on-line commissioning experiments using No isotopes, an extraction efficiency greater than 30% was achieved from the cryogenic gas cel. In FY2016, mass measurements of more than 80 nuclides, including short-lived ($T_{1/2} = 10$ ms) isotopes of Ra and several isotopes of the trans-uranium elements Fm, Es, No, and Md were performed at GARIS-II in collaboration with the KEK Wako Nuclear Science Center and the Super Heavy Element Synthesis team of RIKEN. The highest precisions, achieved for Ga isotopes, reached a level of 0.03 ppm. For most of the well-known nuclides, agreement with the literature mass values was found. However, discrepancies were found in some literature values derived from pre-1980 indirect measurements. This suggests that such indirect measurements must be revised with comprehensive direct mass measurements. The masses of four isotopes of Es and Md were measured for the first time, allowing for confirmation of the $N = 152$ shell closure in Md. Using these new mass data as anchor points, the masses of seven isotopes of super-heavy elements up to Mt were indirectly determined and comparisons with various nuclear mass models were performed.

For comprehensive mass measurements of all available nuclides, multiple units of gas catchers and MR-TOF devices will be placed at the new GARIS-II, KISS, as well as the BigRIPS + SLOWRI facilities of RIBF.

(4) Development of collinear fast beam apparatus for nuclear charge radii measurements

The root-mean-square charge radii of unstable nuclei have been determined exclusively by isotope shift measurements of the optical transitions of singly charged ions or neutral atoms by laser spectroscopy. Many isotopes of alkali, alkali-earth, and noble-gas elements in addition to several other elements have been measured by collinear laser spectroscopy since these ions all have good optical transitions and are available at conventional ISOL facilities. However, isotopes of other elements, especially refractory and short-lived ones, have not been investigated so far.

In SLOWRI, isotopes of all atomic elements will be provided as well collimated, mono-energetic ion beams. This should expand the range of nuclides available for laser spectroscopy. In the first years of the RIBF project, elements in the vicinity of Ni, such as Ni, Co, Fe, Cr, Cu, Ga, and Ge are planned to be investigated. They all have possible optical transitions in the ground states of neutral atoms with presently available laser systems. Some of them have so called recycling transitions, which enhance the detection probabilities noticeably. Furthermore, the multistep resonance ionization (RIS) method can be applied to the isotopes of Ni as well as those of some other elements. The required minimum intensity for this method can be as low as 10 atoms per second.

An off-line mass separator and a collinear fast beam apparatus with a large solid-angle fluorescence detector was built previously. A 617-nm transition of the metastable Ar^+ ion at 20 keV was measured with both collinear and anti-collinear geometry, which allowed determination of the absolute resonant frequency of the transition at rest with a relative accuracy better than 10^{-8}. A new setup is under preparation at the SLOWRI experiment area in collaboration with the Ueno nuclear spectroscopy laboratory.

(5) Development of parasitic slow RI-beam production scheme using resonance laser ionization

More than 99.9% of RI ions produced in projectile fission or fragmentation are simply dumped in the first dipole magnet and the slits. A new scheme, named PALIS, meant to rescue such precious RIs using a compact gas catcher cell and resonance laser ionization, was proposed as a part of SLOWRI. The thermalized RI ions in a gas cell filled with Ar gas can be quickly neutralized and transported to the exit of the cell by gas flow. Irradiation of resonance lasers at the exit ionizes neutral RI atoms efficiently and selectively. The ionized RI ions can be further selected by a magnetic mass separator and transported to the SLOWRI experimental area for various experiments. The resonance ionization scheme itself can also be a useful method to perform hyperfine structure spectroscopy of RIs of many elements.

A prototype setup has been used to test resonance ionization schemes of several elements, extraction from the cell, and transport to a high-vacuum chamber. An online setup was fabricated in FY2013 and the first online commissioning took place in FY2015. It was confirmed that the PALIS gas cell is not deleterious for BigRIPS experiments, and a reasonable amount of radioactive Cu isotopes were extracted from the cell by gas flow.　Technical developments are in progress in on- and off-line commissioning.

(6) Development of highly charged ion trap for fundamental physics

Some particular transitions in highly charged ions (HCI) are sensitive to the temporal variation of the fine structure constant. High precision spectroscopy of such transitions can be a probe for the verification of fundamental physics. A cryogenic ion trap setup consisting of a micro electron beam ion trap (μEBIT) and a linear RFQ ion trap in a compact cryogenic enclosure is under development in collaboration with Quantum Metrology Laboratory. First candidate HCIs, such as Ba^{7+} or Ho^{14+} can be produced in the μEBIT and sympathetically cooled by laser cooled Be^+ ions in the linear RFQ trap, following which the "clock" transition can be measured by electron-shelving spectroscopy. The final target is $^{249}Cf^{15+}$, which is known to have the most sensitive transition to the temporal variation of the fine structure constant.

Members

Team Leader
Michiharu WADA

Research & Technical Scientist
Takao KOJIMA (Senior Research Scientist)　　　　　　　　　　　　Aiko TAKAMINE (concurrent; UENO laboratory)

Nishina Center Research Scientists

Tetsu SONODA

Kensuke KUSAKA (concurrent; BigRIPS Team)

Nishina Center Technical Scientist

Takeshi MAIE (concurrent; Cryogenic Technology Team)

Special Postdoctoral Researcher

Yuta ITO

Marco ROSENBUSCH

Part-time Workers

Shigeaki ARAI

Sota KIMURA

Ichiro KATAYAMA

Visiting Scientists

Hans A SCHUESSLER (Texas A&M Univ.)

Kunihiro OKADA (Sophia Univ.)

Hermann WOLLNIK (Univ. of Giessen)

Volker SONNENSCHEIN (Nagoya Univ.)

Hideki IIMURA (JAEA)

Mikael REPONEN (JYFL)

Hideki TOMITA (Nagoya Univ.)

Student Trainees

Naoki KIMURA (Sophia Univ.)

Takahide TAKAMATSU (Nagoya Univ.)

Masaya OOHASHI (Nagoya Univ.)

Daiki MATSUI (Nagoya Univ.)

Yoshitaka ADACHI (Nagoya Univ.)

List of Publications & Presentations

Publications

[Journal]

(Original Papers) *Subject to Peer Review

Y. Ito, P. Schury, M. Wada, F. Arai, H. Haba, Y. Hirayama, S. Ishizawa, D. Kaji, S. Kimura, H. Koura, M. MacCormick, H. Miyatake, J. Y. Moon, K. Morimoto, K. Morita, M. Mukai, I. Murray, T. Niwase, K. Okada, A. Ozawa, M. Rosenbusch, A. Takamine, T. Tanaka, Y. X. Watanabe, H. Wollnik, S. Yamaki, "First direct mass measurements of nuclides around $Z = 100$ with a multireflection time-of-flight mass spectrograph," Phys. Rev. Lett. **120**, 152501 (2018) .*

M. Mukai, Y. Hirayama, Y.X. Watanabe, P. Schury, H.S. Jung, M. Ahmed, H. Haba, H. Ishiyama, S.C. Jeong, Y. Kakiguchi, S. Kimura, J.Y. Moon, M. Oyaizu, A. Ozawa, J.H. Park, H. Ueno, M. Wada, H. Miyatake, "High-efficiency and low-background multi-segmented proportional gas counter for be-ta-decay spectroscopy," Nucl. Instrum. Methods Phys. Res. A **884**, 1−10 (2018) .*

T. Sonoda, H. Iimura, M. Reponen, M. Wada, I. Katayama, V. Sonnenschein, T. Takamatsu, H. Tomita, T.M. Kojima, "The laser and optical system for the RIBF-PALIS experiment," Nucl. Instrum. Methods Phys. Res. A **877**, 118−123 (2018) .*

Y. Hirayama, Y.X. Watanabe, M. Mukai, M. Oyaizu, M. Ahmed, H. Ishiyama, S.C. Jeong, Y. Kakiguchi, S. Kimura, J.Y. Moon, J.H. Park, P. Schury, M. Wada, H. Miyatake, "Doughnut-shaped gas cell for KEK Isotope Separation System," Nucl. Instrum. Methods Phys. Res. B **412**, 11−18 (2017) .*

H. Suzuki, L. Sinclair, P.-A. Söderström, G. Lorusso, P. Davies, L. S. Ferreira, E. Maglione, R. Wadsworth, J. Wu, Z. Y. Xu, S. Nishimura, P. Doornenbal, D. S. Ahn, F. Browne, N. Fukuda, N. Inabe, T. Kubo, D. Lubos, Z. Patel, S. Rice, Y. Shimizu, H. Takeda, H. Baba, A. Estrade, Y. Fang, J. Henderson, T. Isobe, D. Jenkins, S. Kubono, Z. Li, I. Nishizuka, H. Sakurai, P. Schury, T. Sumikama, H. Watanabe, and V. Werner, "Discovery of ^{72}Rb : A nuclear sandbank beyond the proton drip line ," Phys. Rev. Lett. **119**, 192503 (2017).*

Y. Hirayama, M. Mukai, Y. Watanabe, M. Oyaizu, M. Ahmed, Y. Kakiguchi, S. Kimura, H. Miyatake, P. Schury, M. Wada, S.C. Jeong, "Ionization cross section, pressure shift and isotope shift measurements of osmium," J. Phys. B: At. Mol. Opt. Phys. **50**, 215203 (2017) .*

T. Nakajima, K. Okada, M. Wada, V.A. Dzuba, M.S. Safronova, U.I. Safronova, N. Ohmae, "Visible spectra of highly charged holomium ions observed with a compact electron beam ion trap," Nucl. Instrum. Methods Phys. Res. B **408**, 118−121 (2017) .*

P. Schury, M. Wada, Y. Ito, D. Kaji, H. Haba, Y. Hirayama, S. Kimura, H. Koura, M. MacCormick, H. Miyatake, J.Y. Moon, K. Morimoto, K. Morita, I. Murray, A. Ozawa, M. Rosenbusch, M. Reponen, A. Takamine, T. Tanaka, Y.X. Watanabe, H. Wollnik, "Observation of doubly-charged ions of francium isotopes extracted from a gas cell," Nucl. Instrum. Methods Phys. Res. B **407**, 160−165 (2017) .*

K. Okada, Y. Takeda, N. Kimura, M. Wada, H.A. Schuessler, "Development of a wavy Stark velocity filter for studying interstellar chemistry," Rev. Sci. Instrum. **88**, 0813106 (2017) .*

Y. Hirayama, M. Mukai, Y.X. Watanabbe, M. Ahmed, S.C. Jeong, H.S. Jung, Y. Kakiguchi, S. Kanaya, J.Y. Moon, T. Nakatsukasa, M. Oyaizu, J.H. Park, P. Schury, A. Taniguchi, M. Wada, K. Wahiyama, H. Watanabe, H. Miyatake, "In-gas-cell laser spectroscopy of the magnetic dipole moment of the N≈126 isotope 199Pt," Phys. Rev. C **96**, 014307 (2017) .*

[Proceedings]
 (Original Papers) *Subject to Peer Review
  M. Commara, M. Mazzocco, A. Boiano, C. Boiano, C. Manea, C. Parascandolo, D. Pierroutsakou, C. Signorini, E. Strano, D. Torresi, H. Yamaguchi,
   D. Kahl, P.D. Meo, J. Grebosz, N. Imai, Y. Hirayama, H. Ishiyama, N. Iwasa, S.C. Jeong, H.M. Jia, Y.H. Kim, S. Kimura, S. Kubono, C.J. Lin,
   H. Miyatake, M. Mukai, T. Nakao, M. Nicoletto, Y. Sakaguchi, A.M. Sánchez-Benítez, F. Soramel, T. Teranishi, Y. Wakabayashi, Y.X. Watanabe,
   L. Yang, Y.Y. Yang, "^{8}B + ^{208}Pb elastic scattering at Coulomb barrier energies," EPJ Web Conf. **163**, 00032 (2017) .*

Oral Presentations
 [International Conference etc.]
  M. Wada, "High precision spectroscopy of low-energy short-lived nuclei," Turkish Physical Society 33rd International Physics Congress (TPS33), Bodrum,
   Turkey, Sept. 9, 2017.
  M. Wada, "Toward mass measurement of super-heavy nuclei using MRTOF," Workshop for Einsteinium Campaign, Tokai, Japan, Nov. 7, 2017.
  M. Wada, "Mass measurements of short-lived nuclei with a multi-reflection time-of-flight mass spectrograph −recent results and future plans−," The 10th
   International Conference on Nuclear Physics at Storage Rings (STORI'17), Kanazawa, Japan, Dec. 5, 2017.
  S. Kimura, "High precision mass measurements of intermediate-mass neutron-deficient nuclei via MRTOF-MS," The 10th International Conference on
   Nuclear Physics at Storage Rings (STORI'17), Kanazawa, Japan, Nov. 15, 2017.
  M. Rosenbusch, "Direct mass measurements of neutron-deficient Actinium and Radium isotopes; Probing indirect mass links in the region of heavy nuclei,"
   The 10th International Conference on Nuclear Physics at Storage Rings (STORI'17), Kanazawa, Japan, Nov. 15, 2017.
  M. Wada, "Precision mass measurements of short-lived heavy nuclei, present and future toward comprehensive measurement," International symposium on
   RI beam physics in the 21st century: 10th anniversary of RIBF, Wako, Japan, Dec. 5, 2017.
  M. Wada, "KEK MRTOF Efforts," KEK-TRIUMF Scientific Symposium, Vancouver, Canada, Dec. 14−15, 2017.

[Domestic Conference]
  M. Wada,「MRTOF 質量分光器を用いた重元素の網羅的高精度質量測定」, 2017 年度核データ研究会, 東海村, 2017 年 11 月 17 日.
  N. Kimura,「多価イオン共同冷却実験に向けたイオン生成と捕捉」, 日本物理学会 2017 年秋季大会, 岩手大学, 2017 年 9 月 21–24 日.
  N. Kimura,「多価イオン共同冷却実験に向けたイオン生成と捕捉 II」, 日本物理学会第 73 回年次大会, 野田, 2018 年 3 月 22–25 日.

RIBF Research Division
Instrumentation Development Group
Rare RI-ring Team

1. Abstract

Mass measurement is one of the most important contributions to a nuclear property research especially for short-lived unstable nuclei far from the beta-stability line. In particular, a high-precision mass measurement for nuclei located around the r-process pass (rare-RI) is required in nucleosynthesis point of view. We chose a method of time-of-flight isochronous mass spectrometry (IMS) to make a measurement time shorter than 1 ms. Heavy-ion storage ring named "Rare-RI Ring (R3)" has been constructed until the end of 2014 and commissioning experiments were successfully performed in 2015. Our target performance in the mass determination is to achieve accuracy of the order of 1 ppm (~100 keV) even if we get only one event. Since an isochronism in R3 is established over a wide range of the momentum, rare-RIs with a large momentum spread, $\Delta p/p = \pm 0.5\%$, are acceptable. Another significant feature of the R3 system is an individual injection scheme in which a produced rare-RI itself triggers the injection kicker. In the first commissioning experiment using primary ^{78}Kr beam, we demonstrated a high ability of R3 as a storage ring and succeed in establishing the individual injection scheme for the first time. In 2016, we performed the third commissioning experiment using isotopes around ^{78}Ge. We successfully extracted several kinds of isotopes, ^{79}As, ^{77}Ga, ^{76}Zn, and ^{75}Cu from the R3 in the same setting and established the mass measurement method. In 2017, we were able to improve the extraction efficiency by a factor of 10 and be ready to conduct the first mass measurement experiment with R3. We have plan to measure masses for isotopes around ^{75}Ni and ^{124}Pd regions in 2018.

2. Major Research Subjects

(1) Developments of heavy-ion storage ring
(2) Precision mass measurement for rarely produced isotopes related to r-process.

3. Summary of Research Activity

Since the lattice design of R3 is based on the cyclotron motion, it can provide an isochronism in a wide range of the momentum. We expect a great improvement in mass resolution in IMS as long as the isochronous field is precisely formed in R3. Therefore, IMS using R3 is capable of both a high-precision measurement and a fast measurement. All the devices in R3 was designed under the assumption that an incoming beam has an energy of less than 200 MeV/nucleon and a charge to mass ratio, m/q, of less than 3. The ring structure was designed with a similar concept of a separate-sector ring cyclotron. It consists of six sectors and 4.02-m straight sections, and each sector consists of four rectangular bending magnets. A radially homogeneous magnetic field is produced in the magnet, and a magnetic rigidity is 6.5 Tm at maximum, for instance, ^{78}Ni with the magnetic rigidity of 5.96 Tm. Two magnets at both ends of each sector are additionally equipped with ten trim coils to form a precise isochronous magnetic field. For $\Delta p = 0$ particle, the circumference is 60.35 m and the betatron tunes are $v_x = 1.21$ and $v_y = 0.84$ in horizontal and vertical directions, respectively. The momentum acceptance is $\Delta p/p = \pm 0.5\%$, and the transverse acceptances are 150π mmmrad and 30π mmmrad in horizontal and vertical directions with $\Delta p/p = 0.0\%$, respectively.

Another performance required for R3 is to efficiently seize hold of an opportunity of the measurement for rare-RIs produced unpredictably. We adopted an individual injection scheme in which the produced rare-RI itself triggers the injection kicker magnets. Full activation of the kicker magnetic field has to be completed within the flight time of the rare-RI from an originating point (F3 focal point in BigRIPS) of the trigger signal to the kicker position in R3. We successfully developed an ultra-fast response kicker system working with the repetition rate of 100 Hz.

Since R3 accumulates, in principle, only single ion, we need high-sensitive beam diagnostic devices in the ring, and they should be applicable even for a single particle circulation. One of them is a cavity type of Schottky pick-up installed for tuning of isochronous field. A resonance frequency is 171 MHz, a measured quality factor is about 1945, and shunt impedance is 190 kΩ. Another is a timing monitor, which detects secondary electrons emitted from thin carbon foil placed on the accumulation orbit. The thickness of the foil will be 50 μg/cm^2. The rare-RI with the energy of 200 MeV/nucleon survives only for first 100 turns because of an energy loss at the foil.

In 2015, we had two times of commissioning experiments. In the first commissioning, we used primary ^{78}Kr^{36+} beam with the energy of 168 MeV/nucleon. We succeeded in beam injection particle by particle in individual injection scheme, beam extraction after 700-μs accumulation (~1860 turns), and measurements of the TOF from the injection to the extraction. It was demonstrated that R3 works well as a storage ring and a single particle is certainly manipulated in this storage ring system. The individual injection scheme was established for the first time in the world. In addition, the Schottky pick-up monitored a single ^{78}Kr^{36+} particle circulation with the measuring time of less than 10 ms. That demonstrated that our pick-up is world most sensitive non-destructive monitor. In this experiment, we could tune completely the first order isochronism, but higher order components were remained, consequently, the 10-ppm accuracy of the isochronism was obtained. More precise tuning is possible with reference the Schottky data. In the second commissioning, we injected two isotopes, ^{36}Ar and ^{35}Cl, selected in the secondary beams into the ring, in which the isochronism is tuned for ^{36}Ar. It was obviously demonstrated that the mass of ^{35}Cl relative to ^{36}Ar is determined by comparing the TOF values for both isotopes, and the accuracy was ~20 ppm, which is one-order less than our target value of a few ppm. We found that the imperfection of isochronism significantly contributes to the time resolution of measured TOF values.

In 2016, we performed the third commissioning experiment using unstable nuclei. In this experiment, the 5-ppm accuracy of isochronism was obtained for the reference isotope ^{78}Ge by adjusting the isochronism up to second order. In addition, we derived the masses of ^{79}As, ^{77}Ga, ^{76}Zn, and ^{75}Cu relative to ^{78}Ge by determining its revolution time with beta correction. We found that not only the imperfection of isochronism but also the insufficient resolution of beta measurement significantly contributes to the mass resolution.

Detailed analysis is ongoing. In 2017, we performed the forth commissioning experiment using ^{78}Ge. In this experiment, we improved the extraction efficiency to 2% by considering the emittance matching. Since R3 is ready for mass measurement experiments, we will measure masses for isotopes around ^{75}Ni and ^{124}Pd regions in 2018.

Members

Team Leader
Masanori WAKASUGI (concurrent; Group Director, Instrumentations Development Gr.)

Nishina Center Research Scientists
Yoshitaka YAMAGUCHI

Nishina Center Technical Scientists
Takeshi MAIE (concurrent; Cryogenic Technology Team)

Special Postdoctoral Researcher
Yasushi ABE

Research Consultant
Akira NODA

List of Publications & Presentations

Publications
[Journal]
(Review)
Y. Yamaguchi, M. Wakasugi, Y. Abe, F. Suzaki, D. Nagae, S. Omika, S. Naimi, Z. Ge, T. Yamaguchi, A. Ozawa, and T. Uesaka, "Recent progress on the rare-RI ring at RIKEN RI Beam Factory," J. Part. Acc. Soc. Jpn. (in Japanese) **14**, 23−27 (2017).

Oral Presentations
[International Conference etc.]
S. Naimi, "The Rare-RI Ring ready to explore terra incognita," International Conference on Advances in Radioactive Isotope Science (ARIS2017), Colorado, USA, May−June 2017.

A. Ozawa, "Rare-RI Ring in RIKEN RI Beam Facrtory," China-Japan collaboration workshop on Nuclear mass and life for unravelling mysteries of r-process, Tsukuba, Japan, June 2017.

S. Suzuki, A. Ozawa, T. Moriguchi, M. Amano, D. Kamioka, Y. Ichikawa, Y. Tajiri, K. Hiraishi, T. Matsumoto, D. Nagae, Y. Abe, S. Naimi, T. Yamaguchi, S. Omika, Z. Ge, K. Wakayama, N. Tadano, H. Arakawa, K. Inomata, T. Kobayashi, A. Kitagawa, S. Sato, and H. Li, "Performance of time-of-flight detector and demonstration of completely new position detector for mass measurements with the Rare-RI Ring," 10th International Conference on Nuclear Physics at Storage Rings (STORI2017), Kanazawa, Japan, November 2017.

Y. Abe, and rare-RI ring collaborators, "Analysis of isochronism in Rare-RI Ring," 10th International Conference on Nuclear Physics at Storage Rings (STORI2017), Kanazawa, Japan, November 2017.

F. Suzaki, Y. Abe, M. Wakasugi, T. Yamaguchi, and Y. Yamaguchi, "Observation of ^{78}Kr stored in Rare-RI Ring with a resonant Schottky pick-up," 10th International Conference on Nuclear Physics at Storage Rings (STORI2017), Kanazawa, Japan, November 2017.

D. Nagae, and rare-RI ring collaborators, "Mass measurement of exotic nuclei using Rare-RI Ring," 10th International Conference on Nuclear Physics at Storage Rings (STORI2017), Kanazawa, Japan, November 2017.

A. Ozawa, "Past and future of Rare-RI Ring," 10th International Conference on Nuclear Physics at Storage Rings (STORI2017), Kanazawa, Japan, November 2017.

T. Yamaguchi, "Storage ring mass spectrometry of exotic nuclei," International symposium on RI beam physics in the 21st century: 10th anniversary of RIBF, Wako, Japan, December 2017.

T. Yamaguchi, "Status of storage rings in Japan," NUSTAR annual meeting, Darmstadt, Germany, February 2018.

S. Naimi, "Rare-RI Ring (R3) at RIBF/RIKEN: Mass measurement of r-process nuclei," Nuclear Astrophysics at Rings and Recoil Separators, Darmstadt, Germany, March 2018.

[Domestic Conference]
大甕舜一朗, 長江大輔, 山口貴之, 只野奈津生, 鈴木健, 若山清志, 荒川裕樹, 伊五澤涼, 猪股玖美, 西室国光, 藤居朋也, 三ツ井俊哉, 阿部康志, 上坂友洋, S. Naimi, Z. Ge, 洲嵜ふみ, 馬場秀忠, 柳澤善行, 矢野安重, 山口由高, 若杉昌徳, 天野将道, 小沢顕, 上岡大起, 鈴木伸司, 森口哲朗, 大田晋輔, 道正新一郎, G. Lorusso, Yu. A. Litvinov,「稀少 RI リングの質量測定の現状」, 日本物理学会 2017 年秋季大会, 宇都宮市, 2017 年 9 月.

鈴木伸司, 小沢顕, 森口哲朗, 天野将道, 上岡大起, 長江大輔, 阿部康志, S. Naimi, H. F. Li, 山口貴之, 大甕舜一朗, Z. Ge, 若山清志, 猪俣玖美, 荒川裕樹, 北川敦志, 佐藤眞二,「質量測定用非行時間検出器の大型実機の開発」, 日本物理学会 2017 年秋季大会, 宇都宮市, 2017 年 9 月.

大甕舜一朗, 長江大輔, 小沢顕, 山口貴之, 鈴木健, 荒川裕樹, 伊五澤涼, 猪股玖美, Z. Ge, 只野奈津生, 西室国光, 藤居朋也, 若山清志, 阿部康志, 上坂友洋, N. Sarah, 洲嵜ふみ, 鈴木宏, 馬場秀忠, Hongfu Li, 山口由高, 若杉昌徳, 天野将道, 上岡大起, 鈴木伸司, 森口哲朗, 大田晋輔, 道正新一郎, G. Lorusso, Yuri. A. Litvinov,「稀少 RI リングを用いたウラン核破砕片の質量測定実験のデータ解析」, 日本物理学会第 73 回年次大会, 野田市, 2018 年 3 月.

鈴木伸司, 小沢顕, 森口哲朗, 天野将道, 上岡大起, 長江大輔, 阿部康志, S. Naimi, H. F. Li, 山口貴之, 大甕舜一朗, Z. Ge, 若山清志, 猪俣玖美, 荒川裕樹, 北川敦志, 佐藤眞二,「RI 質量測定用の薄膜を用いた準非破壊的位置検出器の開発」, 日本物理学会第 73 回年次大会, 野田市, 2018 年 3 月.

Poster Presentations

[International Conference etc.]

D. Nagae, S. Omika, Y. Abe, Y. Yamaguchi, F. Suzaki, S. Naimi, Z. Ge, S. Suzuki, T. Moriguchi, K. Wakayama, N. Tadano, S. Michimasa, S. Ota, G. Lorusso, Yu. A. Lotvinov, T. Yamaguchi, T. Suzuki, A. Ozawa, T. Uesaka, M. Wakasugi, and Rare-RI collaborators, "First mass measurement using Rare-RI Ring," International Conference on Advances in Radioactive Isotope Science (ARIS2017), Colorado, USA, May−June 2017.

K. Inomata, T. Yamaguchi, H. Arakawa, T. Fujii, S. Omika, T. Suzuki, K. Wakayama, Y. Abe, H. Li, D. Nagae, M. Amano, D. Kamioka, T. Moriguchi, A. Ozawa, S. Suzuki, A. Kitagawa, and S. Sato, "Basic study on delta-ray detection for in-ring revolution time determination," 10th International Conference on Nuclear Physics at Storage Rings (STORI2017), Kanazawa, Japan, November 2017.

K. Inomata, T. Yamaguchi, H. Arakawa, K. Nishimuro, S. Omika, T. Suzuki, N. Tadano, K. Wakayama, D. Nagae, A. Kitagawa, and S. Sato, "Beam test of a long scintillating fiber as a position sensor for storage ring facility," 10th International Conference on Nuclear Physics at Storage Rings (STORI2017), Kanazawa, Japan, November 2017.

H. Arakawa, T. Yamaguchi, Y. Abe, M. Amano, K. Inomata, D. Kamioka, A. Kitagawa, H. Li, T. Moriguchi, D. Nagae, S. Omika, A. Ozawa, S. Sato, S. Suzuki, T. Suzuki, and K. Wakayama, "Properties of a thin YAP(Ce) scintillation counter for heavy ions," 10th International Conference on Nuclear Physics at Storage Rings (STORI2017), Kanazawa, Japan, November 2017.

Z. Ge, T. Uesaka, M. Wakasugi, H. Li, T. Yamaguchi, Y. Yamaguchi, S. Naimi, F. Suzaki, S. Suzuki, A. Ozawa, Y. Abe, D. Nagae, K. Wakayama, S. Omika, N. Tadano, T. Moriguchi, K. Inomata, T. Kobayashi, H. Arakawa, A. Kitagawa, and S. Sato, "Development of electrostatic mirror type MCP detector at Rare Ri Ring," 10th International Conference on Nuclear Physics at Storage Rings (STORI2017), Kanazawa, Japan, November 2017.

K. Wakayama, T. Yamaguchi, Y. Abe, M. Amano, H. Arakawa, H. Li, K. Inomata, D. Kamioka, A. Kitagawa, T. Kobayashi, D. Nagae, T. Moriguchi, S. Omika, A. Ozawa, S. Sato, S. Suzuki, T. Suzuki, N. Tadano, and Z. Ge, "A simple readout method of a position-sensitive detector using plastic scintillation bars," 10th International Conference on Nuclear Physics at Storage Rings (STORI2017), Kanazawa, Japan, November 2017.

H. Li, Z. Ge, S. Naimi, Y. Abe, T. Uesaka, and D. Nagae, "A large area position sensitive TOF MCP detector at the Rare RI Ring," 10th International Conference on Nuclear Physics at Storage Rings (STORI2017), Kanazawa, Japan, November 2017.

S. Omika, and rare-RI ring collaborators, "Development of experimental devices for precise mass measurements at the Rare-RI Ring facility," 10th International Conference on Nuclear Physics at Storage Rings (STORI2017), Kanazawa, Japan, November 2017.

RIBF Research Division
Instrumentation Development Group
SCRIT Team

1. Abstract

The SCRIT Electron Scattering Facility has been constructed at RIKEN RIBF. This aims at investigation of internal nuclear structure for short-lived unstable nuclei by means of electron scattering. SCRIT (Self-Confining RI Ion Target) is a novel method to form internal targets in an electron storage ring. This is a unique method for making electron scattering experiments for unstable nuclei possible. Construction of the facility has been started in 2009. This facility consists of an electron accelerator (RTM), a SCRIT-equipped electron storage ring (SR2), an electron-beam-driven RI separator (ERIS), and a window-frame spectrometer for electron scattering (WiSES) which consists of a large window-frame dipole magnet, drift chambers and trigger scintillators. Installation of all components in the facility was completed in 2015. After the comprehensive test and tuning, the luminosity was reached to $3\times10^{27}/(cm^2s)$ with the number of injected ions of 3×10^8. In 2016, we successfully completed a measurement of diffraction of scattered electrons from ^{132}Xe nuclei and determined the charge density distribution for the first time. The facility is now under setting up to move the first experiment for unstable nuclei.

2. Major Research Subjects

Development of SCRIT electron scattering technique and measurement of the nuclear charge density distributions of unstable nuclei.

3. Summary of Research Activity

SCRIT is a novel technique to form internal target in an electron storage ring. Positive ions are three dimensionally confined in the electron beam axis by transverse focusing force given by the circulating electron beam and applied electrostatic longitudinal mirror potential. The created ion cloud composed of RI ions injected from outside works as a target for electron scattering. Construction of the SCRIT electron scattering facility has been started in 2009. The electron accelerators RTM and the storage ring SR2 were successfully commissioned in 2010. Typical accumulation current in SR2 is 250−300 mA at the energy range of 100−300 MeV that is required energy range in electron scattering experiment. The SCRIT device was inserted in the straight section of SR2 and connected to an ISOL named ERIS (Electron-beam-driven RI separator for SCRIT) by 20-m long low energy ion transport line. A buncher system based on RFQ linear trap named FRAC (Fringing-RF-field-Activated dc-to-pulse converter) was inserted in the transport line to convert the continuous beam from ERIS to pulsed beam, which is acceptable for SCRIT. The detector system WiSES consisting of a high-resolution magnetic spectrometer, drift chambers and trigger scintillators, was constructed, and it has a solid angle of 100 msr, energy resolution of 10^{-3}, and the scattering angle coverage of 25−55 degrees. A wide range of momentum transfer, 80−300 MeV/c, is covered by changing the electron beam energy from 150 to 300 MeV.

We successfully measured a diffraction pattern in the angular distribution of scattered electron from ^{132}Xe isotope at the electron beam energy of 150 MeV, 200 MeV, and 300 MeV, and derived the nuclear charge distribution by assuming two-parameters Fermi model for the first time. At this time, luminosity was reached to $3\times10^{27}/(cm^2s)$ at maximum and the averaged value was $1.2\times10^{27}/(cm^2s)$ with the number of injected target ions of 3×10^8.

We are now under preparation for going to the experiments for unstable nuclei. There are some key issues for that. They are increasing the intensity of the RI beams from ERIS, efficient DC-to-pulse conversion at FRAC, improving the transmission efficiency from FRAC to SCRIT, and effective suppression of the background in measurement of scattered electrons. RI beam intensity will be improved by upgrading the electron beam power from 10 W to 60 W, increasing the contained amount of U in the target ion source, and some modifications in mechanical structure in the ion source. For upgrading the electron beam power, the RF system of RTM has been maintained intensively, and we will continue the development of RTM. For efficient DC-to-pulse conversion, we established the two-step bunching method, which is time compression at FRAC in combination with pre-bunching at the ion source using grid action. Furthermore, we will improve the conversion efficiency and the transmission efficiency from FRAC to the SCRIT device by cooling the trapped ions using minuscule amounts of a buffer gas. These improvements on FRAC were already confirmed in off-line test. Since one of significant contribution to the background for scattered electron is scattering from massive structural objects around the trapping region originated from halo components of the electron beam, we will remodel the SCRIT electrodes. The vacuum pump system at the SCRIT device will be upgraded to reduce the contribution of residual gases. Luminosity for radioactive Xe isotopes is expected to be more than $10^{26}/(cm^2s)$ after these improvements. Then, we will be able to start experiments for unstable nuclei. When further upgrading in the RTM power planed to be 3 kW will be achieved, we can extend the measurements to more exotic nuclei.

In 2017, several developments were started. One is the introduction of the surface-ionization type ion source at ERIS in order to increase kinds of radioactive beam and to produce high intensity beam. Another development is the upgrading of the drift chamber located in front of the magnetic spectrometer of WiSES to improve the momentum resolution and angular acceptance. These developments are in progress and they help to realize experiments for unstable nuclei.

Members

Team Leader

Masanori WAKASUGI (concurrent; Group Director, Instrumentations Development Gr.)

Research & Technical Scientists

Masamitsu WATANABE (Senior Research Scientist)   Tetsuya OHNISHI (Senior Technical Scientist)

Nishina Center Research Scientist
Akitomo ENOKIZONO

Research Consultants
Tadaaki TAMAE

Masahiro HARA

Shin-ichi ICHIKAWA

Takashi EMOTO

Senior Visiting Scientist
Toshitada HORI (Hiroshima University)

Visiting Scientists
Shuo WANG (Shandong University)

Ryo OGAWARA (National Institute of Radiological Sciences)

Yuki HONDA (Tohoku University)

Toshimi SUDA (Tohoku University)

Kyo TSUKADA (Tohoku University)

Kazuyoshi KURITA (Rikkyo University)

Research Fellow
Mamoru TOGASAKI (Rikkyo University)

Student Trainees
Keita KASAMA (Tohoku University)

Mitsuki HORI (Rikkyo University)

Kazuki NAMBA (Tohoku University)

Nobuaki UCHIDA (Rikkyo University)

Taihei AOYAGI (Tohoku University)

Shinnosuke SASAMURA (Rikkyo University)

Syota TAKAYAMA (Tohoku University)

List of Publications & Presentations

Publications
[Journals]

K. Tsukada, A. Enokizono, T. Ohnishi, K. Adachi, T. Fujita, M. Hara, M. Hori, T. Hori, S. Ichikawa, K. Kurita, K. Matsuda, T. Suda, T. Tamae, M. Togasaki, M. Wakasugi, M. Watanabe, and K. Yamada, "First elastic electron scattering from ^{132}Xe at the SCRIT facility," Phys. Rev. Lett. **118**, 262501 (2017).

T. Suda and Haik Simon, "Prospects for electron scattering on unstable, exotic nuclei," Prog. Part. Nucl. Phys, **96** 1−31, (2017).

A. Enokizono, T. Ohnishi, and K. Tsukada, "The SCRIT electron scattering facility at RIKEN: The world's first electron femtoscope for short-lived unstable nuclei," Nucl. Phys. News, in press.

[Proceedings]

(Original Papers) *Subject to Peer Review

T. Ohnishi, A. Enokizono, M. Hara, M. Hori, S. Ichikawa, M. Wakasugi, M. Watanabe, K. Adachi, T. Fujita, T. Hori, K. Kurita, M. Togasaki, N. Uchida, K. Yamaa, T. Suda, T. Tamae, and K. Tsukada, "The SCRIT electron scattering facility project at the RIKEN RI Beam Factory," Acta Phy. Pol. B **49,** 483−493, (2018).

A. Enokizono, K. Adachi, T. Fujita, M. Hori K. Kurita, S. Sasamura, M. Togasaki, N. Uchida, K. Yamada, K. Kasama, K. Namba, T. Suda, T. Tamae, K. Tsukada, M. Hara, T. Hori. S. Ichikawa, T. Ohnishi, M. Wakasugi, M. Watanabe, S. Wang, "The performance of the SCRIT detectors for electron-RI scattering experiment," Proc. Sci. **INPC2016**, 092 (2017).

T. Ohnishi, M. Hara, T. Hori, S. Ichikawa, M. Watanabe, M. Wakasugi, K. Adachi, A. Enokizono, T. Fujita. M. Hori, S. Ichikawa, M. Togasaki, N. Uchida, K. Yamada, K. Kurita, K. Kasama, K. Namba, K. Tsukada, T. Tamake, T. Suda, S. Wang, T. Kikuchi, "The SCRIT Electron Scattering Facility at the Riken RI Beam Factory," Proc. Sci. **INPC2016**, 088 (2017).

K. Tsukada, K. Kasama, K. Namba, T. Suda, T. Tamae, M. Hara, S. Ichikawa, T. Ohnishi, M. Wakasugi, M. Watanabe, K. Adachi, A. Enokizono, T. Fujita, M. Hori, K. Kurita, S. Sasamura, M. Togasaki, N. Uchida, K. Yamada, and S. Wang, "First result from SCRIT electon scattering facility: Charge density distribution of ^{132}Xe," Proc. Sci. **INPC2016**, 007 (2017).

Oral Presentations
[International Conference etc.]

K. Tsukada, "First result from SCRIT electron scattering facility with ^{132}Xe target," 10th International Conference on Nuclear Physics at Storage Rings (STORI17), Kanazawa, Japan, November 13−17, (2017).

A. Enokizono, "Properties of ion trapping inside the electron storage ring at the SCRIT experiment," 10th International Conference on Nuclear Physics at Storage Rings (STORI17), Kanazawa, Japan, November 13−17, (2017).

T. Ohnishi, "The SCRIT Electron scattering Facility project at the RIKEN RI Beam Factory," XXXV Mazurian Lakes Conference on Physics, Piaski, Poland, September 3−9, (2017).

T. Suda, "Electron scattering for neutron-rich exotic nuclei," ECT* workshop "Walk on the neutron-rich side," Trento, Italy, April 10−13, (2017).

T. Suda, "The SCRIT electron scattering facility − the world's first electron-scattering facility for short-lived exotic nuclei," The International Symposium on Physics of Unstable Nuclei 2017 (ISPUN17), Halong City, Vietnam, September 25−30, (2017).

A. Enokizono, K. Adachi, T. Fujita, M. Hara, M. Hori, T. Hori, S. Ichikawa, K. Kasama, K. Kurita, K. Namba, T. Ohnishi, S. Sasamura, T. Suda, T. Tamae, K. Tsukada, M. Togasaki, N. Uchida, M. Wakasugi, S. Wang, M. Watanabe, K. Yamada, "Results of the first physics experiment with 132Xe and 208Pb targets at the SCRIT facility," ARIS2017, Keystone, Colorado, May 30th, (2017).

A. Enokizono, K. Adachi, T. Fujita, M. Hara, M. Hori, T. Hori, S. Ichikawa, K. Kasama, K. Kurita, K. Namba, T. Ohnishi, S. Sasamura, S. Wang, T. Suda, T. Tamae, K. Tsukada, M. Togasaki, N. Uchida, M. Wakasugi, M. Watanabe, K. Yamada, "The performance of the SCRIT detectors for electron-ri scattering experiment," International Nuclear Physics Conference (INPC2016), Adelaide Convention Centre, Australia, September 11−16, (2016).

T Ohnishi, M. Hara, T. Hori, S. Ichikawa, M. Watanabe, M. Wakasugi, K. Adachi, A. Enokizono, T. Fujita, M. Hori, S. Sasamura, M. Togasaki, N. Uchida, K. Yamada, K. Kurita, K. Kasama, K. Namba, K. Tsukada, T. Tamae, T. Suda, S. Wang, T. Kikuchi, "The SCRIT electron scattering facility at the RIKEN RI Beam Factory," International Nuclear Physics Conference (INPC2016), Adelaide Convention Centre, Australia, September 11−16, (2016).

K. Tsukada, K. Kasama, K. Namba, T. Suda, T. Tamae, M. Hara, T. Hori, S. Ichikawa, T. Ohnishi, M. Wakasugi, M. Watanabe, K. Adachi, A. Enokizono, T. Fujita, M. Hori, K. Kurita, S. Sasamura, M. Togasaki, N. Uchida, K. Yamada, "First result from SCRIT electron scattering facility: Charge density distribution of ^{132}Xe," International Nuclear Physics Conference, Adelaide Convention Centre, Australia, September 11−16, (2016).

K. Kurita, "How SCRIT came into reality," International Symposium on Modern technique and its Outlook in Heavy Ion Science (MOTO16), Rikkyo University, Tokyo, Japan, June (2016).

T. Suda, "SCRIT electron scattering facility: present status and future perspectives," Neutron Skin of Nuclei, Mainz, Germany, May 17–27, (2016).

T. Suda, "Electron scattering off short-lived nuclei at SCRIT facility," Seminar at GANIL, CAEN, France. April 29, 2016.

K. Tsukada, "Physics program with SCRIT," Electron-radioactive ion collisions: theoretical and experimental challenges, Saclay, France, April 25–27, (2016).

T. Suda, "Future perspectives of the SCRIT facility," Electron-radioactive ion collisions: theoretical and experimental challenges, Saclay, France, April 25−27, (2016).

M. Wakasugi, "The SCRIT Facility at RIKEN," Int. Workshop on Electron Radioactive Collision, Apr. 25−27, CEA Saclay, France (2016).

[Domestic Conference]

内田信昭, 足立江介, 市川進一, 榎園昭智, 大西哲哉, 笠間桂太, 栗田和好, 須田利美, 玉江忠明, 塚田暁, 戸ケ崎衛, 原雅弘, 藤田峻広, 堀充希, 堀利匡, 山田耕平, 若杉昌徳, 渡邊正満, 「SCRIT 実験における捕獲されたイオンのモジュレーション依存性」, 日本物理学会, 3 月, 東京理科大学, 千葉 (2018).

堀充希, 榎園昭智, 大西哲哉, 原雅弘, 栗田和好, 若杉昌徳, 渡邊正満, 「電子蓄積リングにおける二光子相関を用いたバンチ長モニター開発」, 日本物理学会, 3 月, 東京理科大学, 千葉 (2018).

高山祥汰, 須田利美, 塚田暁, 本多佑記, 玉江忠明, 笠間桂太, 青柳泰平, for the SCRIT collaboration, 「SCRIT 電子スペクトロメーター性能向上に向けた飛跡検出器の開発」, 日本物理学会, 3 月, 東京理科大学, 千葉 (2018).

塚田暁, 市川進一, 内田信昭, 榎園昭智, 大西哲哉, 栗田和好, 笹村薪ノ介, 須田利美, 玉江忠明, 戸ケ崎衛, 原雅弘, 堀利匡, 堀充希, 若杉昌徳, 渡邊正満, 「SCRIT 実験：安定核標的による成果と今後", 日本物理学会, 9 月, 宇都宮大学, 栃木 (2017).

山田耕平, 大西哲哉, 栗田和好, 戸ケ崎衛, 鳥羽僚太, 原雅弘, 渡邊正満, 若杉昌徳 SCRIT 実験のためのイオンビームバンチャーの開発」, 日本物理学会, 3 月, 大阪大学, 大阪 (2017).

藤田峻広, 足立江介, 市川進一, 内田信昭, 榎園昭智, 大西哲哉, 笠間桂太, 栗田和好, 笹村薪之介, 須田利美, 玉江忠明, 塚田暁, 戸ケ崎衛, 南波和希, 原雅弘, 堀利匡, 堀充希, 松田一衛, 山田耕平, 若杉昌徳, 渡邊正満, 「電子蓄積リングにおける電子散乱実験の制動輻射を用いたルミノシティ測定」, 日本物理学会, 3 月, 大阪大学, 大阪 (2017).

塚田暁, 足立江介, 市川進一, 榎園昭智, 大西哲哉, 笠間桂太, 栗田和好, 笹村薪之介, 須田利美, 玉江忠明, 戸ケ崎衛, 南波和希, 原雅弘, 藤田峻広, 堀利匡, 堀充希, 松田一衛, 山田耕平, 若杉昌徳, 渡邊正満, 「SCRIT法を用いた ^{132}Xe の電荷分布測定」, 日本物理学会, 9 月, 宮崎大学, 宮崎 (2016).

藤田峻広, 足立江介, 市川進一, 榎園昭智, 大西哲哉, 栗田和好, 須田利美, 玉江忠明, 塚田暁, 戸ケ崎衛, 原雅弘, 堀利匡, 堀充希, 松田一衛, 山田耕平, 若杉昌徳, 渡邊正満, 「SCRIT 法を用いた Xe 同位体標的・電子散乱実験における ルミノシティ測定」, 日本物理学会, 9 月, 宮崎大学, 宮崎 (2016).

塚田暁, 足立江介, 市川進一, 榎園昭智, 大西哲哉, 栗田和好, 須田利美, 玉江忠明, 水流輝明, 戸ケ崎衛, 原雅弘, 藤田峻広, 堀利匡, 堀充希, 松田一衛, 山田耕平, 若杉昌徳, 渡邊正満, 「SCRIT 法を用いた Xe 同位体標的における電子散乱の角度分布測定」, 日本物理学会, 3 月, 東北学院大, 仙台 (2016).

榎園昭智, 足立江介, 市川進一, 大西哲哉, 栗田和好, 須田利美, 玉江忠明, 塚田暁, 水流輝明, 戸ケ崎衛, 原雅弘, 藤田峻広, 堀利匡, 堀充希, 松田一衛, 山田耕平, 若杉昌徳, 渡邊正満, 「SCRIT 法を用いた電子・不安定 Xe 核散乱実験におけるルミノシティの測定」, 日本物理学会, 3 月, 東北学院大, 仙台 (2016).

Poster Presentations
[International Conference etc.]

T. Ohnishi, K. Adachi, A. Enokizono, T. Fujita, M. Hara, M. Hori, T. Hori, S. Ichikawa, K. Kasama, K. Kurita, T. Suda, T. Tamae, M. Togasaki, K. Tsukada, N. Uchida, M. Wakasugi, M. Watanabe, K. Yamada, "THE SCRIT electron scattering facility at RIKEN RI Beam Factory," 10th International Conference on Nuclear Physics at Storage Rings (STORI17), Kanazawa, Japan, November 13−17, (2017).

RIBF Research Division
Research Instruments Group

1. Abstract

The Research Instruments Group is the driving force at RI Beam Factory (RIBF) for continuous enhancement of activities and competitiveness of experimental research. Consisting of four teams, we are in charge of the operation, maintenance, and improvement of the core research instruments at RIBF, such as the BigRIPS in-flight RI separator, ZeroDegree spectrometer and SAMURAI spectrometer, and the related infrastructure and equipment. We are also in charge of the production and delivery of RI beams using the BigRIPS separator. The group also conducts related experimental research as well as R&D studies on the research instruments.

2. Major Research Subjects

Design, construction, operation, maintenance, and improvement of the core research instruments at RIBF and related R&D studies. Experimental studies on exotic nuclei.

3. Summary of Research Activity

The current research subjects are summarized as follows:

(1) Production and delivery of RI beams and related research

(2) Design, construction, operation, maintenance, and improvement of the core research instruments at RIBF and their related infrastructure and equipment

(3) R&D studies on the core research instruments and their related equipment at RIBF

(4) Experimental research on exotic nuclei using the core research instruments at RIBF

Members

Group Director
Hideki UENO

Junior Research Associate
Momo MUKAI (Tsukuba University)

Senior Visiting Scientists
Toshio KOBAYASHI (Tohoku University)   Jerry NOLEN (Argonne National Laboratory)

Visiting Scientist
Toshiyuki KUBO (Michigan State University)

Student Trainee
Katrina Elizabeth KOEHLER (West Michigan University)

RIBF Research Division
Research Instruments Group
BigRIPS Team

1. Abstract

This team is in charge of design, construction, development and operation of BigRIPS in-flight separator and its related research instruments at RI beam factory (RIBF). They are employed not only for the production of RI beams but also the experimental studies using RI beams.

2. Major Research Subjects

Design, construction, development and operation of BigRIPS in-flight separator, RI-beam transport lines, and their related research instruments

3. Summary of Research Activity

This team is in charge of design, construction, development and operation of BigRIPS in-flight separator, RI-beam transport lines, and their related research instruments such as ZeroDegree spectrometer at RI beam factory (RIBF). They are employed not only for the production of RI beams but also various kinds of experimental studies using RI beams.

The research subjects may be summarized as follows:

(1) General studies on RI-beam production using in-flight scheme.
(2) Studies on ion-optics of in-flight separators, including particle identification of RI beams
(3) Simulation and optimization of RI-beam production.
(4) Development of beam-line detectors and their data acquisition system.
(5) Experimental studies on production reactions and unstable nuclei.
(6) Experimental studies of the limits of nuclear binding.
(7) Development of superconducting magnets and their helium cryogenic systems.
(8) Development of a high-power production target system.
(9) Development of a high-power beam dump system.
(10) Development of a remote maintenance and remote handling systems.
(11) Operation, maintenance and improvement of BigRIPS separator system, RI-beam transport lines, and their related research instruments such as ZeroDegree spectrometer and so on.
(12) Experimental research using RI beams.

Members

Team Leader
Koichi YOSHIDA

Research & Technical Scientists
Yoshiyuki YANAGISAWA (Senior Research Scientist)   Masao OHTAKE (Senior Technical Scientist)
Naohito INABE (Senior Technical Scientist)

Nishina Center Research Scientists
Hiroyuki TAKEDA   Naoki FUKUDA
Kensuke KUSAKA

Contract Researchers
Yohei SHIMIZU   Hiroshi SUZUKI

Postdoctoral Researchers
Deuk Soon AHN   Zeren KORKULU

Research Consultant
Hidekazu KUMAGAI

Part-time Worker
Tetsuro KOMATSUBARA

Visiting Scientists
Daisuke KAMEDA (TOSHIBA Corp.)   Michael Andrew FAMIANO (Western Michigan University)

Daniel Pierre BAZIN (NSCL, MSU)

Oleg Borisovich TARASOV (NSCL, MSU)

Hans GEISSEL (GSI)

David Joseph MORRISSEY (NSCL, MSU)

Bradley Marc SHERRILL (NSCL, MSU)

Yutaka MIZOI (Osaka Elec.-Com. University)

Naohito IWASA (Tohoku University)

Tuomas Arne Santeri GRAHN (University of Jyvaskyla)

Alfredo ESTRADE VAZ (Central Michigan University)

Mauricio PORTILLO (NSCL, MSU)

Alan Matthew AMTHOR (Bucknell University)

Kazuo IEKI (Rikkyo University)

Student Trainees

Daichi MURAI (Rikkyo University)

Ha JEONGSU (Seoul National University)

Kousei ASADA (Tohoku University)

Junki AMANO (Rikkyo University)

Takahiro SAKAKIBARA (Tohoku University)

Shunki ISHIKAWA (Tohoku University)

List of Publications & Presentations

Publications

[Journal]

(Original Papers) *Subject to Peer Review

J. Wu, S. Nishimura, G. Lorusso, P. Möller, E. Ideguchi, P.-H. Regan, G. S. Simpson, P.-A. Söderström, P. M. Walker, H. Watanabe, Z. Y. Xu, H. Baba, F. Browne, R. Daido, P. Doornenbal, Y. F. Fang, N. Fukuda, G. Gey, T. Isobe, Z. Korkulu, P. S. Lee, J. J. Liu, Z. Li, Z. Patel, V. Phong, S. Rice, H. Sakurai, L. Sinclair, T. Sumikama, M. Tanaka, A. Yagi, Y. L. Ye, R. Yokoyama, G. X. Zhang, D. S. Ahn, T. Alharbi, N. Aoi, F. L. Bello Garrote, G. Benzoni, A. M. Bruce, R. J. Carroll, K. Y. Chae, Z. Dombradi, A. Estrade, A. Gottardo, C. J. Griffin, N. Inabe, D. Kameda, H. Kanaoka, I. Kojouharov, F. G. Kondev, T. Kubo, S. Kubono, N. Kurz, I. Kuti, S. Lalkovski, G. J. Lane, E. J. Lee, T. Lokotko, G. Lotay, C.-B. Moon, D. Murai, H. Nishibata, I. Nishizuka, C. R. Nita, A. Odahara, Zs. Podolyák, O. J. Roberts, H. Schaffner, C. Shand, Y. Shimizu, H. Suzuki, H. Takeda, J. Taprogge, S. Terashima, Z. Vajta, and S. Yoshida, "94 β-Decay half-lives of neutron-rich ^{55}Cs to ^{67}Ho: Experimental feedback and evaluation of the r-process rare-earth peak formation," Phys. Rev. Lett. **118**, 072701 (2017).*

H. Suzuki, L. Sinclair, P.-A. Söderström, G. Lorusso, P. Davies, L.S. Ferreira, E. Maglione, R. Wadsworth, J. Wu, Z.Y. Xu, S. Nishimura, P. Doornenbal, D.S. Ahn, F. Browne, N. Fukuda, N. Inabe, T. Kubo, D. Lubos, Z. Patel, S. Rice, Y. Shimizu, H. Takeda, H. Baba, A. Estrade, Y. Fang, J. Henderson, T. Isobe, D. Jenkins, S. Kubono, Z. Li, I. Nishizuka, H. Sakurai, P. Schury, T. Sumikama, H. Watanabe, and V. Werner, "Discovery of ^{72}Rb: A nuclear sandbank beyond the proton drip line," Phys. Rev. Lett. **119**, 192503 (2017).*

R. Yokoyama, S. Go, D. Kameda, T. Kubo, N. Inabe, N. Fukuda, H. Takeda, H. Suzuki, K. Yoshida, K. Kusaka, K. Tanaka, Y. Yanagisawa, M. Ohtake, H. Sato, Y. Shimizu, H. Baba, M. Kurokawa, D. Nishimura, T. Ohnishi, N. Iwasa, A. Chiba, T. Yamada, E. Ideguchi, T. Fujii, H. Nishibata, K. Ieki, D. Murai, S. Momota, Y. Sato, J. W. Hwang, S. Kim, O. B. Tarasov, D. J. Morrissey, B. M. Sherrill, G. Simpson, and C. R. Praharaj, "New K isomers in the neutron-rich N =100 isotones ^{162}Sm, ^{163}Eu, and ^{164}Gd," Phys. Rev. C **95**, 034313, (2017).*

B. Moon, C.-B. Moon, P.-A. Söderström, A. Odahara, R. Lozeva, B. Hong, F. Browne, H. S. Jung, P. Lee, C. S. Lee, A. Yagi, C. Yuan, S. Nishimura, P. Doornenbal, G. Lorusso, T. Sumikama, H. Watanabe,.I. Kojouharov, T. Isobe, H. Baba, H. Sakurai, R. Daido, Y. Fang, H. Nishibata, Z. Patel,. Rice, L. Sinclair, J. Wu, Z. Y. Xu, R. Yokoyama, T. Kubo, N. Inabe, H. Suzuki, N. Fukuda, D. Kameda, H. Takeda, D. S. Ahn, Y. Shimizu, D. Murai, F. L. Bello Garrote, J. M. Daugas, F. Didierjean, E. Ideguchi, T. Ishigaki, S. Morimoto, M. Niikura, I. Nishizuka, T. Komatsubara, Y. K. Kwon, and K. Tshoo, "Nuclear structure and β-decay schemes for Te nuclides beyond N = 82," Phys. Rev. C **95**, 044322 (2017).*

T. Sumikama, S. Nishimura, H. Baba, F. Browne, P. Doornenbal, N. Fukuda, S. Franchoo, G. Gey, N. Inabe, T. Isobe, P. R. John, H. S. Jung, D. Kameda, T. Kubo, Z. Li, G. Lorusso,. Matea, K. Matsui, P. Morfouace, D. Mengoni, D. R. Napoli, M. Niikura, H. Nishibata, A. Odahara, E. Sahin, H. Sakurai, P.-A. Söderström, G. I. Stefan, D. Suzuki, H. Suzuki, H. Takeda, R. Taniuchi, J. Taprogge, Zs. Vajta, H. Watanabe, V. Werner, J. Wu, Z. Y. Xu, A. Yagi, and K. Yoshinaga, "Observation of new neutron-rich Mn, Fe, Co, Ni, and Cu isotopes in the vicinity of ^{78}Ni," Phys. Rev. C **95**, 051601(R) (2017).*

A. I. Morales, A. Algora, B. Rubio, K. Kaneko, S. Nishimura, P. Aguilera, S. E. A. Orrigo, F. Molina, G. de Angelis, F. Recchia, G. Kiss, V. H. Phong, J. Wu, D. Nishimura, H. Oikawa, T. Goigoux, J. Giovinazzo, P. Ascher, J. Agramunt, D. S. Ahn, H. Baba, B. Blank, C. Borcea, A. Boso, P. Davies, F. Diel, Zs. Dombrádi, P. Doornenbal, J. Eberth, G. de France, Y. Fujita, N. Fukuda, E. Ganioglu, W. Gelletly, M. Gerbaux, S. Grévy, V. Guadilla, N. Inabe, T. Isobe, I. Kojouharov, W. Korten, T. Kubo, S. Kubono, T. Kurtukián Nieto, N. Kurz, J. Lee, S. Lenzi, J. Liu, T. Lokotko, D. Lubos, C. Magron, A. Montaner-Pizá, D. R. Napoli, H. Sakurai, H. Schaffner, Y. Shimizu, C. Sidong, P.-A. Söderström, T. Sumikama, H. Suzuki, H. Takeda, Y. Takei, M. Tanaka, and S. Yagi, "Simultaneous investigation of the T = 1 (J^π = 0$^+$) and T = 0 (J^π = 9$^+$) β decays in ^{70}Br," Phys. Rev. C **95**, 064327 (2017).*

B. Moon, C.-B. Moon, A. Odahara, R. Lozeva, P.-A. Söderström, F. Browne, C. Yuan, A. Yagi, B. Hong, H. S. Jung, P. Lee, C. S. Lee, S. Nishimura, P. Doornenbal, G. Lorusso, T. Sumikama, H. Watanabe, I. Kojouharov, T. Isobe, H. Baba, H. Sakurai, R. Daido, Y. Fang, H. Nishibata, Z. Patel, S. Rice, L. Sinclair, J. Wu, Z. Y. Xu, R. Yokoyama, T. Kubo, N. Inabe, H. Suzuki, N. Fukuda, D. Kameda, H. Takeda, D. S. Ahn, Y. Shimizu, D. Murai, F. L. Bello Garrote, J. M. Daugas, F. Didierjean, E. Ideguchi, T. Ishigaki, S. Morimoto, M. Niikura, I. Nishizuka, T. Komatsubara, Y. K. Kwon, and K. Tshoo, "β-decay scheme of ^{140}Te to ^{140}I: Suppression of Gamow-Teller transitions between the neutron h$_{9/2}$ and proton h$_{11/2}$ partner orbitals," Phys. Rev. C **96**, 014325 (2017).*

F. Browne, A. M. Bruce, T. Sumikama, I. Nishizuka, S. Nishimura, P. Doornenbal, G. Lorusso, P.-A. Söderström, H. Watanabe, R. Daido, Z. Patel, S. Rice, L. Sinclair, J. Wu, Z. Y. Xu, A. Yagi, H. Baba, N. Chiga, R. Carroll, F. Didierjean, Y. Fang, N. Fukuda, G. Gey, E. Ideguchi, N. Inabe, T. Isobe, D. Kameda, I. Kojouharov, N. Kurz, T. Kubo, S. Lalkovski, Z. Li, R. Lozeva, N. Nishibata, A. Odahara, Zs. Podolyák, P. H. Regan, O. J. Roberts, H. Sakurai, H. Schaffner, G. S. Simpson, H. Suzuki, H. Takeda, M. Tanaka, J. Taprogge, V. Werner, and O. Wieland, "K selection in the decay of the (ν5/2[532]⊗3/2[411])4$^-$ isomeric state in ^{102}Zr," Phys. Rev. C 96, 024309 (2017).*

Z. Patel, P. M. Walker, Zs. Podolyák, P. H. Regan, T. A. Berry, P.-A. Söderström, H. Watanabe, E. Ideguchi, G. S. Simpson, S. Nishimura, Q. Wu, F. R.

Xu, F. Browne, P. Doornenbal, G. Lorusso, S. Rice, L. Sinclair, T. Sumikama, J. Wu, Z. Y. Xu, N. Aoi, H. Baba, F. L. Bello Garrote, G. Benzoni, R. Daido, Zs. Dombrádi, Y. Fang, N. Fukuda, G. Gey, S. Go, A. Gottardo, N. Inabe, T. Isobe, D. Kameda, K. Kobayashi, M. Kobayashi, T. Komatsubara, I. Kojouharov, T. Kubo, N. Kurz, I. Kuti, Z. Li, M. Matsushita, S. Michimasa, C.-B. Moon, H. Nishibata, I. Nishizuka, A. Odahara, E. S¸ahin, H. Sakurai, H. Schaffner, H. Suzuki, H. Takeda, M. Tanaka, J. Taprogge, Zs. Vajta, A. Yagi, and R. Yokoyama, "Isomer-delayed γ-ray spectroscopy of A = 159–164 midshell nuclei and the variation of K-forbidden E1 transition hindrance factors," Phys. Rev C **96**, 034305 (2017).*

H. Suzuki, T. Kubo, N. Fukuda, N. Inabe, D. Kameda, H. Takeda, K. Yoshida, K. Kusaka, Y. Yanagisawa, M. Ohtake, H. Sato, Y. Shimizu, H. Baba, M. Kurokawa, K. Tanaka, O. B. Tarasov, D. Bazin, D. J. Morrissey, B. M. Sherrill, K. Ieki, D. Murai, N. Iwasa, A. Chiba, Y. Ohkoda, E. Ideguchi, S. Go, R. Yokoyama, T. Fujii, D. Nishimura, H. Nishibata, S. Momota, M. Lewitowicz, G. DeFrance, I. Celikovic, and K. Steiger, "Discovery of new isotopes ^{81,82}Mo and ^{85,86}Ru and a determination of the particle instability of ^{103}Sb," Phys. Rev. C **96**, 034604 (2017).*

J. Park, R. Krücken, D. Lubos, R. Gernhäuser, M. Lewitowicz, S. Nishimura, D. S. Ahn, H. Baba, B. Blank, A. Blazhev, P. Boutachkov, F. Browne, I. ˇCelikoviˊ, G. de France, P. Doornenbal, T. Faestermann, Y. Fang, N. Fukuda, J. Giovinazzo, N. Goel, M. Górska, H. Grawe, S. Ilieva, N. Inabe, T. Isobe, A. Jungclaus, D. Kameda, G. D. Kim, Y.-K. Kim, I. Kojouharov, T. Kubo, N. Kurz, G. Lorusso, K. Moschner, D. Murai, I. Nishizuka, Z. Patel, M. M. Rajabali, S. Rice, H. Sakurai, H. Schaffner, Y. Shimizu, L. Sinclair, P.-A. Söderström, K. Steiger, T. Sumikama, H. Suzuki, H. Takeda, Z. Wang, H. Watanabe, J. Wu, and Z. Y. Xu, "Properties of γ-decaying isomers and isomeric ratios in the ^{100}Sn region," Phys. Rev. C **96**, 044311 (2017)

N. Nakatsuka, H.Baba, T.Aumann, R.Avigo, S.R.Banerjee, A.Bracco, C.Caesar, F.Camera, S.Ceruti, S.Chen, V.Derya, P.Doornenbal, A.Giaz, A.Horvat, K.Ieki, T.Inakura, N.Imai, T.Kawabata, N.Kobayashi, Y.Kondo, S.Koyama, M.Kurata-Nishimura, M.Masuoka, M.Matsushita, S.Michimasa, B.Million, T.Motobayashi, T.Murakami, T.Nakamura, T.Ohnishi, H.J.Ong, S.Ota, H.Otsu, T.Ozaki, A.Saito, H.Sakurai, H.Scheit, F.Schindler, P.Schrock, Y.Shiga, M.Shikata, S.Shimoura, D.Steppenbeck, T.Sumikama, I.Syndikus, H.Takeda, S.Takeuchi, A.Tamii, R.Taniuchi, Y.Togano, J.Tscheuschner, J.Tsubota, H.Wang, O.Wieland, K.Wimmer, Y.Yamaguchi, K.Yoneda, J.Zenihiro, Observation of isoscalar and isovector dipole excitations inneutron-rich ^{20}O, Phys. Lett. B **768**, 387 (2017).*

J.W.Hwang, S.Kim, Y.Satou, N.A.Orr, Y.Kondo, T.Nakamura, J.Gibelin, N.L.Achouri, T.Aumann, H.Baba, F.Delaunay, P.Doornenbal, N.Fukuda, N.Inabe, T.Isobe, D.Kameda, D.Kanno, N.Kobayashi, T.Kobayashi, T.Kubo, S.Leblond, J.Lee F.M.Marqués, R.Minakata, T.Motobayashi, D.Murai, T.Murakami, K.Muto, T.Nakashima, N.Nakatsuka, A.Navin, S.Nishi, S.Ogoshi, H.Otsu, H.Sato, Y.Shimizu, H.Suzuki, K.Takahashi, H.Takeda, S.Takeuchi, R.Tanaka, Y.Togano, A.G.Tuff, M.Vandebrouck, K.Yoneda, "Single-neutron knockout from ^{20}C and the structure of ^{19}C," Phys. Lett. B **769**, 503 (2017).*

A. Jungclaus, H. Grawe, S. Nishimura, P. Doornenbal, G. Lorusso, G.S. Simpson, P.-A. Söderström, T. Sumikama, J. Taprogge, Z.Y. Xu, H. Baba, F. Browne, N. Fukuda, R. Gernhäuser, G. Gey, N. Inabe, T. Isobe, H.S. Jung, D. Kameda, G.D. Kim, Y.-K. Kim, I. Kojouharov, T. Kubo, N. Kurz, Y.K. Kwon, Z. Li, H. Sakurai, H. Schaffner, Y. Shimizu, K. Steiger, H. Suzuki, H. Takeda, Zs. Vajta, H. Watanabe, J. Wu, A. Yagi, K. Yoshinaga, G. Benzoni, S. Bönig, K.Y. Chae, L. Coraggio, J.-M. Daugas, F. Drouet, A. Gadea, A. Gargano, S. Ilieva, N. Itaco, F.G. Kondev, T. Kröll, G.J. Lane, A. Montaner-Pizá, K. Moschner, D. Mücher, F. Naqvi, M. Niikura, H. Nishibata, A. Odahara, R. Orlandi, Z. Patel, Zs. Podolyák, A. Wendt, "Observation of a γ-decaying millisecond isomeric state in ^{128}Cd$_{80}$," Phys. Lett. B **772**, 483 (2017).*

H. Wang, H. Otsu, H. Sakurai, D. Ahn, M. Aikawa, T. Ando, S. Araki, S. Chen, N. Chiga, P. Doornenbal, N. Fukuda, T. Isobe, S. Kawakami, S. Kawase, T. Kin, Y. Kondo, S. Koyama, S. Kubono, Y. Maeda, A. Makinaga, M. Matsushita, T. Matsuzaki, S. Michimasa, S. Momiyama, S. Nagamine, T. Nakamura, K. Nakano, M. Niikura, T. Ozaki, A. Saito, T. Saito, Y. Shiga, M. Shikata, Y. Shimizu, S. Shimoura, T. Sumikama, P.-A. Söderström, H. Suzuki, H. Takeda, S. Takeuchi, R. Taniuchi, Y. Togano, J. Tsubota, M. Uesaka Y. Watanabe, Y. Watanabe, K. Wimmer, T. Yamamoto, K. Yoshida, "Spallation reaction study for the long-lived fission product ^{107}Pd," Prog. Theor. Exp. Phys. **2017**, 021D01 (2017).

S. Kawase, K. Nakano, Y. Watanabe, H. Wang, H. Otsu, H. Sakurai, D. S. Ahn, M. Aikawa, T. Ando, S. Araki, S. Chen, N. Chiga, P. Doornenbal, N. Fukuda, T. Isobe, S. Kawakami, T. Kin, Y. Kondo, S. Koyama, S. Kubono, Y. Maeda, A. Makinaga, M. Matsushita, T. Matsuzaki, S. Michimasa, S. Momiyama, S. Nagamine, T. Nakamura, M. Niikura, T. Ozaki, A. Saito, T. Saito, Y. Shiga, M. Shikata, Y. Shimizu, S. Shimoura, T. Sumikama, P. Soderstrom, H. Suzuki, H. Takeda, S. Takeuchi, R. Taniuchi, Y. Togano, J. Tsubota, M. Uesaka, Y. Watanabe, K. Wimmer, T. Yamamoto, K. Yoshida, "Study of proton- and deuteron-induced spallation reactions on the long-lived fission product ^{93}Zr at 105 MeV/nucleon in inverse kinematics," Prog. Theor. Exp. Phys. **2017**, 093D03 (2017).

K. Sekiguchi, Y. Wada, A. Watanabe, D. Eto, T. Akieda, H. Kon, K. Miki, N. Sakamoto, H. Sakai, M. Sasano, Y. Shimizu, H. Suzuki, T. Uesaka, Y. Yanagisawa, M. Dozono, S. Kawase, Y. Kubota, C. S. Lee, K. Yako, Y. Maeda, S. Kawakami, T. Yamamoto, S. Sakaguchi, T. Wakasa, J. Yasuda, A. Ohkura, Y. Shindo, M. Tabata, E. Milman, S. Chebotaryov, H. Okamura, T. L. Tang, "Deuteron analyzing powers for dp elastic scattering at intermediate energies and three-nucleon forces," Few-Body Syst. **58**, 48 (2017).*

[Proceedings]
(Original Papers) *Subject to Peer Review

L.A. Gurgi, P.H. Regan, P.-A. Söderström, H. Watanabe P.M. Walker, Zs. Podolyák, S. Nishimura, T.A. Berry, P. Doornenbal, G. Lorusso, T. Isobe, H. Baba, Z.Y. Xu, H. Sakurai, T. Sumikama, W.N. Catford, A.M. Bruce, F. Browne, G.J. Lane, F.G. Kondev, A. Odahara, J. Wu, H.L. Liu, F.R. Xu, Z. Korkulu, P. Lee, J.J. Liu, V.H. Phong, A. Yagi, G.X. Zhang, T. Alharbi, R.J. Carroll, K.Y. Chae, Zs. Dombradi, A. Estrade, N. Fukuda, C. Griffin, E. Ideguchi, N. Inabe, H. Kanaoka, I. Kojouharov, T. Kubo, S. Kubono, N. Kurz, I. Kuti, S. Lalkovski, E.J. Lee, C.S. Lee, G. Lotay, C.B. Moon, I. Nishizuka, C.R. Nita, Z. Patel, O.J. Roberts H. Schaffner, C.M. Shand, H. Suzuki, H. Takeda, S. Terashima, Zs. Vajta, S. Kanaya, J.J. Valiente-Dobón, "Isomer spectroscopy of neutron-rich ^{165,167}Tb," Acta Phys. Pol. B **48**, 601 (2017).*

L.A. Gurgi, P.H. Regan, P.-A. Söderström, H. Watanabe P.M. Walker, Zs. Podolyák, S. Nishimura, T.A. Berry, P. Doornenbal, G. Lorusso, T. Isobe, H. Baba, Z.Y. Xu, H. Sakurai, T. Sumikama, W.N. Catford, A.M. Bruce, F. Browne, G.J. Lane, F.G. Kondev, A. Odahara, J. Wu, H.L. Liu, F.R. Xu, Z. Korkulu, P. Lee, J.J. Liu, V.H. Phong, A. Yagi, G.X. Zhang, T. Alharbi, R.J. Carroll, K.Y. Chae, Zs. Dombradi, A. Estrade, N. Fukuda, C. Griffin, E. Ideguchi, N. Inabe, H. Kanaoka, I. Kojouharov, T. Kubo, S. Kubono, N. Kurz, I. Kuti, S. Lalkovski, E.J. Lee, C.S. Lee, G. Lotay, C.B. Moon, I. Nishizuka, C.R. Nita, Z. Patel, O.J. Roberts H. Schaffner, C.M. Shand, H. Suzuki, H. Takeda, S. Terashima, Zs. Vajta, S. Yoshida, J.J. Valiente-Dobón, "Isomer spectroscopy of neutron-rich ^{168}Tb$_{103}$," Radiat. Phys. Chem. **140**, 493 (2017).*

Oral Presentations

[International Conference etc.]

K. Kusaka, "RadiationEffects in Superconducting Quadruoles for BigRIPS In-flight Separator at RIKEN," 13th European Conference on Applied Superconductivity, Geneva, Switzerland, September 17–21, 2017.

[Domestic Conference]

本間彰, 武智麻耶, 大坪隆, 田中聖臣, 福田光順, 鈴木健, 西村太樹, 森口哲朗, 安得順, A.S. Aimaganbetov, 天野将道, 荒川裕樹, S. Bagchi, K.-H. Behr, N. Burtebayev, 親跡和弥, 杜航, 藤井朋也, 福田直樹, H. Geissel, 堀太地, 星野寿春, 伊五澤涼, 池田彩夏, 稲辺尚人, 猪股玖美, 板橋健太, 泉川卓司, 上岡大起, 神田直人, 加藤郁磨, I. Kenzhina, Z. Korkulu, Ye. Kuk, 日下健祐, 三原基嗣, 宮田恵理, 長江大輔, 中村翔健, M. Nassurlla, 西室国光, 西塚賢治, 大甕舜一朗, 大西康介, 大竹政雄, 王恵仁, 小沢顕, A. Prochazka, 櫻井博儀, C. Scheidenberger, 清水陽平, 杉原貴信, 炭竃聡之, 鈴木伸司, 鈴木宏, 竹田浩之, 田中悠太郎, 田中良樹, 和田太郎, 若山清志, 八木翔一, 山口貴之, 柳原陸斗, 柳澤善行, 吉田光一, T.K. Zholdybayev,「中性子過剰側 Ni 同位体の相互作用断面積測定」, 日本物理学会　第 72 回年次大会 (2017), 大阪大学、大阪府、3/17–20, 2017.

中村翔健, 武智麻耶, 田中聖臣, 本間彰, 鈴木健, 福田光順, 西村太樹, 森口哲朗, 安得順, A.S. Aimaganbetov, 天野将道, 荒川裕樹, S. Bagchi, K.H. Behr, N. Burtebayev, 親跡和弥, 杜航, 藤井朋也, 福田直樹, H. Geissel, 堀太地, 星野寿春, 伊五澤涼, 池田彩夏, 稲辺尚人, 猪股玖美, 板橋健太, 泉川卓司, 上岡大起, 神田直人, 加藤郁磨, I. Kenzhina, Z. Korkulu, Ye. Kuk, 日下健祐, 松多健策, 三原基嗣, 宮田恵理, 長江大輔, M. Nassurlla, 西室国光, 西塚賢治, 大甕舜一朗, 大西康介, 大竹政雄, 大坪隆, 王恵仁, 小沢顕, A. Prochazka, S. K. Sakhiyev, 櫻井博儀, C. Scheidenberger, 清水陽平, 杉原貴信, 炭竃聡之, 鈴木伸司, 鈴木宏, 竹田浩之, 田中良樹, 田中悠太郎, 谷畑勇夫, 和田太郎, 若山清志, 八木翔一, 山口貴之, 柳原陸斗, 柳澤善行, 吉田光一, T.K. Zholdybayev,「Ni 領域中重核の陽子標的相互作用断面積測定」, 日本物理学会　第 72 回年次大会(2017), 大阪大学、大阪府, 3/17–20, 2017.

田中聖臣, 武智麻耶, 本間彰, 鈴木健, 田中悠太郎, 福田光順, 西村太樹, 森口哲朗, 安得順, A.S. Aimaganbetov, 天野将道, 荒川裕樹, S. Bagchi, K.-H. Behr, N. Burtebayev, 親跡和弥, 杜航, 藤井朋也, 福田直樹, H. Geissel, 堀太地, 星野寿春, 伊五澤涼, 池田彩夏, 稲辺尚人, 猪股玖美, 板橋健太, 泉川卓司, 上岡大起, 神田直人, 加藤郁磨, I. Kenzhina, Z. Korkulu, Ye. Kuk, 日下健祐, 松多健策, 三原基嗣, 宮田恵理, 長江大輔, 中村翔健, M. Nassurlla, 西室国光, 西塚賢治, 大甕舜一朗, 大西康介, 大竹政雄, 大坪隆, 王恵仁, 小沢顕, A. Prochazka, S.K. Sakhiyev, 櫻井博儀, C. Scheidenberger, 清水陽平, 杉原貴信, 炭竃聡之, 鈴木伸司, 鈴木宏, 竹田浩之, 田中良樹, 谷畑勇夫, 和田太郎, 若山清志, 八木翔一, 山口貴之, 柳原陸斗, 柳澤善行, 吉田光一, T.K. Zholdybayev,「Ca, Ni 同位体の荷電変化断面積測定」, 日本物理学会　第 72 回年次大会 (2017), 大阪大学、大阪府, 3/17–20, 2017.

田中悠太郎, 武智麻耶, 田中聖臣, 本間彰, 鈴木健, 福田光順, 西村太樹, 森口哲朗, 安得順, A.S. Aimaganbetov, 天野将道, 荒川裕樹, S. Bagchi, K.-H. Behr, N. Burtebayev, 親跡和弥, 杜航, 藤井朋也, 福田直樹, H. Geissel, 堀太地, 星野寿春, 伊五澤涼, 池田彩夏, 稲辺尚人, 猪股玖美, 板橋健太, 泉川卓司, 上岡大起, 神田直人, 加藤郁磨, I. Kenzhina, Z. Korkulu, Ye. Kuk, 日下健祐, 松多健策, 三原基嗣, 宮田恵理, 長江大輔, 中村翔健, M. Nassurlla, 西室国光, 西塚賢治, 大甕舜一朗, 大西康介, 大竹政雄, 大坪隆, 王恵仁, 小沢顕, A. Prochazka, S.K. Sakhiyev, 櫻井博儀, C. Scheidenberger, 清水陽平, 杉原貴信, 炭竃聡之, 鈴木伸司, 鈴木宏, 竹田浩之, 田中良樹, 谷畑勇夫, 和田太郎, 若山清志, 八木翔一, 山口貴之, 柳原陸斗, 柳澤善行, 吉田光一, T.K. Zholdybayev,「Ca 同位体の相互作用断面積と核構造」, 日本物理学会　第 72 回年次大会 (2017), 大阪大学、大阪府, 3/17–20, 2017.

小山俊平, 大津秀暁, 清水陽平, 米田健一郎, 佐藤広海, 本林透, 西村美月, 銭廣十三, 櫻井博儀, 武内聡, 磯部忠昭, 馬場秀忠, 日下健祐, 大西純一, 笹野匡紀, P. Doornenbal, 福田直樹, 小林俊雄, 炭竃聡之, 松田洋平, 佐藤義輝, J. Hwang, 近藤洋介, 中村隆司, 栁野泰宏, 南方亮吾, 生越駿, 村上哲也, 中塚徳継, J Gibelin, L Sylvain, 新倉潤, 小林信之, H. Liu, J. Lee, E. Nikolskii, 坂口聡志, D. Beaumel,「^{16}C のクラスター構造」, 日本物理学会　第 72 回年次大会 (2017), 大阪大学、大阪府, 3/17–20, 2017.

S. Chebotaryov, S. Sakaguchi, T. Uesaka, T. Akieda, Y. Ando, M. Assie, D. Beaumel, N. Chiga, M. Dozono, A. Galindo-Uribarri, B. Heffron, A. Hirayama, T. Isobe, S. Kawase, W. Kim, T. Kobayashi, H. Kon, Y. Kondo, Y. Kubota, S. Leblond, H. Lee, T. Lokotko, Y. Maeda, Y. Matsuda, K. Miki, E. Milman, T. Motobayashi, T. Mukai, S. Nakai, T. Nakamura, A. Ni, T. Noro, S. Ota, H. Otsu, T. Ozaki, V. Panin, S. Park, A. Saito, H. Sakaguchi, H. Sakai, M. Sasano, H. Sato, K. Sekiguchi, Y. Shimizu, I. Stefan, L. Stuhl, M. Takaki, K. Taniue, K. Tateishi, T. Teranishi, S. Terashima, Y. Togano, T. Tomai, Y. Wada, T. Wakasa, T. Wakui, A. Watanabe, Y. Yamada, Z. Yang, J. Yasuda, M. Yasuda, K. Yoneda, and J. Zenihiro, "Status of data analysis from experiment on p-^{6}He elastic scattering at 200 MeV/nucleon," 日本物理学会　第 72 回年次大会 (2017), 大阪大学、大阪府, 3/17–20, 2017.

平山晃大, 中村隆司, 武内聡, 近藤洋介, 栁野泰宏, 四方瑞紀, 坪田潤一, 尾崎友志, 齊藤敦美, 斗米貴人, 大津秀暁, Wang He, 渡辺幸信, 川瀬頌一郎, ImPACT Collaboration,「^{79}Se,^{80}Se のクーロン分解反応」, 日本物理学会　第 72 回年次大会 (2017), 大阪大学、大阪府, 3/17–20, 2017.

福田光順, 田中聖臣, 武智麻耶, 本間彰, 神田直人, 鈴木健, 西村太樹, 森口哲朗, 安得順, A.S. Aimaganbetov, 天野将道, 荒川裕樹, S. Bagchi, K.-H. Behr, N. Burtebayev, 親跡和弥, 杜航, 藤井朋也, 福田直樹, H. Geissel, 堀太地, 星野寿春, 伊五澤涼, 池田彩夏, 稲辺尚人, 猪股玖美, 板橋健太, 泉川卓司, 上岡大起, 加藤郁磨, I. Kenzhina, Z. Korkulu, Ye. Kuk, 日下健祐, 松多健策, 三原基嗣, 宮田恵理, 長江大輔, 中村翔健, M. Nassurlla, 西室国光, 西塚賢治, 大甕舜一朗, 大西康介, 大竹政雄, 大坪隆, 王恵仁, 小沢顕, A. Prochazka, S.K. Sakhiyev, 櫻井博儀, C. Scheidenberger, 清水陽平, 杉原貴信, 炭竃聡之, 鈴木伸司, 鈴木宏, 竹田浩之, 田中悠太郎, 田中良樹, 谷畑勇夫, 和田太郎, 若山清志, 八木翔一, 山口貴之, 柳原陸斗, 柳澤善行, 吉田光一, T.K. Zholdybayev,「$Z = 20$ および 28 近傍領域の核子ピックアップ断面積」, 日本物理学会　2017 年秋季大会, 宇都宮大学、栃木県, 9/12–15, 2017.

田中聖臣, 武智麻耶, 本間彰, 福田光順, 神田直人, 鈴木健, 西村太樹, 森口哲朗, 安得順, A.S. Aimaganbetov, G, 天野将道, 荒川裕樹, S. Bagchi, K.-H. Behr, N. Burtebayev, 親跡和弥, 杜航, 藤井朋也, 福田直樹, H. Geissel, 堀太地, 星野寿春, 伊五澤涼, 池田彩夏, 稲辺尚人, 猪股玖美, 板橋健太, 泉川卓司, 上岡大起, 加藤郁磨, I. Kenzhina, Z. Korkulu, Ye. Kuk, 日下健祐, 松多健策, 三原基嗣, 宮田恵理, 長江大輔, 中村翔健, M. Nassurlla, 西室国光, 西塚賢治, 大甕舜一朗, 大西康介, 大竹政雄, 大坪隆, 王恵仁, 小沢顕, A. Prochazka, S.K. Sakhiyev, 櫻井博儀, C. Scheidenberger, 清水陽平, 杉原貴信, 炭竃聡之, 鈴木伸司, 鈴木宏, 竹田浩之, 田中悠太郎, 田中良樹, 谷畑勇夫, 和田太郎, 若山清志, 八木翔一, 山口貴之, 柳原陸斗, 柳澤善行, 吉田光一, T.K. Zholdybayev,「$Z = 20$ および 28 近傍領域の荷電変化断面積測定」

平山晃大, 中村隆司, 武内聡, 近藤洋介, 栁野泰宏, 四方瑞紀, 坪田潤一, 尾崎友志, 齊藤敦美, 斗米貴人, 大津秀明, 王赫, 渡辺幸信, 川瀬頌一郎, 他 ImPACT Collaboration,「^{79}Se,^{80}Se のクーロン分解反応断面積」, 日本物理学会　2017 年秋季大会, 宇都宮大学、栃木県、9/12–15, 2017.

親跡和弥, 武智麻耶, 大坪隆, 王赫, 大津秀暁, 櫻井博儀, 安得順, 合川正幸, P. Doornenbal, 福田直樹, 磯部忠明, 川上駿介, 小山俊平, 久保

敏幸, 久保野茂, G. Lorusso, 前田幸重, 牧永綾乃, 籾山悟至, 中野敬太, 新倉潤, 志賀慶明, P. A.Söderström, 鈴木宏, 竹田浩之, 武内聡, 谷内稜, 渡部康, 渡辺幸信, 山崎隼汰, 吉田光一,「^{90}Sr および ^{89}Rb, ^{88}Kr, ^{91}Y の相互作用断面積測定」, 日本物理学会　2017 年秋季大会, 宇都宮大学、栃木県、9/12–15, 2017.

本間彰, 武智麻耶, 大坪隆, 田中聖臣, 福田光順, 鈴木健, 西村太樹, 森口哲朗, 安得順, A.S. Aimaganbetov, G, 天野将道, 荒川裕樹, S. Bagchi, K.-H. Behr, N. Burtebayev, 親跡和弥, 杜航, 藤井朋也, 福田直樹, H. Geissel, 堀太地, 星野寿春, 伊五澤涼, 池田彩夏, 稲辺尚人, 猪股玖美, 板橋健太, 泉川卓司, 上岡大起, 神田直人, 加藤郁磨, I. Kenzhina, Z. Korkulu, Ye. Kuk, 日下健祐, 三原基嗣, 宮田恵理, 長江大輔, 中村翔健, M. Nassurlla, 西室国光, 西塚賢治, 大甕舜一朗, 大西康介, 大竹政雄, 王恵仁, 小沢顕, A. Prochazka, 櫻井博儀, C. Scheidenberger, 清水陽平, 杉原貴信, 炭竈聡之, 鈴木伸司, 鈴木宏, 竹田浩之, 田中悠太郎, 田中良樹, 和田太郎, 若山清志, 八木翔一, 山口貴之, 柳原陸斗, 柳澤善行, 吉田光一, T.K. Zholdybayev,「中性子過剰側 Ni 同位体の相互作用断面積と中性子スキン厚」, 日本物理学会　2017 年秋季大会, 宇都宮大学、栃木県、9/12–15, 2017.

神田直人, 武智麻耶, 大坪隆, 本間彰, 田中聖臣, 福田光順, 鈴木健, 西村太樹, 森口哲朗, 安得順, A.S. Aimaganbetov, G, 天野将道, 荒川裕樹, S. Bagchi, K.-H. Behr, N. Burtebayev, 親跡和弥, 杜航, 藤井朋也, 福田直樹, H. Geissel, 堀太地, 星野寿春, 伊五澤涼, 池田彩夏, 稲辺尚人, 猪股玖美, 板橋健太, 泉川卓司, 上岡大起, 加藤郁磨, I. Kenzhina, Z. Korkulu, Ye. Kuk, 日下健祐, 三原基嗣, 宮田恵理, 長江大輔, 中村翔健, M. Nassurlla, 西室国光, 西塚賢治, 大甕舜一朗, 大西康介, 大竹政雄, 王恵仁, 小沢顕, A. Prochazka, 櫻井博儀, C. Scheidenberger, 清水陽平, 杉原貴信, 炭竈聡之, 鈴木伸司, 鈴木宏, 竹田浩之, 田中悠太郎, 田中良樹, 和田太郎, 若山清志, 八木翔一, 山口貴之, 柳原陸斗, 柳澤善行, 吉田光一, T.K. Zholdybayev,「K 同位体相互作用断面積測定」, 日本物理学会　2017 年秋季大会, 宇都宮大学、栃木県、9/12–15, 2017.

西村太樹, 笈川浩之, 藤田佳孝, B. Rubio, W. Gelletly, J. Agramunt, A. Algora, F, V. Guadilla, A. Montaner-Piza, A.I. Morales, S.E.A. Orrigo, G.G. Kiss, 西村俊二, P.-A. Söderström, P. Doornenbal, V.H. Phong, J. Wu, B. Blank, T. Goigoux, 千葉順成, 武井悠稀, 田中聖臣, 八木翔一, Zs. Dombrádi, 安得順, 馬場秀忠, 福田直樹, 郷慎太郎, 稲辺尚人, 磯部忠昭, 久保敏幸, 久保野茂, 櫻井博儀, 清水陽平, C. Sidong, 炭竈聡之, 鈴木宏, 竹田浩之, P. Ascher, M. Gerbaux, J. Giovinazzo, S. Grévy, T. Kurtukian Nieto, C. Magron, K. Wimmer, P. Aguilera, F. Molina, F. Diel, J. Eberth, D. Lubos, G. de Angelis, D. Napoli, C. Borcea, A. Boso, R.B. Cakirli, E. Ganioglu, and G. de France,「^{58}Zn のベーターガンマ分光で探る質量数 58 体系のアイソスピン対称性」, 日本物理学会　2017 年秋季大会, 宇都宮大学、栃木県、9/12–15, 2017.

ムハマドハルーン, 八木彩祐未, 小田原厚子, 西村俊二, J. Wu, R. Lozeva, C.-B. Moon, 方一帆, 大道理恵, 西畑洸希, 金岡裕志, P. Lee, 下田正, P. Doornenbal, G. Lorusso, 炭竈聡之, 渡辺寛, P. A. Söderström, F. Brown, Z.Y. Xu, 横山輪, 磯部忠昭, 馬場秀忠, 櫻井博儀, 鈴木宏, 稲辺尚人, 亀田大輔, 福田直樹, 竹田浩之, 安得順, 清水陽平, 佐藤広海, 久保敏幸, 石垣知樹, 森本翔太, 井手口栄治, 小松原哲郎, 新倉潤, 西塚一平, and the EURICA collaborators,「β-decay isomer をプローブとする A～140 中性子過剰核の構造研究」, 日本物理学会　2017 年秋季大会, 宇都宮大学、栃木県、9/12–15, 2017.

RIBF Research Division
Research Instruments Group
SAMURAI Team

1. Abstract

In collaboration with research groups in and outside RIKEN, the team designs, develops and constructs the SAMURAI spectrometer and relevant equipment that are and will be used for reaction experiments using RI beams at RI Beam Factory. The SAMURAI spectrometer consists of a large superconducting dipole magnet and a variety of detectors to measure charged particles and neutrons. After the commissioning experiment in March 2012, the team prepared and conducted, in collaboration with researchers in individual experimental groups, the first series of experiments with SAMURAI in May 2012. Then, several numbers of experiments were well performed until now utilizing the property of SAMURAI. The team also provides basis for research activities by, for example, organizing collaboration workshops by researchers who are interested in studies or plan to perform experiments with the SAMURAI spectrometer.

2. Major Research Subjects

Design, operation, maintenance and improvement of the SAMURAI spectrometer and its related research instruments. Support and management for SAMURAI-based research programs. Generate future plans for next generation instruments for nuclear reaction studies.

3. Summary of Research Activity

The current research subjects are summarized as follows:

(1) Operation, maintenance and improvement of a large superconducting dipole magnet that is the main component of the SAMURAI spectrometer.
(2) Design, development and construction of various detectors that are used for nuclear reaction experiments using the SAMURAI spectrometer.
(3) Preparation for planning experiments using SAMURAI spectrometer.
(4) Maintenance and improvement of the SAMURAI beam line.
(5) Formation of a collaboration platform called "SAMURAI collaboration.
(6) Preparation for next generation spectrometer for nuclear reaction studies.

Members

Team Leader
Hideaki OTSU

List of Publications & Presentations

Publications

[Journal]

(Original Papers)

S Chebotaryov et al., "Proton elastic scattering at 200 A MeV and high momentum transfers of 1.7–2.7 fm-1 as a probe of the nuclear matter density of ^{6}He," Prog. Theo. Exp. Phys., Volume **2018**, Issue 5, 1, 053D01 (20 pages).

J.W. Hwang, S. Kim, Y. Satou, N.A. Orr, Y. Kondo, T. Nakamura, J. Gibelin, N.L. Achouri, T. Aumann, H. Baba, F. Delaunay, P. Doornenbal, N. Fukuda, N. Inabe, T. Isobe, D. Kameda, D. Kanno, N. Kobayashi, T. Kobayashi, T. Kubo, S. Leblond, J. Lee, F.M. Marqués, R. Minakata, T. Motobayashi, D. Murai, T. Murakami, K. Muto, T. Nakashima, N. Nakatsuka, A. Navin, S. Nishi, S. Ogoshi, H. Otsu, H. Sato, Y. Shimizu, H. Suzuki, K. Takahashi, H. Takeda, S. Takeuchi, R. Tanaka, Y. Togano, A.G. Tuff, M. Vandebrouck, K. Yoneda, "Single-neutron knockout from ^{20}C and the structure of ^{19}C," Phys. Lett. B **769**, 503 (2017).

P.Lasko et al., "KATANA - A charge-sensitive triggering system for the SπRIT experiment," Nucl. Instrum. Methods Phys. Res. A **856**, 92(7 pages) (2017).

S. Tangwancharoen et al., "A gating grid driver for time projection chambers," Nucl. Instrum. Methods Phys. Res. A **853**, 44(9 pages) (2017).

J. Kahlbow, C. Caesar, T. Aumann, V. Panin, S. Paschalis, H. Scheit, H. Simon, "Neutron radioactivity—Lifetime measurements of neutron-unbound states," Nucl. Instrum. Methods Phys. Res. A **866**, 265（7 pages）(2017).

(Review)

T. Nakamura, H. Sakurai, H. Watanabe, "Exotic nuclei explored at in-flight separators," Prog. Part. Nucl. Phys. **97**, 53–122 (2017).

(Proceedings)

Tadaaki Isobe for the SπRIT Collabortion, "Constraint on Nuclear Symmetry Energy through Heavy RI Collision Experiment by Using SπRIT Device at RIBF–SAMURAI," Proc. 14th Int. Symp. on Nuclei in the Cosmos (NIC2016), JPS Conf. Proc. **14**, 010803 (2017).

Oral Presentations

[International Conference etc.]

Y. Kondo, (Invited) "Studies of neutron-neutron correlation near the drip line with SAMURAI at RIBF," International symposium on RI beam physics in the 21st century: 10th anniversary of RIBF, December 4–5, 2017, RIKEN.

S. Koyama, (Invited) "Study of cluster structure in ^{16}C," Workshop on Nuclear Cluster Physics 2017, 25th October, Sapporo, Japan.

V. Panin, (Invited) "Dissociation of proton-rich nuclei at SAMURAI as a method to study the most critical (p,γ) reaction rates in stellar nucleosynthesi," KPS 2017 meeting, Daejeon, South Korea, Apr, 2017.

Y. Kubota, (Invited) "Probing neutron-neutron correlation in ^{11}Li via the quasi-free (p,pn) reaction," Hadrons and Nuclear Physics meet ultracold atoms: a French Japanese workshop, Paris, France, 29 January–2 February, 2018.

Y. Kubota, (Invited) "Probing neutron-neutron correlation in ^{11}Li through the quasi-free (p,pn) reaction," The 244th RIKEN RIBF Nuclear Physics Seminar, Saitama, Japan, December 19, 2017.

Y. Kubota, (Invited) "Dineutron correlation in Borromean nuclei," 3rd International Workshop on Quasi-Free Scattering with Radioactive-Ion Beams: QFS-RB 17, York, United Kingdom, July, 24–27, 2017.

T.Nakamura, (Invited) "Spectroscopy of drip-line nuclei using the large acceptance spectrometer SAMURAI," October 19–20, 2017, Collaboration Workshop on RI and Heavy-ion Sciences, Ewha Womans University, Seoul, South Korea.

T.Nakamura, (Invited) "Exploring Neutron Drip Line and Beyond by Breakup Reactions," June 18–23, 2017, Nuclear Chemistry, Gordon Research Conference, Colby-Sawyer College, New London, NH, USA, Ewha Womans University, Seoul, South Korea.

T.Nakamura, (Invited) "Correlated neutron states near and beyond the neutron drip line," December 18–22, 2017, International Workshop on Hadron and Nuclear Physics (HNP2017), RIKEN, Wako, Japan.

T.Nakamura, (Invited) "Study of neutron drip line nuclei by breakup reactions," May 14–19, 2017, Int. Conf. on Isospin, STructure, Reactions and energy Of Symmetry (ISTROS), Casta Papiernicka, Slovakia.

T.Nakamura, (Invited) "Clustering phenomena of nuclei near the neutron drip line," October 25–27, 2017, Workshop on Nuclear Cluster Physics (WNCP2017), Hokkaido Univ., Sapporo, Hokkaido, Japan.

T.Nakamura, (Invited) "Exploring Nuclei beyond the Neutron Drip Line," November 1–4, 2017, IIRC Symposium, Perspectives of the Physics of Nuclear Structure, Koshiba-Hall, U. of Tokyo, Tokyo, Japan.

A. Corsi, "Dineutron correlation in ^{14}Be and Spectroscopy of ^{13}Be probed via QFS reactions," QFS workshop, York, July 24–26 2017.

T.Nakamura, "Exclusive Coulomb breakup of neutron drip-line nuclei," August 8–11, 2017, SAMURAI International Collaboration Workshop, Lichtenberghus, Darmstadt, Germany.

Y. Kubota, "Neutron-neutron correlation in Borromean nucleus ^{11}Li," SAMURAI International Collaboration Workshop 2017, Darmstadt, Germany, August 8–11, 2017.

S. Sakaguchi for SAMURAI13 collaboration, "Elastic scattering of polarized proton from ^{6}He," SAMURAI International Collaboration Workshop 2017, Darmstadt, Germany, August 8–11, 2017.

Y. Kondo, "Status report of the SAMURAI21 experiment," SAMURAI International collaboration workshop 2017, Darmstadt Germany, 8–11 August.

Y. Togano, "Progress report on the electric dipole response of n-ich Ca isotopes," SAMURAI International collaboration workshop 2017, Darmstadt Germany, 8–11 August.

A. Saito, "Development of high resolution neutron detector HIME," SAMURAI International collaboration workshop 2017, Darmstadt Germany, 8–11 August.

T. Tomai, "The SAMURAI27 experiment: Spectroscopy of ^{31}Ne using breakup reactions," SAMURAI International collaboration workshop 2017, Darmstadt Germany, 8–11 August.

[Domestic Conference]

T.Nakamura, "Clustering and hierarchical structure of strongly-interacting systems," 2017 年 9 月 13 日, 日本物理学会秋の分科会シンポジウム "Clustering as a window on the hierarchical structure of quantum systems," 宇都宮.

近藤洋介 他, 「魔法数 $N=20$ 近傍の非束縛酸素同位体の研究」, 日本物理学会 2017 年秋季大会, 2017 年 9 月 12–15 日, 宇都宮.

栂野泰宏, 中村隆司, 小林俊雄 他 3 名, SAMURAI09 Collaboration, 「^{50,52}Ca の E1 応答測定」, 2017 年 9 月, 日本物理学会秋季大会, 宇都宮.

平山晃大, 中村隆司 他 12 名, ImPACT–RIBF Collaboration, 「^{79}Se,^{80}Se のクーロン分解反応断面積」, 2017 年 9 月, 日本物理学会秋季大会, 宇都宮.

斗米貴人, 中村隆司 他 10 名, SAMURAI27 Collaboration, 「分解反応を用いた ^{31}Ne の核分光 II」, 2017 年 9 月, 日本物理学会秋季大会, 宇都宮.

安田昌弘, 中村隆司, 近藤洋介, SAMURAI21 Collaboration, 「陽子標的との反応による中性子過剰 F, Ne のインビーム γ 線核分光」, 2017 年 9 月, 日本物理学会秋季大会, 宇都宮.

松本真由子, 中村隆司 他 9 名, 「逆転の島領域にある中性子過剰核 ^{32}Ne の核分光」, 2017 年 9 月, 日本物理学会秋季大会, 宇都宮.

山田啓貴, 中村隆司 他 10 名, SAMURAI27 Collaboration, 「核子剥離反応を用いた逆転の島近傍核の分光」, 2017 年 9 月, 日本物理学会秋季大会, 宇都宮.

栂野泰宏, 「^{50,52}Ca の E1 応答測定」, 2017 年 9 月, 日本物理学会秋季大会, 宇都宮.

武内聡 他 5 名, 「^{79,80}Se および ^{93,94}Zr のクーロン分解反応による光吸収断面積の導出」, 2017 年 9 月日本原子力学会秋の大会, 札幌.

近藤洋介, 「RIBF における非束縛酸素同位体 $^{25-28}$O の質量測定実験」, 第 6 回「中性子星の核物質」研究会, 2017 年 12 月 1–3 日, 理化学研究所, 和光市.

三輪海彩 他 15 名, 「重水素標的を用いた二陽子ノックアウト反応による中性子過剰核の生成」, 2018 年 3 月 日本物理学会第 73 回年次大会, 野田.

安田昌弘, 近藤洋介, 中村隆司, SAMURAI21 Collaboration, 「逆転の島近傍ネオン同位体のインビーム γ 線核分光」, 日本物理学会第 73 回年次大会, 野田.

斗米貴人, 中村隆司 他 7 名, SAMURAI27 Collaboration, 「^{31}Ne のクーロン分解反応」, 日本物理学会第 73 回年次大会, 野田.

松本真由子, 中村隆司 他 7 名, SAMURAI27 Collaboration, 「中性子過剰核 ^{32}Ne の非束縛準位の探索」, 日本物理学会第 73 回年次大会, 野田.

武内聡 他 6 名, ImPACT–RIBF Collaboration, 「クーロン分解反応による ^{79,80}Se および ^{93,94}Zr の光吸収断面積導出」, 2018 年 3 月 日本物理学会第 73 回年次大会, 野田.

藤野佑亮, 「^{50,52}Ca の束縛 1-励起状態探索」, 2018 年 3 月 日本物理学会第 73 回年次大会, 野田.

武内聡 他 5 名，「^{79, 80}Se および，^{93, 94}Zr のクーロン分解反応断面積の統計崩壊モデルを使った解析」，2018 年 3 月 日本原子力学会年会，大阪.

中村隆司，"Clustering as a window on the hierarchical structure of quantum systems," 2018 年 2 月 13–14 日「物質階層の原理を探求する統合的実験研究」研究報告会，理化学研究所，埼玉県和光市.

中村隆司，「原子核の実験でさぐる中性子星の核物質」，2017 年 6 月 30 日「原子・分子・光科学(AMO)討論会」，電気通信大学，東京都調布市.

中村隆司，「量子クラスターで読み解く物質の階層構造-序」，2018 月 3 月 30–31 日 研究会「量子クラスターで読み解く物質の階層構造」，東京工業大学.

栂野泰宏，「中性子過剰核"の E1 応答測定による対称エネルギーの制限」，2017 年 12 月，理化学研究所.

Poster Presentation

[International Conference.]

T. Tomai, "Spectroscopy of ^{31}Ne using breakup reactions," Joliot Curie School, 24–29, Sep. 2017, Les Issambres, France.

[Domestic Conference]

島田哲朗，中村隆司，他 9 名，SAMURAI27 Collaboration，「中性子過剰非束縛核 ^{30}F の探索」，2018 年 3 月 日本物理学会第 73 回年次大会，野田.

Master Thesis

斗米貴人，「変形誘因型ハロー核 ^{31}Ne の分解反応」，東京工業大学理学院物理学系.

平山晃大，「^{79,80}Se のクーロン分解反応断面積測定」，東京工業大学理学院物理学系.

Bachelor Thesis

島田哲朗，「中性子過剰非束縛核 ^{30}F の探索」，東京工業大学.

受賞

斗米貴人，「東京工業大学物理学コース優秀修士論文賞」，2017 年 3 月.

RIBF Research Division
Research Instruments Group
Computing and Network Team

1. Abstract

This team is in charge of development, management and operation of the computing and network environment, mail and information servers and data acquisition system and management of the information security of the RIKEN Nishina Center.

2. Major Research Subjects

(1) Development, management and operation of the general computing servers
(2) Development, management and operation of the mail and information servers
(3) Development, management and operation of the data acquisition system
(4) Development, management and operation of the network environment
(5) Management of the information security

3. Summary of Research Activity

This team is in charge of development, management and operation of the computing and network environment, mail and information servers and data acquisition system and management of the information security. The details are described elsewhere in this progress report.

(1) Development, management and operation of the general computing servers

We are operating Linux/Unix NIS/NFS cluster system for the data analysis of the experiments and general computing. This cluster system consists of eight computing servers with 64 CPU cores and totally 200 TB RAID of highly-reliable Fibre-channel interconnection. Approximately 700 user accounts are registered on this cluster system. We are adopting the latest version of the Scientific Linux (X86_64) as the primary operating system, which is widely used in the accelerator research facilities, nuclear physics and high-energy physics communities in the world.

(2) Development, management and operation of the mail and information servers

We are operating RIBF.RIKEN.JP server as a mail/NFS/NIS server. This server is a core server of RIBF Linux cluster system. Postfix has been used for mail transport software and dovecot has been used for imap and pop services. These software packages enable secure and reliable mail delivery. Because seven years have passed since the installation of this sever (HP-DL380G7), we replaced the server to HP-DL380G9 and RAID file system in January 2018. The current OS is Scientific Linux 7.5. Sophos Email Security and Control (PMX) installed on the mail front-end servers which tags spam mails and isolates virus-infected mails. The probability to identify the spam is approximately 95-99%. We noticed that virus-infected mails were occasionally not detected by PMX in the case of new types of virus. Therefore, we added a new rule to PMX to isolate and remove executable image files attached in mail because they are often aimed at virus infection. As a result, most of the viruses in mails are successfully blocked by PMX. We are operating several information servers such as Web servers, Integrated Digital Conference (INDICO) server, Wiki servers, Groupware servers, Wowza streaming servers. An anonymous ftp server, FTP.RIKEN.JP , is managed and operated at the RNC. Major Linux distributions, including Scientific Linux, Ubuntu and CentOS, are mirrored daily for the convenience of their users and for facilitating high-speed access. An HP PloLiant DL-380G6 server was installed in 2009, and it was replaced by DL-380G9 in June 2017. Simultaneously, the OS was upgraded from SL 5.11 to SL 7.3. We have been operating approximately 70 units of wireless LAN access points in RNC. Almost the entire radiation-controlled area of the East Area of RIKEN Wako campus is covered by wireless LAN for the convenience of experiments and daily work. Since the devices used for the Wireless LAN access points became obsolete, all of them were replaced by WAPM-1166D in 2016 and 2017, which supports the protocols of 802.11b, 11g, 11a, 11n, and 11ac. The UPS system of RIBF 1F server room (20KVA) was replaced in the summer of 2017 because they were installed in 2005 and exceeded the design life of 10 years.

(3) Development, management and operation of the data acquisition system

We have developed the standard data-acquisition system named as RIBFDAQ. This system can process up to 40 MB/s data. By using parallel readout from front-end systems, the dead time could be small. To synchronize the independent DAQ systems, the time stamping system has been developed. The resolution and depth of the time stamp are 10 ns and 48 bit, respectively. This time stamping system is very useful for beta decay experiments such as EURICA and BRIKEN projects. The current main task is the DAQ coupling, because detector systems with dedicated DAQ systems are transported to RIBF from foreign facilities. In case of SAMURAI Silicon (NSCL/TUM/WUSTL), the readout system is integrated into RIBFDAQ. The projects of MUST2 (GANIL), MINOS (CEA Saclay), NeuLAND (GSI) and TRB3 (TUM) cases, data taken by their DAQ systems are transferred to RIBFDAQ. For SPIRIT (RIKEN/GANIL/CEA Saclay/NSCL), RIBFDAQ is controlled from the NARVAL-GET system that is a large-scale signal processing system for the time projection chamber. EURICA (GSI), BRIKEN (GSI/Univ. Liverpool/IFIC), VANDLE (UTK) and OTPC (U. Warsaw) projects, we adopt the time stamping system to use individual trigger for each detector system. In this case, data are merged in offline. In addition to the development DAQ system, we are developing intelligent circuits based on FPGA. Mountable Controller (MOCO) is a very fast readout controller for VME modules. General Trigger Operator (GTO) is an intelligent triggering NIM module. Functions of "common trigger management", "gate and delay generator", "scaler" are successfully implemented. The trigger system in BigRIPS DAQ has been successfully upgraded by 5 GTO modules.

(4) Development, management and operation of the network environment

We have been managing the network environment collaborating with Advanced Center for Computing and Communications (ACCC). All the Ethernet ports of the information wall sockets are capable of the Gigabit Ethernet connection (10/100/1000BT). In addition, a 10

Gbps network port has been introduced to the RIBF Experimental area in for the high speed data transfer of RIBF experiment to ACCC in near future.   Approximately 65 units of wireless LAN access points have been installed to cover the almost entire area of Nishina Center.

(5) Management of the information security
It is essential to take proper information security measures for information assets.
We are managing the information security of Nishina Center collaborating with ACCC.

Members

Team Leader
Takashi ICHIHARA (concurrent; Vice Chief Scientist, RI Physics Lab.)

Research & Technical Scientist
Yasushi WATANABE (concurrent; Senior Research Scientist, Radiation Lab.)

Nishina Center Research Scientist
Hidetada BABA

List of Publications & Presentations

Publications
[Journal]
(Original Papers) *Subject to Peer Review
C. Aidala *et al*. (PHENIX Collaboration), "B-meson production at forward and backward rapidity in p+p and Cu+Au collisions at √sNN=200 GeV," Phys. Rev. C **96**, 064901 (2017).

A. Adare *et al*. (PHENIX Collaboration), "Measurements of e^+e^- pairs from open heavy flavor in p+p and d+A collisions at √sNN=200 GeV," Phys. Rev. C **96**, 024907 (2017).

C. Aidala *et al*. (PHENIX Collaboration), "Cross section and transverse single-spin asymmetry of muons from open heavy-flavor decays in polarized p+p collisions at √s = 200 GeV," Phys. Rev. D **95**, 112001 (2017).

A. Adare *et al*. (PHENIX Collaboration), "Angular decay coefficients of J/ψ mesons at forward rapidity from p+p collisions at √s=510 GeV," Phys. Rev. D **95**, 092003 (2017).

C. Aidala *et al*. (PHENIX Collaboration), "Measurements of B→J/ψ at forward rapidity in p+p collisions at √s=510 GeV, Phys. Rev. D **95**, 092002 (2017).

A. Adare *et al*. (PHENIX Collaboration), "Nonperturbative-transverse-momentum effects and evolution in dihadron and direct photon-hadron angular correlations in p+p collisions at √s=510 GeV," Phys. Rev. D **95**, 072002 (2017).

Oral Presentations
[International Conference]
H. Baba, "Study of low-lying states in unstable oxygen isotopes using isoscalar and isovector probes," IVth Topical Workshop on Modern Aspects in Nuclear Structure, Bormio, Italy, 19−25th February, 2018 (Invited).
[Domestic Conference]
H. Baba, "Development of the multihost-type DAQ front-end system," JPS Annual Meeting, 22−25th March, Noda, Chiba, Japan, 2018.

RIBF Research Division
Research Instruments Group
Detector Team

1. Abstract

This team is in charge of development, fabrication, and operation of various detectors used for nuclear physics experiments at RIBF. Our current main mission is maintenance and improvement of detectors which are used at BigRIPS separator and its succeeding beam lines for beam diagnosis and particle identification of RI beams. We are also engaged in R&D of new detectors that can be used for higher-intensity RI beams. In addition, we are doing the R&D which uses the pelletron accelerator together with other groups.

2. Major Research Subjects

Development, fabrication, and operation of various detectors for nuclear physics experiments, including beam-line detectors which are used for the production and delivery of RI beams (beam diagnosis and particle identification). R&D which uses the pelletron accelerator.

3. Summary of Research Activity

The current research subjects are summarized as follows:
(1) Maintenance and improvement of the beam-line detectors which are used at BigRIPS separator and its succeeding beam lines.
(2) Development of new beam-line detectors with radiation hardness and tolerance for higher counting rates
(3) Management of the pelletron accelerator and R&D which uses the pelletron

Members

Team Leader
Hiromi SATO

Research and Technical Scientist
Tokihiro IKEDA (Senior Research Scientist)

Special Temporary Employee
Manabu HAMAGAKI

Visiting Scientist
Takeshi KOIKE (Tohoku University)

Student Trainee
Itaru HAKAMADA (Tokyo University)　　　　　　　　　　　　Kanji HIROSE (Toho University)
Kenta SATO (Toho University)

List of Publications & Presentations

Publications

[Journal]

(Original Papers) *Subject to Peer Review

J.W. Hwang, S. Kim, Y. Satou, N.A. Orr, Y. Kondo, T. Nakamura, J. Gibelin, N.L. Achouri, T. Aumann, H. Baba, F. Delaunay, P. Doornenbal, N. Fukuda, N. Inabe, T. Isobe, D. Kameda, D. Kanno, N. Kobayashi, T. Kobayashi, T. Kubo, S. Leblond, J. Lee, F.M. Marques, R. Minakata, T. Motobayashi, D. Murai, T. Murakami, K. Muto, T. Nakashima, N. Nakatsuka, A. Navin, S. Nishi, S. Ogoshi, H. Otsu, H. Sato, Y. Shimizu, H. Suzuki, K. Takahashi, H. Takeda, S. Takeuchi, R. Tanaka, Y. Togano, A.G. Tuff, M. Vandebrouck, K. Yoneda, "Single-neutron knockout from C-20 and the structure of C-19," Phys. Lett. B **769**, 503−508 (2017). *

H. Suzuki, T. Kubo, N. Fukuda, N. Inabe, D. Kameda, H. Takeda, K. Yoshida, K. Kusaka, Y. Yanagisawa, M. Ohtake, H. Sato, Y. Shimizu, H. Baba, M. Kurokawa, K. Tanaka, O.B. Tarasov, D. Bazin, D.J. Morrissey, B.M. Sherrill, K. Ieki, D. Murai, N. Iwasa, A. Chiba, Y. Ohkoda, E. Ideguchi, S. Go, R. Yokoyama, T. Fujii, D. Nishimura, H. Nishibata, S. Momota, M. Lewitowicz, G. DeFrance, I. Celikovic, K. Steiger, "Discovery of new isotopes Mo-81,Mo-82 and Ru-85,Ru-86 and a determination of the particle instability of Sb-103," Phy. Rev. C **96**, 034604 (2017). *

N. Fukuda, T. Kubo, D.,Kameda, N. Inabe, H. Suzuki, Y. Shimizu, H. Takeda, K. Kusaka, Y. Yanagisawa1 M. Ohtake, K. Tanaka, K. Yoshida, H. Sato, H. Baba, M. Kurokawa, T. Ohnishi, N. Iwasa, A. Chiba, T. Yamada, E. Ideguchi, S. Go, R. Yokoyama, T. Fujii, H. Nishibata, K. Ieki, D. Murai, S. Momota, D. Nishimura, Y. Sato, J.W. Hang, S. Kim, O.B. Tarasov, D.J. Morrissey, G. Simpson, "Identification of New Neutron-Rich Isotopes in the Rare-Earth Region Produced by 345 MeV/nucleon U-238," J Phys. Soc. Jpn. **87**, 014202 (2018). *

Y. Shimizu, T. Kubo, N. Fukuda, N. Inabe, D. Kameda, H. Sato, H. Suzuki, H. Takeda, K. Yoshida, G. Lorusso, H. Watanabe, G.S. Simpson, A. Jungclaus, H. Baba, F. Browne, P. Doornenbal, G. Gey, T. Isobe, Z. Li, S. Nishimura, P.A. Söderström, T. Sumikama, J. Taprogge, Z. Vajta, J. Wu, Z. Xu, A. Odahara, A. Yagi, H. Nishibata, R. Lozeva, C. Moon, H.S. Jung, "Observation of New Neutron-rich Isotopes among Fission Fragments from

In-flight Fission of 345 MeV/nucleon U-238: Search for New Isotopes Conducted Concurrently with Decay Measurement Campaigns," J Phys. Soc. Jpn. **87**, 014203 (2018). *

J. A. Tanis, D. Keerthisinghe, S. Wichhramarachchi, T. Ikeda, and N. Stolterfoht, "Charge deposition dependence of electron transmission through PET nanocapillaries and a tapered glass microcapillary," Nucl. Instrum. Methods Phys. Res. **B** 423, 1−6 (2018). *

Oral Presentations
[International Conference etc.]

H. Sato, "SAMURAI magnet," CBM Dipole Conceptual Design Review, (GSI), Darmstadt, Geramany, May (2017).

M. Ohno, T. Irimatsugawa, Y. Miura, H. Takahashi, T. Ikeda, C. Otani, M. Sakama, and N. Matsufuji, "Calorimetry of Heavy Charged Particle by superconducting transition edge sensor," 17th International Workshop on Low Temperature Detectors (LTD17), (Kyusyu University), Fukuoka, July (2017).

T. Ikeda, T. M. Kojima, Y. Natsume, J. Kimura, and T. Abe, "Active discharging method for stable transmission of slow highly-charged ions through sub-micron glass capillary," The 25th International Symposium on Ion-Atom Collisions (ISIAC 2017), (Hotel Grand Chancellor), Palm Cove, Queensland, Australia, July (2017).

T. Ikeda, T. M. Kojima, Y. Natsume, J. Kimura, and T. Abe, "Active discharging method for stable transmission of keV highly charged ion microbeams through tapered glass capillary," 22nd International Workshop on Inelastic Ion-Surface Collisions (IISC-22), (Hotel Schloss Eckberg), Dresden, Germany, September (2017).

[Domestic Conference]

池田時浩, 浜垣 学, 佐藤 広海, 小林知洋,「理化学研究所におけるタンデム加速器の現状（2016−2017 年度）」, 第 30 回「タンデム加速器及びその周辺技術の研究会」,（セラトピア土岐）, 岐阜県土岐市, 7 月 (2017).

ムハマドハルーン, 八木彩祐未, 小田原厚子, 西村俊二, J. Wu, R. Lozeva, C.-B. Moon, 方一帆, 大道理恵, 西畑洸希, 金岡裕志, P. Lee, 下田正, P. Doornenbal, G. Lorusso, 炭竃聡之, 渡辺寛, P.A. Söderström, F. Brown, Z.Y. Xu, 横山輪, 磯部忠昭, 馬場秀忠, 櫻井博儀, 鈴木宏, 稲辺尚人, 亀田大輔, 福田直樹, 竹田浩之, 安得順, 清水陽平, 佐藤広海, 久保敏幸, 石垣知樹, 森本翔太, 井手口栄治, 小松原哲郎, 新倉潤, 西塚一平, and the EURICA collaborators,「β-decay isomer をプローブとする A～140 中性子過剰核の構造研究 」, 日本物理学会 2017 年秋季大会,（宇都宮大学）, 宇都宮市, 9 月 (2017).

池田時浩, 幸島美輝子, 松原充芳, 増山貴文, 佐藤謙太, 廣瀬寛士, 箕輪達哉, 金衛国,「ガラスキャピラリーによる細胞照射のための励起光レーザー照準装置の開発」, 日本物理学会 2017 年秋季大会,（岩手大学）, 盛岡市, 9 月 (2017).

池田時浩, 松原充芳, 増山貴文, 佐藤謙太, 廣瀬寛士, 箕輪達哉, 金衛国,「紫外線への応用に向けたガラスキャピラリーによるレーザーマイクロビームの生成」, 日本物理学会 2017 年秋季大会,（岩手大学）, 盛岡市, 9 月 (2017).

佐藤謙太, 池田時浩, 廣瀬寛士, 松原充芳, 増山貴文, 箕輪達哉, 金衛国,「ガラスキャピラリー光学系による細胞照射用マイクロレーザービームの開発：ミクロンオーダー照射距離でのプロファイル測定」, 第 60 回放射線化学討論会,（産業技術総合研究所）, つくば市, 9 月 (2017).

廣瀬寛士, 池田時浩, 佐藤謙太, 松原充芳, 増山貴文, 箕輪達哉, 金衛国,「ガラスキャピラリー光学系による マイクロ励起光ピンポイント照射法の開発 ：ビームパワー密度分布測定」, 第 60 回放射線化学討論会,（産業技術総合研究所）, つくば市, 9 月 (2017).

池田時浩,「ガラスキャピラリーを使ったイオンマイクロビーム小型生成装置による細胞内小器官ピンポイント損傷法」, ビーム物理研究会 2017／分子研研究会「量子ビームの物質生命科学への応用の新展開」,（自然科学研究機構岡崎コンファレンスセンター）, 岡崎市, 11 月 (2017).

佐藤謙太, 池田時浩, 廣瀬寛士, 松原充芳, 増山貴文, 箕輪達哉, 金衛国,「ガラスキャピラリーによる細胞照射のための フレネル型ピンポイントレーザー照準法の開発」, ビーム物理研究会 2017／分子研研究会「量子ビームの物質生命科学への応用の新展開」,（自然科学研究機構岡崎コンファレンスセンター）, 岡崎市, 11 月 (2017).

廣瀬寛士, 池田時浩, 佐藤謙太, 松原充芳, 増山貴文, 箕輪達哉, 金衛国,「ガラスキャピラリー光学系による レーザーマイクロビームピンポイント照射法開発 ：ビームパワー密度分布測定」, ビーム物理研究会 2017／分子研研究会「量子ビームの物質生命科学への応用の新展開」,（自然科学研究機構岡崎コンファレンスセンター）, 岡崎市, 11 月 (2017).

池田時浩, 入松川知也, 三浦義隆, 中田直樹, 小島隆夫, 袴田格, 松藤成弘, 坂間誠, 三輪海彩, 大野雅史,「テーパー型ガラス管による 100 MeV/u 炭素イオンビーム通過テスト」, 日本物理学会 第 73 回年次大会（2018 年）,（東京理科大学）, 野田市, 3 月 (2018).

福田直樹, 清水陽平, 鈴木宏, AHN DeukSoon, 竹田浩之, 炭竃聡之, 宮武宇也, 渡辺裕, 稲辺尚人, 西村俊二, 大津秀暁, 吉田光一, 上野秀樹, 佐藤広海, 鈴木大介, 笹野匡紀, 磯部忠昭, 平山賀一, 家城和夫, 天野順貴,「^{238}U の入射核破砕反応を用いた $N = 126$ 近傍の中性子過剰核の生成 」, 日本物理学会第 73 回年次大会,（東京理科大学）, 野田市, 3 月 (2018).

Poster Presentations
[International Conference etc.]

M. Koushima, T. Ikeda, M. Matsubara, T. Masuyama, T. Minowa, and W.-G.Jin, "Development of laser target sight-on system based on multiple transmission through a tapered glass capillary for ion microbeam irradiation," the 30th International Conference on Photonic, Electronic and Atomic Collisions (ICPEAC XXX), (Cairns Convention Centre), Cairns, Queensland, Australia, August (2017).

T. Ikeda, T. M. Kojima, Y. Natsume, J. Kimura, and T. Abe, "Active discharging method for stable sub-micron sized beams of slow highly charged ions using tapered glass capillary with electrodes," the 30th International Conference on Photonic, Electronic and Atomic Collisions (ICPEAC XXX), (Cairns Convention Centre), Cairns, Queensland, Australia, August (2017).

M. Matsubara, T. Masuyama, T. Ikeda, T. Minowa, and W.-G.Jin, "Propagation of Laser Light Through Glass Capillaries for Ultraviolet Microbeams," International Conference on Quantum Atomic, Molecular and Plasma Physics, (Hilton Glasgow Grosvenor Hotel), Glasgow, UK, September (2017).

J. Tanis, D. Keerthisinghe, S. Wichhramarachchi, T. Ikeda, and N. Stolterfoht, "Charge (time) dependence of electron transmission through PET and tapered glass capillaries," 22nd International Workshop on Inelastic Ion-Surface Collisions (IISC-22), (Hotel Schloss Eckberg), Dresden, Germany, September (2017).

RIBF Research Division
Accelerator Applications Research Group

1. Abstract

This group promotes various applications of ion beams from RI Beam Factory (RIBF). Ion Beam Breeding Team studies various biological effects of fast heavy ions and develops new technology to breed plants and microbes by heavy-ion irradiations. RI Applications Team studies production and application of radioisotopes for various research fields, development of trace element analysis and its application, and development of chemical materials for ECR ion sources of RIBF accelerators.

2. Major Research Subjects

Research and development in biology, chemistry and materials science utilizing heavy-ion beams from RI Beam Factory.

3. Summary of Research Activity

  (1) Biological effects of fast heavy ions
  (2) Molecular nature of DNA alterations induced by heavy-ion irradiation
  (3) Research and development of heavy-ion breeding
  (4) RI application researches
  (5) Research and development of RI production technology at RIBF
  (6) Developments of trace elements analyses
  (7) Development of chemical materials for ECR ion sources of RIBF accelerators

Members

Group Director
Tomoko ABE

List of Publications & Presentations

Publications and presentations for each research team are listed in subsections.

RIBF Research Division
Accelerator Applications Research Group
Ion Beam Breeding Team

1. Abstract

Ion beam breeding team studies various biological effects of fast heavy ions. It also develops new technique to breed plants and microbes by heavy-ion irradiations. Fast heavy ions can produce dense and localized ionizations in matters along their tracks, in contrast to photons (X rays and gamma rays) which produce randomly distributed isolated ionizations. These localized and dense ionization can cause double-strand breaks of DNA which are not easily repaired and result in mutation more effectively than single-strand breaks. A unique feature of our experimental facility at the RIKEN Ring Cyclotron (RRC) is that we can irradiate living tissues in atmosphere since the delivered heavy-ion beams have energies high enough to penetrate deep in matter. This team utilizes a dedicated beam line (E5B) of the RRC to irradiate microbes, plants and animals with beams ranging from carbon to iron. Its research subjects cover physiological study of DNA repair, genome analyses of mutation, and development of mutation breeding of plants by heavy-ion irradiation. Some new cultivars have already been brought to the market.

2. Major Research Subjects

(1) Study on the biological effects by heavy-ion irradiation
(2) Study on the molecular nature of DNA alterations induced by heavy-ion irradiation
(3) Innovative applications of heavy-ion beams

3. Summary of Research Activity

We study biological effects of fast heavy ions from the RRC using 135A MeV C, N, Ne ions, 95A MeV Ar ions, 90A MeV Fe ions and from the IRC using 160A MeV Ar ions. We also develop breeding technology of microbes and plants. Main subjects are:

(1) Study on the biological effects by heavy-ion irradiation

Heavy-ion beam deposits a concentrated amount of dose at just before stop with severely changing the linear energy transfer (LET). The peak of LET is achieved at the stopping point and known at the Bragg peak (BP). It is well known to be good for cancer therapy to adjust the BP to target malignant cells. On the other hand, a uniform dose distribution is a key to the systematic study for heavy-ion mutagenesis, and thus to the improvement of the mutation efficiency. Therefore plants and microbes are treated using ions with stable LET. We investigated the effect of LET ranging from 23 to 640 keV/μm, on mutation induction using dry seeds of the model plants *Arabidopsis thaliana*. The most effective LET (LETmax) was 30 keV/μm. LETmax irradiations showed the same mutation rate as that by chemical mutagens, which typically cause high mutation rate. The LETmax of imbibed rice (*Oryza sativa* L.) seeds, dry rice seeds and dry wheat (*Triticum monococcum*) seeds were shown to be 50−63 keV/μm, 23−30 keV/μm and 50 keV/μm, respectively. In the case of microbe (*Mesorhizobium lothi*), the results showed a higher incidence of deletion mutations for Fe ions at 640 keV/μm than for C ions at 23−40 keV/μm. Thus, the LET is an important factor to be considered in heavy-ion mutagenesis.

(2) Study on the molecular nature of DNA alterations induced by heavy-ion irradiation

Detailed analyses on the molecular nature of DNA alterations have been reported as an LET-dependent effect for induced mutation. The most mutations were deletions ranging from a few to several tens of base pairs (bp) in the *Arabidpsis thaliana* mutants induced by irradiation with C ions at 30 keV/μm and rice mutants induced by irradiation with C ions at 50 keV/μm or Ne ions at 63 keV/μm. LETmax is effective for breeding because of its very high mutation frequency. Since most mutations are small deletions, these are sufficient to disrupt a single gene. Thus, irradiation can efficiently generate knockout mutants of a target gene, and can be applied to reverse genetics. On the other hand, irradiation with Ar ions at 290 keV/μm showed a mutation spectrum different from that at LETmax: the proportion of small deletions (<1 kbp) was low, while that of large deletions ranging from several to several tens of kbp, and rearrangements was high. Many genes in the genome (> 10%) are composed of tandem duplicated genes that share functions. For knockout of the tandem duplicated genes, large deletions are required, and the appropriate deletion size is estimated to be around 5−10 kbp and 10−20 kbp based on the gene density in *Arabidpsis* and rice, respectively. No method is currently available to efficiently generate deletion mutants of this size. As such, higher LET irradiation is promising as a new mutagen suitable for the functional analysis of tandem duplicated genes.

(3) Innovative application of heavy-ion beams

We have formed a consortium for ion-beam breeding. It consisted of 24 groups in 1999, in 2017, it consisted of 176 groups from Japan and 11 from overseas. Breeding was performed previously using mainly flowers and ornamental plants. We have recently put a new sweet-smelling onion cultivar with tearless and non-pungent, 'Smile Balls' on the market. Beneficial variants have been grown for various plant species, such as high yield rice, semi-dwarf early rice, semi-dwarf buckwheat, semi-dwarf barley, hypoallergenic peanut, spineless oranges, non-flowering Eucalyptus and lipids-hyperaccumulating unicellular alga. The target of heavy-ion breeding is extended from flowers to crops so that it will contribute to solve the global problems of food and environment. We collaborate with the National Research and Development Agency, Japan Fisheries Research and Education Agency and Nagasaki University. The monogonont rotifer (*Brachionus* spp.) is a complex species and an essential food source for finfish aquaculture. The *B. plicatilis* is divided into three major clades (small, medium and large(L)) based on body length. Although the body size ranges from 100 to 300 μm in length, a mutation breeding of rotifers with larger size is expected for the purpose of productivity improvement in the aquaculture industry. Therefore, we conducted a large-scale screening to isolate gigantic rotifers by heavy-ion-beam irradiation to L-type rotifers. Then we have established some dozens of mutant lines that have an average length of over 350 μm (a maximum length reached 394 μm) through over ten thousand of individual mutagenized lines. These data will be useful to choose the suitable lines that satisfies the request of the aquaculture industry.

Members

Team Leader
Tomoko ABE (concurrent: Group Director, Accelerator Applications Research Gr.)

Research & Technical Scientist

Kazuhide TSUNEIZUMI (Senior Research Scientist)   Katsunori ICHINOSE (Senior Technical Scientist)
Masako IZUMI (Senior Research Scientist)   Hiroshi ABE (Senior Technical Scientist)
Teruyo TSUKADA (Senior Research Scientist)   Ryouhei MORITA (Technical Scientist)
Tokihiro IKEDA (concurrent)

Contract Researchers

Hiroyuki ICHIDA   Yusuke KAZAMA
Kotaro ISHII

Technical Staff I

Yoriko HAYASHI   Yuki SHIRAKAWA

Technical Staff II

Sumie OHBU   Mieko YAMADA
Taeko WAKANA

Research Consultants

Masahiro MII

Part-time Workers

Hideo TOKAIRIN   Sachiko KOGURE

Visiting Scientist

Makoto FUJIWARA (Univ. of Tokyo)   Eitaro FUKATSU (Forestry and Forest Products Res. Inst.)
Masao WATANABE (Tohoku Univ.)   Tomonari HIRANO (Univ. of Miyazaki)
Hisashi TSUJIMOTO (Tottori Univ.)   Yoichi SATO (Riken Food Co., Ltd.)
Yutaka MIYAZAWA (Tohoku Univ.)   Ali FERJANI (Tokyo Gakugei Univ.)
Toshinari GODO (Flower & Garden Bank)   Katsutomo SASAKI (Nat'l Agric. and Food Res. Org.)
Masanori TOMITA (CRIEPI)   Kunio SUZUKI (Technoflora, Co., Ltd.)
Toshikazu MORISHITA (Nat'l. Inst. Agric. Res.)   Kazumitsu MIYOSHI (Chiba. Univ.)
Koji MURAI (Fukui Pref. Univ.)   Makoto UBUKATA (Hokkaido Univ.)
Hinako TAKEHISA (Nat'l. Inst. Agric. Sci.)   Tadashi SATO (Tohoku Univ.)
Akiko HOKURA (Tokyo Denki Univ.)   Takeshi YAMAKI (Riken Vitamin Co., Ltd.)
Norihiro OHTSUBO (Kyoto Pref. Univ.)   Ayumi DEGUCHI (Chiba Univ.)

Visiting Technicians

Takuji YOSHIDA (Takii Seed Co., Ltd.)   Keiji IKEDA (KK SeaAct)
Daisuke SAITO (Riken Food Co., Ltd.)

Research Fellows

Naoji WAKITA (Wadomari Cho Agr. Exp. Station)   Yoshiharu TAKE (Wadomari Cho)
Tadahito OOTUBO (Wadomari Cho Agr. Exp. Station)   Hiroshi ASATO (Wadomari Cho)
Shunsuke IMANISHI (Natl. Inst.Veg. and Tea Sci.)   Kenji OOYOSHI (Wadomari Cho)
Tomihiro TAKESHITA (Wadomari Cho)   Hironari UCHIDA (Saitama Pref. Res. Inst.)

Student Trainees

Yu IMAMURA (Tokyo Denki Univ.)   Koichi NAMBU (Tokyo Denki Univ.)
Kazuki TAKANASHI (Tokyo Denki Univ.)   Naoko HIROSE (Tokyo Denki Univ.)
Yoshihiro TAKAHASHI (Kitazato Univ.)   Koya INOUE (Tokyo Denki Univ.)
Takuya NISHINOBO (Tokyo Denki Univ.)

List of Publications & Presentations

Publications

[Journal]
(Original Papers) *Subject to Peer Review

M. Amino, K. Yoshioka, Y. Furusawa, S. Tanaka, N. Kawabe, T. Hishida, T. Tsukada, M. Izumi, S. Inokuchi, T. Abe, T. Tanabe, Y. Ikari, "Inducibility of Ventricular Arrhythmia 1 Year Following Treatment with Heavy Ion Irradiation in Dogs with Myocardial Infarction," Pacing Clin. Electrophysiol. **40**(4), 379−390 (2017). *

Y. Sato, T. Hirano, H. Ichida, M. Murakami, N. Fukunishi, T. Abe, S. Kawano, "Morphological and physiological differences among cultivation lines of *Undaria pinnatifida* in a common garden experiment using a tank culture system," J. Appl. Phycol. **29**(5), 2287−2295 (2017). *

M. T. Fujiwara, M. Yasuzawa, S. Sasaki, T. Nakano, Y. Niwa, S. Yoshida, T. Abe, R. D. Itoh, "The Arabidopsis minD mutation causes aberrant FtsZ1 ring placement and moderate heterogeneity of chloroplasts in the leaf epidermis," Plant Signal Behav., e1343776 (2017). *

玉木克知, 山中正仁, 林依子, 阿部知子, 小山佳彦,「キクの品種特性が炭素イオンビーム照射による花色突然変異体の出現に及ぼす影響", 園学研. **16**(2), 117−123 (2017). *

M. Izumi, T. Mizuno, K. Yanagi, K. Sugimura, K. Okumura, N. Imamoto, T. Abe, F. Hanaoka, "The Mcm2-7 -interacting domain of human mini-chromosome maintenance 10(Mcm10) protein is important for stable chromatin association and origin firing," J. Biol. Chem. **292**(31), 13009−13021 (2017). *

K. Niwa, T. Abe, A. Kobiyama, "Possibility of polyploidy breeding using cryptic species in the marine crop *Pyropia yezoensis* (Bangiales, Rhodophyta)," J. Appl. Phycol. **30**(2), 1197−1205 (2017). *

Y. Kazama, Ishii K., T. Hirano, T. Wakana, M. Yamada, S. Ohbu, T. Abe, "Different mutational function of low- and high-linear energy transfer heavy-ion irradiation demonstrated by whole-genome resequencing of Arabidopsis mutants," Plant J. **92**(6), 1020−1030 (2017). *

Y. Sato, M. Yamaguchi, T. Hirano, N. Fukunishi, T. Abe, S. Kawano, "Effect of water velocity on *Undaria pinnatifida* and *Saccharina japonica* growth in a novel tank system designed for macroalgae cultivation," J. Appl. Phycol. **29**(3), 1429−1436 (2017). *

Y. Yamamoto, H. Ichida, A. Hieno, O. Daich, M. Tokizawa, M. Nomoto, Y. Tada, K. Kusunoki, H. Koyama, N. Hayami, "Prediction of bipartite transcriptional regulatory elements using transcriptome data of Arabidopsis," DNA Res. **24**, 271–278, 2017.

Y. Koide, A. Ogino, T. Yoshikawa, Y. Kitashima, N. Saito, Y. Kanaoka, K. Onishi, Y. Yoshitake, T. Tsukiyama, H. Saito, M. Teraishi,Y. Yamagata, A. Uemura, H. Takagi, Y. Hayashi, T. Abe, Y. Fukuta, Y. Okumoto, A. Kanazawa, "Lineage-specific gene acquisition or loss is involved in interspecific hybrid sterility in rice," Proc. Natl. Acad. Sci. **115**(9), E1955−E1962 (2018). *

H. Murata, T. Abe, H. Ichida, Y. Hayashi, T. Yamanaka, T. Shimokawa, K. Tahara, "Heavy-ion beam mutagenesis of the ectomycorrhizal agaricomycete *Tricholoma matsutake* that produces the prized mushroom 'matsutake' in conifer forests," Mycorrhiza **28**, 171−177 (2018). *

H. Yamatani, K. Kohzuma, M. Nakano, T. Takami, Y. Kato, Y. Hayashi, Y. Monden, Y. Okumoto, T. Abe, T. Kumamaru, A. Tanaka, W. Sakamoto, M. Kusaba, "Impairment of Lhca4, a subunit of LHCI, causes high accumulation of chlorophyll and the stay-green phenotype in rice," J. Exp. Bot. **69**(5), 1027−1035 (2018). *

(Review)

阿部知子,「重イオンビーム育種技術の開発─微生物は鉄イオンビームがお好き─」, ふぇらむ **22**(7), 362−365 (2017).

平野智也, 市田裕之, 阿部知子,「重イオンビームで広がる花きの新品種作出　原子核は花の品種改良を加速する」, 化学と生物 **55**, 775−782 (2017). *

Oral Presentations

[International Conference]

T. Ikeda, T. M. Kojima, Y. Natsume, J. Kimura, T. Abe , "Active discharging method for stable transmission of slow highly-charged ions through sub-micron glass capillary," The 25th International Symposium on Ion-Atom Collisions (ISIAC 2017), Palm Cove, Australia, July (2017).

Y. Kazama , "Deletion mapping of the plant huge Y chromosome by employing traveling salesman problem ," Oxford Congress on Plant Sciences 2017, Oxford, UK, September (2017).

[Domestic Conference]

阿部知子,「加速器物理学と農学は平行線：重イオンビーム育種技術の開発秘話」, 原子力平和利用連絡協議会, 仙台, 7 月 (2017).

風間裕介,「重イオンビームの変異特性に関する研究とそれを利用した植物巨大 Y 染色体の精密マッピング」, 日本植物学会第 81 回大会、日本植物学会賞奨励賞受賞講演, 野田, 9 月 (2017).

石井公太郎, 浅野円花, 風間裕介, 佐々木成江, 東山哲也, 阿部知子, 河野重行,「クロレラの内部倍数性機構の解明と鉄イオンビームによる染色体の分断化と再構成」, 日本植物学会第 81 回大会, 野田, 9 月 (2017).

竹下毅, Ivanov I. N., Bišová K., Zachleder V., 石井公太郎, 風間裕介, 阿部知子, 河野重行,「重イオンビーム照射によるクロレラ変異体: オイル増産株の作出と欠失部位ゲノム解析」, 日本植物学会第 81 回大会, 野田, 9 月 (2017).

阿部知子, 市田裕之, 高城啓一, 畑下昌範,「未来を作るイオンビーム育種技術」, 平成 29 年度園芸学会北陸支部大会, 福井, 12 月 (2017).

高城啓一, 畑下昌範, 阿部知子,「北陸にもあるイオンビーム照射施設: 若狭湾エネルギー研究センターでのイオンビーム育種研究」, 平成 29 年度園芸学会北陸支部大会, 福井, 12 月 (2017).

阿部知子,「原子核は生物の進化を加速するか？─異分野交流を楽しむ研究場─」, 平成 29 年度　奈良女子大学環境安全管理センター研修会, 奈良, 12 月 (2017).

風間裕介, 石井公太郎, 平野智也, 若菜妙子, 山田美恵子, 大部澄江, 阿部知子,「シロイヌナズナ変異体の全ゲノムリシーケンスで明らかにした 突然変異誘発への LET の影響」,日本育種学会　第 133 回講演会, 福岡, 3 月 (2018).

市田裕之, 森田竜平, 白川侑希, 林依子, 阿部知子,「イネ無選抜エキソーム解析による重イオンビーム誘発変異の解析」,日本育種学会　第 133 回講演会, 福岡, 3 月 (2018).

R. Tabassum, T. Katsube-Tanaka, T. Abe, "Analysis on White Immature Grains of the Rice Mutant Line 13-45 IV. Quantitative comparison among cultivars," 日本作物学会　第 247 回講演会, つくば, 3 月 (2018).

吉田祐樹, 成田典之, 星野里奈, 矢野覚士, 風間裕介, 阿部知子, 堀口吾朗, 塚谷裕一,「レーザー変位センサ測定によるシロイヌナズナの葉の厚さ変異体の単離と解析」, 第 59 回日本植物生理学会, 札幌, 3 月 (2018).

Poster Presentations
[International Conference]

T. Abe, S. Ishii, Y. Hayashi, Y. Kazama, T. Hirano, "New ornamental cherry cultivars induced by heavy-ion beam irradiation," 8th International Cherry Symposium in YAMAGATA, Yamagata, Japan, June (2017).

K. Suzuki, A. Nakashima, K. Yamada, H. Suzuki, T. Takeuchi, Y. Kazama, S. Mitra, T. Abe, O. Iwata, K. Goda , "FACS-based selective breeding of Euglena gracilis for efficient biofuel production," CYTO 2017: 32nd Congress of the International Society for Advancement of Cytometry, Boston, USA, June (2017).

T. Ikeda, T. M. Kojima, Y. Natsume, J. Kimura, T. Abe , "Active discharging method for stable sub-micron sized beams of slow highly charged ions using tapered glass capillary with electrodes," The 30th International Conference on Photonic, Electronic and Atomic Collisions (ICPEAC XXX), Cairns, Australia, July (2017).

Y. Sato, T. Hirano, H. Ichida, N. Fukunishi, T. Abe, S. Kawano, "Development of elite lines in *Undaria pinnatifida* for diversification of cultivation periods at the coast in the Sanriku region, northern Japan," The 8th Asian Pacific Phycological Forum, Kuala Lumpur, Malaysia, October (2017).

K. Murai, Y. Kazama, T. Abe , "Mutant panels of diploid and teteraploid wheats developed by heavy-ion beam mutagenesis and their application for genetic research," TAIWAN-Japan Plant Biology 2017 Conference, Taipei, Taiwan, November (2017).

[Domestic Conference]

阿部知子,「重イオンビームで染色体を加工して変異体を創る〜新品種育成と遺伝子機能解析〜」, 理化学研究所創立百周年記念交流会, 東京, 4 月 (2017).

Vuong N. Q., 風間裕介, 石井公太郎, 大部澄江, 國武久登, 阿部知子, 平野智也,「シロイヌナズナ大輪変異体 *ohbana*1 における花器官サイズ制御機構の解析」, 日本植物学会第 81 回大会, 野田, 9 月 (2017).

大野豊, 長谷純宏, 佐藤勝也, 野澤樹, 加藤浩, 市田裕之, 森田竜平, 阿部知子,「炭素イオンビームによるイネ変異体の作出と変異解析」, QST 高崎サイエンスフェスタ 2017, 高崎, 12 月 (2017).

佐藤陽一, 萩原亮, 斎藤大輔, 中裕之, 柏谷伸一, 平野智也,市田裕之, 福西暢尚, 阿部知子, 河野重行, 小野克徳,「三陸産ワカメ優良系統開発と実用化に向けた取り組み」, 日本藻類学会第 42 回大会, 仙台, 3 月 (2018).

遠藤貴司, 佐藤浩子, 石森裕貴, 中込佑介, 佐藤雅志, 林依子, 市田裕之, 阿部知子,「重イオンビーム照射によるイネ有用変異体の探索」, 日本育種学会　第 133 回講演会, 福岡, 3 月 (2018).

上田純平, 風間裕介, 阿部知子, 村井耕二,「早生突然変異体コムギ系統における花成遅延復帰変異体 *late-heading* 1 の同定」, 日本育種学会　第 133 回講演会, 福岡, 3 月 (2018).

森田竜平, 市田裕之, 一瀬勝紀, 白川侑希, 林依子, 佐藤雅志, 阿部知子,「重イオンビーム誘発変異の網羅的検出に向けたプログラムの検討」, 日本育種学会　第 133 回講演会, 福岡, 3 月 (2018).

中野絢菜, 相井城太郎, 小森美佳, 阿部知子, 森下敏和, 鈴木達郎, 清水明美, 田中宥司,「イオンビーム照射由来ダッタンソバ半矮性変異体 *sdb* における原因遺伝子の同定」, 日本育種学会　第 133 回講演会,福岡, 3 月 (2018).

大野豊, 市田裕之, 野澤樹, 森田竜平, 加藤浩, 阿部知子, 長谷純宏,「イネ炭素イオンビーム誘発変異体のエキソーム解析」, 第 59 回日本植物生理学会, 札幌, 3 月 (2018).

山谷浩史, 上妻馨梨, 中野道治, 高見常明, 加藤裕介, 林依子, 門田有希, 奥本裕, 阿部知子, 熊丸敏博, 田中歩, 坂本亘, 草場信,「イネ stay-green 突然変異体 dye1 の分子遺伝学的解析」,第 59 回日本植物生理学会, 札幌, 3 月 (2018).

RIBF Research Division
Accelerator Applications Research Group
RI Applications Team

1. Abstract

The RI Applications Team develops production technologies of radioisotopes (RIs) at RIKEN RI Beam Factory (RIBF) for application studies in the fields of physics, chemistry, biology, engineering, medicine, pharmaceutical and environmental sciences. We use the RIs mainly for nuclear and radiochemical studies such as RI production and superheavy element chemistry. The purified RIs such as ^{65}Zn, ^{85}Sr, ^{88}Y, and ^{109}Cd are delivered to universities and institutes through Japan Radioisotope Association. We also develop new technologies of mass spectrometry for the trace-element analyses using accelerator technology and apply them to the research fields such as cosmochemistry, environmental science, archaeology and so on. We also develop chemical materials for ECR ion sources of heavy-ion accelerators in RIBF.

2. Major Research Subjects

(1) Research and development of RI production technology at RIBF
(2) RI application researches
(3) Development of trace element and isotope analyses and their applications to geoscience and environmental science
(4) Development of chemical materials for ECR ion sources of heavy-ion accelerators in RIBF

3. Summary of Research Activity

(1) Research and development of RI production technology at RIBF and RI application studies

Due to its high sensitivity, the radioactive tracer technique has been successfully applied for investigations of the behavior of elements in the fields of chemistry, biology, engineering, medicine, pharmaceutical and environmental sciences. We have been developing production technologies of useful radiotracers at RIBF and conducting their application studies in collaboration with many researchers in various fields. With 14-MeV proton, 24-MeV deuteron, and 50-MeV alpha beams from the AVF cyclotron, we presently produce about 50 radiotracers from ^{7}Be to ^{211}At. Among them, ^{65}Zn, ^{85}Sr, ^{88}Y, and ^{109}Cd are delivered to Japan Radioisotope Association for fee-based distribution to the general public in Japan. Our RIs are also distributed to researchers under the Supply Platform of Short-lived Radioisotopes for Fundamental Research, supported by MEXT KAKENHI. On the other hand, radionuclides of a large number of elements are simultaneously produced from metallic targets such as ^{nat}Ti, ^{nat}Ag, ^{nat}Hf, and ^{197}Au irradiated with a 135-MeV nucl.$^{-1}$ ^{14}N beam from the RIKEN Ring Cyclotron. These multitracers are also supplied to universities and institutes as collaborative researches.

In 2017, we developed production technologies of radioisotopes such as ^{24}Na, $^{42, 43}$K, ^{44m}Sc, $^{48, 51}$Cr, ^{67}Cu, ^{74}As, ^{88}Y, ^{135m}Ba, ^{139}Ce, ^{143}Pm, ^{206}Bi, and ^{211}At which were strongly demanded but lack supply sources in Japan. We also investigated the excitation functions for the ^{64}Ni(α, x), ^{89}Y(α, x), ^{nat}Zr(α, x), ^{nat}In(α, x), ^{169}Tm(α, x), ^{nat}Yb(α, x), ^{nat}Hf(α, x), and ^{nat}W(α, x) reactions to quantitatively produce useful RIs. We used radiotracers of $^{48, 51}$Cr, ^{74}As, ^{88}Y, ^{135m}Ba, ^{139}Ce, ^{143}Pm, ^{206}Bi, and ^{211}At for application studies in chemistry, ^{24}Na, ^{42,43}K, ^{44m}Sc, ^{67}Cu, and ^{211}At in nuclear medicine, and ^{88}Zr and ^{175}Hf in geochemistry. We also produced ^{65}Zn, ^{85}Sr, ^{88}Y, and ^{109}Cd for our scientific researches on a regular schedule and supplied the surpluses through Japan Radioisotope Association to the general public. In 2017, we accepted 2 orders of ^{65}Zn with a total activity of 5.5 MBq, 1 order of ^{85}Sr with 3.7 MBq, and 2 orders of ^{88}Y with 2 MBq. We also distributed ^{44m}Sc (5 MBq × 1), ^{67}Cu (10 MBq × 1), ^{88}Zr (1 MBq × 1 and 2 MBq × 1), ^{121m}Te (2 MBq × 1), and ^{211}At (40 MBq × 3) under the Supply Platform of Short-lived Radioisotopes for Fundamental Research.

(2) Superheavy element chemistry

Chemical characterization of newly-discovered superheavy elements (SHEs, atomic numbers $Z \geq 104$) is an extremely interesting and challenging subject in modern nuclear and radiochemistry. We are developing SHE production systems as well as rapid single-atom chemistry apparatuses at RIBF. Using heavy-ion beams from RILAC and AVF, ^{261}Rf ($Z = 104$), ^{262}Db ($Z = 105$), ^{265}Sg ($Z = 106$) and ^{266}Bh ($Z = 107$) are produced in the ^{248}Cm(^{18}O, $5n$)^{261}Rf, ^{248}Cm(^{19}F, $5n$)^{262}Db, ^{248}Cm(^{22}Ne, $5n$)^{265}Sg, and ^{248}Cm(^{23}Na, $5n$)^{266}Bh reactions, respectively, and their chemical properties are investigated.

We installed a gas-jet transport system to the focal plane of the gas-filled recoil ion separator GARIS at RILAC. This system is a promising approach for exploring new frontiers in SHE chemistry: the background radiation from unwanted products are strongly suppressed, the intense primary heavy-ion beam is absent in the gas-jet chamber, and hence the high gas-jet extraction yield is attained. Furthermore, the beam-free conditions make it possible to investigate new chemical systems. To realize aqueous chemistry studies of Sg and Bh, we have been developing a continuous and rapid solvent extraction apparatus which consists of a continuous dissolution apparatus Membrane DeGasser (MDG), a Flow Solvent Extractor (FSE), and a liquid scintillation detector for α/SF-spectrometry. On the other hand, we installed a gas-jet coupled target system and a safety system for a radioactive ^{248}Cm target on the beam line of AVF. A chemistry laboratory, AVF hot laboratory, was also constructed on the upper floor of AVF. Aqueous chemistry apparatuses for ion exchange, solvent extraction, and electrolysis are under development together with an automated α-particle detection system.

In 2017, we produced radiotracers of ^{88}Zr, $^{92m, 95}$Nb, ^{93m}Mo, ^{95m}Tc, ^{175}Hf, ^{179}Ta, $^{179m, 181}$W, and ^{183}Re at AVF and conducted model experiments for aqueous chemistry studies on Rf, Db, Sg, and Bh.

(3) Development of trace element and isotope analyses and their applications to geoscience and environmental science

We have been developing the ECR Ion Source Mass Spectrometer (ECRIS-MS) for trace element analyses. In 2017, we renovated the detection system of ECRIS-MS and evaluated sensitivity and mass resolution power. We equipped a laser-ablation system with an ion

source and a pre-concentration system to achieve high-resolution analyses for noble gases such as Kr and Xe. This technique is expected to monitor the atmosphere around nuclear power plants.

Using the conventional ICP-MS, TIMS, IRMS and so on, we analyzed sediments such as a ferro-manganese nodule in the Pacific Ocean to elucidate its growth history concerning the environmental changes in the ocean. We also studied lead and sulfur isotope ratios on cinnabar and asphalt samples from ancient ruins in Japan to elucidate the distribution of goods in the archaic society and to reveal the establishment of the Yamato dynasty in the period from Jomon to Tumulus. In 2017, we improved the sensitivity for the sulfur isotope ratios with the "trapping and focusing" techniques using a cryo-system and applied the analyses of pigment from Roman ruins, such as Badalona (Spain).

(4) Development of chemical materials for ECR ion sources of RIBF

In 2017, we prepared metallic ^{238}U rods and ^{238}UO$_2$ on a regular schedule for ^{238}U-ion accelerations with the 28-GHz ECR of RILAC II.

Members

Team Leader
Hiromitsu HABA

Research & Technical Scientist
Kazuya TAKAHASHI (Senior Research Scientist)

Postdoctoral Researchers
Kaustab GHOSH   Takuya YOKOKITA
Yukiko KOMORI

Technical Staff I
Shinya YANOU

Research Consultants
Hisaaki KUDO   Seiichi SHIBATA

Part-time Workers
Michiko KITAGAWA   Minako OSANAI
Yu Vin SAHOO   Nozomi SATO
Keiko WATANABE

Visiting Scientists
Masayuki AIKAWA (Hokkaido Univ.)   Kazuhiko AKIYAMA (Tokyo Met. Univ.)
Hayato IKEDA (Tohoku Univ.)   Hirokazu KAWAMURA (Tohoku Univ.)
Mayeen Uddin KHANDAKER (Univ. Malaya)   Hidetoshi KIKUNAGA (Tohoku Univ.)
Takumi KUBOTA (Kyoto Univ.)   Toshimitsu MOMOSE (International Univ. Health Welfare)
Aya SAKAGUCHI (Univ. of Tsukuba)   Miho TAKAHASHI (Tokyo Univ. Marine Sci. and Tech.)
Yuichi TAKAKU (Institute for Environmental Sci.)   Kazuo TANAKA (Tohoku Univ.)
Masayoshi TODA (Tokyo Univ. Marine Sci. and Tech.)   Atsushi TOYOSHIMA (JAEA)
Naoyuki UKON (Fukushima Med. Univ.)   Akihiko YOKOYAMA (Kanazawa Univ.)
Koji YOSHIMURA (Okayama Univ.)

Visiting Technicians
Yuki TAKEMURA (ATOX)   Shusaku TAZAWA (ATOX)
Zenko YOSHIDA (ATOX)   Mami YUKI (ATOX)

Student Trainees
Yuki HATTORI (Tokyo Univ. Marine Sci. and Tech.)   Akimitsu KANDA (Osaka Univ.)
Takumi IKEDA (Osaka Univ.)   Narumi KONDO (Osaka Univ.)
Saki ITO (Tohoku Univ.)   Risa MOTOYAMA (Niigata Univ.)
Michiko KITAGAWA (Kindai Univ.)   Masahiro NAGASE (Osaka Univ.)
Takuya MORIYAMA (Niigata Univ.)   Hidemi NINOMIYA (Osaka Univ.)
Tomohiro MURATA (Hokkaido Univ.)   Kouki OUCHI (Osaka Univ.)
Yuki NARUSE (Niigata Univ.)   Moemi SAITOH (Hokkaido Univ.)
Sho OKUBO (Okayama Univ.)   Daisuke SATO (Niigata Univ.)
Ryota OZAKI (Okayama Univ.)   Yudai SHIGEKAWA (Osaka Univ.)
Yuta HAYAKAWA (Kanazawa Univ.)   Kenta SUZUKI (Okayama Univ.)
Junpei INAGAKI (Univ. of Tsukuba)   Shota TSUCHIYA (Niigata Univ.)

Eisuke WATANABE (Osaka Univ.)

Tomohiro TOMITSUKA (Niigata Univ.)

Kouhei YAMAMORI (Kanazawa Univ.)

Rufai Ahmed USMAN (Univ. Malaya)

Keita SEKIGUCHI (Univ. of Tsukuba)

Ryohei YAMADA (Niigata Univ.)

Kaori SHIRAI (Niigata Univ.)

Yuki YASUDA (Osaka Univ.)

List of Publications & Presentations

Publications

[Journal]

(Original Papers) *Subject to Peer Review

P. Schury, M. Wada, Y. Ito, D. Kaji, F. Arai, M. MacCormick, I. Murray, H. Haba, S. Jeong, S. Kimura, H. Koura, H. Miyatake, K. Morimoto, K. Morita, A. Ozawa, M. Rosenbusch, M. Reponen, P.-A. Söderström, A. Takamine, T. Tanaka, and H. Wollnik, "First online multireflection time-of-flight mass measurements of isobar chains produced by fusion-evaporation reactions: Toward identification of superheavy elements via mass spectroscopy," Phys. Rev. C **95**, 011305(R) 1–6 (2017).*

D. Kaji, K. Morita, K. Morimoto, H. Haba, M. Asai, K. Fujita, Z. Gan, H. Geissel, H. Hasebe, S. Hofmann, M. Huang, Y. Komori, L. Ma, J. Maurer, M. Murakami, M. Takeyama, F. Tokanai, T. Tanaka, Y. Wakabayashi, T. Yamaguchi, S. Yamaki, and A. Yoshida, "Study of the reaction ^{48}Ca + ^{248}Cm → ^{296}Lv* at RIKEN-GARIS," J. Phys. Soc. Jpn. **86**, 034201 1–7 (2017).*

S. Takács, F. Ditrói, Z. Szűcs, H. Haba, Y. Komori, M. Aikawa, and M. Saito, "Crosschecking of alpha particle monitor reactions up to 50 MeV," Nucl. Instrum. Methods Phys. Res. B **397**, 33–38 (2017).*

M. Saito, M. Aikawa, Y. Komori, H. Haba, and S. Takács, "Production cross sections of ^{169}Yb and Tm isotopes in deuteron-induced reactions on ^{169}Tm," Appl. Radiat. Isotopes **125**, 23–26 (2017).*

A. R. Usman, M. U. Khandaker, H. Haba, N. Otuka, and M. Murakami, "Excitation functions of alpha particles induced nuclear reactions on natural titanium in the energy range of 10.4–50.2 MeV," Nucl. Instrum. Methods Phys. Res. B **399**, 34–47 (2017).*

K. Fujiki, S. Yano, T. Ito, Y. Kumagai, Y. Murakami, O. Kamigaito, H. Haba, and K. Tanaka, "A One-Pot Three-Component Double-Click Method for Synthesis of [^{67}Cu]-Labeled Biomolecular Radiotherapeutics," Sci. Rep. **7**, 1912 1–9 (2017).*

D. Kaji, K. Morimoto, H. Haba, Y. Wakabayashi, M. Takeyama, S. Yamaki, Y. Komori, S. Yanou, S. Goto, and K. Morita, "Decay measurement of ^{283}Cn produced in the ^{238}U(^{48}Ca,3n) reaction using GARIS-II," J. Phys. Soc. Jpn. **86**, 085001 1–2 (2017).*

G. L. Wilson, M. Takeyama, A. N. Andreyev, B. Andel, S. Antalic, W. N. Catford, L. Ghys, H. Haba, F. P. Heßberger, M. Huang, D. Kaji, Z. Kalaninova, K. Morimoto, K. Morita, M. Murakami, K. Nishio, R. Orlandi, A. G. Smith, K. Tanaka, Y. Wakabayashi, and S. Yamaki, "β-delayed fission of ^{230}Am," Phys. Rev. C **96**, 044315 1–7 (2017).*

F. Minato, K. Tsukada, N. Sato, S. Watanabe, H. Saeki, M. Kawabata, S. Hashimoto, and Y. Nagai, "Measurement and estimation of the ^{99}Mo production yield by ^{100}Mo(n,2n)^{99}Mo," J. Phys. Soc. Jpn. **86**, 114803 1–6 (2017).*

羽場宏光,「超重元素化学の新展開－GARIS ガスジェット法によるシーボーギウムのカルボニル錯体の合成－」, 化学と教育 **65**, No. 3,116–119 (2017).

羽場宏光,「GARIS が拓く超重元素の化学 」, 原子核研究 **62**, No. 1, 95–99 (2017).

T. Tanaka, Y. Narikiyo, K. Morita, K. Fujita, D. Kaji, K. Morimoto, S. Yamaki, Y. Wakabayashi, K. Tanaka, M. Takeyama, A. Yoneda, H. Haba, Y. Komori, S. Yanou, B. J.-P. Gall, Z. Asfari, H. Faure, H. Hasebe, M. Huang, J. Kanaya, M. Murakami, A. Yoshida, T. Yamaguchi, F. Tokanai, T. Yoshida, S. Yamamoto, Y. Yamano, K. Watanabe, S. Ishizawa, M. Asai, R. Aono, S. Goto, K. Katori, and K. Hagino, "Determination of fusion barrier distributions from quasielastic acattering cross sections towards superheavy nuclei synthesis," J. Phys. Soc. Jpn **87**, 014201 1–9 (2018).*

M. Mukai, Y. Hirayama, Y. X. Watanabe, P. Schury, H. S. Jung, M. Ahmed, H. Haba, H. Ishiyama, S. C. Jeong, Y. Kakiguchi, S. Kimura, J. Y. Moon, M. Oyaizu, A. Ozawa, J. H. Park, H. Ueno, M. Wada, H. Miyatake, "High-efficiency and low-background multi-segmented proportional gas counter for β-decay spectroscopy," Nucl. Instrum. Methods Phys. Res. A **884**, 1–10 (2018).*

E. Tsantini, T. Minami, K. Takahashi, M. Á. C. Ontiveros, "Analysis of sulphur isotopes to identify the origin of cinnabar in the Roman wall paintings from Badalona (Spain)," J. Archaeol. Sci. **18**, 300–307 (2018).*

[Proceeding]

(Original Paper) *Subject to Peer Review

M. U. Khandaker, H. Haba, N. Otuka, and H. A. Kassim, "Investigation of the ^{27}Al(d,x)^{24}Na nuclear reaction for deuteron beam monitoring purpose," EPJ Web Conf. **146**, 11029 1–4 (2017).*

N. Ukon, M. Aikawa, Y. Komori, and H. Haba, "Activation cross sections of deuteron-induced reactions on natural palladium for ^{103}Ag production," Proceedings of the Eighth AASPP Workshop on Asian Nuclear Reaction Database Development, National University of Mongolia, Ulaanbaatar, Mongolia, Oct. 11–13, 2017, M. Odsuren, G. Khuukhenkhuu, S. Davaa, and N. Otuka (Eds.), INDC(MGL)-0001, 15–18 (2018).

M. Aikawa, M. Saito, S. Ebata, Y. Komori, and H. Haba, "Activation cross sections of alpha-induced reactions on natural zinc for ^{68}Ge production," Proceedings of the 2016 Symposium on Nuclear Data, November 17-18, 2016, High Energy Accelerator Research Organization, Tsukuba, Ibaraki, Japan, JAEA-Conf 2017-001, INDC(JPN)-203, 153–156 (2018).

[Book]

(Original Paper)

桜井 弘,荒野泰,小谷明,高妻孝光,佐治英郎,鈴木晋一郎,寺嶋孝仁,中山祐正,根矢三郎,羽場宏光,廣田俊,藤井敏司,「ブルーバックス 元素 118 の新知識」, 546, 講談社, 2017 年 8 月 20 日.

Oral Presentations

[International Conference etc.]

T. Tanaka, Y. Narikiyo, K. Morita, K. Fujita, D. Kaji, K. Morimoto, S. Yamaki, Y. Wakabayashi, K. Tanaka, M. Takeyama, A. Yoneda, H. Haba, K. Komori, S. Yanou, B. JP. Gall, Z. Asfari, H. Faure, H. Hasebe, M. Huang, J. Kanaya, M. Murakami, A. Yoshida, T. Yamaguchi, F. Tokanai, T. Yoshida, S. Yamamoto, Y. Yamano, K. Watanabe, S. Ishizawa, M. Asai, R. Aono, S. Goto, and K. Katori, "Study of barrier distribution in heavy reaction system at the RIKEN-GARIS," FUSION-17 International Conference on Heavy-Ion Collisions at near-barrier energies, Tasmania, Australia, Feb. (2017).

N. Sato, "Measurement of the first ionization potential of lawrencium (Lr, Z = 103)," The 98th CSJ Annual Meeting, Asian International Symposium –Inorganic and Radiochemistry–, Yokohama, Japan, March (2017).

T. Minami, E. Tsantini, and K. Takahashi, "Effect of Gypsum on Sulfur Isotope Ratio of Vermilion Painted on Gypsum Wall," Colloquium Spectroscopicum Internationale XL, Pisa, Italy, June (2017).

N. Kondo, Y. Kasamatsu, H. Haba, K. Ouchi, M. Nagase, Y. Yasuda, Y. Shigekawa, A. Kanda,Y. Kuboki, Y. Komori, S. Yano, N. Sato, T. Yokokita, and A. Shinohara, "Liquid-liquid extraction of element 104, Rf, in Aliquat 336/HCl system," ACTINIDES2017, Sendai, Japan, July (2017).

K. Morita, K. Morimoto, D. Kaji, H. Haba, and H. Kudo, "Discovery of new element, nihonium, and perspectives," ACTINIDES2017, Sendai, Japan, July (2017).

Y. Oura, M. Ebihara, N. Shirai, H. Tsuruta, T. Nakajima, Y. Moriguchi, T. Ohara, Y. Nagakawa, N. Sakurai, H. Haba, and H. Matsuzaki, "^{129}I/^{137}Cs ratios for atmospheric particular matters collected just after TEPCO FDNPP accident," Goldschmidt 2017, Paris, France, Aug. (2017).

M. Ebihara, Y. Oura, N. Shirai, Y. Nagakawa, N. Sakurai, H. Haba, H. Matsuzaki, H. Tsuruta, and Y. Moriguchi, "A new approach for reconstructing the ^{131}I-spreading triggered by the FDNPS accident in 2011," Goldschmidt 2017, Paris, France, Aug. (2017).

H. Haba, "Present status and perspectives of SHE chemistry at RIKEN, 3rd International Symposium on Super-Heavy Elements "Challenges in the studies of super-heavy nuclei and atoms" (SHE 2017)," Kazimierz Dolny, Poland, Sept. (2017).

H. Haba, F. Fan, D. Kaji, Y. Kasamatsu, H. Kikunaga, Y. Komori, N. Kondo, H. Kudo, K. Morimoto, K. Morita, M. Murakami, K. Nishio, J. P. Omtvedt, K. Ooe, Z. Qin, D. Sato, N. Sato, T. K. Sato, Y. Shigekawa, A. Shinohara, M. Takeyama, T. Tanaka, A. Toyoshima, K. Tsukada, Y. Wakabayashi, Y. Wang, S. Wulff, S. Yamaki, S. Yano, Y. Yasuda, and T. Yokokita, "Production and decay studies of ^{261}Rf, ^{262}Db, ^{265}Sg, and ^{266}Bh for superheavy element chemistry at RIKEN GARIS," 6th Asia-Pacific Symposium on Radiochemistry (APSORC17), Jeju, Korea, Sept. (2017).

Y. Komori, H. Haba, K. Ooe, D. Kaji, Y. Kasamatsu, H. Kikunaga, A. Mitsukai, K. Morimoto, R. Motoyama, J. P. Omtvedt, Z. Qin, D. Sato, N. Sato, Y. Shigekawa, T. Tanaka, A. Toyoshima, K. Tsukada, Y. Wang, K. Watanabe, S. Wulff, S. Yamaki, S. Yano, and Y. Yasuda, "Development of a rapid solvent extraction apparatus coupled to the GARIS gas-jet transport system for aqueous chemistry of the heaviest elements," 6th Asia-Pacific Symposium on Radiochemistry (APSORC17), Jeju, Korea, Sept. (2017).

Z. Qin, Y. Wang, F. L. Fan, S. W. Cao, H. Haba, Y. Komori, S. Yano, D. Kaji, and K. Morimoto, "Gas-phase chemistry of technetium and rhenium carbonyl complexes with short-lived isotopes," 6th Asia-Pacific Symposium on Radiochemistry (APSORC17), Jeju, Korea, Sept. (2017).

H. Haba, F. Fan, D. Kaji, Y. Kasamatsu, H. Kikunaga, Y. Komori, N. Kondo, H. Kudo, K. Morimoto, K. Morita, M. Murakami, K. Nishio, J. P. Omtvedt, K. Ooe, Z. Qin, D. Sato, N. Sato, T. K. Sato, Y. Shigekawa, A. Shinohara, M. Takeyama, T. Tanaka, A. Toyoshima, K. Tsukada, Y. Wakabayashi, Y. Wang, S. Wulff, S. Yamaki, S. Yano, Y. Yasuda, and T. Yokokita, "Production and decay studies of ^{261}Rf, ^{262}Db, ^{265}Sg, and ^{266}Bh for superheavy element chemistry at GARIS," 9th Workshop on the Chemistry of the Heaviest Elements, Ascona, Switzerland, Oct. (2017).

M. Götz, Ch. E. Düllmann, A. Yakushev, M. Asai, J. Ballof, A. Di Nitto, K. Eberhardt, S. Götz, H. Haba, E. Jäger, Y. Kaneya, Y. Komori, J.-V. Kratz, J. Krier, B. Lommel, A. Mitsukai, Y. Nagame, T. Sato, A. Toyoshima, K. Tsukada, V. Wolter, and V. Yakusheva, "In-situ synthesis of volatile transition metal carbonyl complexes with short-lived radioisotopes," 9th Workshop on the Chemistry of the Heaviest Elements, Ascona, Switzerland, Oct. (2017).

Y. Komori, H. Haba, K. Ooe, D. Kaji, Y. Kasamatsu, H. Kikunaga, A. Mitsukai, K. Morimoto, J. P. Omtvedt, Z. Qin, D. Sato, N. Sato, Y. Shigekawa, T. Tanaka, A. Toyoshima, K. Tsukada, Y. Wang, S. Wulff, S. Yamaki, S. Yano, and Y. Yasuda, "Development of a rapid solvent extraction apparatus coupled to the garis gas-jet transport system for aqueous chemistry of Sg and Bh," 9th Workshop on the Chemistry of the Heaviest Elements, Ascona, Switzerland, Oct. (2017).

N. Kondo, Y. Kasamatsu, H. Haba, K. Ouchi, M. Nagase, Y. Yasuda, Y. Shigekawa, A. Kanda, Y. Kuboki, Y. Komori, S. Yano, N. Sato, T. Yokokita, and A. Shinohara, "Liquid-liquid extraction of Rf using flow-type extraction apparatus (ISE) in the aliquat 336/HCl system," 9th Workshop on the Chemistry of the Heaviest Elements, Ascona, Switzerland, Oct. (2017).

A. Yakushev, L. Lens, Ch. E. Düllmann, M. Asai, M. Block, H. David, J. Despotopulos, A. Di Nitto, K. Eberhardt, U. Forsberg, P. Golubev, M. Götz, S. Götz, H. Haba, L. Harkness-Brennan, F. P. Heßberger, R.-D. Herzberg, D. Hinde, J. Hoffmann, A. Hübner, E. Jäger, D. Judson, J. Khuyagbaata, B. Kindler, Y. Komori, J. Konki, J. V. Kratz, J. Krier, N. Kurz, M. Laatiaoui, S. Lahiri, B. Lommel, Ch. Lorentz, M. Maiti, A. K. Mistry, C. Mokry, K. Moody, Y. Nagame, J. P. Omtvedt, P. Papadakis, V. Pershina, D. Rudolph, J. Runke, M. Schädel, P. Scharrer, L. G. Sarmiento, T. Sato, D. Shaughnessy, B. Schausten, J. Steiner, P. Thörle-Pospiech, N. Trautmann, K. Tsukada, J. Uusitalo, A. Ward, M. Wegrzecki, E. Williams, N. Wiehl, and V. Yakusheva, "Recent gas phase chemistry experiments at TASCA," 9th Workshop on the Chemistry of the Heaviest Elements, Ascona, Switzerland, Oct. (2017).

Y. Wang, Z. Qin, J. Yang, J. C. Zhang, H. Haba, and Y. Komori, "Laser ablation mass spectrometry of rhenium carbonyls," 9th Workshop on the Chemistry of the Heaviest Elements, Ascona, Switzerland, Oct. (2017).

Z. Qin, Y. Wang, F. L. Fan, S. W. Cao, H. Haba, Y. Komori, S. Yano, D. Kaji, and K. Morimoto, "Gas-phase chemistry of technetium and rhenium carbonyl complexes with short-lived isotopes," 9th Workshop on the Chemistry of the Heaviest Elements, Ascona, Switzerland, Oct. (2017).

T. Yokokita, Y. Kasamatsu, A. Kino, H. Haba, Y. Shigekawa, Y. Yasuda, K. Nakamura, K. Toyomura, Y. Komori, M. Murakami, T. Yoshimura, N. Takahashi, K. Morita, and A. Shinohara, "Observation of the chemical reaction equilibria of rutherfordium," 9th Workshop on the Chemistry of the Heaviest Elements, Ascona, Switzerland, Oct. (2017).

T. Fukuchi, T. Okauchi, M. Shigeta, H. Haba, S. Yamamoto, Y. Watanabe, and S. Enomoto, "Image Reconstruction Method for Multiple Isotope PET," 2017 IEEE Nuclear Science Symposium and Medical Imaging Conference (NSS/MIC), Atlanta, USA, Oct. (2017).

N. Ukon, M. Aikawa, Y. Komori, and H. Haba, "Activation cross sections of deuteron-induced reactions on natural palladium for ^{103}Ag production," The

8th Workshop on Asian Nuclear Reaction Database Development, Ulaanbaatar, Mongolia, Oct. (2017).

H. Haba, "Production of radioisotopes for application studies at RIKEN RI Beam Factory," 9th International Conference on Isotopes (9 ICI), Doha, Qatar, Nov. (2017).

T. Murata, M. Aikawa, M. Saito, N. Ukon Y. Komori, H. Haba, and S. Takács, "Cross section measurement to produce ^{99}Mo by alpha-induced reactions on natural zirconium," 2017 Symposium on Nuclear Data, Tokai-mura, Japan, Nov. (2017).

H. Haba, "Superheavy Element Nuclear Chemistry at RIBF," International symposium on RI beam physics in the 21st century: 10th anniversary of RIBF, Wako, Japan, Dec. (2017).

H. Haba, "Production of radioisotopes for application studies at RIKEN RI Beam Factory," The 7th Yamada workshop on RI Science Evolution 2018 (RISE18), Suita, Japan, March (2018).

[Domestic Conference]

羽場宏光, "Present status and perspectives of medical radioisotope production at the RIKEN," 第 3 回核医学治療際シンポジウム 医産連携による核学治療の新たな躍進 －福島から世界へ－, 千代田区, 2 月 (2017).

小森有希子,「Fr の錯形成反応」,「第 9 回停止・低速 RI ビームを用いた核分光研究会」&「2017 超重元素の科学研究会」合同研究会, 東海村, 3 月 (2017).

羽場宏光,「GARIS が拓く超重元素化学」,「第 9 回停止・低速 RI ビームを用いた核分光研究会」&「2017 超重元素の科学研究会」合同研究会, 東海村, 3 月 (2017).

小森有希子,「GARIS を用いた Sg と Bh の溶液化学研究」,「第 9 回停止・低速 RI ビームを用いた核分光研究会」&「2017 超重元素の科学研究会」合同研究会, 東海村, 3 月 (2017).

羽場宏光,「超重元素化学の現状と展望」, 日本物理学会 第 72 回年次大会, 豊中市, 3 月 (2017).

伊藤由太, 和田道治, P. Schury, 加治大哉, 森本幸司, 羽場宏光, I. Murray, M. Rosenbusch, 木村創大, 高峰愛子, 宮武宇也, 山木さやか, 新井郁也, H. Wollnik,「MRTOF 質量分析器による八重極変形核 $^{223, 224}$Th の精密原子質量測定」, 日本物理学会 第 72 回年次大会, 豊中市, 3 月 (2017).

庭瀬暁隆, 森田浩介, 藤田訓裕, 山野裕貴, 渡辺健友, 光岡駿, 平野剛, 加治大哉, 森本幸司, 羽場宏光, B. J. P. Gall, Z. Asfari,「^{208}Pb(^{51}V,xn)$^{259-x}$Db 反応における融合障壁分布の測定」, 日本物理学会 第 72 回年次大会, 豊中市, 3 月 (2017).

山野裕貴, 森田浩介, 藤田訓裕, 渡辺健友, 庭瀬暁隆, 平野剛, 光岡駿, 加治大哉, 森本幸司, 羽場宏光,「^{50}Ti, ^{51}V + ^{248}Cm 反応における融合障壁分布の測定」, 日本物理学会 第 72 回年次大会, 豊中市, 3 月 (2017).

羽場宏光,「新元素 ニホニウムの発見 －理研・森田グループからの詳細報告－」, 日本化学会第 97 春季年会, 横浜市, 3 月 (2017).

右近直之, 合川正幸, 小森有希子, 羽場宏光,「重陽子入射によるパラジウム標的での ^{103}Ag 生成放射化断面積の測定」, 日本原子力学会 2017 年春の年会, 平塚市, 3 月 (2017).

高橋和也,「同位体分析法から見た墳墓出土朱の産地変遷－大和政権による朱の政治的利用－」, 日本分析化学会第 77 回分析化学討論会, 京都市, 5 月 (2017).

羽場宏光,「ニホニウム誕生」, 理研和光事業所一般公開 特別講演会, 和光市, 4 月 (2017).

羽場宏光,「ニホニウム誕生」, ニホニウム通り記念イベント（市民講演会）, 和光市, 6 月 (2017).

羽場宏光,「理研 AVF サイクロトロンを利用した応用研究用 RI の製造」, ＡＶＦ合同打ち合わせ, 福島市, 6 月 (2017).

羽場宏光,「新元素ニホニウム発見への道のり」, 日比谷高校 SSH 特別講演会, 千代田区, 7 月 (2017).

海老原充, 大浦泰嗣, 白井直樹, 鶴田治雄, 森口祐一, 永川栄泰, 櫻井昇, 羽場宏光, 松崎浩之,「福島第一原発事故直後に採取された大気浮遊粒子中の放射性核種の測定方法の開発と総合解析：(その 2) 放射性ヨウ素 (I-129) の定量」, 第 54 回アイソトープ・放射線研究発表会, 文京区, 7 月 (2017).

宗兼将之, 上田真史, 本村信治, 神野伸一郎, 羽場宏光, 吉川豊, 安井裕之, 榎本秀一,「二重標識クリオキノール-亜鉛錯体の生体内挙動と生体内化学形態変化の解析」, 第 15 回次世代を担う若手のためのフィジカル・ファーマフォーラム（PPF2017）, 金沢市, 9 月 (2017).

稲垣純平, 坂口綾, 井上美南, 羽場宏光, 柏原輝彦, 山﨑信哉, 菊池早希子, 金子政志, 小谷弘明, 高橋嘉夫, 臼井朗, 末木啓介,「深海底化学堆積物・鉄マンガンクラストにおける Zr, Hf の分別挙動に関する考察」, 日本地球化学会第 64 回年会, 目黒区, 9 月 (2017).

高橋和也,「遺跡から出土する水銀朱の産地同定のための硫黄, 鉛の同位体分析の試み」, 日本分析化学会第 66 年会, 葛飾区, 9 月 (2017).

後藤真一, 加治大哉, 土谷翔太, 青野竜士, 森本幸司, 羽場宏光, 大江一弘, 工藤久昭,「^{254}Rf の自発核分裂における核分裂片の全運動エネルギー測定」, 2017 日本放射化学会年会・第 61 回放射化学討論会, つくば市, 9 月 (2017).

小森有希子, 羽場宏光, F. Fan, 加治大哉, 笠松良崇, 菊永英寿, 近藤成美, 工藤久昭, 森本幸司, 森田浩介, 村上昌史, 西尾勝久, J. P. Omtvedt, 大江一弘, Z. Qin, 佐藤大輔, 佐藤望, 佐藤哲也, 重河優大, 篠原厚, 武山美麗, 田中泰貴, 豊嶋厚史, 塚田和明, 若林泰生, Y. Wang, S. Wulff, 山木さやか, 矢納慎也, 安田勇輝, 横北卓也,「107 番元素 Bh の化学研究に向けた ^{248}Cm + ^{23}Na 反応による Bh 同位体の合成とその壊変特性」, 2017 日本放射化学会年会・第 61 回放射化学討論会, つくば市, 9 月 (2017).

庭瀬暁隆, 和田道治, P. Schury, 伊藤由太, 木村創大, M. Rosenbusch, 加治大哉, 森本幸司, 羽場宏光, 山木さやか, 田中泰貴, 森田浩介, 高峰愛子, 宮武宇也, 平山賀一, 渡邉 裕, J. Y. Moon, 向井もも, H. Wollnik,「GARIS-II+MRTOF を用いた短寿命核精密質量分析」, 2017 日本放射化学会年会・第 61 回放射化学討論会, つくば市, 9 月 (2017).

矢納慎也, 羽場宏光, 小森有希子, 横北卓也, 高橋和也, 佐藤望, 小山内美奈子,「^{133}Cs(α,pn)^{135m}Ba 反応による精製 ^{135m}Ba の製造」, 2017 日本放射化学会年会・第 61 回放射化学討論会, つくば市, 9 月 (2017).

秋山和彦, 宮内翔哉, 雨倉 啓, 伊藤健太, 菊永英寿, 羽場宏光, 久冨木志郎,「光核反応を用いた ^{143}Pm 製造と ^{143}Pm 内包フラーレンの合成及びその性質」, 2017 日本放射化学会年会・第 61 回放射化学討論会, つくば市, 9 月 (2017).

稲垣純平, 坂口綾, 井上美南, 羽場宏光, 柏原輝彦, 山﨑信哉, 菊池早希子, 金子政志, 小谷弘明, 高橋嘉夫, 臼井朗, 末木啓介,「鉄マンガンクラストにおける Zr, Hf の分別挙動に関する考察」, 2017 日本放射化学会年会・第 61 回放射化学討論会, つくば市, 9 月 (2017).

近藤成美, 笠松良崇, 永瀬将浩, 安田勇輝, 重河優大, 大内昴輝, 神田晃充, 二宮秀美, 渡邉瑛介, 羽場宏光, 久保木祐生, 小森有希子, 横北卓也, 矢納慎也, 佐藤望, 篠原厚,「Aliquat 336/HCl 系における Rf の溶媒抽出実験」, 2017 日本放射化学会年会・第 61 回放射化学討論会, つくば市, 9 月 (2017).

佐藤大輔, 村上昌史, 後藤真一, 大江一弘, 本山李沙, 白井香里, 山田亮平, 土屋翔太, 守山卓也, 羽場宏光, 小森有希子, 矢納慎也, 豊嶋厚史, 水飼秋菜, 菊永英寿, 工藤久昭, 「105 番元素 Db に対する Aliquat 336 樹脂を用いたフッ化水素酸系逆相クロマトグラフィー」, 2017 日本放射化学会年会・第 61 回放射化学討論会, つくば市, 9 月 (2017).

羽場宏光, 「RI 製造の最前線～新元素の化学から核医学の診断・治療まで～」, 研究成果展開事業産学共創プラットフォーム共同研究推進プログラム 安心・安全・スマートな長寿社会実現のための高度な量子アプリケーション技術の創出 キックオフシンポジウム, 豊中市, 3 月 (2018).

Poster Presentations

[International Conference etc.]

K. Tanaka, K. Chiba, K. Akiyama, H. Haba, and S. Kubuki, "Development of metallofullerene separation by chemical reduction," 6th Asia-Pacific Symposium on Radiochemistry (APSORC17), Jeju, Korea, Sept. (2017).

K. Takahashi, "New method for comprehensive detection of trace elements in environmental or biochemical materials using an electron-cyclotron-resonance ion-source mass spectrometer," 4th World Congress on Mass Spectrometry, London, UK, June (2017).

M. Okamura, T. Karino, T. Kanesue, S. Ikeda, Y. Saito, and H. Haba, "Investigate the characteristics of oxide of ^{96}Zr," 17th International Conference on Ion Sources, Geneva, Switzerland, Oct. (2017).

[Domestic Conference]

中野貴志, 福田光宏, 青井考, 鈴木智和, 高橋成人, 酒見泰寛, 羽場宏光, 上垣外修一, 渡部浩司, 伊藤正俊, 菊永英寿, 「短寿命 RI プラットフォームの紹介」, 第 54 回アイソトープ・放射線研究発表会, 文京区, 7 月 (2017).

神原正, 吉田敦, 羽場宏光, 「回転体上のガンマ線源分布の検査法」, 第 54 回アイソトープ・放射線研究発表会, 文京区, 7 月 (2017).

田中康介, 秋山和彦, 羽場宏光, 久冨木志郎, 「化学的還元反応を用いた金属内包フラーレン分離の条件検討-2」, 2017 日本放射化学会年会・第 61 回放射化学討論会, つくば市, 9 月 (2017).

加治大哉, 森本幸司, 羽場宏光, 「スパッタ法による厚い金属ウラン標的の調整と照射試験」, 2017 日本放射化学会年会・第 61 回放射化学討論会, つくば市, 9 月 (2017).

大江一弘, 草刈駿, 後藤真一, 工藤久昭, 羽場宏光, 小森有希子, 「Rf の同族元素 Zr, Hf の 2-フロイルトリフルオロアセトンを用いた溶媒抽出」, 2017 日本放射化学会年会・第 61 回放射化学討論会, つくば市, 9 月 (2017).

菊永英寿, 小森有希子, 羽場宏光, 柴田誠一, 矢納慎也, 「^{27}Al(α,3p)反応で製造した ^{28}Mg の担体無添加化学分離法の再検討」, 2017 日本放射化学会年会・第 61 回放射化学討論会, つくば市, 9 月 (2017).

横北卓也, 矢納慎也, 小森有希子, 羽場宏光, 「イオン交換繊維による Zr、Hf 及び Th のイオン交換挙動 –イオン交換繊維を用いた Rf のイオン交換実験の検討–」, 2017 日本放射化学会年会・第 61 回放射化学討論会, つくば市, 9 月 (2017).

RIBF Research Division
User Liaison and Industrial Cooperation Group

1. Abstract

The essential mission of the "User Liaison and Industrial Cooperation (ULIC) Group" is to maximize the research activities of RIBF by attracting users in various fields with a wide scope.

The ULIC Group consists of two teams.

The RIBF User Liaison Team provides various supports to visiting RIBF users through the User's Office. The Industrial Cooperation Team supports potential users in industries who use the beams for application purposes or for accelerator related technologies other than basic research. Production of various radioisotopes by the AVF cyclotron is also one of the important mission. The produced radioisotopes are distributed to researchers in Japan for a charge through the Japan Radioisotope Association.

In addition the ULIC Group takes care of laboratory tours for RIBF visitors from public. The numbers of visitors amounts to 2,300 per year.

Members

Group Director
Hideyuki SAKAI

Special Temporary Employee
Tadashi KAMBARA

Senior Visiting Scientists
Ikuko HAMAMOTO (Lund Univ.)   Munetake ICHIMURA (Univ. of Tokyo)

Assistants
Tomomi OKAYASU   Yu NAYA
Yoko FUJITA   Midori YAMAMOTO

RIBF Research Division
User Liaison and Industrial Cooperation Group
RIBF User Liaison Team (User Support Office)

1. Abstract

To enhance synergetic common use of the world-class accelerator facility, the Radioisotope Beam Factory (RIBF), it is necessary to promote a broad range of applications and to maximize the facility's importance. The facilitation and promotion of the RIBF are important missions charged to the team. Important operational activities of the team include: i) the organization of international Program Advisory Committee (PAC) meetings to review experimental proposals submitted by RIBF users, ii) RIBF beam-time operation management, and iii) promotion of facility use by hosting outside users through the RIBF Independent Users program, which is a new-user registration program begun in FY2010 at the RIKEN Nishina Center (RNC) to enhance the synergetic common use of the RIBF. The team opened the RIBF Users Office in the RIBF building in 2010, which is the main point of contact for Independent Users and provides a wide range of services and information.

2. Major Research Subjects

(1) Facilitation of the use of the RIBF
(2) Promotion of the RIBF to interested researchers

3. Summary of Research Activity

(1) Facilitation of the use of the RIBF

The RIBF Users Office, formed by the team in 2010, is a point of contact for user registration through the RIBF Independent User program. This activity includes:

- registration of users as RIBF Independent Users,
- registration of radiation workers at the RIKEN Wako Institute,
- provision of an RIBF User Card (a regular entry permit) and an optically stimulated luminescence dosimeter for each RIBF Independent User, and
- provision of safety training for new registrants regarding working around radiation, accelerator use at the RIBF facility, and information security, which must be completed before they begin RIBF research.

The RIBF Users Office is also a point of contact for users regarding RIBF beam-time-related paperwork, which includes:

- contact for beam-time scheduling and safety review of experiments by the In-House Safety Committee,
- preparation of annual Accelerator Progress Reports, and
- maintaining the above information in a beam-time record database.

In addition, the RIBF Users Office assists RIBF Independent Users with matters related to their visit, such as invitation procedures, visa applications, and the reservation of on-campus accommodation.

(2) Promotion of the RIBF to interested researchers

- The team has organized an international PAC for RIBF experiments; it consists of leading scientists worldwide and reviews proposals in the field of nuclear physics (NP) purely on the basis of their scientific merit and feasibility. The team also assists another PAC meeting for material and life sciences (ML) organized by the RNC Advanced Meson Laboratory. The NP and ML PAC meetings are organized twice a year.
- The team coordinates beam times for PAC-approved experiments and other development activities. It manages the operating schedule of the RIBF accelerator complex according to the decisions arrived at by the RIBF Machine Time Committee.
- To promote research activities at RIBF, proposals for User Liaison and Industrial Cooperation Group symposia/mini-workshops are solicited broadly both inside and outside of the RNC. The RIBF Users Office assists in the related paperwork.
- The team is the point of contact for the RIBF users' association. It arranges meetings at RNC headquarters for the RIBF User Executive Committee of the users' association.
- The Team conducts publicity activities, such as arranging for RIBF tours, development and improvement of the RNC official web site, and delivery of RNC news via email and the web.

Members

Team Leader
Ken-ichiro YONEDA

Deputy Team Leader
Yasushi WATANABE (concurrent: Senior Research Scientist, Radiation Lab.)

Technical Staff I
Narumasa MIYAUCHI

RIBF Research Division
User Liaison and Industrial Cooperation Group
Industrial Cooperation Team

1. Abstract

Industrial cooperation team handles non-academic activities at RIBF corresponding to industries and to general public.

2. Major Research Subjects

(1) Fee-based distribution of radioisotopes produced at RIKEN AVF Cyclotron
(2) Support of industrial application using the RIBF accelerator beam and its related technologies including novel industrial applications.
(3) Development of real-time wear diagnostics of industrial material using RI beams

3. Summary of Research Activity

(1) Fee-based distribution of radioisotopes

This team has been handling fee-based distribution of radioisotopes since 2007. Radionuclides of Zn-65, Sr-85, Y-88 and Cd-109, which are produced by the RI application team at the AVF cyclotron, are distributed to nonaffiliated users under a Material Transfer Agreement (MTA) between Japan Radioisotope Association and RIKEN. In FY 2017, we delivered 2 shipments of Zn-65 with a total activity of 4.2 MBq, one shipment of Y-88 with an activity of 1 MBq and one shipment of Sr-85 with an activity of 3.7 MBq. The final recipients of the RIs were two universities and two research institutes.

(2) Support of Industrial application using RIBF

RNC promote facility-sharing program "Promotion of applications of high-energy heavy ions and RI beams." In this program, RNC opens the old part of the RIBF facility, which includes the AVF cyclotron, RILAC, RIKEN Ring Cyclotron and experimental instruments, to non-academic proposals from users including private companies. The proposals are reviewed by a program advisory committee, industrial PAC (InPAC). The proposals which have been approved by the InPAC are allocated with beam times and the users pay RIKEN the beam time fee. The intellectual properties obtained by the use of RIBF belong to the users. In order to encourage the use of RIBF by those who are not familiar with utilization of ion beams, the first two beam times of each proposal can be assigned to trial uses which are free of beam time fee.

In January 2018, the seventh InPAC met and reviewed one fee-based proposal from a private company. In February 2018, a fee-based beamtime was performed with a Kr-84 (70 MeV/A) beam at the E5A beamline for 4 days. The client used the beam to simulate single-event effects of space-use semi-conductors by heavy-ion components of cosmic rays. In the same month, we performed a test beamtime at the same beamline to study the characteristics of a higher LET Xe-136 (10.75 MeV/A) beam.

(3) Development of real-time wear diagnostics using RI beams

We are developing a method to determine the spatial distribution of gamma-ray emitting RIs on periodically-moving objects, named "GIRO" (Gamma-ray Inspection of Rotating Object), that is based on the same principle as the medical PET imaging but is simpler and less expensive. This method can be used for real-time inspection of a closed system in a running machine. In 2017, we performed single-photon emission computer tomography (SPECT) mode measurement with sources of Cs-137, Eu-152 and Na-22.

Members

Team Leader
Atsushi YOSHIDA

Contract Researcher
Tadashi KAMBARA

Technical Staff I
Shinya YANOU (concurrent: RI Application Team)

List of Publications & Presentations

Publications
[Journal]
(Original Papers) *Subject to Peer Review
T. Kambara, "Gamma-Ray Inspection of Rotating Object (GIRO)," Nucl. Phys. News **26**, No.4, 26−29 (2016).

Oral Presentations
[Domestic Conference]
T. Kambara,「イオン照射による材料改質と摩耗試験」, 日本物理学会 年次大会, 東北学院大学 仙台, 03/19−22 (2016).
A.Yoshida,「重イオン加速器の産業利用」, 理研と未来を創る会 第 25 回 講演会・見学会, 和光, 07/26, (2017).

Poster Presentations

[Domestic Conference]

A. Yoshida, T. Kambara,「ＲＩビームでオンライン精密摩耗量測定〜摩耗のイメージング〜」, nano tech 2016 第 15 回国際ナノテクノロジー総合展・技術会議, 01/27−29, 東京, 2016 年 1 月 27−29 日.

T. Kambara, A. Yoshida, H. Haba,「陽電子放出核種による回転体検査法の開発」, 2016 日本放射化学会年会・第 60 回放射化学討論会, 新潟, 2016 年 9 月 10−12 日.

T. Kambara, A. Yoshida, H. Haba,「回転体上のガンマ線源分布の検査法」, 第 54 回　アイソトープ・放射線研究発表会, 東京, 2017 年 7 月 5−7 日.

List of Intellectual Properties

Patents

A. Yoshida, T. Kambara, R. Uemoto, A. Nagano, H. Uno, N. Takahashi, "Wear diagnostics method and instrument, " 2015-1490 patent applied.

T. Kambara, A. Yoshida, H. Takeichi, "Gamma-ray measurement method and instrument, " 2014-034417, patent registered.

RIBF Research Division
Safety Management Group

1. Abstract

The RIKEN Nishina Center for Accelerator-Based Science possesses one of the largest accelerator facilities in the world, which consists of two heavy-ion linear accelerators and five cyclotrons. This is the only site in Japan where uranium ions are accelerated. The center also has electron accelerators of microtron and synchrotron storage ring. Our function is to keep the radiation level in and around the facility below the allowable limit and to keep the exposure of workers as low as reasonably achievable. We are also involved in the safety management of the Radioisotope Center, where many types of experiments are performed with sealed and unsealed radioisotopes.

2. Major Research Subjects

(1)   Safety management at radiation facilities of Nishina Center for Accelerator-Based Science
(2)   Safety management at Radioisotope Center
(3)   Radiation shielding design and development of accelerator safety systems

3. Summary of Research Activity

Our most important task is to keep the personnel exposure as low as reasonably achievable, and to prevent an accident. Therefore, we daily patrol the facility, measure the ambient dose rates, maintain the survey meters, shield doors and facilities of exhaust air and wastewater, replenish the protective supplies, and manage the radioactive waste. Advice, supervision and assistance at major accelerator maintenance works are also our task.

The radiation shield on the beam line between SRC and BigRIPS was installed. Though there was future risk of radiation dose level higher than legal limit, it was reduced to about 1/10.

The radiation control system for RILAC accelerator were newly developed. The RILAC accelerator will be upgraded and new radiation control system is required. The software development was completed. It will set in the next year.

Minor improvements of the radiation safety systems were also done. The radiation monitors at the Nishina building has been replaced annually from 2015 because they get older, which were installed in 1986.

Members

Group Director
Yoshitomo UWAMINO

Deputy Group Director
Kanenobu TANAKA

Nishina Center Technical Scientists
Rieko HIGURASHI   Hisao SAKAMOTO

Technical Staff I
Atsuko AKASHIO   Tomoyuki DANTSUKA (concurrent; Cryogenic Technology Team)

Research Consultant
Masaharu OKANO (Japan Radiation Res. Soc.)

Visiting Scientists
Noriaki NAKAO (Shimizu Corp.)   Nobuhiro SHIGYO (Kyushu Univ.)
Koji OHISHI (Shimizu Corp.)   Hee Seock LEE (POSTECH)
Arim LEE (Pohang Accelerator Laboratory POSTECH)   Joo-Hee OH (POSTECH)
Nam-Suk JUNG (POSTECH)

Student Trainees
Kenta SUGIHARA   Shougo IZUMITANI
Eunji LEE

Assigned Employee
Hiroki MUKAI

Temporary Staffing
Ryuji SUZUKI

Part-time Workers
Hiroshi KATO   Naoko USUDATE
Satomi IIZUKA   Shin FUJITA
Kimie IGARASHI   Yukiko SHIODA
Hiroko AISO

Assistant
Tomomi OKAYASU

List of Publications & Presentations

Oral Presentations
[International Conference etc.]
K. Tanaka, "Improvement of emergency evacuation from underground at RIBF accelerator facility", International Technical Safety Forum 2017 (ITSF2017), Vancouver, Canada, September (2017).

[Domestic Conference]
上蓑義朋,「RIBF における放射線安全教育とクレーン利用に関する報告」, 第 5 回加速器施設安全シンポジウム, 東海村, 1 月,(2018).
赤塩敦子, 杉原健太, 執行信寛, 田中鐘信,「345MeV/u ウランビームを用いた放射線評価」, 日本原子力学会 2018 年春の年会, 吹田市, 3 月 (2018).

Partner Institutions

The Nishina Center established the "Research Partnership System" in 2008. This system permits an external institute to develop its own projects at the RIKEN Wako campus in equal partnership with the Nishina Center. At present, three institutes, Center for Nuclear Study, the University of Tokyo (CNS); Institute of Particle and Nuclear Studies, KEK (KEK); and the Institute of Science and Technology, Niigata University (Niigata) are conducting research activities under the Research Partnership System.

CNS and the Nishina Center signed the partnership agreement in 2008. Until then, CNS had collaborated in joint programs with RIKEN under the "Research Collaboration Agreement on Heavy Ion Physics" (collaboration agreement) signed in 1998. The partnership agreement redefines procedures related to the joint programs while keeping the spirit of the collaboration agreement. The joint programs include experimental nuclear physics activities using CRIB, SHARAQ, and GRAPE at RIBF, theoretical nuclear physics activities with ALPHLEET, accelerator development, and activities at RHIC PHENIX.

The partnership agreement with the Niigata University was signed in 2010. The activity includes theoretical and experimental nuclear physics, and nuclear chemistry.

KEK started low-energy nuclear physics activity at RIBF in 2011 under the Research Partnership System. The joint experimental programs are based on KISS (KEK Isotope Separator). After the R&D studies on KISS, it became available for users from 2015. In this year, a new KEK branch, Wako Nuclear Science Center (WNSC) has been launched at the Wako campus to enhance the scientific activities of KISS.

The experimental proposals that request the use of the above-noted devices of CNS and KEK together with the other RIBF key devices are screened by the Program Advisory Committee (PAC). The PAC meetings are co-hosted by CNS and KEK.

The activities of CNS, Niigata, and KEK are reported in the following pages.

Partner Institution
Center for Nuclear Study, Graduate School of Science
The University of Tokyo

1. Abstract

The Center for Nuclear Study (CNS) aims to elucidate the nature of nuclear system by producing the characteristic states where the Isospin, Spin and Quark degrees of freedom play central roles. These researches in CNS lead to the understanding of the matter based on common natures of many-body systems in various phases. We also aim at elucidating the explosion phenomena and the evolution of the universe by the direct measurements simulating nuclear reactions in the universe. In order to advance the nuclear science with heavy-ion reactions, we develop AVF upgrade, CRIB and SHARAQ facilities in the large-scale accelerators laboratories RIBF. The OEDO facility has been developed as an upgrade of the SHARAQ, where a RF deflector system has been introduced to obtain a good quality of low-energy beam. We added a new group for fundamental symmetry by using heavy RIs. We promote collaboration programs at RIBF as well as RHIC-PHENIX and ALICE-LHC with scientists in the world, and host international meetings and conferences. We also provide educational opportunities to young scientists in the heavy-ion science through the graduate course as a member of the department of physics in the University of Tokyo and through hosting the international summer school.

2. Major Research Subjects

(1) Accelerator Physics
(2) Nuclear Astrophysics
(3) Nuclear spectroscopy of exotic nuclei
(4) Quark physics
(5) Nuclear Theory
(6) OEDO/SHARAQ project
(7) Exotic Nuclear Reaction
(8) Low Energy Nuclear Reaction Group
(9) Active Target Development
(10) Fundamental Physics

3. Summary of Research Activity

(1) Accelerator Physics

One of the major tasks of the accelerator group is the AVF upgrade project that includes development of ion sources, upgrading the AVF cyclotron of RIKEN and the beam line to CRIB. In 2017, the operating time of the HyperECR was 2414 hours, which is 61 % of the total operating time of the AVF cyclotron. The beam extraction system of the HyperECR is under development to realize a high intensity and low emittance beam. We have succeeded to suppress $^{12}C^{4+}$ beam which contaminated $^{18}O^{6+}$ beam by measuring the light intensity of the C_{IV} line spectrum. The calculation model of injection beam orbit of the AVF cyclotron was completed and the adjustment of the positon and angle deviation between the measured beam orbit and the calculated beam orbit is carried on. The detailed studies on ion optics of the beamline to CRIB from AVF cyclotron were performed with beam diagnosis system and simulation code, and it turned out the loss of the beam intensity is occurred at the entrance of the vertical deflection bending magnet.

(2) Nuclear Astrophysics

The main activity of the nuclear astrophysics group in CNS is experimental studies on astrophysical reactions and special nuclear clustering using the low-energy RI beam separator CRIB. In 2017, a strong indication of an exotic linear-chain cluster structure in ^{14}C nucleus was presented based on the $^{10}Be + \alpha$ resonant scattering measurement at CRIB. To give a solution to the cosmological ^{7}Li abundance problem, two experimental projects are in progress. One is to determine the $^{7}Be(n, \alpha)/(n, p)$ astrophysical reaction rates with the Trojan Horse method, and another is the measurement of $^{7}Be(d, p)$ with a ^{7}Be-implanted target. The latter project is in collaboration with RCNP, Osaka Univ. and JAEA, and CRIB was used for the ^{7}Be target production. Based on the interest of the galactic γ-ray production, a proton resonant scattering experiment with ^{26}Al isomeric beam was performed at CRIB in Mar. 2017. With the analysis followed that, the isomeric purity was found to be about 50%. Resonances in ^{27}Si are observed in the relevant energy range of supernovae, and we may be able to discuss possible destruction of ^{26}Al in supernovae.

(3) Nuclear structure of exotic nuclei

The NUSPEQ (NUclear SPectroscopy for Extreme Quantum system) group studies exotic structures in high-isospin and/or high-spin states in nuclei. The CNS GRAPE (Gamma-Ray detector Array with Position and Energy sensitivity) is a major apparatus for high-resolution in-beam gamma-ray spectroscopy. Missing mass spectroscopy using the SHARAQ is used for another approach on exotic nuclei. In 2017, the following progress has been made. Experimental data taken under the EURICA collaboration has been analyzed for studying octupole deformation in neutron-rich Ba isotopes and preparing publication. A new experiment measuring the $^{4}He(^{8}He, ^{8}Be)4n$ reaction was performed for better statistics and better accuracy in order to verify a candidate of the ground state of the tetra neutrons just above the 4n threshold, which is under analysis.

(4) Quark Physics

Main goal of the quark physics group is to understand the properties of hot and dense nuclear matter created by colliding heavy nuclei at relativistic energies. The group has been involved in the PHENIX experiment at Relativistic Heavy Ion Collider (RHIC) at Brookhaven National Laboratory, and the ALICE experiment at Large Hadron Collider (LHC) at CERN. As for ALICE, the group has involved in the data analyses, which include the measurement of low-mass lepton pairs in Pb-Pb and p-Pb collisions, J/ψ measurements in p-Pb collisions, long range two particle correlations in p-Pb collisions, and searches for thermal photons in p-Pb collisions. The group has involved in the ALICE-TPC upgrade using a Gas Electron Multiplier (GEM). Development of the new data readout system for the upgrade, which aims online data processing by utilizing FPGA and GPU, has been ongoing in 2017.

(5) Nuclear Theory

The nuclear theory group participates a project, "Priority Issue 9 to be tackled by using the Post-K Computer" and promotes computational nuclear physics utilizing supercomputers. In FY2017, we performed the Monte Carlo shell model calculations of the Sn isotopes and revealed that the anomalous enhancement of the B(E2) transition probabilities in the neutron-deficient region is caused by the proton excitation from the $1g_{9/2}$ orbit, and found that the second-order quantum phase transition occurs around $N = 66$. We also investigated the double Gamow-Teller strength distribution of double-beta decay emitters, such as ^{48}Ca. We theoretically predict a linear relation between the nuclear matrix elements of the double Gamow-Teller transition and the neutrinoless double beta decay. In parallel, we have been promoting the CNS-RIKEN collaboration project on large-scale nuclear structure calculations and performed shell-model calculations under various collaborations with many experimentalists for investing the exotic structure of neutron-rich nuclei, such as ^{35}Mg, ^{136}Ba, ^{138}Ce, and ^{135}La.

(6) OEDO/SHARAQ project

The OEDO/SHARAQ group pursues experimental studies of RI beams by using the high-resolution beamline and the SHARAQ spectrometer. A mass measurement by TOF-$B\rho$ technique for very neutron-rich successfully reaches calcium isotopes beyond $N = 34$, $^{55-57}$Ca, and the preparation of publication is ongoing. The experimental study of 0^- strength in nuclei using the parity-tansfer charge exchange (^{16}O, ^{16}F) is on progress and the data analysis is on the final stage. The OEDO beamline, which was an upgrade of the high-resolution beamline to produce low-energy RI beams, has started the operation in June and has successfully achieved the designed ion-optical performance. The first and second experiments were performed in October and November, and new data for nuclear transmutation of long lived fission products (LLFPs) were successfully obtained.

(7) Exotic Nuclear Reaction

The Exotic Nuclear Reaction group studies various exotic reactions induced by beams of unstable nuclei. One subject is inverse-kinematics (p, n) reaction. In 2017 a set of neutron counters PANDORA was used for the first time at HIMAC facility for the study of the ^{6}He(p, n) reaction. Candidate nuclei to study are high spin isomers such as ^{52}Fe(12$^+$). Development of isomer beam was carried out.

(8) Low Energy Nuclear Reaction Group

A recoil particle detector for missing mass spectroscopy, named TiNA, had been developed under the collaboration with RIKEN and RCNP. TiNA consists of 6 sector telescopes. Each of which as a stripped-type SSD and 2 CsI(Tl) crystals. After the test experiment at the tandem facility of Kyushu Univ., TiNA was employed at the physics experiment with OEDO. Development of the tritium target is still on-going. Several deuterium doped Ti targets were fabricated at the Toyama Univ. They were tested by using $d(^{12}$C, $d)$ reaction at the tandem facility at Kyushu. The amount of deuterium was found to be scattered. The optimum condition to make the target will be sought for. The production cross section ^{178m2}Hf was evaluated for the mass production in the future. The digital signal processing devices for the GRAPE have been developed to measure the cascade transitions from the isomeric state. After chemical separation of Hf at the hot laboratory at RIBF. The week cascade decay was successfully measured.

(9) Active Target Development

Two types of gaseous active target TPCs called CAT's and GEM-MSTPC are developed and used for the missing mass spectroscopy. The CAT's are employed for the study of equation of state of nuclear matter. The measurement of giant monopole resonance in ^{132}Sn at RIBF with CAT-S and the data analysis is ongoing. In 2017, we developed a larger active target called CAT-M, which has 10-times larger active volume than that of CAT-S. The CAT-M was commissioned at HIMAC and the excitation energy spectrum of ^{136}Xe for proton scattering was measured. The GEM-MSTPC is employed for the nuclear astrophysics study. The data analysis of (α, p) reaction on ^{18}Ne and ^{22}Mg and the β-decay of ^{16}Ne followed by α emission are ongoing.

(10) Fundamental Physics

Although the Standard Model of particle physics is being steadily and successfully verified, the disappearance of the antimatter in the universe could not be sufficiently explained; a more fundamental framework is required and has to be studied. In order to understand the mechanism of matter-antimatter symmetry violation, we are developing the next generation experiments employing ultracold atoms to search for the electron electric dipole moment (EDM) using heavy element francium (Fr) in an optical lattice at RIBF. The developments of a high intensity surface ionizer to produce Fr and a magneto-optical trap (MOT) are in progress, and Fr-MOT experiments are going on at present at CYRIC.

Members

Director
Susumu SHIMOURA

Scientific Staff
Susumu SHIMOURA (Professor)
Yasuhiro SAKEMI (Professor)
Kentaro YAKO (Associate Professor)
Nobuaki IMAI (Associate Professor)
Noritaka SHIMIZU (Project Associate Professor)

Hidetoshi YAMAGUCHI (Lecturer)
Shin'ichiro MICHIMASA (Assistant Professor)
Taku GUNJI (Associate Professor)
Shinsuke OTA (Assistant Professor)
Hiroki NAGAHAMA (Assistant Professor)

Guest Scientists
Yutaka UTSUNO (Guest Professor)

Yutaka MIZOI (Guest Associate Professor)

Technical Staff
Yasuteru KOTAKA

Techinical Assistants
Yukimitsu OHSHIRO
Mamoru KATAYANAGI

Reiko KOJIMA
Hiroshi KUREI

Project Research Associates
Togashi TOMOAKI
Ichikawa TAKATOSHI

Olga BELIUSKINA

Post Doctoral Associates
ShinIchi HAYASHI
Philipp SCHROCK
Laszlo STUHL
Masanori DOZONO
Javier MENENDEZ SANCHEZ
Zhang NINGTAO

Seiya HAYAKAWA
Chihiro IWAMOTO
Lei YANG
Tsunoda YUSUKE
Jongwon HWANG
Takayuki MIYAGI

Graduate Students
Hiroshi TOKIEDA
Yuko SEKIGUCHI
Ryo NAKAJIMA
Noritaka KITAMURA
Hideki SHIMIZU

Motonobu TAKAKI
Soichiro MASUOKA
Keita KAWATA
Rieko TSUNODA

Administration Staff
Mikio OKI
Takako ENDO

Ikuko YAMAMOTO
Yukino KISHI

List of Publications & Presentations

Publications

[Journal]

(Original Papers) *Subject to Peer Review

A.I. Morales, G. Benzoni, H. Watanabe, Y. Tsunoda, T. Otsuka, S. Nishimura, F. Browne, R. Daido, P. Doornenbal, Y. Fang, G. Lorusso, Z. Patel, S. Rice, L. Sinclair, P. A. Soderstrom, T. Sumikama, J. Wu, Z. Y. Xu, A. Yagi, R. Yokoyama, H. Baba, R. Avigo, F. L. Bello Garrote, N. Blasi, A. Bracco, F. Camera, S. Ceruti, F.C.L. Crespi, G. De Angelis, M. -C. Delattre, Zs. Dombradi, A. Gottardo, T. Isobe, I. Kojouharov, N. Kurz, I. Kuti, K. Matsui, B. Melon, D. Mengoni, T. Miyazaki, V. Modamio-Hoybjor, S. Momiyama, D. R. Napoli, M. Niikura, R. Orlandi, H. Sakurai, E. Sahin, D. Sohler, H. Schaffner, R. Taniuchi, J. Taprogge, Zs. Vajta, J. J. Valiente-Dobón, O. Wieland, M. Yalcinkaya, "Type II shell evolution in $A = 70$ isobars from the $N \geq 40$ island of inversion,'' Phys. Lett. B **765**, 328−333 (2017).*

S. Kawase, T. Uesaka, TL. Tang, D. Beaumel, M. Dozono, T. Fukunaga, T. Fujii, N. Fukuda, A. Galindo-Uribarri, S. Hwang, N. Inabe, T. Kawabata, T. Kawahara, W. Kim, K. Kisamori, M. Kobayashi, T. Kubo, Y. Kubota, K. Kusaka, C. Lee, Y. Maeda, H. Matsubara, S. Michimasa, H. Miya, T. Noro, Y. Nozawa, A. Obertelli, K. Ogata, S. Ota, E. Padilla-Rodal, S. Sakaguchi, H. Sakai, M. Sasano, S. Shimoura, S. Stepanyan, H. Suzuki, T. Suzuki, M. Takaki, H. Takeda, A. Tamii, H. Tokieda, T. Wakasa, T. Wakui, K. Yako, J. Yasuda, Y. Yanagisawa, R. Yokoyama, K. Yoshida, K. Yoshida, J. Zenihiro, "Exclusive quasi-free proton knockout from oxygen isotopes at intermediate energies,'' Prog. Theor. Exp. Phys. **2018**, 021D01 (2018).*

D. Steppenbeck, S. Takeuchi, N. Aoi, P. Doornenbal, M. Matsushita, H. Wang, H. Baba, S. Go, JD. Holt, J. Lee, K. Matsui, S. Michimasa, T. Motobayashi, D. Nishimura, T. Otsuka, H. Sakurai, Y. Shiga, P.-A. Soderstrom, S. R. Stroberg, T. Sumikama, R. Taniuchi, J. A. Tostevin, Y. Utsuno, J. J. Valiente-Dobon, K. Yoneda, "Structure of ^{55}Sc and development of the $N = 34$ subshell closure,'' Phys. Rev. C **96**, 064310 (2017).*

S. Momiyama, P. Doornenbal, H. Scheit, S. Takeuchi, M. Niikura, N. Aoi, K. Li, M. Matsushita, D. Steppenbeck, H. Wang, H. Baba, E. Ideguchi, M.

Kimura, N. Kobayashi, Y. Kondo, J. Lee, S. Michimasa, T. Motobayashi, N. Shimizu, M. Takechi, Y. Togano, Y. Utsuno, K. Yoneda, H. Sakurai, "In-beam gamma-ray spectroscopy of ^{35}Mg via knockout reactions at intermediate energies,'' Phys. Rev. C **96**, 034328 (2017).

Z. Patel, P. M. Walker, Z. Podolyak, P. H. Regan, T. A. Berry, P.-A. Soderstrom, H. Watanabe, E. Ideguchi, G. S. Simpson, S. Nishimura, Q. Wu, F. R. Xu, F. Browne, P. Doornenbal, G. Lorusso, S. Rice, L. Sinclair, T. Sumikama, J. Wu, Z. Y. Xu, N. Aoi, H. Baba, F. L. Bello Garrote, G. Benzoni, R. Daido, Z. Dombradi, Y. Fang, N. Fukuda, G. Gey, S. Go, A. Gottardo, N. Inabe, T. Isobe, D. Kameda, K. Kobayashi, M. Kobayashi, T. Komatsubara, I. Kojouharov, T. Kubo, N. Kurz, I. Kuti, Z. Li, M. Matsushita, S. Michimasa, C. -B. Moon, H. Nishibata, I. Nishizuka, A. Odahara, E. Sahin, H. Sakurai, H. Schaffner, H. Suzuki, H. Takeda, M. Tanaka, J. Taprogge, Zs. Vajta, A. Yagi, R. Yokoyama, "Isomer-delayed gamma-ray spectroscopy of A=159-164 midshell nuclei and the variation of K-forbidden E1 transition hindrance factors,'' Phys. Rev. C **96**, 034305 (2017).*

S. Kawase, K. Nakano, Y. Watanabe, H. Wang, H. Otsu, H. Sakurai, D. S. Ahn, M. Aikawa, T. Ando, S. Araki, S. Chen, N. Chiga, P. Doornenbal, N. Fukuda, T. Isobe, S. Kawakami, T. Kin, Y. Kondo, S. Koyama, S. Kubono, Y. Maeda, A. Makinaga, M. Matsushita, T. Matsuzaki, S. Michimasa, S. Momiyama, S. Nagamine, T. Nakamura, M. Niikura, T. Ozaki, A. Saito, T. Saito, Y. Shiga, M. Shikata, Y. Shimizu, S. Shimoura, T. Sumikama, P. -A. Soderstrom, H. Suzuki, H. Takeda, S. Takeuchi, R. Taniuchi, Y. Togano, J. Tsubota, M. Uesaka, Y. Watanabe, K. Wimmer, T. Yamamoto, K. Yoshida, "Study of proton- and deuteron-induced spallation reactions on the long-lived fission product ^{93}Zr at 105 MeV/nucleon in inverse kinematics,'' Prog. Theor. Exp. Phys. **2018**, 093D03 (2017).*

N. Nakatsuka, H. Baba, T. Aumann, R. Avigo, SR. Banerjee, A. Bracco, C. Caesar, F. Camera, S. Ceruti, S. Chen, V. Derya, P. Doornenbal, A. Giaz, A. Horvat, K. Ieki, T. Inakura, N. Imai, T. Kawabata, N. Kobayashi, Y. Kondo, S. Koyama, M. Kurata-Nishimura, S. Masuoka, M. Matsushita, S. Michimasa, B. Million, T. Motobayashi, T. Murakami, T. Nakamura, T. Ohnishi, HJ. Ong, S. Ota, H. Otsu, T. Ozaki, A. Saito, H. Sakurai, H. Scheit, F. Schindler, P. Schrock, Y. Shiga, M. Shikata, S. Shimoura, D. Steppenbeck, T. Sumikama, I. Syndikus, H. Takeda, S. Takeuchi, A. Tamii, R. Taniuchi, Y. Togano, J. Tscheuschner, J. Tsubota, H. Wang, O. Wieland, K. Wimmer, Y. Yamaguchi, K. Yoneda, J. Zenihiro, "Observation of isoscalar and isovector dipole excitations in neutron-rich ^{20}O," Phys. Lett. B **768**, 387−392 (2017).*

P. Doornenbal, H. Scheit, S. Takeuchi, Y. Utsuno, N. Aoi, K. Li, M. Matsushita, D. Steppenbeck, H. Wang, H. Baba, E. Ideguchi, N. Kobayashi, Y. Kondo, J. Lee, S. Michimasa, T. Motobayashi, T. Otsuka, H. Sakurai, M. Takechi, Y. Togano, K. Yoneda, "Low-Z shore of the 'island of inversion' and the reduced neutron magicity toward ^{28}O," Phys. Rev. C **95**, 041301 (2017).*

H. N. Liu, J. Lee, R. Doornenbal, H. Scheit, S. Takeuchi, N. Aoi, KA. Li, M. Matsushita, D. Steppenbeck, H. Wang, H. Baba, E. Ideguchi, N. Kobayashi, Y. Kondo, G. Lee, S. Michimasa, T. Motobayashi, A. Poves, H. Sakurai, M. Takechi, Y. Togano, J. A. Tostevin, Y. Utsuno, "Intruder configurations in the ground state of ^{30}Ne,'' Phys. Lett. B **767**, 58−62 (2017).*

H. Wang, H. Otsu, H. Sakurai, D. Ahn, M. Aikawa, T. Ando, S. Araki, S. Chen, N. Chiga, P. Doornenbal, N. Fukuda, T. Isobe, S. Kawakami, S. Kawase, T. Kin, Y. Kondo, S. Koyama, S. Kubono, Y. Maeda, A. Makinaga, M. Matsushita, T. Matsuzaki, S. Michimasa, S. Momiyama, S. Nagamine, T. Nakamura, K. Nakano, M. Niikura, T. Ozaki, A. Saito, T. Saito, Y. Shiga, M. Shikata, Y. Shimizu, S. Shimoura, T. Sumikama, P. -A. Soderstrom, H. Suzuki, H. Takeda, S. Takeuchi, R. Taniuchi, Y. Togano, J. Tsubota, M. Uesaka, Y. Watanabe, Y. Watanabe, K. Wimmer, T. Yamamoto, K. Yoshida, "Spallation reaction study for the long-lived fission product ^{107}Pd,'' Prog. Theor. Exp. Phys. **2017**, 021D01 (2017).*

Hideshi Muto, Yukimitsu Ohshiro, Yasuteru Kotaka, Hidetoshi Yamaguchi, Yasuhiro Sakemi, Kiyoshi Kobayashi, Makoto Nishimura, Michihiro Oyaizu, Shigeru Kubono, Masayuki Kase, Toshiyuki Hattori Susumu Shimoura: "Note: An innovative method for ^{12}C^{4+} suppression in ^{18}O^{6+} beam production in an electron cyclotron resonance ion source,'' Rev. Sci. Instrum **89**, 016103 (2018).*

H. Suzuki, T. Kubo, N. Fukuda, N. Inabe, D. Kameda, H. Takeda, K. Yoshida, K. Kusaka, Y. Yanagisawa, M. Ohtake, H. Sato, Y. Shimizu, H. Baba, M. Kurokawa, K. Tanaka, O. B. Tarasov, D. Bazin, D. J. Morrissey, B. M. Sherrill, K. Ieki, D. Murai, N. Iwasa, A. Chiba, Y. Ohkoda, E. Ideguchi, S. Go, R. Yokoyama, T. Fujii, D. Nishimura, H. Nishibata, S. Momota, M. Lewitowicz, G. DeFrance, I. Celikovic, and K. Steiger: "Discovery of new isotopes ^{81,82}Mo and ^{85,86}Ru and a determination of the particle instability of ^{103}Sb,'' Phys. Rev. C **96**, 034604 (2017).*

B. Moon, C.-B. Moon, A. Odahara, R. Lozeva, P.-A. Soderstrom, F. Browne, C. Yuan, A. Yagi, B. Hong, H. S. Jung, P. Lee, C. S. Lee, S. Nishimura, P. Doornenbal, G. Lorusso, T. Sumikama, H. Watanabe, I. Kojouharov, T. Isobe, H. Baba, H. Sakurai, R. Daido, Y. Fang, H. Nishibata, Z. Patel, S. Rice, L. Sinclair, J. Wu, Z. Y. Xu, R. Yokoyama, T. Kubo, N. Inabe, H. Suzuki, N. Fukuda, D. Kameda, H. Takeda, D. S. Ahn, Y. Shimizu, D. Murai, F. L. Bello Garrote, J. M. Daugas, F. Didierjean, E. Ideguchi, T. Ishigaki, S. Morimoto, M. Niikura, I. Nishizuka, T. Komatsubara Y. K. Kwon, K. Tshoo: "Beta-decay scheme of ^{140}Te to ^{140}I: Suppression of Gamow-Teller transitions between the neutron h$_{9/2}$ and proton $h_{11/2}$ partner orbitals,'' Phys. Rev. C **96**, 014325 (2017).*

B. Moon, C.-B. Moon, P.-A. Soderstrom, A. Odahara, R. Lozeva, B. Hong, F. Browne, H. S. Jung, P. Lee, C. S. Lee, A. Yagi, C. Yuan, S. Nishimura, P. Doornenbal, G. Lorusso, T. Sumikama, H. Watanabe, I. Kojouharov, T. Isobe, H. Baba, H. Sakurai, R. Daido, Y. Fang, H. Nishibata, Z. Patel, S. Rice, L. Sinclair, J. Wu, Z. Y. Xu, R. Yokoyama, T. Kubo, N. Inabe, H. Suzuki, N. Fukuda, D. Kameda, H. Takeda, D. S. Ahn, Y. Shimizu, D. Murai F. L. Bello Garrote, J. M. Daugas, F. Didierjean E. Ideguchi, T. Ishigaki, S. Morimoto, M. Niikura, I. Nishizuka, T. Komatsubara, Y. K. Kwon, K. Tshoo: "Nuclear structure and beta-decay schemes for Te nuclides beyond $N = 82$,'' Phys. Rev. C **95**, 044322 (2017).*

K. Win, Y. Fujita, Y. Y. Oo, H. Fujita, Y. F. Niu, T. Adachi, G. P. A. Berg, G. Colo, H. Dohmann, M. Dozono, D. Frekers, E. -W. Grewe, K. Hatanaka, D. Ishikawa, R. Kehl, N. T. Khai, Y. Kalmykov, H. Matsubara, P. von Neumann-Cosel, T. Niizeki, T. Ruhe, Y. Shimbara, K. Suda, A. Tamii, J. Thies, and H. P. Yoshida: "High-resolution study of $T_Z = +1 \rightarrow 0$ Gamow-Teller transitions in the ^{26}Mg(^{3}He, t)^{26}Al reaction,'' Phy. Rev. C **96**, 064309 (2017).*

K. Sekiguchi, H. Witala, T. Akieda, D. Eto, H. Kon, Y. Wada, A. Watanabe, S. Chebotaryov, M. Dozono, J. Golak, H. Kamada, S. Kawakami, Y. Kubota, Y. Maeda, K. Miki, E. Milman, A. Ohkura, H. Sakai, S. Sakaguchi, N. Sakamoto, M. Sasano, Y. Shindo, R. Skibinski, H. Suzuki, M. Tabata, T. Uesaka, T. Wakasa, K. Yako, T. Yamamoto, Y. Yanagisawa, and J. Yasuda: "Complete set of deuteron analyzing powers from dp elastic scattering at 190 MeV/nucleon,'' Phy. Rev. C **96**, 064001 (2017).*

T. Wakasa, J. Yasuda, M. Dozono, T. Fukunaga, S. Gotanda, K. Hatanaka, K. Ishibashi, S. Kimura, Y. Maeda, Y. Maeda, Y. Nishio, T. Noro, T. Nozoe, K. Ohnaka, S. Sakaguchi, Y. Sakemi, K. Sekiguchi, T. Taguchi, and Y. Wada: "Cross sections and analyzing powers for (p, np) reactions of ^{2}H, ^{6}Li, and ^{12}C at 296 MeV,'' Phy. Rev. C **96**, 014604 (2017).*

J.W. Hwang, S. Kim, Y. Satou, N.A. Orr, Y. Kondo, T. Nakamura, J. Gibelin, N. L. Achouri, T. Aumann, H. Baba, F. Delaunay, P. Doornenbal, N. Fukuda, N. Inabe, T. Isobe, D. Kameda, D. Kanno, N. Kobayashi, T. Kobayashi, T. Kubo, S. Leblond, J. Lee, F. M. Marqués, R. Minakata, T.

Motobayashi, D. Murai, T. Murakami, K. Muto, T. Nakashima, N. Nakatsuka, A. Navin, S. Nishi, S. Ogoshi, H. Otsu, H. Sato, Y. Shimizu, H. Suzuki, K. Takahashi, H. Takeda, S. Takeuchi, R. Tanaka, Y. Togano, A. G. Tuff, M. Vandebrouck, K. Yoneda, "Single-neutron knockout from ^{20}C and the structure of ^{19}C,'' Phys. Lett. B **769**, 503−508 (2017).*

R. Yokoyama, S. Go, D. Kameda, T. Kubo, N. Inabe, N. Fukuda, H. Takeda, H. Suzuki, K. Yoshida, K. Kusaka, K. Tanaka, Y. Yanagisawa, M. Ohtake, H. Sato, Y. Shimizu, H. Baba, M. Kurokawa, D. Nishimura, T. Ohnishi, N. Iwasa, A. Chiba, T. Yamada, E. Ideguchi, T. Fujii, H. Nishibata, K. Ieki, D. Murai, S. Momota, Y. Sato, J. W. Hwang, S. Kim, O. B. Tarasov, D. J. Morrissey, B. M. Sherrill, G. Simpson, and C. R. Praharaj, "New K isomers in the neutron-rich N = 100 isotones ^{162}Sm, ^{163}Eu, and ^{164}Gd," Phys. Rev. C **95** 034313 (2017).*

N. Fukuda, T. Kubo, D. Kameda, N. Inabe, H. Suzuki, Y. Shimizu, H. Takeda, K. Kusaka, Y. Yanagisawa, M. Ohtake, K. Tanaka, K. Yoshida, H. Sato, H. Baba, M. Kurokawa, T. Ohnishi, N. Iwasa, A. Chiba, T. Yamada, E. Ideguchi, S. Go, R. Yokoyama, T. Fujii, H. Nishibata, K. Ieki, D. Murai, S. Momota, D. Nishimura, Y. Sato, J. Hwang, S. Kim, Oleg B. Tarasov, D. J. Morrissey, and G. Simpson, "Identification of new neutron-rich isotopes in the rare-earth region produced by 345 MeV/nucleon ^{238}U," J. Phys. Soc. Jpn. **87** 014202 (2017).*

J.C. Zamora *et al*., "Nuclear-matter radius studies from ^{58}Ni(α, α) experiments at the GSI Experimental Storage Ring with the EXL facility," Phys. Rev. C **96**, 034617 (2017). *

K. Sekiguchi *et al*., "Complete set of deuteron analyzing powers from dp elastic scattering at 190 MeV/nucleon," Phys. Rev. C 96, 064001 (2017). *

L. Stuhl, M. Sasano, K. Yako, J. Yasuda, T. Uesaka, "PANDORA, a large volume low-energy neutron detector with real-time neutron–gamma discrimination," Nucl. Instrum. Methods Phys. Res. A **864**, 164−171 (2017). *

S. Acharya *et al*. [ALICE Collaboration], "First measurement of Ξ_c^0 production in pp collisions at $\sqrt{s}$ = 7 TeV," Phys. Lett. B **781**, 8 (2018).*

S. Acharya *et al*. [ALICE Collaboration], "Measurement of Z^0-boson production at large rapidities in Pb-Pb collisions at $\sqrt{s_{NN}}$ = 5.02 TeV," Phys. Lett. B **780**, 372 (2018).*

S. Acharya *et al*. [ALICE Collaboration], "Longitudinal asymmetry and its effect on pseudorapidity distributions in Pb-Pb collisions at $\sqrt{s_{NN}}$ = 2.76 TeV," Phys. Lett. B **781**, 20 (2018).*

S. Acharya *et al*. [ALICE Collaboration], "Production of ^{4}He and ^{4}anti-He in Pb-Pb collisions at $\sqrt{s_{NN}}$ = 2.76 TeV at the LHC," Nucl. Phys. A **971**, 1 (2018).*

S. Acharya *et al*. [ALICE Collaboration], "Production of deuterons, tritons, ^{3}He nuclei and their antinuclei in *pp* collisions at $\sqrt{s}$ = 0.9, 2.76 and 7 TeV," Phys. Rev. C **97**, 024615 (2018).*

S. Acharya *et al*. [ALICE Collaboration], "Search for collectivity with azimuthal J/ψ-hadron correlations in high multiplicity *p*-Pb collisions at $\sqrt{s_{NN}}$ = 5.02 and 8.16 TeV," Phys. Lett. B **780**, 7 (2018).*

S. Acharya *et al*. [ALICE Collaboration], "J/ψ elliptic flow in Pb-Pb collisions at $\sqrt{s_{NN}}$ = 5.02 TeV," Phys. Rev. Lett. **119**, 242301 (2017).*

S. Acharya *et al*. [ALICE Collaboration], "Constraining the magnitude of the Chiral Magnetic Effect with Event Shape Engineering in Pb-Pb collisions at $\sqrt{s_{NN}}$ = 2.76 TeV," Phys. Lett. B **777**, 151 (2018).*

S. Acharya *et al*. [ALICE Collaboration], "The ALICE Transition Radiation Detector: construction, operation, and performance," Nucl. Instrum. Methods Phys. Res. A **881**, 88 (2018).*

S. Acharya *et al*. [ALICE Collaboration], "Kaon femtoscopy in Pb-Pb collisions at $\sqrt{s_{NN}}$ = 2.76 TeV," Phys. Rev. C **96**, 064613 (2017).*

S. Acharya *et al*. [ALICE Collaboration], "Systematic studies of correlations between different order flow harmonics in Pb-Pb collisions at $\sqrt{s_{NN}}$ = 2.76 TeV," Phys. Rev. C **97**, 024906 (2018).*

S. Acharya *et al*. [ALICE Collaboration], "π^0 and η meson production in proton-proton collisions at $\sqrt{s}$ = 8 TeV," Eur. Phys. J. C **78**, 263 (2018).*

C. Aidala *et al*. [PHENIX Collaboration], "Measurements of azimuthal anisotropy and charged-particle multiplicity in *d* + Au collisions at $\sqrt{s_{NN}}$ = 200, 62.4, 39, and 19.6 GeV," Phys. Rev. C **96**, 064905 (2017).*

S. Acharya *et al*. [ALICE Collaboration], "Charged-particle multiplicity distributions over a wide pseudorapidity range in proton-proton collisions at $\sqrt{s}$ = 0.9, 7, and 8 TeV," Eur. Phys. J. C **77**, 852 (2017).*

S. Acharya *et al*. [ALICE Collaboration], "Measurement of deuteron spectra and elliptic flow in Pb–Pb collisions at $\sqrt{s_{NN}}$ = 2.76 TeV at the LHC," Eur. Phys. J. C **77**, 658 (2017).*

C. Aidala *et al*. [PHENIX Collaboration], "Measurements of Multiparticle Correlations in *d* + Au Collisions at 200, 62.4, 39, and 19.6 GeV and *p* + Au Collisions at 200 GeV and Implications for Collective Behavior," Phys. Rev. Lett. **120**, 062302 (2018).*

S. Acharya *et al*. [ALICE Collaboration], "Searches for transverse momentum dependent flow vector fluctuations in Pb-Pb and *p*-Pb collisions at the LHC," JHEP **1709**, 032 (2017).*

S. Acharya *et al*. [ALICE Collaboration], "*D*-meson azimuthal anisotropy in midcentral Pb-Pb collisions at $\sqrt{s_{NN}}$ =5.02 TeV," Phys. Rev. Lett. **120**, 102301 (2018).*

S. Acharya *et al*. [ALICE Collaboration], "Measuring $K^0_S K^\pm$ interactions using Pb-Pb collisions at $\sqrt{s_{NN}}$ =2.76 TeV," Phys. Lett. B **774**, 64 (2017).*

S. Acharya *et al*. [ALICE Collaboration], "Linear and non-linear flow modes in Pb-Pb collisions at $\sqrt{s_{NN}}$ = 2.76 TeV," Phys. Lett. B **773**, 68 (2017).*

D. Adamová *et al*. [ALICE Collaboration], "*J/ψ* production as a function of charged-particle pseudorapidity density in *p*-Pb collisions at $\sqrt{s_{NN}}$ = 5.02 TeV," Phys. Lett. B **776**, 91 (2018).*

C. Aidala *et al*. [PHENIX Collaboration], "Nuclear dependence of the transverse-single-spin asymmetry for forward neutron production in polarized *p* + A collisions at $\sqrt{s_{NN}}$ =200 GeV," Phys. Rev. Lett. **120**, 022001 (2018).*

C. Aidala *et al*. [PHENIX Collaboration], "Cross section and transverse single-spin asymmetry of muons from open heavy-flavor decays in polarized *p* + *p* collisions at $\sqrt{s}$ =200 GeV," Phys. Rev. D **95**, 112001 (2017).*

J. Adam *et al*. [ALICE Collaboration], "Flow dominance and factorization of transverse momentum correlations in Pb-Pb collisions at the LHC," Phys. Rev. Lett. **118**, 162302 (2017).*

D. Adamova *et al*. [ALICE Collaboration], "Azimuthally differential pion femtoscopy in Pb-Pb collisions at $\sqrt{s_{NN}}$ = 2.76 TeV," Phys. Rev. Lett. **118**, 222301 (2017).*

S. Acharya *et al*. [ALICE Collaboration], "Production of muons from heavy-flavour hadron decays in *p*-Pb collisions at $\sqrt{s_{NN}}$ = 5.02 TeV," Phys. Lett. B **770**, 459 (2017).*

C. Aidala *et al*. [PHENIX Collaboration], "B-meson production at forward and backward rapidity in *p* + *p* and Cu + Au collisions at √s_{NN} =200 GeV," Phys. Rev. C **96**, 064901 (2017).*

A. Adare *et al*. [PHENIX Collaboration], "Measurements of *e*⁺*e*⁻ pairs from open heavy flavor in *p* + *p* and *d* + A collisions at √s_{NN} =200 GeV," Phys. Rev. C **96**, 024907 (2017).*

S. Acharya *et al*. [ALICE Collaboration], "Production of π⁰ and ηmesons up to high transverse momentum in *pp* collisions at 2.76 TeV," Eur. Phys. J. C **77**, 339 (2017).*

S. Acharya *et al*. [ALICE Collaboration], "First measurement of jet mass in Pb-Pb and *p*-Pb collisions at the LHC," Phys. Lett. B 776, 249 (2018).*

S. Acharya *et al*. [ALICE Collaboration], "Measurement of *D*-meson production at mid-rapidity in *pp* collisions at √*s* =7 TeV," Eur. Phys. J. C **77**, 550 (2017).*

S. Acharya *et al*. [ALICE Collaboration], "Energy dependence of forward-rapidity *J/ψ* and *ψ*(2S) production in *pp* collisions at the LHC," Eur. Phys. J. C **77**, 392 (2017).*

J. Adam *et al*. [ALICE Collaboration], "*K**(892)⁰ and *φ*(1020) meson production at high transverse momentum in *pp* and Pb-Pb collisions at √s_{NN} = 2.76 TeV," Phys. Rev. C **95**, 064606 (2017).*

D. Adamova *et al*. [ALICE Collaboration], "Production of *Σ*(1385)± and *Ξ*(1530)⁰ in *p*-Pb collisions at √s_{NN} = 5.02 TeV," Eur. Phys. J. C **77**, 389 (2017).*

C. Aidala *et al*. [PHENIX Collaboration], "Measurements of *B*→ *J/ψ* at forward rapidity in *p* + *p* collisions at √*s* = 510 GeV," Phys. Rev. D **95**, 092002 (2017).*

J. Adam *et al*. [ALICE Collaboration], "Insight into particle production mechanisms via angular correlations of identified particles in pp collisions at √*s* = 7 TeV," Eur. Phys. J. C **77**, 569 (2017).*

J. Adam *et al*. [ALICE Collaboration], "Centrality dependence of the pseudorapidity density distribution for charged particles in Pb-Pb collisions at √s_{NN} = 5.02 TeV," Phys. Lett. B **772**, 567 (2017).*

A. Adare *et al*. [PHENIX Collaboration], "Angular decay coefficients of *J/ψ* mesons at forward rapidity from *p* + *p* collisions at √*s* =510 GeV," Phys. Rev. D **95**, 092003 (2017).*

L. Yang, C.J. Lin, H.M. Jia, D.X. Wang, N.R. Ma, L.J. Sun, F. Yang, X.X. Xu, Z.D. Wu, H.Q. Zhang, and Z.H. Liu: "Is the dispersion relation applicable for exotic nuclear systems? The abnormal threshold anomaly in the ⁶He + ²⁰⁹Bi system," Phys. Rev. Lett. **119**, 042503 (2017).*

L. Yang, C.J. Lin, H.M. Jia, D.X. Wang, N.R. Ma, L.J. Sun, F. Yang, X.X. Xu, Z.D. Wu, H.Q. Zhang, and Z.H. Liu: "Abnormal behavior of the optical potential for the halo nuclear system ⁶He + ²⁰⁹Bi," Phys. Rev. C **96**, 044615 (2017).*

I. Indelicato, M. La Cognata, C. Spitaleri, V. Burjan, S. Cherubini, M. Gulino, S. Hayakawa, Z. Hons, V. Kroha, L. Lamia, M. Mazzocco, J. Mrazek, R. G. Pizzone, S. Romano, E. Strano, D. Torresi, A. Tumino, "New improved indirect measurement of the ¹⁹F(*p*, *α*)¹⁶O reaction at energies of astrophysical relevance,'' Astrophysical Journal, **845**, 19, 13 pages, (2017).*

D. Kahl, H. Yamaguchi, S. Kubono, A.A. Chen, A. Parikh, D.N. Binh, J. Chen, S. Cherubini, N. N. Duy, T. Hashimoto S. Hayakawa, N. Iwasa, H. S. Jung, S. Kato,Y. K. Kwon S. Nishimura, S. Ota, K. Setoodehnia, T. Teranishi, H. Tokieda, T. Yamada, C. C. Yun and L. Y. Zhang, "First measurement of ³⁰S + *α* resonant elastic scattering for the ³⁰S(*α*, *p*) reaction rate," Phys. Rev. C **97**, 015802 (2018).*

T. Aoki, Y. Torii, B.K. Sahoo, B.P. Das, K. Harada, T. Hayamizu, K. Sakamoto, H. Kawamura, T. Inoue, A. Uchiyama, S. Ito, R. Yoshioka, K.S. Tanaka, M. Itoh, A. Hatakeyama, Y. Sakemi, "Parity-nonconserving interaction-induced light shifts in the 7S₁/₂-6D₃/₂ transition of the ultracold ²¹⁰Fr atoms to probe new physics beyond the standard model," Appl. Phys. **123**, 120 (2017).*

T. Wakasa, J. Yasuda, M. Dozono, T. Fukunaga, S. Gotanda, K. Hatanaka, K. Ishibashi, Y. Kanaya, S. Kimura, Y. Maeda, Y. Maeda, Y. Nishio, T. Noro, T. Nozoe, K. Ohnaka, S. Sakaguchi, Y. Sakemi, K. Sekiguchi, K. Taguchi, Y. Wada , "Cross sections and analyzing powers for (*p*⃗, *np*) reactions of H2, Li6 , and C12 at 296 MeV," Phys. Rev. C **96**, 014604 (2017).*

N. Shimizu, J. Menendez and K. Yako, "Double Gamow-Teller transition and its relation to neutrinoless decay," Phys. Rev. Lett. **120**, 142502 (2018).*

T. Mizusaki, M. Oi and N. Shimizu, "Why does sign problem occur in Onishi formula?" Phys. Lett. B **779**, 237 (2018).*

S. Ansari, J.-M. Régis, J. Jolie, N. Saed-Samii, N. Warr, W. Korten, M. Zielińska, M.-D. Salsac, A. Blanc, M. Jentschel, U. Köster, P. Mutti, T. Soldner, G. S. Simpson, F. Drouet, A. Vancraeyenest, G. de France, E. Clément, O. Stezowski, C. A. Ur, W. Urban, P. H. Regan, Zs. Podolyák, C. Larijani, C. Townsley, R. Carroll, E. Wilson, H. Mach, L. M. Fraile, V. Paziy, B. Olaizola, V. Vedia, A. M. Bruce, O. J. Roberts, J. F. Smith, M. Scheck, T. Kröll, A.-L. Hartig, A. Ignatov, S. Ilieva, S. Lalkovski, N. Mărginean, T. Otsuka, N. Shimizu, T. Togashi, and Y. Tsunoda, "Experimental study of lifetime and phase transition in neutron-rich ⁹⁸, ¹⁰⁰, ¹⁰²Zr," Phys. Rev. C **96**, 054323 (2017).*

M. Queiser, A. Vogt, M. Seidlitz, P. Reiter, T. Togashi, N. Shimizu, Y. Utsuno, T. Otsuka, M. Honma, P. Petkov, K. Arnswald, R. Altenkirch, B. Birkenbach, A. Blazhev, T. Braunroth, A. Dewald, J. Eberth, C. Fransen, B. Fu, H. Hess, R. Hetzenegger, R. Hirsch, J. Jolie, V. Karayonchev, L. Kaya, L. Lewandowski, C. Müller-Gatermann, J.-M. Régis, D. Rosiak, D. Schneiders, B. Siebeck, T. Steinbach, K. Wolf, and K.-O. Zell, "Cross-shell excitations from the pf shell: Lifetime measurements in ⁶¹Zn," Phys. Rev. C **96**, 044313 (2017).*

S. Momiyama, P. Doornenbal, H. Scheit, S. Takeuchi, M. Niikura, N. Aoi, K. Li, M. Matsushita, D. Steppenbeck, H. Wang, H. Baba, E. Ideguchi, M. Kimura, N. Kobayashi, Y. Kondo, J. Lee, S. Michimasa, T. Motobayashi, N. Shimizu, M. Takechi, Y. Togano, Y. Utsuno, K. Yoneda, and H. Sakurai, "In-beam gamma-ray spectroscopy of ³⁵Mg via knockout reaction at intermediate energies," Phys. Rev. C **96**, 034328 (2017).*

J.-M. Régis, J. Jolie, N. Saed-Samii, N. Warr, M. Pfeiffer, A. Blanc, M. Jentschel, U. Köster, P. Mutti, T. Soldner, G. S. Simpson, F. Drouet, A. Vancraeyenest, G. de France, E. Clément, O. Stezowski, C. A. Ur, W. Urban, P. H. Regan, Zs. Podolyák, C. Larijani, C. Townsley, R. Carroll, E. Wilson, L. M. Fraile, H. Mach, V. Paziy, B. Olaizola, V. Vedia, A. M. Bruce, O. J. Roberts, J. F. Smith, M. Scheck, T. Kröll, A.-L. Hartig, A. Ignatov, S. Ilieva, S. Lalkovski, W. Korten, N. Mărginean, T. Otsuka, N. Shimizu, T. Togashi, and Y. Tsunoda, "Abrupt shape transition at neutron number *N* = 60: *B*(E2) values in 94,96,98Sr from fast gamma-gamma timing," Phys. Rev. C **95**, 054319 (2017).*

N. Shimizu, T. Abe, M. Honma, T. Otsuka, T. Togashi, Y. Tsunoda, Y. Utsuno and T. Yoshida, "Monte Carlo shell model studies with massively parallel supercomputers," Phys. Scr. **92**, 063001 (2017).*

T. Miyagi, T. Abe, R. Okamoto, and T. Otsuka, "Introduction of the one-body correlation operator in the unitary-model-operator approach," Phys. Rev. C **96**, 054312 (2017).*

C.Wraith, X.F.Yang, L.Xie, C.Babcock, J.Bieroń, J.Billowes, M.L.Bissell, K.Blaum, B.Cheal, L.Filippin, R.F.Garcia Ruiz, W.Gins, L.K.Grob, G.Gaigalas,

M.Godefroid, C.Gorges, H.Heylen, M.Honma, P.Jönsson, S.Kaufmann, M.Kowalska, J.Krämer, S.Malbrunot-Ettenauer, R.Neugart, G.Neyens, W.Nörtershäuser, F.Nowacki, T.Otsuka, J.Papuga, R.Sánchez, Y.Tsunoda, D.T.Yordanov, "Evolution of nuclear structure in neutron-rich odd-Zn isotopes and isomers," Phys. Lett. B **771**, 385 (2017).*

E. Sahin, F. L. Bello Garrote, Y. Tsunoda, T. Otsuka, G. de Angelis, A. Görgen, M. Niikura, S. Nishimura, Z. Y. Xu, H. Baba, F. Browne, M.-C. Delattre, P. Doornenbal, S. Franchoo, G. Gey, K. Hadyńska-Klęk, T. Isobe, P. R. John, H. S. Jung, I. Kojouharov, T. Kubo, N. Kurz, Z. Li, G. Lorusso, I. Matea, K. Matsui, D. Mengoni, P. Morfouace, D. R. Napoli, F. Naqvi, H. Nishibata, A. Odahara, H. Sakurai, H. Schaffner, P.-A. Söderström, D. Sohler, I. G. Stefan, T. Sumikama, D. Suzuki, R. Taniuchi, J. Taprogge, Z. Vajta, H. Watanabe, V. Werner, J. Wu, A. Yagi, M. Yalcinkaya, and K. Yoshinaga, "Shell evolution towards ^{78}Ni: Low-Lying States in ^{77}Cu," Phys. Rev. Lett. **118**, 242502 (2017).*

R. P. de Groote, J. Billowes, C. L. Binnersley, M. L. Bissell, T. E. Cocolios, T. Day Goodacre, G. J. Farooq-Smith, D. V. Fedorov, K. T. Flanagan, S. Franchoo, R. F. Garcia Ruiz, Á. Koszorús, K. M. Lynch, G. Neyens, F. Nowacki, T. Otsuka, S. Rothe, H. H. Stroke, Y. Tsunoda, A. R. Vernon, K. D. A. Wendt, S. G. Wilkins, Z. Y. Xu, and X. F. Yang, "Dipole and quadrupole moments of $^{73-78}$Cu as a test of the robustness of the $Z = 28$ shell closure near 78Ni," Phys. Rev. C **96**, 041302(R) (2017).*

C. M. Shand, Z. Podolyák, M. Górska, P. Doornenbal, A. Obertelli, F. Nowacki, T. Otsuka, K. Sieja, J. A. Tostevin, Y. Tsunoda, G. Authelet, H. Baba, D. Calvet, A. Château, S. Chen, A. Corsi, A. Delbart, J. M. Gheller, A. Giganon, A. Gillibert, T. Isobe, V. Lapoux, M. Matsushita, S. Momiyama, T. Motobayashi, M. Niikura, H. Otsu, N. Paul, C. Péron, A. Peyaud, E. C. Pollacco, J.-Y. Roussé, H. Sakurai, C. Santamaria, M. Sasano, Y. Shiga, D. Steppenbeck, S. Takeuchi, R. Taniuchi, T. Uesaka, H. Wang, K. Yoneda, T. Ando, T. Arici, A. Blazhev, F. Browne, A. M. Bruce, R. J. Carroll, L. X. Chung, M. L. Cortés, M. Dewald, B. Ding, Z. Dombrádi, F. Flavigny, S. Franchoo, F. Giacoppo, A. Gottardo, K. Hadyńska-Klęk, A. Jungclaus, Z. Korkulu, S. Koyama, Y. Kubota, J. Lee, M. Lettmann, B. D. Linh, J. Liu, Z. Liu, C. Lizarazo, C. Louchart, R. Lozeva, K. Matsui, T. Miyazaki, K. Moschner, M. Nagamine, N. Nakatsuka, S. Nishimura, C. R. Nita, C. R. Nobs, L. Olivier, S. Ota, R. Orlandi, Z. Patel, P. H. Regan, M. Rudigier, E. Şahin, T. Saito, P.-A. Söderström, I. Stefan, T. Sumikama, D. Suzuki, Z. Vajta, V. Vaquero, V. Werner, K. Wimmer, J. Wu, and Z. Y. Xu, "Shell evolution beyond $Z = 28$ and $N = 50$: Spectroscopy of $^{81, 82, 83, 84}$Zn," Phys. Lett. B **773**, 492 (2017).*

L. Olivier, S. Franchoo, M. Niikura, Z. Vajta, D. Sohler, P. Doornenbal, A. Obertelli, Y. Tsunoda, T. Otsuka, G. Authelet, H. Baba, D. Calvet, F. Château, A. Corsi, A. Delbart, J. M. Gheller, A. Gillibert, T. Isobe, V. Lapoux, M. Matsushita, S. Momiyama, T. Motobayashi, H. Otsu, C. Péron, A. Peyaud, E. C. Pollacco, J. Y. Roussé, H. Sakurai, C. Santamaria, M. Sasano, Y. Shiga, S. Takeuchi, R. Taniuchi, T. Uesaka, H. Wang, K. Yoneda, F. Browne, L. X. Chung, Z. Dombradi, F. Flavigny, F. Giacoppo, A. Gottardo, K. Hadyńska-Klęk, Z. Korkulu, S. Koyama, Y. Kubota, J. Lee, M. Lettmann, C. Louchart, R. Lozeva, K. Matsui, T. Miyazaki, S. Nishimura, K. Ogata, S. Ota, Z. Patel, E. Sahin, C. Shand, P. A. Söderström, I. Stefan, D. Steppenbeck, T. Sumikama, D. Suzuki, V. Werner, J. Wu, and Z. Xu, "Persistence of the $Z = 28$ Shell Gap Around ^{78}Ni: First Spectroscopy of ^{79}Cu," Phys. Rev. Lett. **119**, 1 (2017).*

S. Bottoni, S. Zhu, R. V. F. Janssens, M. P. Carpenter, Y. Tsunoda, T. Otsuka, A. O. Macchiavelli, D. Cline, C. Y. Wu, A. D. Ayangeakaa, B. Bucher, M. Q. Buckner, C. M. Campbell, C. J. Chiara, H. L. Crawford, M. Cromaz, H. M. David, P. Fallon, A. Gade, J. P. Greene, J. Harker, A. B. Hayes, C. R. Hoffman, B. P. Kay, A. Korichi, T. Lauritsen, J. Sethi, D. Seweryniak, W. B. Walters, D. Weisshaar, and A. Wiens, "Nucleon correlations and the structure of $^{71}_{30}$Zn$_{41}$," Phys. Lett. B **775**, 271 (2017).*

S. Yoshida, Y. Utsuno, N. Shimizu, and T. Otsuka, "Systematic shell-model study of β-decay properties and Gamow-Teller strength distributions in A ~ 40 neutron-rich nuclei," Phys. Rev. C **97**, 054321 (2018).*

B. Fernández-Domínguez, B. Pietras, W. N. Catford, N. A. Orr, M. Petri, M. Chartier, S. Paschalis, N. Patterson, J. S. Thomas, M. Caamaño, T. Otsuka, A. Poves, N. Tsunoda, N. L. Achouri, J.-C. Angélique, N. I. Ashwood, A. Banu, B. Bastin, R. Borcea, J. Brown, F. Delaunay, S. Franchoo, M. Freer, L. Gaudefroy, S. Heil, M. Labiche, B. Laurent, R. C. Lemmon, A. O. Macchiavelli, F. Negoita, E. S. Paul, C. Rodríguez-Tajes, P. Roussel-Chomaz, M. Staniou, M. J. Taylor, L. Trache, and G. L. Wilson, "Re-examining the transition into the $N = 20$ island of inversion: Structure of ^{30}Mg," Phys. Lett. B **779**, 124 (2018).*

J. Menéndez, "Neutrinoless ββ decay mediated by the exchange of light and heavy neutrinos: the role of nuclear structure correlations," J. Phys. G Nucl. Part. Phys. **45**, 014003 (2018).*

H. L. Crawford, A. O. Macchiavelli, P. Fallon, M. Albers, V. M. Bader, D. Bazin, C. M. Campbell, R. M. Clark, M. Cromaz, J. Dilling, A. Gade, A. Gallant, J. D. Holt, R. V. F. Janssens, R. Krücken, C. Langer, T. Lauritsen, I. Y. Lee, J. Menéndez, S. Noji, S. Paschalis, F. Recchia, J. Rissanen, A. Schwenk, M. Scott, J. Simonis, S. R. Stroberg, J. A. Tostevin, C. Walz, D. Weisshaar, A. Wiens, K. Wimmer, and S. Zhu, "Unexpected distribution of ν1$_{f7/2}$ strength in ^{49}Ca," Phys. Rev. C **95**, 064317 (2017).*

P. Klos, A. Carbone, K. Hebeler, J. Menéndez, and A. Schwenk, "Uncertainties in constraining low-energy constants from ^{3}H β decay," Eur. Phys. J. A **53**, 168 (2017).*

M. Hoferichter, P. Klos, J. Menéndez, and A. Schwenk, "Improved limits for Higgs-portal dark matter from LHC searches," Phys. Rev. Lett. **119**, 181803 (2017).*

H. Muto, Y. Ohshiro, Y. Kotaka, H. Yamaguchi, Y. Sakemi, K. Kobayashi, M. Nishimura, M. Oyaizu, S. Kubono, M. Kase, T. Hattori, and S. Shimoura, "An innovative method for ^{12}C^{4+} suppression in ^{18}O^{6+} beam production in an electron cyclotron resonance ion source," Rev. Sci. Instrum. **89**, 016103 (2018).

[Proceedings]

(Original Papers) *Subject to Peer Review

T. Gunji [ALICE Collaboration], "Low mass dielectron measurements in pp, p-Pb, and Pb-Pb collisions with ALICE at the LHC," Nucl. Part. Phys. Proc. **289−290**, 181 (2017).*

T. Otsuka, Y. Tsunoda, T. Togashi N. Shimizu and T. Abe, "Quantum self-organization and nuclear collectivities," J. Phys.: Conf. Ser. **966** 012027 (2018).*

S. Michimasa, S. Ota, M. Dozono, M. Takaki, K. Kisamori, H. Miya, M. Kobayashi, Y. Kiyokawa, H. Baba, N. Fukuda, N. Inabe, S. Kawase, T. Kubo, Y. Kubota, C.S. Lee, M. Matsushita, H. Sakai, A. Stolz, H. Tokieda, T. Uesaka, K. Yako, Y. Yanagisawa, R. Yokoyama, K. Yoshida, S. Shimoura, "SHARAQ spectrometer: High-resolution spectroscopy using exotic beams and reactions," PoS **INPC2016**, 106, (2017).*

D. Steppenbeck, S. Takeuchi, N. Aoi, P. Doornenbal, M. Matsushita, H. Wang, H. Baba, S. Go, J. Lee, K. Matsui, S. Michimasa, T. Motobayashi, D. Nishimura, T. Otsuka, H. Sakurai, Y. Shiga, P.-A. Soderstrom, T. Sumikama, R. Taniuchi, Y. Utsuno, J.J. Valiente-Dobon, K. Yoneda, "Low-lying structures of exotic Sc isotopes and the evolution of the $N = 34$ subshell closure," PoS **INPC2016**, 030, (2017).*

R. Yokoyama, E. Ideguchi, G. Simpson, Mn. Tanaka, S. Nishimura, P. Doornenbal, P.-A. Soderstrom, G. Lorusso, Z.Y. Xu, J. Wu, T. Sumikama, N. Aoi, H. Baba, F. Bello, F. Browne, R. Daido, Y. Fang, N. Fukuda, G. Gey, S. Go, S. Inabe, T. Isobe, D. Kameda, K. Kobayashi, M. Kobayashi, T. Komatsubara, T. Kubo, I. Kuti, Z. Li, M. Matsushita, S. Michimasa, C. B. Moon, H. Nishibata, I. Nishizuka, A. Odahara, Z. Patel, S. Rice, E. Sahin, L. Sinclair, H. Suzuki, H. Takeda, J. Taprogge, Zs. Vajta, H. Watanabe, A. Yagi, "Role of hexadecupole deformation in the shape evolution of neutron-rich Nd isotopes," PoS **INPC2016**, 015, (2017).*

Y. Togano, T. Nakamura, Y. Kondo, N. Kobayashi, R. Tanaka, R. Minakata, S. Ogoshi, S. Nishi, D. Kanno, T. Nakashima, J. Tsubota, A. T. Saito, J. A. Tostevin, N. A. Orr, J. Gibelin, F. Delaunay, F. M. Marques, N. L. Achouri, S. Leblond, Q. Deshayes, K. Yoneda, T. Motobayashi, H. Otsu, T. Isobe, H. Baba, H. Sato, Y. Shimizu, T. Kubo, N. Inabe, N. Fukuda, D. Kameda, H. Suzuki, H. Takeda, J. H. Lee, P. Doornenbal, S. Takeuchi, T. Kobayashi, K. Takahashi, K. Muto, T. Murakami, N. Nakatsuka, Y. Sato, S. Kim, J. Hwang, T. Aumann, D. Murai, A. Navin, A. G. Tuff, M. Vandebrouck, "Reaction cross section of the two-neutron halo nucleus ^{22}C at 235 MeV/nucleon," PoS **INPC2016**, 281, (2017).*

H. Wang, H. Otsu, H. Sakurai, D. Ahn, N. Chiga, P. Doornenbal, N. Fukuda, T. Isobe, T. Kubo, S. Kubono, G. Lorusso, P.-A. Soderstrom, H. Suzuki, H. Takeda, Y. Watanabe, K. Yoshida, T. Matsuzaki, Y. Shimizu, T. Sumikama, M. Uesaka, S. Kawase, K. Nakano, Y. Watanabe, S. Araki, T. Kin, S. Takeuchi, Y. Togano, T. Nakamura, Y. Kondo, T. Ozaki, A. Saito, J. Tsubota, M. Aikawa, A. Makinaga, T. Ando, S. Koyama, S. Momiyama, S. Nagamine, M. Niikura, T. Saito, R. Taniuchi, K. Wimmer, S. Kawakami, Y. Maeda, T. Yamamoto, Y. Shiga, M. Matsushita, S. Michimasa, S. Shimoura, "Spallation reaction study for the long-lived fission products in nuclear waste: Cross section measurements for ^{137}Cs, ^{90}Sr and ^{107}Pd using inverse kinematics method," Energy Procedia **131** 127−132 (2017).*

S. Kawase, Y. Watanabe, H. Wang, H. Otsu, H. Sakurai, S. Takeuchi, Y. Togano, T. Nakamura, Y. Maeda, D. S. Ahn, M. Aikawa, S. Araki, S. D. Chen, N. Chiga, P. Doornenbal, N. Fukuda, T. Ichihara, T. Isobe, S. Kawakami, T. Kin, Y. Kondo, S. Koyama, T. Kubo, S. Kubono, M. Kurokawa, A. Makinaga, M. Matsushita, T. Matsuzaki, S. Michimasa, S. Momiyama, S. Nagamine, K. Nakano, M. Niikura, T. Ozaki, A. Saito, T. Saito, Y. Shiga, M. Shikata, Y. Shimizu, S. Shimoura, T. Sumikama, P.-A. Soderstrom, H. Suzuki, H. Takeda, R. Taniuchi, J. Tsubota, Y. Watanabe, K. Wimmer, T. Yamamoto, K. Yoshida, "Cross section measurement of residues produced in proton- and deuteron-induced spallation reactions on ^{93}Zr at 105 MeV/u using the inverse kinematics method," EPJ Web of Conf. **146**, 03012 (2017).*

K. Nakano, Y. Watanabe, S. Kawase, H. Wang, H. Otsu, H. Sakurai, S. Takeuchi, Y. Togano, T. Nakamura, Y. Maeda, D. S. Ahn, M. Aikawa, S. Araki, S. Chen, N. Chiga, P. Doornenbal, N. Fukuda, T. Ichihara, T. Isobe, S. Kawakami, T. Kin, Y. Kondo, S. Koyama, T. Kubo, S. Kubono, M. Kurokawa, A. Makinaga, M. Matsushita, T. Matsuzaki, S. Michimasa, S. Momiyama, S. Nagamine, M. Niikura, T. Ozaki, A. Saito, T. Saito, Y. Shiga, M. Shikata, Y. Shimizu, S. Shimoura, T. Sumikama, P.-A. Soderstrom, H. Suzuki, H. Takeda, R. Taniuchi, J. Tsubota, Y. Watanabe, K. Wimmer, T. Yamamoto, K. Yoshida, "Cross sections for nuclide production in proton- and deuteron-induced reactions on ^{93}Nb measured using the inverse kinematics method," EPJ Web of Conf. **146**, 11046 (2017).*

K. Sekiguchi, Y. Wada, A. Watanabe, D. Eto, T. Akieda, H. Kon, K. Miki, N. Sakamoto, H. Sakai, M. Sasano, Y. Shimizu, H. Suzuki, T. Uesaka, Y. Yanagisawa, M. Dozono, S. Kawase, Y. Kubota, C. S. Lee, K. Yako, Y. Maeda, S. Kawakami, T. Yamamoto, S. Sakaguchi, T. Wakasa, J. Yasuda, A. Ohkura, Y. Shindo, M. Tabata, E. Milman, S. Chebotaryov, H. Okamura, and T. L. Tang: "Deuteron analyzing powers for dp elastic scattering at intermediate energies and three-nucleon forces," Few Body Syst. **58**, 48 (2017).*

H. Yamaguchi, D. Kahl, S. Hayakawa, Y. Sakaguchi, K. Abe, T. Nakao, T. Suhara, N. Iwasa, A. Kim, D. H. Kim, S. M. Cha, M. S. Kwag, J. H. Lee, E. J. Lee, K. Y. Chae, Y. Wakabayashi, N. Imai, N. Kitamura, P. Lee, J. Y. Moon, K. B. Lee, C. Akers, H. S. Jung, N. N. Duy, L. H. Khiem and C. S. Lee, "Study on a-cluster levels in non-4n nuclei using low-energy RI beams," J Phys.: Conf. Ser. **863**, 012025 (2017).*

D. Kahl, H. Shimizu, H. Yamaguchi, K. Abe, O. Beliuskina, S. M. Cha, K. Y. Chae, A. A. Chen, Z. Ge, S. Hayakawa, N. Imai, N. Iwasa, A. Kim, D. H. Kim, M. J. Kim, S. Kubono, M. S. Kwag, J. Liang, J. Y. Moon, S. Nishimura, S. Oka, S. Y. Park, A. Psaltis, T. Teranishi, Y. Ueno and L. Yang, "Isomer beam elastic scattering: ^{26m}Al(p, p) for astrophysics," EPJ Web Conf. **165**, 01030 (2017).*

H. Yamaguchi, D. Kahl, S. Hayakawa, L. Yang, H. Shimizu, Y. Sakaguchi, K. Abe, T. Nakao, T. Suhara, N. Iwasa, A. Kim, D.H. Kim, S.M. Cha, M.S. Kwag, J.H. Lee, E.J. Lee, K.Y. Chae, Y. Wakabayashi, N. Imai, N. Kitamura, P. Lee, J.Y. Moon, K.B. Lee, C. Akers, H.S. Jung, N.N. Duy, L.H. Khiem, C.S. Lee, T. Hashimoto, S. Kubono, T. Kawabata, T. Teranishi, Y.K. Kwon and D.N. Binh, "Nuclear astrophysics projects at the low-energy RI beam separator CRIB," EPJ Web Conf. **165**, 01056 (2017).*

Umakanth Dammalapati, Ken-ichi Harada, Tomohiro Hayamizu, Kosuke Sakamoto, Ko Kato, Takahiro Aoki, Sako Ito, Takeshi Inoue, Aiko Uchiyama, Hirokazu Kawamura, Masatoshi Itoh, Takatoshi Aoki, Atsushi Hatakeyama, Yasuhiro Sakemi, "Francium: Tool for Fundamental Symmetry Investigations," JPS Conf. Proc. **18**, 011046 (2017).*

M. Itoh, S. Ando, T. Aoki, H. Arikawa, S. Ezure, K. Harada, T. Hayamizu, T. Inoue, T. Ishikawa, K. Kato, H. Kawamura, Y. Sakemi, A. Uchiyama, "Measurement of the 3-α decay from the Hoyle and the broad 10 MeV states in ^{12}C," J. Phys. Conf. Ser. **863**, 012019 (2017).*

Oral Presentations

[International Conference etc.]

Y.Sakemi (invited), "Fundamental physics with ultracold radioactive atoms and molecules," MITP program "Low energy probes of new physics (LEPONP2017)," Mainz, Germany, May 14−24, 2017.

Y.Sakemi (invited), "Fundamental physics with cooled radioactive atoms ~ possible extension of Fr-EDM~," 10th International Conference on Nuclear Physics at Storage Rings (STORI2017), Kanazawa, Japan, Nov. 13−18, 2017.

H. Yamaguchi, "Nuclear astrophysics projects at the low-energy RI beam separator CRIB," The 8th Nuclear Physics in Astrophysics International conference (NPA8), INFN-LNS, Catania, Italy, Jun. 18–23, 2017.

S. Hayakawa, "Measurements of the ^{7}Be+n Big-Bang nucleosynthesis reactions at CRIB by the Trojan Horse method," The 8th Nuclear Physics in Astrophysics International Conference (NPA8), Catania, Italy, June 18–23, 2017.

H. Yamaguchi, "Indirect studies on astrophysical reactions at the low-energy RI beam separator CRIB," The 14th International Symposium on Origin of Matter and Evolution of the Galaxies (OMEG2017), Hotel ICC, Daejeon, Korea, Jun. 27–30, 2017.

S. Hayakawa, "Measurements of the neutron-induced reactions on ^{7}Be with CRIB by the Trojan Horse method," The 14th international symposium on Origin of Matter and Evolution of Galaxies (OMEG2017), Daejon, Rep. of Korea, Jun. 27–30 2017.

H. Yamaguchi (invited), "Direct measurements and detection techniques with low-energy RIBs," 9th European Summer School on Experimental Nuclear Astrophysics (Santa Tecla School), Hotel Santa Tecla Palace, Acireale, Italy, Sep. 17–24, 2017.

H. Shimizu, "Isomeric 26mAl Beam Production with CRIB," The 9th European Summer School on Experimental Nuclear Astrophysics, Hotel Santa Tecla Palace, Acireale, Italy, Sep. 17–24, 2017.

H. Yamaguchi (invited), "Studying nuclear astrophysics and nuclear clustering at the low-energy RI beam separator CRIB," The International Symposium on Physics of Unstable Nuclei 2017 (ISPUN2017), Wyndham Legende Halong Hotel, Halong, Vietnam, Sep. 25–30, 2017.

H. Yamaguchi (oral, invited), "Study on alpha-cluster states via resonant scattering with low-energy RI beams," Workshop on Nuclear Cluster Physics 2017 (WNCP2017), Hokkaido University, Sapporo, Japan, Oct. 25–27, 2017.

H. Yamaguchi, "CRIB and OEDO − the low energy RI beam facilities of CNS, the University of Tokyo," Nuclear Physics Seminar, Beihang University, Beijing, China, Nov. 10, 2017.

K. Yako(invited) "Exploring nuclear structure by double charge exchange reactions in Japan," Conference on Neutrino and Nuclear Physics (CNNP2017), University of Catania, Catania, Italy, Oct. 15–21, 2017.

S. Shimoura (Oral), "Reduction and resource recycling of high-level radioactive wastes through nuclear transmutation − Nuclear reaction data of long-lived fission products," International Nuclear Fuel Cycle Conference (GLOBAL2017), September 24–29, 2017, Seoul, Korea.

S. Shimoura (Invited), "New energy-degrading beam line OEDO in RIKEN RI beam factory," The International Symposium on Physics of Unstable Nuclei 2017 (ISPUN17), Halong City, Vietnam, September 25–30, 2017.

P. Schrock (oral), "Shell structure at the border of the island of inversion: Spectroscopy of neutron-rich Al isotopes." The International Symposium on Physics of Unstable Nuclei 2017 (ISPUN17), Halong City, Vietnam, September 25–30, 2017.

S. Shimoura (invited), "Tetra-neutron system studied by (^{8}He, ^{8}Be) reaction," Workshop on Nuclear Structure and Reaction Theories: Building Together for the Future, GANIL, Caen, France, October 9–13, 2017.

S. Shimoura (Invited), "Tetra-neutron system populated by RI-beam experiments," Critical Stability of Quantum Few-Body Systems (crit17), MPIPKS, Dresden, Germany, October 16–20, 2017.

S. Shimoura (invited), "Experimental studies of the tetra-neutron system by using RI-beam," The 23rd European Conference on Few-Body Problems in Physics, Aarhus, Denmark, Aug. 8–12, 2016.

S. Shimoura (invited), "Exotic nuclei studied by exotic reaction," Ito International Research Center (IIRC) Symposium "Perspectives of the Physics of Nuclear Structure," University of Tokyo, Tokyo, Japan, November 1–4, 2017.

S. Michimasa (invited), "Direct mass measurement of Calcium isotopes beyond $N = 34$," International symposium "Perspectives of the physics of nuclear structure," the University of Tokyo, Hongo, Tokyo, Japan, November 1–4, 2017.

S. Shimoura (invited), "Tetra-neutron system studied by ^{4}He(^{8}He, ^{8}Be)," Workshop on Nuclear Cluster Physics (WNCP2016), Kanto-Gakuin University, Yokohama, Japan, Oct. 17–21, 2016.

S. Shimoura (invited), "Tetra-neutron system populated by using RI-beam induced reaction," 第 6 回「中性子星の核物質」研究会, RIKEN Nishina Cenger, Wako, Saitama, Japan, Dec. 1–3, 2017.

N. Imai (Invited),「将来計画ＷＧ不安定核班第 2 期からの報告", RIBF 理論若手放談会：エキゾチック核物理の広がり」，理研神戸・融合連携イノベーション推進棟，Jul. 31–Aug. 2, 2017.

N. Imai, "Surrogate reaction of ^{79}Se(n,gamma)^{80}Se," ImPACT-OEDO workshop, RIBF conference room, Wako, Saitama, Japan, 2017/7/13-14.

M. Dozono, "p/d iduced reaction of ^{107}Pd," ImPACT-OEDO workshop, RIBF conference room, Wako, Saitama, Japan, 2017/7/13-14.

S. Michimasa, "Preliminary report of OEDO commissioning", ImPACT-OEDO workshop, 2017/7/13-14, RIBF conference room, Wako, Saitama, Japan.

N. Imai (invited), "Energy-degraded beam line at RIBF, OEDO," International Workshop on "Physics Opportunities using CAGRA and RCNP tracking Ge detector" (CAGRA17) Sigma Hall, Toyonaka Campus, Osaka University, Osaka, Japan, Oct 10-12, 2017.

P. Schrock (invited), "Transfer Reactions with CAGRA at OEDO," International Workshop on "Physics Opportunities using CAGRA and RCNP tracking Ge detector (CAGRA17)" Sigma Hall, Toyonaka Campus, Osaka University, Osaka, Japan, Oct 10−12, 2017.

O. Beliuskina, "The ultrafast dE-ToF sc diamond detector," International Workshop on "Physics Opportunities using CAGRA and RCNP tracking Ge detector (CAGRA17)" Sigma Hall, Toyonaka Campus, Osaka University, Osaka, Japan, Oct 10−12, 2017.

N. Imai (Invited),「OEDO を用いた低エネルギーLLFP の核反応データ取得」，東海村産業・情報プラザ (アイヴィル), 2017/11/16−17.

N. Imai (Invited), "Nuclear Data of LLFP and Future prospect of a new energy degraded beam line OEDO," RIBF Users group meeting, RIBF Conference Room, 2017/12/6.

O. Beliuskina (oral), "The ultrafast dE-ToF single crystal diamond detector", The 6th ADAMAS Workshop, November 27−28, 2017, Zagreb, Croatia.

S. Shimoura, "Direct Reaction," Rewriting Nuclear Physics Textbooks: Basic nuclear interactions and their link to nuclear processes in the cosmos and on earth, Pisa, Italy, July 24−28, 2017.

S. Ota, "Nuclear matter from low-energy reaction," OEDO Workshop, CNS Wako campus, Saitama, Japan, Jul.15, 2017.

S. Ota, "Equation of state of nuclear matter from direct reactions," Workshop on RI and Heavy-ion science, Ewha womans university, Seoul, Korea, Oct. 19−20, 2017.

S. Ota, "Active targets CAT's for missing mass spectroscopy with high-intensity beams," Workshop on active targets and time projection chambers for high-intensity and heavy-ion beams in nuclear physics, Santiago de Compostela University, Spain, Jan. 17−19.

T. Otsuka, "Quantum self-organization and nuclear shapes," Advances in Radioactive Isotope Science, ARIS2017, USA, June 2017.

T. Otsuka, "Twenty years ago, twenty years later," Perspectives of physics of nuclear structure, Tokyo, Japan, November 2017.

T. Otsuka, "Impact to shell model, impact of shell model," Probing fundamental interactions by low energy excitations, Stockholm, Sweden, June 2017.

T. Otsuka, "Single-particle states vs. collective modes: friends or enemies," Shapes and symmetries in nuclei: from experiment to theory, France,

November 2017.

T. Otsuka, "Quantum self-organization and the structure evolution of atomic nuclei," international symposium on physics of unstable nuclei 2017, Hanoi, Vietnam, September 2017.

T. Otsuka, "Suppression of double-beta decay and quadrupole pairing," Nuclear ab initio theories and neutrino physics, Seattle, USA, March 2018.

T. Otsuka, "Quantum self-organization and nuclear collectivity," IVth Topical workshop on modern aspects in nuclear structure, Bormio Italy, February 2018.

T. Otsuka, "Single-particle states vs. collective modes: friends or enemies?" 16th International symposium on capture gamma-ray spectroscopy and related topics (CGS16), Shanghai, China, September 2017.

T. Otsuka, "Beauty and the Quantum," Academia Europaea Section Initiated Workshop - Inaugural Lectures by New Members of Physics and Engineering Sciences, Budapest Hungary, September 2017.

T. Otsuka, "Quantum self-organization and nuclear collectivities," 12th International spring seminar on nuclear physics, current problems and prospects for nuclear structure, Ischia Italy, May 2017.

T. Otsuka, "Shell-model challenges to gamma-ray spectroscopy," NUSPIN2017, GSI, Germany, June 2017.

T. Otsuka, "Shape coexistence and quantum phase transition in the Monte-Carlo Shell Model," Shape coexistence and electric monopole transitions, Salay, France, October 2017.

T. Otsuka, "Cluster and molecular structure emerging from ab initio Monte Carlo Shell Model calculations," 2nd International Workshop on Nuclear Cluster Physics (WNCP2017), Sapporo, Japan, October 2017.

T. Otsuka, "Quantum self-organization in atomic nuclei," The COPIGAL Meeting on recent results and future projects involving PARIS, AGATA, NEDA, and FAZIA detectors, Krakow, Poland, December 2017.

T. Otsuka, "Perspectives of the shell model on and beyond monopole," First Workshop on Nuclear Shell Model Developments and Applications in Eastern Asia (NuSEA2018), Shanghai, China, March 2018.

N. Shimizu, "Double Gamow-Teller transition and its relation to neutrinoless double beta decay," Nuclear ab initio Theories and Neutrino Physics, Seattle, USA, March 2018.

N. Shimizu, "Shell model study on a double-beta decay nucleus ^{48}Ca," Probing Fundamental Interactions by Low Energy Excitations, KTH Royal Institute of Technology, Stockholm, Sweden, June 2017.

T. Miyagi, "Recent progress in the unitary-model-operator approach," TRIUMF workshop on Progress in Ab Initio Techniques in Nuclear Physics, Vancouver, Canada, March 2018.

T. Miyagi, "Unitary-model-operator approach calculations with the chiral NN+3N forces," 16th CNS Summer School, RIKEN, Wako, Japan, August 2017.

T. Miyagi, "Ground-state energies and radii from the unitary-model-operator approach," Probing fundamental interactions by low energy excitations -Advances in theoretical nuclear physics, Royal Institute of Technology, Stockholm, Sweden, June 2017.

Y. Utsuno, "Shell-model study for the $A \sim 130$ region," Gif-Sur-Yvette, France (Conference "Shapes and Symmetries in Nuclei: from Experiment to Theory (SSNET'17)"), November 2017.

Y. Utsuno, "Consistent description of shell gaps and deformed states around O-16 and Ca-40," Mumbai, India (Conference "Frontiers in Gamma Ray Spectroscopy (FIG18)"), March 2018.

T. Abe, "Advances in the Monte Carlo Shell Model for Understanding Nuclear Structure," Ito International Center (IIRC) Symposium "Perspectives of the Physics of Nuclear Structure," Ito Hall, the University of Tokyo, November 2017.

T. Abe, "Recent advances in the no-core Monte Carlo shell model," Progress in Ab Initio Techniques in Nuclear Physics, TRIUMF, Canada, March 2018.

Y. Tsunoda, "Monte Carlo shell model calculations for structure of nuclei around $Z = 28$," IVth Topical Workshop on Modern Aspects in Nuclear Structure, Bormio, Italy, February 2018.

Y. Tsunoda, "Nuclear structure studied by Monte Carlo shell model calculations," NUSTAR Annual Meeting 2018, GSI, Darmstadt, Germany, March 2018.

N. Tsunoda, "Exotic neutron-rich medium-mass nuclei with realistic nuclear force," Keystone ARIS2017, May 2017.

N. Tsunoda, "Structure of exotic nuclei based on nuclear force," Perspective of physics of nuclear structure, Tokyo, Japan, November 2017.

N. Tsunoda, "Many body perturbation theory for the effective interaction for the shell model calculation and its application to island of inversion," Leuven-Tokyo mini workshop, Tokyo, Japan, March 2018.

J. Menéndez, "Nuclear matrix elements for double-beta decay: present and future," Solvay workshop "Beyond the Standard model with Neutrinos and Nuclear Physics", Brussels (Belgium), November 30, 2017.

J. Menéndez, "Nuclear Matrix Elements for Fundamental Symmetries," Perspective of the Physics of Nuclear Structure Conference, Tokyo (Japan), November 4, 2017.

J. Menéndez, "Double Gamow-Teller transition of ^{48}Ca and its relation to neutrinoless double-beta decay," Conference on Neutrino and Nuclear Physics (CNNP2017), Catania (Italy), October 17, 2017.

J. Menéndez, "The interplay of nuclear structure with β and double-β decays," International Symposium on Physics of Unstable Nuclei 2017 (ISPUN17), Halong City (Vietnam), September 26, 2017.

J. Menéndez, "Status of neutrinoless double-beta decay nuclear matrix elements," Recent developments in neutrino physics and astrophysics workshop, Gran Sasso (Italy), September 6, 2017.

J. Menéndez, "Which nuclear data and correlations can constrain neutrinoless double-beta decay matrix elements?" INT Program "Neutrinoless Double-beta Decay," Seattle (USA), June 21, 2017.

[Domestic Conference]

S. Hayashi, "J/psi production in heavy ion collisions," Heavy Ion Café, RIKEN, Wako, Japan, January 13, 2018.

S. Hayakawa, 「CRIB での ^{7}Be ビームを用いたビッグバン元素合成反応の測定」, X 線天体と元素合成を中心とする宇宙核物理研究会, RIKEN,

Wako, Japan, July 20–21, 2017.

H.Shimizu,「CRIB における ^{26}Al 核異性体の陽子弾性共鳴散乱実験」, X 線天体と元素合成を中心とする宇宙核物理研究会, RIKEN, Wako, Japan, July 20–21, 2017.

山口英斉, 「α 共鳴散乱による不安定核クラスター状態の研究」, RCNP 研究会「核子・ストレンジネス多体系におけるクラスター現象」大阪大学核物理研究センター, Aug 3−5, 2017.

S. Michimasa *et al.*,「LLFP 安定核種化・短寿命化のための核変換法の開発 (6) OEDO ビームラインの性能評価」, AESJ Fall meeting, Hokkaido University, Sapporo, Hokkaido, Japan, Sept. 13–15.

S. OTA, "Matter dominant universe through nuclear physics,'' High school lecture for Fukuoka Prefectural Chikushigaoka High School, CNS Wako campus, Saitama, Japan, Aug. 1, 2017.

S. Michimasa, 「SHARAQ スペクトロメータを用いた中性子過剰核の直接質量測定」, 第 7 回先導原子力研コロキウム, Tokyo Institute of Technology, Meguro, Tokyo, Japan, July 21, 2017.

S. Shimoura, 「エキゾチック原子核の世界」, 集中講義, 立教大学, June 9, 16, 23, 2017.

N. Imai, 「不安定核物理の将来,'' JPA Fall meeting, Utsunomiya University, Utsunomiya, Tochigi, Japan, Sept. 12−15, 2017.

T. Gunji, 「高エネルギー重イオン衝突による物理の将来」, JPA Fall meeting, Utsunomiya University, Utsunomiya, Tochigi, Japan, Sept. 12–15, 2017.

S. Hayashi, "Inclusive J/psi measurement in *p*-Pb collisions with the ALICE detector," JPS Autumn Meeting 2017, Utsunomiya University, Utsunomiya, Japan, September 12–15, 2017.

Y. Sekiguchi for the ALICE collaboration, "Study of particle correlations in *p*-Pb collisions with ALICE detector," 日本物理学会 2017 年秋季大会, 宇都宮大学, 峰キャンパス, 2017 年 9 月 12–15 日.

H. Murakami for the ALICE collaboration, "Status of direct photon measurement in small systems with ALICE," 日本物理学会 2017 年秋季大会 宇都宮大学, 2017 年 9 月 12–15 日.

早川勢也 (oral), 「トロイの木馬法による ^{7}Be+n ビッグバン元素合成反応の測定 II」, 日本物理学会　2017 年秋季大会, 宇都宮大学, 2017 年 9 月 12–15 日.

N. Kitamura *et al.*,「TRIUMF におけるトリチウム標的の評価」, JPS Fall meeting, Utsunomiya University, Utsunomiya, Tochigi, Japan, Sept. 12–15, 2017.

K. Kawata *et al.*,「^{58}Ni の入射核破砕反応による高スピンアイソマービームの生成」, JPS Fall meeting, Utsunomiya University, Utsunomiya, Tochigi, Japan, Sept. 12–15, 2017.

C. Iwamoto *et al.*,「ガスアクティブ標的 CAT の大型化に向けた二重増幅率抑制型多層 THGEM の開発」, JPS Fall meeting, Utsunomiya University, Utsunomiya, Tochigi, Japan, Sept. 12–15, 2017.

S. Michimasa *et al.*,「低速 RI ビームを用いた LLFP 核の核反応断面積測定」, AESJ Spring meeting, Osaka University, Osaka, Japan, Mar. 26–28.

M. Dozono *et al.*, 「低速 RI ビームを用いた ^{107}Pd, ^{93}Zr の陽子および重陽子誘起反応測定」, AESJ Spring meeting, Osaka University, Osaka, Japan, Mar. 26–28.

大塚孝治, 「核力と原子核の基本的性質」, 「原子核多体問題の進展と展望」, 軽井沢, 2017 年 6 月.

清水則孝, 「ベイズ統計による殻模型計算の解析」, 素粒子・原子核・宇宙「京からポスト京に向けて」シンポジウム, 筑波大学文京校舎, 2017 年 12 月.

清水則孝, 「殻模型計算による核準位密度の微視的記述」, 2017 年度核データ研究会, 茨城県東海村, 東海駅前・アイヴィル, 2017 年 11 月.

清水則孝, 「ボゴリューボフ準粒子基底によるモンテカルロ殻模型」, 日本物理学会 2017 年秋季大会 (宇都宮大学峰キャンパス), 2017 年 9 月.

宮城宇志, 「3 体力効果を取り込んだ UMOA 計算」, 日本物理学会 2017 年秋季大会, 宇都宮大学, 峰キャンパス, 2017 年 9 月.

宮城宇志, 「中重核における 3 体力の効果」, RIBF 理論若手放談会：エキゾチック核物理の広がり, 理化学研究所, 神戸キャンパス, 2017 年 8 月.

角田佑介, 「モンテカルロ殻模型による原子核形状の研究」, RIBF 理論若手放談会：エキゾチック核物理の広がり, 理化学研究所神戸キャンパス, 2017 年 7 月.

角田佑介, 「モンテカルロ殻模型による Sm 同位体の形状変化の研究」, 日本物理学会 2017 年秋季大会, 宇都宮大学峰キャンパス, 2017 年 9 月.

角田佑介, 「中重核・重い原子核の形状のモンテカルロ殻模型による研究」, 素粒子・原子核・宇宙「京からポスト京に向けて」シンポジウム, 筑波大学東京キャンパス文京校舎, 2017 年 12 月.

角田佑介, 「Sm 同位体の形状変化のモンテカルロ殻模型による研究」, 日本物理学会第 73 回年次大会, 東京理科大学野田キャンパス, 2018 年 3 月.

角田佑介, 「量子自己組織化と原子核の集団性」, 研究会「量子クラスターで読み解く物質の階層構造」, 東京工業大学大岡山キャンパス, 2018 年 3 月.

角田直文, 「Medium-mass nuclei from nuclear force」, 京都大学 基研研究会「核力に基づく核構造・核反応物理の展開」, 2017 年 3 月.

角田直文, 「核力と中性子過剰核の構造」, 理研神戸・融合連携イノベーション推進棟 RIBF 若手放談会「エキゾチック核物理の広がり」, 2017 年 7–8 月.

角田直文, 「中性子過剰な Mg 同位体の新たな様相」, 宇都宮大学 日本物理学会 2017 年秋季大会, 2017 年 9 月.

角田直文, 「原子核殻模型における統計力学的考察」, 宇都宮大学 日本物理学会 2017 年秋季大会, 2017 年 9 月.

角田直文, 「現実的核力に基づく多殻有効相互作用の構築と中性子過剰核への適用」, 東京理科大学 日本物理学会第 73 回年次大会, 2018 年 3 月.

富樫智章, 「Zr 同位体近傍における形の量子相転移のモンテカルロ殻模型による研究」, 宇都宮大学, 日本物理学会 2017 年秋季大会, 2017 年 9 月.

富樫智章, 「大規模殻模型計算による中性子過剰 N=82 近傍の半減期の計算」, 宇都宮大学, 日本物理学会 2017 年秋季大会, 2017 年 9 月.

富樫智章, 「モンテカルロ殻模型による Sn 同位体の系統的研究」, 東京理科大学, 日本物理学会第 73 回年次大会, 2018 年 3 月.

小高康照他, 「空間電荷効果を導入した理研 AVF サイクロトロン入射軌道解析」, 第 14 回日本加速器学会年会, 北海道札幌市, 北海道大学,

2016 年 8 月 1–3 日.

大城幸光(oral),「CNS イオン源の現状」, 第 14 回 AVF 合同打合せ, 福島県立医科大学, 2017 年 6 月 29−30 日.

小高康照(oral),「4 次元エミッタンス測定値を用いた AVF 入射軌道解析(2)」, 第 14 回 AVF 合同打合せ, 福島県立医科大学, 2017 年 6 月 29–30 日.

大城幸光(oral),「CNS イオン源の現状」, 第 15 回 AVF 合同打合せ, 大阪大学 RCNP, 2018 年 2 月 26–27 日.

小高康照(oral),「AVF 入射軌道解析の現状」, 第 15 回 AVF 合同打合せ, 大阪大学 RCNP, 2018 年 2 月 26–27 日.

Poster Presentations

[International Conference etc.]

T. Miyagi, "Nuclear ab initio calculations with the unitary-model-operator approach," Perspective of the physics of the nuclear structure, Tokyo, Japan, November 2017.

Y. Tsunoda, "Shapes of medium and heavy nuclei studied by Monte Carlo shell model calculations," Ito International Research Center (IIRC) symposium "Perspectives of the physics of nuclear structure," Tokyo, Japan, November 2017.

H. Shimizu: "^{26m}Al beam production and decay measurement at CRIB," The 14th international symposium on Origin of Matter and Evolution of Galaxies (OMEG2017), Jun. 27–30, 2017, Daejeon, Korea.

Partner Institution
Center for Radioactive Ion Beam Sciences
Institute of Natural Science and Technology, Niigata University

1. Abstract

   The Center for Radioactive Ion Beam Sciences, Niigata University, aims at uncovering the properties of atomic nuclei and heavy elements and their roles in the synthesis of elements, with use of the advanced techniques of heavy ion and radioactive ion beam experiments as well as the theoretical methods. Main research subjects include the measurements of various reaction cross sections and moments of neutron- or proton-rich nuclei, synthesis of super-heavy elements and radio-chemical studies of heavy nuclei, and theoretical studies of exotic nuclei based on quantum many-body methods and various nuclear models. In addition, we promote interdisciplinary researches related to the radioactive ion beam sciences, such as applications of radioactive isotopes and radiation techniques to material sciences, nuclear engineering and medicine. Many of them are performed in collaboration with RIKEN Nishina Center and with use of the RIBF facilities. The center emphasizes also its function of graduate education in corporation with the Graduate School of Science and Technology, Niigata University, which invites three researchers in RIKEN Nishina Center as visiting professors.

2. Major Research Subjects

(1) Reaction cross section and radii of neutron-rich nuclei
(2) Production of superheavy nuclei and radiochemistry of heavy elements
(3) Nuclear theory

3. Summary of Research Activity

(1) Measurements of matter and charge radii of exotic nuclei

   The experimental nuclear physics group has studied the nuclear structures of exotic nuclei through the measurements of nuclear matter radii. The nuclear matter radii can be determined from interaction cross sections with the use of nuclear reaction model. At RIBF, RIKEN, we have performed experiments to measure interaction cross sections of F, Ne, Na, Mg, and Al isotopes and clarified the halo structure of ^{31}Ne, and also the development of strong deformation in those isotopes, $^{28-32}$Ne, $^{32-38}$Mg, which are located around and beyond the "island of inversion" region. Recently our new project to explore the equation of state (EOS) of nuclear matter has been started. For the understanding of the EOS of asymmetric nuclear matter, either highly proton deficient or neutron deficient, the investigation of the development of neutron skin thickness in the exotic nuclei give the crucial information. We have measured interaction cross sections and charge changing cross sections for $^{58-78}$Ni using BigRIPS fragments separator at RIBF in FY2016. While nuclear matter radii can be determined from interaction cross sections, the proton distribution radii will be determined from charge-changing cross sections, thus neutron skin thickness will be obtained. The data analysis are in progress.

(2) Production of superheavy nuclei and radiochemistry of heavy elements

The nuclear chemistry group has been investigating decay properties of super-heavy nuclei, measured the excitation functions of rutherfordium isotopes, and clarified the ambiguity of the assignment of a few-second spontaneously fissioning isotope of ^{261}Rf. The new equipment designed for measurement of short-lived alpha emitters is under development.

For the chemistry research of super-heavy elements, preparatory experiments, such as solvent extraction for the group 4, 5, and 6th elements and gaseous phase chemistry for group-4 elements, have been performed using radioisotopes of corresponding homolog elements.

(4) Nuclear theory

   One of the main activities of the nuclear theory group concerns with developments of the nuclear density functional theory and exploration of novel correlations and excitations in exotic nuclei. A fully selfconsistent scheme of the (quasiparticle) random phase approximation (QRPA) on top of the Skyrme-Hartree-Fock-Bogoliubov mean-field has been applied not only for spherical nuclei but also for deformed nuclei. The model is used to study the low-lying dipole excitation in neutron-rich nuclei in order to investigate the relation between the low-lying strength and the equation of state (EOS) of asymmetric nuclear matter. The QRPA in the density functional framework has been developed in various directions. The continuum QRPA, which describes not only collective correlations but also coupling to unbound continuum states of nucleons, has been applied to describe the direct neutron capture reaction in the r-process nucleosynthesis. The QRPA is recently applied to describe collective excitation in inner crust of neutron stars. The continuum quasiparticle states are also analyzed to study possible pairing effects on low-lying p-wave resonances and s-wave scattering states in unbound odd-N nuclei. Cluster structure and the ab initio studies of light nuclei are also important research subjects of the theory group. A new direction of theoretical study is initiated in this fiscal year toward a fully microscopic description of low-energy heavy ion dynamics using the time-dependent Hartree-Fock theory. The model has been applied to describe multi-nucleon transfer reaction to form heavy neutron-rich nuclei, and fusion process to form superheavy nuclei.

Members

Director
Masayuki MATSUO (Professor)

Scientific Staff
Takashi OHTSUBO (Associate Professor)
Shin-ichi GOTO (Associate Professor)
Shigeyoshi AOYAMA (Associate Professor)
Takuji IZUMIKAWA (Associate Professor)

Kazuyuki SEKIZAWA (Assistant Professor)
Kazuhiro OOE (Assistant Professor)
Jun GOTO (Assistant Professor)
Maya TAKECHI (Assistant Professor)

Post Doctoral Associates
Tsunenori INAKURA

List of Publications & Presentations

Publications
[Journal]
(Original Papers) *Subject to Peer Review

J. Goto, M. Oshima, M. Sugawara, Y. Yamaguchi, C. Bi, S. Bamba, T. Morimoto, "Introduction of multiple γ-ray detection to charged particle activation analysis", J. Radioanal. Nucl. Chem. **314**, 1707–1714 (2017).*

H.N. Liu , J. Lee, P. Doornenbal, H. Scheit, S. Takeuchi, N. Aoi, K.A. Li, M. Matsushita, D. Steppenbeck, H. Wang, H. Baba, E. Ideguchi, N. Kobayashi, Y. Kondo, G. Lee, S. Michimasa, T. Motobayashi, A. Poves, H. Sakurai, M. Takechi, Y. Togano, J.A. Tostevin, Y. Utsuno: "Intruder configurations in the ground state of ^{30}Ne", Phys. Lett. B **767**, 58 (2017).*

P. Doornenbal, H. Scheit, S. Takeuchi, Y. Utsuno, N. Aoi, K. Li, M. Matsushita, D. Steppenbeck, H. Wang, H. Baba, E.Ideguchi, N. Kobayashi, Y. Kondo, J. Lee, S.Michimasa, T. Motobayashi, T. Otsuka, H. Sakurai, M. Takechi, Y. Togano, and K. Yoneda : "Low-Z shore of the "island of inversion" and the reduced neutron magicity toward ^{28}O", Phy. Rev. C **95**, 041301(R) (2017).*

D. Kaji, K. Morimoto, H. Haba, Y. Wakabayashi, M. Takeyama, S. Yamaki, Y. Komori, S. Yanou, S. Goto, K. Morita, "Decay Measurement of ^{283}Cn Produced in the ^{238}U(^{48}Ca, 3n) Reaction Using GARIS-II", Journal of Physical Society of Japan **86**, 085001(2) (2017).*

N. Nakatsuka, H. Baba, T. Aumann, R. Avigo, S.R. Banerjee, A. Bracco, C. Caesar, F. Camera, S. Ceruti, S. Chen, V. Derya, P. Doornenbal, A. Giaz, A. Horvat, K. Ieki, T. Inakura, N. Imai, T. Kawabata, N. Kobayashi, Y. Kondo, S. Koyama, M. Kurata-Nishimura, S. Masuoka, M. Matsushita, S. Michimasa, B. Million, T. Motobayashi, T. Murakami, T. Nakamura, T. Ohnishi, H.J. Ong, S. Ota, H. Otsu, T. Ozaki, A. Saito, H. Sakurai, H. Scheit, F. Schindler, P. Schrock, Y. Shiga, M. Shikata, S. Shimoura, D. Steppenbeck, T. Sumikama, I. Syndikus, H. Takeda, S. Takeuchi, A. Tamii, R. Taniuchi, Y. Togano, J. Tscheuschner, J. Tsubota, H. Wang, O. Wieland, K. Wimmer, Y. Yamaguchi, K. Yoneda, J. Zenihiro, "Observation of isoscalar and isovector dipole excitations in neutron-rich ^{20}O", Phys. Lett. B **768**, 387–392 (2017).*

Oral Presentations
[International Conference etc.]

K. Shirai, S. Goto, K. Ooe, H. Kudo, "Influence of Surface Condition of Quartz Column for Gas Chromatoraphic Behaviors of $ZrCl_4$ and $HfCl_4$", 6th Asia-Pacific Symposium on Radiochemistry (APSORC17), Jeju, Korea, September 17–22, 2017.

T. Tomitsuka, Y. Kaneya, T. K. Sato, M. Asai, K. Tsukada, A. Toyoshima, A. Mitsukai, A. Osa, K. Nishio, Y. Nagame, K. Ooe, M. Sakama, S. Miyashita, M. Shibata, Y. Kasamatsu, R. Eichler, C. E. Düllmann, N. Trautmann, J. V. Kratz, M. Schädel, "Adsorption of Lawrencium (Z = 103) on a Tantalum Surface", 6th Asia-Pacific Symposium on Radiochemistry (APSORC17), Jeju, Korea, September 17–22, 2017.

K. Shirai, S. Goto, K. Ooe, H. Kudo, "Off-line experiment of gas chromatography for $ZrCl_4$ and $HfCl_4$ using a chlorinated column", 9th Workshop on the Chemistry of the Heaviest Element (CHE9), Ascona, Switzerland, October 8–11, 2017.

T. Inakura, M. Matsuo, Anderson-Bogoliubov phonon in inner crust of neutron star, Interdisciplinary symposium on modern density functional theory (iDFT), RIKEN, June 19–23, 2017.

[Domestic Conference]

J. Goto, T. Takahashi, R. Endo, Y. Fukushima, H. Yoshida, M. Nishikata, Y. Shobugawa and M. Naito,「ASURA を用いた最近の調査の紹介」, 第 5 回「原発事故被災地域における放射線量マッピングシステムの技術開発・運用とデータ解析に関する研究会」, 京都大学原子炉実験所, 2018 年 2 月 27 日.

J. Goto, T. Takahashi, R. Endo, Y. Fukushima and H. Yoshida,「常磐自動車道における放射線の分布状況調査（4）ASURA を用いた道路上の放射性セシウム沈着量調査」, 日本原子力学会 2018 年春の年会, 大阪大学吹田キャンパス, 2018 年 3 月 26–28 日.

S. Goto, D. Kaji, S. Tsuchiya, R. Aono, K. Morimoto, H. Haba, K. Ooe, H. Kudo,「^{254}Rf の自発核分裂における核分裂片の全運動エネルギー測定」, 第 61 回放射化学討論会, 筑波大学筑波キャンパス, 9 月 (2017).

D. Sato, M. Murakami, S. Goto, K. Ooe, R. Motoyama, K. Shirai, R. Yamada, S. Tsuchiya, T. Morimoto, H. Haba, Y. Komori, S. Yano, A. Toyoshima, A. Mitsukai, H. Kikunaga, H. Kudo,「105 番元素 Db に対する Aliquat336 樹脂を用いたフッ化水素酸系逆相クロマトグラフィー」, 第 61 回放射化学討論会, 筑波大学筑波キャンパス, 9 月 (2017).

S. Goto,「新潟大における Zr,Hf および Rf 塩化物の気相化学研究および今後の計画」, 東北大学ワークショップ「アクチノイド元素の科学と技術」・第 9 回アルファ放射体実験室利用研究会, 東北大学金属材料研究所 2 号館講堂, 11 月 (2017).

稲倉恒法,「中性子星内殻における超流動中性子と原子核の集団運動」, 新学術領域「実験と観測で解き明かす中性子星の核物質」第 6 回「中性子星の核物質」研究会, 理研, 12 月 (2017).

稲倉恒法, 「中性子星内殻における超流動中性子と原子核の集団運動：双極モードと四重極モード」, 新学術領域「実験と観測で解き明かす中性子星の核物質」理論班主催研究会「中性子星核物質」, 熱海, 2 月 (2018).

Poster Presentations

[International Conference etc.]

J. Goto, M. Oshima, H. Kumada, Y. Yamaguchi, S. Bamba, C. Bi and T. Morimoto, "Study of charged particle activation analysis -optimal configuration of γ-ray detectors for a sample with strong background from positron annihilation-," YBNCT9, Kyoto, Japan, November 13–15, 2017.

[Domestic Conference]

K. Shirai, S. Goto, K. Ooe, H. Kudo,「Zr, Hf 塩化物の等温クロマトグラフィにおけるカラム通過挙動に対する分子数の影響」, 第 61 回放射化学討論会, 筑波大学筑波キャンパス, 9 月 (2017).

K. Ooe, S. Kusakari, S. Goto, H. Kudo, H. Haba, Y. Komori,「Rf の同族元素 Zr, Hf の 2-フロイルトリフルオロアセトンを用いた溶媒抽出」, 第 61 回放射化学討論会, 筑波大学筑波キャンパス, 9 月 (2017).

T. Tomitsuka, K. Tokoi, T. Sato, M. Asai, K. Tsukada, A. Toyoshima, N. M. Ciera, Y. Kamata, Y. Nagame, S. Goto,「103 番元素ローレンシウムの価電子構造決定に向けた低速原子ビーム取り出し技術の開発」, 第 61 回放射化学討論会, 筑波大学筑波キャンパス, 9 月 (2017).

Partner Institution
Wako Nuclear Science Center, IPNS (Institute of Particle and Nuclear Studies)
KEK (High Energy Accelerator Research Organization)

1. Abstract

The KEK Isotope Separation System (KISS) has been constructed to experimentally study the β-decay properties of unknown neutron-rich nuclei near the neutron magic number $N = 126$, which are of interest in astrophysics. A new rotating target system was introduced and higher yields and more stable operational conditions were achieved. Resonance ionization spectroscopy for the hyperfine structure of ^{199}Pt was performed at KISS. An international collaboration with the Institute of Basic Science (IBS), Korea, has been organized. As part of this collaboration, an array of super-clover germanium detectors was installed. A new project for comprehensive mass measurements with MRTOF mass spectrograph at KISS and other devices has started in collaboration with the RIKEN SLOWRI team.

2. Major Research Subjects

(1)   Production and manipulation of radioactive isotope beams for nuclear experiments.
(2)   Explosive nucleosynthesis (r- and rp-process).
(3)   Heavy ion reaction mechanism for producing heavy neutron-rich nuclei.
(4)   Development of MRTOF mass spectrograph for short-lived heavy nuclei.
(5)   Development of RNB probes for materials science applications.

3. Summary of Research Activity

KISS is an element-selective isotope separator, combining the use of a magnetic mass separator with in-gas-cell resonant laser ionization. The gas cell, filled with argon gas at 75 kPa, is a central component of KISS, from which only the elements of interest are extracted as an ion beam for subsequent mass separation. In the cell, nuclei primarily produced by low-energy heavy-ion reactions are stopped (thermalization and neutralization), transported by a buffer gas (gas flow of ~75 kPa argon in the present case), and then re-ionized by laser irradiation just before the exit. The gas cell was fabricated to efficiently collect the reaction products produced by multi-nucleon transfer (MNT) reactions in the ^{136}Xe + ^{198}Pt system. For the first extraction of the reaction products, the ^{136}Xe beam energy and ^{198}Pt target thickness were set at 10.8 MeV/nucleon and 6 mg/cm^2, respectively. In FY2014, the half-life of ^{199}Pt was measured with β-ray telescopes and a tape transport system located at the focal point of KISS. The β-ray telescopes were composed of three double-layered thin plastic scintillators; the thicknesses of the first and second layers were 0.5 mm and 1 mm, respectively. In order to reduce the background, low-activity lead blocks and a veto counter system consisting of plastic scintillator bars surrounded the telescopes. The background rate of these β-ray telescopes was measured to be 0.7 counts per second. For further reduction of the background rate to as low as 0.1 counts per hour, a gas counter-based beta-ray telescope system was installed in FY2016. An array of germanium detectors consisting of four super-clover germanium crystals was also brought into operation in FY2016. Using these setups, new isomeric state in ^{195}Os were discovered and the half-lives of ^{197}Os and ^{198}Os, respectively, were revised and determined for the first time.

For higher primary beam intensities and a higher extraction efficiency, a doughnut-shaped gas cell with a rotating target wheel setup has been developed for KISS. Using this setup, resonance ionization spectroscopy of the ground-state hyperfine structure of Pt and Ir was performed. The nuclear g-factor and charge radius of the ground state and an isomeric state of ^{199}Pt were deduced from the experimental results. For further improvement of spectral resolution of the hyperfine structure measurements, an in-gas-jet laser ionization setup utilizing an S-shaped RF ion guide and a new laser system consisting of a 10 kHz Nd:YAG pump laser and a dye amplifier seeded by a narrow-band diode laser have been installed.

Cross-section measurements were performed at GANIL in 2012 to investigate the feasibility of using MNT in the reaction system of ^{136}Xe on ^{198}Pt to produce heavy neutron-rich isotopes around a mass number of 200 with the neutron magic number 126; the analysis of the data has been completed. The cross sections of target-like fragments around $N=126$ were comparable to those estimated using the GRAZING code, and their main contributions appear to be from the reactions having a low total energy loss with weak N/Z equilibration and particle evaporation. This suggests the use of the MNT reactions with a heavy projectile at energies above the Coulomb barrier could be a promising means for the production of neutron-rich isotopes around $N = 126$.

The multi-reflection time-of-flight mass spectrograph (MRTOF-MS) has been developed for direct mass measurements of short-lived heavy nuclei at KISS and other facilities. In FY2016, mass measurements of more than 80 nuclides, including short-lived ($T_{1/2} = 10$ ms) isotopes of Ra and several isotopes of the trans-uranium elements Es and Md were performed at GARIS-II in collaboration with the SLOWRI team and the Super Heavy Element Synthesis team of RIKEN. The highest precisions, achieved for Ga isotopes, reached a level of 0.03 ppm. For most of the well-known nuclides, agreement with the literature mass values was found. However, discrepancies were found in some literature values derived from pre-1980 indirect measurements. This suggests that such indirect measurements must be revised with comprehensive direct mass measurements. The masses of four isotopes of Es and Md were measured for the first time, allowing for confirmation of the $N = 152$ shell closure in Md. Using these new mass data as anchor points, the masses of seven isotopes of super-heavy elements up to Mt were indirectly determined and comparisons with various nuclear mass models were performed.

The diffusion coefficient of lithium in solid materials used in secondary Li-ion batteries is one of the key parameters that determine how fast a battery can be charged. The reported Li diffusion coefficients in solid battery materials scatter over several orders of magnitude. An in-situ nanoscale diffusion measurement method using α-emitting radioactive ^{8}Li as a tracer has been developed. In this method, while implanting

a pulsed 8 keV beam of ^{8}Li, the α-particles emitted at small angles ($\theta = 10 \pm 1\circ$) relative to the sample surface were detected as a function of time. The Li diffusion coefficient could then be determined from the time-dependent yields of the α particles, the energy loss of which can be converted to nanometer-scale position information of diffused ^{8}Li. The method has been successfully applied to measure the lithium diffusion coefficients for amorphous Li_4SiO_4-Li_3VO_4 (LVSO) which was used as a solid electrolyte in a solid-state Li thin-film battery, well demonstrating that the present method is sensitive to diffusion coefficients down to the level of 10^{-12} cm^2/s, which corresponds with nanoscale Li diffusion. In FY2016, this method was used to determine Li diffusion coefficients in a spinel-type Li compound $LiMn_2O_4$ (LMO), which is used as the anode of Li batteries in electric vehicles. A significant change in the time dependent yields of the α particles was observed at a sample temperature of approximately 623 K and the measurements will be continued in order to obtain the temperature dependence of Li diffusion coefficients in LMO.

Members

Group Leader
Hiroari MIYATAKE

Researchers
Michiharu WADA   Yoshikazu HIRAYAMA
Yutaka WATANABE   Peter SCHURY

Technical Staff
Yutaka KAKIGUCHI   Michihiro OYAIZU

Visiting Researchers
Jun-young Moon (IBS)   Hyun-suk Choi (Seoul National University)
Jin-hyung Park (IBS)

Student Trainees
Momo MUKAI (PhD. Student, Tsukuba Univ.)   Murad AHMED MD (PhD. Student, Tsukuba Univ.)
Sota KIMURA (PhD. Student, Tsukuba Univ.)

Assistant
Machiko IZAWA

List of Publications & Presentations

Publications
[Journal]
(Original Papers) *Subject to Peer Review

Y. Ito, P. Schury, M. Wada, F. Arai, H. Haba, Y. Hirayama, S. Ishizawa, D. Kaji, S. Kimura, H. Koura, M. MacCormick, H. Miyatake, J. Y. Moon, K. Morimoto, K. Morita, M. Mukai, I. Murray, T. Niwase, K. Okada, A. Ozawa, M. Rosenbusch, A. Takamine, T. Tanaka, Y. X. Watanabe, H. Wollnik, and S. Yamaki, "First direct mass measurements of nuclides around $Z = 100$ with a multireflection Time-of-flight mass spectrograph," Phys. Rev. Lett. **120**, 152501 (2018).*

M. Mukai, Y. Hirayama, Y.X. Watanabe, P. Schury, H.S. Jung, M. Ahmed, H. Haba, H. Ishiyama, S.C. Jeong, Y. Kakiguchi, S. Kimura, J.Y. Moon, M. Oyaizu, A. Ozawa, J.H. Park, H. Ueno, M. Wada, H. Miyatake, "High-efficiency and low-background multi-segmented proportional gas counter for beta-decay spectroscopy," Nucl. Instrum. Methods Phys. Res. A **884**, 1−10 (2018).*

T. Sonoda, H. Iimura, M. Reponen, M. Wada, I. Katayama, V. Sonnenschein, T. Takamatsu, H. Tomita, T.M. Kojima, "The laser and optical system for the RIBF-PALIS experiment," Nucl. Instrum. Methods Phys. Res. A **877**, 118−123 (2018) .*

Y. Hirayama, Y.X. Watanabe, M. Mukai, M. Oyaizu, M. Ahmed, H. Ishiyama, S.C. Jeong, Y. Kakiguchi, S. Kimura, J.Y. Moon, J.H. Park, P. Schury, M. Wada, H. Miyatake, "Doughnut-shaped gas cell for KEK Isotope Separation System," Nucl. Instrum. Methods Phys. Res. B **412**, 11−18 (2017) .*

H. Suzuki, L. Sinclair, P.-A. Söderström, G. Lorusso, P. Davies, L. S. Ferreira, E. Maglione, R. Wadsworth, J. Wu, Z. Y. Xu, S. Nishimura, P. Doornenbal, D. S. Ahn, F. Browne, N. Fukuda, N. Inabe, T. Kubo, D. Lubos, Z. Patel, S. Rice, Y. Shimizu, H. Takeda, H. Baba, A. Estrade, Y. Fang, J. Henderson, T. Isobe, D. Jenkins, S. Kubono, Z. Li, I. Nishizuka, H. Sakurai, P. Schury, T. Sumikama, H. Watanabe, and V. Werner, "Discovery of ^{72}Rb : A nuclear sandbank beyond the proton drip line," Phys. Rev. Lett. **119**, 192503 (2017) .*

Y. Hirayama, M. Mukai, Y. Watanabe, M. Oyaizu, M. Ahmed, Y. Kakiguchi, S. Kimura, H. Miyatake, P. Schury, M. Wada, S.C. Jeong, "Ionization cross section, pressure shift and isotope shift measurements of osmium," J. Phys. B: At. Mol. Opt. Phys. **50**, 215203 (2017) .*

T. Nakajima, K. Okada, M. Wada, V.A. Dzuba, M.S. Safronova, U.I. Safronova, N. Ohmae, "Visible spectra of highly charged holomium ions observed with a compact electron beam ion trap," Nucl. Instrum. Phys. Res., B **408**, 118−121 (2017).*

P. Schury, M. Wada, Y. Ito, D. Kaji, H. Haba, Y. Hirayama, S. Kimura, H. Koura, M. MacCormick, H. Miyatake, J.Y. Moon, K. Morimoto, K. Morita, I. Murray, A. Ozawa, M. Rosenbusch, M. Reponen, A. Takamine, T. Tanaka, Y.X. Watanabe, H. Wollnik, "Observation of doubly-charged ions of francium isotopes extracted from a gas cell," Nucl. Instrum. Methods Phys. Res. B **407**, 160−165 (2017).*

K. Okada, Y. Takeda, N. Kimura, M. Wada, H.A. Schuessler, "Development of a wavy Stark velocity filter for studying interstellar chemistry," Rev. Sci. Instrum. **88**, 0813106 (2017).*

Y. Hirayama, M. Mukai, Y.X. Watanabbe, M. Ahmed, S.C. Jeong, H.S. Jung, Y. Kakiguchi, S. Kanaya, J.Y. Moon, T. Nakatsukasa, M. Oyaizu, J.H. Park, P. Schury, A. Taniguchi, M. Wada, K. Wahiyama, H. Watanabe, H. Miyatake, "In-gas-cell laser spectroscopy of the magnetic dipole moment of the $N \approx 126$ isotope ^{199}Pt," Phys. Rev. C **96**, 014307 (2017).*

[Proceedings]
 (Original Papers) *Subject to Peer Review

M. Commara, M. Mazzocco, A. Boiano, C. Boiano, C. Manea, C. Parascandolo, D. Pierroutsakou, C. Signorini, E. Strano, D. Torresi, H. Yamaguchi, D. Kahl, P.D. Meo, J. Grebosz, N. Imai, Y. Hirayama, H. Ishiyama, N. Iwasa, S.C. Jeong, H.M. Jia, Y.H. Kim, S. Kimura, S. Kubono, C.J. Lin, H. Miyatake, M. Mukai, T. Nakao, M. Nicoletto, Y. Sakaguchi, A.M. Sánchez-Benítez, F. Soramel, T. Teranishi, Y. Wakabayashi, Y.X. Watanabe, L. Yang, Y.Y. Yang, "^{8}B + ^{208}Pb elastic scattering at coulomb barrier energies," EPJ Web Conf. **163**, 00032 (2017) .*

Oral Presentations
[International Conference etc.]

M. Wada, "High Precision Spectroscopy of low-energy short-lived nuclei," Turkish Physical Society 33rd International Physics Congress; TPS33, Bodrum, Turkey, Sept. 9, 2017.

Y. Watanabe, "Production of neutron-rich nuclei by multinucleon transfer reactions at KISS project," 3rd International Symposium on Super-Heavy Elements (SHE 2017), Kazimierz Dolny, Poland, Sept. 11, 2017.

H. Miyatake, "Present status of the KISS project," RCNP International workshop on Physics Opportunities using CAGRA and RCNP tracking Ge detector (CAGRA17), Osaka, Japan, Oct. 10, 2017.

H. Miyatake, "Recent KISS activities and future's plan," Workshop for Einsteinium Campaign, Tokai, Japan, Nov. 7, 2017.

Y. Watanabe, "Nuclear production by multinucleon transfer reactions with neutron-rich heavy ion beams," Workshop for Einsteinium Campaign, Tokai, Japan, Nov. 7, 2017.

M. Wada, "Toward mass measurement of super-heavy nuclei using MRTOF," Workshop for Einsteinium Campaign, Tokai, Japan, Nov. 7, 2017.

M. Wada, "Mass measurements of short-lived nuclei with a multi-reflection time-of-flight mass spectrograph −recent results and future plans−," The 10th International Conference on Nuclear Physics at Storage Rings(STORI'17), Kanazawa, Japan, Dec. 5, 2017.

S. Kimura, "High precision mass measurements of intermediate-mass neutron-deficient nuclei via MRTOF-MS," The 10th International Conference on Nuclear Physics at Storage Rings (STORI'17), Kanazawa, Japan, Nov. 15, 2017.

H. Miyatake, "Present status of the KISS project," BUAA Workshop "Impact of Exotic Nuclear Structure on Explosive Nucleosynthesis," Beijing, China, Nov. 23, 2017.

M. Wada, "Precision mass measurements of short-lived heavy nuclei, present and future toward comprehensive measurement," International Symposium on RI beam Physics in the 21st Century: 10th Anniversary of RIBF, Wako, Japan, Dec. 5 2017.

Y. Hirayama, "Nuclear spectroscopy of r-process nuclei around $N \approx 126$ by using KISS," International Symposium on RI beam Physics in the 21st Century: 10th Anniversary of RIBF, Wako, Japan, Dec. 5, 2017.

Y. Hirayama, "Nuclear spectroscopy of r-process nuclei around $N = 126$ by using KISS," KEK-TRIUMF Scientific Symposium, Vancouver, Canada, Dec. 14–15, 2017.

M. Wada, "KEK MRTOF Efforts," KEK-TRIUMF Scientific Symposium, Vancouver, Canada, Dec. 14–15, 2017.

H. Miyatake, "Scientific activities of KEK-WNSC at RIBF in 2017," KEK-TRIUMF Scientific Symposium, Vancouver, Canada, Dec. 14–15, 2017.

[Domestic Conference]

Y.X. Watanabe, "Multinucleon transfer reactions with low-energy neutron-rich heavy ion beams," ImPACT-OEDO Workshop, Wako, Jul. 13–14, 2017.

Y. Hirayama,「KISS I: ^{199}Pt のレーザー共鳴イオン化核分光」, 日本物理学会, Utsunomiya, Sep. 10–14, 2017.

M. Mukai,「KISS II：$^{196-198}$Ir のレーザー共鳴イオン化核分光」,日本物理学会, Utsunomiya, Sep. 10–14, 2017.

M. Wada,「MRTOF 質量分光器を用いた重元素の網羅的高精度質量測定」, 2017 年度核データ研究会, 東海村, Nov. 17, 2017.

H. Miyatake,「KISS、超微細構造測定と質量測定の現状」,平成 29 年度 KUR 専門研究会 短寿命 RI を用いた核分光と核物性研究 Ⅳ, Kumatori, Dec. 20–21, 2017.

Events (April 2017—March 2018)

RNC

Apr. 22	Wako Open Campus
Jun. 15	The 23rd RBRC Management Steering Committee (MSC)
Jul. 3	The 14th Program Advisory Committee for Materials and Life Science Researches at RIKEN Nishina Center (ML-PAC)
Jul.24–Aug.4	Nishina School
Aug. 4	Review of the Safety Management Group
Oct. 30	Review of the Accelerator Applications Research Group
Nov. 2	Review of the Instrumentation Development Group, the Research Instruments Group and the User Liaison and Industrial Cooperation Group
Dec. 7–9	The 18th Program Advisory Committee for Nuclear Physics Experiments at RI Beam Factory (NP-PAC)
Jan. 11–12	The 15th Program Advisory Committee for Materials and Life Science Researches at RIKEN Nishina Center (ML-PAC)
Jan. 19	The 7th Industrial Program Advisory Committee (In-PAC)

CNS

Aug. 23–29	16th CNS International Summer School CNSSS17 https://indico2.cns.s.u-tokyo.ac.jp/event/8/
Dec. 19	Completion Ceremony for the Construction of OEDO（OEDO 完成記念式典）

Niigata Univ.

Sep. 4–5	3rd Workshop on Many-body Correlations in Microscopic Nuclear Model

KEK

	not held in FY2017

Press Releases (April 2017–March 2018)

RNC

May. 17	Gamma decay of unbound neutron-hole states in ^{133}Sn	P. Doornenbal, H. Sakurai, Radioactive Isotope Physics Laboratory
May. 19	Auroral brightening at Jupiter observed by the Hisaki satellite and Hubble Space Telescope during approaching phase of the Juno spacecraft	T. Kimura, High Energy Astrophysics Laboratory
Jun. 13	Shapes evolution in neutron-rich krypton isotopes beyond $N = 60$: First spectroscopy of $^{98, 100}$kr	The SEASTAR collaboration group
Jun. 28	First elastic electron scattering from ^{132}Xe at the SCRIT facility	M. Wakasugi, SCRIT Team
Jul. 18	Success in producing and accelerating high intensity vanadium beam	T. Nakagawa, Y. Higurashi, Ion Source Team
Jul. 18	Decay measurement of ^{283}Cn produced in the ^{238}U(^{48}Ca, ^{3}n) reaction using GARIS-Ⅱ	D. Kaji, K. Morimoto, Superheavy Element Research Device Development Team
Nov. 1	Discovery of ^{72}Rb: A nuclear sandbank beyond the proton drip-line	H. Suzuki, BigRIPS Team, S. Nishimura, H. Sakurai, Radioactive Isotope Physics Laboratory
Dec. 21	Identification of new neutron-rich isotopes in the rare-earth region produced by 345 MeV/nucleon ^{238}U	N. Fukuda, K. Yoshida, BigRIPS Team
Jan. 5	Nuclear dependence of transverse single spin asymmetry for forward neutron production in polarized p + A collisions at $\sqrt{s_{NN}}$ = 200 GeV	Y. Akiba, Experimental Group, I. Nakagawa, Radiation Laboratory

WNSC

Mar. 29	First direct mass measurements of 6 nuclides of trans-uranium elements nuclides, Md and Es	M. Wada, P. Schury, Y. Ito, D. Kaji

VII. LIST OF PREPRINTS

List of Preprints (April 2017 — March 2018)

RIKEN NC-NP

178	Atomic masses of intermediate-mass neutron-deficient nuclei with relative uncertainty down to 35-ppb via multireflection time-of-flight mass spectrograph	S. Kimura, Y. Ito *et al.*
180	Hidden-charm and bottom meson-baryon molecules coupled with five-quark states	Y. Yamaguchi, A. Giachino *et al.*
181	Mesic nuclei with a heavy antiquark	Y. Yamaguchi, S. Yasui
182	Testing the constant-temperature approach for the nuclear level density	N. Dinh Dang, N. Quang Hung *et al.*
183	Level density and thermodynamics in the hot rotating ^{96}Tc nucleus	B. Dey, D. Pandit *et al.*
184	Bubble nuclei within the self-consistent Hartree-Fock mean field plus pairing approach	L. Tan Phuc, N. Quang Hung, N. Dinh Dang
185	Interplay between isoscalar and isovector correlations in neutron-rich nuclei	I. Hamamoto, H. Sagawa
186	Development of co-located ^{129}Xe and ^{131}Xe nuclear spin masers with external feedback scheme	T. Sato, Y. Ichikawa *et al.*
187	Nuclear surface diffuseness revealed in nucleon-nucleus diffraction	S. Hatakeyama, W. Horiuchi, A. Kohama

RIKEN NC- AC

	Not Applicable	

RIKEN MP

	Not Applicable	

RIKEN QHP

306	Observation of an alternative $\chi_{c0}(2P)$ candidate in $e^+e^- \to J/\psi D\bar{D}$	K. Chilikin, I. Adachi *et al.*
307	$p\Xi^-$ Correlation in relativistic heavy ion collisions with nucleon-hyperon interaction from lattice QCD	T. Hatsuda, K. Morita *et al.*
308	Structure of virtual photon polarization in ultrarelativistic heavy-ion collisions	G. Baym, T. Hatsuda, M. Strickland
309	Fully self-consistent relativistic Brueckner-Hartree-Fock theory for finite nuclei	S. Shen, H. Liang *et al.*
310	The limits of the nuclear landscape explored by the relativistic continuum Hatree-Bogoliubov theory	X. W. Xia, Y. Lim *et al.*
311	Complete random matrix classification of SYK models with $N = 0, 1$ and 2 supersymmetry	T. Kanazawa, T. Wettig
312	Renormalization group flows of the N-component Abelian Higgs model	G. Fejos, T. Hatsuda
313	Dirac-mode expansion of quark number density and its implications of the confinement-deconfinement transition	T. M. Doi, K. Kashiwa
314	Goldstino in supersymmetric Bose-Fermi mixtures in the presence of Bose Einstein condensate	J. P. Blaizot, Y. Hidaka, D. Satow
315	Edge states and thermodynamics of rotating relativistic fermions under magnetic field	M. Chernodub, S. Gongyo
316	From hadrons to quarks in neutron stars	G. Baym, T. Hatsuda *et al.*
317	Correlations of energy-momentum tensor via gradient flow in SU(3) Yang-Mills theory at finite temperature	M. Kitazawa, T. Iritani *et al.*
318	Vortex continuity from the hadronic to the color-flavor locked phase	M. Alford, G. Baym *et al.*

319	Sanity check for NN bound states in lattice QCD with Lüscher's finite volume formula – Exposing Symptoms of Fake Plateaux –	S. Aoki, T. Doi, T. Iritani
320	Most strange dibaryon	S. Gongyo, K. Sasaki *et al.*
321	General formulae for dipole Wilson line correlators with the Color Glass Condensate	K. Fukushima, Y. Hidaka
322	Hidden-charm and bottom meson-baryon molecules coupled with five-quark states	Y. Yamaguchi, A. Giachino *et al.*
323	Measurement of branching fraction and direct CP asymmetry in charmless $B^+ \to K^+K^-\pi^+$ decays at Belle	C. L. Hsu, D. Dossett *et al.*
324	Search for CP violation and measurement of the branching fraction in the decay $D^0 \to K_S^0 K_S^0$	N. Dash, S. Bahinipati *et al.*
325	Production cross sections of hyperons and charmed baryons from e^+e^- annihilation near $\sqrt{s} = 10.52$ GeV	M. Niiyama, M. Sumihama *et al.*
326	Invariant-mass and fractional-energy dependence of inclusive production of di-hadrons in e^+e^- annihilation at $\sqrt{s} = 10.58$ GeV	R. Seidl, I. Adachi *et al.*
327	Evidence for isospin violation and measurement of CP asymmetries in $B \to K^*(892)\gamma$	T. Horiguchi, A. Ishikawa *et al.*
328	Search for $\Lambda_c^+ \to \phi p \pi^0$ and branching fraction measurement of $\Lambda_c^+ \to K^-\pi^+ p \pi^0$	F. Okiharu, T. Doi *et al.*
329	Study of η and dipion transitions in $\Upsilon(4S)$ decays to lower bottomonia	E. Guido, R. Mussa *et al.*
330	Angular analysis of the $e^+e^- \to D^{(*)\pm}D^{*\mp}$ process near the open charm threshold using initial-state radiation	V. Zhukova, G. Pakhlova *et al.*
331	Mesic nuclei with a heavy antiquark	Y. Yamaguchi, S. Yasui
332	Functional renormalization group and Kohn-Sham scheme in density functional theory	H. Liang, Y. Niu, T. Hatsuda
333	Multi modification method toward solving sign problem	T. M. Doi, S. Tsutsui
334	Electric conductivity of hot and dense quark matter in a magnetic field with Landau level resummation via kinetic equations	K. Fukushima, Y. Hidaka
335	$\Lambda_c N$ interaction from lattice QCD and its application to Λ_c hypernuclei	T. Miyamoto, S. Aoki *et al.*
336	Two-baryon systems from HAL QCD method and the mirage in the temporal correlation of the direct method	T. Iritani, for HAL QCD Collaboration
337	The $I = 2$ $\pi\pi$ s-wave scattering phase shift from lattice QCD	S. R. Beane, E. Chang *et al.*
338	Baryon interactions from lattice QCD with physical quark masses – Nuclear forces and $\Xi\Xi$ forces –	T. Doi, T. Iritani *et al.*
339	Application of a Coulomb energy density functional for atomic nuclei: Case studies of local density approximation and generalized gradient approximation	T. Naito, R. Akashi, H. Liang
340	Baryon interactions from lattice QCD with physical masses – $S = -3$ sector: $\Xi\Sigma$ and $\Xi\Lambda - \Xi\Sigma$ –	N. Ishii, S. Aoki *et al.*
341	Baryon interactions from lattice QCD with physical masses – strangeness $S = -1$ sector –	H. Nemura, S. Aoki *et al.*
342	Comment on "Relation between scattering amplitude and Bethe-Salpeter wave function in quantum field theory"	S. Aoki, T. Doi *et al.*
343	Lattice QCD studies on baryon interactions in the strangeness -2 sector with physical quark masses	K. Sasaki, S. Aoki *et al.*
344	Matrix model with a topological effect	T. Kanazawa, M. Kieburg, J. Verbaarschot
345	Revised and improved value of the QED tenth-order electron anomalous magnetic moment	T. Aoyama, T. Kinoshita, M. Nio
346	Conformal quantum mechanics and sine-square deformation	T. Tada
347	Nuclear mass predictions based on Bayesian neural network approach with pairing and shell effects	Z. M. Niu, H. Z. Liang
348	Search for $B^- \to \mu^-\bar{\nu}_\mu$ decays at the Belle experiment	A. Sibidanov, K. E. Varvell *et al.*
349	Measurements of the absolute branching fractions of $B^+ \to X_{c\bar{c}}K^+$ and $B^+ \to \bar{D}^{(*)0}\pi^+$ at Belle	Y. Kato, T. Iijima *et al.*
350	Measurement of the τ lepton polarization and $R(D^*)$ in the decay $B^- \to D^*\tau^-\bar{\nu}_\tau$ with one-prong hadronic τ decays at Belle	S. Kisaka, K. Asano *et al.*

351	Observation of excited Ω_c^0 charmed baryons in e^+e^- collisions	J. Yelton, I. Adachi *et al.*
352	Measurement of branching fractions of hadronic decays of the Ω_c^0 baryon	J. Yelton, I. Adachi *et al.*
353	Search for light tetraquark states in $\Upsilon(1S)$ and $\Upsilon(2S)$ decays	S. Jia, C. P. Shen *et al.*
354	Study of K_S^0 pair production in single-tag two-photon collisions	M. Masuda, S. Uehara *et al.*
355	Observation of $\Xi_c(2930)^0$ and updated measurement of $B^- \to K^- \Lambda_c^+ \overline{\Lambda}_c^-$ at Belle	Y. B. Li, C. P. Shen *et al.*
356	Effects of tensor forces in nuclear spin-orbit splittings from ab initio calculations	S. Shen, H. Liang *et al.*
357	Gamow-Teller transitions from high-spin isomers in $N = Z$ nuclei	H. Z. Liang, H. Sagawa *et al.*
358	Combination of complex momentum representation and Green's function methods in relativistic mean-field theory	M. Shi, Z. M. Niu, H. Liang
359	Spin susceptibility and effects of a harmonic trap in the BCS-BEC crossover regime of an ultracold Fermi gas	H. Tajima, R. Hanai, Y. Ohashi
360	Superfluid Fermi atomic gas as a quantum simulator for the study of the neutron-star equation of state in the low-density region	P. van Wyk, H. Tajima *et al.*
361	Many Fermi polarons in a strongly interacting polarized mixture	H. Tajima, S. Uchino
362	Precursor of superfluidity in a strongly interacting Fermi gas with negative effective range	H. Tajima
363	Relativistic Brueckner-Hartree-Fock theory for neutron drops	S. Shen, H. Liang *et al.*
364	Spin symmetry in the Dirac sea derived from the bare nucleon-nucleon interaction	S. Shen, H. Liang *et al.*
365	Stress-tensor distribution in Yang-Mills flux tube – Direct observation on the Lattice with gradient flow –	R. Yanagihara, T. Iritani *et al.*
366	On the observer dependence of the Hilbert space near the horizon of black holes	K. Gotoa, Y. Kazama
367	Continuity of vortices from the hadronic to the color-favor-locked phase in dense matter	M. G. Alford, G. Baym et al.
368	Non-equilibrium chiral magnetic/vortical effects in viscous fluids	D. Yang, Y. Hidaka
369	Effects of tensor force in the relativistic scheme: A case study of neutron drops	S. Shen, H. Liang *et al.*
370	Systematics of the HAL QCD potential at low energies in lattice QCD	T. Iritani, S. Aoki *et al.*
371	Heavy quark spin multiplet structure of $\bar{P}^{(*)}\Sigma_Q^{(*)}$ molecular states	Y. Shimizu, Y. Yamaguchi, M. Harada
372	Image-processing the topological charge density in the $\mathbb{C}P^{N-1}$ model	Y. Abe, K. Fukushima *et al.*

CNS-REP

96	CNS Annual Report 2016	T. Gunji, Y. Kishi

Nishina Center Preprint server (not including Partner Institution) can be found at
   http://nishina-preprints.riken.jp/

VIII. LIST OF SYMPOSIA, WORKSHOPS & SEMINARS

List of Symposia & Workshops (April 2017—March 2018)

RNC

1	Saturation: Recent Developments, New Ideas and Measurements https://www.bnl.gov/sdim17/	BNL	Apr. 26–28
2	Interdisciplinary Symposium on Modern Density Functional Theory — iDFT https://indico2.riken.jp/event/2498/	Okochi Hall	Jun. 19–23
3	Synergies of pp and pA Collisions with an Electron-Ion Collider https://www.bnl.gov/pppa17/	BNL	Jun. 26–28
4	ImPACT-OEDO workshop 2017 https://indico2.riken.jp/event/2534/	RIBF Conference Room	Jul. 13–14
5	X-ray Objects and Element Synthesis https://indico2.riken.jp/event/2530/	RIBF Conference Room	Jul. 20
6	RIBF 理論若手放談会：エキゾチック核物理の広がり https://indico2.riken.jp/event/2509/	RIKEN IIB	Jul. 31– Aug. 2
7	International Workshop on Organic Molecule Systems http://www.riken.jp/~/media/riken/pr/events/symposia/20170801/20170801_p.pdf	Parkroyal Hotel Malaysia	Aug. 1–3
8	The 3rd Emallia Conference 2017 http://phys.sci.hokudai.ac.jp/rikensympo/Emallia2/	National Pusan U. Busan City	Sep. 7–8
9	STORI'17—10th International Conference on Nuclear Physics at Storage Rings https://indico2.riken.jp/event/2581/	Kanazawa Theatre	Nov. 13–18
10	International Symposium on RI Beam Physics in the 21st Century: 10th Anniversary of RIBF https://indico2.riken.jp/event/2541/	RIBF Conference Room	Dec. 4–5
11	RIBF Users Meeting 2017 https://indico2.riken.jp/event/2637/	RIBF Conference Room	Dec. 6
12	イオンビーム品種改良プラットフォームの形成 http://www.riken.jp/~/media/riken/pr/events/symposia/20180125/20180125p.pdf	Suzuki Umetaro Hall	Jan. 25–26

CNS

1	Ito International Research Center (IIRC) Symposium "Perspectives of the Physics of Nuclear Structure"	CNS	Nov. 1–4
2	ImPACT-OEDO Workshop	RIBF Conference Room	Jul. 13–14

List of Seminars (April 2017—March 2018)

Nuclear Physics Monthly Colloquium

1	Atsushi Mochizuki (RIKEN)	Dynamical behaviors of complex biological systems https://indico2.riken.jp/event/2466/	Apr. 18
2	Yoshiharu Mori (Kyoto U.)	Advanced FFAG accelerator https://indico2.riken.jp/event/2622/	Nov. 28
3	Satoshi Nakamura (Tohoku U.)	Study of hypernuclei with electron beams https://indico2.riken.jp/event/2667/	Dec. 26
4	Yasuo Arai (KEK)	Quantum imaging with 3D semiconductor detector https://indico2.riken.jp/event/2725/	Mar. 13

RIBF Nuclear Physics Seminar

1	Minori Abe (Tokyo Metropolitan U.)	HPC in precision relativistic quantum chemistry and recent applications to physics and chemistry https://indico2.riken.jp/event/2471/	Apr. 4
2	Nguyen Dinh Dang (RNC)	Simultaneous microscopic description of nuclear level density and radiative strength function https://indico2.riken.jp/event/2465/	Apr. 11
3	Marco Rosenbusch (RNC)	Online application of multi-reflection time-of-flight mass spectrometry — nuclear masses and beyond https://indico2.riken.jp/event/2497/	May. 9
4	Paer-Anders Soederstroem (TU Darmstadt)	Evolution of nuclear structure and collectivity in the rare-earth region https://indico2.riken.jp/event/2495/	May. 12
5	Newcomers to Nishina Center in 2017	Newcomers' Seminar https://indico2.riken.jp/event/2506/	May. 16
6	Masaaki Kimura (Hokkaido U.)	Nuclear clustering probed by nuclear responses https://indico2.riken.jp/event/2538/	Jun. 13
7	Kyo Tsukada (Tohoku U.)	First result of the SCRIT electron scattering facility https://indico2.riken.jp/event/2544/	Jul. 11
8	Kazunari Yamada (RNC)	Construction of superconducting LINAC at RNC https://indico2.riken.jp/event/2578/	Jul. 25
9	Yuki Kubota (RNC)	Probing neutron-neutron correlation in ^{11}Li through the quasi-free (p,pn) reaction https://indico2.riken.jp/event/2663/	Dec. 19
10	Shigehiro Yasui(TokyoTech)	Impurity physics of heavy flavor in quark matter at low temperature and high density —QCD Kondo effect— https://indico2.riken.jp/event/2687/	Jan. 23
11	Tomoki Kimura (RNC)	Transient brightening of Jupiter's aurora observed by the Hisaki satellite and Hubble Space Telescope during approach phase of the Juno spacecraft https://indico2.riken.jp/event/2689/	Jan. 30
12	Yasuhiro Togano (Rikkyo U.)	Interaction cross section of two-neutron halo nucleus ^{22}C at 235 MeV/nucleon https://indico2.riken.jp/event/2690/	Feb. 20
13	Sohtaro Kanda (RNC)	Precision microwave spectroscopy of the ground-state hyperfine splitting in muonium atom https://indico2.riken.jp/event/2731/	Mar. 6
14	Masayuki Matsuo (Niigata U.)	Di-neutron correlation, pairing collectivity and pair transfer in neuron-rich systems https://indico2.riken.jp/event/2741/	Mar. 20

Lecture Series on Nuclear Physics

	not held in FY2017	-	

Seminar by Each Laboratory

Theoretical Research Division

1	Tilo Wettig (U. Regensburg)	QHP Seminar: HPC in precision medicine	Apr. 11
2	Hyun-Chul Kim (Inha U.)	SNP Seminar: Heavy Baryons and excited baryons in the pion mean fields	Apr. 18
3	Ulugbek Yakhshiev (Inha U.)	SNP Seminar: Topological models and their applications	Apr. 18
4	Kochi Murase (U. Tokyo)	QHP Seminar: Fixed points and flow analysis of the boson Boltzmann equation	May. 2
5	Daisuke Satow (Frankfurt U.)	QHP Seminar: Viscosities and electrical conductivity of QGP in strong magnetic fields	May. 9
6	Yudai Suwa (Kyoto U.)	SNP Seminar: Formation of neutron stars	May. 29
7	Noriaki Sannomiya (U. Tokyo)	QHP Seminar: Spontaneous supersymmetry breaking and Nambu-Goldstone fermions in extended Nicolai models	May. 30
8	Chihiro Matsui (U. Tokyo)	QHP Seminar: Hidden supersymmetry in the Fateev-Zamolodchikov spin chain	Jun. 6
9	Emi Yukawa (RIKEN CEMS)	QHP Seminar: Classification, generation, and application of spin squeezing	Jun. 13
10	Mitsunori Fukuda (Osaka U.)	SNP Seminar: Study of surface structure of nuclei via reaction cross sections	Jun. 16
11	Takaya Miyamoto (Kyoto U.)	SNP Seminar: $\Lambda_c N$ interaction from lattice QCD and its application to Λ_c hypernuclei	Jul. 5
12	Kenji Sasaki (Kyoto U.)	SNP Seminar: Lattice QCD study on baryon-baryon interactions	Jul. 5
13	Hidehiko Shimada (OIST)	QHP Seminar: String field theory for tensionless strings and $N = (2, 0)$ superconformal theory in six-dimensions	Jul. 11
14	Hyeon-Deuk Kim (Kyoto U.)	SNP Seminar: Quantum molecular dynamics simulation method for hydrogen molecules —From a small molecule to condensed phases—	Sep. 15
15	Sophia Han (U. Tennessee)	QHP Seminar: Constraining dense matter properties from thermal and spin evolution of neutron stars	Sep. 25
16	Enrico Rinaldi (RBRC)	QHP Seminar: The nucleon axial charge from Lattice QCD	Oct. 3
17	Naoki Yamamoto (Keio U.)	QHP Seminar: Topological transport of photons and gravitons	Oct. 6
18	Keisuke Fujii (Tokyo Tech)	QHP Seminar: Effective field theory approach to superfluid ^{3}He-B	Oct. 17
19	Utku Can (RNC)	QHP Seminar: Charmed baryon structure in Lattice QCD	Oct. 24

20	Shigehiro Yasui (Tokyo Tech)	QHP Seminar: QCD Kondo effect in quark matter with heavy flavor	Oct. 31
21	Shun Uchino (RIKEN CEMS)	QHP Seminar: Mesoscopic transport with an ultracold atomic gas	Nov. 7
22	Takeru Yokota (Kyoto U.)	QHP Seminar: Tachyonic instability of the scalar mode prior to the QCD critical point based on the functional renormalization-group method in the two-flavor case	Nov. 14
23	Shoichiro Tsutsui (KEK)	QHP Seminar: Thermalization of overpopulated systems	Nov. 21
24	Yang-Ting Chien (MIT)	QHP Seminar: Probing heavy ion collisions using quark and gluon jet substructure with machine learning	Nov. 24
25	Kouji Kashiwa (YITP)	QHP Seminar: Sign problem as optimization problem: Application of neural-network via path optimization method	Nov. 28
26	Shinji Shimazaki (Keio U.)	QHP Seminar: New developments in the complex Langevin method and its application to finite density QCD	Jan. 23
27	Arata Yamamoto (U. Tokyo)	QHP Seminar: Computation of the Berry curvature in QCD and in condensed matter physics	Jan. 30
28	M. Tachikawa (Yokohama City U.)	SNP Seminar: Ab initio calculation for positronic compounds	Feb. 20
29	Michio Kohno (Osaka U.)	SNP Seminar: Hyperons in nuclear matter from YN and YNN interactions in ChEFT and hyperon puzzle	Feb. 21
30	Yuichiro Sekiguchi (Toho U.)	QHP Seminar: Foundations of Gravitational waves and electro-magnetic emissions from NS-NS merger with application to nuclear/hadron physics	Feb. 26
31	Yang-Ting Chien (MIT)	QHP Seminar: Telescoping Jet Substructure	Mar. 6

QHP Seminar -> http://ribf.riken.jp/QHP/seminar.html
SNP Seminar -> http://snp.riken.jp/seminar.html

Sub Nuclear System Research Division

1	Zohreh Davoudi (MIT)	A Special HET/RIKEN Lunch Seminar: The road to nuclear physics from standard model	Apr. 6
2	Dirk Rischke (Johann Wolfgang Goethe U.)	Nuclear Theory/RIKEN Seminar: Anisotropic dissipative fluid dynamics — foundations & applications in heavy-ion physics	Apr. 7
3	Laura Tolos (CSIC-IEEC)	RBRC Lunch Seminar: Charm and beauty @ extremes	Apr. 13
4	Ajit M. Srivvastava (Emory U.)	Nuclear Theory/RIKEN Seminar: Effect of magnetic field on flow fluctuations in	Apr. 14
5	Tuomas Lappi (U. Jyväskylä)	Nuclear Theory/RIKEN Seminar: Forward particle production in pA: implementing the NLO hybrid formalism	Apr. 21
6	Simon Caron-Huot (McGill U.)	Nuclear Theory/RIKEN Seminar: Analyticity in spin and causality in conformal theories	Apr. 28
7	Ethan Neil (RBRC)	RIKEN Lunch Seminar: Lattice study of gauge theory with multiple fermion representations	May. 4
8	Scott Moreland (Duke U.)	Nuclear Theory/RIKEN Seminar: Probing nucleon substructure with Bayesian parameter estimation	May. 5

9	Enrico Rinaldi (RBRC)	RIKEN Lunch Seminar: The nucleon axial charge from lattice QCD	May. 11
10	Jonathan Kozaczuk (U. Mass Amherst)	HET/RIKEN Seminars: Collider and cosmological signatures of a strong electroweak phase transition	May. 17
11	Dima Kharzeev (BNL / Stony Brook U.)	RIKEN Lunch Seminar: Probing quantum entanglement at the Electron Ion Collider	May. 18
12	Patrick Fox (Fermilab)	HET/RIKEN Seminar: Cosmology in mirror twin Higgs and neutrinos	May. 24
13	Yuya Tanizaki (RBRC)	RIKEN Lunch Seminar: Mixed anomaly and global consistency	May. 25
14	Damir Bosnar (U. Zagreb)	Investigations of nucleon and nuclei properties in electron scattering experiments at MAMI	May. 29
15	Derek Teaney (Stony Brook U.)	Nuclear Theory/RIKEN Seminar: Hydrodynamic fluctuations in heavy ion collisions	Jun. 2
16	Zohar Komargodski (Stony Brook U.)	RIKEN Lunch Seminar: Anomalies and exact results in massive quantum chromodynamics	Jun. 8
17	Phiala Shanahan (MIT)	Nuclear Theory/RIKEN Seminar: Gluon structure of hadrons and nuclei	Jun. 9
18	Daniel Stolarski (Carleton U.)	HET/RIKEN Seminars Searching for new physics with Higgs decays	Jun. 14
19	Jan Pawlowski (Heidelberg)	Nuclear Theory/RIKEN Seminar: Exploring the phase structure and dynamics of QCD	Jun. 16
20	Pasi Huovinen (U. Wroclawski)	Nuclear Theory/RIKEN Seminar: Better fitting through (fictitious) chemistry	Jun. 19
21	Feng Yuan (LBL)	Nuclear Theory/RIKEN Seminar: Probing transverse momentum broadening in heavy ion collisions	Jun. 30
22	Ismail Zahed (Stony Brook U.)	Nuclear Theory/RIKEN Seminar: Holographic Pomeron: Scattering, saturation, entropy and black hole	Jul. 7
23	Kenji Fukushima (U. Tokyo)	Nuclear Theory/RIKEN Seminar: General formulae for dipole Wilson line correlators with the Color Glass Condensate	Aug. 4
24	Yoshitaka Hatta (Kyoto U.)	Nuclear Theory/RIKEN Seminar: Resummation of nonglobal logarithms in QCD	Aug. 11
25	Ming Li (U. Minnesota)	RIKEN Lunch Seminar: Revisit the energy density and the gluon spectrum in the boost-invariant Glasma from a semi-analytic approach	Aug. 17
26	Ignazio Scimemi (U. Complutense de Madrid)	Nuclear Theory/RIKEN Seminar: Factorization and phenomenology for transverse momentum dependent distributions	Aug. 18
27	Werner Vogelsang (Tuebingen U.)	Nuclear Theory/RIKEN Seminar: QCD corrections to high-p_T hadron production in ep scattering	Aug. 25
28	Mayank Singh (McGill U.)	RIKEN Lunch Seminar: Thermal fluctuations in hydrodynamic simulations of QGP	Sep. 14
29	Elena Petreska (NIKHEF)	Nuclear Theory/RIKEN Seminar: TMD gluon distributions for dijet production and their behavior at small x	Sep. 15
30	Monica Pate (Harvard U.)	RIKEN Lunch Seminar: Color memory, large gauge transformations, and soft theorems in Yang-Mills theory	Sep. 28
31	Aleksey Cherman (U. Washington)	Nuclear Theory/RIKEN Seminar: QCD on a small circle	Sep. 29

32	Jacquelyn Noronha-Hostler (Rutgers U.)	Nuclear Theory/RIKEN Seminar: What can we learn from flow observables in heavy-ion collisions?	Oct. 12
33	Aaron Meyer (HET Group)	RIKEN Lunch Seminar: Lattice QCD and neutrino physics	Oct. 19
34	Maxim Mai (George Washington U.)	Nuclear Theory/RIKEN Seminar: Quantization of three-body scattering amplitude in isobar formulation	Oct. 20
35	Xiaojun Yao (BNL)	RIKEN Lunch Seminar: Approach to equilibrium of quarkonium in quark-gluon plasma	Oct. 26
36	Andrea Shindler (Michigan State U.)	HET/RIKEN Seminar: Calculation of the electric dipole moment with the gradient flow	Nov. 1
37	Yizhuang Liu (Stony Brook U.)	RIKEN Lunch Seminar: Rotating Dirac fermion in Magnetic field in 1+2 and 1+3 dimensions	Nov. 2
38	Gerald Miller (U. Washington)	Nuclear Theory/RIKEN Seminar: Proton radius puzzle	Nov. 3
39	Mario Mitter (BNL)	RIKEN Lunch Seminar: QCD from gluon, quark, and meson correlators	Nov. 16
40	Yacine Mehtar-Tani (U. Washington)	Nuclear Theory/RIKEN Seminar: Higher-order corrections to jet quenching	Nov. 17
41	Shanshan Cao (Wayne State U.)	Nuclear Theory/RIKEN seminar: Medium modification of jet and jet-induced medium excitation	Dec. 1
42	Jorge Noronha (Columbia U.)	RIKEN Lunch Seminar: Pushing the boundaries of relativistic fluid dynamics	Dec. 7
43	Nobuo Sato (Jlab / U. Connecticut)	Nuclear Theory/RIKEN Seminar: Simultaneous extraction of spin-dependent parton distributions	Dec. 15
44	Sourav Raha (U. Florida)	Nuclear Theory/RIKEN Seminar: Thermodynamics of string bits	Jan. 5
45	Nikhil Karthik (BNL)	RIKEN Lunch Seminar: Three-dimensional gauge theories using lattice regularization	Jan. 11
46	Niklas Mueller (BNL)	RIKEN Lunch Seminar: World-line approach to chiral kinetic theory and the chiral magnetic effect	Jan. 18
47	Felix Ringer (LBL)	Nuclear Theory/RIKEN Seminar: Semi-inclusive jet cross sections within SCET	Jan. 19
48	Yuya Tanizaki (RBRC)	RIKEN Lunch Seminar: Exact results on massless 3-flavor QCD through new anomaly matching	Jan. 25
49	Kiminad Mamo (Stony Brook U.)	RIKEN Lunch Seminar: The Coulomb branch of $N = 4$ SYM and its gravity dual as a new holographic model to QCD	Feb. 1
50	Mohamed Anber (Lewis & Clark College)	Nuclear Theory/RIKEN Seminar: New nonperturbative scales and glueballs in confining gauge theories	Feb. 2
51	Adrian Dumitru (Baruch College / BNL)	RIKEN Lunch Seminar: Biased nuclear gluon distribution from a reweighted JIMWLK small-x ensemble	Feb. 8
52	Stebel Tomasz (BNL)	RIKEN Lunch Seminar: Drell-Yan process beyond collinear approximation	Feb. 22
53	Benedikt Hegner (CERN)	High-Energy Physics & RIKEN Theory Seminar: Preparing high energy physics software for the future - the community white paper	Feb. 28
54	Matt Sievert (LANL)	Nuclear Theory/RIKEN Seminar: Quark / Antiquark correlations in heavy-light ion collisions	Mar. 2

55	Anna Stasto (Penn State U.)	Nuclear Theory/RIKEN Seminar: Yang-Mills action on the light front: MHV amplitudes and Wilson lines	Mar. 9
56	Kazunori Itakura (KEK)	Basics of pomerons and reggeons	Mar. 14
57	Andreas Nyffeler (U. Mainz)	RIKEN Lunch Seminar: Hadronic light-by-light scattering in the muon $g-2$	Mar. 15
58	Ian Balitsky (Jefferson National Lab.)	Nuclear Theory/RIKEN Seminar: Correlators of twist-2 light-ray operators in the BFKL approximation	Mar. 16

RIKEN/BNL Lunch Seminar -> https://www.bnl.gov/riken/events/

RIBF Research Division

1	Teruaki Enoto (Kyoto U.)	High Energy Astrophysics Lab. Seminar: Cloud and crowd science: High-energy physics in thunderstorms	Apr. 3
2	Turriziani Sara (RIKEN)	High Energy Astrophysics Lab. Seminar: Active galactic nuclei in the multi-wavelength, multi-messanger era	May. 1
3	Keita Kawata (CNS)	NSL Seminar: Development of isomer beam by fragmentation reactions	May. 17
4	Momo Mukai (U. Tsukuba)	NSL Seminar: The development of a low-background gas-counter and hyperfine structure measurement for neutron-rich iridium isotopes	May. 17
5	Tomoki Kimura (RNC)	High Energy Astrophysics Lab. Seminar: Transient brightening of Jupiter's aurora observed by the Hisaki satellite and Hubble Space Telescope during approach phase of the Juno spacecraft	Jun. 5
6	Hiroshi Yamakawa (Kyoto U.)	High Energy Astrophysics Lab. Seminar: Research for tackling hazardous space environment	Jul. 10
7	Toshikazu Morishita (NARO)	重イオンビームによるダッタンソバの変異誘発と有用系統の選抜	Jul. 11
8	Ryosuke Hirai (Waseda U.)	High Energy Astrophysics Lab. Seminar: The influence of supernovae on the evolution of binary systems	Oct. 2
9	Yasuyuki Nagashima (Tokyo U. of science)	Ps⁻ photodetachment spectroscopy and its application https://indico2.riken.jp/indico/conferenceDisplay.py?confId=2610	Oct. 18
10	Toru Tamagawa (RNC)	The dawn of the gravitational wave astronomy and the discovery of the neutron star merger https://indico2.riken.jp/event/2621/	Oct. 31
11	Ayako Yamamoto (SIT)	NSL Seminar: Cuprate high-T_c superconductors: Materials and Properties	Jan. 26
12	Alberto Mengoni (ENEA/INFN)	Exploring a neutron channel solution for the cosmological lithium problem at CERN/n_TOF https://indico2.riken.jp/event/2742/	Mar. 13

High Energy Astrophysics Lab. Seminar -> http://astro.riken.jp/wordpress/?page_id=65